Postclosure Safety Assessment of a Used Fuel Repository in Crystalline Rock

NWMO TR-2017-02

December 2017

NUCLEAR WASTE MANAGEMENT ORGANIZATION
SOCIÉTÉ DE GESTION DES DÉCHETS NUCLÉAIRES

Nuclear Waste Management Organization
22 St. Clair Avenue East, 6^{th} Floor
Toronto, Ontario
M4T 2S3
Canada

Tel: 416-934-9814
Web: www.nwmo.ca

EXECUTIVE SUMMARY

For decades Canadians have been using electricity generated by nuclear power reactors in Ontario, Quebec and New Brunswick. The used nuclear fuel removed from these reactors is a highly radioactive waste product requiring careful short and long-term management. Although its radioactivity decreases with time, the used fuel will remain a potential health risk for many hundreds of thousands of years. Canada's used nuclear fuel is now safely stored on an interim basis at licensed facilities located where it is produced.

The Nuclear Waste Management Organization (NWMO) is responsible for the implementation of Adaptive Phased Management (APM), the federally-approved plan for safe long-term management of Canada's used nuclear fuel. Under the APM plan, used nuclear fuel will ultimately be placed within a deep geological repository in a suitable rock formation.

A deep geological repository is a multi-barrier system designed to protect people and the environment in the long term. The barriers are the durable wasteform, long-lived corrosion resistant containers, engineered sealing materials and the surrounding geosphere.

A site selection process is currently underway to identify a safe site for a deep geological repository in an informed and willing host community. The process of site selection will take several years. As potentially suitable sites are identified with interested communities, detailed field studies and geoscientific site characterization activities will be conducted to assess whether the APM multi-barrier repository concept could be safely implemented to meet rigorous regulatory requirements.

At this early stage in the process, before specific sites have been identified for detailed examination, NWMO has been conducting generic studies to understand and illustrate the long-term performance and safety of the multi-barrier repository system within various geological settings.

This report provides an illustrative case study of postclosure safety for a deep geological repository in a hypothetical crystalline Canadian Shield setting. Its purpose is to illustrate a postclosure safety assessment consistent with the Canadian Nuclear Safety Commission (CNSC) Guide G-320 on Assessing the Long Term Safety of Radioactive Waste Management. For a licence application for an actual candidate site, a full safety case would be prepared that would include the results of site-specific geoscience investigations, a site specific deep geological repository design, and a more comprehensive safety assessment than described in this document.

Design Concept

The current conceptual design for crystalline rock consists of a repository constructed at a nominal depth of 500 m. The repository contains a network of placement rooms for the estimated inventory of 4.6 million used fuel bundles encapsulated in about 100,000 long-lived used fuel containers. The container design consists of an outer corrosion-resistant material (copper) and an inner supporting material (steel). The copper provides resistance to container corrosion under deep geological conditions, while the steel provides strength for the container to withstand expected hydraulic and mechanical loads, including those arising from glaciation.

Within each placement room, used fuel containers, encased in bentonite clay buffer boxes, are placed and separated from adjacent containers by bentonite clay spacer blocks. Containers will

be staggered and stacked in two rows in a retreating manner, and void will be backfilled with bentonite based gapfill material.

Bentonite is a durable natural clay material that swells on contact with water, resulting in a self-sealing property that renders it essentially impervious to flowing water.

Geosphere

A reference geosphere has been derived for this report, in part, from historic experience gained in the Canadian program. It is not based on any specific site, and it represents one example of a possible crystalline rock setting. In combination with the other Canadian case studies for alternative geologic settings, this work illustrates a basis for the long-term safety of a deep geologic repository under a range of settings.

The geosphere is an important part of the multi-barrier system. It provides a natural barrier that is hydrogeologically, geomechanically and geochemically stable on timeframes relevant to repository safety (i.e., one million years). The geosphere isolates the repository from surface conditions and provides an environment conducive to long container life.

Postclosure Safety Assessment

The primary safety objective of a deep geological repository is the long-term containment and isolation of used nuclear fuel. The safety of the repository will be based on a combination of the geology, properties of the waste material, the engineered design, careful operations, and quality assurance processes including review and monitoring.

The purpose of a postclosure safety assessment is to determine the potential effects of the repository on the health and safety of people and the environment during the postclosure period. The assessment timeframe is one million years based on the time period needed for the radioactivity of the used fuel to decay to essentially the same level as that in an equivalent amount of natural uranium. This timeframe is also within a reasonable extrapolation of the geological stability of the surrounding rocks.

The postclosure safety assessment adopts scientifically informed, physically realistic assumptions for processes and data that are understood and can be justified on the basis of the results of research and/or future site investigations. Where there are high levels of uncertainty associated with processes and data, conservative assumptions are adopted and documented to allow the impacts of uncertainties to be bounded.

Scope of the Postclosure Safety Assessment

The scope is developed to demonstrate postclosure safety methods and techniques as applied to the most recent container and placement room design. As such, analysis cases are limited to those needed to provide a demonstration of the overall approach and to those needed to reach possible conclusions for the hypothetical site. Items excluded from the scope but which might be included in a licence submission as part of a more comprehensive assessment are also discussed.

Consistent with specifications in CNSC G-320, both Normal Evolution and Disruptive Event Scenarios are considered.

The Normal Evolution Scenario

The Normal Evolution Scenario is based on a reasonable extrapolation of present day site features and receptor lifestyles. It includes the expected evolution of the site and expected degradation of the repository system. Its purpose is to illustrate the anticipated effects of the repository on people and on the environment.

In this report, the Normal Evolution Scenario is described in terms of a “Reference Case”, a “Base Case” sensitivity study and a series of additional sensitivity studies around the “Base Case”.

Sensitivity studies illustrate repository performance for a range of reasonably foreseeable deviations from key Reference Case assumptions. These deviations arise as a result of components placed in the repository that either (a) do not meet their design specification or (b) do not fully function as anticipated.

The likelihood of such deviations will be very low. Care is being taken to design, develop and test a robust fabrication and placement technology which will ultimately be implemented under a comprehensive quality assurance program. A key element of the quality assurance program will be an inspection process designed to ensure all placed components meet design specification. Similarly, component performance is supported by an extensive research and testing program, such that the behaviour of all materials placed in the repository will also be well understood.

Reference Case

The Reference Case represents the situation in which all repository components meet their design specification and function as anticipated. As such, the used fuel containers remain intact essentially indefinitely and no contaminant releases occur in the one million year time period of interest. Radiological doses to the public and the environment are therefore zero.

Base Case

It is plausible to anticipate that some containers will fail. To illustrate repository performance in the presence of failed containers, the “Base Case” sensitivity study assumes a small number of containers are fabricated with sizeable defects in their copper coating, and that a smaller number of these off-specification containers escape detection by the quality assurance program and are unknowingly placed in the repository.

Studies are underway to determine the likelihood and number of off-specification containers that could potentially be present; however, the results of this work are presently not available. In the meantime, 10 containers with large undetected defects in the copper coating are assumed present. Postclosure studies assuming 10 defective containers are sufficient to illustrate repository performance and to provide a measure of the consequences that could be expected should such an event (or a similar one) actually occur.

The defects are assumed sufficiently large to cause each of the 10 containers to fail within one million years. As the actual nature (size, location) of each defect will vary, it is highly unlikely that 10 containers would all fail simultaneously. The failure times are assumed to be evenly spread over the one million year time period of interest, with the first failure occurring at 1000 years and subsequent failures occurring every 100,000 years.

Failures of the fabrication, placement and quality assurance systems could also affect other repository components. For example, off-specification material could unknowingly be used in the fabrication of buffer box bentonite, placement room spacer blocks or bentonite pellets. Off-specification material could also unknowingly be used in the construction of repository tunnel seals and repository shaft seals. Placement rooms and access tunnels could exceed their design dimensions because blasting removes too much rock in some places leading to the use of more bentonite pellets and potentially establishing conditions that are more conducive to microbial growth.

The principal end result of such failures would be either (a) nothing adverse happens, or (b) early container failure(s). Studies are underway to determine the likelihood and number of repository components that could potentially be out of compliance with their design requirements; however, the results of this work are also not presently available. In the meantime, for this postclosure safety assessment, other fabrication and quality assurance system failures that lead to container failure are assumed to be covered by the Base Case and relevant sensitivity cases.

To further define the Base Case, a number of bounding assumptions are made to account for uncertainties affecting case definition. A "bounding assumption" is an assumption that results in a greater consequence than the entire range of uncertainty, usually at the expense of realism. To illustrate, the Base Case replaces the uncertainty associated with the location and lifestyle of people living in the vicinity of the repository in the future with an assumption that instead has people unknowingly living on top of the repository and obtaining all of their drinking and crop irrigation water from a deep well, with the well positioned in the location that maximizes the uptake of any potential contaminant release.

The adoption of bounding assumptions is a common technique in safety assessment. It allows for complex problems to be reduced to much simpler ones, with the downside being that the resulting case is no longer the most realistic. While this is acceptable from a licensing viewpoint (provided results meet acceptance criteria), it can make repository performance appear to be much worse than it really is. This report therefore also includes a discussion of key bounding / conservative assumptions and compares them to what is most likely to occur in reality.

Sensitivity Studies for the Base Case

A deep geological repository is a multi-barrier system. The following deterministic sensitivity cases are examined to illustrate the effect of deviations in barrier performance on the Base Case results:

Fuel Barrier:

- Fuel dissolution rate increased by a factor of 10; and
- Instant release fractions for fuel contaminants set to 0.10 for all radionuclides (i.e., 10% of the entire inventory is instantly released).

Zircaloy Sheath Barrier:

No credit is taken in the postclosure safety assessment for the presence of the Zircaloy fuel sheath as a barrier to contaminant release from the fuel. However, because the sheath itself contains contaminants and because the screening analysis identifies some of these contaminants as potentially important, the following Zircaloy specific sensitivity cases are simulated:

- Zircaloy dissolution rate increased by a factor of 10; and
- Instant release fractions for Zircaloy sheath contaminants set to 0.10 for all contaminants.

Container Barrier:

- All 10 containers fail at 1000 years;
- 50 containers fail at 1000 years;
- 50 and 1000 containers fail at 10,000 years;
- Low sorption in the engineered barrier materials with coincident high solubility limits in the container; and
- No solubility limits in the container.

Buffer and Backfill and Seals Barrier:

- Hydraulic conductivities of all materials (including tunnel backfill, concrete and all shaft materials) increased by a factor of 10;
- Low sorption in the engineered barrier materials with coincident high solubility limits in the container; and
- No sorption in the near field.

Geosphere Barrier:

- Hydraulic conductivities increased by a factor of 10;
- Hydraulic conductivities decreased by a factor of 10;
- Hydraulic conductivity in the excavation damaged zones (EDZ) increased by a factor of 10;
- Fracture standoff distance reduced from 100 m to 50 m, 25 m and 10 m;
- Sorption parameters set to two standard deviations below the mean; and
- Dispersivity increased and decreased by a factor of 5.

Additional cases (not listed here) are also examined to illustrate the effect of well assumptions (in particular, “no well” with water obtained from surface waters) and the effect of modelling parameter assumptions (e.g., time-step and mesh size).

To provide an indication of repository response allowing for uncertainty in multiple parameters, two types of probabilistic sensitivity studies are also performed. In these simulations, random sampling is used to simultaneously vary input parameters for which probability distribution functions are available. Radionuclide release and transport parameters are varied with the fixed reference geosphere.

The specific probabilistic cases are:

- Number, locations and failure times for defective containers fixed at their Base Case values, with all other available parameters varied; and
- Number, locations and failure times for the defective containers varied, with all other parameters maintained at their Base Case values.

All sensitivity cases assume a constant temperate climate; however, during the past one million years, much of Canada has been covered by kilometre-thick ice sheets. The main factors that initiated these cycles (i.e., solar insolation variation due to Earth orbital dynamics and the location and size of the continents) are still present. Current levels of greenhouse gases in the atmosphere may delay the onset of the next glaciation, however, glacial cycles are expected to reassert themselves in the time period of interest to this postclosure safety assessment.

To address the effects of glaciation, a discussion is presented which is based on the analysis of a glaciation scenario carried out as part of previous work for a different geosphere and different repository design. The important features of this glaciation study are described and its applicability to the current study is discussed.

Disruptive Event Scenarios

Disruptive Event Scenarios postulate the occurrence of unlikely events leading to possible penetration of barriers and abnormal loss of containment.

The following Disruptive Scenarios are applicable to the conceptual design and hypothetical geosphere in this study. These have been identified through consideration of the features, events and processes that are important to the repository system, and through consideration of the key barriers:

- Inadvertent Human Intrusion;
- All Containers Fail;
- Repository Seals Failure;
- Poorly Sealed Borehole;
- Undetected Fault;
- Container Failure; and
- Partially Sealed Repository.

The first three scenarios are analyzed in this illustrative safety assessment. It is recognized that for an actual site, the full set of scenarios would need to be evaluated.

The Inadvertent Human Intrusion scenario considers the possibility of a future deep borehole drilled at the site. This scenario is a special case, as recognized in CNSC G-320, since it bypasses the multiple barrier system. The likelihood of this event occurring is very small due to institutional controls and markers that would be placed on the site, as well as placing the used fuel containers deep underground in a location with no currently economically viable mineral resources nor potable groundwater resources to encourage drilling. Furthermore, normal deep drilling practices (e.g., control of drilling fluids, use of gamma logging, etc.) would reduce consequences relative to those estimated here.

The All Container Fail scenario looks at the consequences of all containers failing at 10,000 years and at 60,000 years. This scenario also considers the consequences of gas generation caused by decomposition of organics and by corrosion of steel.

The Repository Seals Failure scenario considers the consequences of the tunnel and shaft seals being less effective than designed.

The Poorly Sealed Borehole scenario is also a Disruptive Scenario because it creates a pathway that bypasses the low-permeability geosphere. However, as long as the boreholes are kept sufficiently far from the repository underground structures, they are unlikely to be important due to the small size of the borehole and the limits of diffusive transport. It would be analyzed as part of a real site, when the borehole distances are known; however, the consequences are expected to be low.

For the Undetected Fault scenario, it is anticipated that any large fractures intercepting the repository not identified during site characterization would be discovered during construction such that appropriate mitigating measures could be taken. These measures could include possible redesign of the repository layout to avoid large transmissive features.

The Container Failure scenario considers failure of some containers due to unexpected in-situ conditions. It is different from the Normal Evolution Base Case which considers a defect unknowingly present in some containers as the initiating event. Although a detailed analysis of the Container Failure Scenario was not included in this study, the peak dose arising from this event is anticipated to be significantly less than that associated with the All Containers Fail scenario due to the much reduced number of affected containers.

The Partially Sealed Repository scenario considers the consequences if the repository is abandoned and the shafts are not sealed. It implies a near-future loss-of-society.

All Disruptive Event Scenarios are analysed with deterministic methods since the basic parameters defining the scenarios are chosen conservatively.

Results for the Normal Evolution Scenario

For the purpose of this Executive Summary, only results for cases measured against the interim acceptance criteria for the radiological protection of persons are presented. In the main body of this report, results are also presented for cases measured against the interim criteria for the protection of persons from hazardous substances, the interim criteria for the radiological protection of the environment, and the interim criteria for the protection of the environment from hazardous substances.

Results are also presented in the main body for two complementary radiological indicators (i.e., radionuclide concentrations in the biosphere and radionuclide transport to the biosphere).

Deterministic Results

The results from the Normal Evolution Scenario and selected sensitivity studies are illustrated in Figure E1.

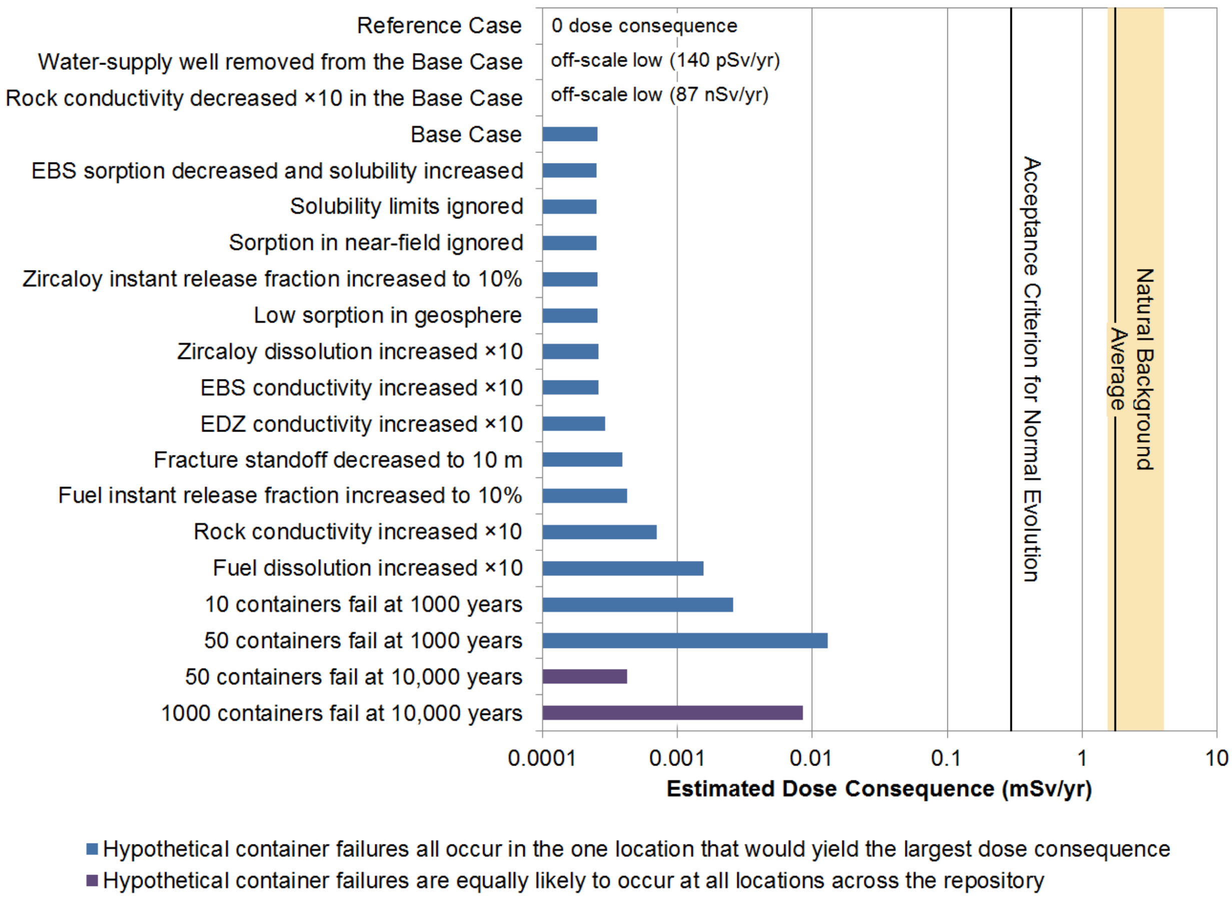

Figure E1: Results from Sensitivity Analyses and Bounding Assessments

The dose rate is zero for the Reference Case.

For the other cases, the results shows that I-129 is the dominant dose contributor. This is because I-129 has a sizeable initial inventory, a non-zero instant release fraction, a very long half-life, no solubility limit, is non-sorbing in the buffer, backfill and geosphere and has a radiological impact on humans. All other fission products and actinides either decay away, or are released very slowly as the fuel dissolves and are thereafter sorbed in the engineered barriers and geosphere.

For the Base Case, the peak dose rate is 2.5×10^{-4} mSv/a occurring at 23,300 years. This is well below the average Canadian background dose rate of 1.8 mSv/a and is a factor of 1200 times less than the 0.3 mSv/a interim dose rate acceptance criterion established in this report for the radiological protection of persons.

The actual dose rate could be many orders of magnitude lower, depending on the location of the defective containers, whether or not a well is present, and where that well is located with respect to the defective containers. Results indicating this are presented in the main body of the report.

Of the remaining sensitivity cases illustrating the effect of deviations in barrier performance, most have little to no effect on the dose consequence. Sensitivity cases that lead to higher dose rates include:

- 10 Containers Fail at 1000 Years, leading to a potential dose increase of 10 times;
- Fuel Dissolution Rates increased by a Factor of 10, leading to a potential dose increase of 6.2 times;
- Geosphere Hydraulic Conductivities increased by a factor of 10, leading to a potential dose increase of 2.6 times;
- Fracture Standoff Distance reduced to 10 m, leading to a potential dose increase of about 1.5 times; and
- Geosphere Dispersivity Decreased by a Factor of 5, leading to a potential dose increase of 1.5 times.

As the 10 Containers Fail sensitivity case shows, having all 10 containers fail at the same time and same place as the first container failure in the Base Case effectively results in a proportionately higher release and therefore dose.

The cases with more failed containers, notably with 50 and 1000 failed containers, show that the dose rate could be higher or lower than the Base Case, depending strongly on where the failed containers are located in the repository with respect to the well.

The Glaciation Sensitivity shows that a potential dose increase of 10 times could occur. This is caused by the accumulation of radionuclides during the glacial period, which are then released when people arrive and dig a well that intersects the contaminants. In reality, the effect could be much less, depending on when and where the well is established.

Probabilistic Results

The probabilistic cases examine the effect of simultaneous variation in multiple parameters.

The first case, in which the number, location and failure times of the 10 defective containers are fixed at the same values as in the Base Case while all other available parameters are varied, gives a measure of the overall uncertainty in the Base Case. The 95th percentile dose rate emerging from 100,000 simulations is 9.1×10^{-4} mSv/a or 3.6 times the Base Case value. This is a factor of 330 times less than the interim dose rate criterion of 0.3 mSv/a.

The second probabilistic case, in which the number, location and failure times of the defective containers are varied while all other available parameters are fixed, gives an indication of the effect of different container failure times and different container failure locations, relative to the well location adopted in the Base Case. The 95th percentile dose rate emerging from 100,000 simulations is 2.2×10^{-4} mSv/a, a value less than that of the Base Case. This is because, while more containers can fail, the random distribution of the failures around the repository results in less impact through the main receptor well at the one location.

Results for the Disruptive Event Scenarios

Key features arising from the analysis of the All Containers Fail Disruptive Event Scenario and the Repository Seals Failure Disruptive Event Scenario are:

- Failure of all containers at 60,000 years results in a maximum dose rate of 0.63 mSv/a while failure of all containers at 10,000 years results in a maximum dose rate 0.81 mSv/a. Both results are below the 1 mSv/a interim dose rate acceptance criterion for Disruptive Events established in this report.
- The Repository Seals Failure scenario has no effect on the dose consequence as compared to the Base Case if the well / defective container locations are maintained in their Base Case positions. For different well positions, it is anticipated that even lower doses would arise.

The Inadvertent Human Intrusion scenario bypasses all barriers and brings used fuel material directly to surface via a borehole. The consequences for the case where the intrusion is promptly recognized is a dose to the drill crew of about 100 mSv, and no dose to public as the site would be remediated. If the intrusion was not recognized, and if used fuel material was left on the site at surface, and if a person were to live on the site, then that person could receive a dose of several hundred mSv per year. However the repository siting, design and land use controls make the probability of this very low.

Other Potential Impacts

The results for cases examining the protection of persons from hazardous substances, the radiological protection of the environment, and the protection of the environment from hazardous substances are also all within their associated interim acceptance criteria.

Conclusion

This report describes the reference design for a deep geological repository in crystalline rock and provides an illustrative postclosure safety assessment approach which is structured, systematic and consistent with CNSC Guide G-320. The illustrative assessment includes a description of the repository system, systematically identifies scenarios, models and methods for evaluating safety, uses different assessment strategies, addresses uncertainty, and compares the results of the assessment with interim acceptance criteria.

The postclosure safety assessment shows, for the Normal Evolution Scenario and associated sensitivity cases, that all radiological and non-radiological interim acceptance criteria are met with substantial margins during the postclosure period. This result is consistent with previous assessments of a deep geological repository in Canada, as well as with safety assessment studies by other national radioactive waste management organizations.

TABLE OF CONTENTS

LIST OF TABLES

Page

LIST OF FIGURES

Page

THIS PAGE HAS BEEN LEFT BLANK INTENTIONALLY

1. INTRODUCTION

1.1 Purpose and Scope

The Nuclear Waste Management Organization (NWMO) is responsible for the implementation of Adaptive Phased Management (APM), the federally-approved plan for safe long-term management of Canada's used nuclear fuel. Under the APM plan, used nuclear fuel will ultimately be placed within a deep geological repository in a suitable rock formation. The repository and its surroundings comprise a system that is designed to protect people and the environment through multiple barriers.

This report provides an illustrative case study of the postclosure safety for NWMO's engineered barrier system in a deep geological repository in a hypothetical crystalline rock setting (previously referred to as the Mark II design in the early development phase). The purpose of this case study is to present and illustrate a postclosure safety assessment consistent with the Canadian Nuclear Safety Commission (CNSC) Guide G-320, Assessing the Long Term Safety of Radioactive Waste Management (CNSC 2006).

It presents a case study that illustrates the NWMO's approach to conducting a safety assessment of a repository for used CANada Deuterium-Uranium reactor (CANDU) fuel within a hypothetical Canadian Shield setting. As part of the case study, NWMO's Adaptive Phased Management (APM) facility is described and assessed. The APM facility is a self-contained complex with a combination of surface and underground engineered structures designed to provide multiple isolation barriers and passive systems to provide long-term containment and isolation. It consists of the surface facilities and the Deep Geological Repository (DGR). The approach, methods and tools for conducting a postclosure safety assessment, which contribute to the repository safety case, are fully described. The results of the safety assessment for a hypothetical site are presented to illustrate the multi-barrier deep geological repository concept and provide evidence of how Canadian regulatory requirements would be addressed.

A licence application to prepare the site and to construct a used fuel repository will be supported by a safety case. A safety case is defined as the integration of arguments and evidence that describe, quantify and substantiate the safety, and the level of confidence in the safety, of the deep geological repository and associated facilities. It includes the collection of scientific and technical arguments and evidence in support of the safety of the APM facility covering the site characterization and geosynthesis, the design, construction and operation of the facility, the assessment of radiation risk during operation and postclosure, and quality assurance of all safety-related work associated with the facility.

This definition is consistent with the CNSC Guide G-320 as well as international guidance. The International Atomic Energy Agency (IAEA) also provides guidance in SSG-23 – The Safety Case and Safety Assessment for the Disposal of Radioactive Waste (IAEA 2012), where it notes that the primary objective of a safety case is to allow for informed decisions to be made that are commensurate with the lifecycle phase of the project.

The level of detail in the current study is consistent with the pre-licensing stage of the APM facility and is not a full safety case. It considers a hypothetical site for a deep geological repository in crystalline rock. It identifies and analyzes key scenarios sufficient to understand and illustrate postclosure safety.

For an actual licence application, site-specific information would be used. Further environmental impacts and preclosure safety, including transportation safety, and conventional safety, would be assessed. However, at this pre-licensing stage and in place of site-specific information, data representing a crystalline Canadian Shield setting are used to illustrate how the postclosure safety assessment can be carried out consistent with Canadian regulatory requirements.

1.2 Background and Project Overview

Investigations into the long-term management of used nuclear fuel have a long history in Canada. The deep geological repository concept was identified at the start of the Canadian nuclear program. In 1977, a task force commissioned by Energy, Mines and Resources Canada recommended burial in geological formations with a preference for crystalline rock of the Canadian Shield, but noted that other rock types such as sedimentary rock and salt should also be studied (Hare et al. 1977). Also in 1978, the Porter Commission for Electricity Planning in Ontario recommended that an independent committee be established to report on progress on waste disposal research and demonstration. Subsequently, the governments of Canada and Ontario initiated the Canadian Nuclear Fuel Waste Management Program in 1980.

From this Canadian program and parallel international work, the concept for a deep geological repository was developed by Atomic Energy of Canada Limited (AECL). The work included an underground research laboratory in Manitoba, in which approaches and materials were tested. The AECL concept was then submitted for review by a federal environmental assessment panel. For this review, AECL completed two case studies illustrating the deep geological repository concept in crystalline Canadian Shield settings. AECL submitted its Environmental Impact Statement to the federal review panel in 1994. In 1998, the panel made a number of recommendations and identified the following key conclusions (CEAA 1998):

- *"From a technical perspective, safety of the AECL concept has been on balance adequately demonstrated for a conceptual stage of development, but from a social perspective, it has not.*
- *As it stands, the AECL concept for deep geological disposal has not been demonstrated to have broad public support. The concept in its current form does not have the required level of acceptability to be adopted as Canada's approach for managing nuclear fuel wastes."*

After 1995, research on the deep geological repository concept continued under Ontario Power Generation funding. As part of this, Ontario Power Generation completed a case study identified as the "Third Case Study" in 2004, which considered a third hypothetical Canadian Shield site and used current design concepts, data and assessment methodologies (Gierszewski et al. 2004).

The NWMO was created by Canada's nuclear energy generators as a requirement of the *Nuclear Fuel Waste Act* in 2002, which largely incorporated the recommendations from the earlier federal review panel. The Act required the NWMO to study possible approaches, recommend an approach, and then implement the approved plan for the long-term management of Canada's used nuclear fuel.

In 2005, based on extensive discussions across Canada, the NWMO recommended the APM approach, which consists of both a technical method and a management system. Its key attributes include:

- Ultimate centralized containment and isolation of used nuclear fuel in an appropriate geological formation;
- Phased and adaptive decision-making; and
- Citizen engagement throughout all phases of implementation.

In 2007, the Government of Canada accepted APM as the recommended approach. The NWMO is implementing this approach that is consistent with Canadian federal government policy and with international best practice in its development of a deep geological repository.

APM includes the development of a deep geological repository, associated surface facilities and a used fuel transportation system. The repository system is a multiple-barrier concept designed to safely contain and isolate used nuclear fuel over the long term.

An extensive study of options was conducted to update and optimize the repository design and engineered barriers for used CANDU fuel. The new reference design concept assessed in this study consists of a repository constructed for an inventory of 4.6 million used CANDU fuel bundles at a depth of approximately 500 metres and placed in a network of placement rooms (see Figure 1-1). The actual depth of the repository will depend on geologic characteristics at the specific site.

Used fuel will be loaded into licensed transport packages at the interim storage facilities at the reactor sites and transported to the deep geological repository facility where it will be repackaged in corrosion-resistant containers for placement underground. In the reference concept, the used fuel containers are encased in a bentonite clay buffer box will be transferred underground via a shaft. These boxes will be placed into underground placement rooms stacked in two rows, with bentonite clay pellets used to fill any gaps.

1.3 APM Project Phases

This section briefly describes the phases of APM, along with the milestones and the assumed timeline associated with each, in the context of the broader implementation plan. The timeline illustrating these phases is provided in Figure 1-2. The legal framework that governs these licensing activities is further described in Section 1.5.

1.3.1 Site Selection

The site selection process was launched by the NWMO in 2010. It has been designed to identify an informed and willing host community for the APM facility and to ensure that the site selected to host the facility will safely contain and isolate used nuclear fuel. The site selection process is a nine-step process based on social and technical considerations. Screening criteria have been established to ensure that safety is considered from the start of the siting process. Section 1.6.3 of this report highlights the evaluation factors used in the process. The timeframe associated with completing surface and subsurface investigations at a candidate site is about 5 years.

A licence application would be submitted for a selected site. Licences are issued under the *Nuclear Safety and Control Act* as described in Section 1.5.

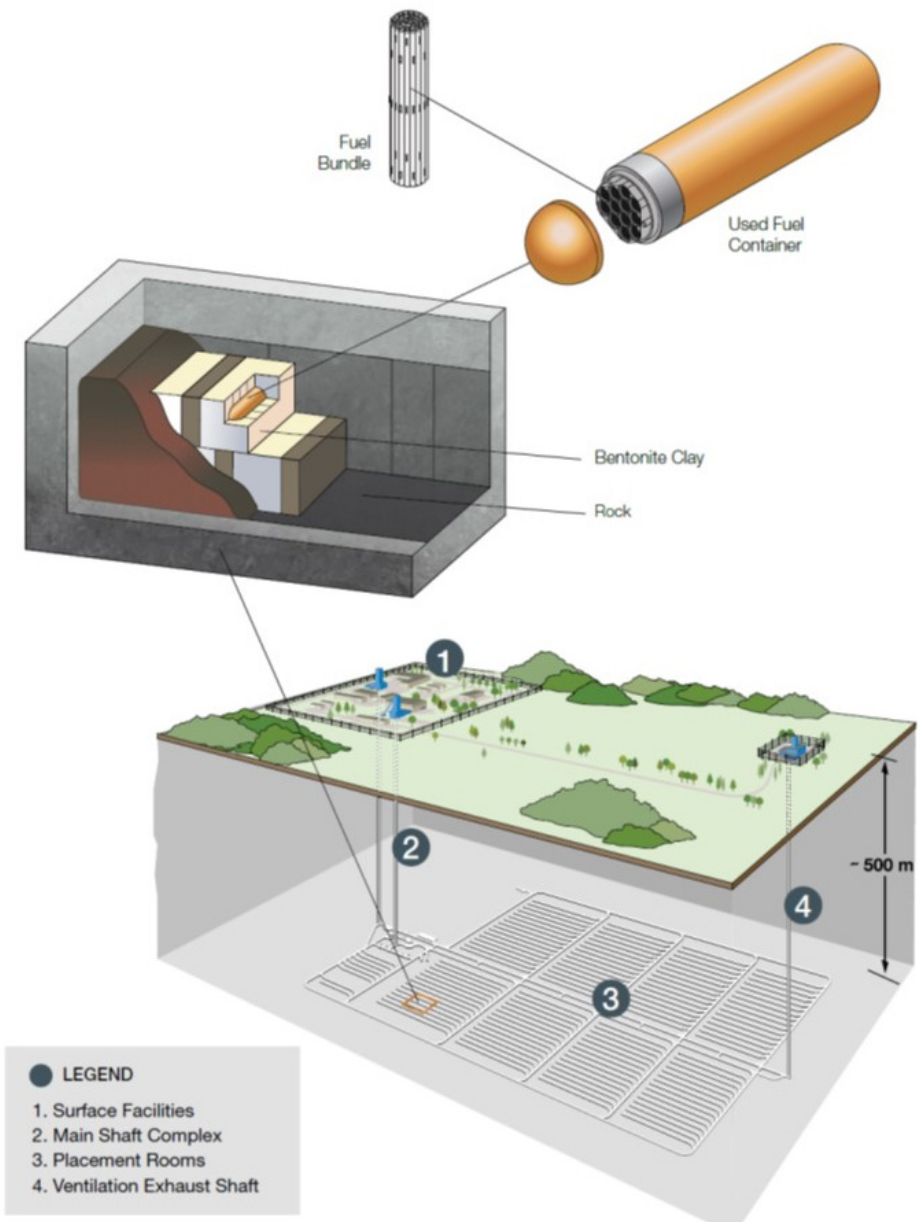

Note: This figure is not to scale.

Figure 1-1: Illustration of Deep Geological Repository Concept

1.3.2 Site Preparation and Construction

The site will be prepared for construction by clearing, site grading, installing fencing, installing temporary construction services, and establishing a stormwater management system. The first phase of construction will be to excavate the shafts and an underground demonstration facility. This phase is expected to last about five years, the time needed to sink the shafts, construct the demonstration facility, complete the detailed design and update the safety case. It is described in more detail in Chapter 4.

After the final design is completed, the construction of the full-scale underground repository and associated surface facilities can begin. The purpose of this construction phase is to excavate and erect all of the facilities necessary for the operation of the repository. This phase is expected to last about five years.

Therefore, the total site preparation and construction phase could be about 10 years.

1.3.3 Operation

Operation will consist of receiving used nuclear fuel transported to the site, re-packaging the used fuel into long-lived containers, placing the used fuel containers in the repository, and continued underground development. All activities will be executed in compliance with supporting documents.

For a reference used fuel inventory of 4.6 million used CANDU fuel bundles, these operational activities are expected to last about 40 years. The actual duration of repository operation will depend on the total inventory of used fuel to be managed at the site and the timing of its production, transportation considerations and other operational factors.

1.3.4 Extended Monitoring

Following placement of used fuel in the repository, a period of monitoring is assumed to continue for an extended period of time. The duration of extended monitoring will be decided in collaboration with a future society. For planning purposes, the period of extended monitoring is assumed to be up to 70 years.

Towards the end of the extended monitoring period (i.e., during the last five years), a detailed decommissioning plan will be prepared and the detailed design of the shaft sealing system will be finalized.

1.3.5 Decommissioning

The decommissioning of the facility will include sealing of access tunnels and shafts, and removal of surface facilities. The site will be restored to a defined end-state that will depend largely on future plans for the site (e.g., industrial, park). For planning purposes, the period of decommissioning is assumed to be 30 years.

It is anticipated that appropriate institutional controls will be put in place at that time.

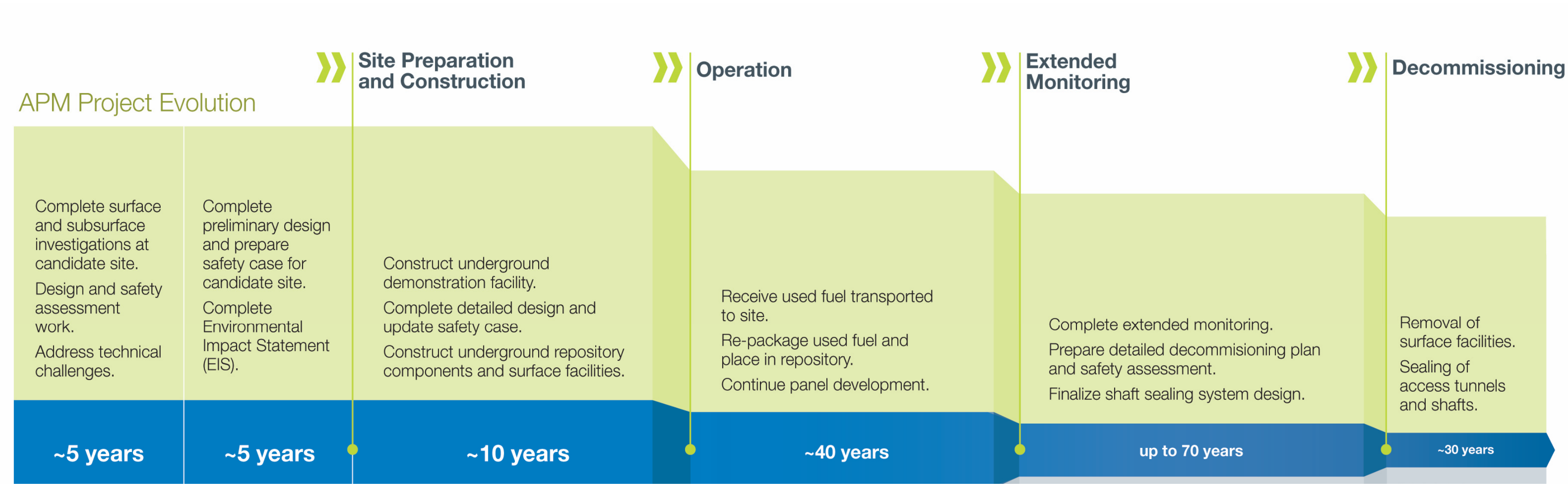

Figure 1-2: Illustrative APM Implementation Schedule for Planning Purposes

1.4 Repository Timeframes

In this safety assessment the potential impact of a repository is assessed in accordance with the CNSC Policy P-290 (CNSC 2004), which requires that, “the assessment of future impacts of radioactive waste on the health and safety of persons and the environment encompasses the period of time when the maximum impact is predicted to occur.” In discussing the long-term evolution of a repository system, it is helpful to consider a sequence of timeframes during which certain events or processes dominate in the postclosure period.

1.4.1 Preclosure Period

The preclosure period is intended to cover the activities described in Sections 1.3.1 to 1.3.5 and is assumed to last up to about 150 years (see Figure 1-2).

During this time, the reference inventory of 4.6 million used nuclear fuel bundles will be transported to the APM facility, encapsulated in approximately 100,000 long-lived used fuel containers, transferred to the underground repository and surrounded by clay-based sealing materials. The total radioactivity will increase as more used fuel is placed in the repository, and then start to decrease due to radioactive decay.

1.4.2 Postclosure Period

The postclosure period starts at the end of decommissioning, after the shafts have been sealed and the surface facilities have been dismantled.

In the postclosure period, the site is assumed to remain under institutional controls for a period of time. Based on CNSC Guide G-320 (CNSC 2006) institutional controls can be defined as, “the control of residual risks at a site (by a designated Institution or Authority) after it has been decommissioned.” These controls can include both active measures (requiring activities on the site such as monitoring and maintenance) and passive measures (that do not require activities on the site, such as land use restrictions, as well as measures taken to support societal memory). Such measures should prevent inappropriate land use, including drilling, deep excavation, or disruption of the shaft seals.

Although there is no specific date at which institutional controls or societal memory would end, it is assumed for safety assessment purposes that these institutional controls and societal memory are effective for about 300 years.

The postclosure period is described in four timeframes. Each of the timeframes is also described in this section. To provide context for these timeframes, Figure 1-3 highlights timescales for relevant past events and expected future events in the Earth’s history.

<u>Up to 1,000 years</u>

At the beginning of this time, the facility is decommissioned. Distinct physical and chemical gradients exist between the various components of the repository, and between the repository and the geosphere. The containers reach their peak temperature. Slow saturation of the repository by groundwater occurs, which is accompanied by swelling of bentonite sealing materials. Especially during the first 500 years, radioactivity and heat in the used fuel decrease significantly due to the decay of most of the fission products.

<u>1,000 - 60,000 years</u>

This time period represents conditions with no glaciation coverage of the site. During this period, the initial sharp physical and chemical gradients around the repository slowly diminish. The surrounding crystalline rock reaches its peak temperature and largely cools back down to natural ambient temperatures. Surface conditions are likely to change reflecting human activities and natural evolution, possibly in response to climate change. Although the overall climate is likely to remain temperate, climate changes could include global warming in the near term, and the advent of cooler climate in the long term.

<u>60,000 - 1,000,000 years</u>

Over this timescale, the main perturbations in the system cease to be repository-driven. Instead, there are regional-scale changes in the geosphere that in turn may be transmitted to the repository. In particular, during this timeframe, climate change initiated by broad changes in solar insolation patterns may occur leading to initiation of a new glaciation cycle. Based on past history, several cycles of glaciation are likely to occur over the next million years.

<u>1,000,000 years and beyond</u>

Beyond this timescale, the repository will be a relatively passive feature of the geosphere, in quasi-equilibrium with the surrounding rock. The dominant processes will be regional perturbations to the geosphere that in turn affect the repository. Over this longer time period, the changes will mainly be the result of slow-acting tectonic forces, and cumulative erosion or deposition processes.

In the safety analysis presented in this report, the discussion of the evolution of a repository focuses on the interval covered by the first three postclosure timeframes, i.e., up to one million years. It will be during this period that the differences between the natural environment and an engineered repository for used fuel are noticeable. Beyond one million years, the level of radioactivity in the used fuel bundles is similar to that of an equivalent amount of natural uranium (see Section 5.3.1). Thereafter, the total amount of radioactivity in the repository is similar to that of a naturally occurring uranium ore body.[1] As part of the safety case prepared for an actual candidate site, geoscientific arguments and evidence supporting the long-term stability and resilience to change of a crystalline rock environment would also be presented.

---

[1] With about 90,000 Mg of uranium, it will be similar to large ore bodies like Cigar Lake and MacArthur River in Saskatchewan.

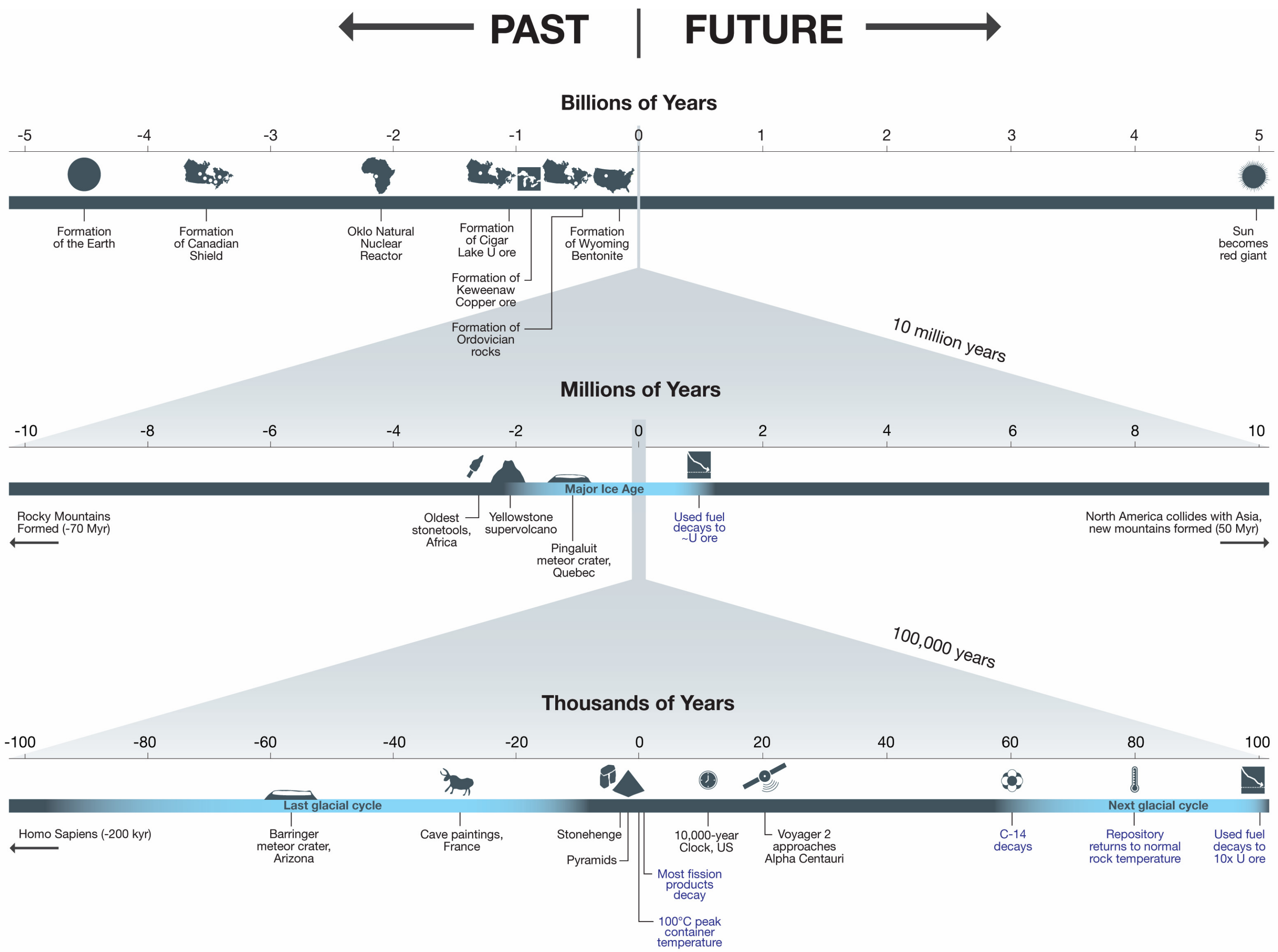

Figure 1-3: Perspective of Past Events and Expected Future Events in Earth's History Including Repository Events

1.5 Relevant Legislation

The intention is for the deep geological repository to meet or exceed all Canadian regulatory requirements, and to be consistent with international practices during site preparation, construction, operation and beyond.

The primary legislations are the *Canadian Environmental Assessment Act* (CEAA) and the *Nuclear Safety and Control Act.* CEAA has been completed. This would require an Environmental Impact Statement (EIS) and other supporting documents, as set out in the *Canadian Environmental Assessment Act*.

1.5.1 CNSC Regulatory Requirements

In accordance with paragraph 2(g) of *Nuclear Safety and Control Act* and paragraph 1(e) of the Class I Nuclear Facilities Regulations, the repository is a Class 1B nuclear facility.

Paragraph 26(e) of the Act states that, “subject to the Regulations, no person shall, except in accordance with a licence…prepare a site for, construct, operate, modify, decommission or abandon a nuclear facility”. The following licences are required over the life of the repository:

- Site Preparation Licence;
- Construction Licence;
- Operating Licence;
- Decommissioning Licence; and
- Abandonment Licence.

The detailed requirements to obtain a licence are described in Section 3 of the General Nuclear Safety and Control Regulations and in the Class I Nuclear Facilities Regulations. Other applicable regulations include the Nuclear Security Regulations, Radiation Protection Regulations, Packaging and Transport of Nuclear Substances Regulations, which apply to all nuclear facilities, and the Uranium Mines and Mills Regulations – due to similarities of some aspects of the APM facility (i.e., deep geological repository) to a mining project.

In addition to the regulations, a number of CNSC regulatory documents in the following categories are also applicable:

- Regulatory policies – describe general principles applied by the CNSC in their review;
- Regulatory documents and standards – establish regulatory standards; and
- Regulatory guides – set out regulatory expectations.

In Canada, the primary regulatory requirements and expectations for the assessment of long-term safety of radioactive waste management are given in the CNSC Policy P-290 (CNSC 2004) and CNSC Guide G-320 (CNSC 2006) and these are the focus of this pre-project report. More generally, the regulatory framework for a licence is organized into 14 Safety and Control Areas. These areas, and examples of regulatory documents that will apply to the APM project, are listed in Table 1-1.

Table 1-1: CNSC Regulatory Documents Applicable to the APM Project

Document Number	Topic
Key references related to safety assessment	
P-290	Managing Radioactive Waste (CNSC 2004)
G-320	Assessing the Long Term Safety of Radioactive Waste Management (CNSC 2006)
Other areas relevant to a licence application	
P-119	Policy on Human Factors
P-211	Compliance
P-299	Regulatory Fundamentals
R-72	Geological Considerations in Siting a Repository for Underground Disposal of High-Level Radioactive Waste
REGDOC-2.3.1	Conduct of Licensed Activities: Construction and Commissioning Programs
REGDOC-2.9.1	Environmental Protection: Environmental Principles, Assessments and Protection Measures
G-129 Rev.1	Keeping Radiation Exposures and Doses "As Low as Reasonably Achievable (ALARA)"
REGDOC-2.10.1	Nuclear Emergency Preparedness and Response, version 2
REGDOC-2.12.2	Site Access Security Clearance
REGDOC-3.1.2	Reporting Requirements for Non-Power Reactor Class I Facilities and Uranium Mines and Mills
REGDOC-3.2.2	Aboriginal Engagement
G-206	Financial Guarantees for the Decommissioning of Licensed Activities
G-208	Transportation Security Plans for Category I, II or III Nuclear Material
G-219	Decommissioning Planning for Licensed Activities
G-221	A Guide to Ventilation Requirements for Uranium Mines and Mills
G-274	Security Programs for Category I or II Nuclear Material or Certain Nuclear Facilities
G-276	Human Factors Engineering Program Plans
G-278	Human Factors Verification and Validation Plans
RD/GD-99.3	Public Information and Disclosure
RD-327/ GD-327	Nuclear Criticality Safety
RD-336/ GD-336	Accounting and Reporting of Nuclear Material
RD-363	Nuclear Security Officer Medical, Physical, and Psychological Fitness

Note: Current versions of the CNSC regulatory documents can be found on the CNSC website (www.cnsc-ccsn.gc.ca).

CNSC Policy P-290 (CNSC 2004) identifies the need for long-term management of radioactive waste and hazardous waste arising from licensed activities. The principles espoused by CNSC Policy P-290 that relate to long-term management are the following:

- The management of radioactive waste is commensurate with its radiological, chemical, and biological hazard to the health and safety of persons and the environment, and to national security;
- The assessment of future impacts of radioactive waste on the health and safety of persons and the environment encompasses the period of time when the maximum impact is predicted to occur; and
- The predicted impact on the health and safety of persons and the environment from the management of radioactive waste is no greater than the impact that is permissible in Canada at the time of the regulatory decision.

Key objectives for long-term management are *containment* and *isolation* of the waste, in accordance with the CNSC Guide G-320 (CNSC 2006). The guide states that:

> *"containment can be achieved through a robust design based on multiple barriers providing defence-in-depth. Isolation is achieved through proper site selection and, when necessary, institutional controls to limit access and land use".*

CNSC Guide G-320 identifies expectations for *"developing a long term safety case that includes a safety assessment complemented by various additional arguments based on:*

1. *Appropriate selection and application of assessment strategies;*
2. *Demonstration of system robustness;*
3. *The use of complementary indicators of safety; and*
4. *Any other evidence that is available to provide confidence in the long term safety of radioactive waste management."*

Guidance is also provided for defining acceptance criteria and performing long-term assessments that includes considerations for: selection of methodology, assessment context, system description, assessment timeframes, assessment scenarios, assessment models, and the interpretation of results.

A mapping that shows how the content of this report is consistent with aspects of CNSC Guide G-320 is shown at the end of this chapter and described in more detail in Chapter 11.

1.5.2 Transportation of Used Nuclear Fuel

The safe and secure transportation of used nuclear fuel is regulated through a comprehensive multi-agency framework of regulations, oversight, and inspections. The process builds on the roles of federal, provincial, and local agencies.

The regulatory oversight of safe transportation of used nuclear fuel in Canada is jointly shared by the CNSC and Transport Canada. Transport Canada's *Transportation of Dangerous Goods Regulations,* and the *Transportation of Dangerous Goods Act,* and CNSC's *Packaging and Transport of Nuclear Substances Regulations,* associated with *Nuclear Safety and Control Act,* and the *Nuclear Security Regulations* apply to all persons who handle, offer for transport, transport or receive nuclear substances.

Transport Canada and CNSC regulations follow the IAEA regulations (SSR-6) for the safe transport of radioactive materials and cover certification of the package used to transport the used fuel, the licence to transport, the security planning, training requirements for the shipper and the transporter, emergency response planning, and communications. These are in addition to the normal commercial vehicle and rail operating regulations and are similar to those used internationally. Packages designed for the transport of used nuclear fuel require certification by the CNSC before they can be used in Canada.

The provinces are responsible for developing, maintaining, and operating the highway infrastructure and for inspecting the commercial vehicles and their drivers. Local governments provide law enforcement and emergency response to incidents. The interaction and cooperation between these agencies facilitates comprehensive regulation and oversight of all transportation of used nuclear fuel.

1.5.3 Canadian Codes and Standards

A number of Canadian codes and standards apply to a deep geological repository project. Compliance with these will be demonstrated in the future in support of a licence application. For example, requirements exist in the following areas and include the following:

- Civil structures will comply with the National Building Code of Canada and the National Fire Code of Canada;
- Electrical installations and components will be in accordance with the Canadian Electrical Code and associated Canadian Standards Association (CSA) standards;
- The management system will comply with the CSA N286 series of standards as well as International Standards Organization (ISO) 9001;
- The environmental management and monitoring programs will comply with the CSA N288 series of standards as well as ISO 14001; and
- The occupational health and safety management programs will comply with the CSA Z1000 standard.

Some regulatory requirements from the provincial jurisdiction will also be applicable. For example, the health and safety program will comply with provincial Occupational Health and Safety Requirements. Although there is presently no specific site, relevant Ontario provincial standards have been used, such as the Ontario water quality objectives (MoEE 1994) and the soil, groundwater and sediment standards (MoE 2011).

1.5.4 Safeguards

Canada’s international safeguards obligations are the result of treaty commitments (IAEA 1970, IAEA 1972, and IAEA 2000). The specific legal requirements to implement these commitments come in the form of licence conditions that are included in a CNSC licence. Compliance with these requirements will be demonstrated in support of a future licence application.

1.5.5 Indigenous Knowledge

NWMO respects the status and rights of First Nations and understands that interweaving of Indigenous Knowledge in the implementation of APM benefits the long-term management of used nuclear fuel. Early in the project this includes recognizing the importance of water, the relationships between various aspects of the environment, as well as the health, trade and spiritual needs of people. The NWMO's Site Selection Process will look to Indigenous peoples as practitioners of Indigenous Knowledge to be active participants in the process, and to share that knowledge with the NWMO to the extent they wish to in order to help guide the decisions involved in site selection and ensure safety and the long-term well-being of the community.

1.5.6 International Guidance

A number of technical documents are available that provide guidance on best international practices with respect both to achieving safety, and on the demonstration of safety. Particular international documents relevant to development and safety for a repository are listed in Table 1-2.

Table 1-2: International Guidance Applicable to Safety Assessment

Document Number	Title
IAEA SSR-5	Disposal of Radioactive Waste (IAEA 2011)
IAEA SSG-23	The Safety Case and Safety Assessment for Radioactive Waste Disposal (IAEA 2012)
ICRP 103	The 2007 Recommendations of the International Commission on Radiological Protection (ICRP 2007)

Note: The latest version of international guidance can be found on the associated agency's website (www.iaea.org, www.icrp.org).

1.6 Safety Case

CNSC Guide G-320 states "*Demonstrating long term safety consists of providing reasonable assurance that waste management will be conducted in a manner that protects human health and the environment. This is achieved through the development of a safety case, which includes a safety assessment complemented by various additional arguments*".

The safety case has been defined in Section 1.1 as: the integration of arguments and evidence that describe, quantify and substantiate the safety, and the level of confidence in the safety, of the deep geological repository and associated facilities. It includes the collection of scientific and technical arguments and evidence in support of the safety of the APM facility covering the site characterization and geosynthesis, the design, construction and operation of the facility, the assessment of radiation risk during operation and postclosure, and quality assurance of all safety-related work associated with the facility.

This report documents components of a safety case, but is not in itself a full safety case; as discussed later, it represents information at a very early stage before a site has been selected. The report contains a description of these various components, and in some cases, an illustration of how the design of the repository will meet Canadian regulatory requirements and will be consistent with international practice.

CNSC Guide G-320 (CNSC 2006) recommends following a structured approach for preparing a safety case and safety assessment. The safety assessment is defined as: the process of systematically analyzing the hazards associated with the facility, and the ability of the site and design to provide the safety functions and meet technical requirements.

The most recent international guidance is included in the IAEA's SSG-23 (IAEA 2012). This guidance is used to present the safety case components for this study. The guidance also acknowledges applying the concept of defence in depth to disposal facilities by stating that: *"the host environment shall be selected, the engineered barriers of the disposal facility shall be designed… to ensure that safety is provided by means of multiple safety functions. Containment and isolation of the waste shall be provided by means of a number of physical barriers of the disposal system. The performance of these physical barriers shall be achieved by means of diverse physical and chemical processes…The capability of the individual barriers…shall be demonstrated. The overall performance of the disposal system shall not be unduly dependent on a single safety function."* It further recommends that the number and extent of required barriers depends on the type of waste and should be commensurate with the hazard potential of the waste, in accordance with the graded approach.

Figure 1-4 is largely consistent with the IAEA's components of a safety case (IAEA 2012). This figure is used to illustrate the current phase and to identify the further phases that will be included as part of a project at the final selected site. The discussion of each of these components is included in the following subsections.

1.6.1 Safety Case Context

The Canadian regulatory framework presented in Section 1.5 provides the context for a deep geological repository safety case.

The primary *safety objective* of the deep geological repository is: to provide safe long-term management of used fuel without posing unreasonable risk to the environment or health and safety of humans.

This objective is consistent with the *Nuclear Safety and Control Act* (subparagraph 9(a) (i)) and IAEA guidance in SSR-5 (IAEA 2011), which notes that the geological disposal of radioactive waste is aimed at:

- Containing the waste until most of the radioactivity, and especially that associated with shorter-lived radionuclides, has decayed;
- Isolating the waste from the biosphere and substantially reducing the likelihood of inadvertent human intrusion into the waste;
- Delaying any significant migration of radionuclides to the biosphere until a time in the far future when much of the radioactivity will have decayed; and
- Ensuring that any levels of radionuclides eventually reaching the biosphere are such that possible radiological impacts in the future are acceptably low.

As described in Section 1.1, this study presents a conceptual design and illustrative safety assessment for a deep geological repository at a hypothetical site. The level of detail is consistent with the pre-project stage, i.e., before a final site has been selected. It is not a full safety case. It considers a hypothetical site, and therefore does not include a geosynthesis. It identifies and analyzes key scenarios, but does not assess all relevant scenarios.

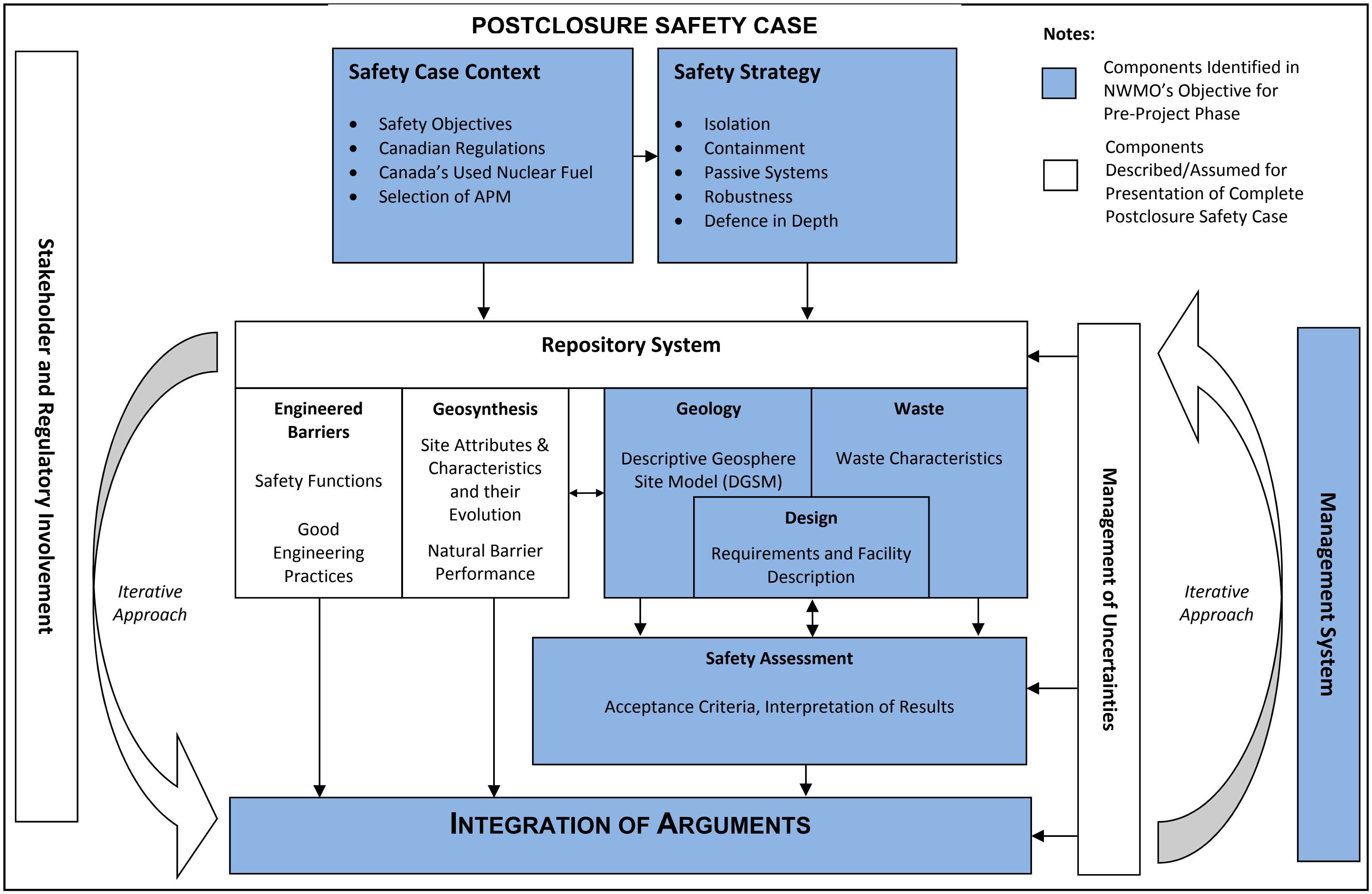

Figure 1-4: Components of the Safety Case

1.6.2 Safety Strategy

Used nuclear fuel is hazardous for long periods of time and its characteristics are used as an input to the design of the repository. The safety strategy is to provide long-term containment and isolation through the use of multiple barriers and passive systems, including in particular a stable and robust geosphere. The geosphere has characteristics that will also delay significant migration of radionuclides to ensure that the impacts in the future are acceptably low.

In this study, a set of safety relevant features are assumed to be present in this hypothetical site. The geological features will need to be confirmed at any future candidate site as part of the Site Selection Process (NWMO 2010). The design concept includes engineered barriers that have properties that also allow a set of safety functions to be fulfilled.

The geological characteristics and the engineered barrier's safety attributes are consistent with the concept of defence in depth and are further described in the following section on the deep geological repository system.

1.6.3 Deep Geological Repository System

The DGR system includes the DGR facility, its geological setting, and the surrounding surface environment. The system includes the engineered and the natural barriers that provide containment and isolation of the waste. The repository system includes the waste, containers, sealing systems and the near-field geosphere around the repository.

Figure 1-4 represents the system across three main areas for which safety arguments are presented: 1) the geology, 2) the waste characteristics, and 3) the design. This section includes a summary of the type of information that needs to be considered.

In this study for a hypothetical site, no specific description of communities is considered, although that will be important for any candidate site.

1.6.3.1 Geology

A key part of the safety case is the geosphere.

The NWMO's siting process (NWMO 2010) includes technical evaluations of a candidate site. The factors affecting safety that were addressed in this process are:

- The containment and isolation characteristics of the host rock;
- The long-term stability of the site;
- The ability of the site to support repository construction, operation and closure;
- The likelihood of future human intrusion;
- The confidence in the site characteristics; and
- The ability to safely transport used fuel to the site.

Site characterization activities for an actual site in crystalline rock would include a thorough and systematic assessment of the site with respect to the above factors. This would be documented in:

- A Descriptive Geosphere Site Model (DGSM) that provides a description of the present day three-dimensional physical and chemical characteristics of a specific site as related to implementation of the repository; and
- A Geosynthesis that provides a geoscientific explanation of the overall understanding of site characteristics, attributes and evolution as they relate to demonstrating long-term performance and safety.

For the purpose of this report and for conducting the illustrative safety assessment, this type of information is presented in Chapter 2.

For the purpose of this report, the key attributes assumed for the hypothetical site in the Canadian Shield are:

- The repository is located at a depth of 500 m;
- There is sufficient volume of rock at the site and depth to host the repository;
- Groundwater at repository depth has low salinity;
- Groundwater at repository depth provides a chemically reducing environment and a low concentration of potentially corrosive agents;
- The host rock is capable of withstanding mechanical and thermal stresses;
- Seismic activity and the risk of volcanism are low, consistent with general Canadian Shield conditions;
- Rates of land uplift, subsidence and erosion at the site are low enough that they will not adversely impact the isolation of the repository; and
- This host rock formation does not contain economically exploitable natural resources at repository depth.

1.6.3.2 Waste Characteristics

The waste characteristics are an input to the safety assessment and guide the design of the DGR facility.

In addition, the waste form itself has safety features that contribute to the safety case. In particular, used CANDU fuel is a barrier which contributes to the containment of contaminants as follows.

- Most radionuclides are immobile within the uranium oxide (UO_2) grains of used fuel;
- The used CANDU fuel grains are mechanically durable and not significantly impacted by radiation effects;
- The used fuel has low solubility under conditions of a failed container in contact with groundwater;
- The Zircaloy cladding provides a barrier to contact between groundwater and used fuel in a failed container; and
- The Zircaloy cladding corrodes slowly under conditions of a failed container with contact with groundwater.

The waste characteristics are further described in Chapter 3 and the evolution of used fuel is described in Chapter 5.

1.6.3.3 Design

The design is largely guided by the geological characteristics and features of a candidate site and also by the characteristics of the waste that will be placed in the repository. For the pre-project report, a hypothetical crystalline site on the Canadian Shield is considered. Representative characteristics of the crystalline site are used to guide specific repository design requirements which include engineered barriers to fulfill specific safety functions. Design requirements are used as an input to the safety assessment.

The safety strategy acknowledges that properties of the engineered barriers are selected to fulfill safety functions. Passive engineered barriers of the used fuel container (UFC), buffer and sealing systems contribute to the isolation and containment of contaminants as follows:

- The used fuel container is a barrier for the underground conditions at timeframes relevant to repository safety;
- Inspection methods would ensure the container is built consistent with design specifications;
- The in-room buffer system holds and protects the containers;
- Engineered seals isolate the placement room from the access tunnels; and
- Shaft backfill and seals isolate the repository from the surface.

The repository design is described in Chapter 4 at a conceptual level of detail. The description focuses on the underground portions relevant to postclosure safety.

The purpose of the design concept presented here is to provide information to support the postclosure safety assessment. This design concept is expected to be further refined once a site has been selected and site specific information becomes available.

1.6.3.4 Institutional Controls

Institutional controls have been described in Section 1.4.2 where it is stated that institutional controls are assumed for a period of time. The safety feature associated with this assumption includes: institutional controls will limit the potential for human encounter with the repository in the near term after closure.

And finally, Chapter 5 discusses the evolution of the deep geological repository system, including how the different components of the system will interact with each other and the environment in the long term, consistent with CNSC Guide G-320 (CNSC 2006).

1.6.4 Safety Assessment

The safety assessment has been defined as: the process of systematically analyzing the hazards associated with the facility, and the ability of the site and design to provide the safety functions and meet technical requirements. As noted in the scope of this report, it focuses on the illustrative postclosure safety assessment, which is discussed in detail in Chapter 7. The scenarios, assessment tools and methods and assessment results are presented. Both radiological and non-radiological impacts are assessed and the safety assessment results are compared against acceptance criteria.

1.6.5 Management of Uncertainties

The report describes the assessment of uncertainties associated with numerical analyses at a level that is reasonable for a conceptual design at a hypothetical site. The discussion is consistent with the CNSC guidance for analyzing uncertainties and addresses such things as: degree of conservatism, conceptual model uncertainty, parameter value uncertainty, and scenario uncertainty. The illustrative safety assessment provides examples of approaches used to assess and understand the relevance of uncertainties in scientific knowledge, data or analysis that support statements of reliability in calculated repository performance.

As noted in Section 1.6.3.1, the geoscience program for a future candidate site will be designed to support the safety case and to produce a Descriptive Geosphere Site Model (DGSM) and a Geosynthesis.

The DGSM and Geosynthesis will be developed in the phased site characterization work program. The work program will allow for the iterative development, testing and refinement of a site-specific model that will contribute to managing uncertainties in scientific understanding, data or models.

The iterative approach described below also highlights how the assessment of uncertainties will be incorporated in the process of developing a safety case for a future candidate site.

1.6.6 Iterative Approach

Consistent with international guidance, the NWMO plans to use an iterative approach in the strategies for management, site characterization, design and assessments of a candidate site. The documentation process to support this iterative approach is included in Figure 1-5. On the left hand side of this figure, two key documents that will support licence applications and that will document the safety case are identified as the Preliminary Safety Report and Final Safety Report.

As noted in Section 1.6.3.3, the design concept presented is illustrative and intended for the safety assessment methodology to be demonstrated. The actual design is expected to be refined once a specific site has been selected, site-specific information becomes available, and design optimization is implemented.

Furthermore, once a site has been selected, Figure 1-5 assumes that the characterization and engineered design programs will go through iterations based on increased knowledge of site characteristics and safety assessment input during detailed site investigations. A few iterations are expected during the phase of detailed investigations.

Some of the key activities in this approach include:

- National and international peer reviews;
- Using site characterization results as an input to repository design and safety assessment, and in building the safety case;

- Conducting complementary geoscience analogue studies to assist with the explanation of geoscience phenomena related to, and to enhance confidence in, the understanding of long-term repository safety;
- Using proven technology in the design;
- Continuing to make use of a range of safety and performance indicators in safety analyses;
- Assessing associated uncertainties and identification of any significant deficiencies in scientific understanding, data or analysis that might affect the analysis results that are presented; and
- Using the results of safety assessment, in particular the preclosure safety assessment and occupational radiation dose ALARA[2] assessment and conventional safety considerations in the design.

1.6.7 Integration of Safety Arguments

The safety arguments will be integrated as part of a complete safety case. These arguments will be supported by evidence and multiple lines of reasoning gathered in the site characterization work program and documented in a Geosynthesis for a candidate site.

For the purpose of this report and to present the illustrative safety assessment, a number of safety arguments have been assumed in Section 1.6.3. These assumptions are made to show how site characteristics or attributes and safety functions are used to illustrate the robustness of a multi-barrier system.

The assessment results presented in Chapter 7 will be used to support safety arguments resulting from the postclosure assessment.

1.6.8 Stakeholder and Regulatory Involvement

As noted in Section 1.1, the purpose of this report is to present a case study involving an illustrative safety assessment of a deep geological repository in a representative crystalline Canadian Shield setting.

This report considers a hypothetical site and is not being prepared for a licensing process, so there are no direct stakeholders. However, it will be available to the CNSC, to provide background information on NWMO’s approach to safety assessment and on the potential performance of its current design concept in the context of a repository system. It will be publicly available and also used as a basis for discussion

[2] ALARA: As low as reasonably achievable, social and economical factors taken into account.

1.6.9 Management System

A project quality plan describes how APM design and technical work activities are conducted under an appropriate management system framework. The plan covers the following elements:

- The project organization and responsibilities;
- NWMO and project-specific governance;
- Quality requirements;
- Verification requirements;
- Requirements for consultant or contractor quality management system;
- Records requirements;
- Program's periodic assessment activities; and
- Annual assessment activities.

Chapter 10 describes the elements of the project quality plan in more detail.

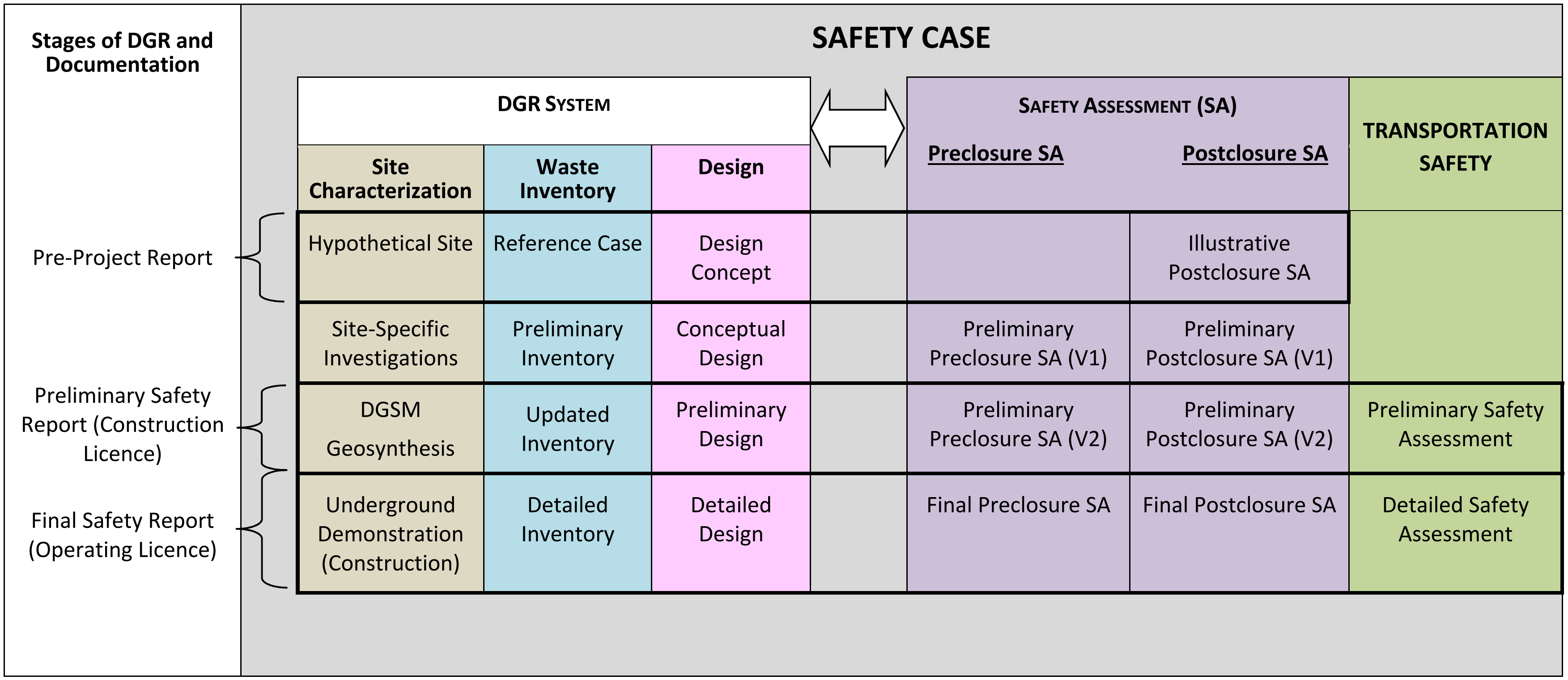

Figure 1-5: Iterative Process for Developing the Safety Case

1.7 International Status of Deep Geological Repositories

The concept of using a deep geological repository for long-term management of used fuel is consistent with other national plans for high-level waste as summarized in Table 1-3. In-service dates for other geological repository projects have been included, where available.

Table 1-3: Status of National Plans for High-Level Waste

Country	National Plan for High-Level Waste	Potential Rock Type	Repository Status
Finland	Geological Repository	Crystalline Rock	- Willing host community selected - Underground demonstration facility at site - 2015: construction licence - 2020s: plan in-service date
Sweden	Geological Repository	Crystalline Rock	- Willing host community selected - Underground demonstration facility operating at generic site - 2011: construction licence application - 2025: plan in-service date
France	Geological Repository	Sedimentary Rock	- General geological region identified - Underground demonstration facility operating at generic site - 2025: plan in-service date
Switzerland	Geological Repository	Sedimentary Rock	- Underground demonstration facilities operating at generic sites - General geological regions identified - 2050: plan in-service date
China	Geological Repository	Crystalline Rock	- 2050: plan in-service date
Germany	Geological Repository	Salt, Crystalline, and Sedimentary Rock	- 2050: earliest in-service date
South Korea	Geological Repository	To be decided	- 2053: plan in-service date
United Kingdom	Geological Repository	Crystalline Rock	- 2075: plan in-service date
Japan	Geological Repository	Crystalline and Sedimentary Rock	- Underground research facilities operating at generic sites - No official date
USA	Geological Repository	To be decided	- No planned date

1.8 Report Structure and Content

The structure of this pre-project review report is as follows:

Chapter 1 Introduction: An overview of the APM project and the context for the report.

Chapter 2 Description of a Hypothetical Site: Information related to a hypothetical site is presented.

Chapter 3 Used Fuel Characteristics: Information on the reference fuel bundle adopted in the postclosure safety assessment is presented.

Chapter 4 Repository Facility – Conceptual Design: Description of conceptual design for a deep geological repository.

Chapter 5 Long-Term Evolution of the Multiple Barrier System: Description of the deep geological repository system, including the interaction of different components of the system.

Chapter 6 Scenario Identification and Description: Description of the systematic scenario identification process used to identify Normal Evolution and Disruptive Event Scenarios.

Chapter 7 Postclosure Safety Assessment: Provides an evaluation of potential impacts during Normal Evolution and Disruptive Event Scenarios.

Chapter 8 Treatment of Uncertainties: Description of scenario, model and data uncertainties.

Chapter 9 Natural Analogues: Description of natural analogues that illustrate material integrity and identification of the role of site-specific analogues.

Chapter 10 Quality Assurance: Description of the APM quality assurance plan.

Chapter 11 Summary and Conclusions: Summary of information presented in the pre-project report and overall conclusion on meeting the pre-project report objective.

Chapter 12 Special Terms: Includes units, abbreviations and acronyms.

The IAEA's structured approach presented in the recent guidance on The Safety Case and Safety Assessment for the Disposal of Radioactive Waste (IAEA 2012) was used to describe the components of a safety case in Section 1.6. This guidance is complimentary to the CNSC Guide G-320 (CNSC 2006) and its structure is used to present the information in this report. To illustrate how the content of G-320 is captured in this report, a mapping of the report sections to the content in G-320 is included in Table 1-4.

Table 1-4: Pre-Project Report Content Mapped to CNSC Guide G-320

G-320 Content	Relevant Section(s) in Report
Developing a Long-Term Safety Case	
Safety Assessment	Chapter 7
Use of Different Assessment Strategies	Section 7.2
Robustness and Natural Analogues	Chapters 7 and 9
Use of Complementary Indicators to Safety	Section 7.13
Defining Acceptance Criteria	
Overview	Section 7.1
Criteria for Protection of Persons and the Environment	Section 7.1
Performing Long-Term Assessments	
Selection of Appropriate Methodology	Sections 7.2 and 7.5
Assessment Context	Sections 7 and 7.2
System Description	Chapters 2 to 5
Assessment Time Frame	Section 1.4 and 6.1
Assessment Scenarios	Chapter 6
Developing and Using Assessment Models	Chapter 7
Interpretation of Results	
Comparing Assessment Results with Acceptance Criteria	Section 7.14
Analyzing Uncertainties	Chapter 8

1.9 References for Chapter 1

CEAA. 1998. Nuclear Fuel Waste Management and Disposal Concept: Report of the Nuclear Fuel Waste Management and Disposal Concept Environmental Assessment Panel. Canadian Environmental Assessment Agency. Ottawa, Canada.

CNSC. 2004. Regulatory Policy P-290: Managing Radioactive Waste. Canadian Nuclear Safety Commission. Ottawa, Canada.

CNSC. 2006. Regulatory Guide G-320: Assessing the Long Term Safety of Radioactive Waste Management. Canadian Nuclear Safety Commission. Ottawa, Canada.

Gierszewski, P., J. Avis, N. Calder, A. D'Andrea, F. Garisto, C. Kitson, T. Melnyk, K. Wei and L. Wojciechowski. 2004. Third-Case Study – Postclosure Safety Assessment. Ontario Power Generation Report 06819-REP-01200-10109-R00. Toronto, Canada.

Hare, F.K., A.M. Aikin and J.M. Harrison. 1977. The Management of Canada's Nuclear Wastes. Report of a Study Prepared under Contract for the Minister of Energy, Mines and Resources Canada. Report EP 77-6. Energy, Mines and Resources Canada. Ottawa, Canada.

IAEA. 1970. Treaty on the Non-Proliferation of Nuclear Weapons. International Atomic Energy Agency INFCIRC/140. Vienna, Austria.

IAEA. 1972. Agreement Between the Government of Canada and the International Atomic Energy Agency for the Application of Safeguards in Connection with the Treaty on the Non-Proliferation of Nuclear Weapons. International Atomic Energy Agency INFCIRC/164. Vienna, Austria.

IAEA. 2000. Protocol Additional to the Agreement between Canada and the International Atomic Energy Agency for the Application of Safeguards in Connection with the Treaty on the Non-Proliferation of Nuclear Weapons. International Atomic Energy Agency INFCIRC/164/Add. 1. Vienna, Austria.

IAEA. 2011. IAEA Safety Standards: Disposal of Radioactive Waste. International Atomic Energy Agency. Specific Safety Requirements IAEA SSR-5. Vienna, Austria.

IAEA. 2012. IAEA Safety Standards: The Safety Case and Safety Assessment for the Disposal of Radioactive Waste. International Atomic Energy Agency. Specific Safety Guide IAEA SSG-23. Vienna, Austria.

ICRP. 2007. The 2007 Recommendations of the International Commission on Radiological Protection. ICRP Publication 103. Ann. ICRP 37 (2-4).

MoEE. 1994. Water Management Policies Guidelines Provincial Water Quality Objectives of the Ministry of Environment and Energy. Ministry of Environment and Energy. Ontario, Canada.

MoE. 2011. Soil, Ground Water and Sediment Standards for Use under Part XV.1 of the Environmental Protection Act. Ontario Ministry of Environment. Ontario, Canada.

NWMO. 2010. Moving Forward Together: Process for Selecting a Site for Canada's Deep Geological Repository for Used Nuclear Fuel. Nuclear Waste Management Organization. Toronto, Canada.

2. DESCRIPTION OF A HYPOTHETICAL SITE

2.1 Introduction

The purpose of this chapter is to describe the characteristics of a hypothetical crystalline site that could be encountered during geoscientific site characterization activities on the Canadian Shield. The description is provided in-lieu of geoscientific information that would be derived through site-specific surface and sub-surface investigations. The intent is to provide information necessary to support an illustrative safety assessment, the focus of which is to demonstrate a methodology to assess the postclosure safety of a deep geological repository for Canada's used nuclear fuel in a crystalline geosphere at an approximate depth of 500 m. The characteristics of the hypothetical crystalline site described in this chapter are based upon those used in NWMO (2012) and, in most instances, the characteristics have been adopted fully and remain unchanged.

Although the data represent a hypothetical Shield site, the information is consistent with reported values obtained from site-specific investigations during the Canadian Nuclear Fuel Waste Management Program on the Canadian Shield (Garisto et al. 2010, Sykes et al. 2004, 2009, Normani et al. 2007). The following sections describe characteristic surface Shield features through the presentation of descriptive geologic (Section 2.2.1), hydrogeologic (Section 2.2.2) and geochemical (Section 2.2.3) site models. The site models are used as a basis for numerical simulations that are intent on illustrating groundwater system behaviour and evolution at time frames relevant to the long-term performance of a deep geological repository. The numerical groundwater simulations are described in Section 2.3.

2.2 Conceptual Model for Hypothetical Site

The following section describes the geosphere model for a hypothetical crystalline site, including information on: the site geology, surface features (topography and hydrology), hydrogeological and geochemical conditions. The long-term stability and natural evolution of the geosphere, including potential geological disturbances (e.g., seismicity) and climate change are discussed in Chapter 5, Section 5.1.

2.2.1 Descriptive Geologic Site Model

The geologic site model describes the geologic composition and structural features of the geosphere, as well as provides the basis for geoscientific understanding of the current conditions and their evolution.

2.2.1.1 Geologic Description

The geology of the site is defined by a layer of Quaternary-aged glacial drift, as well as lake and river sediments (consisting of clay, silt and sand) up to 10 m depth, which overlie crystalline rock of the Canadian Shield. The Canadian Shield consists of a variety of igneous and metamorphic rock types, including volcanic, plutonic, metasedimentary and gneissic (Hoffman 1988, Card 1990). Exposed bedrock areas range from several km^2 to hundreds of km^2. The crystalline rocks vary in composition from gabbros and diorites (which contain many mafic minerals) to granites and granodiorites (which contain mostly felsic minerals). The crystalline rocks for this case study consist of granodiorite and granite, as well as tonalite, and are Archean in age (OGS 2000). The granitic rocks are composed of microcline, plagioclase and quartz, with minor biotite and trace amounts of opaques, epidote, muscovite, chlorite and sphene.

The geothermal gradient is assumed to be 12 °C/km, as is typical for the Canadian Shield (Perry et al. 2010).

For the purposes of this case study, the geology is divided into three rock mass permeability zones and three fracture zones: shallow, intermediate and deep, as described in Section 2.2.2.2. Physical characteristics, including the density and porosity of the geosphere, are also described in Section 2.2.2.2.

2.2.1.2 Surface Features

2.2.1.2.1 Topography

A representative regional area encompassing a watershed with Shield topography was selected for this case study, and is shown in Figure 2-1 with an area of 5734 km^2. The average topographic gradient across the domain is estimated at 0.007. Within this region, an illustrative sub-regional area has been selected to provide a basis for the postclosure safety assessment (refer to Figure 2-1 and Figure 2-2). The boundaries for the sub-regional domain were selected to correspond with surface divides, which represent planes across which groundwater flow is not expected to occur.

The top surface of the domain was defined by a 30 m hydrologically corrected Digital Elevation Model (DEM) (MNRF 2015). The DEM was upscaled to 50 m resolution to coincide with the sub-regional model grid.

The sub-regional watershed and hydrogeologic conditions are described in Section 2.3 and in Sykes et al. (2004). Detailed topography for the sub-regional site is shown in Figure 2-2. The sub-regional watershed corresponds to topographic divides to the north and south, and local topographic highs along other perimeter boundaries.

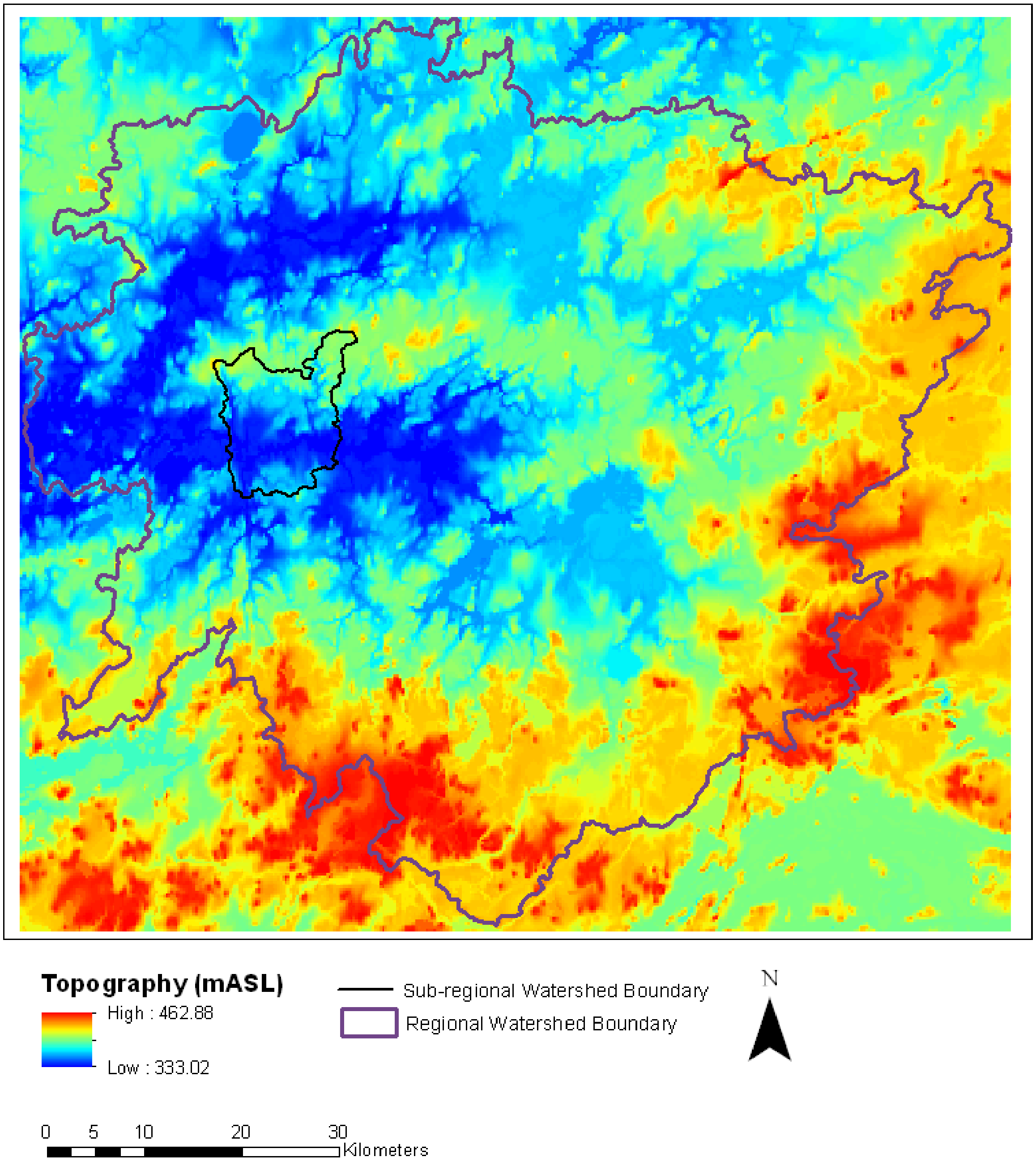

Note: Elevation is given in metres Above Sea Level (mASL).

Figure 2-1: Regional Watershed Boundary and Sub-regional Domain Boundary

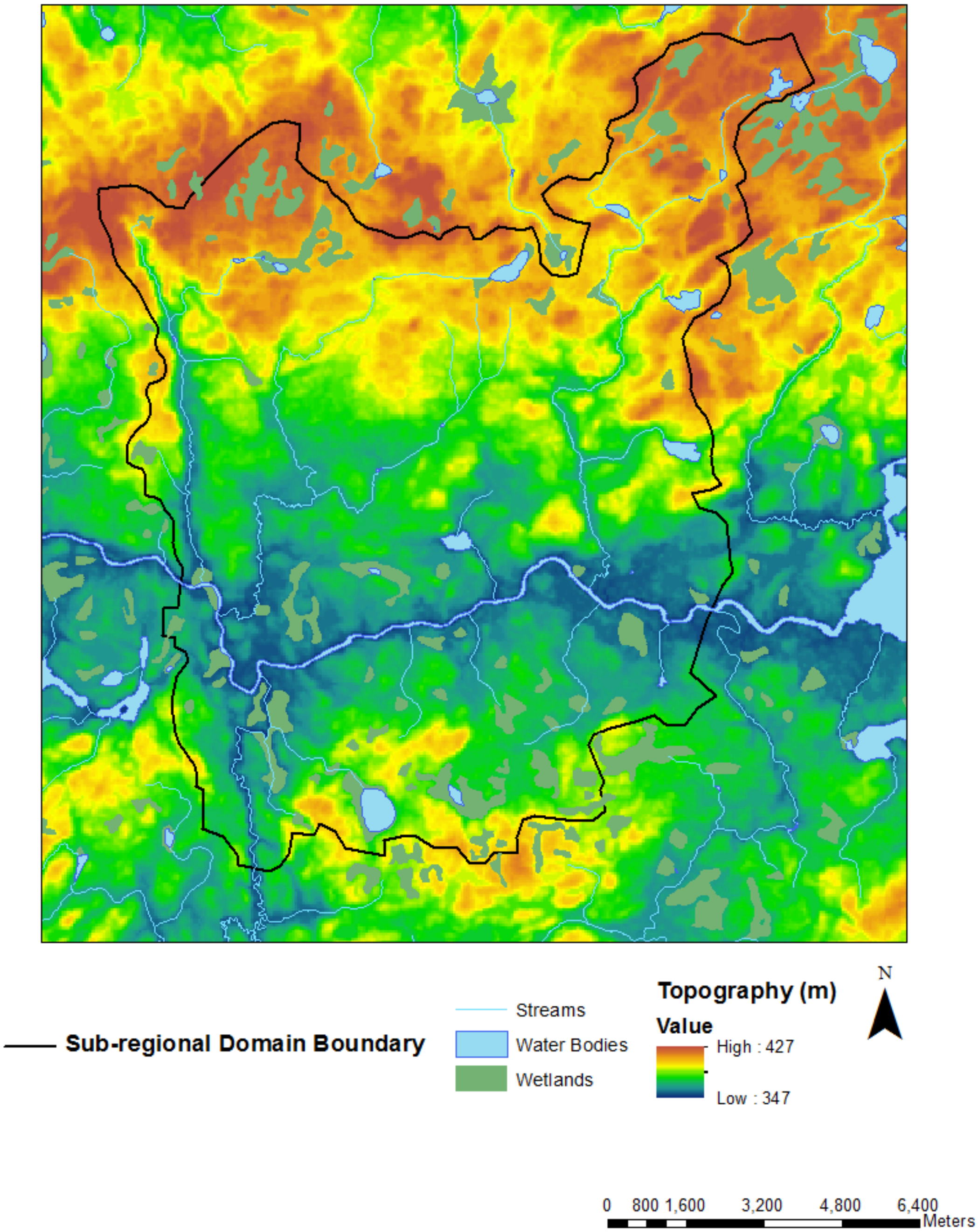

Figure 2-2: Sub-regional Watershed including Topography and Surface Hydrology

2.2.1.2.2 Surface Hydrology

The surface-water features, along with the domain boundary, are also shown in Figure 2-2. The east-west trending river corresponds with a topographic low. This river divides the domain and will act as the convergence point for local surface water patterns. The sub-regional watershed contains smaller rivers, which flow into the main east-west trending river, as well as wetlands.

2.2.1.3 Discrete Fracture Network

Srivastava (2002a) generated a fracture network model for a sub-regional area of the Canadian Shield that was used in the Third Case Study (Garisto et al. 2004) and Fourth Case Study (NWMO 2012). The fracture network was based on a surface lineament analysis that coincided with surface drainage features, and extended underground using a geostatistical fracture propagation process that respected fracture statistics from the Canadian Shield. The network included all fractures with scale length larger than about 500 m.

The fracture network model created by Srivastava (2002a) was informed by a combination of site-specific lineament data and statistical parameter distributions obtained from studies of the Whiteshell Research Area (WRA) on the Canadian Shield. The conditioning data used to determine the fracture distribution and characteristics are from Sikorsky et al. (2002). The conditioning data used would be typical of that available during initial surface-based site characterization activities. Near the surface of the crystalline rock site, fracture zones can be grouped into either sub-vertical fracture zones or low-dip fracture zones. In this case study, the low-dip fracture zones truncate against the sub-vertical fracture zones. At depth, the low-dip fracture zones will not be frequent and the sub-vertical fracture zones will tend to converge, resulting in a decrease in fracture density with depth (Srivastava 2002a).

As part of this pre-project review, the fracture network model from Srivastava (2002a) was recreated using the NWMO's latest generation fracture network modelling code, MoFrac. MoFrac is based upon the legacy FXSIM3D code, created by Mohan Srivastava (Srivastava 2002a, 2002b, Srivastava and Frykman 2006). A collaborative development program has been undertaken to re-implement the functionalities of the legacy FXSIM3D code into a more user-friendly platform. The development of MoFrac is being undertaken as nuclear grade software following the NWMO's technical computing software procedure (NWMO 2015). MoFrac is capable of creating discrete fracture network models at the tunnel, site and regional scale. The modelling of deterministic features allows MoFrac to be directly linked to field observations.

The MoFrac-generated discrete fracture zone network is processed for inclusion in the numerical model following the methodology of Normani et al. (2014) to represent fracture zones using quadrilateral elements, which are defined between neighbouring hexahedral elements of the three-dimensional numerical model. Additional capabilities were added to the pre-processor software to accommodate vertical undulation in the MoFrac fracture zones as well as degenerate triangles resulting from processing the MoFrac discrete fracture zone network in the ParaView visualization software.

The distribution and locations of the fracture zone elements, as applied in the numerical groundwater model (see Section 2.3), are shown in Figure 2-3 and Figure 2-4. The fracture zone network consists of a large number of intersecting features within the first few hundred metres, and significantly fewer features (larger and/or more vertical) extending to greater depths. Characterizing fracture zones with a high degree of detail can be difficult. Major fracture zones can be identified at surface, but the location and distribution of smaller fracture zones, as well as their interconnectedness, will be less certain.

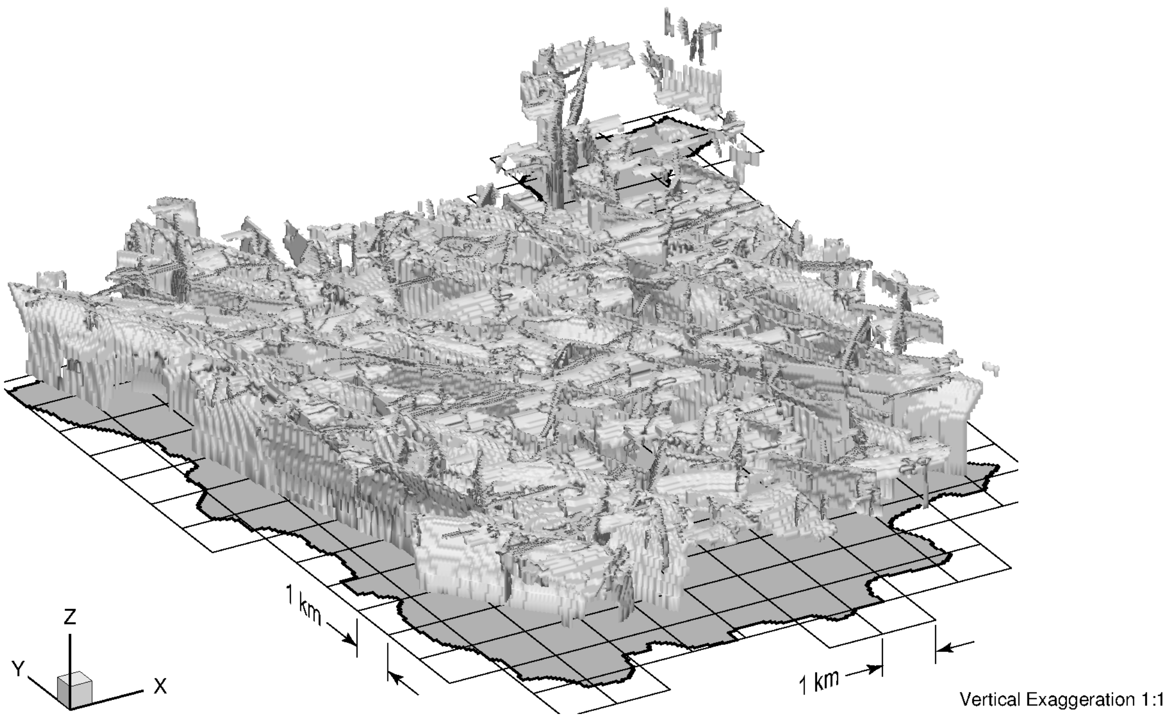

Figure 2-3: Fracture Network Model Elements

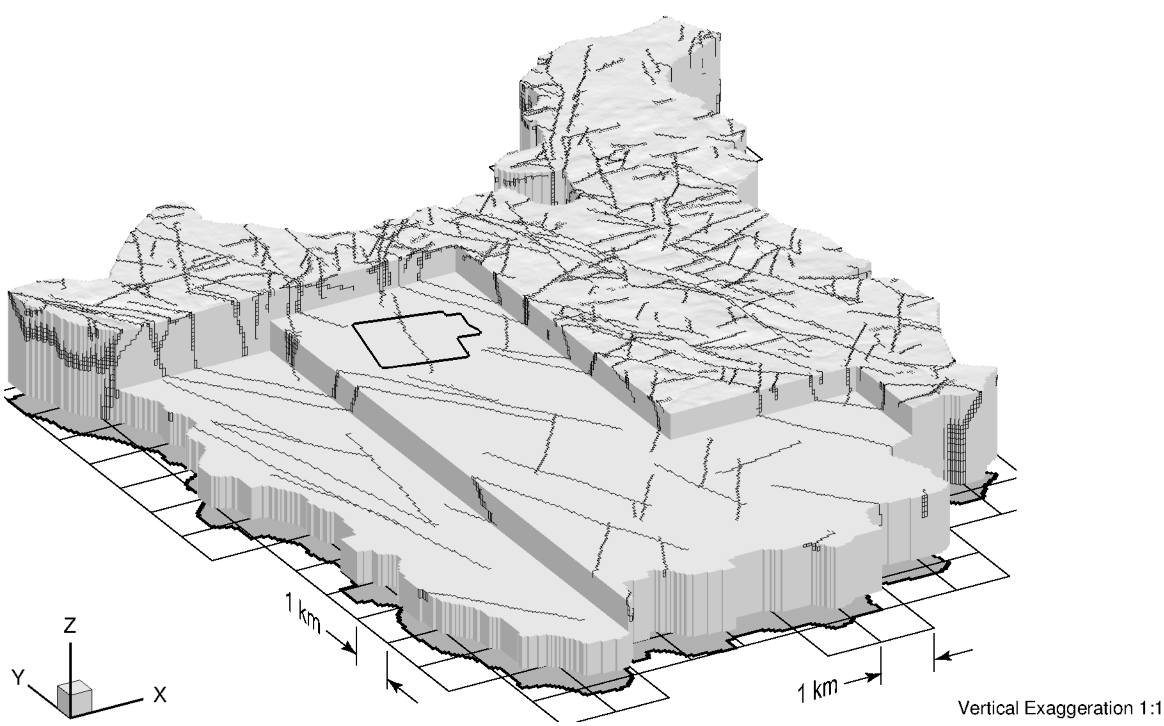

Note: Cut away sections are at 500 metres below ground surface (mBGS) and 1000 mBGS.

Figure 2-4: Distribution of Fracture Zones

2.2.2 Descriptive Hydrogeologic Site Model

Groundwater flow paths and residence times within a crystalline groundwater system are governed to a large extent by site-specific conditions. Key factors influencing groundwater movement include the nature, spatial variability and anisotropy of the permeability field (comprised of the rock matrix and transmissive structural discontinuities), the direction and magnitude of hydraulic gradients resulting from topographic and spatial fluid density differences, and hydraulic boundary conditions. Hydraulic gradients on the Canadian Shield are often on the order of 10^{-3} due to the low topographic relief (Sykes et al. 2009, Ophori et al. 1995). With respect to the latter, at longer time scales, external perturbations, such as hydromechanical ice-sheet loading and permafrost, can influence groundwater system evolution.

The hydrogeologic system at a specific crystalline site, including the existing fracture systems, would be investigated as part of detailed site characterization activities. For the hypothetical crystalline site considered in this study, the conceptual hydrogeological model, including information on the groundwater systems and hydraulic parameters, is described in this section.

2.2.2.1 Groundwater Systems

In the hypothetical Canadian Shield site, three groundwater systems are considered: shallow, intermediate and deep. These systems are identified, in part, by rock mass hydraulic conductivities, as observed at Atikokan and the Whiteshell Research Areas, as well as groundwater total dissolved solids (TDS) concentrations and redox conditions (a detailed, geochemical conceptual model is presented in Section 2.2.3). The primary characteristics for the three groundwater systems are tabulated in Table 2-1 and described below. For the purpose of this study, the hydraulic conditions were assumed to be hydrostatic with respect to the variable density fluids.

<u>Shallow Groundwater System (0-150 mBGS)</u>

The shallow groundwater system, located near surface, is predominately driven by local- and sub-regional-scale topographic changes. Within this system, the rate of movement of groundwater reflects, in part, the heterogeneous three-dimensional network of near-surface vertical and horizontal fracture zones. Meteoric water, in the form of rain or snowmelt, initially recharges the groundwater system by infiltration in fractures from topographic highs, and flows near the surface before discharging into streams or rivers, lakes, swamps or bogs associated with local topographic lows. The velocities in the shallow groundwater zone result in advection dominating contaminant transport processes (Normani et al. 2007). The average travel time for groundwater to recharge, and then subsequently discharge, in the shallow zone is typically less than 1,000 years. The groundwater in the shallow groundwater zone is fresh and oxygen-rich, with low TDS concentrations (further discussion of which can be found in Section 2.2.3).

<u>Intermediate Groundwater System (150-700 mBGS)</u>

The groundwater in the intermediate groundwater system transitions from fresh and oxygen-rich, to more mineralized and chemically reducing with depth. At the hypothetical site, the shift from oxidizing to reducing conditions occurs at around 150 mBGS. In the intermediate groundwater system, larger domains of low permeability rock tend to decrease mass transport rates.

Deep Groundwater System (>700 mBGS)

In contrast with the shallow and intermediate groundwater zones, the groundwaters in the deep system have higher TDS concentrations and, hence, fluid densities. Geochemical redox potential is reducing. The increased fluid density will influence both energy gradients within the groundwater regime and vertical upward movement of groundwater between the shallow/intermediate and deep groundwater zones (Park et al. 2009).

The transition between the shallow and deep systems is, in part, a function of the occurrence, frequency and interconnectivity of discrete fractures and fracture zones within the rock mass. In the deeper regions of the groundwater system, the hydraulic conductivity of the rock mass tends to decrease as the structural discontinuity frequency and interconnectivity diminish (Stevenson et al. 1996, see Figure 2-5).

2.2.2.2 Hydraulic Parameters

Rock mass hydraulic conductivity data from Canadian Shield research sites in the Whiteshell Research Area (Stevenson et al. 1996) and the Atikokan Research Area (Ophori and Chan 1996) were used to define reference case and sensitivity case hydraulic conductivity versus depth profiles for the hypothetical site. The hydraulic conductivity versus depth profiles were grouped into three depth ranges based upon observable trends in the rock mass data. When organized in this manner, the data indicate a trend of decreasing rock mass hydraulic conductivity with depth (Sykes et al. 2004).

The hydraulic conductivity of fracture zones in crystalline rock has a high degree of influence on the development and evolution of groundwater systems at depth (Normani et al. 2007). Normani et al. (2007) developed probabilistic permeability vs. depth profiles for fracture zones based on field data from the Whiteshell Research Area and the Finnish Olkiluoto site. The median fracture zone hydraulic conductivity varies from 10^{-6} m/s at surface to 10^{-9} m/s at approximately 700 m depth and greater. For this case study, however, the fracture zone hydraulic conductivity is assigned a reference value of 10^{-6} m/s (≈ 30 m/a) and is independent of depth. Fracture zone width is assumed to be 1 m. For the purpose of this illustrative case study, smaller fractures and joints are accounted for by the effective hydraulic conductivity assigned to the rock mass between the fracture zones.

An equivalent porous media (EPM) fracture zone representation is used in one of the sensitivity cases (fr-epm). The hydraulic conductivity of a matrix block intersected by a fracture zone is computed using arithmetic averaging, using a 50 m block width of which 1 m is associated with the fracture zone. The computed hydraulic conductivity is assigned isotropically. Furthermore, porosity is calculated using a volumetric average (volume weighted arithmetic average), of which the fracture zone occupies 1/50 of the matrix block. A fracture zone represented as EPM skews the averaged hydraulic conductivity toward the value for the fracture zone, while the average porosity is skewed toward the matrix porosity.

The reference and sensitivity case rock mass and reference case fracture zone hydraulic conductivity profiles are plotted versus depth in Figure 2-5. The key hydraulic parameters (hydraulic conductivity, specific storage, fluid density, rock porosity and effective diffusion coefficients) for the hypothetical site are provided in Table 2-1. At 500 m below ground surface, the reference hydraulic conductivity in the rock mass surrounding the repository is assumed to be 4 x 10^{-11} m/s (≈ 0.001 m/a). Additional parameters are required to perform mass transport simulations and hydro-mechanically coupled paleohydrogeological sensitivity cases.

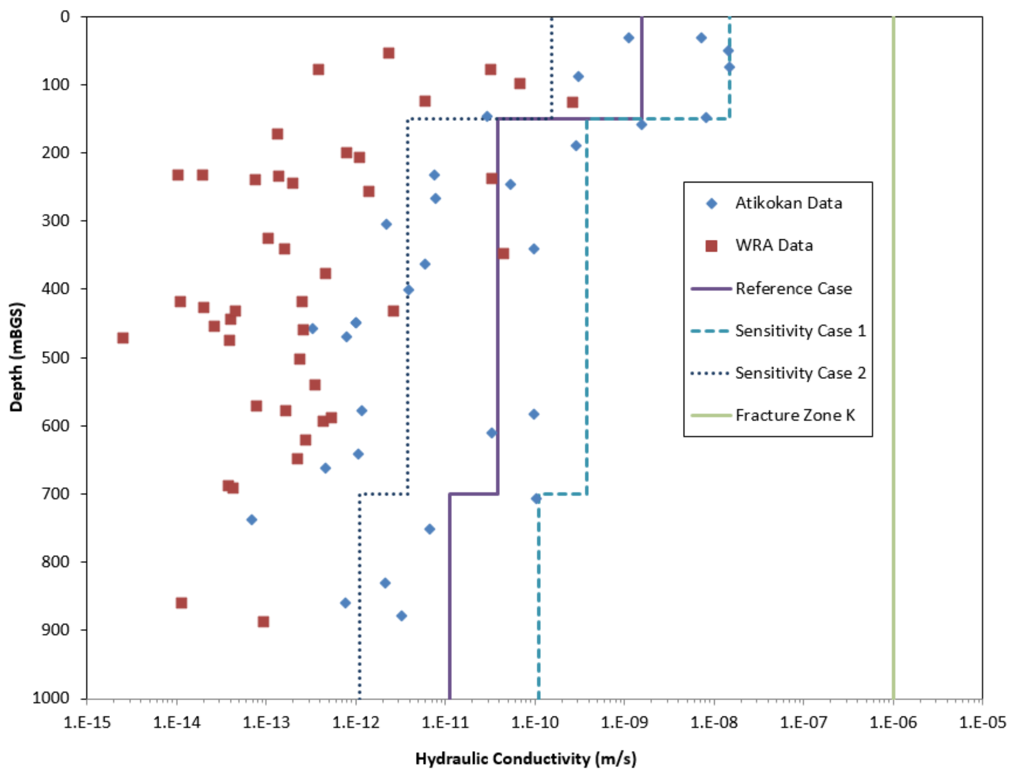

Note: WRA data are from Stevenson et al. (1996). Atikokan data are from Ophori and Chan (1996).

Figure 2-5: Rock Mass and Fracture Zone Hydraulic Conductivity Profile

Table 2-1: Physical Hydrogeological Parameters

Zone	Layer	Depth (mBGS)	Thickness (m)	Conductivity (m/s)			Bulk Density (kg/m^3)[2]	Porosity[3] (-)	Specific Storage (m^{-1})	Effective Diffusion (m^2/s)	Redox Conditions
				Ref. Case	Sens. Case 1	Sens. Case 2[1]					
Shallow Groundwater Zone	Sediment	0 – 10	0 – 10	$1x10^{-5}$	$1x10^{-5}$	$1x10^{-5}$	1250	0.5	$1x10^{-7}$	$1x10^{-12}$	Oxidizing
	Overburden	0 – 10	0 – 10	$1x10^{-8}$	$1x10^{-8}$	$1x10^{-8}$	1537	0.42			
	Rock mass permeability Zone 1	10 – 150	140	$2x10^{-9}$	$2x10^{-8}$	$2x10^{-10}$	2700	0.003			
	Shallow Fracture Zone	10 – 150	150	$1x10^{-6}$			2400	0.1			
Intermediate Groundwater Zone	Rock mass permeability Zone 2	150 – 700	550	$4x10^{-11}$	$4x10^{-10}$	$4x10^{-12}$	2700	0.003	$1x10^{-7}$	$1x10^{-12}$	Reducing
	Intermediate Fracture Zone	150 – 700	550	$1x10^{-6}$			2400	0.1			
Deep Groundwater Zone	Rock mass permeability Zone 3	700 – 1500	800	$1x10^{-11}$	$1x10^{-10}$	$1x10^{-12}$	2700	0.003	$1x10^{-7}$	$1x10^{-12}$	Reducing
	Deep Fracture Zone	700 – 1500	800	$1x10^{-6}$			2400	0.1			

Notes: 1) Sensitivity Case 2 is not reported as the decrease in rock mass hydraulic conductivity by an order-of-magnitude will act to improve geosphere stability.
2) Bulk density values taken from Davison et al. (1994), App. D.
3) The porosity value of 0.003 represents the rock matrix porosity. The porosity value of 0.1 represents the porosity of the fracture zone. Porosity values taken from Davison et al. (1994), App. D. Effective diffusion coefficient for Iodide taken from Vilks et al. (2004).

The parameters required for hydro-mechanical paleohydrogeologic sensitivity cases are provided in Table 2-2. For the reference case, the fluid modulus is calculated to be 3600 MPa based on a pressure of 14.7 MPa, a temperature of 20˚C and a fluid density of 1200 kg/m^3 (Batzle and Wang 1992), assuming the presence and influence of brine, although the reference case does not simulate brine transport. The grain modulus of 50 GPa for crystalline rock was obtained from Lau and Chandler (2004). Given a Poisson's Ratio of 0.25 and a specific storage of 1x10^{-7} m^{-1}, the Young's Modulus is calculated to be 51.8 GPa. The resulting Biot coefficient is 0.309, with a loading efficiency of 0.59. A loading efficiency of 1.0 is specified for glacial drift.

Table 2-2: Hydromechanical Coupling Parameters

Simulation Case	Young's Modulus (GPa)	Grain Modulus (GPa)	Biot Coefficient	Specific Storage (m^{-1})	Loading Efficiency (-)
Reference Case	51.8	50.0	0.309	1.00x10^{-7}	0.59
Biot Coefficient = 1.0	51.8	Infinity	1.0	1.99x10^{-7}	0.95
Biot Coefficient = 0.5	37.5	50.0	0.5	1.92x10^{-7}	0.68

2.2.2.3 Paleohydrogeology Boundary Conditions

Paleohydrogeological simulations are used to illustrate the long-term evolution and stability of the geosphere to external perturbations. Glaciation is expected to be the largest external perturbation to which a repository would be subject.

Over the past 900,000 years, the crystalline rocks of the Canadian Shield have been subjected to nine glaciation events, each lasting for a period of approximately 100,000 years (Peltier 2002). During the last glacial advance and retreat, up to 4 km of ice overrode the Canadian Shield. In assessing the long-term stability and evolution of groundwater systems at depth in a crystalline rock site in the Canadian Shield, the loading and unloading of the geosphere by a glacier will represent one of the most significant perturbations to the present-day conditions.

The University of Toronto (UofT) Glacial Systems Model (GSM) provides the hydraulic and mechanical paleoclimate boundary conditions and permafrost depths for the paleohydrogeologic sensitivity cases (Peltier 2006). Paleoclimate scenario nn2008 represents a single example of a glacial cycle, as predicted by the GSM. A plot of various nn2008 GSM outputs for the grid cell containing the sub-regional modelling domain is shown in Figure 2-6. These outputs include ice thickness, meltwater production rate, lake depth, permafrost depth, and ice-sheet basal temperature relative to the pressure melting point of ice. Only the ice thickness and permafrost depth outputs are applied to the paleohydrogeologic groundwater simulations. Similarly, the alternate paleoclimate scenario, nn2778, GSM model outputs for the grid cell containing the sub-regional modelling domain are shown in Figure 2-7. The main difference between the two glaciation scenarios is the duration of permafrost during the 121,000 years GSM simulation; the length of time nn2778 is subject to permafrost conditions is less than that of nn2008. Permafrost first thaws at approximately 14,000 years before present in the nn2008 GSM scenario and can be considered a cold bottom glacier. A best estimate paleoclimate scenario “Peltier 2015”, presented in Figure 2-8, was developed using the updated UofT GSM (Stuhne and Peltier 2015). The paleoclimate boundary conditions presented in Figure 2-6, Figure 2-7 and Figure 2-8 are applied to the paleoclimate sensitivity cases described in Section 2.3.5.3. A permafrost hydraulic conductivity of $5x10^{-11}$ m/s, from McCauley et al. (2002), as determined experimentally for frozen soils, was applied.

2.2.3 Descriptive Geochemical Site Model

The groundwater chemistry in crystalline rocks of the Canadian Shield shows a general pattern in chemical evolution with respect to depth or distance along the flow path (Gascoyne and Kamineni 1994). Singer and Cheng (2002) suggest, in general, that within the Canadian Shield there are two main groundwater systems: a shallow fresh water system (0-150 m) and an underlying deep system with increased groundwater salinity. Crystalline rocks occupy vast geographic distances, and therefore it is unlikely that the shallow groundwater system has the same vertical extent across all Canadian Shield regions (Singhal and Gupta 2010). Site-specific characterization would delineate the nature and extent of different groundwater systems at any potential repository site.

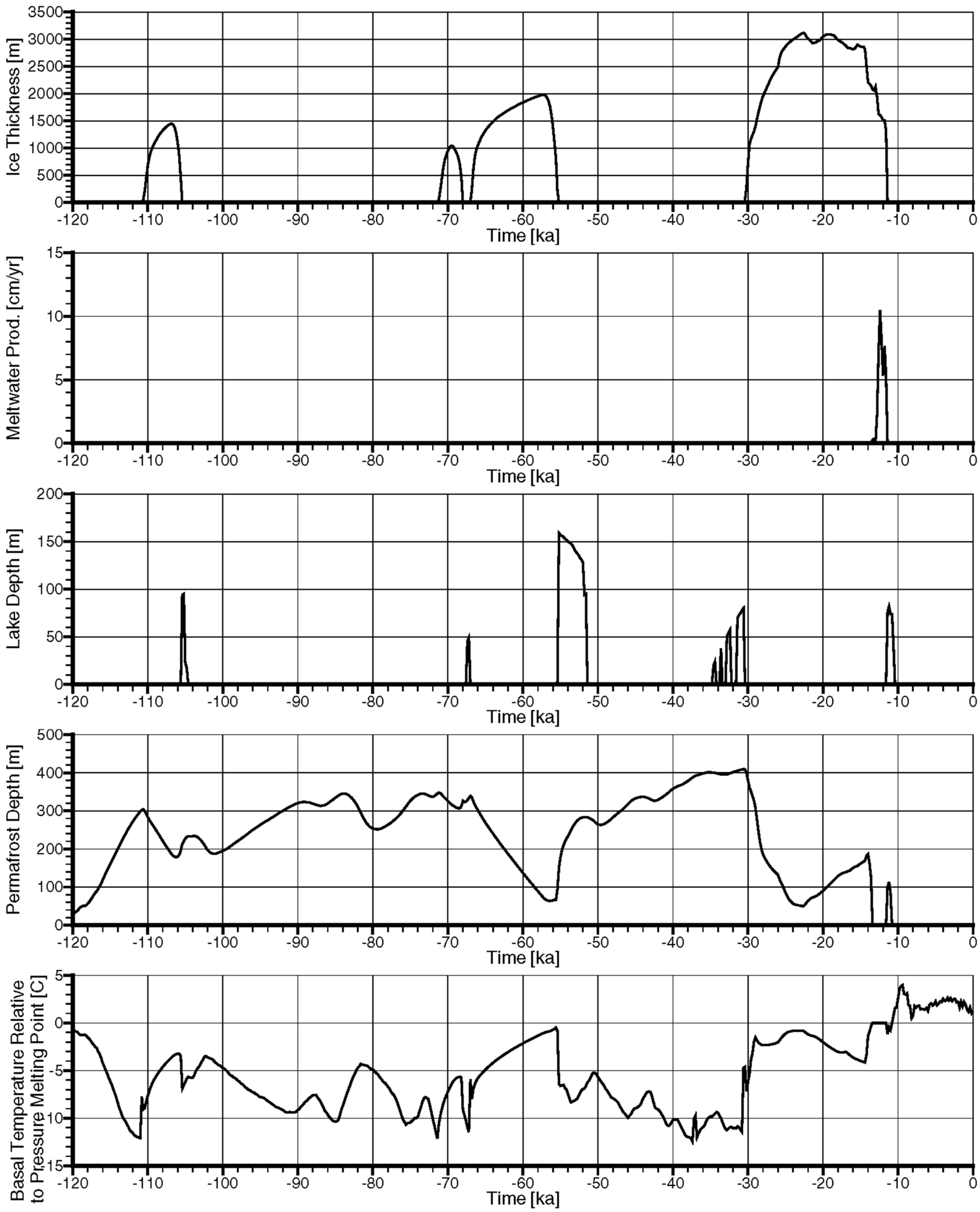

Figure 2-6: GSM Outputs from Scenario nn2008 for the Grid Cell Containing the Sub-Regional Modelling Domain

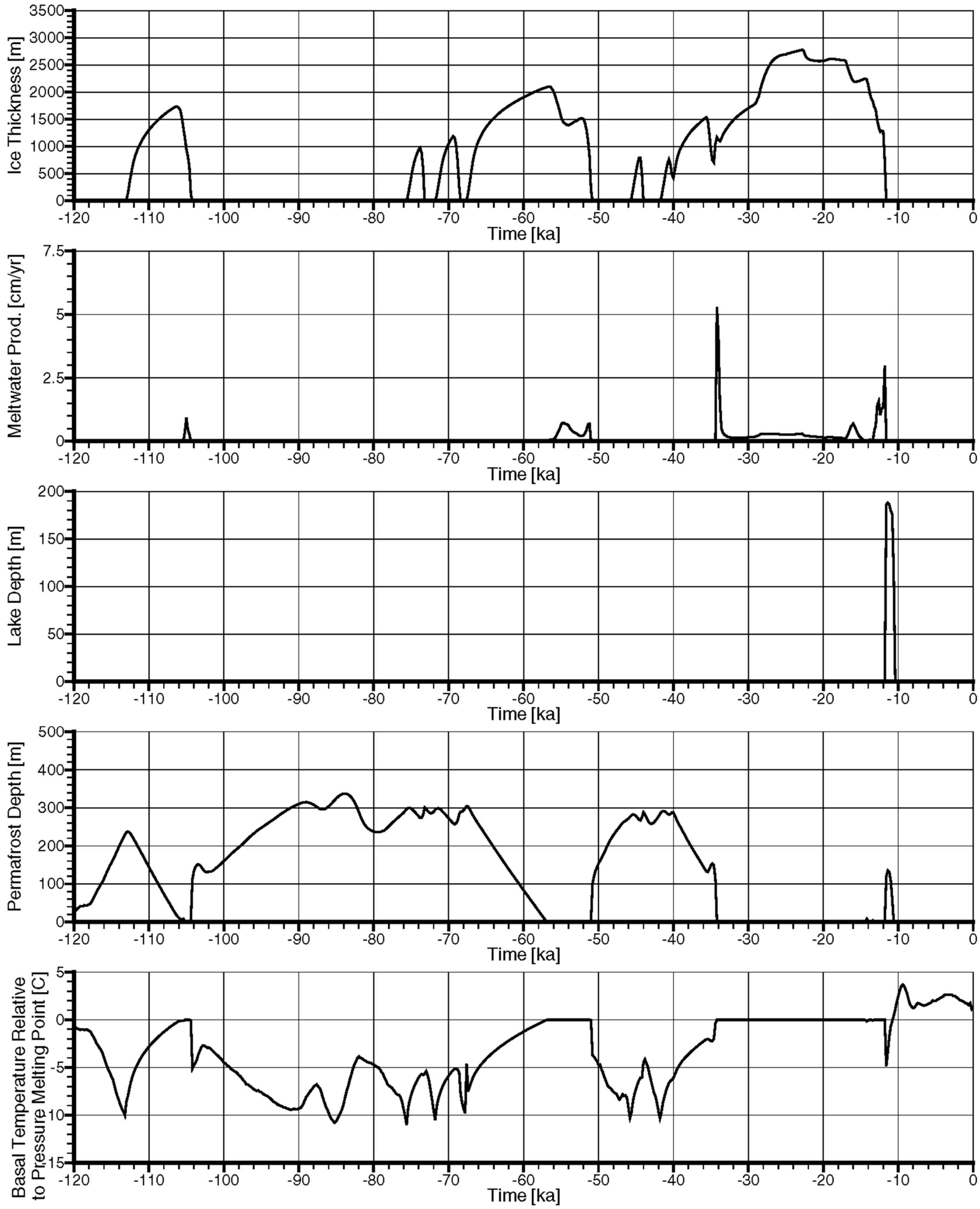

Figure 2-7: GSM Outputs from Scenario nn2778 for the Grid Cell Containing the Sub-Regional Modelling Domain

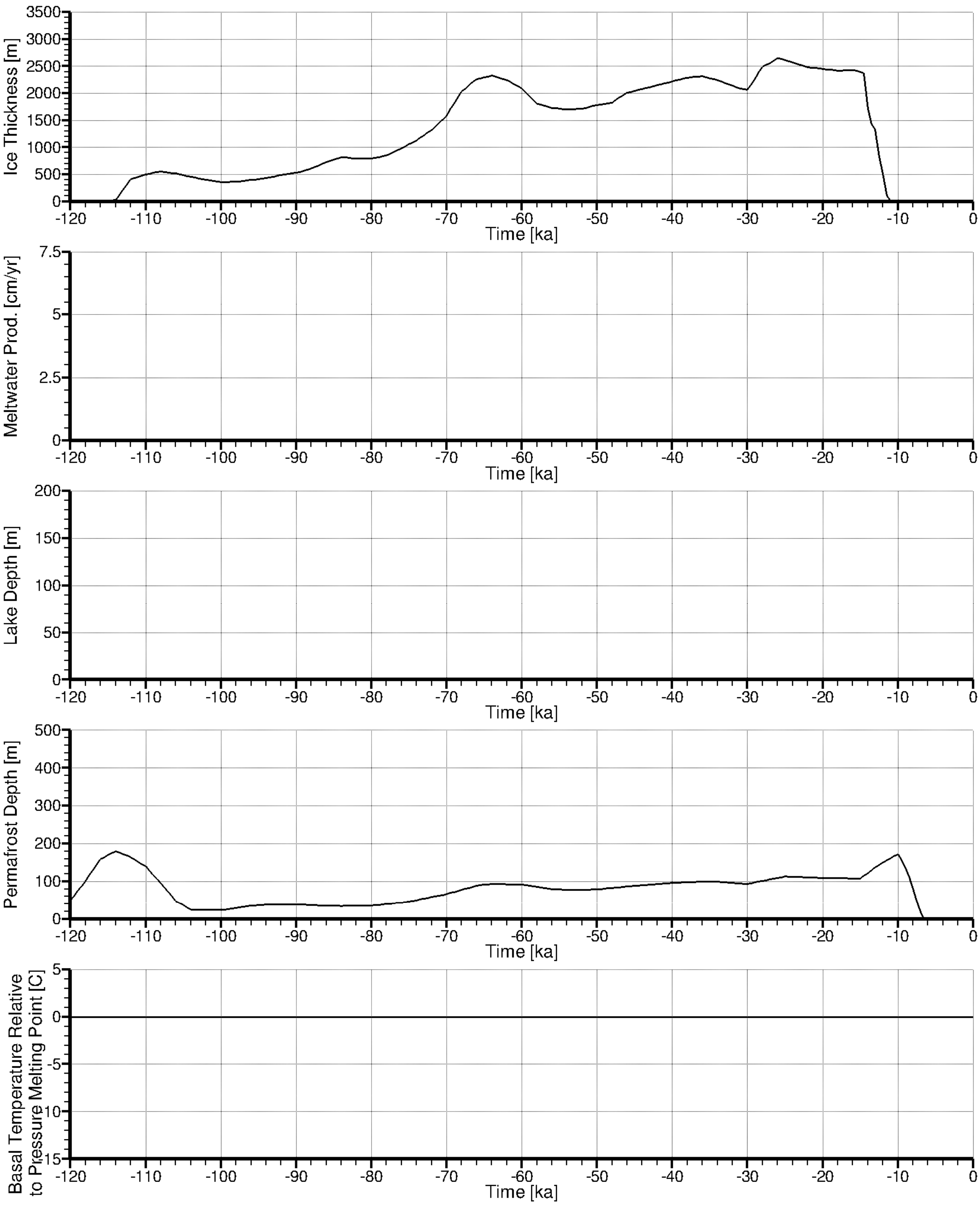

Figure 2-8: GSM Outputs from Scenario "Peltier 2015" for the Grid Cell Containing the Sub-Regional Modelling Domain

In low temperature environments, dissolution rates are very low for the major rock-forming minerals in granitic rocks. The most abundant chemical components in groundwater in granitic rocks are the cations Ca, Na, and Mg, and the anions HCO_3, SO_4, and Cl (Bucher and Stober 2000). Cations such as K, Al, Si, and Fe, which are important components of the most abundant minerals in the rock, are less abundant in solution because they tend to be associated with relatively insoluble secondary minerals. Groundwater geochemistry is modified over time and space by rock-water interactions, mixing with other waters in the system, and by microbially-mediated reactions. In crystalline rocks, vertical zoning in groundwater chemical composition has been reported from several areas, with a progression from dilute near-surface waters, to brackish waters and, in some instances, to saline waters at depths ≥ 500 m (Singhal and Gupta 2010, and references therein).

Information on the geochemical conditions collected as part of detailed site characterization activities would be combined with available regional information to define site-specific conditions. The geochemical conditions in the shallow, intermediate and deep groundwater systems assumed for the hypothetical site (Section 2.2.2.1) are described below. The microbial conditions and expected colloid concentrations in groundwaters within crystalline settings are also described.

2.2.3.1 Geochemical Conditions at the Hypothetical Site

The geochemical conditions described here pertain to both the groundwater present in fractures and to porewaters within the rock matrix.

Shallow Groundwater System (0-150 mBGS)

McMurry et al. (2003) reported that shallow groundwaters in crystalline rock generally are dilute and oxidizing. The pH values are buffered by carbonate equilibria to near-neutral pH values of about 6 to 8. Reactions with organic material and bacteria tend to consume dissolved oxygen rapidly along the flow path, promoting reducing conditions in the subsurface within tens of metres, in most cases (Gascoyne 1997). The shallow groundwaters in the crystalline rocks of the hypothetical Canadian Shield site remain largely separate from stagnant, geochemically distinct groundwaters at depth, consistent with data collected from actual Canadian Shield environments.

Intermediate Groundwater System (150-700 mBGS)

With increased depth, rock-water interactions, such as the precipitation and dissolution of calcite and ion exchange on clay minerals, cause the groundwaters to become slightly more mineralized (e.g., McMurry 2004, Gascoyne and Kamenini 1994). Hydrolysis reactions, particularly those involving amphiboles and plagioclase feldspar, in some cases, cause pH values to increase to about 9 for granitic rocks, or to about 10 for rocks such as gabbros, which contain large amounts of Ca-rich plagioclase. Reactions with ferrous minerals, sulphides, reduced sulphur aqueous species and dissolved organics promote and maintain reducing conditions. Many of these redox reactions are microbially-mediated. The depth of the redox divide is typically 150 mBGS (Gascoyne 2000).

Gascoyne et al. (1988) investigated the saline brines within several Precambrian plutons and identified a chemical transition around 300 m depth, marked by a rapid rise in TDS. This was attributed to advective mixing above 300 m, with a shift to diffusion-controlled transport below that depth. It was noted that major fracture zones within the bedrock can, where present, extend the influence of advective processes to greater depth. In the deeper regions, groundwater transport in the intact rock tends to be very slow, resulting in long residence times (Gascoyne and Kamineni 1994, Gascoyne 2004).

A reference groundwater composition, CR-10 (Table 2-3), has been defined to represent the saline groundwater conditions at the depth of the hypothetical repository (500 mBGS). It is based on the understanding that the typical groundwater chemistry at this depth in crystalline rock is Na-Ca-Cl or Ca-Na-Cl saline water under reducing conditions (McMurry 2004, Gascoyne and Kamenini 1994). The CR-10 water was derived from the WRA reference water WN-1M, which, in turn, was derived from data at depths ranging from 350-800 mBGS at the WRA in crystalline rocks of the Canadian Shield (Gascoyne 1988, McMurry 2004).

CR-10 is a Ca-Na-Cl type water with a TDS concentration of 11.3 g/L and is under reducing conditions. The density of the groundwater is 1.006 kg/L. The concentration of key chemical solutes is shown in Table 2-3.

The reducing environment at depth is, in part, the result of microbial reactions involving organic carbon, and rock-water interactions between dissolved oxygen and iron- and sulphur-rich minerals (see Table 2-4). These reactions consume dissolved oxygen, resulting in a reducing groundwater environment (Davison et al. 1994). The assumed colloid concentration in groundwater at repository depth is 0.34 mg/L (Davison et al. 1994). Further discussion of colloids can be found in Section 2.2.3.3 and Section 5.5.8.

Table 2-3: CR-10 Porewater Parameters

Composition	CR-10
pH	7.0
Environment type	Reducing
Eh (mV)	-200
Density	1.006
Solutes (mg/L)	
Na	1900
K	15
Ca	2130
Mg	60
HCO_3	70
SO_4	1000
Cl	6100
Br	-
Sr	25
Li	-
F	2
I	-
B	-
Si	5
Fe	1
NO_3	<1
PO_4	0
TDS	11,300

Note: The charge balance error (CBE) for water CR-10 in Table 2-3 is 0.08%

Table 2-4: Geosphere Redox Conditions

Depth(mBGS)	Redox Condition
0-10	Oxidizing
10-150	Oxidizing
150-300	Reducing
300+	Reducing

Deep Groundwater System (>700 mBGS)

Groundwater research carried out at the Atomic Energy of Canada Limited (AECL) Underground Research Lab (URL) found that groundwaters and seepage waters in the crystalline rocks at depths of 300 to 1000 m possessed TDS concentrations values ranging between 3 and 90 g/L (Gascoyne 2000, Gascoyne 2004). However, as summarized in Stotler et al. (2012), TDS concentrations exceeding 250 g/L have been reported in some regions of the Canadian Shield at depths below 500 m. There are a number of potential sources of salinity, including: prolonged interactions of pore fluids with the rock, salt enrichment by freezing or evaporation, and mixing with hydrothermal saline fluids that may have persisted in fractures for hundreds of millions of years. In crystalline rocks that were adjacent to, or covered by, marine waters at some time in the geological past, there is also evidence that seawater or evaporative brines have migrated into the fractures along regional flow paths (Bottomley et al. 1999).

2.2.3.2 Microbial Conditions in Crystalline Environments

Cell densities in Canadian groundwaters have been reported between 103 and 105 cells/mL (Stroes-Gascoyne and West 1997). Microbial metabolism requires a carbon source, terminal electron donor and terminal electron acceptor. Additional nutrients required for growth and maintenance include N, P, S, K, Mg, Na, Ca and Fe, as well as a suite of other trace elements.

Subsurface microbial communities are capable of using an array of terminal electron accepting processes. The dominant species in a given environment tend to be those bacteria that generate the most energy from the available nutrient sources. As summarized in the review by Sherwood Lollar (2011) and references therein, acetogens, iron-reducing and sulphate-reducing bacteria and methanogens (using either dissolved inorganic carbon or acetate) are often the dominant component of the population in Canadian Shield groundwaters. In addition, studies of Canadian Shield groundwaters have shown microbial assemblages containing heterotrophic aerobes and anaerobes, denitrifying, N_2-fixing and iron-precipitating bacteria (Jain et al. 1997).

Microbial processes in the geosphere that are relevant to a DGR for used nuclear fuel are summarized in Humphreys et al. (2010) and Sherwood Lollar (2011), and references therein. The consumption of oxygen by aerobic microbial activity has been identified as the most significant effect of microorganisms on base scenario processes related to the evolution of the geosphere (McMurry et al. 2003).

Microbial processes play an important role in O_2 reduction in the subsurface and are able to catalyze reactions that would not otherwise take place at low temperatures (SKB 2006). Oxygen is a versatile electron acceptor and is energetically favourable for many microorganisms. As summarized in SKB (2006), several in-situ and laboratory experiments have demonstrated the consumption of oxygen in granitic environments. These studies have shown that there is a substantial increase in microbial activity where surface water containing O_2 encounters stagnant groundwater systems, and that the time scale for complete microbial oxygen reduction in typical fractures is on the order of a few days (SKB 2006). In crystalline rock environments, oxygen concentrations have been shown to decrease with depth due to microbial processes. For example, at the crystalline site of Olkiluoto, Finland, oxygen concentration decreases have been correlated to methanotrophic (methane metabolizing) bacteria, suggesting that these bacteria could constitute an effective barrier against oxygen intrusion in the presence of methane (Pedersen 2006).

Gas production is a natural abiotic and biotic process in crystalline rock environments (Sherwood Lollar et al. 1993a, 1993b, 2007). From a microbial energy production perspective, methane and hydrogen are perhaps the most important deep subsurface gases. Methane concentrations ranging from 1 µM to 18,600 µM have been reported in Canadian Shield and Fennoscandian Shield groundwaters (Sherwood Lollar et al. 1993a, 1993b). The fixation of CO_2 to organic molecules by autotrophic methanogens and acetogens under anaerobic conditions is an important process in the deep subsurface, resulting in the formation of methane and acetate, respectively. This provides a renewable source of organic carbon to continually fuel the consumption of oxygen (if present) in the deep subsurface (SKB 2006). Hydrogen is a versatile electron donor in subsurface environments. H_2 concentrations tend to increase in deeper, more saline fracture waters (Sherwood Lollar et al. 2007). Between 2 µM and 1600 µM of hydrogen in groundwater from Canadian Shield and Fennoscandian Shield rocks has been reported (Sherwood Lollar et al. 1993a, 1993b, 2014). Hydrogen from deep geological processes contributes to the redox stability of deep groundwater by acting as an electron donor for microbial metabolism (Pedersen 2000).

2.2.3.3 Colloids

Particles between 1 µm and 1 x 10^{-3} µm are termed colloids and include both inorganic mineral particles (in particular clays) and organic particles, such as microbial cells, viruses or organic matter (Hallbeck and Pedersen 2008). They are suspended in groundwater and are sufficiently small so that interfacial forces are significant controls on their transport and fate. Depending on their composition and physical characteristics, among other factors, colloids may be transported at approximately the same velocity as groundwaters.

Colloids typically are present in low concentrations (less than 1 mg/L) in groundwaters (McMurry et al. 2003). The natural colloid concentration in deep groundwaters in the Canadian Shield is expected to be low. See, for example, data from Whiteshell and Atikokan on total colloids (Davison et al. 1994, Vilks and Bachinski 1997, Vilks et al. 1998) and also on organic colloids in Fennoscandian Shield groundwaters (Andersson 1999). In such settings, the assumed reference natural colloid concentration in deep groundwaters is between 0.2 and 0.4 mg/L. The concentration of colloids in the near-field geosphere will be influenced to some extent by repository-related changes in temperature, interactions with clay and cementitious sealing materials, as well as groundwater salinity.

2.2.3.4 Sorption

The sorption of radionuclides onto mineral surfaces within the geosphere is a potential mechanism for slowing the transport of radionuclides from repository depth to the surface environment. There are many factors that impact radionuclide sorption processes in the geosphere, such as rock type, mineral surface area, groundwater salinity, pH, redox conditions, temperature, the presence or absence of complexing ligands, and radionuclide concentration. The sorption partition coefficient (K_d) of radionuclides is used to describe their sorption behaviour. In fractures, the presence of alteration minerals will generally result in higher sorption capacities (K_d values) than in non-altered rock (Byegård et al. 2008, Crawford et al. 2006).

Sorption of radionuclides is generally reduced in groundwaters with high salinity (Vilks 2009). In particular, radionuclides that are retarded by cation exchange mechanisms (i.e., Cs and Sr) are more strongly adsorbed in groundwaters with lower ionic strengths (Byegård et al. 2008, Crawford et al. 2006). This effect is not as important for either the elements that adsorb by surface complexation, or for the moderately saline groundwater conditions at repository level for this hypothetical Canadian Shield site. Sorption coefficients for the hypothetical site considered in this study are presented in Chapter 7.

2.2.4 Descriptive Geomechanical Site Model

2.2.4.1 Rock Mass Strength

The conceptual repository is assumed to be constructed at a nominal depth of 500 m in fractured crystalline rock (Geological Strength Index =79) of granitic origin. The rock is also homogenous and behaves isotropically. Its characteristics match those of a typical Canadian Shield rock in northern Ontario. Uniaxial compression tests are the most widely-performed tests for classification and determination of rock strength to be used in geomechanical analysis. These tests provide the basis stress-strain parameters of an intact rock, such as the uniaxial compressive strength (UCS), modulus of elasticity and Poisson's ratio. They also allow examination of the damage development within the granite and are used to select the appropriate long-term rock strength of rock. The crack initiation and crack damage stress states are assumed to be about 40% and about 85% of UCS, respectively (Itasca 2015). The properties of intact rock and the estimated rock mass strength are tabulated in Table 2-5 and Table 2-6, respectively.

Table 2-5: Intact Rock and Hoek-Brown Rock Mass Properties

Property	Value
UCS	210 MPa
Young's Modulus	45 GPa
Poisson's Ratio	0.25
Density	2700 kg/m^3

Note: Properties are from Itasca (2015).

Table 2-6: Mechanical Properties of Granite Rock Mass with Geological Strength Index of 79

Property	Value
Rock Mass Peak UCS	105 MPa
Cohesion	14 MPa
Friction Angle	59°
Tensile Strength	1.7 MPa

Note: Properties are from Itasca (2015).

The thermal properties of granite rock mass are listed in Table 2-7. The rock is assumed to be homogeneous and isotropic.

Table 2-7: Thermal Properties of Granite Rock Mass

Property	Value
Thermal Conductivity	3.00 Wm/K
Specific Heat Capacity	845 J/kgK
Linear Coefficient of Thermal Expansion	10^{-5} 1/K

Note: Properties are from Itasca (2015).

2.2.4.2 Ground Stresses

Kaiser and Maloney (2005) complied a representative ground stress database (tensor; magnitudes and orientations) of northern Ontario's Canadian Shield region for the sighting of a nuclear waste deep geologic repository (DGR). The study involved the collection and review of data in available stress measurement databases, as well as stress measurements from mining locations across the study area. Related reports and publications were collected and examined to assess the quality of the data. Effects of nearby mining, core damage, stress measurements and data interpretation approaches were used to evaluate and constrain such ground stress measurements. Based on the study, the Canadian Shield can be divided into three domains. In undisturbed zones, the local stress in Domain 3 directly reflects the virgin stress at depth, while near the surface, the stresses (Domain 1) are disturbed, and virgin stresses are relaxed and modified, leading to lower stresses, and, in between, there is a transition zone (Domain 2). Hence, it is necessary to define the stress state in Domains 1 and 3, and the thickness, as well as the nature of the anticipated transition zone. The in-situ stress regimes for the crystalline geosphere, based on Kaiser and Maloney (2005), are tabulated below in Table 2-8.

Table 2-8: In-situ Stress State (Kaiser and Maloney 2005)

Domain	Depth range (m)	Stresses
1	0 – 300	σ_H = 0.071 MPa/m + 5.768 MPa σ_h = 0.043 MPa/m + 3.287 MPa σ_v = 0.034 MPa/m
2	300 – 600	stresses assumed to increase linearly from values at base of Domain 1 to values corresponding to top of Domain 3.
3	600 - 1500	σ_H = 0.026 MPa/m + 23.636 MPa σ_h = 0.016 MPa/m + 17.104 MPa σ_v = 0.020 MPa/m + 1.066 MPa

An update of the Canadian Shield stress database is currently underway. All new in-situ stress data collected falls within the range of those reported in 2005 study (Yong and Maloney 2015).

2.3 Sub-Regional Scale Hydrogeologic Modelling

In order to illustrate the role of key geosphere parameters and processes, such as rock mass and fracture hydraulic conductivity, on geosphere and groundwater system stability at repository depth, a suite of sub-regional scale numerical groundwater models was developed. The following sections describe the strategy behind the modelling conducted.

2.3.1 Modelling Strategy

The behaviour, stability and resilience to change of the geosphere at repository depth is illustrated through the use of 21 comparative sensitivity cases, contrasted with a reference case based upon the conceptual model described in Section 2.2. In the sensitivity cases, key geosphere parameters are varied to illustrate the role they play in influencing groundwater flow and mass transport. The reference case and the geosphere parameters varied in the sensitivity cases are shown in Table 2-9.

The reference case simulates current site conditions at the sub-regional scale. For the purpose of this illustrative case study, the discrete fracture zone network realization is simulated using a dual continuum representation in which 2D quadrilateral elements representing fracture zones are assigned between adjacent 3D hexahedral elements in the numerical model mesh following Normani et al. (2014). A dual continuum, as implemented in this analysis, is different than a dual porosity formulation whereby the matrix and fracture domains overlap. Fracture zones are characterized by their hydraulic conductivity, porosity, and width (Normani et al. 2007, Normani et al. 2014).

Sensitivity cases, in which the hydraulic conductivity of the rock mass and discrete fracture zone networks is varied within an expected range of uncertainty, are performed in order to illustrate the sensitivity of estimated groundwater performance measures and, in particular, designation of mass transport regimes. An equivalent porous medium representation for the fracture zones is included in the sensitivity analysis to examine the role of the assumed fracture zone characteristics on groundwater performance measures. The distributions of TDS are varied to examine the role of spatially variable groundwater densities on groundwater system stability and dominant mass transport processes. In addition, the sensitivity to effective diffusion coefficients, dispersivities, and a recharge surface boundary condition are included.

The paleohydrogeologic sensitivity cases conducted as a part of this study are shown in Table 2-10. The purpose of the paleohydrogeologic sensitivity cases is to assess the influence of a glacial event on groundwater system stability. In particular, these cases explore transient hydraulic gradients, groundwater velocities, and the depth of penetration by glacial recharge, which are relevant to illustrating long-term DGR safety. The paleohydrogeologic boundary conditions are varied to include cold and warm based glaciers in order to illustrate groundwater system resilience to external perturbations. An additional best estimate paleohydrogeological case “Peltier 2015” was undertaken based upon paleoclimate simulations from the updated UofT GSM (Stuhne and Peltier 2015). In addition to the cold and warm based glaciers, the parameters used to represent the hydromechnical effects of hydrologeologic surface boundary conditions are varied to illustrate the effect on system performance measures and groundwater system stability at depth.

The effect of hydromechanical coupling during the paleohydrogeologic sensitivity cases is investigated in two ways: i) the loading efficiency is varied from the calculated reference value to 0 in order to illustrate the role of hydromechanical coupling; and, ii) the Biot coefficient is varied from 1.0 to 0.5 to illustrate the role of the assumed grain compressibility on groundwater system response.

2.3.2 Computational Models

The numerical groundwater modelling was performed using HydroGeoSphere (HGS) revision 1540 (Aquanty 2013). It is a computational model capable of solving three-dimensional variably-saturated groundwater flow and solute transport in discretely-fractured media. The model includes a dual continuum formulation, while discrete fractures are represented as idealized two-dimensional parallel plates, or as fracture zones defined by hydraulic conductivity and width. The numerical solution to the governing equations is based on implementations of both the control volume finite-element method and the Galerkin finite-element method. HGS couples fluid flow with salinity transport through fluid density, which is dependent on the TDS concentration. Details of the HGS model that are pertinent to the study are described in Aquanty (2013). HGS, as a successor to FRAC3DVS-OPG, is maintained as nuclear grade software in a Quality Assurance framework in accordance with NWMO Technical Computing Software Procedure document number NWMO-PROC-EN-0002.

Important attributes of HGS include: its ability to describe arbitrary combinations of porous, discretely fractured and dual porosity media; its flexible pre- and post-processing capabilities; the accurate handling of fluid and mass exchanges between fracture zones and matrix, including matrix diffusion effects and solute advection in the matrix; fluid and solute mass balance tracking; and, adaptive time-stepping schemes with automatic generation and control of time steps. Additionally, algorithms to estimate performance measures of groundwater age and life expectancy for the domain groundwater are also present (Cornaton and Perrochet 2006a, 2006b; Park et al. 2008). Further information on the performance measures can be found in Section 2.3.3.

Table 2-9: Table of Sub-regional Scale Temperate Reference and Sensitivity Cases

		fr-base	fr-sens	fr-EPM	fr-De	fr-Neumann	fr-disp2	fr-brine-frac-7	fr-brine-frac-8	fr-brine-frac-9	fr-sens-brine-frac-7	fr-base-frac-7
Rock Mass Hydraulic Conductivity	Reference Case	•		•	•	•	•	•	•	•		•
	Sensitivity Case 1		•								•	
Surface BC	Dirichlet at surface	•	•	•	•		•	•	•	•	•	•
Neumann	Neumann at surface					•						
Effective Diffusion Coefficient	Reference Case	•	•	•		•	•	•	•	•	•	•
	Reference Case x10				•							
Fracture Representation	DFN	•	•		•	•	•	•	•	•	•	•
	EPM			•								
Fracture Hydraulic Conductivity	10^{-6} m/s	•	•	•	•	•	•					
	10^{-7} m/s							•			•	•
	10^{-8} m/s								•			
	10^{-9} m/s									•		
Density	Brine							•	•	•	•	
	no brine	•	•	•	•	•	•					•
Dispersivity	Reference Case	•	•	•	•	•						
	Reference Case x10						•					

Table 2-10: Table of Sub-regional Scale Paleohydrogeologic Reference and Sensitivity Cases

		fr-base-paleo	fr-base-paleo-nn2778	Fr-base-paleo-Peltier	fr-base-paleo-80	fr-base-paleo-30	fr-base-paleo-0	fr-base-paleo-biot10	fr-base-paleo-biot05	fr-base-paleo-le1	fr-base-paleo-le0	fr-base-paleo-0-le1
Paleo Simulation	nn2008	•			•	•	•	•	•	•	•	•
	nn2778		•									
	Peltier 2015			•								
Paleo Surface BC	Dirichlet 100%	•	•	•				•	•	•	•	
	Dirichlet 80%				•							
	Dirichlet 30%					•						
	Dirichlet 0%						•					•
Hydromechanical Coupling	Biot Calculated Reference Value (0.309)	•	•	•	•	•	•			•	•	•
	Biot 1.0							•				
	Biot 0.5								•			
Loading Efficiency	Calculated Reference Value (0.59)	•	•	•	•	•	•	•	•			
	1.0									•		•
	0.0										•	

2.3.3 System Performance Measures

The safety case for a potential deep geological repository will rely, in part, on the ability of the geosphere to provide a long-term barrier to solute transport. The behaviour and stability of the groundwater flow and transport regimes found at repository depth can be illustrated by determining and quantifying what impact, if any, the variability of model parameters will have on the model results. By demonstrating and determining the sensitivity of the model to perturbations in model parameters, insight into the understanding of groundwater system behaviour influencing deep geological repository performance can be obtained.

Common measures of the performance of a groundwater system include the flow state variables of equivalent freshwater head or environmental head and the derived porewater velocity, the solute concentration for a conservative tracer and, as shown in Normani et al. (2007), mean life expectancy (MLE) and groundwater age. Life expectancy is estimated by determining the Probability Density Function (PDF) for the time required for water particles at a spatial position in a groundwater system to reach outflow points. Particles can migrate to the boundary by both advection and hydrodynamic dispersion; particles originating from a given point in the system will not follow the same path to the boundary due to hydrodynamic dispersion. In this case study, the first moment of the PDF for life expectancy is estimated with the value being expressed as the MLE. Groundwater age of water particles at a spatial position can be determined by the PDF for time elapsed since the water particles entered the system from a boundary.

2.3.4 Sub-Regional Scale Conceptual Model

2.3.4.1 Model Domain and Spatial Discretization

The top surface of the domain was defined by a 30 m hydrologically corrected Digital Elevation Model (DEM) (MNRF 2015). Further description of the DEM and corrections made can be found in Section 2.2.1.2. The lateral boundaries were chosen to be coincident with topographic divides.

2.3.4.2 Model Parameters

The physical hydrogeological parameters are given in Section 2.2.2.2, Table 2-1. The approach used to define additional model parameters is described below.

In-situ diffusion experiments, conducted within low-permeability crystalline rock, estimated effective diffusion coefficients (D_e) for iodide in the range of 1.4×10^{-13} m^2/s to 1.1×10^{-12} m^2/s. Evidence obtained during the in-situ experiments did not identify any apparent trend related to sample depth or stress conditions (Vilks et al. 2004). An effective diffusion coefficient value of 1×10^{-12} m^2/s is applied at the hypothetical site (as listed in Table 2-1). To estimate this D_e value, zonal tortuosity values were calculated using porosity and a brine diffusion coefficient (NaCl at 1 mol/L) of 1.5×10^{-9} m^2/s (Weast 1983). For paleohydrogeologic simulations with a tracer, the free-water diffusion coefficient for the tracer ($H_2{}^{18}O$) of 2.7×10^{-9} m^2/s in Singh and Kumar (2005) was used with the tortuosity value previously calculated. Longitudinal dispersivity values for brine and tracer transport, and for MLE[1], were set to 120 m, while both transverse horizontal

[1] Mean Life Expectancy (MLE): Mean Life Expectancy is the mean time for discharge of a non-decaying, non-sorbing solute from a given point in the groundwater system based upon advective-dispersive mass transport.

and transverse vertical dispersivities were set to 12 m. Smaller dispersivity values resulted in numerical artifacts and oscillations in the transport and MLE solutions.

2.3.4.3 Flow Boundary Conditions

For the solution of the groundwater flow equation, a specified head (Dirichlet) boundary condition is applied to all surface nodes to set the head equal to elevation for the reference case and sensitivity cases, but not for the paleohydrogeologic simulations. Zero flux boundary conditions are applied to both the lateral and bottom boundaries of the modelling domain. For simulations involving coupled density-dependent flow and transport of brine, a Dirichlet boundary condition equal to the TDS value at the bottom of the modelling domain is applied to all bottom nodes, and a mixed (Cauchy) boundary condition with zero concentration for recharging waters is applied to all surface nodes. A tracer representing recharge waters is used in the paleohydrogeologic simulations and its boundary conditions are set to zero concentration for all bottom nodes and a concentration of unity using a Cauchy boundary condition for all surface nodes.

2.3.4.4 Initial Conditions and Solution of Density-Dependent Flow

Salinity plays an important role with regard to fluid flow at repository depth. An increase in the concentration of TDS will result in an increase in the fluid density, which will then act as an inhibiter of active flow at depth (Park et al. 2009). The methodology for developing a solution for density-dependent flow is described in Sykes et al. (2011), Normani and Sykes (2012) and Normani et al. (2014). The following paragraphs summarize the methodology.

In the absence of a source term for salinity, a transient analysis is required to determine a pseudo-equilibrium solution at a time, *t,* for density-dependent flow. The analysis requires the specification of an initial distribution throughout the spatial domain for both freshwater heads and TDS concentrations. In a transient analysis, the initial prescribed salinity distribution is allowed to evolve to a new state that reflects the boundary conditions, hydraulic properties and transport properties of the sub-regional scale domain. For the coupled density-dependent flow and transport system, fresh water can recharge at the surface, reducing the TDS concentration in the shallow groundwater system. The time to flush TDS from a fracture zone or the matrix is a function of the hydraulic conductivity of the unit and the energy potential of the displacing fluid as compared to the energy potential of the fluid being displaced. Fluids with lower TDS, such as recharging water, will have a lower energy potential when compared to higher TDS fluids with the same elevation and pressure. Therefore, for low-permeability regions with a relatively high TDS concentration, the time to flush the region or displace the fluids can be very long (millions of years). Complete flushing may only occur as a result of diffusion because energy gradients and/or low permeabilities may yield low fluid fluxes that may not be sufficient for advective displacement to occur. In using this method to synthesize a spatial salinity distribution, the total mass of dissolved solids and its distribution in the model domain is assumed to be known and will be a maximum initially because there are no internal sources to generate dissolved solids resulting from rock-water interaction. With this approach, as time progresses, the dissolved solids will gradually reduce as the groundwater discharges from the system.

A plot of TDS with depth is provided in Figure 2-9, and represents an upper bound for the TDS distribution. A linear relationship is assumed between fluid density and TDS such that a fluid density of 1200 kg/m^3 is equal to 300 g/L. Further discussion of the linear relationship between fluid density and TDS can be found in Normani et al. (2007).

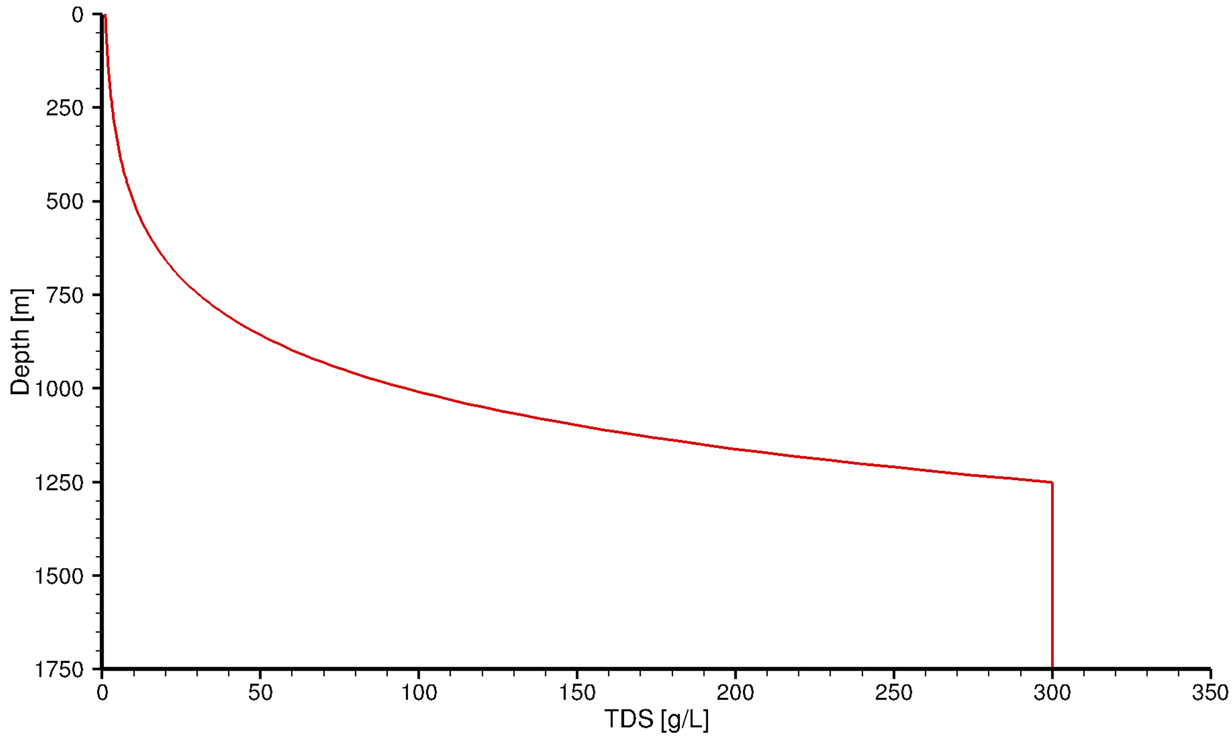

Note: Figure is based on Frape and Fritz (1987).

Figure 2-9: Initial Total Dissolved Solids Concentrations (g/L) versus Depth

For this study, the final freshwater head distribution for the sensitivity cases: fr-brine-frac-7, fr-brine-frac-8, fr-brine-frac-9, and fr-sens-brine-frac-7 was calculated using the following three-step process.

i) The distribution of freshwater heads was calculated for density-independent steady-state flow.
ii) A TDS concentration distribution was assigned throughout the domain as an initial condition using the procedure described in the preceding paragraph. The density-independent freshwater heads were allowed to equilibrate to the assigned TDS distribution in a transient analysis, while not allowing the TDS distribution to evolve. This step allowed the freshwater heads to reflect the variation of fluid density as specified by the initial TDS distribution.
iii) The TDS distribution was allowed to vary with the freshwater heads in a one million year transient analysis.

Generally, pseudo-equilibrium is reached when then the model TDS reasonably matches field measurements (for detailed discussion, see Normani 2009). In recharge areas, brine will be flushed because of a combination of the absence of a source term for brine and the effect of meteoric recharge. This is contrasted with discharge locations, which tend to transport higher concentration brines from deeper in the groundwater system. Brine is excluded from the reference case and sensitivity cases with uniform 10^{-6} m/s fracture zone hydraulic conductivities.

A depth-dependent initial TDS distribution was applied, based on Frape and Fritz (1987) for the sensitivity cases: fr-brine-frac-7, fr-brine-frac-8, fr-brine-frac-9, and fr-sens-brine-frac-7. These sensitivity cases are developed using a dual-continuum approach for the discrete fracture zone networks with uniform hydraulic conductivities ranging from 10^{-7} to 10^{-9} m/s.

2.3.5 Sub-regional Scale Analyses

2.3.5.1 Reference Case Simulation

The reference case is comprised of steady-state groundwater flow with a uniform fracture zone hydraulic conductivity of 10^{-6} m/s and no brine. The very high fracture zone hydraulic conductivity resulted in numerical instabilities such as oscillations, overshoot and undershoot in the calculation of brine concentrations. The steady-state freshwater heads, as a block-cut view, are shown in Figure 2-10. The fresh-water steady-state heads shown are calculated without the influence of density. The discrete fracture zone network is shown in two block-cuts at approximately 500 mBGS and 1000 mBGS. The freshwater heads at depth are controlled by the major east-west trending river that crosses the modelling domain.

Porewater velocity magnitudes in the rock matrix are shown in Figure 2-11. The highest velocities occur within fracture zones and in the more permeable shallow groundwater system. Velocity magnitudes tend to decrease with increasing depth, generally due to the decreasing hydraulic conductivity with depth in the rock matrix. At the repository, the porewater velocity magnitudes are between 10^{-2} and 10^{-3} m/a, except within or immediately adjacent to a fracture zone.

The performance measure selected for the evaluation of the groundwater system at repository depth is the MLE, as shown in Figure 2-12. The shallow groundwater system has significantly shorter mean life expectancies compared to the deep groundwater system. The areas of surficial recharge versus discharge can be identified in the figure because the recharge areas have a high MLE while the discharge areas have low MLEs. The MLEs within the repository outline are between one thousand years and one million years, depending on the proximity to fracture zones, with a median MLE 1.8×10^5 years. Mean life expectancies are lower in regions near fracture zones, due primarily to their higher hydraulic conductivity.

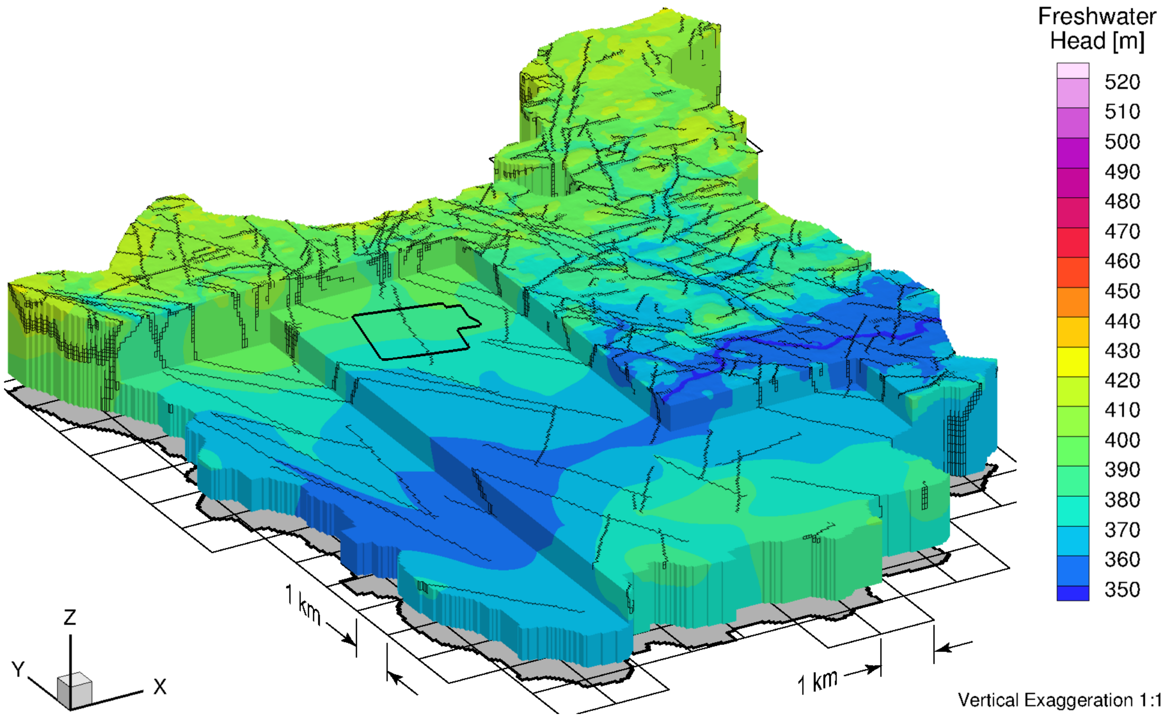

Note: Block-cuts occur at 500 mBGS and 1000 mBGS. The black outline in the centre of the figure delineates the repository location.

Figure 2-10: Reference Case Block Cut View of Steady-State Freshwater Heads

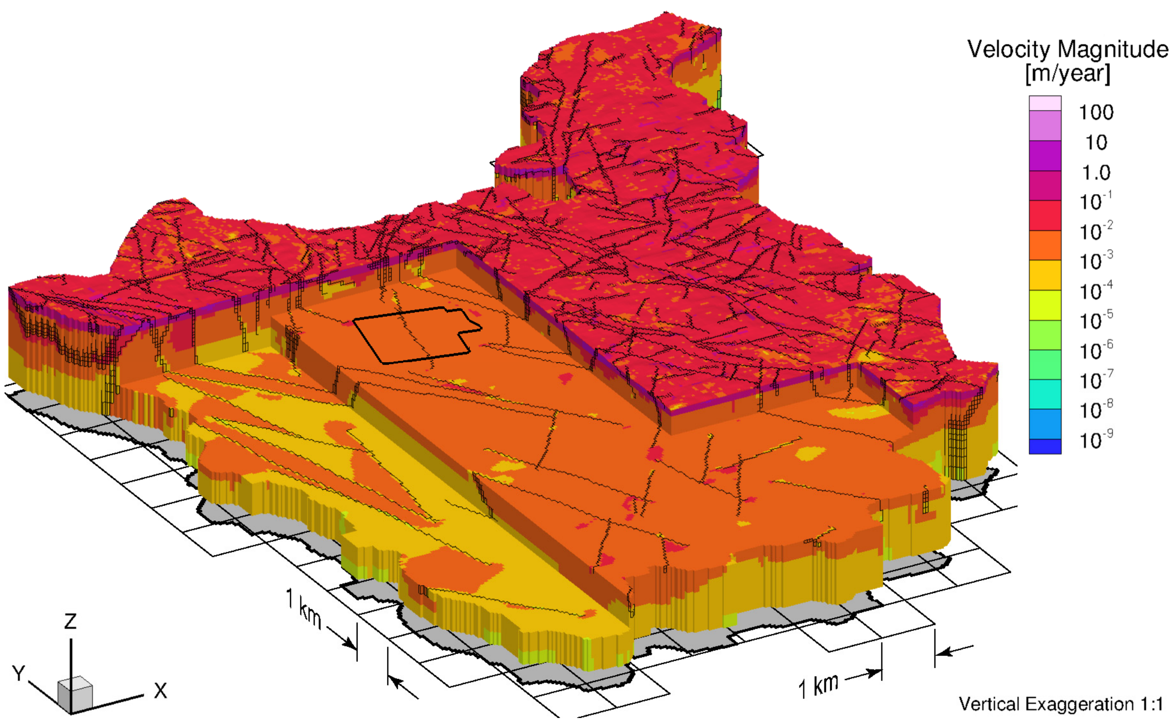

Figure 2-11: Reference Case Porewater Velocity Magnitudes

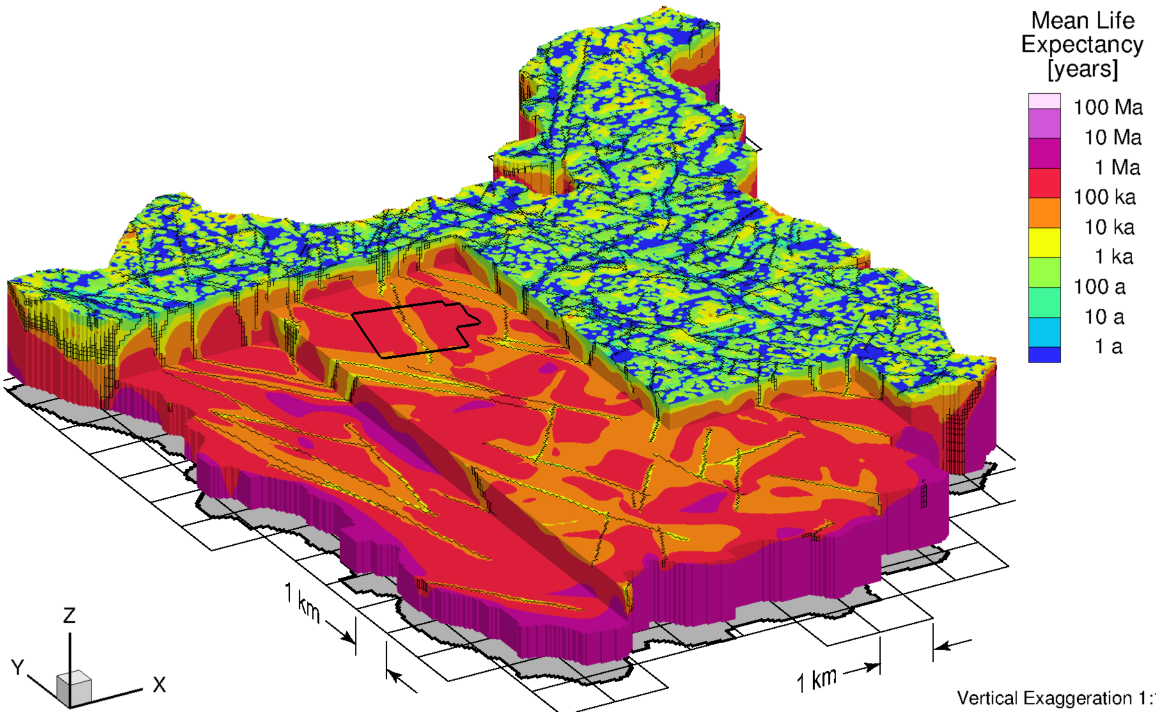

Figure 2-12: Reference Case Mean Life Expectancies

2.3.5.2 Temperate Transient Sensitivity Cases

Increasing the rock mass hydraulic conductivities by an order-of-magnitude significantly affects the groundwater system. The difference in freshwater heads between sensitivity case 1 and the reference case are shown in Figure 2-13. Within the repository, freshwater heads generally increase and the differences are predominantly within 4 m.

The ratio of porewater velocities between sensitivity case 1 and the reference case are shown in Figure 2-14. Porewater velocities generally increase by an order-of-magnitude within the rock mass. The MLE ratios shown in Figure 2-15 generally indicate a decrease in the MLE values of approximately one order-of-magnitude for the sensitivity case, resulting in a 50th percentile MLE for the repository of 2.3×10^4 years, whereas the reference case yields a 50th percentile MLE for the repository of 1.8×10^5 years. MLE ratios are closer to unity in the vicinity of fracture zones.

Figure 2-16 shows a cumulative density function of MLE values within the repository for the temperate sensitivity cases (steady-state groundwater system without brine) and a case illustrating the impact of brines on MLE. The most discernible difference is the impact of the rock-mass hydraulic conductivity in sensitivity case 1. Decreasing fracture zone hydraulic conductivity generally tends to increase the MLEs within the repository.

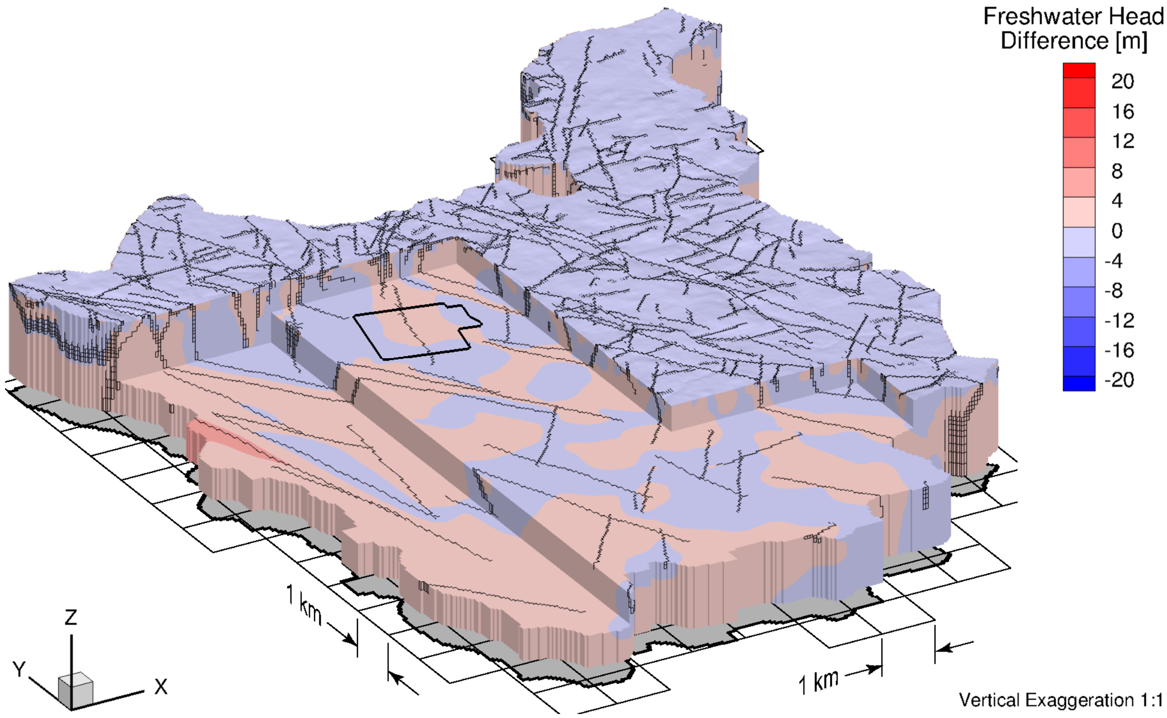

Figure 2-13: Difference in Freshwater Heads between Sensitivity Case 1 and the Reference Case

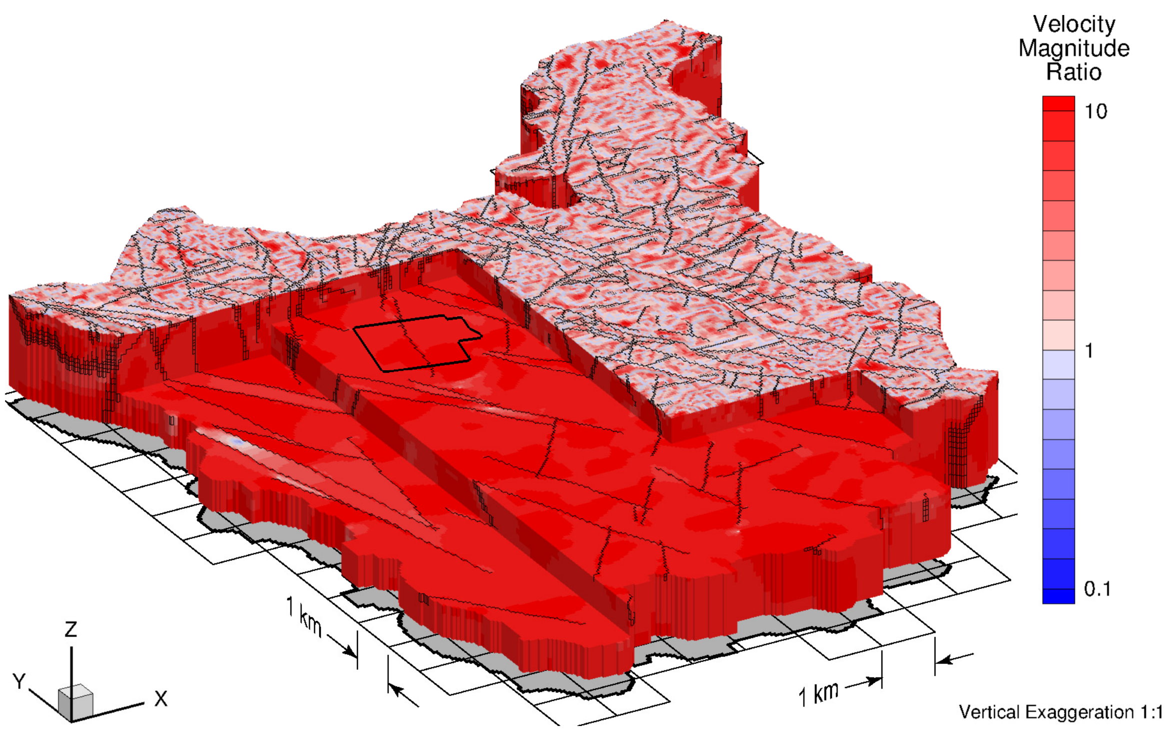

Figure 2-14: Ratio of Velocity Magnitudes for Sensitivity Case 1 to the Reference Case

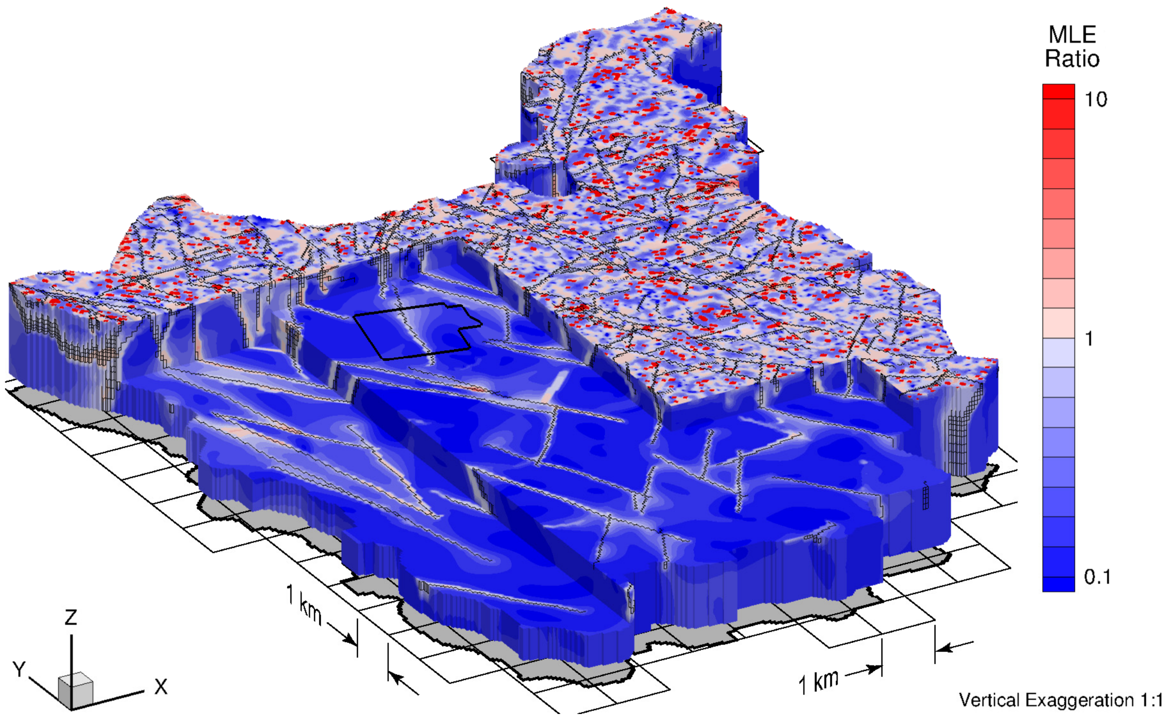

Figure 2-15: Ratio of MLE for Sensitivity Case 1 to the Reference Case

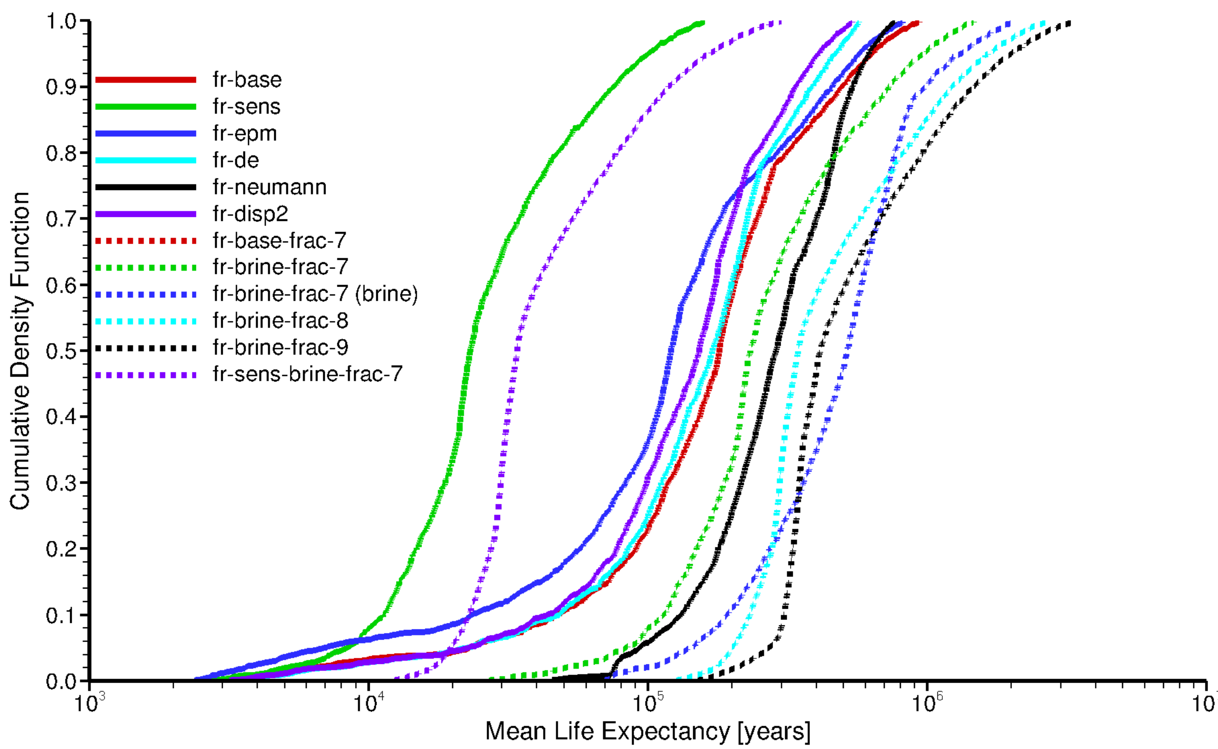

Figure 2-16: Cumulative Density Function of Mean Life Expectancy within Repository Outline at Repository Depth for Temperate Sensitivity Cases

The impact of an equivalent porous media (EPM) representation is investigated by comparing freshwater heads, porewater velocity magnitudes and mean life expectancies for steady-state groundwater systems. Figure 2-17 shows the freshwater head difference, Figure 2-18 shows the porewater velocity ratio and Figure 2-19 shows the MLE ratio. Little difference in freshwater heads is noted in Figure 2-17, while significant variation exists in both the porewater velocity ratios and MLE ratios, predominantly related to matrix blocks which are used to represent fracture zones. Porewater velocity ratios are generally greater within the repository outline for the EPM case, leading to lower MLE values as shown in Figure 2-19. The 50th percentile MLE for the repository of 1.2x10^5 years is less than for the reference case. The CDF for the repository MLE, shown in Figure 2-16, is consistently lower for the EPM representation than for the reference case. This result is likely due to the way in which EPM is calculated for a matrix block intersected by a fracture zone in this study, namely using arithmetic averaging for hydraulic conductivity and volumetric averaging for porosity. An EPM approach is predicated on an REV (representative elementary volume) concept. However, a single discrete fracture zone does not follow this model.

The migration of solutes in porous media is affected by diffusion and hydrodynamic dispersion. The impact of increasing the free solution diffusion coefficient by an order-of-magnitude and increasing the dispersivity by a factor of two is investigated with two sensitivity cases. Figure 2-20 shows the MLE ratio for an order-of-magnitude increase in the diffusion coefficient while Figure 2-21 shows the MLE ratio for a doubling of the dispersivity. Within the repository outline, the MLE ratios are generally less than unity for the sensitivity cases, except near the fracture zone that intersects the repository. Both an increase in the diffusion coefficient or in dispersivity values will tend to reduce MLE values in the matrix and increase MLE near fracture zones. The 50th percentile MLE for the repository of 1.7x10^5 years for an increase in the diffusion coefficient is lower than the reference case. The CDF curves of MLE in Figure 2-16 show similarity between the diffusion sensitivity case and the reference case. Greater differences are noted in the dispersivity case where the 50th percentile MLE for the repository of 1.5x10^5 years is less than for the reference case. The lowering of MLE values, due to an increase in the diffusion coefficient, is more pronounced in the deeper regions of the groundwater system due to the very low hydraulic conductivities at depth, which means that diffusion is an increasingly important transport process, when compared with advection, as depth increases in the rock mass.

A recharge surface boundary condition with a net recharge rate of 1 mm/a over the entire surface of grid cells, with a surface area of 50 m by 50 m each, is developed to demonstrate the impact on the groundwater system. Freshwater head Dirichlet nodes are specified for the significant water features such as lakes, wetlands, and rivers, and are set equal to elevation. The net recharge for grid cells is transferred vertically to the underlying cell or horizontally to adjacent grid cells; the cumulative net recharge for multiple grid cells will discharge at the model areas with defined Dirichlet nodes that represent the discretization of surface water bodies. For this conceptual model of a granitic environment, a significant portion of the point recharge will discharge to the surface at sub-grid cell features such as small rills, gullies, ditches, creeks, brooks and streams that are important in the surface flow system. Figure 2-22 shows the difference in heads compared to the reference case. Freshwater heads in regions of topographic highs are significantly lower when compared to the reference case. This has the impact of reducing hydraulic gradients, and hence, lowering porewater velocities as shown in Figure 2-23 with ratio values generally less than unity within the repository outline. Correspondingly, MLE ratios in Figure 2-24 generally increase within the repository outline. The median MLE value of 2.9×10^5 years is greater than the reference case. Figure 2-16 shows the MLE CDF is generally to the right of the reference case.

Although the inclusion of coupled density-dependent flow and transport can be computationally burdensome, it is an important physical attribute of the groundwater system, both from a geochemical and hydrogeologic perspective. The impact of density-dependent flow is investigated by comparing mean life expectancies between a steady-state groundwater flow simulation and the one million year transient density-dependent flow simulation for a uniform fracture zone hydraulic conductivity of 10^{-7} m/s. Calculating the ratio of MLE between a steady-state freshwater system without brine and the one million year transient brine simulation, as shown in Figure 2-18, shows changes across the domain generally within an order-of-magnitude. The 50th percentile MLE for the repository location for the case without salinity is 2.3×10^5 years, compared to the 50th percentile MLE for the case including salinity, which is 5.1×10^5 years. However, within the repository location, the MLEs are generally reduced in freshwater simulations. In the deeper portions of the groundwater system, especially along or near fracture zones, mean life expectancies can be an order-of-magnitude less for the freshwater simulation when compared to the brine simulation. In general, the average MLE will be greater for cases including salinity, as the presence of higher density fluids will act to increase stability of the groundwater system at depth.

MLE ratios for a uniform fracture zone hydraulic conductivity of 10^{-7} m/s relative to the reference case is provided in Figure 2-26. MLE ratios are generally greater by approximately one order-of-magnitude near fracture zones. Within the repository outline, the 50th percentile MLE is 2.3×10^5 years. Figure 2-16 shows a greater MLE for the CDF line as compared to the reference case. MLE ratios for decreases in fracture zone hydraulic conductivities to 10^{-8} m/s and 10^{-9} m/s, as compared to the reference case, are shown in Figure 2-27 and Figure 2-28, respectively. Decreasing fracture zone hydraulic conductivity leads to progressively larger MLE values. The 50th percentile MLE values for the 10^{-8} m/s, and 10^{-9} m/s cases are 3.4×10^5 years, and 4.1×10^5 years, respectively. Figure 2-16 shows the CDF MLE curves for these cases for the 10^{-8} m/s and 10^{-9} m/s cases. The greatest difference between these two curves is in the lower percentile range, dominated by the fracture zone that intersects the repository. The sensitivity case 1 simulation was also simulated with an order-of-magnitude decrease in the fracture zone hydraulic conductivity. Figure 2-16 shows this case plotting to the right of the sensitivity case with 10^{-6} m/s fracture zone hydraulic conductivity. The 50th percentile MLE value of 3.4×10^4 years is greater than the sensitivity case of 2.3×10^4 years.

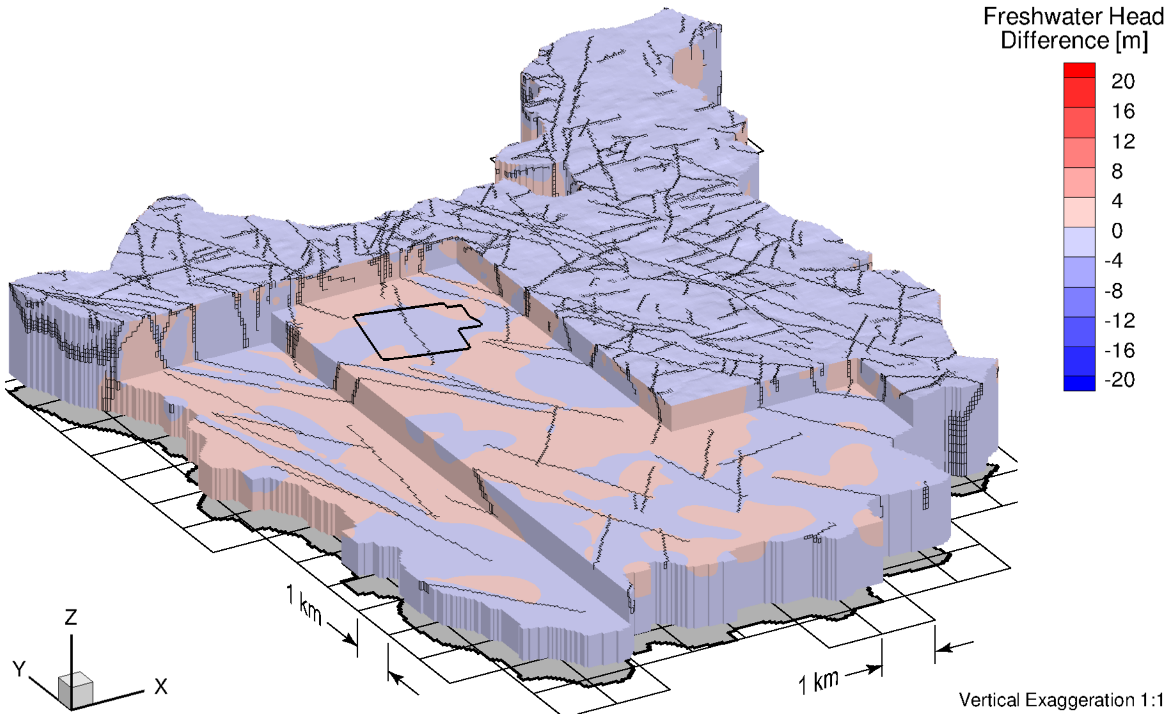

Figure 2-17: Difference in Freshwater Heads between the EPM Case and the Reference Case

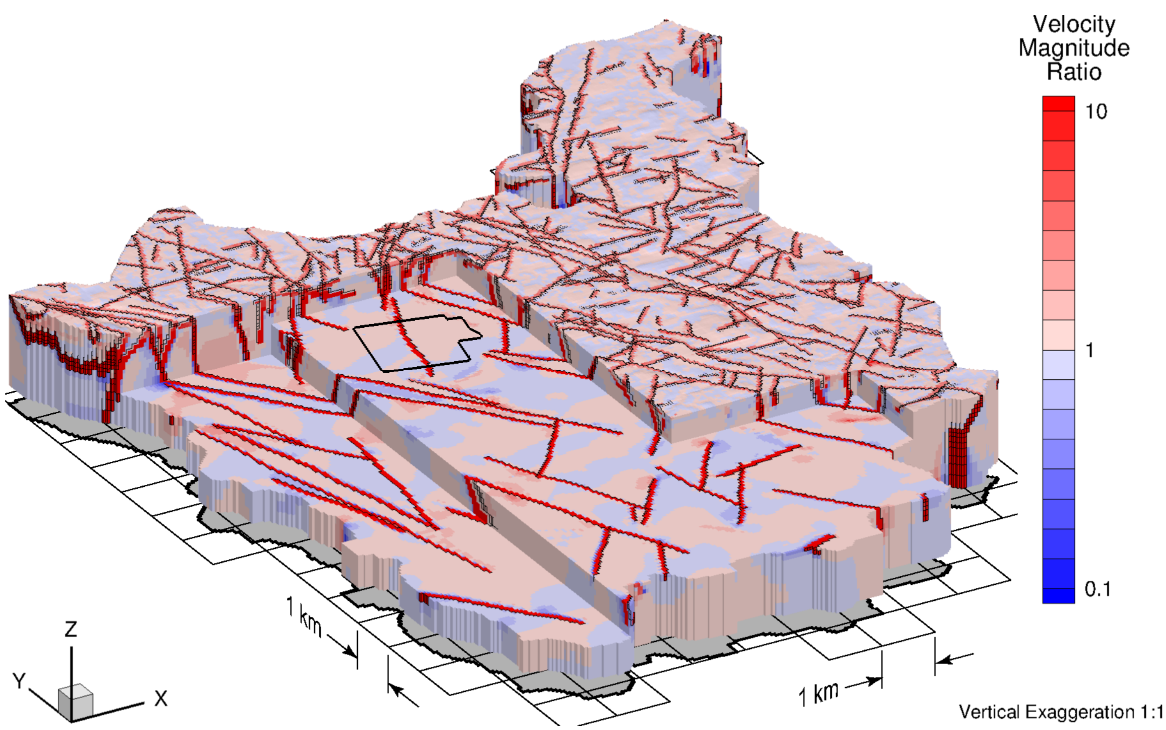

Figure 2-18: Ratio of Velocity Magnitudes for the EPM Case to the Reference Case

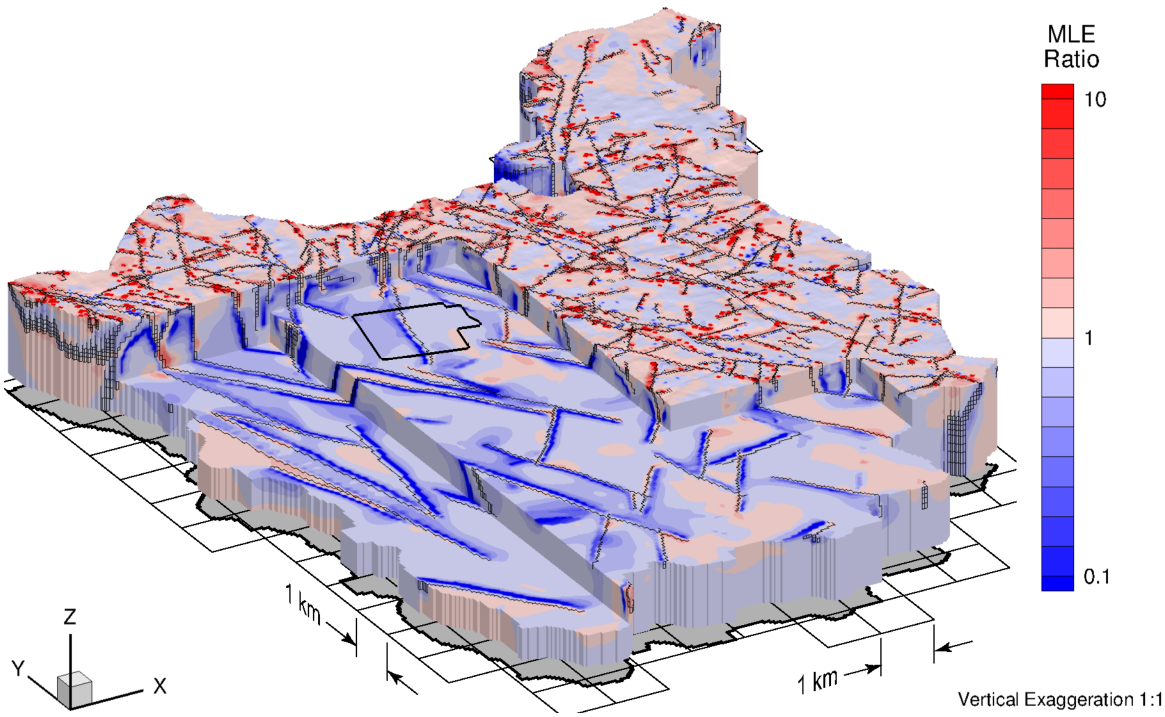

Figure 2-19: Ratio of MLE for the EPM Case to the Reference Case

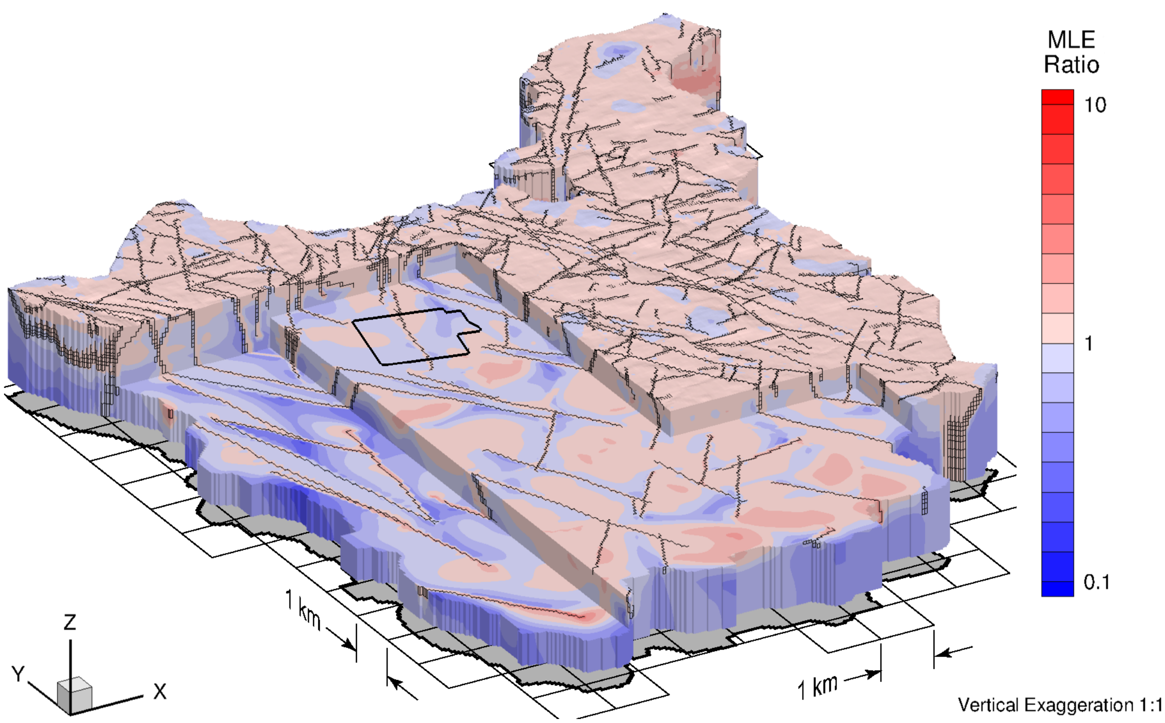

Figure 2-20: Ratio of MLE for an Order-of-Magnitude Increase in the Diffusion Coefficient Relative to the Reference Case

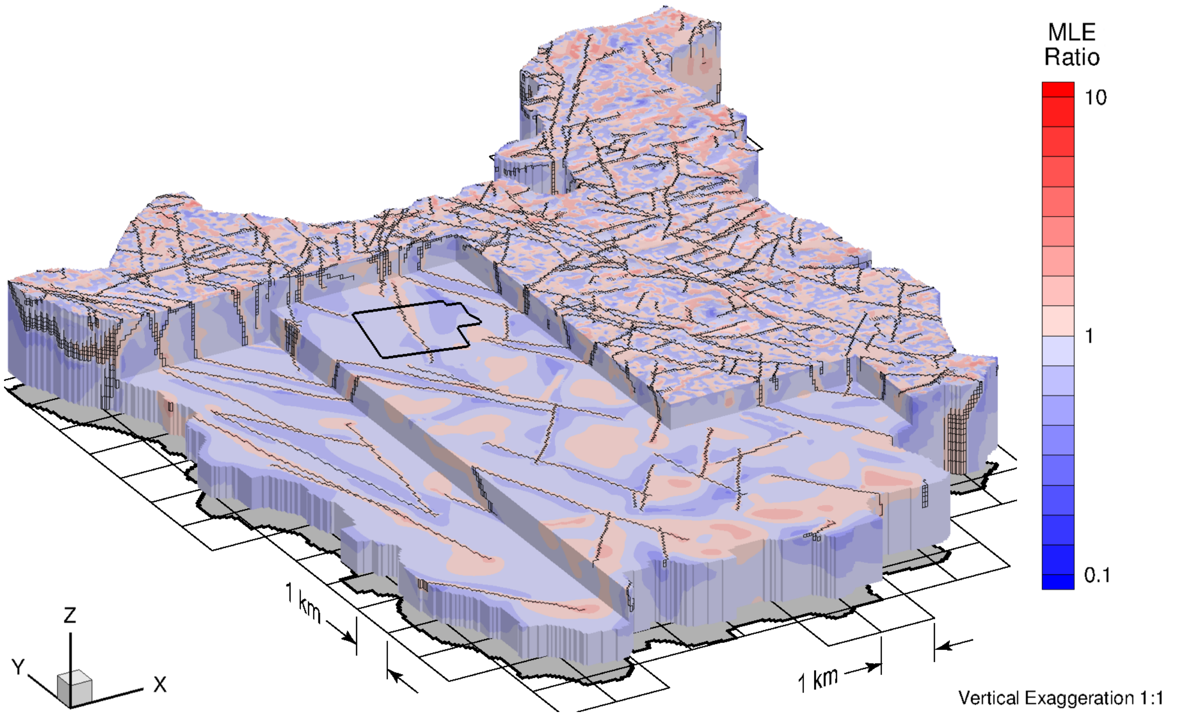

Figure 2-21: Ratio of MLE for a Doubling of Dispersivity Relative to the Reference Case

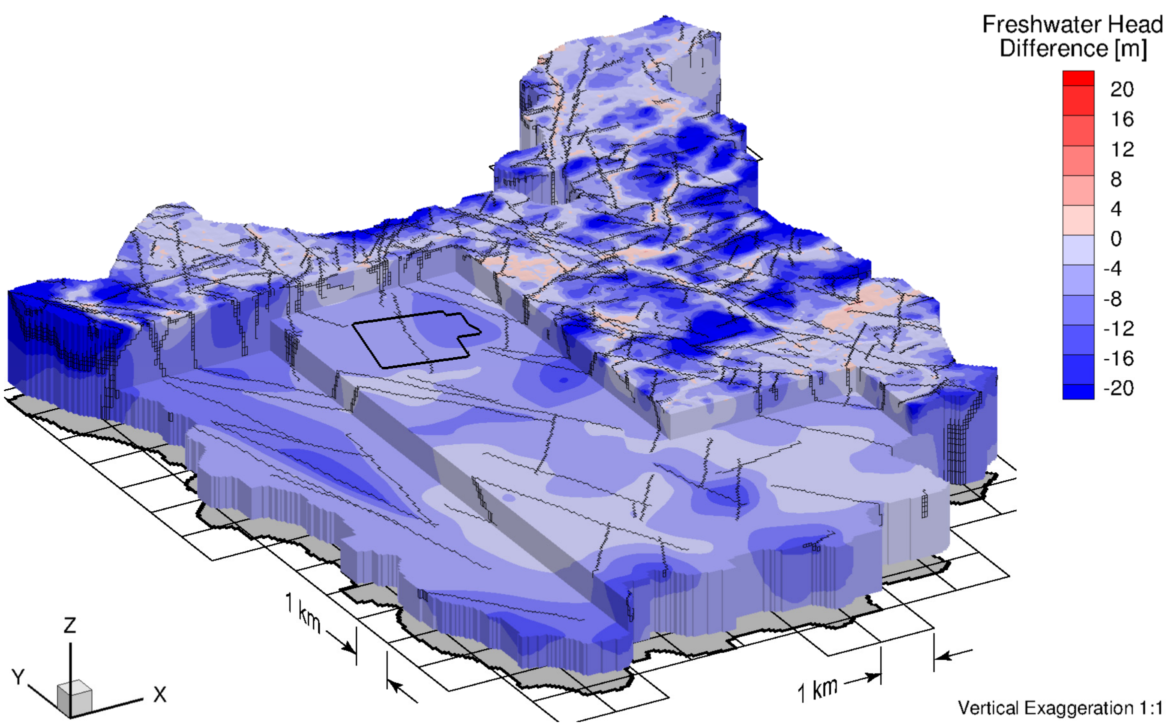

Figure 2-22: Difference in Freshwater Heads for a Recharge Surface Boundary Condition Relative to the Reference Case

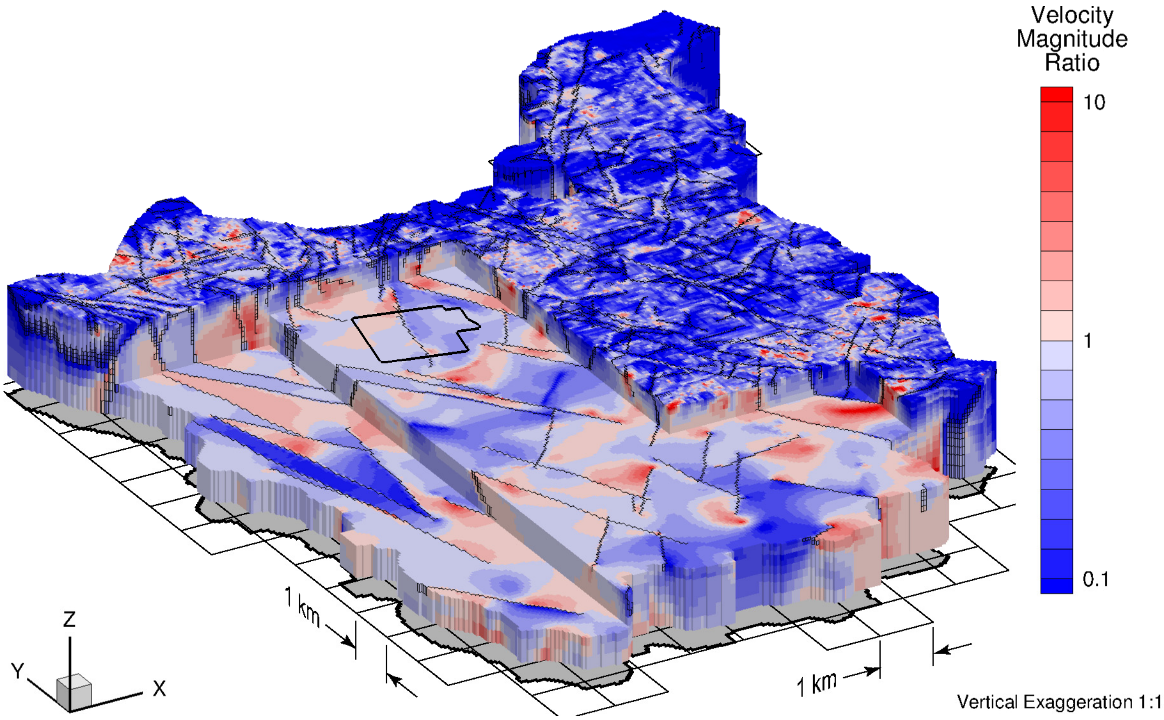

Figure 2-23: Ratio of Velocity Magnitudes for a Recharge Surface Boundary Condition Relative to the Reference Case

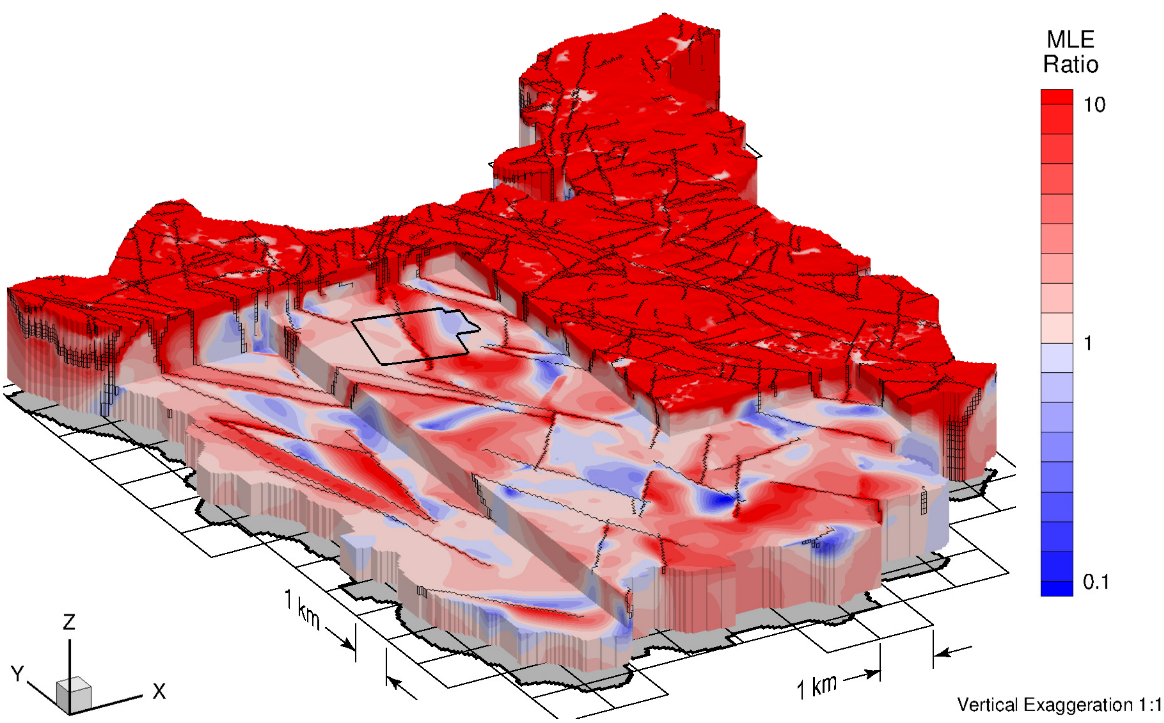

Figure 2-24: Ratio of MLE for a Recharge Surface Boundary Condition Relative to the Reference Case

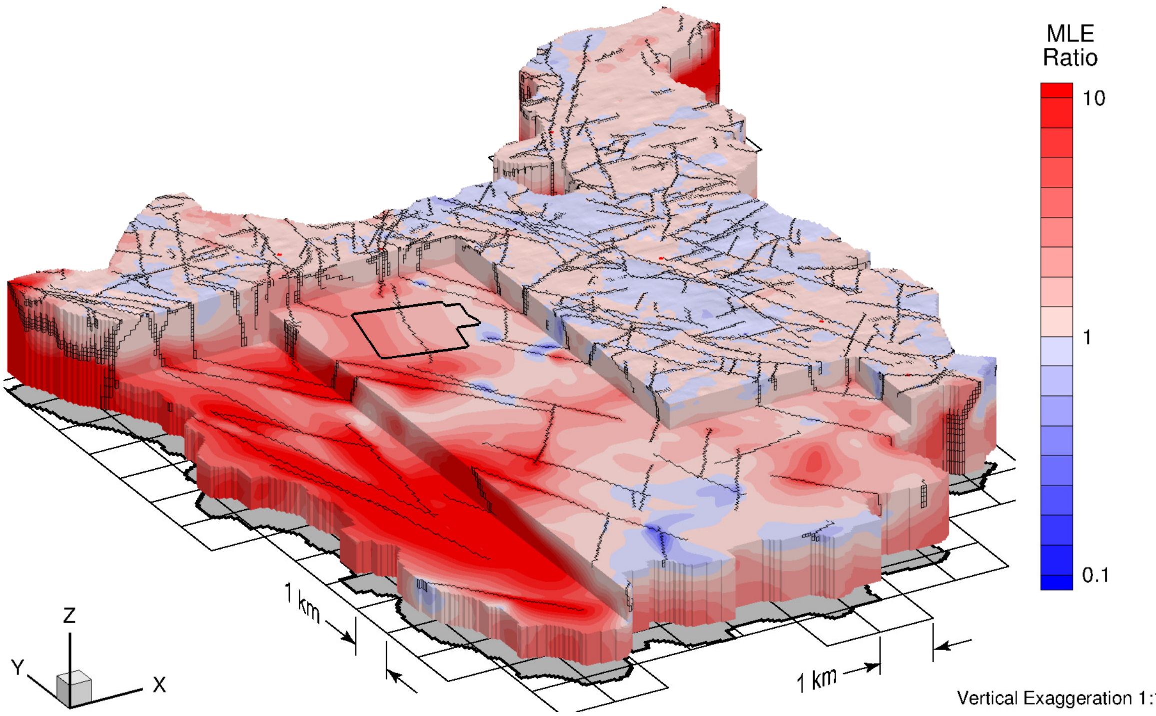

Figure 2-25: Ratio of MLE for a Density-Dependent Groundwater Flow Case to a Steady-State Case for Uniform Fracture Zone Hydraulic Conductivity of 10^{-7} m/s

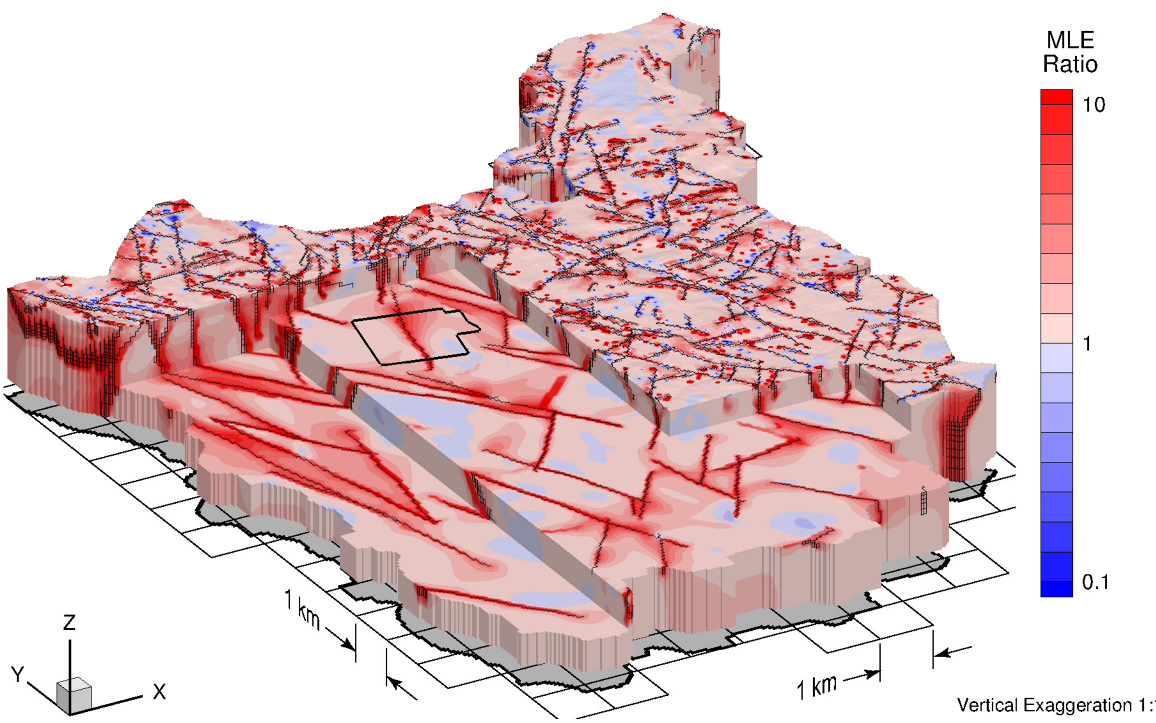

Figure 2-26: MLE Ratio of Uniform Fracture Zone Hydraulic Conductivity of 10^{-7} m/s Relative to Reference Case Simulation

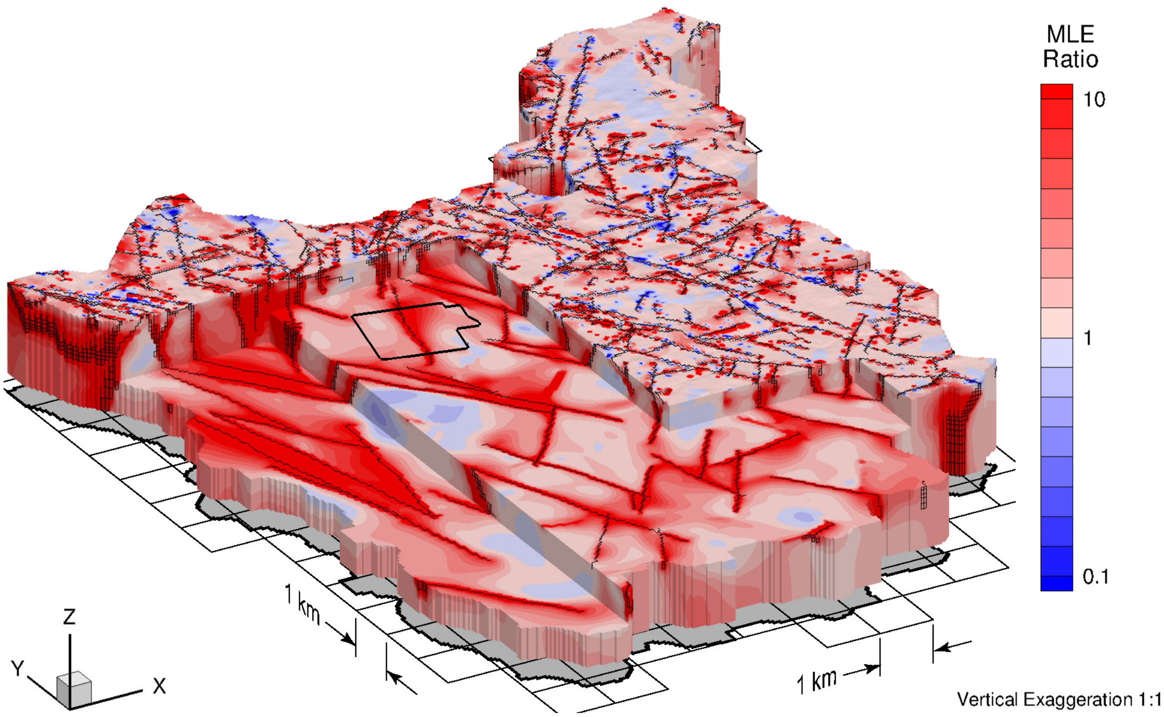

Figure 2-27: MLE Ratio of Uniform Fracture Zone Hydraulic Conductivity of 10^{-8} m/s Relative to Reference Case Simulation

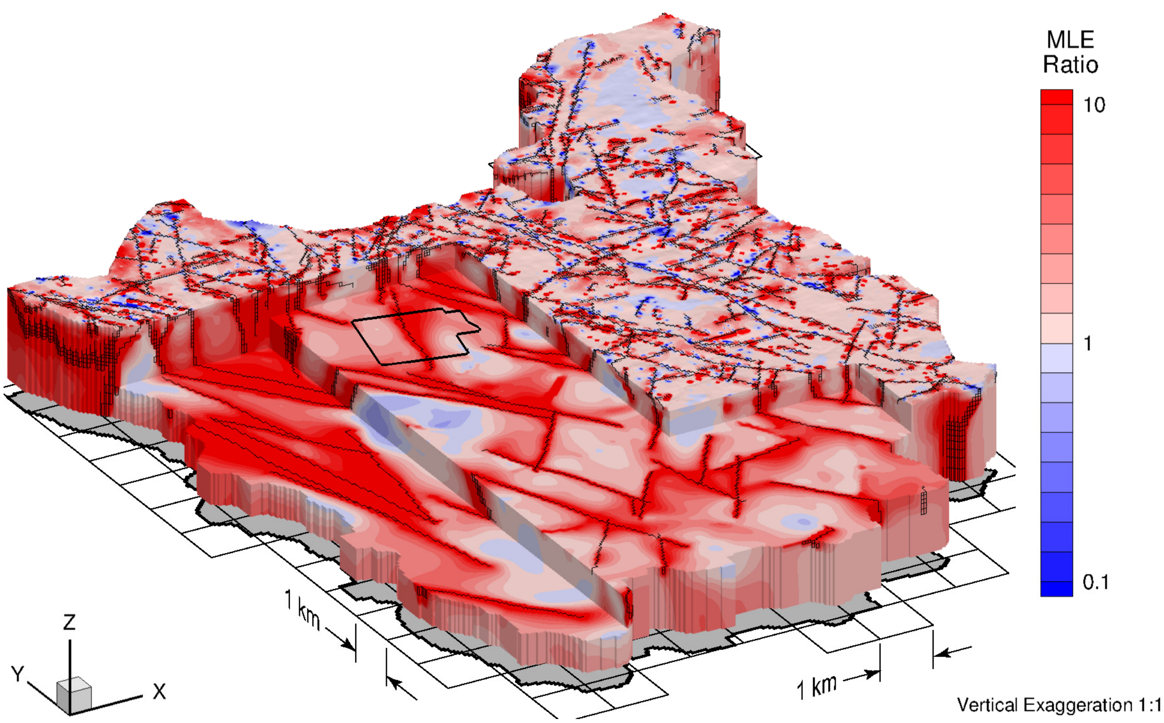

Figure 2-28: MLE Ratio of Uniform Fracture Zone Hydraulic Conductivity of 10^{-9} m/s Relative to Reference Case Simulation

2.3.5.3 Paleohydrogeologic Sensitivity Cases

A total of eleven paleohydrogeologic simulations were performed to investigate the role of varying paleoclimate boundary conditions and the characterization of hydromechanical coupling. These simulations are summarized in Table 2-10. The reference case model is used as the basis for all simulations and the initial conditions for freshwater heads, as described in Section 2.3.5.1.

The performance measure chosen to compare the paleohydrogeologic simulations is the movement of a conservative unit tracer applied with a Cauchy boundary condition at the top surface of the model domain. This tracer represents the migration of recharge waters into the groundwater system over the course of a 121,000 year simulation. Comparisons between simulations are made using block-cut three-dimensional figures, as well as calculating the cumulative density function (CDF) for the depth of the 5% isochlor at the end of the calculation period. The 5% isochlor represents a pore fluid containing 5% recharge water; it provides an indication of recharge water migration into the subsurface, which can be used to compare alternative paleohydrogeologic sensitivity cases. The 5% isochlor illustrates a potential depth of penetration of glacial meltwater. However, the dissolved oxygen content of these waters will likely be consumed within the shallow groundwater system by mineralogical and/or microbial reactions (see also Section 2.2.3.2).

The tracer migration at 120,000 years for the paleohydrogeologic reference case simulation (fr-base-paleo) is shown in Figure 2-29. Deeper migration can occur in fracture zones; however, it depends on whether that portion of the fracture zone is associated primarily with a recharge area or a discharge area. The portion of the domain within the repository shows a variation in tracer concentration of approximately 50% compared with less than 5% elsewhere. The 50th percentile of tracer depth (5% isochlor) for the reference case is at a depth of 865 m. Higher concentrations are generally associated with recharge areas and fracture zones. A cumulative density function of 5% isochlor depth for this case is shown in Figure 2-30. All other simulations are plotted on the same figure for comparison purposes.

As discussed in Section 2.2.2.3, multiple plausible paleoclimate reconstructions can be developed from the UofT GSM model (Peltier 2006). The reference case paleohydrogeologic simulation uses paleoclimate simulation nn2008, representing a cold based ice-sheet condition with extensive permafrost. An alternate paleoclimate simulation nn2778 (fr-base-paleo-nn2778) represents a greater extent of ice-sheet coverage over the domain, but less permafrost is predicted to form in the subsurface over the 121,000 year simulation period. Figure 2-31 shows the tracer migration at 120,000 years for the nn2778 paleoclimate boundary conditions. In comparison to the reference case simulation, there is a significant increase in the depth to which the tracer migrates, 973 mBGS versus 865 m in the reference case, as shown in Figure 2-30. Increased migration results from less permafrost and more ice-sheet advance/retreat cycles. A second alternate paleoclimate simulation “Peltier 2015” (fr-base-peltier), shown in Figure 2-32, represents a best estimate based upon the updated formulation of the University of Toronto Glacial Systems Model (Stuhne and Peltier 2015). This case has the greatest ice coverage and results in the least median tracer migration depth of 792 mBGS.

The top surface hydraulic boundary condition can be varied, as various percentages of ice-sheet thickness and a range of conditions were used for the sensitivity analyses. The reference case uses 100% of ice-sheet thickness in calculating the equivalent freshwater head.

One paleohydrogeologic scenario for each of 0%, 30%, and 80% (named fr-base-paleo-0, fr-base-paleo-30, and fr-base-paleo-80, respectively) of ice-sheet thickness were performed; the CDF versus depth relationship for tracer migration is shown in Figure 2-30. For the 0% case, representing zero fluid pressure, slightly shallower migration than the reference case (800 mBGS) is noted and is attributed to the larger upward gradients resulting from a zero pressure surface boundary condition. The 30% and 80% cases result in CDF versus depth relationships that approach values for the reference case (790 mBGS and 842 mBGS, respectively).

In addition to the surface hydraulic boundary condition, an equally important parameter is the one-dimensional loading efficiency. The loading efficiency is calculated based on the pore fluid and rock matrix compressibilities (see also Section 2.2.2.2). In the reference case simulation, the one-dimensional loading efficiency is calculated to be 0.59 for the rock mass. In two paleohydrogeologic sensitivity cases, the one-dimensional loading efficiencies are set to zero (fr-base-paleo-le0) and unity (fr-base-paleo-le1) while maintaining the specific storage at $1x10^{-7}$ m^{-1}. The purpose of these sensitivity cases is to illustrate the role of the one-dimensional loading efficiencies. Both the loading efficiency and specific storage values are affected by the choice of Biot coefficient. The following sensitivity cases investigate the role of the Biot coefficient on hydromechanical coupling. For a Biot coefficient of 1.0 (fr-base-paleo-biot10), a one-dimensional loading efficiency of 0.95 results, while a Biot coefficient of 0.5 (fr-base-paleo-05) yields a one-dimensional loading efficiency of 0.68. In both Biot sensitivity cases, the specific storage approximately doubles from the reference case value. The final sensitivity case (fr-base-paleo-0-le1) uses a loading efficiency of unity and a 0% of ice-sheet thickness equivalent freshwater head for the surface hydraulic boundary condition. For the nn2008 paleoclimate boundary conditions, fr-base-paleo-le1 (Figure 2-33) represents a predicted tracer migration, to a median depth of 886 mBGS, while fr-base-paleo-le0 (Figure 2-34) represents a median depth of 858 mBGS. These results are counter-intuitive because as the one-dimensional loading efficiency is decreased, vertical gradients increase. The increase in vertical gradients occurs due to in-situ pore pressures, which are reduced during ice-sheet loading for the same 100% of ice-sheet thickness equivalent freshwater head surface hydraulic boundary condition. This may be attributed to the bimodal nature of Figure 2-30, representing both a fracture and a matrix domain. Migration to a depth of 858 mBGS, occurs in the fr-base-paleo-0-le1 (Figure 2-35) sensitivity case, very similar to fr-base-paleo-le1 (shown in Figure 2-30 and Figure 2-33).

Insight into the depth of penetration by glacial meltwaters within the sub-regional groundwater domain is based on the spatial distribution of the 5% isochlor for eleven paleohydrogeologic sensitivity cases. Within the discretely fractured groundwater system, median depths of penetration ranged between approximately 790 mBGS and 983 mBGS. Within the rock matrix at the repository horizon for the reference case simulation, tracer meltwater concentrations range between approximately 3% and 37%. Significantly higher meltwater concentrations occurred to greater depth (> 1000 m) within the discrete higher permeability fracture zones. Although predicted glacial meltwater recharge depths may approach the repository level, it is expected that groundwater conditions will remain reducing.

Plots of the velocity magnitude versus time at five locations within the repository (centre and four corners) for the reference case paleohydrogeologic scenario (fr-base-paleo) are shown in Figure 2-36. These results illustrate the stability of geosphere during glacial advances and retreats. The grey regions in the figure represent upward groundwater movement. Select sensitivity cases illustrating the velocity magnitude versus time are also shown in Figure 2-37 through Figure 2-39. The figures were chosen, based upon the 5% isochlor migration CDF plot shown in Figure 2-30, to show the widest range of results. As illustrated in Figure 2-37 and Figure 2-39, rates of mass transport remain predominantly low for the duration of the glacial cycles. However, for the nn2778 paleoclimate scenario, advective transport in the rock matrix occurs during times of significant glacial unloading (see Figure 2-37). The centre and west locations show the greatest velocity magnitudes, due to their proximity to a fracture zone. Areas in the rock mass away from fracture zones show increased stability. During glacial unloading, fluid pressures in fracture zones will decrease much more rapidly than in the rock mass, resulting in hydraulic gradients above unity, acting to advect fluid from the rock mass toward the fracture zones. The combination of using either a loading efficiency of 0 (Figure 2-40), or a loading efficiency of 1 and a 0% of ice-sheet thickness equivalent freshwater head for the surface hydraulic boundary condition (Figure 2-41), result in advection and diffusion both occurring to a similar degree.

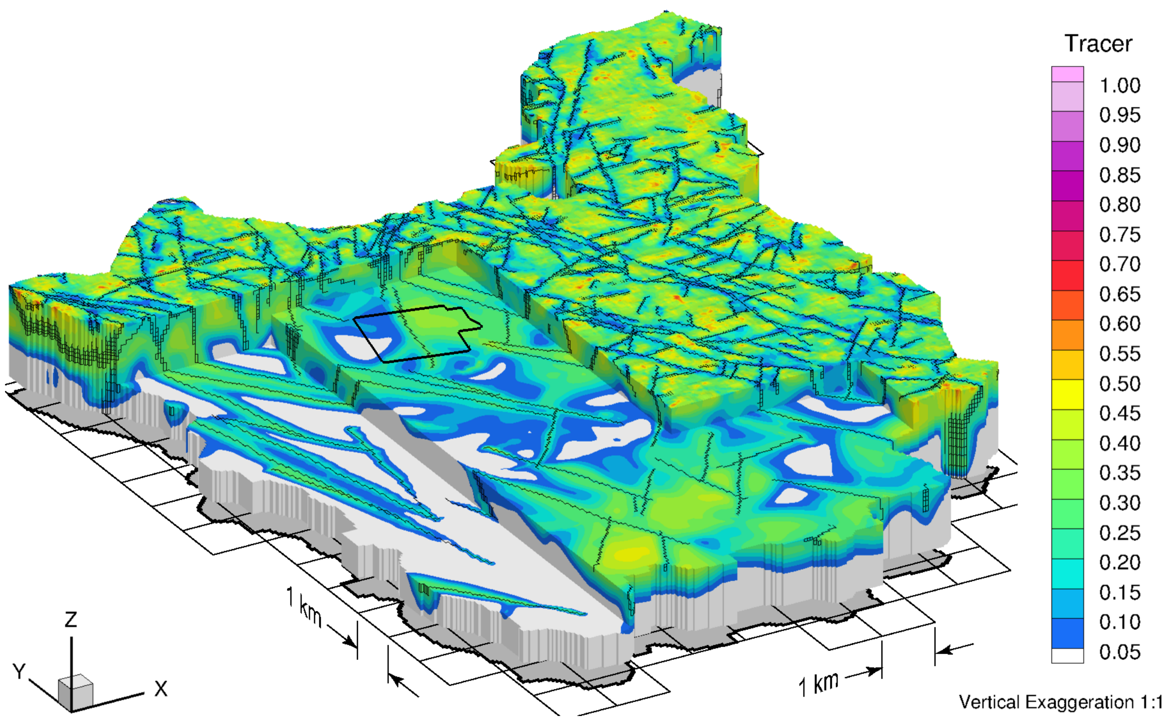

Figure 2-29: Tracer Migration after 120,000 Years for nn2008 Reference Case Paleohydrogeologic Scenario (fr-base-paleo)

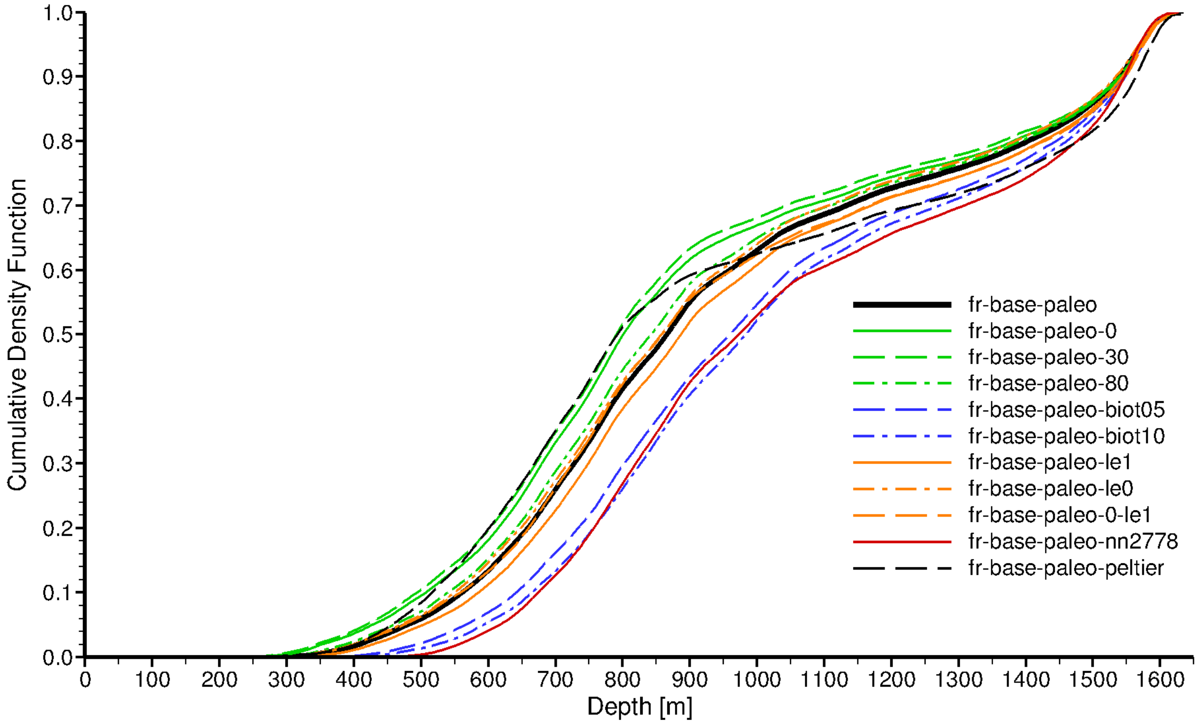

Figure 2-30: Cumulative Density Function of 5% Isochlor Depth for Paleohydrogeologic Sensitivity Cases

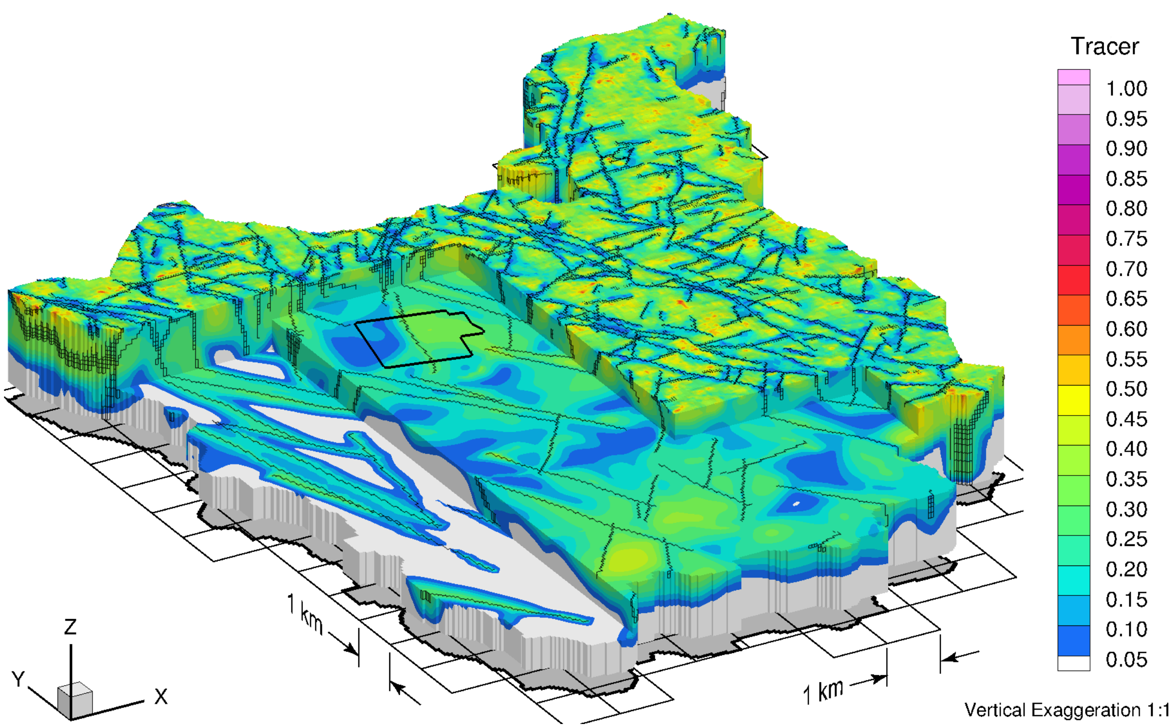

Figure 2-31: Tracer Migration at 120,000 Years for the nn2778 Paleoclimate Boundary Conditions (fr-base-paleo-nn2778)

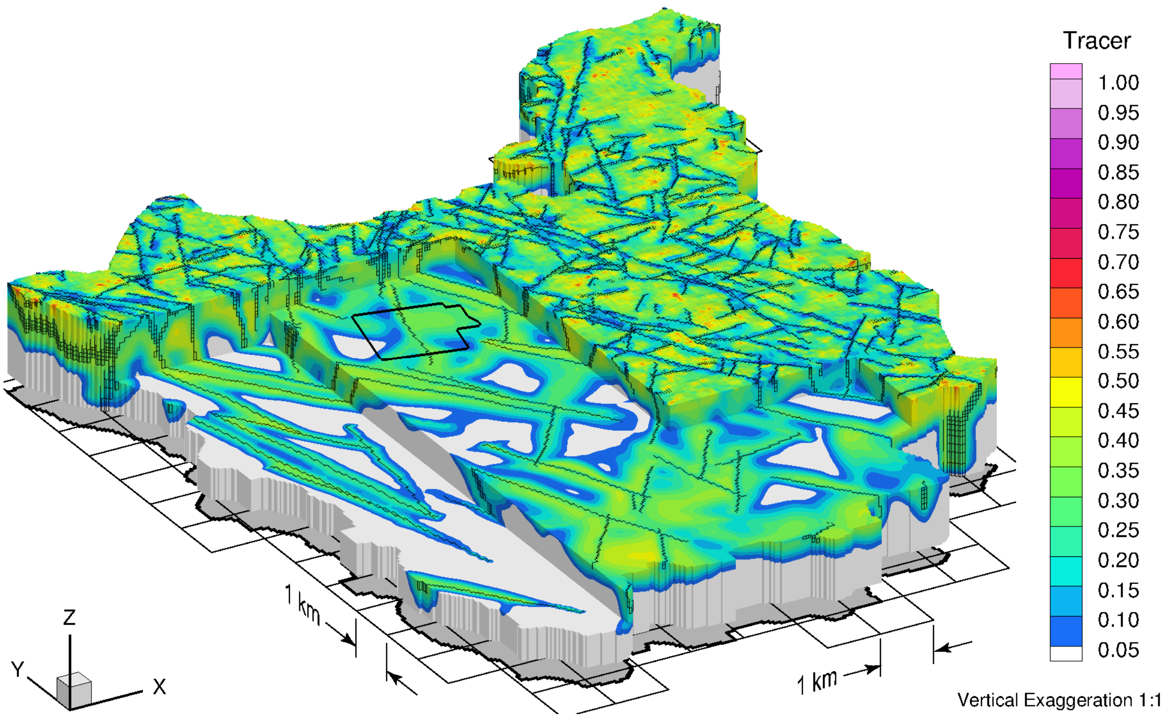

Figure 2-32: Tracer Migration at 120,000 Years for the "Peltier 2015" Paleoclimate Boundary Conditions (fr-base-paleo-peltier)

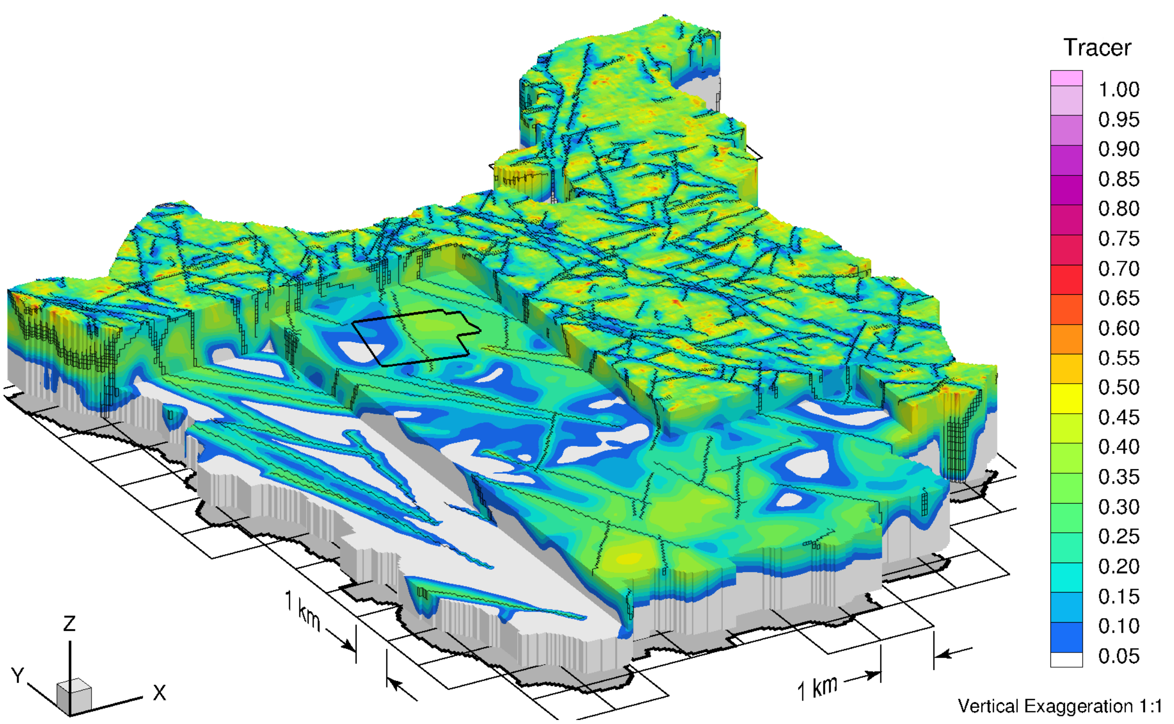

Figure 2-33: Tracer Migration at 120,000 Years for nn2008 Paleoclimate Boundary Conditions and a Loading Efficiency of 1 (fr-base-paleo-le1)

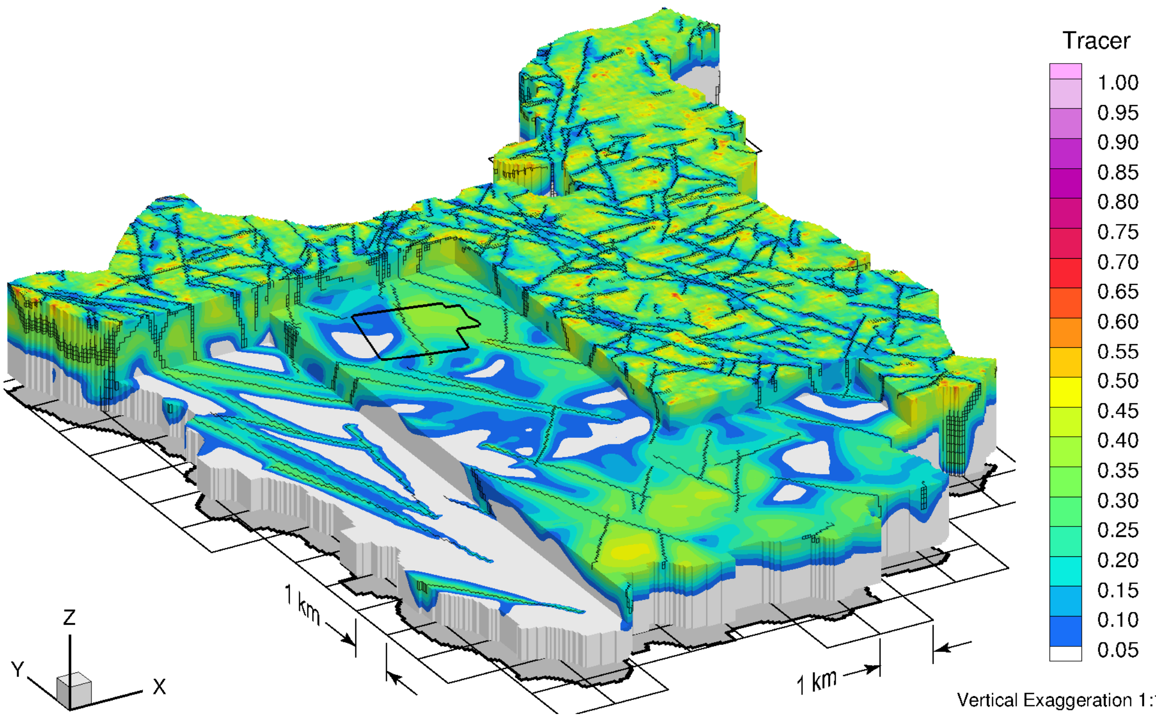

Figure 2-34: Tracer Migration at 120,000 Years for nn2008 Paleoclimate Boundary Conditions and a Loading Efficiency of 0 (fr-base-paleo-le0)

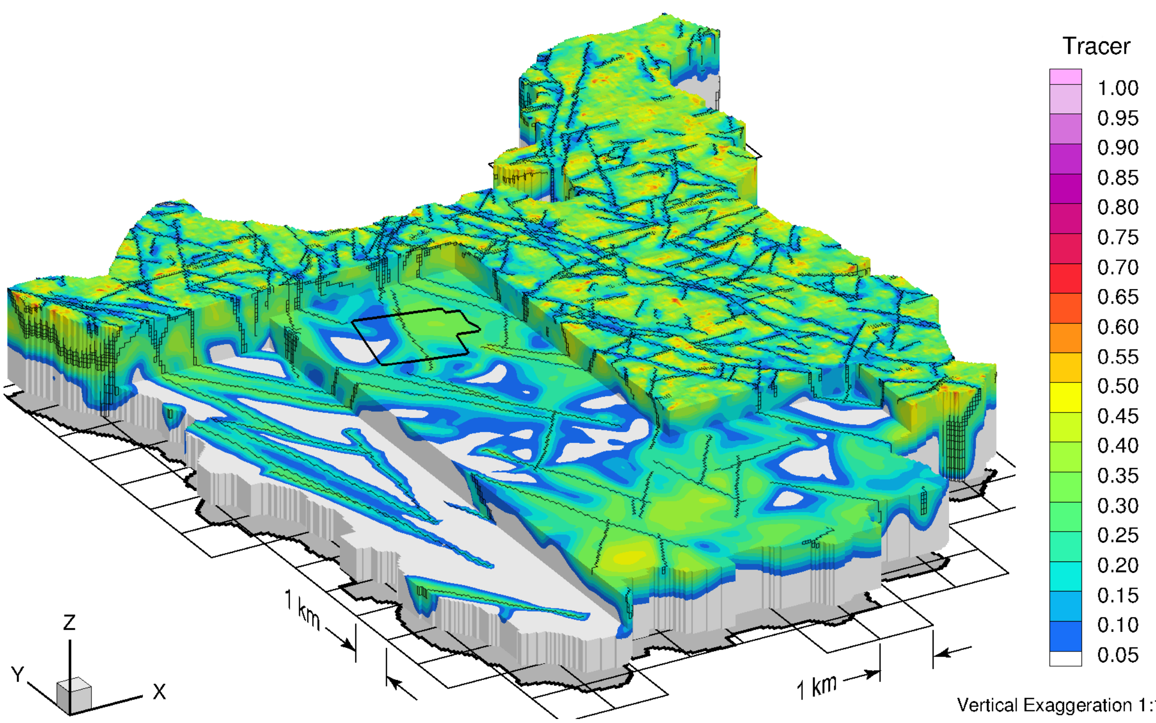

Figure 2-35: Tracer Migration at 120,000 Years for nn2008 Paleoclimate Boundary Conditions Loading Efficiency of 1 and a 0% of Ice-Sheet Thickness Equivalent Freshwater Head for the Surface Hydraulic Boundary Condition (fr-base-paleo-0-le1)

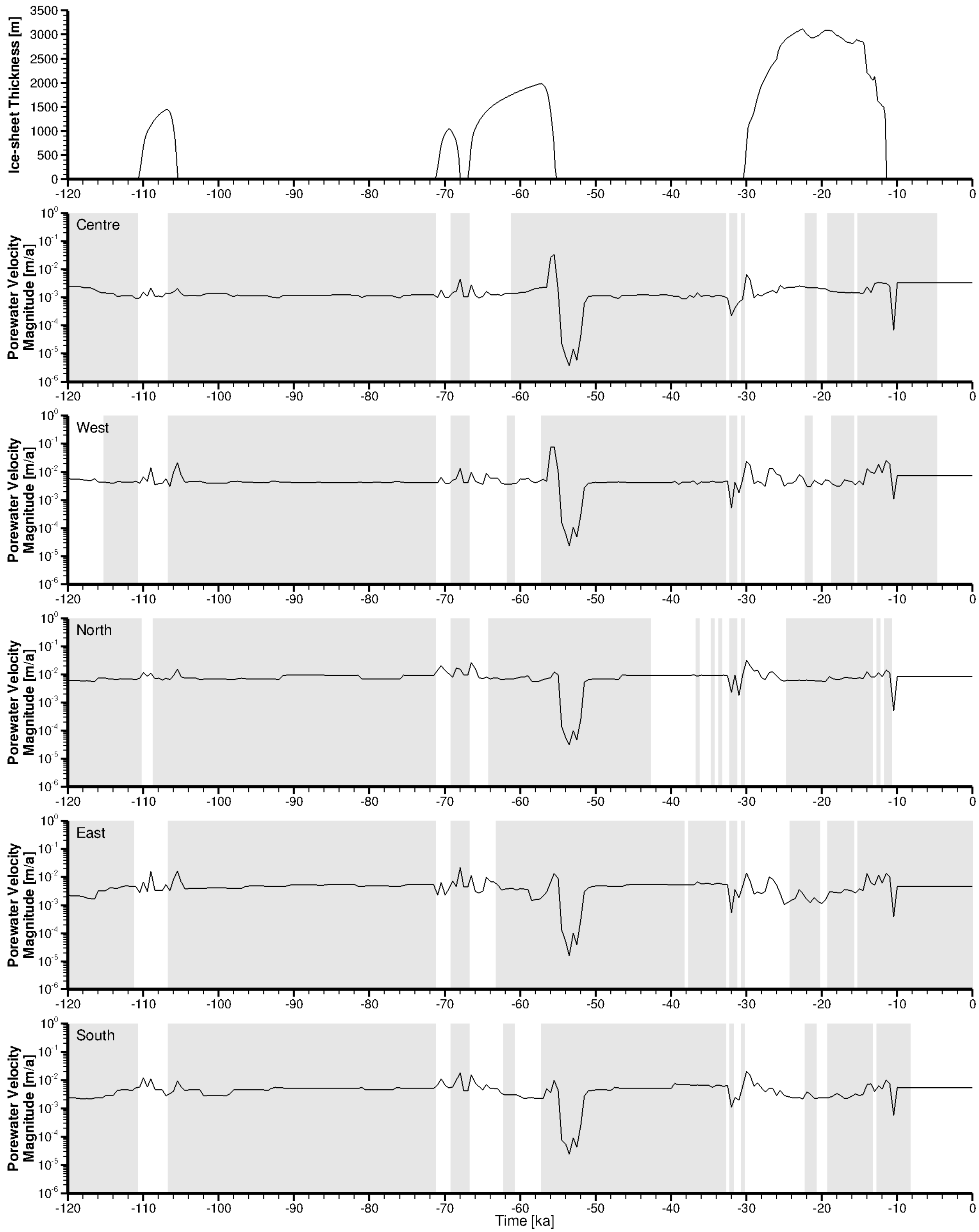

Figure 2-36: Velocity Magnitude versus Time for the nn2008 Reference Case Paleohydrogeological Scenario (fr-base-paleo)

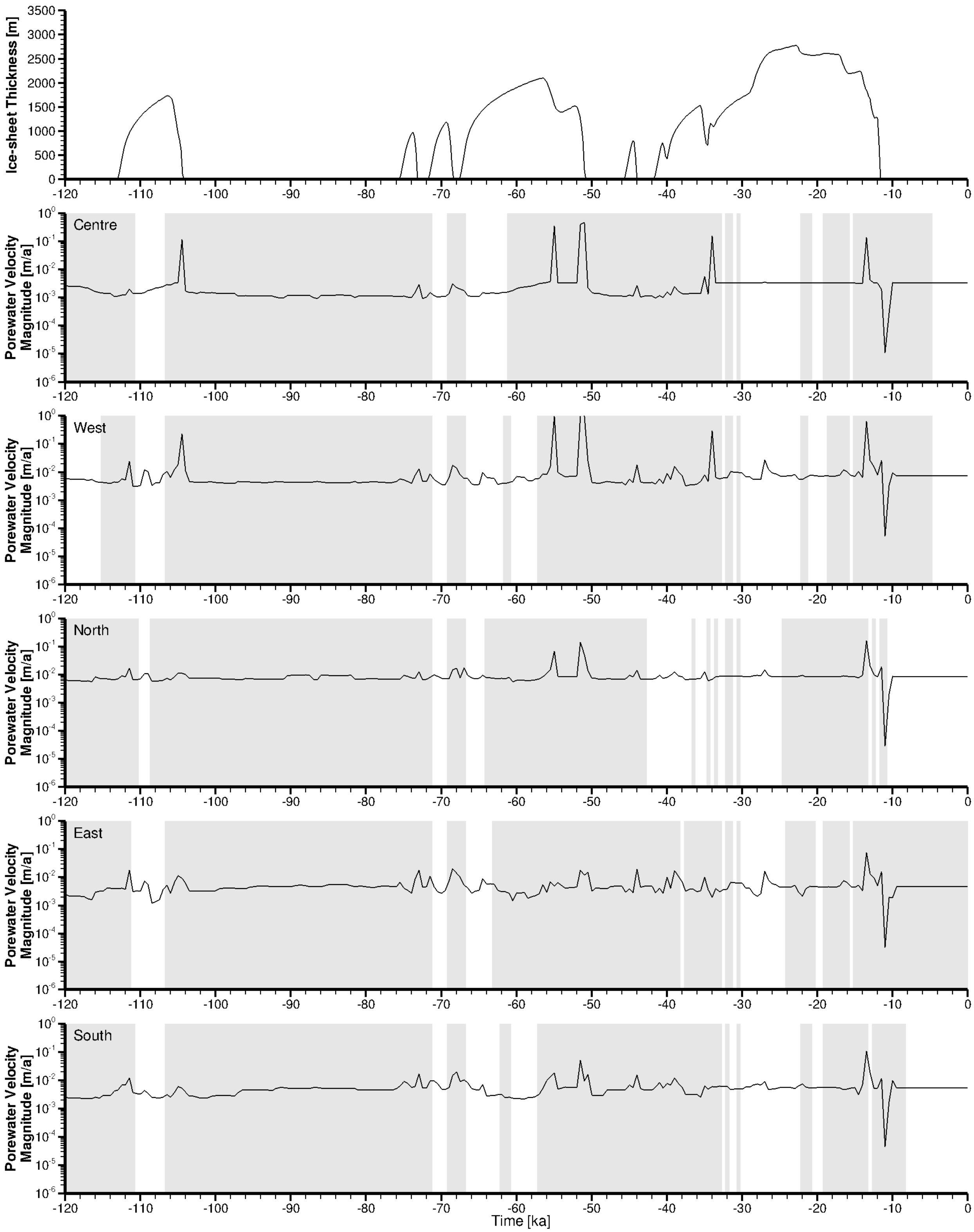

Figure 2-37: Velocity Magnitude versus Time for the nn2778 Paleoclimate Boundary Conditions (fr-base-paleo-nn2778)

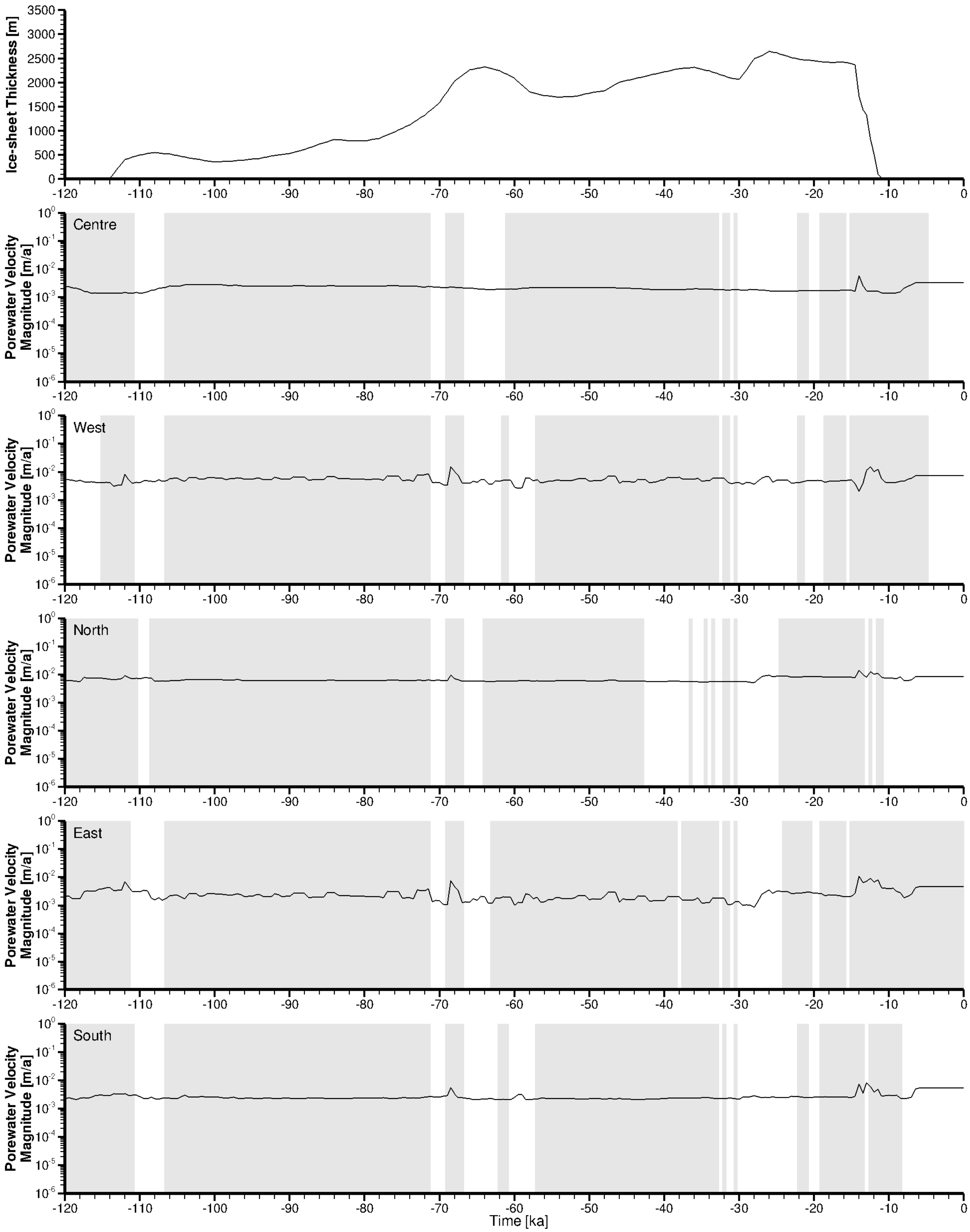

Figure 2-38: Velocity Magnitude versus Time for the "Peltier 2015" Paleoclimate Boundary Conditions (fr-base-paleo-peltier)

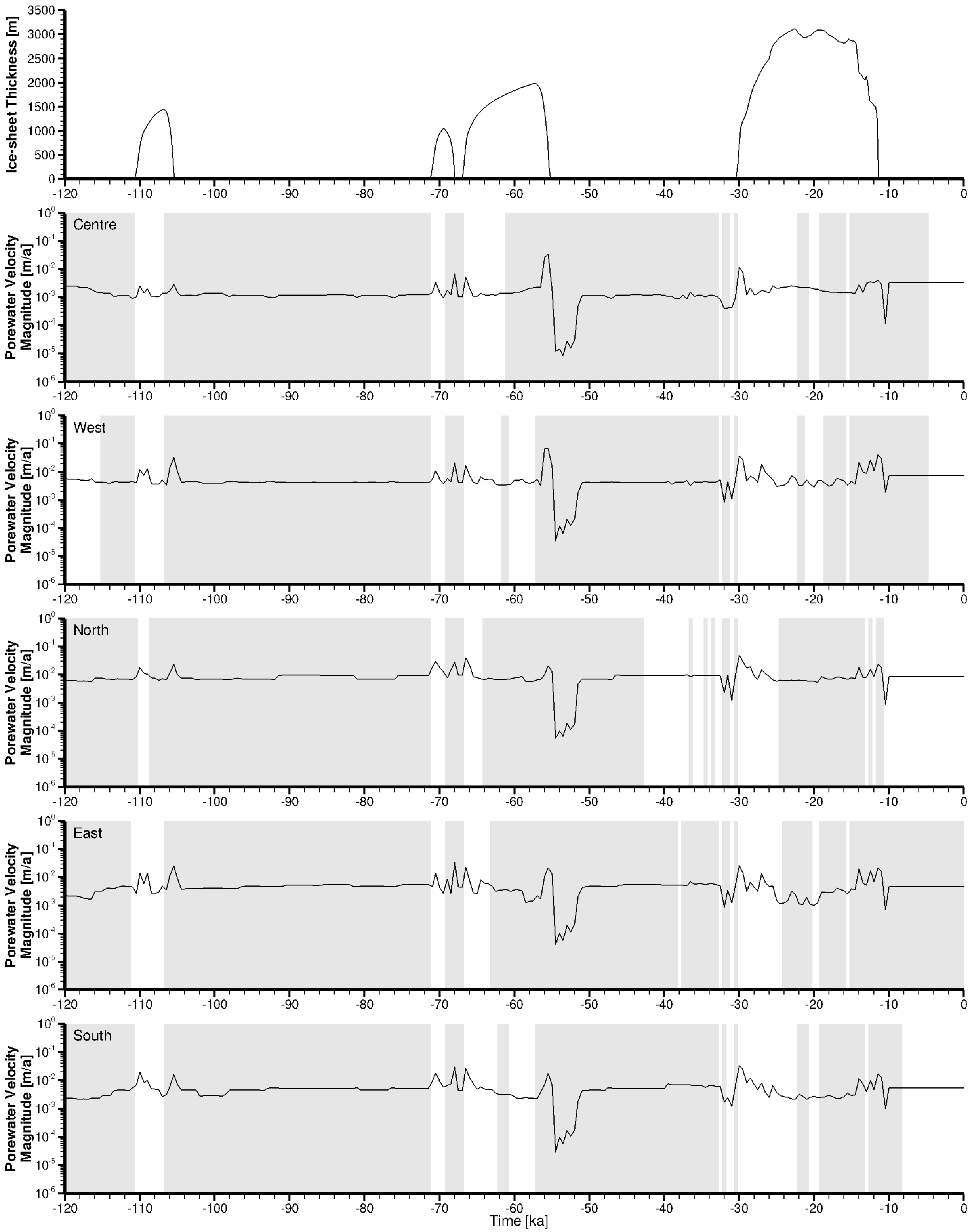

Figure 2-39: Velocity Magnitude versus Time for nn2008 Paleoclimate Boundary Conditions and a Loading Efficiency of 1 (fr-base-paleo-le1)

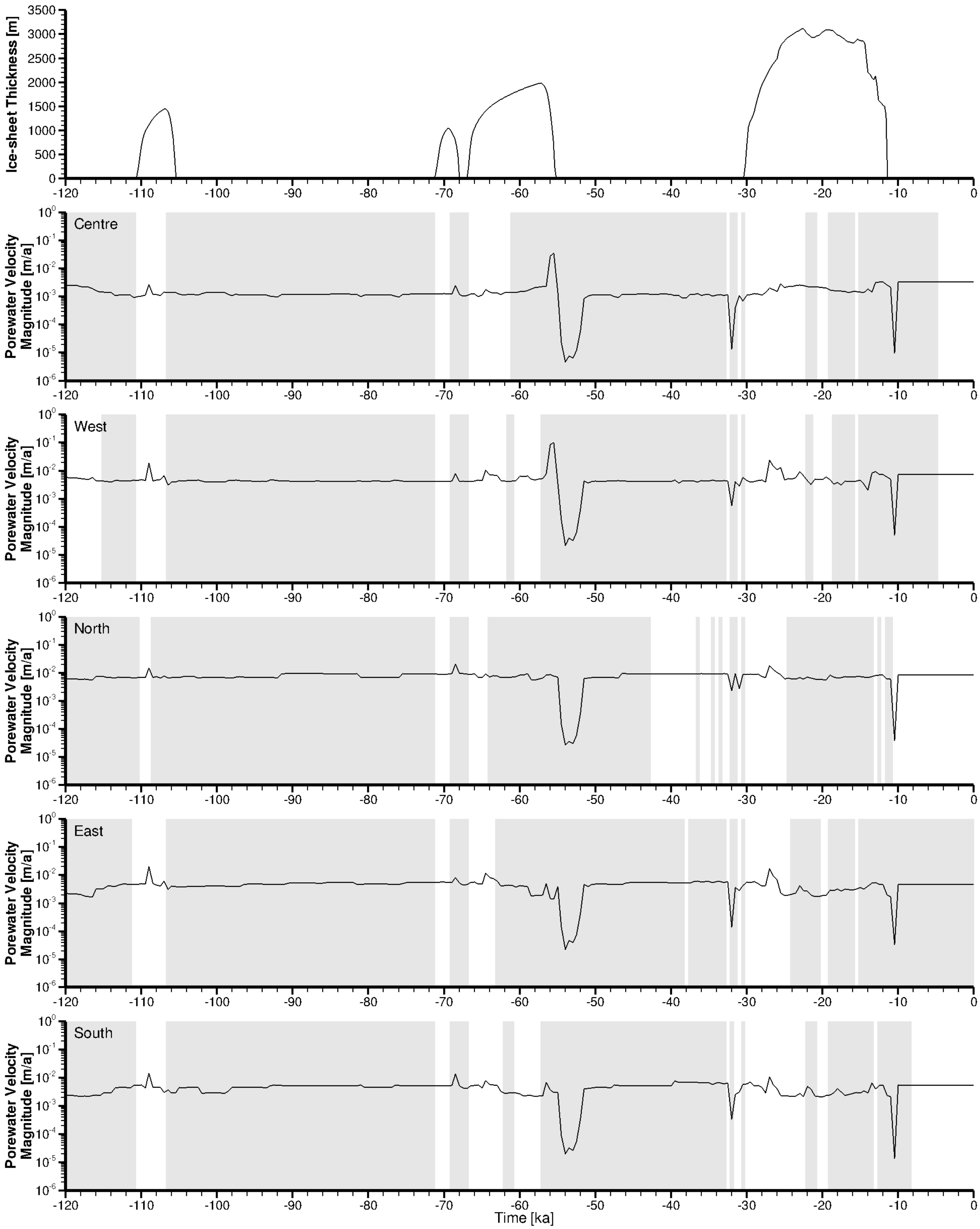

Figure 2-40: Velocity Magnitude versus Time for nn2008 Paleoclimate Boundary Conditions and a Loading Efficiency of 0 (fr-base-paleo-le0)

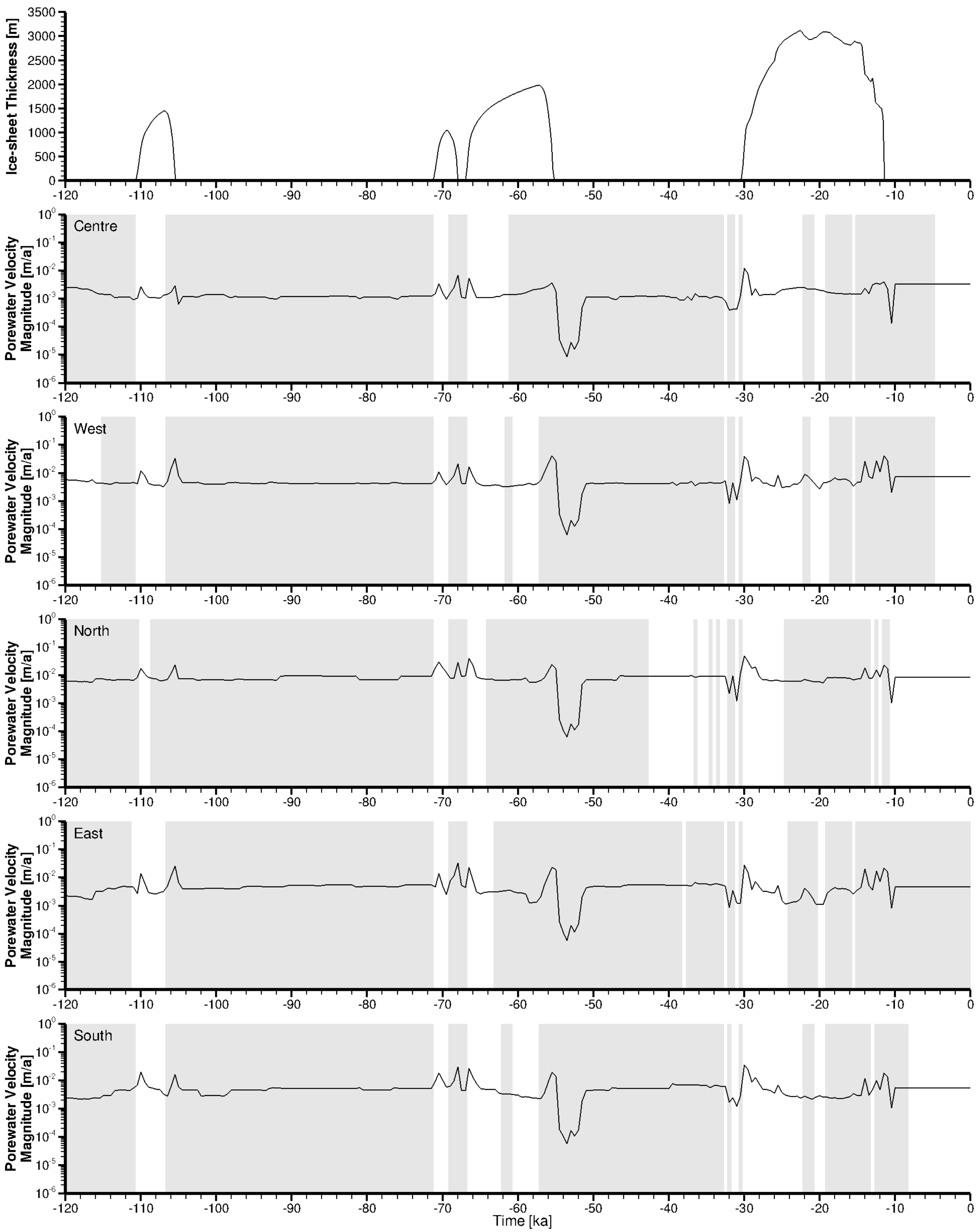

Figure 2-41: Velocity Magnitude versus Time for nn2008 Paleoclimate Boundary Conditions a loading efficiency of 1 and a 0% of ice-sheet thickness equivalent freshwater head for the surface hydraulic boundary condition (fr-base-paleo-0-le1)

2.4 Summary and Conclusions

This chapter describes a geosphere dataset for a hypothetical crystalline site on the Canadian Shield. The dataset was developed from historical work conducted during the Canadian Nuclear Fuel Waste Management Program on the Canadian Shield, as summarized, in part, by Sykes et al. (2004, 2009) and Normani et al. (2007). The geosphere data set described in this chapter was provided for the purpose of performing an illustrative postclosure safety assessment. The behaviour of the groundwater systems during temperate and glacial conditions was explored through a suite of 22 sensitivity cases.

The hydrogeological domain for the geosphere described in this chapter is divided into three groundwater systems: shallow (0 – 150 mBGS), intermediate (150 – 700 mBGS) and deep (700 - 1500 mBGS). These systems are identified, in part, by rock mass hydraulic conductivities, as observed at the Atikokan and the Whiteshell Research Areas, as well as groundwater TDS concentrations and redox conditions. The shallow groundwater zone occurs in the upper 150 m and comprises glacial sediment overlying a relatively permeable fractured rock mass. In the shallow system, groundwater is considered to be fresh and oxygen-rich. The intermediate groundwater system is a transition zone in which the groundwater becomes progressively more mineralized and reducing with depth. Within the deep groundwater system, groundwater conditions are saline and reducing. With increasing depth, the general increase in salinity, and decrease in rock mass hydraulic conductivities, leads to improved groundwater system stability at time frames relevant to repository safety. Mean life expectancies were used as illustrative performance measures to gain insight into the processes most influencing mass transport. For an assumed reference case, the shallow groundwater system is advective, whereas at greater depths, the low permeability rock mass and decreased interconnectivity of the fracture network decreases mass transport rates. Further groundwater system stability occurs as a result of salinity gradients within the intermediate and deep groundwater systems. The rock mass hydraulic conductivity played the most significant role in governing MLEs at depth. For a given representation of the discrete fracture network (DFN), decreases in the fracture zone hydraulic conductivity resulted in increases in MLE at depth.

Paleohydrogeological sensitivity cases were used to illustrate the long-term evolution and stability of the geosphere and groundwater systems to external perturbations. The distribution and duration of permafrost at the repository location play a role in governing the depth to which meltwater penetrates. The paleohydrogeologic sensitivity cases suggest that glacial meltwaters may recharge to median depths of 790 to 983 mBGS. The depth of recharge estimated within the more permeable discrete fractures can exceed 1000 mBGS. Glacial recharge penetrating below the shallow groundwater system is not expected to be oxygenated or influence redox conditions at the repository horizon. For the paleohydrogeologic sensitivity cases performed, the glacial perturbations did not materially change mass transport rates at repository depth.

2.5 References for Chapter 2

Andersson, J. 1999. SR97 Data and data uncertainties. SKB Technical Report TR-99-09. Stockholm, Sweden.

Aquanty, 2013. HGS 2013: HydroGeoSphere User Manual, Release 1.0. Aquanty Inc., Waterloo, Ontario, Canada.

Batzle, M. and Z. Wang. 1992. Seismic properties of pore fluids. Geophysics 57, 1396–1408.

Bottomley, D.J., A. Katz, L.H. Chan, A. Starinsky, M. Douglas, I.D. Clark and K.G. Raven. 1999. The origin and evolution of Canadian Shield brines: evaporation or freezing of seawater? New lithium isotope evidence from the Slave craton. Chemical Geology 155, 295-320.

Bucher, K. and I. Stober. 2000. The Composition of Groundwater in the Continental Crystalline Crust. In Hydrogeology of Crystalline Rocks. Kluwer Academic Publishers, Netherlands, 141-175.

Byegård, J., E. Selnert and E.L. Tullborg. 2008. Bedrock Transport Properties, Data Evaluation and Retardation Model, Site Descriptive Modeling SDM-Site Forsmark. Swedish Nuclear Fuel and Waste Management Company Report SKB R-08-98. Stockholm, Sweden.

Card, K.D. 1990. A review of the Superior Province of the Canadian Shield, a product of Archean accretion. Precambrian Research 48, 99-156.

Cornaton, F., and P. Perrochet. 2006a. Groundwater age, life expectancy and transit time distributions in advective-dispersive systems: 1. generalized reservoir theory, Advances in Water Resources 29, 1267–1291.

Cornaton, F., and P. Perrochet. 2006b. Groundwater age, life expectancy and transit time distributions in advective-dispersive systems; 2. reservoir theory for sub-drainage basins, Advances in Water Resources 29, 1292–1305.

Crawford J., I. Neretnieks and M. Malmström. 2006. Data and Uncertainty Assessment for Radionuclide Kd Partitioning Coefficients in Granitic Rock for Use in SR-Can Calculations. Swedish Nuclear Fuel and Waste Management Company Report SKB R-06-75. Stockholm, Sweden.

Davison, C.C., T. Chan, A. Brown, M. Gascoyne, D. Kamineni, G. Lodha, T. Melnyk, B.W. Nakka, P. O'Connor, D. Ophori, N. Scheier, N. Soonawala, F. Stanchell, D. Stevenson, G. Thorne, T. Vandergraaf, P. Vilks and S. Whitaker. 1994. The Disposal of Canada's Nuclear Fuel Waste: The Geosphere Model for Postclosure Assessment. Atomic Energy of Canada Limited Report AECL-10719, COG-93-9. Pinawa, Canada.

Frape, S.K. and P. Fritz. 1987. Geochemical trends for groundwaters from the Canadian Shield. In Saline Water and Gases in Crystalline Rocks (P. Fritz and S.K. Frape, eds.). Number 33 in Geological Association of Canada Special Paper, 19–38.

Garisto, F., J. Avis., T. Chshyolkova, P. Gierszewski, M. Gobien, C. Kitson, T. Melnyk, J. Miller, R. Walsh and L. Wojciechowski. 2010. Glaciation Scenario: Safety Assessment for a Used Fuel Geological Repository. Nuclear Waste Management Organization Report NWMO TR-2010-10. Toronto, Canada.

Garisto, F., A. D'Andrea, P. Gierszewski and T. Melnyk. 2004. Third Case Study – Reference Data and Codes. Ontario Power Generation Report 06819-REP-01200-10107-R00. Toronto, Canada.

Gascoyne, M. 1988. Reference Groundwater Composition for a Depth of 500 m in the Whiteshell Research Area – Comparison with Synthetic Groundwater WN-1. Atomic Energy of Canada Limited Report AECL TR-463. Pinawa, Canada.

Gascoyne, M. and D.C. Kamineni. 1994. The Hydrogeochemistry of Fractured Plutonic Rocks in the Canadian Shield. Applied Hydrogeology, 2, 43-49.

Gascoyne, M. 1997. Evolution of redox conditions and groundwater composition in recharge-discharge environments on the Canadian Shield. Hydrogeological Journal 5, 4-18.

Gascoyne, M. 2000. Hydrogeochemistry of the Whiteshell Research Area. Ontario Power Generation, Nuclear Waste Management Report 06819-REP-01200-10033-R00. Toronto, Canada.

Gascoyne, M. 2004. Hydrogeochemistry, groundwater ages and sources of salts in a granitic batholith on the Canadian Shield, southeastern Manitoba. Applied Geochemistry 19, 519-560.

Hallbeck, L. and K. Pedersen. 2008. Explorative Analyses of Microbes, Colloids, and Gases together with Microbial Modelling. Site Description Model SDM-Site Laxemar. Swedish Nuclear Fuel and Waste Management Company Report SKB TR-08-109. Stockholm, Sweden.

Hoffman, P.F. 1988. United plates of America, the birth of a craton Early Proterozolc assembly and growth of Laurentia. Annual Review of Earth and Planetary Sciences 16, 543-603.

Humphreys, P.N., J.M. West, and R. Metcalfe. 2010. Microbial effects on repository performance. Prepared by Quintessa Ltd. for the Nuclear Decommissioning Authority, Oxfordshire, United Kingdom. Report No. QRS-1378Q-1.

Itasca. 2015. Long-term Stability Analysis of APM Mark II Conceptual Design in Sedimentary and Crystalline Rocks. Nuclear Waste Management Organization Report NWMO TR-2015-27. Toronto, Canada.

Jain, D.K., S. Stroes-Gascoyne, M. Providenti, C. Tanner and I. Cord. 1997. Characterization of microbial communities in deep groundwater from granitic rock. Canadian Journal of Microbiology 43, 272-283.

Kaiser, P.K. and S. Maloney. 2005. Review of Ground Stress Database for the Canadian Shield. NWMO Report No: 06819-REP-01300-10107-R00.

Lau, J.S.O. and N.A. Chandler. 2004. Innovative laboratory testing. International Journal of Rock Mechanics & Mining Sciences 41, 1427-1445.

McCauley, C. A., D. M. White, M. R. Lilly, and D. M. Nyman. 2002. A comparison of hydraulic conductivities, permeabilities and infiltration rates in frozen and unfrozen soils. Cold Regions Science and Technology 34, 117–125.

McMurry, J. 2004. Reference Water Compositions for a Deep Geologic Repository in the Canadian Shield. Ontario Power Generation Report 06819-REP-01200-10135-R01, Toronto, Canada.

McMurry, J., D.A. Dixon, J.D. Garroni, B.M. Ikeda, S. Stroes-Gascoyne, P. Baumgartner and T.W. Melnyk. 2003. Evolution of a Canadian Deep Geologic Repository: Base Scenario. Ontario Power Generation Report 06819-REP-01200-10092-R00. Toronto, Canada.

Ministry of Natural Resources and Forestry (MNRF). 2015. User Guide for the Ontario Integrated Hydrology Data – Elevation and Mapped Water Features for Provincial Scale Hydrology Applications. Spatial Data Infrastructure, Mapping Information Resources Branch, Corporate Management and Information Division, Ministry of Natural Resources and Forestry.

Normani, S.D., Y.-J. Park, J.F. Sykes and E.A. Sudicky. 2007. Sub-Regional Modelling Case Study 2005-2006 Status Report. Nuclear Waste Management Organization Report NWMO TR-2007-07. Toronto, Canada.

Normani, S.D. 2009. Paleoevolution of Pore Fluids in Glaciated Geologic Settings. Ph.D. Thesis, Department of Civil Engineering, University of Waterloo. Ontario, Canada.

Normani, S. D., and J. F. Sykes. 2012. Paleohydrogeologic simulations of Laurentide ice-sheet history on groundwater at the eastern flank of the Michigan Basin, Geofluids, 12, 97-122.

Normani, S. D., J. F. Sykes, and Y. Yin. 2014. Methodology to generate orthogonal fractures from a discrete, complex, and irregular fracture zone network, in Fractured Rock Hydrogeology, IAH Selected papers on hydrogeology 20, 197–210, CRC Press/Balkema, The Netherlands.

NWMO. 2012. Used Fuel Repository Conceptual Design and Postclosure Safety Assessment in Crystalline Rock, Pre-Project Report, NWMO-TR-2012-16. Toronto, Canada.

NWMO. 2015. Technical Computing Software Procedure. NWMO-PROC-EN-0002. Toronto, Canada.

Ontario Geological Survey (OGS). 2000. Bedrock Geology of Ontario. ERLIS Data Set 6, Queens Printer for Ontario. ISBN 0-7778-9309-6. Ontario, Canada.

Ophori, D.U., D.R. Stevenson, M. Gascoyne, A. Brown, C.C. Davison, T. Chan, and F.W. Stanchell. 1995. Revised Model of Regional Groundwater Flow of the Whiteshell Research Area: Summary. AECL-11286.

Ophori, D.U. and T. Chan. 1996. Regional Groundwater Flow in the Atikokan Research Area: Model Development and Calibration. Atomic Energy of Canada Limited Report AECL-11081, COG-93-183. Pinawa, Canada.

Park, Y.-J., F.J. Cornaton, S.D. Normani, J.F. Sykes and E.A. Sudicky. 2008. Use of groundwater lifetime expectancy for the performance assessment of a deep geologic radioactive waste repository: 2. Application to a Canadian Shield environment. Water Resources Research, 44.

Park, Y. J., E. A. Sudicky, and J. F. Sykes. 2009. Effects of Shield brine on the safe disposal of waste in deep geologic environments. Advances in Water Resources 32, 1352–1358.

Pedersen, K. 2006. Microbiology of transitional groundwater of the porous overburden and underlying shallow fractured bedrock aquifers in Olkiluoto 2004, Finland. POSIVA Working Report 2006-09.

Pedersen, K. 2000. Microbial processes in radioactive waste disposal. SKB TR-00-04.

Peltier, W.R. 2002. A Design Basis Glacier Scenario. Ontario Power Generation Report 06819-REP-01200-10069-R00. Toronto, Canada.

Peltier, W.R. 2006. Boundary Conditions Data Sets for Spent Fuel Repository Performance Assessment. Nuclear Waste Management Report 06819-REP-01200-10154-R00. Toronto, Canada.

Perry, C., C. Rosieanu, J.-C. Mareschal and C. Jaupart. 2010. Thermal Regime of the Lithosphere in the Canadian Shield. Canadian Journal of Earth Sciences 47, 389-408.

Sherwood Lollar, B., S.K. Frape, P. Fritz, S.A. Macko, J.A. Welhan, R. Blomqvist and P.W. Lahermo. 1993a. Evidence for bacterially-generated hydrocarbon gas in Canadian and Fennoscandian Shield rocks. Geochimica et Cosmochimica Acta 57, 5073-5085.

Sherwood Lollar, B., S.K. Frape, S.M. Weise, P. Fritz, S.A. Macko and J.A. Welhan. 1993b. Abiogenic methanogenesis in crystalline rocks. Geochimica et Cosmochimica Acta 75, 5087-5097.

Sherwood Lollar, B. 2007. Hydrogeologic controls on episodic H_2 release from Precambrian fractured rocks – Energy for deep subsurface life on Earth and Mars. Astrobiology 7, 971-986.

Sherwood Lollar, B. 2011. State of Science Review: Far-field microbiological considerations relevant to a Deep Geological Repository for used nuclear fuel. Nuclear Waste Management Organization Report NWMO TR-2011-09, Toronto, ON.

Sikorsky, R.I., M. Serzu, D. Tomsons and J. Hawkins. 2002. A GIS-based Methodology for Lineament Interpretation and its Application to a Case Study at AECL's Whiteshell Research Area in Southeastern Manitoba. Ontario Power Generation Report 06819-REP-01200-10073-R00, Toronto, Canada.

Singer S.N. and C.K. Cheng. 2002. An Assessment of the Groundwater Resources of Northern Ontario. Hydrogeology of Ontario Series (Report 2). Ministry of the Environment: Environmental Monitoring and Reporting Branch. Page 255. Ontario, Canada.

Singh, B.P. and B. Kumar. 2005. Isotopes in Hydrology, Hydrogeology, and Water Resources. Narosa Publishing House Pvt. Ltd., New Delhi, India.

Singhal, B.B.S. and R. P. Gupta. 2010. Chapter 13: Hydrogeology of Crystalline Rocks. In Applied Hydrogeology of Fractured Rocks. Springer Science and Business Media. 237-255.

SKB. 2006. Geosphere process report for the safety assessment of SR-Can. Swedish Nuclear Fuel and Waste Management Company Report TR-06-19. Stockholm, Sweden.

Srivastava, R.M. 2002a. The discrete fracture network model in the local scale flow system for the Third Case Study. Ontario Power Generation Report 06819-REP-01200-10061-R00. Toronto, Ontario.

Srivastava, R.M. 2002b. Probabilistic Discrete Fracture Network Models for the Whiteshell Research Area. Ontario Power Generation Report 06819-REP-01200-17001-R00. Toronto, Canada.

Srivastava, R. M. and P. Frykman. 2006. Fracture Network Modelling: Verification of Procedures and Validation using Lägerdorf Quarry Field Data. Ontario Power Generation Report 06819-REP-01200-10122-R00. Toronto, Ontario.

Stevenson, D.R., E.T. Kozak, C.C. Davison, M. Gascoyne and R.A. Broadfoot. 1996. Hydrogeologic Characteristics of Domains of Sparsely Fractured Rock in the Granitic Lac du Bonnet Batholith, Southeastern Manitoba, Canada. Atomic Energy of Canada Limited Report AECL-11558, COG-96-17. Pinawa, Canada.

Stotler, R.L., S.K. Frape, T. Ruskeeniemi, P. Pitkänen and D.W. Blowes. 2012. The interglacial–glacial cycle and geochemical evolution of Canadian and Fennoscandian Shield groundwaters. Geochimica et Cosmochimica Acta 76, 45-67.

Stroes-Gascoyne, S., and J.M. West. 1997. Microbial studies in the Canadian nuclear fuel waste management program. FEMS Microbiology Reviews 20, 573-590.

Stuhne, G. and W.R. Peltier. 2015. Surface Boundary Conditions During Long-Term Climate Change. Nuclear Waste Management Organization Report NWMO TR-2015-16. Toronto, Canada.

Sykes, J.F., S.D. Normani, E.A. Sudicky and R.G. McLaren. 2004. Sub-regional Scale Groundwater Flow within an Irregularly Discretely Fractured Canadian Shield Setting. Ontario Power Generation Report 06819-REP-01200-10133-R00. Toronto, Canada.

Sykes, J.F., S.D. Normani, M.R. Jensen and E.A. Sudicky. 2009. Regional-scale groundwater flow in a Canadian Shield setting. Canadian Geotechnical Journal 46, 813–827.

Sykes, J. F., S. D. Normani, and Y. Yin. 2011. Hydrogeologic modelling. Nuclear Waste Management Organization Report NWMO DGR-TR-2011-16 R000. Toronto, Canada.

Vilks, P. and D. Bachinski. 1997. Natural colloids in groundwater from granite and their potential impact on radionuclide transport. Atomic Energy of Canada Limited Report AECL-11635, COG-96-311-I. Pinawa, Canada.

Vilks, P., F. Caron and M. Haas. 1998. Potential for the formation and migration of colloidal material from a near-surface waste disposal site. Applied Geochemistry 13, 31-42 (AECL-11935).

Vilks, P., N.H. Miller and F.W. Stanchell. 2004. Phase II In-Situ Diffusion Experiment. Ontario Power Generation Report 06819-REP-01200-10128-R00. Toronto, Canada.

Vilks, P. 2009. Sorption in Highly Saline Solutions – State of the Science Review. Nuclear Waste Management Organization Report NWMO TR-2009-18. Toronto, Canada.

Wang, H.F. 2000. Theory of Linear Poroelasticity with Applications to Geomechanics and Hydrogeology. Princeton University Press. Princeton, USA.

Weast, R.C. (Ed.). 1983. CRC Handbook of Chemistry and Physics. 64th edition. CRC Press Inc., Boca Raton, Florida, USA.

Yong, S. and S. Maloney. 2015. An Update to Canadian Shield Stress Database. Nuclear Waste Management Organization Report NWMO TR-2015-18. Toronto, Canada.

THIS PAGE HAS BEEN LEFT BLANK INTENTIONALLY

3. USED FUEL CHARACTERISTICS

3.1 Used Fuel Description

3.1.1 Used Fuel Type and Amount

The inventory of used fuel in interim storage consists primarily of 28-element and 37-element natural uranium CANDU fuel bundles and their variants. Variants include the 37-element long length bundle and the 37m bundle[1], while additionally there are some older bundles that do not have the CANLUB coating (i.e., a thin graphite layer between the fuel pellet and the fuel sheath). Other fuel bundles in storage include small quantities of 18-element bundles[2], 19-element bundles[3], and 43-element CANFLEX LVRF bundles[4].

The storage inventory also includes very small quantities of more experimental fuel types (including some enriched in U-235) developed by AECL in prior decades. This fuel is currently the subject of ongoing characterization studies.

Given the overwhelming predominance of CANDU fuel in interim storage, the used fuel waste form adopted for this assessment is a post-discharge natural uranium UO_2 CANDU fuel bundle. The AECL experimental fuel types mentioned above are not included due to the lack of data describing the fuel characteristics. These will be included in future work as the characterization studies come to fruition.

The conceptual repository is assumed to contain 4.6×10^6 used bundles. This quantity is slightly greater (5 percent more) than the total used fuel inventory projected over the expected lifetime of the current Canadian fleet of CANDU power reactors (Garamszeghy 2015)[5,6]. Because the inventory projections indicate there will be 3.6×10^6 37-element bundles and only 8.1×10^5 28-element bundles, the standard 37-element (Bruce) fuel bundle is selected as the reference fuel bundle for this assessment. Sensitivity studies in Tait et al. (2000) show the differences in radionuclide inventories between the 28-element and 37-element designs are small enough to be ignored. Specifically:

- Radionuclide inventories calculated for a discharge burnup of 250 MWh/kgU differ by less than 3%, with the most significant differences occurring for Ra-225, Ac-225, Ra-225, Th-229, U-233, Np-237, Pu-239, Pu-242, and Cm-244.

---

[1] A modified 37-element bundle (37m) will be entering service in some stations; however, the changes are minor and do not significantly affect inventory.

[2] A small quantity of 18-element fuel is currently in dry storage after use in the Gentilly 1 CANDU-BLW boiling water reactor prototype.

[3] A small quantity of the 19-element fuel is currently in dry storage after use in the Douglas Point CANDU PHWR reactor prototype.

[4] A 43-element bundle with a central element composed of Dysprosium used in a limited fashion in Bruce B reactors and is an option for use in EC-6 reactors.

[5] The 4.6 $\times 10^6$ value assumes refurbishment of Bruce A, Darlington, Point Lepreau and Gentilly-2, no further refurbishment of Pickering or Bruce B, and no new build. Because Gentilly-2 has decided to not proceed with refurbishment, the current projected used fuel inventory is slightly reduced to about 4.4×10^6 bundles.

[6] After the analysis was completed, the inventory estimate of 4.6 $\times 10^6$ bundles in Garamszeghy (2015) was revised upwards to 5.224×10^6 bundles (Garamszeghy 2016). This revised value, and any future revisions, will be incorporated in future safety assessments.

- For most fission products, inventories for the 37-element bundles are greater those for the 28-element bundles.
- For most actinides, inventories for the 37-element bundles are generally less than those for the 28-element bundles.

Note that the age of the fuel when placed in the repository will vary. Because the earliest bundles date back to 1970 and because the repository is unlikely to open before 2035, some fuel will be over 60 years old at the time of placement. For this assessment, all fuel bundles are assumed to have an out-of-reactor decay time of 30 years.

3.1.2 Geometry

Fuel pellets formed from natural uranium UO_2 are placed inside a fuel sheath made of a zirconium-tin alloy (Zircaloy-4) with a thin CANLUB graphite coating on the inside. The ends of the sheath are closed by a welded zirconium alloy plug to produce a sealed fuel element. Fuel elements are welded to zirconium alloy end plates to form a fuel bundle as shown in Figure 3-1.

The number of pellets in a fuel element, and the number and dimensions of the fuel elements in a fuel bundle depend on the particular CANDU reactor. As noted previously, the most common bundle contains 37 fuel elements, each of which is 13.1 mm in diameter and 486 mm long. This fuel bundle weighs 23.9 kg, of which 21.7 kg is UO_2 and 2.2 kg is Zircaloy (Tait et al. 2000). This is the bundle that has been selected as the reference bundle for this assessment.

Upon discharge, less than 0.015% of the bundles are expected to have minor damage or defects (such as pinhole failures in the fuel sheaths) based on statistics from 1994 to 2006 (IAEA 2010), although pre-1994 bundle defect rates were approximately 0.1% (Tait et al. 2000). Analysis of the integrity of used fuel bundles indicates that they are unlikely to fail during storage (Freire-Canosa 2011). A small percentage may have increased susceptibility to integrity failure during subsequent transport to permanent storage. While the specific value may be relevant to the packaging plant design, the postclosure safety assessment is not sensitive to this value since no credit is taken for fuel integrity.

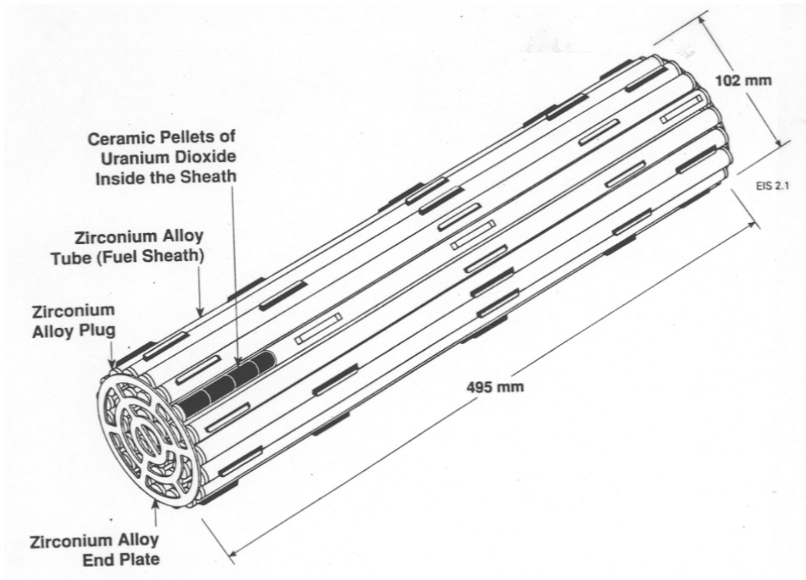

Figure 3-1: Typical CANDU Fuel Bundle

3.1.3 Discharge Burnup and Linear Power

Discharge Burnup:

Discharge burnup is a measure of the total energy produced by the used fuel bundle while it is still in the reactor. The radioactivity level, heat generation rate, and radionuclide composition all depend on this value. The discharge burnup itself depends on many factors including the type of reactor, the location of the bundle in the core, the bundle residence time, and bundle shifts that occur during fuelling operations. Although each bundle has a unique irradiation history, used fuel from all CANDU reactors is similar enough that it is not necessary to know individual detailed characteristics to assess the overall behaviour of the used fuel assemblies in the repository.

Figure 3-2 shows the distribution of discharge burnup for all CANDU used fuel bundles in interim storage for the time period up to and including 2012 (Wilk 2013). The aggregate 95th percentile value is 254 MWh/kgU, with some exceptional fuel elements experiencing burnups as high as 706 MWh/kgU. The median value is 192 MWh/kgU, while on a per station per decade basis, the 95th percentile values vary between 224 MWh/kgU and 286 MWh/kgU. At these burnup levels, about 2% of the initial uranium is converted into other elements.

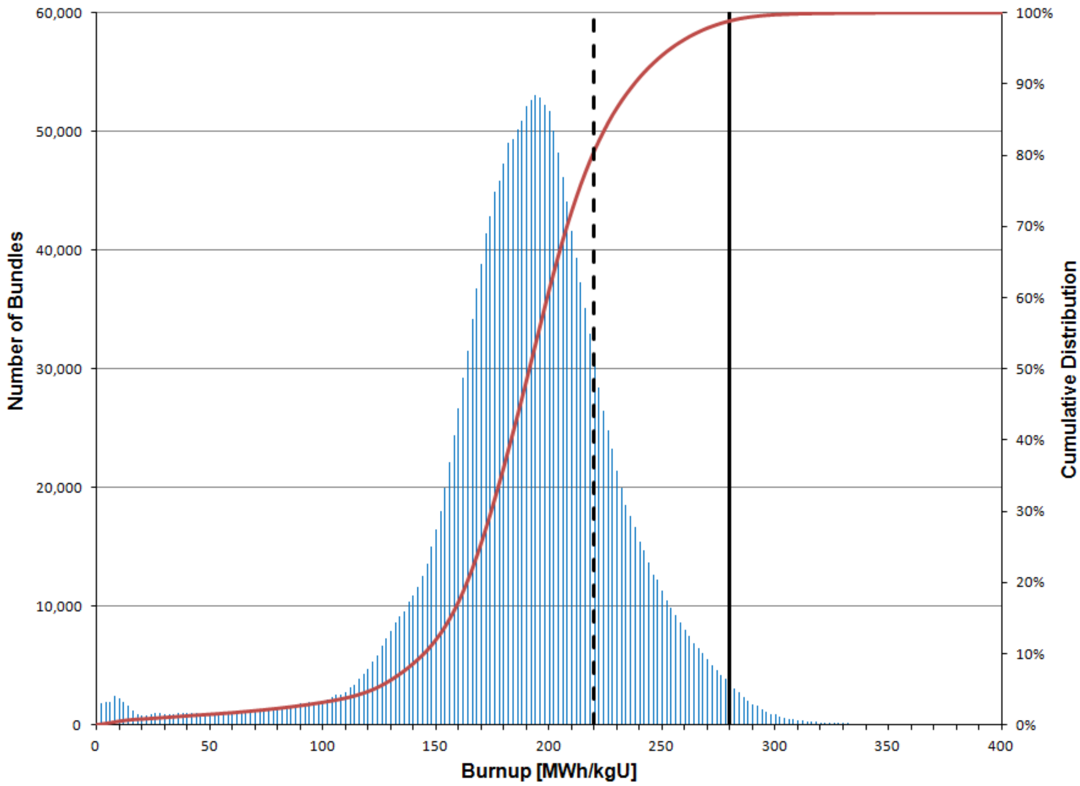

Note: The vertical dashed and solid black lines correspond to burnup values of 220 MWh/kgU and 280 MWh/kgU, while the red line represents the cumulative distribution. The figure is based on data in Wilk (2013).

Figure 3-2: Used Fuel Discharge Burnup

Table 3-1 shows the corresponding discharge burnup percentiles using lifetime aggregate values on a per station basis for burnup values of 220 MWh/kgU and 280 MWh/kgU (Wilk 2013).

Table 3-1: Discharge Burnup Percentiles on a Per Station Basis

Reactor	Burnup Percentile for 220 MWh/kgU	Burnup Percentile for 280 MWh/kgU
Bruce A	62.9	96.7
Bruce B	92.3	99.7
Darlington A	75.3	99.7
Gentilly-2	93.3	99.9
Point Lepreau	93.0	99.9
Pickering A	71.5	95.0
Pickering B	87.3	99.8
Aggregate	80.7	98.8

Linear Power:

Linear power is a measure of the energy production rate per unit length of the fuel. Linear power primarily affects the operating temperatures, which typically range from around 400^{o}C on the outside of the fuel sheath to between 800^{o}C and 1700^{o}C at the fuel centreline, well below the UO_2 melting temperature of 2865^{o}C.

Figure 3-3 shows the distribution of maximum linear power for all CANDU used fuel bundles in interim storage for the time period up to and including 2012 (Wilk 2013). Tait et al. (2000) show that the differences in radionuclide inventories between typical minimum and maximum power levels (200 kW/bundle and 900 kW/bundle) are generally less than about 2% for the same burnup. Tait et al. (2000) therefore adopted a mid-range value of 455 kW/bundle for reference inventory calculations.

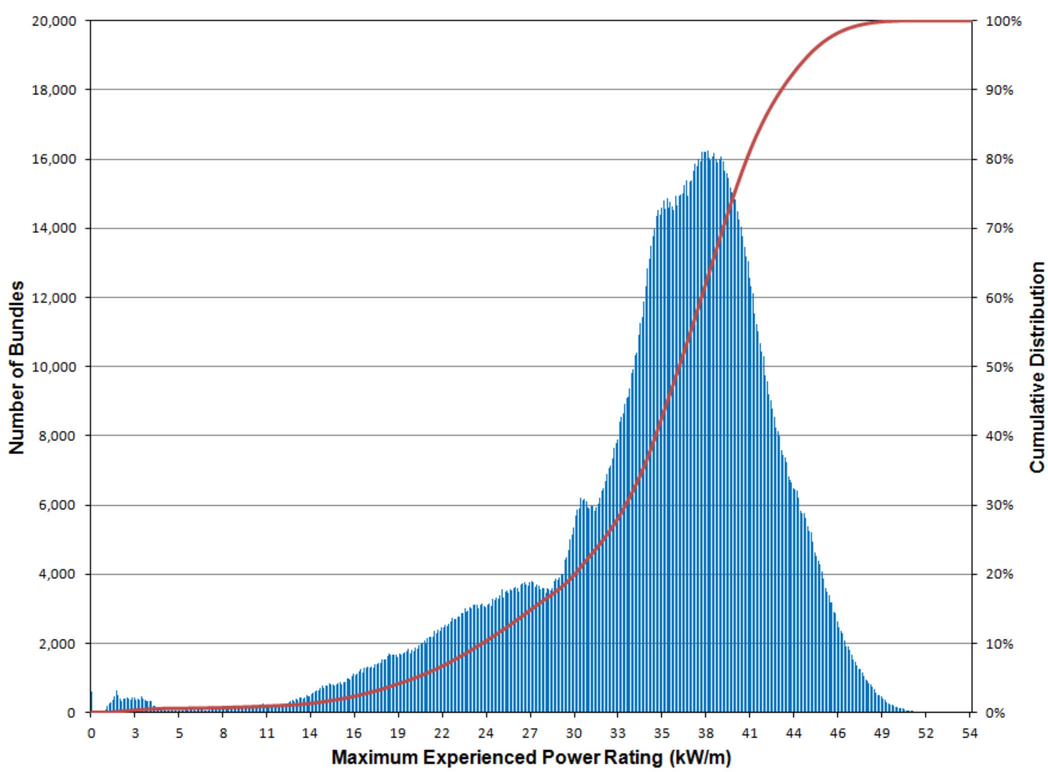

Note: The standard deviation of the distribution is approximately 7.4 kW/m or 140 kW/bundle. The figure is based on data in Wilk (2013).

Figure 3-3: Maximum Fuel Bundle Linear Power

Given these burnup and linear power data, the following values are adopted in this assessment:

- For scenarios involving a small number of used fuel containers (such as the Normal Evolution Scenario – see Chapter 6), the discharge burnup is 280 MWh/kgU and the maximum linear power level is 455 kW/bundle. Table 3-1 shows this burnup value corresponds to at least the 95th (and up to 99.9th) percentile discharge burnup, depending on the station.

- For scenarios involving a large number of used fuel containers (such as the All Containers Fail Scenario – see Chapter 6), the discharge burnup is 220 MWh/kgU and the maximum linear power level is 455 kW/bundle. Table 3-1 shows this burnup value corresponds to the 80th percentile discharge burnup across the entire inventory, with values for individual stations both above and below this percentile.

The higher value is adopted for events involving a small number of containers to address the potential situation in which the container is fully loaded with high burnup fuel bundles. This is conservative, in part because it is unlikely that all the bundles in a given load are high burnup, but also because such a container could have a high heat load, and would be deliberately monitored to avoid this situation during the container filling stage. For events involving a large number of containers, it is not physically possible for all containers to be fully loaded with 95th percentile burnup bundles and therefore a lower (yet still conservative) value is adopted.

3.1.4 Effect of Irradiation

The fuel undergoes a number of microstructural changes during irradiation, as illustrated by the sequence of photographs in Figure 3-4. Unirradiated fuel has a cohesive, interlocking microstructure and many grains have some internal sintering porosity from the fuel fabrication process. During irradiation, the sintering porosity is largely eliminated, boundaries between individual grains become more distinct, and some volatile elements diffuse out of the fuel grains to form fission gas bubbles at the interfaces between grains. At linear power ratings higher than approximately 50 kW/m (i.e., higher than achieved in most CANDU bundles), the fission gas bubbles enlarge and begin to coalesce, leading in some cases to the formation of gas tunnels along grain boundaries.

Unirradiated fuel pellets are very fine-grained, but at linear power ratings higher than approximately 50 kW/m equiaxial grain growth occurs in the pellet interior where temperatures are highest (Figure 3-5). Grain growth is typically accompanied by the diffusion and segregation of non-volatile fission products, some of which form small metallic particles at grain boundaries as shown in Figure 3-6.

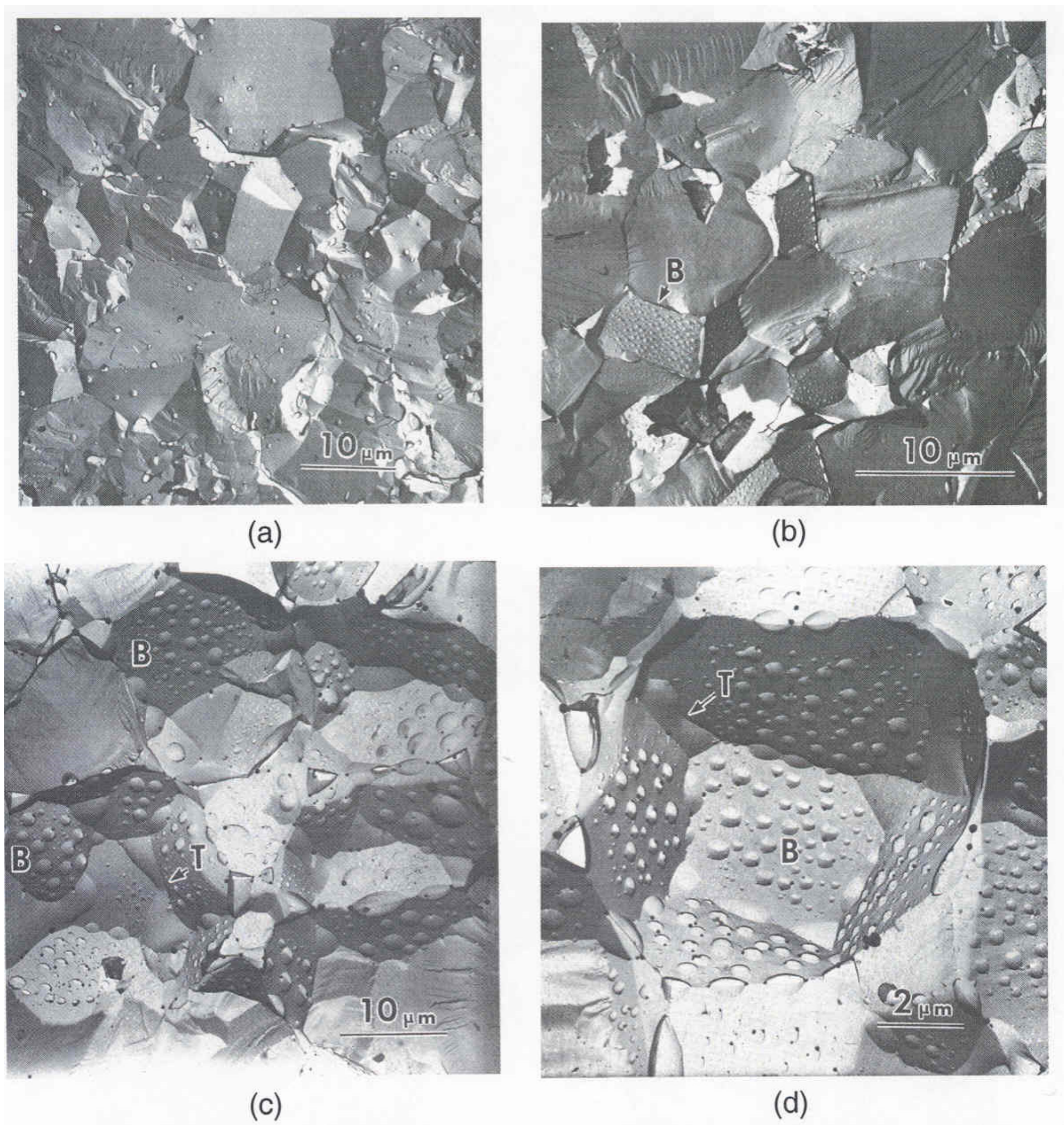

Notes: a) Typical microstructure of unirradiated UO_2. Small inclusions = sintering porosity.
b) Irradiated at low power (< 45 kW/m). Note loss of sintering porosity and development of small intergranular fission gas bubbles (B).
c) Irradiated at higher power (≥ 50 kW/m), showing growth of fission gas bubbles (B) and initiation of tunnels (T).
d) Magnified view of irradiated higher power fuel. Note the grain-edge tunnels (T) and the development of fission gas bubbles (B) on all faces of the “pull-out” of a single grain.
Ref.: Hastings (1982).

Figure 3-4: Typical Microstructure of Unirradiated and Irradiated UO_2 Fuel

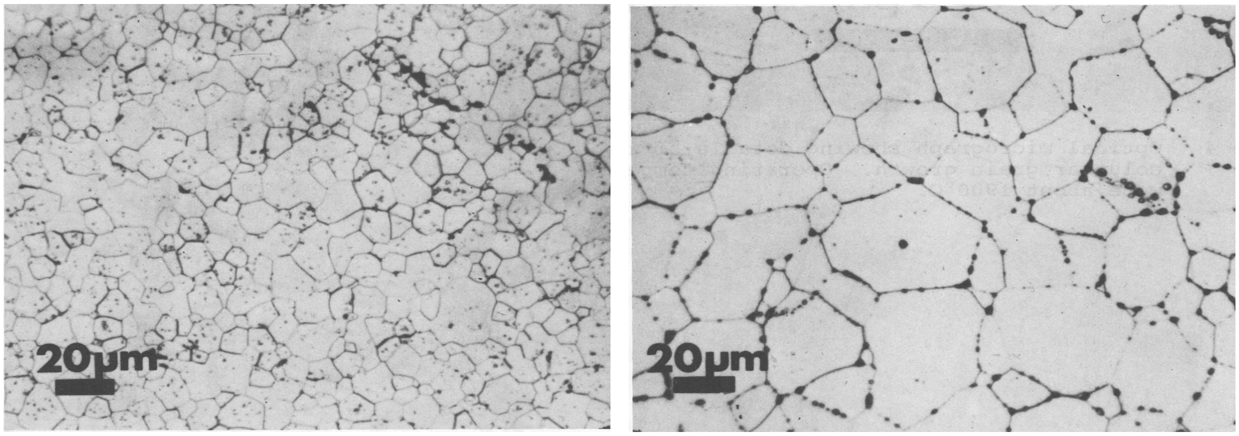

(a) (b)

Notes: a) Unirradiated UO_2. Note sintering porosity in grain interiors.
b) Irradiated UO_2 at low burnup and high power (20 MWh/kgU at 50 kW/m). Note increase in grain size, loss of sintering porosity, and formation of fission gas bubbles and tunnels along boundaries.
Ref.: Hastings (1982).

Figure 3-5: Grain Growth in Irradiated UO_2 Fuel

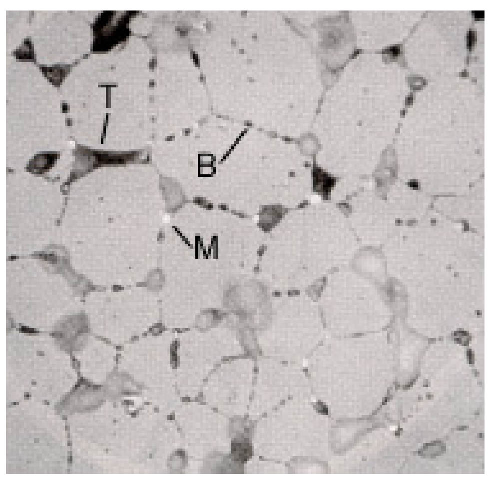

Ref: Novak and Hastings (1991).

Notes: Optical micrograph of polished and etched UO_2 fuel irradiated to very high burnup (770 MWh/kgU at 52 kW/m), showing small white particles at grain boundaries (M) that are formed from incompatible metals such as Mo, Ru, and Pd that have diffused out of the UO_2 grains. Well-developed fission gas bubbles (B) and tunnels (T) are also present at grain boundaries. Scale is approximately same as shown for Figure 3-5.

Figure 3-6: Segregation of Metallic Fission Products from UO_2 Fuel

Compared to fresh bundles, used bundles contain new elements (approximately 2% by mass), including fission products, activation products and actinides other than uranium. Of these, more than 95% remain within the UO_2 grains very close to the location of their formation (Gobien et al. 2016 and references therein).

As indicated in Figure 3-7, the species produced can be grouped according to their chemical behaviour into the following categories (Kleykamp 1985):

1. Species such as He, Kr, Ar, Cs and I that are gaseous or somewhat volatile at fuel operating temperatures (i.e., 400-1700°C). Due to their relatively high diffusion coefficients, during reactor operation a small fraction of each species migrates out of the fuel grains and into fuel element void spaces (i.e., into the fuel sheath gap and into cracks in the fuel pellets). At the same time, another small fraction moves to the grain boundaries within the fuel pellets and forms fission gas bubbles. The remainder (roughly 95%) of the fission gases are held in the UO_2 crystal lattice.
2. Species such as the metals Mo, Ru, and Pd that are non-volatile but have a low solubility in UO_2. At high in-reactor temperatures, small quantities of these species can diffuse from the fuel grains and segregate as metallic alloy phases at grain boundaries, particularly in areas of UO_2 grain growth. The majority of incompatible species remain trapped within the fuel grains due to their low diffusion coefficients in UO_2 at fuel operating temperatures.
3. Species that are compatible with UO_2, including the lanthanide elements and actinides such as Pu, Am, Np. These elements can substitute chemically for uranium in UO_2, and the atoms are then structurally bound as trace elements in the UO_2 crystal lattice.

The Zircaloy-4 fuel sheath consists of more than 98 wt% Zr and approximately 1.5 wt% Sn, with a number of other elements present as impurities (Tait et al. 2000). During irradiation, the cladding receives a neutron fluence of around 10^{25} n/m^2 (Truant 1983). The irradiated metal cladding is a fine-grained material (grain size typically 10 μm, thickness typically 0.4 mm) with neutron activation products, such as C-14, Ni-59 and Ni-63, present at concentrations less than 1 mg/kg Zr. Due to the low temperature of the cladding material during irradiation (< 400°C), activation products in the Zircaloy cannot diffuse any significant distance from the site of their formation, and they are therefore likely to be distributed uniformly throughout the metal. While in-reactor, coolant pressure causes the fuel cladding to collapse onto the fuel pellets, the heat generated in the fuel causes the pellets to expand slightly into an hourglass shape, which leads to the formation of minor cylindrical ridges in the cladding. This effect is more pronounced at high linear power and when fuel is in the reactor for long times.

Corrosion products formed within the primary coolant circuit of a reactor can deposit on the surfaces of fuel bundles in the reactor core. Neutron activation of some of these corrosion products can generate radioactive isotopes. In addition, fission products and UO_2 fuel particulates released from defective fuel bundles can also deposit on fuel bundle surfaces. In the context of a geological repository for used fuel, these surface deposits provide a small additional source of radionuclides. Information compiled on radionuclide concentrations on the external surfaces of fuel bundles (Gobien et al. 2016) indicates that the fission product, uranium and transuranium inventories in these surface deposits are very low (< 0.001%) compared to the corresponding inventories within the fuel bundle itself (Chen et al. 1986) and they can therefore be neglected in postclosure safety assessment calculations. The compilation also indicates that the inventories of Fe, Ni, Cu, and Cr on the outside surfaces of the fuel bundles are approximately 1.5%, 1%, 2.5% and 1% of the corresponding inventories in the fuel itself. If these chemical elements are of concern (i.e., potentially hazardous (see Section 3.2)), then their inventories on the external bundle surfaces should be included in the safety assessment calculations. This is achieved by increasing the instant release fractions of these elements.

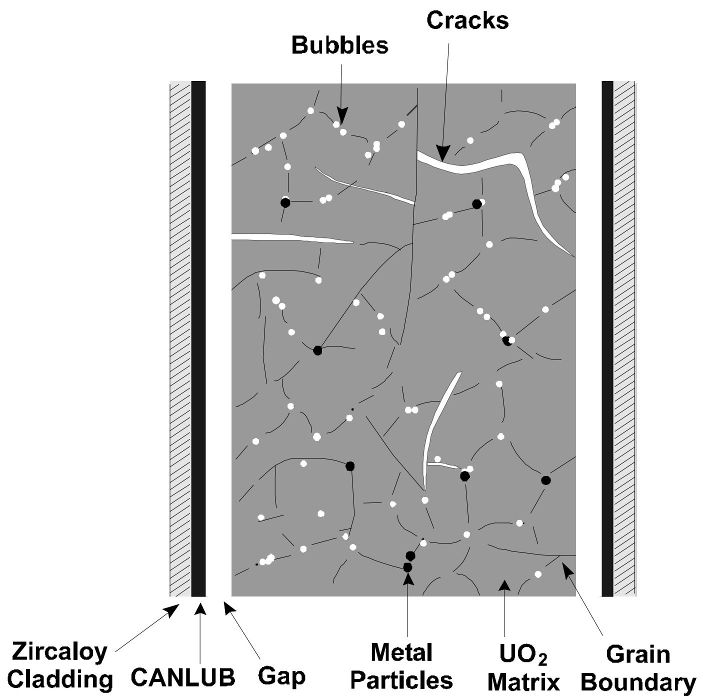

Zircaloy Cladding	CANLUB	Gap	Metal Particles	UO_2 Matrix	Grain Boundary
^{14}C	^{14}C	^{14}C	Mo	Actinides	^{14}C
^{59}Ni	^{129}I	^{129}I	Ru	~98% Fission	^{129}I
	^{135}Cs	^{135}Cs	Pd	Products	
	^{79}Se	^{79}Se	Rh		
	^{125}Sn	^{99}Tc	Tc		
	^{3}H	^{125}Sn			
	^{39}Ar	^{3}H			
	^{4}He	^{39}Ar			
	^{85}Kr	^{4}He			
		^{85}Kr			

Figure 3-7: Illustrative Distribution of Some Fission Products and Actinides within a Used Fuel Element

3.1.5 Reference Used Fuel Parameters

Table 3-2 summarizes the characteristics of the reference used fuel bundle adopted in this assessment.

Table 3-2: Reference Used Fuel Parameters

Parameter	Value	Comment
Waste Form	37-element UO_2 fuel bundle	Standard fuel bundle from Bruce and Darlington stations
Mass U/bundle	19.25 kg	Initial mass (before irradiation)
Mass Zircaloy/bundle	2.2 kg	Includes cladding, spacers, end plates
Initial U-235	0.72 wt% U	Natural uranium is used in all CANDU fuel, except a small number of research or test bundles.
Burnup	220 MWh/kgU	For events affecting a large number of containers (such as the All Containers Fail Disruptive Event Scenario – see Chapter 6)
	280 MWh/kgU	For events affecting a small number of containers (such as the Base Case of the Normal Evolution Scenario – see Chapter 6)
Power Rating	455 kW/bundle	Nominal mid-range value
Fuel Age (when placed in repository)	30 years	e.g., 10 years in pools, 20 years in dry storage
Fuel Pellet Geometric Surface Area	8.47 cm^2	Surface area of undamaged pellet (37 element design)

Note: Fuel data from Tait et al. (2000), burnup data from Wilk (2013).

3.2 Radionuclide and Chemical Element Inventories and Uncertainties

3.2.1 Potentially Hazardous Radionuclides and Elements

When discharged from the reactor, the used fuel bundle initially contains hundreds of different radionuclides; however, many of these decay quickly. Moreover, following placement in a deep geological repository, only a small fraction of these pose a potential radiological hazard to humans or the environment. The subset of radionuclides of potential concern for safety is identified via a screening analysis.

The screening analysis, described in Chapter 7, identifies 26 radionuclides from the UO_2 fuel and 2 radionuclides from the Zircaloy sheath as potentially important. Eleven additional radionuclides are included to ensure ingrowth is properly accounted for so that a total of 39 radionuclides are included in the detailed safety assessment calculations described in Chapter 7.

Table 3-3 shows the included radionuclides and their associated decay chains.

Table 3-3: Potentially Significant Radionuclides Included in the Assessment

Radionuclides	
Fuel	
Single Nuclides	Cl-36, I-129, C-14, Cs-135, Ca-41, Se-79, Sr-90
Chain Nuclides	Pu-239 → U-235 = Th-231 → Pa-231 = Ac-227 = Th-227 = Ra-223
	Pu-240 → U-236 → Th-232 = Ra-228
	Pu-242 → U-238 = Th-234 → U-234 → Th-230 → Ra-226 = Rn-222 = Pb-210 = Bi-210 = Po-210
	Am-241 → Np-237 = Pa-233 → U-233 → Th-229 = Ra-225 = Ac-225
	Sn-126 → Sb-126
Zircaloy	
Single Nuclides	C-14, Cl-36

Note: Red shows the screened-in radionuclides. The '→' indicates decay is modelled while the '=' indicates the species is modelled in secular equilibrium with the parent. Radionuclides in black are added to account for ingrowth.

At the time of discharge the used fuel also contains essentially the entire periodic table of elements ranging from hydrogen to californium; however, only a small fraction of these could potentially pose a non-radiological hazard to humans or to the environment. The subset of chemical elements of potential concern is identified via a screening analysis.

This screening analysis is also described in Chapter 7. The analysis identifies 13 elements of potential concern arising from the fuel and two from the Zircaloy, where multiple isotopes of an element (e.g., U) are considered as one element. To ensure that ingrowth is properly accounted for (leading to formation of these elements), an additional 18 radionuclides are also included in the chemical hazard analysis.

Table 3-4 shows the included chemical elements and their associated decay chains.

Table 3-4: Potentially Hazardous Elements Included in the Assessment

Chemically Hazardous Elements	
Fuel	
Elements	Cd, Hg, I, Mo, Sb, Se, Tc, W
Chains	Pu-239 → U-235
	Pu-240 → U-236
	Pu-242 → U-238 = Th-234 → U-234 → Th-230 → Ra-226 = Rn-222 = Pb-210 = Bi-210
	Am-241 → Np-237 = Pa-233 → U-233 → Th-229 = Ra-225 = Ac-225 → Bi
Misc	Pd-107 → Ag Se-79 → Br Sn-126 → Sb-126 → Te
Zircaloy	
Elements	Te

Note: Red shows the screened-in elements. The '→' indicates decay is modelled while the '=' indicates secular equilibrium is assumed. Radionuclides in black are added to account for ingrowth.

3.2.2 Inventories of Potentially Hazardous Radionuclides and Elements

Table 3-5 and Table 3-6 list all the radionuclides shown in either Table 3-3 or Table 3-4 together with their half lives, their inventories at the assumed time of placement in the repository, and various uncertainties associated with the inventories (discussed in the next section). The inventories are taken from Tait and Hanna (2001).

Tait and Hanna (2001) and Tait et al. (2000) calculated radionuclide inventories using an average burnup calculation (i.e., all fuel elements in the bundle are assumed to experience the same average neutron flux and, hence, the same average burnup). However, since elements in each ring of the bundle will see a different neutron flux because of shielding by the surrounding elements, the actual burnup in each ring will be different. A more accurate but computationally more difficult calculation can be done by performing an inventory calculation for each bundle ring and summing the results to derive an average bundle inventory. Tait et al. (2000) carried out such a sensitivity study to determine the differences between radionuclide inventories calculated using an average fuel bundle burnup and by summing inventories produced in individual bundle rings. For this postclosure safety assessment, corrections have been made to the inventories calculated by Tait and Hanna (2001) to account for the difference in the bundle average and "ring sum"[7] inventories wherever those differences exceed +1%, as described in Gobien et al. (2016).

[7] "Ring sum" refers to a radionuclide inventory calculation performed with different neutron fluxes and, hence, different burnup assumptions in the individual fuel bundle 'rings' (Tait et al. 2000)

Table 3-5: Inventories of Potentially Hazardous Radionuclides in UO_2 Fuel for 30 Year Decay Time

Nuclide	Half-life* [a]	280 MWh/kgU Inventory [moles/kgU initial]	220 MWh/kgU Inventory [moles/kgU initial]	σ_{OR} [%]	σ_{PR} [%]	σ_{Total} [%]
Ac-225	2.7380E-02	1.856E-14	1.662E-14	-	-	NA1
Ac-227	2.1770E+01	1.872E-11	1.573E-11	3	-	3
Am-241	4.3260E+02	1.544E-03[&]	1.155E-03[&]	15	-	15
Bi-210	1.3720E-02	5.225E-18	5.296E-18	-	-	NA1
[1]C-14	5.7000E+03	5.600E-06	5.600E-06	-	-	NA2
Ca-41	1.0200E+05	3.041E-06	2.354E-06	7	-	7
[1]Cl-36	3.0100E+05	5.423E-06	5.423E-06	-	-	NA3
Cs-135	2.3000E+06	3.455E-04	2.675E-04	7	7.9	14.5
I-129	1.5700E+07	5.486E-04	4.228E-04	7	-	7
Np-237	2.1440E+06	2.218E-04	1.708E-04	20	-	20
Pa-231	3.2760E+04	4.473E-08	3.820E-08	3	-	3
Pa-233	7.3850E-02	7.662E-12	5.901E-12	-	-	NA1
Pb-210	2.2200E+01	8.488E-15	8.604E-15	55	-	55
Pd-107	6.5000E+06	9.866E-04	6.901E-04	7	-	7
Po-210	3.7890E-01	1.443E-16	1.463E-16	-	-	NA1
Pu-239	2.4110E+04	1.152E-02	1.123E-02	3	-	3
Pu-240	6.5610E+03	6.788E-03	5.339E-03	4	-	4
Pu-242	3.7350E+05	7.773E-04	4.257E-04	7	-	7
Ra-223	3.1290E-02	2.669E-14	2.243E-14	-	-	NA1
Ra-225	4.0790E-02	2.747E-14	2.460E-14	-	-	NA1
Ra-226	1.6000E+03	2.282E-12	2.354E-12	55	-	55
Ra-228	5.7500E+00	8.309E-13	8.370E-13	-	-	NA1
Rn-222	1.0470E-02	1.493E-17	1.541E-17	-	-	NA1
Sb-126	3.3810E-02	3.356E-12	2.462E-12	-	-	NA1
Se-79	2.9500E+05	2.216E-05	1.762E-05	7	-	7
Sn-126	2.3000E+05	7.063E-05	5.182E-05	7	-	7
Sr-90	2.8790E+01	8.966E-04	7.561E-04	4	-	4
Tc-99	2.1110E+05	3.021E-03	2.409E-03	10	-	10
Th-227	5.1140E-02	4.308E-14	3.620E-14	-	-	NA1
Th-229	7.3400E+03	5.341E-09	4.783E-09	20	-	20
Th-230	7.5380E+04	1.571E-08	1.636E-08	55	-	55
Th-231	2.9110E-03	1.932E-14	2.944E-14	-	-	NA1

Nuclide	Half-life* [a]	280 MWh/kgU Inventory [moles/kgU initial]	220 MWh/kgU Inventory [moles/kgU initial]	σ_{OR} [%]	σ_{PR} [%]	σ_{Total} [%]
Th-232	1.4050E+10	2.078E-03	2.095E-03	4	-	4
Th-234	6.5980E-02	6.074E-11	6.091E-11	-	-	NA1
U-233	1.5920E+05	4.004E-05	3.608E-05	20	-	20
U-234[&]	2.4550E+05	2.166E-04[&]	2.089E-04[&]	50	-	50
U-235	7.0380E+08	4.748E-03	7.238E-03	3	-	3
U-236	2.3420E+07	3.845E-03	3.501E-03	4	-	4
U-238	4.4680E+09	4.114E+00	4.125E+00	0	-	0

Notes:
NA1 = Nuclide assigned a constant inventory because it has a short half-life.
NA2 = Nuclide inventory is based on an impurity level of 5.6×10^{-6} mol/kgU and assigned a uniform distribution with maximum value 1.43x the impurity inventory and minimum value equal to 0.4x the impurity level. Limits are based on measured values from Stroes-Gascoyne et al. (1994).
NA3 = Nuclide inventory is assigned a uniform distribution with maximum impurity level from Tait et al. (2000) and minimum value equal to maximum/10.
*Half-life from ENDF/B VII.1 (Chadwick et al. 2011) and converted as required using 365.25 days = 1 year.
[&]Incl. inventory of short-lived precursor: Am-241 (Pu-241, 2.737E-4 mol/kgU) and U-234 (Pu-238, 2.259E-5 mol/kgU).
[1]Analyses erroneously assumed median 220 MWh/kgU and 280 MWh/kgU inventories of 5.6×10^{-6} mol/kgU and 5.2423×10^{-6} mol/kgU for C-14 and Cl-36 instead of 6.725×10^{-6} mol/kgU and 5.207×10^{-6} mol/kgU. Differences in results were assessed and found to be inconsequential. Correct values will be adopted in future case studies.

Table 3-6: Inventories of Potentially Hazardous Radionuclides of Interest in Zircaloy for 30 Years Decay Time

Nuclide	Half-life* [a]	280 MWh/kgU Inventory [moles/kgU initial]	220 MWh/kgU Inventory [moles/kgU initial]	σ_{OR} [%]	σ_{PR} [%]	σ_{Total} [%]
C-14	5.7000E+03	2.457E-05	2.180E-06	-	-	NA1
Cl-36	3.0100E+05	1.489E-05	9.860E-06	-	-	NA1

Notes:
NA1 = Nuclide assigned a constant inventory because it is formed by activation of impurity in the fuel, and impurity levels were assigned high values in Tait et al. (2000).
*Half-life from ENDF/B VII.1 (Chadwick et al. 2011) and converted as required using 365.25 days = 1 year.

Table 3-7 and Table 3-8 list the chemical elements included in Table 3-4, their inventories at the assumed time of placement in the repository, and the various associated uncertainties. The inventory of an element shown in Table 3-7 excludes the concentration of all short-lived isotopes of the element.

The inventories are from Tait and Hanna (2001) with corrections applied to account for the difference in the bundle average and “ring sum” inventories if differences exceed +1%, as described in Gobien et al. (2016).

Table 3-7: Inventories of Potentially Hazardous Elements for 30 Year Decay Time

Nuclide	Main Source[1]	280 MWh/kgU Inventory [moles/kgU initial]	220 MWh/kgU Inventory [moles/kgU initial]	σ_{OR} [%]	σ_{PR} [%]	σ_{Total} [%]
Ag	FP	4.628E-04	3.348E-04	7	-	7
Bi	IMP	9.603E-05	9.595E-05	-	-	NA1
Br	FP	1.475E-04	1.309E-04	7	-	7
Cd	FP	2.870E-04	1.928E-04	7	-	7
Hg	IMP	7.105E-06	6.719E-06	-	-	NA1
I	FP	7.024E-04	1.144E-04	7	-	7
Mo	FP	1.195E-02	9.488E-03	7	-	7
Sb	FP	3.686E-05	2.977E-05	7	-	7
Se	IMP	4.795E-04	4.185E-04	-	-	NA1
Te	FP	1.351E-03	1.048E-03	7	-	7
W	IMP	6.093E-05	5.956E-05	-	-	NA1

Notes:

[1] Source of chemical element in fuel is either fission product (FP) or impurity in fuel (Imp).

NA1 = Nuclide assigned a constant inventory because it is formed by activation of impurity in the fuel, and impurity levels were assigned high values in Tait et al. (2000).

Table 3-8: Inventories of Potentially Hazardous Elements in Zircaloy for 30 Year Decay Time

Nuclide	Main Source[1]	280 MWh/kgU Inventory [moles/kgU initial]	220 MWh/kgU Inventory [moles/kgU initial]	σ_{OR} [%]	σ_{PR} [%]	σ_{Total} [%]
Te	IMP	2.569E-05	2.157E-05	-	-	NA1

Notes:

[1] Source of chemical element in Zircaloy is an impurity in Zircaloy (Imp).

NA1 = Nuclide assigned a constant inventory because it is formed by activation of impurity in the fuel, and impurity levels were assigned high values in Tait et al. (2000).

3.2.3 Uncertainties in Isotope Inventories

Regarding uncertainty in the isotope inventory calculations, it should be noted that what is important for safety assessment is the uncertainty in the total inventory inside the used fuel container. With 48 fuel bundles in a container, the overall percentage uncertainty is less than that for a single fuel bundle. The uncertainties in total container inventory are shown in Table 3-5 to Table 3-8.

Uncertainty arises due to the accuracy of the ORIGEN-S calculations when compared against measurements (σ_{OR}), and due to the use of an average power rating (σ_{PR}) in the calculation of initial radionuclide inventories. The latter uncertainty is small for the radionuclides of interest except for Cs-135 (Gobien et al. 2016).

There is no need to account for the distribution or uncertainty in burnup of the fuel bundles in a given container because the reference burnups of 280 MWh/kgU or 220 MWh/kgU are already conservative as described in Section 3.1.3. Since inventories generally increase with relevant burnups (Tait et al. 2000), the calculated inventories are conservative.

Validation studies (Tait et al. 1995) indicate that ORIGEN-S predictions generally agree with measured actinide and fission product inventories, with the residual uncertainty in many cases related more to the accuracy of the measurements. A comparison of measured and predicted values for a range of relevant radionuclides in a Pickering fuel bundle is shown in Table 3-9.

More recent comparisons by SKB (2010) for PWR fuel, indicates that the ratio of measured to ORIGEN calculated inventories is 1.01 for U and Pu isotopes, 1.01 for fission products and 1.11 for actinides other than U and Pu. Again, the agreement is good and within the uncertainty of the measured data.

Further information on the derivation of the uncertainties is available in Appendix A of Gobien et al. (2016).

Table 3-9: ORIGEN-S: Pickering Fuel Measure and Calculated Inventory Comparison

Isotope	Measured[1,2] (g/kg U)	ORIGEN-S (g/kg U)	Ratio (calc/meas)
Cm-244	7.12E+08 ± 15%	7.44E+08	1.05
Am-241	1.86E+10 ± 20%	1.92E+10	1.03
Np-237	1.00E+06 ± 20%	8.51E+05	0.85
H-3	2.07E+09 ± 7%	2.23E+09	1.08
Sr-90	4.86E+11 ± 4%	5.03E+11	1.03
Tc-99	1.08E+08 ± 10%	1.50E+08	1.39
Ru-106	8.72E+07 ± 5%	2.52E+08	2.89
Sb-125	2.20E+09 ± 18%	2.56E+09	1.16
I-129	2.44E+05	3.62E+05	1.48
Cs-134	4.16E+09 ± 7%	4.03E+09	0.97
Cs-137	8.05E+11 ± 5%	7.88E+11	0.98
Eu-154	8.14E+09 ± 5%	9.07E+09	1.11
Eu-155	3.35E+09 ± 8%	3.13E+09	0.93
Isotope	**Measured[1,2] (g/kg U)**	**ORIGEN-S (g/kg U)**	**Ratio (calc/meas)**
U-233	< 0.01	2.22E-07	--
U-234	0.0339 ± 55%	0.0423	1.25
U-235	1.64 ± 2.4%	1.64	1.00
U-236	0.802 ± 3.7%	0.813	1.01
U-238	983.5 ± 0.01%	983.5	1.00
Pu-238	0.0058 ± 5.6%	0.0053	0.91
Pu-239	2.69 ± 2.5%	2.72	1.01
Pu-240	1.22 ± 37%	1.25	1.03
Pu-241	0.134 ± 9%	0.142	1.06
Pu-242	0.094 ± 6.8%	0.0972	1.03

Notes:

[1]Data from Tait et al. (1995)

[2]Analytical or measurement uncertainty, σ_{meas}, expressed as a percentage.

3.3 References for Chapter 3

Chadwick, M.B., M. Herman, P. Obložinský, M.E. Dunn, Y. Danon, A.C. Kahler, D.L. Smith, B. Pritychenko, G. Arbanas, R. Arcilla, R. Brewer, D.A. Brown, R. Capote, A.D. Carlson, Y.S. Cho, H. Derrien, K. Guber, G.M. Hale, S. Hoblit, S. Holloway, T.D. Johnson, T. Kawano, B.C. Kiedrowski, H. Kim, S. Kunieda, N.M. Larson, L. Leal, J.P. Lestone, R.C. Little, E.A. McCutchan, R.E. MacFarlane, M. MacInnes, C.M. Mattoon, R.D. McKnight, S.F. Mughabghab, G.P.A. Nobre, G. Palmiotti, A. Palumbo, M.T. Pigni, V.G. Pronyaev, R.O. Sayer, A.A. Sonzogni, N.C. Summers, P. Talou, I.J. Thompson, A. Trkov, R.L. Vogt, S.C. van der Marck, A. Wallner, M.C. White, D. Wiarda and P.G. Young. 2011. ENDF/B-VII.1 Nuclear data for science and technology: Cross section, covariances, fission product yields, and decay data. *Nuclear Data Sheets*: 112-12, 2887-2996 (2011).

Chen, J.D., P.A. Seeley, R. Taylor, D.C. Hartrick, N.L. Pshhyshlak, K.H. Wasywich, A. Rochon and K.I. Burns. 1986. Characterization of corrosion deposits and the assessment of fission products released from used CANDU fuel. Proceedings 2nd International Conference on Radioactive Waste Management. Winnipeg, Canada, 7-11 September 1986. Canadian Nuclear Society, Canada.

Freire-Canosa, J. 2011. Used Fuel Integrity Program: Summary Report. Nuclear Waste Management Organization Report NWMO TR-2011-04. Toronto, Canada.

Garamszeghy, M. 2015. Nuclear Fuel Waste Projections in Canada - 2014 Update. Nuclear Waste Management Organization Report NWMO TR-2015-19. Toronto, Canada.

Garamszeghy, M. 2016. Nuclear Fuel Waste Projections – 2016 Update. Nuclear Waste Management Organization Report NWMO-TR-2016-09. Toronto, Canada.

Gobien, M., F. Garisto, E. Kremer and C. Medri. 2016. Sixth Case Study: Reference Data and Codes. Nuclear Waste Management Organization Report NWMO TR-2016-10. Toronto, Canada.

Hastings, I.J. 1982. Structures in Irradiated UO_2 Fuel from Canadian Reactors. Atomic Energy of Canada Limited Report AECL-MISC-249. Chalk River, Canada.

IAEA (International Atomic Energy Agency). 2010. Review of Fuel Failures in Water Cooled Reactors. IAEA Nuclear Energy Series No. NF-T-2.1. Vienna, Austria.

Kleykamp, H. 1985. The chemical state of the fission products in oxide fuels. Journal of Nuclear Materials 131, 221-246.

Novak, J. and I.J. Hastings. 1991. Ontario Hydro Experience with Extended Burnup Power Reactor Fuel. Atomic Energy of Canada Limited Report AECL-10388. Chalk River, Canada.

SKB. 2010. Spent nuclear fuel for disposal in the KBS-3 repository. Swedish Nuclear Fuel and Waste Management Company Report SKB TR-10-13. Stockholm, Sweden.

Stroes-Gascoyne, S., J.C. Tait, R.J. Porth, J.L. McConnell and W.J. Lincoln. 1994. Releases of ^{14}C from the gap and grain-boundary regions of used CANDU fuels to aqueous solutions. Waste Management 15, 385-392.

Tait, J.C., I.C. Gauld and A.H. Kerr. 1995. Validation of the ORIGEN-S code for predicting radionuclide inventories in used CANDU fuel. Journal of Nuclear Materials 223, 109-121.

Tait, J.C. and S. Hanna. 2001. Characteristics and radionuclide inventories of used fuel from OPG nuclear generating stations, Volume 3 - Radionuclide inventory data. Ontario Power Generation Report 06819-REP-01200-10029-R00. Toronto, Canada.

Tait, J.C., H. Roman and C.A. Morrison. 2000. Characteristics and Radionuclide Inventories of Used Fuel from OPG Nuclear Generating Stations, Volumes 1 and 2. Ontario Power Generation Report 06819-REP-01200-10029. Toronto, Canada.

Truant, P.T. 1983. CANDU Fuel Performance: Power Reactor Experience. Atomic Energy of Canada Limited Report AECL-MISC-250, Rev. 1. Chalk River, Canada.

Wilk, L. 2013. CANDU Fuel Burnup and Power Rating – 2012 Update. Nuclear Waste Management Organization Report NWMO-TR-2013-02. Toronto, Canada.

4. REPOSITORY FACILITY – CONCEPTUAL DESIGN

4.1 General Description

The Adaptive Phased Management (APM) facility includes an underground repository for used fuel and a number of surface facilities designed to support the construction and operation of the repository (Noronha 2016). The primary function of the surface facilities is to receive used fuel that is shipped from reactor-site storage facilities, to place fuel in durable containers and prepare used fuel containers (UFC) for transfer to the underground repository. The underground repository consists of several panels of used fuel containers in placement rooms which are connected to the surface via a network of access tunnels and three vertical shafts. An illustration of the APM facility in crystalline rock is shown in Figure 4-1.

The reference used fuel container is designed with a corrosion-resistant copper barrier and an inner supporting steel vessel to provide long-term containment of the fuel in the repository. Before transfer underground, the containers are placed inside highly compacted bentonite blocks called “buffer boxes”. Each fully assembled buffer box is transferred inside a shielded transfer cask to a placement room where the buffer box is unloaded and then stacked underground.

The site selection process initiated in 2010 is ongoing and, although a repository site has not yet been selected, the assumptions made for development of the site model reflect the properties of crystalline rock found in the Canadian Shield. Therefore, a generic repository design is described here for the purpose of preparing an illustrative postclosure safety assessment for a hypothetical APM facility in crystalline rock. The two key safety objectives are (1) containment of Canada’s used nuclear fuel and isolation from people and the surface environment and (2) passive safety. In this case, passive safety means that once the operational phase is complete and the repository is backfilled and sealed, no further actions are needed to ensure its safety.

For the purpose of this study, the repository is assumed to be constructed in crystalline rock at a depth of 500 m. The used fuel container, the sealing systems surrounding the container and the rock mass in which the repository is constructed provide protective barriers that are capable of containing and isolating the used fuel indefinitely. In the repository, the used fuel containers will be surrounded by engineered, highly compacted bentonite (HCB) that will provide protection against possible mechanical, chemical and biological agents that could cause container damage. The containers are expected to remain intact while the used fuel presents a hazard during the repository’s evolution. The repository engineered barriers will also create a chemical and physical environment that would limit the mobility of contaminants during postulated long-term disruptive scenarios that deviate from the expected, normal evolution of the repository.

Monitoring systems for verification of safety performance are provided as part of the repository system design. Retrievability of the fuel containers is another design feature of the APM repository.

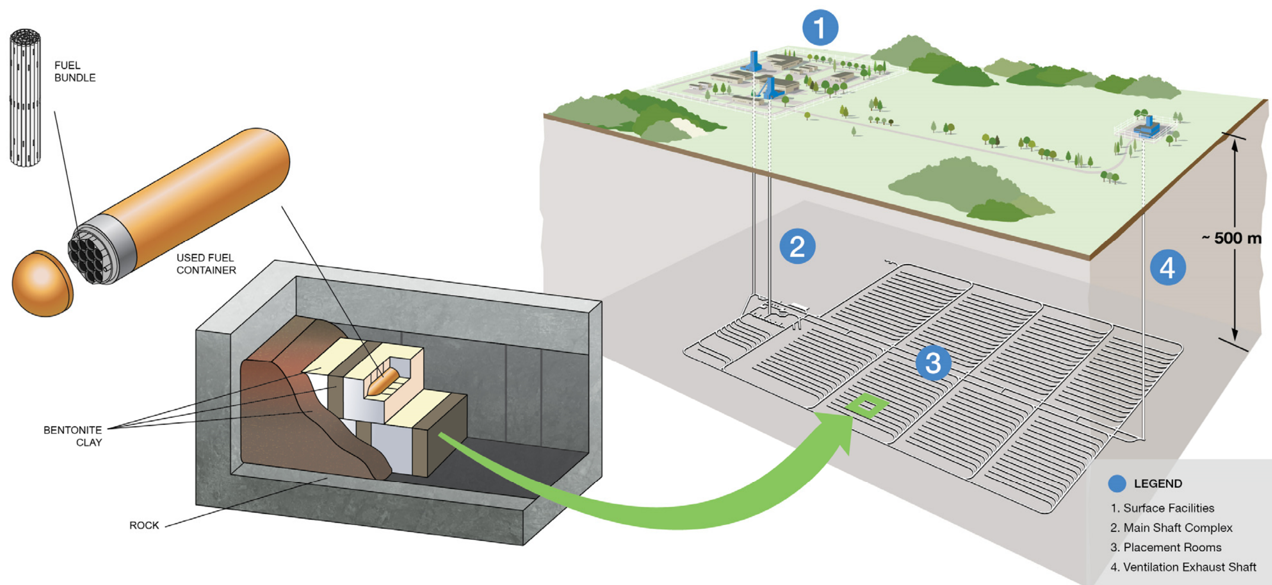

Figure 4-1: Illustration of APM Facility in Crystalline Rock

4.2 Design Requirements

4.2.1 Canadian Acts, Regulations and Codes

The DGR facility falls under federal jurisdiction. Thus, Canadian federal acts, regulations and codes apply to all aspects of the DGR facility. Under the Nuclear Safety and Control Act (NSCA) and its associated Regulations, Class 1 Nuclear Facility Regulations apply, and the DGR facility is classified as a Class 1B nuclear facility under these regulations as described in Chapter 1.

The following Canadian acts, regulations and codes apply to a deep geological repository project. Compliance with these will be demonstrated in the future in support of a licence application:

1. Above-ground civil structures will comply with the National Building Code of Canada and the National Fire Code of Canada;

2. Nuclear aspects of the facility will be designed to comply with the Nuclear Safety and Control Act and its associated regulations;

3. Electrical installations and components will be in accordance with the Canadian Electrical Code and associated Canadian Standards Association (CSA) standards;

4. The management system will comply with the CSA N286 series of standards as well as ISO 9001;

5. The environmental management and monitoring programs will comply with the CSA N288 series of standards as well as ISO 14001; and

6. The occupational health and safety management programs will comply with the CSA Z1000 standard.

By Canadian Federal Regulation 98-180, responsibility for workplace health and safety at all nuclear facilities in Ontario (including nuclear waste management facilities) has been delegated to the Province of Ontario. It is expected that workplace health and safety during the construction and operation of the DGR facility will also be regulated under the Ontario Occupational Health and Safety Act (OHSA) and its associated regulations. In particular, it is assumed that underground aspects (e.g. shafts, tunnels and placement rooms) will comply with relevant requirements in Ontario Regulation 854/90, Mines and Mining Plants, which is a regulation under OHSA.

4.2.2 Safeguards

Canada's international safeguards obligations are the result of treaty commitments (IAEA 1970, IAEA 1972, and IAEA 2000). The specific legal requirements to implement these commitments come in the form of licence conditions that are included in a Canadian Nuclear Safety Commission (CNSC) licence. Compliance with these requirements will be demonstrated in support of a future licence application.

4.2.3 Facility Requirements

1. The deep geological repository shall accommodate the intact, damaged and defective used fuel bundles arising from the nuclear reactors currently operating or previously operated in Canada.

2. The deep geological repository shall be sized to contain the used fuel, plus a contingency allowance (to be determined). This contingency shall consider the possibility of additional Canadian non-standard fuel and high-level radioactive waste. For the purpose of conceptual facility design updates, the reference inventory is 4.6 million used fuel bundles.

3. It shall also be assumed that the placement rate for the used fuel in the deep geological repository will be 120,000 used fuel bundles per year. This allows the reference inventory of 4.6 million bundles to be placed within approximately 40 years.

4. The deep geological repository shall be sited and designed to provide passive containment and isolation of used fuel using the multiple-barrier concept.

5. The deep geological repository shall be constructed at a depth within the host geological media that will provide a stable environment for excavation and operation, provide environmental conditions that contribute to used fuel isolation, and contribute to the safety. The depth of the placement rooms will be established based on the analyses of actual site

information. For conceptual facility design updates, the preliminary requirement is that the depth of the used-fuel placement rooms is a nominal 500 m below ground surface.

6. The deep geological repository shall be designed to allow for an extended period of personnel access to the major underground service areas and access tunnels for continued monitoring after the placement of all used fuel containers is completed and before decommissioning and closure is initiated. Such access will be provided without compromising the long-term postclosure safety performance of the sealed repository.

7. The deep geological repository facility shall be designed to allow the safe construction of placement rooms to occur concurrently with placement of used fuel containers.

8. The deep geological repository shall be designed to allow retrieval of some or all placed used fuel containers prior to the decommissioning of the repository. Design of the deep geological repository shall consider measures to assist postclosure retrieval insofar as these measures do not compromise safe repository performance and nuclear material safeguard measures.

9. Following closure of the deep geological repository, monitoring to observe the performance of the repository and to verify the non-diversion of used fuel, by deterrence and detection as required by nuclear material safeguards agreements, shall be possible without compromising the long-term postclosure safety of the repository.

10. The repository layout will be designed to maintain the surface temperature of the used fuel container below 100°C to ensure that the properties of the surrounding bentonite and the copper are not adversely affected.

4.2.4 Engineered Barrier Requirements

4.2.4.1 Container Requirements

1. The used fuel container shall provide containment for used fuel (as well as other high level radioactive waste deemed acceptable for the repository) from the time of loading through handling, transfer operations, placement in the repository, potential retrieval operations, and during the postclosure period as required to ensure postclosure safety.

2. The used fuel container shall be designed with sufficient mechanical stability and strength to withstand mechanical loads (including hydrostatic pressures due to glaciation) based on temperatures that could arise at the repository at depth and maintain mechanical integrity to provide containment.

3. The used fuel container shall be designed with sufficient corrosion allowance for corrosion processes (internal and external to the UFC) to maintain mechanical stability and strength and to prevent through-wall corrosion penetration.

4.2.4.2 Room and Tunnel Sealing Requirements

1. Each used fuel container shall be completely surrounded by a buffer material. The buffer material shall restrict groundwater flow around the container, create a stable chemical

environment that minimizes corrosion of the container and act as a mechanical buffer to dampen external loading (e.g. due to rock movements).

2. Each placement room in the deep geological repository shall be filled with a placement room sealing system as the used fuel containers are placed and the entrance closed with a bulkhead sealing system after the room is filled. The placement room sealing system shall act to minimize the movement of groundwater within the placement room. The bulkhead sealing system will include a cut-off trench through the excavation damage zone EDZ to impede the migration of groundwater from the placement room, provide shielding to mitigate the radiation fields in adjacent unsealed areas, contribute to maintaining the integrity of the buffer materials surrounding each used-fuel container within the room and provide access control to filled and sealed rooms.

4.2.4.3 Shaft Sealing Requirements

1. The shaft sealing materials and design shall be compatible with chemical and mechanical conditions within the host rock surrounding the shafts and the chemical conditions of the pore fluid in the host rock and repository sealing system components.

2. The sealing system applied in a shaft shall maintain its function during the postclosure period without need for maintenance or replacement.

3. Each shaft shall be completely filled by the sealing system in order to minimize subsidence of sealing materials that have been placed in the shaft and to reduce likelihood of future inadvertent intrusion.

4. The sealing systems applied in a shaft shall be designed to prevent flow and mixing of groundwater between permeable bedrock formations connected via the vertical shaft(s).

4.3 Description of Engineered Barriers

Within the deep geological repository, a series of engineered and natural barriers will work together to safely contain and isolate used nuclear fuel from people and the environment.

The first barrier in the multiple-barrier system is the used nuclear fuel which is described in Chapter 3. This chapter describes the characteristics of the engineered barriers. Used fuel bundles will be placed into large, very durable containers. In 2014, the NWMO refined its container design to one that is optimized for the used CANDU fuel produced by Canadian nuclear power reactors. Together with the bentonite clay buffer box, the container is a key part of the engineered barrier system. The container isolates and contains the used nuclear fuel from the underground environment, leaving most of the radionuclide inventory fixed in the ceramic matrix of the fuel and preventing radionuclides in the fuel from being released into the underground environment. Each container holds 48 used fuel bundles in a steel basket within a carbon steel pipe. This steel pipe has the mechanical strength to withstand pressures of the overlying rock and loading from glaciers much higher than those evidenced in Canada’s glacial history. The container is protected by a corrosion-resistant copper coating. The container has spherical heads that are welded to the core of the container. This hemispherical shape can withstand significant pressure.

Each used nuclear fuel container will be encased in a highly compacted bentonite clay buffer box before placement in the repository. Bentonite clay is a natural material evolved from volcanic ash. Compacted bentonite is proven to be a powerful barrier to water flow. It swells when exposed to water, making it an excellent sealing material. Bentonite is also very stable, as seen in natural deposits formed millions to hundreds of millions of years ago. In the repository, the chemical properties of the bentonite clay, backfill, and sealing materials would also help to trap any radionuclides in the unlikely event they were released from the container. Each buffer box will be placed and separated from horizontally adjacent boxes with spacer blocks. Containers will be stacked in two layers. After the used nuclear fuel containers are placed in the repository, all open spaces in each placement room will be filled with bentonite clay. A 6 metre-thick highly compacted bentonite clay seal and a 10 metre-thick concrete bulkhead will be used to seal the entrance to each placement room.

Before closing the repository, all tunnels and shafts will be filled with backfill and sealing materials, isolating the repository from the environment. The performance of the repository will be monitored during placement operations and during an extended monitoring period.

The geosphere forms a natural barrier of rock, which will protect the repository from disruptive natural and anthropogenic events, water flow, surface-based human activities and human intrusion. The repository will be approximately 500 metres underground - the exact depth will depend on the site. It could be excavated within a crystalline rock formation that meets the technical and safety requirements of the project. The rock formation selected will have favourable permeability to limit groundwater movement as described in Chapter 2, Section 2.2.2.2 of this report.

4.3.1 Used Fuel Container

The used fuel container incorporates a steel core for structural strength and an exterior copper coating for corrosion protection. The capacity of the UFC is 48 used CANDU fuel bundles for a fuel mass of 1200 kg. The inner vessel wall thickness is 46 mm and it is designed to sustain a maximum external isotropic pressure of 45 MPa which is a conservative estimate of maximum loads the container would experience in the repository during a glaciation cycle as described in Chapter 5, Section 5.4.1.3 of this report. To ensure best practices consistent with the principles of CSA N285.0-12, the components of the used fuel container will be designed and manufactured following the intent of ASME BPVC (Boiler Pressure Vessel Code), Section III, Division 3, Subsection WC: Class SC Storage Containments, except those identified as exempt and/or modified.

The UFC has been designed with a 3-mm-thick outer copper coating for corrosion resistance. Under repository conditions, corrosion of the copper barrier is predicted to be much less than 2 mm over a period of one million years (Kwong 2011), which is approximately the time required for the radioactivity of the used CANDU fuel to decay to levels comparable to those of natural uranium deposits. The fabrication materials selected for the manufacturing of the UFC structural vessel will have a suitable thermodynamic performance for the anticipated facility environment to ensure penetration of the corrosion barrier will not occur with the expected ground water chemistry as described in Chapter 5, Section 5.4.1.5 of this report. The UFC structural vessel will be designed with sufficient corrosion allowance for all postulated corrosion processes (internal and external to the UFC).

The UFCs will be fabricated at qualified vendor sites in accordance with pre-approved manufacturing processes and procedures, many of which are being developed under NWMO proof testing program. An example is the factory copper coating, which will be accomplished by electrodeposition, and is illustrated on the left-hand side of Figure 4-2. The UFCs will be fabricated and inspected to meet the requirements listed in pre-approved technical specification and will employ standard commercially available components, materials and manufacturing techniques to the extent practical.

In contrast, some manufacturing operations will be conducted in a hot cell at the site, during fuel repackaging. This includes fuel loading, welding, welding inspection, cold spray application over the weld zone with copper, coating inspection, and all relevant heat treatments. The right side of Figure 4-2 illustrates a simplified scheme of hot cell operations.

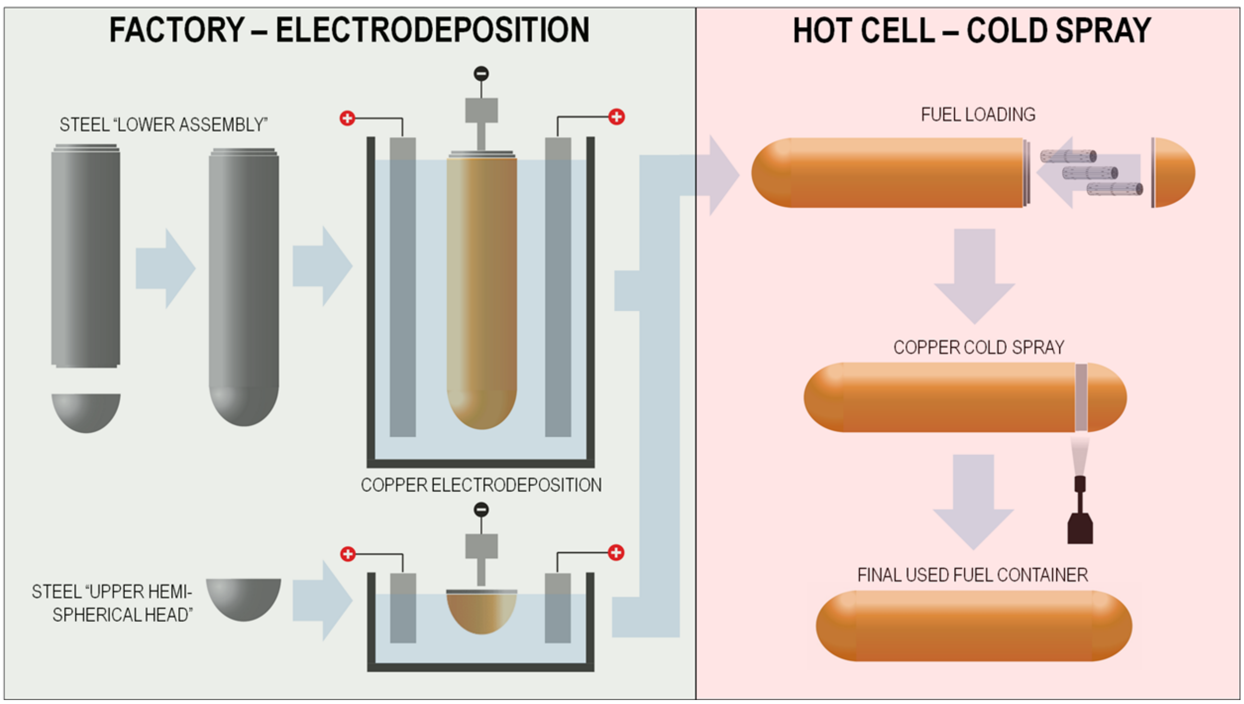

Note: This figure shows the two processes used for copper-coating the container: 1) the lower assembly and the upper hemispherical head are electroplated in a factory environment; and 2) the final steel zone is welded after the used fuel is loaded in the hot cell and then cold-sprayed with copper.

Figure 4-2: Used Fuel Container Manufacturing Process

Copper coating and base material inspections, weld inspections and hydrostatic pressure testing are examples of things being tested under NWMO's proof testing program. Various Non-destructive Examination (NDE) techniques like Eddy Current, Ultrasonic Examination and Liquid Penetrant Examination are being developed for quality assurance testing of coatings, base materials and weld inspections, for future manufacturing.

UFCs will be inspected at various stages of fabrication to ensure minimal defects in the final product. Inspections will be performed systematically in accordance with preapproved written procedures or applicable industry standards. Where required, fabrication hold points will be imposed to allow witnessing of tests/inspections. The tests and inspection results will be recorded in the Inspection and Test Plan document, which will be archived for future reference.

The design parameters of the copper coating and the inner steel vessel are given in Table 4-1. Figure 4-3 is an illustration of the used fuel container. The total mass of a loaded used fuel container is about 2800 kg.

Table 4-1: Reference Used Fuel Container and Copper Coating Parameters

Used Fuel Container – Design Parameters		
Assembled Used Fuel Container	Container capacity	48 CANDU fuel bundles
	Overall container diameter	564 mm (nominal)
	Overall container length	2514 mm (apex head-to-head)
	Loaded container mass	2805 kg (with fuel)
Steel Vessel	Outer diameter	556 mm
	Shell length	1950 mm
	Shell thickness	46.2 mm (nominal)
	Hemispherical head thickness	30 mm (nominal)
	Overall length	2506 mm (apex head-to-head)
	Mass	1343 kg
	Material	A/SA-106 Gr. C (shell), A/SA-516 Gr. 70 (hemispherical head)
Copper Coating	Thickness	3mm (minimum)
	Mass	157 kg (nominal)
	Material	Low oxygen, high purity copper
Insert for Used Fuel Bundles	Mass	105 kg (estimated, prototype)
	Material	Low carbon steel

Note: The values presented here are from the data clearance process used to conduct this safety assessment.

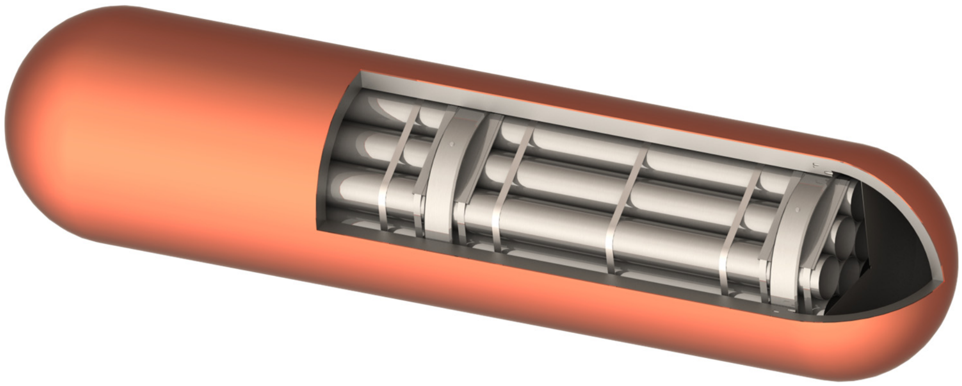

Figure 4-3: Copper Coated Used Fuel Container

4.3.2 Room, Tunnel and Shaft Sealing Materials

The key functions for various components of the repository sealing system are to:

- Fill the entire excavated volume of each area being sealed;
- Resist physical and chemical deterioration by the local environment, which includes the preclosure and postclosure geochemical conditions;
- Limit the rate of groundwater flow to and from the sealed placement rooms; and
- Limit the rate of potential radionuclide migration from the sealed placement rooms and, if released from the rooms, radionuclide migration along various underground tunnels and within the shafts.

Clay-based materials will be used to backfill most of the underground space. At the entrance to each placement room and at strategic locations in the tunnels, seals comprising highly compacted bentonite blocks would be keyed through the EDZ. These seals will be held in place by a concrete bulkhead.

Each shaft will be backfilled with a bentonite/sand mixture. At strategic locations in each shaft, concrete bulkheads will be constructed. In addition, asphalt may be used as a component in the shaft sealing system.

The following sections describe the various materials that will be used to seal the underground repository. Additional information about the configuration of sealing materials in the placement rooms is presented in Section 4.8.1. The possible arrangement of sealing materials to be placed in the tunnels and shafts during decommissioning and closure is described in Section 4.12.

4.3.2.1 Highly Compacted Bentonite

Highly compacted bentonite will be used to create buffer boxes, machined to accept the cylindrical UFCs and for spacer blocks. The HCB buffer boxes will completely surround each

UFC (see Figure 4-4). HCB will also be used as a component in the construction of room and tunnel seals. Dimensions of various HCB products will vary depending on the application.

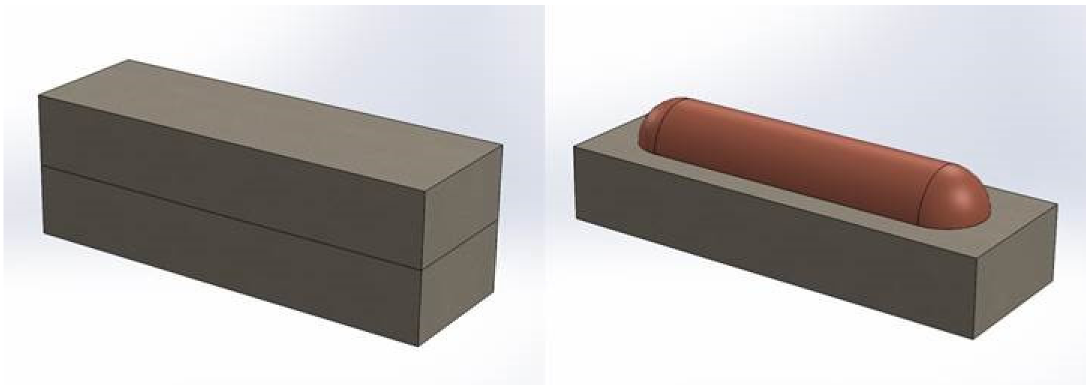

Figure 4-4: Buffer Box

HCB contains only bentonite, the commercial name given to a naturally occurring clay-rich sediment that evolves from volcanic ash (McMurry et al. 2003). The main mineral phase in bentonite is montmorillonite, a smectitic clay mineral that has expandable layers and a high cation-exchange capacity. Montmorillonite is responsible for the most distinctive property of bentonite, which is that it can swell to many times its original volume when placed in fresh water. In a confined space, swelling of compacted bentonite during resaturation can apply a substantial swelling pressure on its confinement, producing tight surface contacts and providing very effective sealing of fractures. Bentonite-based materials also have the advantage of very low permeability, reducing mass transport in the vicinity of the container and, at high density, providing an unfavourable environment for microbial activity.

Bentonite deposits in many parts of the world (e.g., Wyoming, Saskatchewan, Greece, India, China, Korea, Japan) have been assessed for their potential use as buffer material in a deep geological repository. The proportion and composition of montmorillonite varies with the source of the bentonite, with corresponding differences in swelling and mass transport properties. Bentonite that contains a high proportion of montmorillonite and whose main exchangeable cation is sodium (Na) (i.e., Na-bentonite) generally has the greatest swelling and sealing properties. Depending on its source, bentonite also contains some non-expandable clays, such as illite, and other minerals such as quartz, feldspars, calcite and gypsum, which generally are inert filler materials that do not actively affect buffer behaviour. Some bentonites are not chemically dominated by Na^+ (e.g., Ca, Mg, Fe). These non-Na clays generally have a lower swelling capacity, higher hydraulic conductivity and some (e.g., Fe varieties) have the potential to interact adversely with their surroundings. It is also anticipated that ultimately Na-bentonites will evolve towards a calcium bentonite (Ca-bentonite) as ion exchange occurs with calcium-rich groundwater. However for the critical period immediately following container placement, the buffer behaviour will be that of a Na-bentonite. Like Na-bentonites, Ca-bentonites exhibit a swelling capacity (< Na-varieties) and low permeability, making them suitable for use as buffer materials.

Important functions of the highly compacted bentonite that surrounds the used fuel containers are:

- The buffer prevents damage to the UFCs by acting as mechanical protection against stresses;
- The buffer controls groundwater flow in the area around the UFC and furthermore, controls the chemistry of the groundwater and other substances in the vicinity of the UFC;
- The buffer controls microbial activity in the vicinity of the UFC, therefore reducing the potential for microbial-induced corrosion of the container; and
- The buffer keeps the container in place.

In the case of a breach of the container, the buffer system provides a hydraulic and chemical environment which would limit the mobility of contaminants in defective UFCs.

Table 4-2: Physical Composition and As-Placed Properties of Clay-Based and Asphalt Materials for Room, Tunnel and Shaft Sealing

Material[1]	Nominal Dry density [kg/m^3]	Saturation [%]	Porosity [%]	Bulk density [kg/m^3]	Water content [kg/kg][2]	Effective montmorillonite dry density [kg/m^3][3]
Highly compacted bentonite (100% bentonite; MX-80 or equivalent)	1700	67	38.2	1955	0.15	1550
Dense backfill (5:25:70 bentonite:clay:aggregate)	2120	80	19.4	2276	0.074	376
Gap fill (100% bentonite; MX-80 or equivalent)	1410	6	48.6	1439	0.021	1261
Light backfill (50:50 bentonite:granitic sand)	1240	33	53.7	1418	0.143	692
Shaft backfill (70:30 bentonite:granitic sand)	1600	80	41.1	1930	0.205	1220
Asphalt	--	--	2	1960	--	n/a

Notes:
1. Actual backfill compositions and their engineered physical properties will depend on the site-specific design requirements for a repository.
2. Water content calculated by using the formula [Bulk Density - Dry Density] / [Dry Density].
3. To provide for comparison of sealing materials prepared using different bentonite source materials and amounts, these relationships are expressed in terms of a parameter called the effective montmorillonite dry density, which normalizes bentonites and bentonite-sand mixtures in terms of their active component, montmorillonite clay. Effective montmorillonite dry densities (EMDD) are determined using calculations illustrated in Baumgartner (2006).

4.3.2.2 Gap Fill

The gap fill's sole constituent is bentonite. Gap fill material will also be placed on the floor of each room before buffer boxes are stacked in the room. The gap fill will be used to fill the nominal 100-mm-thick gap that will exist between the stacks of buffer boxes, with their accompanying HCB spacer blocks, and the surrounding rock walls. The 100 percent bentonite gap fill will swell when saturated with water and seal the gap.

4.3.2.3 Dense Backfill

Dense backfill, as currently formulated, is a mixture of bentonite, naturally-occurring glacial lake clay and crushed rock, formed into blocks. Dense backfill blocks and gap fill will be used to fill the various horizontal access tunnels at the time of repository decommissioning and closure.

4.3.2.4 Light Backfill

Light backfill (LBF), as currently formulated, is a mixture of bentonite and sand-sized material that can be placed pneumatically ("blown in"). LBF provides many of the same functions as dense backfill except that it is not load-bearing. It would contain less crushed rock and more bentonite than dense backfill, as indicated in Table 4-2. The LBF would be used during closure of various tunnels and other horizontal openings. It will be used to fill the sides and upper (crown) regions of tunnels where it would not be possible to place dense backfill due to geometric or other constraints. Because the LBF will likely be emplaced pneumatically, it would not be as highly compacted as DBF blocks.

4.3.2.5 Shaft Backfill

Shaft backfill is a mixture of bentonite and sand that will be delivered in bulk to each shaft at the time of repository closure. It will be placed in layers and each layer will be compacted in-situ to the required density. Once saturated, the compacted bentonite/sand materials will act as a low permeability barrier to minimize groundwater flow and resist the movement of radionuclides out of the repository. Compacted clays or clay/sand mixtures are the most commonly proposed sealing materials for nuclear waste repositories. Sand will be added to the bentonite to act as a filler without compromising the low hydraulic conductivity and swelling potential of the bentonite-dominant material. The use of sand will improve workability during placement, ease compaction and improve dust control. As the compacted bentonite/sand materials saturate with groundwater from the surrounding rock, they will generate swelling pressures, which will aid in the development of a tight seal against the shaft wall and provide a confining pressure to the rock surface.

4.3.2.6 Asphalt

Asphalt may be used as one component in the shaft sealing system. Asphalt has been selected because it has the ability to flow and make good contact with host rock. Immediately upon emplacement, the asphalt will create an effective barrier to water flow. Furthermore, the use of another low permeability sealing material provides an additional level of redundancy to the sealing system against upward or downward fluid flow.

4.3.2.7 Concrete

During operations concrete is used to construct shaft liners and tunnel floors, and to construct bulkheads at the entrance to each placement room. During closure of the repository concrete will also be used to create bulkheads in the tunnels and shafts, and to create a concrete monolith at the base of each shaft. The concrete would be mass-poured. The shaft liners would be constructed using standard high performance concrete, which will be removed during the decommissioning and closure of the repository. The bulkheads will be constructed using low-heat high-performance concrete and these bulkheads will remain in place after repository closure.

Table 4-3: Composition of Various Concretes for the Repository

Ingredients	Standard High-Perf. Concrete [kg/m^3]	Low-Heat High-Perf. Concrete [kg/m^3]	Cement Grout [kg/m^3]
Portland Cement	497 (CSA Type 50)	97 (CSA Type 50)	1208 - 950 (CSA Type 50)
Silica Fume	49.7	97	136 - 107
Fly Ash	0	0	0
Silica Flour	0	194	0
Superplasticizer	7.1	10.3	14 - 11
Fine Aggregate	703	895	0
Coarse Aggregate	1100	1040	0
Water	124	97	543 - 640
Water/Cement Ratio	0.23	0.5	0.4 - 0.6

Note: Table from McMurry et al. (2003).

Interactions between concrete and water in a repository have the potential over the long term to produce alkaline chemical conditions that are detrimental to the swelling properties of bentonite; therefore, a special low-heat, high-performance concrete has been developed for use in the concrete bulkheads. Such a concrete has much lower lime content than regular concrete, giving it a lower pH in reactions with water. This lower alkalinity would limit the potential for adverse chemical reactions within the repository. In addition, the low-heat, high-performance concrete generates less heat during curing than regular concrete. The poured concrete would be less likely to crack due to thermal expansion and subsequent contraction during cooling.

4.3.2.8 Grout

Grouting is a short-term expedient that allows excavation and construction to be carried out in localized regions where groundwater inflow would otherwise be unacceptably high, or to limit seepage around or into engineered structures. Clay-based grouting materials may be an option under some conditions in a repository, but cement or silica-based grouts are more likely to be used. Low-viscosity cement grouts, grouts having a low cement content and silica rather than lime bases, have been developed for use in conditions anticipated to be encountered in a repository environment. One potential grout for use in a repository environment is presented in Table 4-3 (McMurry et al. 2003).

4.4 Surface Facilities

The surface facilities require a dedicated surface area of about 650 metres by 550 metres for the main buildings and about 100 metres by 170 metres for the ventilation exhaust shaft.

The site layout is shown in Figure 4-5 and individual buildings and other surface facilities are listed in Table 4-4. The site is surrounded by a perimeter fence; and the facilities within this perimeter are arranged into two areas:

a) the Protected Area, which is a high-security zone; and

b) the Balance of Site, a zone which includes facilities that do not require high security.

The main facilities included in the Protected Area are the Used Fuel Packaging Plant (UFPP), the main shaft and service shaft buildings as well as the auxiliary building, quality control offices, laboratory, radioactive waste handling facilities, switchyard, transformer area and emergency generators. The ventilation shaft complex is also a protected area. All activities pertaining to handling and storage of used fuel are conducted in the UFPP. A description of the UFPP and its operation is given in Section 4.5.

The Balance of Site zone includes the administration building, the fire hall, as well as ancillary facilities such as the cafeteria, garage, warehouse, water and sewage treatment plants, and helicopter pad. Fuel and water storage tanks and an air compressor building are also found in this zone.

Balance of Site also includes the concrete batch plant and the sealing materials compaction plant. The concrete batching plant will produce the concrete mixes that are required in the repository, including the low-heat, high-performance (LHHP) concrete required for the bulkheads to be placed at entrance of the container-filled placement rooms. At the sealing materials compaction plant, externally sourced aggregate, lake clay and bentonite will be mixed to produce compacted bentonite blocks and gap-fill material required for sealing the used fuel containers inside the placement rooms.

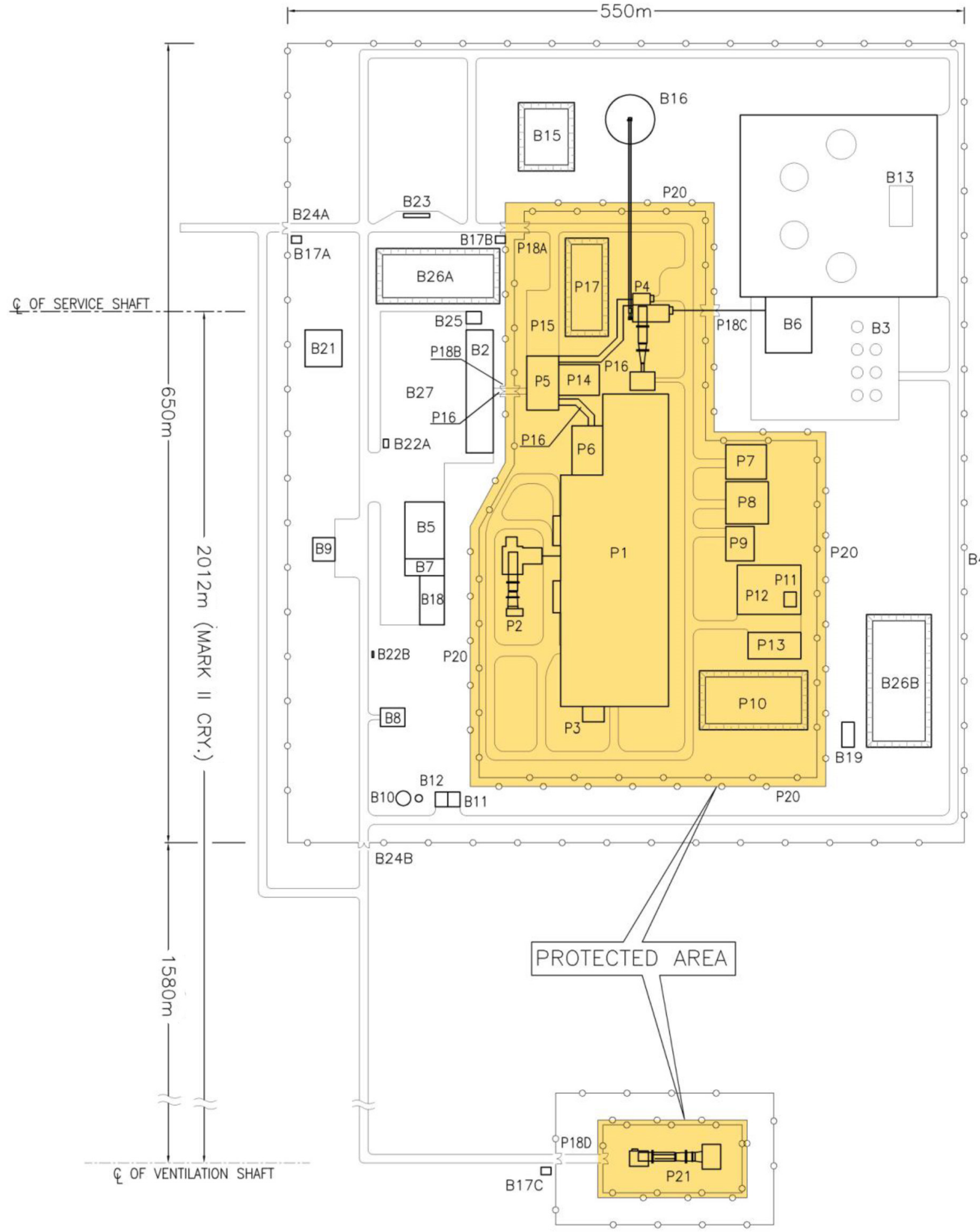

Figure 4-5: APM Surface Facilities Layout

Table 4-4: APM Facility Number and Description

Area	Protected Area	Area	Balance of Site
P1	Used Fuel Packaging Plant	B1	Excavated Rock Management Area*
P2	Main Shaft Complex	B2	Administration Building including Firehall and Cafeteria
P3	Stack	B3	Sealing Material Storage Bins
P4	Service Shaft Complex	B4	Perimeter Fence
P5	Auxiliary Building	B5	Garage
P6	Active Solid Waste Handling Facility	B6	Sealing Materials Compaction Plant
P7	Waste Management Area	B7	Warehouse and Hazardous Materials Storage Building
P8	Active Liquid Waste Treatment Building	B8	Air Compressor Building
P9	Low-Level Liquid Waste Storage Area	B9	Fuel Storage Tanks
P10	Storm Water Management Pond	B10	Water Storage Tanks
P11	Switchyard	B11	Water Treatment Plant
P12	Transformer Area	B12	Pump House
P13	Emergency Generators	B13	Concrete Batch Plant
P14	Quality Control Offices and Laboratory	B14	Not Used
P15	Parking Area	B15	Process Water Settling Pond
P16	Covered Corridor / Pedestrian Routes	B16	Excavated Rock Stockpile
P17	Mine Dewatering Settling Pond	B17	Guardhouse (B17A, B17B & B17C)
P18	Security Checkpoint (P18A, P18B, P18C, P18D)	B18	Storage Yard
P19	Not Used	B19	Sewage Treatment Plant
P20	Double Security Fence	B20	Storm Water Management Pond*
P21	Ventilation Shaft Complex	B21	Helicopter Pad
		B22	Bus Shelters (B22A, B22B)
		B23	Weigh Scale
		B24	Security Checkpoints (B24A, B24B)
		B25	Security Monitoring Room
		B26	Storm water Management Ponds (B26A, B26B)
		B27	Parking Area

Note: *Refers to off-site facilities

The APM facility will also require a storage area of about 0.18 km^2 for the excavated rock (Area B1). Its location would be selected in consultation with the community and surrounding region. The area will initially be prepared using dumped crusher wastes to directly fill any low-lying depressions. Additional excavated rock will then be placed in layers on the prepared ground surface. Access routes and paths will be prepared for loaders, dumpers and trucks to move around and up the piles easily.

The excavated rock management area will include a storm water management pond (Area B20) to collect and monitor the run-off water before being released to the receiving water body. The potential contaminants of concern in the run-off will likely be various chemical constituents due to leaching of minerals in the excavated rock and nitrogen compounds from residual explosives on the excavated rock. The surface water run-off from the excavated rock pile will be monitored and appropriate effluent control procedures will be implemented based on the monitoring results.

4.5 Used Fuel Packaging Plant

The UFPP is identified as Area P1 on Figure 4-5 and the layout is shown in Figure 4-6. This single storey building is a reinforced concrete structure and has a basement. It will include all necessary provisions for receiving used fuel bundles in Used Fuel Transportation Packages (UFTPs), transferring used fuel bundles from the UFTPs to the UFCs. The UFPP has equipment for sealing, inspecting and assembly of UFCs into buffer boxes, and for dispatching of the buffer boxes for placement in the underground repository. Any defective UFCs would require repacking into a new container. Figure 4-6 also includes preliminary radiological zones for the movement of staff and materials, including required maintenance activities, to keep doses As Low As Reasonably Achievable (ALARA).

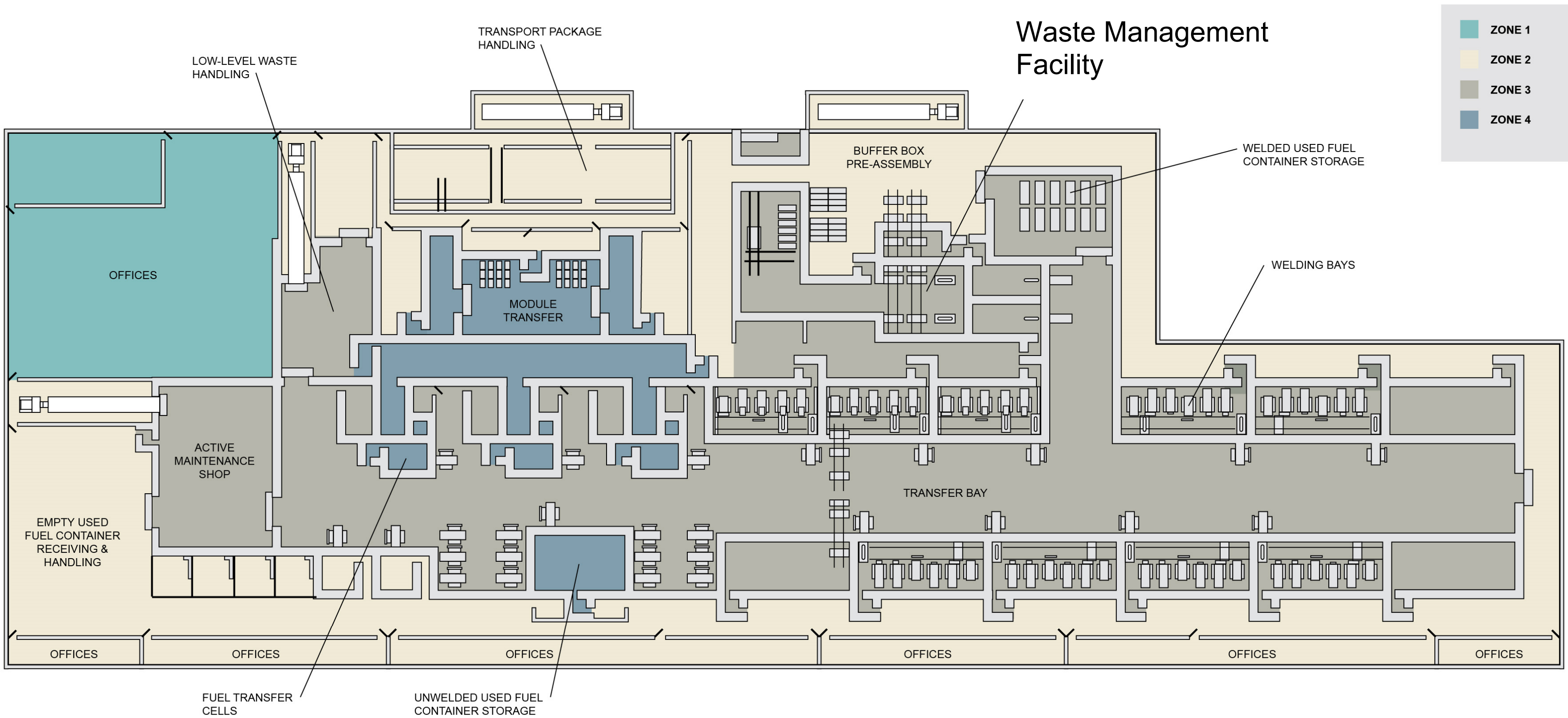

Figure 4-6: Overview of the UFPP Layout

There are processing lines for receiving and unloading UFTPs and handling the UFCs. The processing line for UFCs is designed so that several containers can be in process simultaneously. Key data for the UFPP throughput is provided in Table 4-5. The UFPP also includes auxiliary systems, such as ventilation, electrical power systems, a central control room, waste management facility, and facilities for personnel and visitors.

Table 4-5: Key Data for Average UFPP Throughput

	Bundles per Unit	Throughput		
		Base Case Total	Annual	Daily *
Bundles	1	4,600,000	120,000	480
Modules	96	47,917	1,250	5.0
UFTP	192	23,958	625	2.5
UFC	48	95,833	2500	10

Note: * Based on assumption of 250 working days per year.

Most steps in the packaging process are remotely operated. However, after removal of the radiation source and decontamination by remote-controlled processes, all areas can be accessed by maintenance personnel. Areas and equipment for handling used fuel bundles and filled UFCs are radiation shielded. The fuel receiving and transfer area will be kept at a negative pressure to prevent the spread of airborne contamination.

4.5.1 Used Fuel Transport Package Receipt and Unloading

To achieve the specified daily throughput, an average of three UFTPs will need to be processed each day. To achieve this throughput, the system will incorporate two parallel and independent processing lines. Each line will process between 1 and 2 UFTPs per day. Fuel-filled modules will be placed into temporary dry storage, as required, until modules can be accepted for processing inside the UFPP. It is assumed that wet storage is not required because all fuel received at the UFPP will be sufficiently cool for dry storage.

Used fuel inside a UFTP arrives at the UFPP from the interim storage facilities at reactor sites via the ground transportation system and is transferred to one of two parallel UFTP handling cells which are located on the basement level of the plant (see Figure 4-7). After the impact limiter is removed, the UFTP loaded with modules is raised and connected to an opening in the ground-level floor. The UFTP lid is removed and modules are lifted out of the package and then transferred to the respective module handling cell on the ground level of the plant. There will be a process in place to clearly distinguish and track the empty and filled transportation packages, and to keep these packages in separate locations.

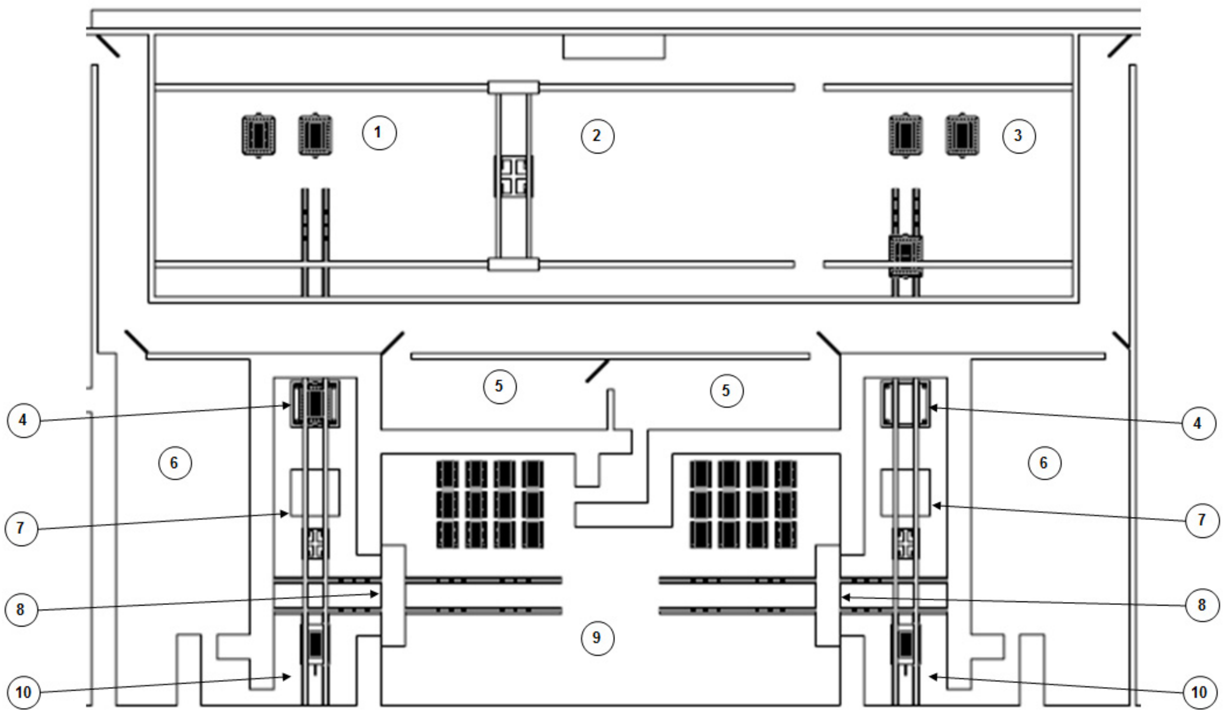

Figure 4-7: UFTP Receiving and Fuel Module Handling

The UFTP Handling Cells illustrated in Figure 4-7 consist of the following areas or components (numbers refer to locations in the figure):

1. UFTP Storage area
2. UFTP Shipping and Receiving Hall
3. Impact Limiter Removal area
4. UFTP Lid Removal
5. Control Room
6. Operator Room
7. Module Transfer Cell
8. Module Transfer to Dry Storage
9. Dry Storage area
10. Module Transfer to Distribution Hall

4.5.2 Used Fuel Container Loading and Sealing

To ensure the specified daily throughput listed on Table 4-5 is achieved, a total of 12 UFCs are planned to be loaded per day, which corresponds to 6 fuel modules. To accomplish this, the system will utilize three parallel and independent processing lines, each processing an average of 2 modules and 4 UFCs per day (Figure 4-8).

The three processing lines will be isolated from one another with airlocks and concrete shielding walls to create “hot cells”. The ‘hot cell’ areas will have lead glass windows and will be equipped with closed circuit cameras for remote viewing.

Empty containers will be produced off-site at a dedicated UFC factory and delivered to the UFPP. Fuel will be received, unloaded and transferred into used fuel containers in a hot cell process. Once the fuel is loaded into the used fuel container, the top hemispherical head will be temporarily installed and the assembly is transferred to the used fuel container processing cell (as illustrated in Figure 4-2). The UFC is welded, examined, copper-cold-sprayed and annealed prior to being placed inside a buffer box in the UFPP. The buffer box is placed inside a shielded cask for transfer underground. Figure 4-8 to Figure 4-11 illustrate the key steps in the process to load and seal the UFC.

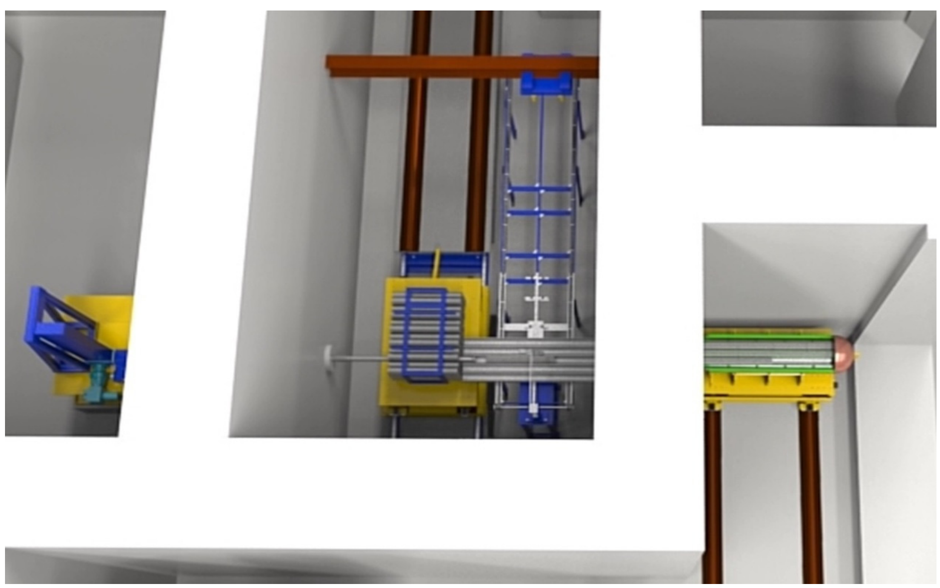

Notes:

1. Room at left of figure houses the equipment to operate the push rod that penetrates the hot cell shield wall.
2. Module loaded with fuel bundles is located in hot cell at center of figure.
3. Bundles are pushed by the rod into the UFC located in hot cell at right of figure. The UFC is shown in a cut-away view with top half of the UFC removed for the purpose of this illustration.

Figure 4-8: Fuel Transfer into Used Fuel Container

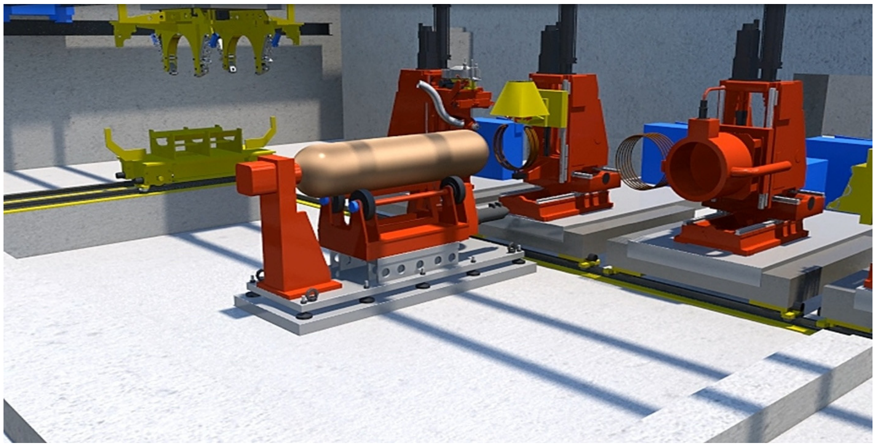

Figure 4-9: Automated Work Tables inside Processing Cell

Inside the processing cell shown in Figure 4-9, automated work tables are responsible for:

1. Welding the hemispherical head to the shell (Figure 4-10)
2. Clean-up machining of the weld (if required)
3. Non-destructive examination of the weld (Figure 4-10)
4. Copper cold spray over weld area (Figure 4-11)
5. Clean-up machining of the copper cold spray (if required)
6. Annealing of copper cold spray (Figure 4-11)
7. Non-destructive examination of the copper cold spray

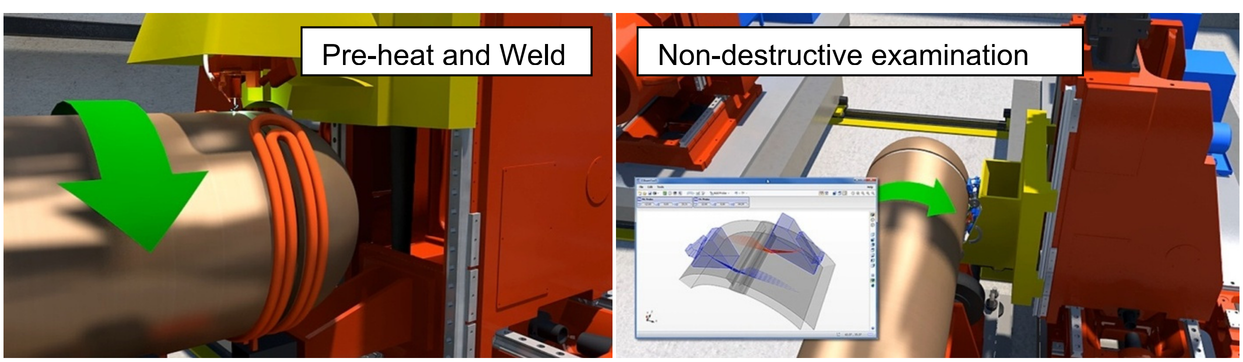

Figure 4-10: Weld Worktable and Non-Destructive Examination Worktable

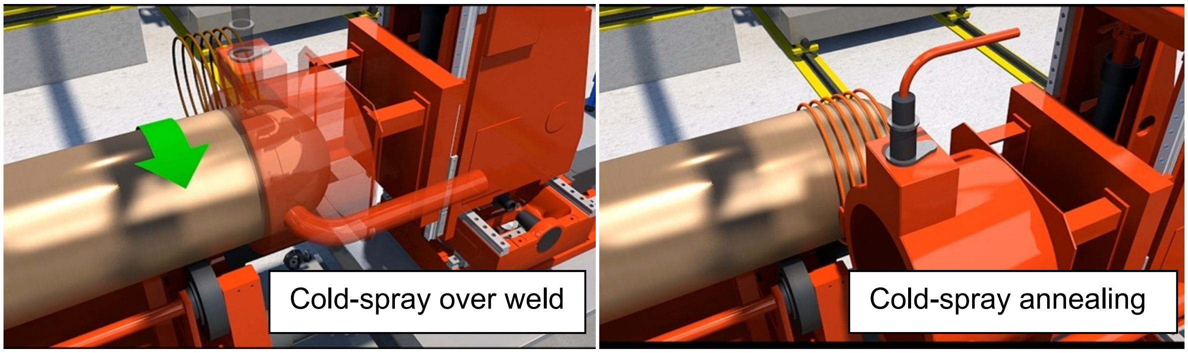

Figure 4-11: Copper Cold Spray and Copper Annealing Worktable

4.5.3 Used Fuel Container Intra-Plant Transfer System

The UFC intra-plant transfer system is comprised primarily of an Automated Guided Vehicle (AGV) system and the UFC transfer hall where four AGVs will operate. The transfer hall contains three Work in Progress (WIP) storage areas:

- WIP Storage Area #1 for loaded UFCs – UFCs loaded with used fuel;
- WIP Storage Area #2 for post-weld UFCs - UFCs that have just completed the welding operation; and
- WIP Storage Area #3 for completed UFCs – UFCs that have successfully been coated with copper and are ready for dispatch to buffer box assembly area.

The hall allows AGVs to access the active maintenance shop, waste management facility, fuel loading cells, process contingency manual work cell, UFC weld cell, UFC copper application cell and the UFC final decontamination cells.

All areas of the transfer hall will be shielded from radiation fields given off by the UFC using concrete shielding walls between processing areas, or by the use of a shielded UFC transfer flask. The main transfer hall is expected to be classed as Zone 2. However because there is risk that contamination could spread from the unsealed UFCs to inside and outside of the UFC flask, this area may have to be designated Zone 3. Hot cells in this facility can be considered as Zone 4 for control purposes.

The used fuel packaging plant illustrated in Figure 4-6 consists of the following areas or components:

1. UFC Transfer Hall
2. Fuel Handling Cell Docking
3. UFC Weld Cell Docking
4. UFC Copper Application Cell Docking
5. WIP Storage Area #1 - Loaded UFCs

6. WIP Storage Area #2 – Post-Weld UFCs
7. WIP Storage Area #3 - Completed UFCs
8. UFC Decontamination Cell Docking
9. Process Contingency Manual Work Cell Docking

4.6 Sealing Materials Production Facilities

The sealing materials are produced in the sealing materials compaction plant (Area B6 in Figure 4-5) and the concrete batch plant (Area B13 in Figure 4-5). For logistics reasons the sealing materials facilities are situated outside the Protected Area but as close as possible to the service shaft.

4.6.1 Sealing Materials Compaction Plant

During repository operations the sealing materials compaction plant will be used to manufacture the following materials:

- HCB blocks, spacers and bricks; and
- Gap fill

The presses used to produce the HCB material are a specialized item that will need to be designed to suit this purpose. Two compaction options exist for the very large HCB blocks (a uniaxial compaction approach and an isostatic compaction approach).

Examples of the large presses that would be required for production of some of the bentonite components are shown in Figure 4-12 and Figure 4-13.

All raw materials used in the sealing materials compaction plant will be externally sourced.

Figure 4-12: Example of a Closed-Die Forging Press (Uniaxial Compaction)

Figure 4-13: Cold Isostatic Press for Production of Highly Compacted Bentonite Blocks

During closure of the underground repository, the sealing materials compaction plant will be reconfigured, as required, to produce different categories of clay based sealing materials:

- Dense backfill blocks,
- Light backfill.
- Gap fill,
- Highly Compacted Bentonite blocks, and
- Bentonite/sand mixture.

Additional information about tunnel and shaft sealing is presented in Section 4.12.

4.6.2 Concrete Batch Plant

The concrete batch plant will produce two different qualities of high-performance concrete mixes, one used for the shaft liners and the other for tunnel floors, placement room bulkheads and shaft seals. Externally sourced raw materials will be used to produce the concrete including aggregate and binders. The concrete batch plant will also be used during closure of the underground repository.

4.6.3 Aggregate Supply

Due the relatively small quantity of aggregate required by the sealing materials compaction plant and concrete batch plant during repository operations, an on-site rock crushing plant is not required and all aggregate will be imported to the site. Modified granular A (a graded crushed stone) and fine sand will also be delivered and used to produce aforementioned sealing materials in the sealing material compaction plant. Aggregate (sand and stone) will be delivered to the site for use in the concrete batch plant.

4.7 Shafts and Hoists

Access to the repository is via shafts serviced by hoisting facilities. Three shafts will be constructed, the main shaft, the service shaft, and the ventilation shaft (Figure 4-14) each serving specific functions during construction and operations of the repository facility. Their primary functions are the transport of materials and personnel, and providing ventilation to the repository. The shafts will be constructed using techniques that minimize host rock damage, to enhance the effectiveness of postclosure shaft seals.

The shafts diameters are as follows:

- Main shaft finished diameter is 7 metres;
- Service shaft finished diameter is 6.5 metres; and
- Ventilation shaft finished diameter is 5.6 metres.

The headframes for the three shafts will be of slip-formed concrete construction for durable and easily maintainable structures. All the shafts will be concrete lined and the lining will be removed during sealing of the shafts following the end of operations.

The three shaft structures (including head frames and hoisting plants) provide a number of support functions during construction and operation of the underground repository:

- The main shaft serves as the exclusive means for transfer of used fuel containers from the surface to the underground repository. Conversely, it could also be used for transfer of a retrieved used fuel container from the repository to the surface, if this was required. Finally, the main shaft is used to deliver fresh air to the underground;
- The service shaft serves as the principal conveyance for personnel, materials and equipment to the underground as well as for transport of excavated rock to the surface. It is also used to exhaust some underground air to surface; and
- The ventilation shaft, located about 2 km outside the main surface facilities fence is the primary route to exhaust underground air and also serves as a second emergency exit from the repository.

4.8 Underground Facility Design

For the purpose of conceptual design and safety studies for a hypothetical site in crystalline rock, the used fuel repository is assumed to be developed on a single level, at a depth of approximately 500 m, in a setting capable of withstanding mechanical and thermal stresses. The actual layout for a selected repository site will be adapted to suit the specific site conditions.

The geology of the hypothetical site used in this study is described in Chapter 2. The volume of available competent rock in this hypothetical geosphere allows sufficient distance from unfavourable geological features. However the repository was intentionally placed near a feature, by setting the closest distance from a placement room to a water conducting fracture to 100 m, to assess the impact of a nearby fracture. A possible layout for a repository designed to accommodate a reference inventory of 4.6 million used fuel bundles is shown in Figure 4-14 and it covers an area of about 3.4 km^2.

It is possible that the various crystalline rock sites in Northern Ontario will have widely-spaced major geologic structures. Thus an underground repository layout that has the flexibility to easily avoid these structures with a good margin is currently being developed.

Other countries, such as Finland and Sweden, have identified their hosting locations. This has allowed them to start developing site-specific layouts which are adaptive (flexible) layouts in that the layouts can be adjusted to suit the conditions encountered underground. NWMO has recognized the necessity for this flexibility in the layouts, and has started the process of identifying the challenges and options to be faced in achieving this design flexibility.

4.8.1 Underground Layout

The reference repository layout is a rectangular configuration, with two central access tunnels and two perimeter tunnels connected by perpendicular tunnels, called panel access tunnels, which provide access to the placement rooms.

The placement rooms are a series of parallel tunnels arranged in eight panels, as shown in Figure 4-14. Within each panel, the placement rooms have a centre-to-centre spacing of 20 m to satisfy thermal constraints, and each room has a single access from the corresponding panel access tunnel. The length of the rooms in the reference design is specified as 304 m where the useable length in each room is 287 m. The used fuel container density is designed to minimize the repository underground footprint while, at the same time, satisfying thermal design requirements. The placement room design is shown in Figure 4-15 and described in further detail in Section 4.8.2.

The repository includes provision for an underground demonstration facility located near the main and service shafts. This facility will be used to support long-term testing and demonstration of repository technology.

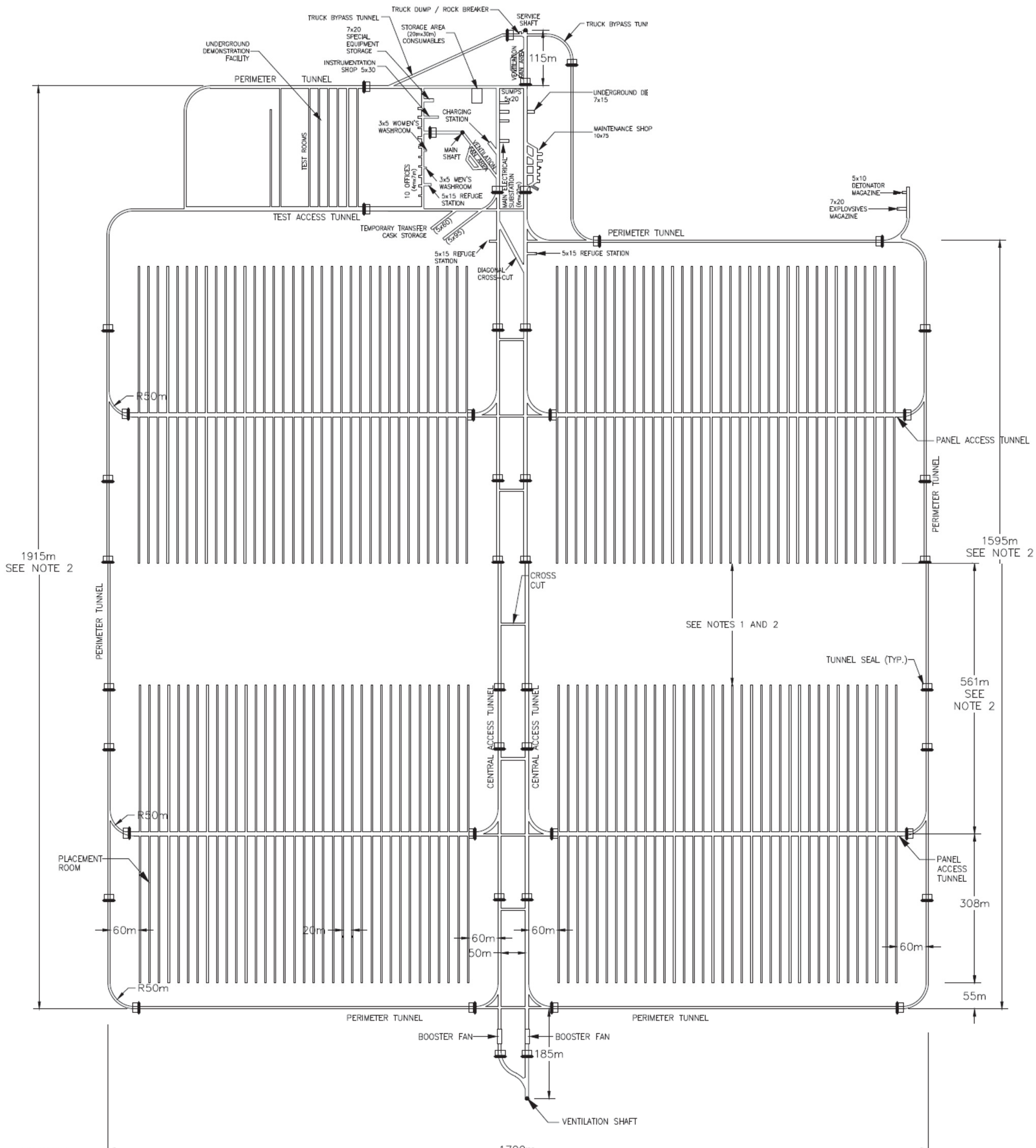

NOTES:

1. 252.8m SEPARATION BETWEEN PANELS IS BASED ON A HYPOTHETICAL FRACTURE ZONE WITH 100m STANDOFF
2. NWMO MAY ADJUST THE SEPARATION IN THE FUTURE BASED ON SITE SPECIFIC SAFETY ANALYSES.

Figure 4-14: Underground Repository Layout

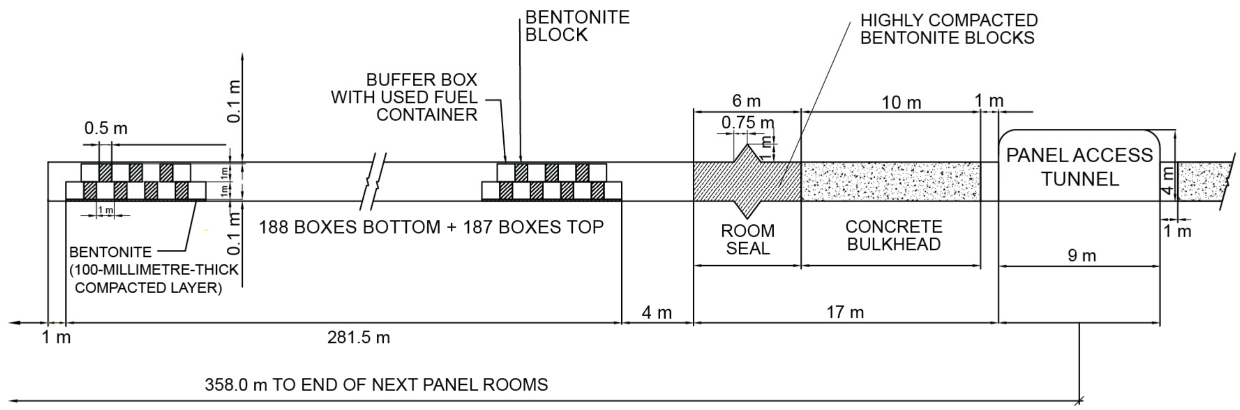

Figure 4-15: Placement Room Longitudinal Section

4.8.2 Placement Room Geometry and Spacing

The size of the buffer box and the placement equipment determines the placement room dimensions and profile. These factors and the need to minimize stresses (to maximize rock stability) were addressed by using room cross-section geometry with a height of 2.2 m and a width of 3.2 m (Figure 4-16).

The sealing materials used in placement rooms are:

- HCB blocks which surround the used fuel containers inside the buffer boxes;
- HCB blocks which act as 0.5-m-thick spacers between the buffer boxes; and
- Gap fill which is placed on the floor before start of placement activities and in the nominal 100-mm-thick gap between stacks of buffer boxes and spacer blocks and the rock wall and roof.

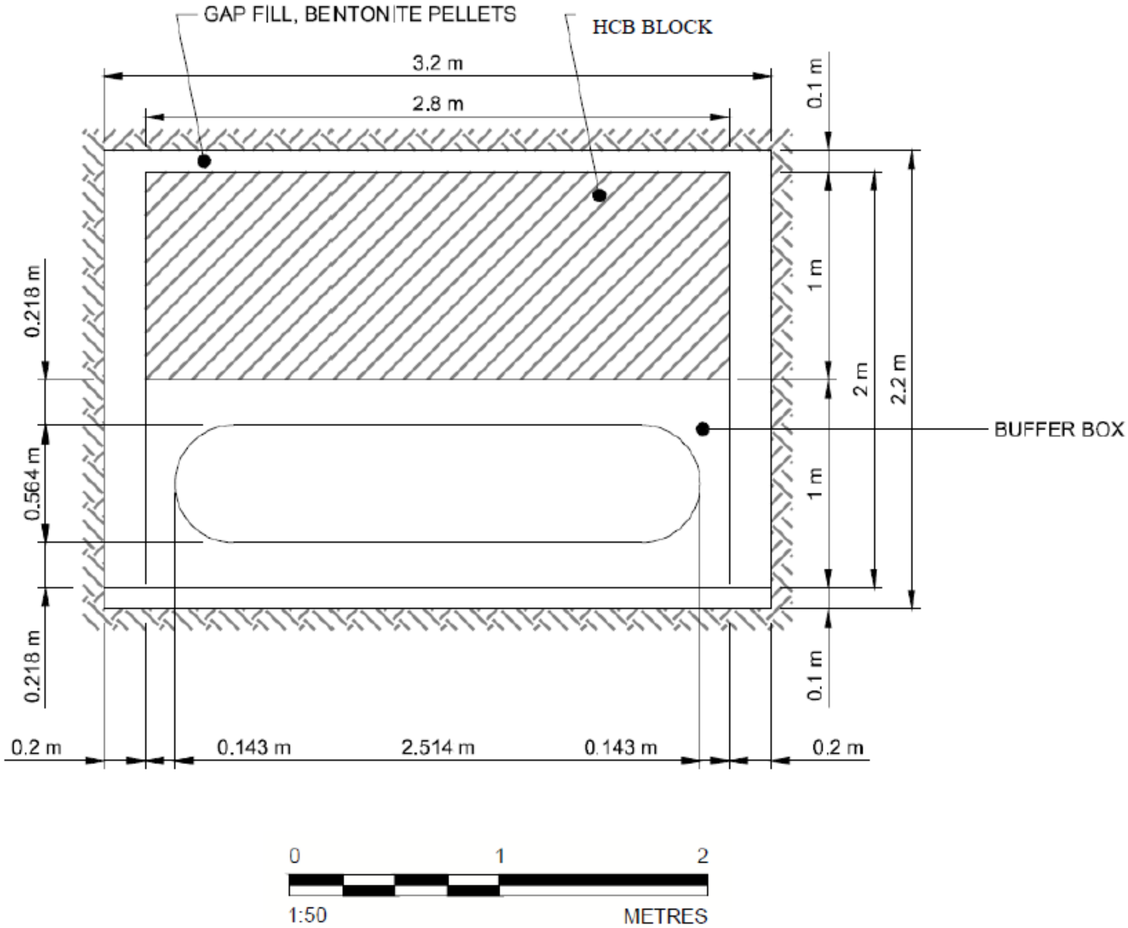

Figure 4-16: Placement Room Geometry (Vertical Section)

Thermal analyses were conducted to establish the temperature regimes for both the engineered barriers and the geosphere. The thermal analysis results were used to optimize both room spacing and container spacing. These parameters were chosen to ensure that the temperature at the container surface will not exceed 100°C at any time. To meet this requirement, the centre-to-centre spacing of placement rooms was set at 20 m and the centre-to-centre spacing of buffer boxes was set at 1.5 m.

Regardless of the room geometry and spacing, some excavation damage is expected to occur in the rock around placement rooms. However, the maximum depth of the damaged zone is not expected to exceed a few tens of centimeters.

Although it is expected that rock support will not be required inside the placement rooms, there may be minor amounts of metal rock bolts and screens used to stabilize excavated walls and ceilings for worker safety.

4.8.3 Placement Room Closure

Once the placement room has been filled with buffer boxes, the room will be closed with a bentonite room seal and concrete bulkhead. This room closure would permit physical isolation of the regions where container emplacement has been completed, improving security and permitting the continued use of the tunnels and access ways for ongoing repository operations in adjacent rooms. The major components of the placement room sealing system are illustrated in Figure 4-17.

Before the room seal is constructed a 4-m length of room between the last stack of buffer boxes and the start of the room seal will be filled with HCB spacer blocks. The void space around the 0.5-m-thick HCB blocks will be filled with gap fill material similar to the process used during buffer box placement.

Upon completion of these activities, a 6-m-thick bentonite room seal will be constructed at the entrance of the placement room. The seal will be constructed with HCB blocks and bricks, as illustrated in Figure 4-17 (HCB blocks in red, HCB bricks in green). The HCB bricks will be placed to create a wedge-shaped ring designed to interrupt the continuity of the excavation damage zone. The void space around the HCB blocks will be filled with gap fill material in parallel with the block placement process.

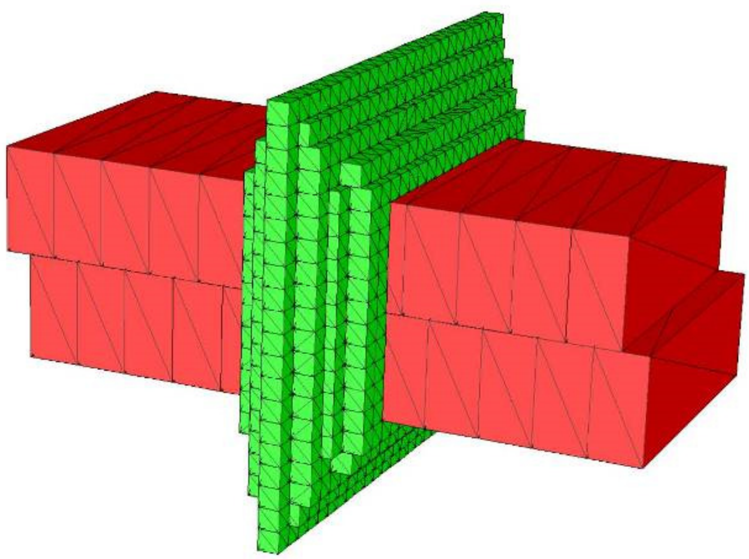

Figure 4-17: Room Seal

After HCB blocks and bricks have been placed, a thick bulkhead of low-heat, high-performance concrete (see Figure 4-15) will be constructed. The purpose of the bulkhead is to provide mechanical restraint against the forces exerted by swelling clay sealing materials. The bulkhead will thereby act to keep the sealing materials isolated in their intended positions while the access tunnels remain unfilled.

4.8.4 Ventilation System

The repository ventilation system utilizes the three shaft complexes and a combination of parallel airways for intake and exhaust. Underground booster fans, ventilation doors and dampers are used to control the airflow distribution. Since the primary repository ventilation system consists of relatively large airways, the overall circuit can be described as having relatively low resistance characteristics in a push-pull type network. Two parallel surface fresh air fans supply air to the main shaft. Air is heated as required during winter months. The fresh air supply reaches the repository level at the main shaft station and is split to the underground services area and the panels of placement rooms. A portion of the exhaust air flow is routed to the service shaft by an exhaust booster fan, installed underground at the service shaft station. The return air is exhausted to atmosphere via service shaft by one exhaust fan installed on the surface in the service shaft area.

The majority of the exhaust air from the repository area is routed to the ventilation shaft by two exhaust booster fans, installed underground in a parallel configuration at the shaft station. Return air is exhausted to atmosphere by two parallel exhaust fans installed on the surface in the ventilation shaft area.

Air distribution in the repository is promoted through the use of fans and regulators. The system will be operated to ensure that the underground work is performed in a fresh air supply stream with the exhaust being directed through unoccupied areas, going generally from clean areas towards operation areas.

During development of individual placement rooms, auxiliary fans will be installed near room entrances to deliver air via ducting to the working face in the rooms. The fans will provide approximately 6 m^3/s of air to the room face and the air will exhaust via cross-section of the room. During operations, the rooms will be ventilated by auxiliary fans in an exhaust configuration where air will be extracted from the working face via a rigid metal duct system. For used fuel container placement activities, the required supply flow per room is expected to be 2 m^3/s. The exhaust air during both room development and operations will be carried to a perimeter tunnel, and then to the underground booster exhaust fans located at the base of the ventilation shaft.

For the purpose of this conceptual design, stand-by HEPA filtration systems are assumed to be installed at the service shaft and ventilation shaft stations only.

4.9 Site Preparation and Construction of the Repository

Implementation of a deep geological repository falls under federal jurisdiction. It will be regulated under the NSCA and its associated regulations as described in Chapter 1, Section 1.5. The following sections describe the site preparation and construction work to be performed at the DGR site.

4.9.1 Site Preparation

Initial site preparation activities, which include clearing and grading, establishing access roads and the installation of basic infrastructure systems would be conducted. The site infrastructure required to support excavation, including electrical delivery systems, headframes, ventilation and excavated rock management systems would also be established.

4.9.2 Shaft Sinking

Controlled construction methods will be used to minimize disturbances to the area surrounding the facility. The three shafts will be developed using a controlled drill and blast shaft sinking approach specifically designed to minimize the excavation damage zone. The shaft sinking process will involve the following steps:

- Collaring or starting the shaft;
- Setting up the equipment needed to sink the shaft;
- Sinking the shaft to its full depth using the drill and blast method; and
- Dismantling the equipment used for sinking.

Conventional blasting operations include drilling blast holes in a converging pattern designed to minimize the quantity of detonated explosive per volume of rock. In order to reduce damage to the perimeter of the opening, a larger number of blast holes with smaller individual explosive charges are used in the outer region of the shaft. This is usually referred to as contour wall blasting, and it will be used to minimize the thickness of the excavation damage zone. Between the blasting cycles, fumes are vented, scaling is done to remove loose rock and ground support is applied as required. This excavation method is expected to result in a rate of advance in the range of 2.5 metres to 3.5 metres per day.

4.9.3 Underground Demonstration Facility

An Underground Demonstration Facility (UDF) will be constructed at the DGR site. Studies that would be conducted as part of the UDF include verification of geological conditions, demonstration of applicable procedures for management of used fuel containers and sealing materials, long-term studies of engineered barrier materials, monitoring instrumentation and ground support system and/or monitoring of specially instrumented emplaced containers.

The UDF is a stand-alone testing location near the Main and Service Shafts. The UDF will be constructed as soon as possible after the Service Shaft reaches the shaft station and a rock handling system is installed. The UDF would operate on a stand-alone basis for about 5 years prior to start of operations and would continue to operate over the complete life of the repository.

The UDF will be designed to integrate with the overall underground repository but will be located so as to be separate from the placement rooms with respect to the test room activities. This will ensure that facilities common to both the UDF and the repository are centrally located to both operations.

The test room excavation work in the UDF will provide an opportunity to demonstrate and refine drilling and blasting techniques intended for the placement rooms. In order to minimize potential pathways for groundwater movement after closure, and to reduce the use of ground support in the placement rooms and tunnels, the blasting damage in the rock surrounding the created openings needs to be minimized. This EDZ can be controlled through the use of careful excavation techniques. Detailed mapping of the rock after excavation, and correlation of the EDZ thickness to the blast-hole pattern and blasting techniques (for example) will ensure that the methods adopted meet all requirements. Excavation methodologies for the various underground openings can, therefore, be optimized.

Geoscience verification activities will be carried out in the UDF and at other locations in the underground repository for the purpose of verifying assumptions and geoscience data used in the safety case. In particular, data will be gathered to confirm that the host rock formation will be able to act as a long-term barrier and will be able to contain and isolate the used fuel. The results of these geoscience investigations and monitoring activities will be used in the application seeking approval for full construction of the repository, and eventually in the application for an operating licence.

The UDF would support the long-term demonstration and monitoring of container placement and sealing systems, and will provide a training area for DGR employees. The test placement rooms would be available for prototype equipment testing five years before the repository is operational.

4.9.4 Lateral Development

The remaining underground excavations, like access tunnels and panels, will be constructed by controlled drilling and blasting after the UDF.

4.9.5 DGR Facility Commissioning

The DGR facility will be commissioned once initial construction of the underground repository is complete.

4.10 Repository Operation

During repository operations, panel development and used fuel placement operations will be performed concurrently and will move from the ventilation shaft end towards the main shaft end of the repository. Retreating towards the main shaft will minimize the need for personnel to enter or pass by completed repository areas. The excavation of new panels will take place as far as possible from the container placement operations which will minimize any possible effects of the excavation activities on container placement operations. The repository development/operation strategy will optimize efficiency while considering both safety and operating factors (e.g., vehicle traffic and ventilation) as well as the potential interactions between repository development and operations.

Each placement room panel will require about 3 years for development to be completed. Placement activities in each panel are expected to require from 3.5 to 4 years. The repository operations will continue until all used fuel has been repackaged in used fuel containers and buffer boxes, all buffer boxes placed into rooms and all placement rooms sealed. This is expected to take about 40 years for a used fuel inventory of 4.6 million bundles.

The following sections describe the preparation of placement rooms to receive buffer boxes (with UFCs), equipment to be used for placement of buffer boxes and the sequence of placement operations.

4.10.1 Preparation of Placement Room

After excavation work is complete and prior to the start of buffer box placement operations the room will be prepared by first placing a 100-mm-thick levelling layer of bentonite pellets on the room floor. Temporary metal plates will be installed on top of the bentonite layer to facilitate equipment access to the work face. The metal plates will be placed over the full length of the room to the near end of the room. The temporary metal plates will have a metal ventilation duct integrated into the design of the plate. Fresh air is delivered into the placement room via the room cross-section. The air is then exhausted ("pulled") from the room via ventilation ducts which remove heat and dust from the room. As placement operations retreat from the end of the room toward the room entrance, the floor plates will be removed to allow stacking of buffer boxes directly on top of the bentonite layer.

4.10.2 Buffer Box Placement

The UFCs will be assembled into buffer boxes inside the UFPP (see Figure 4-6). Fully assembled buffer boxes will be staged inside the UFPP awaiting transfer to the main shaft. After final inspection, each buffer box will be loaded into a shielded transfer cask and then the cask will be loaded onto a rubber-tired trolley. Using a tow vehicle, the trolley with transfer cask will be moved into and secured within the main shaft cage. Upon arrival at the repository level, the trolley with transfer cask will be removed from the cage by another tow vehicle and taken to the shielding canopy at the entrance of a placement room.

Once the transfer cask is mated to the access window of the shielding canopy, an ejection ram will push the buffer box out of the cask onto the placement vehicle waiting inside the shielding canopy. The unmanned and remote-controlled placement vehicle will travel the length of the placement room to the final placement location. Radiation protection controls will be in-place to deny workers entry in the room to protect them from the radiation fields emitted from the UFCs. After two buffer boxes have been stacked, two spacer blocks will be stacked by procedures similar to those used to place the buffer boxes. After two buffer boxes and two spacer blocks are placed, then placement operations will be temporarily stopped to allow placement of gap fill (bentonite pellets).

The placement vehicle will exit the placement room through the shielding canopy. The bentonite pellet placement equipment will enter the placement room and perform the pellet placement operation – injecting loose bentonite pellets in the void spaces between the stacked buffer boxes and dense backfill blocks, and the rock wall. Due to presence of radiation fields, the bentonite pellet placement operation must also be remotely-controlled.

After the bentonite pellet placement equipment has exited the placement room, the placement vehicle, equipped with a magnetic floor plate removal system, would enter the placement room through the shielding canopy, and remove a floor plate segment and then exit the room.
It is expected that the entire buffer box placement process will take approximately four hours per box. Further, it is anticipated that each phase of the process will take four operators to complete (connecting and operating equipment, etc.). Placement operations must be performed concurrently within three rooms in order to achieve a throughput of 2,500 buffer box per year.

4.10.3 Description of Placement Equipment

The key equipment that will be used in the placement operations are described in this section.

Buffer Box Placement Vehicle: This remotely-controlled underground vehicle is based on a highly customized commercial electric forklift with various enhancements including built-in remote operation sensing, lighting, and camera equipment as well as a customized lifting attachment to accommodate the buffer boxes and spacer blocks. It will also have an attachment for removal of the floor plates.

Shielding Canopy: The mobile shielding canopy will permit shielded activities to take place inside rooms, while also allowing use of the panel access tunnel by passing vehicles and personnel. The small void space around the canopy perimeter can be covered by manually placed lead shielding packs to ensure radiation does not escape through the gap between the shield and rock.

The canopy has shielded hinged access doors for vehicle access. It also includes a shielded access window which, when opened, allows passage of buffer boxes and dense backfill spacer blocks.

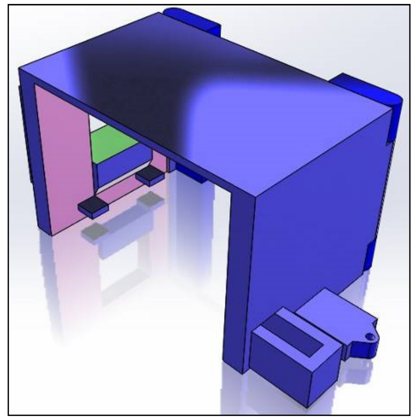

Figure 4-18: Shielding Canopy

Bentonite Pellet Injection System: After two buffer boxes and two spacer blocks are placed, all void spaces around the boxes and blocks will be filled with loosely-placed bentonite pellets (gap fill). The bentonite placement system will be mounted on a vehicle that is similar to the placement vehicle and it will use a pneumatic or auger insertion system for placing loose bentonite.

Floor Plates with Ventilation Ducts: The floor plates will be installed before the start of buffer box placement activities. As placement activities progress towards the room entrance, segments of floor plates will be removed. A magnetic attachment on the placement vehicle would be used to pick up the plate segments and bring them out of the placement room.

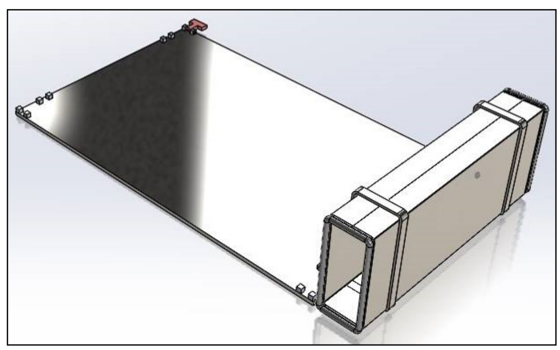

Figure 4-19: Floor Plate with Built-in Ventilation Duct

4.10.4 Storyboard Description of Preparation and Placement Operations

Graphical storyboards showing key steps in room preparation, and the transfer and placement of the buffer boxes are provided in the following figures. Figure 4-20 provides a summary of the placement equipment. Figure 4-21 illustrates, step-by-step, all activities that are required to prepare each room for the receipt of buffer boxes. Figure 4-22 illustrates the steps that would be taken to place the buffer boxes inside a placement room.

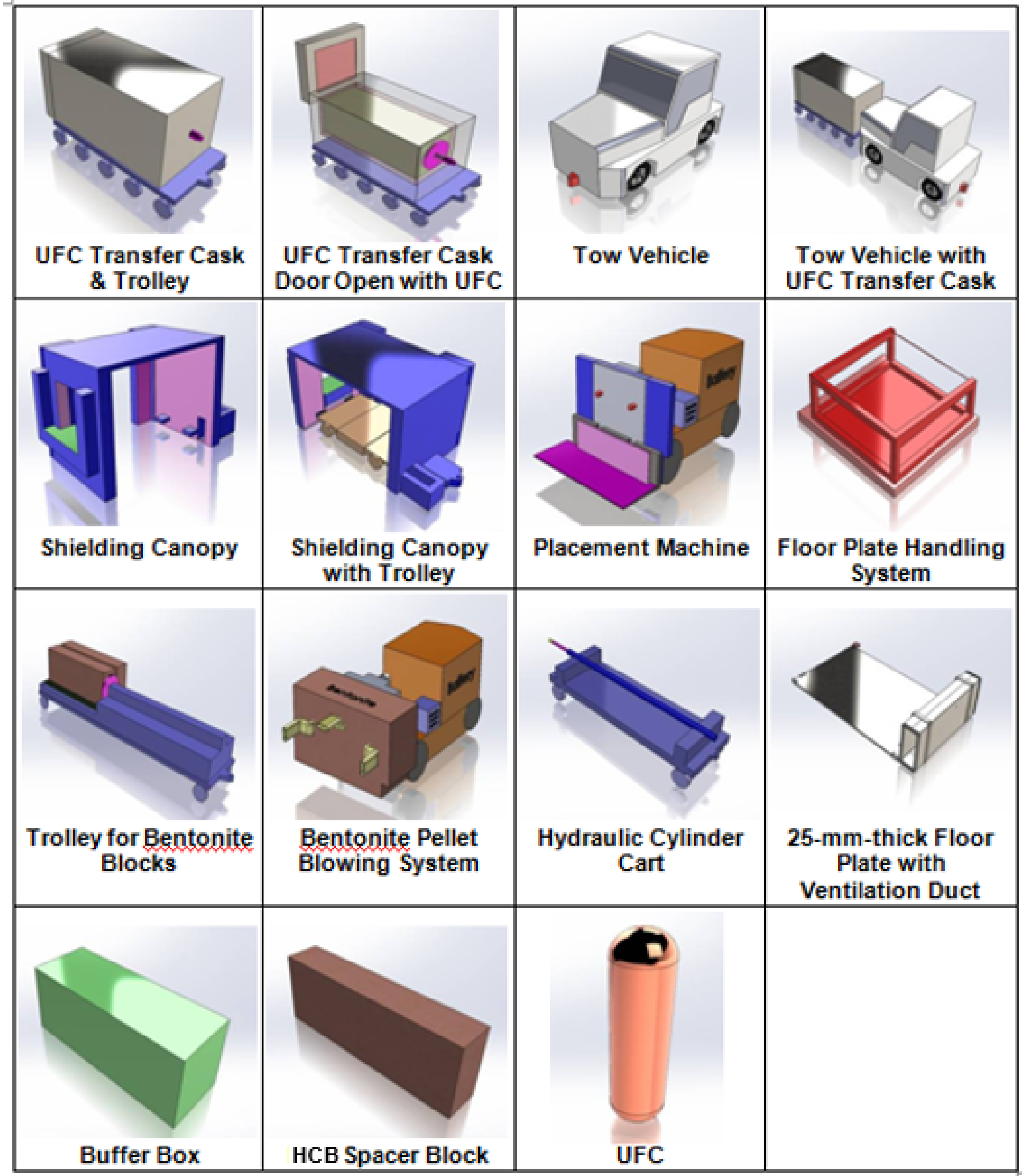

Figure 4-20: Legend for Container Placement Equipment

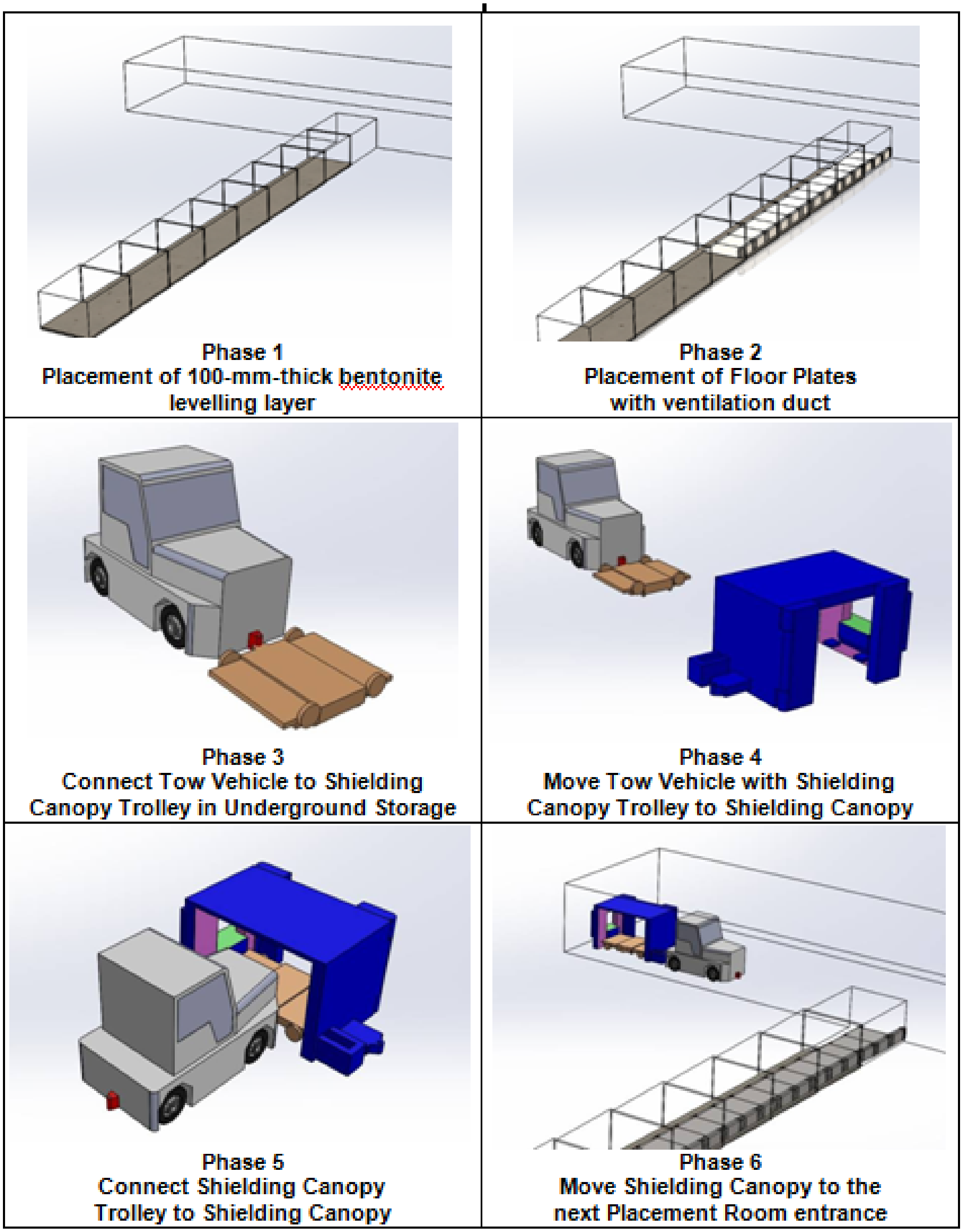

Figure 4-21: Preparation of Placement Room & Shielding Canopy

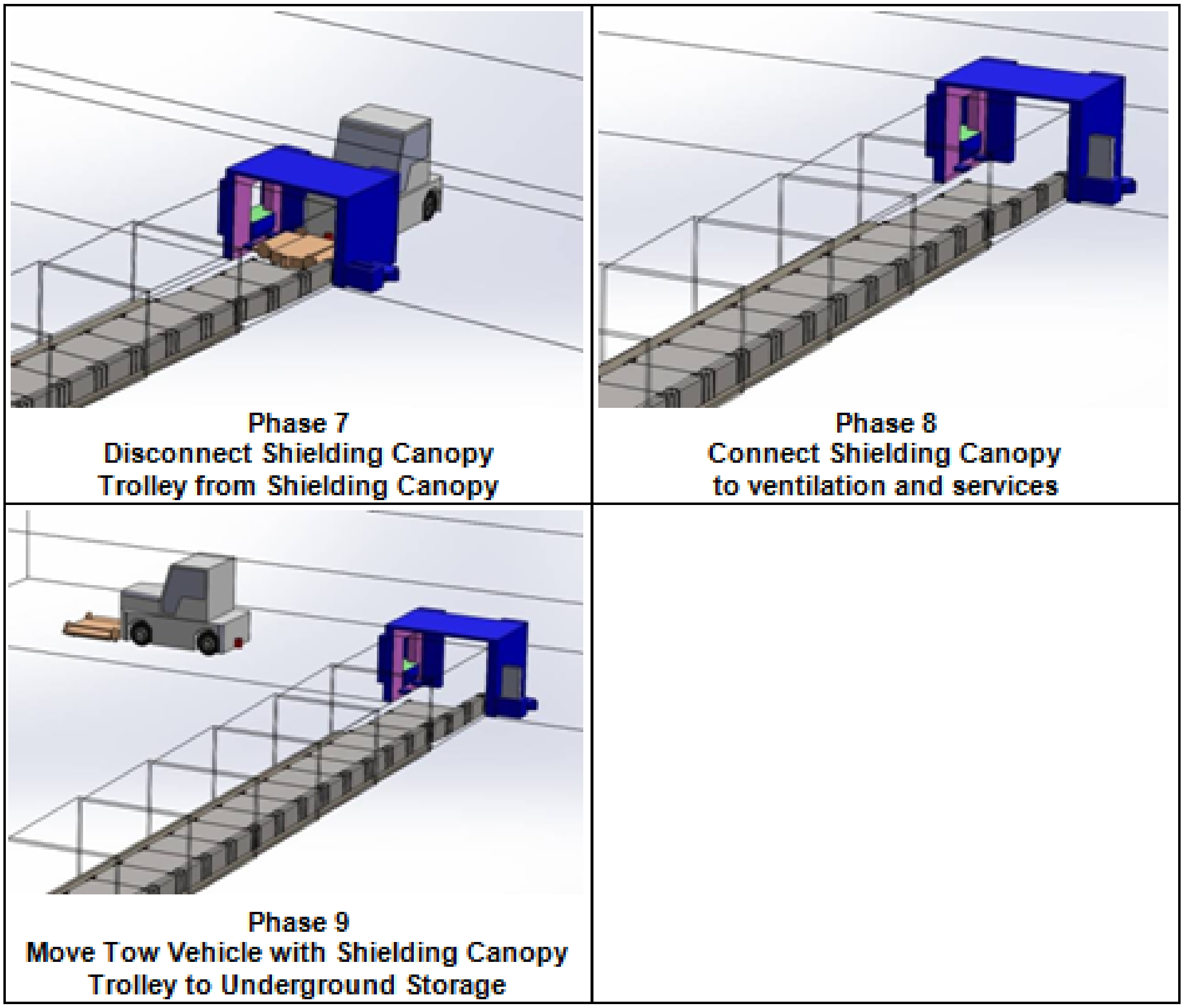

Figure 4-21: Preparation of Placement Room & Shielding Canopy (concluded)

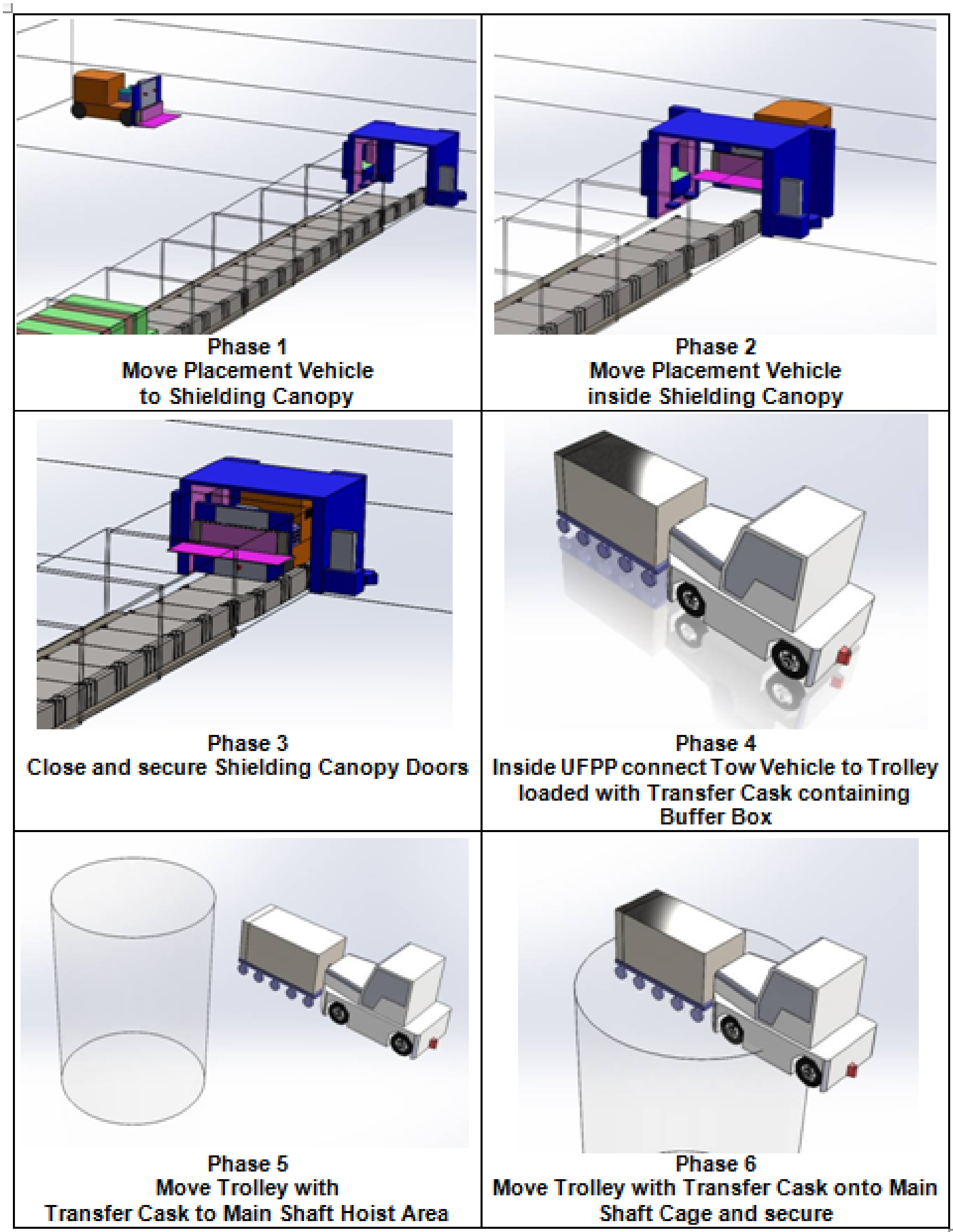

Phase 1
Move Placement Vehicle
to Shielding Canopy

Phase 2
Move Placement Vehicle
inside Shielding Canopy

Phase 3
Close and secure Shielding Canopy Doors

Phase 4
Inside UFPP connect Tow Vehicle to Trolley loaded with Transfer Cask containing Buffer Box

Phase 5
Move Trolley with
Transfer Cask to Main Shaft Hoist Area

Phase 6
Move Trolley with Transfer Cask onto Main Shaft Cage and secure

Figure 4-22: Container/Buffer Box Placement

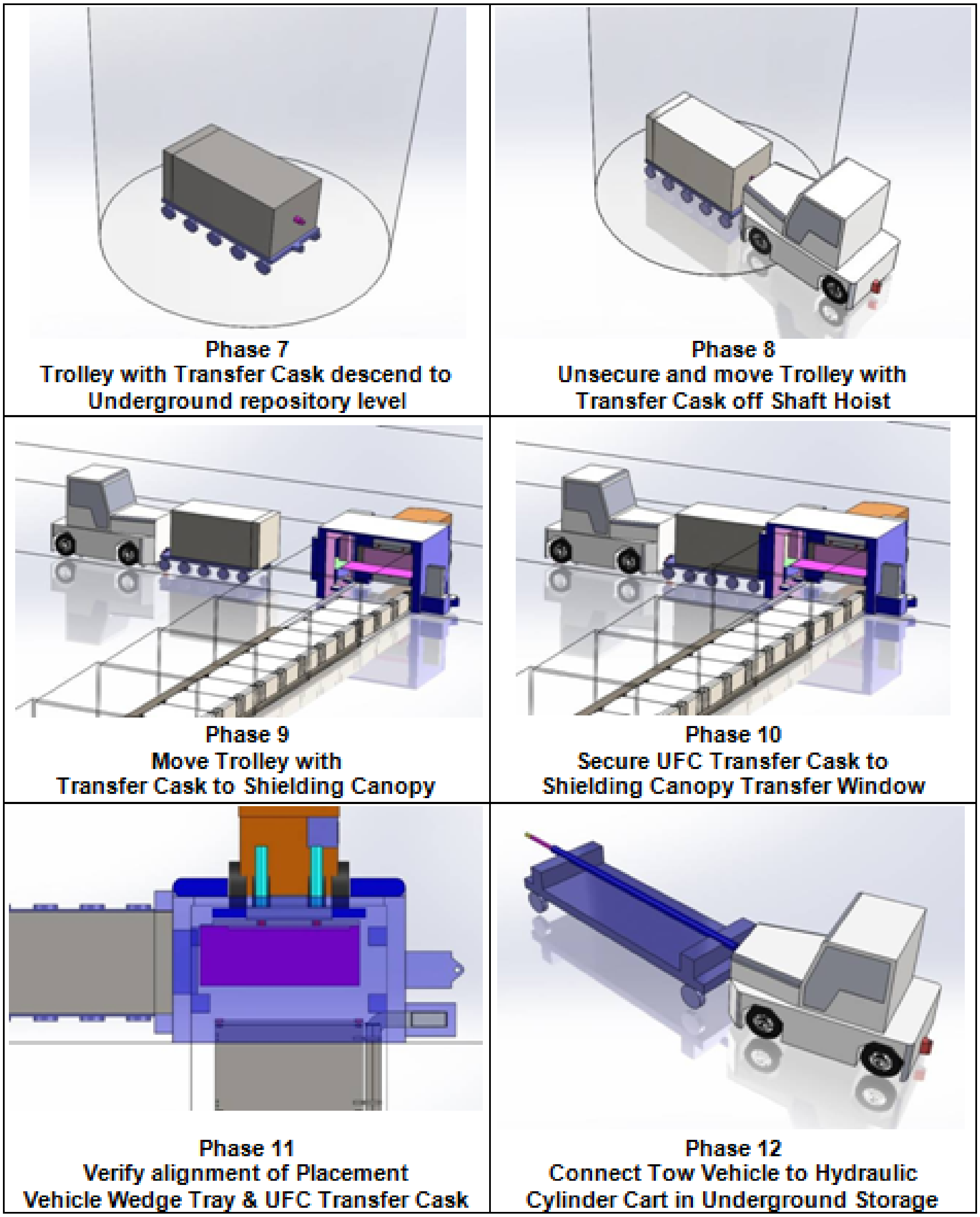

Figure 4-22: Container/Buffer Box Placement (continued)

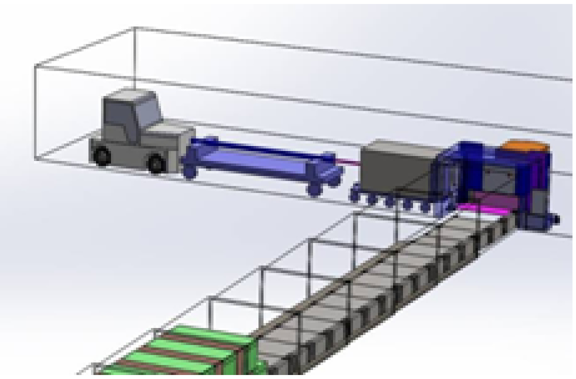

Phase 13
Move Hydraulic Cylinder Cart to
Transfer Cask at Shielding Canopy

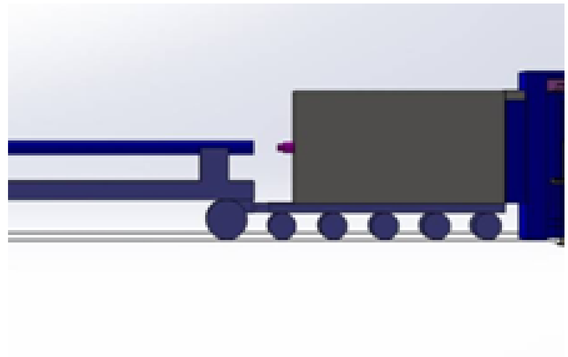

Phase 14
Connect Hydraulic Cylinder
Cart to Transfer Cask Trolley

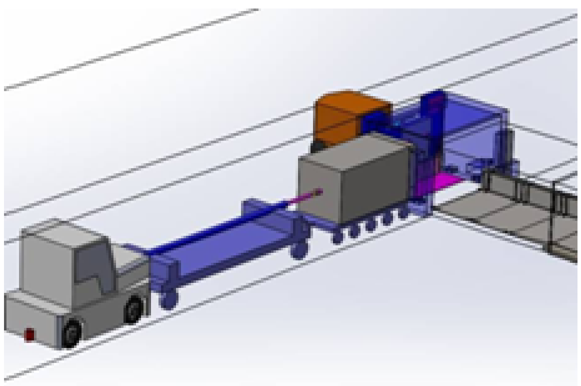

Phase 15
Connect Hydraulic
Cylinder Cart to Services

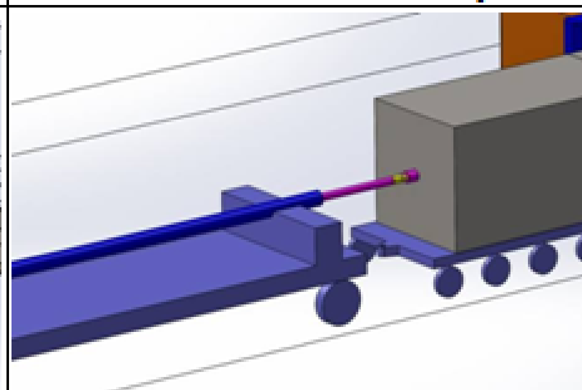

Phase 16
Install Coupling between Cylinder
and Ram on Transfer Cask

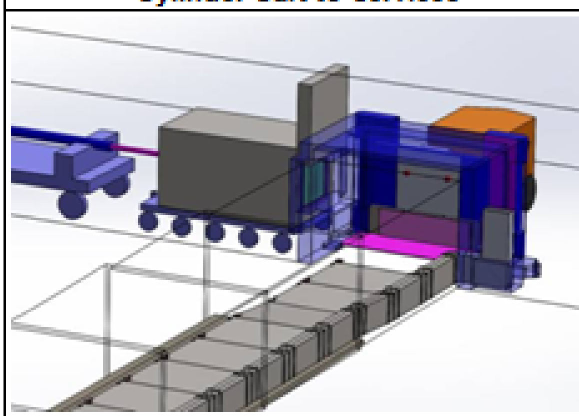

Phase 17
Open Transfer Cask Shielding Door

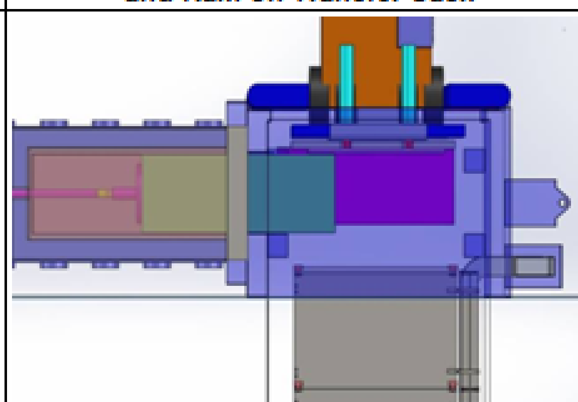

Phase 18
Push Buffer Box from Transfer Cask on low
friction liner and window opening support

Figure 4-22: Container/Buffer Box Placement (continued)

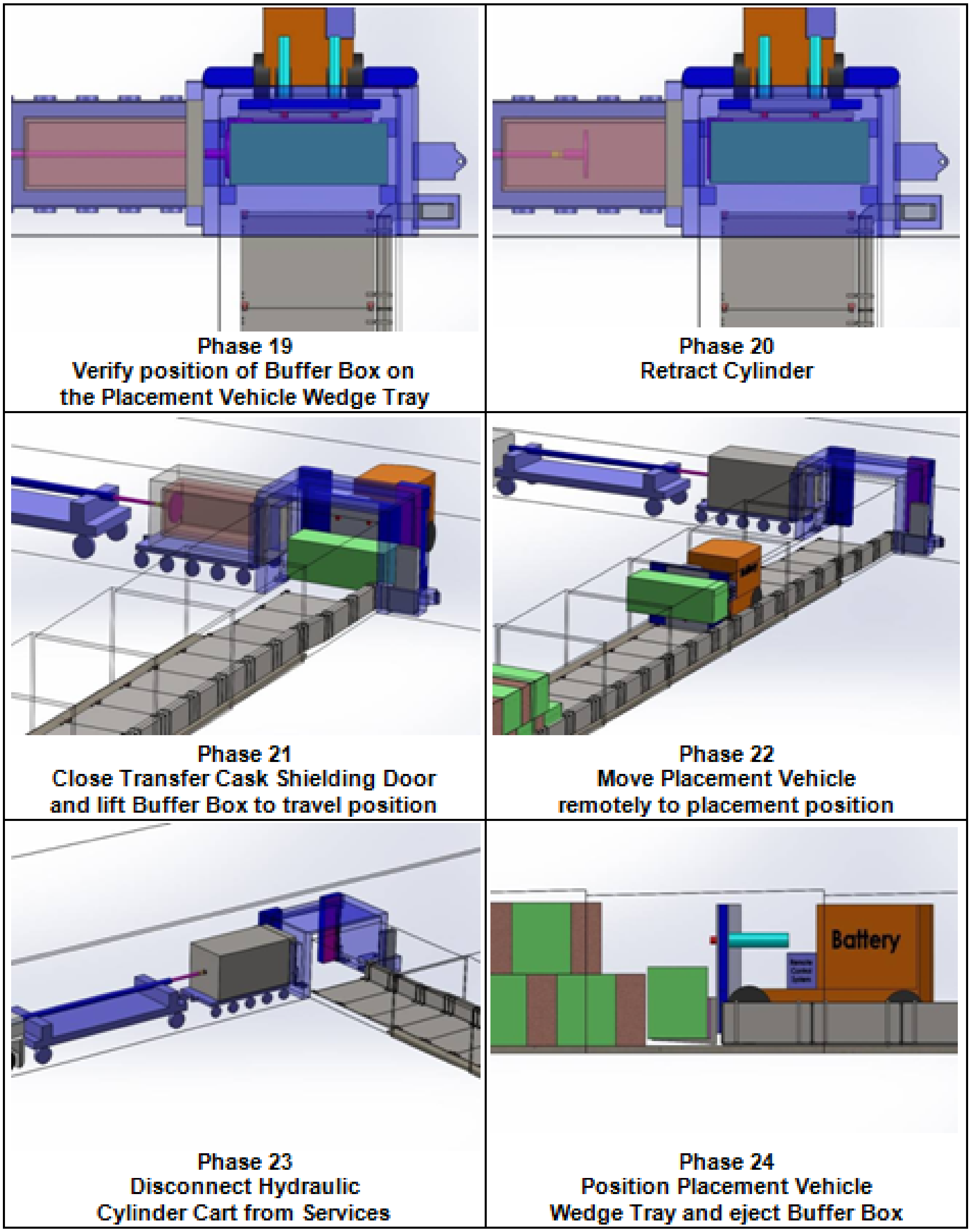

Figure 4-22: Container/Buffer Box Placement (continued)

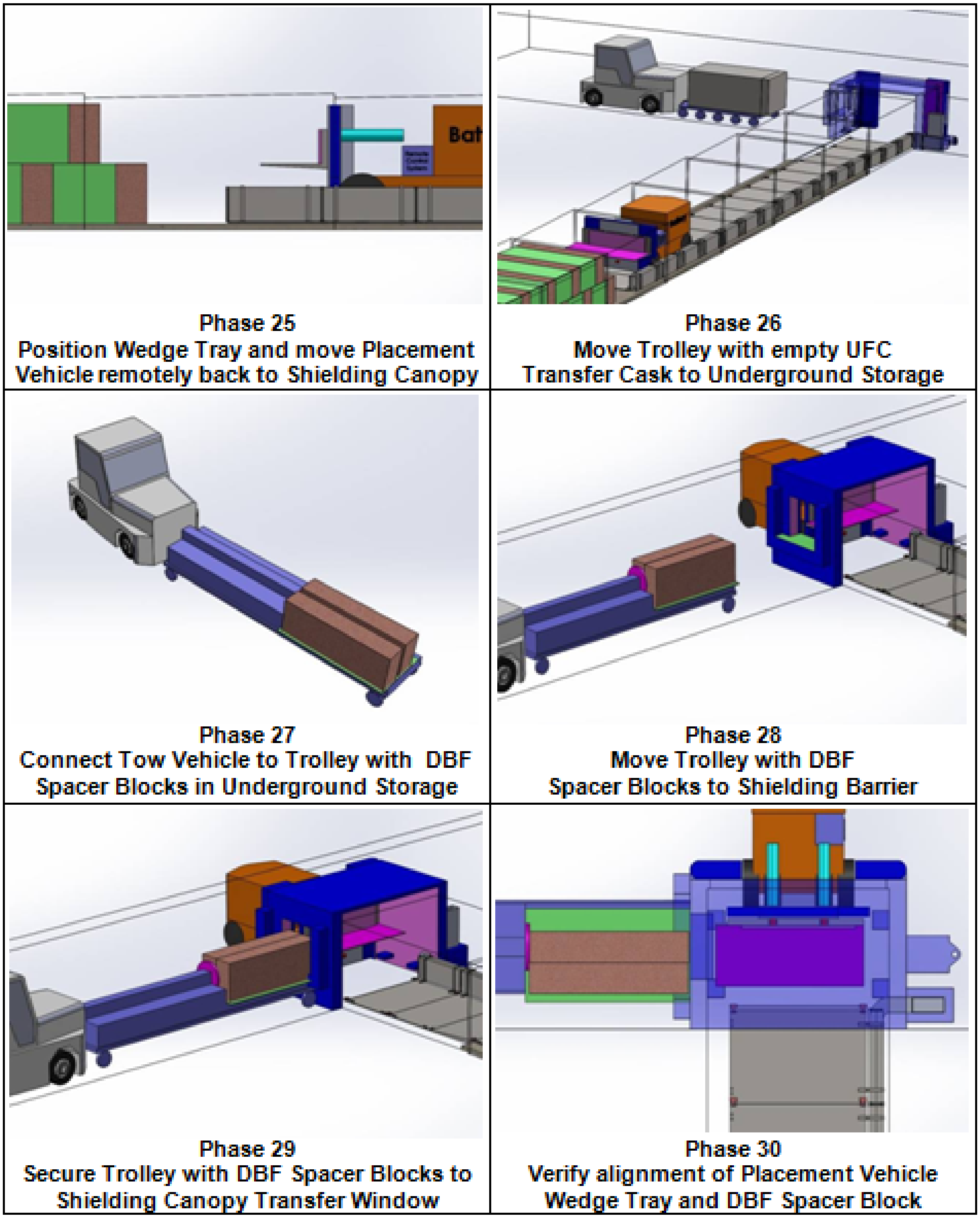

Figure 4-22: Container/Buffer Box Placement (continued)

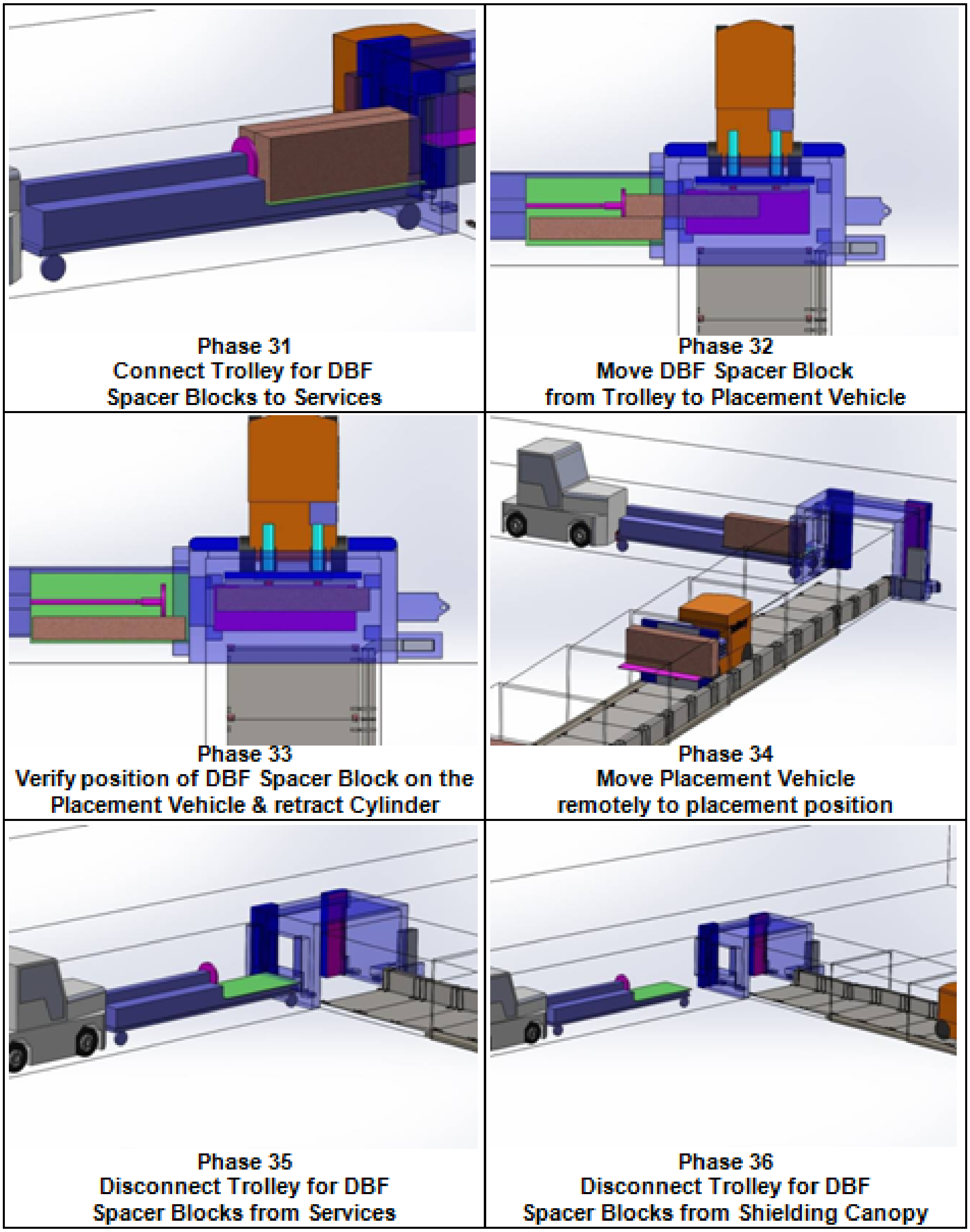

Phase 31
Connect Trolley for DBF Spacer Blocks to Services

Phase 32
Move DBF Spacer Block from Trolley to Placement Vehicle

Phase 33
Verify position of DBF Spacer Block on the Placement Vehicle & retract Cylinder

Phase 34
Move Placement Vehicle remotely to placement position

Phase 35
Disconnect Trolley for DBF Spacer Blocks from Services

Phase 36
Disconnect Trolley for DBF Spacer Blocks from Shielding Canopy

Figure 4-22: Container/Buffer Box Placement (continued)

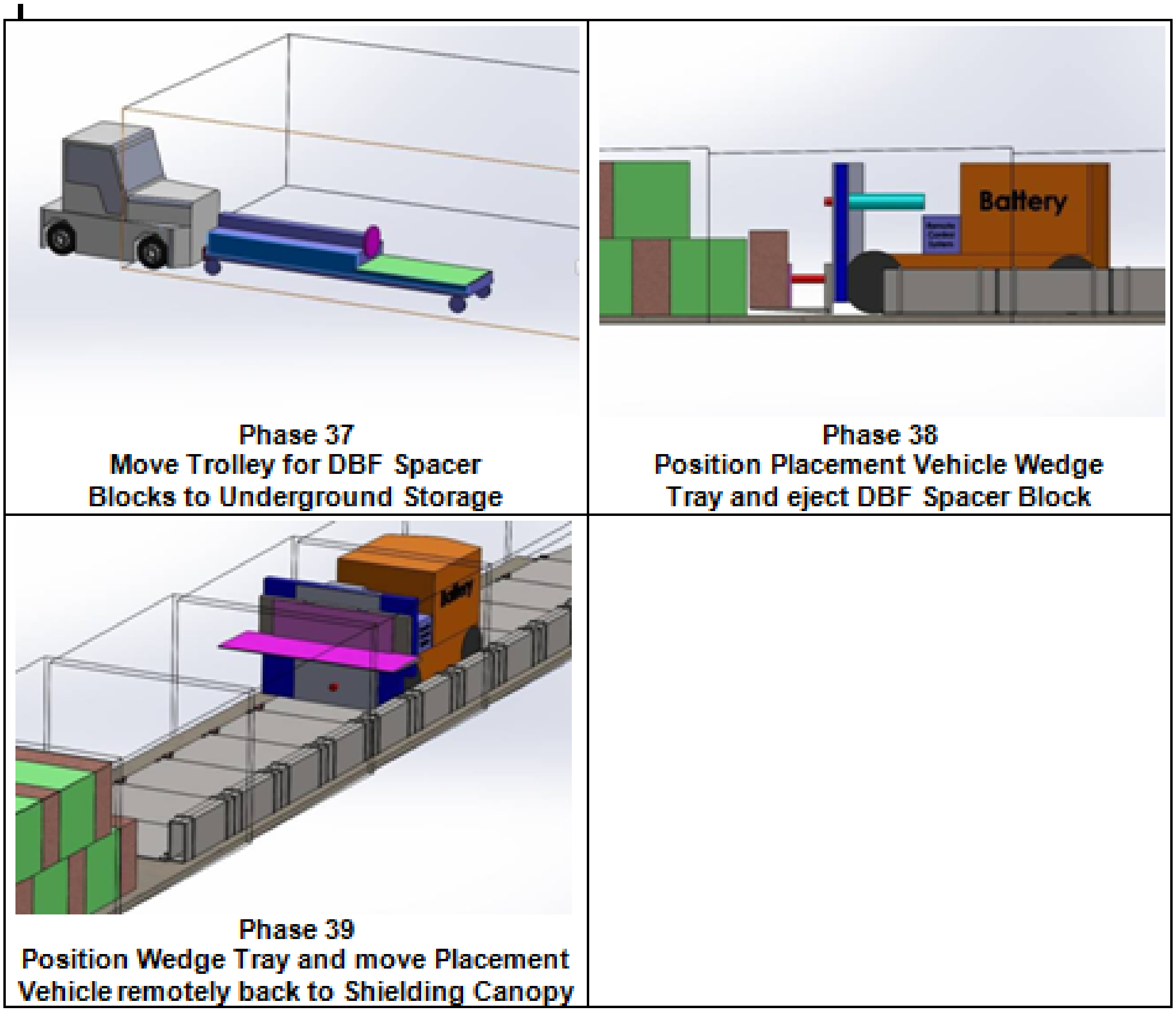

Figure 4-22: Container/Buffer Box Placement (concluded)

4.10.5 Environmental Monitoring Programs

Prior to start of construction the environmental monitoring program will collect data to establish baseline conditions. Thereafter, the program will monitor for any changes that may be imposed on the environment due to construction activities and ultimately the operation of the DGR facility. Monitoring requirements for the postclosure period will need to be re-examined as part of the final plan for decommissioning and closing the site.

The environmental monitoring program will be comprised of the following components:

- Radiological monitoring;
- Groundwater quality and levels monitoring;

- Monitoring of surface water and storm water;
- Air quality monitoring; and
- Meteorological monitoring

The final elements will be developed as part of the formal licensing process for the DGR. The expectation is that the program will provide reliable, accurate and timely data in a fashion that is easily audited.

4.11 Extended Monitoring

Upon completion of used fuel container placement activities all placement rooms will be sealed and closed, but the access tunnels and shafts will remain open. The facility will be placed in an extended care and maintenance program during which monitoring of the repository and surrounding geosphere will continue to confirm the performance of the repository system. The extended monitoring period could have a duration of several decades.

4.12 Decommissioning and Closure

Following the receipt of regulatory approval and the licence to decommission and close the DGR facility, underground facilities are expected to be removed first, in parallel with those surface facilities not required to support the remaining underground decommissioning and closure activities.

Decommissioning of underground facilities involves the removal of operational systems and furnishings, the interim installation of temporary services and furnishings, and the repair and preparation of exposed rock surfaces for sealing. As currently envisaged, the decommissioning and closure activities will be carried out in several stages and will include activities related to removal of material handling systems, the sealing of underground horizontal openings, and the sealing of shafts and boreholes.

As the repository saturates, the sealing materials will swell, forming dense, low-permeability seals throughout the underground repository and in the shafts. These seals will isolate and contain the used fuel located in the placement rooms. The following sections describe the decommissioning and closure of various underground horizontal openings and the three shafts. Descriptions of the sealing materials to be used for the closure of the underground repository are presented in Section 4.3.2.

4.12.1 Sealing of Underground Horizontal Openings

The sealing of underground horizontal openings consists of closing off access tunnels and ancillary facilities. Such activities would commence with the removal of instrumentation and sealing of the boreholes, followed by the preparation of exposed rock surfaces and removing loose rock before backfilling and sealing. The access tunnels would then be backfilled with dense backfill blocks and light backfill, and tunnel bentonite seals with associated concrete bulkheads would be installed at strategic locations. All sealing materials would be created in the sealing materials compaction plant and concrete batch plant.

The bentonite tunnel seals and associated concrete bulkheads would be located at strategic locations through the network of underground access tunnels. The tunnels seals and bulkheads would be designed similar to room seals and associated concrete bulkhead. The primary function of tunnel seals would be to limit fluid flow along the access tunnels.

4.12.2 Sealing of Hydraulically Active Zones

The most robust sealing arrangements in access tunnels would be required at locations where tunnels intersect hydraulically active regions in the rock. A possible seal arrangement including grouting is shown in Figure 4-23. The seals and bulkheads would be required to withstand rapidly developing hydraulic pressures. The properties of clay-based seals and the concrete are presented in Tables 4-2 and 4-3, respectively.

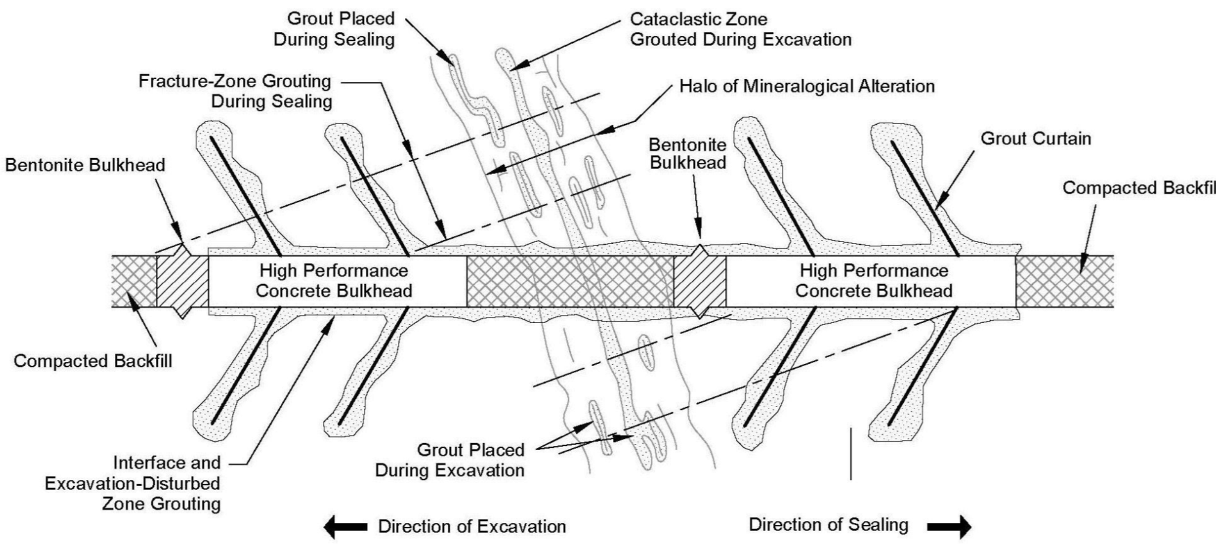

Note: Figure is not to scale.

Figure 4-23: Illustrative Tunnel Plug in a Hydraulically Active Region

4.12.3 Sealing of Shafts

Sealing of the shafts is the last step in the closure of the underground repository. This activity starts after sealing of underground tunnels and ancillary areas is complete, and when the concrete monolith has been constructed in underground openings around the base of each shaft. At that time, the following activities will take place:

- Removal of shaft services including compressed air lines, water lines, power supply, lighting and communication cables;
- Removal of instruments and sealing of any impacted geological investigation boreholes;
- Removal of furnishings including all of the shaft guides and sets, steel support brackets, brattice and lower crash beam assemblies from bottom to top while backfilling;

- Reaming of the shafts (as required) to remove the concrete linings and any degraded wall rock. It is assumed that approximately 0.5 m of rock will be removed from the shaft walls to expose the sound rock; and
- After each shaft is re-equipped with services and staging, placement of sealing materials in each shaft will be initiated.

The proposed design for a shaft seal system is described in Table 4-6. The final design for the shaft seals will depend on the geological conditions of the site. The approach for the shaft seal design focuses on the use of simple, relatively well understood and durable materials, and use of proven methodologies for placement. The shaft seal system consists primarily of a column of compacted bentonite/sand. Sand and bentonite are durable natural materials (see Chapter 9). An asphalt column or HCB may be placed above the first bentonite/sand layer to provide a redundant low permeability sealing material against upward or downward fluid flow. Concrete bulkheads could be used to provide structural components to the column and provide additional (early) sealing capability.

Table 4-6: Proposed Sealing System for Shafts

Depth from Surface	Material
0 – 20 m	Low-heat high-performance concrete– concrete cap at surface
20 – 150 m	Shaft backfill - 70/30 bentonite/sand mixture compacted in-situ
150 – 170 m	Low-heat high-performance concrete for concrete bulkhead keyed into rock / overburden to a distance of 0.5 times the original radius of the shaft
170 – 330 m	Shaft backfill - 70/30 bentonite / sand mixture compacted in-situ
330 – 380 m	Asphalt or highly-compacted bentonite seal
380 – 480 m	Shaft backfill - 70/30 bentonite / sand mixture compacted in-situ
480 – 500 m	Concrete monolith – Low-heat high-performance concrete

The shaft sealing system presented in Table 4-6 is based on the assumption that all shafts will intersect low permeability rock over the full depth of the shafts. However it is possible that the DGR shafts will intersect relatively permeable rock near ground surface. If so, then engineered fill material based on rock excavated during shaft sinking or some other suitable material will be used in the upper portion of each shaft. This engineered fill would likely be placed from surface to a depth where low permeability rock is first encountered.

The shaft seal design concept in Table 4-6 has focused on the use of simple, relatively well understood and durable materials, and use of proven methodologies for placement. Concrete, bentonite/sand mixture and asphalt will be the sealing materials used in each shaft. All shaft sealing materials, except asphalt, would be created in the sealing materials compaction plant (Section 4.6.1) or the concrete batch plant (Section 4.6.2). Asphalt material would be imported to the site. Additional information about each major component of the shaft seal system is presented below.

Concrete monolith will be placed at the base of the seal system. The LHHP concrete will provide a stable foundation for the overlying seal materials (see Section 4.3.2 for properties). The monolith will be constructed in stages beneath each shaft. Each monolith will form a contiguous mass concrete structure with no structural reinforcement within the concrete. All services and utilities will be stripped out of the excavations to be filled by the monolith.

Shaft Backfill: The column of sealing materials in each shaft is largely composed of a compacted bentonite/sand mixture (see Table 4-6 for properties). The mixture will be created in the sealing materials compaction plant and then delivered to shaft as a bulk material. The mixture will be placed in layers and each layer will be compacted to achieve required density. As the compacted bentonite/sand materials saturate with groundwater from the surrounding rock, they will generate swelling pressures, which will aid in the development of a tight seal against the shaft wall and provide a confining pressure to the rock surface.

Asphalt Seal: An asphalt column may be placed above the lowermost bentonite/sand column. Immediately upon emplacement, the asphalt will create an effective barrier to water flow. Furthermore, the use of another low permeability sealing material provides an additional level of redundancy to the sealing system against upward or downward fluid flow.

Highly Compacted Bentonite Seal: As an alternative to the aforementioned asphalt seal, a seal comprised of HCB blocks would be constructed above the lowermost bentonite/sand column. Once saturated and the swelling is complete, this seal would create an additional level of redundancy to the sealing system against upward or downward fluid flow.

Concrete Bulkhead: The primary function of the LHHP concrete bulkhead will be to provide structural support in the column of sealing materials (see Section 4.3.2 for properties). In the short-term the concrete will act as an additional seal and over the long-term the ability to act as a seal will diminish as concrete degrades. As with the monolith, concrete for the bulkhead will be placed in mass and with no reinforcing steel, and using measures to control heat build-up. Contact/seal grouting will be applied around the bulkheads to minimize the potential impacts of shrinkage at the interface with the host rock formation. Concrete will be poured directly onto the bentonite/sand columns located below each bulkhead.

Concrete Cap: A surficial concrete cap will be installed on each shaft to minimize risk of human intrusion into the underground repository via shafts. The cap will be constructed using LHHP concrete (see Section 4.3.2 for properties). Air entrainment within the concrete is required to minimize adverse effects of freeze/thaw action on the concrete cap.

4.12.4 Sealing of Boreholes

Siting, construction, and operation of a repository would require the drilling of numerous exploration and monitoring boreholes, including those drilled from the ground surface in the vicinity of the repository and boreholes drilled from within the repository into the adjacent rock. As part of the final closure of the repository, all boreholes would be sealed to ensure that there are no direct paths for water movement between the repository and the surface environment. The borehole seals would be composite seals made of bentonite, sand and concrete. The borehole seal design would be adjusted, as needed, to compensate for hydraulically active regions in the adjacent rock.

The purpose of removing monitoring wells and then sealing the geological borehole is to inhibit groundwater movement and contaminant transport. A combination of cement-based materials and clay-based materials with low permeability and a high swelling potential will be installed as required to prevent the geological boreholes from becoming preferential transport paths.

4.12.5 End State

A minimized administration area will be maintained during the end of decommissioning to support the post-decommissioning monitoring systems. If at that time it is felt that permanent facilities are no longer required, the monitoring systems could be supported by small enclosures for the electrical equipment, and all other remaining facilities could be removed and the site essentially fully returned to greenfield conditions.

The facility's environmental monitoring carried out during the operational and extended monitoring periods as well as throughout the decommissioning stage may be continued following decommissioning and closure. The scope and duration of such tasks will be decided at the appropriate time by both regulatory entities and society at large.

4.13 References for Chapter 4

Baumgartner, P. 2006. Generic Thermal-Mechanical-Hydraulic (THM) Data for Sealing Materials – Volume 1: Soil-water Relationships. Ontario Power Generation Report 06819-REP-01300-10122-R00. Toronto, Canada.

IAEA. 1970. Treaty on the Non-Proliferation of Nuclear Weapons. International Atomic Energy Agency INFCIRC/140. Vienna, Austria.

IAEA. 1972. Agreement Between the Government of Canada and the International Atomic Energy Agency for the Application of Safeguards in Connection with the Treaty on the Non-Proliferation of Nuclear Weapons. International Atomic Energy Agency INFCIRC/164. Vienna, Austria.

IAEA. 2000. Protocol Additional to the Agreement between Canada and IAEA for the Application of Safeguards in Connection with the Treaty on the Non-Proliferation of Nuclear Weapons. International Atomic Energy Agency INFCIRC/164/Add. 1. Vienna, Austria.

Kwong, G. 2011. Status of Corrosion Studies for Copper Used Fuel Containers under Low Salinity Conditions. Nuclear Waste Management Organization Report NWMO TR-2011-14. Toronto, Canada.

McMurry, J., D.A. Dixon, J.D. Garroni, B.M. Ikeda, S. Stroes-Gascoyne, P. Baumgartner and T.W. Melnyk. 2003. Evolution of a Canadian Deep Geologic Repository: Base Scenario. Ontario Power Generation Report 06819-REP-01200-10092-R00. Toronto, Canada.

Noronha, J. 2016. Deep Geological Repository Conceptual Design Report Crystalline / Sedimentary Rock Environment. Nuclear Waste Management Organization Report APM-REP-00440-0015 R000. Toronto, Canada.

5. LONG-TERM EVOLUTION OF THE MULTIPLE BARRIER SYSTEM

The repository will be sited, designed and contructed in order to provide long-term containment and isolation of the used fuel. It will do so through a multiple-barrier approach, with a combination of natural and engineered barriers. Table 5-1 summarizes the main safety attributes of the repository.

Some of these attributes are important to safety in the preclosure period during construction and operation. This report is focused on the postclosure period, and therefore on those safety attributes relevant in the long-term (i.e., one million years).

Chapters 2, 3, and 4 of this report describe the site, the used fuel waste form and the repository design. Table 5-2 presents a summary of the the key repository components.

This chapter describes how these components of the repository are expected to evolve and interact with their environment during the postclosure period. This includes both their expected behavior as well as a range of unlikely but plausible circumstances.

Additional features, events and processes (FEPs) were assessed and excluded for the reasons outlined in the FEPs report (Garisto 2017), and therefore are not included in the repository evolution described in this chapter.

The NWMO continues technical work in a number of areas in order to increase knowledge and reduce uncertainties associated with the components and processes relevant to long-term containment and isolation. This work is summarized in the NWMO's annual technical reports; see for example the 2015 annual technical report (Crowe et al. 2016).

Table 5-1: Main Safety Attributes

1. The geologic setting provides isolation and containment.
1.1. The repository depth isolates the waste and repository components from surface changes created by human activities or natural events.
1.2. The repository is enclosed by stable, competent and low permeability rock.
1.3. The hydrogeologic setting that encloses the repository restricts groundwater and radionuclide movement.
1.4. The mineralogy of the host rock, and the composition of the ground/porewater, are compatible with the engineered barriers.
1.5. The host rock mineralogy and the composition of the ground/porewater are favourable for mitigating radionuclide movement.
1.6. Natural resource potential is low within the repository geologic setting.
1.7. Seismic hazard is low.
1.8. The host rock is predictable and amenable to characterization.
2. The site geology has long-term stability.
2.1. The hydrogeologic conditions at repository depth are stable and resilent to internal and external perturbations, including glaciation.
2.2. The host rock is capable of withstanding thermal and mechanical stresses induced by internal and external perturbations, including glaciation.
2.3. The repository conditions including chemistry and physical condition important for safety are not influenced by internal and external perturbations, including glaciation.
2.4. Rate of erosion is low.
2.5. Repository safety is not influenced by strong ground motions associated with rare earthquakes.
3. The site supports robust construction and operation.
3.1. Repository host rock conditions allow safe construction and operation.
3.2. Safe transportation route to site.
3.3. Frequency of severe natural events at site during construction and operation is low.
3.4. Robust facility design for safe construction and operation.
3.5. The site is not located in a sensitive ecological environment.
4. The used fuel wasteform is a barrier which contributes to the containment of radionuclides.
4.1 Most radionuclides are immobile within the uranium oxide grains of the used CANDU fuel.
4.2 The used CANDU fuel grains are mechanically durable and not materially impacted by radiation damage or helium gas buildup.
4.3 The used fuel has low solubility under conditions of a failed container with contact with ground/porewater.

	4.4 The Zircaloy cladding provides a barrier to contact between ground/porewater and used fuel in a failed container.
	4.5 The Zircaloy cladding corrodes slowly under conditions of a failed container in contact with ground/porewater.
5.	**Container and sealing systems are barriers which contribute to the isolation and containment of radionuclides.**
	5.1. The container is designed for the underground conditions at timeframes relevant to repository safety.
	5.2. Inspection methods would ensure the container is built consistent with design specifications.
	5.3. The in-room buffer system holds and protects the containers.
	5.4. Engineered seals isolate the placement rooms from the access tunnels.
	5.5. Shaft backfill and seals isolate the repository from the surface.
6.	**Repository construction, operation and closure supports the long term repository performance objective.**
	6.1. Repository layout and spacing are designed for long-term structural stability.
	6.2. Repository design and construction methods minimize the excavation damaged zone.
	6.3. Materials used in repository construction and operation will not compromise long-term performance.
	6.4. Institutional controls and monitoring will verify performance.
7.	**The repository is robust to accidents and unexpected events.**
	7.1. Credible accident during operations would have low effects on public and environment.
	7.2. Postclosure analyses show low effect from normal or expected scenarios, with large safety margin to regulatory criteria.
	7.3. Postclosure analyses show risk from disruptive scenarios to be acceptable.

Table 5-2: General Parameters of Key Repository Features

PROPERTY	REFERENCE VALUE
Used Fuel	
Waste form	Used CANDU fuel bundles
Bundle	37-element standard bundle
Initial mass U	19.25 kg/bundle
Initial mass Zircaloy	2.2 kg/bundle
Burnup (nominal value)	220 MWh/kgU
Power rating (nominal value)	455 kW/bundle
Minimum fuel age at placement	30 years (out of reactor)
Used Fuel Container	
Design	Steel load-bearing vessel coated with high purity copper, fuel bundles held in steel sleeves
Coating material	High-purity copper applied by a combination of electroplating and cold spray
Container material	A106 Grade C cylinder body welded to hemispherical heads fabricated from A516 grade 70 carbon steel
Container fill gas	Ambient air installed at atmospheric pressure
Container capacity	48 bundles
Container dimensions	0.56 m outer diameter x 2.51 m long
Coating thickness	3 mm
Container mass	2805 kg loaded
Thermal output	170 W based on 30 year old, 220 MWh/kgU used fuel
Temperature (outer surface)	Up to 100°C
Buffer/Backfill	
Buffer design	Container is placed between two 1.0 x 0.5 x 2.8 m Highly Compacted Bentonite buffer blocks. The remainder of the placement tunnel is backfilled with 100% bentonite gap fill
Buffer material	100% bentonite clay, MX-80 or equivalent
Buffer density	1,700 kg/m^3 dry density
Gap fill density	1,410 kg/m^3 dry density
Buffer temperature	<100°C
Backfill design	Backfill is used to fill access drifts and perimeter drifts. Primarily a dense backfill material, with 50:50 bentonite:sand gap fill
Concrete	Low-heat, high-performance concrete

PROPERTY	REFERENCE VALUE
Placement Rooms	Horizontal rooms, buffer boxes stacked in two rows Rooms aligned taking account of principal stresses Rooms sealed with end plugs from access tunnels
Repository	
Depth Footprint	500 m (nominal) ~3.2 km^2
Total number of bundles Total number containers Operation phase Extended monitoring phase	4.6 million ~100,000 40 years Nominally 70 years (following placement of all containers)
Geosphere at repository depth	
Predominant rock type Rock structure at depth Geothermal gradient Temperature Rock Mass hydraulic conductivity Rock mass porosity fraction Porewater Total Dissolved Solids	Crystalline (granitic) Discretely fractured low permeability granitic rock 12°C/km ~11°C 4×10^{-11} m/s (repository horizon) 0.003 11 g/L
Surface/Biosphere	
Land surface temperature Air surface temperature Ecosystem	+5°C annual average (present) +5°C annual average (present) Boreal forest (present)

5.1 Long-Term Evolution of the Geosphere

Within the Canadian Shield, natural processes that could potentially affect the geosphere at repository level over one million years are primarily seismicity and glaciation.

Volcanism is not present on the Canadian Shield nor likely to occur on relevant timescales. This and other potential Features, Events and Processes (FEPs) were assessed and excluded, based on the rationale provided in the FEPs report (Garisto 2017), and therefore are not a part of the expected evolution described in this section.

The influence and likelihood of seismicity and glaciation are described in the following sections, in support of the geologic site attributes listed below (see also Section 1.6.3.1):

- The repository depth isolates the waste and components from surface disturbances, as well as from changes induced by human activities and natural events; and
- The site geology provides long-term stability to the repository.

5.1.1 Seismicity

In general, the Canadian Shield is characterized by low seismicity as it is located within the center of the stable North America craton (Adams et al. 2016). Large earthquakes are infrequent, with contemporary seismicity generally confined to pre-existing zones of weakness and faults. Damage to intact rock is not likely to occur, because in-situ tectonic and glacially-induced stresses are not considered sufficient to generate the forces required to create new ruptures within fresh rock (Lund 2006).

Reactivation of existing faults is more likely than creation of new faults. There is evidence from the Scandinavian Shield that the effects of glacial unloading on the lithosphere can lead to fault reactivation. Examples of fault reactivation include the Pärvie fault in northern Sweden, which displays offsets of up to 10 m over distances of 150 km (Kukkonen et al. 2010). In the Canadian Shield, the only known surface rupture was observed at Ungava, northern Quebec, from a M6.3 earthquake in 1989. The event resulted in up to 3 m offset at ground surface of an existing fault over a distance of 7 km (Adam 1989). There is no evidence of surface rupture within Ontario, and no identified structures can be conclusively linked to postglacial reactivation (Fenton 1994).

In the study region (Canadian Shield in Ontario), the probability of having a large enough seismic event that is sufficiently close to affect a deep geologic repository, either through primary or secondary fault displacement or through strong motion, lies within the approximate range from nil to 5×10^{-7} per annum (Atkinson and McGuire 1993).

The impact of shaking from rare, extreme seismic events on the integrity of the respository was assesed by Itasca (2015). The analyses reveal that there is virtually no increase in rock mass damage around placement rooms due to the confinement provided by room backfilling. A more detailed description of seismic simulation results is presented in Section 5.2.2.1.4 and in Itasca (2015).

5.1.2 Glaciation

The last million years of Earth's history has been marked by periods of glaciation (Peltier 2002, 2006). Ice coverage was marked by many cycles of glacial ice sheet advance and retreat, separated by ice-free periods of warmer climate (interglacials), lasting from thousands to hundreds of thousands of years. Nine glacial cycles occurred over the past million years. During the last glaciation, starting approximately 120,000 years before present, over 97% of Canada was covered by ice. The final retreat of the ice sheet occurred between 9000 and 6500 years ago. Numerical realization of this glaciation, as well as discussion of processes that cause glaciations, can be found in Peltier (2002, 2003, 2006, 2011) and Stuhne and Peltier (2015, 2016).

Conditions suitable for the reglaciation of the Canadian land mass will likely occur ~60,000 years from present, and again ~125,000 years from present (Stuhne and Peltier 2015). However, if at that time the concentration of carbon dioxide and other greenhouse gases in the atmosphere are similar to present levels, it is unlikely that a renewed episode of glaciation would occur. As the abililty to predict the atmospheric CO_2 level so far into the future is limited, the possibility of a renewed glacial event cannot be discounted and, therefore, glacial processes must be taken into account when developing the safety case for a used fuel repository in a Canadian Shield environment.

The characteristics of the glaciation process that are relevant to the understanding of repository performance include:

- Groundwater system stability, including deep groundwater chemical conditions, which has the potential to impact rates of mass transport at repository depth;
- Geomechanical stability of the repository system and geosphere, as impacted by the increased ground stresses due to the ice-thickess;
- Erosion, related to the movement of the ice sheet and meltwater across the land surface; and
- Permafrost formation, which will affect groundwater movement, and potentially the repository if it extends to that depth.

The phenomena associated with glaciation are described in detail in Chapter 2 in the context of this site, but are summarized below in four broad categories: glacial loading, glacial erosion, permafrost formation and groundwater system stability.

5.1.2.1 Glacial Loading

As noted in Chapter 2, climate modelling of the late Quaternary indicates that the last glacial episode had a duration of approximately 120,000 years and involved a prolonged glacial advance and retreat. The model predicts ice thicknesses were up to 3 km over northern Canada, and approaching 2 km in southern Ontario (Stuhne and Peltier 2015, 2016). These predictions of ice-thickness are constrained by observations of relative sea-level and isostatic uplift.

The weight of the thick ice sheet acts to depress the Earth's crust over a large area. Stuhne and Peltier (2015) predicted that the maximum crustal depression from the equilibrium level occurred at the Last Glacial Maximum (LGM) and reached approximately 500 m. Removal of the ice load by melting leads to slow crustal rebound, a process that continues today in the Canadian Shield from the last glaciation.

The University of Toronto Glacial Systems Model (UofT GSM), which is a model of continental-scale glaciation events, was used by Stuhne and Peltier (2015, 2016) to develop a description of past glaciation of the Canadian landmass. A time series of ice sheet thickness for the past 120,000 years was developed, as shown in Figure 5-1 (as SP15). The ice thickness time series from previous model results, representing two different glacial potential basal conditions, are also shown in the plot for comparison (nn2008 and nn2778). Ensemble results for sensitivity analyses for SP15 are also shown (Stuhne and Peltier 2016), which give an estimate of the range in variability of the ice thickness and permafrost depths as a result of model parameter sensitivity. In particular, the variability arising from the GSM model parameter sensitivity result in ice-thickness variability at LGM of approximately 50 m for the SP15 simulation.

5.1.2.2 Permafrost Formation

Future glacial conditions at the hypothetical repository site would be accompanied by an extended period with widespread formation of permafrost. The range of permafrost thickness time series applicable to this site is shown in Figure 5-1 (see Section 2.2.2.3).

The repository itself at 500 m would be below the depth of permafrost, so not directly affected. However the presence of permafrost in the geosphere will act to reduce the hydraulic conductivity, thereby limiting recharge from the surface during glaciation. The effects of this permafrost is considered in the next section as part of the analysis of groundwater system evolution.

In regions of permafrost, taliks are regions of perennially unfrozen ground that exist within otherwise continuous permafrost environments. The formation of taliks is dependent on site-specific conditions, and for example may exist under large water bodies. At the repository site, the heat load from the used fuel is expected to have sufficiently dissipated by the time glaciation may be occurring, so this heat load is not expected to significantly influence the permafrost at the site.

5.1.2.3 Glacial Erosion

The primary process expected to result in erosion over the next million years is glacial activity. Glacial ice and water can erode sediment and rock by abrasion, quarrying, and mechanical erosion. Regardless of the mechanism, the rate of surface erosion can be limited by the ability of the meltwater to remove debris (e.g., due either to an insufficient hydraulic head gradient to carry debris-laden subglacial water out of the basin, or the lack of adequate subglacial pathways for water flow). In terms of erosion at a local level, the basal sliding velocity is the primary factor controlling the rate of erosion. However, rapid basal sliding velocity does not necessarily correlate with rapid erosion at the base of the glacier, as the glacier may be decoupled from the bedrock surface by a thin layer of basal melt water.

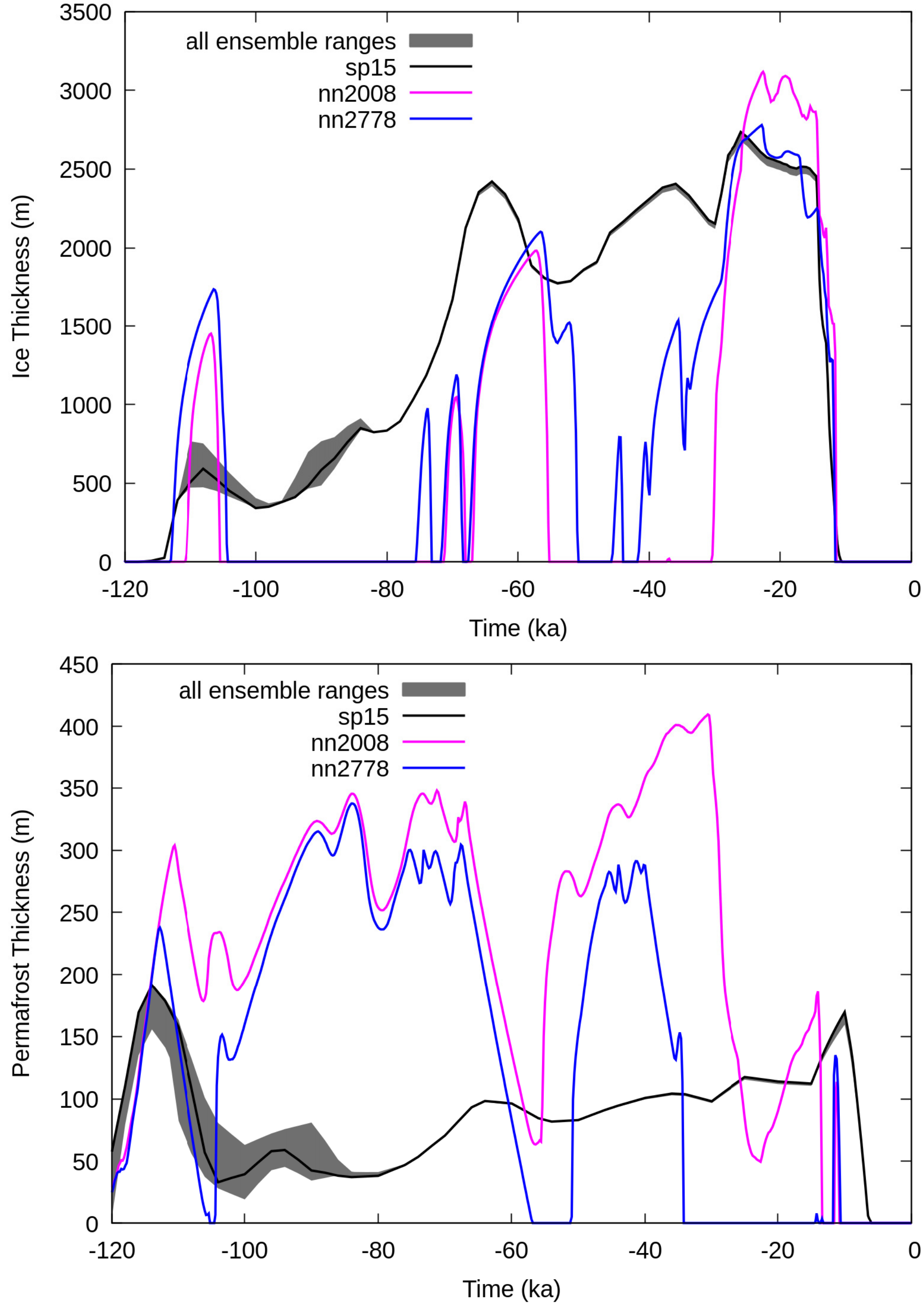

Note: Glaciation scenario nn2008 represents cold based glacial conditions, scenario nn2778 represents warm based glacial conditions, and scenario SP15 represents best estimate conditions (variability in SP15 ensemble shown as shaded area).

Figure 5-1: Three Ice Sheet and Permafrost Thickness Time Series

A number of studies have produced estimates of the amount of erosion by the Laurentide Ice Sheet and Fennoscandian ice sheets. Geomorphic studies indicate many examples where the pre-glacial regoliths or river valleys have been preserved. Most work performed to-date to estimate glacial erosion suggests that total erosion during the Quaternary did not exceed 10 m to 40 m for both the Laurentide Ice Sheet and Fennoscandian ice sheets (Hay et al. 1989, Lidmar-Bergstrom 1997, Ebert 2015, Melanson et al. 2013). Therefore, glacial erosion is not expected to affect a repository located at a depth of 500 m over a 1 million year time frame.

5.1.2.4 Groundwater System Evolution

Glaciation, as the strongest single external perturbation to the geosphere, will impact the long-term evolution and stability of groundwater systems at depth, including:

- Depth of penetration of glacial meltwater,
- Changes to rates of mass transport, and
- Redox stability.

The impact of glaciation on the deep groundwater system at the hypothetical crystalline site was considered in this study. Paleohydrogeological modelling was completed for the Laurentide glacial episode (120,000 to 10,000 years before present) and is presented in detail in Chapter 2 (Section 2.3.5.3). The key insights from the illustrative modelling are summarized below.

Eleven simulations were performed to investigate the role of varying paleoclimate boundary conditions. Details of the paleoclimate modelling scenario can be found in Section 2.3.5.3. The performance measure used to compare these simulations is the movement of a conservative unit tracer applied with a Cauchy boundary condition at the top surface of the model domain. This tracer represents the predicted migration of recharge waters into the groundwater system over the course of a 120,000 year simulation. The depth of the tracer is determined by the 5% isochlor, which represents a pore fluid containing 5% recharge water. The 5% isochlor provides an indication of recharge water migration into the subsurface, which can be used to compare alternative paleohydrogeologic scenarios. The simulations do not consider reactive transport; therefore, although the 5% isochlor provides an indication of the percentage of meltwater, it does not take into account the consumption of oxygen within this meltwater as it penetrates. Reactive transport modelling analyses in fractured crystalline rock conducted in Spiessl et al. (2009) indicate that the ingress of oxygenated water will be limited to the upper 70 m.

The depth of penetration of the tracer is shown in Figure 5-2 for the best estimate glacial systems model boundary conditions (Stuhne and Peltier 2015). The tracer concentrations in Figure 5-2 are shown after 120,000 year simulation time. For the best estimate glacial boundary conditions, the median tracer migration depth for a 5% isochlor is 792 mBGS. However, areas away from the influence of fracture zones remain free of tracer at depth.

The change in rates of mass transport within the deep groundwater system was also assessed as a part of this study in Section 2.3.5.3. Plots of velocity magnitude versus time for the paleoclimate sensitivity analyses indicated that rates of mass transport will remain low in areas of the rock mass away from the influence of fracture zones. Detailed evaluations of the potential effects of glaciation on regional and site groundwater systems in crystalline environments are provided in Walsh and Avis (2010) , Normani (2009) and Normani and Sykes (2014).

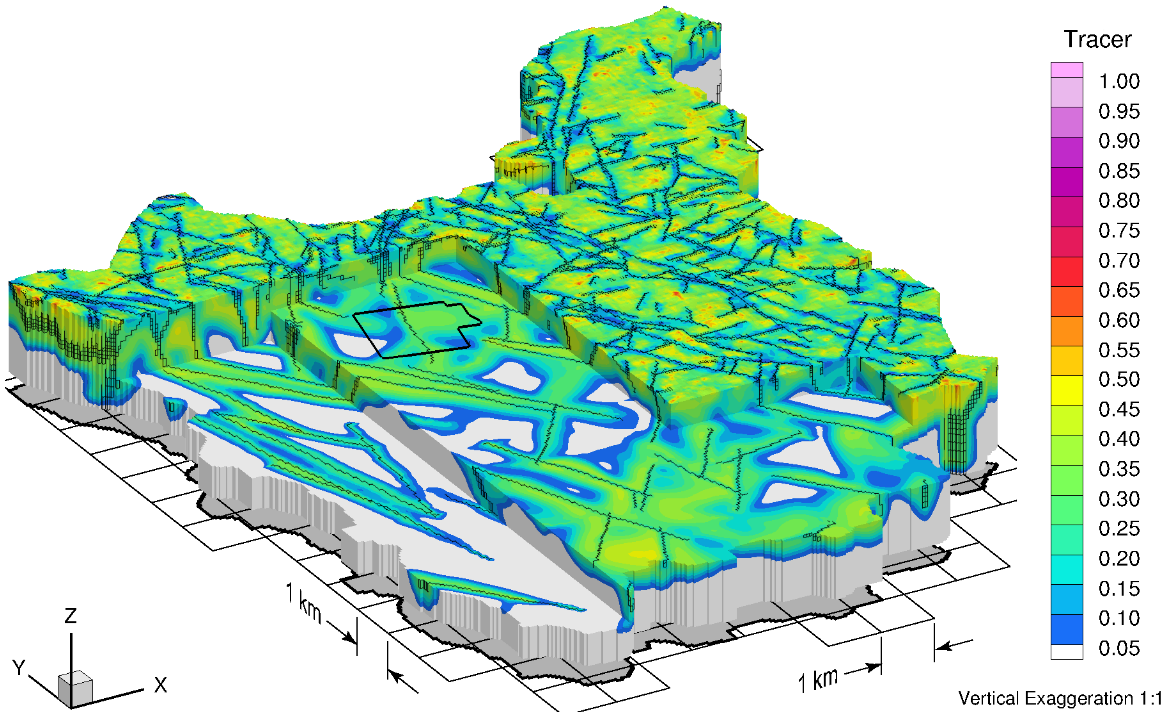

Figure 5-2: Tracer Migration at 120,000 Years for the Best Estimate (SP15) Paleoclimate Boundary Conditions (fr-base-paleo-peltier)

5.1.3 Confidence in Geosphere Evolution

The geosciences program for a candidate site will be designed to support the safety case. A site model and geosynthesis will be developed during a phased site characterization work program. The work program will allow for the iterative development, testing and refinement of a site-specific model that will contribute to managing uncertainties in scientific understanding, data and models.

Seismicity: The host rock would be demonstrably resilient to earthquakes based on its history. The actual repository location would be chosen to avoid fracture zones or faults where future fracture movement is more likely.

Glaciation: Peltier (2011) provides a review of what is known concerning the geologically recent history of long-term climate change, as background to the detailed analysis of the conditions that would be expected to develop at and below the surface of the Earth if the Canadian land mass were to be reglaciated. Results from an appropriately-calibrated model of the most recent glaciation events that occurred in the Late Quaternary period are used as a proxy for a future reglaciation event (Stuhne and Peltier 2015, 2016). The method, additionally, has been validated using recreations of existing ice sheets in Greenland and Antarctica.

Groundwater System Evolution: Evidence gathered during site characterisation activities would minimize uncertainties through a synthesis of geologic, structural geologic, hydrogeochemical and physical hydrogeologic data to assess long-term groundwater system evolution and stability. Such efforts would be aided through the application of numerical methods that provide a systematic framework to integrate independent data sets (Sykes et al. 2004, 2009; Normani et al. 2007, 2014; Normani and Sykes 2014). Such techniques, as supported by field data, can provide insight (i.e., time rates of change and magnitude) into groundwater system response to external events and can constrain uncertainty with regard to geosphere performance.

Uncertainties in the future evolution of groundwater compositions are coupled to uncertainties about the movement of groundwater. Similarly, impacts of glaciation at repository depth will be dependent on site-specific conditions. The age of, and potential influence of glaciation on, groundwaters and porewaters cannot be determined directly; instead, they are inferred from paleohydrogeological evidence, such as fluid inclusion data and stable water isotope ratios. Together with numerical tools, such as reactive transport modelling, this information can be used to illustrate the potential evolution of geochemical conditions at repository depths.

5.2 Long-Term Evolution of the Repository Environment

Although the construction, operation and closure will be conducted so as to avoid compromising the long-term safety of the repository, the repository will be a change in the geosphere setting. Potential disturbances to the geosphere include those induced by excavation itself (e.g. damage to surrounding rock, introduction of blast residue) and those due to placement of the waste and engineered systems (e.g., changes in temperature, saturation, near-field chemistry, gas generation). The relevant changes with respect to long-term safety are described below. Additional Features, Events and Processes (FEPs) were assessed and excluded for the reasons outlined in the FEPs report (Garisto 2017) and thus are not part of the expected evolution described in this section.

5.2.1 Temperature

Among the first changes to occur in a repository after container placement is an increase in temperature of the sealing materials around the containers. Figure 5-3 shows the thermal profiles for several points in the repository. The points range from the exterior surface of a container, out through the buffer and into the near-field rock (revised from Guo 2016).

Key points to note in Figure 5-3 are:

- The temperature of sealing materials adjacent to the surface of the container increases rapidly at first, within days to weeks after placement.
- The maximum temperature of the buffer occurs after 30 years and remains below the targeted maximum of 100°C (note that the calculated peak of 87°C in this simulation is sensitive to the specific conditions of a site and optimizations to the repository layout).
- Within about one hundred years, reflecting in part the decay of the heat source, there is an appreciable reduction in peak temperatures.
- After several thousand years, the thermal evolution is marked by a slow, steady cooling. Temperatures return to near-ambient conditions within 100,000 years.

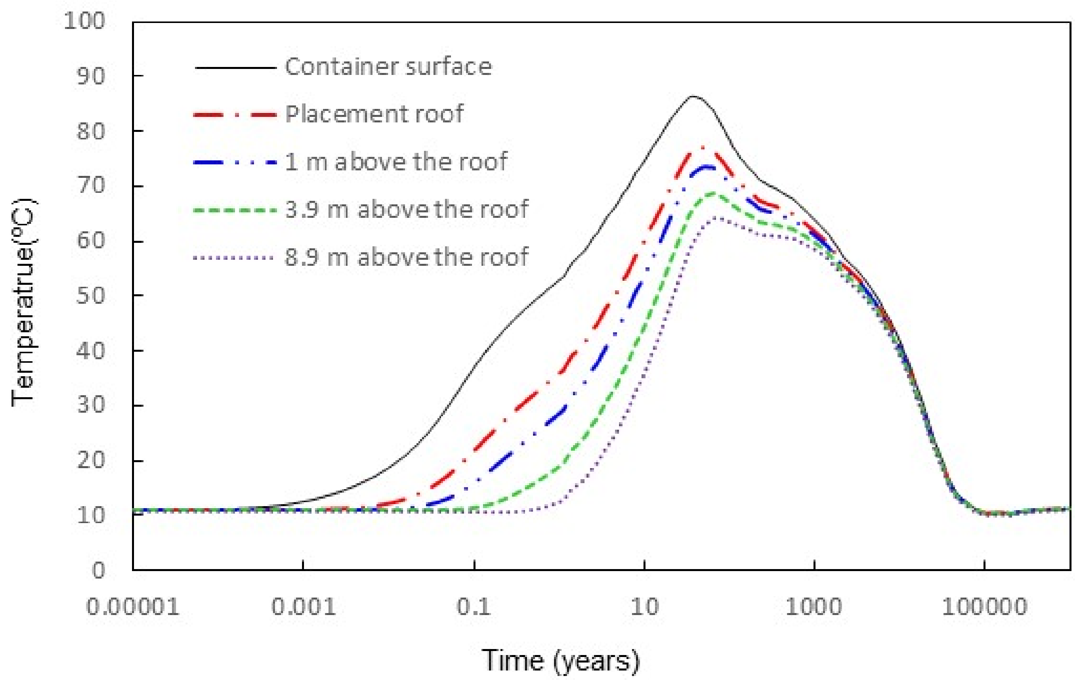

Figure 5-3: Illustrative Example of the Range of Temperature Variation over Time in a Placement Room

5.2.2 Repository Saturation

During the construction and operational phases, groundwater inflows into the excavations will be removed by pumping. At a depth of 500 m below the surface, the hydrostatic pressure within a fresh water-saturated rock mass is about 5 MPa. A sharply defined hydraulic gradient would exist between the geosphere at repository depth and the excavated openings (rooms, cross-cuts and drifts), which would be at atmospheric pressure. This difference would tend to draw groundwater through the rock into the open spaces of the repository. The movement of fluids would occur slowly through the low-permeability rock, but faster through any transmissive fractures. Groundwater seeping into the repository from the surrounding rock will be pumped away to maintain dry conditions within excavated openings, and may also result in drawdown of the groundwater level above the repository. Evaporation would tend to keep the rock surfaces in the excavated openings dry, and may induce partial desaturation of the rock immediately adjacent to the openings (i.e., within the excavation damaged zone and host rock near the repository).

Any dewatering during construction and operation of the repository will be of relatively short duration and will result in groundwater flow(s) toward the repository until pumping activities cease following repository closure. In the postclosure phase, water will flow towards the repository and the near-field will resaturate. Eventually, the flow will stabilize following saturation and will be broadly consistent with the original flow field.

The process of saturation may take a long time, as ingress of water will be restricted because of low host-rock permeabilities and the use of grouting and seals. Furthermore, the rate of wetting will likely vary at different locations within the repository. In saturated rock, high near-field porewater pressures as a result of repository heating could also change the flow field and affect resaturation time. Ovrall, this “pre-saturated period” covers the time period from when the containers are first placed in a repository until their exterior surface is in contact with saturated sealing materials. In fractured crystalline rock, it is likely that this pre-saturated period would last from 100 to 1000 years.

Unsaturated conditions, and the time elapsed before full saturation is attained in different areas of the repository, will be affected by the local temperature, chemistry, stress states (including buffer swelling) and groundwater flow rates. Some sections of rock (and the buffer) may not reach full saturation on relevant timescales. The bentonite buffer and backfill will uptake water during repository saturation, resulting in swelling of these materials. Swelling in response to the addition of water is a natural property of bentonite, resulting in the development of its barrier properties and self-sealing capabilities (low hydraulic conductivity and high swelling pressure).

At the time that the placement rooms are backfilled and sealed, they would contain partially saturated (moistened) buffer and backfill (see Table 4-2). Voids (porosity) in the sealing materials would contain trapped air. Heat from the container would cause the nearby bentonite to dry out, and condensation of the water vapour would occur in cooler portions of the sealing materials. The relative humidity of the trapped air in the sealing materials near a container is of interest because corrosion of copper and iron in air is observed to be slow or nonexistent at relative humidities of less than about 60%. Corrosion of steel under the same conditions produces hydrated iron oxides (“rust”).

5.2.3 Near-Field Chemistry

During repository excavation and operations, oxidizing conditions would develop in the porewaters of the adjacent rock due to exposure to the air in the repository.

However, after the rooms are closed and sealed, the redox conditions within the near-field will evolve back to an anaerobic state. Oxygen is consumed by a number of reactions, including reactions with residual iron in the rooms (e.g., rock bolts) and with copper on the containers (i.e., some combination of Reaction (5-1) and Reaction (5-2)), as well as by reactions with microbes and with redox-sensitive materials throughout the buffer.

$$2\,Cu + {}^{1}/_{2}\,O_2 \rightarrow Cu_2O \qquad (5\text{-}1)$$

$$Cu + {}^{1}/_{2}\,O_2 \rightarrow CuO \qquad (5\text{-}2)$$

Figure 5-4 illustrates the evolution of environmental conditions over time, from warm and oxidizing initially from construction, to cool and anoxic eventually once the oxygen is consumed and the fuel has cooled.

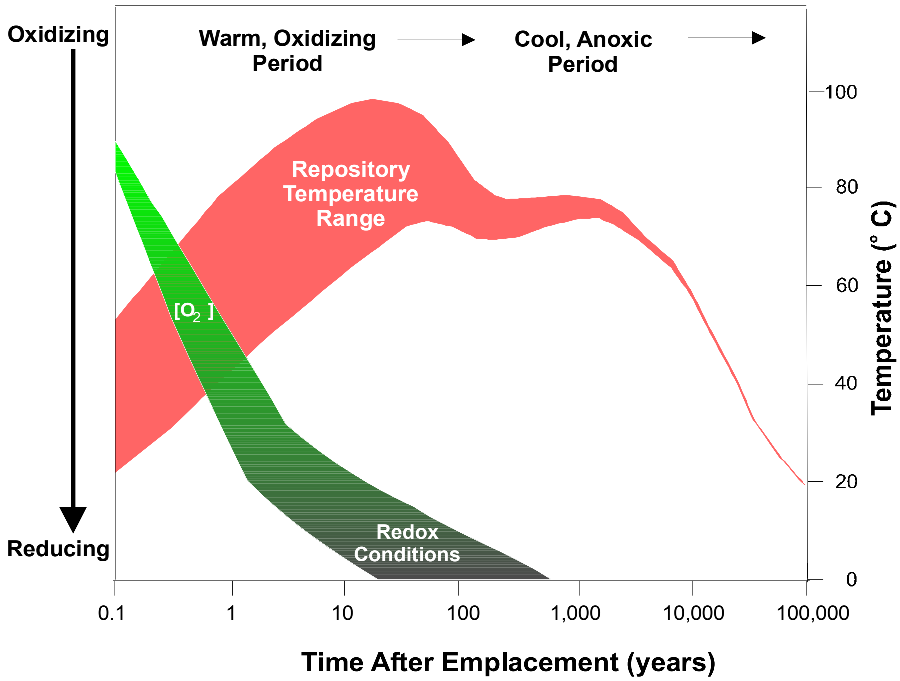

Note: Figure from McMurry et al. (2003).

Figure 5-4: Evolution of the Repository Environment from an Initial Warm, Oxidizing Period to a Prolonged Cool, Anoxic Phase

Most of the repository-related changes in groundwater chemistry would occur at or near the interface between the geosphere and the sealing materials. The diffusion of porewater components, or the mixing of fluids at the repository-geosphere interface, may result in the precipitation of secondary mineral phases at the interface or in nearby fractures in the geosphere. A broader effect would be due to heat from the repository, which would raise the temperature of water in the geosphere. This could result in a slightly greater dissolution rate for some minerals. Later, as the waters cool, the precipitation of secondary phases, such as amorphous silica and calcite, would occur. The extent and significance of the precipitation would depend on site-specific characteristics, such as the distribution and dimensions of the fractures.

In the long term, the geosphere, as a whole, would act as a strong buffer in response to chemical and thermal perturbations from a repository. As the pore fluids in the repository evolve to a composition more similar to that of the surrounding groundwater, and as temperatures in the geosphere gradually return to ambient levels, the chemical conditions in the geosphere would be diminishingly affected by the presence of a repository.

5.2.4 Steel Corrosion and Gas Generation

Small amounts of steel (primarily carbon steel) will be used in construction of the underground facilities. A larger amount is present in the used fuel containers, but this is only exposed in the case of failed containers (see Section 5.4.4.3). This steel will corrode, and relevant effects of steel corrosion are summarized below.

- Dissolved ferrous species, produced as a result of corrosion reactions, can interact with bentonite and convert swelling smectite clays to non-swelling illitic forms, resulting in a partial loss of swelling capacity (Lanson et al. 2015; Osacký et al. 2013; Wersin et al. 2007) near the steel components.
- Anaerobic corrosion will result in the generation of hydrogen (Senior et al. 2017); although it is unlikely that the modest amounts of steel proposed for construction will produce a gaseous H_2 phase in the repository.
- Hydrogen may impact the viability of some microbial species, favouring anaerobic species that can use hydrogen as an energy source.

For the placement rooms, only small amounts of steel are expected to be present, generally as rock bolts. This volume of steel is sufficiently small that the relatively small quantity of hydrogen gas produced does not have the potential to alter the repository characteristics. However, because of the use of carbon steel as a container material, the impact of hydrogen generation on the repository is considered within the All Containers Fail scenario in Chapter 7.

The corrosion behaviour of the steel components will change with time as the environment in the repository evolves (Necib et al. 2017). From a corrosion perspective, the most important environmental factors are the temperature, the redox conditions, the degree of saturation of the repository material, and the composition of the porewater in contact with the steel components. Saturation of the DGR could take a very long time so this transient has led to the conceptual definition of four phases in the evolution of the environment, as described below (see Suckling et al. 2012; King 2013).

<u>Phase 1</u>

Phase 1 represents an early aerobic period prior to the onset of aqueous corrosion. Immediately following closure of the repository, saturation of the Engineered Barrier System (EBS) has not yet occurred, so no liquid water is available for corrosion, and the EBS near the UFCs remains unsaturated. Oxygen is initially present in the unsaturated pore space when the EBS is emplaced. If relative humidity is also low, corrosion will be limited to slow air oxidation. This unsaturated aerobic corrosion is modelled as follows:

$$4Fe + 3O_2 \rightarrow 2\ Fe_2O_3 \tag{5-3}$$

Aqueous corrosion is possible above a critical or threshold relative humidity (RH) that is determined by the nature of the surface and the presence of surface contaminants. As RH increases above a lower threshold value, the consumption of carbon steel by Phase 1 corrosion will decrease until an upper RH threshold is reached, upon which Phase 1 corrosion stops. Presently, the lower RH threshold is about 60% and the upper RH threshold is about 80% (Suckling et al. 2012).

Phase 2

Phase 2 represents an unsaturated aerobic phase, following the condensation of liquid water on the steel surface. During Phase 1, if relative humidity rises above 60-80%, aerobic aqueous corrosion may instead proceed according to the following relationships:

$$4Fe + 3O_2 + 2\,H_2O \rightarrow 4\,FeOOH \tag{5-4}$$

Note that Phase 1 and Phase 2 corrosion overlap as the relative humidity increases from 60% to 80%.

Phase 3

Phase 3 represents an unsaturated anaerobic phase that will occur following the consumption of the oxygen and prior to the full resaturation of the repository; the gaseous phase will be predominantly N_2, H_2 and H_2O vapour. Corrosion during this period is supported by the cathodic reduction of water accompanied by the evolution of hydrogen. Detailed surface analysis indicates that corrosion under unsaturated anaerobic conditions forms magnetite as the predominant corrosion product, as follows:

$$3Fe + 4H_2O \rightarrow Fe_3O_4 + 4H_2 \tag{5-5}$$

The rate of reaction is affected by relative humidity (RH) where the values are dependent on the cationic content of the buffer system, but may be as low as 0.1 and 0.2, respectively, for highly saline systems. Thus, for RHs as low as 20%, the reaction could proceed at its maximum rate.

Phase 4

Phase 4 represents a long-term saturated anaerobic phase, once the EBS material has become completely saturated by groundwater. As in Phase 3, corrosion during Phase 4 is supported by the cathodic reduction of water accompanied by the evolution of hydrogen. In the presence of compacted bentonite under saturated conditions, in addition to the reaction shown in (5-5), where magnetite (Fe_3O_4) is the corrosion product, carbon steel corrodes with the formation of a carbonate-containing corrosion product. The source of carbonate is calcite and other carbonate minerals assumed to be present in the EBS material. Iron carbonate, or some form of $FeCO_3$ incorporating cations from the pore solution, will predominate until such time that all carbonate minerals in the clay have been consumed; after which the predominant corrosion reaction is then likely to be the formation of Fe_3O_4 according to the reaction shown in (5-5).

The overall stoichiometry of the corrosion reaction for Phase 4 is:

$$Fe + CO_3^{2-} + H_2O \rightarrow FeCO_3 + H_2 + 2OH^- \tag{5-6}$$

It is important to note that these four phases do not necessarily occur sequentially. Phases 1 and 2 both occur under aerobic conditions and the degree to which the Phase 1 and Phase 2 corrosion processes are active depends on the relative humidity. The Phase 3 and 4 corrosion processes proceed under anaerobic conditions after Phase 1 and Phase 2. The degree to which the Phase 3 and Phase 4 corrosion processes are active depends on whether or not liquid water is in contact with the steel components or not. As noted above, the Phase 3 process also depends on relative humidity.

The vast majority of H_2 that will be produced in the repository will result from the uniform corrosion of carbon steel during the (unsaturated and saturated) anaerobic phase. Hydrogen can be produced under aerobic conditions due to the reduction of H^+ in acidic environments in pits, crevices, or in porous corrosion products formed as a result of the hydrolysis of Fe(III) species (Akiyama et al. 2010; Tsuru et al. 2005). Local reduction of H^+ may lead to enhanced hydrogen absorption and environmentally assisted cracking (King 2009a), but will not lead to the generation of significant H_2 and is not considered further here.

Hydrogen generated by corrosion can undergo a number of subsequent processes. The H_2 that is evolved could be consumed by microbes (Pedersen 2000) in those parts of the near- and far-fields in which the environment is conducive to microbial activity (namely a water activity greater than 0.96; Stroes-Gascoyne et al. 2006, Stroes-Gascoyne and Hamon 2008). Another fraction of the hydrogen will be absorbed by the carbon steel as atomic H, either from adsorbed H atoms prior to their evolution as H_2, or via the dissociative absorption of gaseous H_2; however, eventually this hydrogen will be released as the steel continues to corrode.

In addition to the evolution of the redox conditions and the degree of saturation, the temperature will also change during these different phases. In general, Phases 1 and 2 will be warmer than Phases 3 and 4, with Phases 3 and 4 encompassing the period of long-term ambient conditions.

The rate of oxidation of carbon steel in dry air (Phase 1) is low at the temperatures of interest (maximum of approximately 120°C) and will result in only a few microns of corrosion. Although the rate of aerobic corrosion in the presence of moisture under unsaturated conditions (Phase 2) is higher, the extent of corrosion is limited by the initial inventory of trapped oxygen in the repository. Therefore, upon the establishment of high humidity Phase 2 conditions, the duration of aerobic corrosion is predicted to be less than 1 year.

Of most interest is the rate of anaerobic corrosion under first unsaturated (Phase 3) and subsequently saturated (Phase 4) conditions. Based on published corrosion studies, these rates are temperature dependent; the corrosion rate decreases with time as the container cools.

A number of other environmental parameters, in addition to the temperature, relative humidity, and redox conditions, also affect the uniform corrosion behaviour, including:

Porewater chemistry: Under saturated conditions, the steel will be in contact with EBS porewater. At least initially, the composition of the porewater may differ from that of the groundwater. Eventually, however, the porewater will equilibrate with the ground water.

pH: Calcite minerals in the bentonite may effectively buffer the pH in the range pH 7-8.

Mass transport: During the aerobic phase, the rate of corrosion may be limited by the rate of transport of O_2 to the steel surface through low-permeability EBS materials.

Radiation: Gamma radiolysis of water will produce oxidizing and reducing radiolysis products. However, the maximum surface absorbed dose rate for a UFC will be <2.3 Gy/h (Morco et al. 2017), for which there is no significant effect on the corrosion rate (Shoesmith and King 1999). Steel components more distant from the UFC will certainly see no effect of radiation/radiolysis.

Microbial activity: Microbial activity is suppressed by the low water activity within the compacted bentonite (Stroes-Gascoyne et al. 2006, Stroes-Gascoyne and Hamon 2008). However, because rock bolts and other steel components will reside outside the UFC engineered barrier system, it is possible that microbial species may accelerate steel corrosion versus a non-microbially active region of the engineered barrier system.

Stress: Applied and residual stresses affect the environmentally assisted cracking behaviour of the steel but have no effect on uniform corrosion.

Mineral impurities: Mineral impurities in the host rock (e.g., pyrite) will have an insignificant effect on the uniform corrosion behaviour of the container.

5.2.5 Excavation Damaged Zone

The rock immediately surrounding the placement rooms, tunnels, shafts and other underground openings is generally disturbed during excavation. This rock zone is often collectively referred to as the “excavation damaged zone”. However, three zones may be defined, as illustrated in Figure 5-5 and defined below based on Tsang et al. (2005) and Fracture Systems (2011):

Highly Damaged Zone (HDZ) is defined as a zone where macro-scale fracturing or spalling may occur. The effective permeability of this zone is dominated by the interconnected fracture system and may be orders of magnitude greater than the undisturbed rock mass.

Excavation Damaged Zone (EDZ) is a zone with hydromechanical and geochemical modifications inducing significant changes in flow and transport properties. These changes can, for example, include one or more orders of magnitude increase in (effective) flow permeability.

Excavation Disturbed Zone (EdZ) is a zone with hydromechanical and geochemical modifications, without major changes in flow and transport properties.

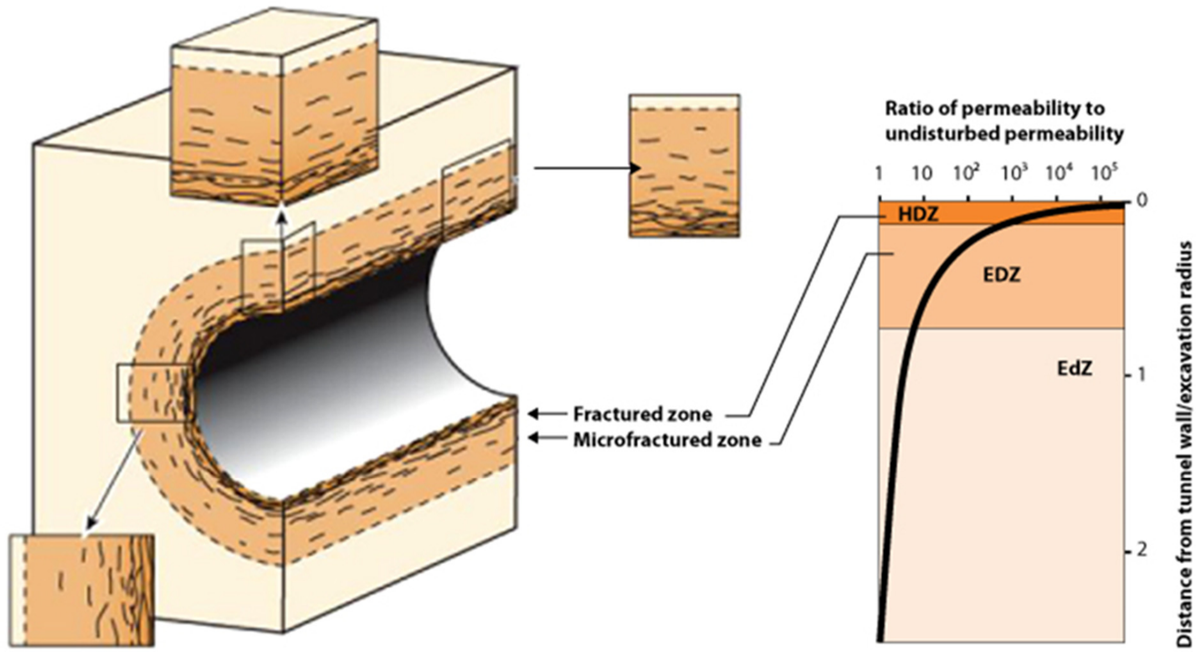

Note: Figure is from Fracture Systems (2011).

Figure 5-5: Illustration Defining Different Excavation Damage Zones for an Unjointed Rock

Further material on the excavation damaged zone is presented in Fracture Systems (2011).

For this repository in crystalline rock, it is assumed that controlled drill-and-blast will be generally used for repository development. Proper control of the drill and blast will minimize this initial excavation damage.

5.2.6 Geomechanical Evolution

The excavation of the placement rooms from the rock, and the subsequent backfilling with used fuel containers and buffer material, will affect the geomechanical conditions around the placement rooms as noted in the previous section.

A numerical analysis was performed to illustrate the stability and integrity of the rock mass enclosing a placement room of the repository during a 1 Ma period (Itasca 2015), and in particular the effects on the excavation damaged zone. The analysis included a sequence of simulations designed to illustrate rock mass response to normal repository evolution and extreme events. Model input parameters were selected based on the geosphere information presented in Chapter 2. A number of conservative assumptions regarding geotechnical conditions were introduced in these analyses in order to provide bounding solutions for the various scenarios.

The results of this assessment is sumamrized in the following subsections. Details are in Itasca (2015). The following conditions were considered for a timeframe of over one million years:

- Time-dependent strength degradation;
- Thermal loading;
- Glaciation;
- Low-probability seismic ground shaking; and
- Combination of loads and perturbations.

5.2.6.1 Impact of Time-Dependent Strength Degradation

The first scenario addresses the base geomechanical performance of the emplacement room, including thermal stresses from the heating due to the containers, as well as time-dependent strength degradation of the rock.

The analysis (Itasca 2015) shows that there is no noticeable change in EDZ extent through the thermal phase of the repository, i.e. during the first 10,000 years. Furthermore, a long-term reduction in strength of the granite rock mass has an insignificant effect on room stability, i.e., a relatively small incremental damage, even with a significant assumed reduction in long-term strength (to 40% of the rock mass Ultimate Compressive Strength).

The main reason for the overall positive performance of the placement rooms, and relatively small effect of low long-term strength, is the backfilling of the placement room. The backfill provides the confining pressure which prevents spalling of the rock and opening of the fractures, and significantly retards the time-dependent strength degradation or stress corrosion processes.

Heating could also cause relatively large displacements of the rock mass. Expansion of the rock mass results in predominantly upward vertical movement. The maximum displacements on the repository level are of the order of 0.04 m. However, this movement is relatively uniform across the entire repository, with relatively small differential displacements that do not affect the performance of the rooms (Itasca 2015).

5.2.6.2 Impact of Glaciation

The assessed site is located in a region that has been subjected to numerous glacial episodes over the past million years. A simulation was conducted assuming that a sequence of glacial events and corresponding histories of rebound stress (Itasca 2015) occurs in the future, starting at about 60,000 years from present (Figure 5-6). A conservative ice thickness of 3 km was selected for the site.

The results show that glacial loading over multiple cycles does not significantly affect the damage zones around the placement room. The lack of damage development around the opening is also attributed mainly to the confinement provided by the backfill in the placement room. The placement room and pillars between rooms remain stable throughout the glacial cycles.

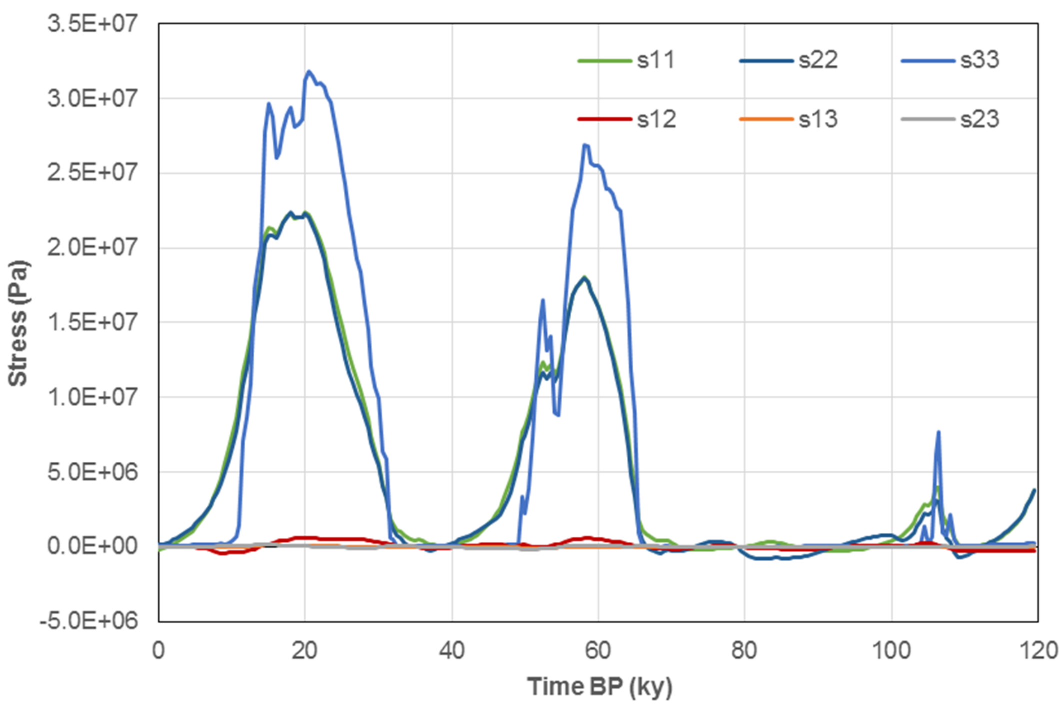

Note: Time BP represents time before present. Glacial boundary conditions from the Laurentide Ice Sheet are used to provide estimates of the impact of future glaciation on the geosphere. (from Itasca 2015)

Figure 5-6: Calculated Glacially-Induced Rebound Stress Histories; S11, S22 & S33 are the Normal Stress Components, S12, S13, & S23 are the Shear Stress Components

5.2.6.3 Impact of Seismic Ground Shaking

The impact of seismic ground motions was also studied as part of Itasca (2015) analysis. Three very low-probability seismic events (with contemporary 10^{-6} per annum probability level) were simulated to evaluate their impact on repository stability. The analysis considered a magnitude 5.5 (M5.5) event at a distance of 20 km, a M6.5 event at a distance of 100 km and a M7.4 event at a distance of 300 km, covering the high, medium and low frequency ranges of the uniform hazard spectrum from AMEC GEOMATRIX (2011) probabilistic seismic hazard analysis (PSHA), respectively. Although the PSHA was prepared for a sedimentary setting in southern Ontario, the spectrally-matched earthquake time histories developed from the PSHA should be a reasonable estimate for the study site on the Canadian Shield (Itasca 2015).

To evaluate the worst-case scenario, the 10^{-6} p.a. seismic loading was applied to the model at two critical instances in time: (1) when peak temperature is reached in the rock, and (2) when maximum glacial loading occurs.

The analysis results indicated that additional rock damage resulting from seismic loading is insignificant.

5.2.7 Confidence in Repository Evolution

Temperature: The thermal conductivity of crystalline rock is primarily influenced by the rock composition and matrix. Many of the uncertainties associated with estimates of heat transport properties of the geosphere would be resolved during site characterization. Temperature distributions in the geosphere would vary on a local scale as a result of repository layout.

However, there is good confidence in results obtained from thermal models over long periods of time, and in conservative estimates at shorter time. Some uncertainties exist in temperature predictions for pre-saturation conditions due to varying physical parameters (such as shrinkage or cracks) and moisture content (affecting thermal conductivity) of the material surrounding the container.

Repository Saturation: The resaturation rate depends on properties of the host rock and engineered barrier materials, temperature, hydraulic gradients, and gas or vapour transport, thus requiring coupled models. The modelling would be supported in part through engineering demonstration tests or monitoring of early placement rooms. While there is some inherent uncertainty, long-term repository performance is not particularly sensitive to the actual time of full saturation.

Near-Field Chemistry: The time at which reducing conditions will be re-established following repository closure is uncertain due to the complex interactions between groundwater, repository components and microbial processes.

Regardless of the amount of time required, the total amount of oxygen is limited and it can confidently be assured that reducing conditions will be re-established at some point in the postclosure period. Conservative assumptions can be applied in the repository design and analysis process that bound the associated uncertainties, to ensure that appropriate conclusions concerning repository performance are made.

Steel Corrosion and Gas Generation: Gas generation and migration depends upon host rock properties, the rate at which water enters the repository, the quantity of organic material present, the number and distribution of rock bolts, the degree to which radiolysis of water occurs, the timing and number of container failures, and the corrosion rates. For the bounding case considered in Chapter 7, gas generation from corrosion of all steel inner containers far exceeds that from other sources, so that some of the related uncertainties are not of special concern.

Excavation Damaged Zone: Estimates of the extent and permeability of the EDZ should be based on site-specific findings for the crystalline rock site, for which data, such as ground stresses and mechanical properties of the host rock, become available during site characterization. Once available, these data will be incorporated into the various assessments, together with appropriate allowances for residual uncertainties.

EDZ predications were based on bounding simulations that consider combinations of loading resulting from extreme geological and repository perturbations. Sensitivity studies to-date indicate that long-term repository stability and performance is not especially sensitive to variations in long-term EDZ development processes.

5.3 Long-Term Evolution of Used Fuel

A description of the used fuel waste form as placed in the repository is provided in Chapter 3. The used fuel assemblies remain isolated and dry within the container. The main long-term process is radioactive decay, including resultant temperature changes, as long as there is no container failure. The processes in a failed container are described in Section 5.4.4 . Additional FEPs were assessed and excluded for the reasons outlined in the FEPs report (Garisto 2017) and thus are not part of the expected evolution described in this section.

5.3.1 Radioactive Decay

When used fuel is first removed from the reactor it is highly radioactive. This activity decreases rapidly over the first year, and more slowly thereafter, as shown in Figure 5-7.

During the first year out of the reactor, the overall radioactivity decreases to about 1% of its initial value, and after about 100 years it decreases to 0.01% of its initial value. For the first 500 years, the total radioactivity of the fuel will be dominated by numerous short-lived fission products, most of which are gamma emitters; thereafter, it will be dominated by long-lived actinides, including uranium, many of which decay by emission of alpha particles.

After about a million years, the total radioactivity in the fuel will have declined to levels that are equivalent to those found in naturally-occurring uranium ore bodies with similar amounts of total uranium. In particular, the repository with 4.6 million fuel bundles will hold about 92,000 Mg of uranium. The Cigar Lake and MacArthur River ore bodies in Saskatchewan held about 90,000 Mg U and 130,000 Mg U, respectively, at an average ore grade of 20%.

Radioactive decay will gradually change the radionuclide composition of the used fuel. The radionuclide inventory, radiation output and heat output can be calculated as a function of time, as illustrated in Figure 5-8 for the radionuclide inventory. The greatest change in the composition of the used fuel is a pronounced decrease in fission products after about 500 years. Nevertheless, over a million-year timeframe all of the changes resulting from radioactive decay will represent only a modest change in the composition of the fuel, of which about 98% would persist as uranium and oxygen.

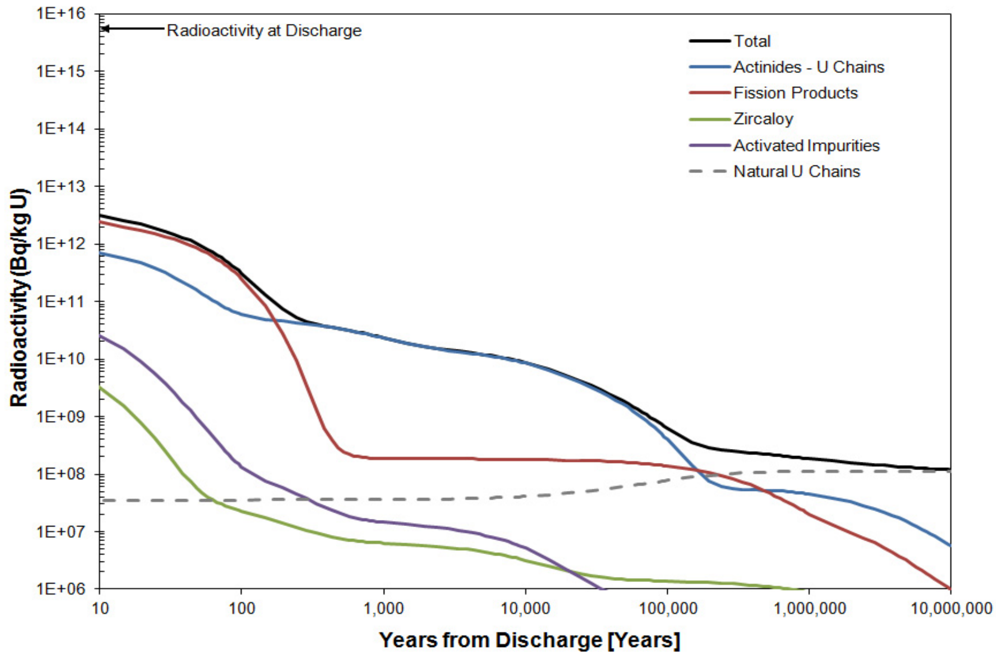

Note: U Chains represent radioactivity from uranium in fuel, including all progeny.

Figure 5-7: Radioactivity of Used CANDU Fuel (220 MWh/kgU burnup)

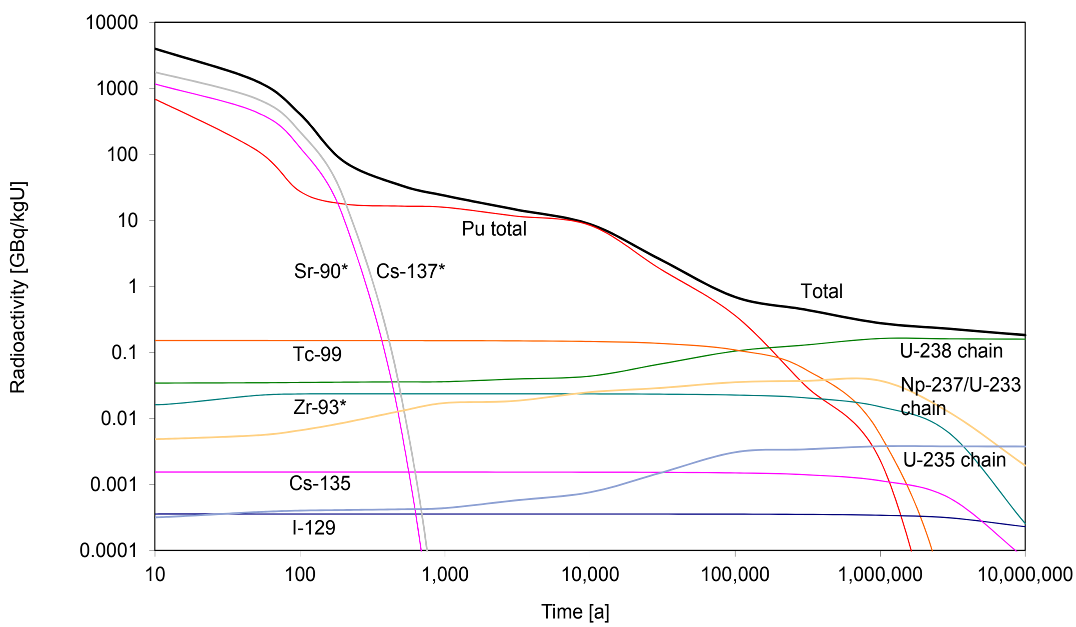

Note: Figure based on data from Tait et al. (2000). * Includes short-lived daughter.

Figure 5-8: Amounts of Key Long-Lived Radionuclides in Used Fuel (220 MWh/kg U burnup)

5.3.2 Changes in Temperature

Radioactive decay of the fuel is accompanied by alpha, beta and gamma radiation that is largely absorbed by the fuel itself and converted to heat. Immediately after being removed from a power reactor, a reference used fuel bundle would release about 27,000 watts of heat. This heat output rapidly decreases. After 10 years, the thermal output has decreased to 5.4 watts and after 30 years about 3.5 watts. In this study, the used fuel age at the time of placement is 30 years out of reactor. For fuel that is 10 years of older, passive cooling is sufficient.

Around 80 years after placement (as 30-year old fuel), the heat output of the entire 48-bundle container will be less than 60 watts.

The temperature of the container's outer surface will initially increase after placement (see Section 5.2.1). The temperature inside the reference container, loaded with 30-year-cooled used CANDU fuel, is expected to remain below 125°C, see Figure 5-9 (Guo 2015). The maximum temperature of the used fuel bundles will be attained within about 15 years after placement in the repository.

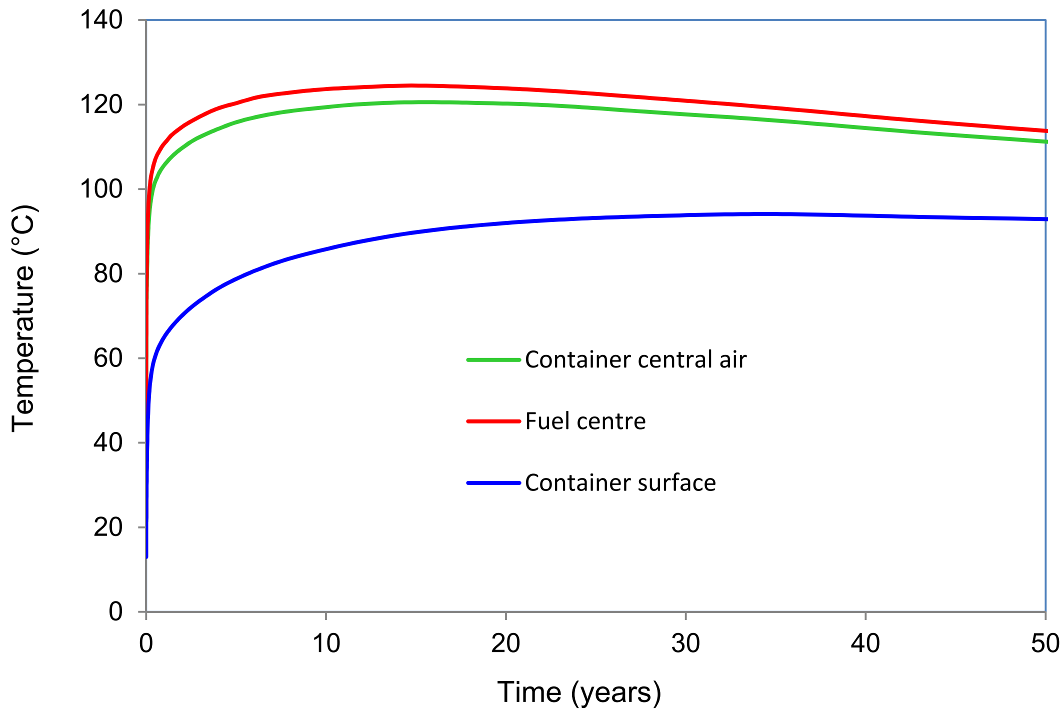

Figure 5-9: Temperature inside Container after Placement in Crystalline Rock [Guo 2015]

5.3.3 Changes in the UO_2

Inside the sealed containers, processes and changes occurring over long timeframes will not materially impact relevant UO_2 properties (i.e., UO_2 grain size, distribution of radionuclides). This is described below.

5.3.3.1 Alpha Radiation Damage

During radioactive decay, the crystalline matrix of the used fuel will experience localized damage to the crystal lattice from the emission of alpha particles, which travel only short distances from the nucleus but have high energy and a relatively large mass. The implications for radionuclide diffusion have been discussed above.

Natural analogue evidence suggests that alpha irradiation damage would not cause used fuel to crumble, even after extremely long times. At Oklo in western Africa, uraninite (UO_2) ore deposits underwent spontaneous nuclear fission reactions more than two billion years ago. Although affected by brecciation during fission and by subsequent hydrothermal alteration in some cases, the uraninite is still granular and massive (Jensen and Ewing 2001).

5.3.3.2 Radionuclide Diffusion

Under repository conditions, the relatively low fuel temperature means that radionuclide movement within the grains towards a grain boundary or fuel element void is slow. This is important because for the bulk of the radionuclides, their release in the case of damaged container then depends on the corrosion of the UO_2 itself.

Radiation damage has the potential to accelerate diffusion beyond normal thermal processes. However, theoretical and experimental assessments (Ferry et al. 2008) indicate that this effect is small, and in particular there is little redistribution of radionuclides within the fuel under repository conditions.

5.3.3.3 Oxidation State of Fuel

In some cases, radioactive decay results in the formation of an element with a higher oxidation valence than that of the parent radionuclide. In principle this could modify the oxygen potential and oxidation state of the UO_2 matrix, in turn affecting diffusion coefficients for radionuclides. Thermal diffusion coefficients of radionuclides are small at repository temperatures, but increase as the oxygen/metal (O/M) ratio of the fuel increases. However, any changes in CANDU fuel are expected to be quite small, from O/M ~ 2.001 to 2.010 or less, and this would not significantly affect thermal diffusion coefficients.

The oxidation state of the fuel potentially could be changed by the reaction of UO_2 and Zr to produce ZrO_2, which is more stable thermodynamically than UO_2. Where the cladding and UO_2 are in direct contact, the Zr eventually would reduce UO_2 to U by solid-state diffusion of oxygen atoms. This process is unlikely to be significant for used fuel due to the small amount of Zr present (10% of UO_2) and very slow solid-state diffusion rates at repository temperatures (Cox 1999). Consequently, the effects of possible galvanic couples are extremely small.

Within the intact container, the fuel cladding will be exposed to ambient air conditions within the container. However, zirconium forms a thin durable oxide layer, which will limit further oxidation of the cladding. And given that oxygen reactivity with the other container internal metals (i.e., steel) is much greater, as well as the limited amount of air present, this will not affect the fuel and cladding.

5.3.4 Zircaloy Cladding

The Zircaloy cladding is a resilient alloy (Freire-Canosa 2011) with a low corrosion rate (Shoesmith and Zagidulin 2010), and therefore can provide a barrier to prevent water from contacting the fuel or to inhibit radionuclide release in a failed container. However this Zircaloy cladding could fail due to processes such as creep, embrittlement and delayed hydride cracking. As the cladding is thin, it is conservatively given no credit within this safety assessment.

5.3.5 Build-Up of Helium Gas

Alpha decay results in the formation of helium (He) atoms in the used fuel. Because helium is stable and unreactive, the total amount of helium in the fuel elements will increase over time. Inventory calculations for high-burnup CANDU fuel (320 MWh/kgU) indicate that the helium content from alpha decay increases from 8×10^{-6} mol/kgU at discharge, to 0.01 mol/kgU at 10 thousand years, to 0.031 mol/kgU at 1 million years, and 0.091 mol/kgU at 10 million years (Tait et al. 2000). This is in addition to the 0.018 mol/kgU of other inert gas fission products present at discharge and largely unchanged with time (Tait et al. 2000).

The fuel pellets are cracked after in-reactor service, and consequently helium released to grain boundaries would be released relatively quickly into the fuel element void. However the majority of the post-discharge helium would be formed within the grains since that is where the radionuclides reside. Under repository temperatures, helium will accumulate within the UO_2 grains since diffusion to the grain boundaries would be slow. For low burnup fuel like CANDU fuel, the quantity of He produced is not sufficient to induce micro-cracking of grains (Ferry et al. 2008).

While much of this inert gas is expected to remain within the UO_2 grains, if all this gas would be released into the container, then after one million years the container pressure would be less than 0.6 MPa even if fully loaded with high-burnup fuel.[1] (As noted above, the fuel element cladding is not credited as a barrier at long times.)

5.3.6 Criticality

Criticality is not an issue for several reasons, the most important of which is that CANDU fuel cannot become critical without the presence of heavy water, regardless of the density or age of the fuel (Garisto et al. 2014). Ordinary water is insufficient to support criticality of used CANDU fuel even if embedded in ordinary water. Furthermore, water would not have access to the used fuel in intact containers anyway.

---

[1] 48 bundles x 19.7 kgU/bundle x (0.031+0.018) mol gas/kgU at 1 Ma ~ 46 mol gas in 0.27 m^3 at 60^oC ~ 0.47 MPa

5.3.7 Mechanical Integrity

As the fuel bundles are supported by steel baskets, they are not subjected to significant load-bearing stresses. If tremors associated with earthquakes caused the fuel bundles to vibrate sufficiently, presumably some of the fuel pellets or the cladding could be damaged. However, the damaged material would still be within an intact container, and the overall evolution of the used fuel bundles would not be significantly changed.

5.3.8 Biological Processes

No changes arising from biological processes are expected because the combination of high temperatures, significant radiation fields, and the absence of water and organic carbon will exclude any biological reactions inside a container.

5.3.9 Confidence

At the time of placement in a deep geological repository, the physical properties of the used fuel and the inventory of radionuclides will be well characterized. Radionuclide decay constants are well defined, and so the changes in the inventory and the related changes in decay heat over time can be calculated with a high degree of confidence.

UO_2 is expected to be a durable material. This is supported by the existence of very old natural uranium deposits, many of which are a form of UO_2. The rates of several processes within the fuel, such as the diffusion of helium in UO_2, are influenced by temperature. These rates would be low because the temperature inside the container will be, at most, about 125°C, and will decrease to ambient host rock temperatures on a 100,000 year timeframe.

In the closed-system environment provided by an intact container, the physical condition of the fuel is not expected to change significantly over long periods of time.

5.4 Long-Term Evolution of a Used Fuel Container

The used fuel container (UFC) is designed to provide long-term containment of the used fuel, preventing contact with groundwater. As described in Section 4.3, the reference container design includes a steel structural vessel that is protected from corrosion with a copper coating. Also, as described in earlier sections, the repository environment will transition from hot (~100°C), dry and aerobic, to cool, water-saturated and anaerobic conditions. Within this environment, specific effects have been examined as they pertain to the evolution of the used fuel container. These are summarized here and described below:

- The copper coating of the UFC will resist external corrosion mechanisms including:
    - Corrosion attributable to oxygen trapped in the repository from placement activities;
    - Corrosion from chloride or other groundwater species that may be present or diffuse into the repository;
    - Corrosion from sulphide that 1) may be present or produced in the undisturbed rock that is capable of migrating to the UFC, 2) may be present in the buffer and 3) may be produced in the near field, including the EDZ, by sulphate-reducing bacteria;
    - Corrosion due to radiation effects (including radiolysis);

- Galvanic corrosion; and
- Stress corrosion cracking.

- Internal degradation mechanisms and processes will not affect the integrity of UFCs over long timeframes.

- The container is designed to withstand an external isotropic pressure of 45 MPa at 50°C. This value would accommodate the normal loads plus the hydrostatic load exerted at repository depth by a glacier above the repository.

Additional FEPs were assessed and excluded for the reasons outlined in the FEPs report (Garisto 2017) and thus are not part of the expected evolution described in this section.

5.4.1 Irradiation of Container Materials

The radioactivity inside the container is at its maximum value when the fuel is first loaded. The radiation field around the container is dominated by the gamma emission from short-lived fission products, which decay almost completely within the first 500 years after placement (see Figure 5-7). Thereafter, the residual radiation field would be very low because most of the remaining radioactivity will be from the alpha emission of long-lived actinides. Alpha particles do not penetrate beyond the fuel cladding.

High levels of neutron radiation, as found in nuclear reactors, can lead to hardening and embrittlement of reactor parts. The neutron flux inside a reactor is on the order of 4×10^{13} n/cm^2·s (neutron per centimetre squared, per second). In comparison, the neutron flux from used fuel is much smaller, about 10^2 -10^3 n/cm^2·s initially in a UFC. Over a million-year timeframe, the total neutron fluence experienced by the container would be less than 10^{15} n/cm^2 (based on Tait et al. 2000). A neutron fluence greater than 10^{22} n/cm^2 would be required to produce measurable displacement effects in metal. Furthermore, a thermal neutron fluence of 10^{19} - 10^{21} n/cm^2 would be needed for defect formation and significant hardening in copper and iron at 70 - 80°C. Consequently, the container metals will not be significantly affected by radiation over a million year exposure to used fuel.

Radiation would be more likely to have an indirect influence on container properties, in terms of changes to the chemical environment that will result from the decomposition (radiolysis) of air and water in the vicinity of the container; this topic is discussed in Section 5.4.3.3.1.

5.4.2 Container Temperature

The repository layout described in Section 4.8.1 is designed to ensure that the exterior surface temperature of the UFCs after placement remain below 100°C (see Figure 5-3), considering the reference horizontal placement concept at a depth of 500 m in crystalline rock.

In practice, only a fraction of the containers in a repository (those with the youngest fuel and / or the highest burnup values) would approach this maximum temperature. In the case of containers that otherwise are identical, those near the edges of a repository would have lower maximum temperatures than those in the centre of a repository because they would be less affected by heat from adjacent containers.

The repository layout is designed based in part on thermal analyses that limit the UFC temperature (Guo 2016). The models used for this analysis have been benchmarked against various heated field experiments (e.g., the full-scale Canister Retrieval Test at the Äspö Hard Rock Laboratory in Sweden; Guo 2009).

5.4.3 Mechanical Integrity

Containers would experience a range of stress conditions over time. The structural design of the container is determined largely by the requirement to provide adequate mechanical strength throughout its design life.

5.4.3.1 Effects of Hydrostatic and Buffer Swelling Pressures

After placement, the external load on the containers initially would consist of little more than the weight of the overlying sealing materials. The load would gradually increase during saturation of the repository. The swelling of the bentonite in the sealing materials is likely to occur unevenly on a local scale because the swelling would be controlled by the supply of water from the rock, by the shape of the room, and by the pathway of water along interfaces. The heterogeneous development of swelling pressures would result initially in non-uniform external loads on the containers, an effect that is expected to diminish as full saturation is achieved. The container design is robust enough to account for this.

By the time a repository is fully saturated, the hydrostatic pressure will have increased up to about 5 MPa at the repository depth of 500 m. As heating progresses, the pressure gradually increases, reaching the peak of 6.6 MPa at about 1000 years. Subsequently, the cooling period begins and the pressure reduces. Buffer swelling pressures could contribute up to 7 MPa to the load on the containers, depending on groundwater salinity and buffer density. The resulting loads are within the container design basis of 7 MPa.

5.4.3.1.1 Effects of Glacial Loading

Additional compressive stresses would be applied to the container by glaciation. It is unlikely that an ice sheet would develop over the repository until at least several tens of thousands of years have elapsed (Peltier 2011). By this time, the buffer saturation-related pressure loads would be fully applied. The loads on the UFC shown in Figure 5-10 are total loads due to effective stresses and pore pressures. In order to obtain the total pressure, the swelling pressure of bentonite backfill of 7.1 MPa (Baumgartner 2006), has been conservatively added.

Major increases in the pressure on the UFC arise during the glaciation period. As a bounding limit, a 3 km ice sheet could potentially add a pure hydrostatic load at the repository equivalent to almost a 3 km column of water (a little less allowing for density difference between water and ice), or about 30 MPa.

However, the loading is more complicated in reality, in part because the ice sheet is solid and much of its weight is carried through the rock structure. Analysis conducted by Itasca (2015) indicated that at the peak glacial load, the mean pressure exerted on the container reaches 17.6 MPa (without fluid migration. This is further mitigated at the container in part, by “stress arching” created when the lower modulus backfill carries less load than the stiffer enclosing rock mass.

The exerted pressure on the UFC is the sum of the initial hydrostatic groundwater pressure (5 MPa), and the change in porewater pressure created by ice sheet loading – representing the resultant total stress change in the far-field. Using a conservative Skempton coefficient of 0.7 to estimate the excess pore pressure, a upper bound pressure on UFC could be 22.7 MPa with fluid migration (Itasca 2015). The pressure will further increase to 29.8 MPa if the swelling pressure of the bentonite backfill is included (Figure 5-10). This estimated value represents a conservative assumption that considers maximum porewater pressure increases allowing for anticipated fluid migration and porewater pressure dissipation. The estimated UFC loading value in this analysis is based on an ice thickness of 3 km. The transient loading on the UFC throughout a glacial cycle is shown in Figure 5-10.

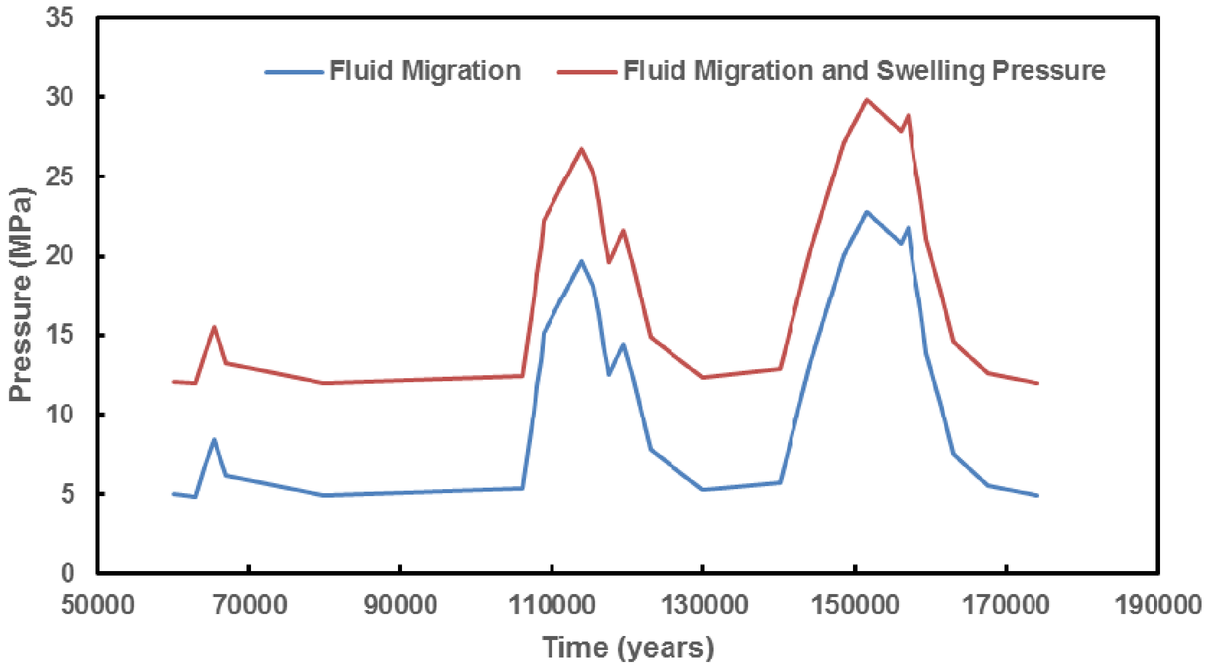

Figure 5-10: Evolution of Pressure on UFC over a Glacial Cycle

5.4.3.1.2 Effect of Seismic Stresses

The Canadian Shield is characterized, in general, by low levels of seismic activity as it is in the center of a stable craton (Atkinson and Martens 2007). Large earthquakes would therefore be very unlikely, although an increase in the number and intensity of earthquakes is likely in response to the reduction in loading as ice sheets retreat.

Earthquakes typically are less destructive at depth than at the surface, diminishing the impact of any seismic activity on a deep geological repository (Bäckblom and Munier 2002), and postglacial faulting is more likely to reactivate an existing zone of weakness in the rock than it is to develop new fractures (see Section 5.1.1).

The present repository site is assumed to be a low seismicity area, consistent with the typical Canadian Shield. The repository is placed away from large fractures, and containers are only placed in rooms without significant local fractures. Normal small earthquakes are unlikely to have significant effect on the site, repository or containers. Large earthquakes could affect the existing fractures, and are considered through the assumption of a high permeability for the existing fractures, which likely is much higher than the in-situ permeability of deep fractures at a real site. Other effects of a very large earthquake are considered within the Disruptive Scenarios.

5.4.3.1.3 Effect of Creep

Creep is the slow deformation of a material under an applied stress that results in a permanent change in shape. For a copper coated vessel, no gap exists between the integrally bonded steel and copper components; thus, the mechanism does not impact either copper or steel independently of each other. For both cylindrical body and hemispherical head components of the UFC, creep is determined by the performance of the steel. As the copper is bonded to the steel, creep rupture of the copper coating is not an issue.

Steel is designed to remain load-bearing over the design lifetime of a container (Werme 1998, Saiedfar and Maak 2002). For example, the maximum stresses developed in the reference steel vessel are only about 30% of its yield strength under normal saturation-related pressures, and approaches the yield strength under peak design-basis glaciation pressures. The creep rate of steel under the anticipated loading conditions (20% of its ultimate tensile strength under saturation-related pressures) and temperature (about 100^{o}C or less) is insignificant. The exact rate is uncertain, but it is expected that it would take at least 100,000 years for any appreciable amount of creep deformation to develop in the steel vessel (Dutton 2006).

5.4.3.2 Effect of Chemical Processes Inside the Container

The containers are expected to remain intact throughout the timeframe of the safety assessment. Chemical changes over time involving those processes that affect the interior of the container (a closed system) may therefore be considered separately from those that affect its exterior surface.

At the time of packaging, which will be conducted in ambient conditions, the container interior is dry, as are the used fuel bundles. It is expected that air and water vapour trapped during the closure of the container will subsequently react with the metals in the container interior (SKB 2011).

The zirconium alloy in the fuel bundles described in Section 5.3.4 will already have a surface film of ZrO_2 that formed at high temperatures in a reactor. This resistant ZrO_2 surface layer on the cladding will inhibit any further reaction with the small amount of air initially available inside the container. This is in contrast to the more porous and reactive air-formed iron oxide layer on steel that is not expected to prevent further oxidation. Thermodynamic and kinetic arguments predict that reaction between the iron and oxygen will occur, even at a very low oxygen partial pressure. Therefore, the steel inner vessel and the steel baskets holding the fuel bundles would tend to react rapidly with any available oxygen, forming iron oxides/hydroxides as corrosion products. This would remove any gaseous oxygen and water from the interior of the container, so that conditions in the interior will become dry and anoxic. Using conservative assumptions with respect to high amounts of water being trapped (e.g., damaged fuel bundles), approximately 1 μm of iron oxide is expected to form from these internal reactions.

In addition, irradiation of air will produce small quantities of oxidized nitrogen by radiolysis. Owing to the limited quantities of oxygen and water, and the reactivity of these species with the carbon steel inside the container, no significant quantities of species such as nitric acid are anticipated. Studies are being directed at localized corrosion within the container, either at welded zones or as a result of radiation/radiolysis processes; no significant issues have been identified (Guo et al. 2016, Morco et al. 2017, Turnbull et al. 2017, Wu et al. 2017).

Fuel elements with defective cladding would also release some fission gases to the container interior, particularly if the cladding fails after the container is sealed. Iodine, which assists stress corrosion cracking of metals under some conditions, is the most noteworthy of these gases. However, the partial pressure and total quantities of any released gases would be small (e.g., $<10^{-7}$ MPa for iodine). Most of the other released gases would be adsorbed onto the internal surfaces of the steel structure, or they would be distributed among the exposed iron, zirconium and copper surfaces, yielding no significant changes to the interior of the container (McMurry et al. 2003).

In summary, the interior of the container would quickly develop a dry, reducing chemical environment that would persist as long as the container remains intact.

5.4.3.3 Effect of Chemical Processes Outside the Container

This section summarizes the current understanding of the corrosion behaviour of copper used fuel containers in a deep geological repository. This understanding has been developed based on an extensive experimental program carried out in Canada, and other parts of the world, over the past 30 years, and on the results of mechanistically-based modelling of various corrosion processes.

The corrosion behaviour of copper depends on the nature of the environmental conditions. For this discussion, the following attributes of the container and reference repository design are important.

- The container corrosion barrier is manufactured from high purity copper.
- The container is placed in the room within clay blocks, capable of sealing the system when in contact with water.
- The containers are surrounded by buffer material comprising dense bentonite block and gap fill, with an average dry density of at least 1.6 Mg/m^3.
- The groundwater is a Ca-Na-Cl solution, with small amounts of sulphate and low levels of carbonate.
- The available O_2 is limited to that trapped initially in the pores of the buffer and backfill materials, and the groundwater itself is O_2-free.
- The container includes a thick inner steel vessel resulting in a maximum surface dose rate of <2 Gy/h.
- The container surface temperature does not exceed 100°C.

- There is a period of unsaturated conditions immediately following container placement and prior to saturation of the repository.
- There is little or no sulphide (HS^-) present in the groundwater.
- The container is subject to external loading from a combination of the hydrostatic load and bentonite swelling pressure.

Experimental research and modelling has considered uniform corrosion, pitting corrosion, stress corrosion cracking (SCC) and microbially-influenced corrosion (MIC). A list of studies conducted in the Canadian copper corrosion program is tabulated in Kwong (2011) and reviewed in Scully and Edwards (2013). A more recent review has been performed of all copper corrosion mechanisms, particularly for active research topics, which further supports the conclusions below (Scully et al. 2016).

Overall, these studies conclude that a used fuel container with an external barrier of copper, placed in a deep geological repository, will be primarily subject to general corrosion, regardless of copper form (i.e. manufacturing method, Standish et al. 2016). The degree of localized attack (pitting), microbial-influenced corrosion and stress corrosion cracking will be negligible, and can be controlled using standard engineering design. All forms of corrosion will be stifled as the repository environment becomes anoxic. The various corrosion mechanisms are discussed in more detail in the following sections.

The important characteristics of the corrosion of copper containers in a deep geological repository are as follows.

- The corrosion behaviour changes with time, largely as a result of the evolution of the repository environment (King and Shoesmith 2010). This environment evolves from an initial period of warm, aerobic conditions to an indefinite period of cool, anoxic conditions. From a corrosion perspective, this environmental evolution means that localized corrosion processes are limited to the early period, with corrosion becoming more uniform in nature as time progresses.

- The nature of the environment at the container surface determines the corrosion behaviour. The surface environment can be different from that in the host rock as a result of the chemical conditioning of the groundwater by the bentonite clay and the slow mass transport of reactants to, and of corrosion products away from, the container surface due to the presence of the bentonite.

- A limited period of time of a few hundred years is available during which gamma radiation from within the container can interact with water in the surrounding media (i.e., buffer) and produce trace amounts of reactive species, such as hydrogen peroxide, that may interact with the container surface.

- In general, groundwater chloride promotes the uniform dissolution of copper and suppresses localized corrosion and SCC (King et al. 2010, 2011a).

- The dense bentonite clay buffer and high groundwater salinity around the container suppress microbial activity.

Specific corrosion processes are described below.

5.4.3.3.1 Uniform Copper Corrosion

The uniform corrosion of copper in the environment expected in a deep geological repository has been extensively studied, and the corrosion mechanism is well understood and summarized in Kwong (2011). Figure 5-11 illustrates the mechanism developed to describe the uniform corrosion of copper in compacted bentonite saturated with oxygen (O_2) and containing chloride (Cl^-) porewaters. The mechanism couples the interfacial electrochemical reactions that occur on the container surface to various processes occurring at or within the bentonite. These processes include: the diffusive mass-transport of species to and from the corroding interface (denoted by the wavy arrows in Figure 5-11); the adsorption and desorption of Cu(II) on the clay; redox reactions involving dissolved O_2, Fe(II), and Cu(I) and Cu(II) species; the dissolution and precipitation of various solid mineral phases and corrosion products; the partitioning of O_2 between the gaseous and aqueous phases; and, in a simplistic manner, the microbial consumption of dissolved O_2. This reaction scheme applies equally to both the buffer and backfill materials, as well as the to host rock, and further details are included below.

Copper can react in dry air as shown in Reaction (5-6). The rate of copper oxidation in dry air at temperatures below 150°C is of the order of nm/a, and, therefore, is effectively negligible.

$$2Cu + {}^{1}\!/_{2}\,O_2 \rightleftharpoons Cu_2O \qquad (5\text{-}6)$$

Copper will corrode in solutions containing O_2 under atmospheric conditions, providing the relative humidity is above that required to form a thin surface water film, i.e., approximately 50 to 70% relative humidity. The rate of corrosion may also depend on the presence of atmospheric contaminants, such as SO_2, NO_2, and CO_2. The ion-containing water film acts as an electrolyte to support electrochemical reactions and the dissolved impurities will further enhance the corrosion process. For instance, in water, SO_2 forms H^+ and HSO_3^-; the latter species can be oxidized to sulphate by oxidants in the air to produce local quantities of sulphuric acid. Similarly NO_2 can be absorbed in the water film as HNO_3, nitric acid. Either of these acidic media can enhance corrosion and copper dissolution; although the effect is very limited in this case, as oxygen is very limited. The corrosion behaviour of copper in O_2-containing Cl^- solution has also been well studied. A detailed reaction mechanism exists that accounts for the various electrochemical, chemical, redox, adsorption/desorption, precipitation/dissolution, and mass transport processes involved in the corrosion process in compacted bentonite. The behaviour of copper over a range of chloride concentrations has also been experimentally evaluated. Kinetic rate constants, equilibrium constants and other thermodynamic parameters required for modelling are available, as summarized in Kwong (2011).

During corrosion, the anodic reaction is coupled to the cathodic reduction of an oxidant such as dissolved O_2; however, it may also be supported by the presence of another oxidizing species such as Cu^{2+}, Fe^{3+}, Pb^{4+}, etc.

$$Cu + O_2 \text{ (or other oxidant)} \rightarrow Cu^+ \text{ or } Cu^{2+} \qquad (5\text{-}7)$$

Both Cu^+ and Cu^{2+} can precipitate as species such as Cu_2O and $CuCl_2{\cdot}3Cu(OH)_2$, respectively (Reactions (5-8) and (5-9)). Such a duplex corrosion product layer could comprise an inner layer of Cu_2O and an outer layer of basic Cu(II) salts, such as $CuCl_2 \cdot 3Cu(OH)_2$) or $Cu_2CO_3(OH)_2$, depending on the specific composition of the porewater.

$$2CuCl_2^- + H_2O \rightleftharpoons Cu_2O + 2H^+ + 4Cl^- \tag{5-8}$$

$$2Cu_2O + O_2 + 2Cl^- + 4H_2O \rightleftharpoons CuCl_2 \cdot 3Cu(OH)_2 + 2OH^- \tag{5-9}$$

While a precipitated surface film of this nature could block surface electrochemical reactions and prevent the permanent separation of anodic and cathodic reactions required for localized corrosion to occur, it is notable that Cu^+ dissolves readily in Cl^--containing solutions. This feature is likely to ensure that the metallic copper will be continuously exposed to the solution, which will enhance general corrosion. In addition, as the repository environment becomes anaerobic, residual $CuCl_2 \cdot 3Cu(OH)_2$ layers will also dissolve owing to the disproportionation of Cu^{2+} with metallic copper (Cu^0) to produce $2Cu^+$, the stable and soluble species.

The radiation field, which begins at < 2.3 Gy/h (Morco et al. 2017) and diminishes over several hundred years, is significantly below the value expected to cause alterations to the copper (i.e., at dose rates >100 Gy/h, see SKB 2010). However, since water radiolysis is known to produce oxidants such as oxygen, there is significant research ongoing to validate this assessment. When high gamma fields are used in experiments designed to accelerate the effect (i.e., 3 kGy/h for 72 h in air), copper oxidation takes the form of deposits that spread laterally (Ibrahim 2015). Despite the absence of evidence for radiolytic-related corrosion, an allowance of 0.1 mm of general corrosion has been assumed for this process.

In the absence of oxygen, corrosion would require a reaction with water to produce hydrogen gas (H_2):

$$2Cu + H_2O \rightleftharpoons Cu_2O + H_2 \tag{5-10}$$

Or

$$Cu + H_2O \rightleftharpoons CuOH + {}^1/_2 H_2 \tag{5-11}$$

Known thermodynamic relationships (Puigdomenech and Taxén 2000) indicate that the equilibrium shown in Reaction (5-10) is very strongly biased towards the reactants: metallic copper and water. Accordingly, upon formation of a very small amount of Cu_2O (i.e., a single monolayer), only a very small amount of hydrogen, with a partial pressure on the order of 10^{-11} mbar, is necessary to suppress the corrosion reaction [i.e., Reaction (5-10) becomes unfavourable in the forward direction]. In addition, the corrosion product in Reaction (5-11) has not been shown to be stable. Therefore, Reactions (5-10) and (5-11) are considered very improbable in water.

Under anaerobic conditions, copper corrosion accompanied by the evolution of H_2 does occur in the presence of sulphide, as per Reaction (5-12).

$$2Cu + H^+ + HS^- \rightleftharpoons Cu_2S + H_2 \tag{5-12}$$

Sulphide is not widely found in groundwaters in crystalline rock in Canada (King et al. 2017). However, owing to the possibility of remote microbial reactions that produce sulphide (see Section 5.4.3.3.5), and the very small dissolution of sulphide from pyrite in the rock and bentonite, a reference value of 1 µmol/L (0.034 mg/L or 34 ppb) has been considered in the absence of site-specific data. This value is less than those projected for Sweden and Finland, where deep groundwaters do contain small amounts of HS^- (typically <1 mg/L; King et al. 2010, 2011a). In all cases, these concentrations result in corrosion rates of well below one nm/a due to the slow transport of sulphide to the container surface through the compacted bentonite buffer (SKB 2011).

Researchers from the Royal Institute of Technology (Sweden) have published experimental results indicating that copper can corrode in pure, oxygen-free water. Their research claims that water is reduced in the anaerobic corrosion process to form hydrogen atoms (Szakálos et al. 2007, Hultquist et al. 2009, 2011), and that a hydroxyl-containing copper corrosion product may be produced. Subsequent expert review (Swedish National Council 2010) concluded that it was necessary to demonstrate that the proposed corrosion product was thermodynamically stable before it could be justifiably claimed that copper could corrode in oxygen and sulphide-free water. An SKB review also concluded that there were possible errors in the original experiments (SKB 2010).

Further studies have been conducted in Sweden, as well as by NWMO. Preliminary results were reported in SSM (2011a) and Hultquist et al. (2013). These have found extremely small quantities of hydrogen in similar experiments, although the tests were not definitive. In addition, careful analysis of the thermodynamics of the reactions between copper, pure water, and sulphide (SSM 2011b) has indicated that copper-water interactions, as described by (5-10) and (5-11), are theoretically possible but would only produce very small quantities of hydrogen, and that reactions with sulphide species are much more important (SSM 2011b). More recent experimentation has focused on preparation and cleaning of copper samples and the effects on measured hydrogen (Johansson et al. 2015), and some truly definitive work by Ottosson et al. (2016) has demonstrated very clear evidence that as-produced/purchased copper contains significant amounts of hydrogen prior to its immersion in water. In this latter work, it was demonstrated that pretreatment of copper prior to experiments can completely remove hydrogen and suppress all hydrogen production during very long-term immersion in ultrapure water.

In addition, while this topic is still being studied, it appears that the hydrogen produced from a copper-water interaction would be self-limiting, and not a significant corrosion mechanism within a repository. If the corrosion mechanism via reaction (5-11) does occur, for example, hydrogen partial pressures of ~1 mbar (Szakálos et al. 2007) and 0.5 mbar (Hultquist et al. 2009) are all this is required at temperatures of 73°C and 45°C, respectively, to suppress the corrosion reaction. In a DGR, sufficient hydrogen could be present from many sources: the copper-water reaction, if it occurs; anaerobic corrosion of steel components; reactions between copper or steel with trace levels of sulphides; and/or native hydrogen levels (SKB 2010). For example, measurements at depth within crystalline rock formations have demonstrated hydrogen concentrations between 2 and 1,600 µmol/L (Sherwood Lollar 2011), equivalent to partial pressures of 2.6 to 2,000 mbar. The source of hydrogen at these depths is predominantly radiolysis reactions of the natural uranium in the host rock material.

The rate-controlling process for the overall uniform corrosion of copper changes as the environmental conditions evolve. Under aerobic conditions, there is evidence that the transport of dissolved Cu away from the corroding interface can be rate controlling (King et al. 2010, 2011a) (i.e., the corrosion reaction is anodically transport limited). As the repository environment becomes anoxic, the corrosion rate must eventually become cathodically transport limited as a result of the slow diffusion of oxidant to the container surface. In the presence of sulphide, if such species were to be found in Canadian groundwaters or produced from sulphates by microbes, then the corrosion rate is limited by the rate of transport of HS^- to the container surface (Chen et al. 2011, King et al. 2011b).

Overall, the uniform corrosion behaviour of copper in conditions expected for a deep geological repository in crystalline rock is well understood. Both the mechanism of copper corrosion in oxygen-containing chloride solution and kinetic and thermodynamic parameters required for modelling are available.

5.4.3.3.2 Uniform Copper Corrosion Modelling

To complement the extensive experimental studies on which the mechanism in Figure 5-11 is based, a detailed reactive-transport model has been developed to predict the long-term uniform corrosion behaviour of copper containers in the repository. The model, referred to as the Copper Corrosion Model for Uniform Corrosion (CCM-UC), is based on the mechanism in Figure 5-11 and couples the corrosion behaviour of the container to the various processes occurring in the near- and far-fields of the repository, specifically the evolution of the environmental conditions. The corrosion behaviour is modelled using electrochemical mixed-potential principles. As a result, the model not only predicts the time-dependent corrosion rate (as a corrosion current density), but also the time-dependent corrosion potential (E_{CORR}). E_{CORR} is a useful parameter for assessing the probability of localized corrosion and stress corrosion cracking, as well as providing information about uniform corrosion.

Various methods have been developed to predict the rate or extent of the uniform corrosion of copper containers. Because uniform corrosion is limited by the availability of oxidant, the rate of corrosion is of less importance than the extent of corrosion. The maximum depth of corrosion can be assessed based on mass-balance principles (SKB 2011) or using the detailed mechanistically-based CCM-UC model (King et al. 2008).

The exact amount of O_2 trapped in a repository placement room during its closure depends on the buffer and backfill material porosity, volume (relative to the total UFC surface area in the room), and, crucially, degree of saturation at the time of closure (the majority of the trapped O_2 is present as gaseous O_2 in the air-filled pores of the buffer and backfill). If all trapped oxygen in the reference placement room, corresponding to 2.6 mol_{O2}/m^2_{Cu}, is consumed by copper corrosion, then the maximum wall penetration of the UFCs in the present design would be 75 µm (0.075 mm). In reality, nearly all of the O_2 will be consumed by aerobic microbial activity in the backfill material and the oxidation of ferrous species, so that the actual depth of uniform copper corrosion will be much lower. Depending upon the relative rates of the different microbial and redox reactions, the model predictions suggest that more than 50% of the trapped O_2 could be consumed by processes other than corrosion. A consequence of the limited availability of oxidant is that, once all of the O_2 (or the Cu^{2+} produced by the oxidation of $CuCl_2^-$ by O_2) has been consumed, and there is sufficient generation of H_2, corrosion of the container ceases.

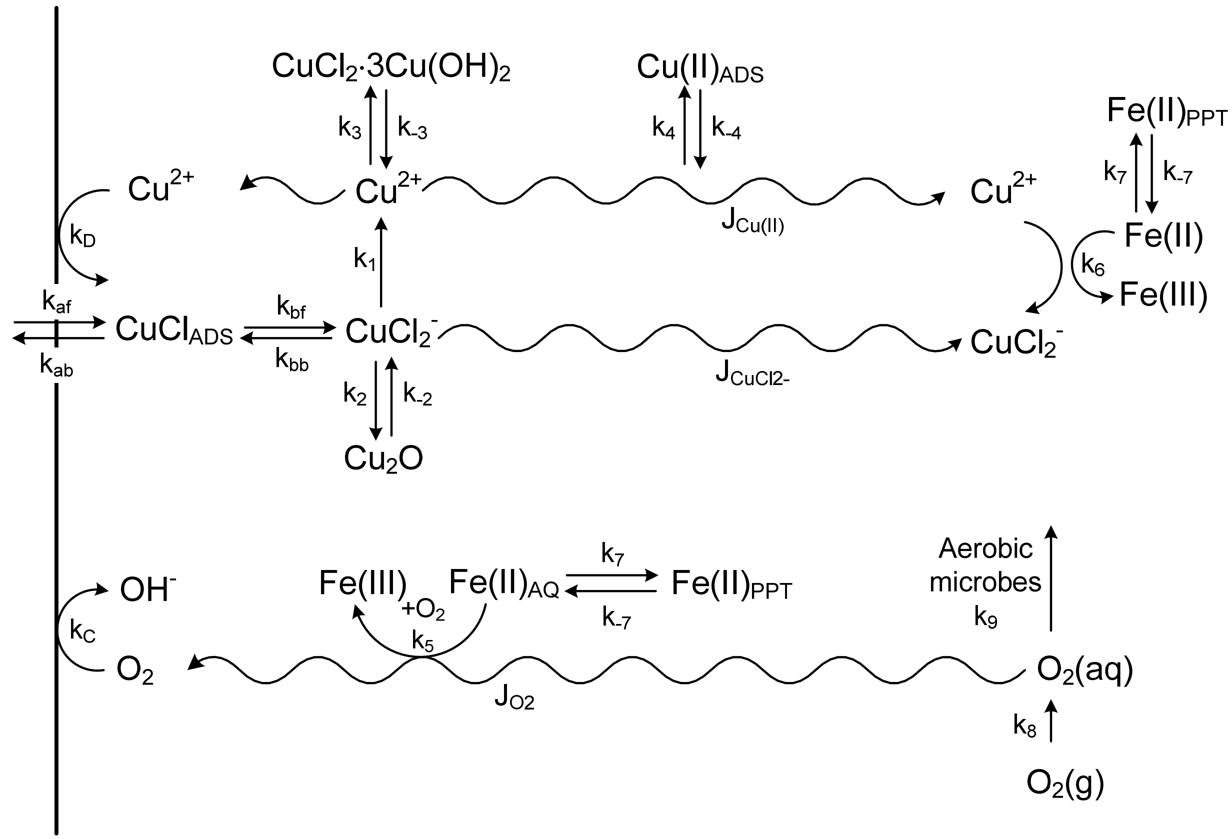

Notes: From King and Kolář (2000) and King et al. (2008, 2010, 2011a). The k's denote rate constants for the various interfacial electrochemical and homogeneous reactions and the J's denote diffusive fluxes.

Figure 5-11: Reaction Scheme for the Uniform Corrosion of Copper in Compacted Bentonite Saturated with O_2-Containing Chloride Solution

5.4.3.3.3 Localized Corrosion

Kwong (2011) and Scully and Edwards (2013) identify that studies designed to specifically examine the surface profile of copper corroded in groundwater-saturated, compacted buffer materials have been completed. Experimental results showed that the copper will only undergo a form of surface roughening as a result of the non-permanent separation of anodic and cathodic processes. A mechanism to account for the observed surface profile, which involved the periodic separation of anodic and cathodic processes through the formation of temporary occluded cells, has since been proposed (King and Kolář 2000). Conceptually, these conditions could exist where there are differences in the flux of O_2 to different parts of the container surface, i.e., where bentonite blocks of different density might be used around the container.

Experimentally and through thermodynamic analysis, it has been shown that any localized corrosion rates would decrease with decreasing oxygen concentration and decreasing container surface temperature. The resultant corroded copper surfaces showed only general corrosion with minor surface roughening and no distinct pitting, and it was concluded that the rate and extent of localized corrosion in a deep geological repository will be very small because there will be a limited supply of oxygen.

More recent work (Qin et al. 2017) has focused on the environmental and surface conditions of copper within a DGR during the early oxidizing period, as coverage by a surface passive film is required for classical pitting. Experimental conditions have included expected groundwater constituents, such as chloride, sulphate and carbonate, over a range of pH and temperature values. Broadly speaking, passive films can be produced on copper in the absence of chloride and low temperatures (i.e., 25°C) for pH < 9. As temperature or chloride are increased, or as pH or carbonate are reduced, passive conditions are lost, and active, general corrosion is favoured. At expected repository conditions, where groundwater is dominated by chloride and temperatures exceed 75°C (i.e., during the oxic period), there is a significant safety margin of at least 2.5 pH units between expected repository pH and the conditions under which passive films can be formed. Work is ongoing to enhance the statistical significance of these data sets.

The long-term localized corrosion behaviour of copper has also been extensively studied in the Swedish / Finnish nuclear waste management programs. They predicted the depth of localized corrosion based on pitting factors and an analysis of empirical pitting data from archaeological artifacts subject to long-term burial in natural environments. Extreme-value statistics have also been applied to estimate the maximum pit depth on a container as a function of exposure time in the repository (King 2006). A pit propagation model was developed for reducing conditions, assuming the pit growth was limited by the transport of HS^- to the copper surface.

Based on the various measurements and models summarized above, it is clear that a copper corrosion barrier in a deep geological repository will not undergo classical pitting corrosion, but only a surface roughening. This process may necessitate provision for a maximum of 0.1 mm of additional copper wall thickness to account for any wall loss due to general oxic corrosion.

5.4.3.3.4 Stress Corrosion Cracking

Considerations for stress corrosion cracking (SCC) of the copper shell have been extensively explored in Kwong (2011). The occurrence of SCC requires a susceptible metal to be exposed to sufficient tensile stress and an active SCC agent. Copper is known to be susceptible to SCC in environments containing ammonia, nitrite ions, acetate, or, possibly, high concentrations of sulphide. Studies focused on SCC have concluded that the SCC of copper requires the prior formation of a thin oxide or tarnish film. When this film does not form, SCC is not observed.

While SCC agents are not normally found in natural groundwater, they can be introduced by either mining or microbial activities. Numerous tests have, therefore, been performed to assess the SCC behaviour of copper in nitrite-, ammonia- and acetate-containing environments. Results indicate that copper SCC susceptibility would decrease with decreasing concentrations of the SCC agents. These studies also suggest a threshold concentration level for each agent below which SCC would not occur. Also observed in these studies is the inhibiting effect of chloride on copper SCC in nitrite, ammonia and acetate environments; the SCC susceptibility decreases with increasing chloride concentration. The ability of chloride to inhibit SCC also appears to be enhanced by elevated temperatures, as exhibited in tests conducted at 100 to 130°C (in nitrite only and nitrite/chloride solutions). This effect can be attributed to the ability of chloride ions to promote general dissolution of copper, which results in more uniform corrosion (see Section 5.4.3.3.3).

Furthermore, tensile stress is needed on a material to initiate SCC. However, the UFC design has been optimized to ensure that stress patterns are predominantly compressive. This design is significantly improved over UFCs that utilize flat heads, as the latter contains regions with tensile stress that result during loading to conservative glacial conditions (i.e., > 40 MPa).

In summary, research results have suggested SCC under aerobic conditions in a deep geological repository is unlikely, as the pre-requisite conditions of corrosion potential, interfacial pH, tensile stress and concentration of SCC agents do not exist simultaneously at the container surface. According to mechanistic arguments, there is also no evidence to indicate that SCC of copper is possible under anaerobic conditions at the sulphide levels expected at the container surface. Based on the nature of the repository environment, SCC does not appear to be a threat to the integrity of a copper used fuel container. Despite the low risk of SCC on copper, suitable engineering procedures can be effectively applied to further minimize the probability of SCC. This will include ensuring that the level of airborne ammonia and nitrite formed during blasting operations are controlled (i.e., below the threshold concentration) in order to preclude the possibility of cracking.

5.4.3.3.5 Microbially-Influenced Corrosion

The historical microbially-influenced corrosion (MIC) program is summarized in Kwong (2011). Similar to other engineering materials, copper is susceptible to this type of corrosion should the environment be hospitable to microbes that produce corrosion-causing species. MIC is largely mitigated within the DGR by ensuring that the water activity of the system is ≤ 0.96 near the container (i.e., within the bentonite buffer). During the evolution of the repository, the water activity will remain low, from the early dry period through to the saturated period, largely owing to the very high average compaction of the bentonite material (> 1,600 kg/m^3) and the nature of the bentonite. As placed, bentonite contains no available water, owing to the modest amounts used in manufacturing and the high suction potential of the material (King et al. 2010). Subsequently, incoming water is tightly bound by the confined material as it swells against the host rock. Section 5.5 describes buffer performance comprehensively, including the rationale for excluding near-field microbial growth as a corrosion mechanism.

In principle, far-field microbial metabolic by-products may affect the SCC behaviour of copper, as microbial activity may form SCC agents, ammonia, nitrite, and acetate ions that traverse the buffer toward the UFC. These species are not likely to be produced in sufficient quantity to affect SCC (see Section 5.4.3.3.4), and the UFC is not under sufficient stress. With respect to MIC, another species often considered is HS^- produced by the reduction of sulphate by sulphate-reducing bacteria. This reaction occurs under anaerobic conditions and requires the presence of simple organic molecules or H_2 as electron donors. Without the formation of biofilms on the container surface, which are prevented via the highly-compacted bentonite material, the only form of MIC possible is that due to the diffusion of remotely-produced metabolic by-products through the bentonite to the container surface. Sulphide ions produced at a location away from the container surface must diffuse through the bentonite sealing materials to have any effect on container corrosion. The maximum corrosion rate is, therefore, limited by the rate of diffusion of sulphide (HS^-) to the container surface, a continued supply of which is required to sustain MIC.

To assess potential damage from sulphide ingress toward the UFCs, the NWMO has modelled the diffusion-based flow for a continuously produced source of sulphide in the far field (Briggs et al. 2017a). Sensitivity studies have been completed for values ranging from the reference groundwater value of 1 µmol/L (0.034 mg/L or 34 ppb) to beyond 300 µmol/L (10 mg/L or 10 ppm), and the relationship between concentration and corrosion rate has proven to be linear, owing to the Fickian diffusion. However, because of the complex shape of the UFC and buffer box, MIC is not uniform; rather, it tends to concentrate its effects on the ends of the UFCs. This result is readily visible in Figure 5-12, which normalizes low flux areas against the highest region (on the end cap, from Briggs et al. 2017b).

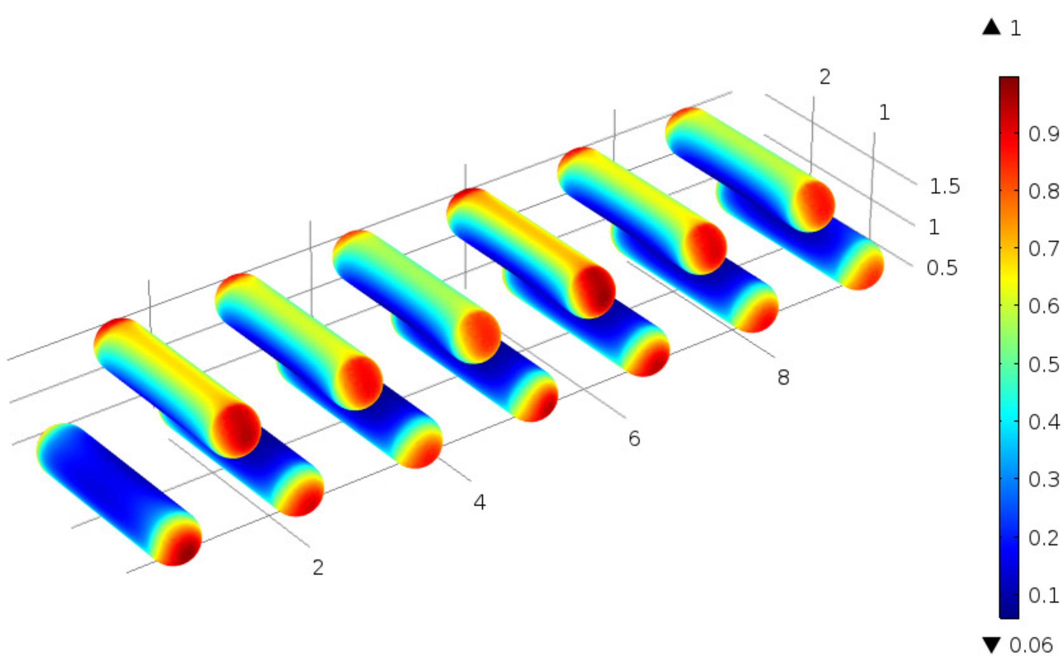

Figure 5-12: Normalized Diffusive Sulphide Flux Ratio for UFCs in Placement Room for a Uniform Background Concentration of Sulphide in the Host Rock

From these results, a simplified equation can be derived for the maximum corrosion rate observed in an placement room:

$$CR_{MAX}\ ,\ {}^{nm}/_{a} = 0.8[HS^{-}]\ ,\ {}^{mg}/_{L} \tag{5-13}$$

Thus, for a groundwater sulphide concentration of 1 µmol/L (i.e., 0.034 mg/L or 34 ppb), the maximum corrosion rate from sulphide diffusion would be 0.026 nm/a, while values of 340 ppb or 3400 ppb produce 0.26 nm/a and 2.6 nm/a, respectively. Over one million years, the wall loss from sulphide corrosion from the scenario of 1 µmol/L sulphide will be just 0.026 mm, a value hardly discernable from the wall loss assumed due to oxic corrosion/localized corrosion of 0.27 mm. This feature can be seen in Figure 5-13, which presents the remaining copper thickness after corrosion as a function of time for a period up to one hundred million years.

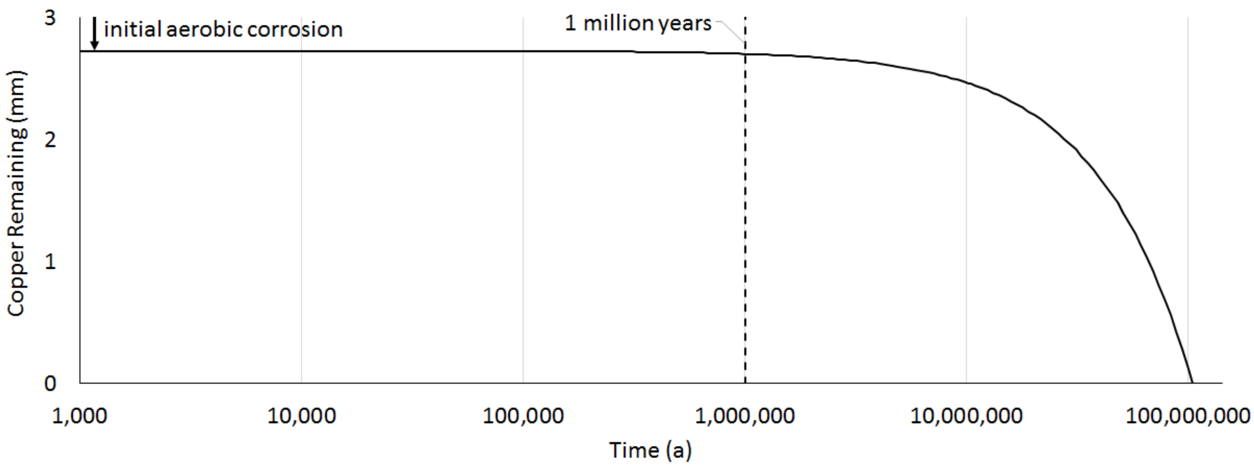

Figure 5-13: Reduction in Thickness of Copper Due to Reaction with Groundwater Sulphide

5.4.3.4 Summary

Research work over the past 30 years has established a good understanding of the long-term performance of copper used fuel containers in a deep geological repository.

In the environments anticipated in crystalline rock, copper will begin to corrode under early atmospheric conditions, provided the relative humidity is above 50-70%. The rate and mechanism of corrosion will be affected by the presence of atmospheric contaminants, such as SO_2 and NO_2, as these species potentially acidify the surface. Maximum damage from these processes is expected to be 70 µm; an additional factor of 100 µm may also be conservatively considered to account for the minor roughening that may occur concurrent with this process. An additional 100 µm allowance is included for radiolysis-related corrosion.

Stress corrosion cracking is highly unlikely, owing to the lack of the pre-requisite conditions for SCC (the required threshold concentration of SCC agents, a suitable interfacial pH, tensile stress and the required corrosion potential on the copper surface).

Microbially-influenced corrosion of copper will be controlled by the use of compacted bentonite around the copper container (and, in some rock types, the high salinity of native groundwater) to suppress microbial activity in the near field and to limit the migration of any corrosive agents produced by microbial activity in the far field. Nonetheless, trace sulphide concentrations of 1 µmol/L account for far-field microbial activity that may impact the UFC.

Although there have been measurements of water acting as an oxidant for copper, the available evidence is not entirely reproducible. Regardless of such uncertainty, there is significant evidence that the hydrogen produced from a copper-water interaction, or steel corrosion, within the repository would compel any such mechanism to be self-limiting, and thus would not be a significant corrosion mechanism within a repository. In addition, any early effects of water corroding copper would be overwhelmed by the interaction of copper and microbiologically-produced sulphide over the long term. Nonetheless, the low rate of this reaction will provide for an extremely long-lived container.

5.4.4 Effects of the Environment on Containers with Defects in the Copper Coating

Containers for a repository will be manufactured according to a process that includes careful fabrication and a series of inspections to preclude significant defects, as described in Section 4.3.1. Failures during manufacturing or quality-assurance practices, while unlikely, present the risk for undetected defects within copper coatings. In addition, although strict protocols and procedures for handling the UFCs will be in place, there is a non-zero probability that a UFC may be damaged during placement, resulting in a copper-coating defect.

Coating defects include the subset of through-copper defects, where the defect extends across the full thickness of the copper coating, exposing the underlying steel to the environment. Probability and consequences of defects are described in the following sections.

5.4.4.1 Impacts of Coating Defects

In general, defects within the coating that do not expose the steel do not significantly impact the performance of the UFC. From a corrosion processes perspective, very little wall loss is expected over 100,000 or even 1,000,000 years (i.e., well below <0.5 mm, see Section 5.4.3.3), which is similar to the conservative Non-Destructive Examination (NDE) detection estimate of 0.8 mm. Accordingly, very long-lived containers can be expected where coating damage does not expose the underlying steel.

In terms of quantifying damage, the impact of an undetected defect on the local corrosion rate will depend partly on the size and shape of the defect. Figure 5-14 proposes some examples of hypothetical defects in a nominal 3 mm copper coating. If a defect results in a locally thinner copper coating, then the steel beneath a defect may be exposed to groundwater earlier than Figure 5-13 suggests. Figure 5-15 and Table 5-3 present the time to exposed steel beneath a defect as a function of the defect size. Calculations assume that defects are oriented for maximum reduction in the local coating thickness.

These results show that any defects passing a quality inspection undetected would lead to exposed steel only after a period greater than 10 million years. Exposed steel upon placement in the repository would require a through-copper defect to pass quality inspection undetected.

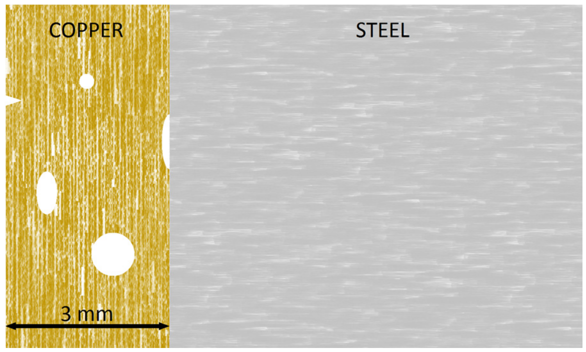

Figure 5-14: Hypothetical Defects in the Copper Coating

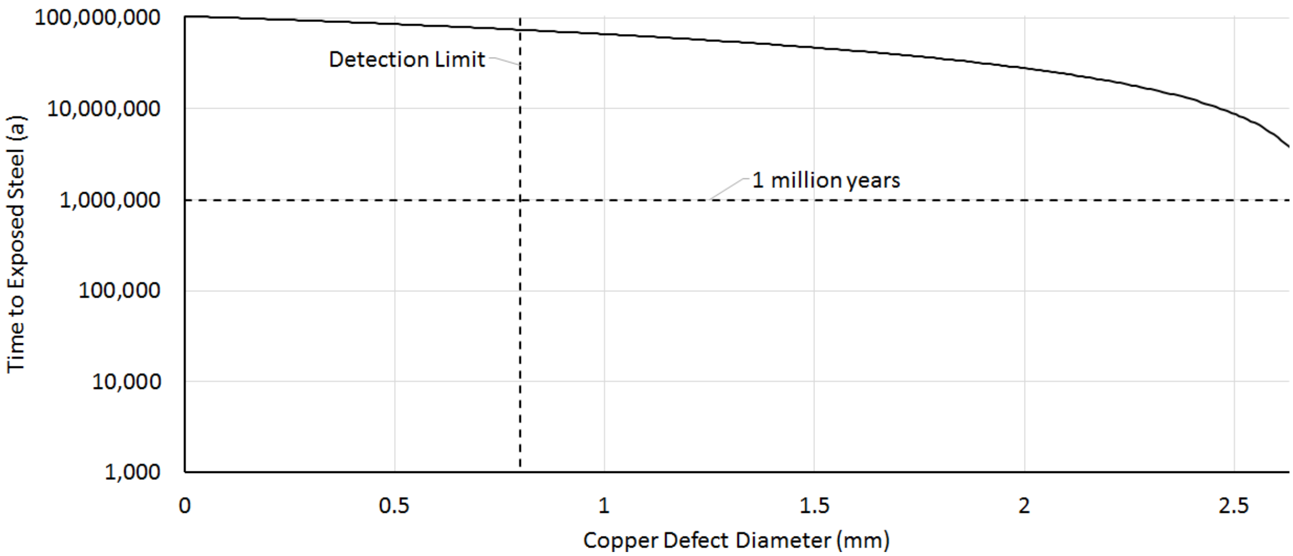

Figure 5-15: Time to Exposed Steel beneath Defects in a Nominal 3 mm Copper Coating

Table 5-3: Time to Exposed Steel Beneath Defects in a Nominal 3 mm Copper Coating

Microbially-Influenced Corrosion	0.026 nm/a
Corrosion = 3 mm	105 Ma
Time to Expose Steel, Defect = 0.8 mm	74 Ma
Time to Expose Steel, Defect = 2 mm	28 Ma

5.4.4.2 Impacts of Through-Copper Defects

Exposure of steel to the environment due to a through-copper defect would leave a (small) region of the container surface without protection from corrosion. As noted in Section 5.2.4, exposed steel can corrode throughout the entire life of the DGR, through a range of mechanisms. The very slow rate at which this process occurs in a DGR has led many countries, such as France and Switzerland, to select steel as their used container material, without any other corrosion barrier. Through a narrow defect in the copper coating, the steel corrosion processes are likely to be further slowed, as steel corrosion products are likely to plug the defect and inhibit contact with water (or oxygen). However, owing to the presence of copper directly on the steel (i.e., electrically connected), galvanic corrosion processes must also be considered for the oxic and anoxic periods, described in Sections 5.4.4.2.1 and 5.4.4.2.2, respectively, and experimentally examined in ongoing work (Standish et al. 2017).

5.4.4.2.1 Oxic Galvanic Corrosion

For galvanic corrosion to occur, one metal performs/catalyzes the cathodic electrochemical reactions, while the other metal performs/catalyzes anodic reactions. In the case of steel (iron) coupled to copper, oxidation of iron at the container breach would be enhanced if the very large intact copper surface could sufficiently support reduction reactions: either oxygen reduction during the aerobic period, or hydrogen reduction during the long anaerobic period.

Experiments conducted by Smart et al. (2004, 2005) have examined both conditions and measured galvanic currents – with the copper behaving as a cathode and the iron behaving as an anode. In aerated conditions, galvanic corrosion rates of iron (coupled to copper) are as high as 100 μm/a. Other research has revealed that copper-steel couples in aerated seawater can cause an enhancement in corrosion of steel (Chen et al. 2007). However, the actual depth of corrosion from this process would be significantly limited by the volume of oxygen available in the repository.

Competing with the galvanic couple during the oxic period is the copper oxidation mechanism (Section 5.4.3.3). While this reaction is not as energetically favourable as the galvanic couple that sees steel oxidized and oxygen reduced on copper, it does not require energy to transfer electrons between the metals or ionic species through the solution. As a result of these energy losses, galvanic couples typically have a small range over which they affect the system – for the UFC described above, this would imply that corrosion damage to the steel from the oxic galvanic couple would be very small compared to the anoxic corrosion of steel that would follow once oxygen is depleted from the system.

5.4.4.2.2 Anoxic Galvanic Corrosion

Smart et al. (2005) measured galvanic coupling currents in a deaerated system and values were much lower: typically 0.1 μm/a at 30°C and 1 μm/a at 50°C. These values are no different from those measured for iron corroding in deaerated groundwater, where water is reduced at the same steel interface at which steel is oxidized. In effect, the copper couple does not alter the corrosion properties of iron in this medium. The interpretation of this result is that the couple between iron and copper does not sufficiently polarize the copper negatively to support enhanced water reduction (King et al. 2010). Accordingly, the copper would be largely inactive in the context of the iron corrosion process.

The low importance of galvanic corrosion is also supported by results from the SKB Minican experiment. Post-test examination (of the first experiment after 4 years in-situ) has indicated extensive corrosion by sulphide present in the groundwater, but no evidence of galvanic corrosion (Smart et al. 2012).

5.4.4.2.3 Anaerobic Corrosion of the Steel Vessel Through a Defect in the Coating

Where water is in contact with the steel, Reaction (5-4) will occur forming an iron corrosion product and, in the absence of oxygen, hydrogen. An amorphous or poorly crystalline solid would be likely to form first, which would gradually transform into a more crystalline phase, likely magnetite, and possibly siderite should sufficient carbonate be carried into the defect, as discussed in Section 5.4.4.3.

Initially, iron corrosion products would form only on the outside surface of the steel (within the coating defect). Literature values for the anaerobic corrosion rate of steel vary over a wide range, between 0.1 and 50 μm/a. The corrosion rate in the defect likely would be at the lower end of the range, given that the water would be chemically buffered by clay, and given that the water would be supplied at a limited rate to the steel; this same limitation would likely mitigate any radiolysis reactions that could potentially impact corrosion. Among other factors, the water ingress would be restricted by 1) low permeability of the bentonite clay around the container, 2) the small aperture of the defect in the copper coating, which may be blocked by swelling bentonite, and 3) slow transport through the porosity of the corrosion products filling the through-copper defect.

5.4.4.3 Modelling Steel Corrosion Beneath a Through-Copper Defect

If defects in the copper coating lead to exposed steel, then groundwater will begin to corrode the exposed steel and may eventually perforate the wall of the container. The time required for groundwater to perforate a container will depend on the thickness of the steel wall (Figure 5-16) and on the steel corrosion rate.

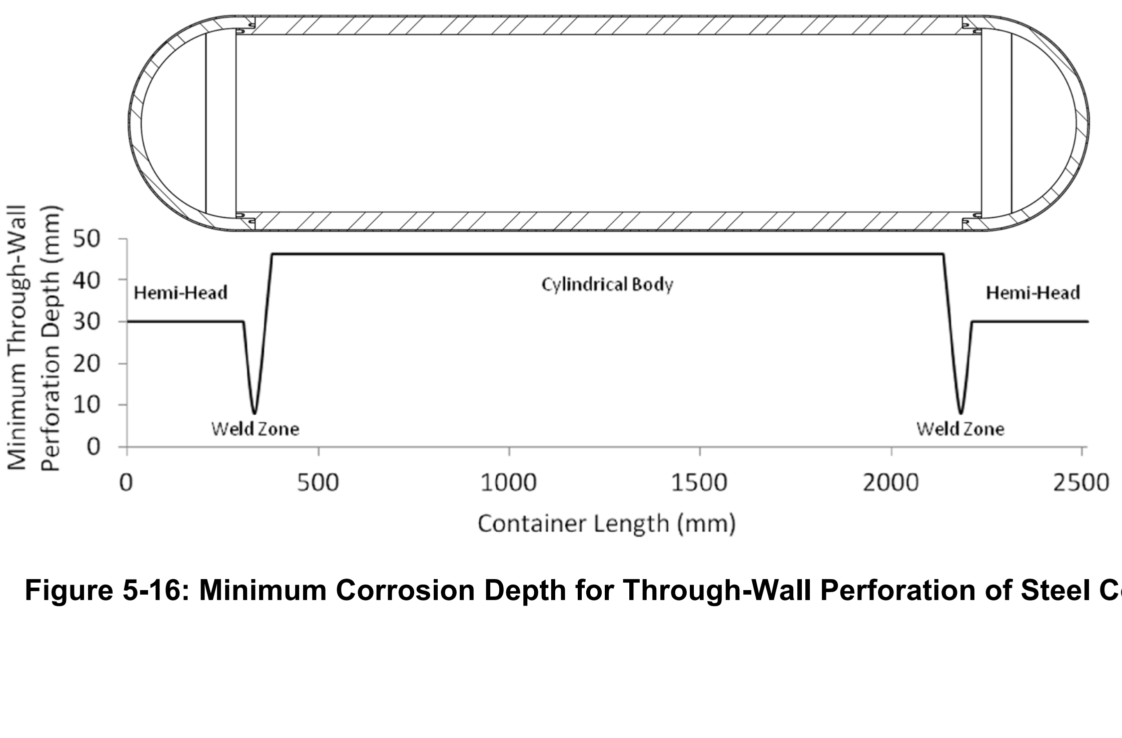

Figure 5-16: Minimum Corrosion Depth for Through-Wall Perforation of Steel Container

As described above, the UFC is protected by a continuous layer of copper. Although the container manufacturing and inspection processes are under development, presently there is no basis to assume there are any locations across the container surface where an undetected copper defect is more or less likely to occur.

Sections of the container wall have different thicknesses. From the information provided in Figure 5-16:

- 70% of the container surface, corresponding to the container body, requires 46.2 mm of corrosion to perforate the steel;

- 25.4% of the container surface, corresponding to the heads, requires 30 mm of corrosion to perforate the steel; and

- 4.6% of the container surface, corresponding to the weld region or zone within a few mm of the weld, requires something less than 30 mm of corrosion to perforate the steel (the partial-penetration weld itself presents the minimum wall thickness of at least 8 mm and accounts for less than 1% of the container surface).

The steel corrosion models used by the NWMO were developed by King (2013). Corrosion rates are temperature-dependent, and the calculations discussed here use the container surface temperatures determined by Guo (2016).

As noted above, the postclosure repository environment will become anoxic within a relatively short time. Under these conditions, magnetite is the likely corrosion product, particularly if the system is carbonate-limited or only partially saturated. The rate of magnetite-generating corrosion is based primarily on work by Newman et al. (2010) and passivation of the steel is implicit. Siderite may be the primary corrosion product if the system has sufficient carbonate available and is fully saturated. The rate of siderite-generating corrosion is based on literature values (King 2013) and passivation is implicit. Rates for both forms of corrosion are shown in Figure 5-17, based on the container temperatures provided in Figure 5-3. Siderite-generating corrosion is much faster than magnetite-generating corrosion – more than 10 times faster if temperatures are below ~40°C. As per Figure 5-3, the temperature becomes less than 40°C around 14,000 years postclosure.

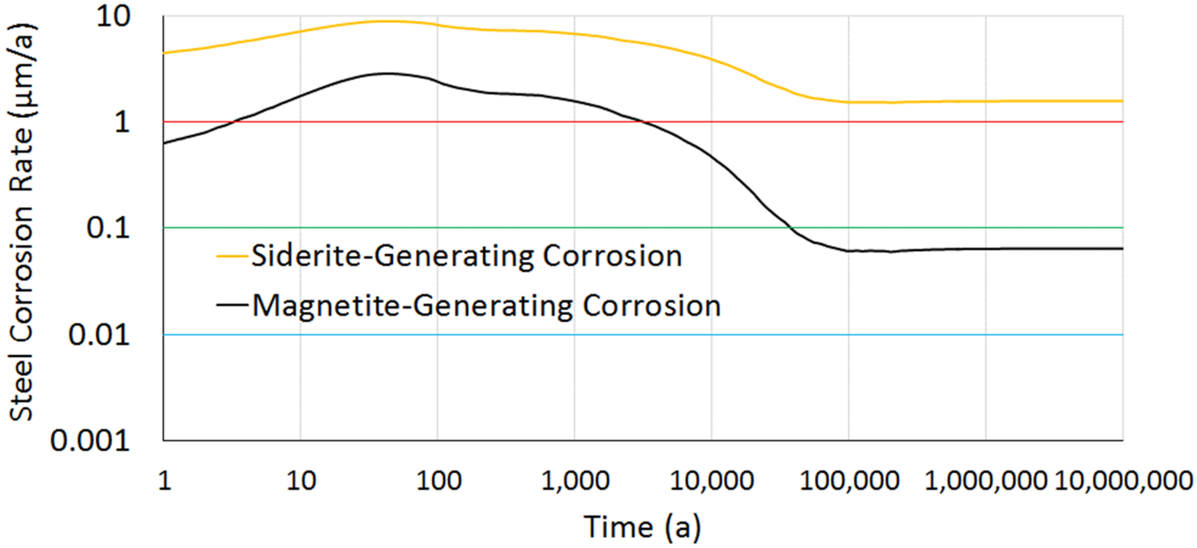

Figure 5-17: Evolution of Steel Corrosion Rates

The steel corrosion models developed by King (2013) apply to an open surface with no protective copper coating, referred to here as open-surface corrosion. The models consider a corrosion front advancing uniformly through steel, where the corrosion product steadily suppresses the corrosion rate. These models may be adapted to reflect corrosion through a defect in the copper coating, referred to here as defect corrosion. Figure 5-18 illustrates how open-surface corrosion differs geometrically from defect corrosion: the corrosion front is expected to advance radially from the defect, resulting in an expanding hemisphere of corroded steel. This is supported by the micrograph included in Figure 5-18, presenting early results from laboratory experiments assessing defect corrosion of copper-coated steel.

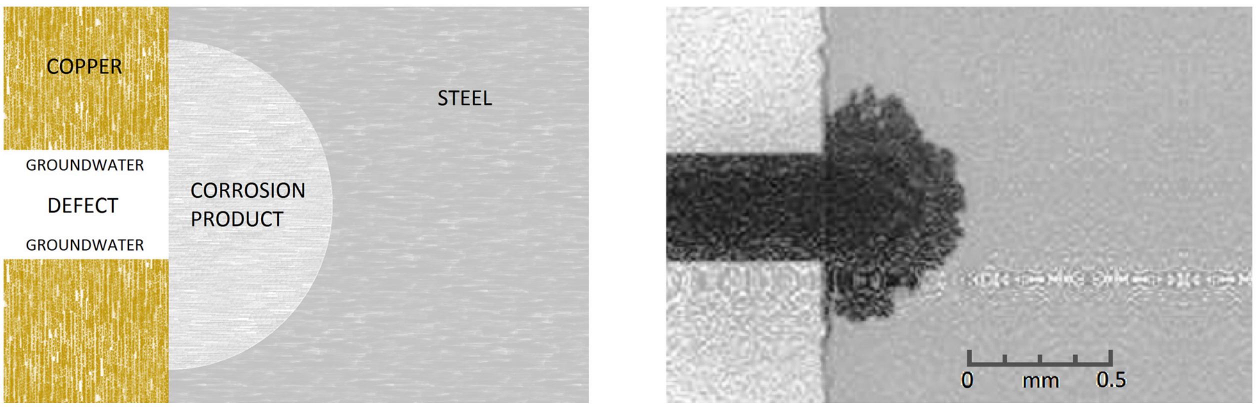

Note: The left panel represents a conceptual illustration and the right micrograph shows early results from laboratory experiments that have been accelerated by utilizing a free-flowing solution, purged with oxygen.

Figure 5-18: Illustration of Defect Corrosion

Assuming the material properties of the corrosion product (bulk porosity, ion diffusivity, etc.) are the same under open-surface and defect corrosion, it is then reasonable to infer that transport of the components of the corrosion reaction becomes dependent on the size of the defect. In this case, the rate of defect corrosion can be shown to relate to open-surface corrosion according to the following equation (Kremer 2017):

$$\frac{\text{Defect Corrosion}}{\text{Open-Surface Corrosion}} = \frac{r_o}{(r - r_o)} \tag{5-14}$$

where r_0 is the radius of the defect and r is the radius of steel lost to corrosion.

This relationship includes several conservatisms:

- For $r \leq r_0$, calculations assume open-surface corrosion;
- Corrosion products grown within the protected environment of the defect may be more homogeneous and, consequently, more resistant to transport of reaction components;
- Expansion of corrosion product relative to corroded steel, confined and compressed between steel and copper boundaries, may increase corrosion-product density and further limit transport; and
- Even if sufficient carbonate is available, this configuration may inhibit siderite-generating corrosion.

In addition, the calculations for defect corrosion presented here respect the lower bounds imposed on the open-surface corrosion models (King 2013); that is, where defect corrosion predicts lower corrosion rates, the assumed corrosion rate is never lower than the lower bound for open-surface corrosion. This addresses the uncertainty implicit in modelled defect corrosion rates not yet confirmed experimentally. Corrosion model calculations for siderite-generating corrosion are shown in Figure 5-19, comparing open-surface corrosion and defect corrosion with the (conservative) assumed corrosion rate used here. Calculations assume a 1 mm diameter through-copper defect.

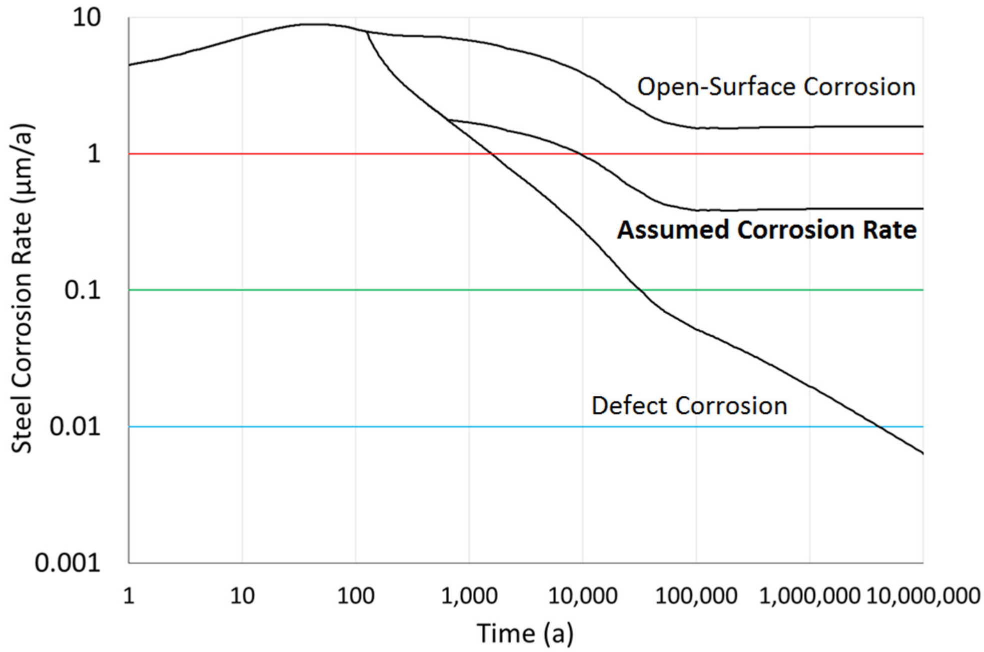

Note: This figure illustrates siderite-generating corrosion.

Figure 5-19: Adaption of Open-Surface Corrosion Models for Defect Corrosion

Figure 5-20 presents the time required to perforate the different thicknesses of steel along the length of the container wall (see Figure 5-16). Table 5-4 provides a summary of perforation times. Depending on the modelled steel corrosion rate and the thickness of the steel wall, the time required for groundwater to perforate a container varies from as short as 1,100 years to well over 10 million years.

It should be noted that these calculations include corrosion rates driven by elevated temperatures associated with the first few thousands of years postclosure. As discussed above, for exposure of steel beneath a defect in the copper coating to occur within one million years, a fairly large defect, greater than 2 mm, as well as elevated groundwater sulphide concentrations, would be required. The steel corrosion calculations presented here assume exposed steel upon placement of containers in the repository. This would require a through-copper defect in the copper coating to pass a quality inspection undetected, which may be unrealistic.

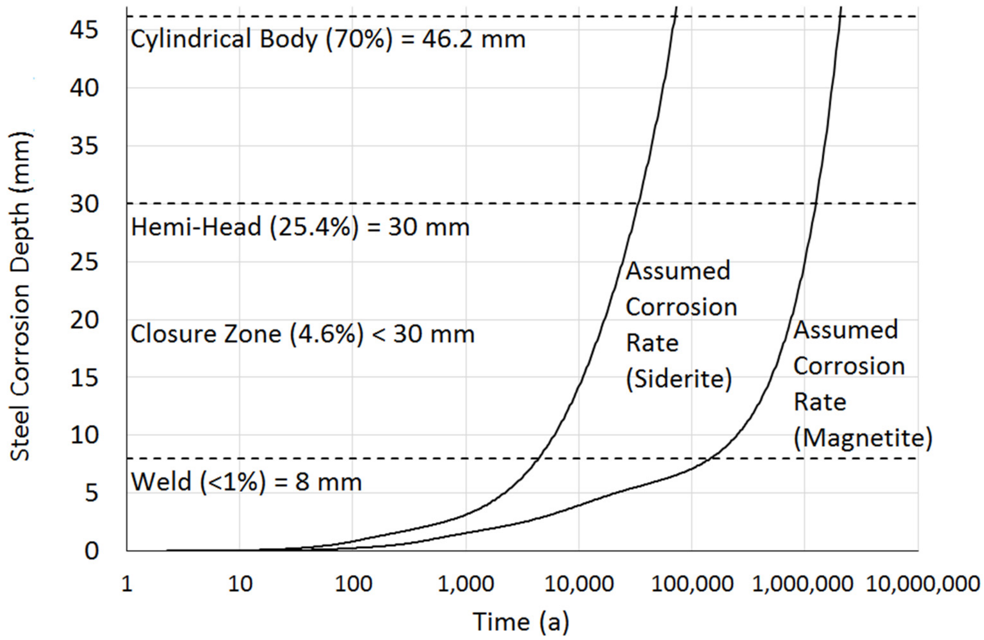

Figure 5-20: Evolution of Steel Corrosion Depth

Table 5-4: Time for Steel Corrosion to Perforate the Container Wall

	Cylindrical Body (46.2 mm) 70% Container Surface Magnetite- / Siderite-Generating Corrosion	**Hemi-Head (30 mm)** 25.4% Container Surface Magnetite- / Siderite-Generating Corrosion	**Weld (8 mm)** < 1% Container Surface Magnetite- / Siderite-Generating Corrosion
Open-Surface Corrosion	530 ka / 8.6 ka	280 ka / 5 ka	7.8 ka / 1.1 ka
Defect Corrosion	>10 Ma / 1.3 Ma	>10 Ma / 510 ka	700 ka / 11 ka
Assumed Corrosion Rate	2 Ma / 71 ka	1.3 Ma / 33 ka	140 ka / 4.4 ka

5.4.4.4 Stresses in the Copper Defect As a Result of Corrosion

As the iron that is exposed through the copper defect is corroded, it will form corrosion products. Iron corrosion products are less dense than the metal itself. Thus, the volume of Fe_3O_4 formed by Reaction (5-5) is about twice the volume of the Fe metal consumed in its formation if it is unconfined (McMurry et al. 2004). As a result of the possible volume change, the formation of corrosion products in a confined space has the potential to exert a force on the adjacent solids.

The resultant stresses would have little preliminary effect on the steel vessel, due to its high mechanical strength. Similarly, while it has less mechanical strength, the copper coating is integrally bonded to the steel; thus it is likely that the surrounding clay buffer would deform more easily if there is a volumetric expansion from corrosion products.

However, there are compelling reasons for the conclusion that there will not be a volumetric expansion as a result of the formation of iron corrosion products, as there is experimental evidence to that effect (Smart et al. 2003, 2006). Specifically, during analysis of stresses produced during anaerobic corrosion over a two-year period, no detectable expansion was observed for bentonite-equililbrated groundwaters under compressive loads (Smart et al. 2006). In addition, the anaerobic corrosion products were easily deformable and were incapable of producing expansion under simulated repository conditions. Only for aerobic conditions, and low applied loads, were expansions measureable due to corrosion products. Similarly, after 4 years in-situ, observations from the first MiniCan experiment indicate no expansion in the SKB outer-copper shell due to corrosion of the cast iron insert, and there is apparent extrusion of iron corrosion products through the defect (Smart et al. 2012). As a result, it is likely that copper coating deformation at a defect would occur very slowly, if at all.

5.4.4.5 Failure of the Steel Vessel During Corrosion at a Defect in Copper Coating

During corrosion of steel below a coating defect, it is expected that there will be a gradually increasing volume of wall loss of steel. Should the defect be a narrow cylindrical pore, the damage would likely resemble a growing hemispherical region, as per Figure 5-18. Because the narrow pore would act as a bottleneck, limiting the amount of water reaching the hemisphere, overall corrosion would be slow, but the result would be a gradual widening of the defect in the steel vs. the initial defect in the copper. Eventually, the steel below the copper coating defect will sufficiently deplete via corrosion, or fail mechanically, and allow water to enter the container.

Owing to the slow rate of steel corrosion, this process may take many thousands of years. Once through-wall penetration occurs, it will permit corrosion to begin on the inside of the container on all of the steel components. This process will gradually thin the container wall, which will weaken it to mechanical loading; however, the incoming water will also equilibrate the interior and exterior pressure of the container. As a result, mechanical requirements for the container will be virtually eliminated, other than those associated with anisotropic loading; however, the development of anisotropic loading is not expected in the crystalline host rock. Regardless, interactions between the incoming water and the materials inside the “breached” container need to be considered for all steel vessel failure scenarios.

5.4.4.6 Corrosion and Deformation of the Zircaloy Cladding

At the time of placement in a repository, virtually all of the used fuel elements will have intact Zircaloy cladding. A few of the cladding sheaths would have become defective during their use in a reactor (historical estimates of this number ranged from approximately 1 per 10,000 to 1 per 100,000 fuel elements, Frescura and Wight 1979). This is supported by more recent statistics from 1994 to 2006, which indicate that upon discharge, less than 0.015% of CANDU fuel bundles have minor damage or defects (such as pinhole failures in the fuel sheaths, IAEA 2010), Some others may have developed defects during post-reactor storage, transportation, or packaging into containers. In a breached container, one of the most significant changes in the used fuel bundles over time will be mechanical failure of the cladding, mainly in association with corrosion of the steel vessel. In addition, the cladding will be subjected to hydrogen embrittlement, corrosion, and creep, as described below.

Over time, hydrogen gas would be produced inside a breached container by two separate processes: the anaerobic corrosion of steel and the radiolysis of water. Hydrogen-induced cracking is a potential failure mechanism for Zircaloy cladding. Studies of the durability of used fuel bundles in dry or moist air have found no evidence of cladding failures (Lovazic and Gierszewski 2005). Given that significant partial pressures of hydrogen gas would not develop in a container until saturation of the repository had occurred, lifetimes of the Zircaloy cladding in a breached container could exceed thousands of years.

On observable time scales, the uniform corrosion of Zircaloy cladding is negligible (likely between 1 and 5 nm/a, with an upper limit of 20 nm/a), even in contact with water, which is due largely to the corrosion resistance of a passive oxide film on the Zircaloy surface (Shoesmith and Zagidulin 2010).

In a breached container, pitting and crevice corrosion of cladding would be inhibited by the rapid consumption of oxidizing agents (residual oxygen and radiolysis products) by the iron and copper container materials. In addition, iodine-induced stress corrosion cracking would be inhibited because most of the iodine in the fuel gap in CANDU fuel exists as cesium iodide, preventing it from forming the zirconium iodides that are thought to be the chemical precursors to stress corrosion cracking in Zircaloy.

Using the above values, a general corrosion lifetime for a 0.5 mm cladding is calculated to exceed 25,000 years when presuming the highest corrosion rate of 20 nm/a; a more realistic value of >100,000 years is calculated for expected corrosion rates (i.e., those at or below 5 nm/a).

5.4.4.7 Dissolution of the Used Fuel Matrix

After the cladding is breached and the fuel pellets exposed to water, the next barrier against radionuclide release is the UO_2 fuel matrix, which contains most of the radionuclides and has a very low solubility. Dissolution of the UO_2 matrix of the used fuel would progress according to two general methods: oxidative dissolution (i.e., corrosion) and chemical dissolution. Radiolysis of water in contact with the fuel pellets would produce oxidizing conditions at or near the used fuel surface, contributing initially to oxidative dissolution of the UO_2. If water is able to contact the fuel while radiation fields are high, this process would tend to promote the dissolution of the used fuel at a higher rate than would be expected solely on the basis of the chemical solubility of UO_2 in the near-field porewater. The production rate of oxidants by radiolysis would decrease with time as the strength of the radiation field decreases (Gobien et al. 2016).

At the fuel-water interface, the alpha dose rate exceeds the gamma and beta dose rates for most of the fuel history (Figure 5-21) and is the main contributor to radiolysis, producing molecular oxidants such as H_2O_2. Other potential sources of oxidants, such as any O_2 trapped inside the container when it was sealed, would already have been consumed by Fe and Cu corrosion processes before the fuel cladding was breached, because these corrosion reactions are much faster than the reaction with UO_2. In principle, the radiolytically-produced oxidants would be consumed by reaction with container materials, rather than by reaction with used fuel; however, for alpha radiolysis, the oxidants would only be produced within

20 μm of the fuel-water interface and would have difficulty diffusing through openings in the cladding to react with container materials.

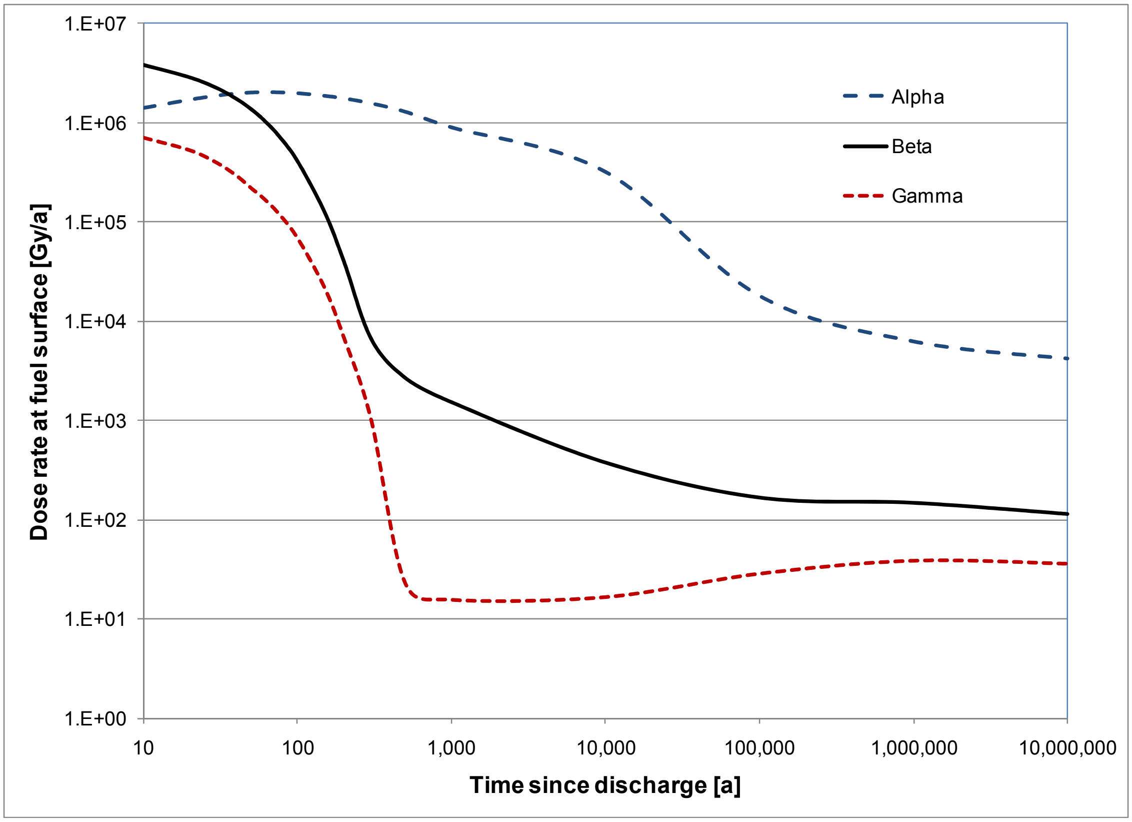

Figure 5-21: Radiation Dose Rate in Water at the Fuel Surface (220 MWh/kgU burnup)

Oxidative dissolution of the fuel continues as long as the alpha radiation field is sufficiently high. However, the actual dissolution rate of the fuel decreases over time, as the alpha radiation field decreases due to decay. Experiments and mechanistic models have been developed to describe this corrosion rate, and results indicate that the dissolution of the used fuel would take more than one million years (Gobien et al. 2016).

Furthermore, in UO_2 and used fuel dissolution experiments, the dissolution rate decreases by several orders of magnitude in the presence of even modest hydrogen gas pressures (Shoesmith 2008), which would certainly be present due to corrosion of the iron vessel. A number of mechanisms have been either demonstrated or proposed to explain these effects, all of which involve the activation of hydrogen to produce the strongly reducing $H^\bullet$ radical – which scavenges radiolytic oxidants and suppresses fuel oxidation and corrosion (Shoesmith 2008).

After the alpha radiation field has decreased substantially after many thousands of years, chemical dissolution of the fuel proceeds according to the reaction,

$$UO_2 + 2H_2O \rightarrow U(OH)_4 \qquad (5\text{-}15)$$

under the anaerobic conditions expected in the repository. This reaction occurs very slowly, as illustrated by the age of uraninite ore (largely UO_2) deposits, such as those in northern Saskatchewan (Alexandre et al 2009).

5.4.4.8 Radionuclide Release from the Fuel Pellets and Cladding

Extensive studies of the interactions between used fuel and groundwater have established that radionuclide release from the used fuel occurs by two main processes. Instant-release refers to the initial and comparatively rapid release of a small fraction (typically a few percent) of the inventory of a selected group of radionuclides that are either very soluble (such as ^{137}Cs, ^{129}I, ^{14}C and ^{36}Cl) or gaseous (such as Xe), and that are residing in the fuel sheath gap or at grain boundaries which are relatively quickly accessed by water. The second and slower release process comprises release of radionuclides from the UO_2 fuel matrix as the matrix itself corrodes or dissolves, and is referred to as congruent dissolution.

The instant-release fractions for various important radionuclides in used CANDU fuel are given in Gobien et al. (2016) and typical values for selected radionuclides are presented in Table 7-13. Note that the use of the term “instant-release” with reference to the gap and grain boundary inventories is a simplification. In reality, it would take a finite time for water to penetrate into the grain boundaries and for the radionuclides located there to diffuse out. However, compared to the much longer time required for dissolution of the UO_2 matrix itself, grain boundary releases are so much faster that they can be considered “instantaneous”. Therefore, in conceptual models of radionuclide release, both locations – the gap and grain boundary inventories – are considered to contribute to the instant-release fraction. Ferry et al. (2008) have shown that the instant-release fractions do not change with time, with processes such asathermal diffusion of radionuclides induced by alpha-particle recoil displacements having negligible effects.

In addition to the bulk of the radionuclides in the used fuel pellets, there would be a small quantity of radionuclides present in the irradiated Zircaloy from neutron activation. These radionuclides are generally distributed uniformly through the cladding and would only be released as the cladding itself dissolves. However, evidence suggests that some of the C-14 in the Zircaloy is present within the zirconium oxide film (Gobien et al. 2016). Zircaloy is corrosion-resistant in water due to the stability of its oxide coating, and thus would corrode at a slow rate (as described in Section 5.4.4.6).

5.4.4.9 Fate of Released Radionuclides

As radionuclides are released to solution, some would become oversaturated and secondary radionuclide-bearing phases would precipitate on the fuel surface (e.g., ThO_2) or on other surfaces nearby, such as those provided by metal corrosion products. Aside from the low overall amount of such nuclides in a container, it is expected that their concentration in a precipitate would be diluted by the co-precipitation of other elements. Precipitation of a large mass of fissile nuclides, in particular, would be hindered by the intergrowth of such mixed-isotope precipitates along with iron corrosion products or buffer clays.

The radionuclides that remained in solution as aqueous species, and solids suspended in colloidal form, would diffuse through the various metal corrosion products inside the container. The corrosion products would also provide a surface for sorption of many of the radionuclides. In some cases, the sorption would be irreversible because the radionuclides would be incorporated into the crystal lattice of the corrosion product (i.e., if it undergoes a transformation to a more stable solid phase).

Dissolved radionuclides would diffuse, by a tortuous path through, what was left of the container, through the low-permeability sealing materials, and finally enter the host rock surrounding the repository. Migration of radionuclides away from the repository, and their transport rate through the geosphere as a whole, would be controlled by the local hydrogeological conditions. For the current hypothetical geosphere, groundwater velocities are low and transport is diffusion controlled. Radionuclides in colloid form or sorbed to colloids would be filtered by the buffer and would not reach the geosphere.

5.4.4.10 Summary

The postclosure safety assessment presented in Chapter 7 will consider a failure in the copper coating and inspection process that could lead to containers placed in the repository with small defects. Corrosion modelling results presented here suggest it may be reasonable and conservative to assume that defects passing a quality inspection undetected would lead to exposed steel only after more than 10 million years. Once steel is exposed to groundwater, corrosion model calculations find that the additional time required for groundwater to perforate a container may vary from as little as 1,100 years to well over 10 million years.

From these results, used fuel containers are expected to remain intact essentially indefinitely, with no releases (and no dose consequences) within the one million year timeframe of the postclosure safety assessment.

5.4.5 Confidence

Extensive corrosion experiments have been carried out to improve the confidence in the ability to predict the corrosion behaviour and lifetime of copper-coated used fuel containers in a deep geological repository in Canada.

<u>Container Corrosion:</u> Because of the extensive experimental database on the corrosion of copper, and the level of mechanistic understanding that has been developed over the past 30 years, in addition to the existence of natural and archaeological analogues, there is significant confidence in the prediction of the long-term corrosion behaviour of copper containers. Both the predictive models for corrosion processes that are expected to occur, such as uniform corrosion and localized surface roughening, and the reasoned arguments against those that are not thought to be possible, such as stress corrosion cracking, are robust. Where uncertainty exists, such as the mechanism and exact corrosion rate that describe copper corrosion in anaerobic water or brine solutions, these uncertainties do not compromise arguments for container integrity since the total corrosion possible from these processes is very small over the container design life.

The evidence from natural and man-made analogues builds confidence in the conclusions drawn from experimental and modelling studies. Man-made analogues, such as Bronze Age artifacts or more-recent anthropogenic objects (discussed in Chapter 9), also provide useful supporting evidence that copper corrodes slowly, even in near-surface aerobic environments. The existence of native metallic copper deposits indicates that, under certain environmental conditions, metallic copper is stable over geological time scales. The fact that the majority of copper deposits in the Earth's crust are in the form of sulphide minerals is also evidence of the potential role of HS^- species in the corrosion of copper containers. Although it is not a pre-requisite that the groundwater at repository depth be free of sulphide, as the programs in Sweden and Finland demonstrate, there are clear advantages to selecting a site with little or no sulphide in groundwater, as appears to be the case in Canadian crystalline rock.

Confidence in long-term predictions is supported by the robustness of those predictions and on the underlying information on which they are based. This confidence arises, for example, from achieving the same result from different modelling approaches. For example, the conclusion that the maximum depth of uniform corrosion is of the order of a few hundred micrometres is predicted by both simple mass-balance models (SKB 2011) and from detailed mechanistically-based reactive-transport modelling (King et al. 2008). These detailed reactive-transport models have been validated against experimental data and evidence from archaeological analogues (King et al. 2001).

Confidence results from having a sound mechanistic understanding of corrosion processes. For example, the proposed mechanism to explain observations discussed in Section 5.4.3.3.3 is the strong evidence that under repository conditions the localized corrosion of copper containers will take the form of surface roughening rather than pitting. This understanding is equally important for processes that are not considered likely to occur, such as stress corrosion cracking. The approach for stress corrosion cracking provides multiple lines of argument against this behaviour, and it is not considered feasible that all of the pre-requisite conditions for stress corrosion cracking would exist in the repository at the same time.

There are also multiple lines of argument for why MIC will have a minimal impact on the container (King 2009b, Sherwood Lollar 2011 and Wolfaardt and Korber 2012). However, uncertainties regarding the potential for microbial growth and activity under unsaturated conditions, and at component interfaces, requires further investigation. Because the possibility of remote microbial activity cannot be excluded, a corrosion allowance is made for this in any lifetime assessments (Kwong 2011, Scully and Edwards 2013).

The multi-barrier repository system represents a robust system that is capable of withstanding upset or unexpected conditions whilst still maintaining a high degree of containment. For example, the predicted container lifetimes are insensitive to the groundwater salinity and, in fact, higher Cl^- concentrations promote uniform rather than localized corrosion (King et al. 2010, 2011a). Information from site investigations in crystalline rock in Canada suggest that the there is little or no sulphide in deep groundwaters (INTERA 2011). Experience from the Swedish and Finnish programs demonstrates that the combination of a copper container and dense bentonite buffer provides long-term containment even if sulphide were to be present at low concentrations. Similarly, there is no geological evidence that O_2-containing water has ever reached repository depths, even under glacial conditions (see Section 5.1.2.4).

<u>Container Temperature:</u> The container surface temperature is affected by the container power, placement method, chemical composition, water content and thickness of sealing materials, distance between containers, distance between the placement rooms and tunnels, etc. The thermal responses were successfully modelled and there is good confidence that the evolution of temperatures of the container surface and surrounding bentonite buffer materials can be well estimated by existing computer models.

Container Structural Integrity: To maintain long-term structural integrity during its design life, the UFC is designed to withstand an external isotropic pressure during the interglacial period, which accounts for the 5 MPa hydrostatic pressure up to a 500 m depth, together with bentonite swelling. The container could also withstand an external pressure load during the glaciation period (which corresponds to a 3000 m thick ice sheet) with full load applied as hydrostatic head (i.e., no load carried by the rock matrix). These are conservative assumptions. While glaciation will be a significant load, the earliest site coverage due to an ice sheet would be thousands of years in the future (i.e., at least another 60,000 years from present).

The container would be subjected to uneven bentonite swelling loads during the transient period, before full water saturation, and also, possibly, after saturation (though to a reduced extent) because of density differences that do not entirely homogenize because of internal friction. It is expected that any such uneven swelling pressure loads would not cause container failure, based on the results of analyses for similar SKB and Posiva containers (Werme 1998, Raiko 2005). This will be verified by engineering analyses.

5.5 Long-Term Evolution of Buffer, Backfill and Seals

Each used fuel container will be placed within a buffer box, which will be surrounded by gap fill, other buffer boxes and spacer blocks. Bentonite is a type of clay that swells on contact with water, providing a natural self-sealing ability, and is widely available including as the commercial brand MX-80. Bentonite is a durable natural material that is expected to maintain its properties over the long term. Within the repository, bentonite will: 1) prevent damage to the repository system by acting as mechanical protection against stresses; 2) control groundwater in the area around the UFC and the chemistry of the groundwater and other substances in the vicinity of the UFC; and 3) control microbial activity in the vicinity of the UFC, therefore reducing the potential for microbially-influenced corrosion of the container.

Within ongoing work, there are several programs that are relevant for bentonite. These include: 1) characterization of bentonite from a range of sources for a range of conditions (i.e., temperature, moisture, etc.); 2) interaction of bentonite and other repository components (i.e., container, concrete/grout); as well as a range of other works that explore corrosion and biological processes relevant to bentonite.

The main processes with potential influence on the evolution of the sealing systems are discussed in the succeeding sections.

Additional Features, Events and Processes (FEPs) were assessed and excluded for the reasons outlined in the FEPs report (Garisto 2017) and thus are not part of the expected evolution described in this section.

5.5.1 Changes during Saturation

After the gap fill material is installed, the water seeping into the repository will begin to wet this material and the HCB blocks and the bentonite in the buffer will expand. As this expansion progresses, it will fill the space between the granular particles and restrict water movement. Moreover, the swelling pressure will, in due course, provide mechanical resistance to the local effects of large-scale flexing and crustal rebound processes associated with glacial loading, reducing the severity of damage to the near-field rock surrounding the backfilled openings of the repository. The swelling capacity of the bentonite decreases at high salinity, but the performance requirements for hydraulic conductivity and swelling pressures are met for high salinities, exceeding those expected at 500 m depth, (i.e., a total dissolved solids content of up to 275 g/L).

Figure 5-22 A illustrates the resultant swelling pressures for a range of salinities:

- no salinity (deionized water, DW);
- 50, 100 and 335 g/L of sodium chloride; and
- simulated groundwaters SR160, SR223 and SR335, which correspond to 160, 223 and 335 g/L of salinity, respectively..

Figure 5-22 B illustrates the effect of these same salinities on hydraulic conductivity, as well as the design limit of 10^{-10} m/s.

The Effective Montmorillonite Dry Density (EMDD) is a parameter that allows a comparison of the behaviour of different types and densities of clay-based materials (Man and Martino 2009, Dixon et al. 2011) (see Table 4-2). For the reference gap-fill material, using dense pellets of MX-80 clay and emplaced at an effective dry density of 1410 kg/m^3, the EMDD will be around 1260 kg/m^3.

The timing and rate of saturation of a repository depends on a number of site-specific conditions, as described in Section 5.2.2.

A

B

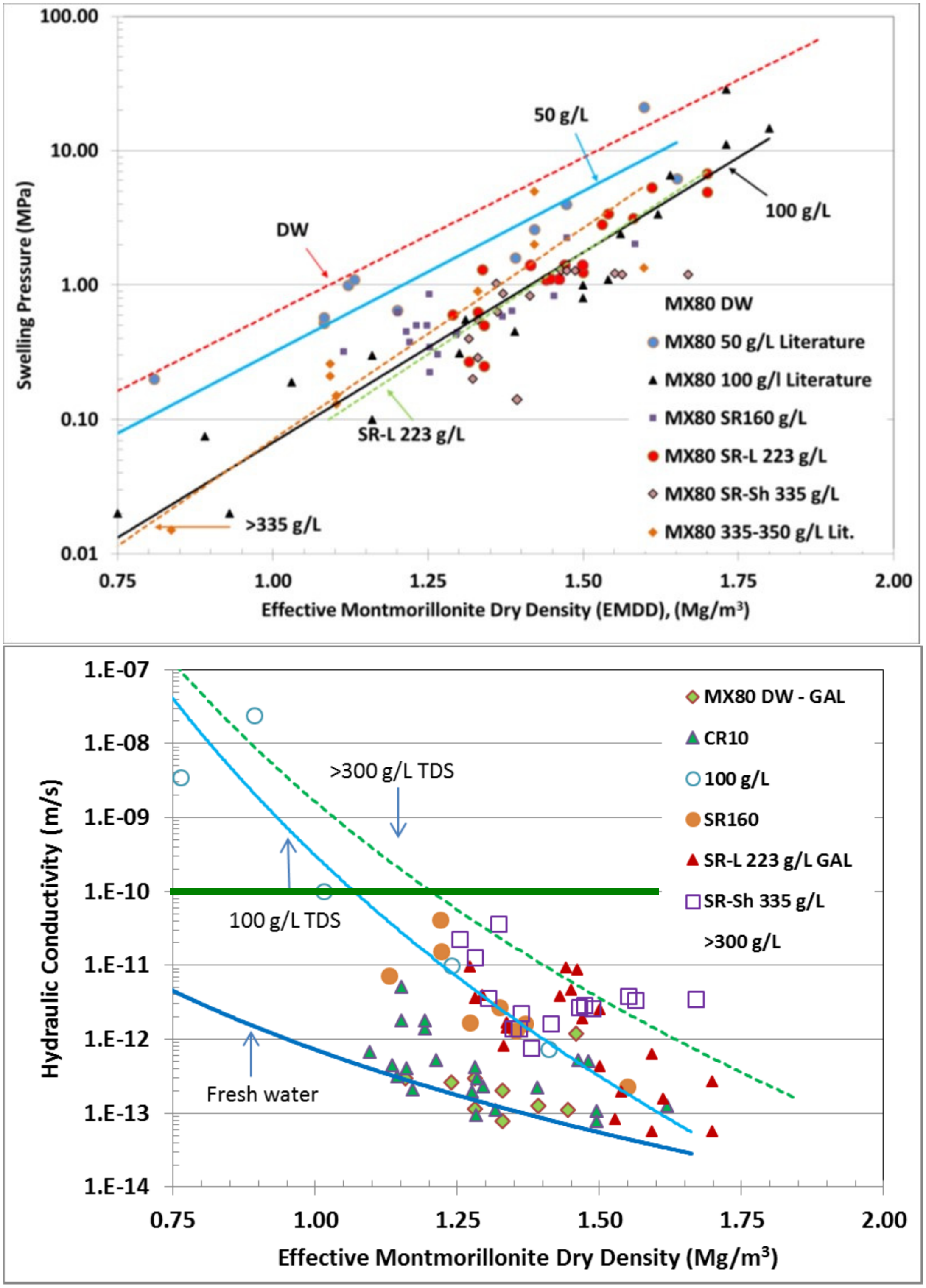

Note: Figures are taken from Dixon et al. (2016)

Figure 5-22: Hydraulic Conductivity and Swelling Pressure under Various Water Conditions: Variation with Effective Montmorillonite Dry Density

5.5.2 Temperature Changes

The thermal conductivity of the various clay-based sealing-system components changes with their degree of water saturation. Figure 5-23 illustrates this relationship for bentonite-only and bentonite-sand compositions. This figure illustrates the effects of sealing material composition and water content on its heat-transfer characteristics. Initially considered for use as the buffer material in the repository concept developed by AECL, a mixture of equal dry weight proportions of sand and bentonite was defined as the reference bentonite-sand buffer for use in filling the region between the container and the surrounding rock. Subsequent review identified bentonite-only clay as the preferred buffer material, such as the 100% bentonite gap-fill material with a dry density of 1410 kg/m^3.

From Figure 5-23, it can be seen that in the region nearest the containers, the thermal conductivity of the buffer will decrease as heat from the containers drives moisture away. In contrast, buffer thermal conductivity will gradually increase as the degree of saturation increases. Good agreement is obtained in modelling of thermal profiles in field experiments, such as the SKB Container Retrieval Test, when the thermal conductivity characteristics provided in Figure 5-23 are used (Guo 2009).

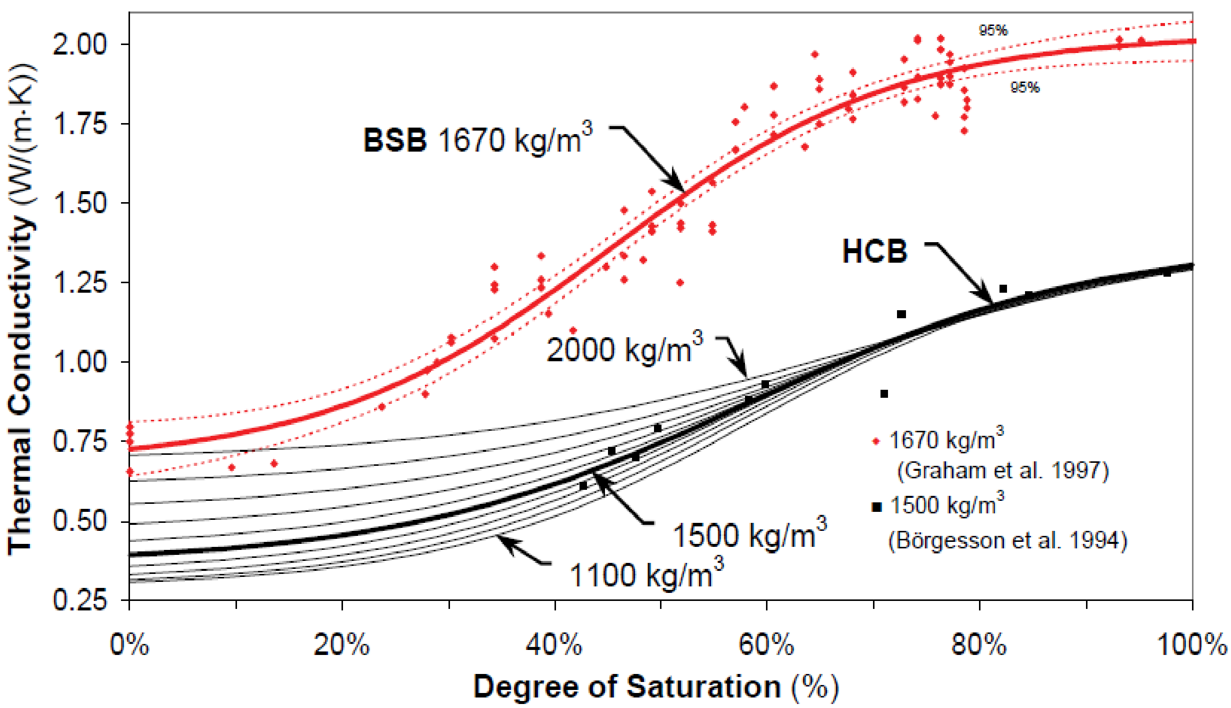

Notes: From Man and Martino (2009). Label units are dry densities.

Figure 5-23: Thermal Conductivity of 50:50 wt% Bentonite-Sand Buffer (BSB) and of 100 wt% MX-80 Bentonite

The maximum near-field temperature is predicted to occur within the first 30 years following placement as shown in Figure 5-3, when the buffer will be unsaturated. The main sealing material that would potentially be affected by thermal expansion is the concrete bulkheads at the ends of placement rooms (Figure 4-15), which could also be affected by heat released during their curing process. These would be installed using low-heat concrete and in a manner that minimized contraction during the concrete-curing process.

Later, as the temperature of the repository declines (Figure 5-3), thermal contraction of the concrete bulkhead is likely to cause some rejuvenation of cracks or the production of new cracks at the rock-concrete interface. This process was observed in the concrete seal portion of the AECL URL Tunnel Sealing Experiment (Chandler et al. 2002). The concept of using a composite HCB-concrete structure in a repository anticipates that, by the time temperatures decrease significantly in this region, the clay gasket that was installed as part of the composite seal should be fully saturated. The clay would expand, providing a tight contact with the concrete and rock, and if water flow is occurring from the backfilled tunnel past the concrete, it is expected that the clay will seal the open interface and reduce mass-transport from any open features.

5.5.3 Chemical Changes

An important function of the buffer is to produce/maintain a chemical environment in the repository that will inhibit corrosion of the containers and, in the case of a breach in a container, would limit the solubility of the used fuel and the subsequent migration of radionuclides. Conversely, the composition of porewater in the repository will affect the mechanical and hydraulic properties of the buffer. The evolution of porewater chemistry in the sealing materials is complex, as it is influenced by many parameters: the compositions and proportions of minerals in the buffer and backfill, the composition of the saturating groundwater, the repository temperature, the relative rates of movement through the clay, the initial proportions of exchangeable cations in the clay minerals, and the composition of the water used during wetting and compaction of the sealing materials. Eventually the porewater in the buffer will resemble the groundwater entering the repository, and the Na in the bentonite will have exchanged with Ca in the groundwater, potentially causing a reduction in the swelling pressure and an increase in the hydraulic conductivity of the buffer. However, such potential effects are accounted for in the design of the repository.

5.5.4 Changes due to Biological Processes

Aerobic biodegradation of concrete is a well-known microbial process (Humphreys et al. 2010). Initially, conditions in the vicinity of the concrete seals and floors in the deep geological repository may be moist and aerobic enough that pyrite or other sulphide minerals present in the sealing materials (as part of the concrete aggregate or as minor components in buffer or backfill) could be converted to sulphuric acid (i.e. H_2SO_4) by sulphate-producing bacteria. The extent of the resulting corrosion would be minor, however, given the relatively short duration of oxidizing conditions in the repository and the likely low abundances of sulphide accessory minerals in the sealing materials.

Clay-based materials have been shown to contain indigenous aerobic and anaerobic microorganisms. Microorganisms could also enter the sealing materials during the operating phase of a repository from the air and human activities in the short term, and from the host rock in the long term. The current understanding of microbiology in the context of a repository is summarized by Wolfaardt and Korber (2012).

Specific biogeochemical processes in the buffer, backfill and seals pertain to:

- Consumption of oxygen and creation of an anaerobic environment;
- Gas production and consumption; and
- Microbially-influenced corrosion (MIC).

As the geosphere of a deep geological repository is nutrient-poor, microbial activity at depth is limited compared to the near-surface environment.

During the time that a repository is open, the engineered barrier system and adjacent rock will be exposed to air, which will facilitate the growth of aerobic bacteria. After the repository is closed, the aerobic bacteria in this zone are expected to actively promote reducing conditions by consuming the remaining oxygen. Anaerobic bacteria, which were likely to have been the main forms of life in the deep subsurface environment prior to repository excavation, will eventually dominate again, and reducing groundwater conditions will be maintained far into the future. Upon establishment of anaerobic repository conditions, a variety of organisms with the capabilities to utilize alternate electron acceptors have the potential to become active. Anaerobic bacteria can both produce and consume gases, which have limited potential to impact both the physical and chemical aspects of the repository. Of particular interest is the potential for microbial activity to cause MIC, as discussed in Section 5.4.3.3.5. As a result, a substantial amount of research has been conducted on the ability of clay buffer materials to inhibit microbial activity (e.g., Stroes-Gascoyne 2010).

In the current Canadian EBS design, 100% HCB buffer material surrounding the waste containers is proposed to prevent or minimize potential negative consequences of microbial activity, such as damage to the container or barrier integrity. Numerous studies have evaluated the survival and activity of microorganisms in clay-based sealing materials under relevant environmental conditions, as summarized in Wolfaardt and Korber (2012). The activity and abundance of microbes in a repository are affected by three main factors: 1) the supply of usable nutrients and energy sources, 2) the availability of water, and 3) elevated temperatures. Radiation fields are not expected to be significant due to the shielding provided by the thick-walled containers.

Sources of nutrients in the sealing materials would include organic matter associated with the clays, nitrates and fuel oil from blasting residues, and hydrocarbons from diesel oils and exhaust gases, all potentially introduced during repository excavation and operation activities, but minimized to the extent possible. As the organic matter in such clays has already persisted in the presence of indigenous microbial assemblages for thousands to millions of years, it is probably unrealistic to assume that all of the organic carbon would be accessible to microbes. It is likely, therefore, that “available” organic carbon would be the limiting nutrient for microbial activity in a repository.

Microbiologists generally use a thermodynamic parameter, water activity (a_w), to express water availability in a quantitative sense. This term corresponds to the ratio of a solution’s vapour pressure to that of pure water at a given temperature. The activity of porewater in sealing materials is affected, in particular, by the salinity of the water, as well as by the affinity of the clay for water. For example, while the water activity in pure water is 1.0, the water activity in a 2 mol/kg solution of $CaCl_2$ is about 0.85 within the buffer material (King and

Stroes-Gascoyne 1997). Bacteria must expend extra effort to grow in a habitat with a low a_w because they must maintain a high internal solute concentration to retain water within their cells. Most bacteria flourish only at or above an a_w of approximately 0.98, the a_w for seawater (see Figure 5-24). In order for the buffer to inhibit bacterial growth, the following criteria have been established: 1) the water activity to be less than or equal to 0.96; and 2) a bentonite dry density of at least 1600 kg/m^3 or a porewater salinity of greater than 60 g NaCl/L (Stroes-Gascoyne et al. 2006, 2007a, 2007b).

Temperatures within the repository are anticipated to range from ambient (10 - 20^{o}C) to ~100^{o}C (i.e., adjacent to a container). Temperatures within this range would have some impact on the viability of most microbes indigenous to the sealing materials. The bacteria in buffer material closest to the container would be subjected to the most intense heat and related buffer desiccation. Experiments assessing the effect of temperature suggest that microbes were not particularly sensitive to a temperatures of 60°C, and some culturability remained after exposure to 80°C at all dry buffer densities studied (0.8 to 2.0 Mg/m^3), but at temperatures ≥ 121°C, culturability was reduced (Stroes-Gascoyne and Hamon 2010). Importantly, the effect of temperature on culturability in low-dry-density bentonite was reversible once the heat source was removed and re-saturation was allowed to occur, highlighting the importance of maintaining high dry density to inhibit/minimize microbial activity (Stroes-Gascoyne and Hamon 2010).

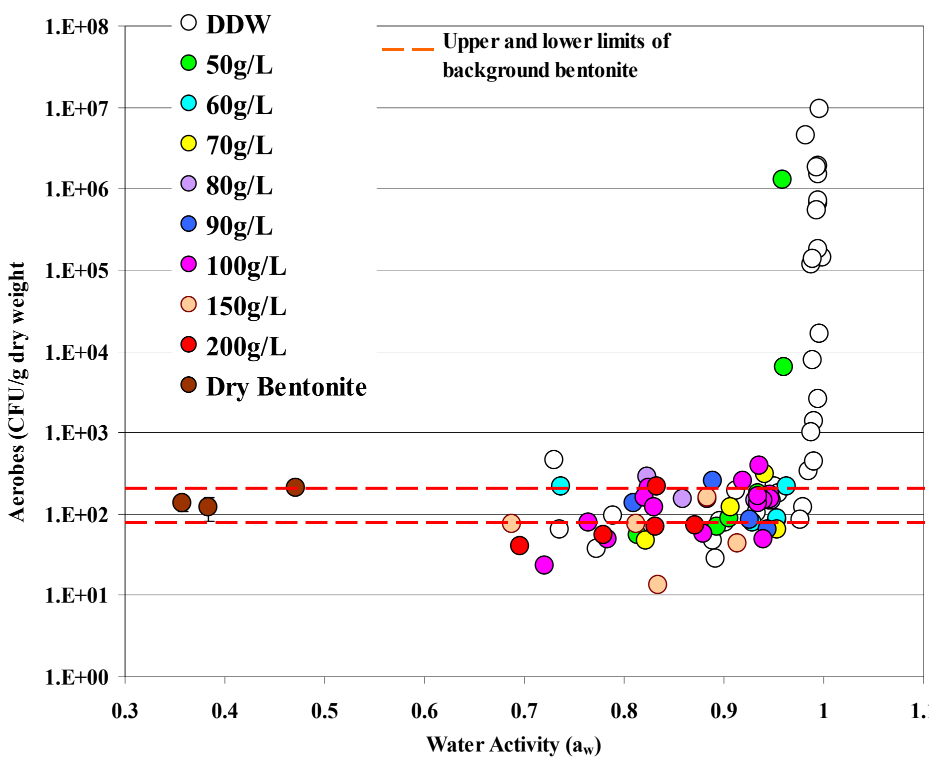

Notes: Stroes-Gascoyne and Hamon (2008). CFU – Colony Forming Units.

Figure 5-24: Effect of Water Activity on Aerobic Culturability in Compacted Bentonite

In summary, experimental evidence indicates that in a low-salinity repository environment, a highly compacted bentonite with a dry density of 1600 kg/m^3 will suppress microbial aerobic culturability to below background levels (Stroes-Gascoyne et al. 2010b). In contrast, in a high-salinity repository environment, with porewater salinities ≥ 50 g/L, salinity will suppress microbial activity over a wider range of bentonite dry densities (~ 800 to 1800 kg/m^3) (Stroes-Gascoyne et al. 2010a, 2011). These studies further indicate that 100% highly-compacted bentonite, when directly in contact with the used fuel containers, will reduce microbial activity to insignificant levels.

5.5.5 Radiation

Radiation will have little effect on the sealing materials, even near the container surfaces. It was estimated that for the reference container, the initial external surface dose rate for 30-year fuel would be ~1 Gy/hr (Morco et al. 2017). The dose rate drops by over four orders of magnitude after 500 years and beyond. Radiation may restrict biological processes in the immediate vicinity of the container, and it may result in minor chemical changes in gas and porewater composition due to radiolysis, but none of these effects are expected to be significant (McMurry et al. 2003).

5.5.6 Sorption

The buffer system provides a chemical environment which will limit the mobility of contaminants in defective UFCs. Sorption is a general term for surface-related processes that involve the transfer of ions from a solution in which they have freedom of movement, to a fixed position on a surface. In addition to ion exchange, sorption includes surface complexation (in which ions form a strong chemical bond with a reactive surface group at the mineral surface without the displacement of any other ions) and surface precipitation (in which a chemical reaction occurs on the surface because conditions there differ from those in solution).

5.5.7 Vertical Movement of Containers

In the horizontal placement concept, used fuel containers are contained within the HCB box and the remaining void space is filled with gap-fill material. One of the design requirements of this buffer is to prevent containers from shifting from their respective as-placed locations within the placement room, which would reduce the buffer thickness.

Upon closure, water is expected to slowly enter the placement rooms, wetting, swelling and compressing the blocks and gap-fill material. The rate of resaturation will depend on the rate and location of water inflow, as well as the actual evolution of the saturation and homogenisation of the buffer. Variability in resaturation is expected to lead to an uneven distribution of swelling pressures within the placement rooms. However, the system will gradually move toward equilibrium very slowly (Kim and Priyanto 2011 and Chandler 2008). In addition, some upward swelling is expected because the gap-fill material has a lower swelling pressure and a certain degree of compressibility. Such small movements of the containers would not affect repository evolution.

5.5.8 Buffer Erosion and Colloid Formation

Colloids are small solid particles, between 1 nm and 1 μm in diameter, that are suspended and dispersed in groundwater. Colloids may form by microbial activity, or as precipitates, due to a change in porewater chemistry. Colloids are of interest in a repository primarily because they have the potential to sorb radionuclides if containers have failed, at which point the transport of the contaminant is controlled by the mobility of the colloid, rather than by the chemical speciation of the radionuclide. These are not expected to be important due to the low permeability of the host rock, such that transport is by diffusion and not advection.

5.5.9 Confidence

The engineered sealing-system components would be installed subject to design, manufacturing and construction specifications, and so their properties would be known with a high degree of confidence. Nevertheless, there are uncertainties about the long-term behaviour of the materials and the processes that would affect them.

Temperature: There is confidence in the results of thermal models over long timeframes. Temperatures in the near-field are generally well predicted in modelling of prototype repository-design experiments over a range of repository saturation levels. Uncertainties would tend to be localized and due to spatial variability in properties.

Repository Saturation: Considerable confidence exists in the ability to describe repository performance in a saturated state, but there would exist a period of potentially tens to hundreds of years in which saturation will not be fully achieved. During this pre-saturation stage of repository evolution, many interactions between repository components will occur, and resaturation of a repository involves coupling of thermal-hydraulic-mechanical processes. Current numerical models are sufficiently able to broadly explain the evolution of saturation conditions.

Swelling Pressures and Stresses: The swelling pressures generated by the buffer will depend on the buffer composition, buffer density, and groundwater conditions. The swelling characteristics of a wide range of bentonite-based sealing materials have been determined through testing, but would need to be confirmed for site-specific conditions. The manner in which stresses develop within a repository would also influence the swelling pressure. Strains within one component of the repository sealing system may affect the density and, hence, the swelling pressure development of another component. The development of thermal stresses, in conjunction with the hydraulic and swelling stresses, within a multi-component system is complex. Although numerical simulations have been conducted to evaluate the near-field stress in the buffer system, further effort is required to refine the results based on the site-specific data and the advanced understanding of the buffer materials. However, the UFC is designed to withstand significant buffer swelling load. The refinement in the near-field stress calculation is not expected to impact the UFC integrity.

Evolution of Material Properties: The properties of light and dense backfill used to close the repository are not yet thoroughly characterized with respect to their performance under repository conditions. Further studies on the long-term evolution of these materials and their interaction with adjacent materials and groundwater are warranted.

Mineralogical Stability of Montmorillonite: Under the expected repository conditions (temperatures less than 100°C, moderate pH levels, moderate potassium concentrations in groundwater), it is very unlikely that substantial conversion of montmorillonite to illite would occur over a million-year timeframe.

Microbiological Processes: Although viable microbes would initally inhabit at least some portions of a deep geological repository, there are a number of uncertainties associated with the extent of changes that would result from their presence. For example, although experimental data indicate it is unlikely that bacteria would become active or able to recolonize saturated, highly-compacted buffer material, their behaviour in gap-fill material needs to be demonstrated.

Redox Conditions: There is some uncertainty about when reducing conditions would be established in the sealing materials. It has also been noted that estimates of the time required to reach anaerobic conditions vary from approximately tens of thousands of years to hundreds of thousands of years, depending on assumptions made in the calculations. Regardless of the amount of time required for oxygen in the repository to be consumed, the total amount of oxygen available for reaction is limited. There are no processes (including radiolysis) that are likely to introduce significant additional quantities of oxygen or other oxidizing species after closure.

Interactions Between Sealing System Components: The interfaces between materials might provide preferential pathways for the migration of water, contaminants or microbes within a repository. Examples of such interfaces include: installation assembly gaps (e.g., between blocks of compacted buffer), shrinkage cracks during the desaturation phase, and the formation of an open space along the top of the room if there is insufficient backfill swelling.

5.6 Summary

The discussion in this chapter describes changes that would occur in the multi-barrier repository system during its lifetime. The discussion is based on reasonable expectations for conditions that are likely to be encountered in crystalline rock.

Many properties of the repository components, and the processes that would affect them, are well characterized. The system is based on durable materials and passive natural processes. Natural and archaeological analogues help to support the descriptions of system behaviour into the future. Of the uncertainties that remain, some questions would be resolved during site characterization activities. Other uncertainties about the future evolution of the system arise from the recognition that simplifying assumptions and simple models may not, in all cases, adequately represent the complexity or heterogeneity of an actual repository over long periods of time. These uncertainties would be addressed by further analyses, by additional experimental or field studies (including extended monitoring in the repository itself), and by using conservative or bounding assumptions in the safety assessment models.

5.7 References for Chapter 5

Adams, J., V. Peci, S. Halchuk and P. Street. 2016. Seismic Activity in the Northern Ontario Portion of the Canadian Shield Annual Progress Report for the Period January 01 – December 31, 2015. Nuclear Waste Management Organization Report DGR-TR-2016-21. Toronto, Canada.

Adam, J. 1989. Postglacial faulting in Eastern Canada: nature, origin and seismic hazard implications. Tectonophysics 163, 323-331.

AMEC GEOMATRIX. 2011. Seismic Hazard Assessment. AMEC Geomatrix, Inc. report for the Nuclear Waste Management Organization Report NWMO DGR-TR-2011-20 R000. Toronto, Canada.

Akiyama, E., K. Matsukado, M. Wang and K. Tsuzaki. 2010. Evaluation of hydrogen entry into high strength steel under atmospheric corrosion. Corrosion Science 52, 2758-2765.

Alexandre, P., Kyser, K., Thomas, D. P. Polito, J. Marlat, 2009. Geochronology of unconformity-related uranium deposits in the Athabasca Basin, Saskatchewan, Canada and their integration in the evolution of the basin. Mineralium Deposita 44, 41.

Atkinson, G.M. and R.K. McGuire. 1993. Probability of damaging earthquakes in northwestern Ontario. Report for Atomic Energy of Canada Ltd, TR-M-0023.

Atkinson, G.M. and S.N. Martens. 2007. Seismic hazard estimates for sites in the stable Canadian craton. Canadian Journal of Civil Engineering 34, 1299-1311.

Bäckblom, G. and R. Munier. 2002. Effects of Earthquakes on the Deep Repository for Spent Fuel in Sweden based on Case Studies and Preliminary Model Results. Swedish Nuclear Fuel and Waste Management Company Report TR-02-24. Stockholm, Sweden.

Baumgartner, P. 2006. Generic Thermal-Mechanical-Hydraulic (THM) Data for Sealing Materials – Volume 1: Soil-water Relationships. Ontario Power Generation Report 06819-REP-01300-10122-R00. Toronto, Canada.

Briggs, S.A., J. McKelvie, P. Keech, B. Sleep, and M. Krol. 2017a. Transient Modelling of Sulphide Diffusion under Conditions Typical of a Deep Geological Repository. Corrosion Engineering, Science and Technology, 52, 200-203.

Briggs, S., J. McKelvie, B. Sleep and M. Krol. 2017b. Multi-dimensional transport modelling of corrosive agents through a bentonite buffer in a Canadian deep geological repository. Science of the Total Environment. 599, 348-354.

Chandler, N.A, A. Cournut, D.A. Dixon, C. Fairhurst, F. Hansen, M. Gray, K. Hara, Y. Ishijima, E. Kozak, J. Martino, K. Masumoto, G. McCrank, Y. Sugita, P. Thompson, J. Tillerson and B. Vignal. 2002. The Five-year Report of the Tunnel Sealing Experiment: An International Project of AECL, JNC, ANDRA and WIPP. Atomic Energy of Canada Limited Report AECL-12727. Pinawa, Canada.

Chandler, N. 2008. Modelling the Compliance of Swelling Clay Sealing Systems: In-Floor Borehole and Horizontal Borehole Numerical Simulations. Nuclear Waste Management Organization Report NWMO TR-2008-13. Toronto, Canada.

Chen, Y., X.H. Wang, J. Li, J.L. Lu, F.S. Wang. 2007. Polyaniline for corrosion prevention of mild steel coupled with copper. Electrochimica Acta 52, 5392-5399.

Chen, J., Z. Qin and D.W. Shoesmith. 2011. Rate controlling reactions for copper corrosion in anaerobic aqueous sulphide solutions. Corrosion Engineering, Science and Technology 46, 138-141.

Cox, B. 1999. Corrosion and hydriding of zircaloy fuel cladding - the inside (and outside) story. Proceedings 6th International Conference on CANDU fuel, Niagara Falls, Canada, 338.

Crowe, R., K. Birch, J. Freire-Canosa, J. Chen, D. Doyle, F. Garisto, P. Gierszewski, M. Gobien, C. Hatton, N. Hunt, S. Hirschorn, M. Hobbs, M. Jensen, P. Keech, L. Kennell-Morrison, E. Kremer, J. McKelvie, C. Medri, M. Mielcarek, A. Murchison, A. Parmenter, R. Ross, E. Sykes and T. Yang. 2016. Technical Program for Long-Term Management of Canada's Used Nuclear Fuel – Annual Report 2015. Nuclear Waste Management Organization Report NWMO TR-2016-01. Toronto, Canada.

Dixon D., T. Sandén, E. Jonsson and J. Hansen. 2011. Backfilling of Deposition Tunnels: Use of Bentonite Pellets. Swedish Nuclear Fuel and Waste Management Company Report SKB P-11-44. Stockholm, Sweden.

Dixon, D.A. A. Man, J. Stone, S. Rimal, G. Siemens, P. Abootalebi and K. Birch. 2016. Backfilling and Sealing Materials for a Deep Geological Repository. 3rd Canadian Conference on Nuclear Waste Management, Decommissioning and Environmental Restoration, Ottawa, Canada, Session T3.

Dutton, D. 2006. Preliminary Evaluation of the Creep Behaviour of the Inner Steel Vessel of a Used-fuel Container. Ontario Power Generation Report 06819-REP-01300-10108-R00. Toronto, Canada.

Ebert, K. 2015. GIS analysis of ice-sheet erosional impacts on the exposed shield of Baffin Island, eastern Canadian Arctic. Can. J. Earth Sci. 52, 966-979.

Fenton, C.H. 1994. Postglacial faulting in eastern Canada: an annotated bibliography, Geological Survey of Canada, Open File 2774, pp. 1–98. Ottawa, Canada.

Ferry, C., J.-P. Piron, A. Poulesquen and C. Poinssot. 2008. Radionuclides release from the spent fuel under disposal conditions: Re-evaluation of the instant release fraction. Materials Research Society Symposium Proceedings 1107, 447-454.

Fracture Systems. 2011. Excavation Damaged Zones Assessment. Nuclear Waste Management Organization Report NWMO DGR-TR-2011-21. Toronto, Canada.

Freire-Canosa, J. 2011. Used Fuel Integrity Program: Summary Report. Nuclear Waste Management Organization Report NWMO TR-2011-04. Toronto, Canada.

Frescura, G.M. and A.L. Wight. 1979. Fuel Management & Reactor Operation Review of Operating Experience. From Canteach Website at: https://canteach.candu.org/Content%20Library/20042116.pdf.

Garisto, F. 2017. Sixth Case Study: Features, Events and Processes. Nuclear Waste Management Organization Report NWMO TR-2017-08. Toronto, Canada.

Garisto, N.C., W. Newmyer and A. Ho. 2014. Criticality Safety Computations for Spent CANDU Fuel in a Deep Geologic Repository. Nuclear Waste Management Organization Report NWMO TR-2014-08. Toronto, Canada.

Gobien, M., F. Garisto, E. Kremer and C. Medri. 2016. Sixth Case Study: Reference Data and Codes. Nuclear Waste Management Organization Report NWMO TR-2016-10. Toronto, Canada.

Guo, R. 2009. Coupled Thermal-Hydraulic-Mechanical Modelling of the Canister Retrieval Test. Nuclear Waste Management Organization Report NWMO TR-2009-31. Toronto, Canada.

Guo, R. 2015. Thermal Modelling of a Mark II Container. Nuclear Waste Management Organization Report NWMO TR-2015-06. Toronto, Canada.

Guo, R. 2016. Thermal Response of a Mark II Conceptual Deep Geological Repository in Crystalline Rock. Nuclear Waste Management Organization Report, NWMO TR-2016-03. Toronto, Canada.

Guo, D., L. Wu, A. Chin, J. J. Noel, and J. C. Wren. 2016. Localized Corrosion of Carbon Steel Nuclear Waste Containers Near Weld Regions in the Presence of γ-Radiation., Corrosion 2016, NACE International, Vancouver, Canada.

Hay, W.W., C.A. Shaw and C.N. Wold. 1989. Mass-balanced paleogeographic reconstructions. Geologishe Rundschau 78, 201-242.

Hultquist G., P. Szakálos, M.J. Graham, A.B. Belonoshko, G.I. Sproule, L. Gråsjö, P. Dorogokupets, B. Danilov, T. AAstrup, G. Wikmark, G.-K. Chuah, J.-C. Eriksson and A. Rosengren. 2009. Water corrodes copper. Catalysis Letters 132, 311-316.

Hultquist G., M.J. Graham, P. Szakálos, G.I. Sproule, A. Rosengren and L. Gråsjö. 2011. Hydrogen gas production during corrosion of copper by water. Corrosion Science 53, 310-319.

Hultquist, G., M.J. Graham, O. Kodra, S. Moisa, R. Liu, U. Bexell and J.L. Smialek. 2013. Corrosion of Copper in Distilled Water without Molecular Oxygen and the Detection of Produced Hydrogen. SSM Technical Note 2013:07. Stockholm, Sweden.

Humphreys, P.N., J.M. West and R. Metcalfe. 2010. Microbial Effects on Repository Performance. Prepared by Quintessa Limited for the Nuclear Decommissioning Authority Report No. QRS-1378Q-1. Oxfordshire, United Kingdom.

IAEA (International Atomic Energy Agency). 2010. Review of Fuel Failures in Water Cooled Reactors. IAEA Nuclear Energy Series No. NF-T-2.1. Vienna, Austria.

Ibrahim, B. 2015. The Corrosion Behaviour of Cu in Irradiated and Non-Irradiated Humid Air. University of Western Ontario, Canada. Electronic Thesis and Dissertation Repository, #3315, http://ir.lib.uwo.ca/etd/3315.

INTERA. 2011. Descriptive Geosphere Site Model. Nuclear Waste Management Organization Report NWMO DGR-TR-2011-24. Toronto, Canada.

Itasca Consulting Group. 2015. Long-term Stability Analysis of APM Mark II Conceptual Design in Sedimentary and Crystalline Rocks. Nuclear Waste Management Organization Report NWMO TR-2015-27. Toronto, Canada.

Jensen, K.A. and R.C. Ewing. 2001. The Okélobondo natural fission reactor, southeast Gabon: Geology, mineralogy, and retardation of nuclear-reaction products. Geological Society of America Bulletin 113, 32-62.

Johansson, J., A. Blom, A. Chukharkina, and K. Pedersen. 2015. Study of H_2 gas emission in sealed compartments containing copper immersed in O_2-free water. SKB Report, SKB TR-15-03. Stockholm, Sweden.

Kim, C-S. and D. Priyanto. 2011. Two-Component Swelling Tests Operated for Three, Nine and Twenty-Seven Months. Nuclear Waste Management Organization Report NWMO TR-2011-15. Toronto, Canada.

King, F. 2006. Review and Gap Analysis of the Corrosion of Copper Containers under Unsaturated Conditions. Ontario Power Generation Report 06819-REP-01300-10124-R00. Toronto, Canada.

King, F. 2009a. Hydrogen Effects on Carbon Steel Used Fuel Containers. Nuclear Waste Management Organization Report NWMO TR-2009-29. Toronto, Canada.

King, F. 2009b. Microbiologically influenced corrosion of nuclear waste container. Corrosion 65, 233-251.

King, F. 2013. Consequences of the General Corrosion of Carbon Steel Used Fuel Containers for Gas Generation in a DGR. Nuclear Waste Management Organization Report NWMO TR-2013-16. Toronto, Canada.

King, F. and S. Stroes-Gascoyne. 1997. Predicting the effects of microbial activity on the corrosion of copper nuclear waste disposal containers. Eds. J.H. Wolfram, R.D. Rogers and L.G. Gazso in Microbial Degradation Processes in Radioactive Waste Repository and in Nuclear Fuel Storage Areas. Volume 11 of NATO ASI Series. Kluwer Academic Publishers, Netherlands. 149-162.

King, F. and M. Kolář. 2000. The Copper Container Corrosion Model Used in AECL's Second Case Study. Ontario Power Generation Report 06819-REP-01200-10041-R00. Toronto, Canada.

King, F., L. Ahonen, C. Taxén, U. Vuorinen and L. Werme. 2001. Copper Corrosion under Expected Conditions in a Deep Geologic Repository. Swedish Nuclear Fuel and Waste Management Company Report SKB TR-01-23. Stockholm, Sweden.

King, F., M. Kolář and P. Maak. 2008. Reactive-transport model for the prediction of the uniform corrosion behaviour of copper used fuel containers. Journal of Nuclear Materials 379, 133-141.

King, F. and D. Shoesmith. 2010. Nuclear waste canister materials, corrosion behaviour and long-term performance in geological repository systems. Eds. J. Ahn and M.J. Apted in Geological Repository Systems for Safe Disposal of Spent Nuclear Fuel and Radioactive Waste. Woodhead Publishing, Cambridge, United Kingdom.

King, F., C. Lilja, K. Pedersen, P. Pitkänen and M. Vähänen. 2010. An Update of the State-of-the-Art Report on the Corrosion of Copper under Expected Conditions in a Deep Geologic Repository. Swedish Nuclear Fuel and Waste Management Company Report SKB TR-10-67. Stockholm, Sweden.

King, F., C. Lilja, K. Pedersen, P. Pitkänen and M. Vähänen. 2011a. An Update of the State-of-the-art Report on the Corrosion of Copper under Expected Conditions in a Deep Geologic Repository. Posiva Oy Report POSIVA 2011-01. Olkiluoto, Finland.

King, F., M. Kolář, M. Vähänen and C. Lilja. 2011b. Modelling long term corrosion behaviour of copper canisters in KBS-3 repository. Corrosion Engineering, Science and Technology 46, 217-222.

King, F., D.S. Hall and P.G. Keech. 2017. Nature of the near-field environment in a deep geological repository and the implications for the corrosion behaviour of the container. Corrosion Engineering, Science and Technology 52, 25-30.

Kremer, E.P. 2017. Estimating the Durability of the Canadian Used Fuel Container. Corrosion Engineering Science and Technology, In Press.

Kukkonen, I.T., O. Olesen, M.V.S. Ask and the PFDP Working Group. 2010. Postglacial faults in Fennoscandia: targets for scientific drilling. Geologiska Föreningens i Stockholm Förhandlingar (GFF) 132, 71–81.

Kwong, G.M. 2011. Status of Corrosion Studies for Copper Used Fuel Containers Under Low Salinity Conditions. Nuclear Waste Management Organization Report NWMO TR-2011-14. Toronto, Canada.

Lanson, B., S. Lantenois, P. A. van Aken, A. Bauer, and A. Plançon. 2015. Experimental investigation of smectite interaction with metal iron at 80 °C: Structural characterization of newly formed Fe-rich phyllosilicates. American Mineralogist, 97, 864–871. doi:10.2138/am.2012.4062.

Lidmar-Bergström, K. 1997. A long-term perspective on glacial erosion. Earth Surface Processes and Landforms 22, 297-306.

Lovasic, Z. and P. Gierszewski. 2005. CANDU Fuel Long-Term Storage and Used Fuel Integrity. Paper at 9th International Conference on CANDU Fuel. Canadian Nuclear Society Bulletin Vol. 26, No. 4.

Lund B. 2006. Stress Variations during a Glacial Cycle at 500 m Depth in Forsmark and Oskarshamn: Earth Model Effects. Swedish Nuclear Fuel and Waste Management Company Report R-06-95. Stockholm, Sweden.

Man, A. and J.B. Martino. 2009. Thermal, Hydraulic and Mechanical Properties of Sealing Materials. Nuclear Waste Management Organization Report NWMO TR-2009-20. Toronto, Canada.

McMurry, J., D.A. Dixon, J.D. Garroni, B.M. Ikeda, S. Stroes-Gascoyne, P. Baumgartner and T.W. Melnyk. 2003. Evolution of a Canadian Deep Geologic Repository: Base Scenario. Ontario Power Generation Report 06819-REP-01200-10092-R00. Toronto, Canada.

McMurry, J., B.M. Ikeda, S. Stroes-Gascoyne, D.A. Dixon and J.D. Garroni. 2004. Evolution of a Canadian Deep Geologic Repository: Defective Container Scenario. Ontario Power Generation Report 06819-REP-01200-10127-R00. Toronto, Canada.

Melanson, A., T. Bell and L. Tarasov. 2013. Numerical modelling of subglacial erosion and sediment transport and its application to the North American ice sheets over the Last Glacial cycle. Quaternary Science Reviews 68, 154-174.

Morco, R.P., J. M. Joseph, C. Medri, D. S. Hall, and J. C. Wren. 2017. Model Calculations of Radiolytic Production of Oxidants Anticipated under Deep Geologic Repository Environments. Corrosion Engineering Science and Technology, In Press.

Necib, S., Y. Linard, D. Crusset, M. Schlegel, S. Daumas, N. Michau. 2017. Corrosion processes of C-steel in long term repository conditions. Corros. Eng. Sci. Techn., In Press.

Newman, R.C., S. Wang and G. Kwong. 2010. Anaerobic Corrosion Studies of Carbon Steel Used Fuel Containers. Nuclear Waste Management Organization Report NWMO TR-2010-07. Toronto, Canada.

Normani, S.D., Y.-J. Park, J.F. Sykes and E.A. Sudicky. 2007. Sub-Regional Modelling Case Study 2005-2006 Status Report. Nuclear Waste Management Organization Report NWMO TR-2007-07. Toronto, Canada.

Normani, S.D. 2009. Paleoevolution of Pore Fluids in Glaciated Geologic Settings. Ph.D. Thesis, Department of Civil Engineering, University of Waterloo. London, Canada.

Normani, S.D., and J.F. Sykes. 2014. Paleoclimate Influences in a Sub-Regional Crystalline Rock Setting. Nuclear Waste Management Organization Report NWMO-TR-2014-24. Toronto, Canada.

Normani, S. D., J. F. Sykes, and Y. Yin. 2014. Methodology to generate orthogonal fractures from a discrete, complex, and irregular fracture zone network, in Fractured Rock Hydrogeology, IAH Selected papers on hydrogeology, vol. 20, edited by J. M. Sharp, Jr., pp. 197–210, CRC Press/Balkema, The Netherlands.

Osacký, M., V. Šucha, A. Czímerová, M. Pentrák, and J. Madejová. 2013. Reaction of smectites with iron in aerobic conditions at 75 °C. Applied Clay Science, 72, 26–36. doi:10.1016/j.clay.2012.12.010.

Ottosson, M., M. Boman, P. Berastegui, Y. Andersson, M. Hahlin, M. Korvela and R. Berger. 2016. Copper in ultrapure water. SKB Report, SKB TR-16-01. Stockholm, Sweden.

Pedersen K. 2000. Microbial Processes in Radioactive Waste Disposal. Swedish Nuclear Fuel and Waste Management Company Report SKB TR 00-04. Stockholm, Sweden.

Peltier, W.R. 2002. A Design Basis Glacier Scenario. Ontario Power Generation Report 06819-REP-01200-10069-R00. Toronto, Canada.

Peltier, W.R. 2003. Long-Term Climate Change – Glaciation. Ontario Power Generation Report 06819-REP-01200-10113-R00. Toronto, Canada.

Peltier, W.R. 2004. Permafrost Influences Upon the Subsurface. Ontario Power Generation Report 06819-REP-01200-10134-R00. Toronto, Canada.

Peltier, W.R. 2006. Boundary Conditions Data Set for Spent Fuel Repository Performance Assessment. Ontario Power Generation Report 06819-REP-01200-10154-R00. Toronto, Canada.

Peltier, W.R. 2011. Long-term Climate Change. Nuclear Waste Management Organization Report NWMO DGR-TR-2011-14 R000. Toronto, Canada.

Puigdomenech, I. and C. Taxén. 2000. Thermodynamic Data for Copper: Implications for the Corrosion of Copper under Repository Conditions. Swedish Nuclear Fuel and Waste Management Company Report SKB TR 00-13. Stockholm, Sweden.

Qin, Z., R. Deljeet, M. Ai, N. Farhangi, J.J. Noel, S. Ramamurthy, D.W. Shoesmith, F. King, and P.G. Keech. 2017. The active/passive conditions for copper corrosion under nuclear waste repository environment. Corrosion Engineering, Science and Technology, 52, 45-49.

Raiko, H. 2005. Disposal Canister for Spent Nuclear Fuel – Design Report. Posiva Oy Report POSIVA 2005-02. Olkiluoto, Finland.

Saiedfar, M. and P. Maak. 2002. Preliminary Assessment of the Deformation and Stresses of Copper Used-fuel Containers in a Hypothetical Deep Geologic Repository. Ontario Power Generation Report, 06819-REP-01300-10049-R00. Toronto, Canada.

Scully, J. and M. Edwards. 2013. Review of the NWMO Copper Corrosion Allowance. Nuclear Waste Management Report NWMO TR-2013-04. Toronto, Canada.

Scully, J.R., D. Féron, and H. Hänninen. 2016. Peer review of the NWMO copper corrosion program. Nuclear Waste Management Organization Report, NWMO-TR-2016-11. Toronto, Canada.

Senior, N., R. Newman, S. Wang, and N. Diomidis. 2017. Understanding and Quantifying the Anoxic Corrosion of Carbon Steel in a Swiss L/ILW Repository Environment. Corrosion Engineering Science and Technology, In Press.

Sherwood Lollar, B. 2011. Far-Field Microbiological Considerations Relevant to a Deep Geological Repository – State of Science Review. Nuclear Waste Management Organization Report NWMO TR-2011-09. Toronto, Canada.

Shoesmith, D.W. 2008. The Role of Dissolved Hydrogen on the Corrosion/Dissoluton of Spent Nuclear Fuel. Nuclear Waste Management Organization Report NWMO TR-2008-19. Toronto, Canada.

Shoesmith, D.W. and F. King. 1999. The Effects of Gamma Radiation on the Corrosion of Candidate Materials for the Fabrication of Nuclear Waste Packages. Atomic Energy of Canada Limited Report AECL-11999. Pinawa, Canada.

Shoesmith, D.W. and D. Zagidulin. 2010. The Corrosion of Zirconium under Deep Geological Repository Conditions. Nuclear Waste Management Organization Report NWMO TR-2010-19. Toronto, Canada.

SKB. 2010. Critical Review of the Literature on the Corrosion of Copper by Water. Swedish Nuclear Fuel and Waste Management Company Report SKB TR-10-69. Stockholm, Sweden.

SKB. 2011. Long-term Safety for the Final Repository for Spent Nuclear Fuel at Forsmark. Main Report of the SR-Site Project. Volume I. Swedish Nuclear Fuel and Waste Management Company Report SKB TR-11-01. Stockholm, Sweden.

Smart N., A. Rance, P. Fennell and L. Werme. 2003. Expansion due to anaerobic corrosion of steel and cast iron: experimental and natural analogue studies. Eds. D. Féron and D.D. Macdonald in Prediction of Long Term Corrosion Behaviour in Nuclear Waste Systems: Proceedings of the International Workshop. Cadarache, France. London: Maney Pub. (European Federation of Corrosion Publications 36), paper 19, pp 280–294.

Smart N., P. Fennell, A. Rance and L. Werme. 2004. Galvanic corrosion of copper-cast iron couples in relation to the Swedish radioactive waste canister concept. Ed. D. Féron in Prediction Of Long Term Corrosion Behaviour in Nuclear Waste Systems: Proceedings of the 2nd International Workshop. European Federation of Corrosion, pp 52–60. Nice, France.

Smart N.R., A.P. Rance and P.A.H. Fennell. 2005. Galvanic Corrosion of Copper-Cast Iron Couples. Swedish Nuclear Fuel and Waste Management Company Report SKB TR-05-06. Stockholm, Sweden.

Smart N.R., A.P. Rance and P.A.H. Fennell. 2006. Expansion due to the Anaerobic Corrosion of Iron. Swedish Nuclear Fuel and Waste Management Company Report SKB TR-06-41. Stockholm, Sweden.

Smart N., A. Rance, B. Reddy, P. Fennell and R. Winsley. 2012. Analysis of SKB MiniCan Experiment 3. Swedish Nuclear Fuel and Waste Management Company Report SKB TR-12-09. Stockholm, Sweden.

Spiessl, S.M., K.U. Mayer, and K.T.B. MacQuarrie. 2009. Reactive Transport Modelling in Fractured Rock – Redox Stability Study. Nuclear Waste Management Organization Report NWMO-TR-2009-04. Toronto, Canada.

SSM. 2011a. Evolution of Hydrogen by Copper in Ultrapure Water without Dissolved Oxygen. Strål Säkerhets Myndigheten Report 2011:34. Stockholm, Sweden.

SSM. 2011b. Is Copper Immune to Corrosion when in Contact with Water and Aqueous Solutions? Strål Säkerhets Myndigheten Report 2011:09. Stockholm, Sweden.

Standish, T., J. Chen, R. Jacklin, P. Jakupi, S. Ramamurthy, D. Zagidulin, P. Keech and D.W. Shoesmith . 2016. Corrosion of Copper-Coated Steel High Level Nuclear Waste Containers Under Permanent Disposal Conditions. Electrochimica Acta, 211, 331–342.

Standish, T.E., D. Zagidulin, S. Ramamurthy, P. Keech, J. Noel and D. Shoesmith. 2017. Galvanic corrosion of copper-coated carbon steel for used nuclear fuel containers. Corrosion Engineering Science and Technology, 52(S1), 65-69.

Stroes-Gascoyne, S. 2010. Microbial occurrence in bentonite-based buffer, backfill and sealing materials from large-scale experiments at AECL's Underground Research Laboratory. Applied Clay Science 47, 36-42.

Stroes-Gascoyne, S., C.J. Hamon, C. Kohle and D.A. Dixon. 2006. The Effects of Dry Density and Porewater Salinity on the Physical and Microbiological Characteristics of Highly Compacted Bentonite. Ontario Power Generation Report 06819-REP-01200-10016 R00. Toronto, Canada.

Stroes-Gascoyne, S., C.J. Hamon, D.A. Dixon and J.B. Martino. 2007a. Microbial analysis of samples from the tunnel sealing experiments at AECL's Underground Research Laboratory. Physics and Chemistry of the Earth: Parts A/B/C 32, 219-231.

Stroes-Gascoyne, S., P. Maak, C.J. Hamon, and C. Kohle. 2007b. Potential Implications of Microbes and Salinity on the Design of Repository Sealing System Components. Nuclear Waste Management Organization Report NWMO TR-2007-10. Toronto, Canada.

Stroes-Gascoyne, S. and C.J. Hamon. 2008. The Effect of Intermediate Dry Densities (1.1-1.5 g/cm^3) and Intermediate Porewater Salinities (60-90 g NaCl/L) on the Culturability of Heterotrophic Aerobic Bacteria in Compacted 100% Bentonite. Nuclear Waste Management Organization Report NWMO TR-2008-11. Toronto, Canada.

Stroes-Gascoyne, S. and C.J. Hamon. 2010. The Effects of Elevated Temperatures on the Viability and Culturability of Bacteria Indigenous to Wyoming MX-80 Bentonite. Nuclear Waste Management Organization Report NWMO TR-2010-08. Toronto, Canada.

Stroes-Gascoyne, S., C.J. Hamon, D.A. Dixon and D.G. Priyanto. 2010a. The Effect of $CaCl_2$ Porewater Salinity (50-100 g/L) on the Culturability of Heterotrophic Aerobic Bacteria in Compacted 100% Bentonite with Dry Densities of 0.8 and 1.3 g/cm^3. Nuclear Waste Management Organization Report NWMO TR-2010-06. Toronto, Canada.

Stroes-Gascoyne, S., C.J. Hamon, P. Maak and S. Russell. 2010b. The effects of the physical properties of highly compacted smectitic clay (bentonite) on the culturability of indigenous microorganisms. Applied Clay Science 47, 155-162.

Stroes-Gascoyne, S., C.J. Hamon and P. Maak. 2011. Limits to the Use of Highly Compacted Bentonite as a Deterrent for Microbiologically Influenced Corrosion in a Nuclear Fuel Waste Repository. Physics and Chemistry of the Earth 36(17-18), 1630-1638.

Stuhne, G. and W.R. Peltier. 2015. Surface Boundary Conditions During Long-Term Climate Change. Nuclear Waste Management Organization Report NWMO-TR-2015-16. Toronto, Canada.

Stuhne, G. and W.R. Peltier. 2016. Sensitivity Analyses of Surface Boundary Conditions During Long-Term Climate Change. Nuclear Waste Management Organization Report NWMO-TR-2016-19. Toronto, Canada.

Suckling, P., J. Avis, N. Calder, P. Humphreys, F. King and R. Walsh. 2012. T2GGM Version 3.1: Gas Generation and Transport Code. Nuclear Waste Management Organization Report NWMO TR-2012-23. Toronto, Canada.

Swedish National Council. 2010. Nuclear Waste State-of-the-Art Report 2010 – Challenges for the Final Repository Programme. Swedish Government Official Reports SOU 2010:6. Stockholm, Sweden.

Sykes, J.F., S.D. Normani, E.A. Sudicky and R.G. McLaren. 2004. Sub-regional Scale Groundwater Flow within an Irregularly Discretely Fractured Canadian Shield Setting. Ontario Power Generation Report 06819-REP-01200-10133-R00. Toronto, Canada.

Sykes, J.F., S.D. Normani, M.R. Jensen and E.A. Sudicky. 2009. Regional-scale groundwater flow in a Canadian Shield setting. Canadian Geotechnical Journal, 46(7), 813–827.

Szakálos P., Hultquist G., Wikmark G. 2007. Corrosion of copper by water. Electrochemical and Solid-State Letters 10, C63–C67.

Tait, J.C., H. Roman and C.A. Morrison. 2000. Characteristics and Radionuclide Inventories of Used Fuel from OPG Nuclear Generating Stations. Ontario Power Generation Report 06819-REP-01200-10029-R00. Toronto, Canada.

Tsang, C.F., F. Bernier and C. Davies. 2005. Geohydromechanical processes in the Excavation Damaged Zone in crystalline rock, rock salt, and indurated and plastic clays—in the context of radioactive waste disposal. International Journal of Rock Mechanics and Mining Sciences 42(1), 109-125.

Tsuru, T., Y. Huang, Md.R. Ali and A. Nishikata. 2005. Hydrogen entry into steel during atmospheric corrosion process. Corrosion Science 47, 2431-2440.

Turnbull, J., R. Szukalo, M. Behazin, D. Zagidulin, S. Ramamurthy, J.C. Wren and D.W. Shoesmith. 2017. Exploring the Effects of Cathodic Reagent Concentration and Small Solution Volumes on the Corrosion of Copper in Dilute Nitric Acid Solutions. Corrosion, https://doi.org/10.5006/2655

Walsh, R. and J. Avis. 2010. Glaciation Scenario: Groundwater and Radionuclide Transport Studies. Nuclear Waste Mangement Organization Report NWMO-TR-2010-09. Toronto, Canada.

Werme, L. 1998. Design Premises for Canister for Spent Nuclear Fuel. Swedish Nuclear Fuel Waste Management Company Report SKB TR-98-08. Stockholm, Sweden.

Wersin, P., M. Birgersson, S. Olsson, O. Karnland and M. Snellman. 2007. Impact of Corrosion-Derived Iron on the Bentonite Buffer within the KBS-3H Disposal Concept – the Olkiluoto Site as Case Study. Posiva Oy Report POSIVA 2007-11. Olkiluoto, Finland.

Wheeler, R.L. 1995. Earthquakes and the cratonward limit of Iapetan faulting in eastern North America. Geology 23, 105-108.

Wolfaardt, G.M. and D.R. Korber. 2012. Near-Field Microbiological Considerations Relevant to a Deep Geological Repository for Used Nuclear Fuel – State of Science Review. Nuclear Waste Management Organization Report NWMO TR-2012-02. Toronto, Canada.

Wu, L., D. Guo, M. Li, J.M. Joseph, J.J. Noël, P.G. Keech, J.C. Wren. 2017. Inverse Crevice Corrosion of Carbon Steel: Effect of Solution Volume to Surface Area, J. Electrochem. Soc., 164, C539.

6. SCENARIO IDENTIFICATION AND DESCRIPTION

Postclosure safety is assessed through consideration of a set of potential future scenarios, where scenarios are descriptions of alternative possible evolutions of the repository system. Scenarios can also be designed with the aim of illustrating the properties of natural or engineered barriers (IAEA 2012). For that purpose, it can be instructive to assign parameter values such that the barrier under consideration is influenced in an exaggerated way so that the robustness of the barriers can be more clearly exhibited. Scenarios of this sort are often called "what-if" scenarios to distinguish them from realistic scenarios.

The purpose of scenario identification is to develop a comprehensive range of possible future evolutions against which the performance of the system can be assessed. Consistent with CNSC Guide G-320 (CNSC 2006), both Normal Evolution and Disruptive Event Scenarios are considered. The Normal Evolution Scenario represents the normal (or expected) evolution of the site and facility, while Disruptive Event Scenarios examine the effects of unlikely events that might lead to penetration of barriers and abnormal degradation and loss of containment.

Scenarios of interest are identified through consideration of the various factors (see Table 6-1) that could affect the repository system and its evolution (IAEA 2012). These factors can be further categorized into Features, Events and Processes (FEPs) as shown in Table 6-1. To provide a method for ensuring that all relevant factors are considered, FEPs are organized in a hierarchical structure with up to 4 levels. The finest discretization of the FEPs occurs at the lowest level. This is illustrated in Table 6-2 where the FEPs are listed down to level 3, the lowest level for these FEPs. This hierarchical structure used here, although reorganized, includes all FEPs listed in the FEPs database of the OECD Nuclear Energy Agency (NEA 2000), an intergovernmental agency that facilitates cooperation among countries with advanced nuclear technology infrastructures.

FEPs can be characterized as either "external" or "internal", depending on whether they are outside or inside the spatial and temporal boundaries of the repository system domain, which here includes the repository, the geosphere and the affected biosphere. The external factors originate outside these boundaries; whereas, waste package, repository, geosphere, biosphere and contaminant factors can be considered as "internal" factors. Hence, the waste package, repository, geosphere, biosphere and contaminant factors and FEPs will be referred to as Internal FEPs and the external factors and FEPs will be referred to as External FEPs.

The External FEPs provide the system with boundary conditions and include influences originating outside the repository system that might cause change. Included in this group are decisions related to repository design, operation and closure since these are outside the temporal boundary of the postclosure behaviour of the repository system. If these External FEPs can significantly affect the evolution of the system and / or its safety functions of isolation and containment, they are considered scenario-generating FEPs in the sense that whether or not they occur (or the extent to which they occur or the form that they take) could define a particular future scenario that should be considered.

The External FEPs are listed in Table 6-2. Those that are likely to affect the repository system and its evolution are discussed in Section 6.1. The effects of less likely External FEPs and certain Internal FEPs that might lead to abnormal degradation and loss of containment are discussed in Section 6.2.

Table 6-1: FEP List Showing FEPs Down to Level 2

FEP Number and Title	
1.	**EXTERNAL FACTORS**
1.1	Repository Issues
1.2	Geological Factors
1.3	Climatic Factors
1.4	Future Human Actions
1.5	Other External Factors
2.	**WASTE PACKAGE FACTORS**
2.1	Waste Package Characteristics
2.2	Waste Form Processes
2.3	Waste Container Processes
2.4	Contaminant Transport – Waste Package
3.	**REPOSITORY FACTORS**
3.1	Repository Characteristics
3.2	Repository Processes
3.3	Contaminant Transport – Repository
4.	**GEOSPHERE FACTORS**
4.1	Geosphere Characteristics
4.2	Geosphere Processes
4.3	Contaminant Transport – Geosphere
5.	**BIOSPHERE FACTORS**
5.1	Surface Environment
5.2	Human Behaviour
5.3	Contaminant Transport – Biosphere
5.4	Exposure Factors
6.	**CONTAMINANT FACTORS**
6.1	Contaminant Characteristics

Note: From Garisto (2017).

6.1 The Normal Evolution Scenario

The Normal Evolution Scenario is based on a reasonable extrapolation of present day site features and receptor[1] lifestyle. It includes the expected evolution of the site and expected degradation of the repository system.

[1] The receptor is a person (or persons) who may be exposed to contaminants potentially released from the repository.

6.1.1 External FEPs

The External FEPs shown in Table 6-2 have been reviewed to identify those that are likely to occur and could potentially affect the repository and, therefore, should be included in the Normal Evolution Scenario. The included / excluded items are also shown in Table 6-2 together with a brief justification for their inclusion / exclusion. Further details are provided in Garisto (2017).

Table 6-2 shows that the repository is largely unaffected by many External FEPs, primarily due to its depth and associated geological characteristics. The main External FEPS that are likely to have an impact are:

- Placement of some containers with undetected defects (FEP 1.1.03);
- Glaciation and its effects (FEPs 1.2.02, 1.2.03, 1.2.07, 1.3.01, 1.3.02, 1.3.04, 1.3.05, 1.3.08 and 1.3.09);
- Earthquakes (FEP 1.2.03);
- Human influence on global climate (FEP 1.4.01) delaying onset of the next glaciation; and
- Social and institutional developments leading to changes of land use at the repository site (FEP 1.4.02), and associated drilling, site development and water management (FEPs 1.4.04, 1.4.08 and 1.4.10).

The containers are robust and there are multiple inspection steps to ensure they are fabricated and placed correctly (Chapter 4). However, with the large number of containers (almost 100,000), it is possible that some containers could unknowingly be placed in the repository with defects (Section 7.2.2). Consequently, for the assessment of the Normal Evolution Scenario, it is assumed that some containers with undetected defects are present in the repository.

An important external influence is glaciation. Although glaciation is likely to cause major changes in the surface and near-surface environment, as discussed below, the repository itself is intentionally isolated by its depth from these changes. Geoscientific observations at some Canadian Shield sites imply that conditions at 500 m depths have been isolated from surface changes through the past nine glacial cycles (i.e., for $>10^6$ years). For example, geochemical data from the Whiteshell Research Area in Manitoba indicate glacial meltwaters have not penetrated below about 350 m (Zhang and Frape 2002, Blyth et al. 2000); deep groundwaters are millions of years old (Gascoyne 2004); and oxygenated waters have not penetrated below about 50 m (Gascoyne et al. 2004, McMurry and Ejeckam 2002, Spiessl et al. 2009).

For the hypothetical site, the paleohydrogeologic simulations described in Chapter 2 indicate that glacial meltwaters may reach the repository horizon. Within the rock matrix at the repository horizon meltwater tracer concentrations ranged between 0% and 35% in the reference case paleohydrogeologic simulation (see Section 2.3.5.3); although significantly higher meltwater concentrations occurred within the discrete higher permeability fracture zones. However, the glacial recharge penetrating below the shallow groundwater system (i.e., > 150 mBGS) is not expected to be oxygenated or influence redox conditions at the repository level (see Section 2.4). The paleohydrogeologic simulations also suggest that glacial perturbations do not materially change mass transport rates at repository depth, i.e., diffusion remains the dominant transport mechanism (see Section 2.3.5.3). These characteristics of the repository system are used in the course of scenario identification.

Table 6-2: Status of External FEPs for the Normal Evolution of the Repository System

External FEP			Status*	Remark
1.1	***Repository Issues***			
	1.1.01	Site Investigation	Included	The repository site is hypothetical. The topography and hydrological properties are consistent with Canadian Shield conditions and the fracture[2] network is based on a statistical representation of Canadian Shield fracture patterns. The hypothetical site is described in Chapter 2. It is assumed that there are no identified commercially viable mineral resources at the site (as per Chapter 1).
	1.1.02	Excavation and Construction	Included	The repository is built consistent with the design basis, as described in Chapter 4. Controlled drill and blast excavation is used, which reduces but does not avoid formation of an excavation damaged zone (see Chapter 4).
	1.1.03	Placement of Wastes and Backfill	Included	The in-room container placement method is used. Rooms are backfilled as containers are placed, as described in Chapter 4. It is assumed that a small fraction of the containers are placed with initial defects that are not detected during the fabrication, inspection and placement processes.
	1.1.04	Closure and Repository Sealing	Included	The repository is closed and sealed as described in Chapter 4. This includes sealing of the fracture passing through the repository footprint (see Figure 7.20), and the shafts.
	1.1.05	Repository Records and Markers	Included	Repository records and markers (and passive societal memory) are assumed sufficient to ensure that inadvertent intrusion would not occur for at least 300 hundred years.
	1.1.06	Waste Allocation	Included	The repository holds 4.6 million CANDU fuel bundles. There is no placement of other radioactive or chemically hazardous material at the site.

[2] Fractures are defined here as significant permeable features of the geosphere that are explicitly included in groundwater modelling simulations. These fractures are represented in modelling simulations as equivalent porous media (see Chapter 7) with a thickness of 1 m.

External FEP			Status*	Remark
	1.1.07	Repository Design	Included	The repository design concept is described in Chapter 4.
	1.1.08	Quality Control	Included	Construction, operation, monitoring and closure of the repository are all undertaken under a project quality plan that ensures that the design and safety basis is met (see Chapter 10). However, due to the large number of containers, it is assumed that some containers are placed with initial defects that are not detected during the fabrication, inspection and placement processes.
	1.1.09	Schedule and Planning	Included	The assumed schedule is ~40 years of operation, 70 years of extended monitoring and 30 years for decommissioning and closure.
	1.1.10	Repository Administrative Control	Included	Administrative controls ensure proper operation and closure of the repository. Institutional controls (e.g., land use restrictions) will be implemented on closure, which, while they remain effective, will prevent inadvertent human intrusion and the drilling of wells.
	1.1.11	Monitoring	Included	The preclosure monitoring period is accounted for in all scenarios. The postclosure monitoring program will not compromise the safety of the repository and is excluded from the assessment.
	1.1.12	Accidents and Unplanned Events	Excluded	The likelihood of preclosure accidents or unplanned events that could affect the long-term safety of the repository will be minimized by good engineering practice and quality control; and the effects of any that do occur will be mitigated before the repository is closed.
	1.1.13	Retrieval of Wastes	Excluded	The repository schedule includes an extended period of monitoring after rooms have been filled but before the access tunnels and shaft are sealed, which would facilitate retrieval if required. However, retrieval after closure is not expected and is not included in this safety assessment.

1.2	***Geological Factors***			
	1.2.01	Tectonic Movement and Orogeny	Excluded	The hypothetical site is in a tectonically stable region away from plate margins, with no tectonic activity over the time scale of interest (i.e., 1 million years).
	1.2.02	Deformation (Elastic, Plastic or Brittle)	Included	The repository site is assumed to be tectonically stable; hence, deformation due to tectonic movement and orogeny is unlikely over the timescales of interest. Thus, over the next million years, the only significant deformation force is that due to ice sheet advance over the site. This could cause crustal depression in excess of 500 m, but would occur on a continental scale (Peltier 2011). Ice sheet weight could also cause local movement along existing faults or fractures zones but would not lead to creation of new fractures.
	1.2.03	Seismicity (Earthquakes)	Included	Earthquakes will occur over the time scale of interest; however, since the site is assumed to be located in a seismically inactive region, the likely magnitude, frequency and distance of earthquakes would limit their impact at the repository location. Earthquakes are in general less destructive at depth than at the surface, diminishing the impact of any seismic activity on a deep repository. Furthermore, the repository is backfilled, preventing rock fall. Larger earthquakes which are more likely during retreat of ice sheets could, in theory, reactive an existing fracture or fault, potentially providing a groundwater pathway to the surface. However, consistent with Chapter 2, all known fractures at the site are open (transmissive) and have high permeability. Thus, it is unlikely that a seismic event would increase fracture permeability; the possibility that a seismic event decreases fracture permeability is conservatively neglected. Hence, seismicity is assumed not to change the fracture network or fracture properties in the Normal Evolution Scenario.
	1.2.04	Volcanic and Magmatic Activity	Excluded	No volcanic or magmatic activity over the time scale of interest due to the site location.

	1.2.05	Metamorphism	Excluded	No processes occur over the time scale of interest that will cause metamorphism.
	1.2.06	Hydrothermal Activity	Excluded	The hypothetical repository is located on the Canadian Shield which is geologically stable with a low geothermal flux. Hydrothermal processes therefore act too slowly to be of concern over the time scale of interest.
	1.2.07	Regional Erosion and Sedimentation	Excluded	The area is topographically relatively flat and the surface is primarily granitic bedrock so there is limited potential for large-scale denudation. This is in part due to the erosion caused by ice-sheet movement over the site over the past million years, which has removed easily erodible material.
	1.2.08	Diagenesis	Excluded	The site contains granitic rock, not sedimentary rock.
	1.2.09	Salt Diapirism and Dissolution	Excluded	No significant salt deposits are in the vicinity of the site because it is in the granitic rock of the Canadian Shield.
	1.2.10	Hydrological Response to Geological Changes	Included	A severe seismic event could potentially change the permeability of fractures or activate a closed fault, thereby changing the local hydrology. Since it is difficult to predict which fractures would be affected by seismicity, a simpler but conservative approach is taken in the assessment, i.e., all known fractures at the repository site are conservatively modelled with high permeability.
1.3	***Climate Factors***			
	1.3.01	Global Climate Change	Included	After a period of global warming, it is assumed that glacial / interglacial cycling will eventually resume since the solar insolation variation driving this cycling will continue.
	1.3.02	Local and Regional Climate Change	Included	In the near term, global warming is likely to cause temperature and precipitation changes, although the local / regional climate is likely to remain generally temperate due to the northerly latitude of the repository site. In the long-term, the local / regional climate will respond to global climate change and will cool or warm with the glacial cycle.
	1.3.03	Sea-level Change	Excluded	Changes in sea level do not affect the site due to its assumed mid-continental location.

	1.3.04	Periglacial Effects	Included	Periglacial effects will occur during the colder climate periods of the glacial cycles that are likely to occur at the site over a one million year timeframe. In particular, this would include permafrost development (see Chapter 2).
	1.3.05	Local Glacial Effects	Included	Ice sheets will cause a range of local effects, including changes in rock stress (FEP 1.2.02), earthquake initiation (FEP 1.2.03), changes in surface and near-surface hydrology (FEP 1.3.07), penetration of glacial waters to depth, and changes to ecosystems (FEP 1.3.08) and human behaviour (FEP 1.3.09).
	1.3.06	Warm Climate Effects (Tropical and Desert)	Excluded	Climate change is unlikely to result in development of tropical or hot desert conditions at the site due to its northerly latitude. An initial period of human-induced global warming is not expected to result in extreme temperature rise resulting in tropical or desert conditions in this region.
	1.3.07	Hydrological Response to Near-term Climate Change	Excluded	Surface and near-surface groundwater systems could be altered by a climatic change to wetter or drier conditions. Specifically, the water table on the Canadian Shield is generally within a few meters of the surface and is maintained by a small influx of the total annual precipitation. The deep groundwater system at the site would not be significantly altered by climatic change to wetter or drier conditions (within expected variation, see FEP 1.3.06), due to its low-permeability and depth (see Chapter 2). Changes in hydrology due to glaciation are discussed separately under Periglacial Effects (1.3.04) and Local Glacial Effects (1.3.05).
	1.3.08	Ecological Response to Climate Changes	Included	Flora and fauna at the site change in response to glacial / interglacial cycling.
	1.3.09	Human Behavioural Response to Climate Change	Included	Human behaviour changes in response to glacial / interglacial cycling.

1.4	***Future Human Actions***			
	1.4.01	Human Influences on Climate	Included	Human actions are a possible cause of global climate change, which is included in the expected evolution of the repoistory system (see FEP 1.3.01, Global Climate Change).
	1.4.02	Deliberate Human Intrusion	Excluded	Deliberate human intrusion into the repository is not considered. It is assumed that any future society choosing to recover materials from the repository would have the technology to understand and manage the hazards. Note that unauthorized deliberate intrusion is unlikely due to the infrastructure needed to excavate to repository depth.
	1.4.03	Non-Intrusive Site Investigation	Excluded	Non-intrusive site investigations would not have any effect because of the repository depth.
	1.4.04	Drilling Activities (Human Intrusion)	Excluded	The drilling of deep exploration boreholes that penetrate to the repository is excluded from the expected evolution due to the repository depth (around 500 m), the relatively small repository footprint <6 km^2), and the assumed lack of commercially viable natural resources at the site. Note that this FEP does not include drilling of shallow wells which are considered under FEP 1.4.07.
	1.4.05	Mining (Human Intrusion)	Excluded	It is assumed that there are no commercially viable mineral resources present at the site (see Chapter 1).
	1.4.06	Surface Environment, Human Activities	Excluded	Surface activities are unlikely to have any direct impact on the repository due to the repository depth.
	1.4.07	Water Management (Wells, Reservoirs Dams)	Included	The drilling of shallow water wells in the area is considered once institutional controls are no longer effective (see FEP 1.1.10). Wells in the deeper groundwater zones are excluded since the groundwater in these zones is not potable. This is consistent with present-day practice for extraction of water from shallow groundwater systems on the Canadian Shield. Construction of dams and reservoirs is unlikely to have significant effects on the deep groundwater system due to the generally low topography around the site and the low permeability of the rock.

	1.4.08	Social and Institutional Developments	Included	Institutional controls ensure appropriate use and control of the site in the near term, but it is assumed that this institutional control is eventually lost. Thereafter, the site is assumed to return to land use typical of the region and the site is occupied, including drilling of wells (see FEP 1.4.07).
	1.4.09	Technological Developments	Excluded	It is assumed that the capabilities of future humans will largely resemble present-day capabilities, consistent with the International Commission on Radiological Protection's (ICRP 2000) recommendations and CNSC (2006). Thus, there is no credit taken for advances that might reduce the risk from the repository.
	1.4.10	Remedial Actions	Excluded	Remedial actions are not expected following closure of the repository.
	1.4.11	Explosions and Crashes	Excluded	Most surface explosions and crashes would have no direct impact on the repository due to its depth. Explosions large enough to affect repository depth would likely have large direct consequences that would be much more significant than any additional harm caused by damage to the repository.
1.5	***Other External Factors***			
	1.5.01	Meteorite Impact	Excluded	Excluded due to low probability (due to relatively small repository footprint) and / or low consequence (due to depth of repository). See FEP 1.5.01 in Garisto (2017). Furthermore, meteorites large enough to affect the repository would likely have large direct consequences that would be much more significant than any additional harm caused by damage to the repository.
	1.5.02	Species Evolution	Excluded	No evolution of humans is assumed, consistent with the ICRP recommendation to apply the concept of (present-day) Reference Man to the management of long-lived solid radioactive waste (ICRP 2000). Similarly, no evolution of non-human biota is assumed. General characteristics of biota are assumed to remain similar to current biota.

	1.5.03	Earth Tides, Reversal of Earth's Magnetic Poles, Polar Wander and other Unusual FEPs	Excluded	Consideration of unusual FEPs such as earth tides, reversal of earth's magnetic poles, polar wander, etc. are excluded because of their low probability or because they have no significant effect on the repository.

Note: * Status – *Included* means this factor is considered in the Normal Evolution Scenario. *Excluded* means this factor is not considered in the Normal Evolution Scenario.

6.1.2 Internal FEPs

Internal FEPs are important aids in defining the expected evolution of the repository. They assist in determining which features and processes are important to include in the conceptual model and related computer codes.

The significant FEPs are accounted for in the description of the Normal Evolution Scenario which appears in the following section.

The internal FEPs are reviewed in Garisto (2017).

Internal FEPs are not usually scenario generating; however, they are considered with respect to Disruptive Event Scenarios in Section 6.2.1.

6.1.3 Description of the Normal Evolution of the Repository System

From consideration of the External FEPs and the Internal FEPs, the following high-level narrative of the expected evolution of the repository system can be developed. This understanding is based on many years of study, including laboratory studies, underground research studies, and observations of analogous natural and long-lived human-made structures and materials. This narrative is used to guide both the subsequent development of the conceptual model for the safety assessment and the variations to this model considered in alternative calculation cases.

The narrative summarizes the main events in the evolution of the repository in broad terms, including the long-term changes in the geosphere and biosphere due to glaciation. It is based on the reference design concept where used fuel is placed in the repository in long-lived copper-and-steel containers. These containers are designed not to fail and will be carefully fabricated and inspected. Most of these containers do not fail in the relevant time scale; however, as noted earlier there could be some containers with undetected defects in the copper shell, potentially leading to early releases of radioactivity. Since defective containers behave differently from intact containers, they are described separately in the following sections.

Most of the processes identified are well understood as discussed in Chapter 5. Key points are that the geosphere isolates the repository from the surface, that the groundwater around the repository level remains within its natural chemistry range and low oxygen state, and that the load-bearing capacity of the containers is sufficient to withstand the effects of glaciation and earthquakes at repository depth.

6.1.3.1 Events Occurring for Intact Containers

0-100 years

The repository is assumed to be open and actively monitored for a period of at least 100 years. The 100 year period consists of the reference design assumption of ~40 years of operation and up to 70 years of monitoring during which access tunnels are kept open. Decommissioning and closure will take a further 30 years. In the operation period, 95,833 containers (containing about 4.6 million used fuel bundles, or about 90,000 Mg of uranium) are placed in the repository with the placement rooms backfilled with clay-based sealing materials. The initial radioactivity in a full repository (assuming 30 year old fuel on average) is about 10^{20} Bq and the initial thermal load is about 16 MW (Figure 6-1).

During the first 100 years after placement:

- Radioactivity drops by a factor of 10 and the thermal output drops by a factor of four. Radionuclides with short half-lives such as tritium (H-3) and Co-60 decay to negligible levels.
- Peak temperatures are reached within the repository, with values less than 100^{o}C at the container outer surface.
- The copper container reacts with oxygen from the buffer to form a very thin corrosion layer.
- Recent experiments indicate that it may be possible for copper to corrode in pure, oxygen-free water (see Section 5.4). However, the hydrogen gas generated by this copper corrosion reaction suppresses further corrosion (e.g., at 73ºC, a hydrogen partial pressure of ~1 mbar (Szakálos et al. 2007) is sufficient to suppress the copper-water reaction).
- Thermal expansion and contraction of the rock and concrete combine to create near-field stresses within the low-permeability rock and the concrete bulkhead at the end of the placement rooms, and a limited amount of microcracking occurs.
- In the rock around the repository, groundwater flow and heads are influenced by the presence of the open tunnels and the high-suction clay, which draw water towards the repository. This is countered by the container thermal power, which redistributes water away from the containers.
- Microbes in the buffer material near the containers die or become dormant because of heat, desiccation, lack of nutrients, or lack of space to be viable.

100 - 1000 years

Shortly after the beginning of this time period, all access tunnels and shafts are backfilled and sealed, with particular attention paid to sealing the shafts. All intrusive monitoring systems and deep boreholes are removed or closed. For several hundred years thereafter, distinct physical and chemical gradients (e.g., temperature, porewater composition) will exist between the various components of the repository, and between the repository and the geosphere. Many of the changes that occur within this timeframe are driven by these gradients. During this period:

- Radioactivity drops by a factor of 30. Most fission products decay to insignificant levels, including Sr-90 and Cs-137.
- Container thermal power drops to around 19 W per container. Residual heat comes from decay of the remaining actinides.
- Temperatures in the buffer material around the container remain at about 83^{o}C.

- The oxygen initially present in the sealing materials (as trapped air) is consumed.
- Groundwater from the geosphere continues to enter the repository. As the clay materials begin to saturate, they start to swell and exert pressure on adjacent materials, including the container. The swelling process proceeds slowly and perhaps non-uniformly. Peak swelling loads are about 7 MPa. The swelling clay fills cracks and voids. The EDZ properties are assumed unaffected by swelling of the clay-based seals.
- By the end of this time, the repository is saturated and anaerobic, conditions typical of deep rock environments.
- Climate change may have occurred. Global warming with higher average temperatures could lead to more or less precipitation at the site. This would affect the surface waters (lakes and rivers) and shallow groundwaters, and also the local ecosystem around the site, but deep groundwaters are unaffected.

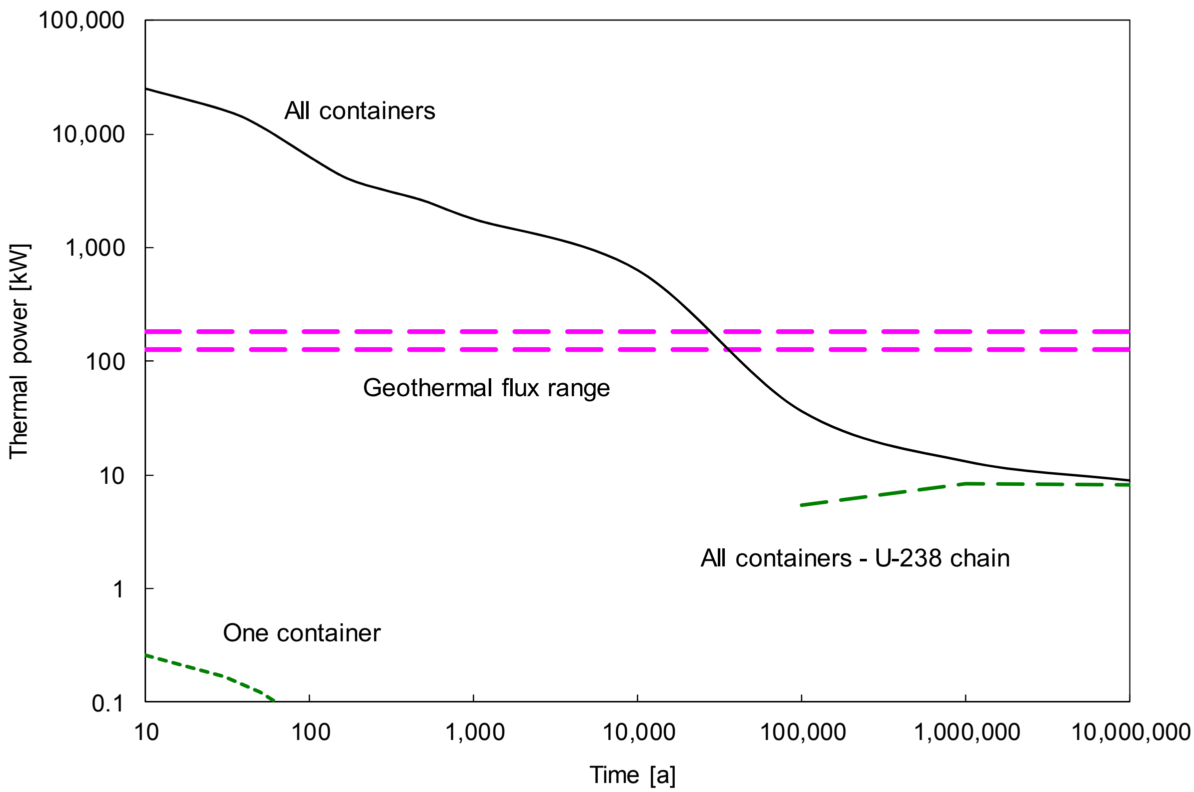

Notes: The power is similar to the natural geothermal flow (Perry et al. 2010) through the repository area after about 30,000 years. After about 1 million years, the residual power is due to radioactive decay of the decay products of uranium.

Figure 6-1: Total Thermal Power of the Repository (Average 220 MWh/kgU Burnup)

1000 - 60,000 years

- Radionuclides like C-14 have decayed.
- Thermal power drops to 1 W per container. The temperatures in and around the repository drop to approximately 10ºC above ambient rock temperatures.
- The highly compacted bentonite and gap fill in the placement rooms become partially homogenized.
- The repository components gradually achieve equilibrium with the surrounding geosphere.
- Corrosion of the container has essentially stopped since the lack of oxygen prevents both uniform and localized corrosion.
- Only minor amounts (< 0.2%) of the montmorillonite in the buffer is converted to illite due to the low potassium concentration present in groundwater and the only slightly elevated temperatures experienced by the buffer over this period.
- The main microbial activity occurring in the repository is due to anaerobic bacteria, including sulphate-reducing bacteria, located mainly at the interfaces with the rock and in the backfill. The buffer remains largely inhospitable because of the high clay density and pressure, which create adverse conditions of low water activity and small pore size.
- Locally near concrete surfaces, a more alkaline porewater develops in the clay-based sealing materials, resulting in an altered layer of clay, several centimetres thick, with a reduced swelling capacity near the interface.
- Changes continue to occur in the surface environment. Climate change due to natural or human influences would likely occur. In particular, the climate might start to cool as part of a long-term glacial cycle with possible formation of permafrost and initiation of glaciation at the site.

60,000 - 1,000,000 years

- Over this timeframe, the perturbations to the system are driven by external events. The most important events are glaciation cycles, which are likely to repeat on a period of roughly every 120,000 years, based on historical trends.
- The residual radioactivity is dominated by the decay of actinides. By the end of this period, all plutonium has decayed.
- The onset of a glaciation cycle starts with a cooling period, with mean surface temperatures over the Canadian Shield dropping to approximately 0ºC. Permafrost develops, disrupting groundwater flow down to a few hundred meters (see Chapter 2).
- Eventually, an ice sheet forms and extends across the site. The hydrological conditions at the edge of the glacier cause major perturbations to the near-surface groundwater flow system. The hydraulic heads at depth also change, but groundwater response is muted due to the low permeability of the deep rock.
- In some areas, glacially driven recharge may penetrate deeper, but reactions with minerals and microbes along the flow path of recharging meltwaters consume dissolved oxygen. Conditions at repository depth remain reducing.
- At its maximum development, the glacial ice sheet could be 2 to 3 kilometres thick above the repository, potentially increasing the hydrostatic pressure at repository depth by 20 to 30 MPa (possibly much less, depending on the rock properties and the nature of the ice sheet). This value is within the design tolerance of the containers.
- During glaciation, the land mass flexes vertically in excess of 500 m in response to the weight of the ice sheets. During glacial retreat, earthquakes may occur. Existing fracture

zones may be reactivated in these locations although there is little change in terms of new fracture development.
- The advancing and retreating ice sheets and their associated meltwater both erode and deposit rock and till. Since the site has already experienced multiple glaciations in the past one million years, the amount of additional bedrock erosion is expected to be limited to meters to tens of meters over a one million year timeframe.
- The chemistry of the porewater within the sealing materials slowly changes to resemble that of the groundwater.
- Along with the porewater chemistry change, the montmorillonite component of the bentonite has lost Na and gained Ca, Mg, and Fe but has still retained its swelling capacity. Due to the lower temperatures and low concentration of potassium in the groundwater, very little additional montmorillonite has converted to illite.
- Microbial activity in the repository is limited in terms of mobility by the impermeable dense buffer around the containers on one side and the low permeability rock on the other; and it is also limited metabolically by the low rate of anaerobic reactions at the ambient temperatures and by the requirement for nutrients to diffuse through the clay-based sealing materials.

Beyond 1,000,000 years

Virtually all the reactor-generated radioactivity has decayed, and most of the residual radioactivity in the used fuel comes from its natural uranium content. The amount of uranium in the repository is comparable to the large uranium ore bodies in north-central Canada. These natural deposits of uranium oxide have been stable for billions of years. Similarly, many ore deposits of metallic copper and sedimentary deposits of bentonite are known that range in age from millions to hundreds of millions of years. The ultimate fate of the repository and the materials it contains will be largely indistinguishable from these natural analogues.

6.1.3.2 Events Occurring for Defective Containers

The evolution of any defective containers will be different from that of intact containers. This evolution is summarized below (see Chapter 5 for a more detailed description).

Only the additional events that may occur in the evolution of these containers are summarized here, since most of the events occurring for the intact containers (e.g., radiation-related changes, thermal changes, etc.) also occur for defective containers. For the purposes of this discussion, it is assumed that (1) some containers are placed in the repository with undetected voids in the copper coating, larger than the expected detection limit of the inspection equipment, that are sufficiently large to cause these containers to be breached within the first one million years; and (2) a pathway through the copper coating to the underlying steel vessel is formed within the first 10,000 years, exposing the underlying steel to groundwater. The time frame for formation of a pathway through the copper coating is expected to be much longer than 10,000 years (see Chapters 5 and 7); in this case, the steel container would be breached at a much later time than described below.

0 - 100 years

Over this period the repository is not fully saturated. Atmospheric corrosion of the copper coating may occur but only to a very limited extent because the relative humidity near the copper container is low and oxygen is consumed by other processes.

<u>100 - 1000 years</u>

During this period the repository becomes saturated, the buffer swells and groundwater contacts the copper shell. Corrosion of copper is slow under the expected anaerobic conditions. The major corrosion mechanism is reaction with sulphide in the groundwater, which reaches the container surface from the surrounding geosphere by diffusion.

<u>1000 - 10,000 years</u>

During this period, it is assumed that the corrosion of the copper coating is sufficiently fast and / or the void in the copper coating is sufficiently large that a pathway through the copper coating to the underlying steel vessel is formed. The buffer may swell into the defect and groundwater contacts the steel inner vessel. Anaerobic corrosion of the steel vessel begins, generating iron corrosion products and hydrogen gas. The most likely iron corrosion products are siderite and magnetite, depending on the carbonate groundwater concentration (see Section 5.4). For the discussion below, it is assumed that the steel corrosion rate is not limited by the availability of carbonate.

<u>10,000 - 60,000 years</u>

- During this period the steel below the defect continues to corrode and the depth of steel corrosion increases with time. If the steel corrosion rate is not carbonate limited, there may be penetration of the steel vessel if the defect occurs in the copper coating covering either the weld region (penetration in 4400 years) or the hemispherical heads (penetration in 33,000 years) of the steel vessel, which are thinner than the main cylindrical body of the steel vessel (see Section 5.4). If the defect is over the thicker parts of the steel vessel, then penetration occurs approximately 70,000 years after repository closure. (Penetration of the steel vessel would take much longer if the steel corrosion rate is carbonate limited, i.e., 140,000 years to 2 million years, depending on the location of the defect.)
- After penetration of the steel vessel, water (and bentonite) move into the interior of the vessel and the inside of the steel vessel also starts to corrode.
- Corrosion of the steel vessel continues and the hydrogen gas pressure increases near the breached container. The timing of events depends on the behaviour of the hydrogen.
- Hydrogen gas generated by steel corrosion forms a bubble or blanket that may inhibit water contact with the container and may inhibit ingress of liquid water into the container. Once the hydrogen pressure is high enough (on the order of the hydrostatic pressure plus swelling pressure), the gas will create a channel through the buffer, and move to the interface with the rock and into the EDZ. The pathway through the buffer re-seals after the gas passes so the effectiveness of the buffer is not impaired. The gas reaching the EDZ would move along the buffer-rock interface until the gas pressure decreases sufficiently that there is no driving force for advective gas movement.
- Water in the steel vessel contacts the fuel bundles. Local failure or corrosion of the Zircaloy cladding allows water to contact the used fuel in some fuel elements. The more soluble radionuclides (typically a few percent) in the fuel / cladding gap and grain boundaries are released into the water inside the steel vessel.
- A small amount of the used fuel dissolves, releasing other radionuclides into the water. The presence of hydrogen gas from corrosion of the steel container sustains conditions that significantly decrease the rate of fuel dissolution.
- Most radionuclides have decayed, or are trapped within the used fuel. Dissolved radionuclides diffuse out of the container and into the buffer surrounding the container.

<u>60,000 - 1,000,000 years</u>

- The steel vessel continues to corrode until all of the steel is consumed.
- Corrosion of the copper vessel continues but only a small fraction of the copper corrodes over this time period.
- Hydrogen gas from steel corrosion present within the excavation damaged zone slowly dissolves in groundwater and slowly diffuses away from the repository. Hydrogen gas remaining in the container also slowly dissolves allowing full saturation of the container.
- At some point, the steel vessel is sufficiently weakened by corrosion that it is no longer load bearing and could collapse, due to the external buffer swelling pressure (i.e., assuming infiltration of mainly water rather than bentonite into the breached container). Any remaining intact fuel bundles are damaged and exposed to water.
- Most of the UO_2 is fractured but intact. About 20% of the fuel has dissolved by the end of this period.
- Some radionuclides migrate out of the container, through the buffer, and into the nearby rock. Most radionuclides decay within or near the repository and surrounding rock. Slow migration of the more mobile, soluble and long-lived species (such as I-129) through the geosphere and into the shallow groundwater system and the biosphere can occur.

6.2 Disruptive Event Scenarios

Disruptive Event Scenarios postulate the occurrence of unlikely events leading to possible penetration of barriers and abnormal loss of containment.

6.2.1 Identification of Disruptive Event Scenarios

A set of Disruptive Event Scenarios has been identified by evaluating the potential for the External FEPs listed in Table 6-2 to compromise the isolation and containment function of the repository system. Specifically, the repository system safety attributes and features in Chapter 1 were checked to see if they could be significantly compromised by any of the External FEPs. This involved brainstorming sessions, and review of disruptive event scenarios identified in previous Canadian and international safety assessments of a geological repository. The results of this assessment are summarized in Table 6-3.

As a further check, the potential for the Internal FEPs to compromise the long-term safety features is also considered, and summarized in Table 6-4. Note that the FEPs considered under the “Biosphere Factors” and “Contaminant Factors” categories are not capable on their own of modifying the repository system to an extent that results in a fundamentally different evolution to that considered in the Normal Evolution Scenario. These are therefore not scenario generating and their effects can be evaluated through different calculation cases for the Normal Evolution Scenario rather than through the development of Disruptive Event Scenarios.

The failure mechanisms identified in Table 6-3 and Table 6-4 can be grouped into seven Disruptive Event Scenarios as discussed below and summarized in Table 6-5. Since the long-term safety of the repository is based on the strength of the geosphere and engineered barriers (including the container and shaft seals), the scenarios focus on events in which these can be degraded or bypassed.

Table 6-3: External FEPs Potentially Compromising Arguments Relating to the Long-Term Safety

Safety Feature	Potentially Compromised by	Consider as Failure Mechanism
1. The depth of the host rock formation should be sufficient for isolating the repository from surface disturbances and changes caused by human activities and natural events.	Meteorite impact (FEP 1.5.01).	**No,** due to low probability of meteor impact capable of compromising safety due to the relatively small repository footprint (<6 km^2) and depth of repository (~500 m). See Garisto (2017) for further discussion of probabilities.
	Exploration borehole penetrates into repository providing enhanced permeability pathway to surface environment and potential for direct exposure to waste (FEP 1.4.04).	**Yes,** although the absence of economically exploitable resources, and the depth (~500 m) and relatively small repository footprint (<6 km^2) mean that the likelihood of such a borehole intruding into the repository would be very low during the period of greatest potential hazard.
	Mining and other underground activities resulting in excavation in the vicinity of the repository (FEP 1.4.05).	**No,** due to assumption of the absence of commercially viable mineral resources near or below repository level. Shallow quarrying or tunnelling activities are unlikely to affect the repository because of repository depth (~500 m). Also, most underground activities would likely be preceded by exploration boreholes, as addressed above.
	Deliberate human intrusion into repository (FEP 1.4.02).	**No,** exclude deliberate human intrusion since it is expected that the intruders would take appropriate precautions. Note that unauthorized deliberate intrusion is unlikely due to the infrastructure needed to excavate to repository depth.

Safety Feature	Potentially Compromised by	Consider as Failure Mechanism
	Could discover resources that were not identified during site investigations (FEP 1.1.01) or exploit existing rocks that have become a commercially viable resource. These new resources are exploited by drilling or mining at or below repository level (FEP 1.4.04 and FEP 1.4.05).	**No,** the lack of resources at the site is assumed to be consistent with regional information. Even if the existing rocks became commercially viable, the repository site is unlikely to become a mine site because similar rocks exist near the surface over a larger lateral extent of the Canadian Shield. Also, deep mining activities would likely be preceded by an exploration borehole, which is considered under FEP 1.4.04.
	Fractures intersecting repository and shafts are not properly sealed providing an enhanced permeability pathway to the surface environment (FEP 1.1.04).	**No**, the fracture and shaft seals are large structures consisting of composite materials that would take months or years, respectively, to install under NWMO quality control and regulatory oversight. A highly improbable failure of the quality control system, lasting many months would be needed for these seals to perform poorly due to improper installation.
	Fracture and shaft seals perform poorly due to unexpected chemical interactions with groundwater and / or glacial meltwater, providing an enhanced permeability pathway to the surface environment (FEP 1.1.04).	**Yes,** although sealing materials will be chosen to be compatible with existing conditions at the repository site, unforeseen chemical interactions could unduly affect performance of seals.
	Repository and shafts not sealed, providing an enhanced permeability pathway to the surface environment (FEP 1.1.04).	**Yes,** due to some severe societal disruption, the repository is not closed as planned but remains open and unsealed, and not maintained.

Safety Feature	Potentially Compromised by	Consider as Failure Mechanism
	Site investigation / monitoring borehole not properly sealed providing an enhanced permeability pathway to the surface environment (FEP 1.1.01 and FEP 1.1.11).	**No**, the boreholes are long and the seals would consist of composite materials that would be installed under enhanced NWMO quality control and regulatory oversight. Given the relatively small number of boreholes to be sealed, a highly improbably failure of the quality control system would be needed for borehole seals to perform poorly due to improper installation.
	Site investigation / monitoring borehole seals perform poorly due to unexpected chemical interactions with groundwater or glacial meltwater, providing an enhanced permeability pathway to the surface environment (FEP 1.1.01 and FEP 1.1.11).	**Yes,** although sealing materials will be chosen to be compatible with existing conditions at the repository site, unforeseen chemical interactions could unduly affect performance of seals.
	Site investigation / monitoring borehole not sealed, providing an enhanced permeability pathway to the surface environment (FEP 1.1.01 and FEP 1.1.11).	**Yes,** due to some severe societal disruption, the repository is not closed as planned but remains open and unsealed but not maintained.
	Poor construction techniques affect the performance of the repository and shaft excavation disturbed zones providing an enhanced permeability pathway to the surface environment (FEP 1.1.02).	**Yes,** although NWMO quality control and regulatory oversight will ensure that poor sealing is very unlikely.
	Site investigations do not identify a permeable fracture zone or fault that provides a connection between the repository horizon and shallow groundwater system (FEP 1.1.01).	**Yes,** although unlikely, such a feature cannot be categorically ruled out due to the limits of current technologies to identify all fracture zones in crystalline rock, and so is considered in a disruptive event scenario. Note that all known fractures are assumed open (i.e., transmissive) in the Normal Evolution Scenario.

Safety Feature	Potentially Compromised by	Consider as Failure Mechanism
	High magnitude seismic event results in reactivation of undetected existing structural discontinuity which provides an enhanced permeability pathway to higher horizons (FEP 1.2.03).	**Yes**, the assessment time scales are such that a significant seismic event may occur even though the annual probability is low. Also, the probability of seismic events increases during periods of glacial retreat. However, the probability that an earthquake could actually reactivate a nearby fracture is very small since it would take a significant amount of energy. Note that all known fractures are assumed open (i.e., highly transmissive) in the Normal Evolution Scenario.
	High magnitude seismic event affects performance of repository and shaft excavation disturbed zones, and /or fracture and shaft seals, providing an enhanced permeability pathway to higher horizons (FEP 1.2.03).	**Yes,** the assessment time scales are such that a significant seismic event may occur even though the annual probability is low. Also, the probability of seismic events increases during periods of glacial retreat.
	Ice sheet erosion removes a significant thickness of rock above repository (FEPs 1.2.07, 1.3.01, 1.3.02, and 1.3.05).	**No,** extrapolating the past rate of erosion implies that on the order of 30 m of granitic bedrock may be eroded over one million years. This would not significantly reduce the geosphere barrier at the site given the depth of the repository.
	Advance / retreat of ice sheets generate large hydraulic gradients which affect groundwater flow velocities in the deep groundwater zone (FEP 1.3.05).	**Yes,** the changing hydraulic head due to ice sheet advance and retreat over the repository site may affect groundwater flow at the repository level, but advective flows will remain low due to the low permeability of the deep rock (see Chapter 2, particularly the discussion of the paleohydrogeologic sensitivity cases). Since glaciation is included in the Normal Evolution Scenario, the normal changes caused by glaciation do not generate additional Disruptive Events.

Safety Feature	Potentially Compromised by	Consider as Failure Mechanism
	Other external geological processes disrupt the repository system, i.e., Tectonic Movement (FEP 1.2.01), Volcanic and Magmatic Activity (FEP 1.2.04), Metamorphism (FEP 1.2.05), Hydrothermal Activity (FEP 1.2.06), Diagenesis (FEP 1.2.08) and Salt Diapirism and Dissolution (FEP 1.2.09).	**No,** since precluded by site's location and assessment time scales.
2. The volume of available competent rock at repository depth should be sufficient to host the repository and provide sufficient distance from active geological features such as zones of deformation or faults and unfavourable heterogeneities.	Site investigations do not identify a permeable fracture zone or fault that provides a connection between the repository horizon and shallow groundwater system (FEP 1.1.01).	**Yes,** although unlikely, such a feature cannot be categorically ruled out due to the limits of current technologies to identify all fracture zones in crystalline rock, and so is considered in a disruptive event scenario. Note that all known fractures are assumed open (i.e., transmissive) in the Normal Evolution Scenario.
	High magnitude seismic event results in reactivation of undetected existing structural discontinuity which provides an enhanced permeability pathway to higher horizons (FEP 1.2.03).	**Yes**, the assessment time scales are such that a significant seismic event may occur even though the annual probability is low. However, the probability that an earthquake could actually reactivate a nearby fracture is very small since it would take a significant amount of energy. Note that all known fractures are assumed open (i.e., transmissive) in the Normal Evolution Scenario.
	High magnitude seismic event affects performance of repository and shaft excavation disturbed zones, and /or repository and shaft seals, providing an enhanced permeability pathway to higher horizons (FEP 1.2.03).	**Yes,** the assessment time scales are such that a significant seismic event may occur even though the annual probability is low.

Safety Feature	Potentially Compromised by	Consider as Failure Mechanism
	Other external geological processes disrupt the repository system, i.e., Tectonic Movement (FEP 1.2.01), Volcanic and Magmatic Activity (FEP 1.2.04), Metamorphism (FEP 1.2.05), Hydrothermal Activity (FEP 1.2.06), Diagenesis (FEP 1.2.08) and Salt Diapirism and Dissolution (FEP 1.2.09).	**No,** since precluded by site's location and assessment time scales.
3. The hydrogeological regime within the host rock should exhibit low groundwater velocities.	High magnitude seismic event results in reactivation of undetected existing structural discontinuity which provides an enhanced permeability pathway to higher horizons (FEP 1.2.03).	**Yes**, the assessment time scales are such that a significant seismic event may occur even though the annual probability is low. However, the probability that an earthquake could actually reactivate a nearby fracture is very small since it would take a significant amount of energy. Note that all known fractures are assumed open (i.e., transmissive) in the Normal Evolution Scenario.
	High magnitude seismic event affects performance of repository and shaft excavation disturbed zones, and /or fracture and shaft seals, providing an enhanced permeability pathway to higher horizons (FEP 1.2.03).	**Yes,** the assessment time scales are such that a significant seismic event may occur even though the annual probability is low.
	Advance / retreat of ice sheets generate large hydraulic gradients which affect groundwater flow velocities in the deep groundwater zone (FEP 1.3.05).	**Yes,** the changing hydraulic head due to ice sheet advance and retreat over the repository site may affect groundwater flow at the repository level, but advective flows will remain low due to the low permeability of the deep rock (see Chapter 2, particularly the discussion of the paleohydrogeologic sensitivity cases). Since glaciation is included in the Normal Evolution Scenario, the normal changes caused by glaciation do not generate additional Disruptive Events.

Safety Feature	Potentially Compromised by	Consider as Failure Mechanism
	Other external geological processes disrupt the repository system, i.e., Tectonic Movement (FEP 1.2.01), Volcanic and Magmatic Activity (FEP 1.2.04), Metamorphism (FEP 1.2.05), Hydrothermal Activity (FEP 1.2.06), Diagenesis (FEP 1.2.08) and Salt Diapirism and Dissolution (FEP 1.2.09).	**No,** since precluded by site's location and assessment time scales.
4. The mineralogy of the rock, the geochemical composition of the groundwater and rock porewater should not adversely impact the expected performance of the repository multi-barrier system. 5. The mineralogy of the host rock, the geochemical composition of the groundwater and rock porewater should be favourable to retarding radionuclide movement.	Infiltration of glacial meltwater (without oxygen) into the repository modifies the hydrogeochemical conditions, affecting, for example, the stability of the buffer and backfill materials (i.e., leads to erosion of these materials due to colloid formation) (FEP 1.3.05).	**No**, the paleohydrogeologic simulations described in Chapter 2 suggest that meltwater tracer concentrations at the repository horizon, including fracture zones, would be in the range 3% to 37%. Such a change in the composition of the porewater should not significantly affect the properties or stability of the engineered barrier system. Repository and boreholes would be located to avoid permeable fractures or, if not possible, such fractures would be sealed.
	Infiltration of oxygenated glacial meltwater into the repository leads to oxidizing conditions in the repository, causing relatively rapid corrosion of copper containers, rapid corrosion of used fuel in any defective containers, and enhanced mobility of redox sensitive nuclides such as U and Tc.	**No**, glacial recharge penetrating below the shallow groundwater system (> 150 mBGS) is not expected to be oxygenated or influence redox conditions at the repository horizon (see Chapter 2). Repository and boreholes would be located to avoid permeable fractures or, if not possible, such fractures would be sealed.
	Other external geological processes disrupt the repository system, i.e., Tectonic Movement (FEP 1.2.01), Volcanic and Magmatic Activity (FEP 1.2.04), Metamorphism (FEP 1.2.05), Hydrothermal Activity (FEP 1.2.06), Diagenesis (FEP 1.2.08) and Salt Diapirism and Dissolution (FEP 1.2.09).	**No,** since precluded by site's location and assessment time scales.

Safety Feature	Potentially Compromised by	Consider as Failure Mechanism
6. The host rock should be capable of withstanding mechanical and thermal stresses induced by the repository without significant structural deformation or fracturing that could compromise the containment and isolation functions of the repository.	Presence of repository weakens rock near repository, potentially making it susceptible to fracturing during earthquakes which could be caused by ice sheet loading / unloading (FEP 1.2.02).	**Yes,** although all known fractures are assumed open (transmissive) in the Normal Evolution Scenario, an unknown fault or fracture could be reactivated by seismic activity particularly if it has been weakened by the presence of the repository.
7. Current and future seismic activity at the repository site should not adversely impact the integrity of the repository during operation and in the very long-term.	High magnitude seismic event results in reactivation of undetected existing structural discontinuity which provides an enhanced permeability pathway to higher horizons (FEP 1.2.03).	**Yes**, the assessment time scales are such that a significant seismic event may occur even though the annual probability is low. However, the probability that an earthquake could actually reactivate a nearby fracture is very small since it would take a significant amount of energy. Note that all known fractures are assumed open (i.e., transmissive) in the Normal Evolution Scenario.
	High magnitude seismic event affects performance of repository and shaft excavation disturbed zones, and /or fracture and shaft seals, providing an enhanced permeability pathway to higher horizons (FEP 1.2.03).	**Yes,** the assessment time scales are such that a significant seismic event may occur even though the annual probability is low.
	Large seismic event results in shearing along an existing fracture that passes through a placement room of the repository. The shearing load causes failure of a used fuel container.	**Yes,** the assessment time scales are such that a significant seismic event may occur even though the annual probability is low. However, the probability that an earthquake would cause failure of a container in a placement room due to a shear load is very small due to the low seismicity at the site, as assumed in Chapter 1; the avoidance of areas in the repository with visible fractures; and the tolerance of the design to some extent of shearing.

Safety Feature	Potentially Compromised by	Consider as Failure Mechanism
8. The expected rates of land uplift, subsidence and erosion at the repository site should not adversely impact the containment and isolation of the repository.	Ice sheet erosion removes a significant thickness of rock above repository (FEPs 1.2.07, 1.3.01, 1.3.02, and 1.3.05).	**No,** extrapolating the past rate of erosion implies that on the order of 30 m of granitic bedrock may be eroded over one million years. This would not significantly reduce the geosphere barrier at the site given the depth of the repository.
	Land uplift decreases depth of repository.	**No,** land uplift occurs on a continental scale so relative depth of repository does not change. Land uplift and large-scale erosion are also not significant factors in affecting repository depth on assessment time scale.
9. The repository should not be located within rock formations containing economically exploitable natural resources such as minerals and other valuable commodities as known today. 10. The repository is not located within geological formations containing groundwater resources at repository depth that could be used for drinking, agriculture or industrial uses.	Mining and other underground activities resulting in excavation in the vicinity of the repository (FEP 1.4.05).	**No,** due to the assumption of the absence of commercially viable resources near or below repository level. Other underground activities are unlikely to affect the repository (e.g., rock quarry) because of repository depth (~500 m). Also, such activities would likely be preceded by exploration boreholes, as addressed above. Even if the host rock itself became commercially viable, the repository site is unlikely to become a mine site because similar rocks exist near the surface over a larger lateral extent of the Canadian Shield.
	Deliberate human intrusion into repository (FEP 1.4.02).	**No,** exclude deliberate human intrusion since it is expected that the intruders would take appropriate precaution.

Safety Feature	Potentially Compromised by	Consider as Failure Mechanism
	Could discover resources that were not identified during site investigations (FEP 1.1.01) or exploit existing rocks that have become a commercially viable resource. These new resources are exploited by drilling or mining at or below repository level (FEP 1.4.04 and FEP 1.4.05).	**No,** the lack of resources at the site is assumed to be consistent with regional information. Even if the host rock itself became commercially viable, the repository site is unlikely to become a mine site because similar rocks exist near the surface over a larger lateral extent of the Canadian Shield. Also, the impact of drilling is already considered under exploration borehole (FEP 1.4.04).
11. The used nuclear fuel is a durable uranium oxide (UO_2); it will dissolve very slowly under the chemical conditions within a failed container. 12. Most of the initial radioactivity is held within the UO_2 grains, where it can only be released as the used fuel dissolves.	Infiltration of oxygenated glacial meltwater into the repository leads to oxidizing conditions in the repository, causing relatively rapid corrosion of copper containers, rapid dissolution of used fuel in any defective containers, and enhanced mobility of redox sensitive nuclides such as U and Tc.	**No,** glacial recharge penetrating below the shallow groundwater system (i.e., depths greater than 150 m) is not expected to be oxygenated or influence the redox conditions at the repository horizon (see Chapter 2).
13. The used fuel container has a design life of at least 100,000 years under the geomechanical and chemical repository conditions expected to exist within the repository.	Defects in the copper coating of some containers are not detected by the quality inspection program, impacting the durability and expected lifetime of these containers (FEP 1.1.03, 1.1.08).	**Yes,** although NWMO's quality control measures will make it very likely that poorly manufactured containers would be discovered and not used, some defective containers may somehow escape detection by the inspection program, given the large number of containers in the repository.
	Unanticipated interactions of the containers with groundwater impact the durability of the used fuel containers (FEP 1.1.03, 1.1.08), significantly reducing their expected lifetime.	**Yes**, although the repository site would be selected to ensure the long-term durability of the containers, unexpected chemical interactions (e.g., due to the presence of sulphides) could impact the lifetime of the containers.

Safety Feature	Potentially Compromised by	Consider as Failure Mechanism
	Used fuel containers fail due to increase in the isostatic load caused by a thick ice sheet passing over the repository site.	**Yes,** although the containers are designed to withstand the total isostatic load from buffer swelling, the current hydrostatic load, and the additional hydrostatic load from a design-basis ice sheet passing over the repository site, the possibility that the design load of the container could be exceeded due to the passage of a beyond design-basis ice sheet needs to be considered.
	Infiltration of oxygenated glacial meltwater into the repository leads to oxidizing conditions in the repository, leading to relatively rapid corrosion of the copper containers (FEP 1.3.05).	**No,** glacial recharge penetrating below the shallow groundwater system (i.e., depths greater 150 m) is not expected to be oxygenated or influence the redox conditions at the repository horizon (see Chapter 2).
14. The container is surrounded by a layer of dense bentonite-based clay that inhibits groundwater movement, has self-sealing capability, inhibits microbial activity near the container, and retards contaminant transport.	Bentonite buffer layer around some containers not properly installed and, therefore, the density of the buffer around these container is lower than the design requirement.	**Yes,** although use of a buffer box and application of NWMO's quality control measures make it very unlikely that the bentonite layer would have substandard properties.
	Infiltration of glacial meltwater (without oxygen) into the repository modifies the hydrogeochemical conditions in the repository, affecting, for example, the stability of the buffer and backfill materials (i.e., leads to erosion of these materials due to colloid formation) (FEP 1.3.05).	**No**, the paleohydrogeologic simulations described in Chapter 2 suggest that meltwater tracer concentrations at the repository horizon, including fracture zones, would be in the range 3% to 37%. Such a change in the composition of the porewater should not significantly affect the properties or stability of bentonite clay.
	A large seismic event causes rock shear along an undetected fracture intersecting the repository at a container location, reducing the buffer thickness between the container surface and the rock.	**Yes,** the assessment time scales are such that a significant seismic event may occur even though the annual probability is low. Even then, the probability that the earthquake could actually reactivate a nearby fracture is very small since it would take a significant amount of energy.

Safety Feature	Potentially Compromised by	Consider as Failure Mechanism
15. Institutional Controls will limit the potential for human encounter with the repository in the near term after closure	Institutional controls on the development of the site are ineffective (FEP 1.4.08). This allows development of the site (FEP 1.4.06) and human intrusion into the repository to occur by drilling (FEP 1.4.04) and / or mining (FEP 1.4.05)	**No,** measures are assumed to be taken in the near term to ensure that information regarding the purpose, location, design and contents of the repository is preserved so that future generations are made aware of the consequences of any actions they may choose to take. With these institutional measures as well as general societal memory, and with the absence of commercially viable natural resources at depth, inadvertent intrusion in the near term after closure is not considered. However, Human Intrusion is considered in the long-term.

Table 6-4: Internal FEPs Potentially Compromising Arguments Relating to Long-Term Safety*

Safety Feature	Potentially Compromised by	Consider as Failure Mechanism
1. The depth of the host rock formation should be sufficient for isolating the repository from surface disturbances and changes caused by human activities and natural events.	No Internal FEP could result in a significant change in the depth of the repository. Note that FEP 5.1.10 relates to the erosion of surficial deposits and not bedrock.	**No.**
2. The volume of available competent rock at repository depth should be sufficient to host the repository and provide sufficient distance from active geological features such as zones of deformation or faults and unfavourable heterogeneities.	An undetected feature (e.g., a fracture zone) in the geosphere provides a relatively high permeability connection between the repository horizon and higher horizons (FEP 4.1.02 and FEP 4.1.03).	**Yes,** a nearby fracture zone or other feature could be missed during site investigation due to the limits of current technologies to identify such features.
3. The hydrogeological regime within the host rock should exhibit low groundwater velocities.	An undetected feature (e.g., a fracture) in the geosphere provides a relatively high permeability connection n between the repository horizon and higher horizons (FEP 4.1.02 and FEP 4.1.03).	**Yes,** a nearby fracture zone or other feature could be missed due to the limits of current technologies to identify such features.
	The failure of most of the containers in the repository, due to an unexpected mechanism, leads to generation of a significant amount of hydrogen gas due to corrosion of the iron inner vessel. The hydrogen pressure could, in theory, exceed the lithostatic pressure leading to rock fracture.	**No,** the threshold capillary pressure of the host rock is less than 3 MPa (see Chapter 7); hence, most of the gas reaching the buffer / rock interface would escape via the host rock after the gas pressure exceeds 3 MPa. This pressure is significantly lower than the lithostatic pressure of the rock.

Safety Feature	Potentially Compromised by	Consider as Failure Mechanism
	A pattern of over- and under-pressure in the groundwater and porewater hydraulic heads at the site is observed during site investigation or forms in the future due to, for example, glaciation. Such pressures would represent a state of disequilibrium.	**No,** such patterns are not common on the Canadian Shield and are assumed not to exist at the hypothetical site.
4. The mineralogy of the rock, the geochemical composition of the groundwater and rock porewater at repository depth should not adversely impact the expected performance of the repository multi-barrier system. 5. The mineralogy of the host rock, the geochemical composition of the groundwater and rock porewater should be favourable to retarding radionuclide movement.	Various repository FEPs (e.g., FEPs 3.1.02, 3.2.01 to 3.2.05), such as temperature rise in the repository, groundwater salinity and groundwater-buffer interactions, and geosphere FEPs (e.g., FEPs 4.2.01 to 4.2.05), such as geothermal gradient and karst formation, have the potential to modify the hydrological, mechanical and chemical conditions at repository depth, affecting seal properties and / or radionuclide movement.	**No,** the effects are likely to be localized to the immediate vicinity of the repository and these FEPs can be evaluated through considering different calculation cases for the Normal Evolution Scenario (e.g., low sorption and high solubility sensitivity cases) rather than through the development of alternative Disruptive Event Scenarios. For conservatism, concrete seals are assumed degraded from the time of repository closure.
	Various waste package FEPs (e.g., FEPs 2.3.01 to 2.3.04) can influence the durability of the used fuel containers, potentially leading to container failures.	**Yes,** poor local conditions (e.g., low buffer density) might cause a limited number of container failures due to, for example, biofilm formation on the copper surface leading to microbial corrosion. Note that the Normal Evolution Scenario already includes a number of containers with pre-existing defects in the copper coating which lead to container failures.
	Various repository FEPs (e.g., FEPs 3.2.01 to 3.2.05), such as temperature rise and groundwater interactions, and geosphere FEPs (e.g., FEPs 4.3.01 to 4.3.08), such as sorption and diffusion, can affect the rate at which contaminants are released from the repository and migrate through the shafts and geosphere.	**No,** the effects of these FEPs can be evaluated through considering different calculation cases for the Normal Evolution Scenario rather than through the development of alternative Disruptive Event Scenarios (e.g., no sorption and high solubility sensitivity cases). The repository and shaft excavation damaged zones are considered in the Normal Evolution Scenario. Also, concrete seals are assumed degraded from the time of repository closure.

Safety Feature	Potentially Compromised by	Consider as Failure Mechanism
	Changes in porewater chemistry in the repository due to, for example, temperature rise in the repository and presence of concrete adversely affects clay seals (FEP 3.1.02 and FEP 3.2.04).	**No,** use of low-temperature, low pH concrete in the repository minimizes interactions with clay seals. Also, the amount of concrete in the repository is small compared to the amount of clay sealing materials.
6. The host rock should be capable of withstanding mechanical and thermal stresses induced by the repository without significant structural deformation or fracturing that could compromise the containment and isolation functions of the repository.	Mechanical and thermal stresses induced by presence of repository are underestimated and cause greater than expected fracturing within the repository, the host rock and shaft excavation damaged zones, providing an enhanced permeability pathway to the surface environment (e.g., FEP 3.2.01 and FEP 3.2.03).	**Yes,** although application of NWMO's quality control measures and engineering safety factors would make it unlikely that stresses are underestimated.
7. Current and future seismic activity at the repository site should not adversely impact the integrity of the repository during operation and in the very long-term.	Relates to External FEPs only (see Table 6-3).	
8. The expected rates of land uplift, subsidence and erosion at the repository site should not adversely impact the containment and isolation of the repository.	Relates to External FEPs only (see Table 6-3).	

Safety Feature	Potentially Compromised by	Consider as Failure Mechanism
9. The repository should not be located within rock formations containing economically exploitable natural resources such as minerals and other valuable commodities as known today. 10. The repository is not located within geological formations containing groundwater resources at repository depth that could be used for drinking, agriculture or industrial uses.	Relates to External FEPs only (see Table 6-3).	
11. The used nuclear fuel is a durable uranium oxide (UO_2); it will dissolve very slowly under the chemical conditions within a failed container.	Various waste package FEPs (e.g., FEP 2.1.02, and FEP 2.2), such as radiation and temperature effects, and rates of used fuel dissolution in groundwater, can affect the rate at which contaminants are released from the used fuel.	**No,** the effects of these FEPs can be evaluated through considering different calculation cases for the Normal Evolution Scenario rather than through the development of alternative Disruptive Event Scenarios (e.g., sensitivity cases with a faster fuel dissolution rate or larger instant release fractions).
12. Most of the initial radioactivity is held within the UO_2 grains, where it can only be released as the used fuel dissolves.	Release due to criticality accident.	**No**, the used fuel is natural uranium based. The fissile content of the used fuel is too low.

Safety Feature	Potentially Compromised by	Consider as Failure Mechanism
13. The used fuel container has a design life of at least 100,000 years under the geomechanical and chemical repository conditions expected to exist within the repository.	Containers are not fabricated to specifications and so are placed in the repository with defects (FEPs 2.3.01 to 2.3.04).	**Yes**, although the fabrication method is designed to be robust and there would be multiple methods of inspection, there is statistically some probability of some defective container not being detected (given the large number of containers) such that a few containers are placed in the repository with defects. The Normal Evolution Scenario assumes some containers with undetected defects are present in the repository at the time of closure, leading to container failures.
	Various waste package and repository FEPs (e.g., FEPs 2.3.03, 2.3.04, 3.1.02, 3.2.01 to 3.2.05), such as uniform corrosion, buffer properties, temperature, and groundwater chemistry, can influence the durability of the used fuel containers, potentially leading to container failures.	**Yes,** although evidence suggests that the copper container would be thermodynamically stable under the reducing conditions expected in the repository, poor local conditions might cause a limited number of container failures. The Normal Evolution Scenario assumes some containers with undetected defects are present in the repository at the time of closure, leading to container failures.
14. The container is surrounded by a layer of dense bentonite-based clay that inhibits groundwater movement, has self-sealing capability, inhibits microbial activity near the container, and retards contaminant transport.	Various repository FEPs (e.g., FEPs 3.1.02, 3.2.01 to 3.2.05), buffer properties, temperature, and groundwater chemistry, can influence the durability of the used fuel containers, potentially leading to container failures.	**Yes,** although evidence suggests that the copper container would be thermodynamically stable under the reducing conditions expected in the repository, poor local conditions might cause a limited number of container failures. The Normal Evolution Scenario assumes some containers with undetected defects are present in the repository at the time of closure, leading to container failures.

Safety Feature	Potentially Compromised by	Consider as Failure Mechanism
	Various repository FEPs (e.g., FEPs 3.1.02, 3.1.03, 3.2.01 to 3.2.05), such as temperature, hydrothermal alteration of the buffer, and buffer-groundwater interactions, have the potential to modify the hydrological, mechanical and chemical conditions at the repository depth, affecting properties of clay-based materials.	**No,** the effects are likely to be localized to the immediate vicinity of the container and these FEPs can be evaluated through considering different calculation cases for the Normal Evolution Scenario (i.e., low sorption and high solubility sensitivity cases) rather than through the development of alternative Disruptive Event Scenarios.
15. Institutional Controls will limit the potential for human encounter with the repository in the near term after closure	Affected by External FEPs relating to Future Human Actions (see Table 6-3) rather than the Internal FEPs relating to human behaviour that responds to the Future Human Actions.	

Note: * the Internal FEPs are shown in Garisto (2017).

Table 6-5: Potential Failure Mechanisms and Associated Scenarios

Failure Mechanism	Associated Disruptive Event Scenario
Exploration borehole penetrates into the repository providing an enhanced permeability pathway to the surface environment and potential for direct exposure to used fuel	Inadvertent Human Intrusion
Poor construction techniques affect the performance of repository and shaft excavation damaged zones providing an enhanced permeability pathway to the surface environment	Repository Seals Failure
Fracture and shaft seals perform poorly due to unexpected chemical interactions with groundwater or glacial meltwater, providing an enhanced permeability pathway to the surface environment	Repository Seals Failure
Site investigation / monitoring borehole seals perform poorly due to unexpected chemical interactions with groundwater or glacial meltwater, providing an enhanced permeability pathway to the surface environment	Poorly Sealed Borehole
The repository is not closed as planned after the monitoring period and tunnels, shafts and monitoring boreholes remain open	Partially Sealed Repository
Site investigations do not identify a permeable fracture zone or fault that provides a connection between the repository horizon and shallow groundwater system	Undetected Fault
Seismic event results in reactivation of an undetected existing fracture zone which provides an enhanced permeability pathway to higher horizons	Undetected Fault
Seismic event affects performance of repository and shaft excavation damaged zones, and /or fracture and shaft seals, providing an enhanced permeability pathway to higher horizons	Repository Seals Failure
Seismic event results in shearing along an existing fracture passing through a placement room, resulting in failure of some container(s) due to the shear load	Container Failure
Mechanical and thermal stresses induced by the presence of the repository cause greater than expected fracturing within the repository and shaft excavation damaged zones, providing an enhanced permeability pathway to surface environment	Repository Seals Failure
Unexpected chemical interactions of the copper coating with groundwater, e.g., due to higher than anticipated sulphide concentrations, affect the durability of a significant number of containers	All Containers Fail
Passage of thicker than design-basis ice sheet over repository site causes isostatic load on all containers to exceed their design load resulting in failure of all containers	All Containers Fail

The repository siting process will ensure that there are no known commercially viable natural resources near or below repository depth. Also, the repository has a relatively small footprint (~2.6 km^2) and the repository is at a depth of around 500 m. These factors limit the range of human activities that could directly affect the closed repository to a borehole unintentionally drilled into the repository as part of a future geological exploration program[3]. Even this situation has a low probability of occurrence. Nevertheless, once controls on the use of the site are no longer effective, the possibility of inadvertent human intrusion by this method cannot be ruled out over long time scales[4]. Such a borehole could provide an enhanced permeability pathway to the surface environment and potential for direct exposure to waste. This scenario is referred to as the **Inadvertent Human Intrusion Scenario**.

A second scenario by which the geosphere barrier can be bypassed is via the shafts (main, service and ventilation shafts) or the fracture passing through the repository footprint (see Figure 7.20). The shafts (with diameters from 7.6 m to 9 m) penetrate the geosphere, but are placed away from the waste panels, as shown in Figure 7.20. Similarly, the fracture intersecting the access tunnels extends from the repository to the near surface environment. The shafts and fractures are carefully sealed during repository closure or repository construction to isolate the repository from its surroundings. The **Repository Seals Failure Scenario** considers the possibility that the long-term performance of the shaft or fracture seals or their surrounding Excavation Damaged Zones (EDZs) is poor due to unexpected physical, chemical and / or biological processes, or that these seals and / or adjacent EDZs are somehow damaged by a seismic event. While these situations could result in an enhanced permeability pathway from the repository to the surface, they are very unlikely due to the quality control measures that will be applied during the selection of the seal materials (i.e., to ensure they are compatible with groundwater at the site), due to the low likelihood of major seismic events and due to the use of durable composite seals.

In the Repository Seals Failure Scenario, it is assumed that the other repository engineered barriers (i.e., the tunnel and room seals, and the backfill and buffer), are not degraded relative to their design properties except for the concrete component of the seals, for which degraded properties are used throughout the simulations, as in the Normal Evolution Scenario. The effects of degradation of these other engineered barriers would be investigated as sensitivity cases of the Repository Seals Failure Scenario.

The geosphere barrier is also bypassed via the shafts in the **Partially Sealed Repository Scenario** in which the repository is assumed not to be sealed following the monitoring period (i.e., after all containers are deposited in the repository and all placement rooms are sealed). In this scenario, the access tunnels and shafts remain open and are not maintained at least for an extended period. Since closing the repository is clearly important and funds would have been set aside for this purpose, this scenario would require a societal collapse or abandonment of the site for other unknown reasons. The likelihood of such a scenario is unknown but is low.

---

[3] The assessment excludes deliberate human intrusion since it is expected that the intruders would take appropriate precaution.

[4] The repository might appear as an anomaly in a surface / air-borne survey of the area, and this could encourage drilling at the site if all records had been lost. However, the absence of interesting minerals or geologic features in the area would argue against deliberate surveys of the area. Furthermore, a cautious approach to drilling might be used if such unexpected anomalies were identified that would minimize the consequences of any intrusion into the repository.

Another way in which the geosphere barrier can be bypassed is through the site characterization / monitoring boreholes. These boreholes are located in the vicinity of the repository down to and below repository depth. These boreholes will be appropriately sealed on completion of site investigation / monitoring activities so they will have no effect on repository performance. However, if the borehole seals were to degrade extensively due to, for example, unexpected chemical interactions with groundwater and / or glacial meltwater, then the borehole would provide a small but relatively permeable pathway for the migration of contaminants from the repository horizon to the environment. The scenario is termed the **Poorly Sealed Borehole Scenario**. Like the Repository Seals Failure Scenario, such a situation is very unlikely due to the adoption of good engineering practices and quality control measures, including the appropriate selection of sealing materials, and the use of durable composite seals.

The fracture zone network at the hypothetical site is based on a geostatistical model that represents a Canadian Shield location consistent with surface lineaments (Chapter 2). In the safety assessment calculations, all the identified fracture zones are assumed to be open and transmissive. However, at a real site in crystalline rock, there will be some uncertainty in the fracture network, and in the properties of the fractures. Site characterization may not identify all existing significant fractures at the site, and therefore a scenario is defined to investigate the safety implications of a hypothetical transmissive fault that is either undetected or formed by the extension of an existing discontinuity. The hypothetical fault is assumed to be in close proximity to the repository and to extend from below the repository level to the shallow groundwater system. This scenario is termed the **Undetected Fault Scenario**.

The copper coated used fuel containers are expected to last considerably more than one million years based on thermodynamic, experimental and natural analogue evidence that copper is stable for very long periods under deep geological repository conditions (see Chapter 5). Nevertheless, there are several mechanisms by which a container could fail sometime after it is installed in the repository. These container failures are in addition to the failures that occur in the Normal Evolution Scenario due to the presence of undetected defects (e.g., voids) in the copper coating. Container failure mechanisms include, but are not limited to, the following:

- After the repository attains reducing conditions, the copper container should be immune to further corrosion. However, unexpected interactions between the groundwater and copper container (e.g., due to higher than expected sulphide concentrations) could damage the copper coating sufficiently over the time frame of interest that the steel vessel would be exposed to water, leading to weakening of the vessel due to corrosion and / or seepage of water into the container.

- A container could be damaged by a sufficiently large shear load. A large seismic event that causes the rock to slip along an undetected fracture intersecting a placement room could produce such a shear load. The probability of such an event depends on the likelihood of an earthquake of a sufficient magnitude; the likelihood that a placement room is intersected by an undetected fracture and the fracture is near a container; and, finally, how the shear load is transmitted through the buffer material, which depends on the buffer thickness and density. The probabilistic analyses in SKB (2011) indicate that, for their repository, on average, one container would fail during a simulation due to shear load over one million years for each 5 simulations that were run.

The specific failure mode is not defined here, but the consequences are evaluated in the **Container Failure Scenario**. This considers failure of containers due to unexpected in-situ conditions, and is different from the Normal Evolution Scenario which considers a defect unknowingly present in some containers as the initiating event.

The containers are designed to be corrosion resistant and to be robust. As noted in Chapter 4, the inner steel vessel is able to sustain an external isostatic load of at least 45 MPa at 100ºC. Thus, the containers are expected to have a long lifetime. However, it is possible that some unexpected event or process may occur in the future such that there are multiple container failures in the repository. For example, the copper coating of the container could fail at long times due to unexpected interactions with groundwater caused by higher than expected sulphide concentrations in groundwater; or, the passage of a beyond design-basis ice-sheet over the repository site causes the load on the containers to exceed their design limit. Consequently, an **All Containers Fail Scenario** is considered in which all the containers in the repository fail at 60,000 years, the time of the assumed first passage of an ice sheet over the site (see Chapter 2). The probability of such a scenario is likely low since site characterization would ensure the absence of groundwater species detrimental to the long life of the container and because the container can withstand beyond-design basis glacial loads before failure. Furthermore, there is no evidence from past glaciations for ice sheets thick enough to exert a load on the containers sufficient to cause failure, even if it is pessimistically assumed that the additional hydrostatic load on the container is equivalent to the height of the ice sheet.

Other potential Disruptive Event Scenarios were considered but ruled out on various grounds as discussed further in the FEPs report (Garisto 2017). No volcanic activity is anticipated in the area over the next one million years. The probability of a large meteor strike, capable of damaging the repository, is remote and the consequences of the impact itself would likely be more significant than those from the repository. Seismic activity is possible, and likely earthquakes are included in the Normal Evolution Scenario. Such seismic activity will not cause rockfall because the repository is backfilled. Large earthquakes are unlikely since it is assumed that the hypothetical site is located in a low-seismicity area. The main effects of an earthquake on the repository are represented by the Repository Seals Failure, the Undetected Fault and the Container Failure Scenarios, so there is no need to consider an additional earthquake scenario. Glaciation, which could affect the repository system, is considered within the Normal Evolution Scenario and is the potential cause of the All Containers Fail Scenario (if the glacial load exceeds the repository design basis.)

Further confidence that an appropriate set of Disruptive Event Scenarios has been identified can be obtained by examining the scenarios (or sensitivity cases) considered in the postclosure safety assessments of deep repositories in other countries. The results of such an examination, summarized in Table 6-6, show that most assessments have identified a limited number of additional scenarios that consider the degradation / failure of engineered and natural barriers by natural processes (e.g., earthquakes, climate change) and human actions (e.g., drilling, poor quality control). Although there are some scenarios that are not considered in the current study, these are either not relevant for the hypothetical site (e.g., volcanic activity, sea-level rise, mining of resources) or have been included in the Normal Evolution Scenario (e.g., climate change, container failure).

Table 6-6: Additional Scenarios Considered in Other Safety Assessments

Assessment	Reference	Additional Scenarios Considered
SR-Site (Sweden)	SKB (2011)	• Canister failure due to corrosion or shear load • Disrupted buffer (due to erosion, advection) • Extended greenhouse effects • Exploratory drilling • Rock facility (e.g., quarry) • Incompletely sealed (or abandoned) repository
Olkiluoto (Finland)	POSIVA (2012)	• Defective canister (early and delayed penetration) • Earthquake/rock shear • Disrupted buffer • Exploratory drilling
Dossier Argile (France)	ANDRA (2005)	• Seal failure and defective plug • Defective waste and spent fuel containers • Borehole penetrating repository • Functioning of repository greatly degraded
H12 (Japan)[1]	JNC (2000)	• Climate and sea-level change • Exploitation drilling (water well) • Engineering defects, including poorly sealed repository
Opalinus (Switzerland)	NAGRA (2002)	• Gas pathways • Exploratory drilling • Poorly sealed repository
GPA (UK)	NIREX (2003)	• Exploratory drilling
WIPP (USA)	DOE (2004)	• Mining • Exploratory drilling
Yucca Mountain (USA)[2]	DOE (2002)	• Exploratory drilling • Seismicity • Volcanic event
SAFIR 2 (Belgium)	ONDRAF/NIRAS (2001)	• Exploratory drilling • Greenhouse effect • Poor sealing of repository • Fault activation • Severe glacial period • Failure of engineered barriers • Gas-driven transport

Notes:

[1] Isolation Failure Scenarios that involve penetration of the repository (including magma intrusion, human intrusion and meteorite impact) were also considered but screened out on the grounds that they are extremely unlikely to occur. Some 'what if' calculations were carried out instead.

[2] The term 'scenario' is used in a way that differs from the other assessments reviewed. Three Thermal Load Scenarios are discussed that are design variants, while two No-action Scenarios refer to futures in which the Yucca Mountain facility does not go ahead.

6.2.2 Description of Disruptive Event Scenarios

The identified Disruptive Event Scenarios are described below. These scenarios are evaluated separately rather than in combination since they have low probability and independent causes, and so the likelihood of simultaneous occurrence is even lower.

6.2.2.1 Inadvertent Human Intrusion Scenario

The Inadvertent Human Intrusion Scenario considers the impact of human intrusion sometime in the future. In this scenario, an exploration borehole is drilled through the geosphere and into the repository with the drill bit intersecting a used fuel container.

It is assumed that the drill crew is unaware of the facility (i.e., the intrusion occurs after institutional controls are no longer effective and societal memory of the site is lost). The investigators will most likely collect samples or conduct measurements at the repository level, due to the unusual nature of the materials. This would identify significant residual radioactivity (e.g., gamma logging is a standard borehole measurement) and the investigators would likely take precautions to prevent further exposure, including appropriate management of any materials released at the surface and sealing of the borehole. Therefore, under normal drilling, there would be little impact after the initial drill crew exposure.

Nevertheless, the reference Inadvertent Human Intrusion Scenario assumes:

- It is not recognized that the drill has intercepted a waste repository so no safety restrictions are applied; and
- The borehole and drill site are not managed and closed to current standards, and material from the borehole is released onto the surface around the drill site.

Contaminants can be released and humans and biota exposed via:

- Retrieval and examination of drill core contaminated with waste; and
- Uncontrolled dispersal of contaminated drill core debris on the site.

This could result in the exposure of the drill crew or other people at the time of intrusion, and people who might occupy the site subsequent to the intrusion event.

A variant of the Inadvertent Human Intrusion Scenario can also be defined in which the drill crew recognizes that the borehole has intercepted a waste repository, immediately ceases operations and vacates the site. The site is then completely remediated by qualified experts. In this case only the drill crew is exposed to a radiation dose.

If the borehole is not properly sealed, it could provide an enhanced permeability pathway to the surface environment or even be used as a well by a future site resident. The impact of this open borehole on future residents of the site can, in theory, be examined as part of the Inadvertent Human Intrusion Scenario.

6.2.2.2 Repository Seals Failure Scenario

The shafts and the fracture through the repository footprint represent potentially important pathways for contaminant release and, therefore, the repository design includes specific measures to provide good shaft and fracture seals, taking into account the characteristics of the geosphere. The Repository Seals Failure Scenario considers the consequences of extensive degradation of the shaft and / or fracture seals and / or their corresponding excavation damaged zones. This scenario, like the other Disruptive Event Scenarios, is a bounding scenario designed to investigate the robustness of the repository system.

The radionuclide exposure pathways (e.g., ingestion, inhalation, etc.) to which the critical group and non-human biota are exposed are the same as those considered in the Normal Evolution Scenario.

6.2.2.3 Partially Sealed Repository Scenario

Another scenario by which the geosphere barrier can be bypassed via the shafts is the Partially Sealed Repository Scenario. The basic assumption in the Partially Sealed Repository Scenario is that the repository is abandoned during the monitoring phase (i.e., after all containers are placed in the repository and all placement rooms are backfilled and sealed), but the main access tunnels and the shafts are still open. This is consistent with normal operations, in which the placement rooms are successively filled with containers and backfilled, and sealed as soon as they are filled.

Abandonment of the repository would require a significant societal breakdown because of the known importance of properly closing the repository.

The radionuclide exposure pathways (e.g., ingestion, inhalation, etc.) to which the critical group and non-human biota are exposed are the same as those considered in the Normal Evolution Scenario.

6.2.2.4 Poorly Sealed Borehole Scenario

Multiple deep site investigation / monitoring boreholes will be drilled in the vicinity of the repository during the site investigation phase. The Poorly Sealed Borehole Scenario considers the consequences of unexpected extensive degradation of the borehole seals. The poorly sealed borehole provides an enhanced permeability connection between the repository level and the overlying groundwater zones and biosphere, bypassing some of the natural geological barriers to contaminant migration from the repository. The exposure pathways are the same as those considered in the Normal Evolution Scenario.

6.2.2.5 Undetected Fault Scenario

The Undetected Fault Scenario considers the impact of an undetected or seismically activated transmissive fault in close proximity to the repository that extends from about the repository level up into the shallow groundwater system. Such a fault could provide an enhanced permeability pathway that bypasses the natural geological barrier.

The radionuclide exposure pathways (e.g., ingestion, inhalation, etc.) to which the critical group and non-human biota are exposed are the same as those considered in the Normal Evolution Scenario.

6.2.2.6 All Containers Fail Scenario

The long-lived used fuel containers are an important feature of the multi-barrier repository concept in this conceptual design. The copper containers are expected to last for a long time because copper is stable under anticipated conditions in a deep geological repository; however, the All Containers Fail Scenario considers the very unlikely and hypothetical case in which all the containers simultaneously fail (i.e., water enters all containers and contacts the fuel) at 60,000 years. This timeframe corresponds to the assumed time scale for glacial cycles to resume and an ice sheet to first cover the site (see Chapter 2). Such an ice sheet could be assumed to cause multiple container failures if the design load of the containers is exceeded or if the containers have been weakened due to penetration of the copper coating and subsequent corrosion of the steel vessel. For simplicity, in this scenario, it is assumed that there are no initially defected containers as in the Normal Evolution Scenario.

A variant case in which all containers are assumed to fail at 10,000 years is also investigated to determine the sensitivity to the assumed failure time.

The radionuclide exposure pathways (e.g., ingestion, inhalation, etc.) to which the critical group and non-human biota are exposed are the same as those considered in the Normal Evolution Scenario. However, the failure of all containers also leads to the generation of significant amounts of hydrogen gas due to corrosion of the inner steel vessel. Consequently, the impact of gas generation on the performance of the repository and the transport of gaseous contaminants is also addressed.

6.2.2.7 Container Failure

The Container Failure Scenario considers the impact of container failure due to several possible mechanisms.

- Corrosion of the copper coating on the container due to, for example, unexpectedly high sulphide concentrations near a small number of containers, allowing eventual corrosion and breach of the steel container.
- A large seismic event (earthquake) in the vicinity of the repository that causes slip along an undetected closed fracture that intersects a placement room. The rock slip along the fracture zone is assumed to be sufficiently large that it causes complete failure of a container. The shearing action could also increase the transmissivity of the fracture. Although the shear movement should not affect the buffer properties, the amount of buffer between the container and the shearing fracture zone would likely be reduced.

The radionuclide exposure pathways (e.g., ingestion, inhalation, etc.) to which the critical group and non-human biota are exposed are the same as those considered in the Normal Evolution Scenario.

6.3 References for Chapter 6

ANDRA. 2005. Dossier 2005 Argile Tome Evaluation de Sûreté du Stockage Géologique. Paris, France.

Blyth, A., S. Frape, R. Blomqvist and P. Nissinen. 2000. Assessing the past thermal and chemical history of fluids in crystalline rock by combining fluid inclusion and isotope investigations of fracture calcite. Applied Geochemistry 13, 1417-1437.

CNSC. 2006. Regulatory Guide G-320: Assessing the Long Term Safety of Radioactive Waste Management. Canadian Nuclear Safety Commission. Ottawa, Canada.

DOE. 2002. Final Environmental Impact Statement for a Geologic Repository for the Disposal of Spent Nuclear Fuel and High-level Radioactive Waste at Yucca Mountain, Nye County, Nevada. United States Department of Energy, Office of Civilian Radioactive Waste Management, DOE/EIS-0250. Nevada, USA.

DOE. 2004. 2004 WIPP Compliance Recertification Application (CRA) - Main Volume. US Department of Energy Report DOE/WIPP 04-3231. Available at: http://www.wipp.energy.gov/library/CRA/CRA_Index.htm. Accessed January 2011.

Garisto, F. 2017. Sixth Case Study: Features, Events and Processes. Nuclear Waste Management Organization Report NWMO TR-2017-08. Toronto, Canada.

Gascoyne, M. 2004. Hydrogeochemistry, groundwater ages and sources of salts in a granitic batholith on the Canadian Shield, southeastern Manitoba. Applied Geochemistry 19, 519-560.

Gascoyne, M., J. McMurry and R. Ejeckam. 2004. Paleohydrogeological Case Study of the Whiteshell Research Area. Ontario Power Generation Report 06819-REP-01200-10121-R00. Toronto, Ontario.

IAEA. 2012. The Safety Case and Safety Assessment for the Disposal of Radioactive Waste. IAEA Safety Standards. Specific Safety Guide No. SSG-23. International Atomic Energy Agency. Vienna, Austria.

ICRP. 2000. Radiation Protection Recommendations as Applied to the Disposal of Long-lived Solid Radioactive Waste. International Commission on Radiological Protection Publication No. 81, Annals of the ICRP 28(4).

JNC. 2000. H12: Project to Establish the Scientific and Technical Basis for HLW in Japan. Japan Nuclear Cycle Development Institute Report JNC TN1410 2000-004. Tokai, Japan.

McMurry, J. and R.B. Ejeckam. 2002. Paleohydrogeological Study of Fracture Mineralogy in the Whiteshell Research Area. Ontario Power Generation Report 06819-REP-01200-10082-R00. Toronto, Canada.

NAGRA. 2002. Project Opalinus Clay: Safety Report, Demonstration of the Disposal Feasibility for Spent Fuel, Vitrified HLW and Long-lived ILW. Nagra Technical Report 02-05. Wettingen, Switzerland.

NEA (Nuclear Energy Agency). 2000. An international database of features, events and processes. Report of the NEA working group on the development of a database of features, events and processes relevant to the assessment of post-closure safety of radioactive waste repositories. OECD Nuclear Energy Agency report. Paris, France.

NIREX. 2003. Generic Repository Studies: Generic Post-closure Performance Assessment. Nirex Report N/080. Harwell, United Kingdom.

ONDRAF/NIRAS. 2001. SAFIR 2: Safety Assessment and Feasibility Interim Report 2. ONDRAF/NIRAS Report NIROND 2001-06E. Brussels, Belgium.

Perry, C., C. Rosieanu, J.-C. Mareschal and C. Jaupart. 2010. Thermal Regime of the Lithosphere in the Canadian Shield, Canadian Journal of Earth Sciences 47, 389-408.

Peltier, W.R. 2011. Long-Term Climate Change. Nuclear Waste Management Organization Technical Report NWMO DGR-TR-2011-14 R000. Toronto, Canada.

POSIVA. 2012. Safety Case for the Disposal of Spent Nuclear Fuel at Olkiluoto – Synthesis 2012. Posiva Report 2012-12. Olkiluoto, Finland.

SKB. 2011. Long-term Safety for the Final Repository for Spent Nuclear Fuel at Forsmark, Main Report of the SR-Site Project. Swedish Nuclear Fuel and Waste Management Report SKB TR-11-01. Stockholm, Sweden.

Spiessl, S.M., K.U. Mayer and K.T.B. MacQuarrie. 2009. Reactive Transport Modelling in Fractured Rock – Redox Stability Study. Nuclear Waste Management Organization Report NWMO TR-2009-04. Toronto, Canada.

Szakálos, P., G. Hultquist and G. Wikmark. 2007. Corrosion of Copper by Water. Electrochemical and Solid-State Letters, 10, pp C63–C67.

Zhang, M. and S.K. Frape. 2002. Permafrost: Evolution of Shield Groundwater Compositions during Freezing. Ontario Power Generation Report 06819-REP-01200-10098-R00. Toronto, Canada.

7. POSTCLOSURE SAFETY ASSESSMENT

This chapter presents an illustrative postclosure safety assessment for a used fuel repository located in the crystalline rock of the Canadian Shield.

The purpose of a postclosure safety assessment is to determine the potential effects of the repository on the health and safety of persons and the environment during the postclosure period. The assessment timeframe is one million years based on the time period needed for the radioactivity of the used fuel to decay to essentially the same level as that in an equivalent amount of natural uranium. This timeframe is also within a reasonable extrapolation of the geological stability of these rocks.

The assessment is conducted by applying computer models to a range of analysis cases. The analysis cases here examine the Normal Evolution Scenario and some of the Disruptive Event Scenarios identified in Chapter 6, together with a series of sensitivity studies performed to examine the importance of various model features and assumptions.

The discussion is arranged as follows:

- Section 7.1 – Interim Acceptance Criteria: four sets of interim acceptance criteria are defined against which the radiological and non-radiological consequences on persons and the environment are assessed.
- Section 7.2 – Scope: a detailed description of the analysis cases and sensitivity studies is described together with the rationale for their selection. Included is a brief discussion of excluded items which might otherwise be included in a more comprehensive licence submission.
- Section 7.3 – Conceptual Model: discusses the conceptualization of the repository evolution.
- Section 7.4 – Computer Codes: introduces the main computer codes used.
- Section 7.5 – Overall Analysis Approach and Selected Data for Groundwater Flow and Radionuclide Transport: outlines the analysis method for groundwater flow and radionuclide transport calculations and provides a selection of data for key parameters.
- Section 7.6 – Modelling and Results for Radionuclide and Chemical Hazard Screening: describes the methods used and results obtained from the work performed to identify the set of radionuclides and chemical elements of potential concern to the postclosure safety assessment.
- Section 7.7 – Modelling and Results for 3D Groundwater Flow and Radionuclide Transport: describes the 3D models used and provides results for I-129, C-14, Ca-41, Cl-36, Cs-135, Se-79 and U-238. I-129 transport results are also provided for those sensitivity studies with the potential to affect the groundwater flow field.
- Section 7.8 – Modelling and Results for the System Model: describes how the System Model is created, and provides results for deterministic and probabilistic simulations of dose consequences for all radionuclides of potential significance for all cases that do not affect the groundwater flow field. A discussion of the anticipated effects of glaciation on the dose consequences for the Normal Evolution Scenario is also included.

- Section 7.9 – Modelling and Results for Disruptive Event Scenarios: describes the analysis and presents results for those scenarios included in the scope of this study.
- Section 7.10 – Modelling and Results for Radiological Protection of the Environment: presents results for the radiological protection of the environment for the Normal Evolution Scenario and the limiting Disruptive Event Scenario.
- Section 7.11 – Modelling and Results for Protection of Persons and the Environment from Hazardous Substances: presents results for the protection of persons and the environment from hazardous substances for the Normal Evolution Scenario and the limiting Disruptive Event Scenario.
- Section 7.12 – Modelling and Results for Gas Generation and Migration: describes the method used and results obtained for the determination of the effects of gas generation and migration in the repository.
- Section 7.13 – Modelling and Results for Complementary Indicators: describes and presents results for two complementary indicators for radiological safety.
- Section 7.14 – Summary and Conclusions.

7.1 Interim Acceptance Criteria

This section presents interim acceptance criteria applicable to the postclosure safety assessment. These criteria are used to judge the acceptability of analysis results.

CNSC Guide G-320 (CNSC 2006) identifies the following be addressed in a postclosure safety assessment:

1. Radiological protection of persons;
2. Protection of persons from hazardous substances;
3. Radiological protection of the environment; and
4. Protection of the environment from hazardous substances.

Interim acceptance criteria are defined for each of the above and discussed in the following sections. These criteria are consistent with current Canadian and international practice; however, these are *interim* criteria because the criteria used in a licence application will need to be accepted by the CNSC at that time, and may be different from the specific values identified here.

7.1.1 Interim Acceptance Criteria for the Radiological Protection of Persons

The main objective of the postclosure safety assessment is to provide reasonable assurance that the regulatory radiological dose limit for public exposure (1 mSv/a) will not be exceeded. To account for the possibility of exposure to multiple sources in the future, a dose constraint below the regulatory limit is adopted.

For the Normal Evolution Scenario, the interim dose rate acceptance criterion is:

- An annual individual effective dose rate of 0.3 mSv/a with the calculation performed to encompass the time of maximum predicted impact to the average adult member of the critical group.

The 0.3 mSv/a dose constraint is consistent with recommendations of the International Commission on Radiation Protection (ICRP) and the International Atomic Energy Agency (IAEA) (ICRP 2007, ICRP 2013, IAEA 2006) and is significantly less than the average Canadian individual dose rate of 1.8 mSv/a received from background radiation (Grasty and LaMarre 2004).

At this dose rate, there is no clear evidence for adverse health effects (NRC 2006, CNSC 2011). However, the Linear-No-Threshold model recommended by international agencies (ICRP 2013) and adopted by the Canadian regulator (CNSC 2013) assumes, for radiation protection purposes, that any dose exposure results in some increase in health risk, notably cancer. This dose constraint ensures that the health risks are small in comparison to the risk from natural background radiation, and to the risk of cancer from all causes.

Calculating the exposure of an adult member of the critical group is consistent with ICRP recommendations which recognize that exposures are expected to occur in the distant future, that exposure would be associated with levels of radionuclides in the environment that change slowly over the time scale of a human lifetime, and that calculated exposures at long times have inherent uncertainties (ICRP 2013). Effective dose rates from ingestion and inhalation of radionuclides are calculated using the dose coefficients from ICRP 72 (ICRP 1995), which are based on a human model that includes male and female organs to ensure that it includes all radionuclide sensitivities and ICRP 60 recommendations (ICRP 1991). Effective dose coefficients for adult ground exposure, air immersion, water immersion and building exposure are also calculated based on ICRP 60 recommendations (Eckerman and Leggett 1996).

For Disruptive Events Scenarios, the interim acceptance criteria are:

- An annual individual effective dose rate target of 1 mSv/a for chronic[1] release scenarios with the calculation performed for the average adult member of the critical group; and
- Acceptability of any scenario with the calculated annual individual effective dose rate for chronic releases exceeding 1 mSv/a to be examined on a case-by-case basis taking into account the likelihood and nature of the exposure, the uncertainty in the assessment and the conservatism in the dose criterion. Where the probability of exposure can be quantified without excessive uncertainty, a measure of risk will be calculated based on the probability of exposure and the consequent health effects. This will be compared with a reference risk value of 10^{-5}/a (ICRP 2013).

A dose rate of 1 mSv/a corresponds to the current regulatory limit for exposure of the public. This is less than the 1.8 mSv/a average natural background dose rate for Canadians.

---

[1] Chronic refers to a release that is sustained over many years.

The reference health risk value of 10^{-5}/a is consistent with ICRP (2013), Health Canada (2010) and IAEA (2006). Based on the ICRP probability coefficient of 0.057 per Sv for stochastic effects (e.g., cancers or hereditary effects) (ICRP 2007), this corresponds to a health risk about a factor of 10 lower than the risk from the natural background dose rate.

Regulatory document G-320 (CNSC 2006) and ICRP (2013) recognizes that inadvertent human intrusion into a repository could result in doses greater than 1 mSv/a because intrusion by definition bypasses the repository barriers. The risk from human intrusion is made low by the site selection criteria which require the facility to be located deep underground in an area known not to have economically exploitable natural resources or potable groundwater resources at repository depth. Institutional controls will also reduce risk in the short-term, when the hazard is greatest.

7.1.2 Interim Acceptance Criteria for the Protection of Persons from Hazardous Substances

Interim acceptance criteria for the protection of persons from hazardous substances are based on Canadian Federal and Provincial guidelines (principally from the Canadian Council of Ministers of the Environment (CCME) and the Ontario Ministry of the Environment (MOE) for concentrations in environmental media relevant to human health and environmental protection, supplemented as needed by internationally developed guidelines. They have been assembled taking into account the guidance of G-320 (CNSC, 2006). The basis for the proposed interim acceptance criteria is discussed in detail in Medri (2015c).

Criteria which are provided for non-radiological contaminants in a used fuel repository for five different environmental media are protective of the following:

Surface water:	Drinking water, aquatic life, agricultural water uses (irrigation and livestock), recreational water uses and aesthetic features.
Groundwater:	Drinking water, agricultural water uses (irrigation and livestock) and surface water bodies from groundwater flow.
Soil:	Ecological receptors and human health for soils for various land uses (agricultural, residential/parkland, commercial and industrial).
Sediment:	Aquatic life, human health and the environment.
Air:	Human health, the environment and nuisance effects (like odour).

The criteria are intended to be cautiously realistic; that is, they ensure the protection of all forms of life (animals, plants and humans) without being excessively conservative. They are intended for postclosure conditions in that they are selected for chronic exposure conditions, and that they are relevant for chemical species that could credibly exist in these media due to release of the elements from the repository.

Estimated environmental concentrations of contaminants are to be compared with the interim acceptance criteria given in Table 7-1. Criteria are not available for all elements in all media, but at least one criterion is available for each listed element. Exceedance of a criterion does not necessarily indicate unacceptable risk. As appropriate, consideration may be given to assessing the conservatism of the criterion through reference to the original sources, to the use of less conservative release and exposure models, to the likelihood and nature of the exposure and to mitigation measures. Additive, synergistic or antagonistic effects from chemical species in mixtures are not considered in this stage.

Table 7-1: Interim Acceptance Criteria for the Protection of Persons and the Environment from Non-Radiological Impacts

Element	Surface Water (µg/L)	Groundwater (µg/L)	Soil (µg/g)	Sediment (µg/g)	Air (µg/m^3)
Ag	0.1	1.2	0.5	0.5	1
Al	=5 if pH<6.5 =100 if pH is ≥6.5	100	50	-	53
As	5	10	11	5.9	0.3
B	200	500	1.5	-	5.8
Ba	1000	1000	210	-	10
Be	=11 if $CaCO_3$ < 75 mg/L =1100 if $CaCO_3$ > 75 mg/L	4	2.5	-	0.01
Bi		-	20	-	100
Br	-	-	10	-	20
Ca	1000 000	1000 000	-	-	200
Cd	0.09	2.1	1	0.6	0.005
Ce	22	-	53	19 000	200
Cl	100 000	100 000	-	-	10
Co	0.6	3.8	22	50	0.1
Cr	1	4.9	0.66	26	10
Cu	=1 $CaCO_3$ ≤ 20 mg/L =5 $CaCO_3$ > 20 mg/L	69	62	12	50
Dy	9.3	-	-	2200	200
Eu	-	-	-	-	200
F	120	1000	200	-	17
Fe	300	300	200	21 000	4
Gd	7.1	-	-	1800	340
Hf	-	-	-	-	10
Hg	0.004	0.12	0.2	0.17	0.5
Ho	-	-	-	-	40
I	100	-	4	-	0.67
K	53 000	-	-	-	15
La	10	-	50	4700	200
Li	2500	2500	2	-	20
Lu	-	-	-	-	8
Mg	82 000	-	-	-	0.11
Mn	50	50	100	460	0.1
Mo	10	10	2	8.3	100
Na	200 000	200 000	-	-	87
Nb	600	-	9	-	200
Nd	1.8	-	-	7500	200

Element	Surface Water (µg/L)	Groundwater (µg/L)	Soil (µg/g)	Sediment (µg/g)	Air (µg/m^3)
Ni	= 25 if $CaCO_3$≤ 60 mg/L =$e^{\{0.76[\ln(\underline{hardness})]+1.06\}}$ if $CaCO_3$> 60 and ≤ 180 mg/L =150 if $CaCO_3$ >180 mg/L	100	37	16	0.02
P	4	-	-	-	-
Pb	=1 if $CaCO_3$ <30 mg/L =3 if $CaCO_3$ is ≥ 30 but ≤80 mg/L =5 if $CaCO_3$ > 80 mg/L	10	45	28	0.2
Pr	9.1	-	-	5800	8
Pt	-	-	-	-	0.2
S	= 170 000 if S exists as sulphate =1.9 if S exists in any other form	=170 000 if S exists as sulphate =50 if S exists in any other form	500	-	7
Sb	6	6	1	3	25
Sc	-	-	-	-	200
Se	1	10	1.2	0.9	10
Sm	8.2	-	-	2500	200
Sn	73	-	5	-	10
Sr	1500	-	33 000	-	100
Ta	-	-	-	-	67
Tb	-	-	-	-	8
Tc	-	-	0.2	-	-
Te	-	-	250	-	10
Ti	-	-	1 000	-	20
Tl	0.3	2	1	-	0.4
Tm	-	-	-	-	200
U	5	20	1.9	32	0.03
V	7	6.2	86	27	2
W	30	-	400	-	67
Y	6.4	-	-	1400	20
Zn	=1000 if soil pH ≤6.5 =5000 if soil pH > 6.5	890	290	120	100
Zr	4	-	97	-	67

Notes: ’-‘ indicates that there are no defined criteria for that element in the given medium.
Detailed information on the individual source documents, speciation and exceptions is available in Medri (2015c)

7.1.3 Interim Acceptance Criteria for the Radiological Protection of the Environment

Protection policies for non-human biota are not as mature as those for humans. There are no internationally agreed upon environmental benchmarks or dose rate criteria against which to assess radiological effects to non-human biota. This stems from the fact that there is a relative lack of data compared to the breadth of parameters involved, such as animal species, type of effect (morbidity, mortality, reproductive success, etc.), type of exposure (internal, external, gamma, alpha, etc.), rate of exposure (chronic or acute) and type of experiment (field or lab). Also, the statistical analysis requires many samples of each data type to achieve statistical relevance. However, while the ICRP (2008) notes that “dose limits” of the form used in human radiological protection would be inappropriate, some form of numerical guidance is required.

As such, the ICRP (2014) recommends the use of the lower end of their Derived Consideration Reference Level (DCRL) bands as points of reference to optimize the level of effort expended on environmental protection. DCRLs are bands of dose rates for each type of reference animal or plant within which there is likely to be some chance of deleterious effects from ionizing radiation. Below the lower end of the DCRL bands, the risks to non-human biota are negligible. Similarly, ERICA (Garnier-Laplace et al. 2006) and PROTECT (Andersson et al. 2009) propose a generic screening criterion for chronic exposures of 10 µGy/h for all biota, which is well accepted and widely used, especially in Europe. The generic screening criterion is typically used in tiered assessments, where exceeding the criterion would highlight the need to consider the level of potential impact in more detail.

In this assessment, a two-tiered approach is adopted as a risk-based method of demonstrating the protection of non-human biota. This is consistent with the approach proposed by BIOPROTA, an international forum which seeks to address key uncertainties in the assessment of radiation doses in the long-term arising from releases of radionuclides as a result of radioactive waste management (Jackson et al. 2014). The first tier criteria are taken to be the lower of the generic ERICA screening criterion of 10 µGy/h and the bottom end of the ICRP DCRL band for each reference non-human biota. Calculated dose rates that fall below the first tier criteria are considered to be of no radiological concern. The second tier criteria are delimited by the upper end of the DCRL band, which are taken to be realistic levels at which some effects to individual non-human biota could be observed, but that would be unlikely to produce significant effects at the population level. Acceptability of dose rates that fall between the first and second tier criteria will be judged within the context of the likelihood of the exposure situation, the conservatisms in the dose rate estimate and the intended protection endpoint. Dose rates that exceed the second tier criteria would need to be investigated in more detail. Taken as a whole, this approach defines the acceptance criteria for this assessment, which is detailed in Table 7-2.

Table 7-2: Interim Acceptance Criteria for the Radiological Protection of the Environment

Biota	Tier 1 Acceptance Criteria[1] (µGy/h)	Tier 2 Acceptance Criteria[2] (µGy/h)
Amphibian	10	400
Aquatic Bird	4	40
Aquatic Mammal	4	40
Aquatic Plants	10	4000
Benthic Invertebrates	10	4000
Fish	10	400
Reptile	10	400
Terrestrial Bird	4	40
Terrestrial Invertebrates	10	4000
Terrestrial Mammals	4	40
Terrestrial Plants (Grasses)	10	400
Terrestrial Plants (Trees)	4	40

1. Dose rates that fall below the Tier 1 criteria are deemed acceptable and require no further discussion.
2. Acceptability of dose rates that fall between Tier 1 and Tier 2 will be judged within the context of the likelihood of the exposure situation, the conservatisms in the dose rate estimate and the intended protection endpoint. Dose rates that exceed Tier 2 would need to be investigated in more detail.

7.1.4 Interim Acceptance Criteria for the Protection of the Environment from Hazardous Substances

For this category, the criteria defined in Section 7.1.2 also apply because the values selected in Table 7-1 are the lowest values relevant to either human health or to the environment.

7.2 Scope

This section presents the scope of work addressed in this postclosure safety assessment.

The scope is defined by taking into account the discussion of the Normal Evolution Scenario and the Disruptive Event Scenarios in Chapter 6 together with experience gained from previous postclosure studies performed for other hypothetical sites and conceptual designs.

The scope is intended to demonstrate postclosure safety methods and techniques as applied to the most recent container and placement room design. As such, analysis cases are limited to those needed to provide a demonstration of the overall approach and to those needed to reach possible conclusions for the hypothetical site. Items excluded from the scope but which might be included in a licence submission as part of a more comprehensive assessment are discussed in Section 7.2.4.

Results for all cases are measured against the interim acceptance criteria for the radiological protection of persons provided in Section 7.1.1.

Results for only the Base Case (see below) of the Normal Evolution Scenario and for the Disruptive Event Scenario with the highest dose consequence are measured against the criteria for the protection of persons from hazardous substances provided in Section 7.1.2, the criteria for the radiological protection of the environment provided in Section 7.1.3, and the criteria for the protection of the environment from hazardous substances provided in Section 7.1.4.

Results are also developed for two complementary radiological indicators (i.e., radionuclide concentrations in the biosphere and radionuclide transport to the biosphere).

All cases considered are shown in Figure 7-1. This figure illustrates the Normal Evolution Scenario and the Disruptive Event Scenarios, together with a series of sensitivity studies performed to examine the effects of degraded barrier performance on the Normal Evolution Scenario. All of these cases are described in detail below.

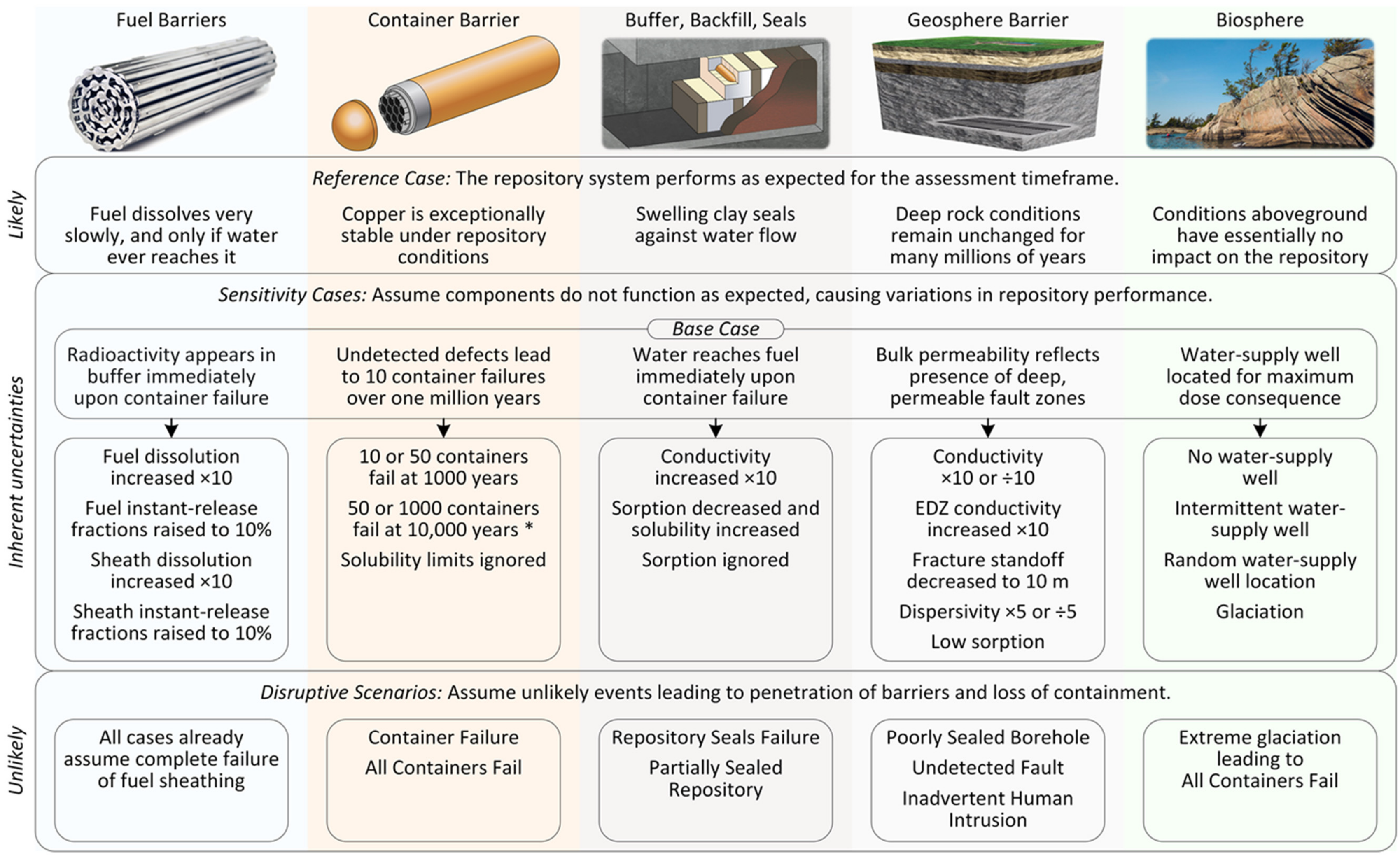

Note: Hypothetical container failures all occur in the one location that would yield the largest dose consequence. The case marked '*' is an exception, where hypothetical container failures are equally likely to occur at all locations across the repository.

Figure 7-1: Illustration showing Normal Evolution Scenario and Sensitivity Studies, and Disruptive Event Scenarios

7.2.1 The Normal Evolution Scenario

The Normal Evolution Scenario is based on a reasonable extrapolation of present day site features and receptor lifestyles. It includes the expected evolution of the site and expected degradation of the repository system. Its purpose is to illustrate the anticipated effects of the repository on people and on the environment.

The Normal Evolution Scenario is described in terms of a “Reference Case” and a series of associated sensitivity studies.

The Reference Case represents the situation in which all repository components meet their design specification and function as anticipated. As such, the used fuel containers remain intact essentially indefinitely (see Chapter 5) and no contaminant releases occur in the one million year time period of interest to the safety assessment.

The associated sensitivity studies illustrate repository performance for a range of reasonably foreseeable deviations from key Reference Case assumptions. These deviations arise as a result of components unknowingly placed in the repository that either (a) do not meet their design specification or (b) do not fully function as anticipated.

The likelihood of such deviations will be very low. Care is being taken to design, develop and proof test a robust placement technology which will ultimately be implemented under a comprehensive quality assurance program. A key element of the quality assurance program will be an inspection process designed to ensure all components cleared for placement meet design specification. Similarly, component performance is supported by an extensive research and testing program, such that the behaviour of all materials placed in the repository will also be well understood.

Because of its importance as a key barrier, every container will be thoroughly inspected using eddy current and ultrasonic techniques together with other methods of surface examination.

7.2.2 Sensitivity Studies for the Normal Evolution Scenario

The most important sensitivity study is the “Base Case”, defined below.

7.2.2.1 The Base Case

The “Base Case” assumes a small number of containers are fabricated with sizeable defects in their copper coating, and that a smaller number of these off-specification containers escape detection by the quality assurance program and are unknowingly placed in the repository.

Studies are underway to determine the likelihood and number of off-specification containers that could potentially be present; however, the results of this work are presently not available. In the meantime, 10 containers with large undetected defects in the copper coating are assumed to be in the repository. Postclosure studies assuming 10 defective containers are sufficient to illustrate repository performance and to provide a measure of the consequences that could be expected should such an event (or a similar one) actually occur.

The defects are assumed sufficiently large to cause each of the 10 containers to fail within one million years. As the actual nature (size, location) of each defect will vary, it is highly unlikely that 10 containers would all fail simultaneously. The failure times are assumed to be evenly spread over the one million year time period of interest, with the first failure occurring at 1000 years and subsequent failures occurring sequentially every 100,000 years. Table 7-3 shows that 1000 years is a very conservative value for the time of first container failure and even more conservative as the assumed time of first radionuclide release

To further define the Base Case, a number of bounding assumptions are made to account for uncertainties affecting case definition. A “bounding assumption” is an assumption that results in a greater consequence than the entire range of uncertainty, usually at the expense of realism. To illustrate, a bounding assumption is created if the uncertainty associated with the location and lifestyle of people unknowingly living in the vicinity of the repository in the future is replaced by an assumption that instead has people unknowingly living on top of the repository and obtaining all of their drinking and crop irrigation water from a deep well, with the well positioned in the location that maximizes the uptake of any potential contaminant release.

The adoption of bounding assumptions is a common technique in safety assessment. It allows for complex problems to be reduced to much simpler ones, with the downside being that the resulting case is no longer the most realistic. While this is acceptable from a licensing viewpoint (provided results meet acceptance criteria), it can make repository performance appear to be much worse than it really is.

To illustrate the degree to which conservatism (and departure from reality) is incorporated in the Base Case, Table 7-3 compares key Base Case assumptions with what might actually occur in reality. For simplicity, the table is focussed only on the 10 defective containers, with separate sections shown for defect, container and dose related assumptions. A discussion of the key parameters in each section is included below the table.

Table 7-3: Conservatisms in Base Case Assumptions

Parameter	Realistic Assumption	Base Case Assumption
When can contaminants escape the container?	After the container is breached and large amounts of water contact the fuel	After the container is breached
Defect Parameters		
What is the defect of concern?	Undetected defect in the copper corrosion barrier	Undetected defect in the copper corrosion barrier
How large is the defect in the copper corrosion barrier?	Random sizes below the Detection Threshold (0.8 mm depth)	>>0.8mm Large enough to cause container failure at the assumed times
Where is the defect located?	Random location • < 1% chance over 8 mm weld • ~5% chance over weld area (8-30 mm steel) • ~25% chance over container head (30 mm steel) • ~70% chance over container body (46 mm steel)	Not applicable Complete container failure occurs at the assumed times
How long does an impaired copper barrier remain effective?	> 74 million years for defects below the 0.8 mm Detection Threshold (see Chapter 5) *Based on an assumed groundwater sulphide concentration of 1* µM	1000 years for the first container One additional container fails every 100,000 years
How many containers are breached prior to 1 million years?	0	10
Container Parameters		
Once the copper barrier is penetrated, how long before the steel inner shell is penetrated due to corrosion?	140,000 years for 8 mm 1,300,000 years for 30 mm 2,000,000 years for 46 mm *Based on 1 mm diameter hole in the copper barrier* *It is anticipated that there will be insufficient amounts of carbonate to promote siderite producing corrosion reactions (see Chapter 5)*	0 years
Once the steel barrier is penetrated, how long before	It could take many tens of thousands of years for the container to fill with water	0 years

Parameter	Realistic Assumption	Base Case Assumption
large amounts of water enter the container?		
Do the Zr fuel sheaths prevent water from contacting fuel elements?	Possibly Some fuel sheaths may still be intact when water enters the container	No
For fuel elements that are contacted by water, how large is the instant release source term?	Depends on the power experienced while in the reactor and on the physical condition of each fuel pellet	Conservative Value
Does H_2 released during steel corrosion and radiolysis inhibit the fuel dissolution rate (and thereby inhibit the contaminant release rate)?	Most likely Yes	No
Do corrosion products accumulate in the defect and obstruct the migration of contaminants?	Yes	No
After the steel barrier is penetrated, how long before the container wall corrodes away and no longer presents any resistance to contaminant release	120,000 years for 8 mm 460,000 years for 30 mm 710,000 years for 46 mm *It is anticipated that there will be insufficient amounts of carbonate to promote siderite producing corrosion reactions (see Chapter 5)*	0 years
Dose Parameters		
Are people living close to the facility?	Unknown The repository footprint is small and the location may be far from populated areas	Yes Living on top of the repository
Are the nearby people using a deep well to obtain their drinking water?	Unlikely Surface water sources or a shallow well are more likely	Yes A 100 m deep well is assumed
If used, where is the well located in relation to the defective containers?	Random	Worst location The location that maximizes contaminant uptake
Where are the hypothetical defective containers located in the repository?	Random	Clustered In the location that maximizes uptake to the well

The following discussion provides contextual information on the contents of Table 7-3.

Defect Assumptions:

The concern is an undetected defect in the copper corrosion barrier.

In the Base Case, 10 containers with defects much greater than the detection threshold of the inspection equipment are assumed to be unknowingly placed in the repository. These defects are of sufficient size that the copper coating is fully penetrated by corrosion within 1000 years to 1,000,000 years.

In reality, defects of size greater than the detection threshold (anticipated to be 0.8 mm) are not expected to be present. Copper defects (voids) smaller than this could exist, and these would be randomly located anywhere in the copper coating. As noted in Chapter 5, containers with a design copper thickness of 3 mm could survive in excess of 74 million years in the type of groundwater conditions anticipated to be present at the hypothetical site, even if a defect in the copper coating of 0.8 mm is assumed.

Container Assumptions:

This portion of Table 7-3 compares Base Case assumptions for container performance following penetration of the copper barrier with what is likely to occur in reality.

Specifically:

- The steel inner container is assumed to be breached immediately upon penetration of the copper barrier. In reality, it could take a minimum of 140,000 additional years (and more likely more than 1 million years) before corrosion sufficient to breach the inner container occurs. The actual length of time would depend on the thickness of the steel barrier at the location of the copper defect and on the steel corrosion rate. The steel corrosion rate in turn depends on the availability of carbonate in the groundwater (see Chapter 5).
- The interior of the container is assumed to fill with water immediately upon penetration of the copper barrier. In reality, it could take many tens of thousands of years before significant quantities of water could pass through the bentonite buffer and enter the container once the steel barrier is penetrated. There could be a further delay due to the generation of gas within the container that could also inhibit water ingress. This is in addition to the time taken to penetrate the steel container discussed above.
- The zirconium fuel sheaths are assumed to not prevent water from coming into contact with the fuel. In reality, many fuel sheaths may be intact when the fuel bundles are placed in the repository, as Zircaloy is a durable metal. As long as the fuel sheaths remain intact, there will be no contaminant release from fuel elements even if the container fills with water. While this may further delay the time at which water contacts the fuel pellets, the likelihood of local hydride related cracking at longer times cannot be easily quantified so no credit is taken for the fuel sheath.
- The entire instant release source term (Section 7.5.2.1) is released immediately upon water contacting the fuel, which is assumed to occur as soon as the container is breached, which in turn is assumed to occur immediately after penetration of the copper barrier. In reality, there will be no instant release until the steel inner shell and Zr fuel sheaths are penetrated

and significant amounts of water contact the fuel. Even then, the instant release would depend on the number of fuel elements exposed to water, the power history of those elements, the fraction of contaminants that have migrated to cracks and grain boundaries, and the fraction of those cracks and grain boundaries that are initially exposed to water. Due to these many variables, a conservative value is adopted in the Base Case.

- A radiolysis-driven fuel dissolution rate is assumed, which allows congruent release of the remaining radionuclides over time. In reality, there is emerging evidence that shows small amounts of dissolved hydrogen can slow down, and even stop the fuel matrix from undergoing radiolysis driven dissolution. If such dissolution does not occur, there is essentially no contaminant release from the fuel matrix other than the instant release source term.
- It is assumed there are no corrosion products present. In reality, corrosion products would accumulate in the penetration and inside the container, thereby providing additional resistance to water and contaminant migration. This will slow down the rate at which contaminants can escape the container; however, because this is difficult to quantify no credit for this behaviour is taken in the Base Case.
- The container itself is assumed to present no resistance to contaminant migration immediately upon penetration of the copper barrier. In reality, even though the container is assumed penetrated, the size of the penetration will be small compared to the size of the container. It could take at least another 120,000 years after the steel shell is breached (and potentially much longer) for the container walls to corrode from the inside to the extent that the container itself no longer presents a resistance to contaminant transport.

Dose Related Assumptions:

The Base Case assumptions are adopted to ensure the highest potential dose rate is calculated, with the intention being that the dose rate to people exhibiting more realistic behaviours or in alternate exposure situations will always be substantially less.

Specifically:

- A self-sufficient farming family is unknowingly living and growing their own food on top of the repository. In reality, given the small footprint and the potential for a crystalline site to be remote from population centres, it is possible that no-one will be living in exactly this location. A greater distance means more opportunity for dilution and dispersion of contaminants leading to lower doses. Furthermore, the Canadian Shield is not generally suitable for self-sufficient farming.
- The family uses a deep well to obtain their drinking water. Given that there are many surface water bodies in the Canadian Shield, it is possible that a well would not be used. Contaminant concentrations in streams and lakes would be much lower than in the well due to greater dilution.
- The drinking water well is assumed to be fairly deep, about 100 m. In reality, it is unlikely that a family would use such a deep well. Current practice is to use more shallow wells for drinking water. Shallow wells allow for lengthier contaminant transport times with associated increased dispersion and dilution in the geosphere.
- The drinking water well is assumed to be in the location that maximizes the uptake of contaminants escaping the repository. In reality, the well would be in a random location with

respect to the hypothetical defective containers. Depending on where the well is actually located, it's possible that no contaminants would be captured by the well.

- The defective containers are assumed to all be clustered in the location that results in the greatest possible contaminant transport to the well. While the defective containers are likely to be randomly distributed, clustering may occur following a temporary lapse of quality control. Even if the containers were clustered, the likelihood that they would be in the location that results in the greatest transport to the well would be low.

Many other assumptions not listed in Table 7-3 are also required before the entire Base Case can be fully defined. For example, values for such things as fuel burnup, radionuclide inventories, fuel dissolution rate, material and transport properties, the geology, the location of surface features, human characteristics and so on, are all required. Most of these assumptions are described in other sections of this report, with more detailed information available in Gobien et al. (2016). The key assumptions for the Base Case are:

- Geosphere properties as per Chapter 2;
- Used fuel inventories as per Chapter 3;
- Repository design as per Chapter 4;
- 10 containers with large defects in the copper coating are present in the repository. The copper coating is penetrated in the first container at 1000 years, with one additional container failing every 100,000 years;
- No other container failures occur;
- Constant temperate climate and steady-state groundwater flow;
- A self-sufficient farming family is unknowingly living on top of the repository, growing crops and raising livestock;
- Drinking and irrigation water for the family is obtained from a 100 m deep well. The well / defective container locations are such that contaminant release to the well is maximized;
- The well is pumped at a rate of 911 m^3/a. This is sufficient for drinking water and irrigation of household crops;
- Input parameters with uncertainty and variability represented by probability distributions are set to either the most probable value (when there is one) or to the median value otherwise.

7.2.2.2 Sensitivity Studies to Illustrate the Effects of Well Assumptions

The Base Case described above in Section 7.2.2.1 assumes the presence of a continuously operating well pumping at a rate of 911 m^3/a throughout the entire one million year period of interest. The sensitivity cases described below are selected to illustrate the sensitivity of Base Case results to some of the well assumptions. The cases considered are:

- No well;
- Intermittent well operation; and
- Random well location.

These cases are further described in Table 7-4.

Table 7-4: Sensitivity Cases to Illustrate the Effects of Well Assumptions

	Base Case Assumption*	Sensitivity Case Assumption	Rationale
Illustrative Cases	Deep well in the location that maximizes uptake of contaminants. The well pumps continuously at a rate of 911 m^3/a throughout the entire one million year period of interest.	No well. The defective containers are in the same location as in the Base Case.	If there are adequate surface sources of water, it is unlikely that a deep well will be used.
		Intermittent well operation. The defective containers are in the same location as in the Base Case.	If a well is used, it will not be pumped continuously over a one million year period.
		Random well location. The defective containers are in the same location as in the Base Case.	If a well is used, it is not likely to be in the location that maximizes contaminant uptake from all of the defective containers in the repository.

Note: * A detailed description of the input data is available in Gobien et al. (2016).

7.2.2.3 Sensitivity Studies to Illustrate the Effect of Deviations in Anticipated Barrier Performance for the Base Case

The Base Case assumes fabrication failures with coincident quality assurance system failures leading to a small number of containers that do not meet design specification being unknowingly placed in the repository.

Coincident failures of this type could also affect other repository components. For example, off-specification material could unknowingly be used in the fabrication of buffer box bentonite, placement room spacer blocks or bentonite pellets. Placement rooms and access tunnels could exceed their design dimensions because blasting removes too much rock in some places. Off-specification material could unknowingly be used in the construction of repository tunnel seals and repository shaft seals.

The principal end result of such failures would be either (a) nothing adverse happens, or (b) the off-specification component eventually leads to early container failure(s). Studies are underway to determine the likelihood and number of repository components that could potentially be out of compliance with their design requirements; however, the results of this work are not presently available. In the meantime, for this postclosure safety assessment, fabrication and quality assurance system failures that lead to container failure are assumed to be covered by the Base Case and relevant sensitivity cases. The Base Case assumes 10 containers fail at various times in the first one million years following repository closure.

Quality assurance failures leading to extreme events such as degraded / ineffective repository seals or degraded / ineffective shaft seals are deemed not credible for the Normal Evolution Scenario. While the sheer number of some repository components (e.g., about 100,000 containers) creates opportunity for unknowingly placing associated non-compliant material in the repository, this opportunity does not exist to the same extent for components present in much reduced numbers, such as for the repository seals and shaft seals. Enhanced vigilance is also anticipated when fabricating and installing these seals to ensure they meet specification. For this reason, degraded repository seals are considered Disruptive Events and described in Section 7.2.3.

The following sensitivity cases are examined to illustrate the effect of deviations in barrier performance on the Base Case:

Fuel Barrier:

- Fuel dissolution rate increased by a factor of 10; and
- Instant release fractions for fuel contaminants set to 0.10 for all radionuclides (i.e., 10% of the entire inventory is instantly released).

Zircaloy Sheath Barrier:

No credit is taken in the postclosure safety assessment for the presence of the Zircaloy fuel sheath as a barrier to contaminant release from the fuel. However, because the sheath itself contains contaminants and because the screening analysis (Section 7.6) identifies some of these contaminants as potentially important, the following Zircaloy specific sensitivity cases are simulated:

- Zircaloy dissolution rate increased by a factor of 10; and
- Instant release fractions for Zircaloy sheath contaminants set to 0.10 for all contaminants.

Container Barrier:

- All 10 containers fail at 1000 years;
- 50 containers fail at 1000 years;
- 50 and 1000 containers fail at 10,000 years;
- Low sorption in the engineered barrier materials with coincident high solubility limits in the container; and
- No solubility limits in the container.

Buffer and Backfill and Seals Barrier:

- Hydraulic conductivities of all materials (including tunnel backfill, concrete and all shaft materials) increased by a factor of 10;
- Low sorption in the engineered barrier materials with coincident high solubility limits in the container; and
- No sorption in the near field.

Geosphere Barrier:

- Hydraulic conductivities increased by a factor of 10;
- Hydraulic conductivities decreased by a factor of 10;
- Hydraulic conductivity in the excavation damaged zones (EDZ) increased by a factor of 10;
- Fracture standoff distance reduced from 100 m to 50 m, 25 m and 10 m;
- Sorption parameters set to two standard deviations below the mean; and
- Dispersivity increased and decreased by a factor of 5.

These sensitivity cases are shown in Table 7-5. The table includes a description of the variation from the Base Case assumptions for each case together with a brief rationale for the case selection.

To provide an indication of repository response allowing for uncertainty in multiple parameters, two types of probabilistic sensitivity studies are also performed. In these simulations, random sampling is used to simultaneously vary input parameters for which probability distribution functions are available. Radionuclide release and transport parameters are varied with the fixed reference geosphere adopted in the System Model (Section 7.8).

The specific probabilistic cases are:

- Number, locations and failure times for defective containers fixed at their Base Case values, with all other available parameters varied; and
- Number, locations and failure times for the defective containers varied, with all other parameters maintained at their Base Case values.

These cases are also described in Table 7-5.

Table 7-5: Sensitivity Cases to Illustrate the Effect of Deviations in Anticipated Barrier Performance for the Base Case

Parameter	Base Case Assumption*	Sensitivity Case Assumption	Rationale
Fuel Barrier			
Fuel Dissolution Rate	Generated via a model that takes into account the effects of radiolysis and chemical dissolution. No credit is taken for the effect of H_2 gas on suppressing dissolution. With this model, ~19% of the fuel dissolves in the first one million years for a burnup of 220 MWh/kgU, and ~21% dissolves for a burnup of 280 MWh/kgU.	The dissolution rate is increased by a factor of 10. With this increase, all of the used fuel dissolves in the first one million years.	The fuel is an important barrier to the release of radionuclides because most radionuclides are contained within the fuel matrix. As the fuel dissolves in the long term these radionuclides become available for transport. The factor of 10 increase roughly corresponds to the 95th percentile value.
Fuel Instant Release Fractions	Instant release fractions are as described in Section 7.5.2. Most radionuclides have no instant release. Instant release fractions for selected radionuclides are: C = 0.027 Ca = 0.0 Cl = 0.06 Cs = 0.04 I = 0.04 Se = 0.006 Np, Pu, Th, U = 0.00	Instant release fractions for all fuel radionuclides are set to 0.10.	Some radionuclides in the used fuel are present initially in the fuel sheath gap and grain boundaries and are therefore available for release early after contact with water. This fraction of the inventory is referred to as the instant release fraction. Assigning a high instant release fraction to all radionuclides (including actinides) ensures the results are bounding as well as providing information on the importance of this term to the overall dose consequence.
Fuel Sheath Barrier			
Zircaloy Dissolution Rate	The fuel sheath itself contains some radionuclides (notably C-14 and Cl-36), which are released as the Zircaloy corrodes.	The dissolution rate of the Zircaloy fuel sheath is increased by a factor of 10.	This is a companion to the fuel dissolution case described above; however, the focus of this case is on radiological contaminants in the Zircaloy fuel sheath.

Parameter	Base Case Assumption*	Sensitivity Case Assumption	Rationale
	Zircaloy dissolution is determined from the corrosion rate of Zr in water (~5 nm/a) and the surface area of Zr in contact with water.		
Zircaloy Instant Release Fractions	C = 0.021 Cl = 0	Instant release fractions for all Zircaloy radionuclides are set to 0.10.	This is a companion to the fuel instant release case described above; however, the focus of this case is on radiological contaminants in the Zircaloy fuel sheath.
Container Barrier			
Container Failure Times	The first container fails after 1000 years, with subsequent containers failing sequentially every 100,000 years.	All 10 containers fail at 1000 years.	This case illustrates repository performance if multiple container failures occur early and all at the same time. At early times, the fuel dissolution rate and the amount of radionuclides present are both greater than for later times. As per the information in Table 7-3, a container failure time of 1000 years is conservative.
Number of Failed Containers	10 containers fail, with the first container failing after 1000 years and subsequent containers failing sequentially every 100,000 years. All failed containers are clustered in the location that yields the highest dose consequence.	50 containers fail at 1000 years. All failed containers are clustered in the location that yields the highest dose consequence.	Because the container manufacturing and inspection processes are still being developed, there is uncertainty in the number of defective containers that could unknowingly be placed in the repository. This case illustrates repository performance for a greater number of defective containers than assumed in the Base Case. For conservatism, and to allow scaling of results from other cases, all 50 containers are assumed to fail early and to be located in the

Parameter	Base Case Assumption*	Sensitivity Case Assumption	Rationale
			position that yields the highest dose consequence. As per the information in Table 7-3, a container failure time of 1000 years is conservative.
Location of Failed Containers	10 containers fail, with the first container failing after 1000 years and subsequent containers failing sequentially every 100,000 years. All failed containers are clustered in the location that yields the greatest dose consequence.	Two cases are considered: i) 50 containers fail at 10,000 years, with the containers uniformly distributed across the repository. ii) 1000 containers fail at 10,000 years, with the containers uniformly distributed across the repository.	If there are larger numbers of defective containers, it is highly unlikely that they will all be located in the position that yields the highest dose consequence. These cases illustrate repository behaviour for larger numbers of defective containers, but with the defective containers assumed to be uniformly distributed across the repository. For simplicity, a 10,000 year failure time is assumed to allow scaling of results from other cases. As per the information in Table 7-3, a container failure time of 10,000 years is conservative.
Low Sorption in the EBS Materials with Coincident High Solubility Limits in the Container	Sorption values for engineered barrier materials are described in Section 7.5.2.6. Solubility limits are as described in Section 7.5.2.4.	“Low” / “High” means the sorption values are set to their respective lower bounds and the solubility limits are set to two standard deviations in the conservative direction.	This case determines the effect of simultaneous pessimistic assumptions affecting the solubility in the container interior and retention in the clay based engineered barriers. This case is identical to that discussed in the Buffer, Backfill and Seals Barrier section of this table. It is included here because this case examines both container assumptions and near-field assumptions.

Parameter	Base Case Assumption*	Sensitivity Case Assumption	Rationale
Solubility Limits	Solubility limits are determined externally from thermodynamic data and specified as input. Solubility limits are as described in Section 7.5.2.4. Solubility limits (mol/m^3) for selected radionuclides are: C = 0.83 Se = 1.3×10^{-5} Np = 1.1×10^{-6} Pu = 9.1×10^{-5} Th = 2.5×10^{-5} U = 3.5×10^{-6} Ca, Cl, Cs, I = no limit The solubility limits are increased in the Base Case by a factor of ten above the values listed here to account for uncertainties in groundwater chemistry and thermodynamic data.	Solubility limits for all radionuclides are set to 2000 mol/m^3. This is equivalent to having no solubility limit since the limit is never reached.	The concentration of a dissolved radionuclide is one of the parameters that can affect the rate of radionuclide release from the defective container. While some radionuclides are highly soluble (e.g., I and Cl), others are not (e.g., Pu and U). Some side species such as organics or colloids may make some radionuclides more soluble than would be expected from straight thermodynamics. Removal of all solubility limits provides information on the importance of this parameter to the overall dose consequence.
Buffer, Backfill and Seals (i.e., the Near-Field) Barrier			
Hydraulic Conductivity of EBS Materials	9×10^{-11} m/s for dense backfill 1×10^{-10} m/s for concrete 5×10^{-13} m/s for bentonite/sand shaft seal 1×10^{-12} m/s for asphalt shaft seal 6×10^{-14} m/s for HCB 4×10^{-13} m/s for gap fill 1×10^{-13} m/s for weighted average These are the reference values at 20ºC. Values are temperature corrected to 85ºC.	Hydraulic conductivities increased by a factor of 10 for all EBS materials. For placement room bentonite, this is roughly equivalent to the upper bound of the measured variations.	EBS materials, especially the HCB bentonite that forms the buffer box, is an important barrier to advective flow. The case illustrates the effect of variation in hydraulic conductivity on barrier performance.

Parameter	Base Case Assumption*	Sensitivity Case Assumption	Rationale
Low Sorption in the EBS Materials with Coincident High Solubility Limits in the Container	Sorption values for engineered barrier materials are described in Section 7.5.2.6. Solubility limits are as described in Section 7.5.2.4.	“Low” / “High” means the sorption values are set to their respective lower bounds and the solubility limits are set to two sigma values in the conservative direction.	This case determines the effect of simultaneous pessimistic assumptions affecting the solubility in the container interior and retention in the clay based engineered barriers. This case is identical to that discussed in the Container Barrier section of this table. It is included here because this case examines both container assumptions and near-field assumptions.
Sorption in the EBS	Use of linear equilibrium sorption model. Sorption coefficients from SKB reviews have been adopted where similar materials and conditions exist. Some elements are non-sorbing (e.g., Cl and I) while others are highly sorbing in the reducing environment (e.g., Np, Pu, Th, and U). Sorption values for engineered barrier materials are described in Section 7.5.2.6.	Sorption coefficients for all near field barrier components including the shafts are set to zero. Sorption coefficients in the geosphere are maintained at their Base Case values.	The clay-based seals have a high surface area and can sorb radionuclides released into the groundwater from the containers. Colloid transport within the dense clay seals is not expected, so it is not included in the Base Case values. Sorption on iron oxides, from corrosion of the steel inner vessel of the container is conservatively neglected. Setting the sorption coefficients to zero results in an unrealistic, yet conservative, case that provides information on the relative importance of sorption in the EBS.
Geosphere Barrier			
Hydraulic Conductivity	Base Case hydraulic conductivity profile as defined in Chapter 2. Zone 1 (10 – 150 m) = $2x10^{-9}$ m/s Zone 2 (150 – 700 m) = $4x10^{-11}$ m/s Zone 3 (700 – 1500 m) = $1x10^{-11}$ m/s	A factor of 10 increase and a factor of 10 decrease relative to the Base Case. *Sensitivity 1:* A factor of 10 increase in hydraulic conductivity:	Geosphere hydraulic conductivity is an important parameter controlling groundwater flow and advective radionuclide transport in the crystalline rock mass. These sensitivity cases cover a range of conductivities. The higher conductivity case corresponds to rock mass conditions under

Parameter	Base Case Assumption*	Sensitivity Case Assumption	Rationale
		Zone 1 (10 – 150 m) = 2×10^{-8} m/s Zone 2 (150 – 700 m) = 4×10^{-10} m/s Zone 3 (700 – 1500 m) = 1×10^{-10} m/s *Sensitivity 2:* A factor of 10 decrease in hydraulic conductivity: Zone 1 (10 – 150 m) = 2×10^{-10} m/s Zone 2 (150 – 700 m) = 4×10^{-12} m/s Zone 3 (700 – 1500 m) = 1×10^{-12}	which advective transport could be important, and therefore tests potential limits for acceptability.
Hydraulic Conductivity of EDZ	The excavation damaged zones are defined with higher hydraulic conductivity than the surrounding rock. Hydraulic conductivity (K/K_{rock}) for selected areas are: *Placement Rooms, Central Access, Panel Access and Perimeter Tunnels:* Inner EDZ = 100 Seal EDZ = 100 Outer EDZ = 10 *Shafts:* Inner EDZ = 100 Outer EDZ = 10 (See Chapter 5)	Hydraulic conductivity of all excavation damaged zones increased by a factor of 10.	The excavation damaged zone is a region of rock damaged during the construction process; potential thermal damage is also taken into account. The EDZ has higher hydraulic conductivity than the surrounding intact rock and could be a pathway for radionuclide transport. Increasing the hydraulic conductivity provides information on the importance of these damage zones to the transport and subsequent release of radionuclides to the surface.

Parameter	Base Case Assumption*	Sensitivity Case Assumption	Rationale
Fracture Location	Fracture intersections with the perimeter drifts and central access tunnels are identified, and repository panels are positioned such that there is 100 m (plus an additional 10 m to account for position uncertainty) from a line connecting the intersection points. For the Base Case, this results in the end of the placement room containing the cluster of defective containers being 167 m from the actual fracture. This extra distance occurs because the fracture 'bends' to the other side of the repository at the location of the room.	Fracture standoff distance decreased to 50 m, 25 m and 10 m. This reduces the distance between the fracture and the end of the placement room containing the defective containers. For the 50 m case, the placement room is 117 m from the actual fracture, for the 25 m case the room is 92 m and for the 10 m case the room is 77 m from the fracture.	The minimum thickness of rock between the repository boundary and a major water conducting feature is a key barrier. A minimum distance of 100 m is currently contemplated for fractures the size of the one intersecting the repository footprint. Reducing this value illustrates the importance of the standoff location to this safety assessment.
Sorption in the Geosphere	Sorption values are described in Section 7.5.2.6. Use of linear equilibrium sorption model. Granite sorption coefficients from the SKB review. Some elements are non-sorbing (e.g., Cl and I) while others are highly sorbing in the saline reducing environment (e.g., Np, Th, and U).	The geosphere sorption coefficients for all elements are set to two standard deviations below the mean. All other near field sorption coefficients (i.e., buffer, backfill and seals) are maintained at their Base Case values.	Radionuclides can be sorbed onto the surfaces of the host rock minerals, thereby retarding their transport to the surface. Setting the sorption coefficients to low values provides information on the relative importance of sorption in the geosphere.
Dispersivity	The Base Case adopts a constant longitudinal dispersivity of 20 m. This is equivalent to 5% of the minimum direct line distance between the repository and the bottom of the well or 1% of the roughly 2000 m transport pathway from the defective containers to the well).	Two sensitivity cases are considered: i) The first increases the dispersivity by a factor of 5 resulting in 100 m longitudinal dispersivity in intact rock and 50 m in EBS materials ii) The second decreases the dispersivity by a factor of 5, to	The dispersivity parameter approximates the spreading of a contaminant plume due to the inherent variability of the local rock and fracture permeability. As a general 'rule of thumb', dispersivity estimates vary from a few percent to 10% of the total path length. A low value of 20 m is adopted in the Base Case because this results in greater plume concentrations and greater transport to the well.

Parameter	Base Case Assumption*	Sensitivity Case Assumption	Rationale
	The transverse dispersivity is defined as 10% of the longitudinal dispersivity (or 2 m). Dispersivity within engineered sealing materials, which are more homogenous and present substantially less variability than rock, is assumed to be 10 m.	4 m in intact rock, and 2 m in EBS materials.	The sensitivity studies explore the effect of variations in this parameter on dose consequences.
Probabilistic Assessment of Uncertainty			
Container Parameters Fixed	There are 10 defective containers all clustered in the location that maximizes contaminant uptake to the well. The containers have defects in their copper coating such that breaching of the first container occurs after 1000 years with breaching of the remaining containers occurring sequentially every 100,000 years. The well is in the location that maximizes contaminant uptake from the clustered containers. Input parameters represented by probability distributions are set to either the most probable value (when there is one) or to the median value otherwise.	The number, location and failure times of the 10 defective containers are identical to those in Base Case. All other available input parameters represented by probability distributions are varied. An important caveat is that these probabilistic simulations are performed in the fixed geosphere of the System Model.	Many of the modelling parameters are uncertain or have a natural degree of variability and as such are more generally characterized by a range or distribution of values. Varying all parameters simultaneously while maintaining the container locations and failure times provides information on the overall uncertainty in the Base Case.
Container Parameters Vary	There are 10 defective containers all clustered in the location that maximizes contaminant uptake to the well. The containers have defects in their copper coating such that	The number, location, and failure times of the containers are varied. No other parameters are varied.	Varying the number, location and failure times of the containers while maintaining all other parameters constant provides information how variations in these

Parameter	Base Case Assumption*	Sensitivity Case Assumption	Rationale
	breaching of the first container occurs after 1000 years with breaching of the remaining containers occurring sequentially every 100,000 years. The well is in the location that maximizes contaminant uptake from the clustered containers. Input parameters represented by probability distributions are set to either the most probable value (when there is one) or to the median value otherwise.	An important caveat is that these probabilistic simulations are performed in the fixed geosphere of the System Model.	parameters could affect the Base Case results.

Note: * A detailed description of the input data is available in Gobien et al. (2016).

7.2.2.4 Sensitivity Studies to Illustrate the Effect of Modelling Attributes and Numeric Parameters on the Base Case

Some additional sensitivity cases have been simulated to illustrate the effect of differing modelling approaches and numeric parameters on the Base Case results. These cases are discussed in Table 7-6 and listed below:

- Increased spatial resolution to confirm convergence for the 3D groundwater and transport models;
- Increased and decreased number of time steps to confirm model results are not sensitive to temporal resolution; and
- Discrete Fracture Network modelling in lieu of Equivalent Porous Media.

Table 7-6: Modelling Attributes and Numeric Parameter Sensitivity Cases

Modelling Attribute or Parameter	Base Case Assumption	Sensitivity Case Assumption	Rationale
Spatial Resolution and Time Step Size	User defined in the Base Case.	Spatial resolution in the finite element model is increased by over 10-fold.	Increasing the spatial resolution provides information on whether the model results are numerically converged.
Time Step Size	User defined in the Base Case.	Time step control in the finite element model is adjusted to change the number of time steps, with the changes resulting in a factor of 2 decrease in one simulation and a factor of 3 increase in another.	Changing the number of time steps provides information on whether the model results are numerically converged.
Discrete Fracture Network	Equivalent Porous Media approach applied in the Base Case.	Element faces that are closest to or intersected by the input fractures are specified as fracture faces and represented as 2D planar elements with property assignments consistent with the fracture definition. All other model features are unchanged from the Base Case.	Discrete Fracture Network modelling (DFN) is more physically representative but is also more computationally demanding than the Equivalent Porous Medium (EPM) approach. This sensitivity case tests whether DFN modelling would be expected to yield significant differences in model results.

7.2.2.5 Sensitivity Study to Illustrate the Effect of Glaciation

During past glacial cycles, much of Canada has been covered by kilometre-thick ice sheets. The main factors that initiated these cycles (i.e., solar insolation variation due to Earth orbital dynamics and the location and size of the continents) are still present. Current levels of greenhouse gases in the atmosphere may delay the onset of the next glaciation (Berger and Loutre 2002); however, glacial cycles are expected to reassert themselves in time period of interest to this postclosure safety assessment.

The scenario identification discussion in Chapter 6 identifies glaciation as an important external factor influencing the behaviour of the Normal Evolution Scenario; however, for this postclosure safety assessment the dose assessment is performed for a constant temperate climate. The purpose of this sensitivity study is to discuss the likely effects of glaciation on the calculated dose rates.

The effect of glaciation is discussed quantitatively based on the analysis of a glaciation scenario carried out as part of the Third Case Study (Garisto et al. 2010; Walsh and Avis 2010). The important features of this glaciation study are described and its applicability to the current study is discussed.

7.2.3 Analysis Cases for Disruptive Event Scenarios

Disruptive Event Scenarios postulate the occurrence of unlikely events leading to possible penetration of barriers and abnormal loss of containment.

Chapter 6 describes the set of Disruptive Scenarios applicable to the conceptual design and hypothetical geosphere in this study. These have been identified through consideration of the features, events and processes that are important to the repository system, and through consideration of the key barriers. The scenarios are:

- Inadvertent Human Intrusion;
- All Containers Fail;
- Repository Seals Failure;
- Poorly Sealed Borehole;
- Undetected Fault;
- Container Failure[1]; and
- Partially Sealed Repository.

The first three scenarios are within the scope of this illustrative safety assessment. Table 7-7 describes each of these three scenarios and includes a description of the parameters changed

[1] This considers delayed but substantive failure of a few containers due to unexpected in-situ conditions, and is different from the Normal Evolution Scenario which considers a defect unknowingly present in some containers as the initiating event.

from the Base Case together with the rationale for the scenario selection. It is recognized that for an actual site, the full set of scenarios would need to be evaluated.

The consequences of gas generation caused by decomposition of organics and by corrosion of steel is assessed for the All Containers Fail Scenario.

The Poorly Sealed Borehole scenario is a Disruptive Scenario because it creates a pathway that bypasses the low-permeability geosphere. However, as long as the boreholes are kept sufficiently far from the repository underground structures, they are unlikely to be important due to the small size of the borehole and the limits of diffusive transport. It would be analyzed as part of a real site, when the borehole distances are known; however, the consequences are expected to be low.

With respect to the Undetected Fault Scenario, it is anticipated that any large fractures intercepting the repository not identified during site characterization would be discovered during construction such that appropriate mitigating measures could be taken. These measures could include possible redesign of the repository layout to avoid large transmissive features.

Although a detailed analysis of the Container Failure Scenario is outside the scope of this study, the peak dose arising from this event is anticipated to be significantly less than that associated with the All Containers Fail Scenario due to the much reduced number of affected containers.

The Improperly Sealed Repository scenario considers the consequences if the repository is abandoned and the shafts are not sealed. It implies a near-future loss-of-society.

All scenarios are analysed with deterministic methods since the basic parameters defining the scenarios are chosen conservatively.

Table 7-7: Analysis Cases for Disruptive Scenarios

Disruptive	Normal Evolution Scenario Base Case Assumption*	Disruptive Case Assumption	Rationale
Inadvertent Human Intrusion	No intrusion.	The engineered and natural barriers are bypassed via the drilling of a borehole into the repository. The borehole intersects a used fuel container with 220 MWh/kgU burnup fuel and used fuel material is brought to the surface. Two stylized events are considered: i) The hazard is identified and the site is vacated (and subsequently mitigated) after 2 days; and ii) The hazard is not identified and the site is vacated after 14 days. The effects of damaging a container with higher (280 MWh/kgU) burnup fuel on the first event are also addressed. The variant case, in which the borehole thereafter remains open, is not considered.	Institutional controls and knowledge of the repository can be lost in the future. This scenario examines the potential consequences to the drill crew and a future resident on the site.
All Containers Fail	There are 10 defective containers all clustered in the location that maximizes contaminant uptake to the well. The containers have defects in their copper coating such that breaching of the first container occurs after 1000 years with the remaining containers failing at a rate of one additional container every 100,000 years.	*Baseline Case* All containers fail 60,000 years after repository closure and no containers fail prior to this time. *Extreme Case* Identical to the above, except the time of container failure is 10,000 years.	The containers are anticipated to last for well in excess of one million years, based on the copper corrosion barrier, sturdy mechanical design and favourable site attributes, including geochemical stability (see Chapter 5). This scenario considers common cause failure of all containers. The Baseline Case corresponds to the likely earliest timeframe for an ice sheet to cover the site, and it is assumed that some unanticipated effect of the ice sheet might cause failure, such as

Disruptive	Normal Evolution Scenario Base Case Assumption*	Disruptive Case Assumption	Rationale
	The well is in the location that maximizes contaminant uptake from the clustered containers.		beyond-design ice thickness and mechanical loading or unexpected changes in groundwater chemistry. The Extreme Case with failure at 10,000 years provides information on the sensitivity of results to the assumed failure time.
Repository Seals Failure	The shaft is filled with a combination of bentonite / sand (70:30), concrete and asphalt with the following hydraulic conductivities (m/s): Bentonite / Sand = 1.6×10^{-11} Concrete = 1.0×10^{-10} Asphalt = 1.0×10^{-12} The fracture seal is a combination of highly compacted bentonite (HCB), concrete and dense backfill with the following hydraulic conductivities (m/s): Dense Backfill = 9×10^{-11} Concrete = 1.0×10^{-10} HCB = 6.0×10^{-14}	The shaft and fracture seals are treated separately. For the shaft seal case, there is a Baseline and Extreme Case, and for the fracture seal case there is a Baseline Case. *Baseline Case* The hydraulic conductivity of seal materials is set to 10^{-9} m/s from the time of repository closure. *Extreme Case* The hydraulic conductivity of all shaft seal materials is further increased by an additional factor of 100. A hydraulic conductivity of 10^{-7} m/s is about equivalent to that of fine silt and sand. The well and defective container locations are maintained at their Base Case locations. A sensitivity study for the shaft seal case considers the effect of having the well and defective containers positioned more closely to the shaft.	This scenario examines the effects of significant degradation in shaft and / fracture seals. For conservatism, this degradation is assumed to occur at the time of repository closure.

Note: * A detailed description of the input data is available in Gobien et al. (2016).

7.2.4 Analysis Exclusions

As noted earlier in Section 7.2, the scope of work is defined for consistency with the objectives of this postclosure safety assessment. As such, the analysis cases are limited to those needed to provide a demonstration of the overall approach and to those needed to reach preliminary conclusions for the hypothetical site.

This section lists scope items that do not appear in this report but which might otherwise be included in a postclosure safety assessment for a licence submission. These are:

- Fracture Uncertainty. In a crystalline rock site, there will be some uncertainty regarding the existence (and location) of fractures. These uncertainties can be reduced through site selection and repository location and depth, and any residual uncertainties can be handled through the adoption of conservative assumptions and / or Disruptive Event Scenarios (such as the Undetected Fault Scenario) within the postclosure analysis.
- Variable Climate Analysis. The effects of permafrost and glaciation are not explicitly determined in this assessment. Instead, the results of a glaciation study previously performed for a less permeable crystalline rock geosphere is described and inferences are drawn about the likely effects of glaciation on the dose assessment for the Normal Evolution Scenario.
- Additional Disruptive Scenarios. As described in Section 7.2.3, a reduced number of Disruptive Event Scenarios is evaluated here. However, the full list of Disruptive Scenarios anticipated for a licence submission is identified.
- Alternative Critical Groups. Other potential critical groups may be considered for a candidate site depending on communities nearby that could be interested in potential impacts - for example, downstream communities and / or First Nation lifestyles. This would be discussed with people in the area.

7.3 Conceptual Model

This section describes the conceptual model associated with key processes occurring in the repository with defective containers present. The presence of defective containers leads to releases of contaminants that eventually enter the biosphere. These biosphere releases have potential impacts on humans and on non-human biota living nearby.

The conceptual model describes the release, migration and fate of contaminants through the identification of key features, events and processes. The model is used to guide the development and application of the computer codes used in the postclosure safety assessment.

Figure 7-2 illustrates the general conceptual model. There are four main elements:

- The used fuel containers;
- The engineered barrier system;
- The geosphere; and
- The biosphere.

Each element is discussed below the figure. The discussion is aligned for consistency with the Base Case of the Normal Evolution Scenario which, as noted in Section 7.2.2.1, assumes a constant temperate climate.

For simplicity, the descriptions of conceptual models are given in terms of radionuclides but the models are also applied to simulate the behaviour of potentially hazardous chemical elements, except that for chemical elements there is no radioactive decay and in the biosphere there is no food chain and no dose rate calculations. Instead, protection of the environment is ascertained by comparison of calculated chemical element concentrations in various biosphere media to the criteria outlined in Table 7-1.

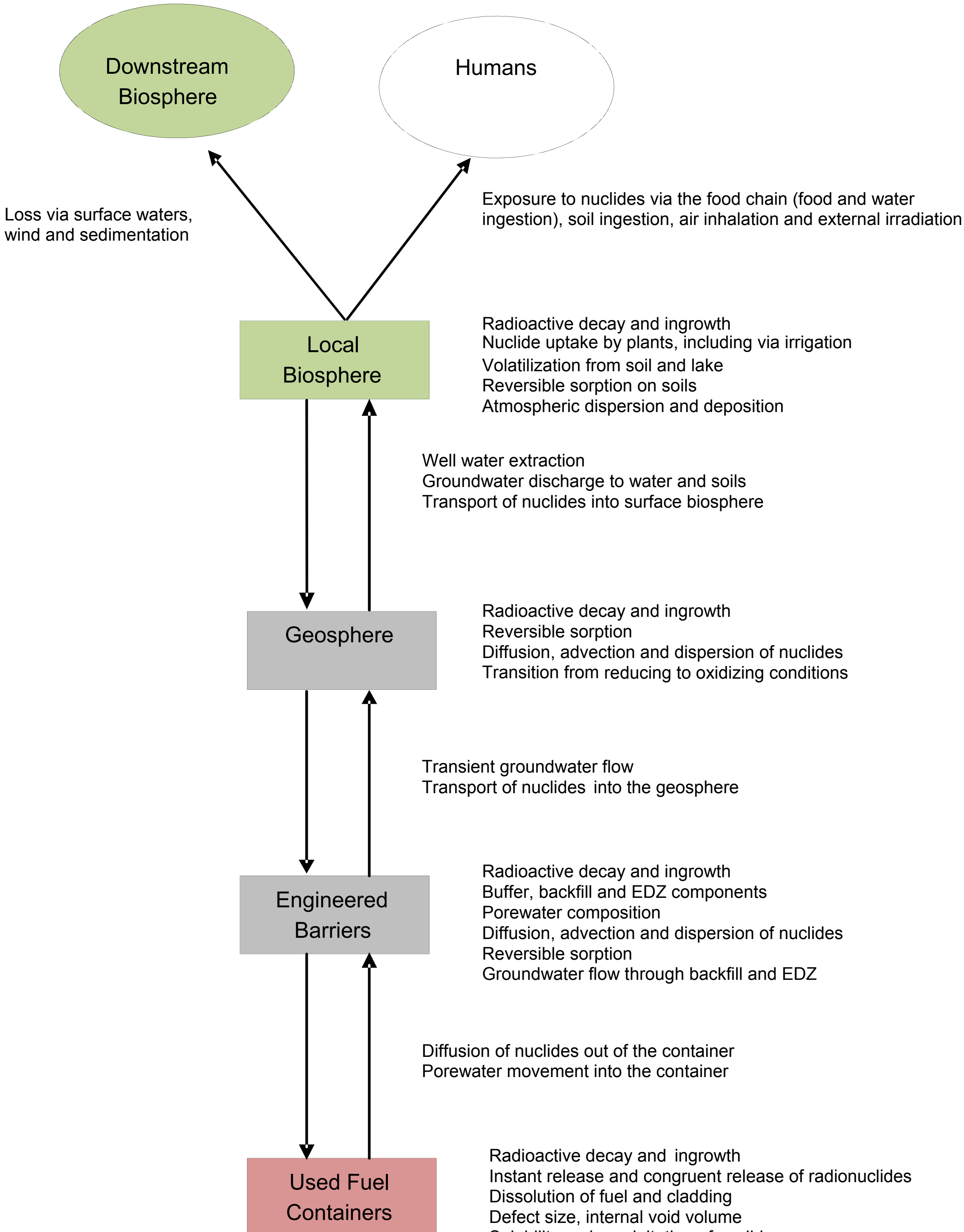

Figure 7-2: General Conceptual Model for Defective Containers

7.3.1 Used Fuel Containers

The principal fuel components and processes for the used fuel containers and waste form are shown in Figure 7-3.

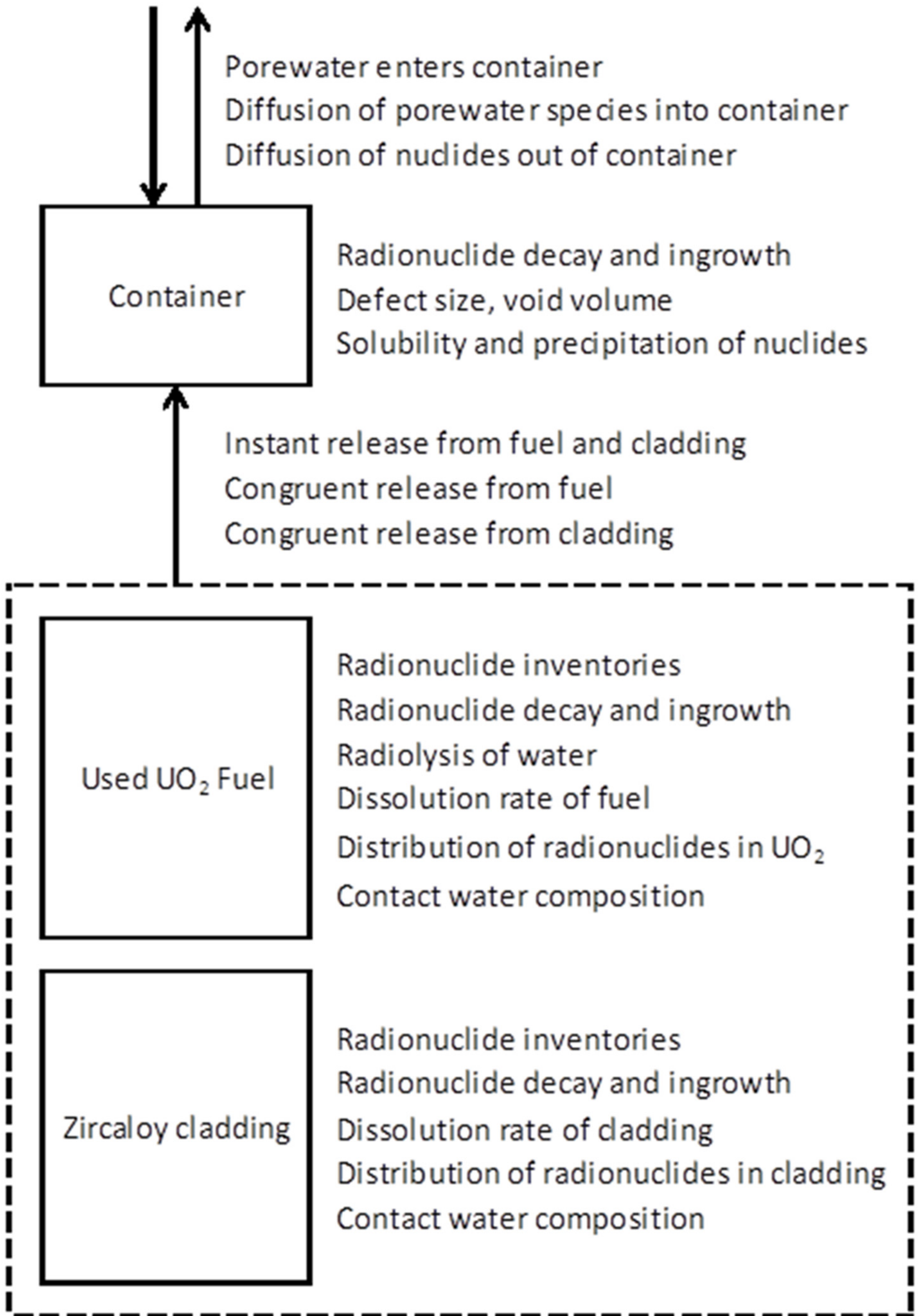

Figure 7-3: Conceptual Model for the Waste Form and Container

The container has a copper outer coating for corrosion protection and a steel inner vessel for structural support.

The inner steel vessel is not specifically included in the conceptual model, except that it is assumed to define the void volume inside the container. In practice, the steel components in any breached container would corrode, producing H_2 gas and iron oxides. The gas could delay water ingress into the container, and also substantially reduce the dissolution rate of the UO_2 fuel; however, this effect is conservatively ignored. Similarly, formation of iron oxides would provide a high surface area for adsorption of some of the radionuclides released from the fuel. These effects are also ignored.

For this conceptual repository and hypothetical geosphere, the temperature at the container surface reaches a peak value of about 84ºC 45 years after container placement, decreases to about 76ºC after 75 years, decreases slowly to about 44ºC at 10,000 years and reaches ambient conditions at around 100,000 years (Guo 2016). The temperature inside the container peaks at about 120ºC within 20 years after placement and then decreases with time (Guo 2015). For a real site, with a different repository design and a different geosphere, the temperatures could be different, but the loading of the container and / or repository design would be adjusted such that container surface temperature would not exceed 100 ºC.

The reference waste form is a standard CANDU 37-element fuel bundle with a burnup of either 220 MWh/kgU (for scenarios involving a large number of bundles) or 280 MWh/kgU (for scenarios involving a small number of bundles) and an average fuel power during operation of 455 kW, as discussed in Chapter 3. The repository holds 4.6 million bundles.

The waste form has two distinct components: the UO_2 fuel and the Zircaloy cladding. Releases of contaminants from these two waste forms are modelled separately.

After water enters the container, the Zircaloy cladding may prevent the water from contacting the fuel for some time. However, the cladding is neglected in the fuel dissolution model and it is assumed that water contacts all the fuel as soon as the container fills with water. The container is conservatively assumed to fill with water immediately after the container fails.

Contaminants within the UO_2 fuel are released by two mechanisms which operate on very different time scales (Grambow et al. 2010), as discussed below.

<u>Instant Release from Fuel</u>

Initially, there will be a comparatively rapid release of a small fraction (typically a few percent) of the inventory of a selected group of radionuclides that are either very soluble (such as C-14, Cl-35, Cs-137 and I-129) or gaseous, and that are residing in the fuel sheath gap or at grain boundaries which are easily and quickly accessed by water. This release process is referred to as “instant-release” and is modelled assuming a certain fraction of the radionuclide inventory in the fuel is released at the same time that water contacts the fuel.

Ferry et al. (2008) have shown that the instant release fractions do not change with time due to, for example, athermal diffusion of radionuclides induced by alpha-particle recoil displacements.

The instant release fractions used in this assessment are given in Section 7.5.2.1.

Fuel Dissolution

The second and slower release process comprises release of radionuclides from the UO_2 fuel matrix as the matrix itself corrodes or dissolves (called "congruent dissolution").

The alpha dose rate at the fuel-water interface, which exceeds the gamma and beta dose rates for most of the fuel history (Figure 7-4), is the main contributor to radiolysis, producing molecular oxidants such as H_2O_2. Other potential sources of oxidants, such as any O_2 trapped in the porewater, will already have been consumed by corrosion processes (e.g., corrosion of the Cu shell) before the fuel cladding is breached because these corrosion reactions are relatively fast (see Chapter 5). In principle, the radiolytically produced oxidants will also be consumed by reaction with container materials rather than by reaction with used fuel; however, for alpha radiolysis, the oxidants (e.g., H_2O_2) are only produced within 20 μm of the fuel-water interface (Garisto 1989), so they are much closer to the fuel than to the container and thus more likely to react with the fuel.

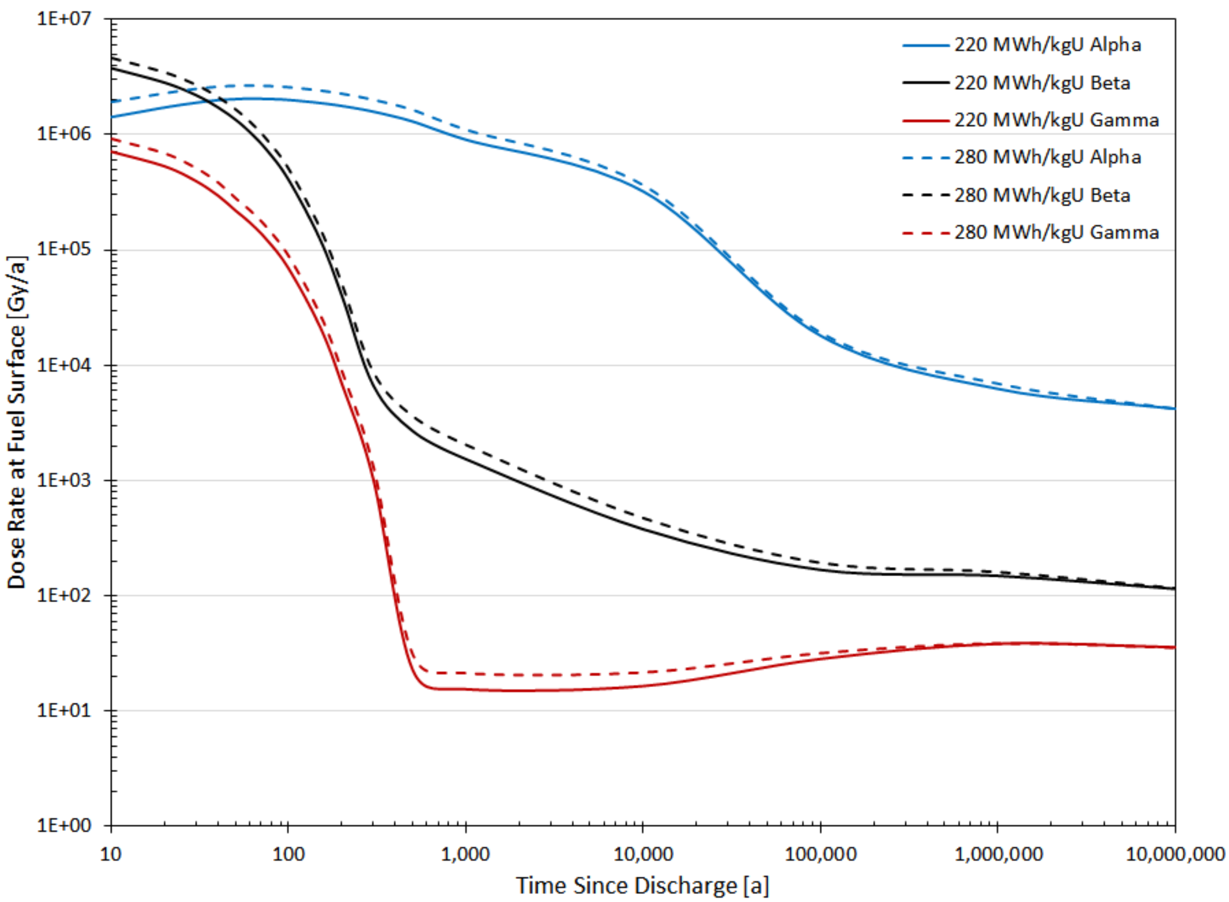

Figure 7-4: Radiation Dose Rate in Water at the Fuel Surface (220 MWh/kgU and 280 MWh/kgU Burnup)

Oxidative dissolution of the fuel continues as long as the alpha radiation field is sufficiently high. Eventually, after about 10 million years (Gobien et al. 2016), chemical dissolution of the fuel dominates according to the reaction:

$$UO_2 + 2H_2O \rightarrow U(OH)_4 \qquad (7\text{-}1)$$

This is a very slow process, as illustrated by the existence of uranium ore bodies that are millions or billions of years old.

The UO_2 dissolution rate would be affected by buildup of hydrogen gas inside the steel vessel generated by anaerobic corrosion of the steel. Experimental and theoretical evidence shows that the dissolution rate drops by several orders of magnitude in the presence of even modest pressures of hydrogen gas (Razdan and Shoesmith 2015, Rollin et al. 2001, Carbol et al. 2005, Wu et al. 2014). This is likely due to the activation of hydrogen by various mechanisms to produce the strongly reducing $H^{\bullet}$ radical, which in turn scavenges radiolytic oxidants and suppresses fuel corrosion (Liu et al. 2016). While this hydrogen effect will suppress fuel dissolution, it is conservatively ignored in the current assessment.

The fuel dissolution rate used in this assessment is shown in Section 7.5.2.1.

Radionuclide Releases from Zircaloy

The Zircaloy sheath surrounding the fuel pellets in a CANDU fuel bundle naturally forms a thin layer of protective ZrO_2 on its surface when in contact with air or water. This oxide layer greatly inhibits the Zircaloy dissolution rate in the postclosure period should water gain access to the used fuel container (Shoesmith and Zagidulin 2010). Because the inventory of certain isotopes such as Cl-36 and C-14 within the fuel sheath can be significant relative to the amount present in the fuel (Gobien and Garisto 2012), dissolution of the Zircaloy is modelled in the postclosure safety assessment. A kinetic dissolution model is used in which the zirconium dissolves at a rate proportional to the corrosion rate of Zircaloy in water and the surface area of the Zircaloy in contact with water. During corrosion, species trapped in the Zircaloy matrix are released congruently with Zircaloy dissolution.

Certain radionuclides (i.e., C-14), may be more concentrated in the zirconium oxide layer on the Zircaloy sheath. Radionuclides in the oxide layer may be released on a faster time scale than those trapped within the cladding. This is included in the Zircaloy release model by introducing an instant release fraction for Zircaloy radionuclides.

7.3.2 Engineered Barrier System

Chapter 4 provides a detailed description of the conceptual repository and engineered barriers assumed in this study.

There is a dense 100% bentonite layer that surrounds the container. The purpose of this layer is to:

- Prevent groundwater flow near the container;
- Mechanically support the container;
- Sorb and delay release of radionuclides from a breached container; and

- Prevent microbial activity that could cause corrosion of the copper shell.

This buffer material has a sufficiently low hydraulic conductivity that transport through it is diffusion dominant (i.e., the advective velocity is negligible).

The excavation damaged zone (or EDZ) extends around the perimeter of excavated spaces and is modelled as a uniform porous medium with higher hydraulic conductivity than the surrounding intact bedrock. Conceptually, the EDZ is divided into two zones, these being an Inner EDZ and Outer EDZ. The Inner EDZ exhibits more damage and has a higher conductivity than the Outer EDZ. Excavation damaged zones along placement rooms, which are narrower, may be less permeable than damage zones along the larger drifts and cross-cuts. As a conservative estimate, the placement room EDZ is assigned the same hydraulic conductivity as the drift and cross-cut EDZ.

The design includes seals at the entrance of each placement room and seals spaced throughout the access drifts and cross cuts. These seals are composed of concrete and clay bulkheads that interrupt the tunnel and placement room Inner EDZs. An additional smaller EDZ associated with excavation of the seals is also assigned the same hydraulic conductivity as the drifts and cross-cut EDZ.

Groundwater contacting the container, and contacting the fuel in a breached container, must pass through the buffer. Initially, the composition of this contact water is similar to the buffer porewater composition which depends strongly on the minor mineral components of the buffer, notably the calcite and gypsum contents (Muurinen and Lehikoinen 1999, Curti and Wersin 2002). In the long term, these minor mineral components would all dissolve and the contact water composition would resemble the geosphere porewater composition.

The time evolution in contact water composition is not explicitly taken into account; rather, two contact water compositions are defined. The first composition is geosphere porewater equilibrated with buffer minerals, and the second composition is geosphere porewater equilibrated with buffer minerals and the steel insert of the container. These compositions are used for the calculation of chemical element solubilities and the highest calculated solubility is used in the safety assessment calculations.

The maximum temperature at the interface between the engineered sealing materials and the host rock is about 76°C, occurring after 75 years, and about 84°C at the interface between the buffer and the container (Guo 2016). Temperature in the placement rooms would be about 44°C after 10,000 years, with ambient rock temperatures returning after 100,000 years. Given this, a temperature of 85°C is selected for the engineered barrier materials as a conservative reflection of the impact of the relatively brief thermal transient on mass transport. Use of a high temperature promotes increased diffusion.

7.3.3 Geosphere

Chapter 2 provides a description of the hypothetical geosphere assumed in this study.

The principal components of the conceptual model are shown in Figure 7-5. The geosphere has a defined fracture network surrounded by a rock mass. The fracture zones are conservatively assigned a uniform high hydraulic conductivity while the rock mass is assigned an effective hydraulic conductivity that decreases with depth.

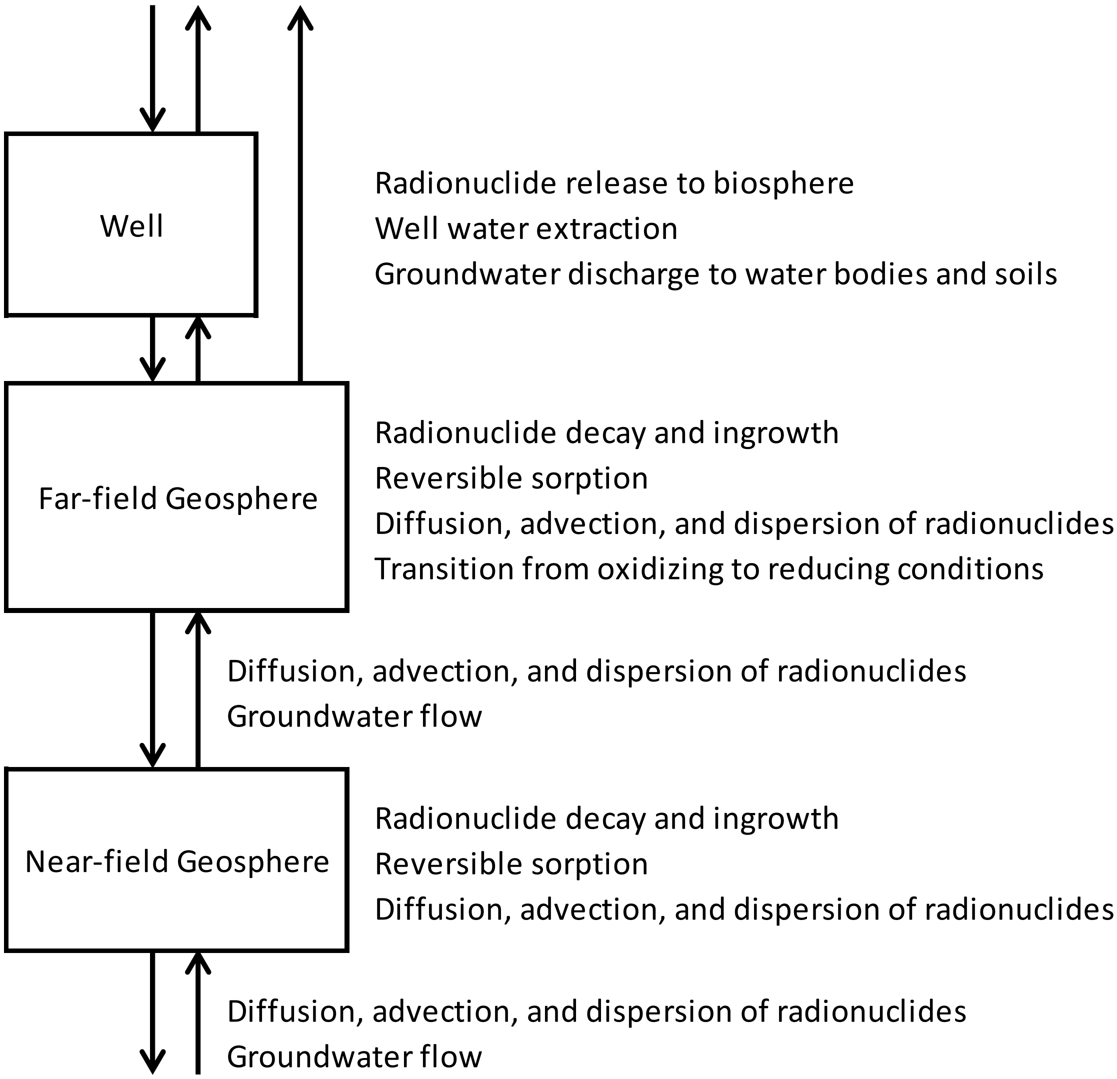

Figure 7-5: Conceptual Model for the Geosphere

The groundwater flow field is calculated assuming constant head boundary conditions at the surface, with the water table following the surface topography and no-flow boundary conditions at the boundaries of the watershed. This is reasonable for this hypothetical site where there is limited topographic relief and conditions can be assumed relatively wet.

The hydrogeological model includes a deep well that intercepts a fracture zone, with the fracture able to supply water at the specified rate. The influence of the well on the overall groundwater flow field is small although the flow field near the well is affected by well drawdown. The groundwater at repository depth is only slightly saline (~12 g/L, Table 7-15), so salinity is not an important factor in the hydrogeological modelling.

In the near-field geosphere (i.e., around the repository), chemically reducing conditions prevail.

The ambient rock temperature at repository level is about 11 ºC. The temperature in the repository will initially be warmer than in the surrounding geosphere due to heat input from the used fuel bundles (caused by radioactive decay). The maximum temperature at the interface between the engineered sealing materials and the host rock is about 76°C, occurring after 75 years (Guo 2016). Temperature in the placement rooms would be about 44ºC after 10,000 years, with rock temperatures after 10,000 years in the area within 35 m and 60 m of the plane of the repository being above 25ºC (and decreasing). In the vertical direction (i.e., towards the surface), at 10,000 years rock temperatures above 25ºC could exist at 190 m above the repository plane, with ambient conditions returning after about 100,000 years. For the contaminant transport times estimated in this study, the bulk of the transport occurs under close to ambient conditions. Values at 20ºC are adopted for geosphere transport parameters.

The physical properties of the rock are described in Chapter 2. The diffusion and sorption coefficients assumed for the rock at repository level are given in Section 7.5.2.5 and Section 7.5.2.6.

7.3.4 Biosphere

The main features of the biosphere model are illustrated in Figure 7-6.

Radionuclides are lost from the local biosphere by outflow with water, by radioactive decay, by atmospheric dispersion and by leaching into deep soil or sediments.

The local biosphere has the characteristics of the Canadian Shield region of central to northern Ontario. As noted in Section 7.2.2.1, a constant temperate climate is assumed. While the properties of the biosphere could vary with time due to global warming in the near term, or due to other natural or human-induced changes, the assumption of a constant biosphere provides a convenient and clear measure of the potential impacts, which can be readily related to what is currently acceptable.

In the long term, it is assumed that glaciation will resume with consequent significant effects as a result of the glaciation itself and the related climate change. The anticipated effects of glaciation on the dose assessment for the Normal Evolution Scenario are discussed in Section 7.8.2.4.

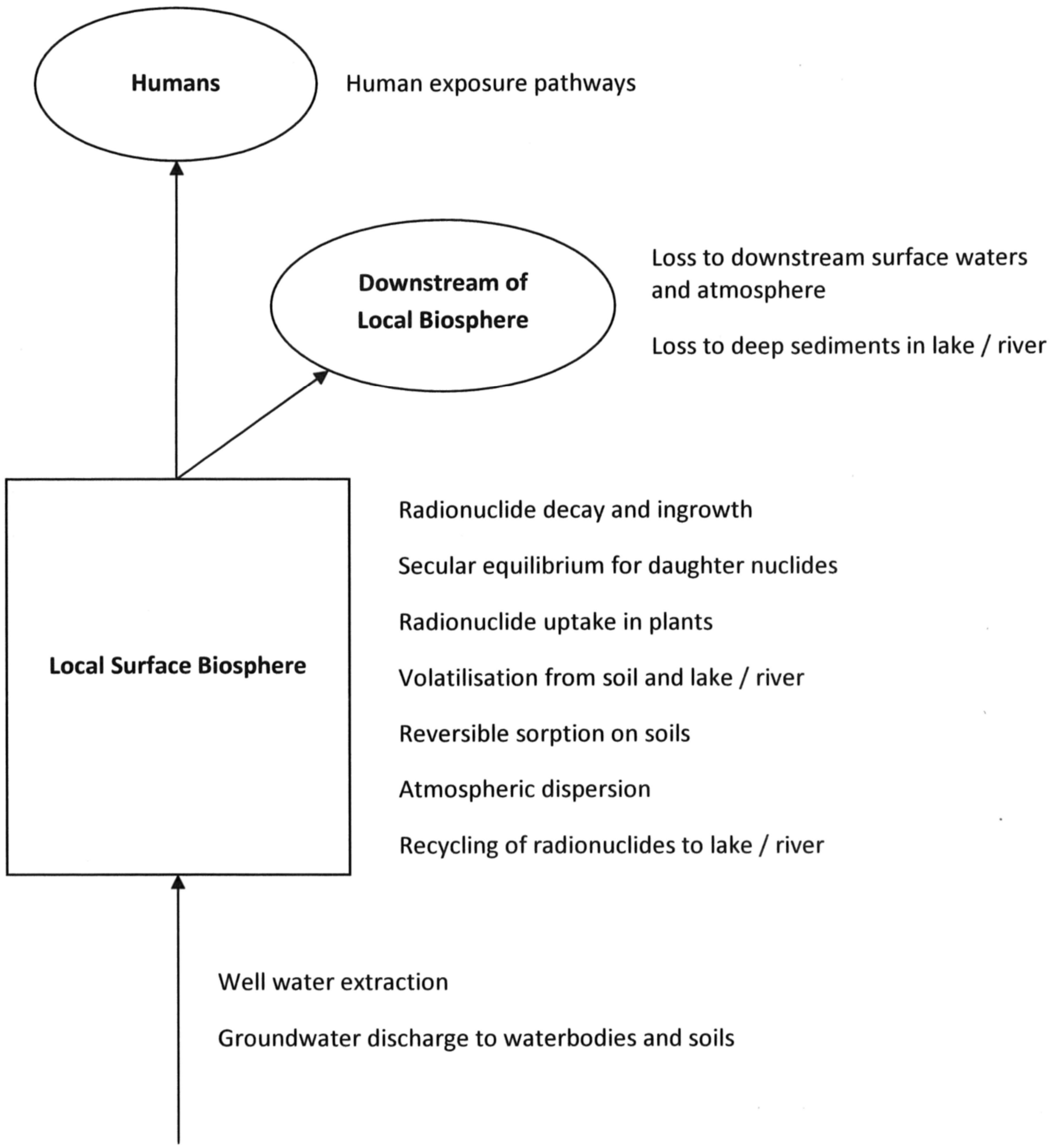

Figure 7-6: Conceptual Model for the Constant Biosphere

Following international practice, the site is assumed occupied by a group of people (i.e., the "critical group") that behaves in a plausible manner but with lifestyle characteristics that maximize their exposure to any radionuclides entering the biosphere. Members of the critical group are assumed to spend all their lives in the local biosphere and obtain all their food, water, fuel and building materials from the local vicinity.

The characteristics of the critical group will change with climate; however, since a constant temperate climate is assumed, a self-sufficient farming family is selected as the critical group.

This group uses a well that intercepts any contaminant plume that might originate in the repository, and grows its own crops and raises animals. Their food includes plants grown in a garden, domesticated animals and local fish. Their lifestyle is more self-sufficient than typical Canadian habits and, because this leads to higher exposure, it is therefore a useful basis for assessing potential repository impacts. However, farming is not very practical on the Canadian Shield, and other lifestyles with more reliance on other food sources would be of interest in future assessments.

Plants growing near the repository can become contaminated directly by atmospheric deposition of radionuclides that reach the biosphere and become volatilized (e.g., I-129) or suspended due to aerosol formation (all nuclides). Plants can also become contaminated due to root absorption of groundwater discharge, irrigation with contaminated surface water (edible crops), and with radionuclides that are deposited to the soil from the atmosphere.

In this safety assessment, a deep groundwater well is assumed to intercept the radionuclide plume, with the well positioned such that the uptake of any radionuclides released from the repository is maximized. Any contaminants not reaching the well are either discharged to surface discharge locations, or decay away before reaching the biosphere.

In the absence of a well, the surface discharge would be much higher; however, the associated doses would still be much less than those with a well because of longer discharge times (i.e., more time available for radioactive decay), more dispersion in the geosphere and much greater dilution in the surface water body.

The biosphere model:

- Describes the movement of contaminants through soil, plants and animals, and the atmosphere in the surface environment near the repository;
- Calculates the concentrations of contaminants in water and air in the local habitat of the critical group; and
- Calculates radiological dose rates to an individual in the critical group due to ingestion and inhalation of radionuclides and by external exposure to radiation from radionuclides in the environment (air immersion, water immersion, building materials and groundshine).

In the model, all radionuclide releases from the geosphere are assumed to enter the primary water body discharge point. In particular, radionuclides captured by the well or directly discharged into soils are not removed from the amount entering the water body. In effect, this assumes the holdup in these paths is relatively short, and the radionuclides eventually do transfer to the water body. This conservatively overestimates the amount of radionuclides in the biosphere, but simplifies the modelling because many processes that recycle radionuclides are accounted for implicitly, such as surface runoff into the water body.

A schematic representation of the environmental transfer model is shown in Figure 7-7. The dose model uses the concentration of radionuclides in the various biosphere compartments (well, soil, plants, animals and air) to calculate the annual dose to a member of the critical group. The critical group is also exposed to sediments from the lake when these sediments are used for soil. In this case, the sediment exposure pathways are the same as those for the soil exposure pathways.

The internal exposure pathways considered are:

- Soil-to-man;
- Soil-to-plant-to-man;
- Soil-to-plant-to-animal-to-man;
- Soil-to-animal-to-man;

- Air-to-man;
- Air-to-plant-to-man;
- Air-to-plant-to-animal-to-man;
- Air-to-animal-to-man;

- Water-to-man;
- Water-to-plant-to-man;
- Water-to-animal (including fish)-to-man; and
- Water-to-plant-to-animal-to-man.

The external exposure pathways considered are:

- Air immersion;
- Water immersion (bathing or swimming if a suitable water body is nearby);
- Groundshine (exposure to radiation from contaminated soil); and
- Building materials (exposure to radiation from building materials).

These exposure pathways are similar to those considered in the guidelines used to calculate derived release limits for normal operation of a nuclear facility (CSA 2014).

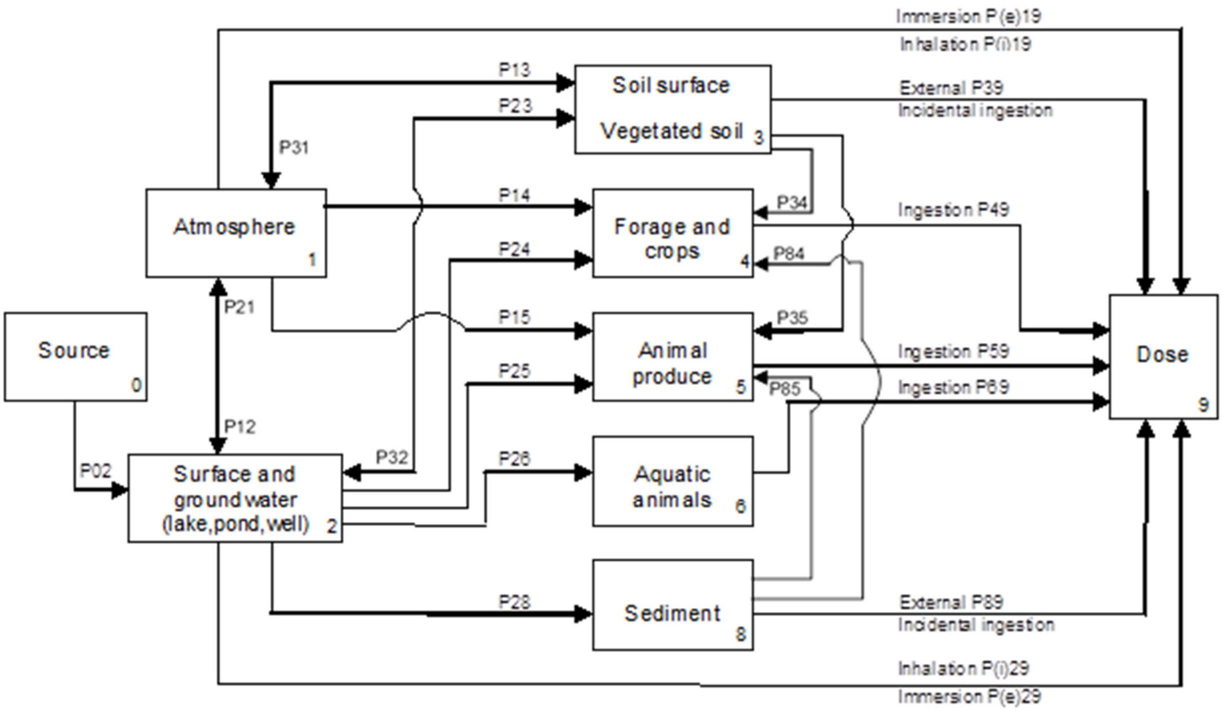

Notes: The nomenclature is from CSA (2014) and the Pij represent transfer parameters from compartment i to compartment j. The biosphere model includes all these environmental transfers and exposure pathways. The building material exposure pathway is not shown here since it is not included in the CSA (2014) dose model.

Figure 7-7: Environmental Transfer Model Showing Critical Group Exposure Pathways

7.4 Computer Codes

The conceptual model for contaminant transport is numerically represented in a suite of computer codes used in postclosure safety assessment modelling.

Figure 7-8 identifies the codes used and their interrelationship. Information from used fuel characteristics, engineering design and site characterization is used to develop site-specific input parameters.

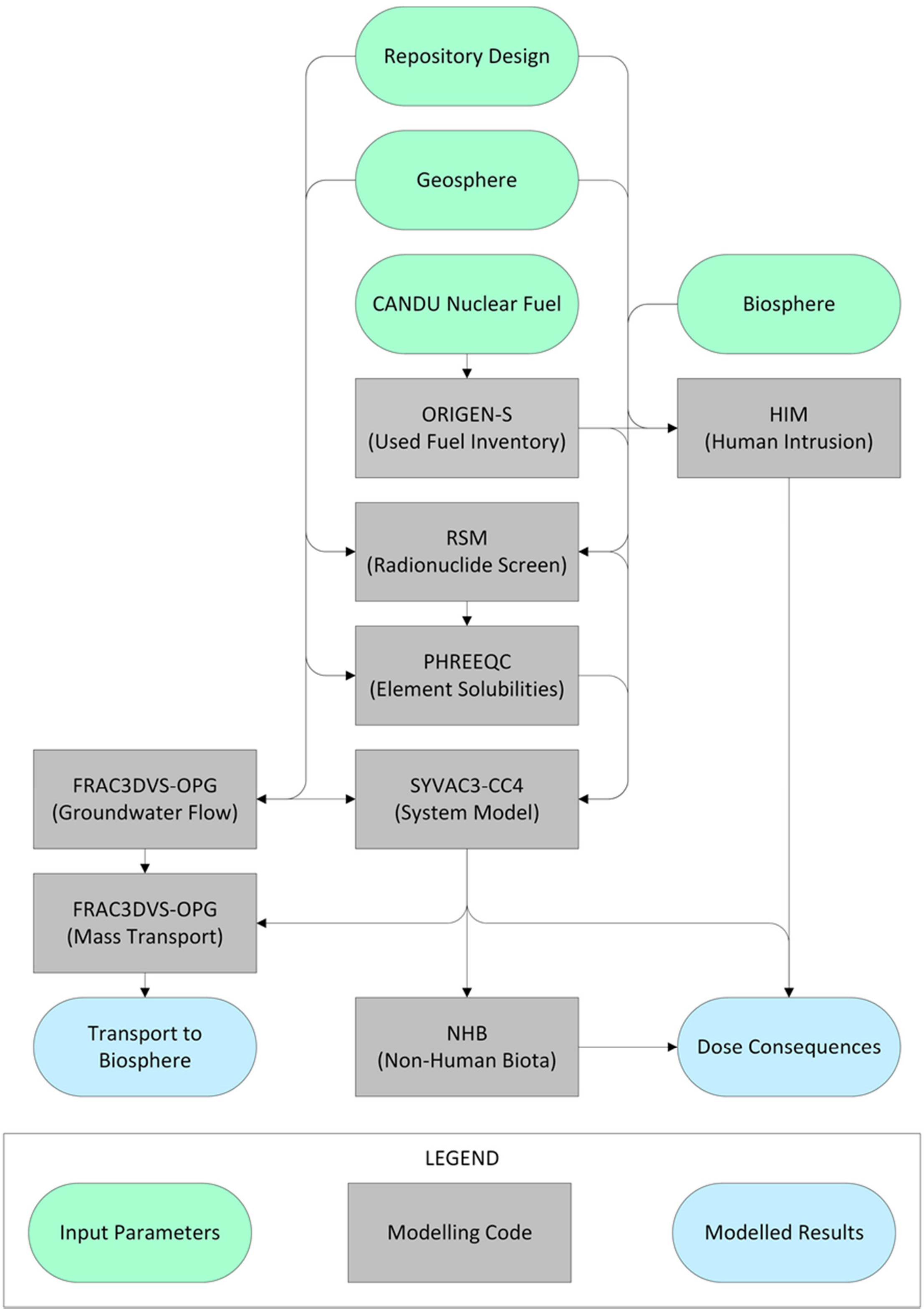

Figure 7-8: Main Computer Codes

ORIGEN-S is a CANDU-industry standard code used to calculate radionuclide inventories in the fuel and Zircaloy cladding at the time of placement, based on a defined reactor exposure scenario (Hermann and Westfall 1995, Tait et al. 1995).

ORIGEN-S was used to derive the used fuel inventories used in this study (see Chapter 3).

PHREEQC is a widely used and tested open source computer program developed by the United States Geological Survey (Parkhurst and Appelo 1999). PHREEQC is based on an ion-association aqueous model and is designed to perform a wide variety of aqueous geochemical calculations.

In this assessment, PHREEQC Version 2.17 has been used for solubility and speciation calculations. The ThermoChimie v.7.b thermodynamic dataset has been used, as described in Gobien et al. (2016).

RSM (Radionuclide Screening Model) is a project-specific simple model of groundwater transport of radionuclides from container to humans via a well. Through a conservative choice of input parameters, a large input set of radionuclides can be screened so as to objectively identify which should be considered further using more detailed models. RSM incorporates data for all radionuclides with half-lives longer than 0.1 years as well as radionuclides with half-lives longer than one day if they have a parent with a half-life longer than 0.1 years.

Table 7-8 provides more information on RSM.

SYVAC3-CC4 is the reference System Model for the assessment of radionuclide release, transport, decay, biosphere transfer and dose assessment. It has been developed for a deep geological repository concept based on used fuel placed in durable containers, surrounded by engineered barrier materials and located deep underground. The code can perform both deterministic and probabilistic calculations.

Table 7-9 provides more information on SYVAC3-CC4.

FRAC3DVS-OPG is the reference Groundwater Flow and Transport code. This is a commercially available 3D finite-element / finite-difference code (Therrien et al. 2010). FRAC3DVS-OPG supports both equivalent porous medium and dual porosity representations of the geologic media.

Table 7-10 provides more information on FRAC3DVS-OPG.

HIMv2.1 is a project-specific code that assesses the consequences of the Inadvertent Human Intrusion Scenario. The model considers a scenario in which a used fuel container is unknowingly intersected by a drilled borehole, resulting in used fuel being brought directly to surface. Dose consequences are estimated for the drill crew and for a resident subsequently using the contaminated area.

Table 7-11 provides more information on HIMv2.1.

NHBv1.0 is a project-specific code that uses as a basis the calculated environmental media concentrations as a function of time from the SYVAC3-CC4 system model to calculate dose rates to non-human biota.

Table 7-12 provides more information on NHBv1.0.

Table 7-8: RSM, Version 1.1

Parameter	Comments
Components:	
SYVAC3	Executive module, Version 3.10.1
RSM	System model, Version 1.1
Main Documents	*RSM Version 1.1 - Theory* (Goodwin et al. 2001) *RSM Version 1.1 Verification and Validation* (Garisto 2001)
Main Features	- Linear decay chains - Radionuclide release by instant release and by congruent dissolution - UO_2 dissolution calculated from user-supplied time-dependent data - Precipitation in container when user-supplied solubility limits exceeded - Durable containers, some fail with small defects - 1D buffer and backfill layer that surrounds the container and inhibits groundwater flow and radionuclide transport - Repository model based on one room containing failed container(s) - Linear sequence of 1D transport segments that connect the repository to a well. Transport segments are user-supplied; transport is solved considering diffusion, advection/dispersion and sorption - Dose impacts to a self-sufficient human household that uses well water, based on conservative model for drinking, immersion, inhalation and ground exposure. Effect of other ingestion pathways is included through a user-input multiplier - Ability to represent all input parameters with a probability density function (PDF) and to run Monte-Carlo type simulations - Time-independent material properties and biosphere characteristics - Database of all radionuclides with half-lives longer than 0.1 years as well as radionuclides with half-lives longer than one day if they have a parent with a half-life longer than 0.1 years

Table 7-9: SYVAC3-CC4, Version SCC4.09.2

Parameter	Comments
Components:	
SYVAC3	Executive module, Version 3.12.1
CC4	System model, Version 4.09.1
ML3	SYVAC3 math library, Version ML3.03
SLATEC	SLATEC Common Mathematical Library, Version 4.1
Main Documents	*SYVAC3-CC4 Theory Manual (NWMO 2012)* *SYVAC3-CC4 User Manual (Kitson et al. 2012)* *SYVAC3-CC4 Verification and Validation Summary (Garisto and Gobien 2013)*
Main Features	- Linear decay chains - Radionuclide release by instant release and by congruent dissolution - UO_2 dissolution rate calculated using radiation dose-rate based model - Precipitation in container when user-supplied solubility limits exceeded - Durable container, but some fail due to small defects - Cylindrical buffer and backfill layer that surrounds the container and inhibits groundwater flow and radionuclide transport - Multiple sector repository connected to the geosphere at sector-specific nodes chosen considering the local groundwater flow - Geosphere network of 1D transport segments that connect the repository to various surface discharge locations, including a well - Transport considers diffusion, advection / dispersion and sorption - Biosphere model that calculates field soil concentrations, well water concentrations, and uses a surface water body as a final collection point - Dose impacts to a self-sufficient human household that uses water body or well water, locally grown crops and food animals, local building materials and heating fuel - Dose impacts to generic non-human biota - Flow-based models in repository and geosphere, concentration-based models in biosphere - Generally time-independent material properties and characteristics for the biosphere and geosphere model. Transitions from one geosphere (or biosphere) state to another at specific times can be accommodated - Ability to represent all input parameters with a probability density function and to run Monte-Carlo type simulations

Table 7-10: FRAC3DVS-OPG, Version 1.3

Parameter	Comments
Components:	
FRAC3DVS-OPG	Main code, Version 1.3
Main Documents	*A Three-dimensional Numerical Model Describing Subsurface Flow and Solute Transport* (Therrien et al. 2010)
Main Features	- Linear decay chains - 3 D groundwater flow and solute transport in saturated and unsaturated media - Variable density (salinity) fluid - 1D hydromechanical coupling - Equivalent porous medium or dual-continuum model; fractures may be represented as discrete 2D elements - Finite-element and finite-difference numerical solutions - Mixed element types suitable for simulating flow and transport in fractures (2D rectangular or triangular elements) and pumping / injection wells, streams or tile drains (1D line elements) - External flow boundary conditions can include specified rainfall, hydraulic head and flux, infiltration and evapotranspiration, drains, wells, streams and seepage faces - External transport boundary conditions can include specified concentration and mass flux and the dissolution of immiscible substances - Options for adaptive time-stepping and sub-gridding

Table 7-11: HIMv2.1

Parameter	Comments
Components:	
AMBER	Executive Code, Version 5.5
HIMv2.1	Main Model Version
Main Documents	*Human Intrusion Model for the Mark II Container in Crystalline and Sedimentary Rock Environments: HIMv2.1 (Medri 2015a)*
Main Features	- Linear decay chains - Dose consequences by external, inhalation and ingestion pathways to drill crew and site resident - Surface contamination decreases with time due to radioactive decay and soil leaching - Time-independent material properties and biosphere characteristics - Includes data for potentially relevant radionuclides

Table 7-12: NHBv1.0

Parameter	Comments
Components:	
AMBER	Executive Code, Version 5.7.1
NHBv1.0	Main Model Version
Main Documents	*Non-Human Biota Dose Assessment Equations and Data (Medri and Bird 2015)*
Main Features	- Uses as a basis the calculated environmental media concentrations as a function of time from the SYVAC3-CC4 system model to calculate dose rates to non-human biota - Media considered are: surface water, groundwater, soil, sediment and air - Considers non-human biota from a range of Canadian ecosystems. - Time-independent material properties and biosphere characteristics - Includes data for potentially relevant radionuclides

7.5 Overall Analysis Approach and Selected Data for Groundwater Flow and Radionuclide Transport

This section describes the overall analysis approach and the manner in which the 3D groundwater and transport models and the System Model are used.

Data for selected parameters are also given to provide context. Additional data are available in Gobien et al. (2016).

7.5.1 Overall Approach

The general approach for conducting the postclosure safety assessment is as follows:

1. Perform Radionuclide and Chemical Hazard Screening

Used nuclear fuel initially contains hundreds of radionuclides and chemically hazardous stable elements; however, most are short lived and / or present in very small amounts. Following placement in a deep geological repository, only a small subset poses a potential risk to humans and the environment. The RSM code is used to identify this subset for more detailed assessment.

The methods used for performing the screening analysis are described in Section 7.6.

2. Perform 3D Groundwater Flow and Radionuclide Transport Modelling

Detailed 3D hydrogeological modelling is performed with the FRAC3DVS-OPG code to determine the groundwater flow field near the repository.

Once the flow field is modelled, detailed 3D diffusive and advective / dispersive radionuclide transport calculations are performed for I-129, C-14, Ca-41, Cl-36, Cs-135, Se-79, and U-238. These radionuclides are typically the most important in terms of potential radiological impact and also represent a range of low-sorption to high-sorption species. Radionuclide releases from the defective containers are obtained from the System Model (implemented in the SYVAC3-CC4 code) and input as a source term to the 3D transport calculation.

Dose consequences cannot be determined in this step because the FRAC3DVS-OPG code does not have biosphere and dose models

Due to the large size of the modelled environment, three different scales of nested models are used. These are:

- Subregional-Scale Model – similar to the model described in Chapter 2, this model encompasses the watershed within which the repository is located together with some of the surrounding area. The model domain is irregularly shaped with an overall east-west extent of 15 km, and a north-south extent of 17.5 km. Vertically, the model extends from ground surface down to a depth of approximately 1550 m.

  No repository features are incorporated at this scale of resolution, although the discretization is refined over the repository footprint to ensure accurate head representation.

This model is used to describe the larger scale flow field and to determine the external head boundary conditions that are applied in the Repository-Scale Models.

- Repository-Scale Models – the model domain includes the repository and a section of the surrounding geosphere large enough to capture all advective transport from the repository to surface. Two Repository-Scale Models are used:

    - The "Full" Repository-Scale Model includes all rooms, tunnels, and shafts with a full representation of the EDZ. The model also supplies head boundary conditions to the Container-Scale Model (described below).
    - The "Rooms-Only" Repository-Scale Model includes just the placement rooms together with a simplified EDZ. The "Rooms-Only" model is much more computationally efficient than the "Full" model and is used extensively in initial assessments determining well and source location, as well as for selected sensitivity cases.

  Individual containers are not modelled at this scale of resolution.

  The models are used for well siting activities and for radionuclide transport calculations. Simulations are performed for those sensitivity studies described in Section 7.2.2 that have the potential to affect the groundwater flow field.

- Container-Scale Models - the model domain consists of a small section of the repository surrounding the defective containers together with the adjacent geosphere. There are four Container-Scale Models, one for each of the four container locations considered for maximizing the dose consequence in the well siting activity (Section 7.7.2.3.2).

  These models incorporate a high level of detail and individual containers are represented at the source location.

  The models are used to calculate radionuclide transport from defective containers into the surrounding rock. The output is used as source term input to the Repository-Scale Models. Simulations are also performed to corroborate results of the Repository-Scale Models and to provide a more complete understanding of repository component functions.

The groundwater flow field obtained using the Repository-Scale Model is also used to guide subsequent development of the SYVAC3-CC4 System Model. To provide data for verifying the System Model, the radionuclide transport calculations performed for I-129, C-14, Ca-41, Cl-36, Cs-135, Se-79, and U-238 are used for comparison purposes. All 3D radionuclide transport simulations are performed for a 10 million year simulation time frame.

Figure 7-9 illustrates the spatial relationships for the Subregional-Scale, the Repository-Scale, and the Container-Scale Models.

The methods used in this phase of the assessment are described in Section 7.7.

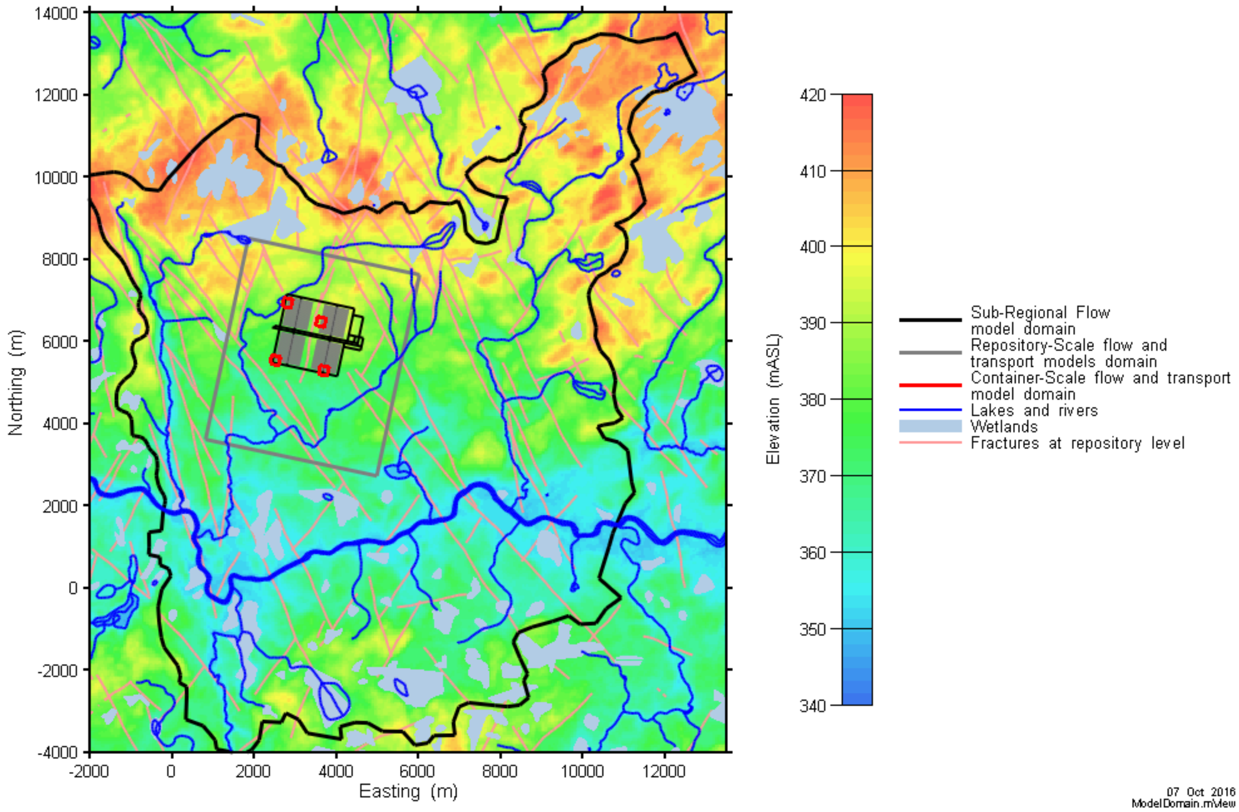

Figure 7-9: 3D Subregional-Scale, Repository-Scale and Container-Scale Model Domains

3. Perform System Modelling

The System Model includes all aspects of the repository – used fuel, container, engineered barrier materials, geosphere, and biosphere. It is implemented in the SYVAC3-CC4 code.

The 3D groundwater advective flow field generated with FRAC3DVS-OPG is used to guide development of the geosphere submodel of the System Model.

Confidence in the geosphere submodel is obtained by comparing radionuclide transport results with similar results from the 3D model. These comparisons are performed for I-129, C-14, Ca-41, Cl-36, Cs-135, Se-79, and U-238, as these represent the key radionuclides for groundwater transport, as well as provide a test of the two models for species that cover a wide range of sorption data.

Other aspects of the System Model - used fuel, container, near-field and biosphere are defined by the case and by input data.

The System Model includes the full suite of contaminants of interest (as identified from the radionuclide and chemical element screening assessment described in Step 1 above).

The System Model is also used for the probabilistic safety assessment, assuming a fixed geosphere. The radionuclide inventory, release and transport properties are varied about the Base Case values, as are the characteristics of the biosphere and dose receptor.

The methods used in this phase of the assessment are described in Section 7.8.

7.5.2 Data for Selected Parameters

This section presents data for a variety of parameters important to the postclosure safety assessment. A full description of the input parameters is available in Gobien et al. (2016).

7.5.2.1 Instant Release Fractions and Fuel Dissolution Rate

Fuel

The reference waste form is a standard CANDU 37-element fuel bundle with a discharge burnup of either 220 MWh/kgU (for scenarios involving releases from a large number of bundles) or 280 MWh/kgU (for scenarios involving releases from a small number of bundles), and an average fuel power during operation of 455 kW. Chapter 3 identifies the inventories for the radionuclides of interest, and provides additional information regarding the two discharge burnup values.

Section 7.3.1 indicates that radionuclides within the UO_2 fuel are released by two distinct mechanisms which operate on very different time scales. These mechanisms are referred to as “instant release” and “congruent release”.

Table 7-13 shows the instant release fractions used in this study.

Table 7-13: Fuel Instant-Release Fractions

Element	PDF Type	PDF Attributes*	Lower Limit	Upper Limit
Ac	constant	0	-	-
Ag	uniform	-	0	0.001
Am	constant	0	-	-
Bi	normal	(0.006, 0.0015)	0.0023	0.03
Br	normal	(0.06, 0.01)	0.01	0.2
C	normal	(0.027, 0.016)	0.0005	0.075
Ca	constant	0	-	-
Cd	normal	(0.006, 0.0015)	0.0023	0.03
Cl	normal	(0.06, 0.01)	0.01	0.2
Cs	normal	(0.04, 0.01)	0.015	0.20
Hg	normal	(0.04, 0.01)	0.015	0.20
I	normal	(0.04, 0.01)	0.015	0.20
Mo	lognormal	(0.01, 2)	0.0005	0.05
Np	constant	0	-	-
Pa	constant	0	-	-
Pb	normal	(0.006, 0.0015)	0.0023	0.03
Pd	lognormal	(0.01, 2)	0.0005	0.05
Po	normal	(0.04, 0.01)	0.015	0.20
Pu	constant	0	-	-
Ra	normal	(0.025, 0.008)	0.001	0.05
Rn	normal	(0.04, 0.01)	0.015	0.20
Sb	normal	(0.006, 0.0015)	0.0023	0.03
Se	normal	(0.006, 0.0015)	0.0023	0.03
Sn	uniform	(0.0, 0.001)	-	-
Sr	normal	(0.025, 0.008)	0.001	0.05
Tc	lognormal	(0.01, 2)	0.0005	0.05
Te	normal	(0.006, 0.0015)	0.0023	0.03
Th	constant	0	-	-
U	constant	0	-	-
W	constant	0	-	-

Note: From Gobien et al. (2016)

*PDF attributes are (mean, standard deviation) for the normal PDF, and (geometric mean, geometric standard deviation) for the lognormal PDF.

Figure 7-10 presents fractional and cumulative information for dissolution of the fuel. Information for both the 220 MWh/kgU and the 280 MWh/kgU burnup values is shown.

The System Model uses the instant release and congruent release together with solubility limits and information on the water volume inside the container to calculate radionuclide concentrations. Radionuclides that escape the container enter the surrounding low hydraulic conductivity buffer material.

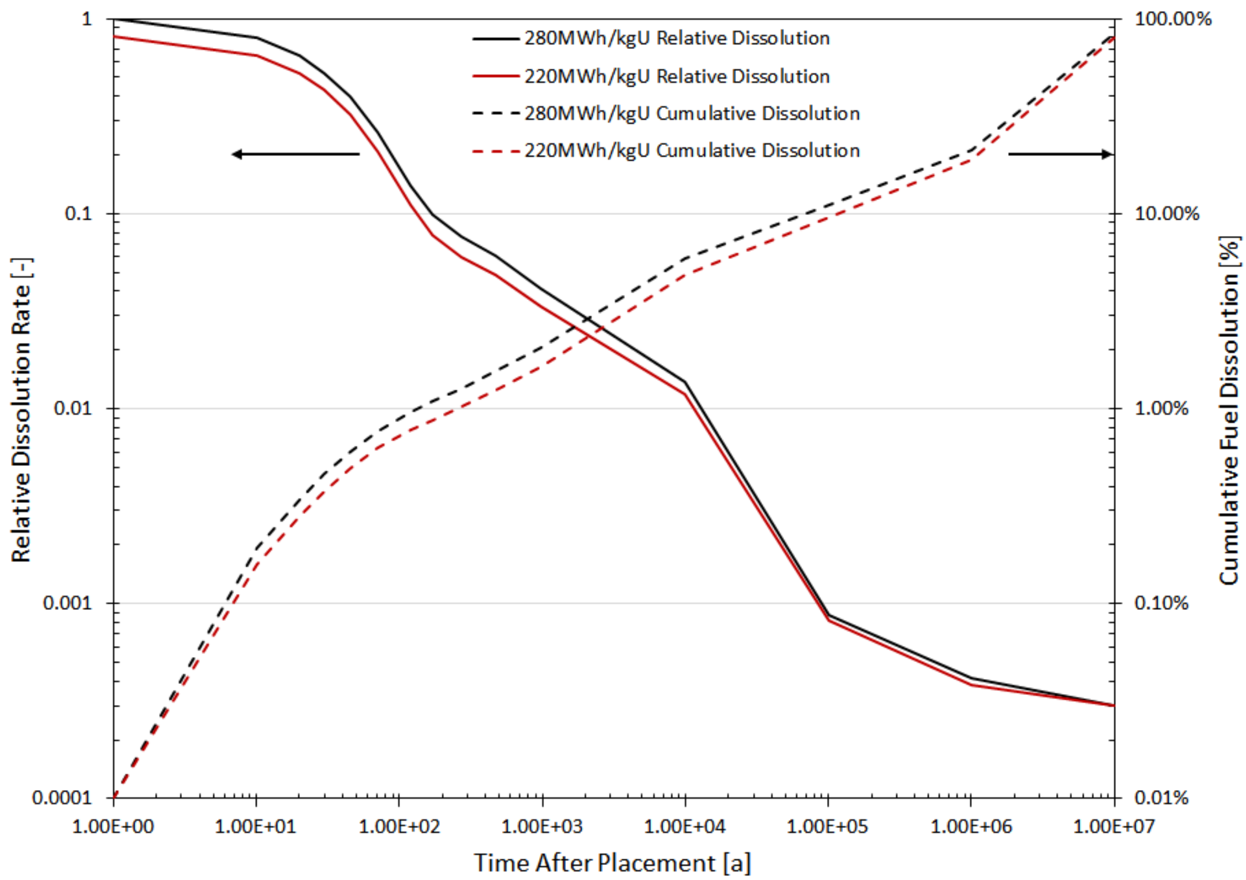

Notes: Relative Dissolution Rate is the ratio of the time-dependent fuel dissolution rate to the maximum fuel dissolution rate. The maximum dissolution rates are 3.12×10^{-3} [mol/m^2/a] for 220 MWh/kgU burnup and 3.84×10^{-3} [mol/m^2/a] for 280 MWh/kgU burnup, where the area is the surface area of the fuel in contact with water. A contact area of 209 m^2 per container is used in this study which assumes the fuel is highly fragmented and the container is full of water.

Figure 7-10: Fuel Dissolution Rate

<u>Zircaloy</u>

The impurities in the Zircaloy cladding are likely uniformly distributed. Because the temperature of the cladding during reactor operation is relatively low, the activation products and impurities in the irradiated Zircaloy would be expected to be likewise uniformly distributed. Hence, for the

Zircaloy, the instant release fractions should be zero and contaminants are released only through congruent dissolution as the Zircaloy corrodes.

Leaching experiments, however, indicate that the C-14 within the oxide film on the Zircaloy is released relatively rapidly compared to the C-14 within the metal itself (Gras 2014, Yamaguichi et al. 1999, Smith and Baldwin 1993). The same leaching experiments do not support the existence of a non-zero C-14 instant release fraction for the Zircaloy metal. Consequently, the fraction of the C-14 within the oxide layer is assumed to be instantly released after water enters a used fuel container and contacts the Zircaloy. Table 7-14 shows the Zircaloy instant release fractions used in this study.

Table 7-14: Zircaloy Instant-Release Fractions

Element	PDF Type	Value
C	Constant	0.021
Other Elements	Constant	0

A kinetic dissolution model in which the zirconium dissolves at a rate proportional to the corrosion rate of Zircaloy in water and the surface area of the Zircaloy in contact with water is used in this work. During corrosion, species trapped in the Zircaloy matrix are released.

7.5.2.2 Radionuclide Source Terms

Figure 7-11 illustrates the source term for I-129, where this represents the source at the interface between the container and the surrounding buffer material. As noted in Table 7-3, this is calculated assuming the container volume is still present but the container walls are not (i.e., the container itself is not a barrier to release from container).

The coloured lines are the individual container source terms, while the dashed line is the combined total. The 10 spikes are due to the instant release term from each the 10 containers assumed to fail in the Base Case.

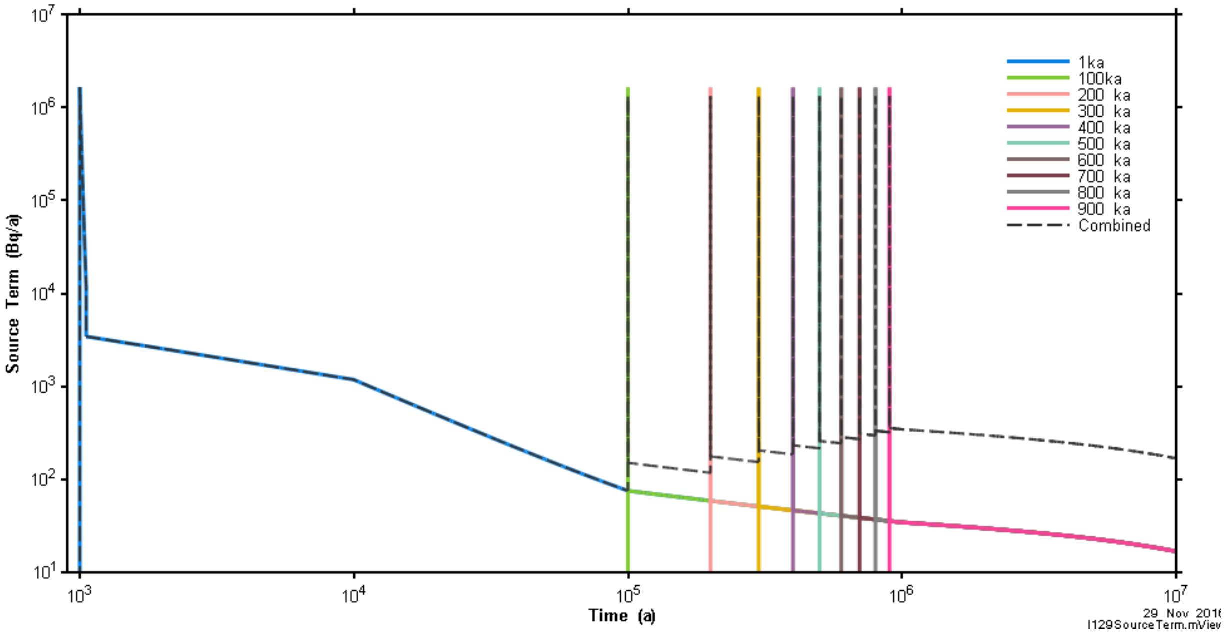

Figure 7-11: I-129 Source Term

Three-dimensional transport calculations are also performed for C-14, Ca-41, Cs-135, Se-79, and U-238. Combined and individual container source terms for these radionuclides are shown in Figure 7-12 through Figure 7-17. Note that the C-14 source term (Figure 7-12) appears for only two containers. This is because the half-life of C-14 (5730 years) is sufficiently short that C-14 has decayed away to insignificant levels at longer times.

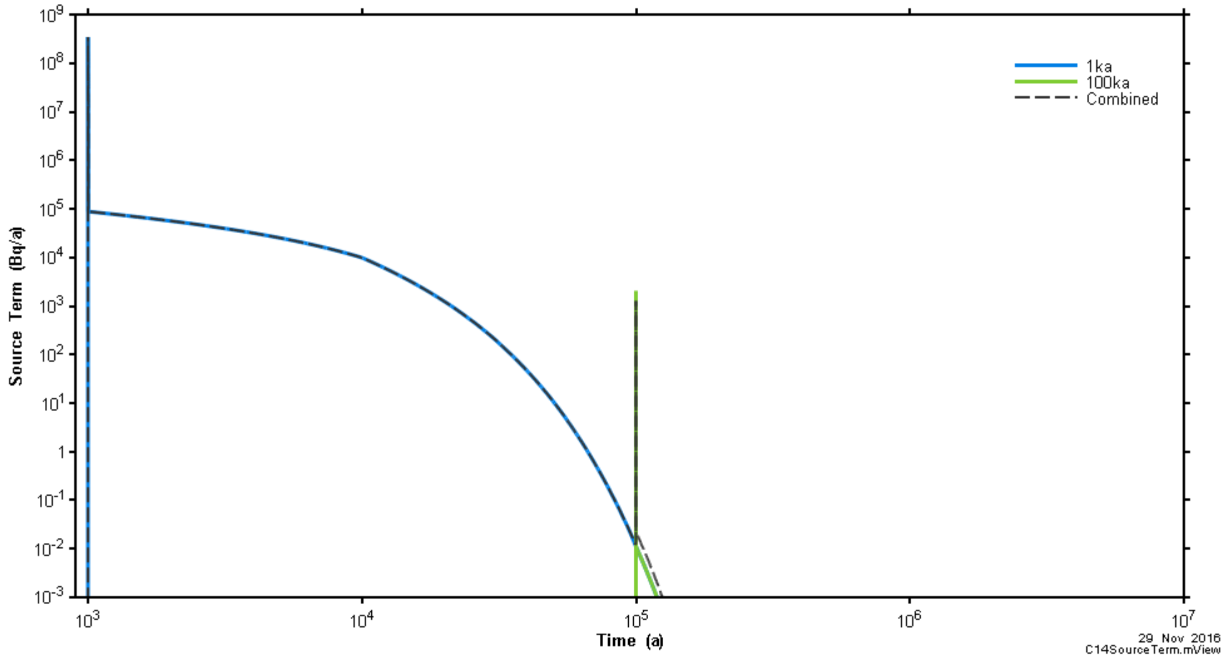

Figure 7-12: C-14 Source Term

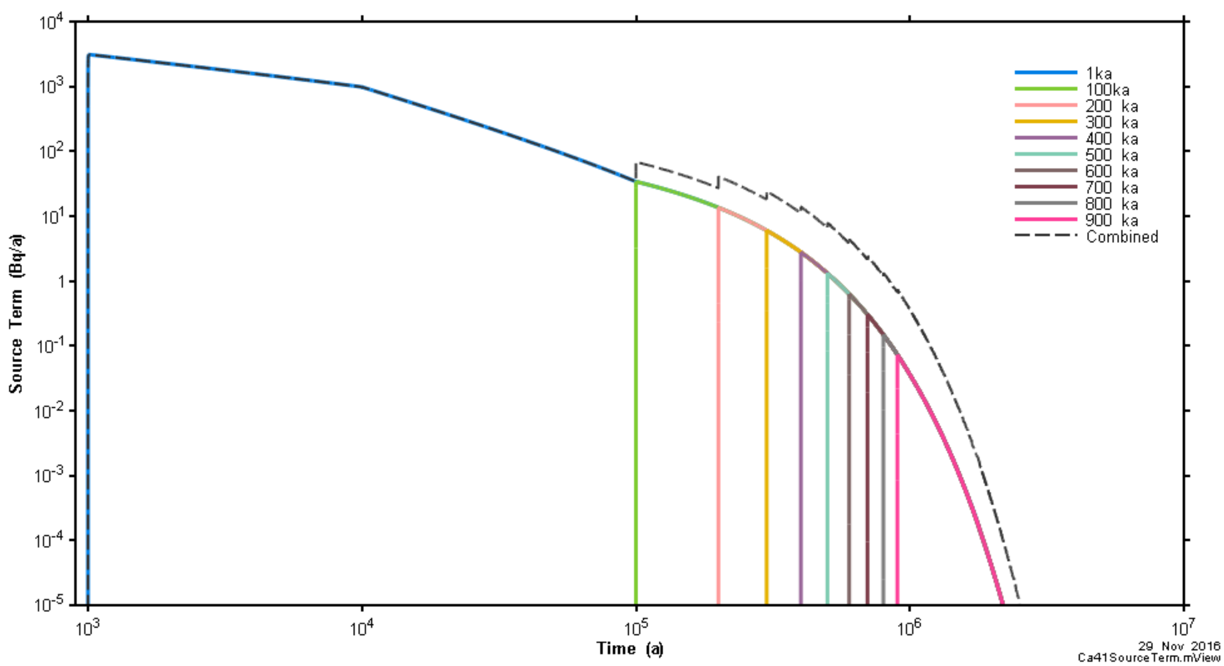

Figure 7-13: Ca-41 Source Term

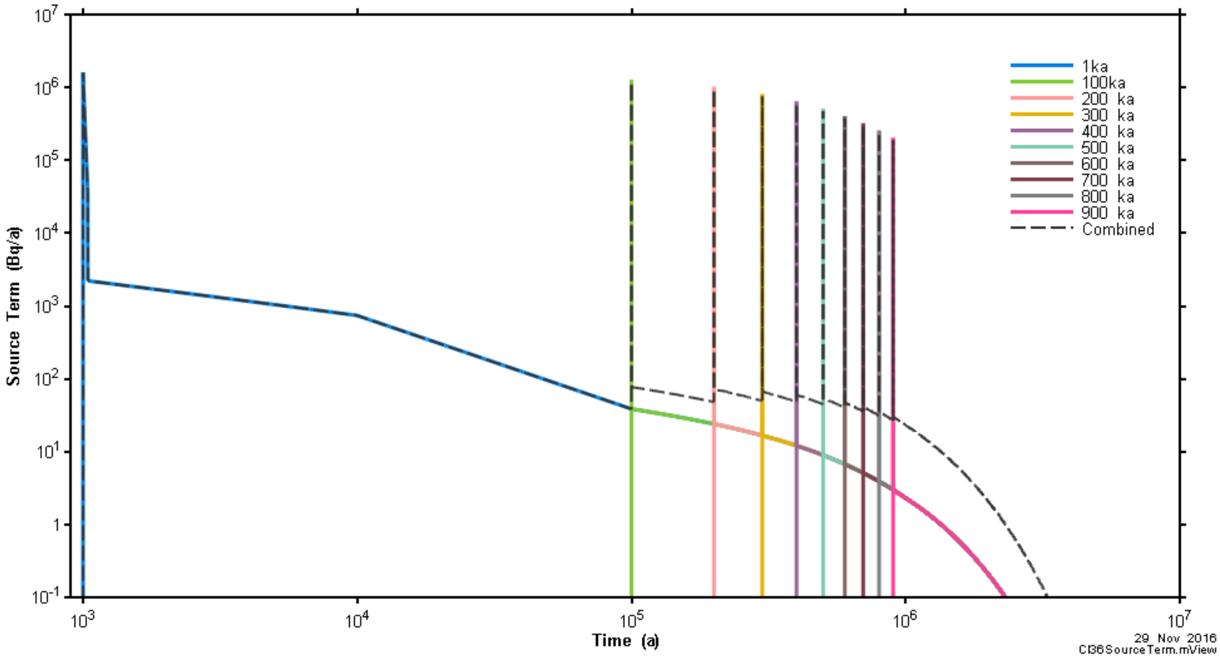

Figure 7-14: Cl-36 Source Term

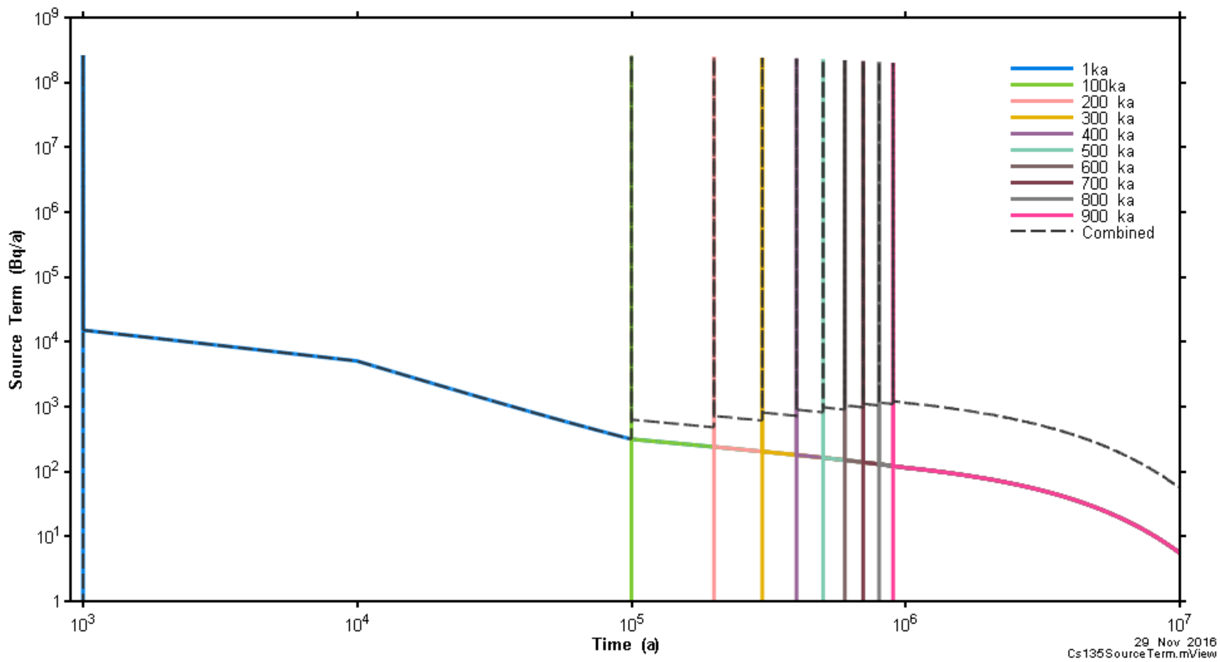

Figure 7-15: Cs-135 Source Term

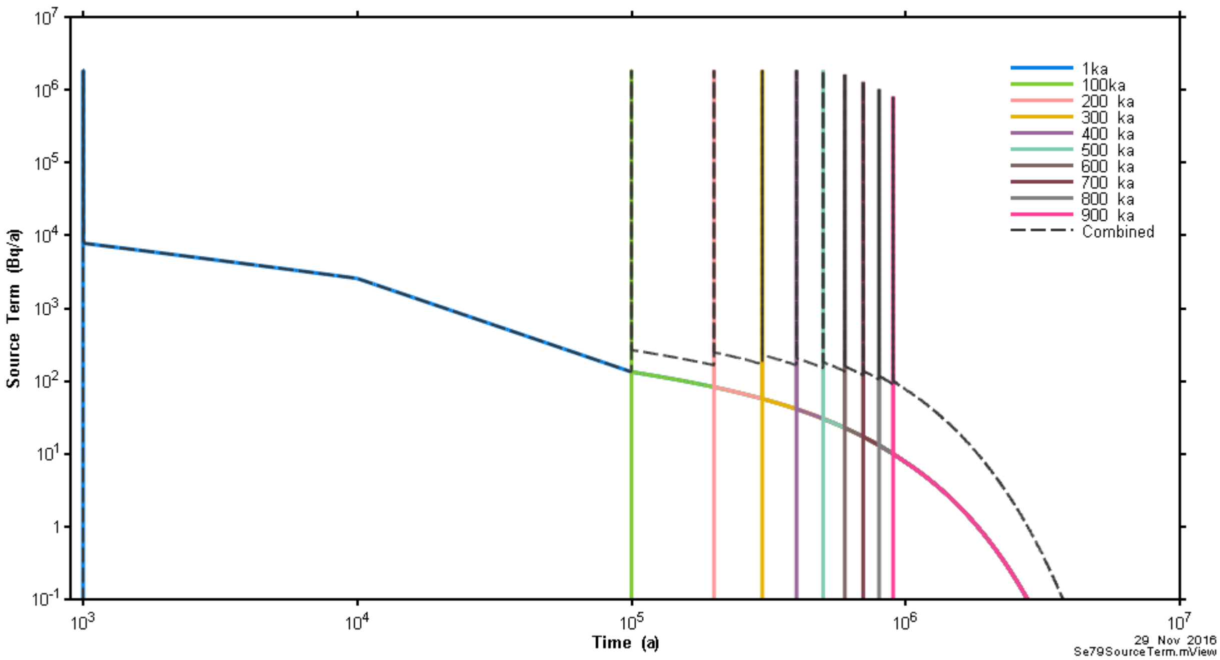

Figure 7-16: Se-79 Source Term

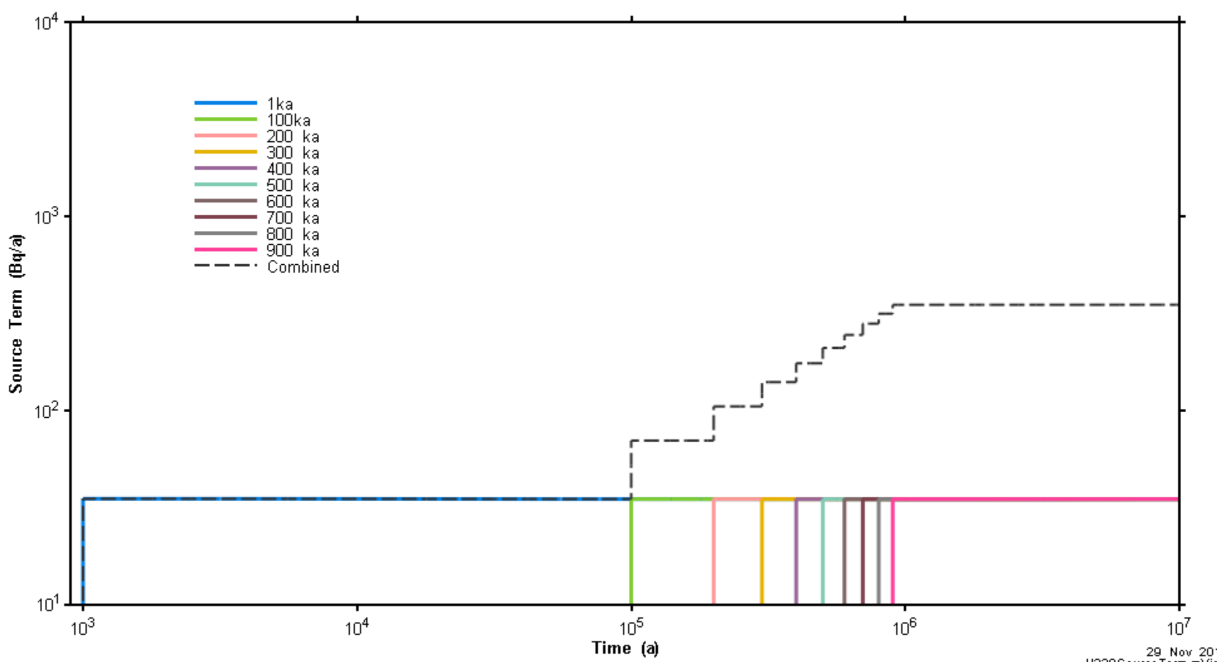

Figure 7-17: U-238 Source Term

Figure 7-18 shows the I-129 source term for the All Containers Fail Disruptive Event Scenarios.

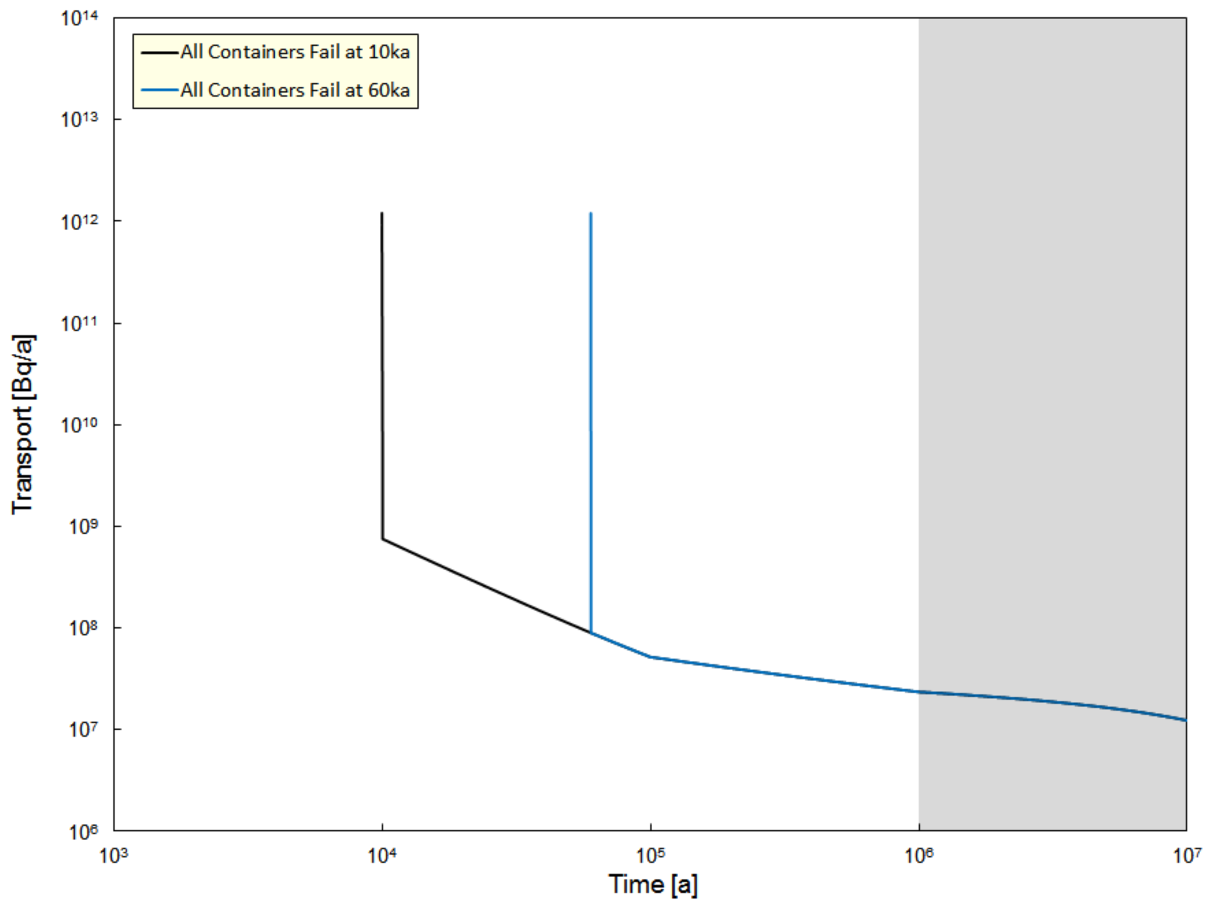

Figure 7-18: I-129 Source Term for the All Containers Fail Cases

7.5.2.3 Reference Groundwater Composition

The groundwater around the repository is slightly saline (see Chapter 2). Table 7-15 shows the reference groundwater composition at repository depth. This shows two compositions, one with rock porewater equilibrated with the host granitic rock, and one with rock porewater equilibrated with the buffer and steel, representing the water that could be seen by the container and used fuel.

Table 7-15: Reference Groundwater Composition at Repository Depth

Groundwater	CR-10 EQ	CR-10 NF
pH	7.1	8.7
Environment	Reducing	Reducing
Eh (mV)	-194	-575
Density (g/mL)	1.006	1.006
Solutes (mg/L)		
Na	1,899	6,255
K	15	80
Ca	2,217	870
Mg	60	182
HCO_3	50	4
SO_4	1,243	4,314
Cl	6,099	6,059
Sr	25	25
F	2	2
Si	5	10
Fe	8	7
NO_3	1	1
PO_4	1	1
Total Dissolved Solids (mg/L)	11,625	17,810

Note: CR-10 EQ is equilibrated with minerals in the host rock (i.e., quartz, gypsum, calcite, magnetite and goethite), and CR-10 NF is CR-10 EQ equilibrated with both the carbon steel insert and bentonite.

From Gobien et al. (2016)

7.5.2.4 Element Solubilities

Element solubilities for all contaminants emerging from the screening assessment (see Section 7.6) are shown in Table 7-16. These have been calculated for the two groundwater compositions shown above at 25ºC, with the higher of the resulting values selected. To account for the higher temperatures in the near field and for uncertainties in the conditions near the container (e.g., pH, salinity, minor species), the solubility values shown in Table 7-16 are 10 times higher than the calculated solubilities.

Any elements not listed are assigned a solubility of 2000 mol/m^3 to ensure they are treated as a fully soluble species.

Table 7-16: Element Solubilities

Element	Value (mol/kg)	GSD	Distribution Type
Ac	2.0	-	Constant
Ag	1.1×10^{-4}	3.2	Lognormal
Am	2.2×10^{-4}	3.2	Lognormal
Bi	1.2×10^{-4}	3.2	Lognormal
Br	2.0	-	Constant
C	8.3×10^{-3}	3.2	Lognormal
Ca	2.0	-	Constant
Cd	7.6×10^{-4}	3.2	Lognormal
Cl	2.0	-	Constant
Cs	2.0	-	Constant
Cu*	1.4×10^{-7}	3.2	Lognormal
Hg	2.0	-	Constant
I	2.0	-	Constant
Mo	2.0	-	Constant
Np	1.1×10^{-8}	3.2	Lognormal
Pa	2.2×10^{-8}	10	Lognormal
Pb	8.0×10^{-5}	3.2	Lognormal
Pd	4.1×10^{-5}	3.2	Lognormal
Po	2.0	-	Constant
Pu	9.1×10^{-7}	3.2	Lognormal
Ra	1.6×10^{-6}	3.2	Lognormal
Rn	2.0	-	Constant
Sb	5.7×10^{-4}	3.2	Lognormal
Se	1.3×10^{-7}	3.2	Lognormal
Sn	9.6×10^{-6}	3.2	Lognormal
Sr	2.0	-	Constant
Tc	2.0	-	Constant
Te	2.0	-	Constant
Th	2.5×10^{-7}	3.2	Lognormal
U	3.5×10^{-8}	3.2	Lognormal
W	2.0	-	Constant

Note: From Gobien et al. (2016)

GSD = Geometric Standard Deviation

*Cu is also included due to the container coating

The values shown are 10 times higher than those in the original references

[3]This current work erroneously assumed solubilities of 2.0 for Mo and Tc instead of 8.7×10^{-8} and 4.0×10^{-8}. Differences in results were assessed and found to be inconsequential. Corrected values will be adopted in future case studies.

7.5.2.5 Effective Diffusion Coefficients

Data for effective diffusion coefficients for 100% bentonite and for the various geosphere units are shown in Table 7-17. The effective diffusivity of all contaminants in concrete is set to 3.9×10^{-3} m^2/a, while the effective diffusivity of all contaminants in asphalt is set to 3.16×10^{-6} m^2/a.

Table 7-17: Effective Diffusion Coefficients, Base Case Values (m^2/a)

Element	100% Bentonite	Deep / Intermediate Rock	Shallow Rock	Fracture	Overburden	Sediment
Ac	4.4×10^{-3}	5.8×10^{-6}	9.6×10^{-5}	3.2×10^{-3}	1.3×10^{-2}	1.2×10^{-2}
Ag	4.4×10^{-3}	9.5×10^{-6}	1.6×10^{-4}	5.3×10^{-3}	2.2×10^{-2}	2.0×10^{-2}
Am	4.4×10^{-3}	5.8×10^{-6}	9.6×10^{-5}	3.2×10^{-3}	1.3×10^{-2}	1.2×10^{-2}
Bi	4.4×10^{-3}	1.2×10^{-5}	2.0×10^{-4}	6.7×10^{-3}	2.8×10^{-2}	2.5×10^{-2}
Br	3.5×10^{-4}	1.1×10^{-5}	1.9×10^{-4}	6.3×10^{-3}	2.6×10^{-2}	2.4×10^{-2}
C	4.4×10^{-3}	6.8×10^{-6}	1.1×10^{-4}	3.8×10^{-3}	1.6×10^{-2}	1.4×10^{-2}
Ca	4.4×10^{-3}	4.5×10^{-6}	7.5×10^{-5}	2.5×10^{-3}	1.1×10^{-2}	9.4×10^{-3}
Cd	4.4×10^{-3}	4.1×10^{-6}	6.9×10^{-5}	2.3×10^{-3}	9.7×10^{-3}	8.6×10^{-3}
Cl	3.5×10^{-4}	1.1×10^{-5}	1.9×10^{-4}	6.3×10^{-3}	2.6×10^{-2}	2.4×10^{-2}
Cs	1.3×10^{-2}	1.2×10^{-5}	2.0×10^{-4}	6.7×10^{-3}	2.8×10^{-2}	2.5×10^{-2}
Hg	4.4×10^{-3}	1.2×10^{-5}	2.0×10^{-4}	6.7×10^{-3}	2.8×10^{-2}	2.5×10^{-2}
I	3.5×10^{-4}	1.1×10^{-5}	1.9×10^{-4}	6.3×10^{-3}	2.6×10^{-2}	2.4×10^{-2}
Mo	4.4×10^{-3}	5.8×10^{-6}	9.6×10^{-5}	3.2×10^{-3}	1.3×10^{-2}	1.2×10^{-2}
Np	4.4×10^{-3}	5.8×10^{-6}	9.6×10^{-5}	3.2×10^{-3}	1.3×10^{-2}	1.2×10^{-2}
Pa	4.4×10^{-3}	5.8×10^{-6}	9.6×10^{-5}	3.2×10^{-3}	1.3×10^{-2}	1.2×10^{-2}
Pb	4.4×10^{-3}	1.2×10^{-5}	2.0×10^{-4}	6.7×10^{-3}	2.8×10^{-2}	2.5×10^{-2}
Pd	4.4×10^{-3}	5.8×10^{-6}	9.6×10^{-5}	3.2×10^{-3}	1.3×10^{-2}	1.2×10^{-2}
Po	4.4×10^{-3}	1.2×10^{-5}	2.0×10^{-4}	6.7×10^{-3}	2.8×10^{-2}	2.5×10^{-2}
Pu	4.4×10^{-3}	5.8×10^{-6}	9.6×10^{-5}	3.2×10^{-3}	1.3×10^{-2}	1.2×10^{-2}
Ra	4.4×10^{-3}	5.0×10^{-6}	8.4×10^{-5}	2.8×10^{-3}	1.2×10^{-2}	1.1×10^{-2}
Rn	4.4×10^{-3}	1.2×10^{-5}	2.0×10^{-4}	6.7×10^{-3}	2.8×10^{-2}	2.5×10^{-2}
Sb	4.4×10^{-3}	1.2×10^{-5}	2.0×10^{-4}	6.7×10^{-3}	2.8×10^{-2}	2.5×10^{-2}
Se	4.4×10^{-3}	5.8×10^{-6}	9.6×10^{-5}	3.2×10^{-3}	1.3×10^{-2}	1.2×10^{-2}
Sn	4.4×10^{-3}	5.8×10^{-6}	9.6×10^{-5}	3.2×10^{-3}	1.3×10^{-2}	1.2×10^{-2}
Sr	4.4×10^{-3}	4.5×10^{-6}	7.5×10^{-5}	2.5×10^{-3}	1.1×10^{-2}	9.4×10^{-3}
Tc	4.4×10^{-3}	5.8×10^{-6}	9.6×10^{-5}	3.2×10^{-3}	1.3×10^{-2}	1.2×10^{-2}
Te	4.4×10^{-3}	1.2×10^{-5}	2.0×10^{-4}	6.7×10^{-3}	2.8×10^{-2}	2.5×10^{-2}
Th	4.4×10^{-3}	5.8×10^{-6}	9.6×10^{-5}	3.2×10^{-3}	1.3×10^{-2}	1.2×10^{-2}
U	4.4×10^{-3}	5.8×10^{-6}	9.6×10^{-5}	3.2×10^{-3}	1.3×10^{-2}	1.2×10^{-2}
W	4.4×10^{-3}	5.8×10^{-6}	9.6×10^{-5}	3.2×10^{-3}	1.3×10^{-2}	1.2×10^{-2}

Note: From Gobien et al. (2016)

7.5.2.6 Sorption Parameters

Data for sorption coefficients for 100% bentonite, backfill, and concrete are shown in Table 7-18. Values for other materials (e.g., soil, sediment, and overburden) can be found in Gobien et al. (2016). Note that owing to a lack of sorption data, and due to the small porosity and limited physical extent of this material, all sorption coefficients for the asphalt shaft seal are conservatively set to zero.

Table 7-18: EBS Sorption Coefficients (K_d), Base Case Values (m^3/kg)

Element	100% Bentonite	Dense Backfill Blocks	Concrete
Ac	61	19	80
Ag	0	3.5×10^{-3}	0
Am	61	19	80
Bi	35	2.5	0
Br	0	0	0
C	0	0	0
Ca	4.5×10^{-3}	1.5×10^{-3}	1.0×10^{-3}
Cd	4.5×10^{-3}	1.5×10^{-3}	1.0×10^{-3}
Cl	0	0	5.0×10^{-3}
Cs	0.093	0.036	5.0×10^{-4}
Hg	0	0	0
I	0	0	0
Mo	0	0	0
Np	63	19	80
Pa	3	0.97	0.1
Pb	74	22	0.5
Pd	5	1.5	0
Po	0.06	0	0
Pu	63	19	80
Ra	4.5×10^{-3}	0	0.05
Rn	0	0	0
Sb	4.5×10^{-3}	1.5×10^{-3}	1.0×10^{-3}
Se	0	7.0×10^{-5}	0.03
Sn	63	19	10
Sr	4.5×10^{-3}	1.5×10^{-3}	1.0×10^{-3}
Tc	63	19	10
Te	0	7.0×10^{-5}	0.03
Th	63	19	80
U	63	19	2
W	0	0	0

Note: From Gobien et al. (2016)

Sorption in the geosphere is based on the values shown in Table 7-19. No distinction is made between sorption values for the bulk granite and for fracture materials in this study, given the absence of site-specific data on the host rock and minerals. More information concerning these values is available in Gobien et al. (2016).

Table 7-19: Geosphere Sorption Coefficients K_d for Fractures and Crushed Rock

Element	Distribution	Salinity / Oxidation	GM [m^3/kg]	GSD [-]	Lower Limit [m^3/kg]	Upper Limit [m^3/kg]
Ac	Lognormal	-	3	1.4	1	5
Ag	Lognormal	Non-Saline	0.5	1.7	0.1	1
		Saline	0.05	1.7	0.01	0.1
Am	Lognormal	-	13	3.9	0.22	190
Bi	Lognormal	-	0.001	2.2	0.0001	0.01
Br	Constant	-	0	-		
C	Lognormal	-	0.001	1.3	5.0×10^{-4}	2.0×10^{-3}
Ca	Lognormal	Non-Saline	1.3×10^{-2}	2.4	1.0×10^{-3}	6.1×10^{-1}
		Saline	9.8×10^{-5}	1.9	1.4×10^{-5}	5.0×10^{-4}
Cd	Lognormal	Non-Saline	0.1	1.3	0.05	0.5
		Saline	0.02	1.3	0.01	0.1
Cl	Constant	-	0	-		
Cs	Lognormal	Non-Saline	0.18	4.7	1.7×10^{-3}	9.6
		Saline	0.042	4.7	4.0×10^{-4}	2.0
Cu	Lognormal	Non-Saline	1.3×10^{-2}	2.4	1.0×10^{-3}	6.1×10^{-1}
		Saline	9.8×10^{-5}	1.9	1.4×10^{-5}	5.0×10^{-4}
Hg	Constant	-	0	-		
I	Constant	-	0	-		
Mo	Constant	-	0	-		
Np	Lognormal	Oxidizing	0.018	2.1	2.0×10^{-3}	2.2×10^{-1}
		Reducing	0.96	2.7	4.7×10^{-2}	20
Pa	Lognormal	-	1	1.3	5.0×10^{-1}	5
Pb	Lognormal	-	1.26	4	0.02	80.6
Pd	Lognormal	-	2.75	5	0.022	344
Po	Lognormal	-	0.1	2.2	0.01	1
Pu	Lognormal	-	5	1.7	1	10
Ra	Lognormal	-	0.175	3.16	5.5×10^{-3}	5.5
Rn	Constant	-	0	-		
Sb	Constant	-	0	-		
Se	Lognormal	-	0.001	1.3	5.0×10^{-4}	5.0×10^{-3}
Sn	Lognormal		0.71	6.3	2.8×10^{-3}	177
Sr	Lognormal	Non-Saline	1.3×10^{-2}	2.4	1.0×10^{-3}	6.1×10^{-1}
		Saline	9.8×10^{-5}	1.9	1.4×10^{-5}	5.0×10^{-4}
Tc	Constant	Oxidizing	0	-		
	Lognormal	Reducing	1	1.3	0.5	3
Te	Constant	-	0	-		
Th	Lognormal	-	1	1.3	5×10^{-1}	10
U	Lognormal	Oxidizing	0.0063	2.3	5.0×10^{-4}	1.2×10^{-1}
		Reducing	6.3	5.1	4.8×10^{-2}	280
W	Constant	-	0	-		

Note: From Gobien et al. (2016)

GM= Geometric Mean

7.6 Modelling and Results for Radionuclide and Chemical Hazard Screening

This section presents results for the radionuclide and chemical hazard screening assessment.

Section 7.5.1 describes how this fits into the overall assessment approach. Note that because the Inadvertent Human Intrusion Disruptive Scenario bypasses the geosphere barrier, the screening assessment described here does not apply and a separate scenario-specific screening assessment is required. This separate assessment is described in Section 7.9.1.

7.6.1 Methods

The Screening Model resembles the System Model used to perform the primary dose assessment; however, a more stylized and conservative representation is adopted. It is implemented in the RSM code. The following discusses the Screening Model in terms of its key features and whether they differ from those in the System Model.

- Solubility limits, diffusion coefficients, sorption coefficients and decay constants are the same.
- The fuel contaminant source term is the same.
- The container release model is the same.
- The EDZ is represented but in a simplified form.
- The near field (the engineered barriers) is represented by a simple one dimensional pathway consisting of a 0.218 m thick layer of bentonite buffer. The gapfill is not modelled.
- The geosphere is based on a one-dimensional diffusion-dispersion-advection transport model representing a single fast transport pathway. This pathway is composed of three zones, these being a segment of intact rock and two segments of transmissive fracture. The second fracture segment is connected to a well in the biosphere.

  The properties used to represent the three geosphere zones are shown in Table 7-20. These properties are selected to ensure a conservative representation of the transport time to the surface.

Table 7-20: Screening Model Geosphere Zone Properties

Geosphere Zone	Material Type	Length (m)	Velocity (m/a)	Porosity (-)	Tortuosity (-)
1	Rock Mass	77.8	5.32×10^{-3}	0.003	0.09
2	Fracture	337	2.11	0.1	0.03
3	Fracture	77.4	33.3	0.1	0.03

- The biosphere includes a limited set of exposure pathways. It calculates doses from water ingestion, groundshine, air immersion and air inhalation. The plant ingestion dose rate is estimated from the drinking water dose rate using an ingestion multiplication factor.

The following assumptions are also incorporated in the biosphere model to ensure conservative results:

- The well demand is set to that corresponding to a single person, excluding irrigation. This ensures the minimum amount of dilution.
- The surface soil is a small irrigated garden large enough to support only a single person. This maximizes the soil concentrations.
- Contaminant concentrations in any surface water present are set equal to those in the well. This maximizes the surface water concentrations.

7.6.1.1 Radionuclide Screening

Prior to running the Screening Model, a pre-screening is done. In this pre-screening, all radionuclides with half-lives longer than 0.1 years are included, as are radionuclides with half-lives longer than one day if they have a parent with a half-life longer than 0.1 years. This results in a total of 251 distinct radionuclides and 96 stable elements in the used fuel and zirconium fuel sheath requiring further consideration.

The Screening Model (i.e., the RSM code) is then run for the analysis cases shown in Table 7-21. A wide range of cases is considered to encompass the full suite of Normal Evolution sensitivity cases described in Section 7.2.2 and to provide confidence that the set of potentially significant radionuclides remains relevant should other sensitivity cases be subsequently identified. The limiting Disruptive Event Scenario (i.e., All Containers Fail) is also included because this is the event most likely to have the greatest consequence. All screening cases are run for a 10 million year simulation time. All cases use the solubility limited Zircaloy model except Cases 17 through 20.

Table 7-21: RSM Cases Considered for the Screening Assessment

Case	Case ID	Case	Case ID
1	Median Case	11	Low (3σ) Sorption Everywhere with High (3σ) Solubility Limits
2	Fuel Dissolution Rate Increased by a Factor of 10	12	All Model Parameters Set to Conservative (High or Low) 3σ Values
3	All Fuel Instant Release Fractions Set to 0.1	13	Advective Velocity of Geosphere Decreased by a Factor of 10
4	No Solubility Limits	14	Geosphere Transport Time Increased to 30,000 Years
5	Geosphere Advective Velocity Increased by a Factor of 10	15	Geosphere Transport Time Increased to 73,000 Years
6	All Containers Fail at 100 Years	16	Geosphere Transport Time Increased to 146,000 Years
7	Fracture Standoff Distance Decreased to 10 m	17	Median Case (with Zircaloy Corrosion Model)

Case	Case ID	Case	Case ID
8	Fracture Standoff Distance Decreased to 25 m	18	Zircaloy Corrosion Model with 10 m Fracture Standoff Distance
9	No Sorption in the EBS	19	Zircaloy Corrosion Model with a Factor of 10 Increase in the Corrosion Rate
10	Low (3σ) Geosphere Sorption with High (3σ) Solubility Limits	20	All Zircaloy Instant Release Fractions Set to 0.1

The set of radionuclides that together contribute 0.1% or less of the total peak dose rate for each case are screened out, and the remaining superset of radionuclides identified over all cases is then carried forward into the postclosure safety assessment.

The results of the radionuclide screening assessment are described in Section 7.6.2.

7.6.1.2 Chemical Element Screening

For chemical element screening, the release rate of a given element from the repository to the biosphere is compared against the release rate arising from natural erosion processes occurring across the repository watershed. A total of 103 elements (from H to Lr) are considered in the screening. Elements that contribute more than 1% of the erosion release rate are screened in.

Erosion release rates are determined using the average of elemental concentrations in granite taken from Bowen (1979), Baumgartner (2000), Flavelle (1996), and Hart and Lush (2004).

Other important parameters are:

- The granite erosion rate is 6.5×10^{-6} m/a (Merrett and Gillespie 1983);
- The repository watershed is about 59 km^2 (Gobien et al. 2016); and
- The granite density is 2700 kg/m^3 (Gobien et al. 2016).

Table 7-22 shows the resulting averaged elemental concentrations in granite and the calculated erosion rates for each of the elements considered.

Table 7-22: Granite Elemental Erosion Rates for the Watershed Area

Element	Average Concentration in Granite [g/kg granite]	Erosion Rate [mol/a]	Element	Average Concentration in Granite [g/kg granite]	Erosion Rate [mol/a]
Ac	5.50×10^{-13}	2.51×10^{-9}	Mn	3.40×10^{-1}	6.42×10^{3}
Ag	4.25×10^{-5}	4.09×10^{-1}	Mo	1.88×10^{-3}	2.03×10^{1}
Al	7.42×10^{1}	2.85×10^{6}	N	1.90×10^{-2}	1.41×10^{3}
Am	0	0	Na	2.80×10^{1}	1.26×10^{6}
Ar	3.50×10^{-3}	9.09×10^{1}	Nb	1.95×10^{-2}	2.18×10^{2}
As	1.88×10^{-3}	2.60×10^{1}	Nd	3.43×10^{-2}	2.46×10^{2}
At	0	0	Ne	5.00×10^{-6}	2.57×10^{-1}
Au	2.00×10^{-6}	1.05×10^{-2}	Ni	1.63×10^{-3}	2.87×10^{1}
B	1.63×10^{-2}	1.56×10^{3}	No	0	0
Ba	6.25×10^{-1}	4.72×10^{3}	Np	0	0
Be	3.40×10^{-3}	3.91×10^{2}	O	4.68×10^{2}	3.03×10^{7}
Bi	9.88×10^{-5}	4.90×10^{-1}	Os	5.00×10^{-8}	2.73×10^{-4}
Bk	0	0	P	5.66×10^{-1}	1.90×10^{4}
Br	7.25×10^{-4}	9.41	Pa	1.40×10^{-9}	6.29×10^{-6}
C	3.28×10^{-1}	2.83×10^{4}	Pb	1.85×10^{-2}	9.26×10^{1}
Ca	1.03×10^{1}	2.65×10^{5}	Pd	5.18×10^{-6}	5.04×10^{-2}
Cd	9.75×10^{-5}	9.00×10^{-1}	Pm	0	0
Ce	1.01×10^{-1}	7.48×10^{2}	Po	2.00×10^{-13}	1.00×10^{-9}
Cf	0	0	Pr	9.73×10^{-3}	7.16×10^{1}
Cl	2.85×10^{-1}	8.34×10^{3}	Pt	2.75×10^{-7}	1.46×10^{-3}
Cm	0	0	Pu	0	0
Co	5.80×10^{-3}	1.02×10^{2}	Ra	8.10×10^{-10}	3.72×10^{-6}
Cr	7.55×10^{-3}	1.51×10^{2}	Rb	1.63×10^{-1}	1.97×10^{3}
Cs	4.75×10^{-3}	3.71×10^{1}	Re	5.80×10^{-7}	3.23×10^{-3}
Cu	2.09×10^{-2}	3.40×10^{2}	Rh	6.00×10^{-7}	6.05×10^{-3}
Dy	4.35×10^{-3}	2.78×10^{1}	Rn	4.00×10^{-16}	1.87×10^{-12}
Er	2.90×10^{-3}	1.80×10^{1}	Ru	5.50×10^{-7}	5.64×10^{-3}
Es	0	0	S	3.88×10^{-1}	1.25×10^{4}
Eu	1.13×10^{-3}	7.70	Sb	1.35×10^{-4}	1.15
F	1.10	6.01×10^{4}	Sc	5.95×10^{-3}	1.37×10^{2}
Fe	2.15×10^{1}	4.00×10^{5}	Se	4.38×10^{-5}	5.75×10^{-1}
Fm	0	0	Si	3.37×10^{2}	1.24×10^{7}
Fr	0	0	Sm	6.95×10^{-3}	4.79×10^{1}
Ga	1.85×10^{-2}	2.75×10^{2}	Sn	3.53×10^{-3}	3.08×10^{1}
Gd	6.18×10^{-3}	4.07×10^{1}	Sr	2.43×10^{-1}	2.87×10^{3}
Ge	1.90×10^{-3}	2.71×10^{1}	Ta	3.13×10^{-3}	1.79×10^{1}

Element	Average Concentration in Granite [g/kg granite]	Erosion Rate [mol/a]	Element	Average Concentration in Granite [g/kg granite]	Erosion Rate [mol/a]
H	5.30×10^{-1}	5.45×10^{5}	Tb	7.28×10^{-4}	4.75
He	8.00×10^{-6}	2.07	Tc	0	0
Hf	5.70×10^{-3}	3.31×10^{1}	Te	5.00×10^{-6}	4.06×10^{-2}
Hg	5.50×10^{-5}	2.84×10^{-1}	Th	3.05×10^{-2}	1.36×10^{2}
Ho	7.70×10^{-4}	4.84	Ti	1.80	3.90×10^{4}
I	1.93×10^{-4}	1.57	Tl	1.10×10^{-3}	5.58
In	4.25×10^{-5}	3.84×10^{-1}	Tm	2.60×10^{-4}	1.60
Ir	3.50×10^{-8}	1.89×10^{-4}	U	4.85×10^{-3}	2.11×10^{1}
K	3.78×10^{1}	1.00×10^{6}	V	4.75×10^{-2}	9.67×10^{2}
Kr	1.00×10^{-7}	1.24×10^{-3}	W	1.50×10^{-3}	8.46
La	5.60×10^{-2}	4.18×10^{2}	Xe	3.00×10^{-8}	2.37×10^{-4}
Li	2.78×10^{-2}	4.15×10^{3}	Y	2.90×10^{-2}	3.38×10^{2}
Lr	0	0	Yb	2.40×10^{-3}	1.44×10^{1}
Lu	3.50×10^{-4}	2.07	Zn	5.33×10^{-2}	8.45×10^{2}
Md	0	0	Zr	3.13×10^{-1}	3.55×10^{3}
Mg	3.18	1.35×10^{5}			

Table 7-22 shows that environmental concentrations in granite (and therefore erosion release rates) are not available for Am, At, Bk, Cf, Cm, Es, Fm, Fr, Lr, Md, No, Np, Pm, Pu and Tc.

- Of these, Am, Bk, Cf, Cm, Es, Fm, Lr, Md, No, Np and Pu are actinides with no stable isotopes. For these, it is reasonable to assume that the hazard is adequately addressed through radiological considerations and these elements are therefore excluded from the non-radiological hazard assessment.
- Of the remaining elements for which no granite data exist (i.e., At, Fr, Pm, and Tc), all isotopes of At, Fr and Pm are relatively short-lived unstable species (e.g., the longest half-life is for Pm at 17.7 years). Given that these elements also have relatively low abundance in the fuel (as compared to I), At, Fr and Pm are also excluded from the non-radiological hazard assessment.
- The remaining element, Tc, also has no stable isotopes; however, it has a few long-lived isotopes and it is present in the fuel in appreciable quantities relative to I. Tc-99 is therefore included in spite of it being excluded in the screening process.

Other elements are screened in (or out) on the basis of RSM simulations of the analysis cases shown in Table 7-21. As done for the radionuclide screening assessment, a wide range of cases is considered to encompass the full suite of Normal Evolution sensitivity cases described in Section 7.2.2 and to provide confidence that the set of potentially significant chemical elements will remain relevant should other sensitivity cases be subsequently identified. The limiting Disruptive Event Scenario (i.e., All Containers Fail) is also included because this is the event most likely to have the greatest consequence. All RSM cases are run for a 10 million year simulation time.

The results of the chemical element screening assessment are described below.

7.6.2 Results

This section presents results of the screening analysis.

Table 7-23 shows the superset of radionuclides and potentially hazardous elements that emerged from the screening assessments described above. There are 26 radionuclides from the fuel and two from the Zircaloy, and 26 chemically hazardous elements from the fuel and two from the Zircaloy.

Table 7-23: Superset of Screened in Radionuclides and Chemically Hazardous Elements

Radionuclides	Chemically Hazardous Elements
Fuel Ac-225, Ac227, Bi-210, C-14, Ca-41, Cl-36, Cs-135, I-129, Np-237, Pa-231, Pb-210, Po-210, Ra-223, Ra-225, Ra-226, Ra-228, Rn-222, Sb-126, Se-79, Sn-126, Sr-90, Th-229, Th-230, U-234, U-236, U-238 **Zircaloy** C-14, Cl-36	**Fuel** Ag, Au[1], Bi, Br, Cd, Hg, I, In[1], Ir[1], Kr[1], Mo, Os[1], Pd[1], Po[1], Pt[1], Ra[1], Rh[1], Rn[1], Ru[1], Sb, Se, Tc[2], Te, U[2], W, Xe[1] **Zircaloy** Pt[1], Te

[1]These elements are excluded from the System Model simulations
[2]These elements are included despite not being identified in the initial screening analysis

Several of the elements in Table 7-23 (i.e., Au, In, Ir, Kr, Os, Pd, Po, Ra, Rh, Rn, Ru and Xe) do not have environmental criteria specified in Canadian or international sources (Medri 2015c and as illustrated by their absence from Table 7-1) and therefore cannot be considered further. Of these elements:

- Kr and Xe are noble gases and their exclusion is justified on the basis that they are effectively inert;
- Po, Ra, and Rn are radionuclides and their exclusion is justified on the basis that they are assumed to be more radiologically hazardous than chemically hazardous; and
- Au is used in jewellery and its exclusion is justified on the basis that it is in common everyday use and it is therefore reasonable to assume its toxicity level is low.

Pt, which has an airborne environmental criterion in Table 7-1, is also excluded on the same basis as Au (i.e., it is in common every day usage in jewellery). Furthermore, Pt is non-volatile and releases from the repository are not likely to establish a significant airborne concentration.

Regarding the remaining elements (i.e., In, Ir, Os, Pd, Rh and Ru), options are being considered for obtaining toxicity information. In the meantime, Table 7-24 shows the ratio comparing environmental release rates from the repository to release rates from granite erosion. For completeness, the elements excluded in the discussion above (Au, Kr, Po, Ra, Rn, Xe, and Pt) are also shown.

Table 7-24: Ratios of Repository Release Rates to Erosion Release Rates for Elements without Environmental Criteria

Element	All Containers Fail Ratio	Normal Evolution Case Ratio
Au	0.76	1.5×10^{-4}
In	0.17	3.4×10^{-5}
Ir	29	5.7×10^{-3}
Kr	2800	0.55
Os	82	0.016
Pd	15	0.003
Po	0	0
Pt	1.31	2.6×10^{-4}
Ra	1.13×10^{-10}	2.2×10^{-14}
Rh	950	0.19
Rn	0	0
Ru	2800	0.56
Xe	1.71×10^{5}	34

Ratio is Transport Release Rate from the Repository / Erosion Rate from the Rock. The Normal Evolution results correspond to the Base Case, as the parameters for this case represent the most likely set.

The table shows that for the Base Case of the Normal Evolution Scenario (i.e., the case with the most likely values for sorption), the release rates for In, Ir, Os, Pd, Rh and Ru are small fractions of the natural erosion rates. For the Normal Evolution Scenario, it is therefore reasonable to conclude that the presence of the repository is not significant in terms of increased non-radiological hazard for these elements.

For the highly unlikely All Containers Fail Disruptive Event Scenario, Table 7-24 shows higher ratios due to the greater number of failed containers. Larger multiples are associated with Ir, Os, Pd, Rh and Ru.

Note that U was not identified in the screening assessment due to the significant amount of U present in granite and due to the immobile nature of U in the repository (i.e., U is essentially insoluble and highly sorbing). Despite this, U has been included in the System Model simulations because of anticipated interest in its behaviour. Also, as noted in Section 7.6.1.2, Tc is included in the system simulations because there is no granite data upon which to exclude it, plus it has a few long-lived isotopes and is present in the fuel in appreciable quantities relative to I.

To summarize, there are 13 chemically hazardous elements included in the System Model simulations. The elements are: Ag, Bi, Br, Cd, Hg, I, Mo, Sb, Se, Tc, Te, U, and W.
To account for radioactive decay and ingrowth, additional parent isotopes must be included.

Table 7-25 and Table 7-26 show the complete sets of potentially significant radionuclides and potentially significant chemically hazardous elements that are carried through into the System Model assessments. Items in red have been identified directly in the screening assessment (i.e., Table 7-23) while items in black have been added to account for in-growth. In all, 11 additional radionuclides are included for the radiological hazard and 18 additional radionuclides are included for the non-radiological hazard.

Table 7-25: List of Potentially Significant Radionuclides

Radionuclides	
Fuel	
Single Nuclides	Cl-36, I-129, C-14, Cs-135, Ca-41, Se-79, Sr-90
Chain Nuclides	Pu-239 → U-235 = Th-231 → Pa-231 = Ac-227 = Th-227 = Ra-223
	Pu-240 → U-236 → Th-232 = Ra-228
	Pu-242 → U-238 = Th-234 → U-234 → Th-230 → Ra-226 = Rn-222 = Pb-210 = Bi-210 = Po-210
	Am-241 → Np-237 = Pa-233 → U-233 → Th-229 = Ra-225 = Ac-225
	Sn-126 → Sb-126
Zircaloy	
Single Nuclides	C-14, Cl-36

Note: '=' means the radionuclides are in secular equilibrium with their parent because of their short half-life

Table 7-26: List of Potentially Significant Chemically Hazardous Elements

Chemically Hazardous Elements	
Fuel	
Elements	Cd, Hg, I, Mo, Sb, Se, Tc, W
Chains	Pu-239 → U-235
	Pu-240 → U-236
	Pu-242 → U-238 = Th-234 → U-234 → Th-230 → Ra-226 = Rn-222 = Pb-210 = Bi-210
	Am-241 → Np-237 = Pa-233 → U-233 → Th-229 = Ra-225 = Ac-225 → Bi
Misc	Pd 107 → Ag Se-79 → Br Sn-126 → Sb-126 → Te
Zircaloy	
Elements	Te

Note: '=' means the radionuclides are in secular equilibrium with their parent because of their short half-life

7.7 Modelling and Results for 3D Groundwater Flow and Radionuclide Transport

This section describes the detailed 3D groundwater flow and transport models illustrated inFigure 7-9 and implemented using FRAC3DVS-OPG. Section 7.5.1 describes how these models fit into the overall assessment approach.

With the exception of the Intermittent Well Sensitivity Case, all flow modelling is steady-state, which is consistent with the Base Case Normal Evolution Scenario constant climate assumption. Small changes in climate may affect the shallow groundwater system, but would not affect the deep groundwater system. The effects of large changes in climate associated with glacial cycles are discussed separately in Section 7.8.2.4.

7.7.1 Methods

7.7.1.1 Subregional-Scale Model

The Subregional-Scale Model simulates flow through the watershed enclosing the repository. The model provides head boundary conditions to the Repository-Scale Models to ensure the flow system within those models is an accurate representation of that in the larger watershed.

Regional-scale groundwater flow modelling of the Canadian Shield has indicated that flow patterns tend to be dominated more by local topography than by large regional flows (Sykes et al. 2003). The Subregional-Scale Model boundaries displayed in Figure 7-9 are therefore placed on topographical highs or lows that will likely form flow divides. These are also sufficiently far from the repository to preclude any interaction with contaminants escaping the repository.

<u>Domain Discretization and Permeability Profile</u>

Horizontally, the Subregional-Scale Model flow domain is discretized in variably sized elements. Discretization ranges from 100 m to 20 m outside the repository footprint, with a constant 20 m within the footprint. There are 336 nodes in the X direction and 342 nodes in the Y direction, for a total of 114,235 elements in each model layer. The complete grid consists of 64 layers for a total of 7.31 million elements, of which 1.78 million are located outside the flow-domain shown in Figure 7-9 and are set inactive. Although the repository footprint is shown in most plan-section figures in this section, there are no repository features or properties specified within the model grid. The repository representation in the figures is only provided to add context.

The bulk rock properties are described as a layered system with permeability decreasing with depth as discussed in Chapter 2. Hydraulic conductivities and model discretization are shown in Table 7-27. Base Case hydraulic conductivities are used in all simulations except for sensitivity studies that examine the effect of different geosphere hydraulic conductivities.

Table 7-27: Property Descriptors for Flow Model Layers

Depth (mBGS) or Elevation (mASL)	Thickness (m)	Hydraulic Conductivity (m/s)*			Model Layers
		Base Case	Sensitivity 1	Sensitivity 2	
Ground surface to 10 mBGS	10	$1x10^{-8}$	$1x10^{-8}$	$1x10^{-8}$	4 layers at 2.5 m
10 mBGS to 150 mBGS (232.5 mASL)	~140	$2x10^{-9}$	$2x10^{-8}$	$2x10^{-10}$	14 layers, variable thickness (6 m to 15 m)
150 – 700 mBGS (232.5 mASL to -317.5 mASL)	550	$4x10^{-11}$	$4x10^{-10}$	$4x10^{-12}$	26 layers, variable thickness (15 m to 35 m)
700 – 1500 mBGS (317.5 mASL to -1117.5 mASL)	800	$1x10^{-11}$	$1x10^{-10}$	$1x10^{-12}$	20 layers, variable thickness (35 to 45 m)

Notes: *Sensitivity 1 and Sensitivity 2 examine the effect of changes in geosphere hydraulic conductivity. See Section 7.2.2.3 and Table 7-5 for a further explanation.

Fracture hydraulic properties are constant with depth, with all fractures having a hydraulic conductivity of 1.0×10^{-6} m/s. Fracture zone thickness is set to 1 m with 10% porosity. The fracture system is implemented as an equivalent porous medium with properties averaged in elements that are intersected by fractures or that share faces with fractures mapped to element faces. Anisotropy in hydraulic conductivity within each fracture element is implemented to model vertical and horizontal fracture tendencies, while porosity is averaged to produce equivalent fracture element advective fluid velocities. Figure 7-19 illustrates fracture and rock mass hydraulic conductivity in an East-West vertical slice through the repository footprint.

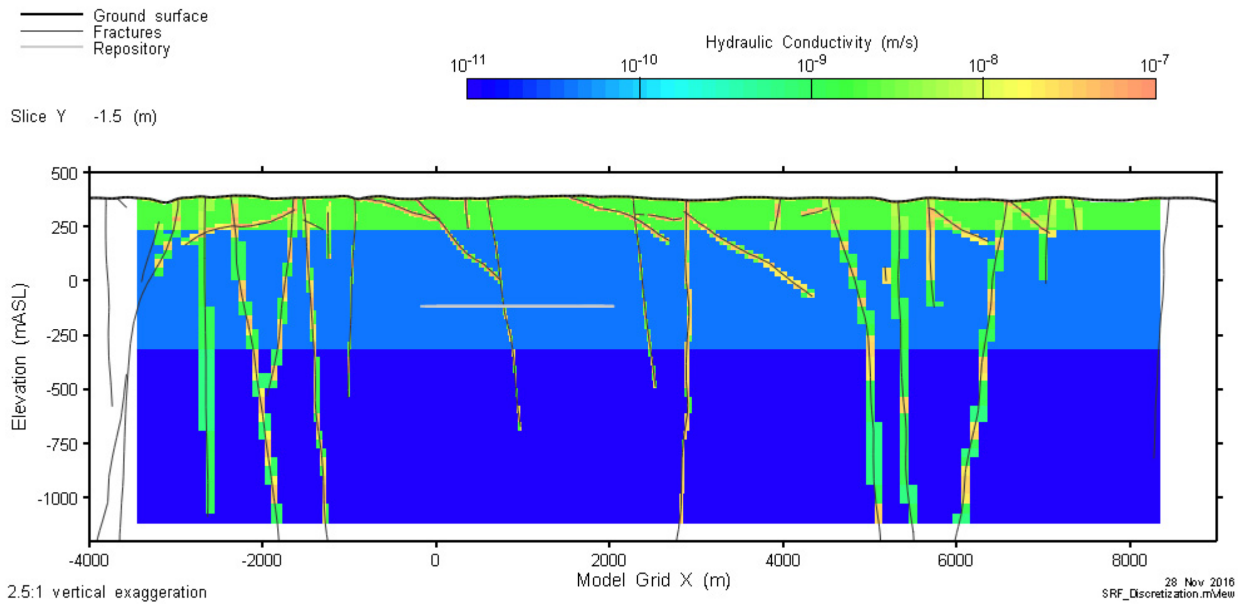

Note: the colour variation in the fracture is an artefact of the property averaging process used in the EPM approach

Figure 7-19: Subregional-Scale Model: EPM Fracture Network and Vertical Permeability Profile

<u>Boundary Conditions</u>

Zero-flow boundary conditions are specified on all external vertical faces and at the lower boundary of the model (about 1500 metres in depth), which are located far from the repository and, in the case of vertical faces, on topographic divides. Fixed head elevation boundary conditions are specified for the top surface of the model, representing a water table close to surface and reflecting the generally low topographic relief.

7.7.1.2 Repository-Scale Models

Repository-Scale Models are used to investigate transport to the well and surface environment for contaminants released from various locations in the repository. The "Full" Repository-Scale Model is discretized for all repository and EBS features except containers, while the "Rooms-Only" Repository-Scale Model includes only placement rooms and a simplified EDZ.

The Full Model is used for Base Case radionuclide transport, and for sensitivity studies related to the EBS, repository EDZ, and fracture and seal functionality. The Rooms-Only Model is used for determining high consequence well / container location pairs, for providing advective transport pathway information for development of the SYVAC3-CC4 System Model, and for all geosphere sensitivity cases. The Rooms-Only Model is used preferentially because the Full Model is computationally demanding, requiring both significantly more memory to execute and significantly more time to simulate. A comparison of the models presented in Section 7.7.2.3.1 shows Rooms-Only Model results are very similar to Full Model results.

The repository is located 500 m below ground surface (mBGS). Since the surface elevation varies slightly across the repository, the horizontal depths are also defined in terms of an absolute measure of m above sea level (mASL). The mean ground surface elevation within the repository footprint and immediate surrounding area is 382.5 mASL. This yields a hypothetical repository elevation of -117.5 mASL. The repository location and layout has been specified to ensure a minimum stand-off distance of 100 m from any sizeable fracture at the repository elevation (Figure 7-20). This required setting the gap between repository panels to 278.8 m. This distance was calculated using the intersection points of the perimeter and main tunnels with the between-panel fracture. The repository layout was adjusted such that the distance from a straight line connecting the fracture intersection points to the end of the placement rooms is no closer than 110 m (100 m plus 10% margin to allow for potential variation in fracture location within the rock).

The Repository-Scale Models are defined with reference to a common model coordinate system with an origin located at the intersection of the longest Central Access Tunnel and the Perimeter Tunnel at the Ventilation Shaft end of the repository, as shown in Figure 7-20. The X and Y axes follow the access tunnel and perimeter tunnel respectively. This allows natural finite-difference discretization of the generally orthogonal repository features. This coordinate system is used for most spatial figures presenting model results.

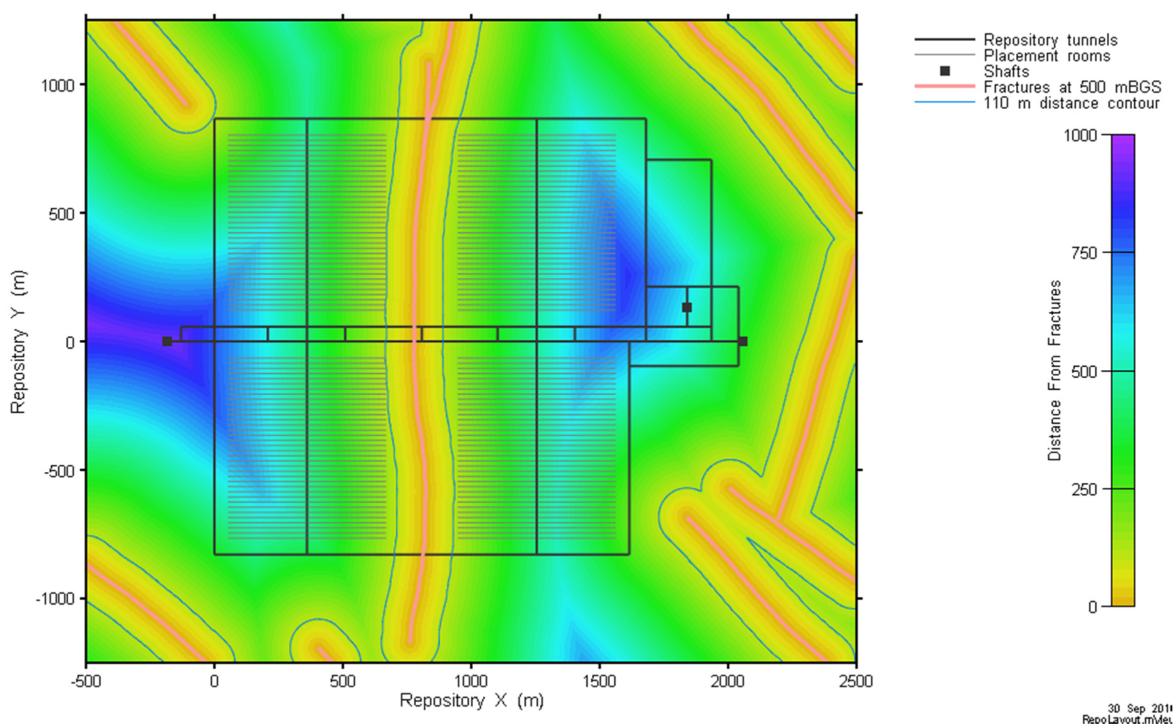

Figure 7-20: Repository Setting with Relation to Fracture System at 500 mBGS

Properties of the engineered barrier system are shown in Table 7-28. Within the repository, excavation-damaged zone (EDZ) properties are derived from the properties of the host rock. All repository tunnels and placement rooms have an Inner EDZ with hydraulic conductivity 100 times higher than the host rock hydraulic conductivity, and porosity twice that of the host rock.

Outer EDZ is assigned hydraulic conductivities 10 times greater than the host rock, while porosity is set equal to the host rock.

An Inner and Outer EDZ is defined for the shafts as well, with Inner EDZ having hydraulic conductivity 100 times greater than that of the host rock and Outer EDZ conductivity increased by a factor of 10 relative to the host rock. Inner EDZ porosity is doubled compared to the host rock. Shaft Inner and Outer EDZ are specified for intermediate and shallow bedrock, but not for overburden. All other EDZ parameters are set equal to those of the host rock.

Table 7-28: Engineered Barrier Hydraulic Properties

Property Identifier	Description	Hydraulic Conductivity (m/s)	Porosity (m)
Tunnel Dense Backfill	Used to backfill repository tunnels	9.0×10^{-11}	0.194
Tunnel Seal Bentonite (Compacted Bentonite)	Used for room seals	1.0×10^{-13}	0.416
Placement Room Bentonite (Homogenized Buffer)	Homogenized mixture of gap fill, buffer box, and spacer blocks in placement rooms at 85C	3.1×10^{-13}	0.415
Concrete, degraded	Low Heat High Performance Concrete (LHHPC) used for room closure and shaft bulkheads	1.0×10^{-10}	0.1
Shaft Bentonite/Sand	Primary Shaft Seal material, 70:30 bentonite to sand	5.0×10^{-13}	0.411
Shaft Asphalt	Additional shaft sealing material	1.0×10^{-12}	0.02

<u>Domain Discretization</u>

The Repository-Scale Model domain was determined from transport pathway analyses performed using the Subregional-Scale Model with Base Case geosphere parameters. Pathways originating within the repository room footprint at the repository elevation discharge to surface south of the repository. Repository-Scale Model extents include the repository footprint, the transport pathway domain plus an additional 1 km of surrounding geosphere (Figure 7-21).

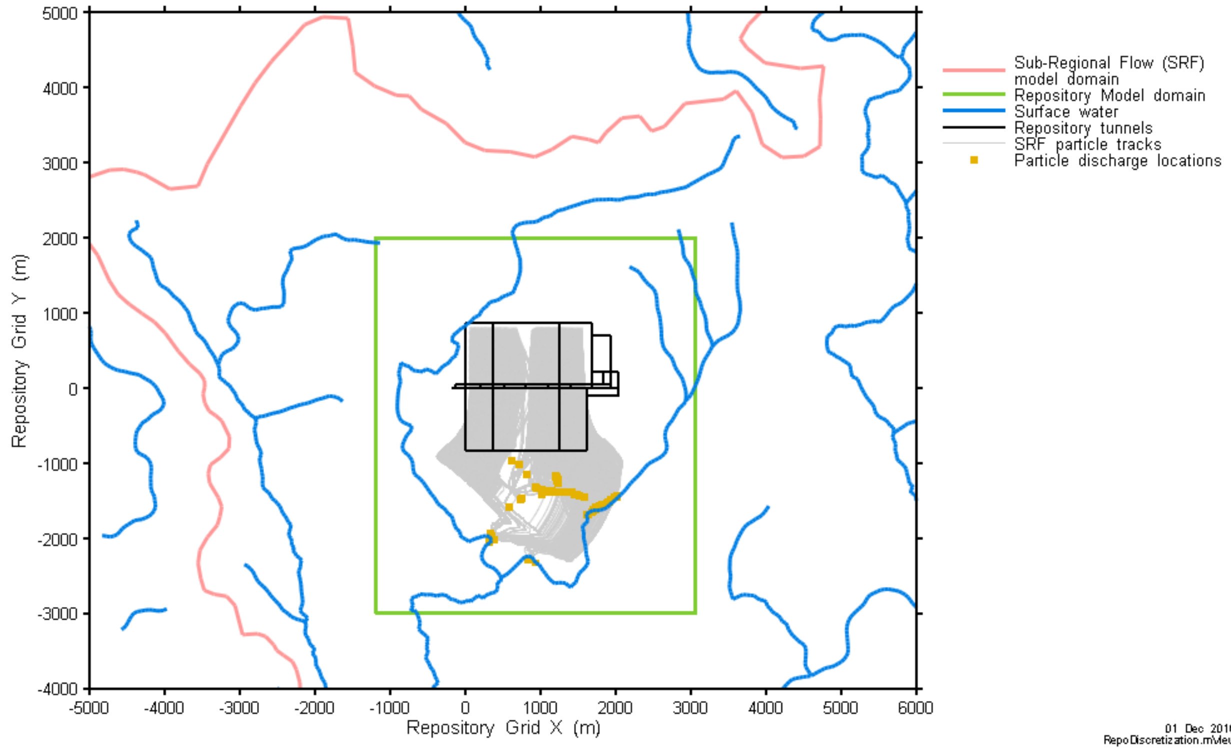

Figure 7-21: Repository-Scale Models: Model Domain Boundary

There are significant differences in horizontal discretization between the Full and Rooms-Only Repository-Scale Models (Figure 7-22) which reflect the different features included in each model. The Full model has 199,576 elements in each layer (405 X nodes, 495 Y nodes), while the Rooms-Only model contains 69,400 elements (200 X nodes, 347 Y nodes) per layer.

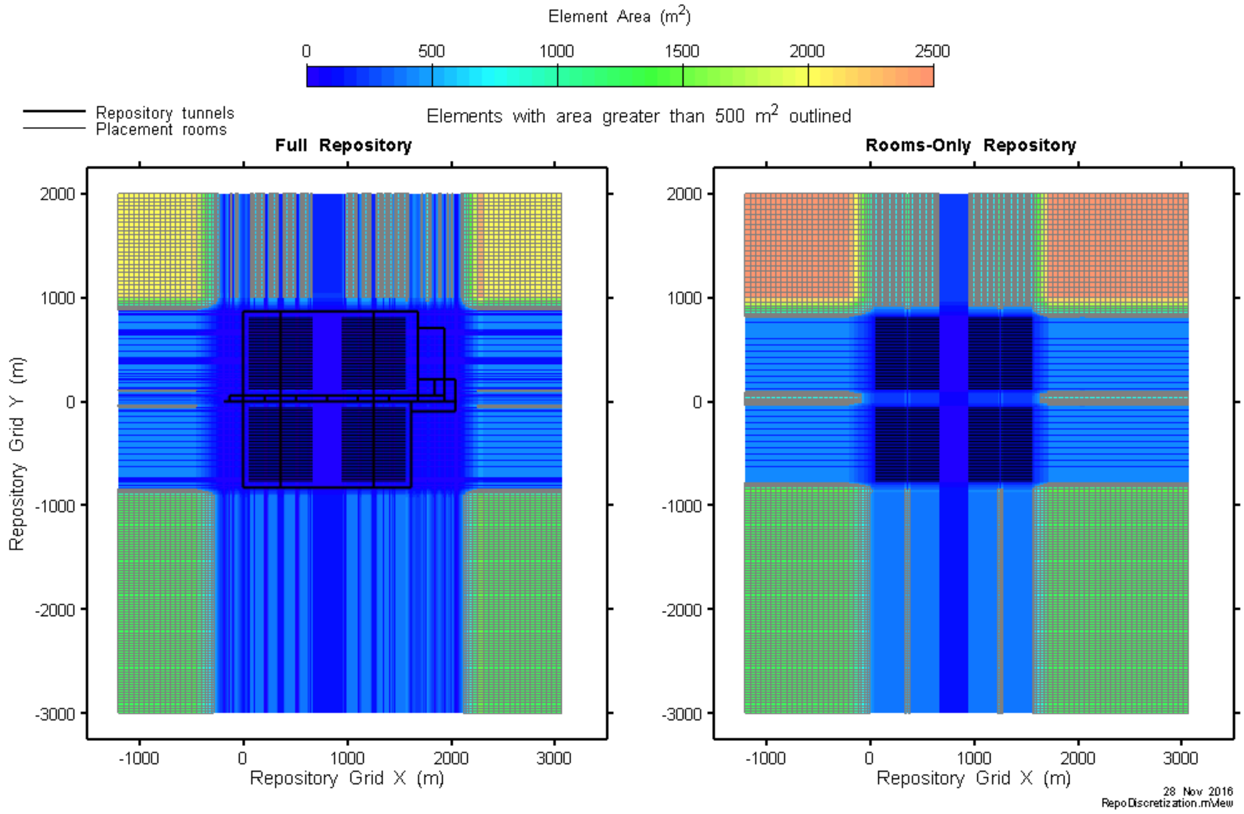

Figure 7-22: Repository-Scale Models: Plan Discretization

The vertical discretization of the two models is similar except in the immediate vicinity of the repository, where the Full Model has several additional layers to incorporate the heights for tunnel features not included in the Rooms-Only Model. Figure 7-23 illustrates overall vertical discretization, while Figure 7-24 shows discretization and property assignments on a section through placement rooms where the rooms meet the Panel Access tunnel. There are 95 layers in the Full Model and 93 layers in the Rooms-Only Model, yielding 19.95M elements for the Full Model and 6.33M elements for the Rooms-Only Model.

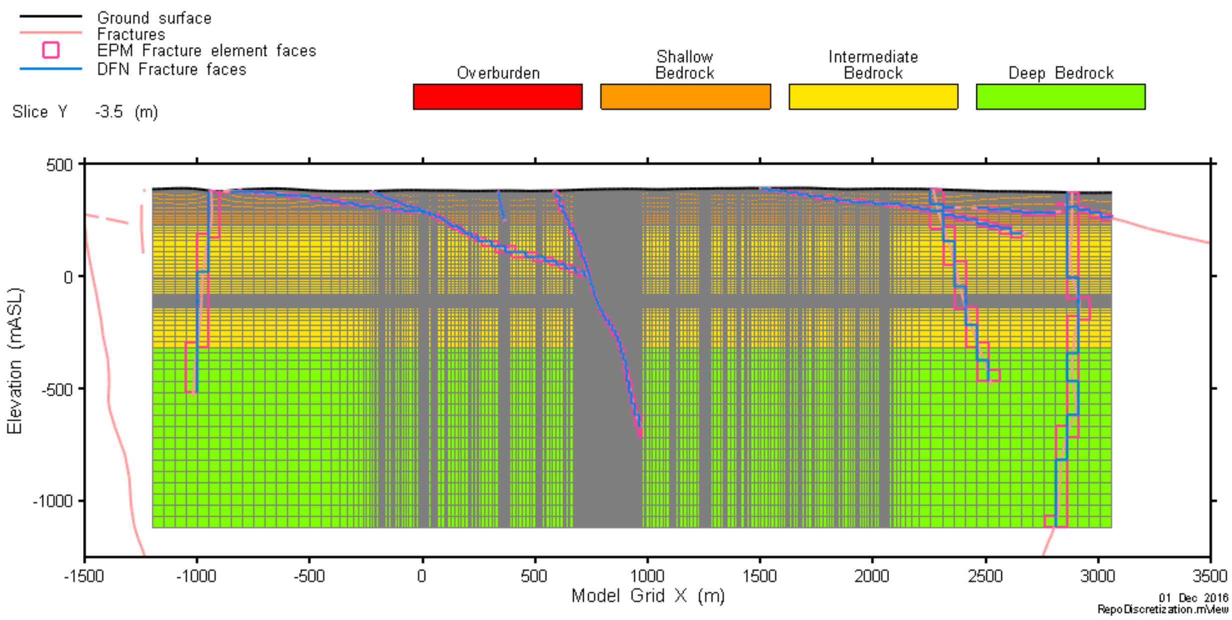

Figure 7-23: Full Repository-Scale Model: Vertical Discretization

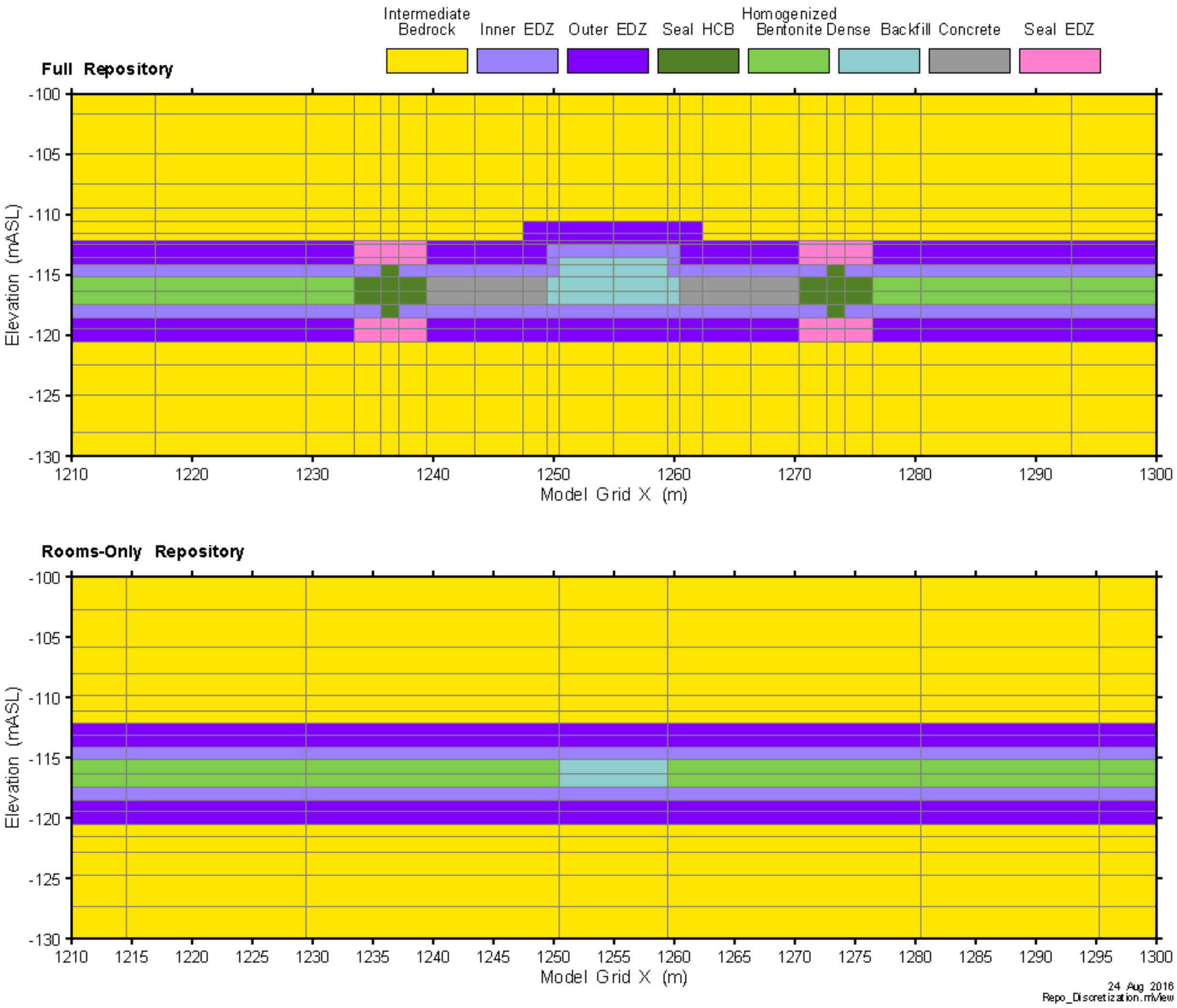

Figure 7-24: Repository-Scale Models: Detailed Vertical Discretization

Full Model discretization and property assignments are further detailed in Figure 7-25 through Figure 7-29. As seen in the figures, only a limited number of placement rooms include both Inner and Outer EDZ on all sides of the room. These rooms include all rooms where defective container sources will be placed (Section 7.7.2.3.2), and rooms adjacent to the selected source rooms. The Full Model discretization was finalized and refined subsequent to the well and source location simulations. All other placement rooms in the Full Model do not have Inner and Outer EDZ on the vertical sides of the room. Instead, Inner and Outer EDZ above and below the rooms are implemented with modified hydraulic conductivity properties to provide the same conductivity x area term as would be present for fully discretized rooms. The Rooms-Only Model uses this approach for all placement rooms.

Room and tunnel seals are slightly simplified in the Full Model. The seals are designed to intercept the bulk of the Inner EDZ with low permeability bentonite, reducing flow through both the Inner EDZ and the adjacent concrete and dense backfill (for tunnel seals). However, a thin (0.1 m) Inner EDZ is expected to remain. Full Model seal details are shown in vertical section in Figure 7-24 (upper panel) and Figure 7-26. The implemented seals cut through the entire Inner EDZ. Outer EDZ elements adjacent to the seals are assigned properties (SealEDZ in figures) consistent with a conductivity x area of the combined 0.1 m Inner EDZ and the specified 2 m Outer EDZ, so that the effective transmissivity of the element includes both Inner and Outer EDZ. A similar approach is used to implement the EDZ around the concrete shaft bulkhead seal at the top of the intermediate bedrock zone in each shaft.

Figure 7-26 and Figure 7-27 show example source nodes where radionuclides are injected for transport simulations. In this case, they are located at the end of a placement room. Source nodes are placed at the interface between the EBS and Inner EDZ, and have a horizontal extent approximately equal to 10 adjacent containers. For the Full Model, the source term is equally divided across 32 nodes, while there are only 8 source nodes at each source location in the Rooms-Only model due to its coarser horizontal discretization and to the lack of Inner EDZ on the sides of the placement rooms.

Figure 7-28 shows a vertical visualization of the main shaft and seals.

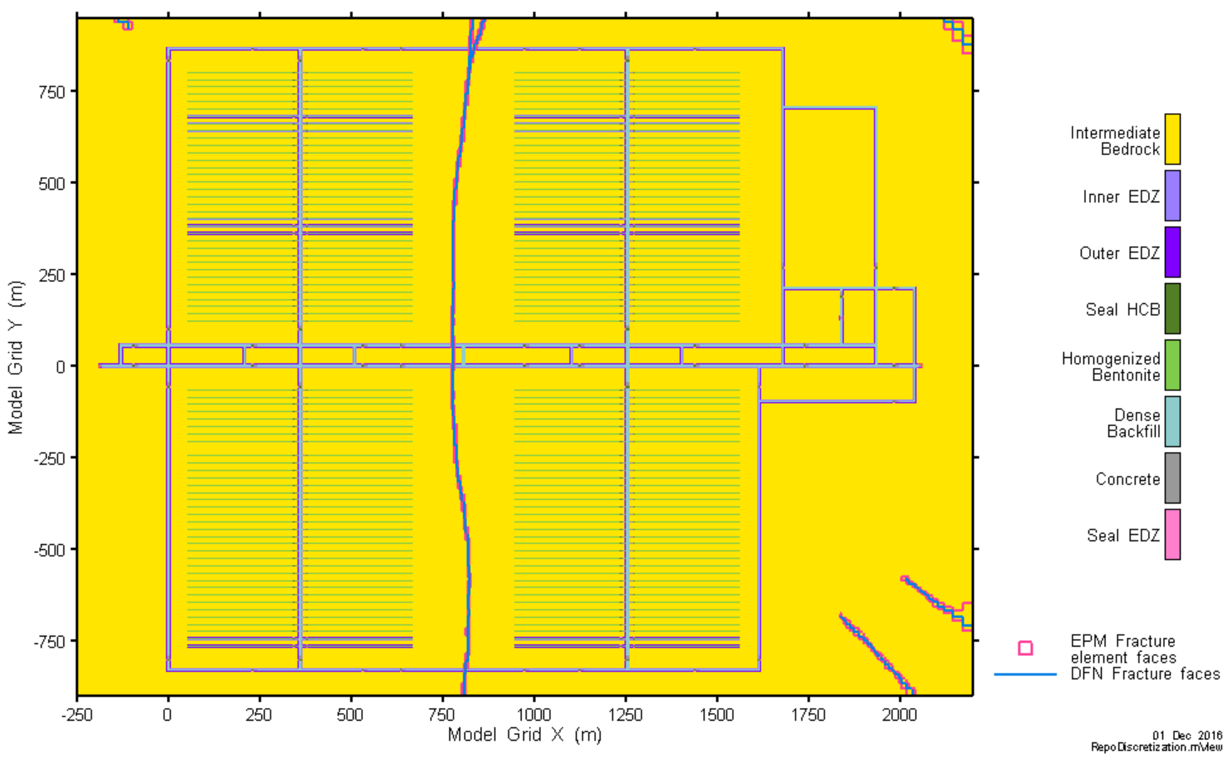

Figure 7-25: Full Repository-Scale Model: Plan View of Repository Property Assignment

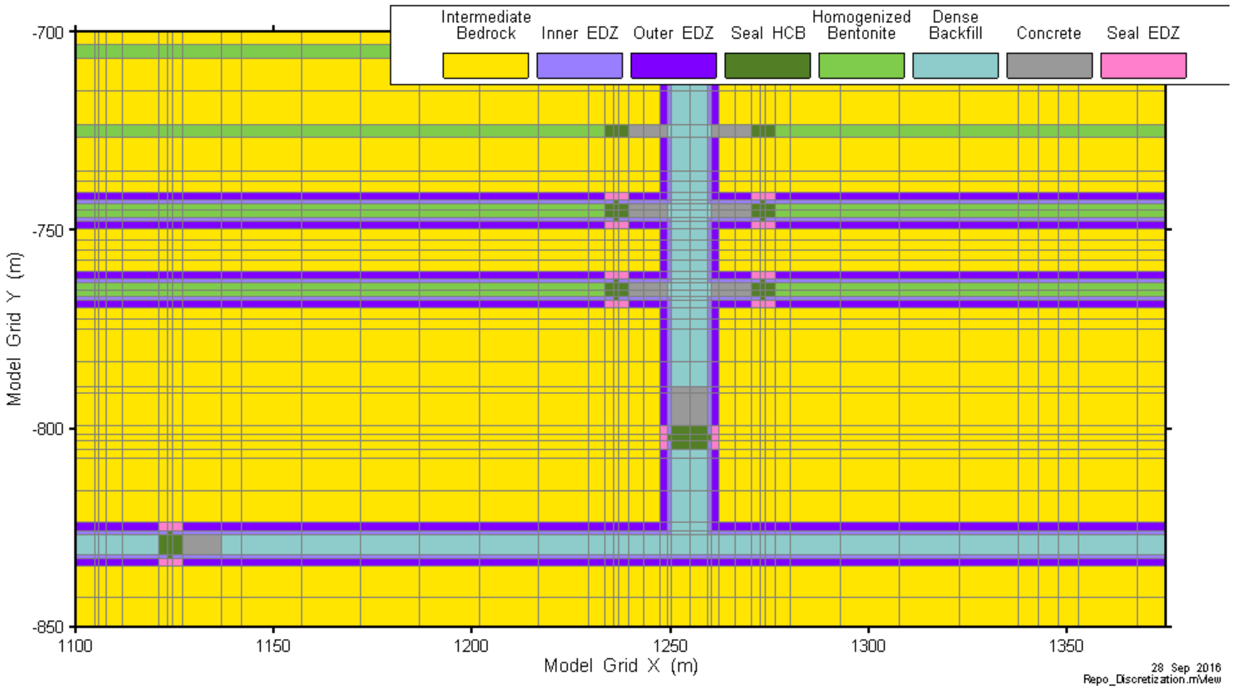

Figure 7-26: Full Repository-Scale Model: Detailed Plan Discretization Showing Seal Implementation

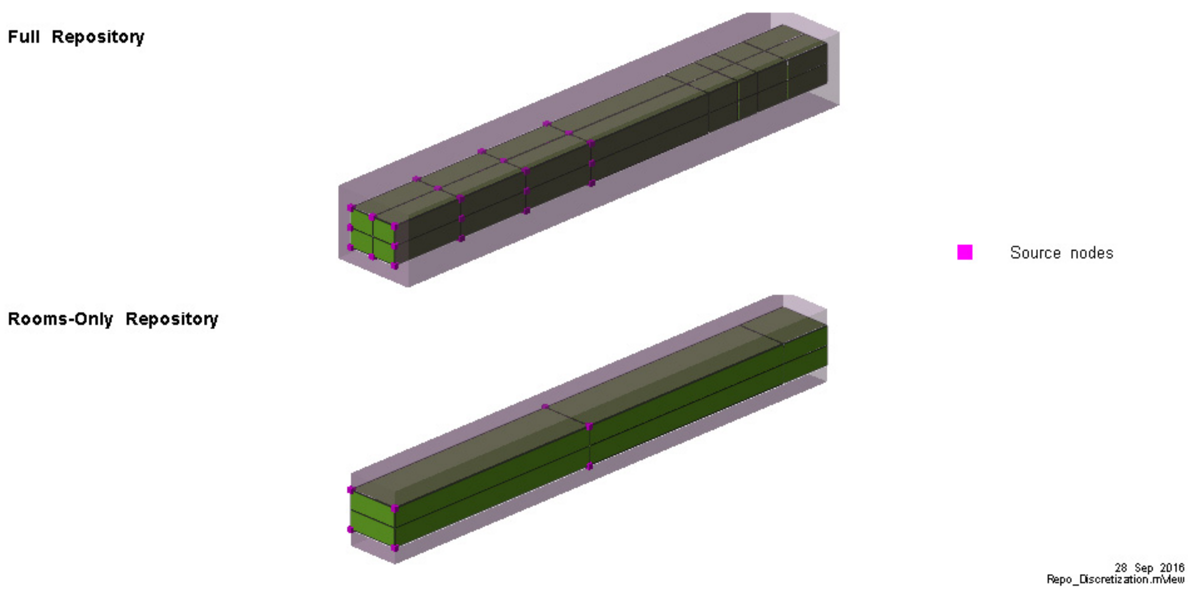

Figure 7-27: Repository-Scale Models: Three-dimensional Visualization of Example Source Nodes

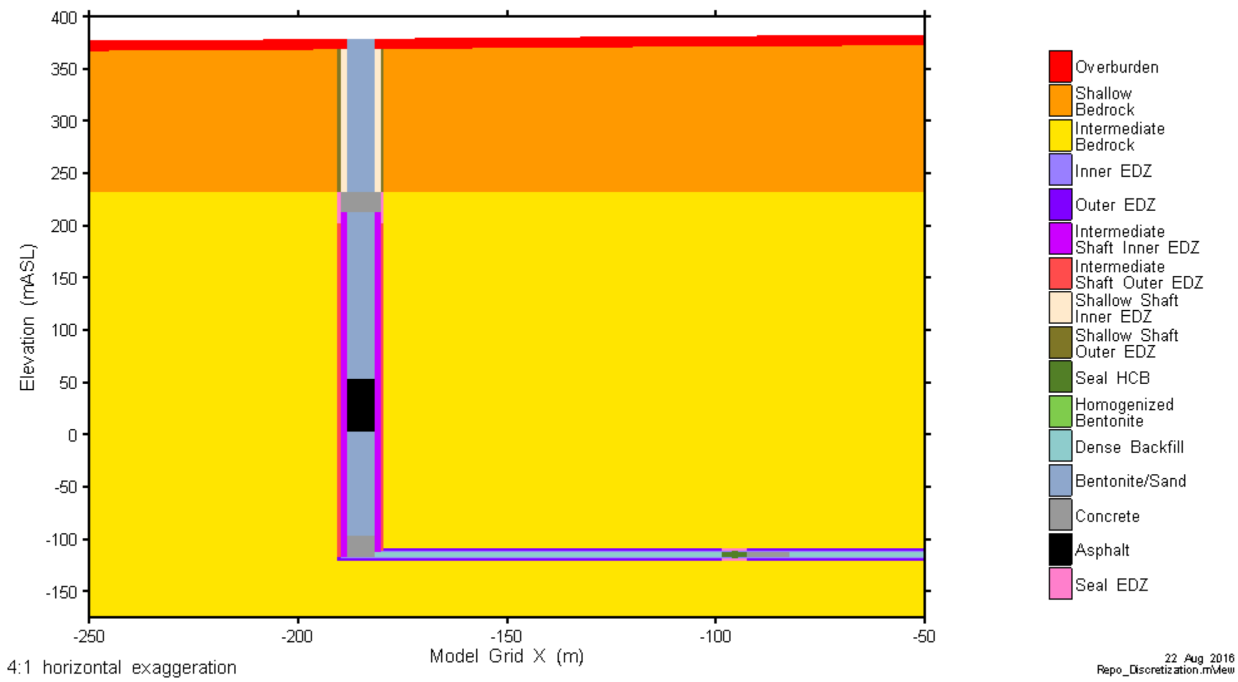

Figure 7-28: Full Repository-Scale Model: Vertical Visualization Showing Shaft and Seals

The three-dimensional difference of total extents for the Full and Rooms-Only Repository models are shown in Figure 7-29.

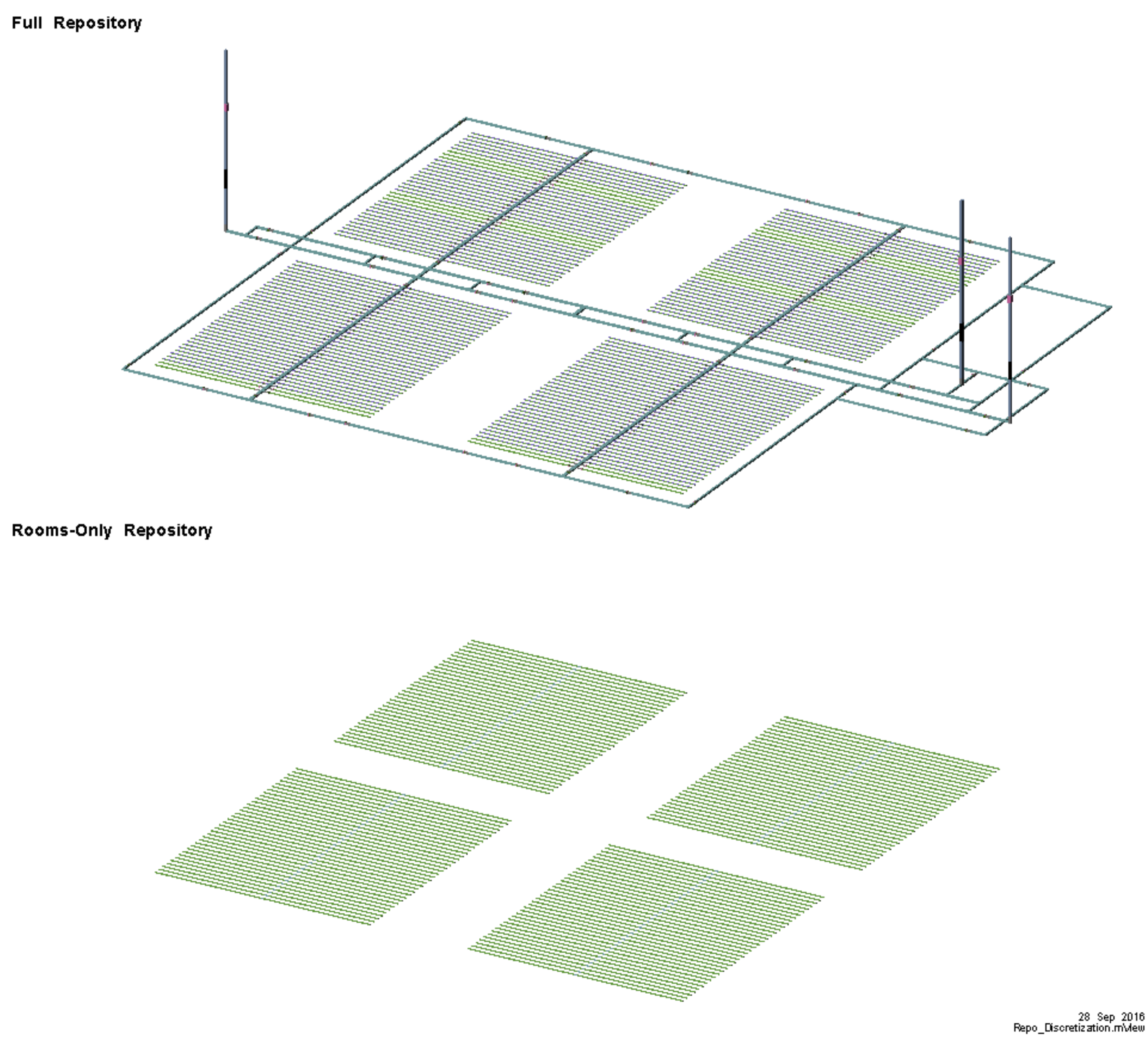

Figure 7-29: Repository-Scale Models: Three Dimensional View

Water Supply Well

The water supply well location is determined concurrently with the location of defective containers and is described in detail in Section 7.7.2.3.2. Wells are screened within the fracture system at a depth of approximately 100 mBGS.

The well is a 2D line element forming a segment, or edge, of a 3D element. Properties appropriate to a nominal 6” diameter well are assigned to the segment to specify the hydraulic conductivity of the well. The lowest node on the segment is defined as the withdrawal node from which water is abstracted.

Hydraulic Head Boundary Conditions

All model top surface nodes are assigned fixed head boundary conditions at topographic elevations. Model bottom boundary conditions are set to zero flow. Fixed head boundary conditions at vertical model sides are interpolated from head fields calculated with the Subregional-Scale Model. Boundary conditions are calculated separately for each well demand and for each high consequence well location. Head values for the Base Case geosphere (with no well) are shown in Figure 7-30.

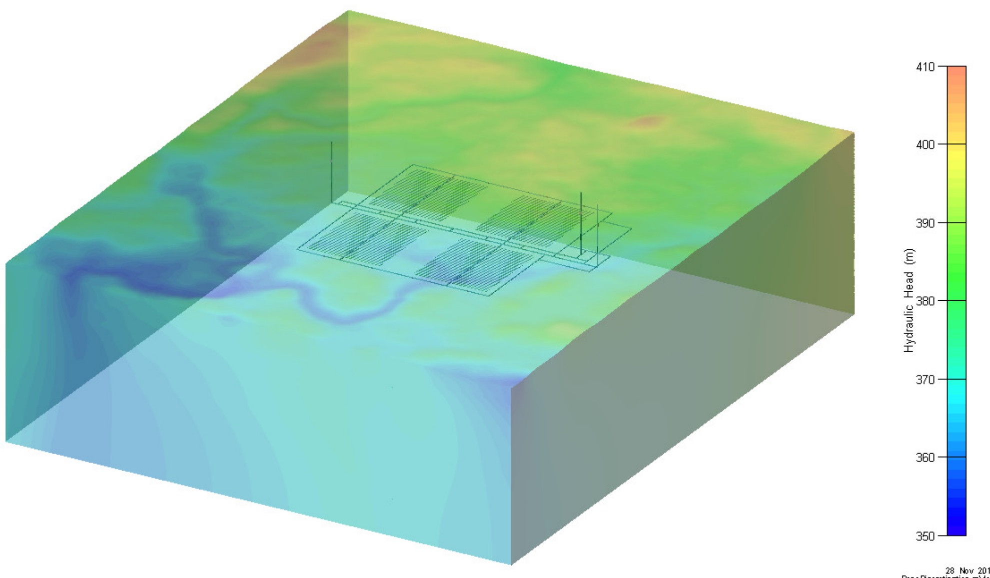

Figure 7-30: Full Repository-Scale Model: Base Case Head Boundaries

7.7.1.3 Container-Scale Models

These models encompass a small section of the repository surrounding the defective container locations and the immediately adjacent geosphere. The models incorporate significant detail and individual containers are represented. The models are used to generate source terms that include the effects of the EBS for input to the Repository-Scale Models. There are four

Container-Scale Models, with each model corresponding to one of the high-consequence release locations (Section 7.7.2.3.2). For purposes of identification, these models are named: Main Model, North-West (or NW) Model, South-West (or SW) Model, and South East (or SE) Model.

The locations of each model with respect to the overall repository are shown in Figure 7-31.

Section 7.7.2.3.2 shows that the Main Model yields the highest dose consequence, and therefore this model is described further below. In the interest of brevity, only cursory information is provided for the other three models as these models are not used once the limiting well / container location has been determined.

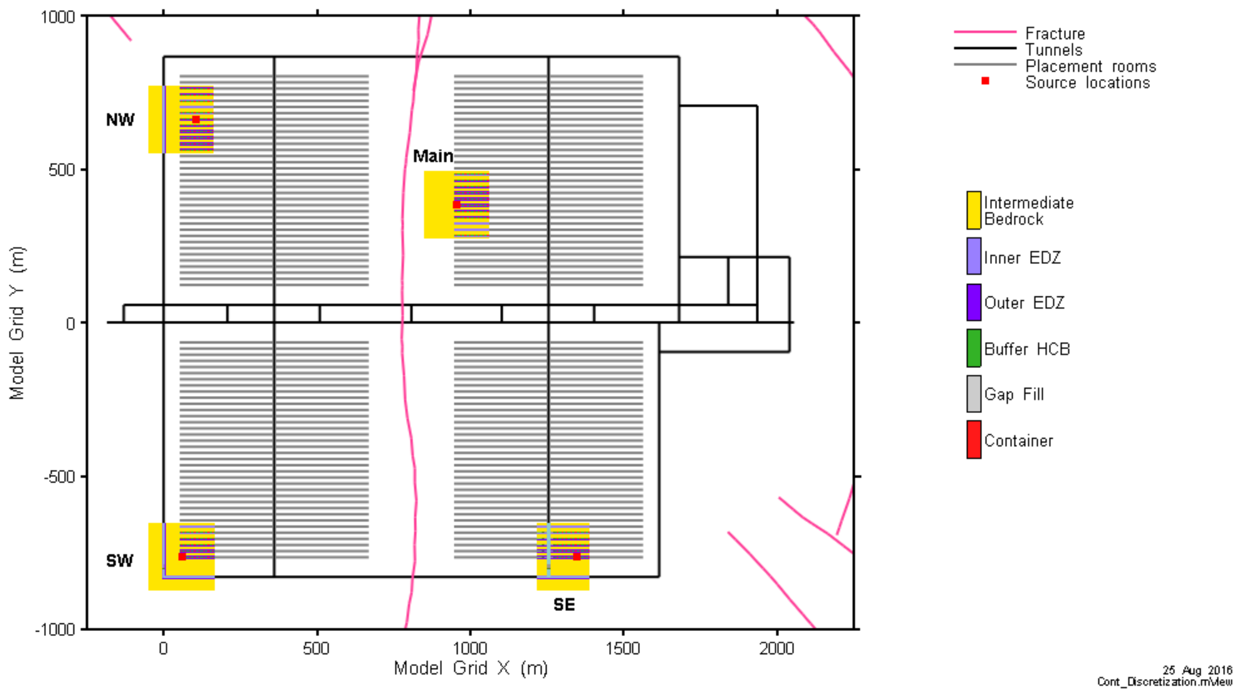

Figure 7-31: Container-Scale Models: Location in Repository

<u>Domain Discretization and Property Assignment</u>

Three of the models have a plan area of approximately 210 by 220 m, with the SE Model being slightly smaller at 170 by 220 metres. The domain is set to include the specified defective container location and any adjacent repository features that may affect the flow system around the defective containers.

Vertically, the model domains are identical, extending from 200 m below the repository (-317.5 mASL) to 150 m above the repository (32.5 mASL). The domain is entirely within the Intermediate Bedrock, with the bottom boundary located at the top of the Deep Bedrock.

Portions of the fracture system can be found in each model and are included in the model properties as equivalent porous media (EPM) elements.

The placement rooms and engineered barrier system are discretized at differing levels of detail. The room containing the radionuclide source is discretized at the highest level and contains representations of the containers in the room. Detailed property assignments for plan, and vertical slices along the room centreline and vertical slices perpendicular to the room are presented for the Main Model in Figure 7-32 through Figure 7-34. The discretization includes a basic representation of the room cross-section and associated EDZ with in-room EBS components (container, gap fill, buffer box, and seal (for SE Model only)) individually discretized. The property assignments used in simulations replace individual bentonite-based room EBS components with homogenized buffer material properties. Variations in room width and height due to construction methods are not incorporated; defined average room widths and heights are used.

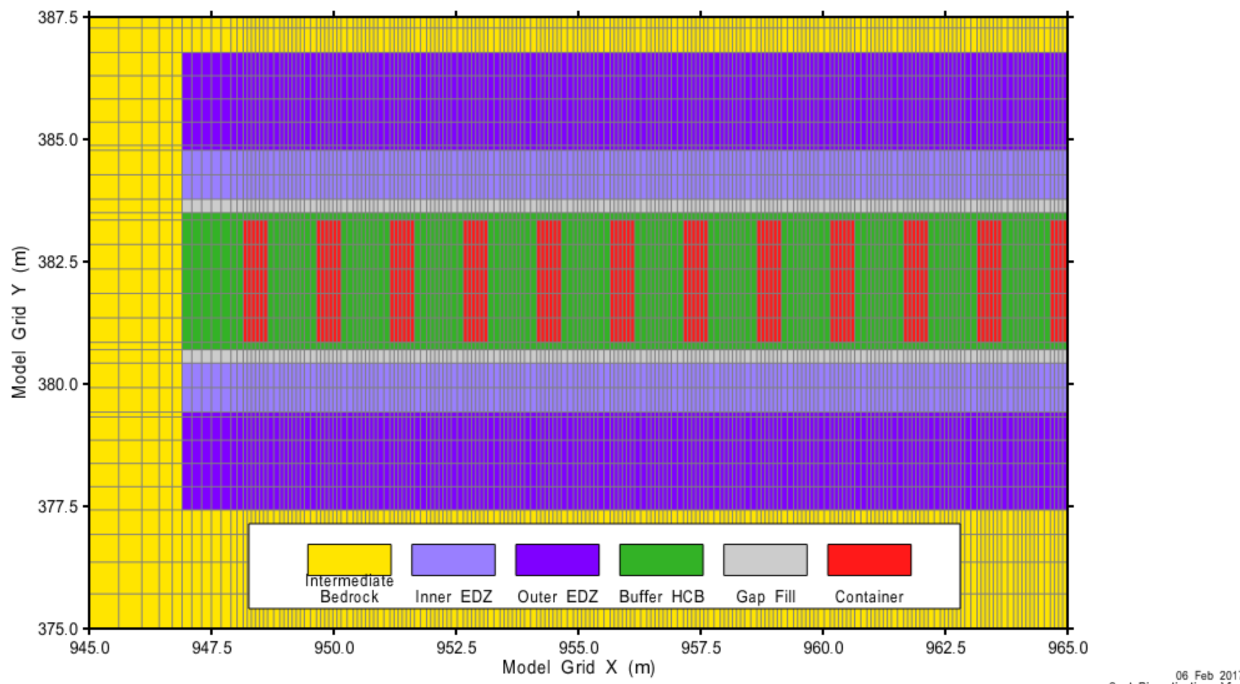

Figure 7-32: Main Container-Scale Model: Plan Property Assignment through the Source Placement Room

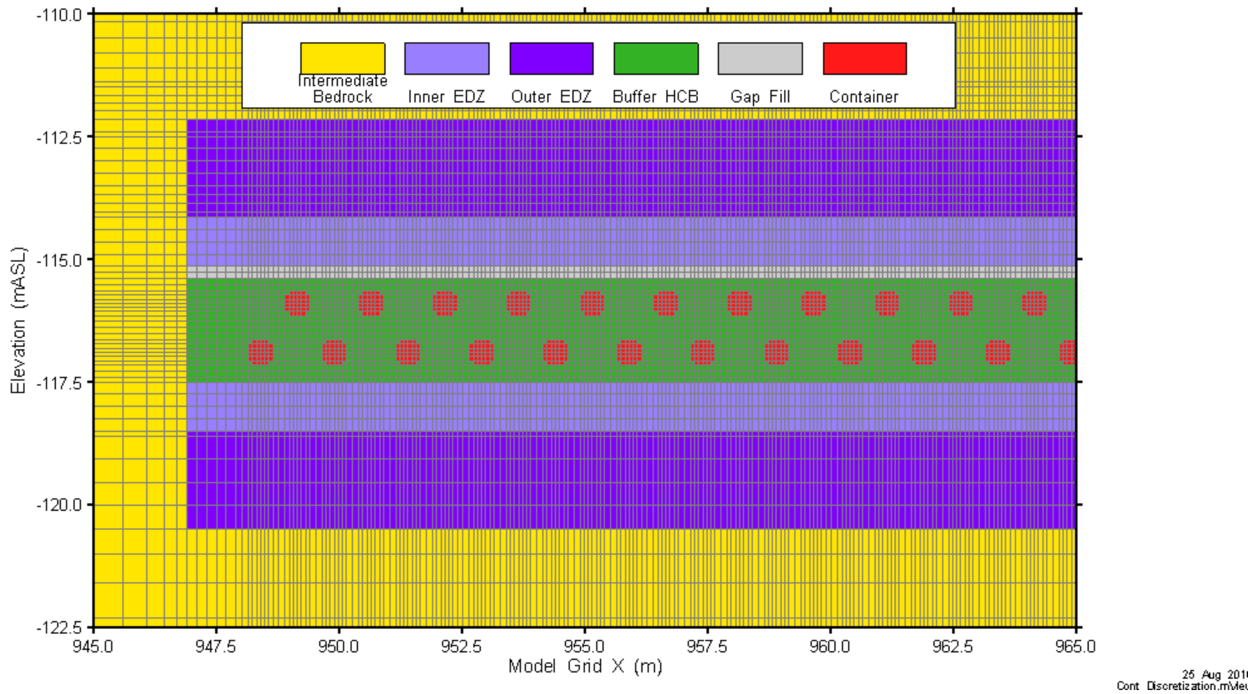

Figure 7-33: Main Container-Scale Model: Vertical Property Assignment Parallel to the Source Placement Room

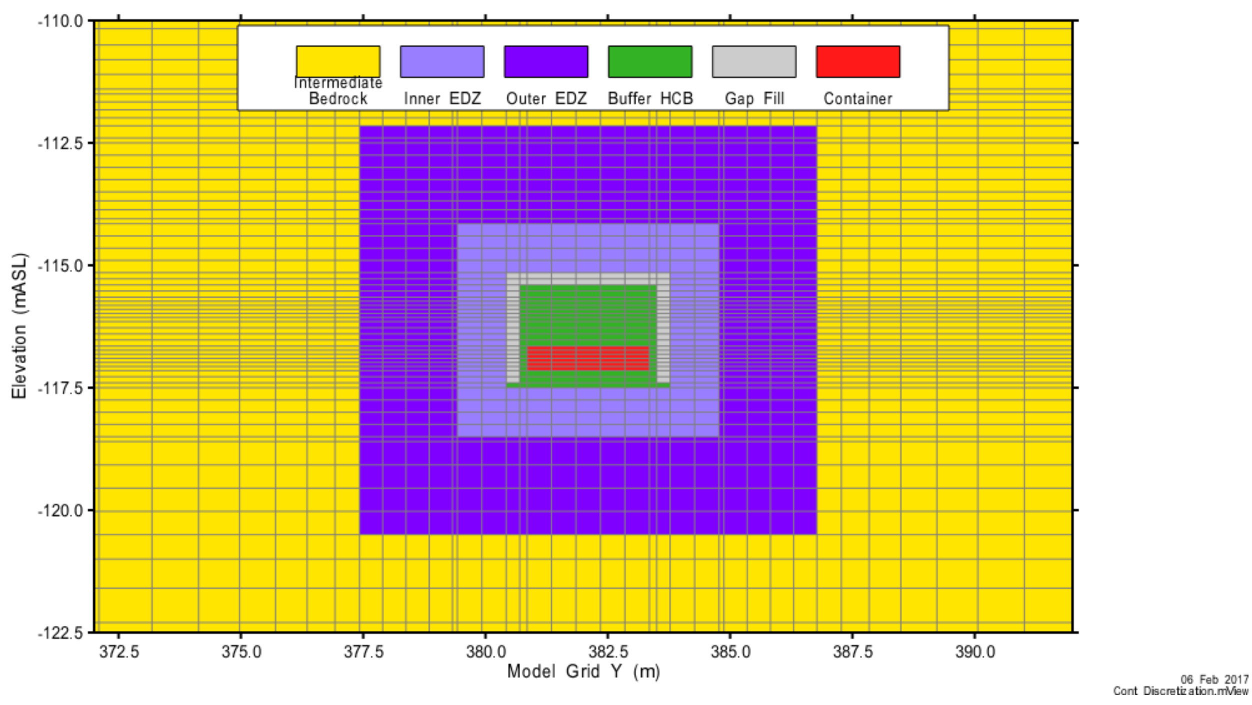

Figure 7-34: Main Container-Scale Model: Vertical Property Assignment Perpendicular to the Source Placement Room

Figure 7-35 illustrates the defective containers at the end of the placement room for the Main Model. There are 144 source nodes allocated over the surface of each container. The figure also shows the transport boundary over which the 10 container release is integrated, for use as a source term in the Repository-Scale Models.

EBS and EDZ elements are shown in Figure 7-36.

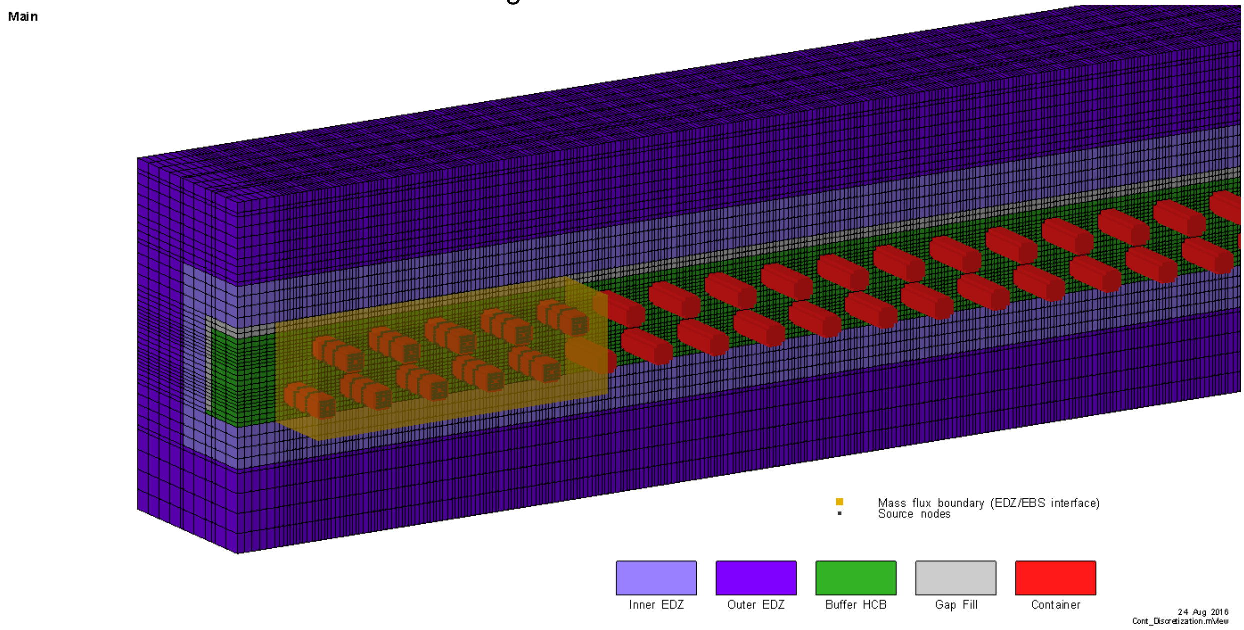

Figure 7-35: Main Container-Scale Model: 3D View of EBS and EDZ near Source Containers

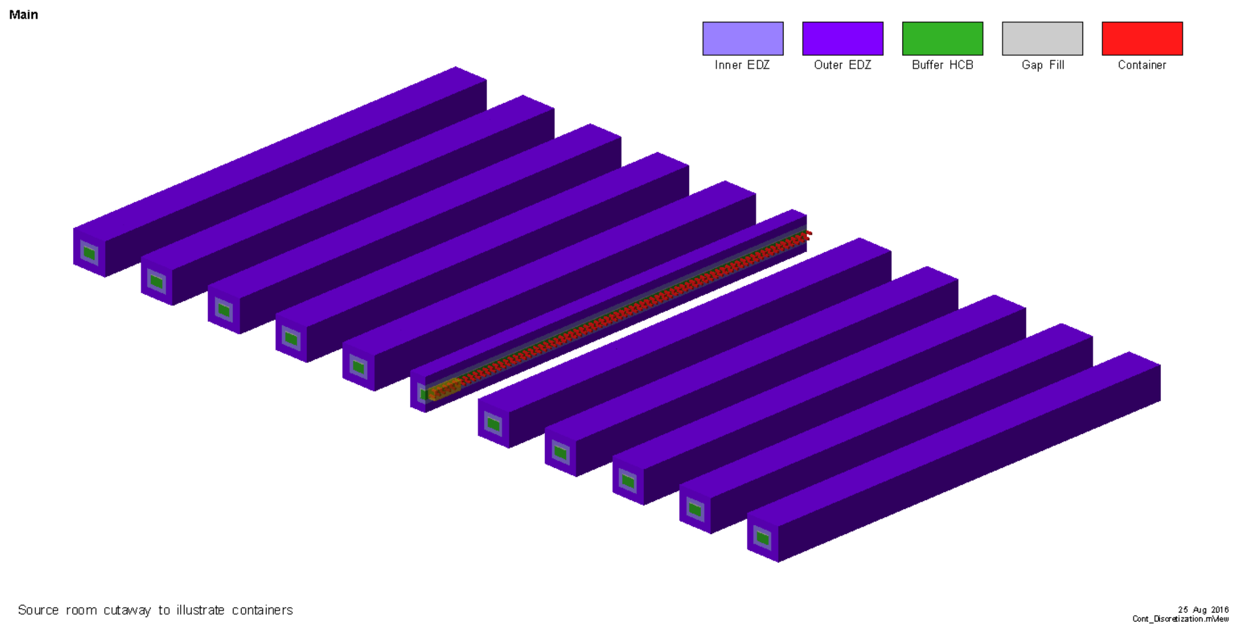

Figure 7-36: Main Container-Scale Model: 3D View of EBS and EDZ

Hydraulic Head Boundary Conditions

Head boundary conditions are extracted from the Full Repository-Scale Model and values are specified for all external model nodes. Base Case Boundary conditions for the Main Container-Scale Model are shown in Figure 7-37.

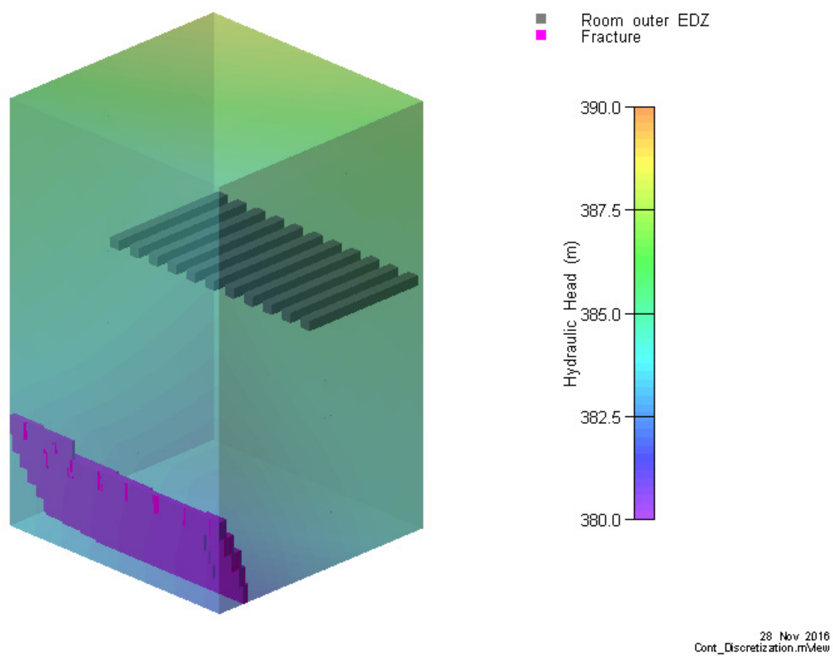

Figure 7-37: Main Container-Scale Model: 3D View of Base Case Head Boundary Conditions

7.7.2 Results

This section presents results of the detailed 3D groundwater flow and radionuclide transport analysis performed for the Base Case of the Normal Evolution Scenario and selected sensitivity studies.

Section 7.2.2.3 and Table 7-5 present the list of sensitivity cases developed to illustrate the effect of deviations in barrier performance. Of these, the following have the potential to affect the groundwater flow field and are therefore not amenable to modelling with the System Model. The System Model cannot be used because the geosphere submodels (Section 7.8.1.2) are based on the constant groundwater flow field associated with the Base Case. Simulation of the following cases is therefore performed with the 3D models:

- Hydraulic conductivities of the engineered barrier system (EBS) increased by a factor of 10;
- Hydraulic conductivities of the host rock increased by a factor of 10;
- Hydraulic conductivities of the host rock decreased by a factor of 10;
- Hydraulic conductivity in the excavation damaged zones (EDZ) increased by a factor of 10;
- Fracture standoff distance reduced to 50, 25 and 10 m; and
- Dispersivity increased and decreased by a factor of 5.

Radionuclide transport is calculated for the Base Case for I-129, C-14, Ca-41, Cl-36, Cs-135, Se-79, and U-238. These radionuclides are typically the most important in terms of potential radiological impact or in representing a range of low-sorption to high-sorption species.

Radionuclide transport for most of the other sensitivity cases is calculated for I-129 only. This is because, as will be seen later in Section 7.8.2.1, I-129 is the overwhelmingly dominant contributor to dose.

Section 7.2.2.4 and Table 7-6 present a list of sensitivity cases developed to illustrate the effect of various FRAC3DVS-OPG modelling attributes and parameters on the Base Case results. These cases, whose results are also presented in this section, are:

- Increased spatial resolution;
- Increased and decreased number of time steps; and
- Discrete fracture modelling (as opposed to equivalent porous media (or EPM) modelling).

Figures in this section show vectors describing the magnitude and direction of velocity of groundwater movement, or advective[1] velocity, in locations where velocities are greater than 10^{-4} m/a.

A description of the various 3D models is provided in Section 7.7.1.

---

[1] Advective velocity is the Darcy velocity (i.e., the volumetric flow rate of water passing through a planar surface divided by the area of that surface) divided by the material porosity. The advective velocity therefore represents the velocity of the fluid within the pore spaces in the rock.

7.7.2.1 Subregional-Scale Model Flow Results

The Subregional-Scale Model is used to determine:

- The groundwater flow field in the vicinity of the repository; and
- The boundary conditions for the Repository-Scale Models.

No repository features are incorporated at this scale of resolution. The repository representation in the figures is provided solely to add context.

Radionuclide transport calculations are not performed with this model.

7.7.2.1.1 Base Case – No Well Flow Results

Figure 7-38 shows groundwater velocity magnitudes and directions together with hydraulic heads for the Base Case geosphere with no operating well. Although the fracture system has a large effect on the head distribution and velocities, gradients across the area of the repository footprint are relatively uniform. Horizontal flow is generally from north of the repository to the south.

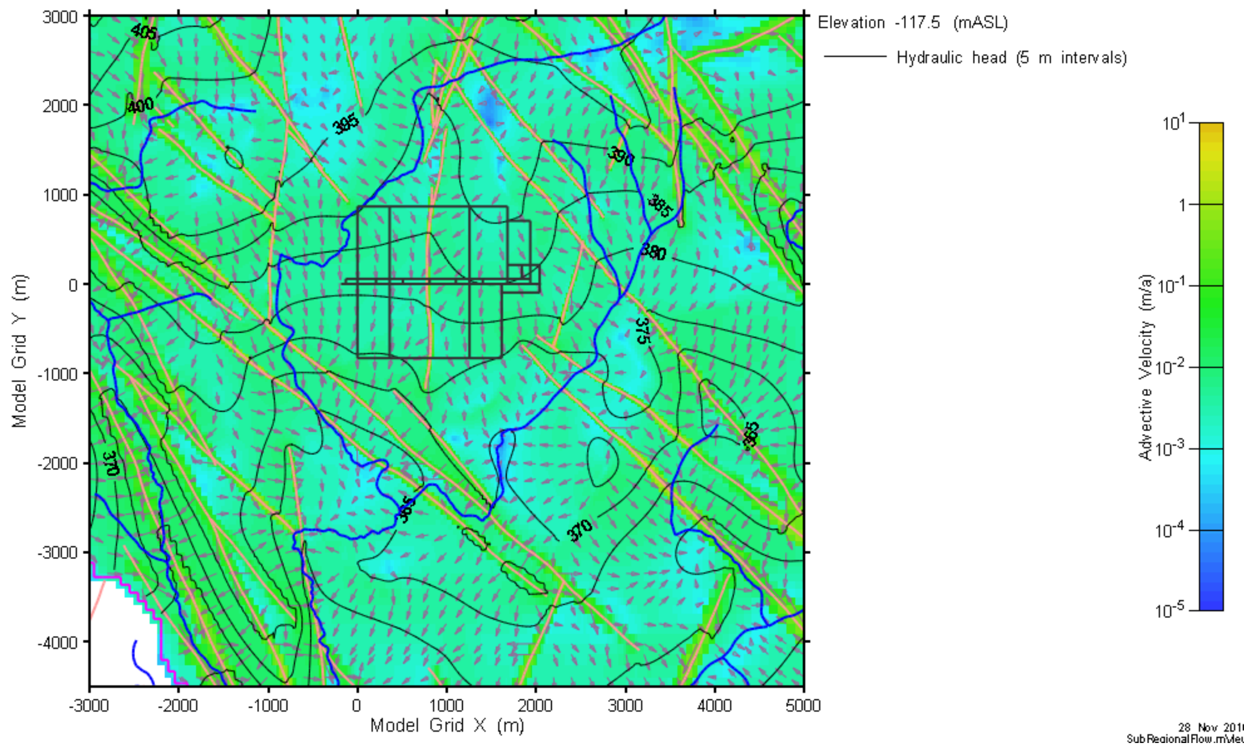

Note: the boundaries of the Subregional-Scale Model are outside the figure edges

Figure 7-38: Subregional-Scale Model: Base Case (No Well) - Advective Velocity and Hydraulic Head at Repository Elevation

Figure 7-39 shows the direction of vertical flow within the same area as Figure 7-38. Flow is upward in the blue to magenta areas while flow is downward in the green to yellowish areas. Within the area of the repository footprint, flow is entirely downwards over the north-eastern quadrant (Panels G and H) and is mixed (upwards and downwards) in other sections. Upward flow is associated with surface water locations and is generally associated with discharge of groundwater to surface.

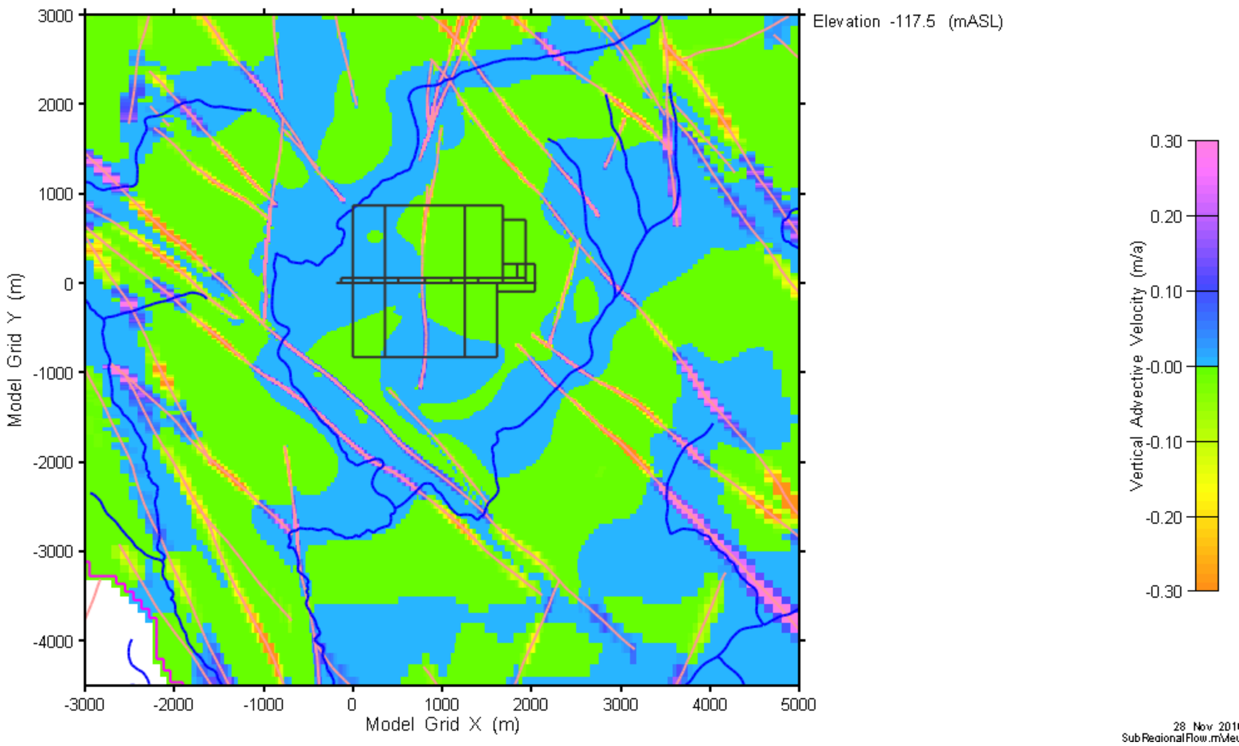

Figure 7-39: Subregional-Scale Model: Base Case (No Well) - Vertical Advective Velocity at Repository Elevation

Mean Life Expectancy (MLE) (Figure 7-40) shows that the mean time to discharge exceeds 100,000 years over the area of the repository footprint except for a small area adjacent to the main fracture.

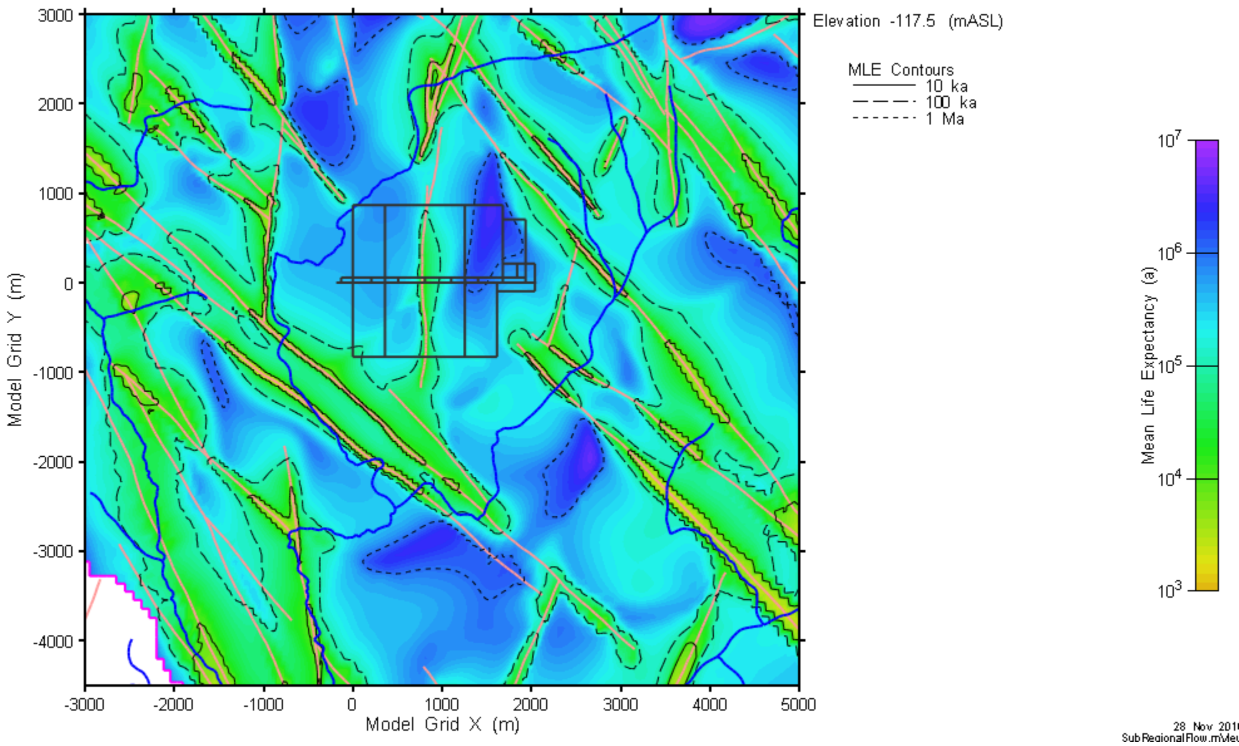

Figure 7-40: Subregional-Scale Model: Base Case (No Well) - Mean Life Expectancy (a) at Repository Elevation

Figure 7-41 shows the vertical flow and head distribution on a XZ section through the repository grid origin (Y = 0). The flow patterns are induced by local topography and are dominated by high flow rates within the fracture system.

Mean Life Expectancy on the vertical slice (Figure 7-42) shows the influence of the fracture system on transport times.

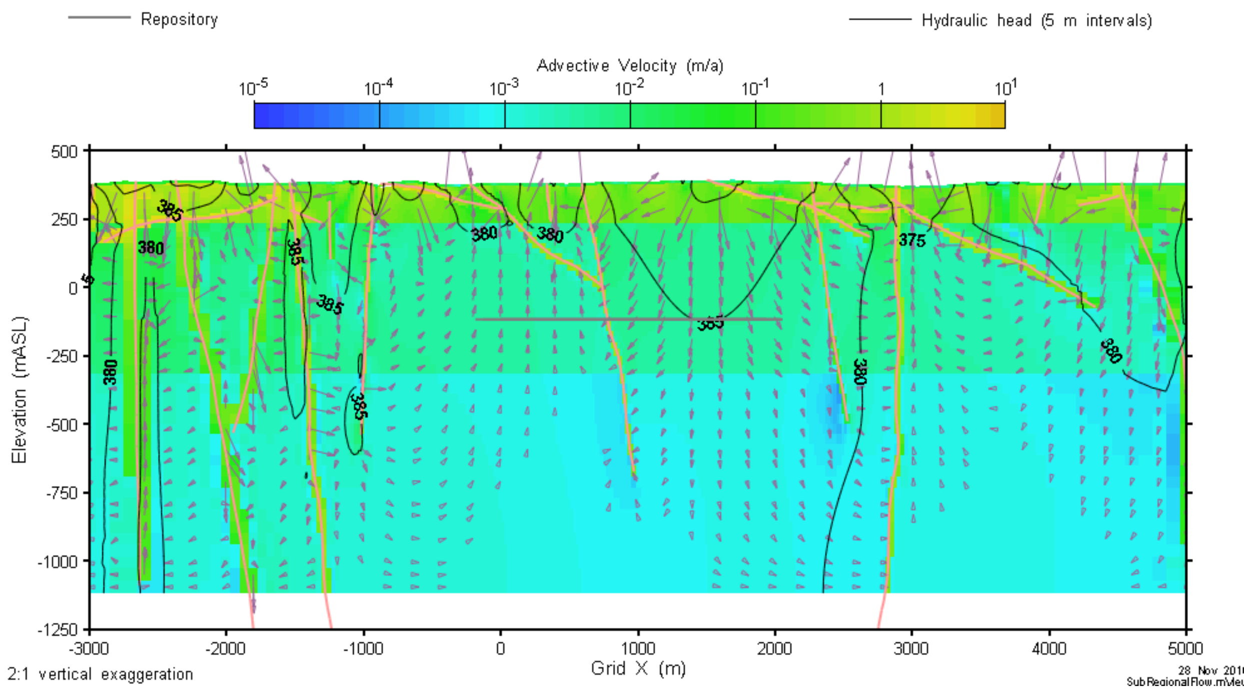

Figure 7-41: Subregional-Scale Model: Base Case (No Well) - Advective Velocity and Hydraulic Head on a Vertical Slice through the Grid Origin

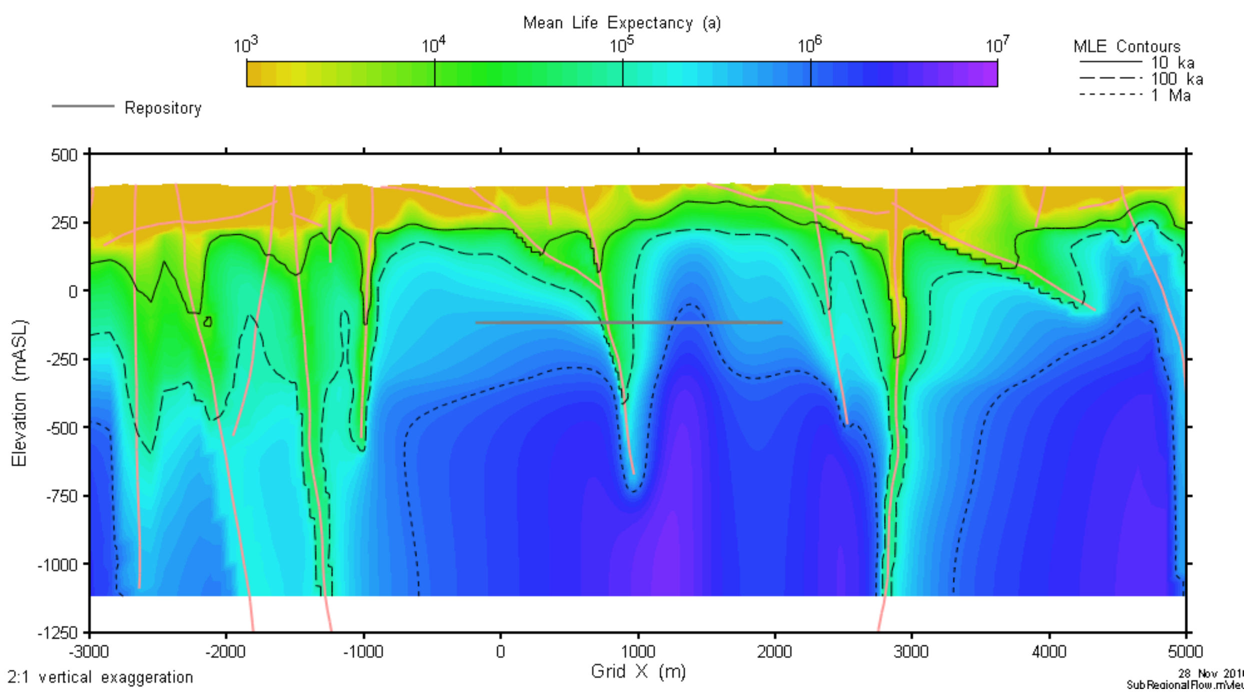

Figure 7-42: Subregional-Scale Model: Base Case (No Well) - Mean Life Expectancy on a Vertical Slice through the Grid Origin

Figure 7-43 provides a three-dimensional view of the advective flow system, with transport pathways originating at the repository horizon within the placement panel footprint. The fracture system is shown as transparent features which collect and channel the transport pathways.

All pathways travel south with discharge to surface water features and to terrestrial locations south of the repository.

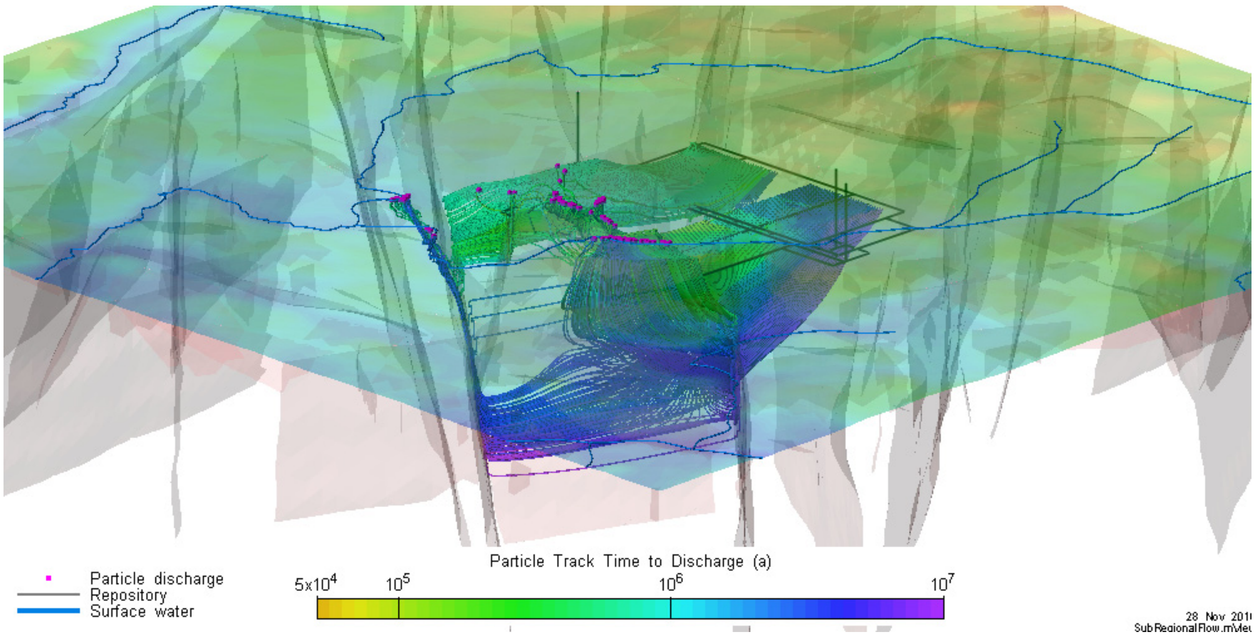

Figure 7-43: Subregional-Scale Model: Base Case (No Well) – Three Dimensional Transport Pathways from Repository to Discharge

Discharge zones can be defined based on common groups of discharge points. Figure 7-44 shows discharge zones together with their pathway origins within the repository footprint. The identified zones are the West River, the Central Wetland, the East River and the South River. The West River discharge zone dominates in terms of area within the footprint with lesser components going to the Central Wetland and East River zones.

A large portion of the West River transport pathways are very long-lived as illustrated in Figure 7-45.

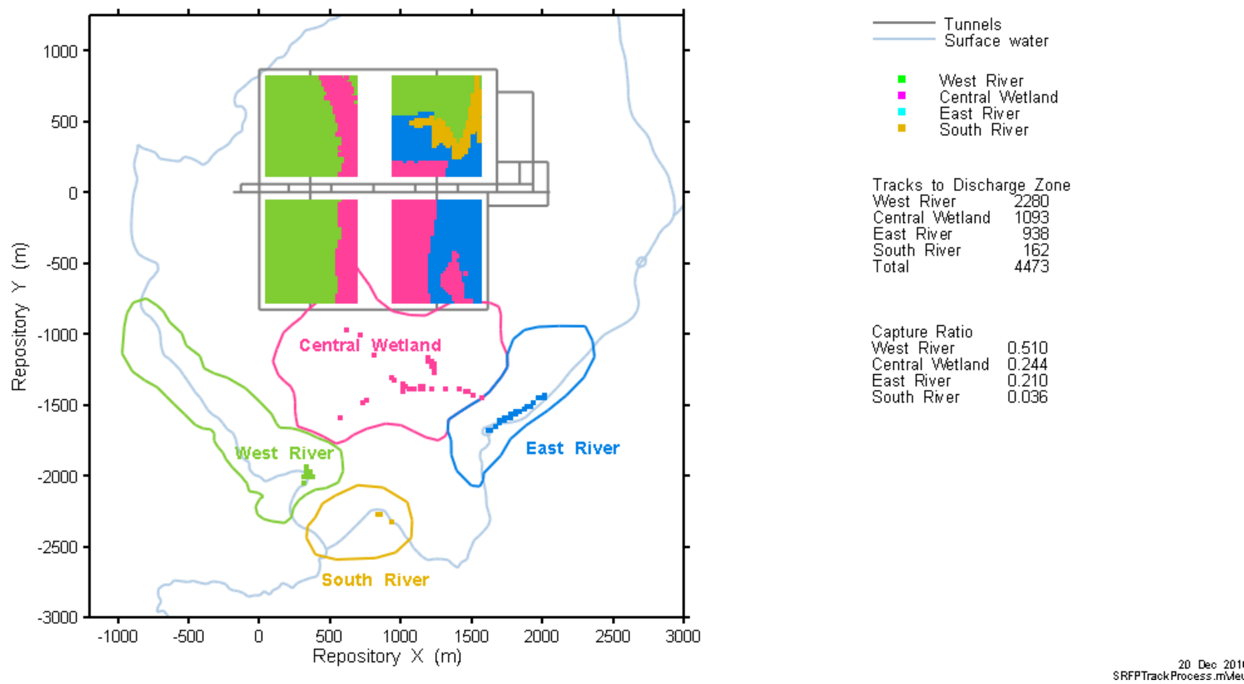

Figure 7-44: Subregional-Scale Model: Base Case (No Well) - Discharge Zones

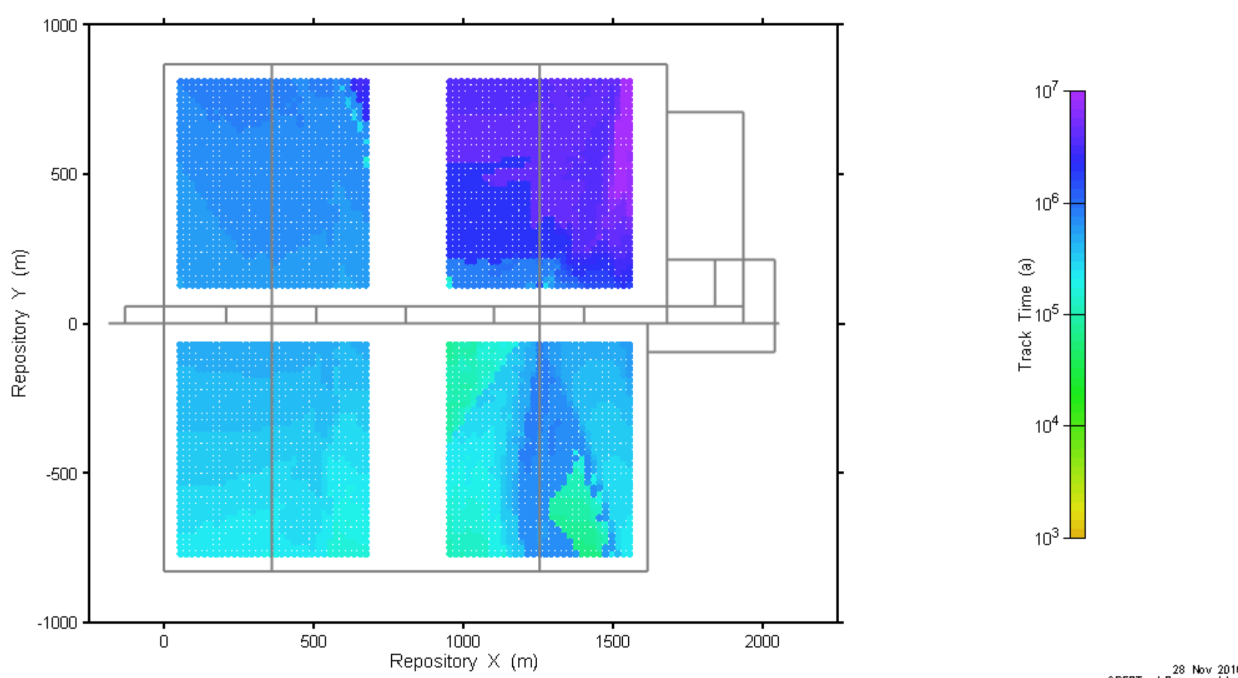

Figure 7-45: Subregional-Scale Model: Base Case (No Well) - Travel Time to Discharge

Cumulative Distribution Functions (CDFs) of transport pathway travel times and total length are shown in Figure 7-46 and Figure 7-47. Central Area pathways are shorter and faster. The West River zone has two separate populations, with about 80% short-lived (from repository panels to the west of the main central fracture) and 20% long-lived (from panels to the east of the fracture). Pathways to the South River zone have the longest distance and travel time.

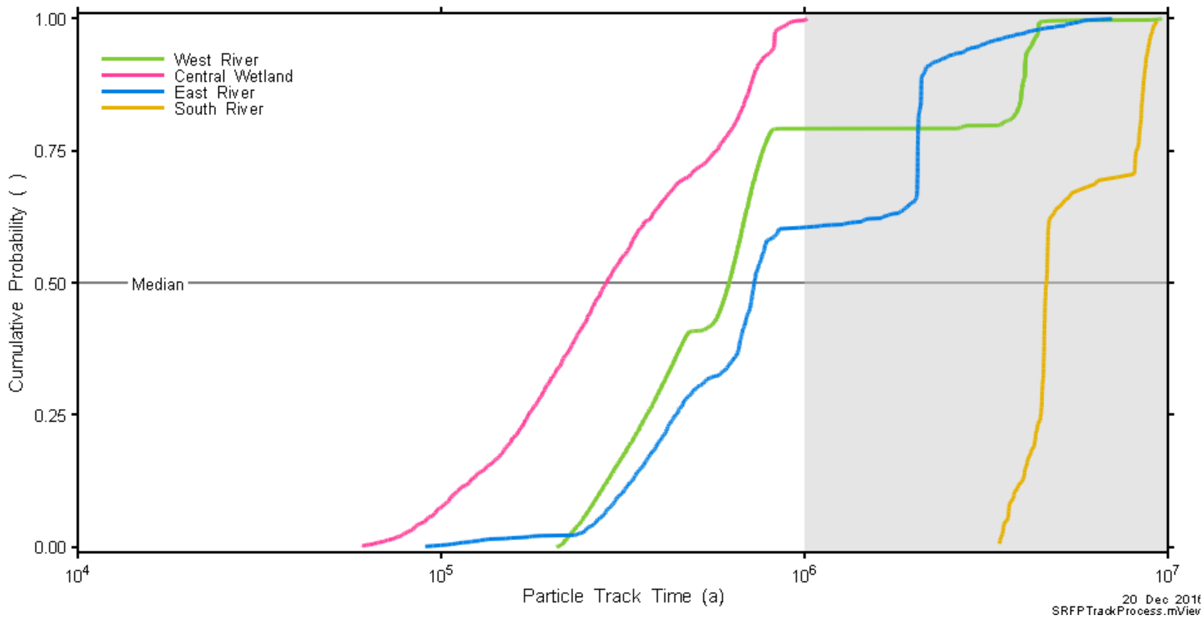

Figure 7-46: Subregional-Scale Model: Base Case (No Well) - Pathway Travel Time Cumulative Distribution Function

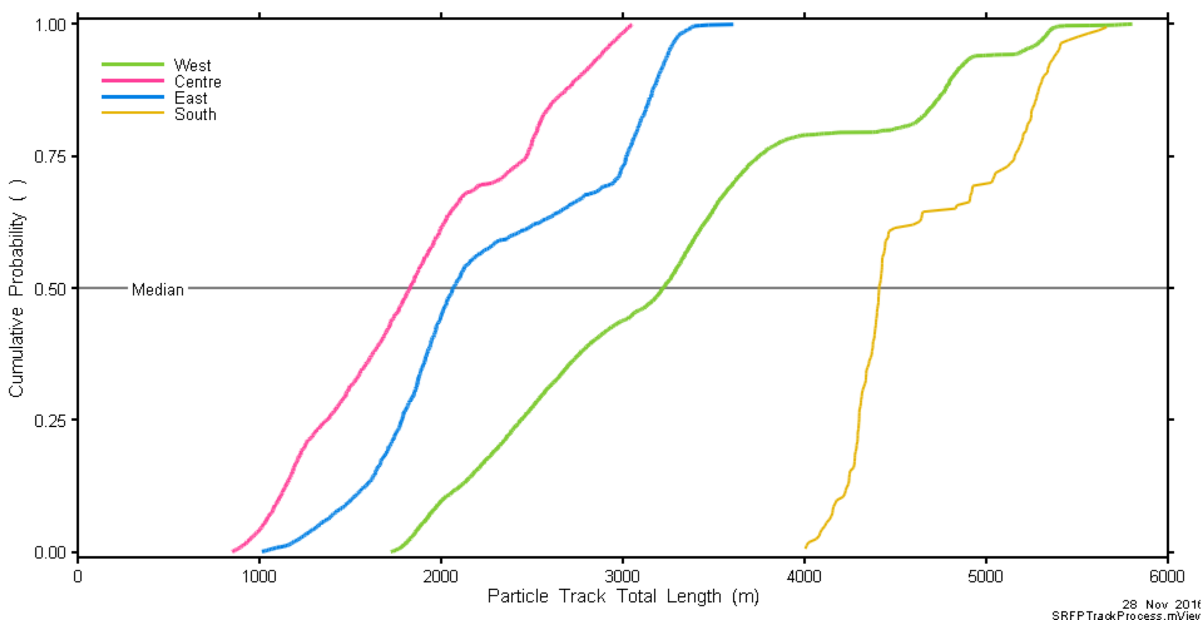

Figure 7-47: Subregional-Scale Model: Base Case (No Well) - Pathway Travel Length Cumulative Distribution Function

Figure 7-48 is a visualization of transport pathways, routes and discharge locations for each discharge zone.

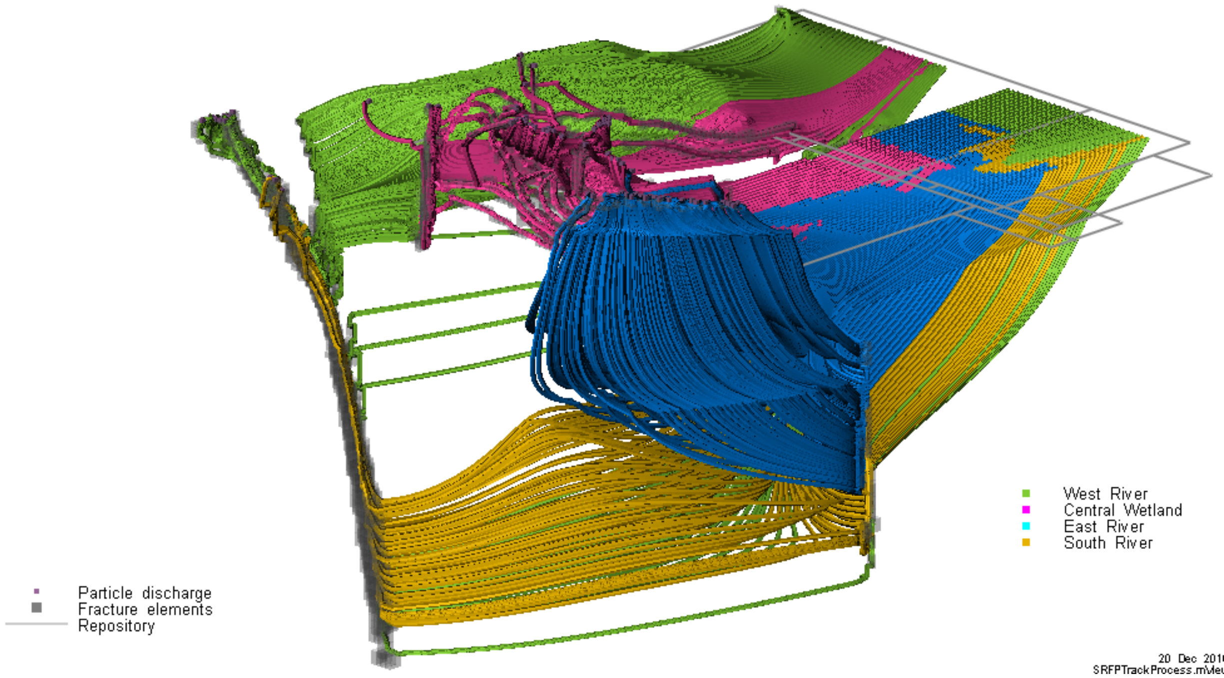

Figure 7-48: Subregional-Scale Model: Base Case (No Well) - Three-Dimensional Pathway Travel and Discharge

7.7.2.2 Repository-Scale Model Flow Results

The Repository-Scale Model domain includes the repository and a portion of the subregional flow system into which groundwater flow from the repository travels and discharges. The model is used to determine:

- Base Case flow results for simulations both with and without the well;
- A comparison of transport results from the Full Repository-Scale Model with results from the Rooms-Only Repository-Scale Model. The effect of some simplifications to the container source term are also examined;
- High consequence well and container locations. These are the locations that result in the fastest and / or highest magnitude radionuclide transport to the well;
- Base Case radionuclide transport results;
- Advective transport pathway and tracer results for use in creating the SYVAC3-CC4 System Model geosphere network;
- Sensitivity case results illustrating the effect of deviations (see Section 7.7.2) affecting the performance of the buffer, backfill and seals barrier and the performance of the geosphere barrier on radionuclide transport;

- Sensitivity case results illustrating the effect of various FRAC3DVS-OPG modelling parameters on radionuclide transport; and
- Boundary conditions for the Container-Scale Models.

Radionuclide transport modelling for I-129, C-14, Cl-36, Ca-41, Cs-135, Sn-126, and U-238 is performed for the Base Case. Other cases typically consider only I-129 because, as will be seen later in Section 7.8.2.1, I-129 is the overwhelmingly dominant contributor to public dose.

As discussed in Section 7.7.1.2, there are two Repository-Scale Models. The “Full” Repository-Scale Model is discretized for all repository and engineered barrier system (EBS) features except containers, while the “Rooms-Only” Repository-Scale Model includes only placement rooms and a simplified EDZ.

The Full Model is used for Base Case radionuclide transport, and for sensitivity studies related to repository EDZ and seal functionality. The Rooms-Only Model is used for determining high consequence well / container location pairs, to provide advective transport pathway and tracer simulations to support development of the SYVAC3-CC4 System Model and for various geosphere sensitivity cases. The Rooms-Only Model is used preferentially because the Full Model is computationally more challenging, requiring both significantly more memory to execute and significantly more time to simulate. Comparison cases presented in Section 7.7.2.3.1 show Rooms-Only Model results are very similar to Full Model results.

Individual containers are not modelled at this scale of resolution.

Figures representing release time histories are shown with shading at times greater than one million years to emphasize that results at these times are illustrative and included only to indicate model behaviour.

7.7.2.2.1 Base Case – No Well Flow Results

Figure 7-49 compares hydraulic head results for the Base Case (with no well) of both Repository-Scale Models with similar results from the Subregional-Scale Model to confirm correct implementation of the boundary conditions. The figure shows continuity of heads at the Repository-Scale Model boundary and close correspondence of results within the model domain. The color shaded portion of the figure shows the ratio of advective velocities from the Full Repository-Scale Model to the Subregional-Scale Model. In areas of intact rock, the ratio is close to 1.0, while more significant differences exist for areas where there are property differences between the Repository-Scale and Subregional-Scale Models.

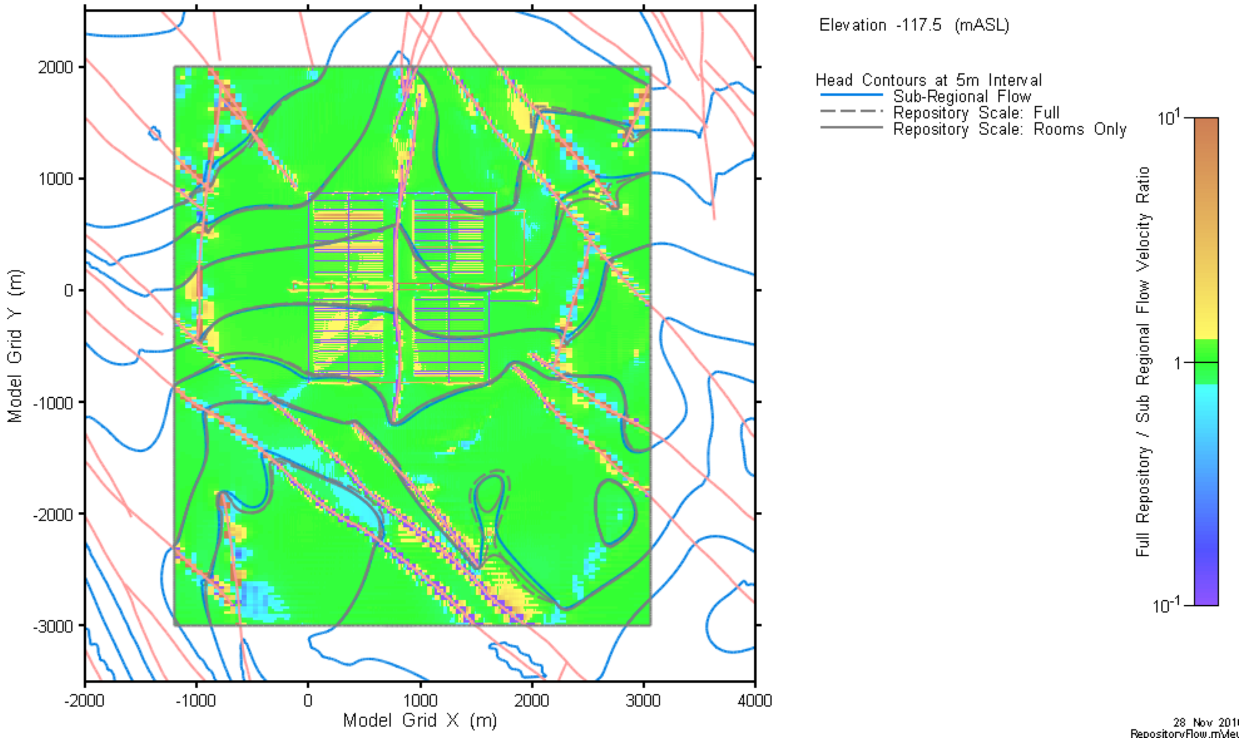

Figure 7-49: Repository-Scale Models: Comparison of Hydraulic Heads and Advective Velocities with Subregional-Scale Model at Repository Elevation

Figure 7-50 shows a more detailed view of the effect of repository features. Velocities in tunnels and placement rooms are lower, while velocities in adjacent EDZ regions are higher. Hydraulic heads are affected by placement rooms for the Rooms-Only Model and also by tunnels for the Full Model.

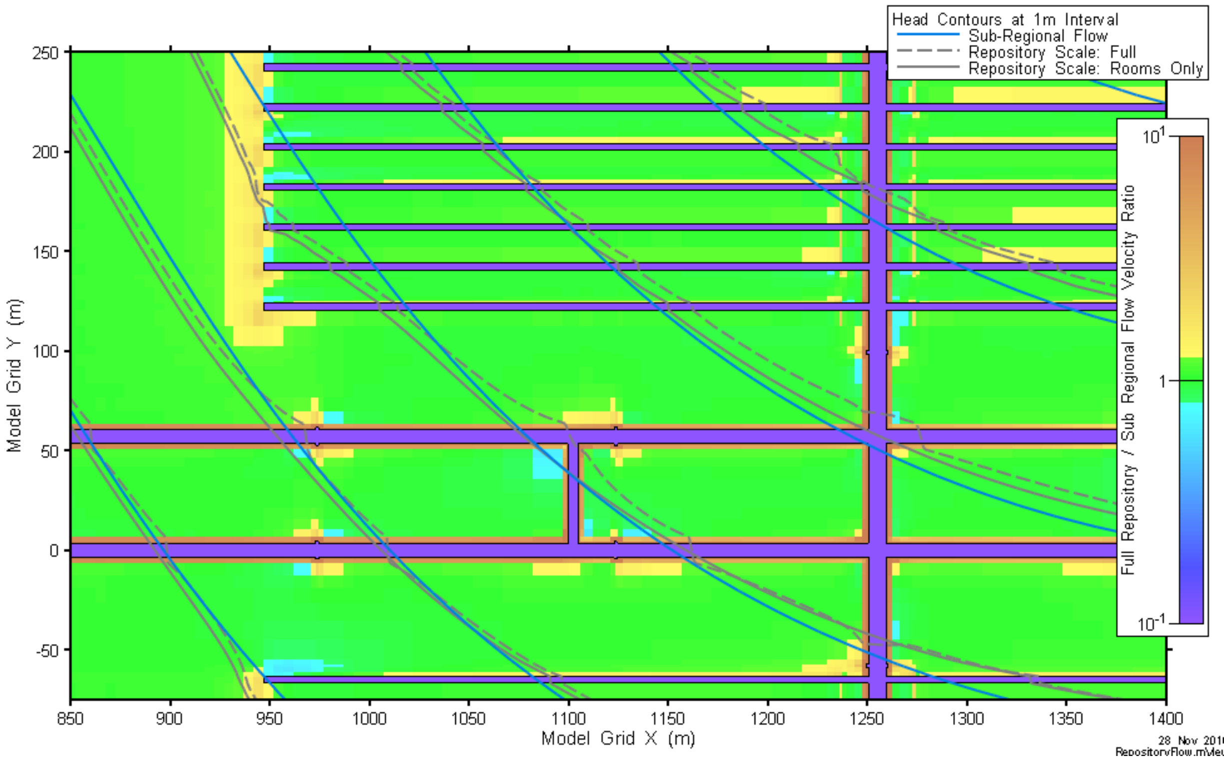

Figure 7-50: Repository-Scale Models: Comparison of Hydraulic Heads and Advective Velocities with Subregional-Scale Model at Repository Elevation

Differences between the Full Repository-Scale Model and the Rooms-Only Repository-Scale Model are shown in Figure 7-51. Velocities are very similar throughout the footprint, except where the Full Repository-Scale Model has features (e.g., tunnels and rooms with vertical EDZ (source rooms)) that are not represented in the Rooms-Only Model.

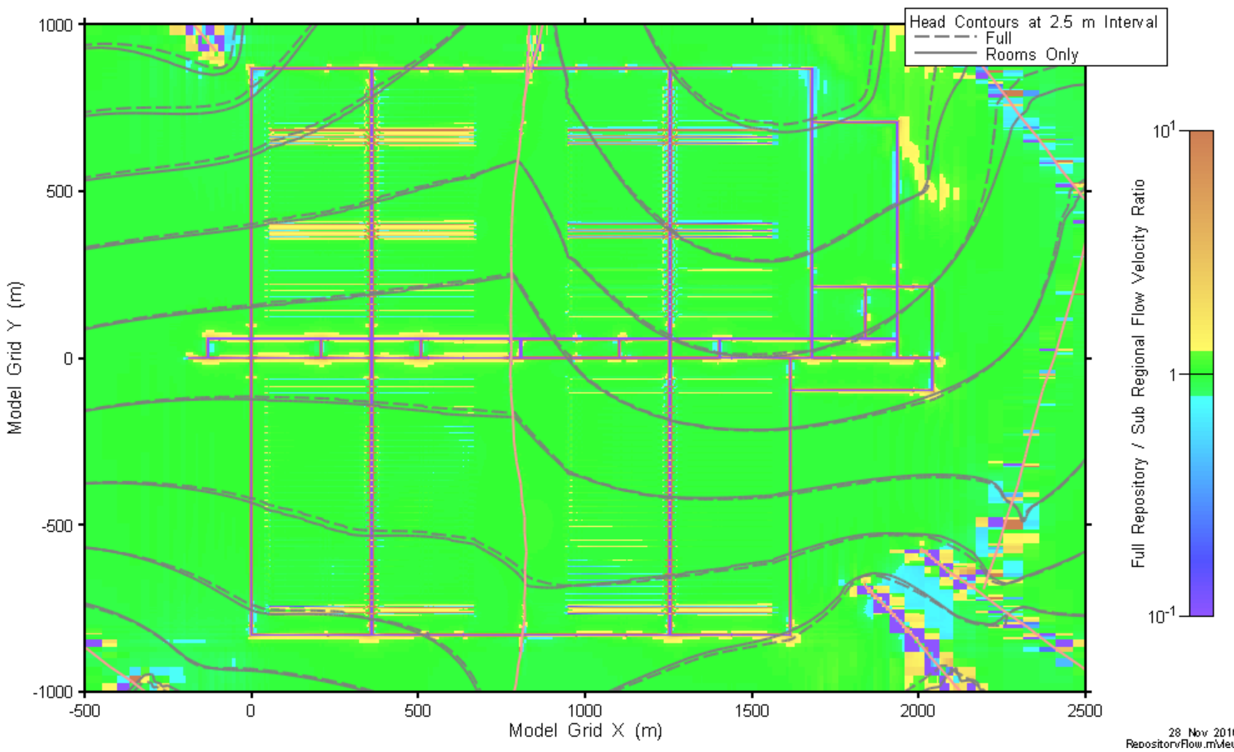

Figure 7-51: Repository Scale Models: Comparison of Hydraulic Heads and Advective Velocities at Repository Elevation

Mean-Life-Expectancy of the Full Repository-Scale Model over the entire domain is shown in Figure 7-52. Comparison to Figure 7-40 shows results are very similar to those for the Subregional-Scale Model.

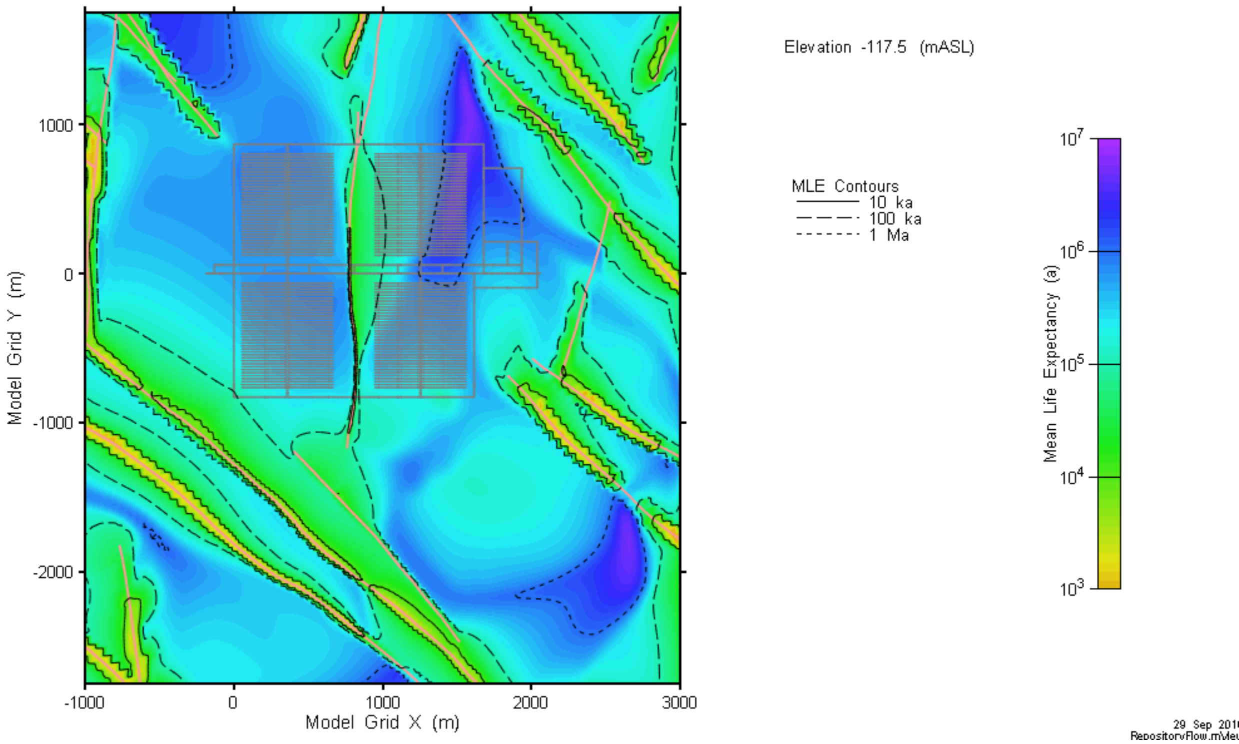

Figure 7-52: Full Repository-Scale Model: Mean Life Expectancy at Repository Elevation

Figure 7-53 is a visualization of the Rooms Only Base Case (with no well) advective transport pathways, for pathways originating within the repository Inner EDZ below the repository placement rooms. Particles are released at approximately 15 m intervals along each room. The figure shows that the pathways taken to the surface discharge locations, with many pathways traveling through the fracture system.

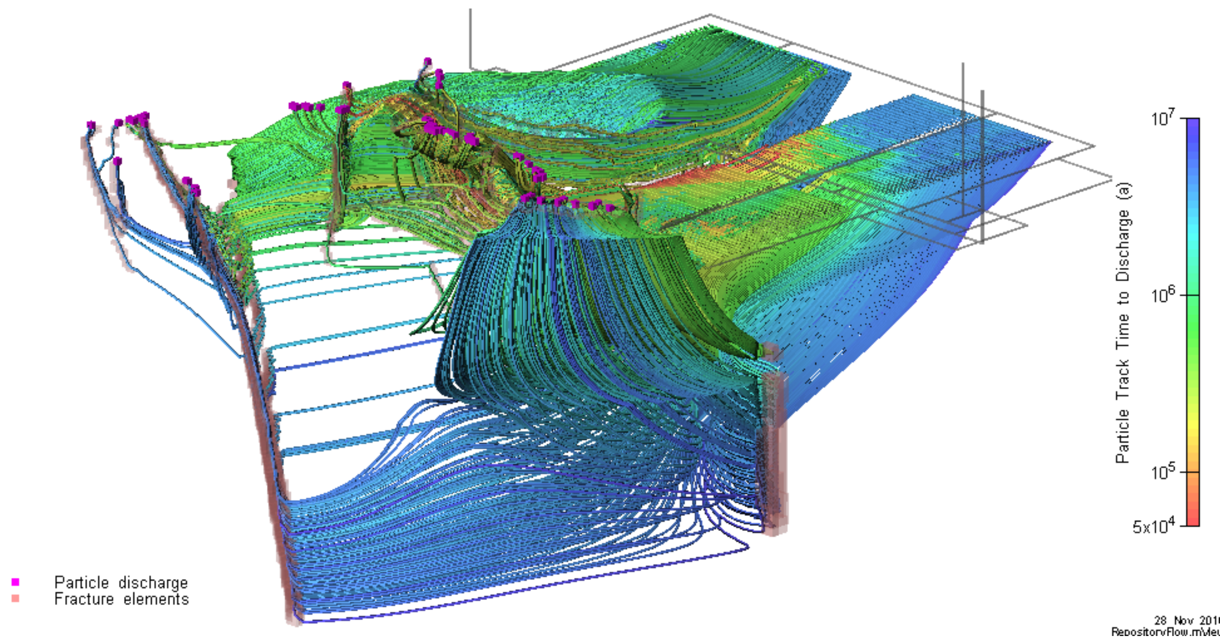

Figure 7-53: Rooms-Only Repository-Scale Model: Base Case No-Well Advective Transport Pathways

These results are similar, but not identical, to the same case for the Subregional-Scale Model (see Figure 7-44 and Figure 7-45). In comparison, transport to the Central Wetland Zone is slightly increased with a corresponding reduction in discharge to the West River as shown in Figure 7-54 and Figure 7-55.

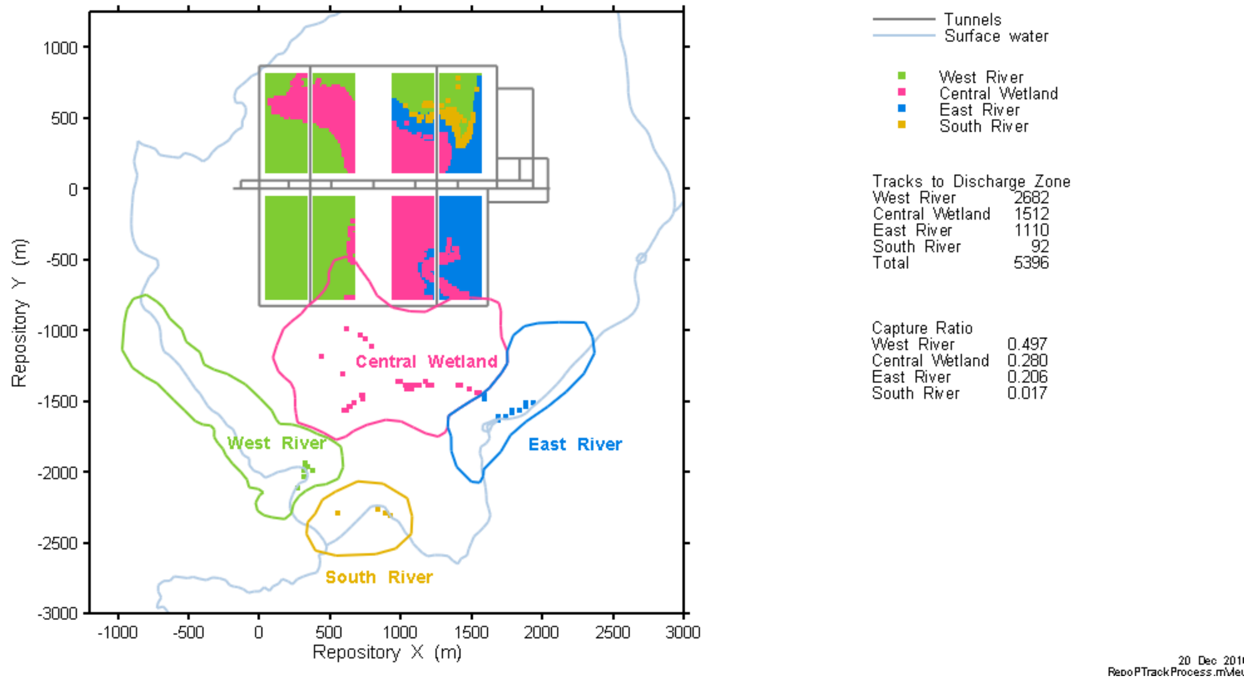

Figure 7-54: Rooms-Only Repository-Scale Model: Base Case No-Well Transport Pathway Discharge Zones

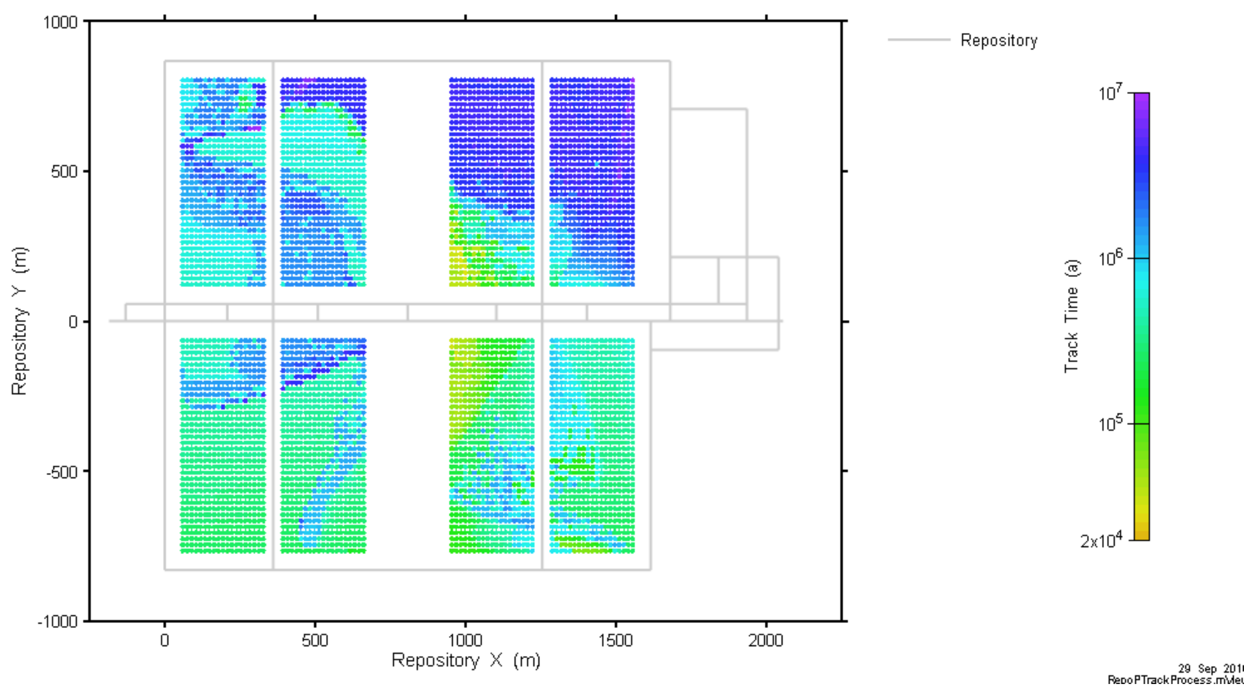

Figure 7-55: Rooms-Only Repository-Scale Model: Base Case No-Well Transport Pathway Travel Time to Discharge

Cumulative Distribution Functions (CDFs) of particle travel time show that the Central Wetland tracks are of longer duration and length (Figure 7-56 and Figure 7-57) than those determined with the Subregional-Scale Model (Figure 7-46 and Figure 7-47).

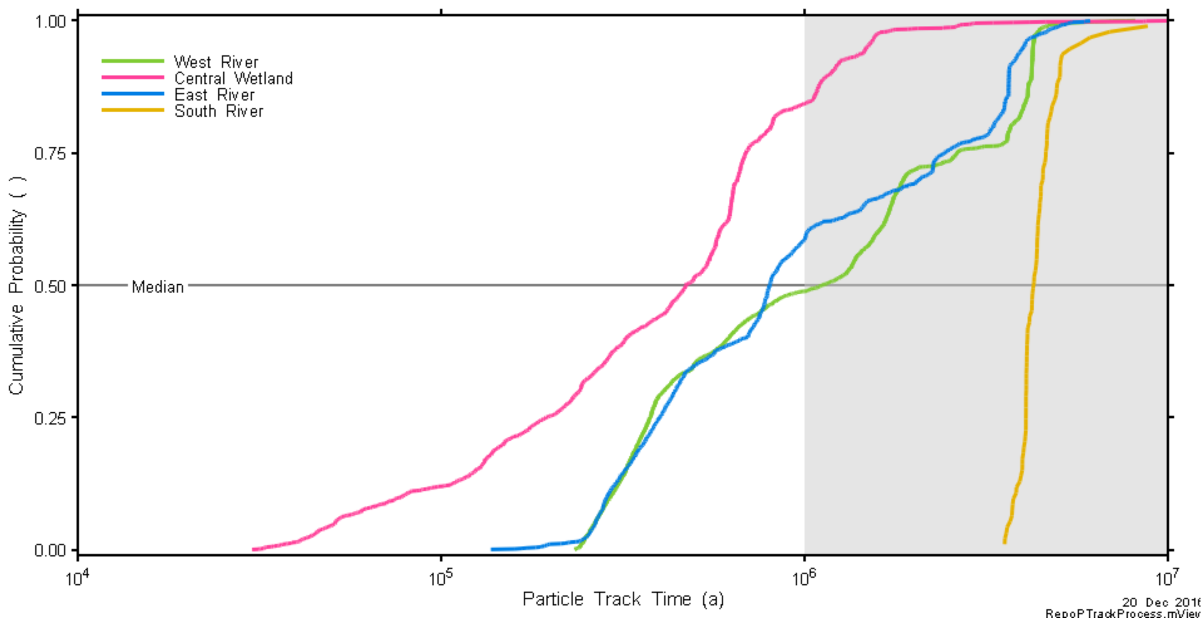

Figure 7-56: Rooms-Only Repository-Scale Model: Base Case No-Well Transport Pathway Travel Time Cumulative Distribution Function

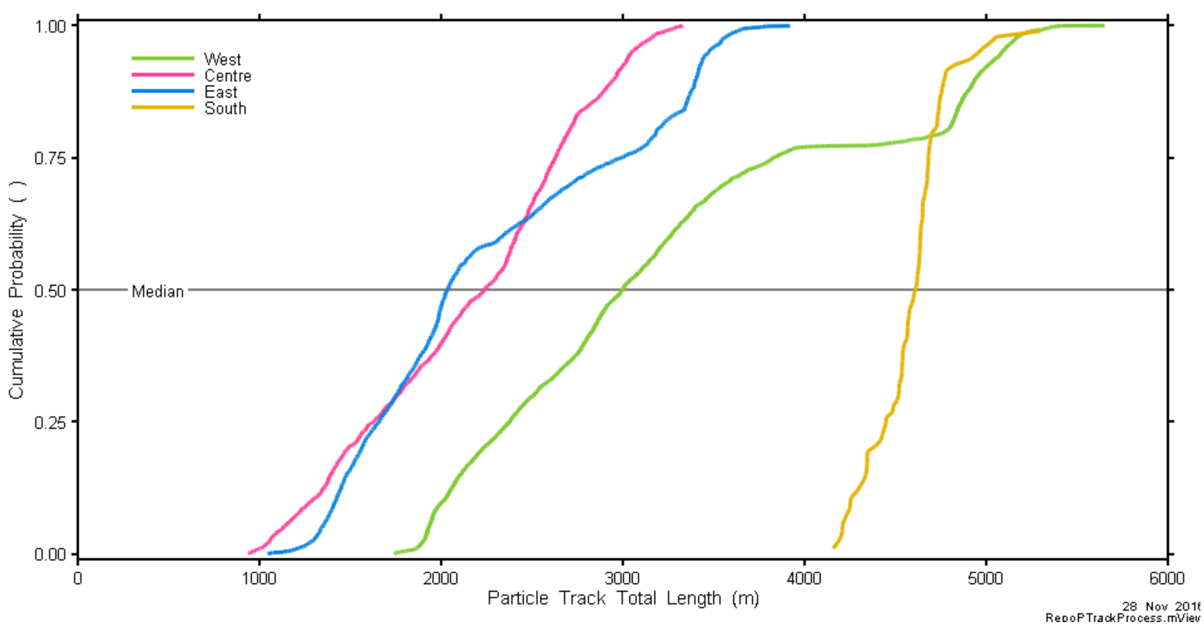

Figure 7-57: Rooms-Only Repository-Scale Model: Base Case No-Well Transport Pathway Total Length Cumulative Distribution Function

7.7.2.2.2 Base Case – With Well Flow Results

The well location for this discussion corresponds to the main fracture well location. As will be shown later (Section 7.7.2.3.2), this is the location that maximizes dose rate to the small farming family that is assumed to be unknowingly living on top of the repository.

Figure 7-58 compares the MLEs and hydraulic head contours with those of the Base Case No Well simulation. The MLE ratios given in the figure are the ratios of the MLEs in the No Well Base Case to the MLEs in the Base Case With Well. Ratios are increased adjacent to the main fracture, indicating a decrease in MLE. Hydraulic head contours are affected near the main fracture with the effect increasing closer to the well.

Figure 7-59 illustrates advective transport pathways.

Figure 7-60 shows that the discharge from a large area of the footprint (29%) would be captured by the well.

Figure 7-61 shows the travel time to discharge for various discharge locations.

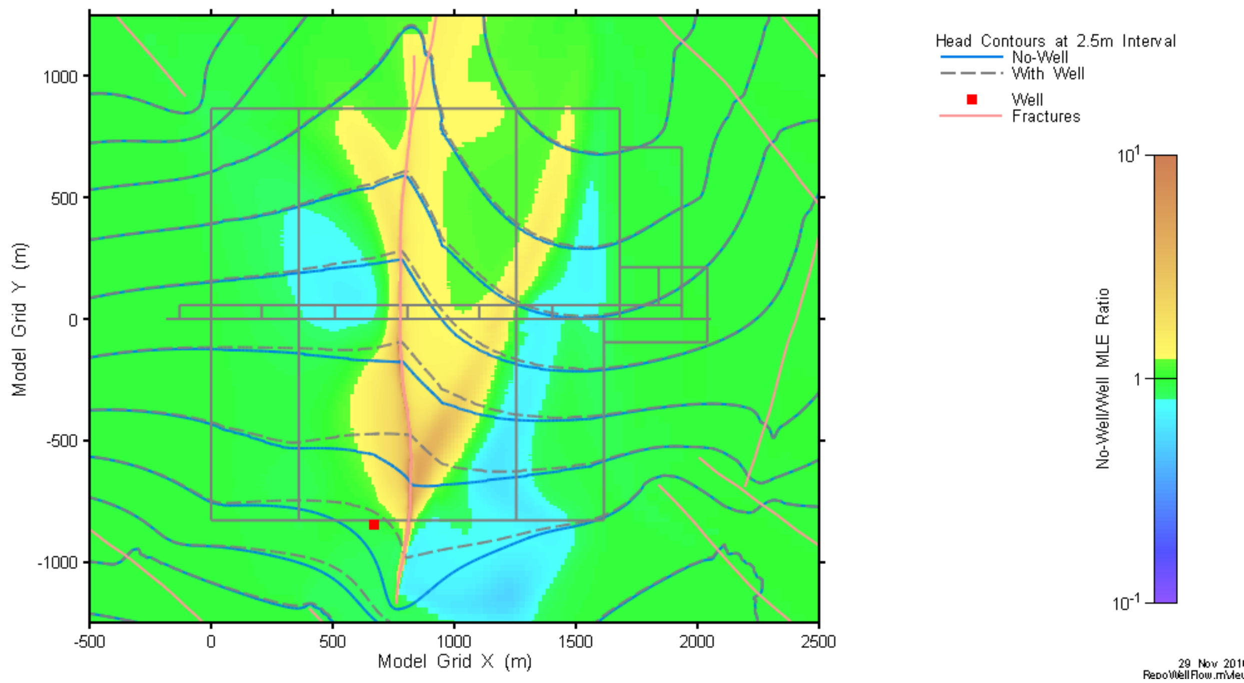

Figure 7-58: Rooms-Only Repository-Scale Model: Comparison of No-Well and Main Fracture Well Hydraulic Heads and MLE Ratios

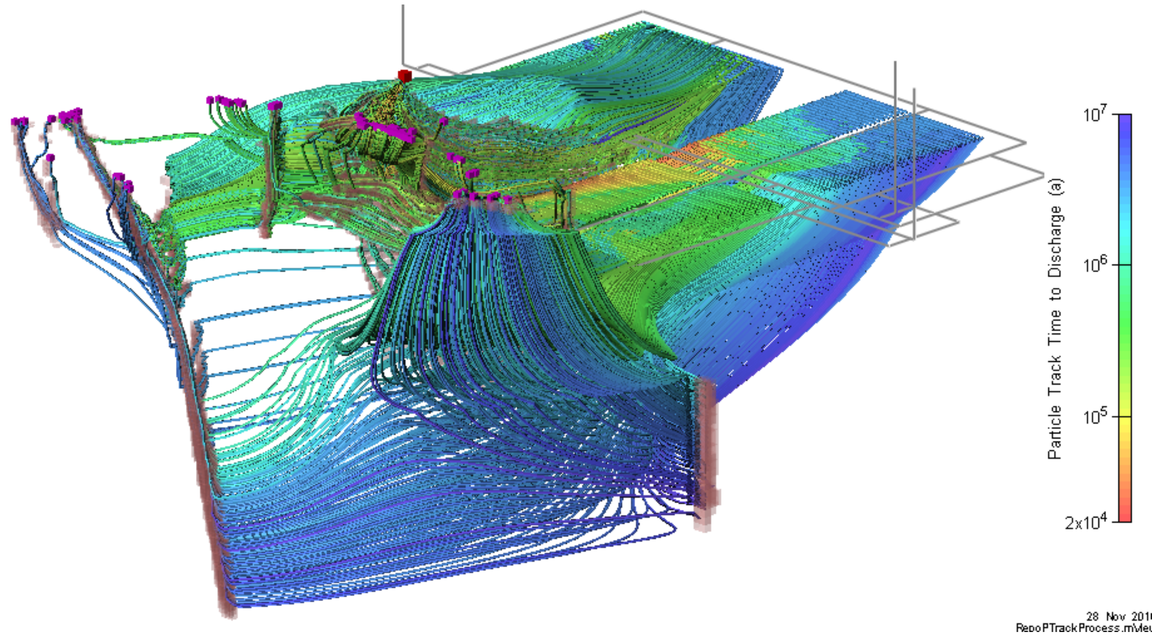

Figure 7-59: Rooms-Only Repository-Scale Model: Main Well Advective Transport Pathways

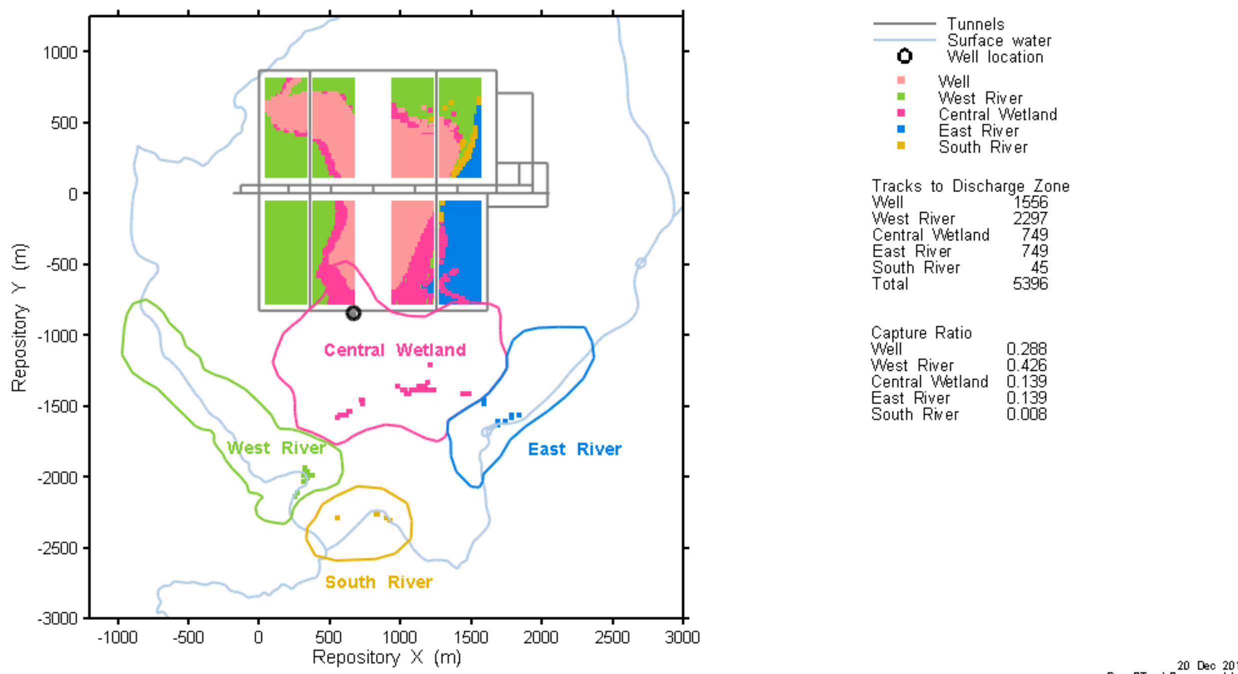

Figure 7-60: Rooms-Only Repository-Scale Model: Main Well Transport Pathway Discharge Zones

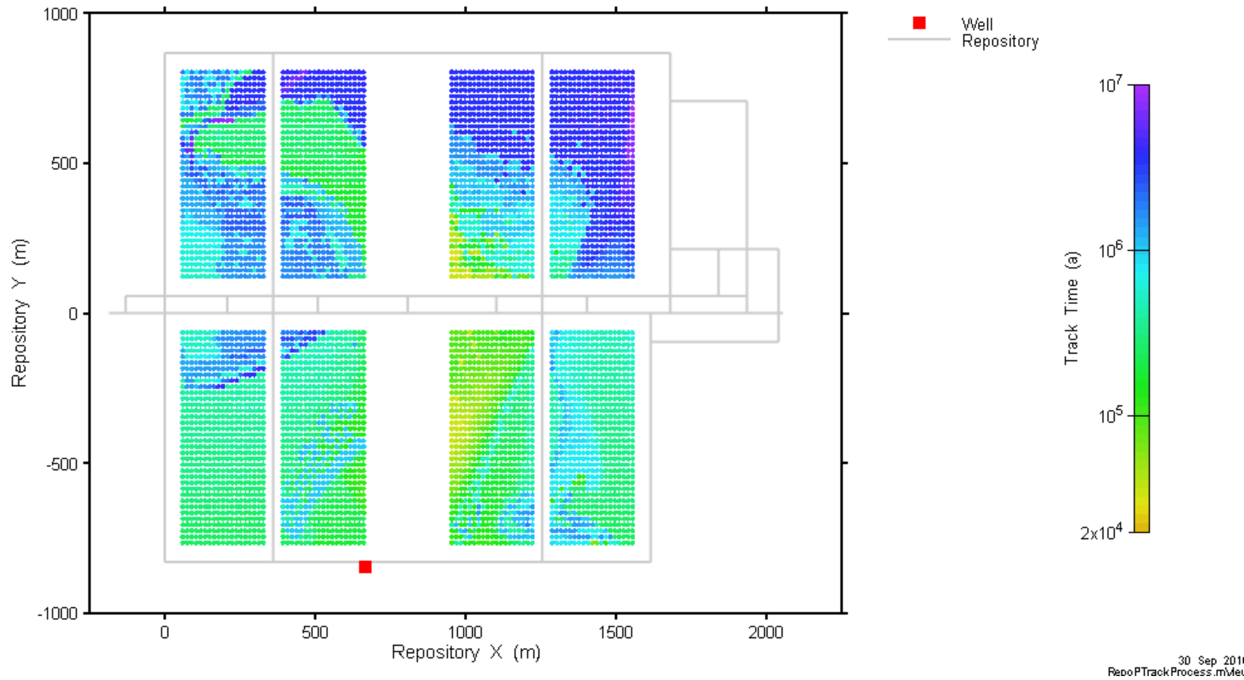

Figure 7-61: Rooms-Only Repository-Scale Model: Main Well Transport Pathway Travel Time to Discharge

Figure 7-62 and Figure 7-63 show the effect of the well on travel times and distances. The fastest travel time to the well (29.1 ka) is very similar to the fastest Central Wetland discharge times for the No-Well case (30.1 ka).

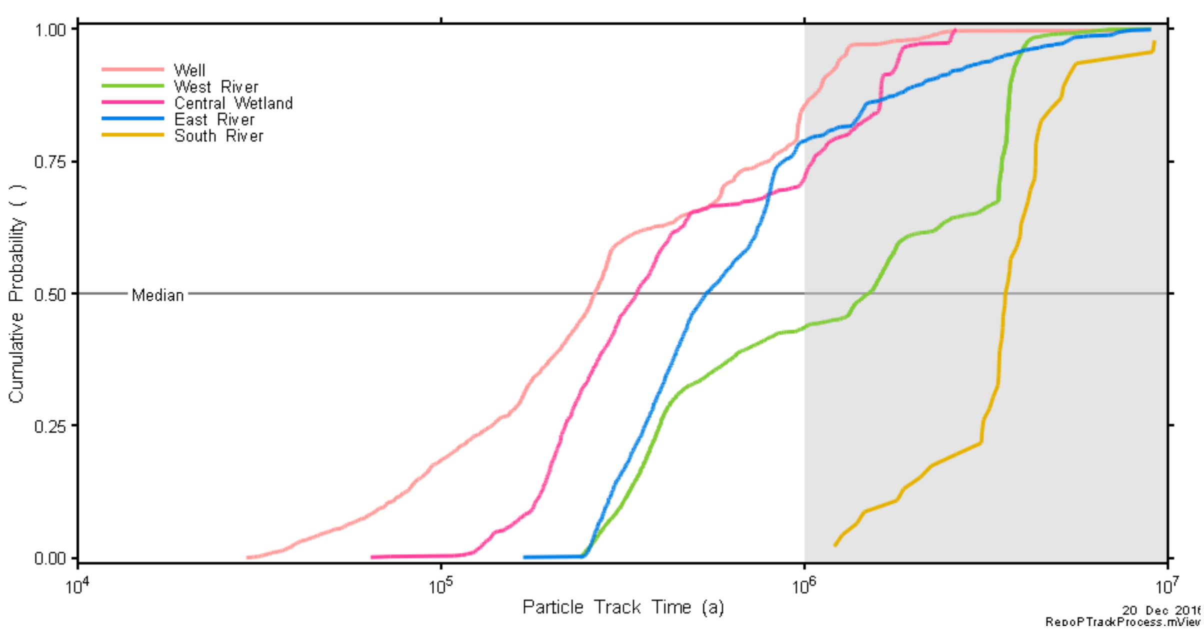

Figure 7-62: Rooms-Only Repository-Scale Model: Main Well Transport Pathway Cumulative Time Distribution Function

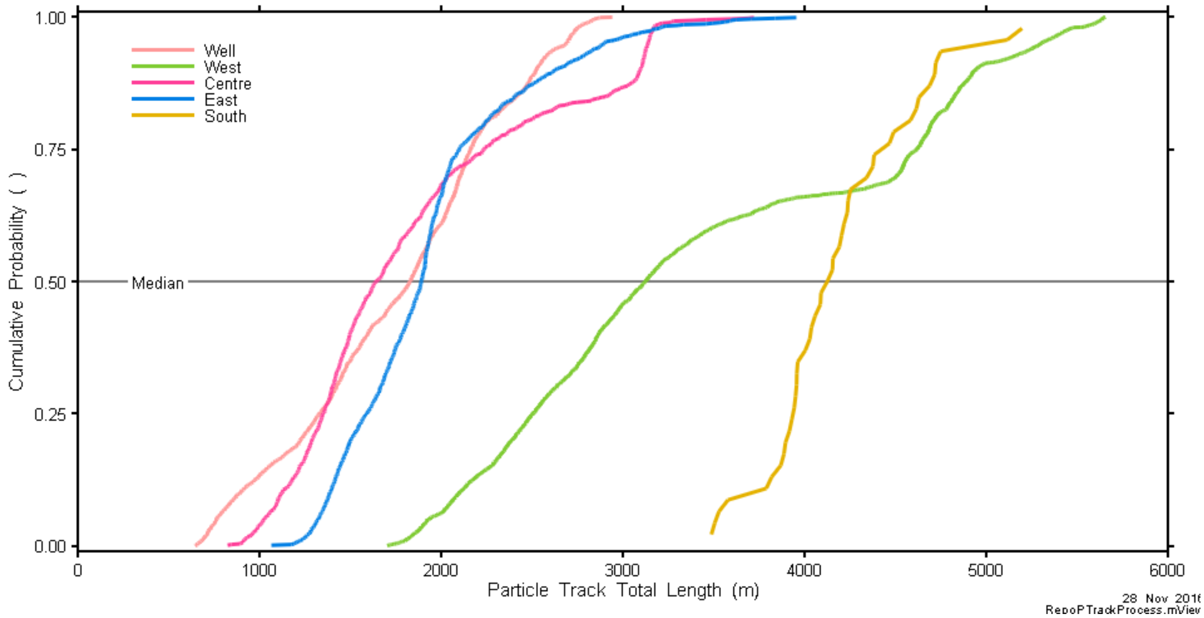

Figure 7-63: Rooms-Only Repository-Scale Model: Main Well Transport Pathway Cumulative Length Distribution Function

In general, overall flow system characteristics are similar to the No Well case, particularly in areas some distance removed from the well and its associated fracture system.

7.7.2.3 Repository-Scale Model Radionuclide Transport Results

This section presents radionuclide transport results as determined using the Repository-Scale Models. The following are described:

- A comparison of results from the Full Repository-Scale Model with results from the Rooms-Only Repository-Scale Model. The effect of different container source terms are also examined;
- High consequence well and container locations. These are the locations that result in the fastest and / or highest magnitude radionuclide transport to the well;
- The Base Case transport results;
- Sensitivity case results illustrating the effect of deviations (see Section 7.7.2) affecting the performance of the buffer, backfill and seals barrier and the geosphere barrier; and
- Sensitivity case results illustrating the effect of various FRAC3DVS-OPG modelling attributes and parameters.

7.7.2.3.1 Comparison of Different Repository-Scale Models

As discussed in Section 7.5.1, two versions of the Repository-Scale Model are used for transport simulations, with the computationally demanding Full Repository-Scale Model used more sparingly. In addition, a further conservatism has been adopted for some cases, this being a direct coupling of the Combined Source Term (i.e., the source term summed over all containers) with the Repository-Scale Models, thereby bypassing the Container-Scale Models and therefore also bypassing the EBS. This conservative approach is adopted where it is impractical to run additional Container-Scale simulations.

Figure 7-64 shows that results for I-129 transport to the well for the various model and source term combinations are virtually identical. The Full Repository-Scale Model has marginally higher and earlier transport than the Rooms-Only Model, while the Combined Source Term results in slightly higher and earlier transport to the well than does the more detailed Container-Scale Model approach. The differences are sufficiently small as to be insignificant, providing confidence in results from either model and source term for I-129 transport. Additional information concerning these results is provided in Section 7.7.2.3.3.

Results for C-14 are also insensitive to the choice of model and to source term combination, as seen in Figure 7-65.

Note that this good agreement applies only to non-sorbing species (or to species with very low sorption coefficients). Contaminants which strongly sorb to EBS components may show different results between the Container-Scale approach and the Combined Source Term, with the Combined Source term showing higher transport to the well and surface.

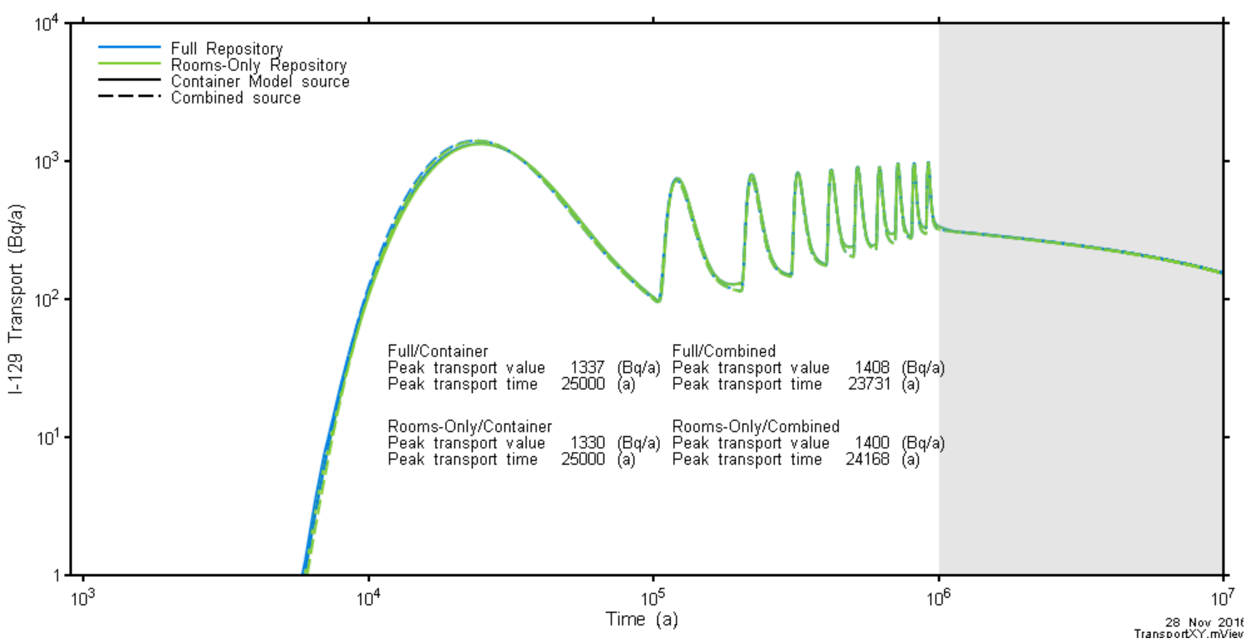

Figure 7-64: Repository-Scale Models: Comparison of Full Model and Rooms-Only Model for the Container Source Term and the Combined Source Term for I-129 Transport to the Main Well

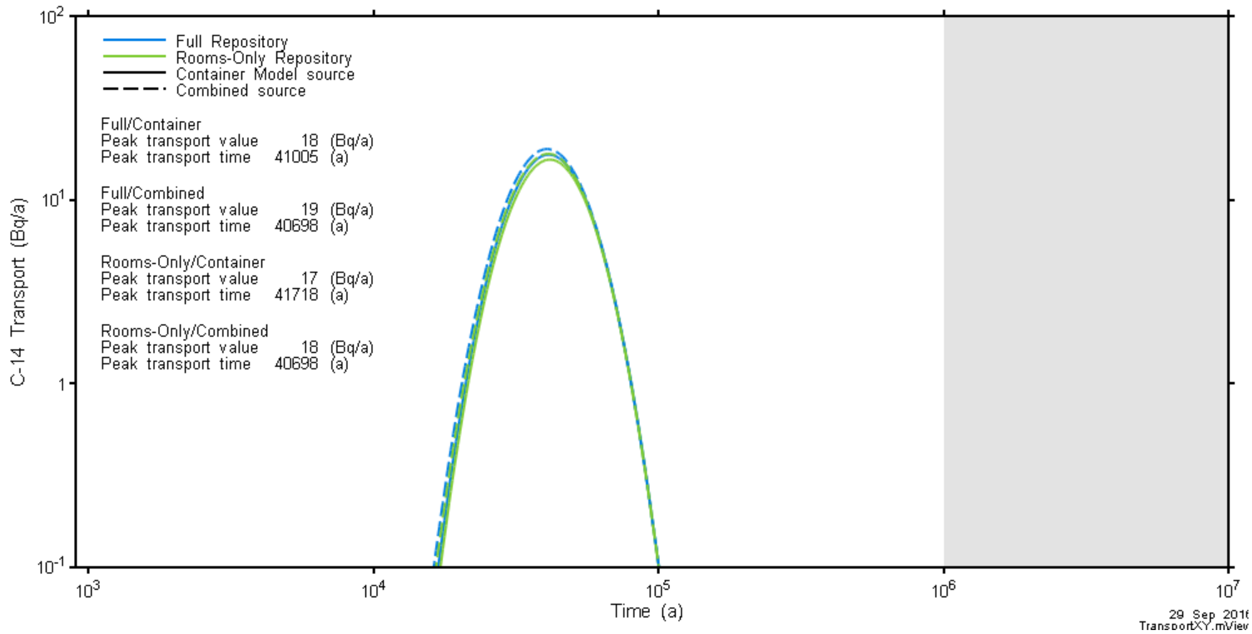

Figure 7-65: Repository Model – Comparison of Model (Full and Rooms-Only) and Source Term (Container model or Combined) C-14 Transport to Main Well

7.7.2.3.2 Location of the Well and Defective Containers

In previous postclosure safety assessments for conceptual repositories, the location of the water supply well was determined through a combination of analytic assessments (i.e., transport pathways and mean life expectancy results) and subjective interpretation of the flow system. Provided that the pathway to the surface from the repository location with the minimum MLE is relatively short, the location of a well that would intercept that pathway is usually obvious. However, this is not the case for the geosphere in the current study where all transport pathways are fairly long, and they terminate in discharge locations outside of the repository footprint.

To address this, an alternate approach has been adopted. In this approach, the selection of well and defective container locations is performed in four stages, as follows:

1. Perform transport simulations with a pulse source term released simultaneously from all possible container locations for one well location, and then repeat for additional well locations until coverage of all possible well locations in the entire repository footprint and surrounding area is achieved.
2. Extract well transport responses with a peak exceeding a threshold value and aggregate by location group.
3. Perform MLE simulations for the maximum transport well in each location group to determine possible defective container locations.
4. Examine well and defective container location pairs with a single container pulse source. Conduct simulations until the maximum well / source pair is determined for each location group.

Figure 7-66 shows all test well locations that have been considered. There are 106 wells spaced at approximately 200 m intervals along all fractures that could potentially intercept repository discharge. All fractures located above / immediately adjacent to the repository footprint are included.

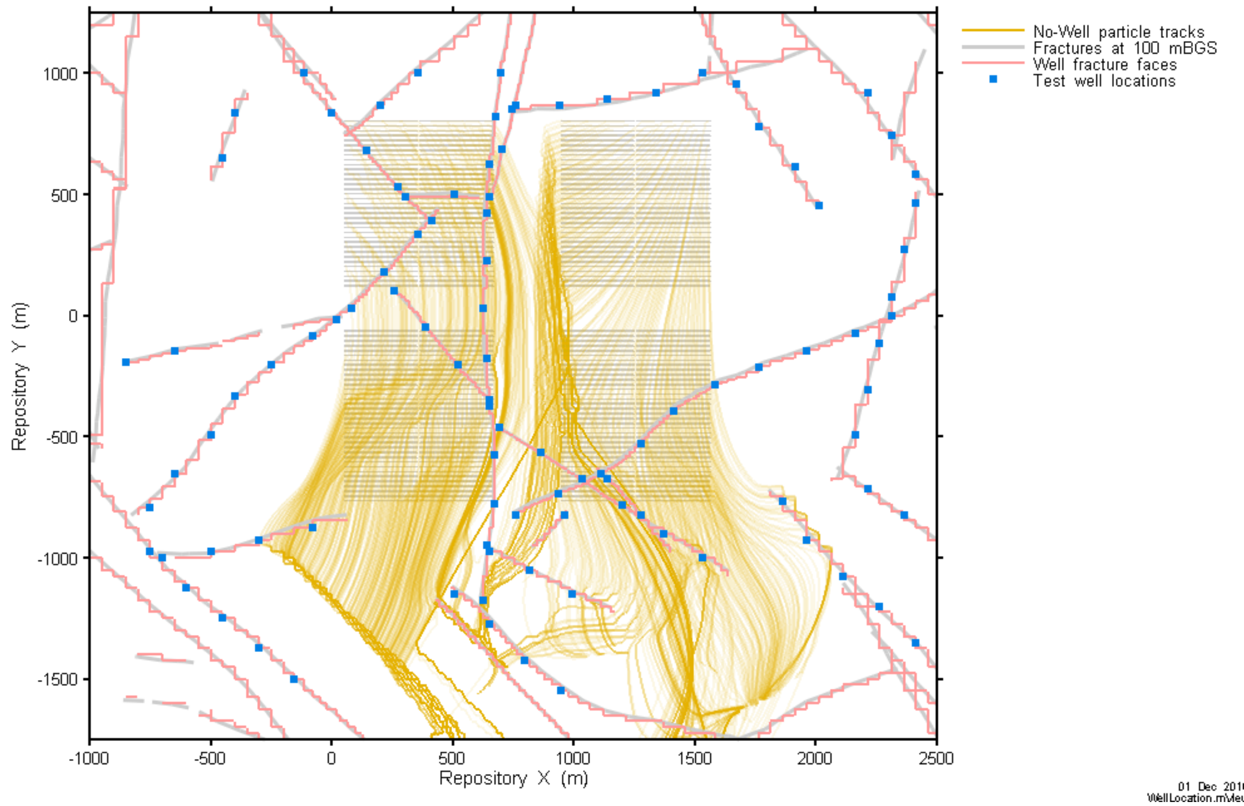

Figure 7-66: Initial Locations for Well Location Simulations

The source term used is a short duration pulse, where 10^9 Bq of I-129 is released at each container location at a constant rate over a 1000 year period starting at t = 0. This is not the same as the I-129 source term from the defective containers, and has only been adopted in this part of the work to simplify the output information so that the effects of different well locations can be more easily determined. Simulations are conducted for 500 ka as this is sufficiently long to identify the time of peak transport at likely well locations. The Rooms-Only Repository-Scale Model was used, and the Base Case reference well demand of 911 m^3/a was adopted.

Figure 7-67 shows well transport versus time results for all 106 wells. The blue dots note the time and magnitude of peak transport.

Figure 7-68 presents a histogram of the peak transport for the 106 locations considered. Most of the considered locations have very low peak transport values.

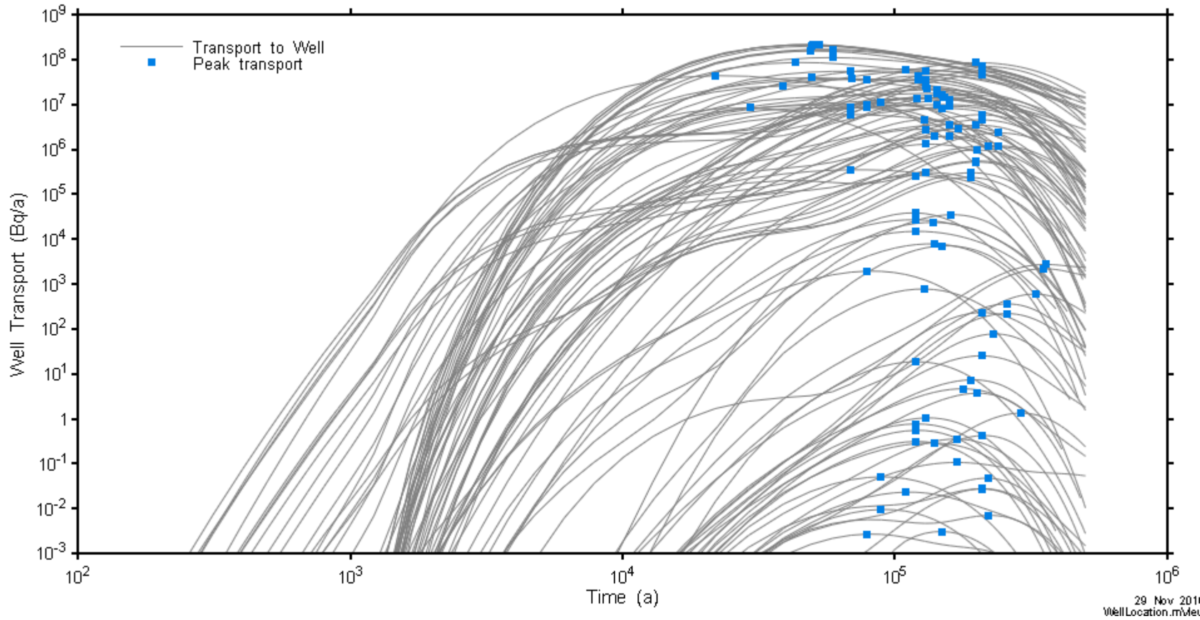

Figure 7-67: Rooms-Only Repository-Scale Model: Well Transport for All Tested Well Locations for the Tracer Source Term

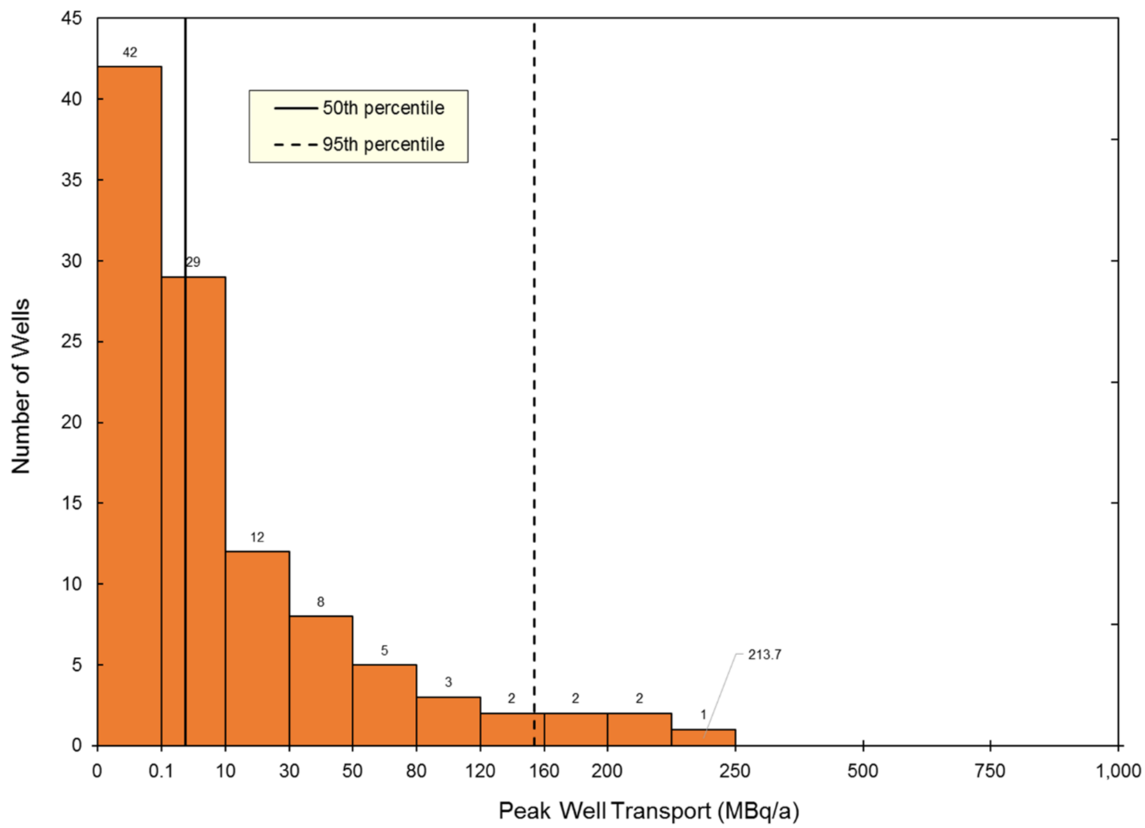

Figure 7-68: Rooms-Only Repository-Scale Model: Histogram of Peak Well Transport for All Tested Well Locations for the Tracer Source Term

Based on these results, four zones of possible higher consequence well locations have been identified. These zones are shown as the circled areas in Figure 7-69.

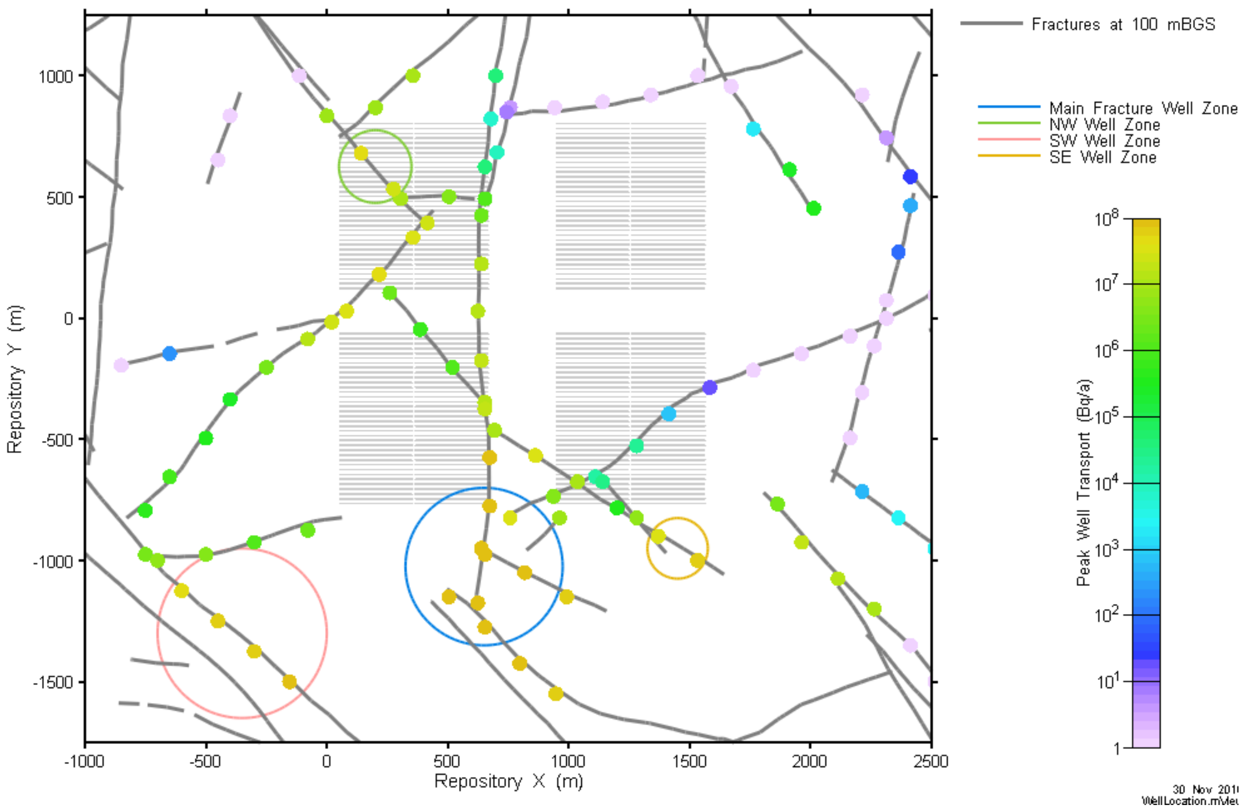

Figure 7-69: Rooms Only Repository-Scale Model: Peak Well Transport at Test Well Locations and Spatial Zone Identification

To guide the selection of possible container source locations, MLE simulations were then generated for the well location within each of the four well zones that results in the highest peak transport. Ratios of the No-Well MLE results, shown in Figure 7-40, divided by With-Well MLE results were then produced to identify those locations affected by the pumping well. Figure 7-70 presents these ratios. Differences from the No-Well results are apparent.

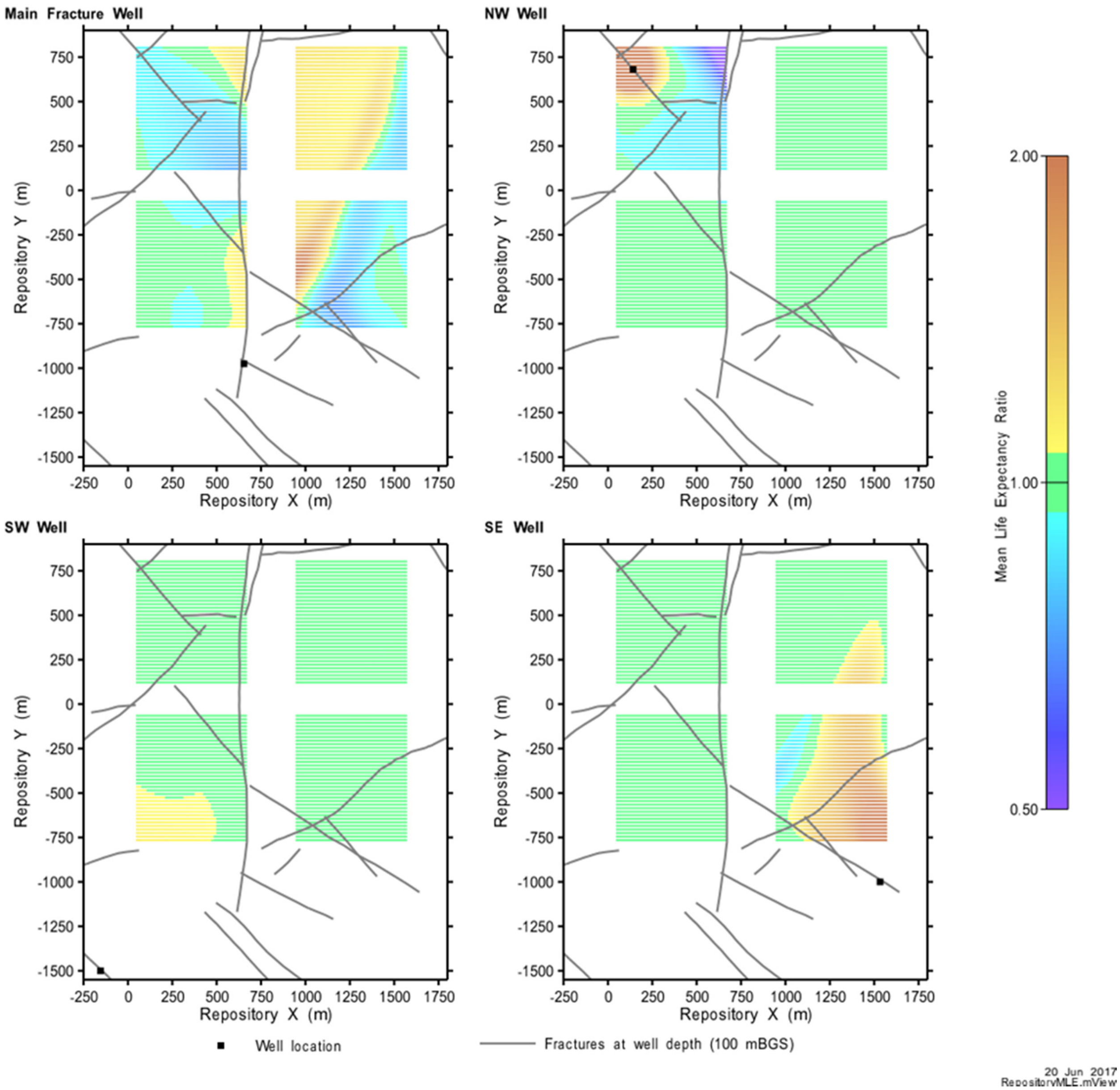

Figure 7-70: Rooms-Only Repository-Scale Model: Mean Life Expectancy Simulations – Interim Peak Well Transport Locations

These results were assessed and potential defective container locations selected. Transport simulations were then conducted again with the pulse source term applied for a single container only at the potential defective container locations. Well and source locations were refined within each of the four zones and new permutations simulated until maximums pairs were identified. Over 300 simulations were performed. Tested well and source locations for each zone are shown in Figure 7-71.

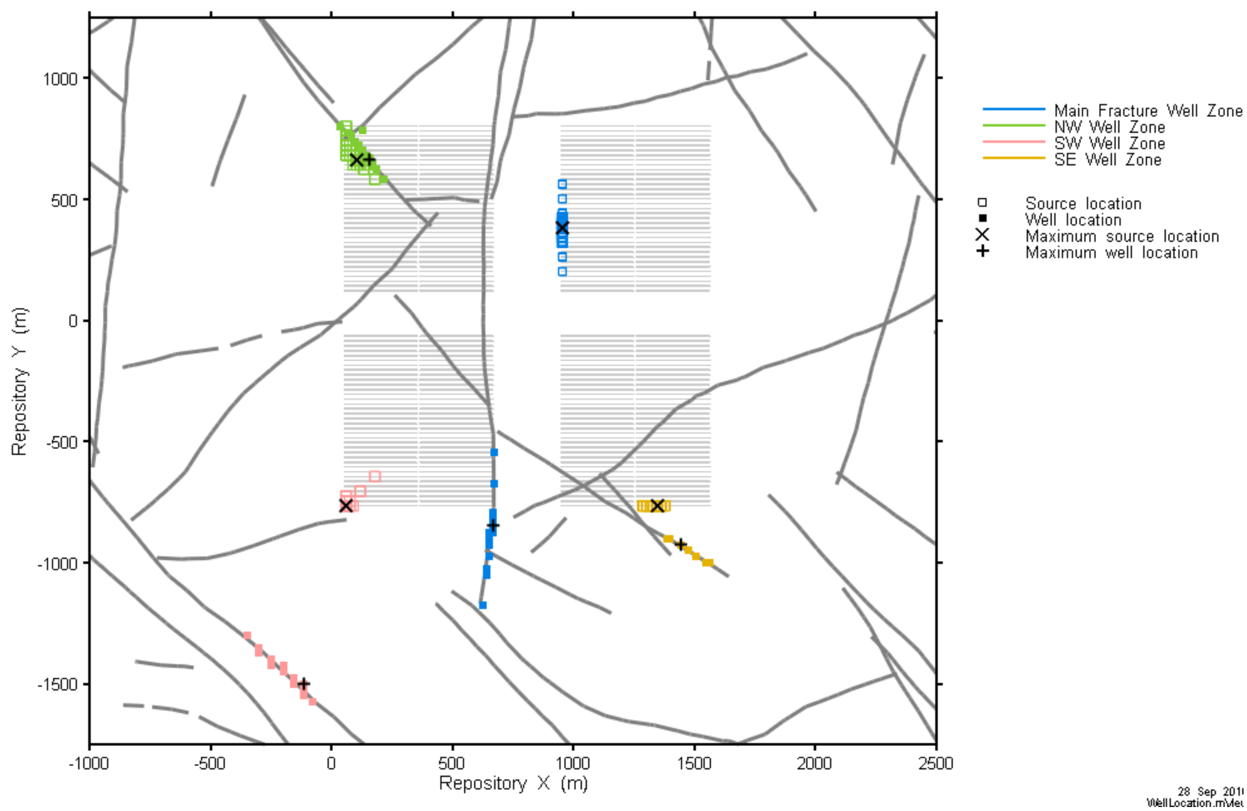

Figure 7-71: Rooms-Only Repository-Scale Model: Well/Source Transport Simulations – Tested and Final Locations

Figure 7-72 shows I-129 transport results for all combinations considered. The Main Fracture Well has the highest peak, although maximum transport is within a factor of two for all zones. The NW Zone pair arrives earlier in time while the SW Zone has the latest peak. The SW Zone has a unique character with a lower early time peak, followed later by the maximum peak. This is indicative of the complexity of the flow system in the SW corner. Differences in maximum peaks between various locations are partially explained by variations in the capture ratio, which is the percentage of the total release (10^9 Bq) that is abstracted by the well. The Main Fracture and SE zone both capture 95% of the source, with slightly lower capture ratios for the NW and SW well zones.

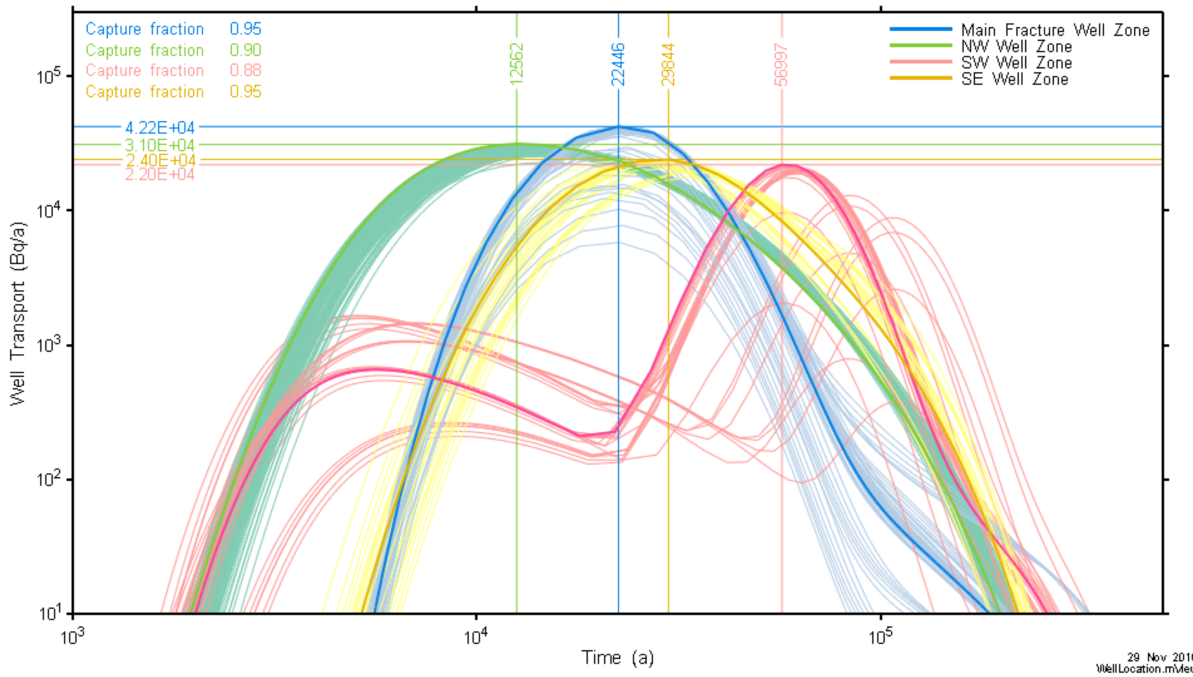

Figure 7-72: Rooms-Only Repository-Scale Model: Well / Source Transport Simulations

Based on these results, the combination of well and defective container locations that result in the highest transport to the well for each zone of interest were selected. These locations are marked in Figure 7-71.

For the marked locations, simulations were then performed using the Combined Source Term for I-129 (i.e., the source term summed for 10 containers) instead of the pulse source term. These results are shown in Figure 7-73.

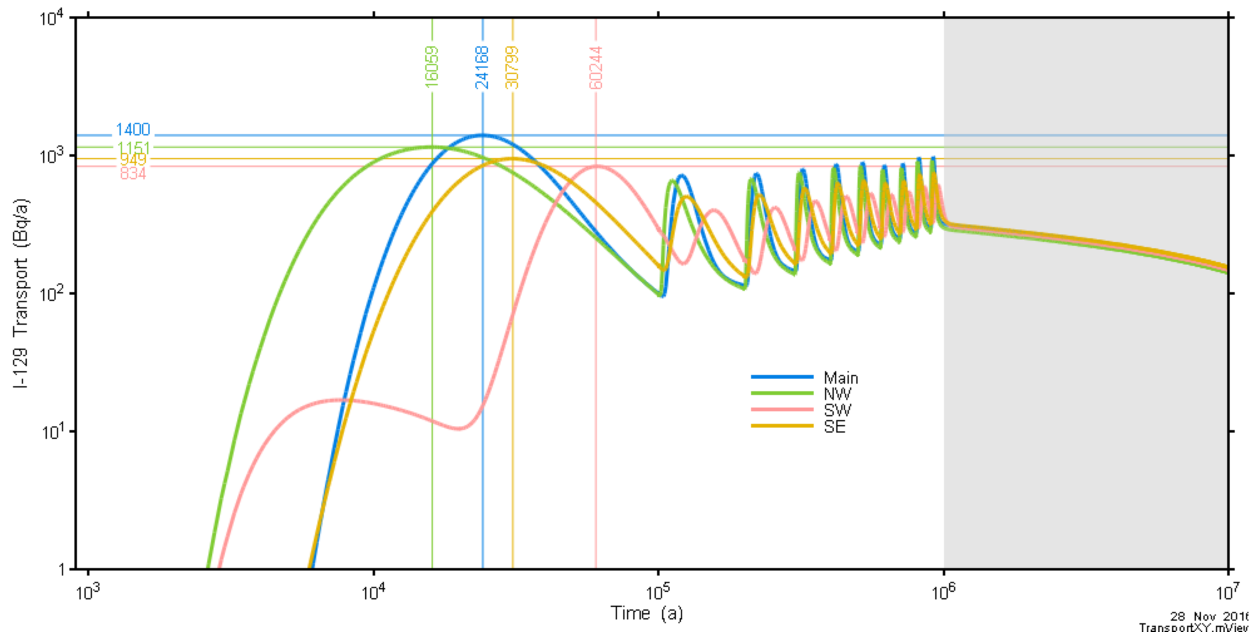

Figure 7-73: Rooms-Only Repository-Scale Model: I-129 Well Transport Comparison of Well/Source Locations

The Figure 7-73 results indicate that maximum I-129 transport to the well occurs for the well / container combination associated with the main fracture. To confirm that this is the most consequential combination for public dose, simulations of C-14 transport were also performed for the Main Fracture Zone and NW Zone well / container combinations. C-14 is of interest as a potential dose contributor because its half-life (5730 years) is sufficiently long that C-14 could also be transported to the NW well with less attenuation by decay than C-14 transported to the Main Fracture Zone. Figure 7-74 and Figure 7-75 show these results.

C-14 transport to the well is greater for the NW Well location due to the shorter transport time; however, this is offset by reduced I-129 transport. Given the relative differences in ingestion dose coefficients between I-129 and C-14, the Main Fracture Zone well / container combination yields the most consequential dose calculations.

With the exception of a no-well sensitivity case, results reported in the remainder of this report are for this dose maximizing combination of well and source location only.

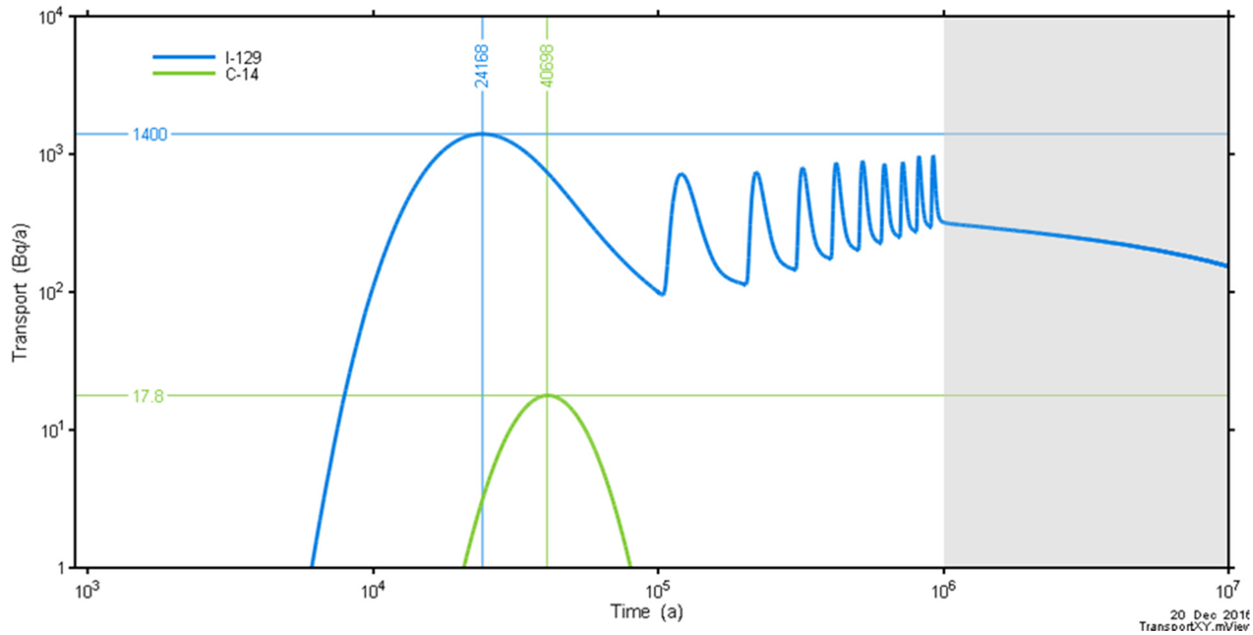

Figure 7-74: Rooms-Only Repository-Scale Model: I-129 and C-14 Well Transport for the Main Fracture Zone

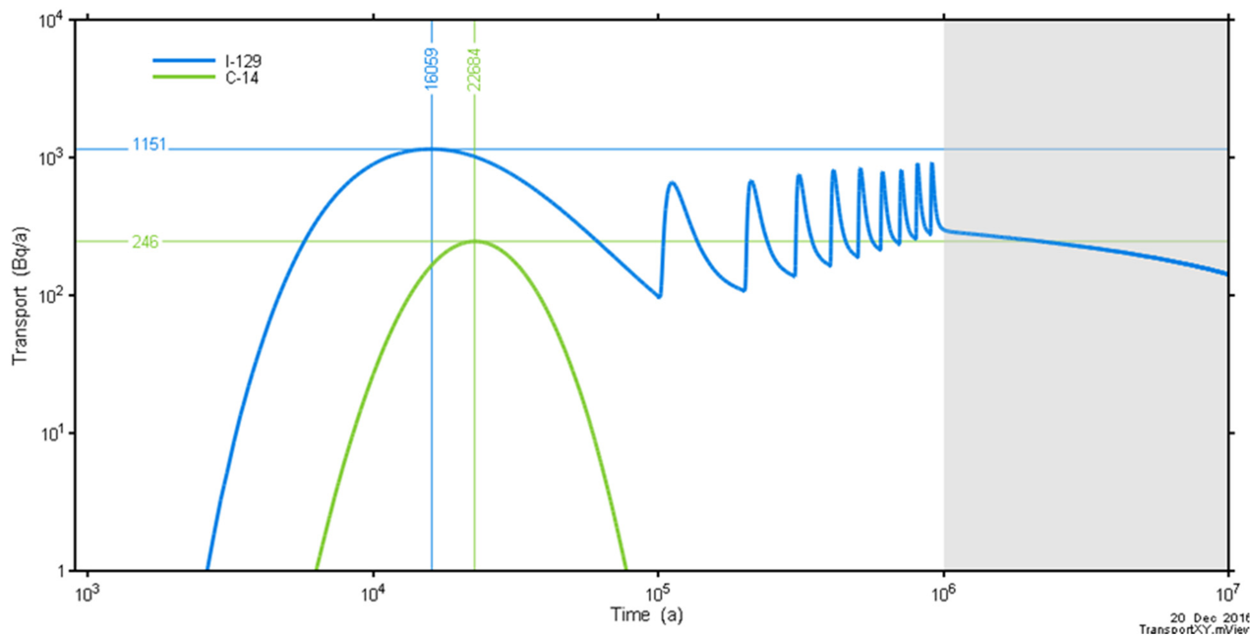

Figure 7-75: Rooms-Only Repository-Scale Model: I-129 and C-14 Well Transport for the NW Zone

7.7.2.3.3 Base Case Results

Transport results for the Base Case are presented here. These are based on 10 containers failing over the first million years, with the first container failing at 1000 years and other containers failing at a rate of one container every 100,000 years.

As described in Section 7.7.2.3.2, the limiting combination of well and defective container location is adopted to ensure contaminant transport to the well is maximized.

In the results presented below, transport from the near-field repository into the rock (at the Inner EDZ boundary) is calculated by the Main Container-Scale Model and imposed as a boundary condition on the Repository-Scale Models, where a time-varying radionuclide mass is injected into the model at nodes surrounding the container location (see Figure 7-27).

Figure 7-76 shows I-129 transport to the well and total discharge to other surface locations over the 10 Ma simulation period. I-129 is selected for this discussion because, as will be seen later in Section 7.8.2.1, essentially all of the dose consequence is due to I-129. The peak transport is 1337 Bq/a occurring at 25,000 years.

There are 10 individual peaks in Figure 7-76 because there are 10 failed containers, and the individual peaks are due to the effect of the instant release contribution to the total source term (see Section 7.3.1). The first transport peak is higher than the others because the radiation field in the container at early times is much greater than at later times, so the used fuel dissolution rate (congruent release rate) is higher.

Overall capture by the well, defined as the integrated transport to the well over 10 Ma divided by the total mass injected into the model, is about 90% of the I-129 originally present in the defective containers. Roughly 2% is discharged to other surface locations, and the remaining I-129 is either retained within the geosphere and repository or lost due to decay.

Note that the results in Figure 7-76 are slightly different from those shown in Figure 7-74 because the Full Repository-Scale Model is used here.

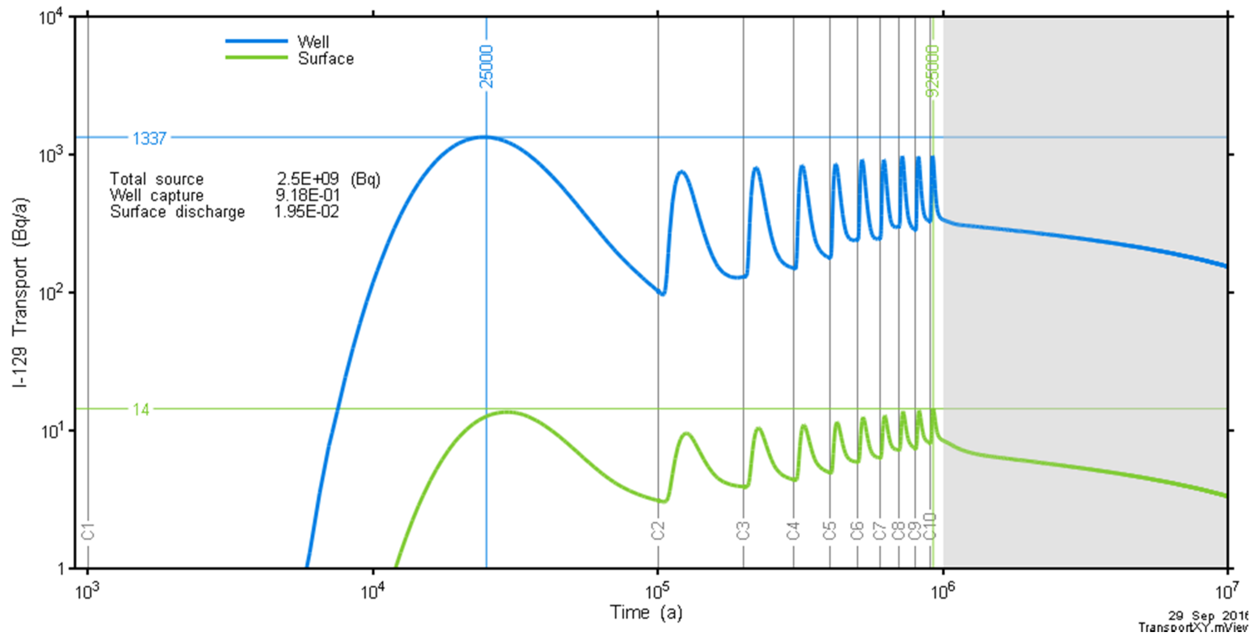

Figure 7-76: Full Repository-Scale Model: I-129 Transport for the Main Fracture Zone

Figure 7-77 through Figure 7-82 illustrate the time dependent behaviour of the I-129 plume on a plan view at the repository elevation and on a vertical slice through the placement room containing the defective containers. The contour plots are on a logarithmic scale. The outer concentration contour, 1 Bq/m^3, corresponds to an effective I-129 drinking water dose of about 0.1 µ /a based on a water consumption of 0.77 m^3/a per person.

After 7500 years (Figure 7-77), the plume encounters the fracture connected to the well. In this context, “encounter” means the radionuclide concentration at the fracture location reaches 1 Bq/m^3. I-129 is thereafter transported along the fracture with maximum extents peaking at 25 ka (Figure 7-78). Subsequently, the reduction in source term causes the concentrations to decrease, although the lower concentration outer edges of the plume, located within the intact rock continue to expand (Figure 7-79). Minimum concentrations are reached at 100 ka (Figure 7-80), just before the time of second container failure. Concentrations peak again at 120 ka (Figure 7-81), when the release from the second container failure reaches the well. This process continues until the final container failure at 900 ka, with near steady-state conditions continuing from 1 Ma (Figure 7-82) until the end of the simulation at 10 Ma.

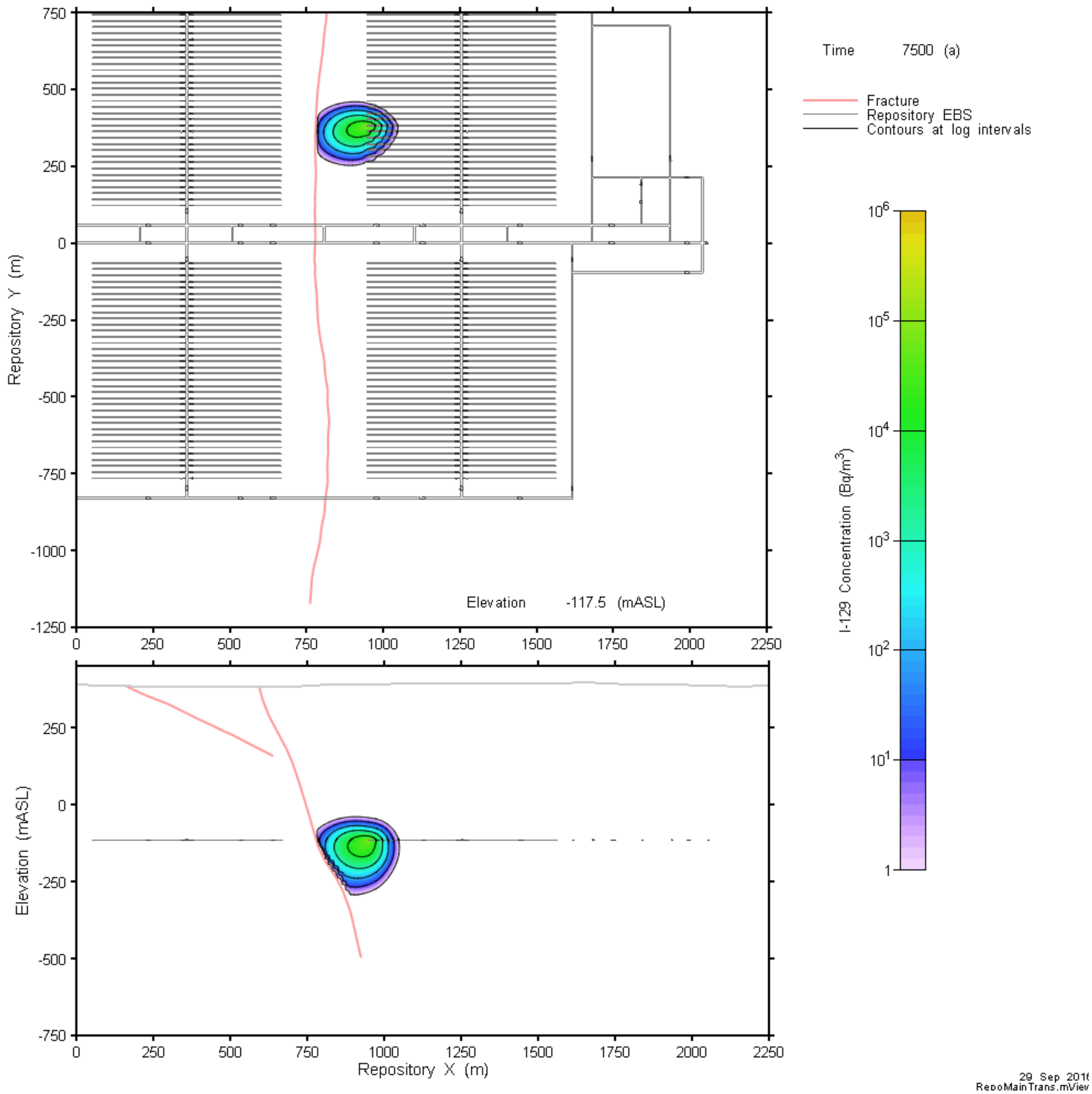

Figure 7-77: Full Repository-Scale Model: Base Case I-129 Concentration at 7,500 Years

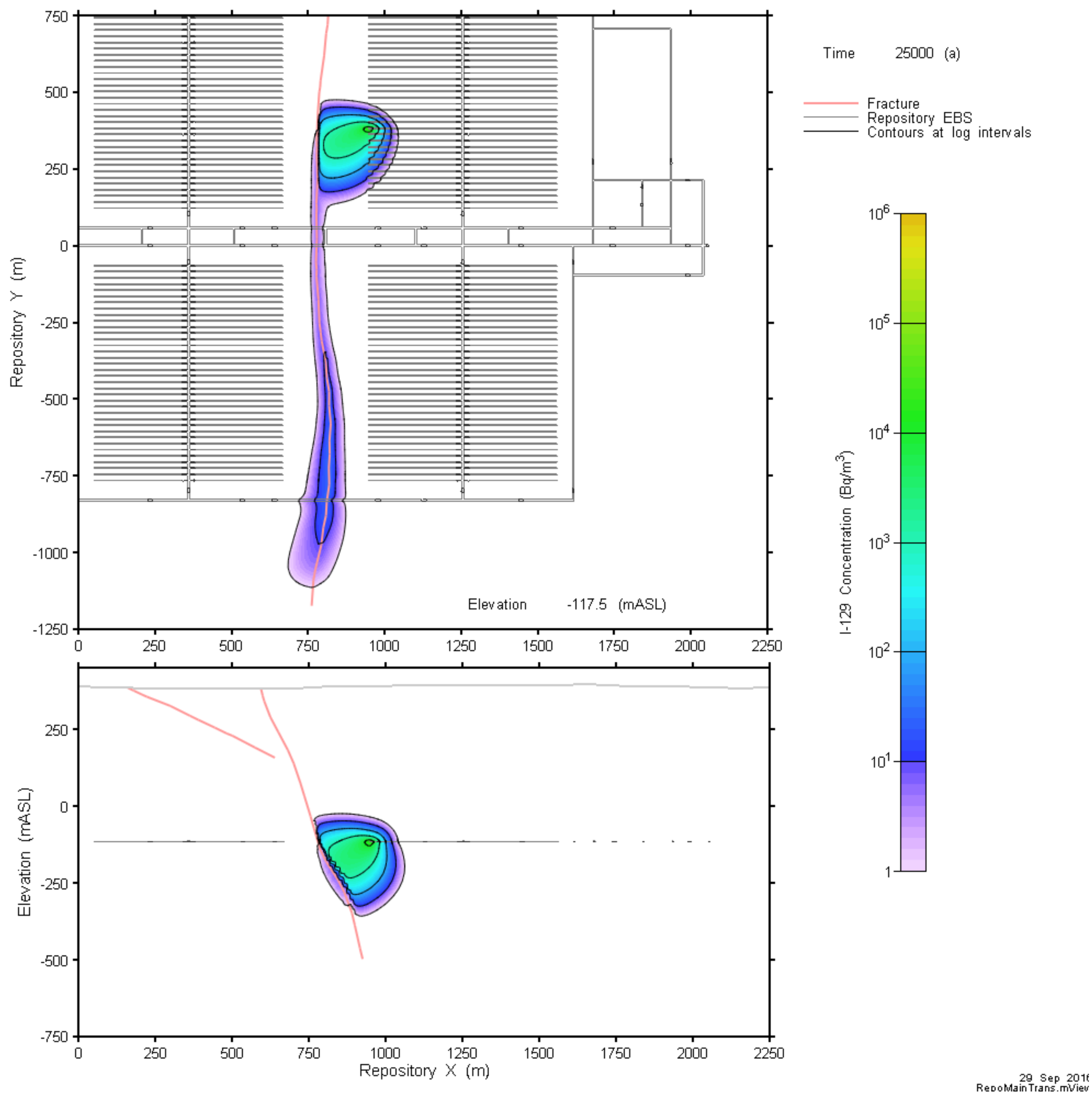

Figure 7-78: Full Repository-Scale Model: Base Case I-129 Concentration at 25 k Years

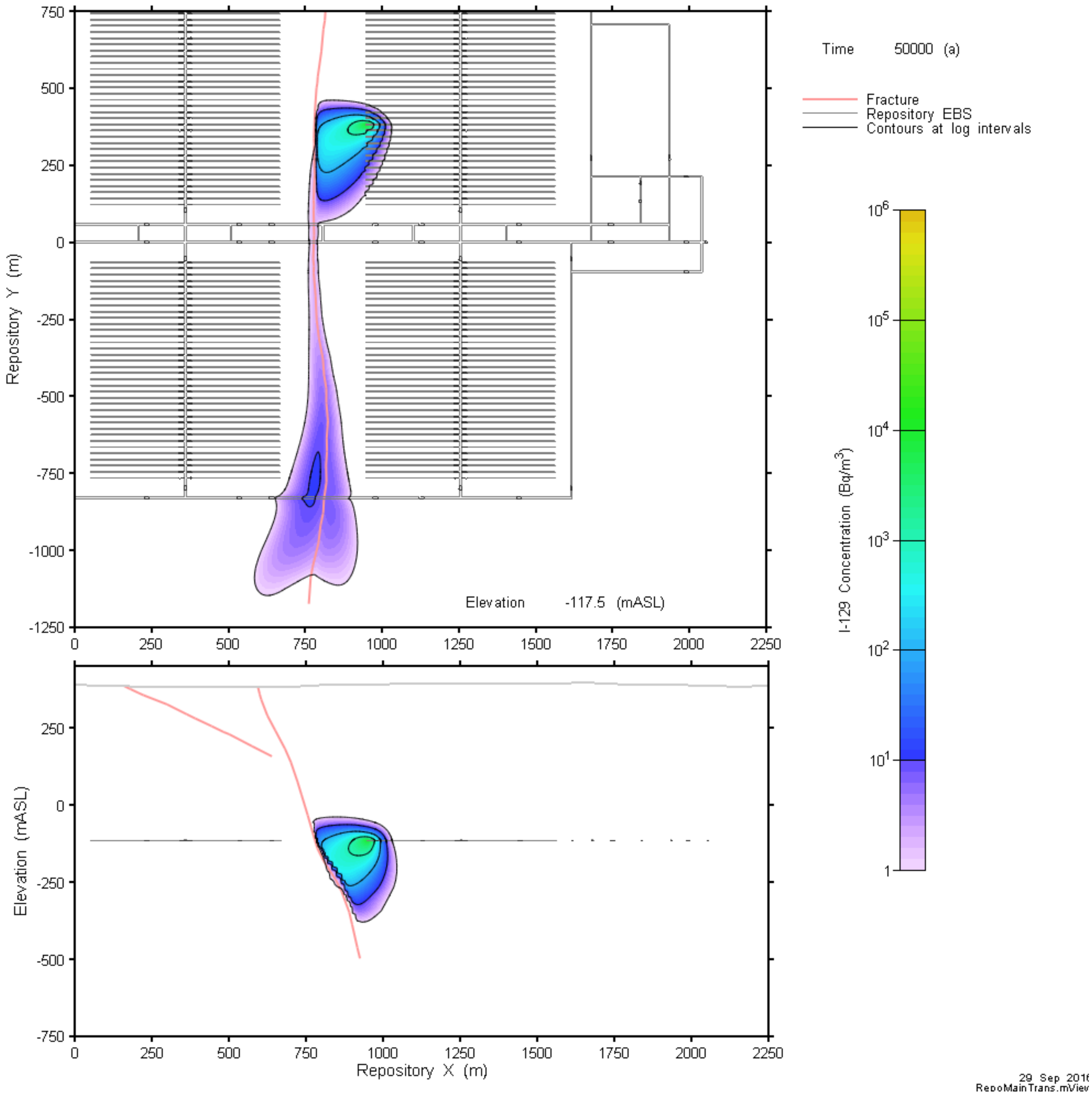

Figure 7-79: Full Repository-Scale Model: Base Case I-129 Concentration at 50 k Years

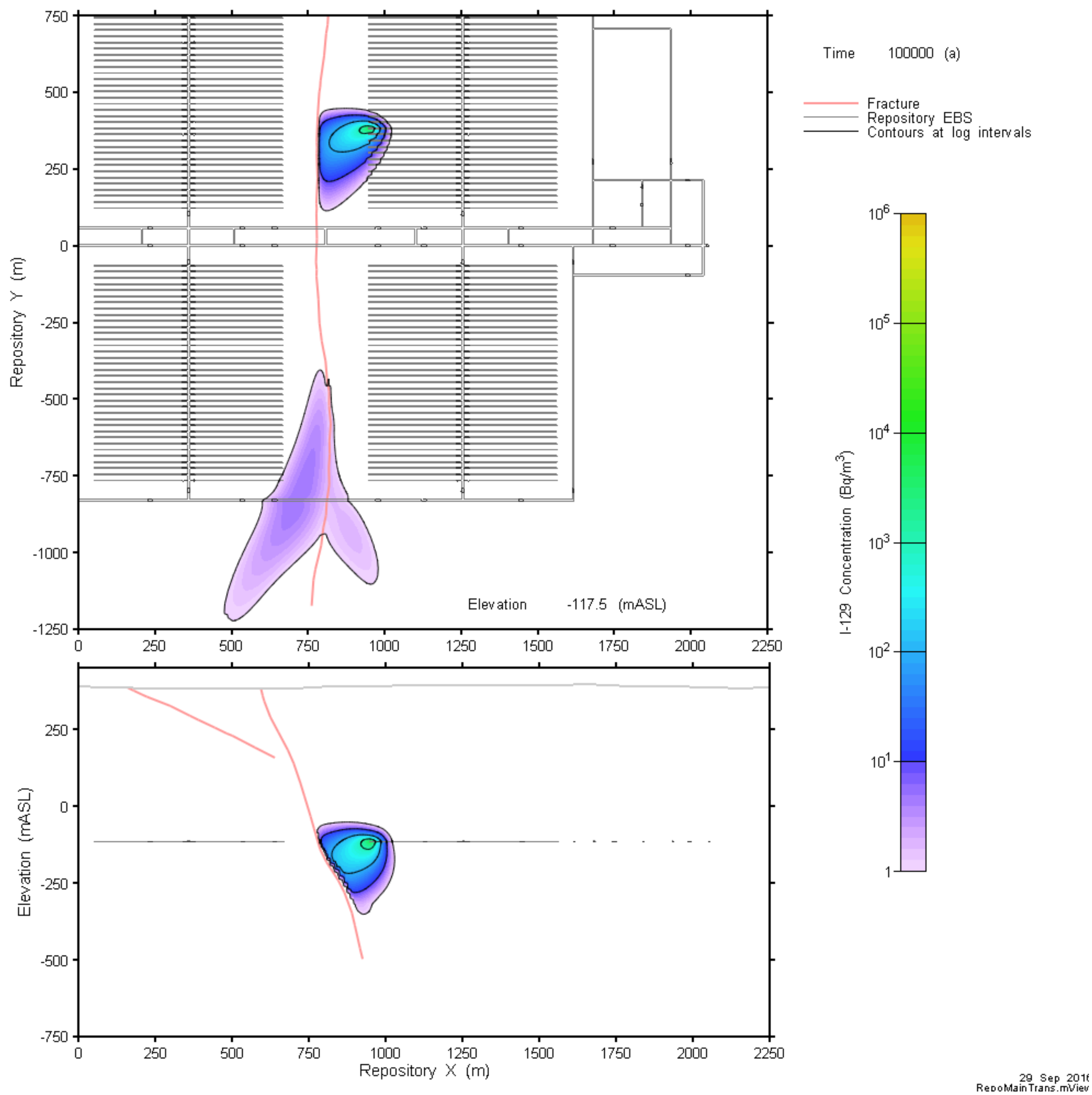

Figure 7-80: Full Repository-Scale Model: Base Case I-129 Concentration at 100 k Years

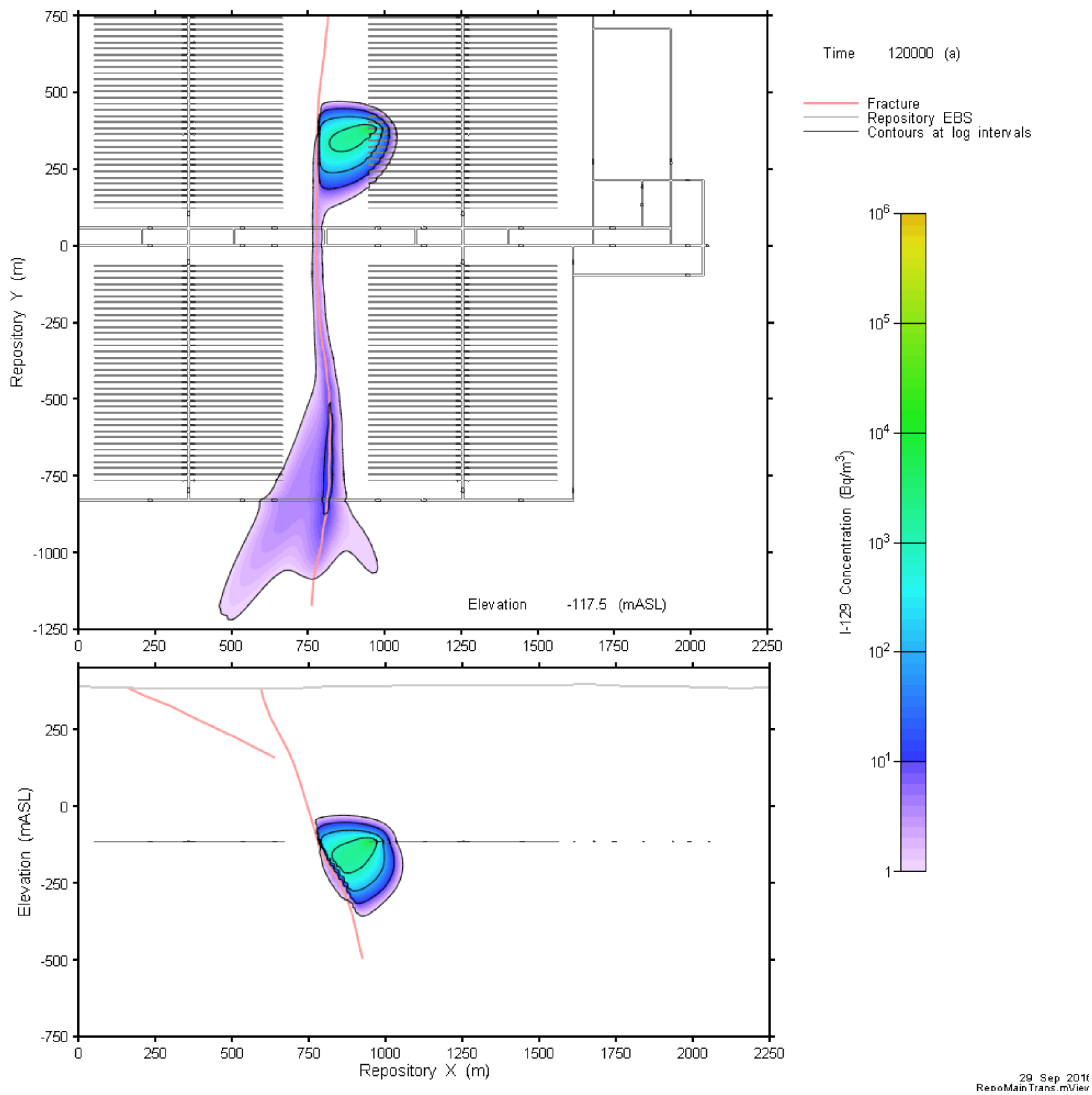

Figure 7-81: Full Repository-Scale Model: Base Case I-129 Concentration at 120,000 Years

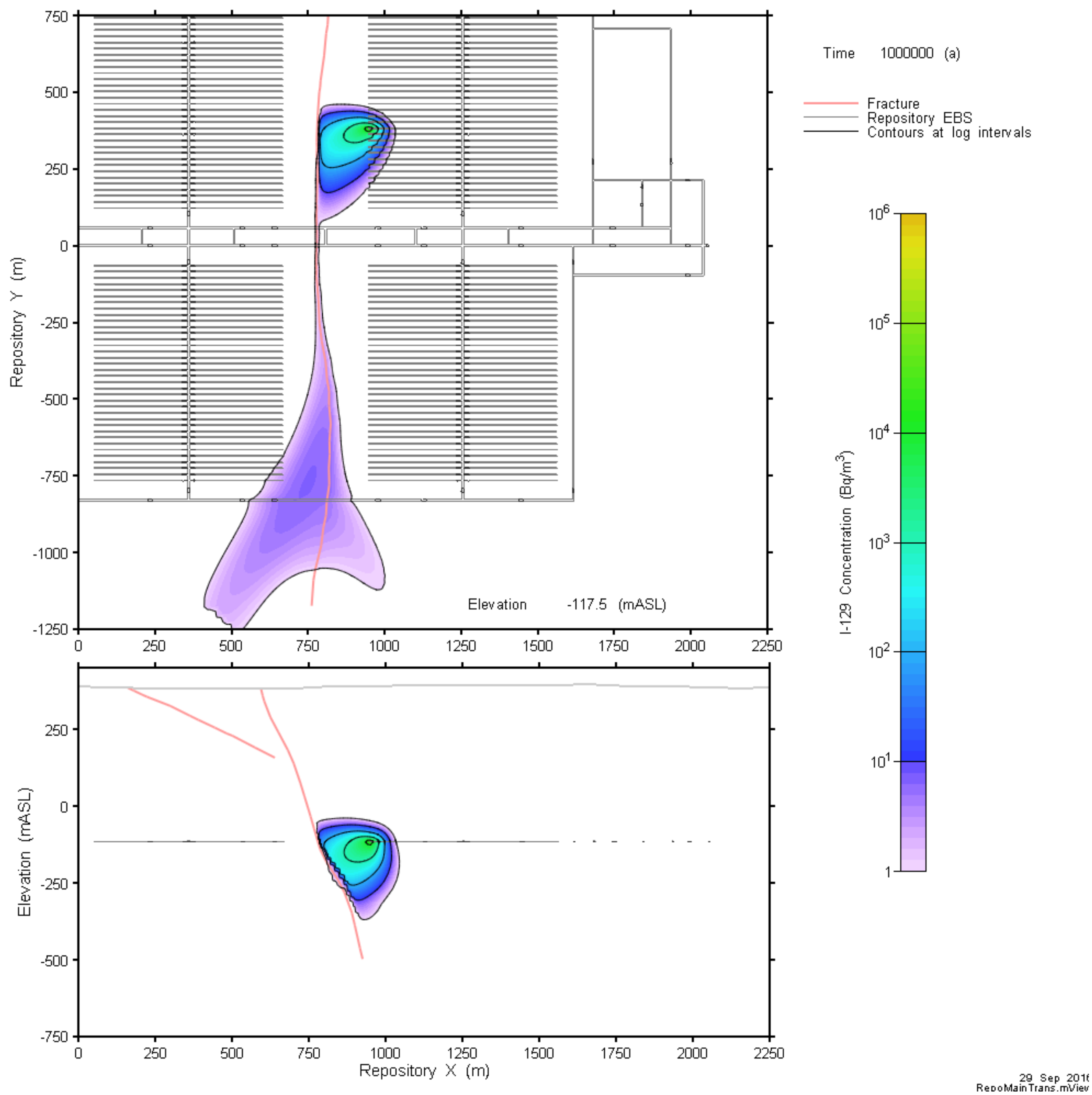

Figure 7-82: Full Repository-Scale Model: Base Case I-129 Concentration at One Million Years

Figure 7-83 and Figure 7-84 illustrate the spatial complexity of the transport processes at the time of peak and initial minimum (i.e., prior to failure of the second container) well transport. Each figure shows two isovolumes, with one corresponding to I-129 concentrations of 1 Bq/m^3

and greater and another to I-129 concentrations of 100 Bq/m^3 and greater. The 100 Bq/m^3 isovolume is largely restricted to the intact rock surrounding the defective container location.

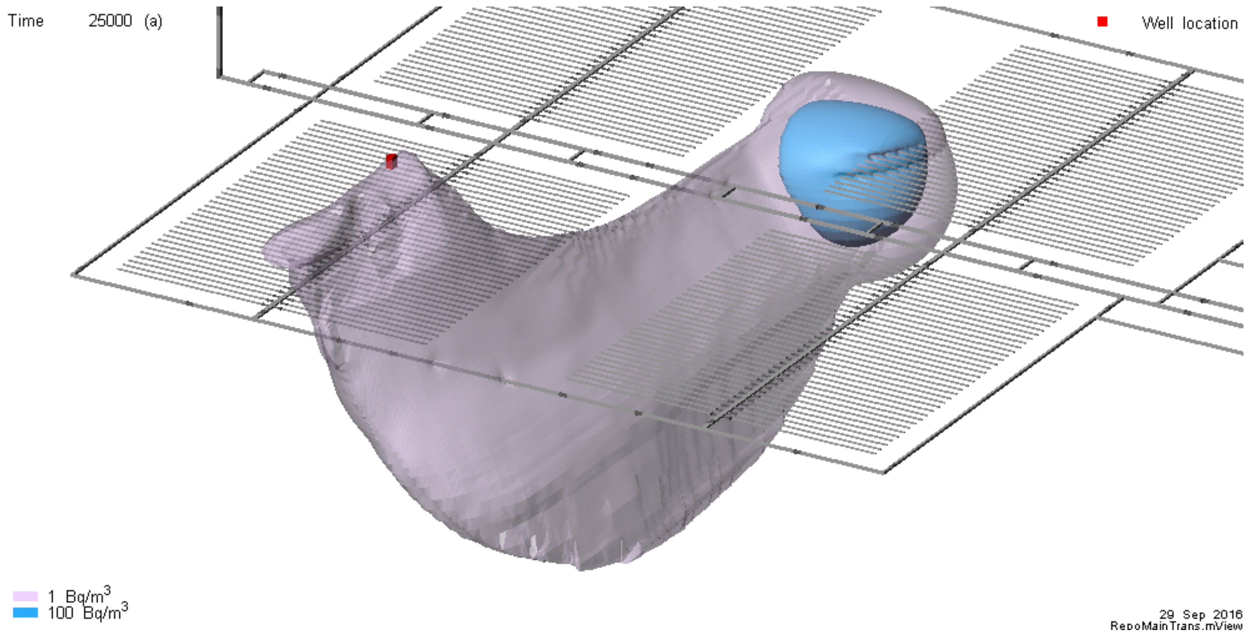

Figure 7-83: Full Repository-Scale Model: Base Case I-129 Concentration in 3D at Time of Peak Well Transport (25 ka)

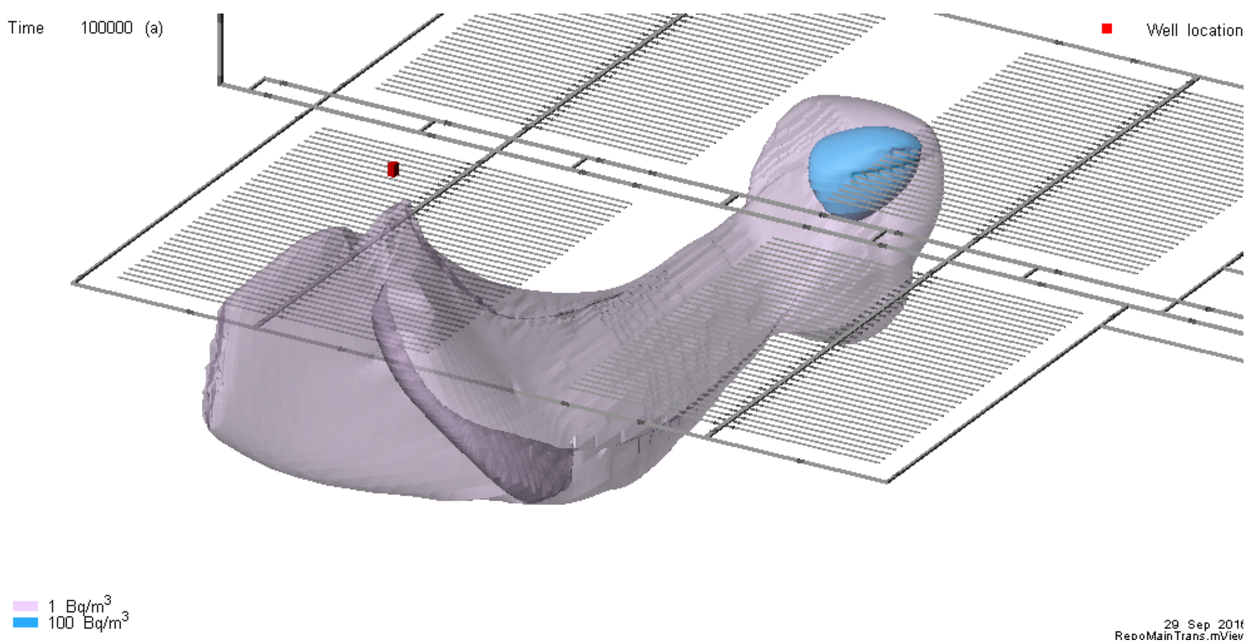

Figure 7-84: Full Repository-Scale Model: Base Case I-129 Concentration in 3D at Time of Initial Minimum Well Transport (100 ka)

Peak I-129 transport to the ground surface occurs at approximately 925 ka and is shown in Figure 7-85. At all times, groundwater discharge concentrations at the surface are below the 1 Bq/m^3 minimum concentration used in the subsurface spatial concentration figures. Surface discharge above 10^{-3} Bq/m^3 is limited to the Central Wetland Zone with a minor amount discharging in the West River Zone. There is no other direct discharge to surface water.

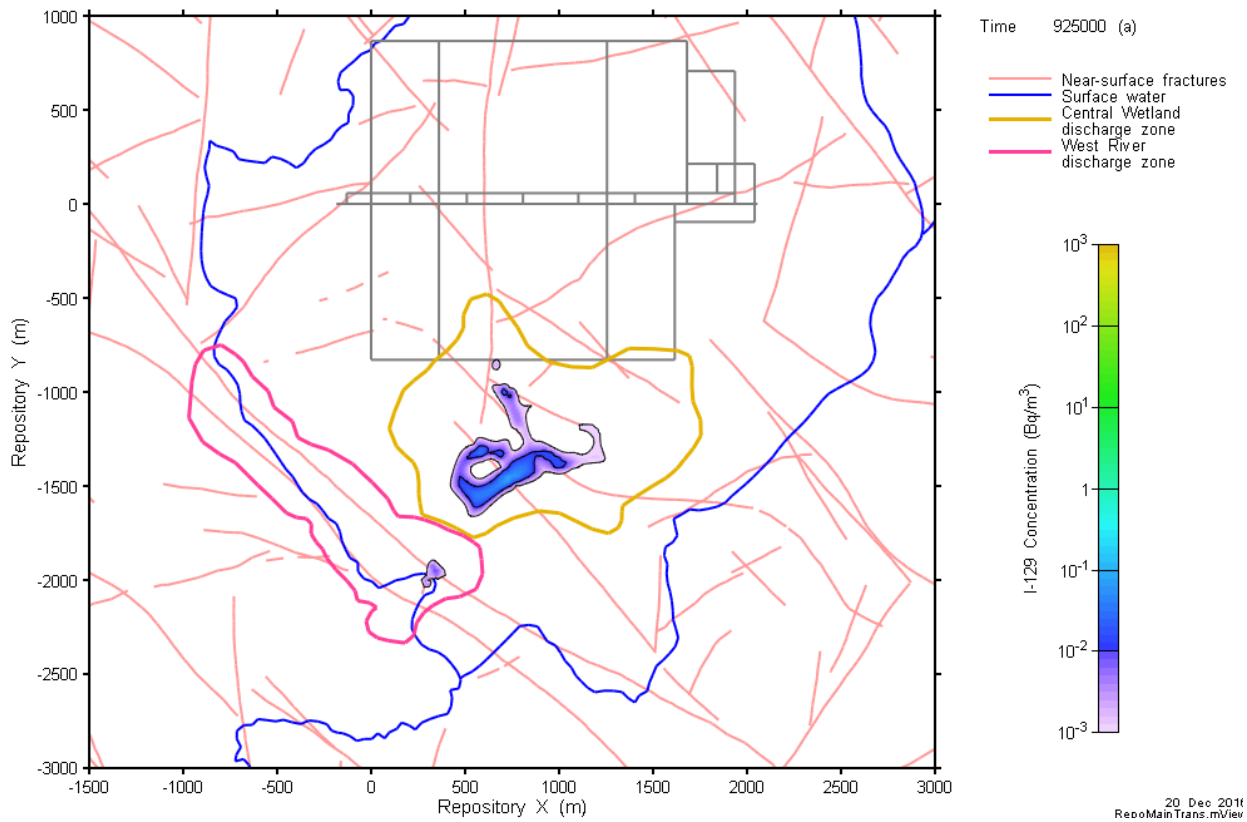

Figure 7-85: Full Repository-Scale Model: Base Case Surface Discharge Concentration at Time of Peak I-129 Transport (925 ka)

Figure 7-86 presents radionuclide transport rates to the well for all simulated nuclides. U-238 is not shown because it does not reach the well due to retention in the engineered barrier system and geosphere near the repository.

The time of peak transport for I-129 and Cl-36 are similar because neither element has any appreciable sorption. Peaks for other nuclides are delayed due to decay and / or sorption in the geosphere or EBS.

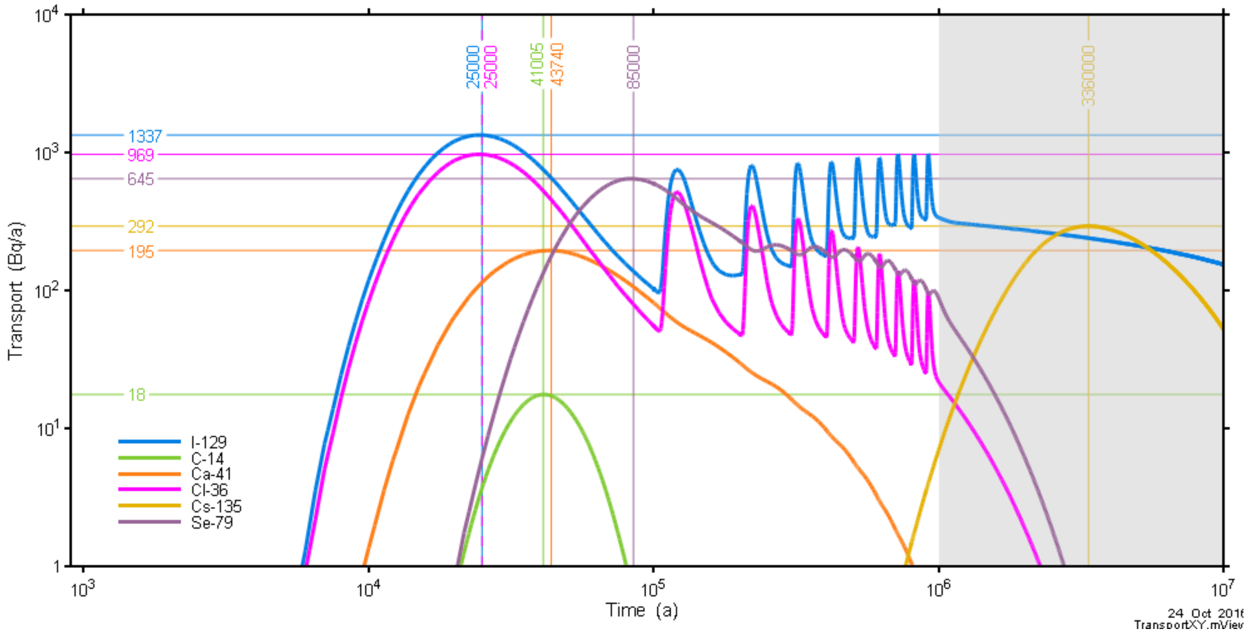

Figure 7-86: Full Repository-Scale Model: Base Case Transport to the Well for all Radionuclides

7.7.2.3.4 Well Assumption Sensitivity Cases

Section 7.8.2.1 shows that the dose consequence for the Base Case is almost entirely due to I-129, with the I-129 dose almost entirely due to the use of well water. In the SYVAC3-CC4 System Model, well water is used for drinking, irrigation of food crops and for watering animals.

Section 7.7.2.3.2 describes the method used to ensure the combination of well and defective container locations is bounding, such that the selected combination is the one that results in the highest possible dose consequence.

As noted earlier in Section 7.2.2.1, the adoption of bounding assumptions (such as the well and defective container location) in safety assessment studies allows for complex problems to be reduced to much simpler ones, but the downside is that this can make repository performance appear to be worse than it really is. To investigate the effect of well assumption on the Base Case, Section 7.2.2.2 defines the following three sensitivity cases:

- No well;
- Intermittent well operation; and
- Random well location.

The latter two sensitivity cases are described below. The No Well case is modelled with the SYVAC3-CC4 System Model and described in Section 7.8.2.2.

Intermittent Well Operation

The Base Case assumes the well is pumping continuously at a rate of 911 m^3/s. This sensitivity study assumes the well and defective containers are present in their bounding Base Case locations, and examines the effect of intermittent well operation.

During periods of non-operation, the transport plume will migrate towards surface discharge locations. When well operation starts, there could be a greater mass of contaminant within the well capture zone than would otherwise be present under conditions of continuous well operation. After some time, the excess would be eliminated through well uptake and the transport processes would re-equilibrate.

The sensitivity case assumes a well operation schedule that has the well ‘on’ for 5000 year periods at times corresponding to peak transport and at times corresponding to near minimum transport after each container failure in the Base Case. A total of 20 periods are considered, resulting in 100 ka of well operation over a 1 Ma time period. Figure 7-87 shows the periods of intermittent well operation in comparison to Base Case I-129 transport.

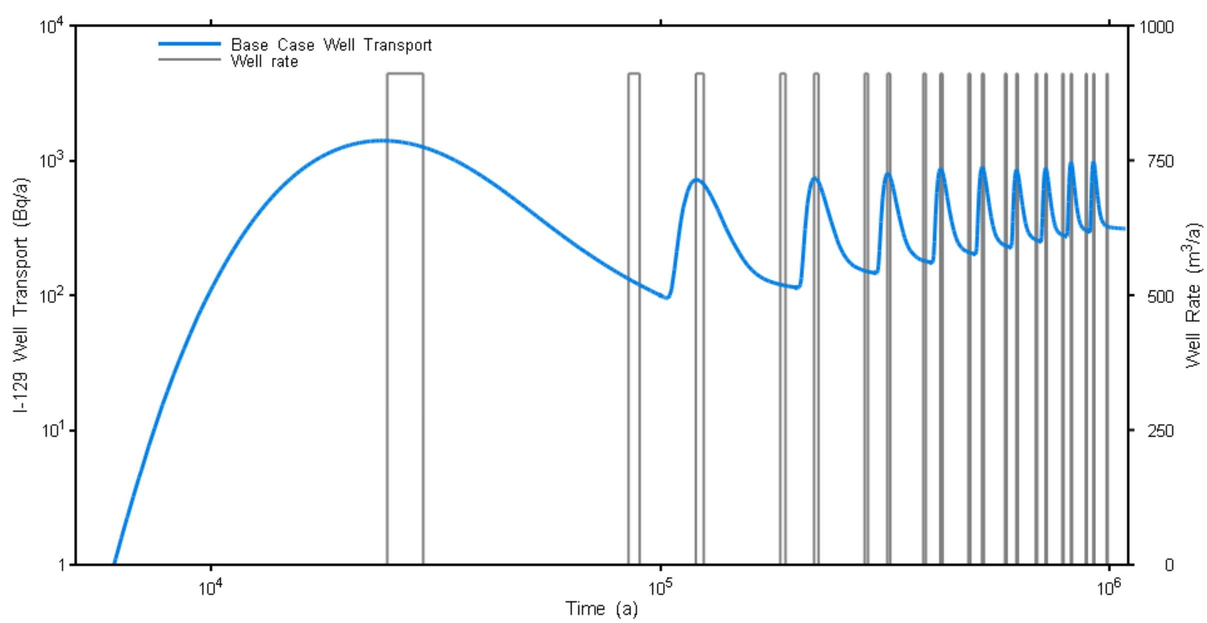

Figure 7-87: Rooms-Only Repository-Scale Model: Intermittent Well Sensitivity - Schedule

Since this case involves transient groundwater flow, analyses are conducted with the Rooms-Only Repository-Scale Model using the Combined Source Term. The flow simulation is transient, with specific storage for all materials set to $1x10^{-7}$ m^{-1}.

Figure 7-88 shows the results. There is a transient increase in peak transport for a short period of time after the well first starts. Increases after subsequent restarts are of similar magnitudes. If the intermittent well is turned on within a fairly short time window encompassing the time of peak I-129 transport, peak transport could increase from 1400 Bq/a to 2492 Bq/a. If the well is off during this time, the dose rate will be much lower as shown in the System Model results discussed in Section 7.7.2.3.4 for the No Well case. Also, if the well is turned on at any time outside this window, the peak transport will likely be less than the 1400 Bq/a peak that arises if the well is assumed to run continuously, and will certainly be less than the 2492 Bq/a value associated with the first container.

Figure 7-88 also compares surface discharge rates. The intermittent case surface discharge is high prior to well operation. After 5000 years of operation, surface discharge is reduced to that of the Base Case as the well interception of the plume is maximized.

Figure 7-89 presents a detailed view of the response to the first well operation. Surface discharge from a Base Case with No Well simulation is also shown for comparison. Note that the figure has a linear Y axis, to better illustrate the processes.

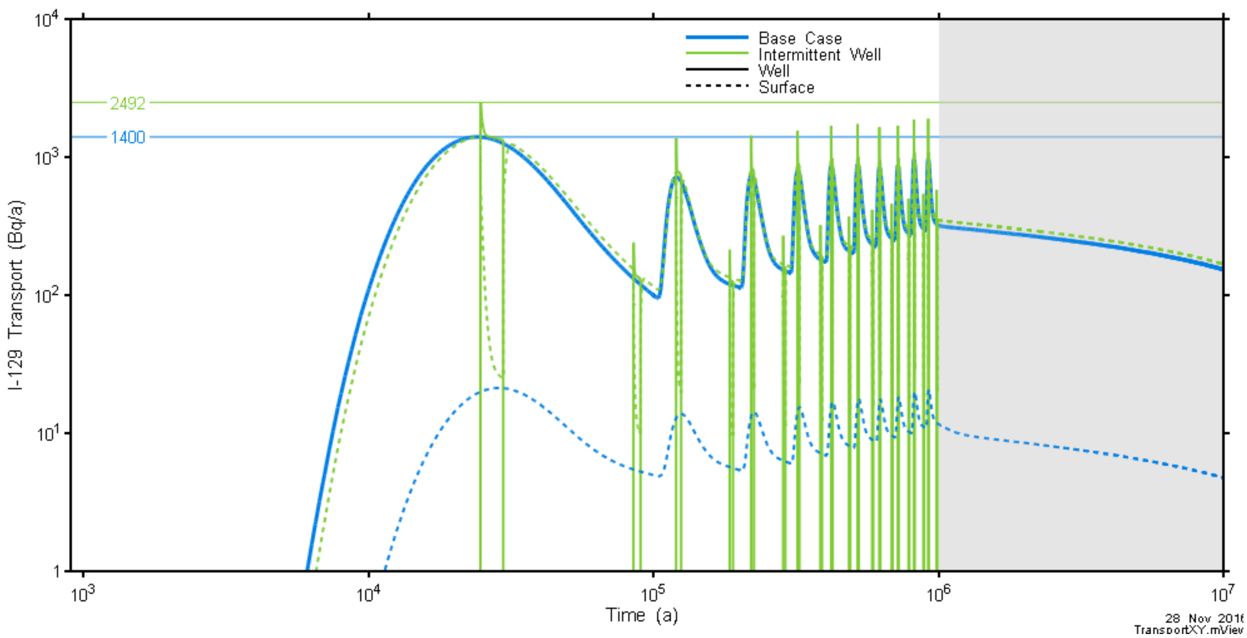

Figure 7-88: Rooms-Only Repository-Scale Model: Intermittent Well Sensitivity – I-129 Comparison to Base Case

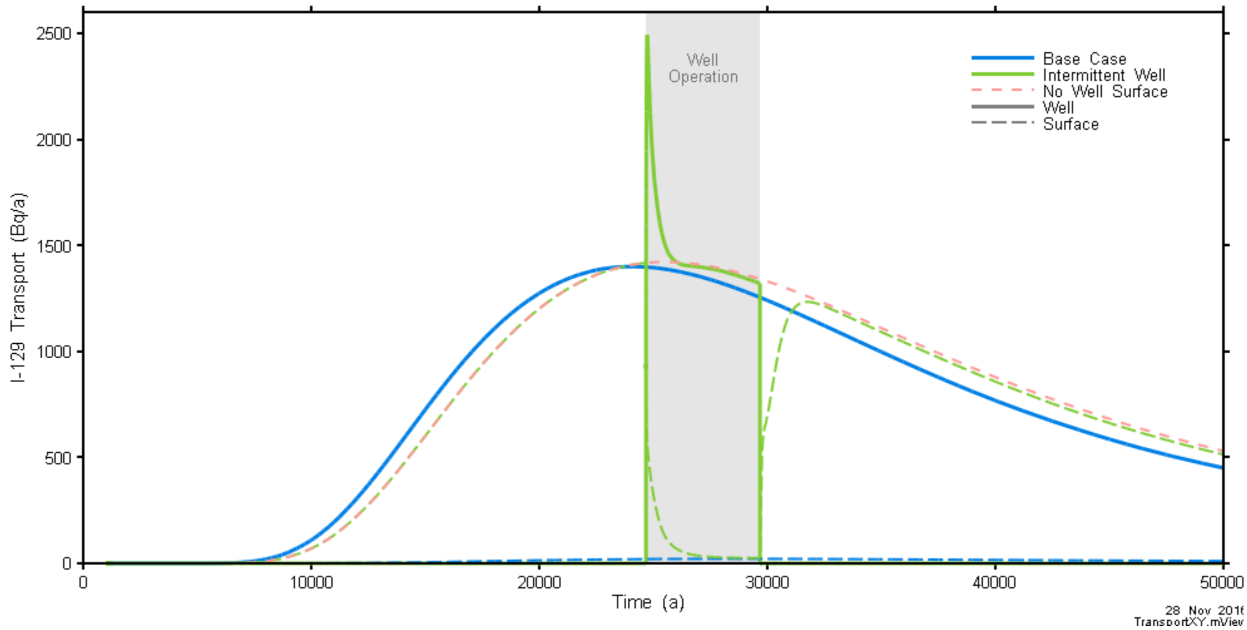

Figure 7-89: Rooms-Only Repository-Scale Model: Intermittent Well Sensitivity – Detail of I-129 Well Transport

<u>Random Well Locations</u>

There are millions of combinations of potential well and defective container locations and it is not practical to test them all. Instead, this sensitivity case uses results generated with the detailed 3D models in Section 7.7.2.3.2 (i.e., for determining the position of the well) to illustrate the effect of well location on dose consequence.

Figure 7-66 shows 106 different well locations that have been tested during the search for the combination of well and defective container locations that result in the highest dose consequence for the Base Case. Each of these locations is used in a simulation in which a tracer source term is released from every container location in the repository. These simulations are similar to All Containers Fail simulations but with a different source term and a different container failure time.

Figure 7-67 shows transport of the tracer to each of the 106 well locations. The blue dots note the point of peak transport in each simulation. Figure 7-68 presents a histogram of the peak transport values.

These results illustrate that there can be many orders of magnitude difference between the maximum and minimum peak values, depending on where the well is located. Large variations would also be expected if the location and number defective containers is also varied. For example, if the well and defective containers are located such that there is no contaminant uptake to the well, the Base Case dose consequence to the small farming family assumed to be unknowingly living on top of the repository would then be similar to that reported in

Section 7.8.2.2 for the No Well sensitivity case (i.e., less than 10^{-6} mSv/a, and over 2 million times less than the average Canadian background dose rate of 1.8 mSv/a).

7.7.2.3.5 Buffer, Backfill and Seals Barrier Sensitivity Cases

This section presents the subset of sensitivity cases identified in Section 7.7.2 that affect the buffer, backfill and seals barrier. One case is considered, in which the hydraulic conductivity of the EBS materials is increased.

Increase in EBS Hydraulic Conductivity

The EBS barrier materials hydraulic conductivities (at 20ºC) are defined for the Base Case (Table 7-5) as:

- $6x10^{-14}$ m/s for HCB
- $4x10^{-13}$ m/s for Gap Fill
- $1x10^{-13}$ m/s for the weighted average of Gap Fill and HCB
- $9x10^{-11}$ m/s for dense backfill
- $1x10^{-10}$ m/s for concrete
- $5x10^{-13}$ m/s for Bentonite/Sand shaft seal
- $1x10^{-12}$ m/s for Asphalt shaft seal

Placement room HCB and Gap Fill are not used as separate materials within any of the transport models. Instead the temperature corrected homogenized, or weighted average, values are used for all placement room homogenized buffer (HBF). With temperature correction to an assumed 85 ºC, the hydraulic conductivity of the HBF is $3.1x10^{-13}$ m/s.

In this sensitivity case, the hydraulic conductivities of all EBS materials are increased by a factor of 10. The simulation is performed using the Full Repository-Scale Model.

Figure 7-90 presents the results for I-129 transport to the well. Comparison with the Base Case shows virtually no difference (an increase from 1337 Bq/a to 1374 Bq/a), confirming the relative unimportance of transport through the EBS for non-sorbing species. This is not unexpected, as even with a factor of 10 increase, the temperature corrected weighted average backfill hydraulic conductivity (Base Case $3.1x10^{-13}$ m/s, High EBS case $3.1x10^{-12}$ m/s, both values at 85ºC) is much lower than the Inner EDZ hydraulic conductivity (Base Case $4.x10^{-9}$ m/s) and therefore does not substantially impact the overall velocity field.

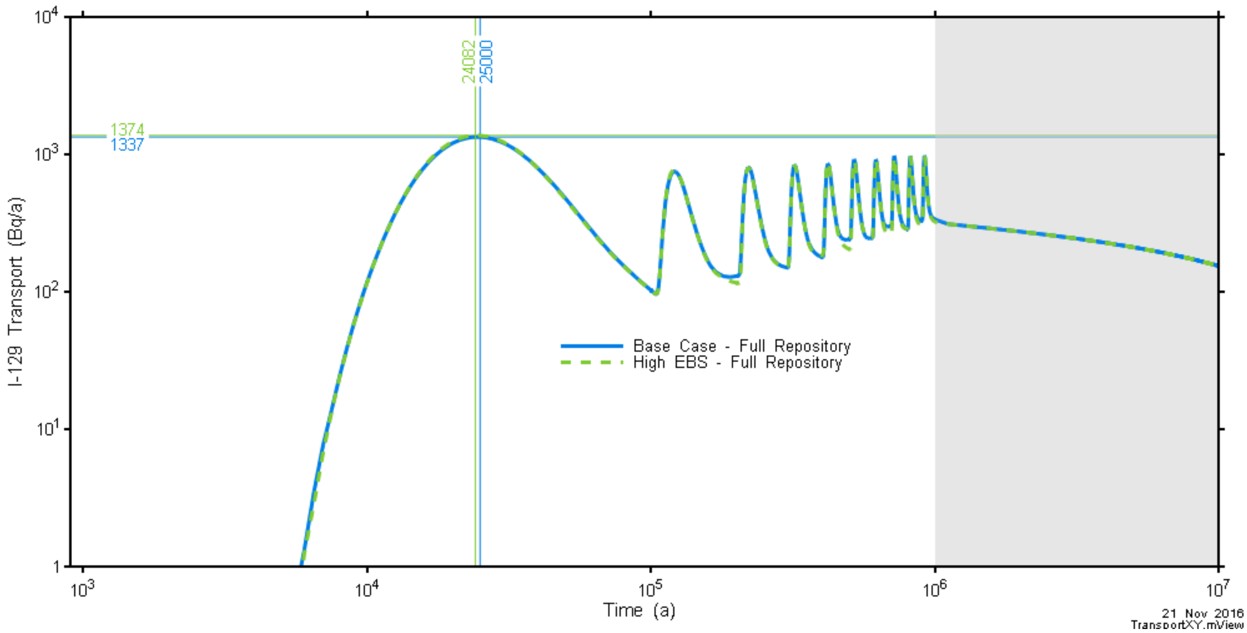

Figure 7-90: Full Repository-Scale Model: EBS Hydraulic Conductivity Sensitivity - I-129 Transport to the Well

7.7.2.3.6 Geosphere Barrier Sensitivity Cases

This section presents the subset of sensitivity cases identified in Section 7.7.2 that affect the geosphere barrier. The cases are:

- Hydraulic conductivities of the host rock increased by a factor of 10;
- Hydraulic conductivities of the host rock decreased by a factor of 10;
- Hydraulic conductivity in the excavation damaged zones (EDZ) increased by a factor of 10;
- Fracture standoff distance reduced to 50, 25 and 10 m; and
- Dispersivity increased and decreased by a factor of 5.

<u>Geosphere Hydraulic Conductivity</u>

Sensitivity 1

This corresponds to the Sensitivity Case 1 profile defined in Chapter 2, with host rock hydraulic conductivities set to 10 times greater those in the Base Case. Specifically:

- Zone 1 (10 – 150 m) is changed from $2x10^{-9}$ to $2x10^{-8}$
- Zone 2 (150 – 700 m) is changed from $4x10^{-11}$ to $4x10^{-10}$
- Zone 3 (700 – 1500 m) is changed from $1x10^{-11}$ to $1x10^{-10}$

Sensitivity 2

This corresponds to the Sensitivity Case 2 profile defined in Chapter 2, with host rock hydraulic conductivities set to 0.1 times those in the Base Case. Specifically:

- Zone 1 (10 – 150 m) is changed from $2x10^{-9}$ to $2x10^{-10}$
- Zone 2 (150 – 700 m) is changed from $4x10^{-11}$ to $4x10^{-12}$
- Zone 3 (700 – 1500 m) is changed from $1x10^{-11}$ to $1x10^{-12}$

Figure 7-91 shows results for I-129 transport as determined using the Rooms-Only Repository-Scale Model with the Combined Source Term. Peak transport to the well is reduced to 725 Bq/a occurring at 4700 years for Sensitivity 1, and to 460 Bq/a occurring at 1.02 Ma for Sensitivity 2. For comparison, Base Case peak transport to the well is 1400 Bq/a occurring at 24,200 years (Figure 7-74).

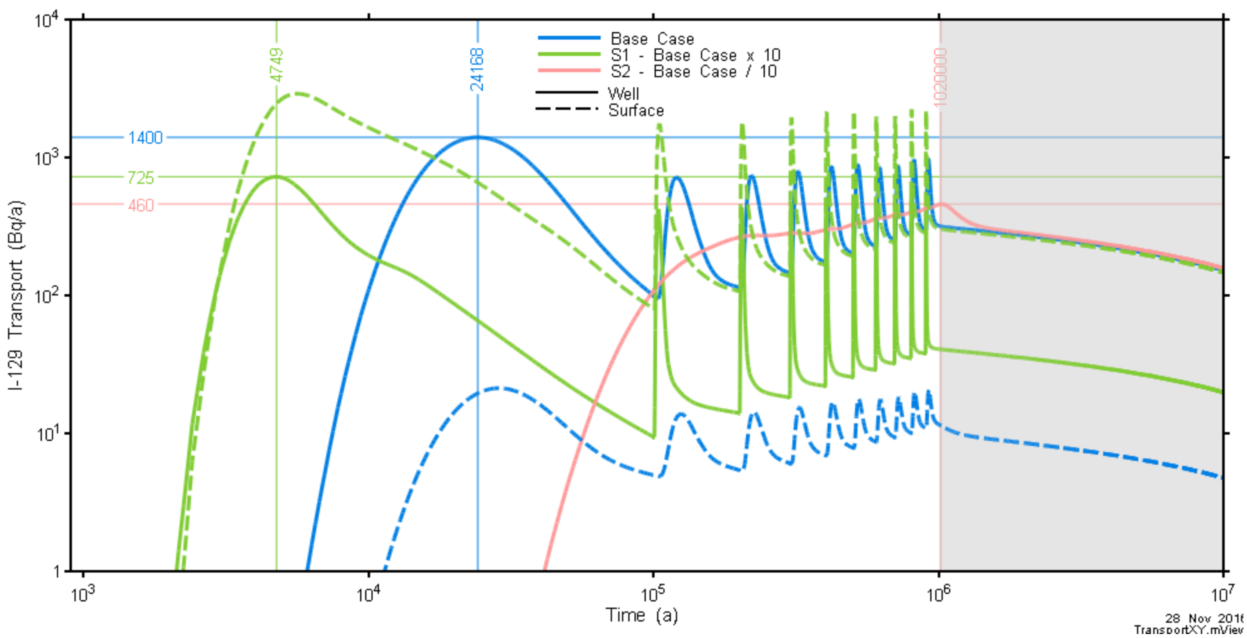

Figure 7-91: Rooms-Only Repository-Scale Model: I-129 Transport for Geosphere Hydraulic Conductivity Sensitivity Cases

Base Case and Sensitivity Case 1 results are advectively dominated with shifts between peak transport times consistent with the changes in hydraulic conductivity. The time shifts are not entirely linear, as the portion of transit time through the fracture remains similar for both cases whereas transport time from the source through the intact rock to the fracture is approximately a factor of ten different. Surface discharge is significantly increased, exceeding transport to the well by a factor of four.

The well capture fraction for the increased hydraulic conductivity case is reduced because of the reduced radius of influence of the well and because of a greater dispersion of the plume. The higher permeability shallow bedrock is able to supply the required well demand with a lower drawdown in the well (7.8 m) compared to the Base Case (15.3 m). A correspondingly smaller volume of geosphere where the well gradient dominates is therefore present. In particular, the well applies a lower hydraulic gradient to the main fracture over which most transport occurs. Consequently, gradients induced by surface topography are relatively more important with the result that a greater percentage of the transport discharges to surface.

The peak transport for the Sensitivity Case 2 occurs after the assumed time of final container failure. The lengthier transport times allow for more dispersion and diffusion of the instant release portion of the source term so the individual transport peaks associated with each container failure are not apparent. Surface discharge is off-scale low.

C-14 transport to the well is also affected by the geosphere hydraulic conductivity. As shown in Figure 7-92, while I-129 transport is decreased in the Sensitivity Case 1 due to the lower well capture fraction, C-14 transport is increased due to reduced decay occurring over the shorter transport time. Peak C-14 transport to the well is 1408 Bq/a occurring at 11,400 years compared to the Base Case value of 18 Bq/a occurring at 40,700 years (Figure 7-74).

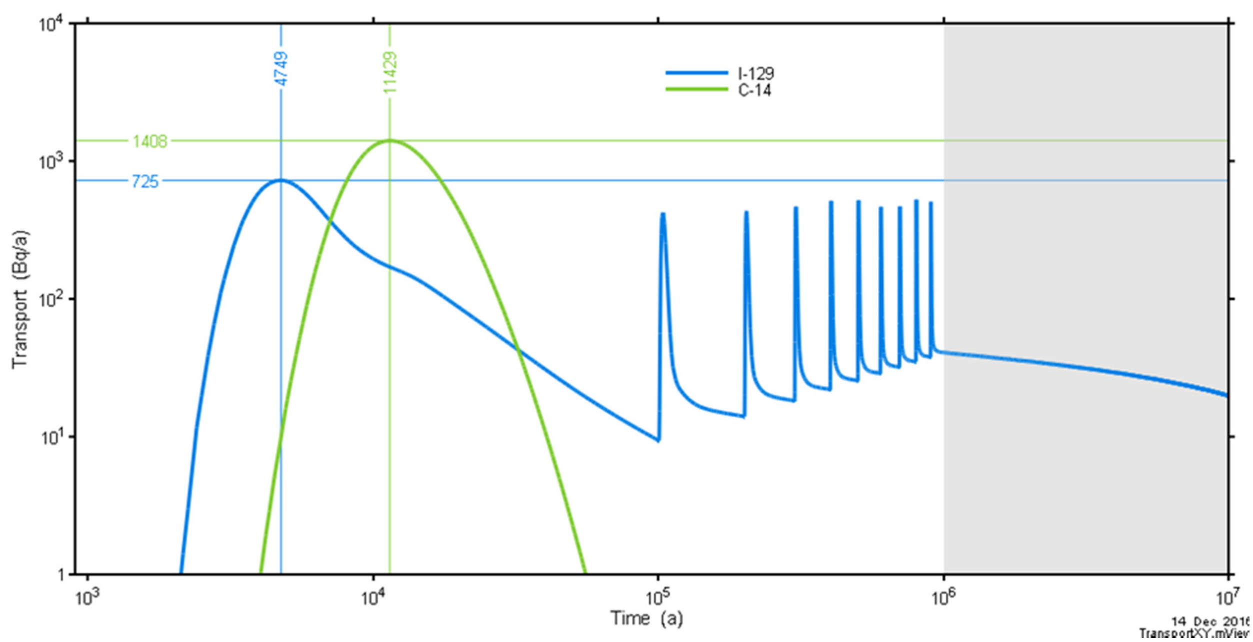

Figure 7-92: Rooms-Only Repository-Scale Model: Base Case Geosphere Hydraulic Conductivity x 10 - I-129 and C-14 Transport to the Well

Because these results show the well capture fracture is dependent upon the geosphere hydraulic conductivity, it is possible that the well / defective container location used in the Base Case may not be the maximum consequence location for other values of hydraulic conductivity. Therefore, additional work was undertaken to reposition the well / defective containers for Sensitivity Case 1 (i.e., with hydraulic conductivity values set to 10 times those of the Base Case).

The process described in Section 7.7.2.3.2 for determining the maximum consequence well / defective container locations was repeated. A total of 785 potential location combinations were tested.

Figure 7-93 shows the maximum consequence location pairs for each of the four potential high consequence zones. The figure also shows the locations adopted in the Base Case for comparison. The results show that although general source and location characteristics are similar, slight changes in source and well locations are apparent for all except the SW source location, which remains at the end of the first placement room. The actual maximum consequence location pair remains associated with the Main Fracture zone.

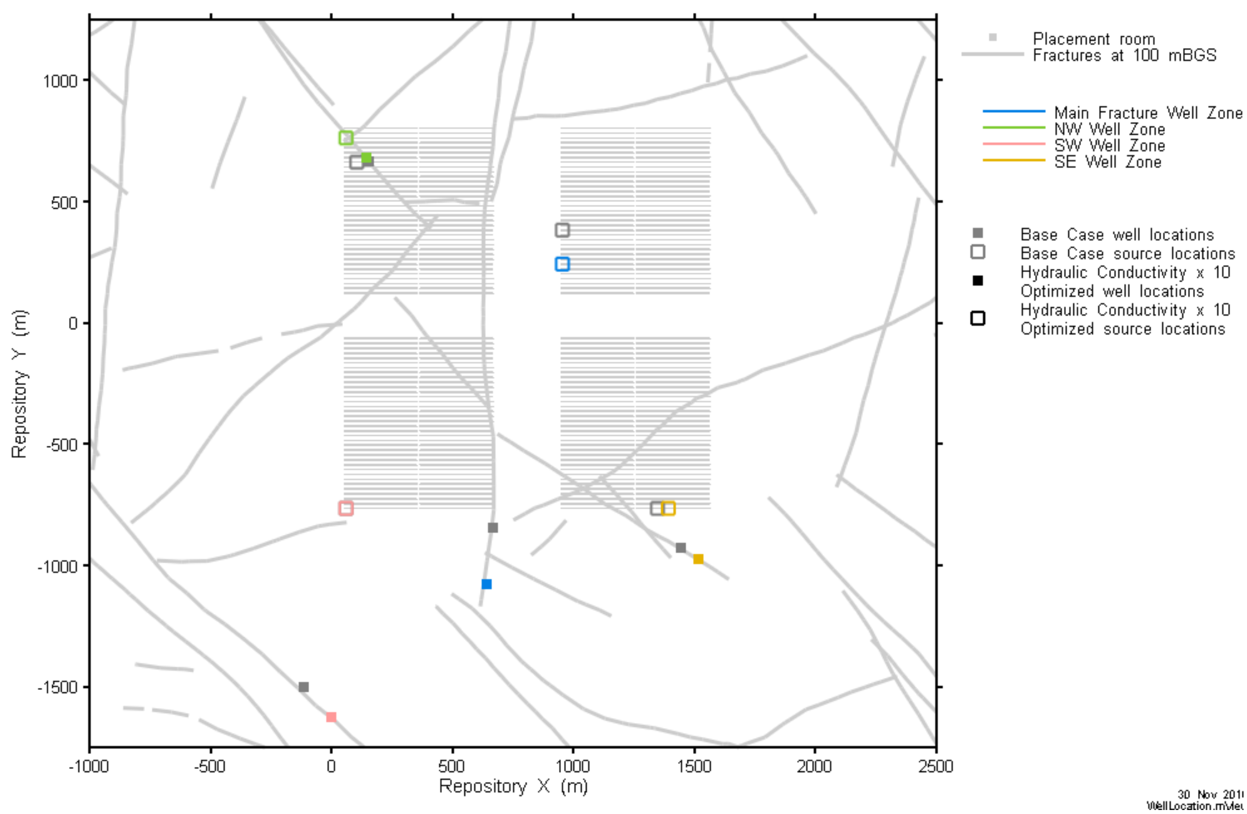

Figure 7-93: Rooms-Only Repository-Scale Model: Base Case Geosphere Hydraulic Conductivity x 10 – Updated Well and Defective Container Locations

Figure 7-94 and Figure 7-95 show results for I-129 and C-14 transport to the well for the revised maximum consequence locations. Also shown for comparison are the transport results for the Base Case and Sensitivity 1 case with the well and defective container locations maintained in their Base Case positions.

The results show peak I-129 transport to the well increases by a factor of about 2.6 as compared to the Base Case (from 1400 Bq/a to 3679 Bq/a), with the time of peak transport decreasing to 5000 years from 24,200 years. For C-14, peak transport to the well increases from 18 Bq/a in the Base Case to 6610 Bq/a, with the time of the peak transport decreasing to 12,100 years from 41,700 years.

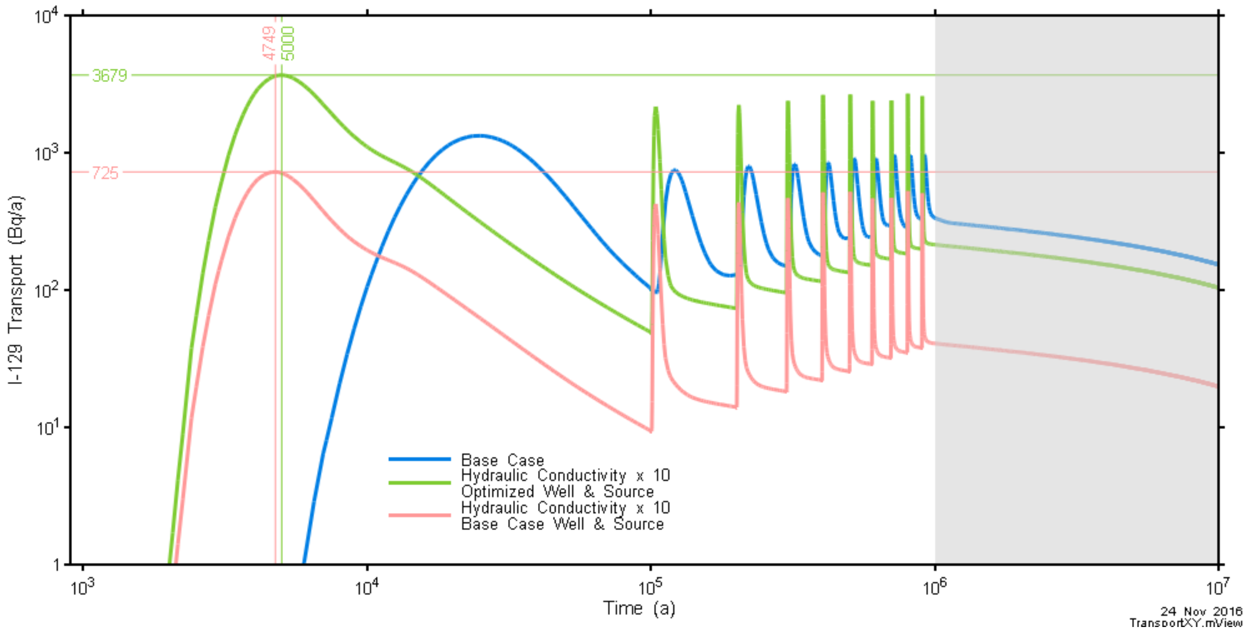

Figure 7-94: Rooms-Only Repository-Scale Model: Base Case Geosphere Hydraulic Conductivity x 10 with Repositioned Well – I-129 Transport to the Well

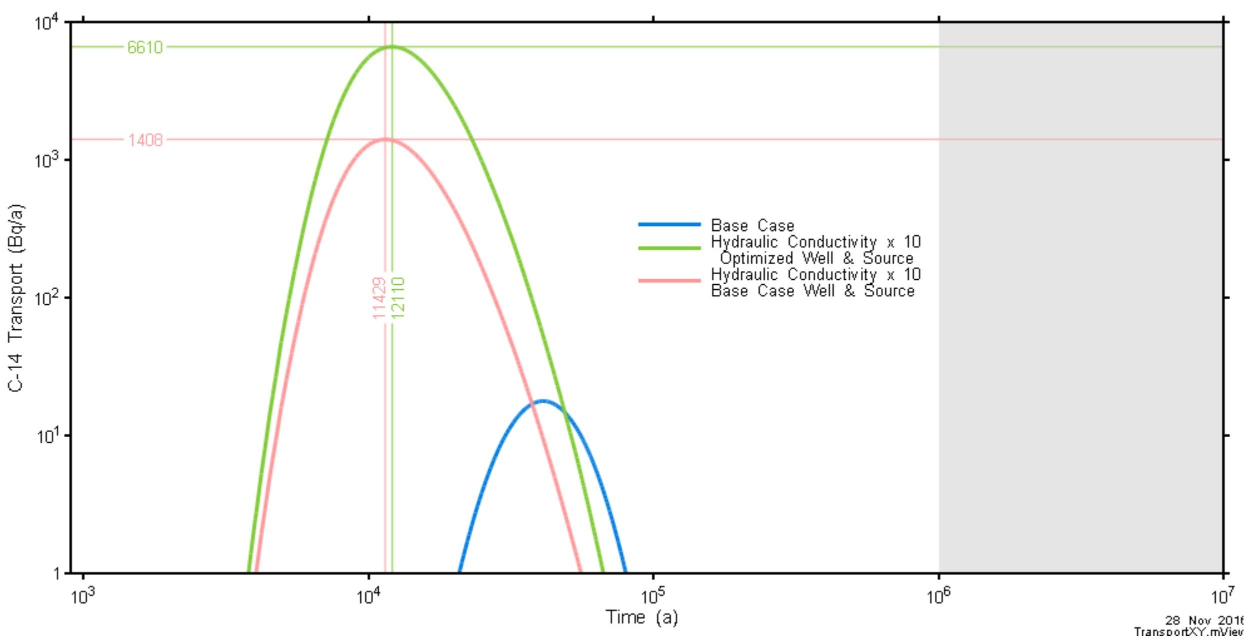

Figure 7-95: Rooms-Only Repository-Scale Model: Base Case Geosphere Hydraulic Conductivity x 10 with Repositioned Well – C-14 Transport to the Well

Increased EDZ Hydraulic Conductivity Sensitivity

The Base Case defines EDZ hydraulic conductivity as a multiple of the host rock hydraulic conductivity. Specifically, values of (K_{EDZ}/K_{ROCK}) for the placement rooms, central access tunnels, panel access tunnels and perimeter tunnels are:

- Inner EDZ = 100
- Seal EDZ = 100
- Outer EDZ = 10

The shaft equivalents are:

- Inner EDZ = 100
- Outer EDZ = 10

In this sensitivity case, all EDZ hydraulic conductivities are increased by a factor of 10. Cases have been simulated using the Full Repository-Scale Model.

Figure 7-96 presents the results. The figure shows that peak I-129 transport to the well increases from 1337 Bq/a (in the Base Case) to 1540 Bq/a, with the time of the peak now occurring at 20,000 years (as compared to 25,000 years). This is due to the effect of the EDZ on the flow field over the placement room panels east of the main fracture. This is illustrated in Figure 7-97 (plan view) and Figure 7-98 (vertical section) which compare hydraulic heads and velocities for the Full Repository Model.

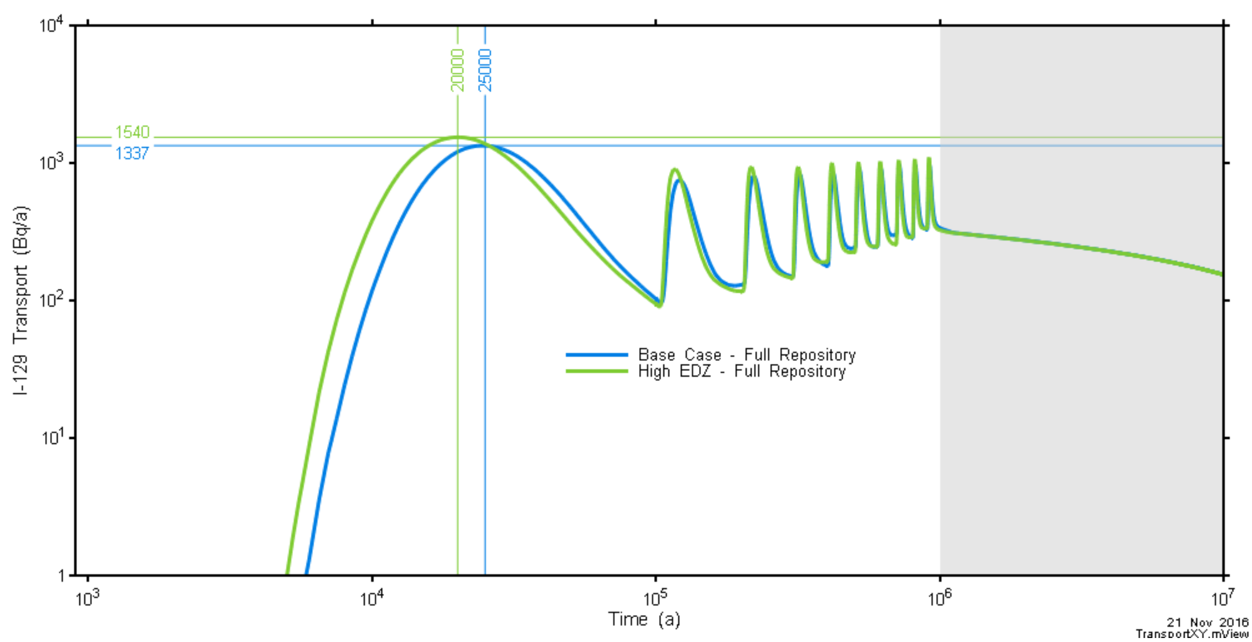

Figure 7-96: Repository-Scale Models: EDZ Hydraulic Conductivity Sensitivity - I-129 Transport to the Well

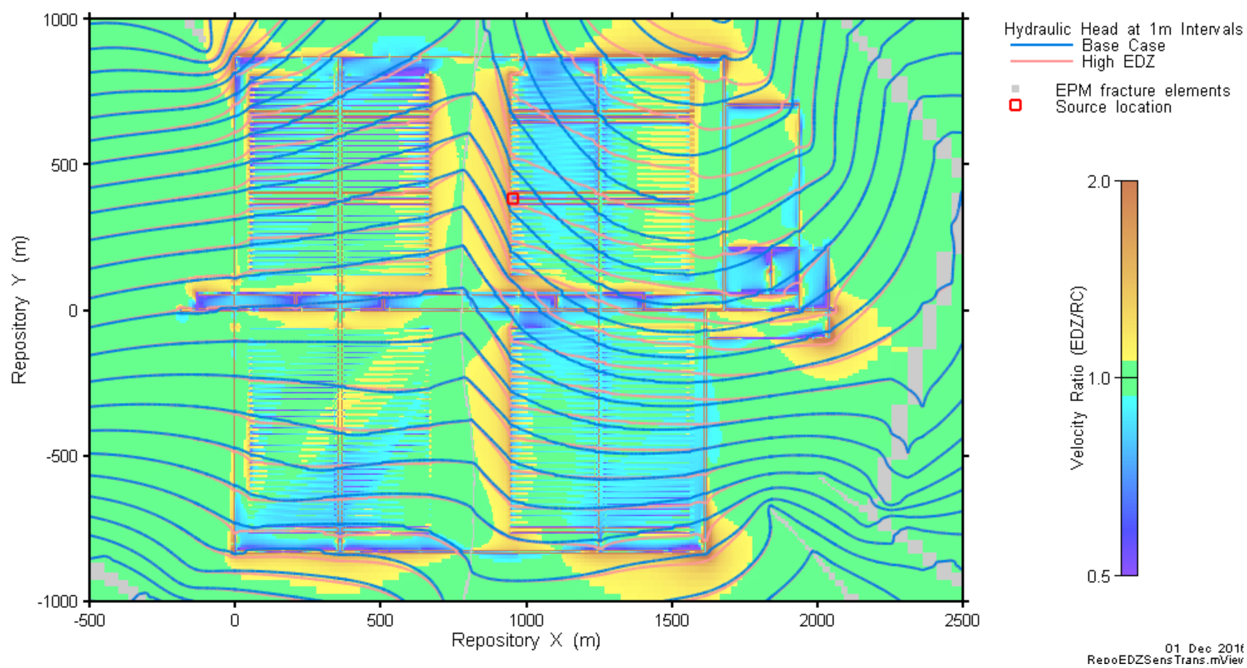

Figure 7-97: Full Repository-Scale Model: EDZ Hydraulic Conductivity Sensitivity - Plan View Velocity Ratio and Hydraulic Head Contours

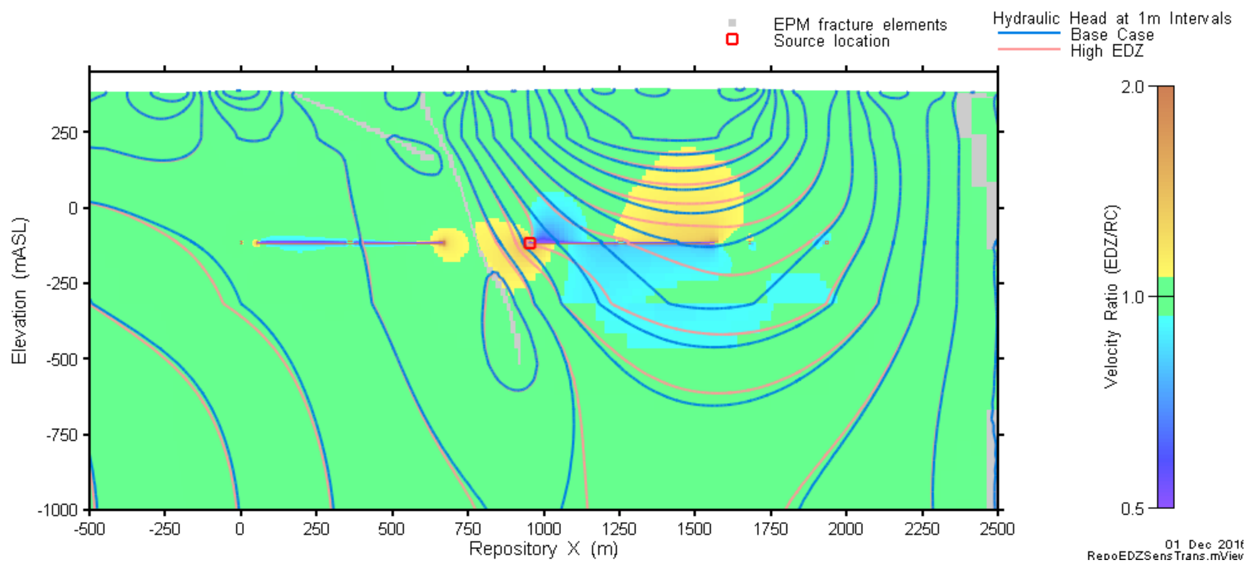

Figure 7-98: Full Repository-Scale Model: EDZ Hydraulic Conductivity Sensitivity Case – Vertical Section View Velocity Ratio and Hydraulic Head Contours

The increased hydraulic conductivity in the placement room EDZ reduces the hydraulic gradient across the rooms, resulting in an increase in the hydraulic gradient between the end of the rooms and the main fracture. This increases velocities in this region by up to a factor of two as indicated by the yellow region on the figures. Consequently, I-129 has a slightly earlier arrival time at the main fracture (leading to the earlier occurrence of the peak) and slightly reduced diffusive transport into the room (leading to the increase in peak transport rate).

Fracture Location Sensitivity

This sensitivity case examines the effect of varying the distance to the conductive fracture intersecting the repository footprint. In the Base Case, the fracture is located such that a minimum 100 m stand-off distance is maintained between the fracture and the placement rooms. This distance is determined using the points at which the perimeter and main tunnels intersect the fracture, and allows for an additional 10 m (10% margin) to account for potential fracture variation within the rock (see Section 7.7.1.2). This results in an actual distance in the model from the nearest defective container to the fracture of 167 m.

Three sensitivity cases are considered, with the main fracture shifted towards the placement room containing the defective containers by 50 m, 75 m, and 90 m to provide minimum stand-off distances of 50 m, 25 m, and 10 m. The cases are simulated with the Rooms-Only Repository-Scale Model.

Figure 7-99 and Figure 7-100 illustrate the locations of the Base Case and sensitivity case fractures in the plan and vertical orientations. For these sensitivity cases the well and defective container locations are the same as in the Base Case, except for small changes as required to ensure the pumping node locations always intersect the fracture.

Figure 7-101 and Figure 7-102 present I-129 and C-14 transport results. For I-129, as the fracture is moved closer to the defective containers the time to reach peak transport decreases; however, the peak magnitude remains similar to the Base Case, with only minor increases apparent. For C-14, peaks are shifted in time, and the transport magnitude is increased due to the reduced decay time associated with the faster transport times. The time differences between peaks represent differences in advective travel time through differing thicknesses of intact bedrock. Fracture travel times are similar for all cases.

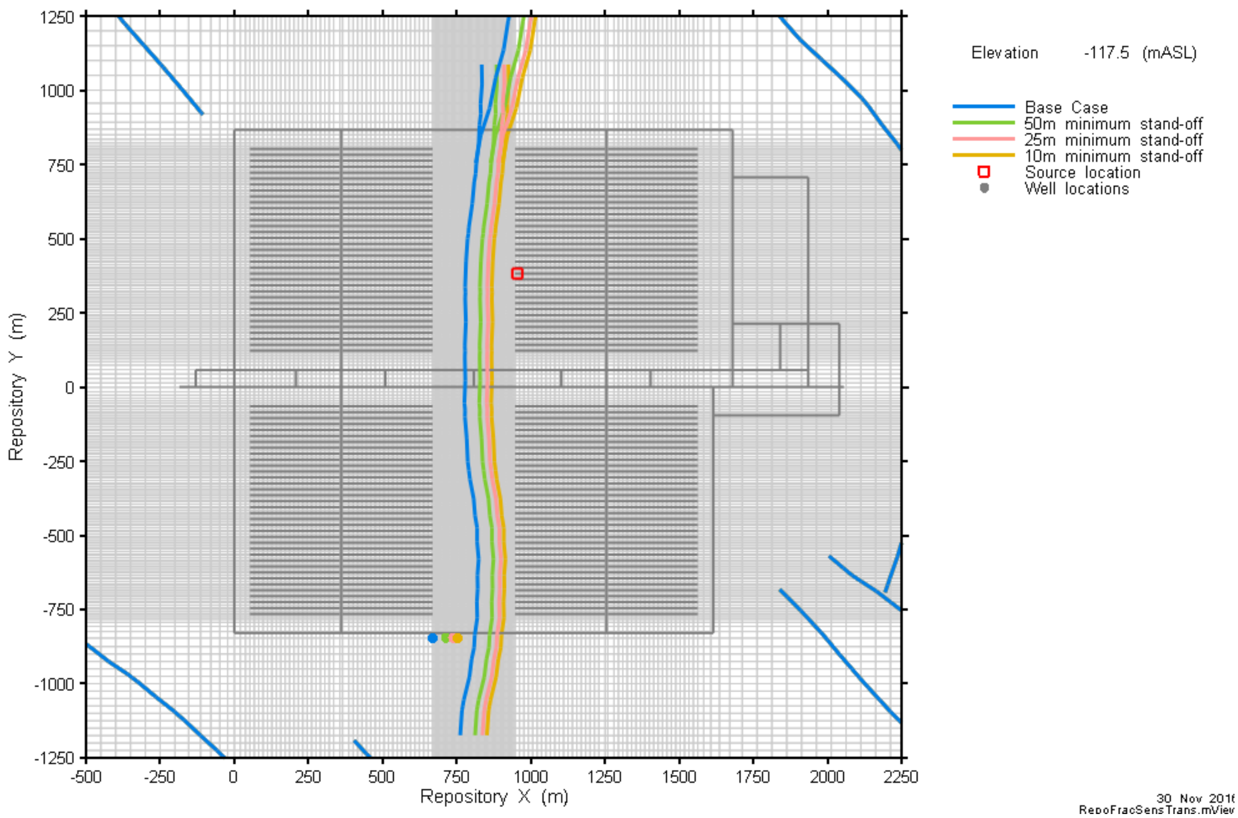

Figure 7-99: Rooms-Only Repository-Scale Model: Fracture Location Sensitivity - Plan View

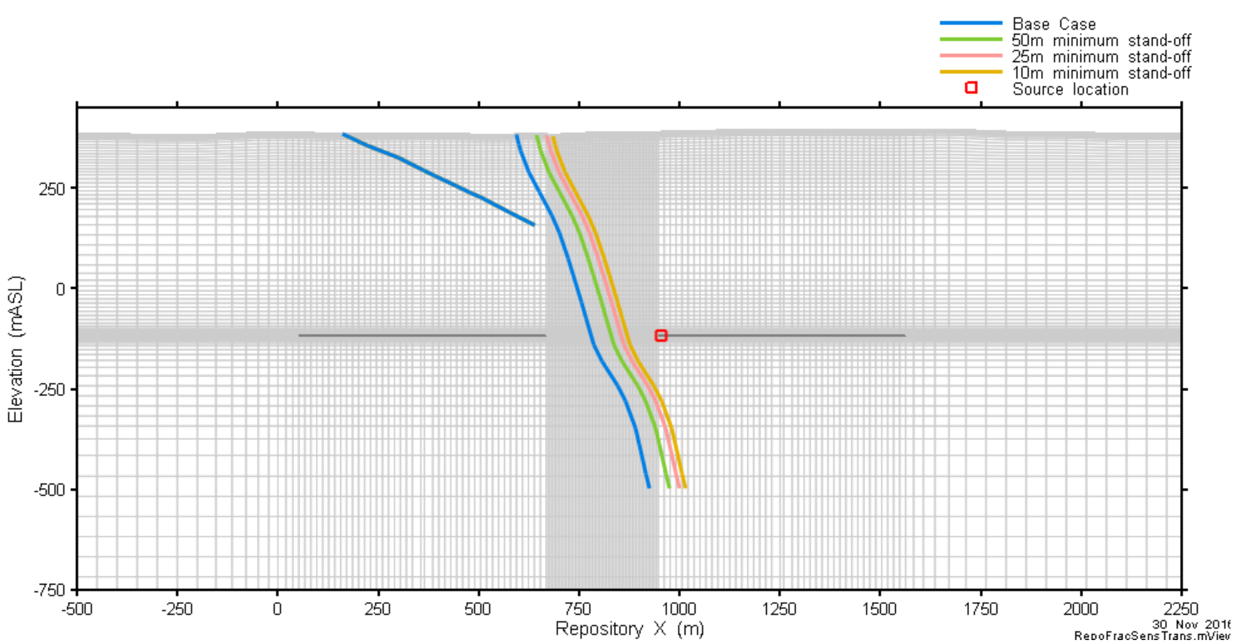

Figure 7-100: Rooms-Only Repository-Scale Model: Fracture Location Sensitivity - Vertical Cross-Section View

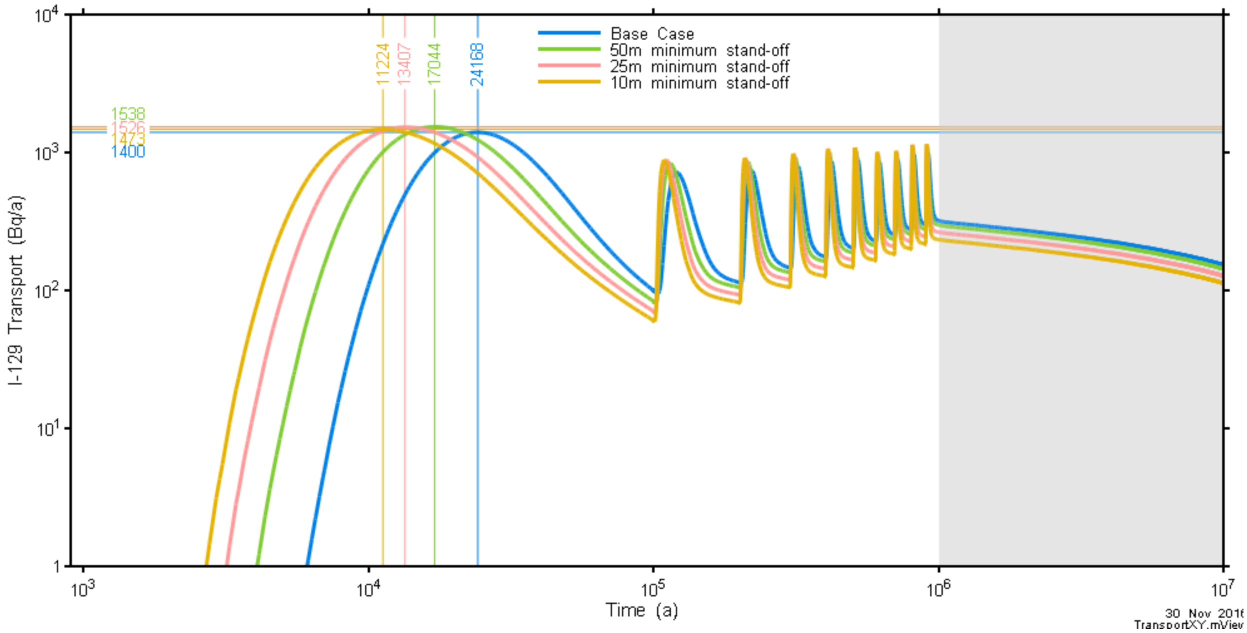

Figure 7-101: Rooms-Only Repository Scale Model: Fracture Location Sensitivity – I-129 Transport to the Well

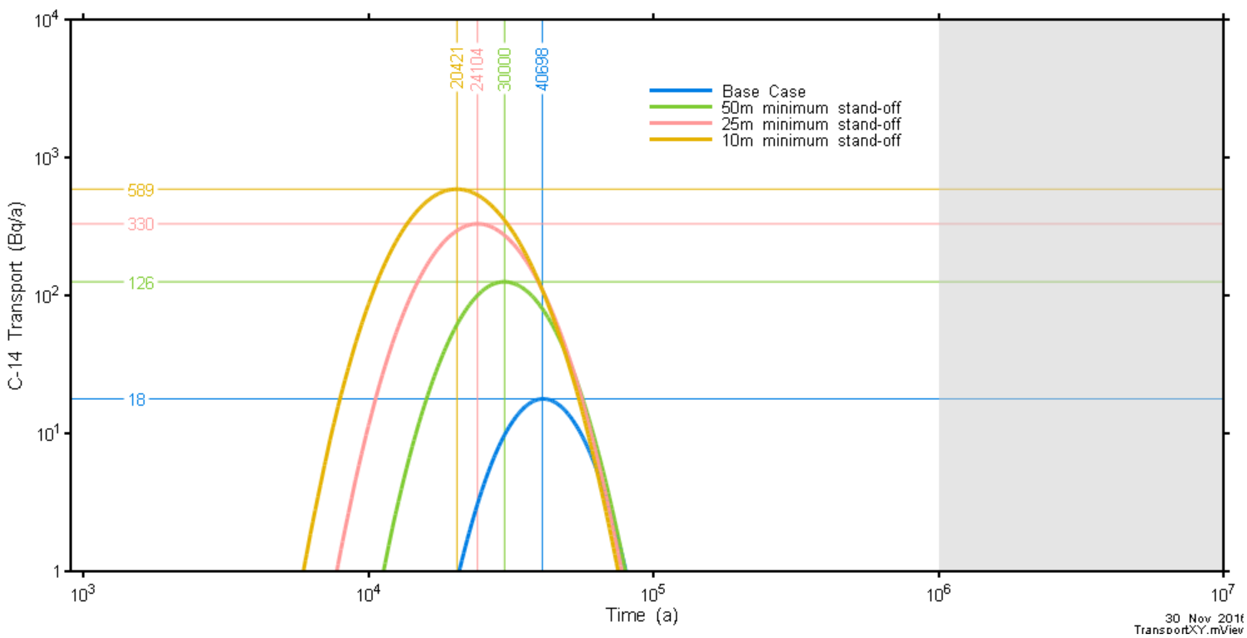

Figure 7-102: Rooms-Only Repository-Scale Model: Fracture Location Sensitivity – C-14 Transport

It is possible that the well / defective container location used in the Base Case may not be the maximum consequence location if the offset distance to the fracture changes. Additional work has therefore been undertaken to reposition the well / defective containers for the case with a 10 m standoff distance.

Figure 7-103 shows the locations investigated together with the well / defective locations that yields the highest dose consequence. The limiting locations are indeed different from those in the Base Case (Figure 7-99).

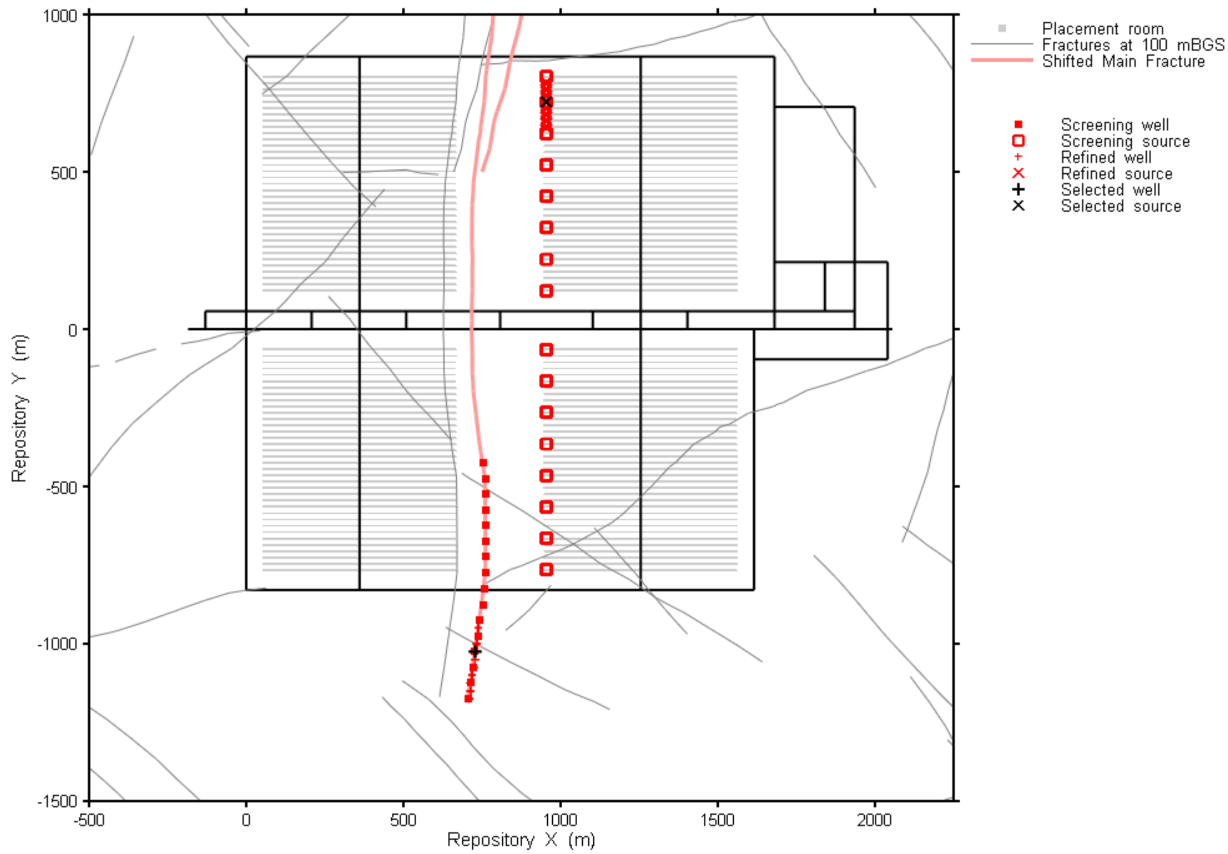

Figure 7-103: Rooms-Only Repository-Scale Model: Fracture Locations Sensitivity – Alternate Well and Defective Container Locations

Figure 7-104 and Figure 7-105 show results for I-129 and C-14 transport to the well for the revised maximum consequence locations. Also shown for comparison are the transport results for the Base Case and for the 10 m offset case with the well and defective container locations maintained in their Base Case positions.

The results show peak I-129 transport to the well increases by a factor of about 1.5 as compared to the Base Case (from 1400 Bq/a to 2046 Bq/a), with the time of peak transport decreasing to 9000 years from 24,200 years. For C-14, peak transport to the well increases from 18 Bq/a in the Base Case to 1865 Bq/a, with the time of the peak transport decreasing to 15,700 years from 41,700 years.

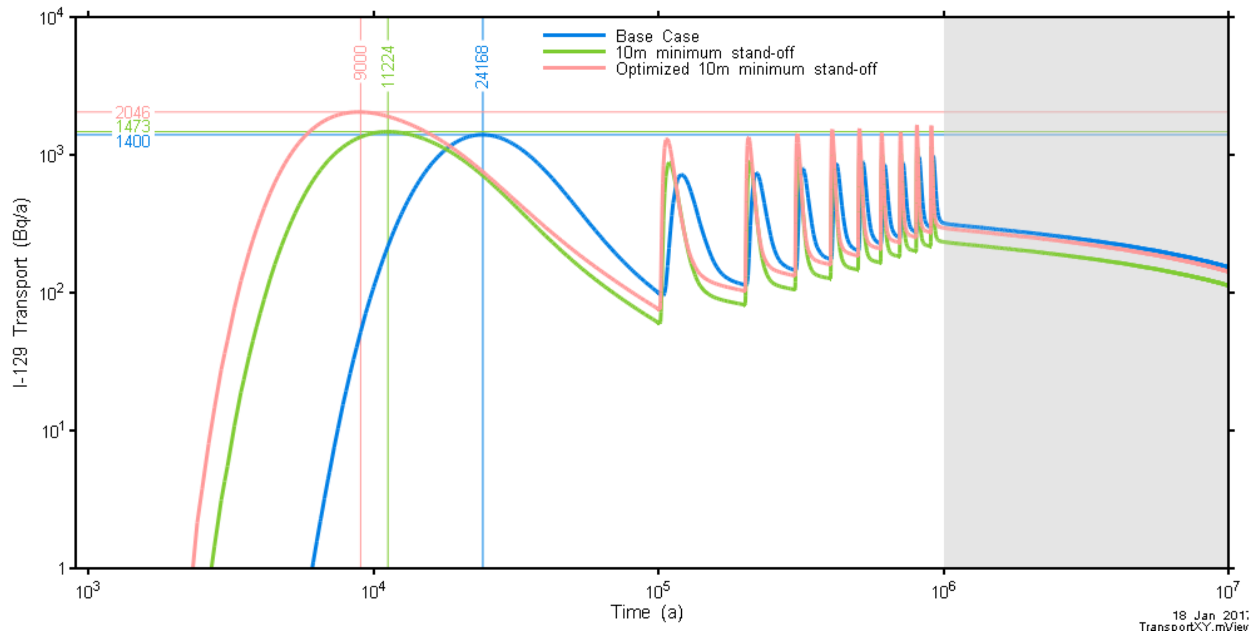

Figure 7-104: Rooms-Only Repository Scale Model: Fracture Location Sensitivity – I-129 Transport to the Well for Alternate Well Location

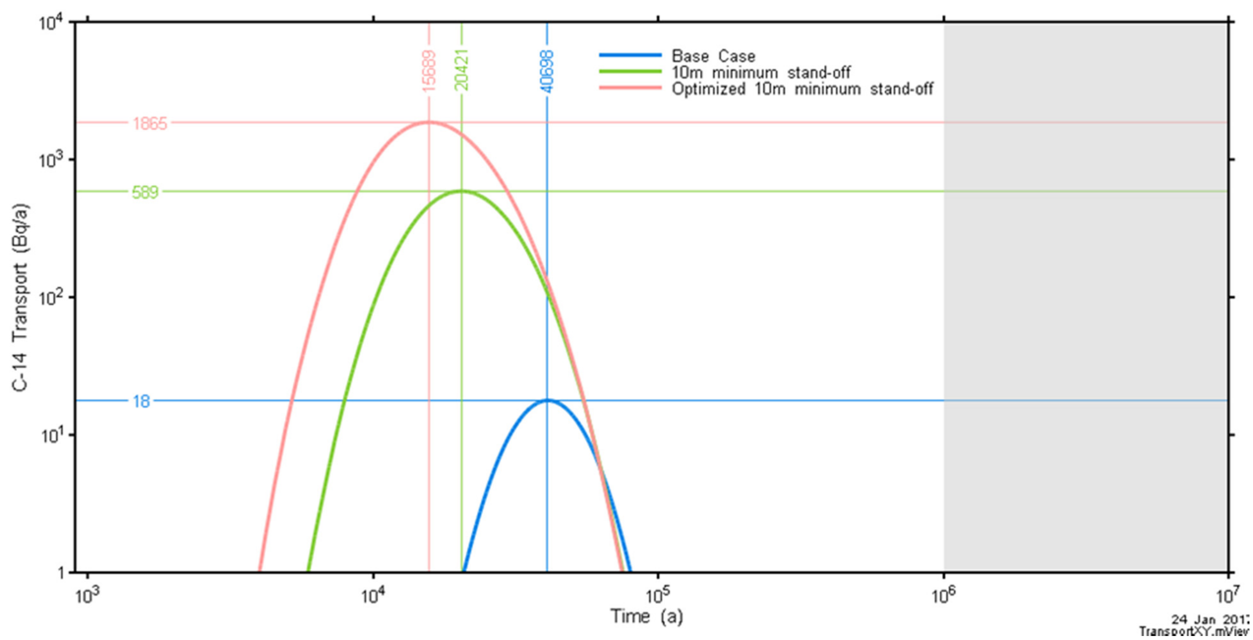

Figure 7-105: Rooms-Only Repository-Scale Model: Fracture Location Sensitivity – C-14 Transport to the Well for Alternate Well Location

The transport metrics for all fracture offset sensitivity cases are summarized in Table 7-29.

Table 7-29: Fracture Distance Sensitivity: Results for I-129 and C-14 Transport

Sensitivity Case*	Peak I-129 Transport Rate at Well (Bq/a)	Time of Peak (a)	Peak C-14 Transport Rate at Well (Bq/a)	Time of Peak (a)
100 m (Base Case)	1400	24,200	18	40,700
50 m	1538	17,000	126	30,000
25 m	1526	13,400	330	24,100
10 m	1473	11,200	589	20,400
10 m**	2046	9000	1865	15,700

*: All results are from the Rooms-Only Repository-Scale Model
**: With alternate well and defective container locations

Dispersivity Sensitivity

Dispersion is an advective process whose effect increases with increasing groundwater velocity. Dispersivity is the specific geosphere parameter that characterizes dispersion. In general, increased dispersivity leads to faster initial arrival of contaminants but with lower peak values, while reduced dispersivity retards initial arrival time, but increases peak values. Dispersivity is a function of porous media heterogeneity and the length scale of transport.

The dispersivity parameter approximates the spreading of a contaminant plume due to inherent variability in the local rock or fracture permeability. As a general “rule of thumb”, dispersivity estimates vary from a few percent to 10% of the total path length (this acknowledges the scale-dependence (Pickens and Grisak 1981)).

For the repository considered here, the path length of interest for the contaminant plume (i.e., when it reaches the surface) ranges from 500 m (the distance from the repository to the surface) to nearly 2 km (the shortest contaminant transport distance in the Base Case). Since assuming lower dispersion is conservative (i.e., less spreading of the contaminant plume results in higher concentrations), the Base Case assumes a constant longitudinal dispersivity of 20 m or 4% of the 500 m repository-to-surface distance. The transverse dispersivity is assumed to be 10% of the longitudinal value or 2 m.

Dispersivity within engineered sealing materials, which are more homogenous and present substantially less variability than rock, is assumed to be 10 m.

Two sensitivity cases to illustrate the effect of dispersivity assumptions are considered. Specifically:

- High Dispersivity – dispersivity increased by a factor of 5, resulting in longitudinal dispersivity of 100 m in intact rock and 50 m in EBS materials; and

- Low Dispersivity – dispersivity reduced by a factor of 5, to 4 m in intact rock, and 2 m in EBS materials.

Simulations were performed for I-129 transport using the Rooms-Only Model with the Combined Source Term, with results as shown in Figure 7-106 and Figure 7-107.

Figure 7-106 illustrates how plume dispersion after 25,000 years is affected by the dispersivity assumption. As expected, there is greater spreading for the increased dispersivity case and reduced spreading for the reduced dispersivity case.

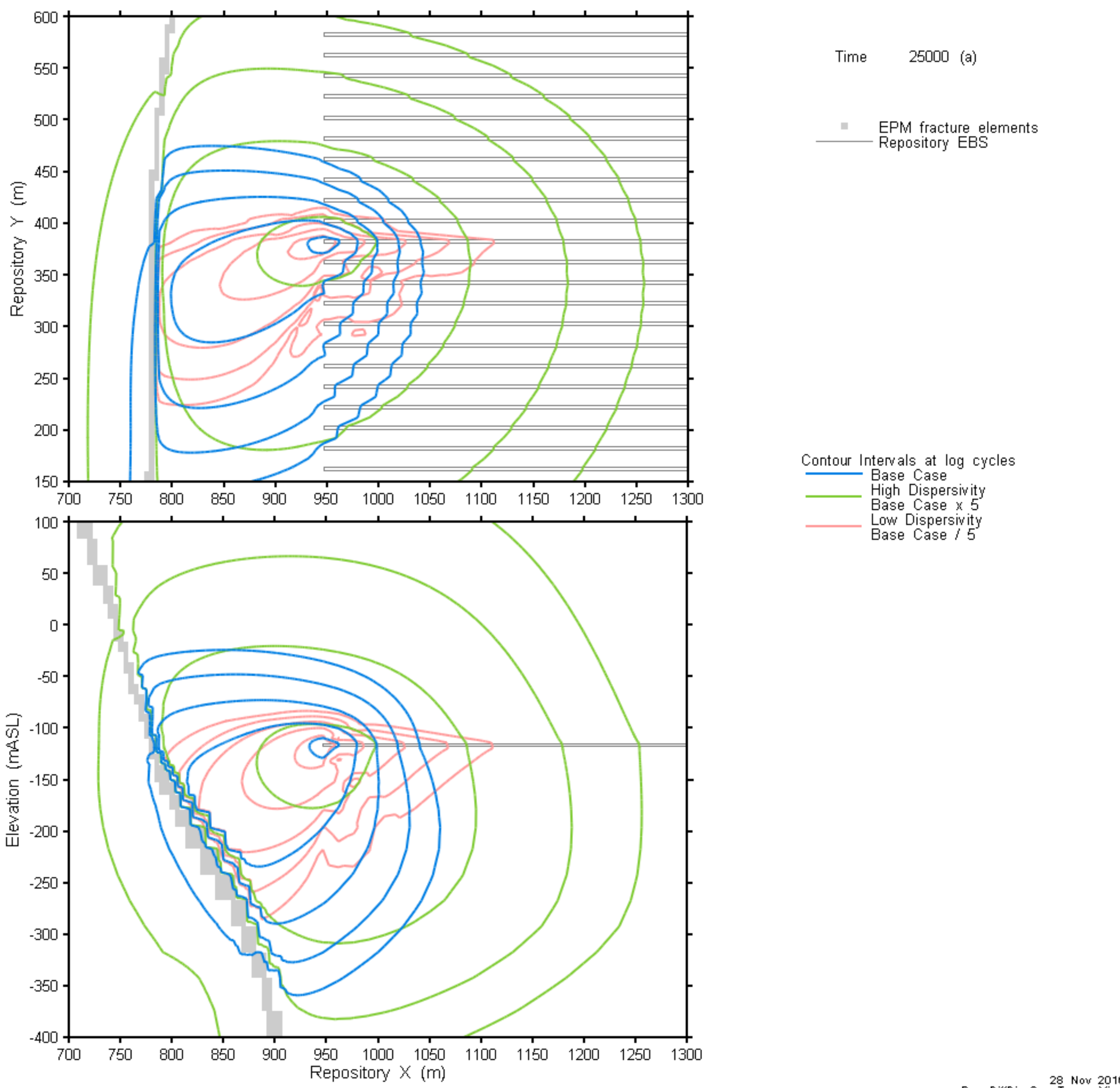

Figure 7-106: Rooms-Only Repository-Scale Model: Dispersivity Sensitivity – Contours of I-129 Concentration in the Geosphere

Figure 7-107 shows that transport time to the well is decreased to 17,000 years for the High Dispersivity case (as compared to 24,200 years for the Base Case). The increased dispersion into the intact rock results in a corresponding reduction in the peak amount of I-129 reaching the well. Peak I-129 transport for this case is 902 Bq/a as compared to 1400 Bq/a for the Base Case.

Similarly, the Low Dispersivity case allows for less dispersion of the plume leading to a greater amount of transport to the well. Peak I-129 transport for this case is 2103 Bq/a occurring at 25,000 years.

For the purpose of this postclosure safety assessment, the Base Case dispersivities are already set to conservative values, at several percent of the transport path length, and further reduction is not warranted.

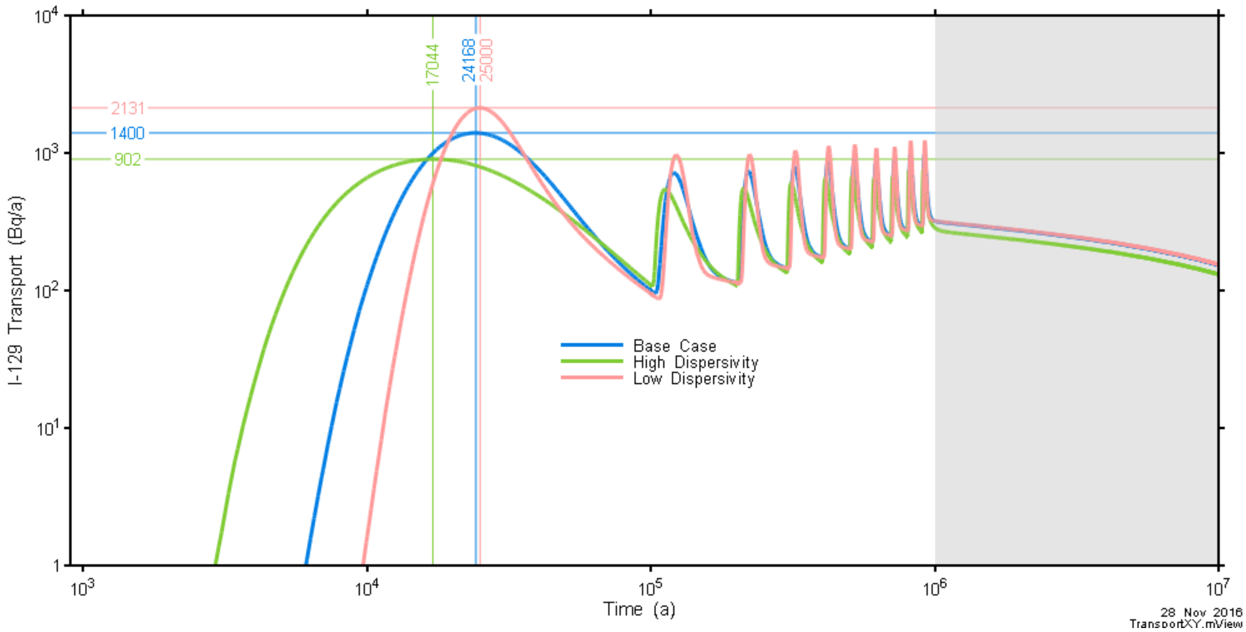

Figure 7-107: Rooms-Only Repository-Scale Model: Dispersivity Sensitivity – I-129 Transport to the Well

7.7.2.3.7 Modelling Attribute and Parameter Sensitivity Cases

This section presents results for sensitivity cases performed to illustrate the effect of various FRAC3DVS-OPG modelling attributes and parameters on the Base Case results. The cases are:

- Increased spatial resolution;
- Increased and decreased number of time steps; and
- Discrete fracture modelling (as opposed to equivalent porous media (or EPM) modelling);

Increased Spatial Resolution

To illustrate the effect of grid size a new version of the Subregional-Scale Model was created using the same domain, parameter distributions and boundary conditions as in the Base Case, but with discretization reduced by a factor of two in the X, Y, and Z directions, thereby increasing the number of active elements and nodes by a factor of eight. Within the repository area, grid size was reduced from a nominal 20 m to 10 m.

Figure 7-108 presents the head difference and compares head contours at the repository horizon. The results show very little difference in calculated heads as compared to the Base Case, indicating that the original spatial discretization is adequate for flow calculations.

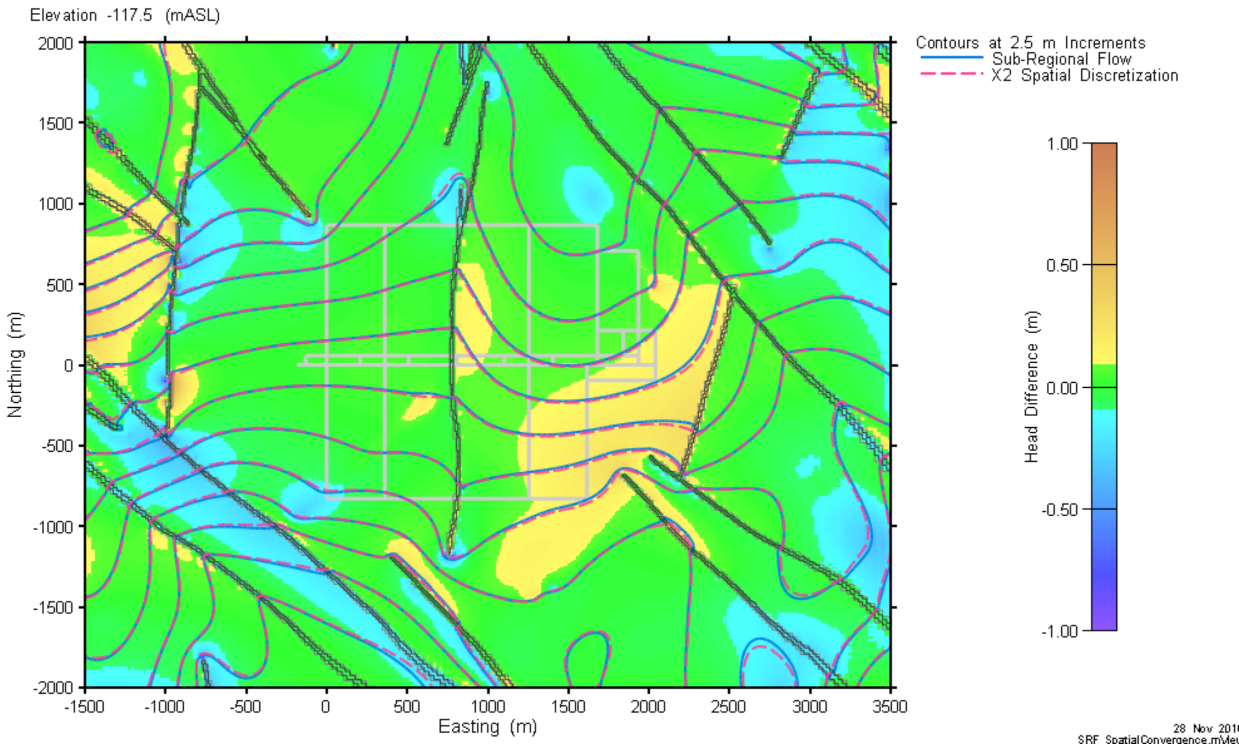

Figure 7-108: Subregional-Scale Model: Spatial Convergence Sensitivity - Comparison of Head Contours

For transport, a similar approach was taken with the Rooms-Only Repository-Scale Model; however, in this case the grid is too large to uniformly double discretization over the entire domain. Instead, discretization was doubled in the plan X and Y directions and in the grid layers within 20 m of the repository horizon. The overall grid increased from 6.45 M nodes to 33.15 M nodes.

Figure 7-109 compares results for I-129 transport at 25,000 years with those in the Base Case version of the model. The figure shows only minor differences in concentration contours, with the largest variation occurring within the placement rooms, upgradient of the source term.

Surface concentrations (Figure 7-110) at peak transport time are also very similar.

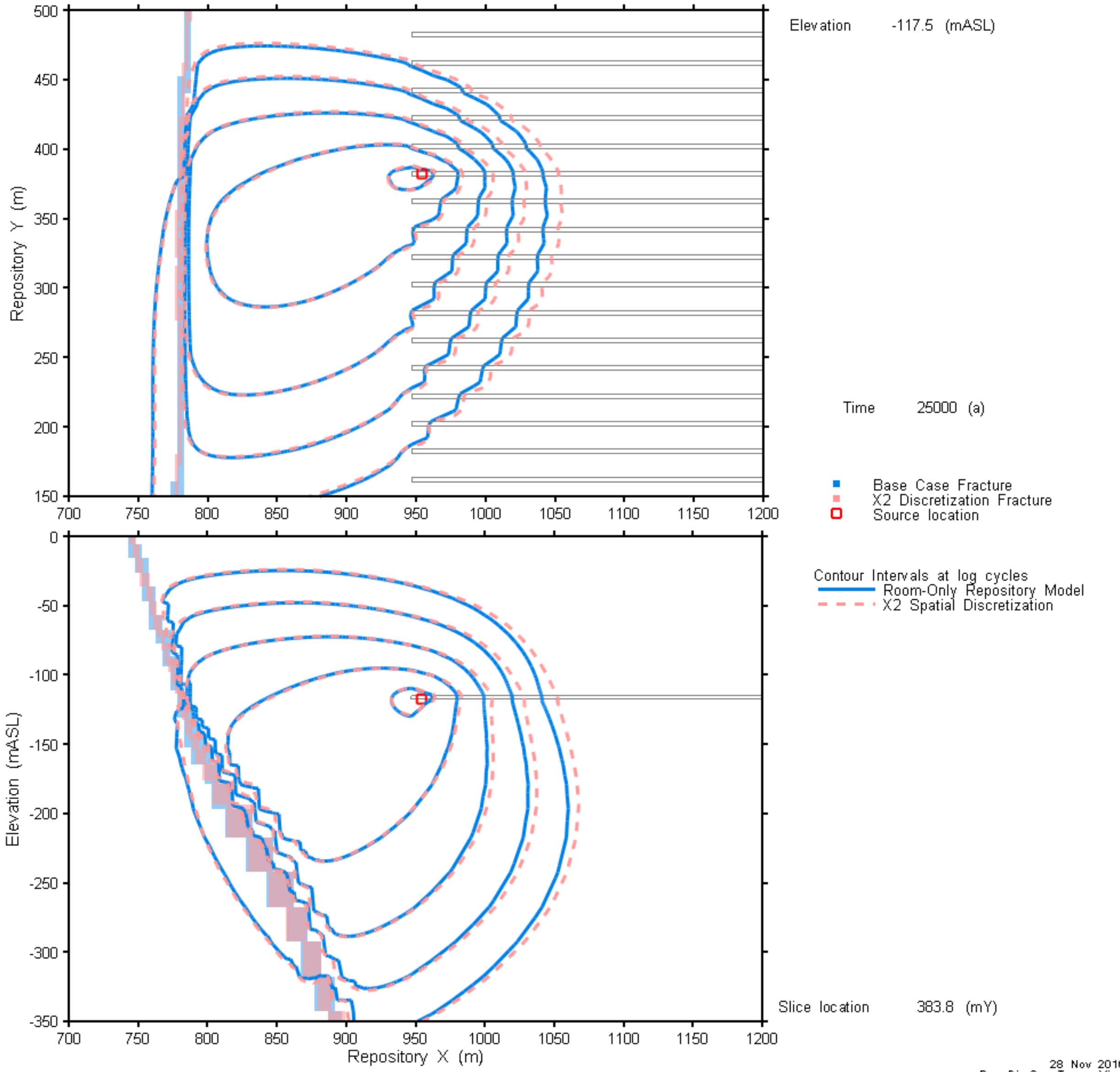

Figure 7-109: Rooms-Only Repository-Scale Model: Spatial Convergence Sensitivity – I-129 Transport

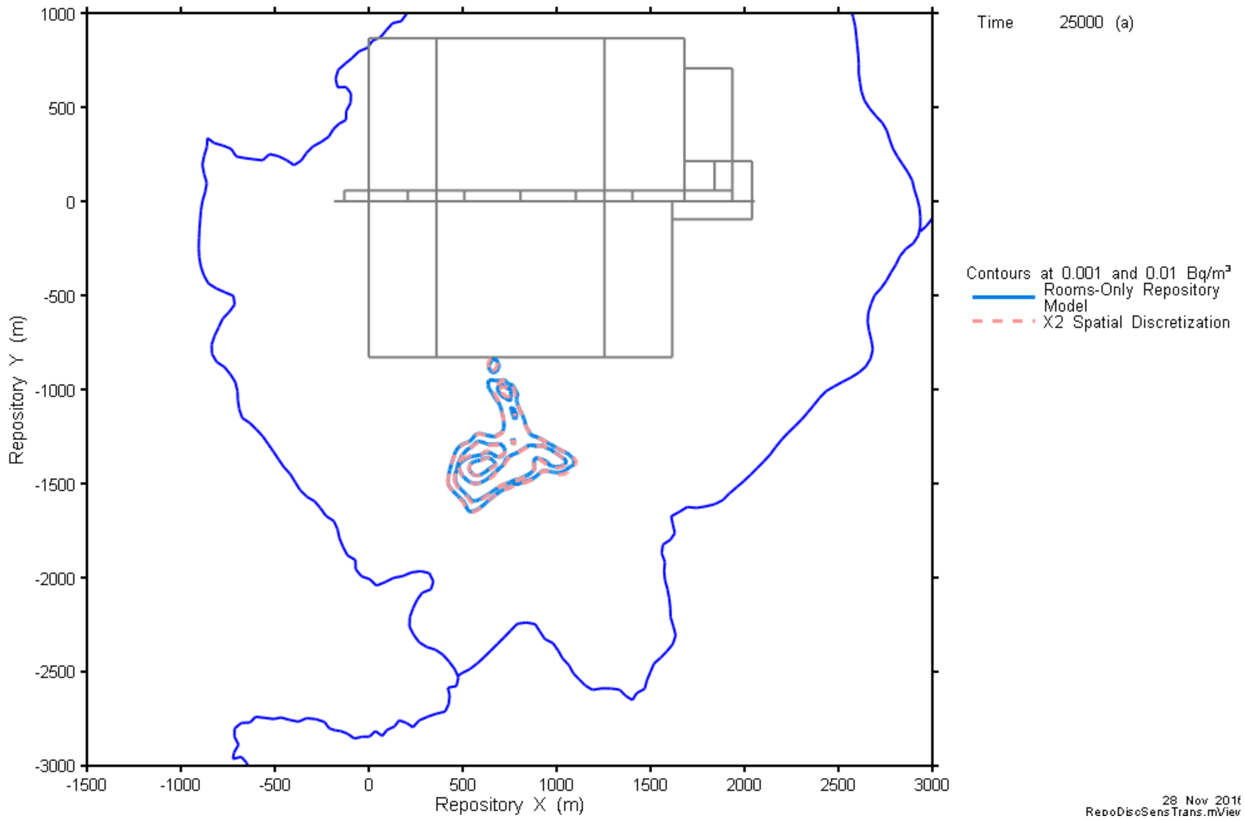

Figure 7-110: Rooms-Only Repository-Scale Model: Spatial Convergence Sensitivity – Peak I-129 Transport at Surface

As shown in Figure 7-111, well transport results from the two models are visually indistinguishable, with the increased discretization resulting in a less than a 1% increase in peak transport. This is not significant in the context of the postclosure safety assessment.

Based on this comparison, it can be concluded that the spatial discretization in the various models is fit for purpose.

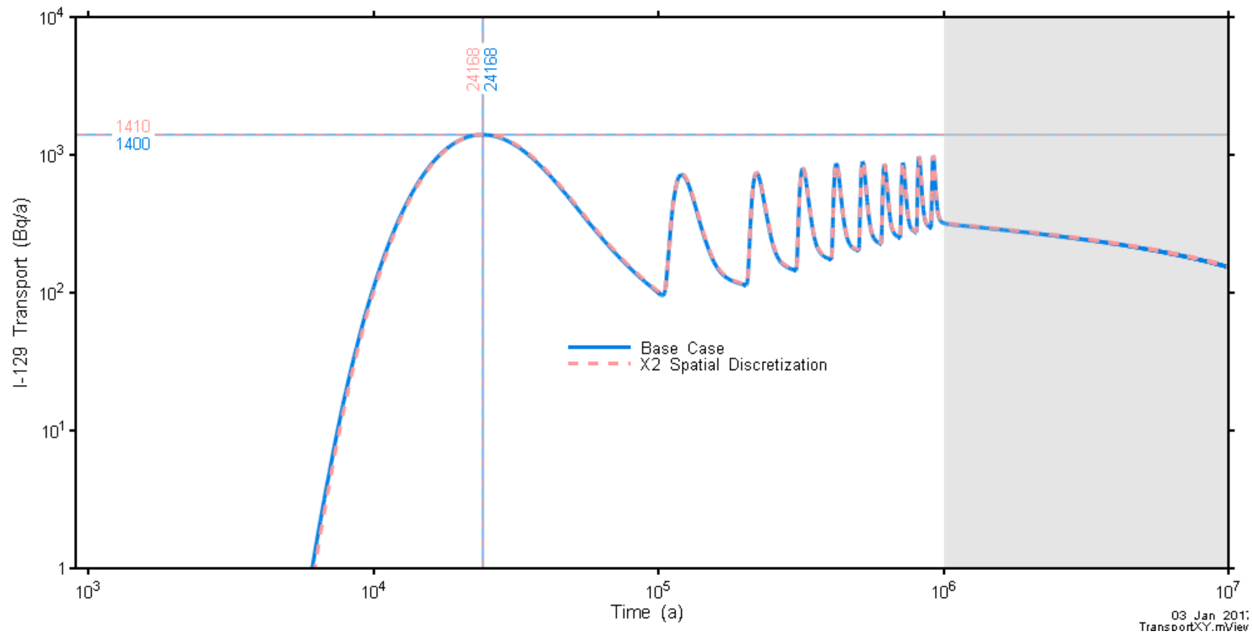

Figure 7-111: Rooms-Only Repository-Scale Model: Spatial Convergence Sensitivity – I-129 Transport to the Well

Temporal Resolution

The effect of time step size was determined by modifying control parameters in Repository-Scale Model simulations. Two tests were performed, the first with the Rooms-Only Model using the Combined Source Term, and the second with the Full-Repository Model using the container source term.

For each test, the following two cases were simulated:

- Increased number of time steps as caused by a reduced convergence factor and maximum time step size parameters relative to the Base Case, and
- Decreased number of time steps as caused by increased values of the same parameters.

Results presented in Figure 7-112 and Figure 7-113 show essentially no sensitivity of peak I-129 transport to the well for the Rooms-Only Model, with a minor decrease in peak well transport occurring when the number of time steps is decreased in the Full Model. For both models a decrease in the number of time steps cause some differences in response after the second container failure (i.e., post 100 ka), likely due to increased coarseness in sampling the source term.

Based on these comparisons it can be concluded that the temporal discretization in the various models is fit for purpose.

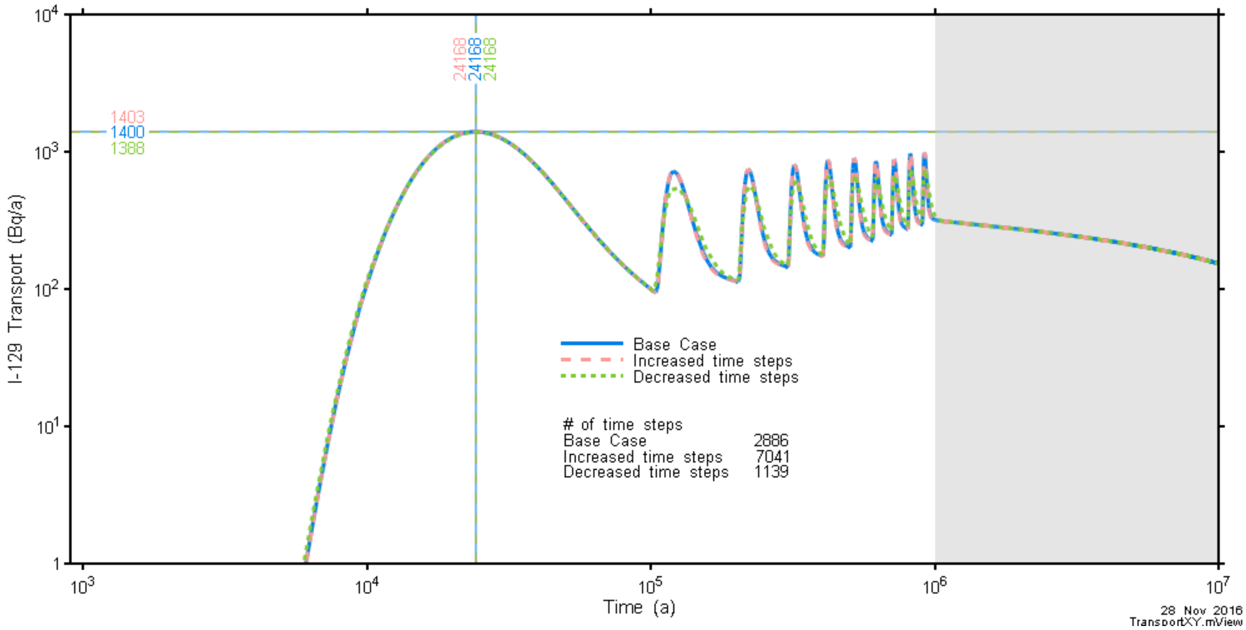

Figure 7-112: Rooms-Only Repository-Scale Model: Time Step Convergence Sensitivity with Combined Source Term – I-129 Transport to the Well

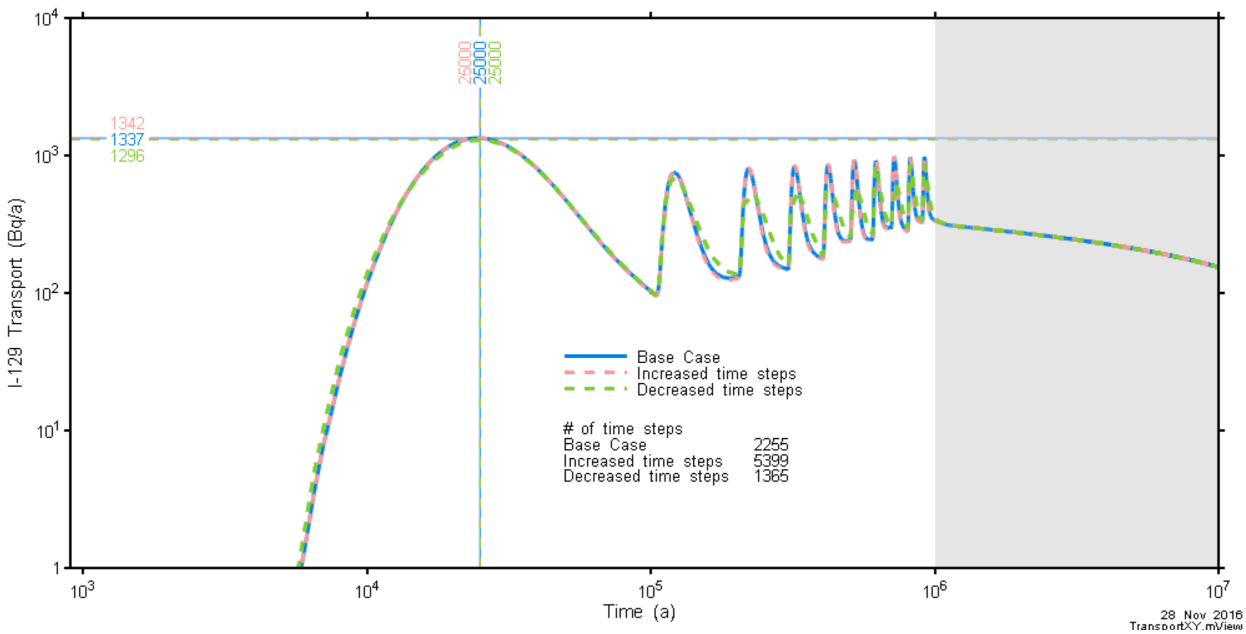

Figure 7-113: Full Repository Scale-Model: Time Step Convergence Sensitivity with Container Source Term – I-129 Transport to the Well

<u>Discrete Fracture Model Sensitivity</u>

The discrete fracture network (DFN) model uses an alternate approach to implementing fractures within the 3D model representing the intact bedrock. As in the EPM approach, the 3D model geometry is processed to determine which elements are intersected by the fracture system. Element faces that are closest to or intersected by the input fractures are specified as fracture faces. These are then specified as rectangular 2D planar elements with property assignments consistent with the fracture description. These 2D elements use the same nodal discretization as the 3D element model and are added to the 3D model during solution matrix assembly by FRAC3DVS-OPG. All other model features (boundary conditions, intact rock properties, source terms, etc.) are identical to the Base Case EPM model.

The resulting DFN model is solved using the finite-element mode, as this is required for correct assembly and solution of the DFN elements. The equivalent porous media (or EPM) approach applied in the Base Case and all other 3D simulations in this assessment uses the finite-difference (FD) mode of solution. This mode is preferred because it is less computationally demanding than the finite-element method; however, to allow a one-to-one comparison with the DFN sensitivity case, the Base Case has been re-simulated using the finite-element approach.

Figure 7-114 compares I-129 transport to the well for the Base Case, the DFN case and the Base Case with finite-element. All simulations were performed with the Rooms-Only Repository-Scale Model using the Combined Source Term.

Both finite-element cases (i.e., the DFN sensitivity and the finite-element Base Case) show slightly earlier I-129 arrival times at the well with reduced peaks as compared to the Base Case. This implies that the finite-element mode results in a greater degree of dispersive / diffusive transport than does the finite-different approach. Based on this, the Base Case results with finite-difference are bounding and the EPM model is deemed fit for purpose.

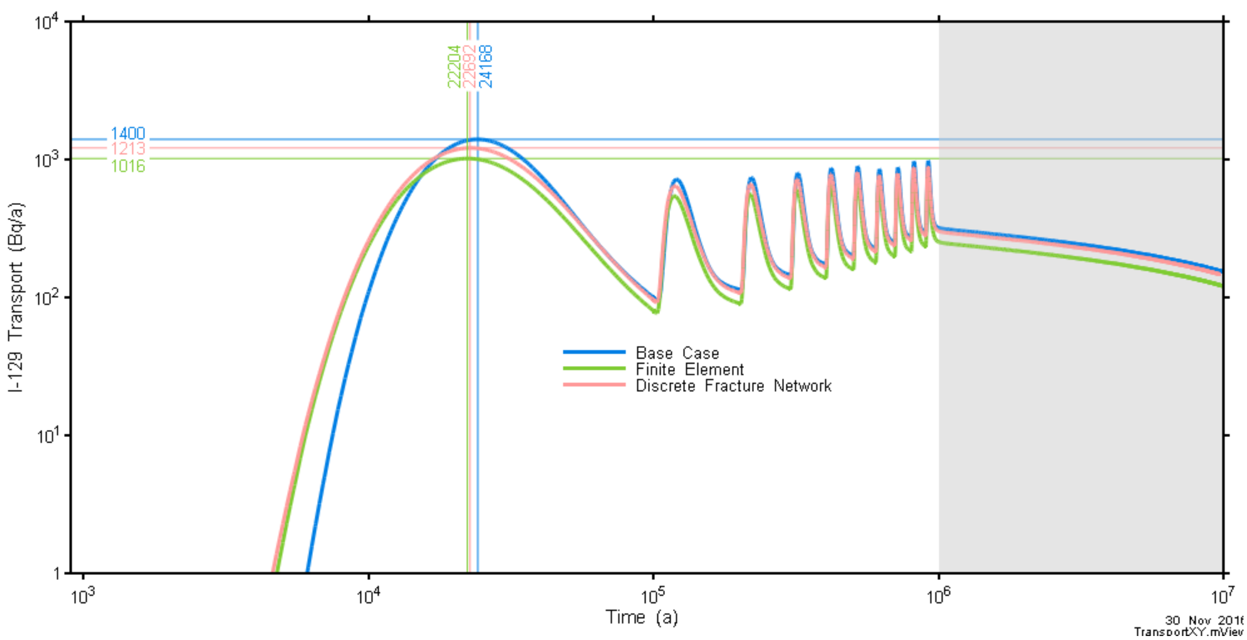

Figure 7-114: Rooms-Only Repository Scale Model: DFN Sensitivity – I-129 Transport to the Well

7.7.2.4 Container-Scale Model Flow Results

The Container-Scale Model represents a small section of the repository surrounding the defective containers and the adjacent geosphere. The model incorporates a high level of detail with individual containers represented.

Four Container-Scale Models have been created in the course of this study, as noted in Section 7.7.1.3, with each model representing a separate potential location for the defective containers. Because Section 7.7.2.3.2 shows that the highest dose consequence occurs for the Main Model, results from only this version of the four models are discussed here in detail. The Main Container model discretization and property assignments are described in Section 7.7.1.3. The location of the defective containers within the repository is indicated by the red dot adjacent to the “Main” label in Figure 7-31.

Base Case and sensitivity case simulations are performed with the Container-Scale Model to generate source terms for the Repository-Scale Models.

Container-Scale Model results are also used to corroborate Repository-Scale Model results and to provide a more detailed understanding of the behaviour of repository components.

Figure 7-115 shows hydraulic head and advective velocities on plan and vertical sections through the middle of the placement room. The Full-Repository Model hydraulic head is also shown. The good agreement confirms correct implementation of the fixed head external boundary conditions. Velocity plots provide insight into the effectiveness of the barrier system in reducing flow rates within the repository system. Flow towards the fracture (lower left corner of the right hand side plot) is evident.

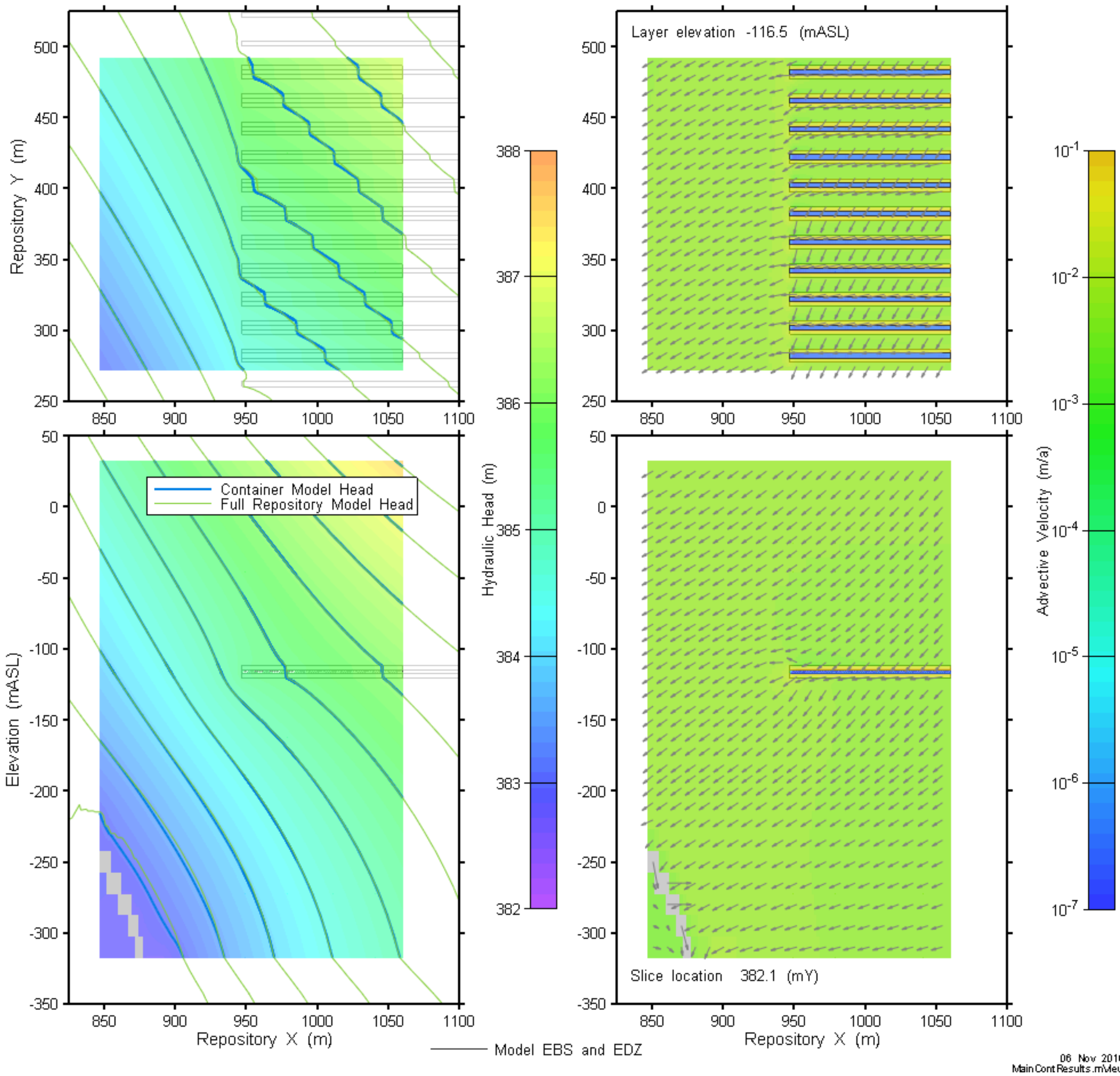

Figure 7-115: Main Container-Scale Model: Hydraulic Head and Advective Velocity on Horizontal Plane through Repository (top) and Vertical Plane through Source Room (bottom)

Figure 7-116 shows advective velocities in a three dimensional view through the EBS and EDZ materials. The cross-section is cut vertically through the centre of the room. The highest velocities are in the Inner EDZ, with much lower velocities within the placement room.

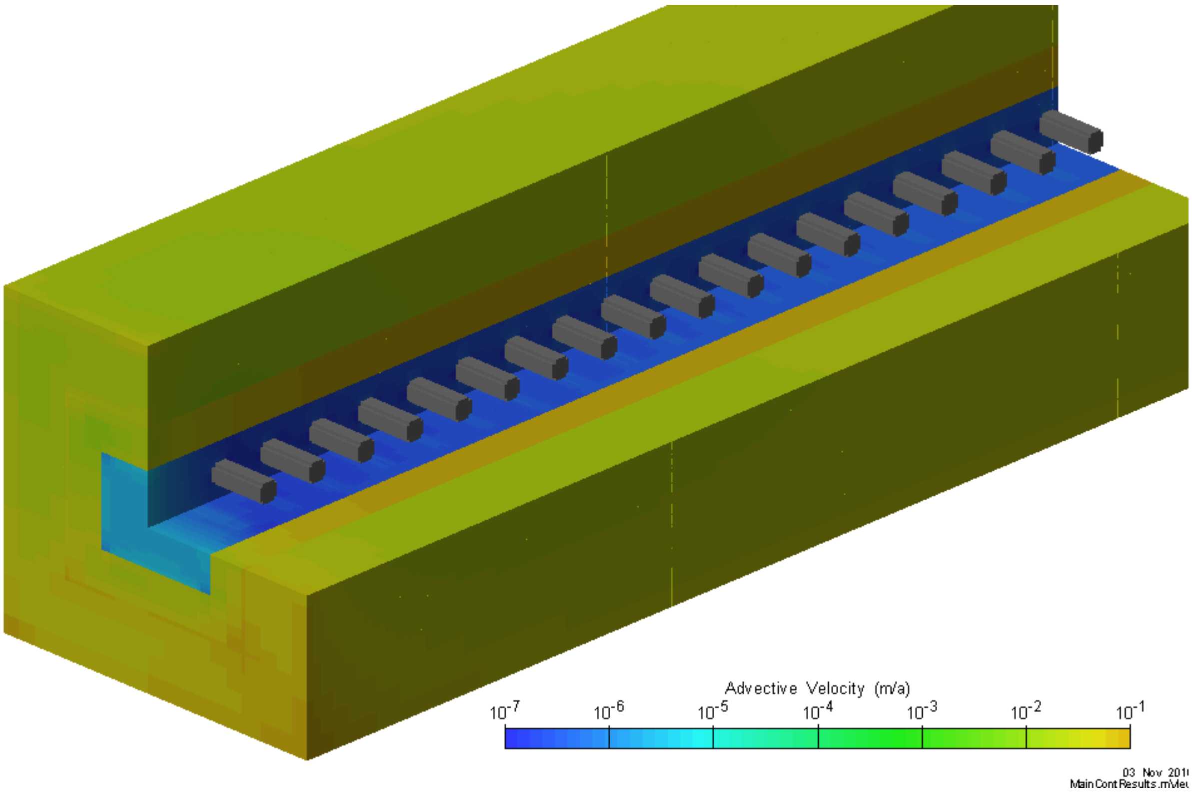

Figure 7-116: Main Container-Scale Model: 3D View of Advective Velocity Magnitudes in EBS and EDZ

7.7.2.5 Container-Scale Model Radionuclide Transport Results

Base Case radionuclide transport modelling is performed for I-129, C-14, Cl-36, Ca-41, Cs-135, Se-79, and U-238. Detailed results are presented here for I-129, U-238 and Cs-135, with summary results presented for the remaining radionuclides. The three selected radionuclides are representative of the behaviours for non-sorbing (I-129), highly sorbing (U-238) and intermediate sorbing (Cs-135) species.

Individual source terms (see Section 7.5.2.2) are applied to each container, with the source distributed equally across 144 nodes on each container surface. The primary output from the model is transport into the Inner EDZ which forms the source term for the Repository-Scale Models.

To provide data for verification of the System Model (Section 7.8.1.4.1), radionuclide transport from the defective containers into the placement room and geosphere (i.e., out of the buffer) is determined over a volume surrounding the defective containers as shown in Figure 7-139.

Figure 7-117 through Figure 7-119 illustrate the I-129 concentration results 500 years after the failure of containers one, six, and ten. Although the location of the maximum concentration shifts, the plume surrounding the room is relatively consistent. The maximum concentration achieved after failure of the first container (Figure 7-117) is slightly higher than for the others due the greater contribution of the congruent release source term at earlier times (see Figure 7-11).

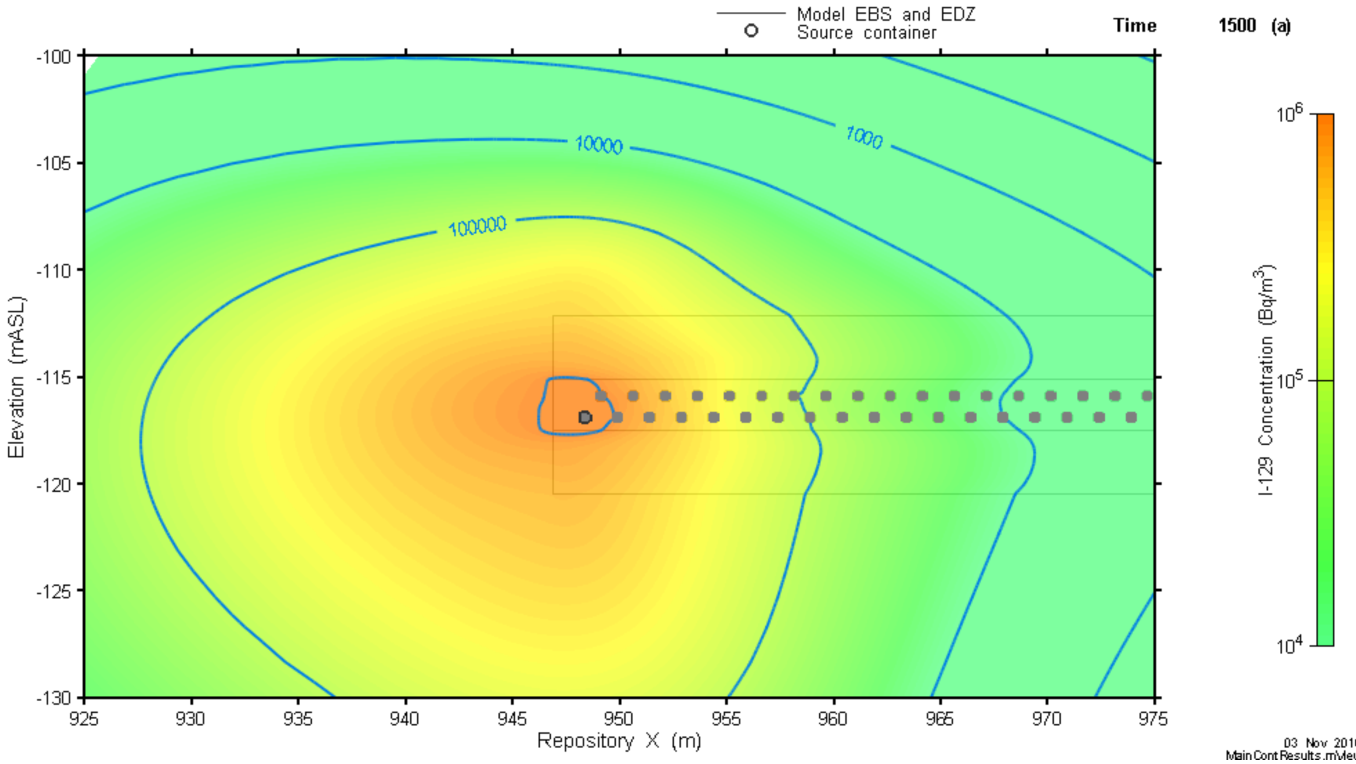

Figure 7-117: Main Container-Scale Model: Detail of I-129 Concentration 500 Years after Failure of the First Container (at 1500 a)

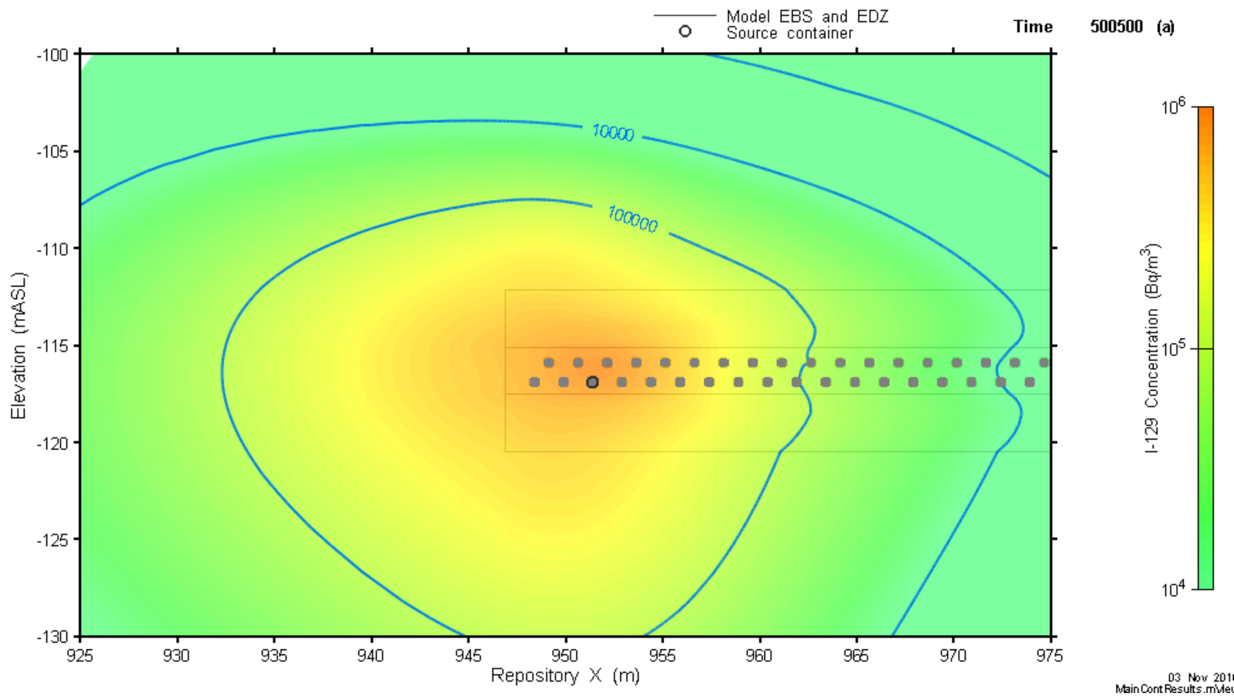

Figure 7-118: Main Container-Scale Model: Detail of I-129 Concentration 500 Years after Failure of the Sixth Container (at 500,500 a)

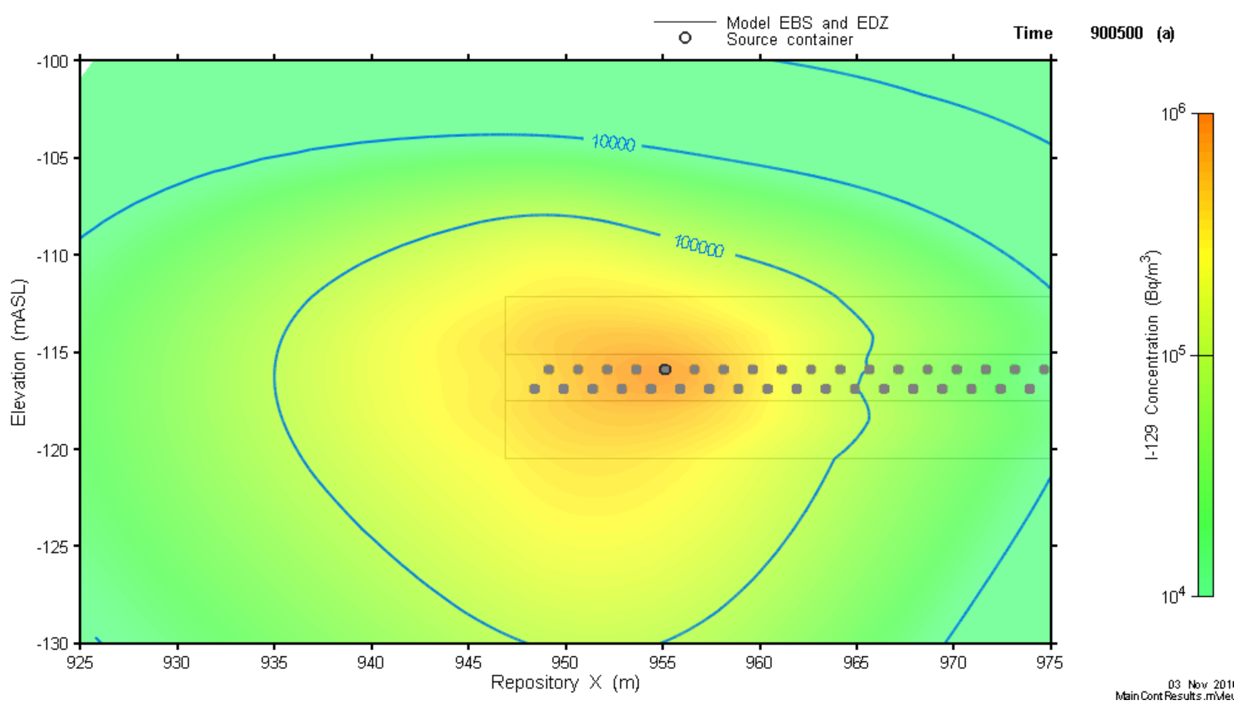

Figure 7-119: Main Source Container-Scale Model: Detail of I-129 Concentration 500 Years after the Failure of the Tenth Container (at 900,500 a)

Figure 7-120 through Figure 7-123 illustrate the time dependent behaviour of the I-129 plume at repository level and on a vertical slice through the placement room. Contours of equivalent results from the Full and Rooms-Only Repository-Scale Models are overlaid for comparison. The results show a very close correspondence between models, again providing confidence in the Repository-Scale Model results.

The outer concentration contour, 1 Bq/m^3, corresponds to an effective I-129 drinking water dose of about 0.1 μSv/a based on a water consumption of 0.77 m^3/a per person.

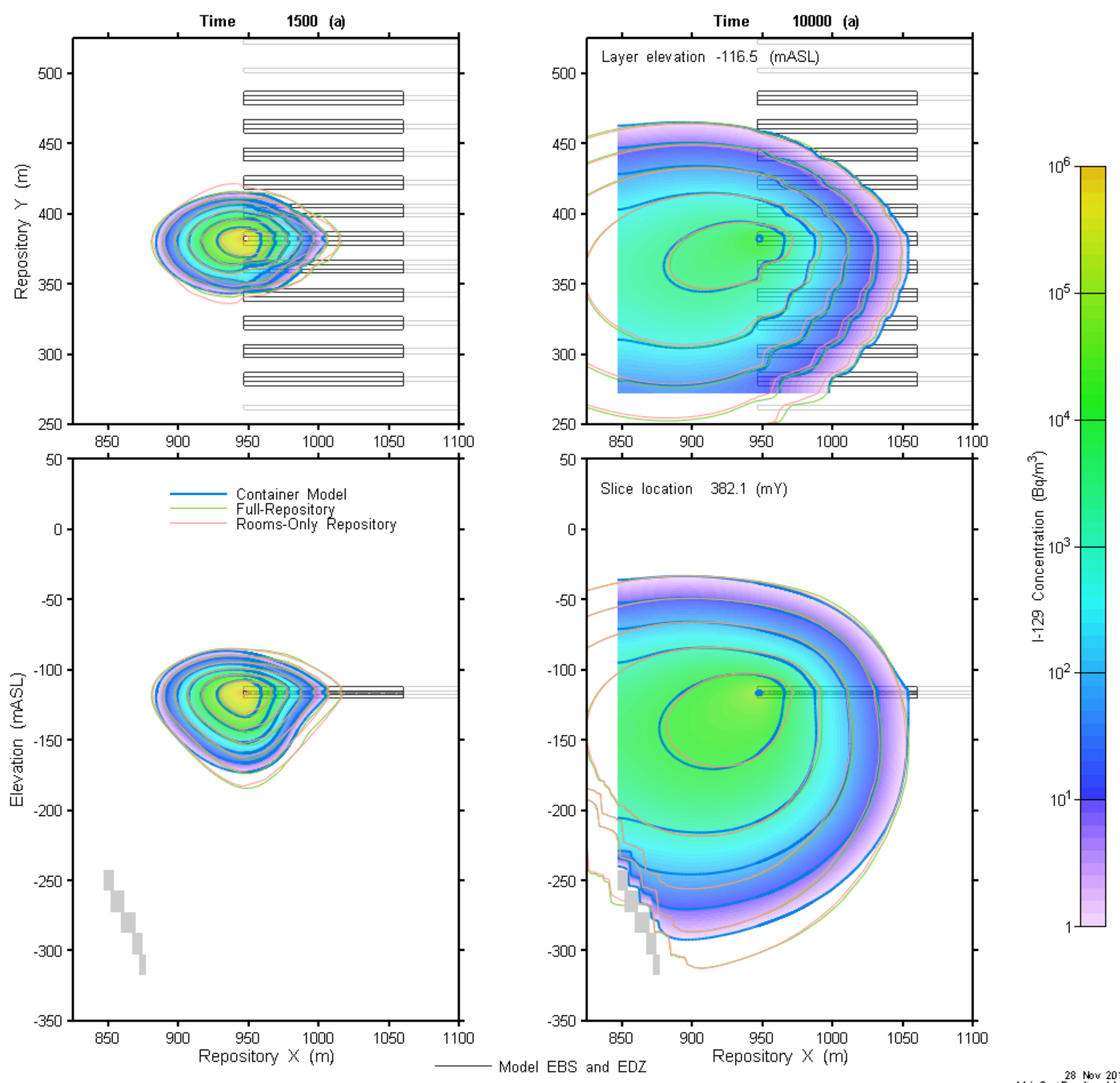

Figure 7-120: Main Container-Scale Model: I-129 Concentration at 1500 a and 10 ka

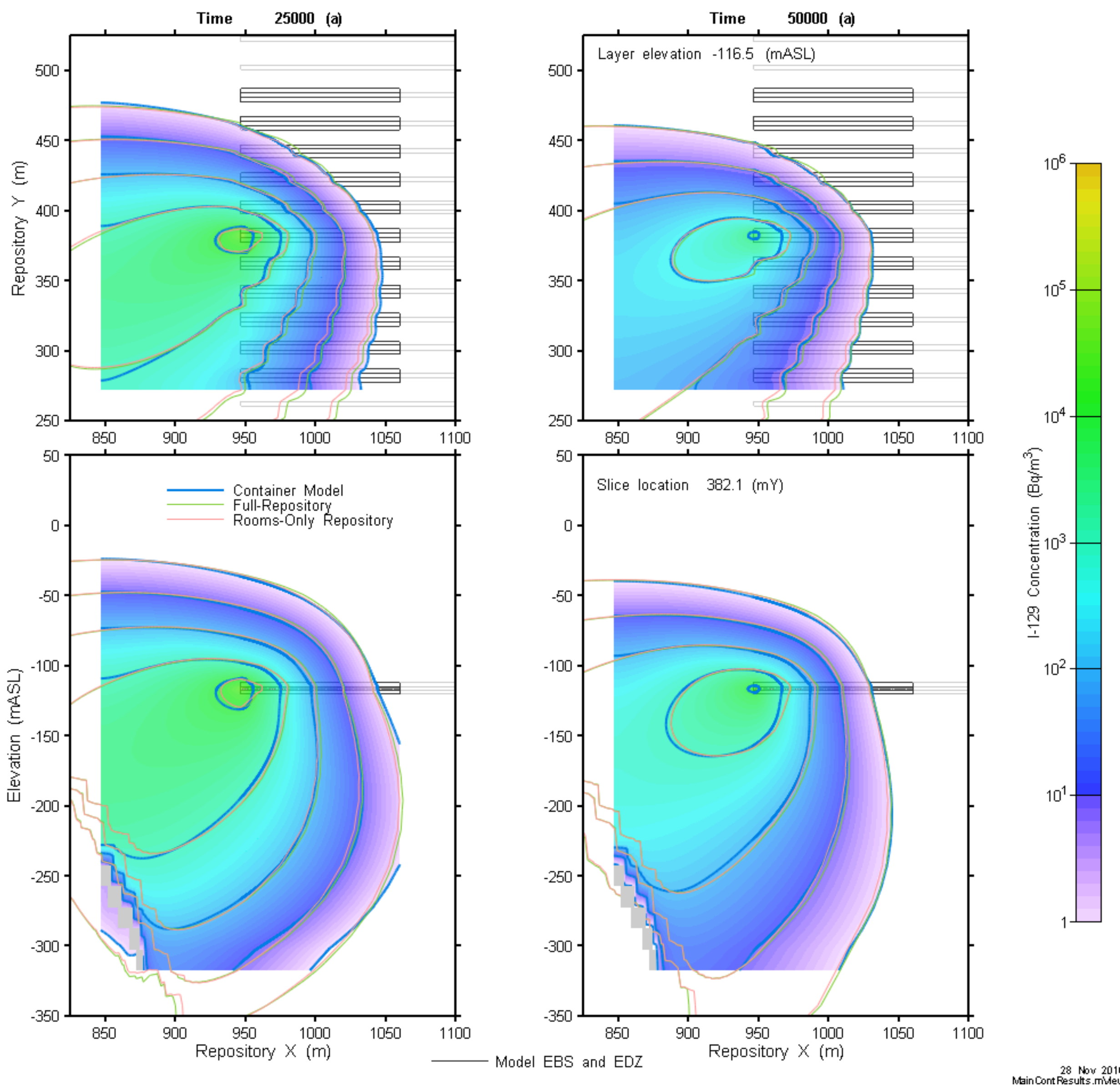

Figure 7-121: Main Container-Scale Model: I-129 Concentration at 25 ka and 50 ka

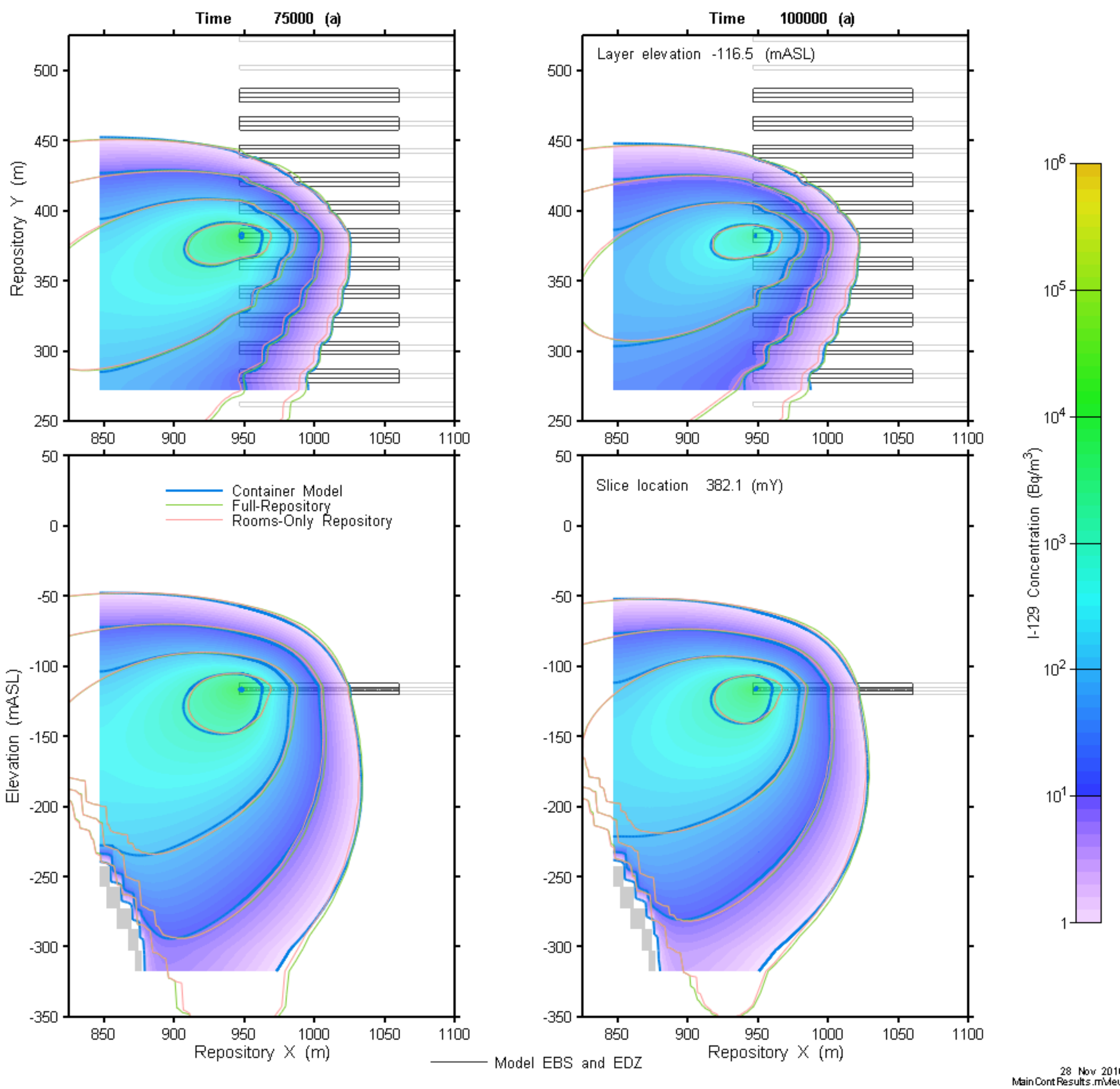

Figure 7-122: Main Container-Scale Model: I-129 Concentration at 75 ka and 100 ka

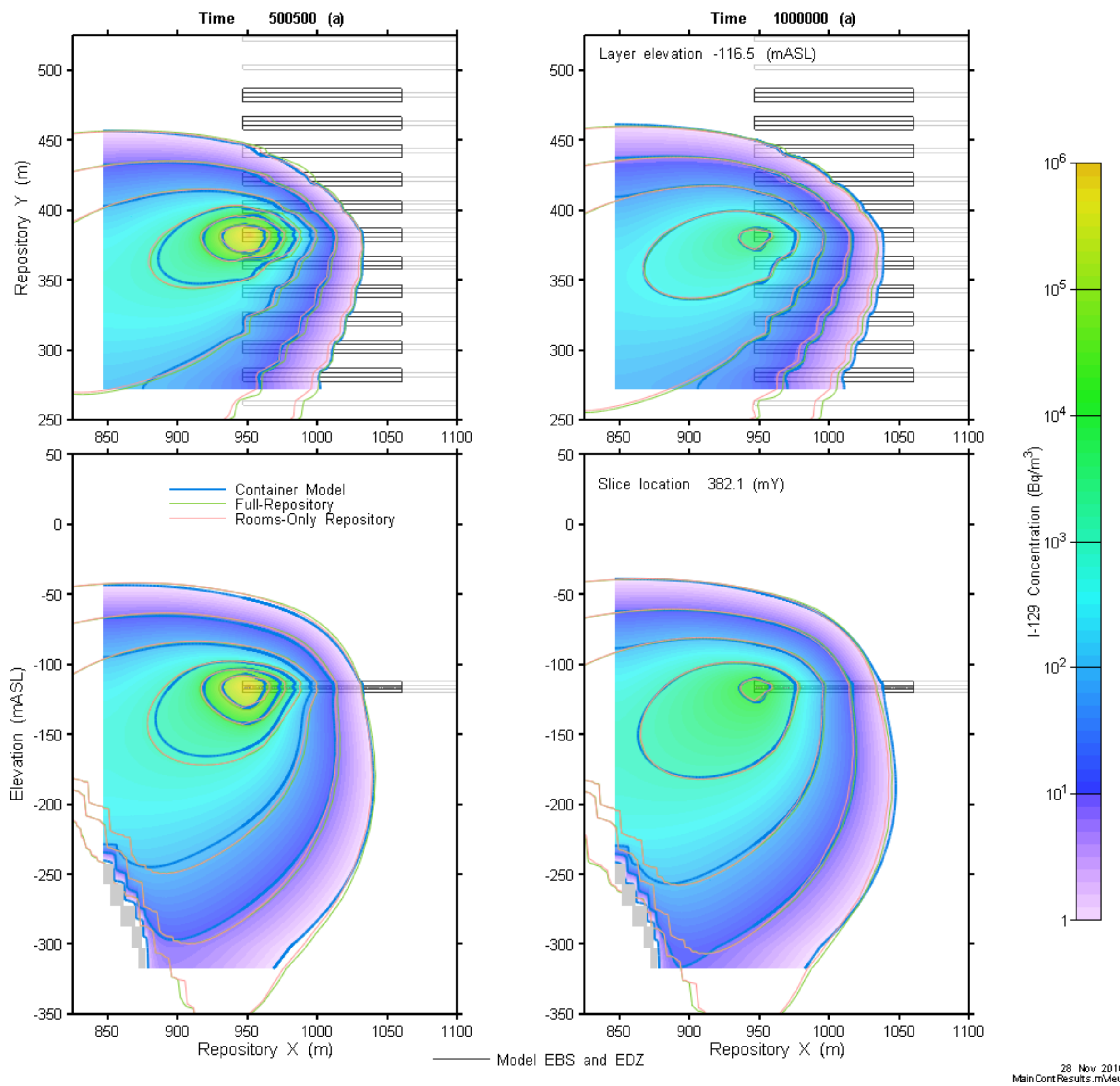

Figure 7-123: Main Container-Scale Model: I-129 Concentration at 500.5 ka and 1 Ma

Changes in the three dimensional plume structure immediately after the first failure, at 5000 a, just before the second failure (at 100,000 years) and 500 years after the sixth failure (at 500,500 years) are shown in Figure 7-124 through Figure 7-127.

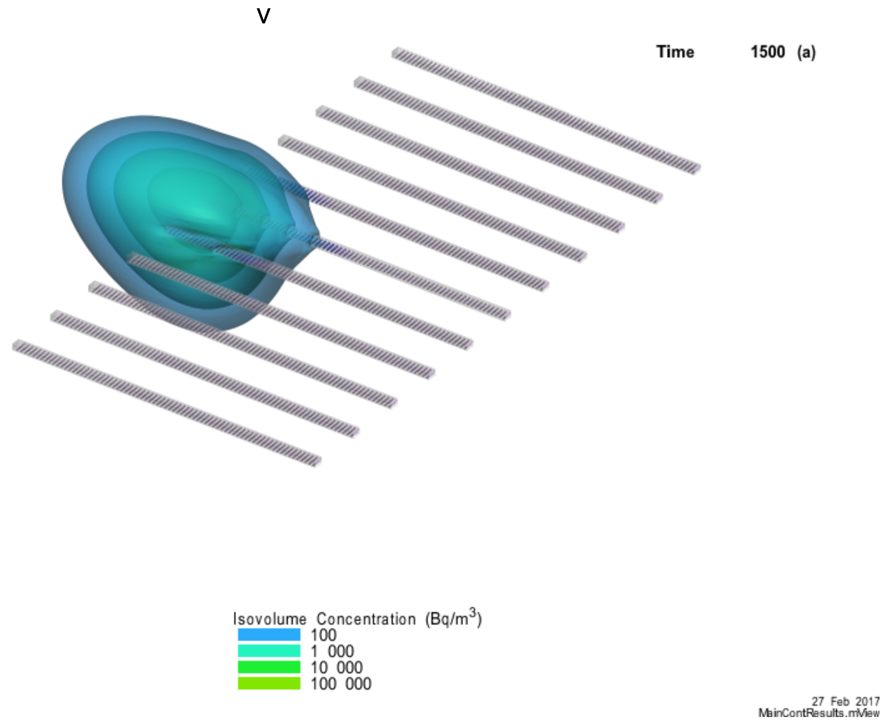

Figure 7-124: Main Container-Scale Model: Three-Dimensional Visualization of I-129 Concentration at 1500 a

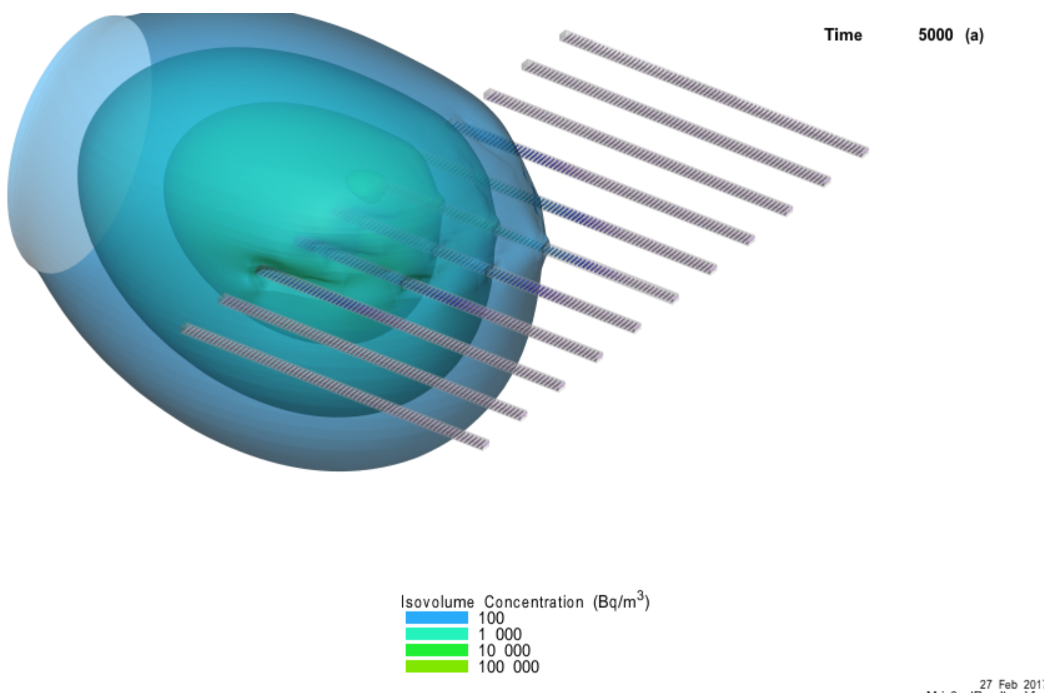

Figure 7-125: Main Container-Scale Model: Three-Dimensional Visualization of I-129 Concentration at 5000 a

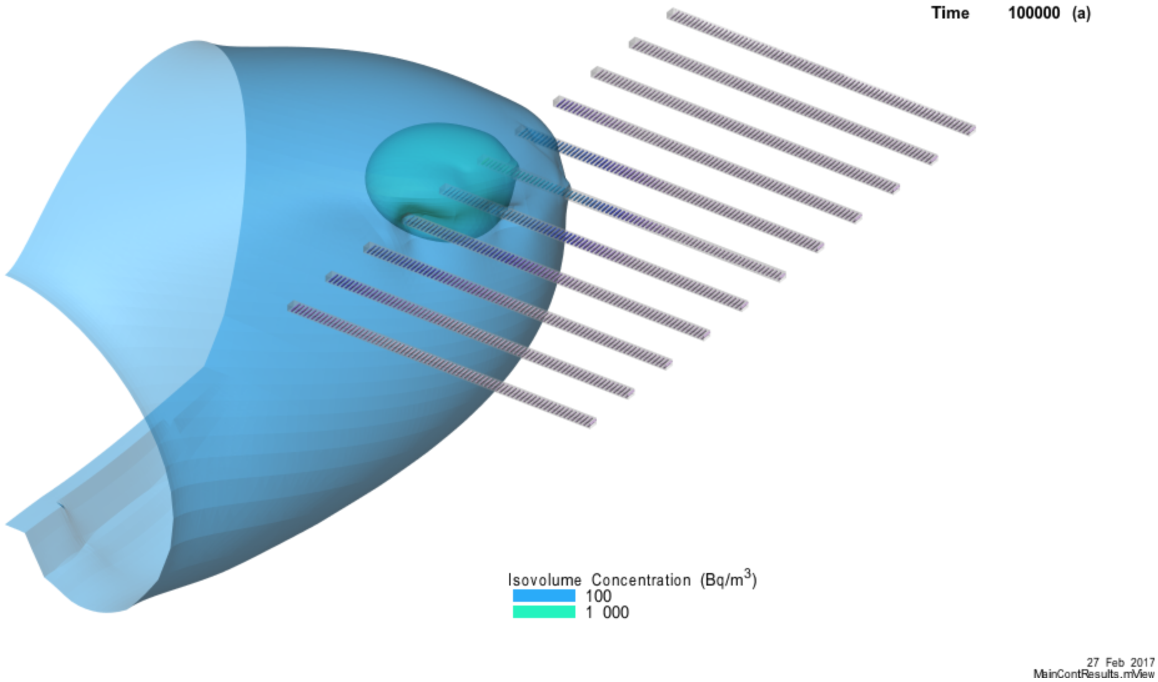

Figure 7-126: Main Container-Scale Model: Three-Dimensional Visualization of I-129 Concentration at 100 ka

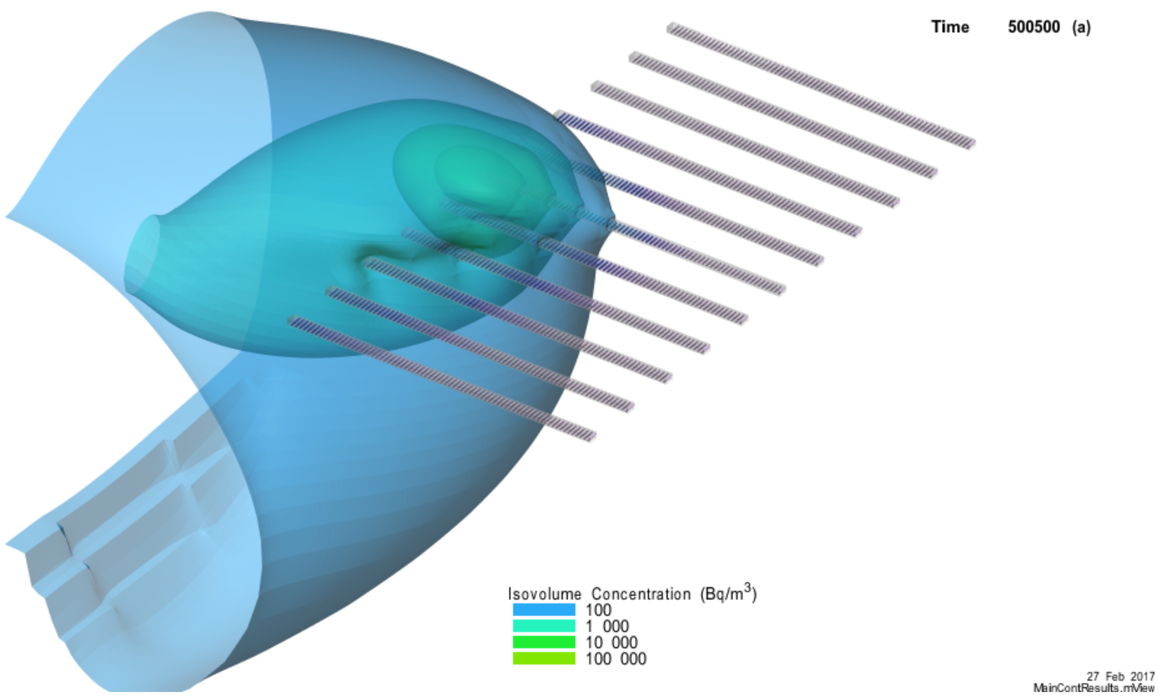

Figure 7-127: Main Container-Scale Model: Three-Dimensional Visualization of I-129 Concentration at 500.5 ka

Unlike I-129, U-238 is strongly sorbed onto sealing materials and the host rock. Consequently, transport of U-238 is limited to a very small domain immediately surrounding the defective container. Figure 7-128 and Figure 7-129 shows sectional views through the release plane and adjacent buffer after the second, third, sixth, and tenth container failures. The different defective container sources are apparent in the plots.

The contour plots are on a logarithmic scale. The 0.001 Bq/m³ concentration contour corresponds to an effective U-238 drinking water dose of about 0.00003 µSv/a (i.e., essentially zero) based on water consumption of 0.77 m³/a per person.

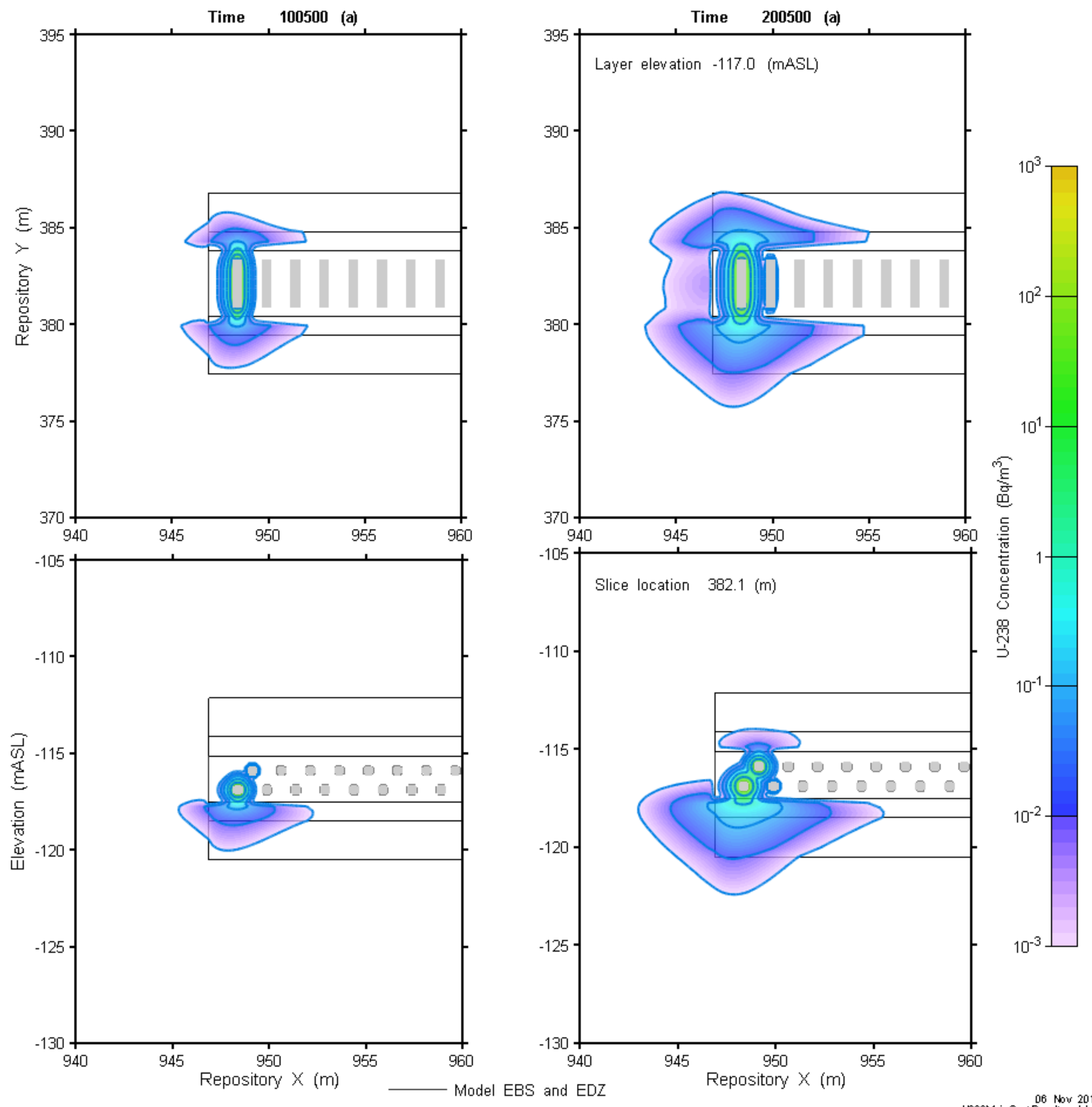

Figure 7-128: Main Container-Scale Model: U-238 Concentration at 100.5 and 200.5 ka

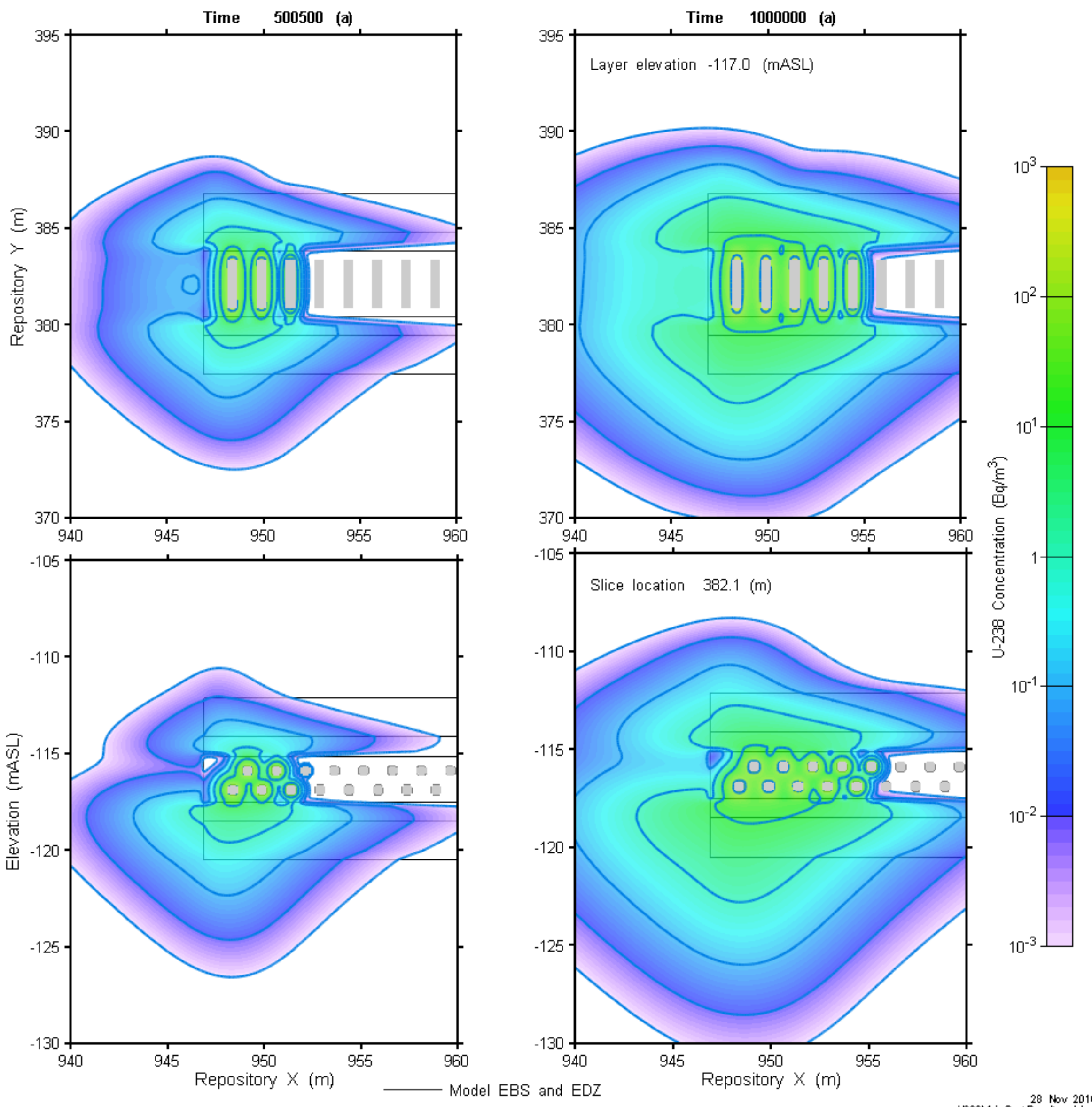

Figure 7-129: Main Container-Scale Model: U-238 Concentration at 500.5 and 1 Ma

Figure 7-130 and Figure 7-131 are three-dimensional views of U-238 plumes at 100.5 ka and 1 Ma, respectively. The limited extent of the plume expansion is evident.

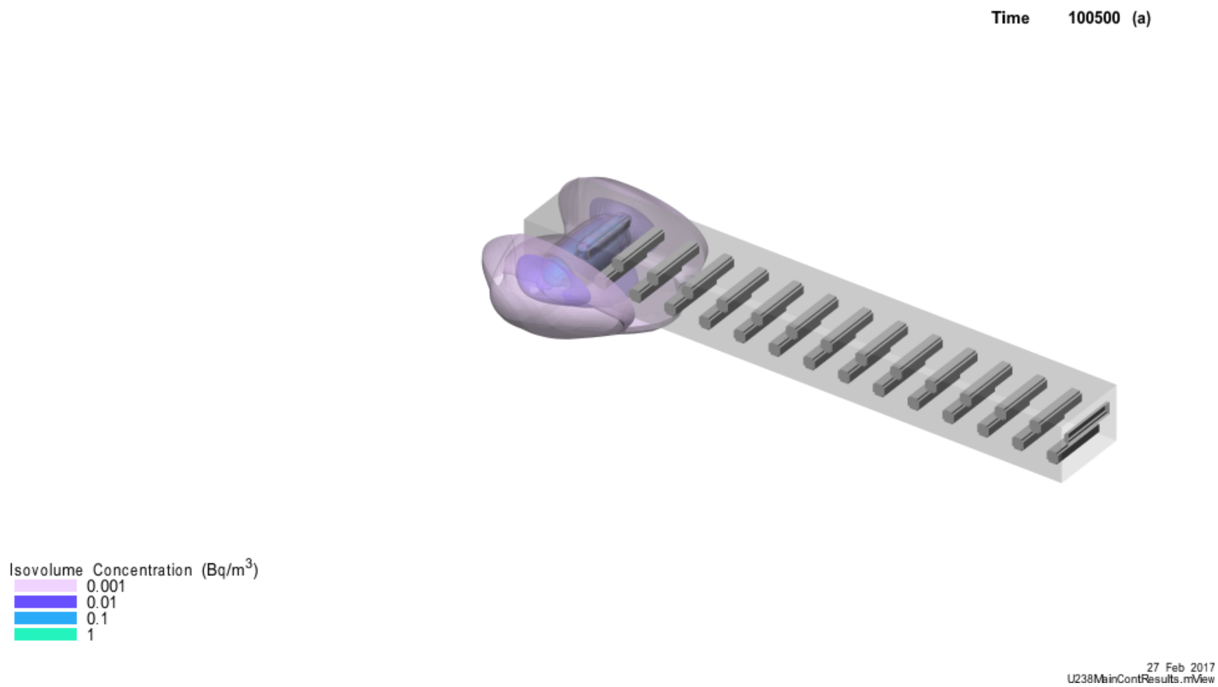

Figure 7-130: Main Container-Scale Model: Three-Dimensional Visualization of U-238 Concentration at 105 ka

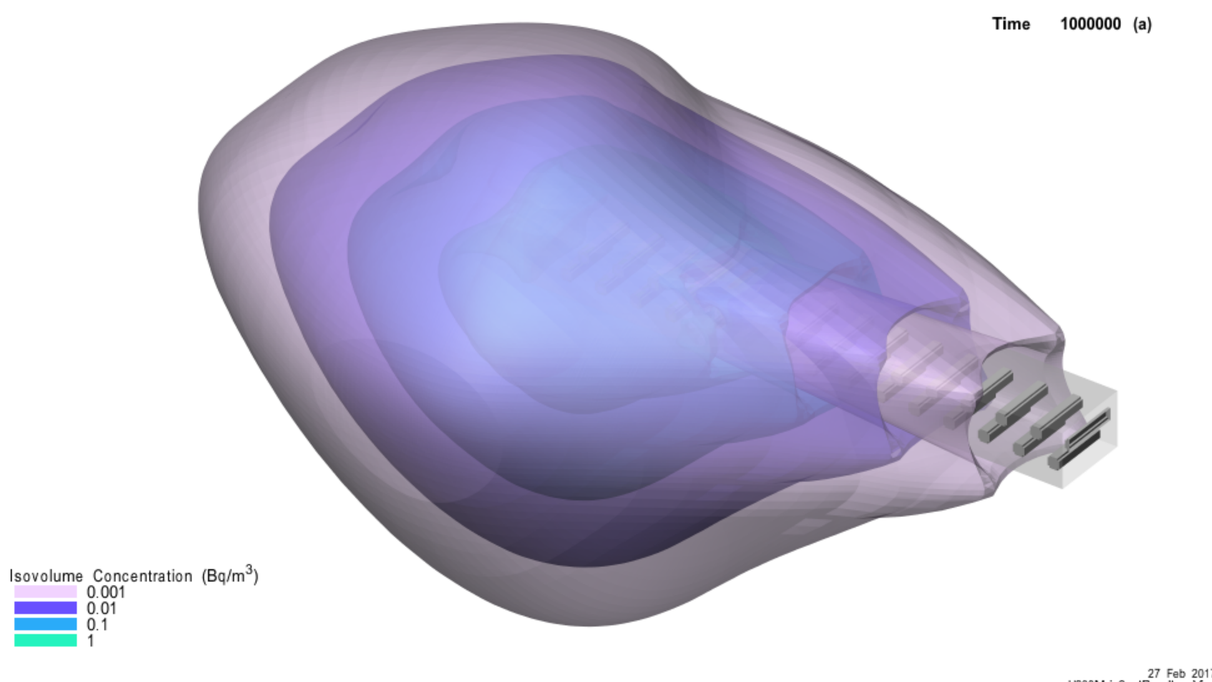

Figure 7-131: Main Container-Scale Model: Three-Dimensional Visualization of U-238 Concentration at 1 Ma

Figure 7-132 shows the Cs-135 plume at 100 and 500 ka. Figure 7-133 is a three-dimensional visualization of the Cs-135 concentration at 100 ka. Cs-135 is less strongly sorbed than U-238 but is still subject to retardation. The results show transport is largely confined to the vicinity of the source placement room. A 1 Bq/m^3 contour line corresponds to a Cs-135 drinking water dose of about 0.00015 μSv/a based on water consumption of 0.77 m^3/a per person.

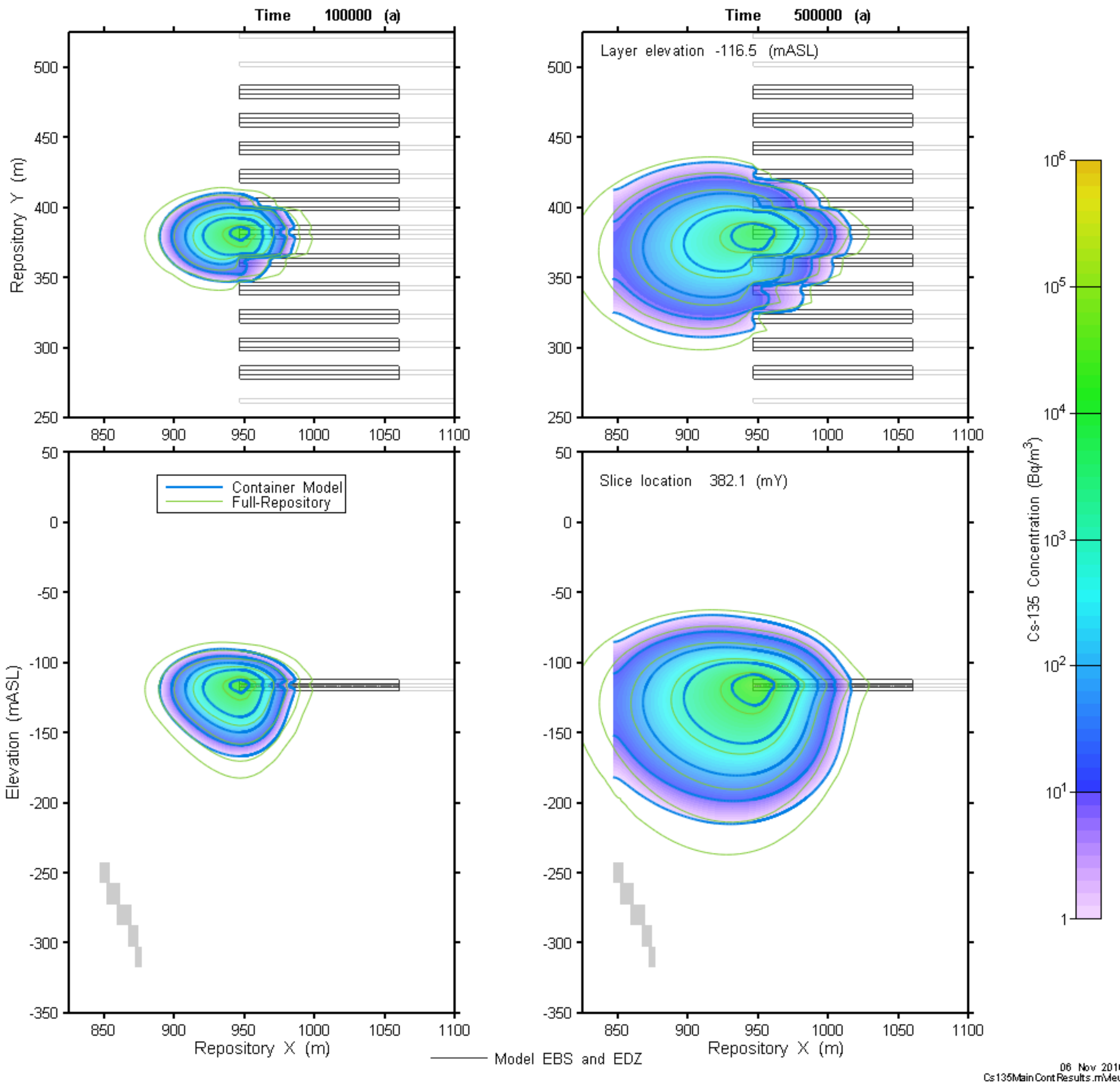

Figure 7-132: Main Container-Scale Model: Cs-135 Concentration at 100 and 500 ka

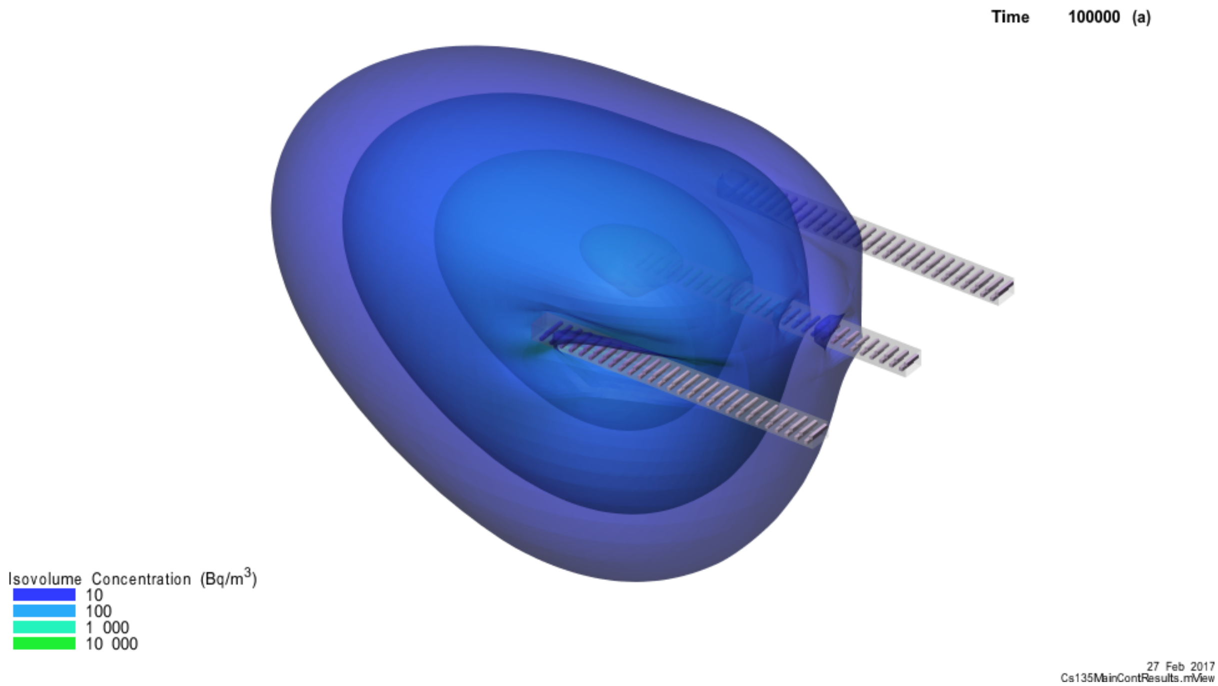

Figure 7-133: Main Container-Scale Model: Three-Dimensional Visualization of Cs-135 Concentration at 100 ka

Figure 7-134 and Figure 7-135 show summary results for all radionuclides considered. These figures show the transport rates out of the EBS and into the Inner EDZ across the inner boundary volume shown in Figure 7-139. The lower part of the figure compares cumulative activity released from the defective containers with that released from the EBS. The difference between the dashed (container release) and solid (EBS release) lines in the lower figure is the amount remaining (or decayed) within the placement room. For non-sorbing species (I-129 and Cl-36) the two curves are nearly indistinguishable, while sorbing species show differing degrees of retention, depending upon radionuclide specific sorption properties.

U-238 is plotted separately in Figure 7-135 because of the differences in activity.

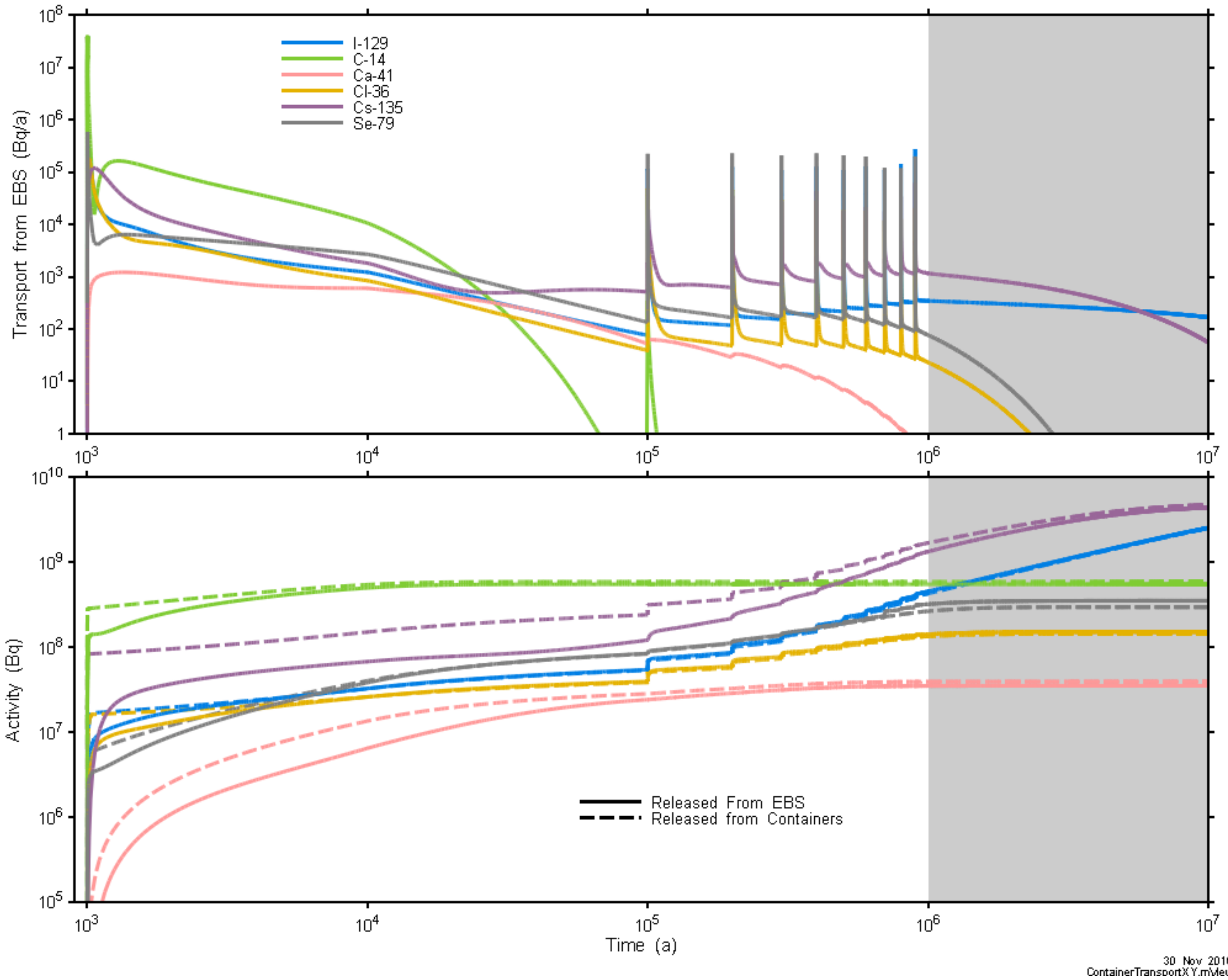

Figure 7-134: Main Container-Scale Model: Transport Rates and Cumulative Release for I-129, C-14, Cl-36, Ca-41, Se-79, and Cs-135

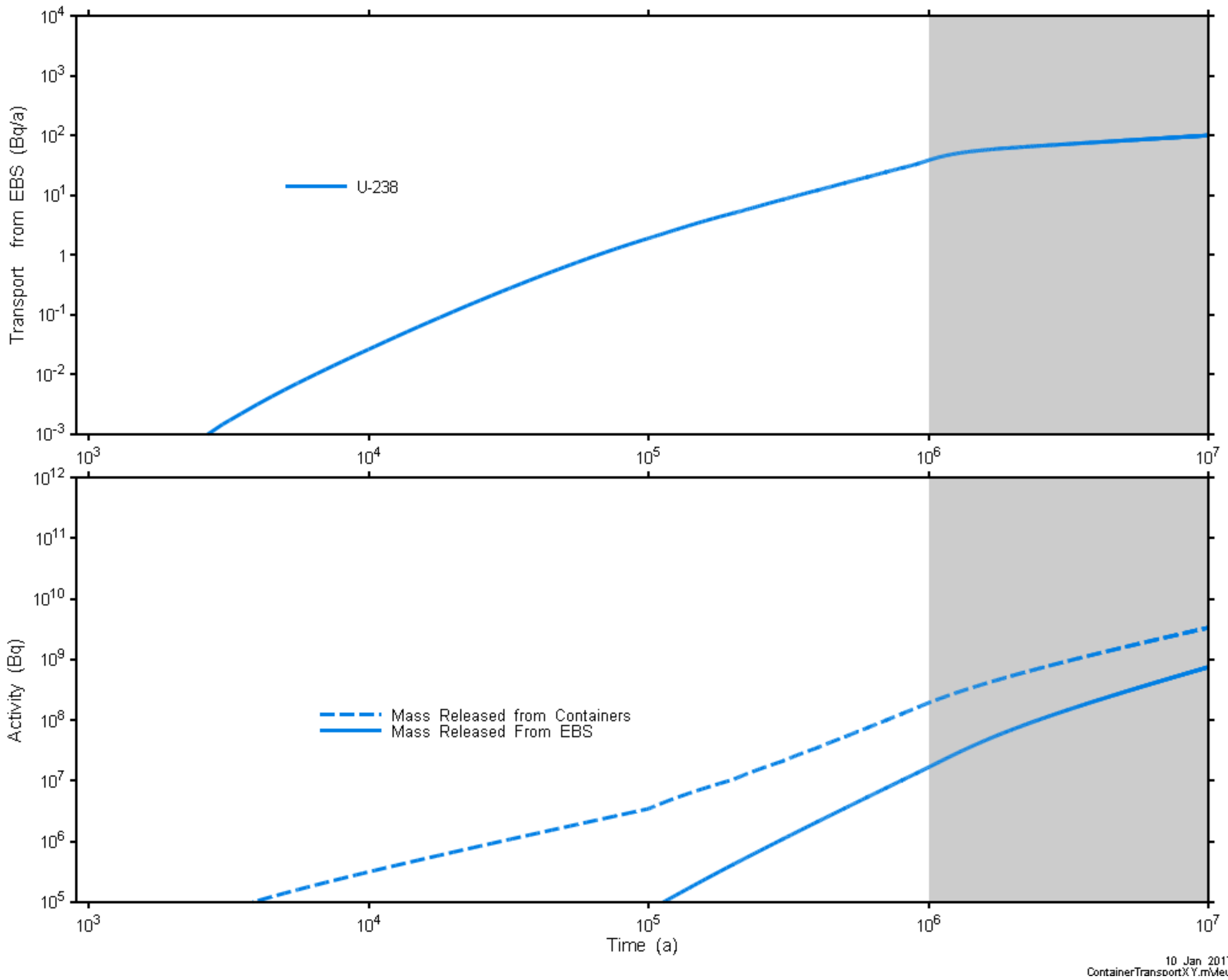

Figure 7-135: Main Container-Scale Model: Transport Rates and Cumulative Release for U-238

7.7.2.6 Effect of Barriers on Radionuclide Transport

This section provides information on the effect of the various barriers on radionuclide transport for the Base Case. Results shown here are determined using the detailed 3D Full Repository-Scale and Main Container-Scale Models.

Figure 7-136 through Figure 7-138 show the transport for I-129 (a non-sorbing fission product), Ca-41 (an intermediate sorbing fission product) and U-238 (a highly sorbing solubility limited actinide) through the various barriers. Each figure shows:

- The release rate from the defective containers. As noted in Section 7.5.1, the source term is determined with the SYVAC3-CC4 System Model and entered as input to the 3D simulations. The source terms are shown Section 7.5.2.2.
- The release rate from the bentonite surrounding the defective containers. This corresponds to transport through the gold hued surface in Figure 7-139.

- The release rate from the repository. In this case transport from the Inner EDZ to Outer EDZ is determined. For the Main Container-Scale Model transport is subsequently out of the EDZ and into the immediately adjacent intact rock at the end of the room. This corresponds to the pink hued surface in Figure 7-139.
- The release rate to the well and all surface locations.

The figures show the retarding effects of the various barriers on the transport of the different radionuclides.

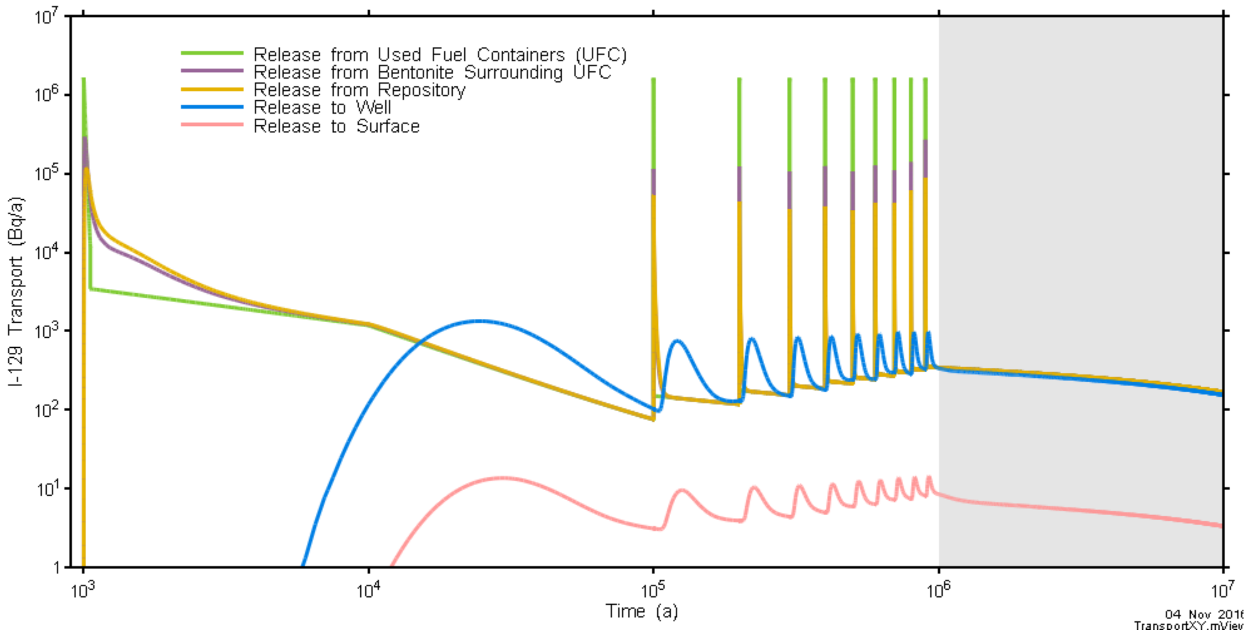

Figure 7-136: Full Repository and Main Container-Scale Models: I-129 Transport through Barriers

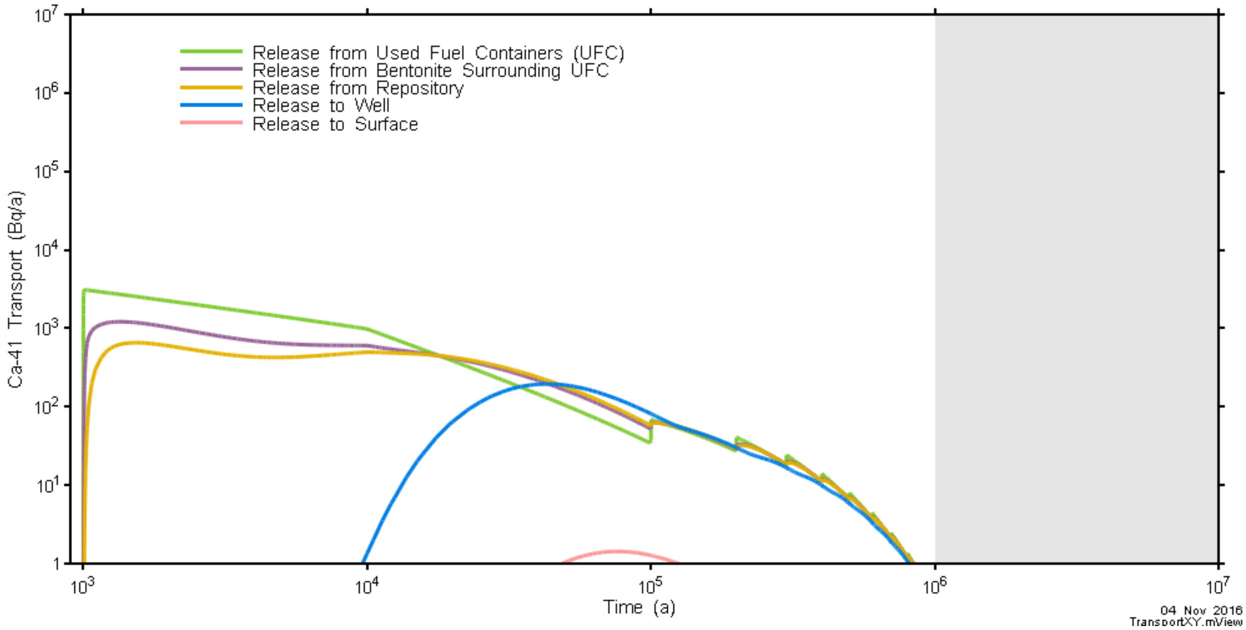

Figure 7-137: Full Repository and Main Container-Scale Models: Ca-41 Transport through Barriers

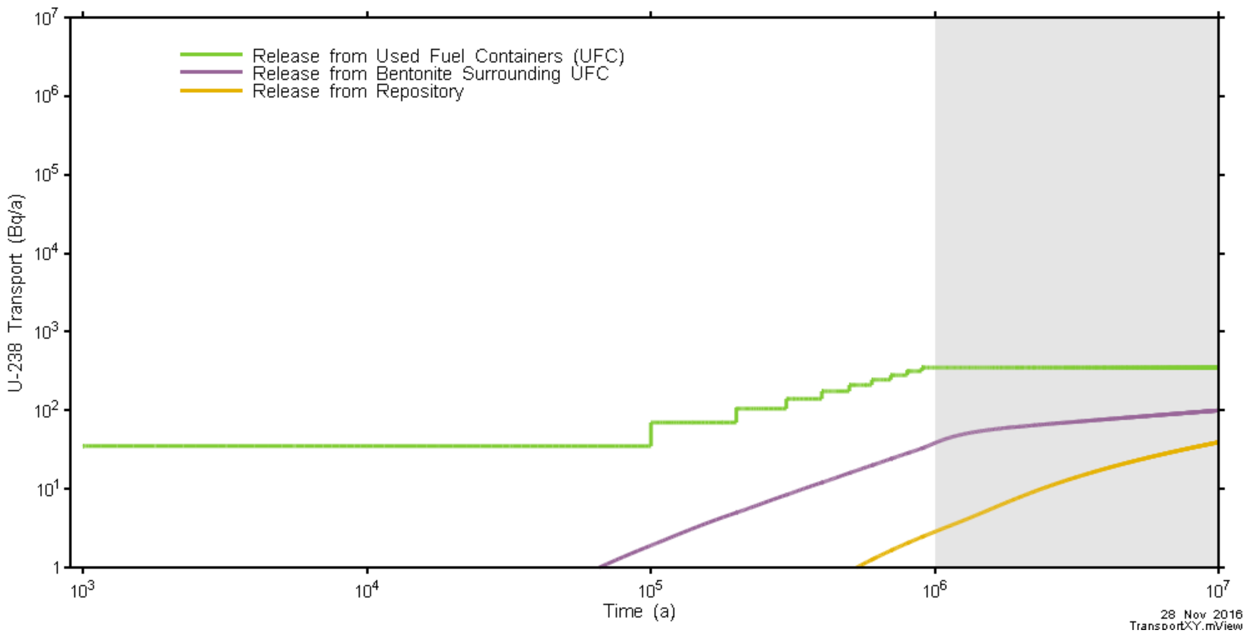

Note: there is no U transport to either the well or the surface

Figure 7-138: Full Repository and Main Container-Scale Models: U-238 Transport through Barriers

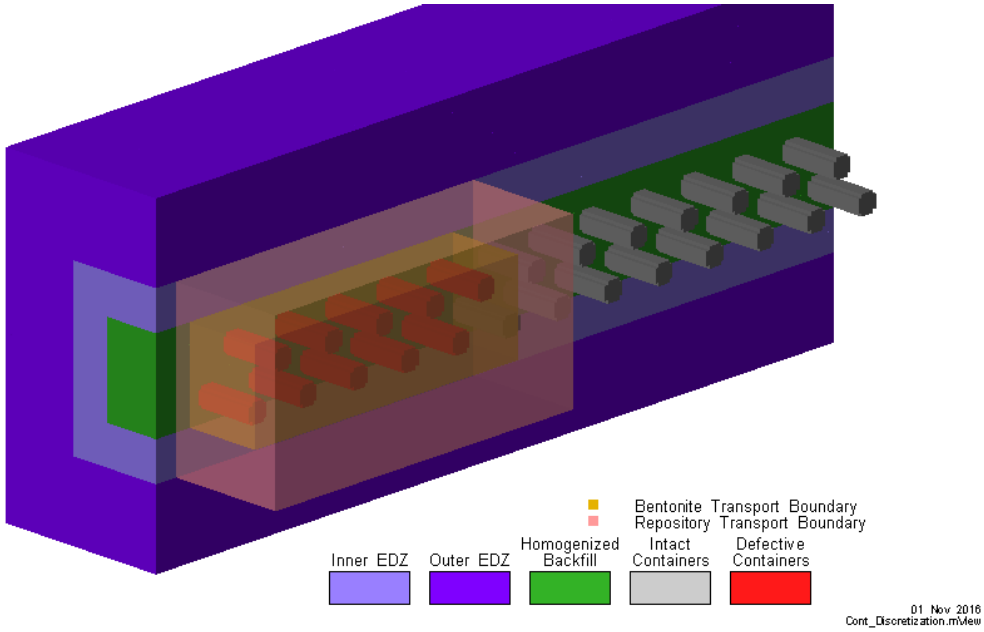

Note: the pink hued surface is set at the boundary between the Inner and Outer EDZ

Figure 7-139: Main Container-Scale Model: Transport Surface for the Bentonite and Repository Release

7.7.2.7 Summary of Results for 3D Modelling

Table 7-30 summarizes results for the sensitivity cases identified for examination with the FRAC3DVS-OPG code in Section 7.7.2. Modelling parameter sensitivity cases are not included.

Table 7-30: Summary of Results for 3D Modelling

Case	Peak I-129 Transport to Well (Bq/a)	Ratio to Base Case	Time of Peak Transport (a)
REFERENCE CASE	**0**	**-**	**-**
Sensitivity Cases			
Base Case (Full Repository-Scale Model)	1337*	-	25,000*
Base Case (Rooms Only Repository-Scale Model)	1400	-	24,200
Base Case – Intermittent Well	No effect for most times but up to 2492 if the well is turned on at the time of I-129 peak		
Base Case – Random Well	Could be many orders of magnitude less than the Base Case depending on the well location		
Buffer, Backfill and Seal Barrier Sensitivity			
EBS Hydraulic Conductivity Increased by a Factor of 10	1374*	1	24,100*
Geosphere Barrier Sensitivity			
Rock Hydraulic Conductivity Increased by a Factor of 10	725	0.52	4700
Rock Hydraulic Conductivity Increased by a Factor of 10 (with repositioned well / defective containers)	3679	2.6	5000
Rock Hydraulic Conductivity Decreased by a Factor of 10	460	0.33	1,020,000
EDZ Hydraulic Conductivity Increased by a Factor of 10	1540*	1.2	20,000*
Fracture Standoff Distance to 50 m	1538	1.1	17,000
Fracture Standoff Distance to 25 m	1526	1.1	13,400
Fracture Standoff Distance to 10 m	1473	1.1	11,200
Fracture Standoff Distance to 10 m (with repositioned well / defective containers)	2046	1.46	9,000
Dispersivity Increased by Factor of 5**	902	0.64	17,000
Dispersivity Decreased by Factor of 5**	2131	1.52	25.000

Note: Cases with '*' have been simulated with the Full Repository-Scale Model
'**': shown for illustration only as the Base Case values are already conservative

7.8 Modelling and Results for the System Model

The System Model combines an idealized geometric description of the repository and a computationally efficient geosphere transport model with more detailed representations of releases from the used fuel and radionuclide transport in the biosphere to compute the radiological consequences. It is implemented in the SYVAC3-CC4 code.

Confidence in the model is provided through comparison with results obtained for selected radionuclides from the detailed 3D Groundwater Flow and Transport Model (Section 7.8.1.4).

The description provided here applies to the situation in which the climate, biosphere and geosphere are constant throughout the simulation. The groundwater flow field is also constant.

7.8.1 Methods

7.8.1.1 Repository Submodel

The System Model represents the placement rooms as a series of concentric cylinders of varying thicknesses as shown in Figure 7-140 to approximate radionuclide transport through the buffer, backfill and excavation damaged zone. This simplification allows for the use of semi-analytical solutions which result in fast computation times suitable for use in probabilistic analyses.

Conceptually, the model represents one container within a placement room surrounded by concentric cylinders of buffer material, backfill material and EDZ. Because the conceptual repository in this study does not have a different placement room backfill, input data for the concentric cylinders are specified such that only homogenized buffer and gap fill (31.8 cm thick – corresponding to the minimum distance between the container and placement room wall) and placement room Inner EDZ (60 cm thick) are represented. The length of the concentric cylinder is about 390 m, corresponding to the length of the placement room. A semi-infinite boundary condition that maintains continuity of concentration and continuity of flux is established at the outer boundary.

The radionuclide release from the defective container is represented by a source that lies along the axis of the nested cylinder. The container is not physically represented.

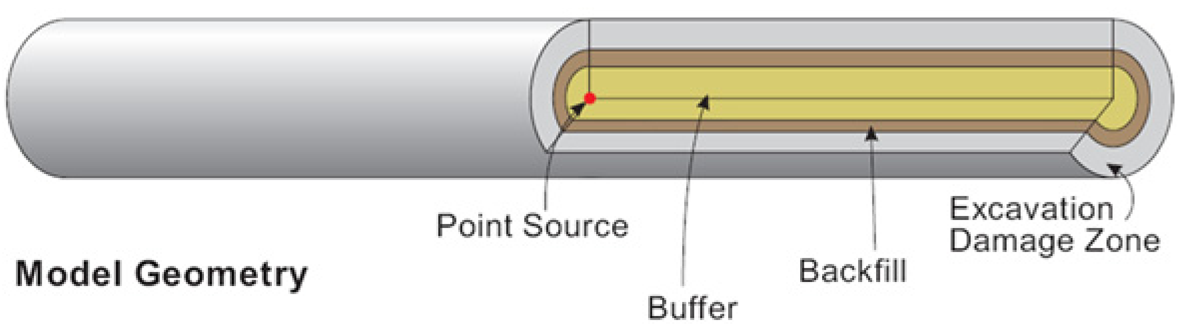

Note: the backfill thickness is 0 cm in the repository model used in this study.

Figure 7-140: System Model, Repository Submodel

The repository submodel simulates the following processes:

- Container Failure – At a specified time some of the containers are assumed to fail.
- Instant Release – A fraction of soluble fission products, representing the radionuclide inventory present at the UO_2 fuel grain boundaries and cladding gap is instantaneously dissolved once the container is breached and water comes into contact with the used fuel. A fraction of the C-14 in the Zircaloy is also released instantaneously when water contacts the Zircaloy.
- Congruent Release – A slow long-term radionuclide release occurs, consistent with the long-term corrosion / dissolution of the ceramic fuel pellet and release of radionuclides trapped within the fuel matrix. Radionuclides are also released from the Zircaloy as it corrodes.
- Precipitation – The precipitation of elements whose concentration in the container exceeds the solubility of the element.
- Radioactive Decay and Ingrowth – Radioactive decay of radionuclides and progeny.
- Transport – The diffusive and advective transport of radionuclides through the engineered barrier system. .

As discussed in Section 7.2.2.1, the defective containers are assumed to fill with water as soon as the steel vessel is breached in the Base Case, which itself is assumed to occur immediately upon full penetration of the copper coating, so that in the Base Case the first container, assumed to fail at 1000 years, is entirely full of water at 1000 years.

7.8.1.2 Geosphere Submodel

The geosphere is represented as a network of 1D transport pathways. Each 1D pathway represents a path in which transport is primarily in one direction, with relatively uniform material properties. This network is defined to approximate the hydrogeological and geochemical features of the geosphere zones located between the repository and the surface biosphere. Transport in each segment is characterized using the 1D advection-diffusion equation, for which robust semi-analytical solutions are available.

The starting point for generation of the System Model geosphere network is a detailed 3D steady-state groundwater flow field determined with the 3D code. From this, a set of pathways is generated that map how a particle released at the repository would move with the advective flow field. Assembly of the transport network, which also includes diffusion, then consists of the following steps:

- Sector Selection – The repository is divided into sectors. A sector is typically defined so that its properties are uniform. For example, it has the same waste form type and room length, and it connects to a portion of the groundwater flow field whose properties are approximately uniform for the entire sector. Different sectors typically have different properties, and often the properties of the surrounding geosphere are the delineating factor.
- Selection of Representative Pathways – A representative pathway for each sector is generally chosen to give the shortest travel time to the surface. In areas of low flow velocity, diffusion towards fractures (if present) may be the shortest travel path. Pathways may

merge with pathways from other sectors and may diverge as portions of the plume are captured by the well or terrestrial discharge areas.

- Selection of Nodes along Pathways – Nodes are generally selected at material property boundaries so that the resulting segments have constant properties.
- Addition of Well and Near-surface Nodes – Additional nodes are required for the well - for example, upper and lower reference nodes define the range of positions for the well and drawdown nodes, which give a better representation of the drawdown cone in the vicinity of the well. Also, near-surface nodes are added to define an overburden and a sediment node for each discharge location, and possibly terrestrial and wetland nodes associated with aquatic discharges.
- Property Assignment – Data needed include the cartesian coordinates of all the nodes, hydraulic heads and temperatures at the nodes, and hydraulic and chemical properties of the different geosphere zones.
- Well Model – The effects of the well drawdown on adjacent node heads is accounted for via an analytical well model within the aquifer, and by a site-specific well-effects model outside the aquifer.

Sector Selection

Since all containers contain the same used fuel waste form and the placement room design is common across the repository, the main distinction between the sectors is the influence of the surrounding groundwater flow field.

For this study, a set of 5396 advective flow transport pathways was generated, with the pathways starting in the placement rooms at the repository horizon. The 3D modelling identified five discharge locations, hereafter referred to as “Well”, “Central Wetland”, “East River”, “West River” and “South River”. The locations of these discharge zones are shown in Figure 7-141.

Figure 7-142 shows a repository map based on the 3D modelling results illustrating which of the 5396 transport pathways connect to each discharge zone (at the reference well demand of 911 m^3/s). This corresponds to the repository part of Figure 7-60.

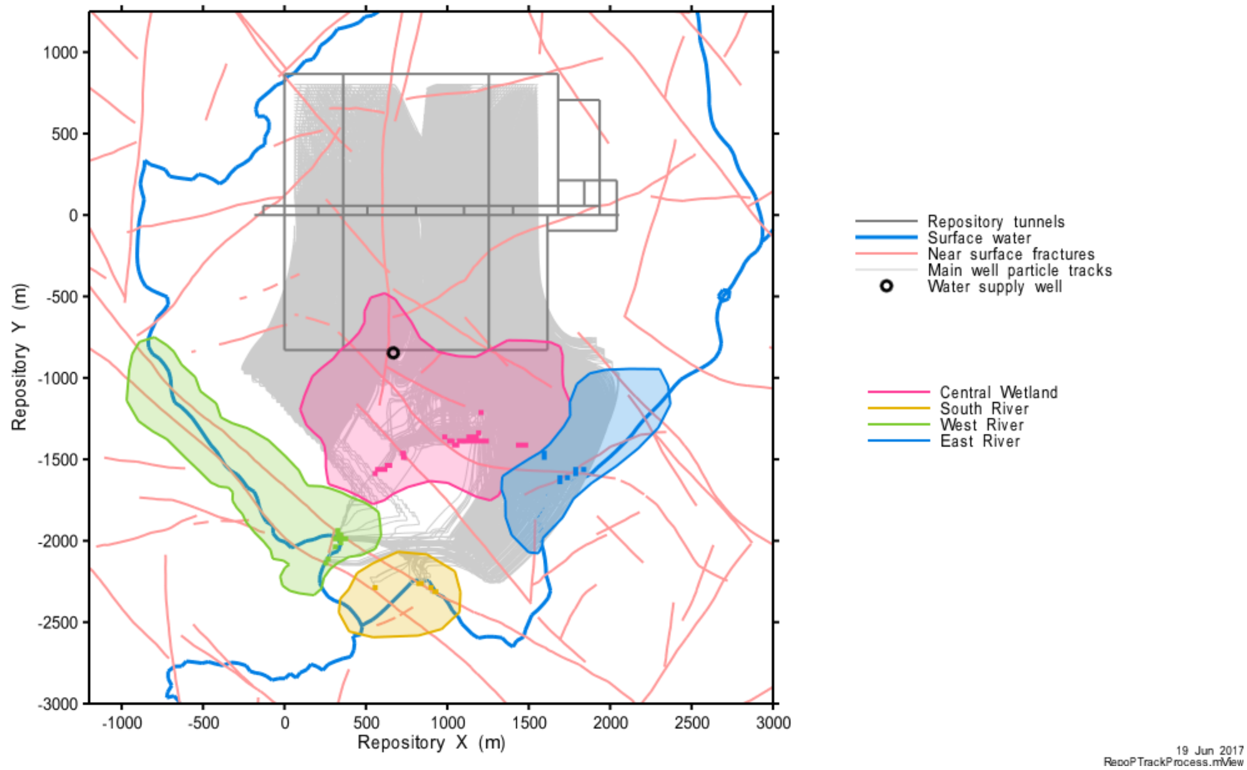

Figure 7-141: Repository-Scale Model: Surface Discharge Zones

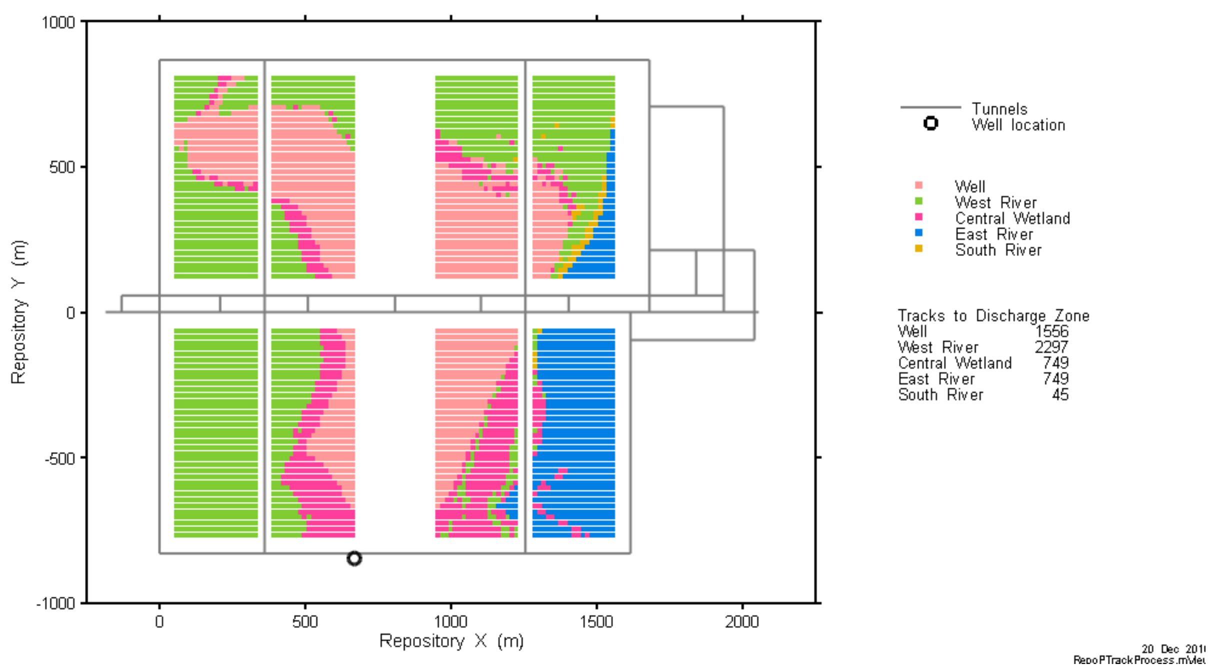

Figure 7-142: Repository-Scale Model: Origin and Discharge Locations of Advective Transport Pathways for a Well Demand of 911 m^3/a

These pathways are then used to create two similar, but different, geosphere submodels:

- Simple Geosphere Submodel: each of the 10 defective containers is modelled as a separate sector to allow for input of specific container failure times. The containers are clustered in the location that maximizes transport to the well, and their contaminants either discharge to the Well or to the Central Wetland area, depending on the well demand. No other containers are represented in this model. This model is used for the Normal Evolution Scenario and associated sensitivity studies, and for one of the two probabilistic assessment cases.
- Full Geosphere Submodel: the entire repository is divided into sectors, where each sector contains multiple containers and where sectorization depends on commonality of transport times and transport endpoints. All containers in the repository are represented in this model. This is used for the All Containers Fail Disruptive Event Scenario and for one of the two probabilistic assessment cases.

Selection of Representative Pathways

For each sector, a representative transport pathway is selected to approximate the transport segment leading to the surface discharge point(s). These pathways may converge and combine on the way to the surface, or conversely may diverge and lead to different discharge points, depending on conditions such as the well demand rate.

When choosing the representative pathway, the pathway from each sector with the shortest advective transport time is selected as a conservative approximation. Since these pathways are based on advective flow, radionuclides may move in different directions in regions where the transport is diffusion dominant. To account for this, in diffusion dominant regions the pathway is conservatively taken as the shortest distance to an area of advective flow that readily leads to the surface.

Selection of Nodes along Pathways

Transport pathways can converge and curve as they lead towards the discharge points. Nodes are defined at material property boundaries and at some intermediate points. Pathways are merged where appropriate, and divergence nodes are located where direction changes occur because of well operation.

Addition of Well, Overburden and Sediment, and Other Features

Four additional nodes are associated with the well. A well discharge node is located at the ground surface immediately above the well aquifer node (the resulting well depth is 100 m). A well capture algorithm determines how much of the contaminant plume is captured by the well.

For proper operation of the code, the surface water system is assumed to have both a terrestrial discharge node and an aquatic discharge node. The aquatic and terrestrial discharges have an overburden and associated sediment / soil node for a total of 4 additional nodes.

Property Assignment

Once the network is defined, physical and chemical properties are assigned to the various rock, fracture, overburden, and sediment nodes and segments.

Values for the hydraulic heads at each node location are obtained from 3D modelling results. Values for transport parameters such as porosity and hydraulic conductivity are supplied for each network segment. Advection is typically the dominant component of geosphere transport at shallow depths and in fractures; however, diffusion and dispersion processes are important in instances of very low advective flow (e.g., in the deep geosphere). The model accounts for both advective and diffusive transport processes.

Finally, retardation due to sorption is calculated using the sorption coefficient (Kd) assigned to each network segment.

Well Model

The well is located in a permeable zone capable of supplying sufficient water. This permeable zone is referred to as an “aquifer” although in the current study the actual location is a permeable subvertical fracture zone.

SYVAC3-CC4 uses an analytical solution to provide the hydraulic head drawdown at the nodes and the capture envelope for the groundwater flowing in the aquifer. The analytical solution is based on a constant head boundary condition at the discharge end of a non-leaky aquifer (where “non-leaky” means there is little inflow from the surrounding rock). The well model allows the assessment of well demands other than that in the Base Case, which is useful in assessing alternative lifestyles or critical groups, and in probabilistic calculations.

The analytical well model is calibrated with the detailed 3D groundwater flow field results. To approximate the groundwater velocities, the thickness of the well aquifer is adjusted, as is the hydraulic conductivity of some segments.

The effects of the well extend outside the well "aquifer". These cannot be calculated with the well model equations so the 3D modelling results for different well demands are used to derive empirical relationships that describe these effects. These include: drawdown at nodes outside the aquifer, plume fractionation towards the well at branching locations outside the well aquifer, and reduction factors for discharge areas due to capture of groundwater by the well.

7.8.1.2.1 Simple Geosphere Submodel

The process described in the previous section has been applied to develop the “Simple” Geosphere Submodel, where “Simple” means the model is developed specifically for the 10 containers assumed to fail in the Base Case. There is a single representative pathway, with this pathway adopting the properties of the pathway having the shortest transport time between the defective container location and the well / surface discharge areas as determined from the detailed 3D modelling.

The complete network for the Simple Geosphere Submodel consists of 40 nodes. The network and its connectivity are shown in Figure 7-143.

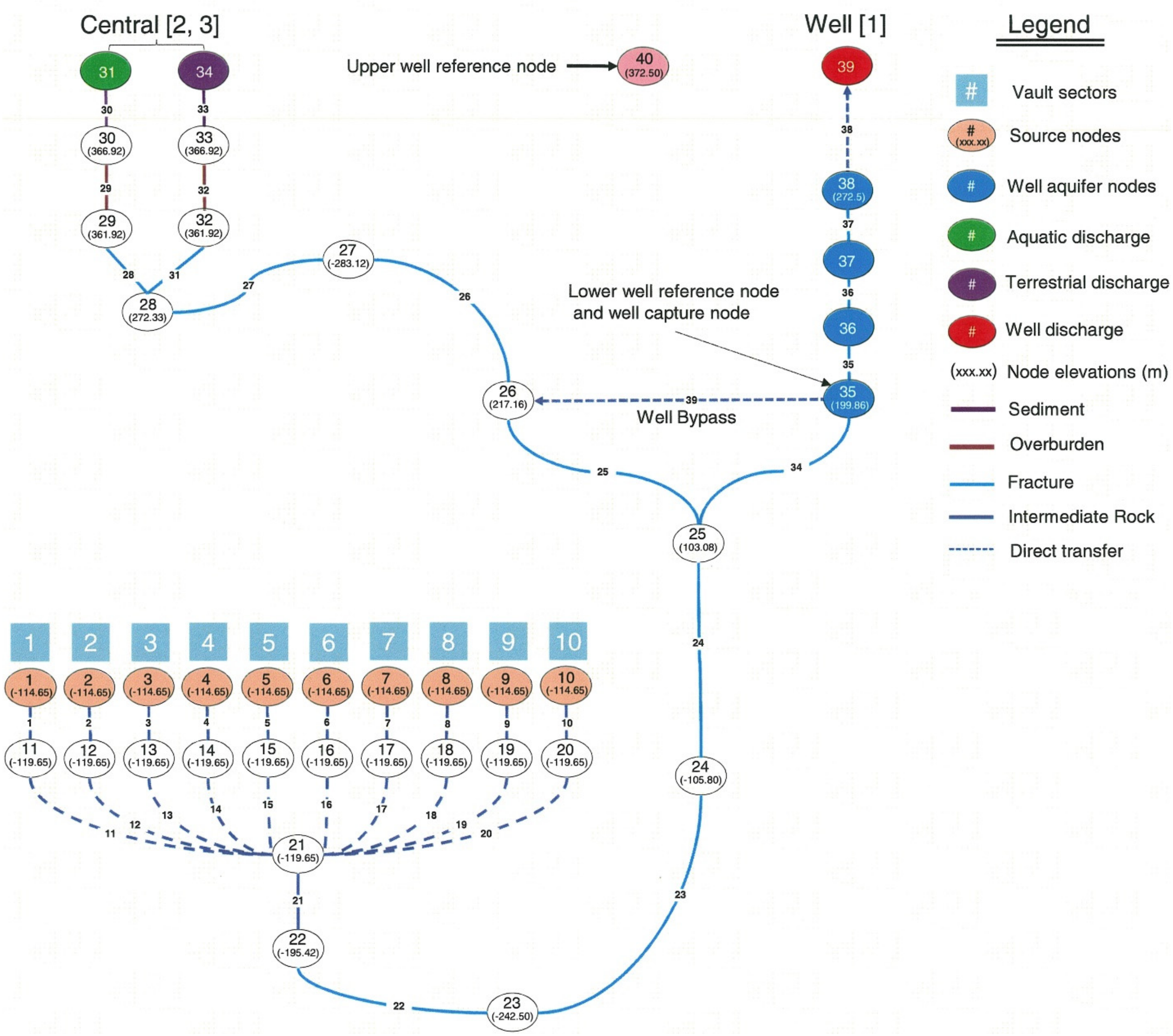

Notes: Only nodes (ellipses) with a particular function are colour coded. The line segments, representing the 1D transport pathways, are colour coded (see legend) to indicate the geosphere zone through which they pass.

Figure 7-143: System Model, Simple Geosphere Submodel: Transport Network Connectivity

Section 7.8.1.4.1 shows transport results generated with this model have good agreement when compared against similar results generated with the detailed 3D model.

7.8.1.2.2 Full Geosphere Submodel

Development of the Full Geosphere Submodel, representing the entire repository, also proceeds along the same lines as outlined in Section 7.8.1.2; however, the process is much more complicated than for the Simple Geosphere Submodel because the entire repository is represented.

Consideration of the discharge patterns from the 3D modelling gives an initial division of the repository into several sectors, these being determined by whether the discharge is to the Well, Central Wetland, East River, West River or South River areas. Further division is made based on consideration of the advective transport pathways and their associated travel times and routes. Because only 64 pathways (out of a total of 5396) terminate in the South River, the South River pathways have been combined with those leading to the other discharge areas to simplify the geosphere submodel.

The final division resulted in 14 unique repository sectors.

Figure 7-144 shows the repository sectorization and the associated discharge areas. Some sectors show multiple discharge areas because the discharge areas change depending on the well pumping rate.

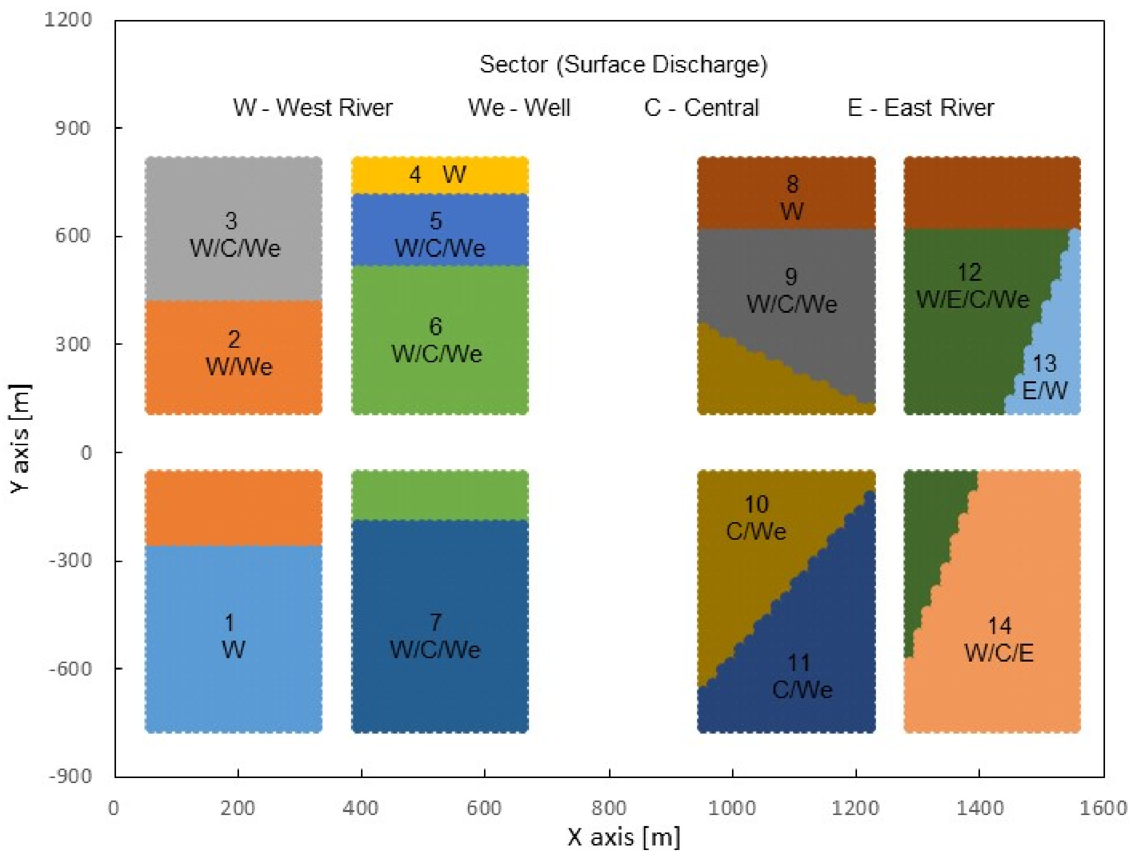

Figure 7-144: System Model, Full Geosphere Submodel: Repository Sectors and Surface Discharge Locations

Over 95,000 containers are distributed among the 14 sectors. The number of containers in each sector is obtained from the fraction of the 5396 total pathways that originate in that sector. Table 7-31 provides information on the number of containers and transport times for each sector.

Table 7-31: System Model, Full Geosphere Submodel: Container Distribution by Repository Sector

Repository Sector	Number of Containers	Well Demand = 0 m^3/a		Well Demand = 911 m^3/a	
		Discharge Location	Travel Time(a)	Well Capture (%)	Travel Time to the Well (a)
1	8773	West	$2.40x10^5$	0.0	-
2	8436	West	$4.86x10^5$	0.0	-
3	6749	West	$7.28x10^5$	53.7	$1.91x10^5$
4	1687	West	$8.55x10^5$	0.0	-
5	3374	Central	$1.81x10^5$	80.0	$1.69x10^5$
6	9111	Central	$4.97x10^5$	50.7	$1.63x10^5$
7	9786	West	$2.34x10^5$	25.4	$1.13x10^5$
8	6749	West	$3.46x10^6$	0.0	-
9	6394	Central	$4.39x10^4$	63.6	$4.96x10^4$
10	7690	Central	$3.03x10^4$	99.1	$3.01x10^4$
11	6500	Central	$1.15x10^5$	2.7	$1.43x10^5$
12	8543	West	$3.34x10^6$	23.5	$2.77x10^5$
13	1918	East	$6.65x10^5$	0.0	-
14	10123	East	$1.39x10^5$	0.0	-

The complete network consists of 181 nodes and 199 segments. This network and its connectivity is shown in Figure 7-145 (Part I) and Figure 7-146 (Part II).

Section 7.8.1.4.2 shows results generated with this model are generally conservative (i.e., releases occur earlier and are greater in magnitude than results obtained in the detailed 3D transport modelling).

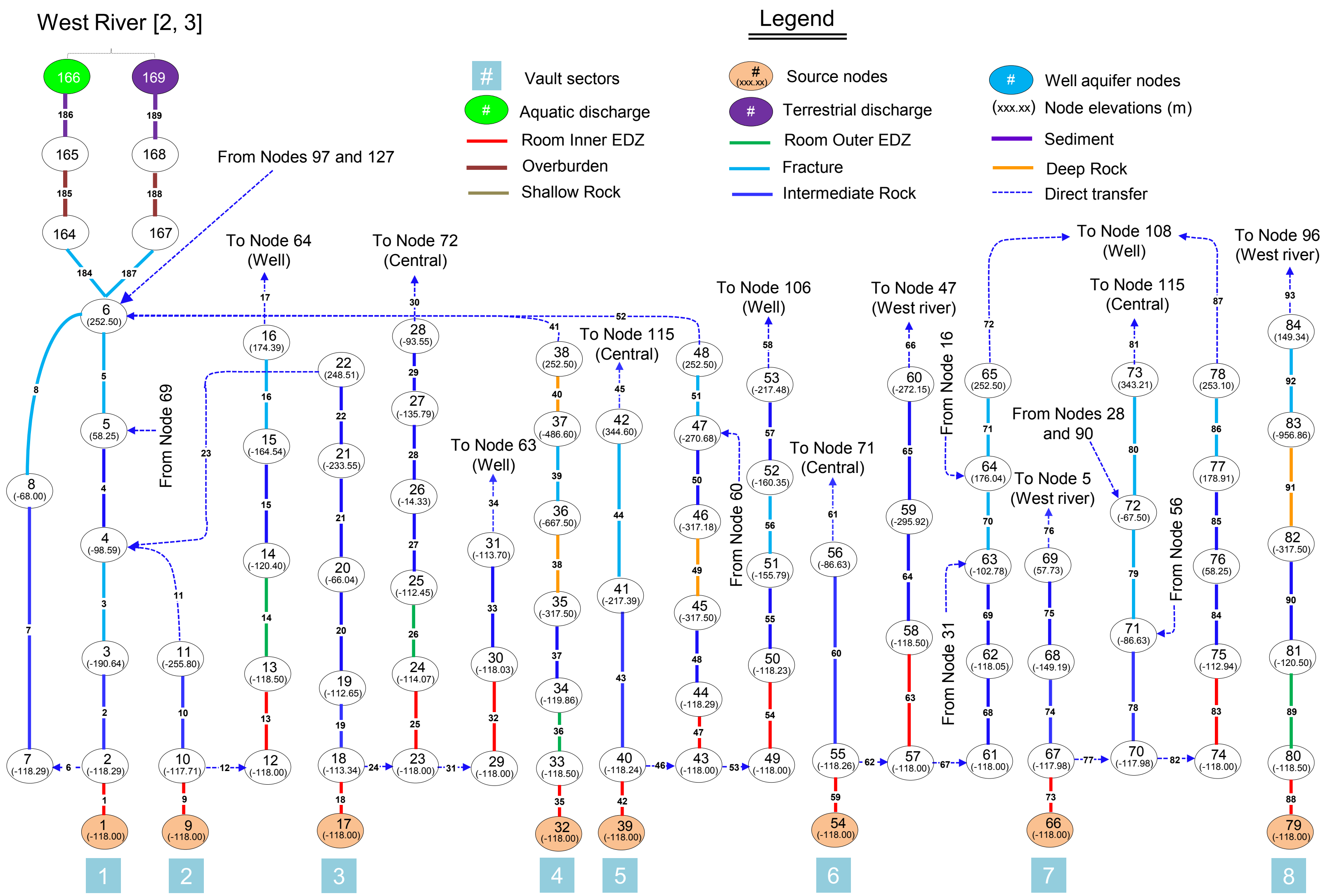

Figure 7-145: System Model, Full Geosphere Submodel: Transport Network Connectivity – Part I

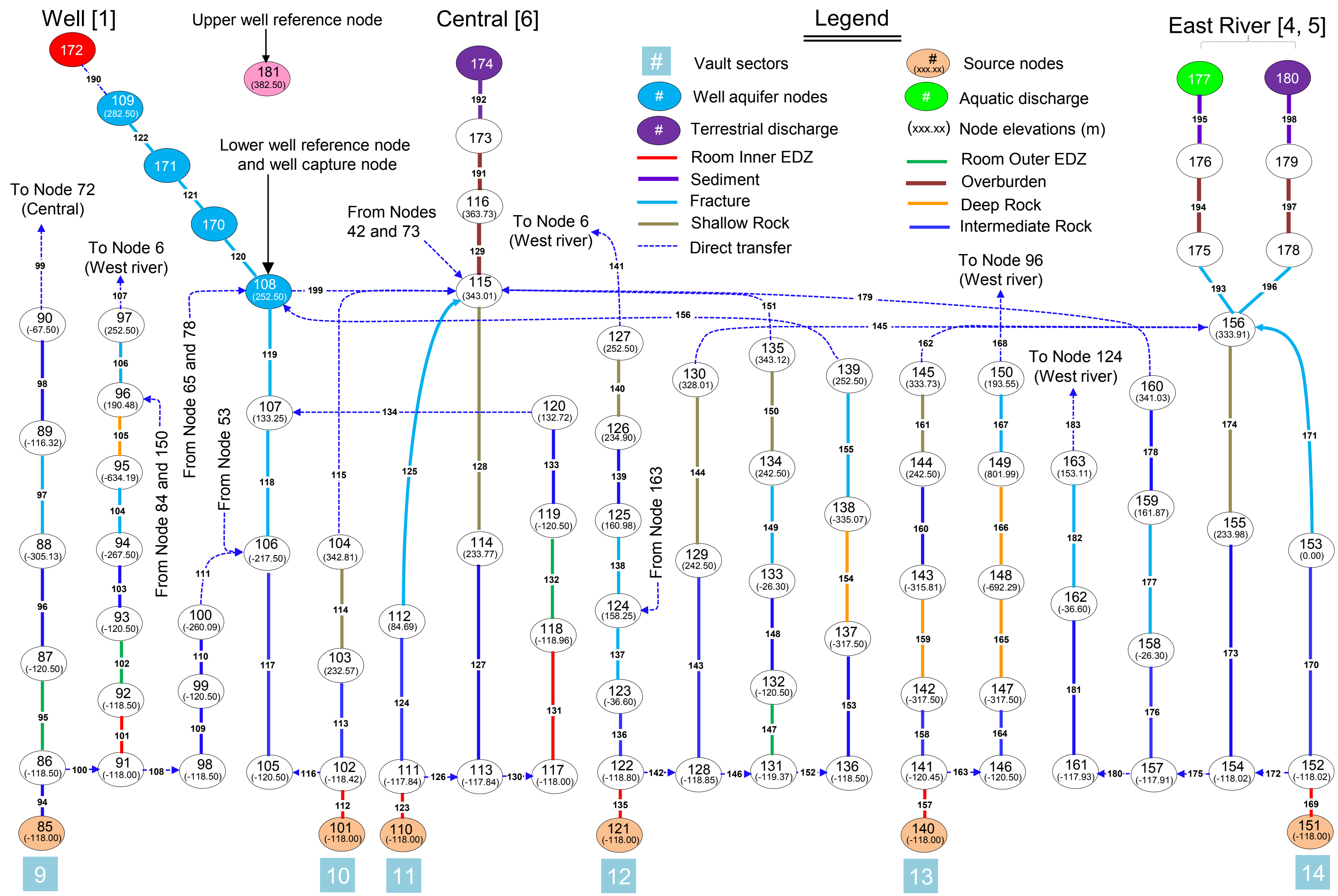

Figure 7-146: System Model, Full Geosphere Submodel: Transport Network Connectivity – Part II

7.8.1.3 Biosphere Submodel

The biosphere model represents a hypothetical but plausible Canadian Shield site.

The topography of the watershed area near the repository is relatively flat as shown in Figure 7-9. The local biosphere is assumed to have the characteristics of the Shield region and its properties are assumed constant during the simulation period. The normal present-day variation of climate and other biosphere parameters is included via the use of probabilistically sampled parameter values.

Key elements of the model are discussed below. A detailed description of the input data used in the model is available in Gobien et al. (2016).

Surface Water

Radionuclides discharging from the geosphere enter one or more topological low points. It is conservatively assumed that radionuclides discharging to the well also simultaneously end up in the West River, East River and Central Wetland discharge areas. This allows local biosphere transfer processes such as runoff, recycling and atmospheric suspension and deposition to be treated very simply. The transport processes considered in the surface water submodel are:

- Discharge to West River, East River and Central Wetland – direct discharge from the geosphere into the rivers, or central wetland area.
- Sedimentation – contamination of sediments by settling of particulates in the water.
- Biological Uptake – uptake of contaminants by plants and animals residing in the surface water bodies.
- Suspension and Volatilization – loss of contaminants from the surface water to the atmosphere.
- Outflow – flow of contaminated water further downstream. The impact of contaminant releases to the downstream environment is not assessed since they are bounded by the site impacts.
- Irrigation – well water or surface water can be used as the water source for irrigation of soil. In the current study well water is used for irrigation of gardens. The forage field is not irrigated.
- Domestic Use – human water use for drinking, cooking, bathing, laundry, and watering livestock.

Table 7-32 shows the surface water discharge areas. Since discharges are to low-lying areas, they may be covered in part by water. Table 7-32 also provides information on the relative proportions of the discharge areas covered by water.

Table 7-32: System Model, Biosphere Submodel, Surface Water Discharge Areas

Discharge Zone	Area of Discharge Zone [m^2]	Range of Discharge Zone Area* [m^2]	Aquatic Discharge Fraction*	Terrestrial Discharge Fraction*
West River	3.4×10^4	1.9×10^4 - 1.46×10^5	0.14 (0.12-0.19)	0.86 (0.81-0.88)
East River	1.5×10^4	6.0×10^3 – 3.7×10^4	0.35 (0.25-0.45)	0.65 (0.55-0.75)
Central Wetland	2.32×10^5	1.05×10^5 - 3.24×10^5	0.0	1.0

Notes: * Discharge area and discharge fractions are described by triangular distributions. The range is determined through consideration of areas defined by concentration profile reaching the surface. See Gobien et al. (2016) for further information

Soil

The soil model calculates the concentration of contaminants in the surface (rooting or cultivated) soil layer. This layer is assumed to be well-mixed due to, for example, plowing in an agricultural field or bioturbation. Two soil models are considered, one for upland soil and one for shallow soil. The upland soil model describes a typical soil layer, with the water table a reasonable distance below the surface soil layer. In the shallow soil model, the water table extends into the surface soil layer on a regular and extended basis (as in the case of marsh or swamp land). The distinction between these two soil types is important in determining how readily contaminated groundwater can reach the surface. In the upland soil model, it must be transported by processes such as capillary action while in the shallow soil model groundwater is discharged directly into the surface soil.

Areas of surface soils have specific designations including use as a vegetable garden, a forage field, and a woodlot. Some of the parameters describing the transport pathways in the soil model are dependent on the type of field (e.g., irrigation rate).

The transport processes considered in the soil model are:

- Irrigation – contaminated water from the well or surface water is added to the soil.
- Groundwater Discharge – direct discharge from a contaminated groundwater water source below the surface soil (shallow soil only).
- Capillary Rise – upwelling of contaminated groundwater from the water table (upland soil only).
- Leaching – contaminants in surface soil migrate to deeper soil layers as water percolates through the soil layer.
- Runoff – precipitation runoff from the watershed area entering the water body.
- Root Uptake – uptake of contaminants by plants and trees.

- Suspension and Volatilization – loss from the soil to the atmosphere due to soil resuspension (wind erosion) and volatilization.
- Deposition – deposition of contaminants from the atmosphere onto surface soils.

For context, some of the physical characteristics of the soil at the hypothetical site are described in Table 7-33 (Gobien et al. 2016). These reflect the values in CSA (2014) where available.

Table 7-33: System Model, Biosphere Submodel, Soil Properties

Parameter	Base Case Value	Comment
Soil types	As per comment column	Distribution of soil types on Canadian Shield: 57% sand, 14% organic, 24% clay, and 5% loam. Soil properties (e.g., sorption coefficient) depend on soil type.
Active surface soil depth	0.2 m	This is the active or root zone layer for which radionuclide concentrations in the soil are determined.
Soil depth to water table	1.5 m	Normal PDF, 1.5 m mean, 0.5 m standard deviation, and bounds of 0.01 to 2.5 m.
Minimum soil depth to water table for upland soil model	0.5 m	This is the minimum depth-to-water-table at which the upland soil model is used. For smaller depths, a shallow soil model is used that allows for flooding of the surface soil by contaminated groundwater.
Upland soil leach rate fraction	0.55	Fraction of net precipitation (precipitation + irrigation - evapotranspiration) that infiltrates into soil. The remainder runs off along the surface. Uniform PDF from 0.1 to 1.

Note: Data taken from Gobien et al. (2016).

Atmosphere

The atmosphere model calculates radionuclide concentrations in air due to the following transport processes:

- Suspension and Volatilization – contamination of the air from particulate or gaseous releases from surface water (if present) and soil.
- Dispersion – reduction in the concentration of contaminants in the air by having them disperse over a larger area.
- Fire – release of contamination into the air from fires assumed to occur on-site. This includes fuel fires used by the critical group as well as natural fires such as a forest fire.

A list of parameters important to the concentration of airborne contaminants is given in Table 7-34 (Gobien et al. 2016). When calculating the concentrations in the atmosphere, all contaminants are conservatively assumed to be located within a couple of metres above the land surface.

Table 7-34: System Model, Biosphere Submodel, Climate and Atmosphere Parameters

Parameter	Base Case Value	Comment
Annual total precipitation	0.76 m/a	Geometric mean of annual averages from 1983 to 2006 in Geraltdon (ON), which was identified as having a climate representative of the Canadian Shield. Normal PDF with a SD of 0.12 and bounds of 0.28 and 1.92 m/a. Lower and upper bounds represent half the minimum and double the maximum annual precipitation.
Annual average runoff	0.31 m/a	This is the balance between total precipitation and evapotranspiration, and includes surface runoff as well as infiltration into the water table. Normal PDF with mean of 0.31 m/a, standard deviation of 0.08 m/a, and bounds of 0.01 and 0.71 m/a.
Average wind speed	2.36 m/s	Normal PDF with mean of 2.36 m/s (8.5 km/h), standard deviation of 0.64 m/s, and bounds of 0.44 and 6 m/s.
Dry deposition velocity	0.006 m/s	Lognormal PDF with geometric mean of 0.006 m/s and geometric standard deviation of 2.
Atmospheric dust load	3.2×10^{-8} $kg_{drysoil}/m^3_{air}$	Lognormal PDF with geometric mean calculated from suspended particulate matter concentrations in Ont, NB, Que and Sask during years 1996 to 2002. Geometric standard deviation (GSD) of 1.7 with bounds of 7.0×10^{-9} and 7.5×10^{-8} $kg_{drysoil}/m^3air$.
Atmospheric aerosol load	2.9×10^{-10} m^3_{water}/m^3_{air}	Lognormal PDF with geometric mean of 2.9×10^{-10} m^3_{water}/m^3_{air}, and GSD of 1.41. Based on estimate for sea salt aerosol over oceans.
Washout Ratio	630 000	CSA (2014) washout ratio for deposition to plants for all elements other than noble gases and iodine. This value is conservative for iodine. CSA (2014) recommends 200 000 for elemental iodine and 8400 for organic iodine.

Note: Data taken from Gobien et al. (2016).

Dose Calculations

The dose model uses the concentrations of radionuclides in the various biosphere compartments to calculate the annual dose to a member of the critical group.

To ensure that dose rates are not underestimated, conservative assumptions are made concerning the characteristics of the critical group. Specifically, it is assumed that the members of the critical group spend all their lives in the local biosphere and obtain all their food, water, fuel and building materials from the local biosphere. The water source for the critical group is a well that intercepts the radionuclide plume. Their food includes plants grown in a garden, domesticated animals and fish. All plant and animal biota used as food are subject to contamination from surface water, soil and air. This lifestyle is consistent with but more self-sufficient than typical current habits and leads to an overestimate of the impact. Because of these characteristics, the hypothetical member of the critical group is referred to as a Self-Sufficient Farmer. The Self-Sufficient Farmer has been found in previous studies to be a good indicator of risk for a range of plausible lifestyles (Garisto et al. 2005).

Some critical group lifestyle characteristics are shown in Table 7-35 (Gobien et al. 2016).

Table 7-35: System Model, Biosphere Submodel, Human Lifestyle Data

Parameter	Reference Case Value	Comment
People per household	3	Piece-wise uniform PDF from 1 to 12 people.
Domestic water demand per person	110 m^3/a	Lognormal PDF with geometric mean 110 m^3/a, geometric standard deviation of 2 and bounds of 40 and 240 m^3/a.
Total energy needs per person	18744 kJ/d	Fixed value, set conservatively high at 90^{th} percentile value.
Man's air inhalation rate	8400 m^3/a	95^{th} percentile
Man's water ingestion rate	840 L/a	90^{th} percentile
Man's meat ingestion rate	103 g/d	Median intake for male adult. Defined as lognormal PDF with geometric mean equal to median and geometric standard deviation equal to 1.65. For a total energy intake of 18744kJ/d, this intake is prorated to 249 g/d.
Man's milk ingestion rate	283 g/d	Median intake for male adult. Defined as lognormal PDF with geometric mean equal to median and geometric standard deviation equal to 1.35. For a total energy intake of 18744kJ/d, this intake is prorated to 685 g/d.
Man's plant ingestion rate	796 g/d	Median intake for male adult. Defined as lognormal PDF with geometric mean equal to median and geometric standard deviation equal to 1.65. For a total energy intake of 18744 kJ/d, this intake is prorated to 1928 g/d.
Man's poultry ingestion rate	53 g/d	Median intake for male adult. Defined as lognormal PDF with geometric mean equal to median and geometric standard deviation equal to 1.65. For a total energy intake of 18744 kJ/d, this intake is prorated to 128 g/d.
Man's fish ingestion rate	7.9 g/d	Median intake for male adult. Defined as lognormal PDF with geometric mean equal to median and geometric standard deviation equal to 4.48. For a total energy intake of 18744 kJ/d, this intake is prorated to 19 g/d.
Soil ingestion rate	0.12 kg/a	95^{th} percentile of incidental soil ingestion rate.
Annual energy consumption per household	$1.2x10^5$ MJ/a	Normal PDF with mean of 1.2×10^5 MJ/a, standard deviation of 8×10^3 MJ/a and bounds of 10^5 MJ/ and 1.3×10^5 MJ/a.
Building occupancy factor	0.8	Fixed value
Building air infiltration rate	0.35 /hr	Fixed value, minimum recommendation for tightly-sealed house.

7.8.1.4 Verification of the System Model

In this section, transport results for the two System Models described above (i.e., one with the Simple Geosphere Submodel and one with the Full Geosphere Submodel) are compared against similar results obtained from the detailed 3D simulations. Comparisons for I-129, C-14, Ca-41, Cl-36, Cs-135, Se-79, and U-238 are made, thereby providing a cross-verification of the SYVAC3-CC4 and the FRAC3DVS-OPG code implementations of each of these models.

The Simple Geosphere Submodel is compared for the Base Case Normal Evolution Scenario, while the Full Geosphere Submodel is compared for the All Containers Fail at 60,000 Years Disruptive Event Scenario.

7.8.1.4.1 Simple Geosphere Submodel - Transport Comparison

“Simple” means the model has been developed specifically for the 10 containers assumed to fail in the Base Case. There is a single representative pathway, with this pathway adopting properties based on those in the detailed 3D simulations for the pathway with the shortest transport time between the defective container location and the well / surface discharge locations.

The 3D transport results used in the comparison are described in detail in Section 7.7.2.3.3.

<u>Near-Field Transport Comparison</u>

Transport from the container to the geosphere for the Base Case is compared with the detailed 3D Container-Scale Model results in Figure 7-147 and Figure 7-148. Transport is across the surface of the pink hued rectangular block in Figure 7-139 while transport in the System Model is across the outer surface of the grey cylinder in Figure 7-140. In both cases, the surface represents the boundary between the Inner EDZ and the rock around a placement room.

The 10 peaks are due to the instant release term from each the 10 containers assumed to fail in the Base Case.

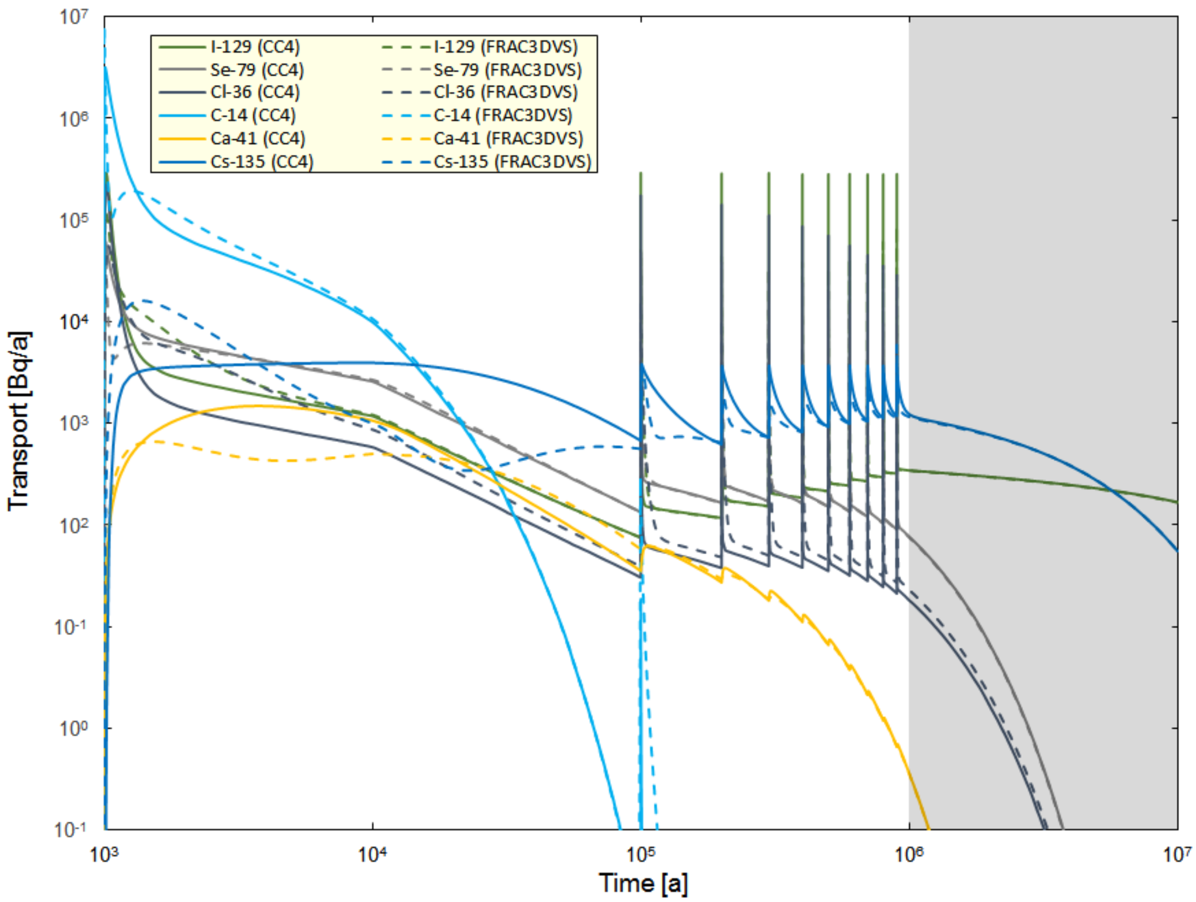

Figure 7-147: System Model, Simple Geosphere Submodel: Comparison of I-129, C-14, Ca-41, Cl-36, Cs-135 and Se-79 Transport to the Geosphere

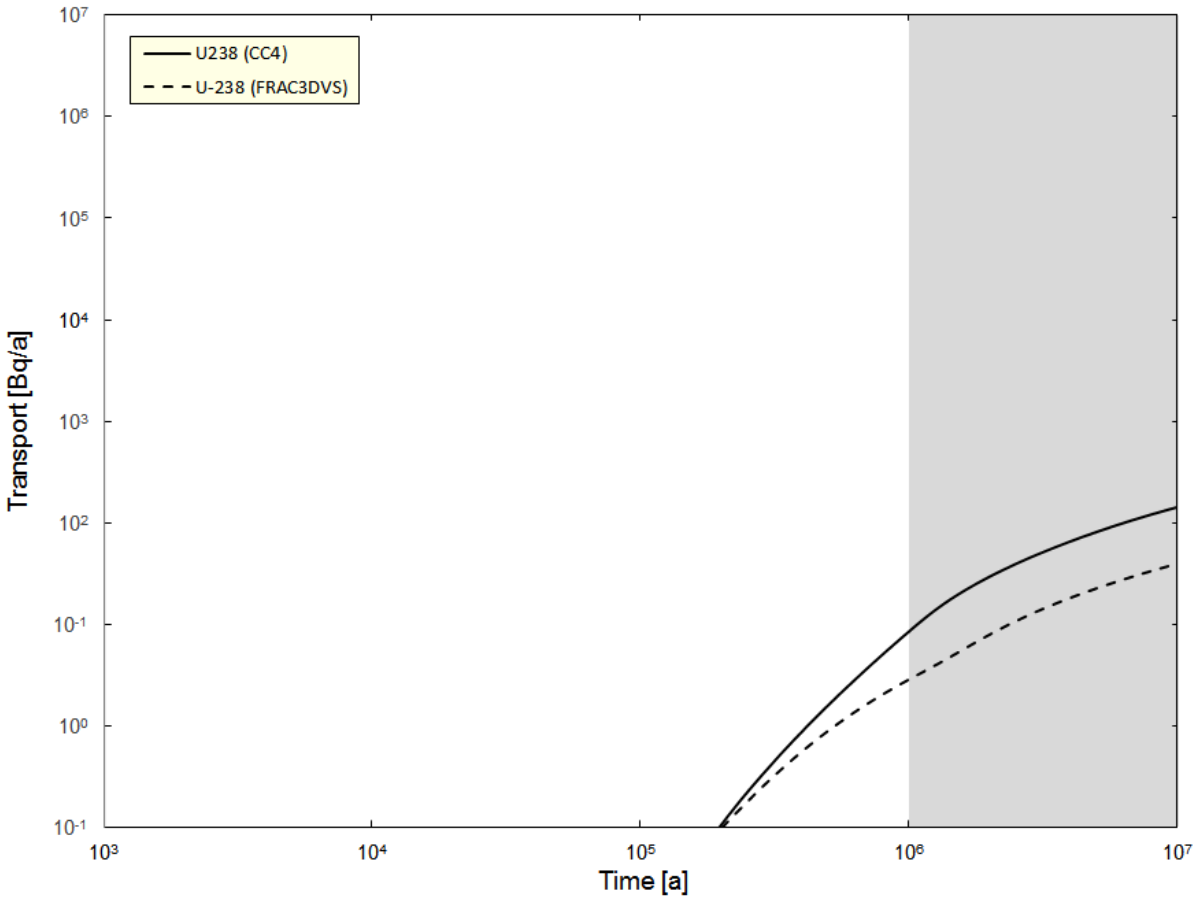

Figure 7-148: System Model, Simple Geosphere Submodel: Comparison U-238 Transport to the Geosphere

The comparison is good for all radionuclides; however, there are some differences in the peak transport between the two models, with results from the 3D model being somewhat greater. The reason for this is that in the 3D model some containers are closer to the boundary over which transport to the geosphere is determined than in the simplified System Model.

<u>Geosphere Transport Comparison</u>

The transport of I-129, C-14, Ca-41, Cl-36, Cs-135, Se-79, and U-238 through the geosphere and to the well for the Base Case is shown in Figure 7-149, with Table 7-36 summarizing the peak transport rates and their associated times.

For U-238, the transport rates are effectively zero due to the highly sorbing nature of these radionuclides.

The comparison is very good, with results showing that peak transport rates in the System Model are slightly conservative when compared to those generated by the 3D Full Repository-Scale model (i.e., the peaks are slightly higher and the time of peak transport is slightly earlier).

It is therefore concluded that the Simple Geosphere Submodel provides a suitable representation of radionuclide transport for key radionuclides.

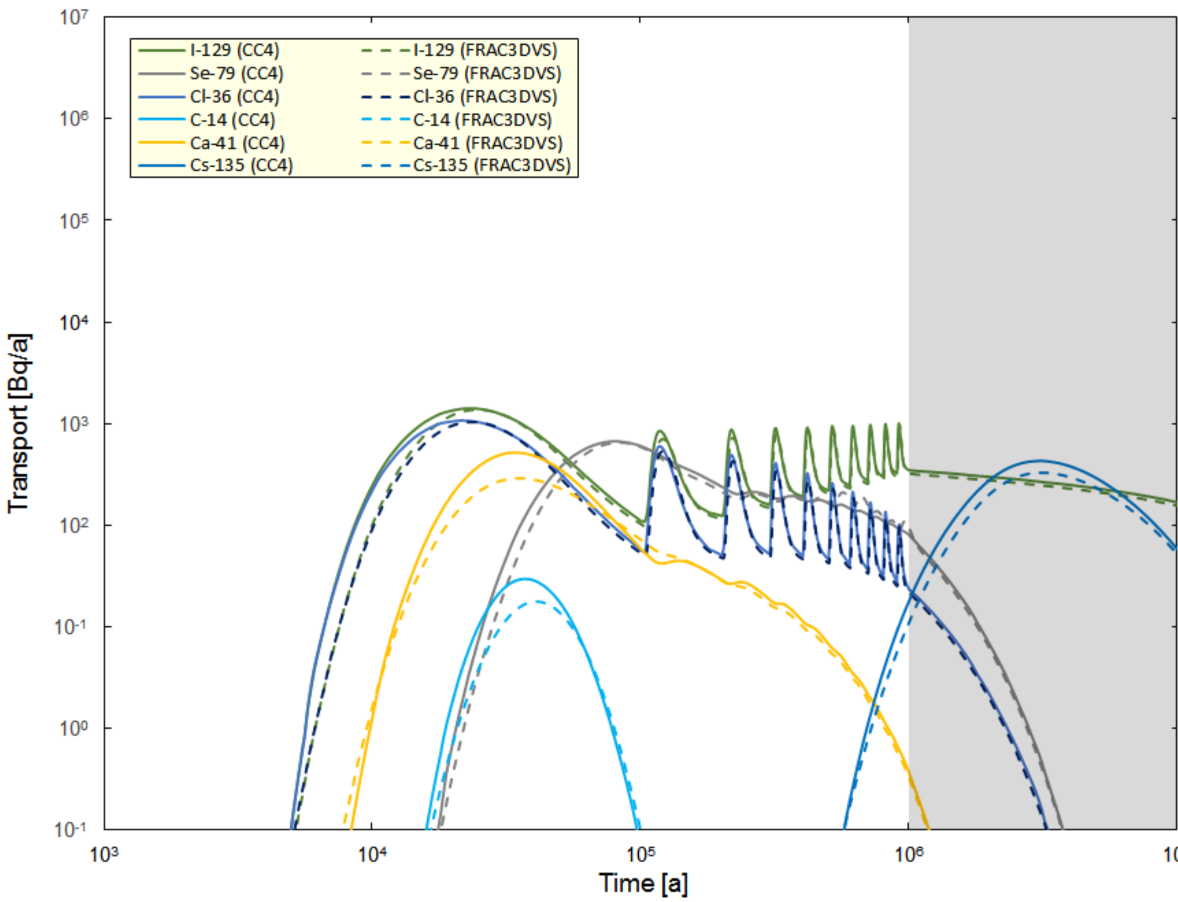

Note: U-238 is off-scale low

Figure 7-149: System Model, Simple Geosphere Submodel: Comparison of I-129, C-14, Ca-41, Cl-36, Cs-135 and Se-79 Transport to the Well

Table 7-36: System Model, Simple Geosphere Submodel: Comparison of Maximum Transport Rates to the Well

Nuclide	Peak Release Rate			Time of Peak Value (a)		
	System Model	3D Model	Ratio[1]	System Model	3D Model	Ratio[1]
I-129	1429	1350	1.05	23,100	24,700	0.94
C-14	29.7	17.8	1.67	36,700	40,700	0.90
Ca-41	520	288	1.81	34,600	35,100	0.99
Cl-36	1070	1020	1.05	21,900	23,600	0.93
Cs-135	430	333	1.29	3.06×10^{6}	3.13×10^{6}	0.98
Se-79	671	661	1.01	7.99×10^{4}	8.32×10^{4}	0.96

Note: [1] Ratio is the System Model value divided by the 3D Model value.

7.8.1.4.2 Full Geosphere Submodel – Transport Comparison

"Full" means the model has been developed to include the entire repository. There are multiple sectors and multiple representative pathways, with different pathways for each repository sector. Pathway properties are based on those in the detailed 3D simulations.

<u>Geosphere Transport Comparison</u>

Transport of I-129, C-14, Ca-41, Cl-36, Cs-135 and Se-79 through the geosphere to the well for the All Containers Fail at 60,000 Years Disruptive Event Scenario is compared with similar 3D model results in Figure 7-150, with Table 7-37 summarizing the peak transport rates and their associated times. The results show that transport to the well is overpredicted in the System Model for all radionuclides considered, with I-129 transport overpredicted by a factor of about 1.6.

For U-238, the release rate is effectively zero due to the highly sorbing nature of these radionuclides.

Figure 7-151 and Table 7-37 show additional comparisons of I-129 transport for the Central Discharge Zone, the West River and the East River. The comparisons are very good, with results showing that peak transport to the Central Discharge Zone and to the West River is slightly less than the 3D model equivalents. Given the relative unimportance of these pathways in comparison to the well (see Section 7.9.2.2) no enhancements have been made to the System Model to obtain better agreement.

It is therefore concluded that the Full Geosphere Submodel provides a conservative representation of radionuclide transport for key radionuclides.

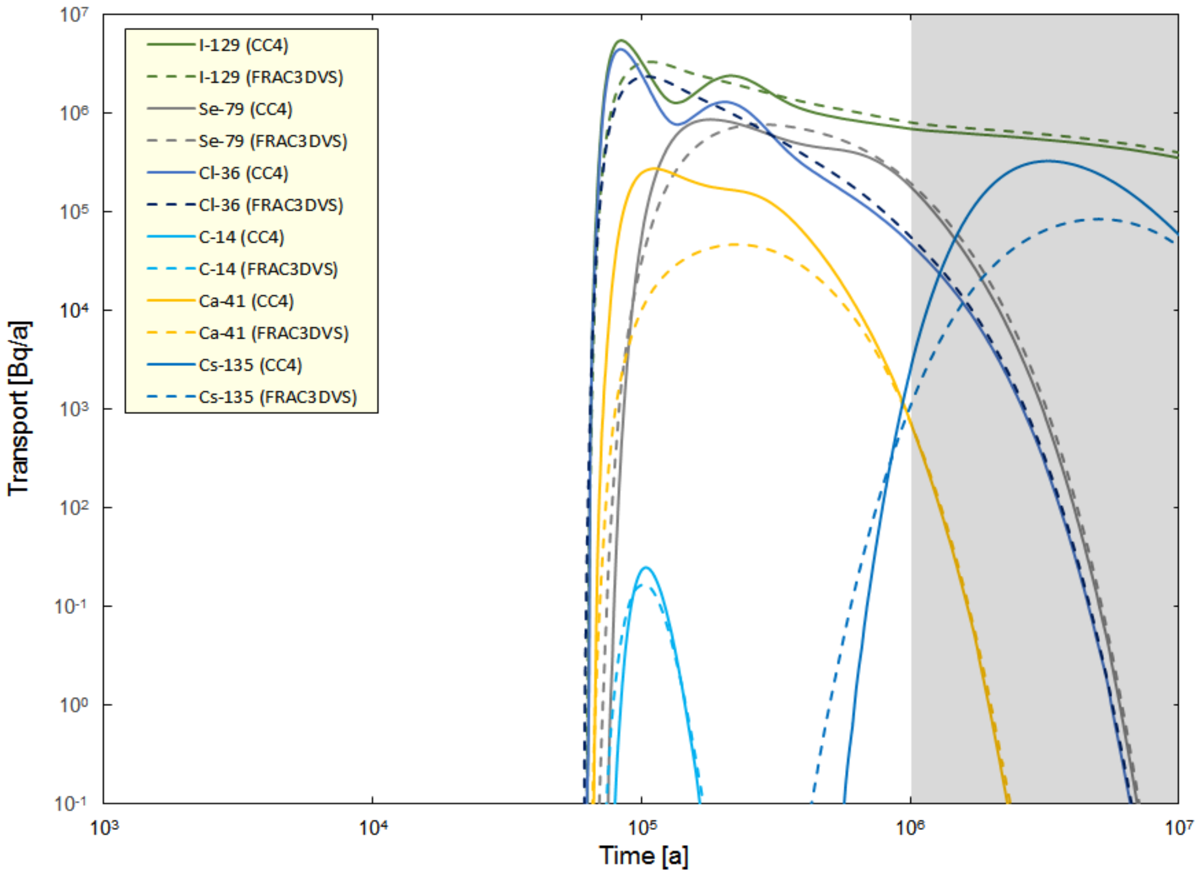

Note: U-238 is off-scale low

Figure 7-150: System Model, Full Geosphere Submodel: Comparison of I-129, C-14, Ca-41, Cl-36, Cs-135 and Se-79 Transport to the Well

Table 7-37: System Model, Full Geosphere Submodel: Comparison of Maximum Transport Rates to the Well

Nuclide	Peak Release Rate (Bq/a)			Time of Peak Value (a)		
	System Model	3D Model	Ratio[1]	System Model	3D Model	Ratio[1]
Well						
I-129	5.50×10^{6}	3.35×10^{6}	1.6	8.41×10^{4}	1.08×10^{5}	0.78
C-14	2.48×10^{1}	1.67×10^{1}	1.5	1.04×10^{5}	1.02×10^{5}	1.0
Ca-41	2.76×10^{5}	4.70×10^{4}	5.9	1.11×10^{5}	2.25×10^{5}	0.49
Cl-36	4.48×10^{6}	2.36×10^{6}	1.9	8.32×10^{4}	1.05×10^{5}	0.79
Cs-135	3.28×10^{5}	8.47×10^{4}	3.9	3.20×10^{6}	5.03×10^{6}	0.64
Se-79	8.66×10^{5}	7.78×10^{5}	1.1	1.82×10^{5}	2.80×10^{5}	0.65
Central Discharge						
I-129	1.02×10^{6}	1.21×10^{6}	0.85	2.38×10^{5}	2.55×10^{5}	0.93
West River						
I-129	1.90×10^{6}	2.00×10^{6}	0.95	1.80×10^{5}	3.01×10^{5}	0.60
East River						
I-129	7.64×10^{5}	4.09×10^{5}	1.87	5.10×10^{5}	5.08×10^{5}	1.00

Note: [1] Ratio is the System Model value divided by the 3D Model value.

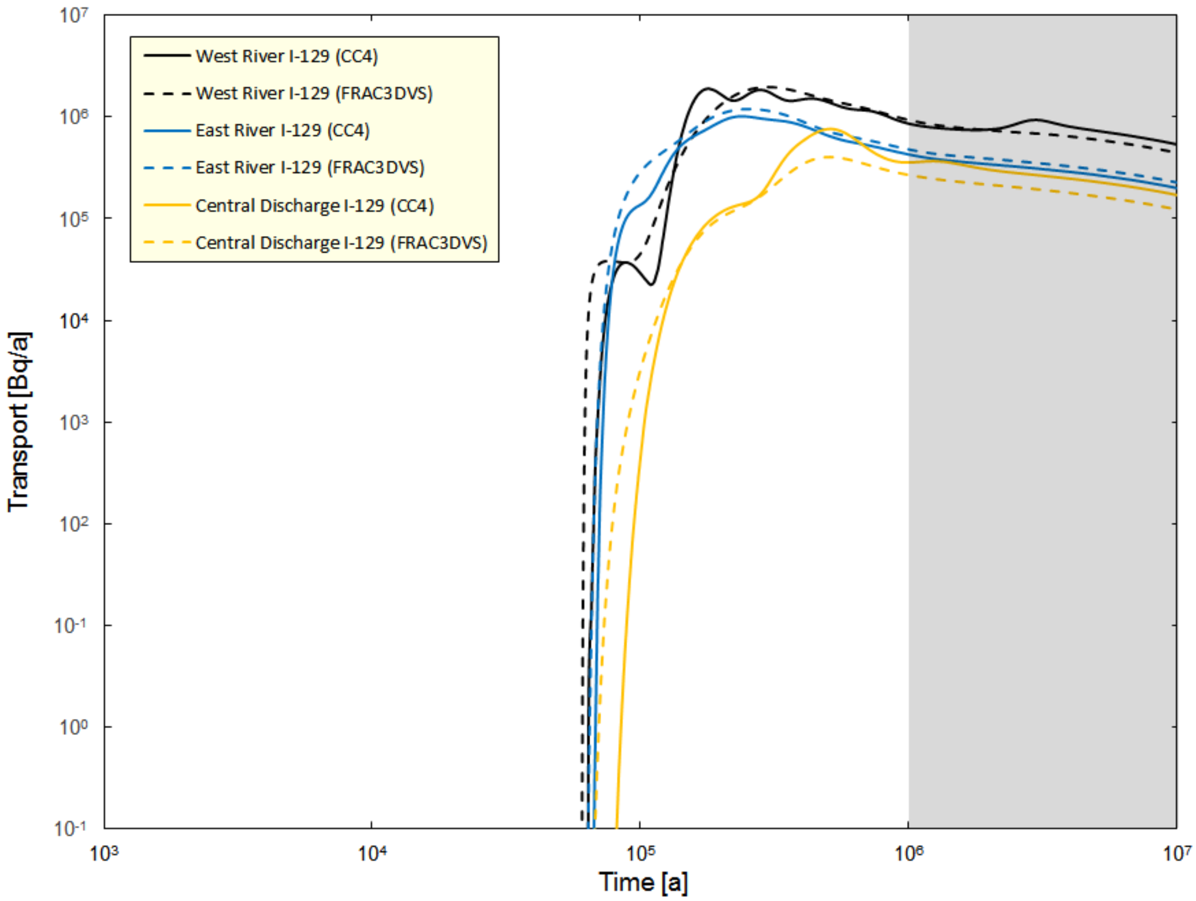

Figure 7-151: System Model, Full Geosphere Submodel: Comparison of I-129 Transport to the Central Wetland, East River and West River Discharge Zones

7.8.2 Results

This section presents the results of deterministic analysis and probabilistic analyses of the Base Case and a set of related sensitivity cases. The purpose of the sensitivity cases is to illustrate the effect of deviations in barrier performance on the Base Case consequences.

For the Reference Case of the Normal Evolution Scenario, all repository components meet their design specification and function as anticipated. As such, the used fuel containers remain intact essentially indefinitely (see Chapter 5) and no contaminant releases occur in the one million year time period of interest to the safety assessment.

Section 7.2.2 and Table 7-5 present the list of barrier sensitivity cases considered. Of these, the following have the potential to affect the groundwater flow field and are not amenable to modelling with the system model (i.e., because the system model is based on the constant 3D groundwater flow field defined in the Base Case). Simulations of these cases are therefore performed with the 3D Transport Model with results as described in Section 7.7.2.3 and associated subsections.

- Hydraulic conductivities of engineered barrier system (EBS) increased by a factor of 10;
- Hydraulic conductivities increased by a factor of 10;
- Hydraulic conductivities decreased by a factor of 10;
- Hydraulic conductivity in the excavation damaged zones (EDZ) increased by a factor of 10;
- Fracture standoff distance reduced to 50, 25 and 10 m; and
- Dispersivity increased and decreased by a factor of 5.

The remaining cases from Table 7-5 (i.e.; those that do not affect the groundwater flow field) are listed below. These cases are simulated with the System Model.

Fuel Barrier:

- Fuel dissolution rate increased by a factor of 10; and
- Instant release fractions for fuel contaminants set to 0.10.

Zircaloy Sheath Barrier:

No credit is taken in the postclosure safety assessment for the presence of the Zircaloy fuel sheath as a barrier to contaminant release from the fuel. However, because the sheath itself contains contaminants and because the screening analysis identifies some of these contaminants as potentially important, the following Zircaloy specific sensitivity cases are simulated:

- Zircaloy dissolution rate increased by a factor of 10; and
- Instant release fractions for Zircaloy sheath contaminants set to 0.10 for.

Container Barrier:

- All 10 containers fail at 1000 years;
- 50 containers fail at 1000 years;
- 50 and 1000 containers fail at 10,000 years;
- Low sorption in the EBS with coincident high solubility limits in the container; and
- No solubility limits in the container.

Buffer, Backfill and Seals Barrier:

- Low sorption in the EBS with coincident high solubility limits in the container; and
- No sorption in the near field.

Geosphere Barrier:

- Sorption parameters set to their two sigma (low) values.

The effect of glaciation is discussed quantitatively based on the analysis of a glaciation scenario carried out as part of the Third Case Study (Garisto et al. 2010; Walsh and Avis 2010). The important features of this glaciation study are described and its applicability to the current study is discussed.

Two probabilistic cases are also simulated. These are:

1) Number, locations and failure times for the defective containers fixed at their Base Case values, with all other available parameters varied; and
2) Number, locations and failure times for the defective containers varied, with all other parameters maintained at their Base Case values.

Figures in this section are shown with shading at times greater than one million years to emphasize that these results are illustrative and included only to indicate peak impacts. Shading for dose rates below 10^{-6} mSv/a indicates these values are negligible and are included to indicate trends.

7.8.2.1 Base Case

Figure 7-152 shows the total dose rate for the Base Case, as determined using the System Model described in Section 7.8.1.2.1. The total dose rate is the sum of the individual contributions from all radionuclides of potential interest and their progeny. The shape of the curve is a result of the assumptions concerning container failure times.

The peak dose rate is 2.5×10^{-4} mSv/a occurring at about 23,300 years. This is a factor of 7200 times less than the average natural background dose rate of 1.8 mSv/a and a factor of 1200 times less than the 0.3 mSv/a interim dose rate acceptance criterion established in Section 7.1.1 for the radiological protection of persons.

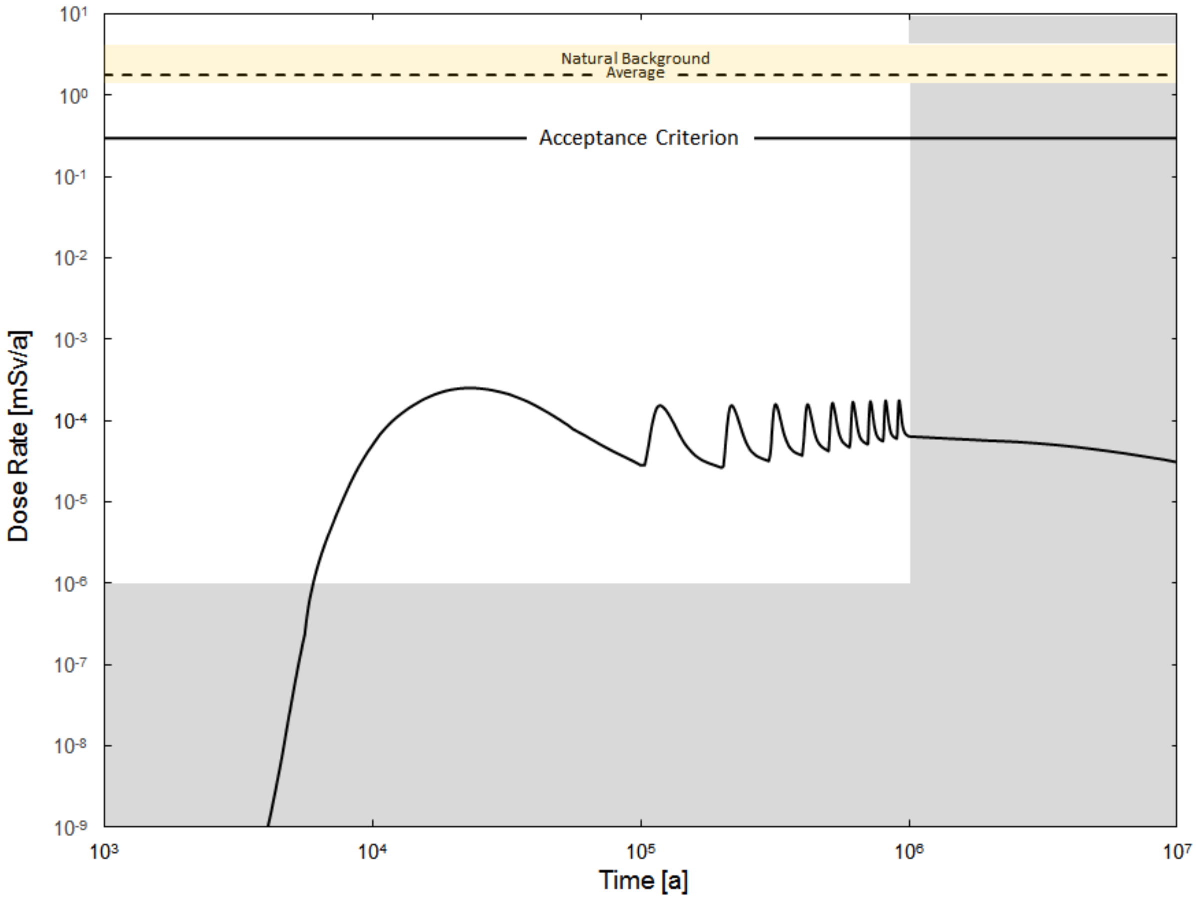

Figure 7-152: System Model: Base Case Total Dose Rate

Figure 7-153 shows the individual contributions to the total dose rate from the most significant radionuclides. I-129 is the dominant contributor, followed to a much lesser extent by Se-79. I-129 is dominant because it has a sizeable initial inventory, a non-zero instant release fraction, a very long half-life, is not solubility limited, is non-sorbing in the buffer, backfill and geosphere and has a radiological impact on humans.

The shape of the curves for individual radionuclides is a function of the radionuclide specific source term, instant release fraction, sorption coefficients and half-life.

Other fission products and actinides either decay away, or are released very slowly as the fuel dissolves and are thereafter sorbed in the engineered barriers and geosphere.

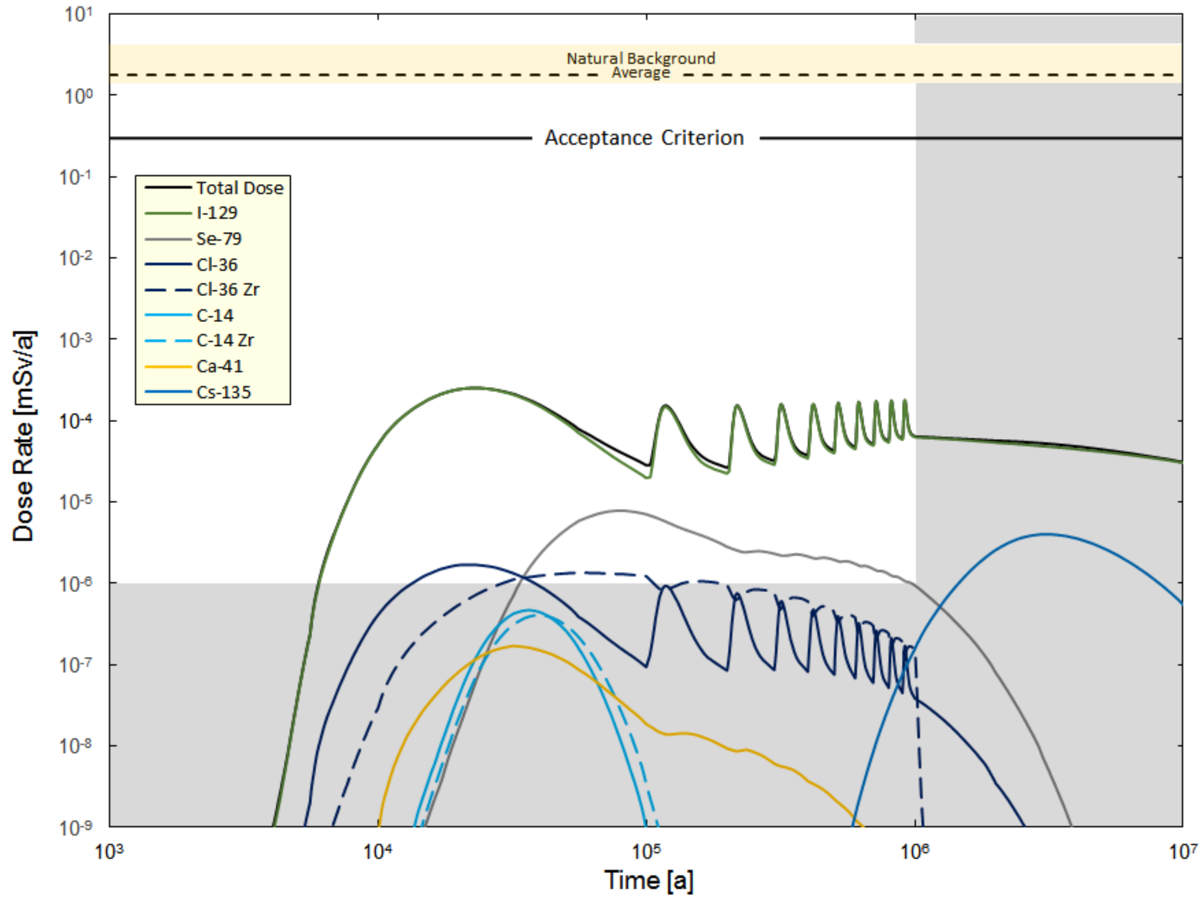

Figure 7-153: System Model: Base Case Individual Radionuclide Dose Rates

Table 7-38 shows a breakdown of radionuclide contributions to the peak dose rate. I-129 is dominant, being responsible for almost 99% of the Base Case dose.

Table 7-38: Radionuclide Dose Contributors for the Base Case

Radionuclide	Peak Dose Rate Contribution [mSv/a]	Percentage of Peak Dose [%]
I-129	2.52×10^{-4}	98.93
Cl-36	1.69×10^{-6}	0.66
Cl-36 Zr	7.29×10^{-7}	0.29
C-14	9.62×10^{-8}	0.04
Ca-41	9.58×10^{-8}	0.04
C-14 Zr	5.55×10^{-8}	0.02
Se-79	4.96×10^{-8}	0.02
Cs-135	0	0
Other	0	0

Table 7-39 shows a breakdown I-129 dose pathways. Essentially all of the I-129 dose is due to internal dose pathways, with drinking water and food ingestion being dominant. Drinking water is supplied by the well, and well water is used to irrigate crops used as food sources by the family.

Table 7-39: Radionuclide Dose Pathways for the Base Case

Pathway	Peak Dose Contribution [mSv/a]	Percentage of the I-129 Peak Dose [%]
Total Dose From all Routes	2.52×10^{-4}	-
Internal Dose Pathways	$\mathbf{2.52 \times 10^{-4}}$	**100**
Drinking Water	1.42×10^{-4}	56.3
Food Ingestion	1.09×10^{-4}	43.3
Inhalation	9.26×10^{-7}	0.37
Soil Ingestion	3.85×10^{-7}	0.15
External Dose Pathways	$\mathbf{4.99 \times 10^{-9}}$	**0.002**
Ground Exposure	3.63×10^{-9}	0.0014
Water Immersion	1.34×10^{-9}	0.00054
Air Immersion	2.72×10^{-11}	0.00001
Building Materials	6.70×10^{-13}	0.0000003

Table 7-40 provides a breakdown of the contributors to the I-129 food ingestion dose rate. Ingestion of leafy vegetables and milk are the largest contributors.

Table 7-40: I-129 Food Ingestion Dose Pathways for the Base Case

Pathway	Peak Dose Contribution [mSv/a]	Percentage of the I-129 Peak Dose [%]
Total Dose From all Routes	2.52×10^{-4}	-
Food Ingestion	1.09×10^{-4}	43.3
Leafy Veg Ingestion	7.09×10^{-5}	28.1
Milk Ingestion	2.42×10^{-5}	9.6
Bird Ingestion	5.96×10^{-6}	2.4
Meat Ingestion	5.75×10^{-6}	2.3
Root Veg Ingestion	2.87×10^{-6}	1.1
Fish Ingestion	1.68×10^{-9}	0.0006

7.8.2.2 Well Assumption Sensitivity Cases

The previous section shows that the dose consequence for the Base Case is almost entirely due to I-129, with the I-129 dose almost entirely due to the use of well water. In the System Model, well water is used for drinking, irrigation of food crops and for watering animals.

The method used to determine the well and defective container locations is described in Section 7.7.2.3.2. Considerable effort has been devoted to ensuring that the combination of well and defective container location maximizes dose consequence.

Given the importance of the well to the overall dose consequence, Section 7.2.2.2 defines three sensitivity cases to illustrate the effects of well assumptions on the Base Case results. These cases are:

- No well;
- Intermittent well operation; and
- Random well location.

This section describes the “No Well” sensitivity case. The other cases have been examined with the 3D models and are described in Section 7.7.2.3.4.

<u>No Well</u>

Given the number of potential arrangements of defective container locations, this sensitivity case has many thousands of different possibilities. To simplify the analysis, the location of the defective containers is assumed to be the same as in the Base Case. This means that all 10 containers are clustered together at the end of a single placement room as indicated by the red dot adjacent to the “Main” label in Figure 7-31. Adoption of this location means the Simple Model described in Section 7.8.1.2.1 can be used for the No Well case dose assessment.

Figure 7-154 shows the results. With no well (and for the specified container location), the peak dose rate is 1.4×10^{-7} mSv/a occurring at 27,700 years. This is about 1800 times less than the peak Base Case dose rate with a well (Section 7.8.2.1), which itself is 1200 times less than the interim dose rate acceptance criterion. The main reason for this difference is the much greater dilution associated with the use of surface water.

Different defective container locations could potentially result in different dose rates because the contaminants could migrate to different surface discharge areas; however, in all cases the no well results are anticipated to be hundreds (if not thousands) of times less than those of the Base Case.

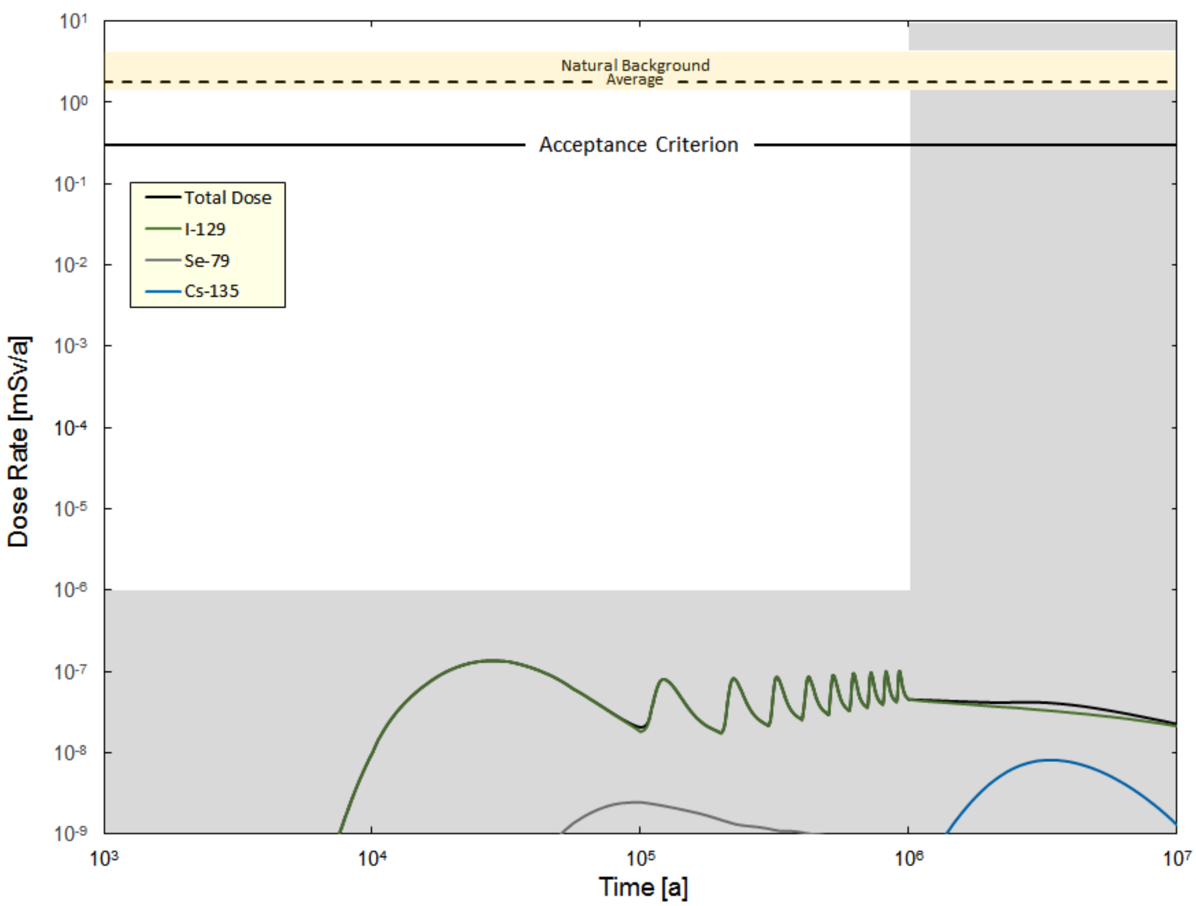

Figure 7-154: System Model: Sensitivity to No Well

7.8.2.3 Barrier Performance Sensitivity Cases

7.8.2.3.1 Fuel Barrier Sensitivity

Sensitivity cases illustrating the effect of deviations in the performance of the fuel barrier are:

- Fuel dissolution rate increased by a factor of 10; and
- Instant release fractions for fuel contaminants set to 0.10.

Figure 7-155 shows the individual contributions to the total dose rate from the most significant radionuclides for the first sensitivity case. For this case, all fuel in the container dissolves within one million years, whereas in the Base Case, only about 21 % of the fuel dissolves (see Figure 7-10).

As in the Base Case, I-129 is the dominant dose rate contributor, followed to a much lesser extent by Se-79, Cl-36 and C-14. The peak dose rate occurs at about 27,900 years and reaches a value of 1.6×10^{-3} mSv or about 6 times that of the Base Case. The peak dose rate does not increase by a factor of 10 because the instant release fraction for I-129 also has an effect and this parameter is independent of the fuel dissolution rate.

Actinide dose rates are zero because they are strongly sorbed in the buffer and geosphere and do not reach the biosphere during the simulation time.

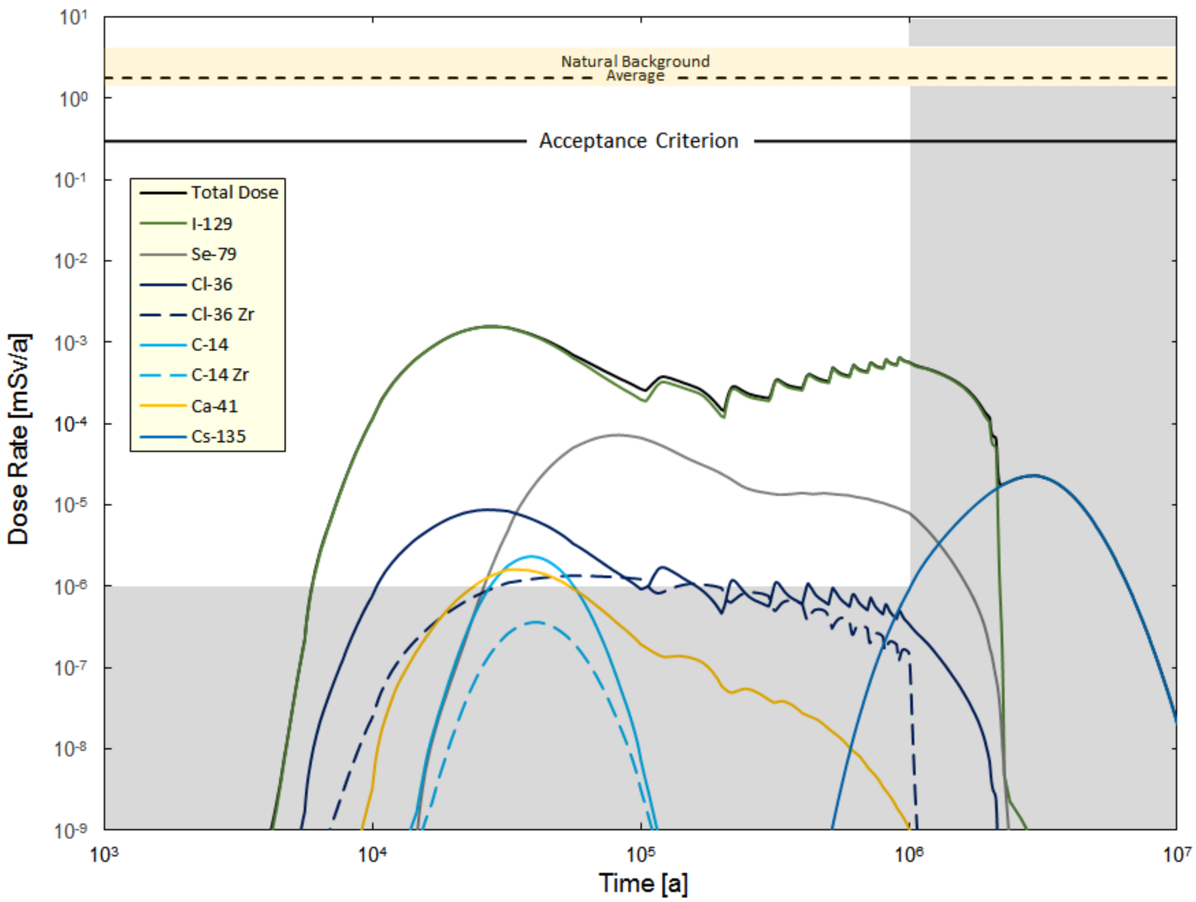

Figure 7-155: System Model: Sensitivity to a Factor of 10 Increase in Fuel Dissolution Rate

Figure 7-156 shows the individual contributions to the total dose rate from the most significant radionuclides for the second sensitivity case (i.e., with the instant release fractions set to 10%).

As in the Base Case, I-129 is the main dose contributor. The peak total dose rate occurs at 21,200 years and reaches a value of about 4.3×10^{-4} mSv or about 1.7 times that of the Base Case. The effect is less than the increase in I-129 instant release (i.e., 0.04 to 0.1 or 2.5 times) due to broadening and dispersion of the pulse as it travels through the clay barriers and the geosphere.

Actinide dose rates are zero because they are strongly sorbed in the buffer and geosphere and do not reach the biosphere during the simulation time.

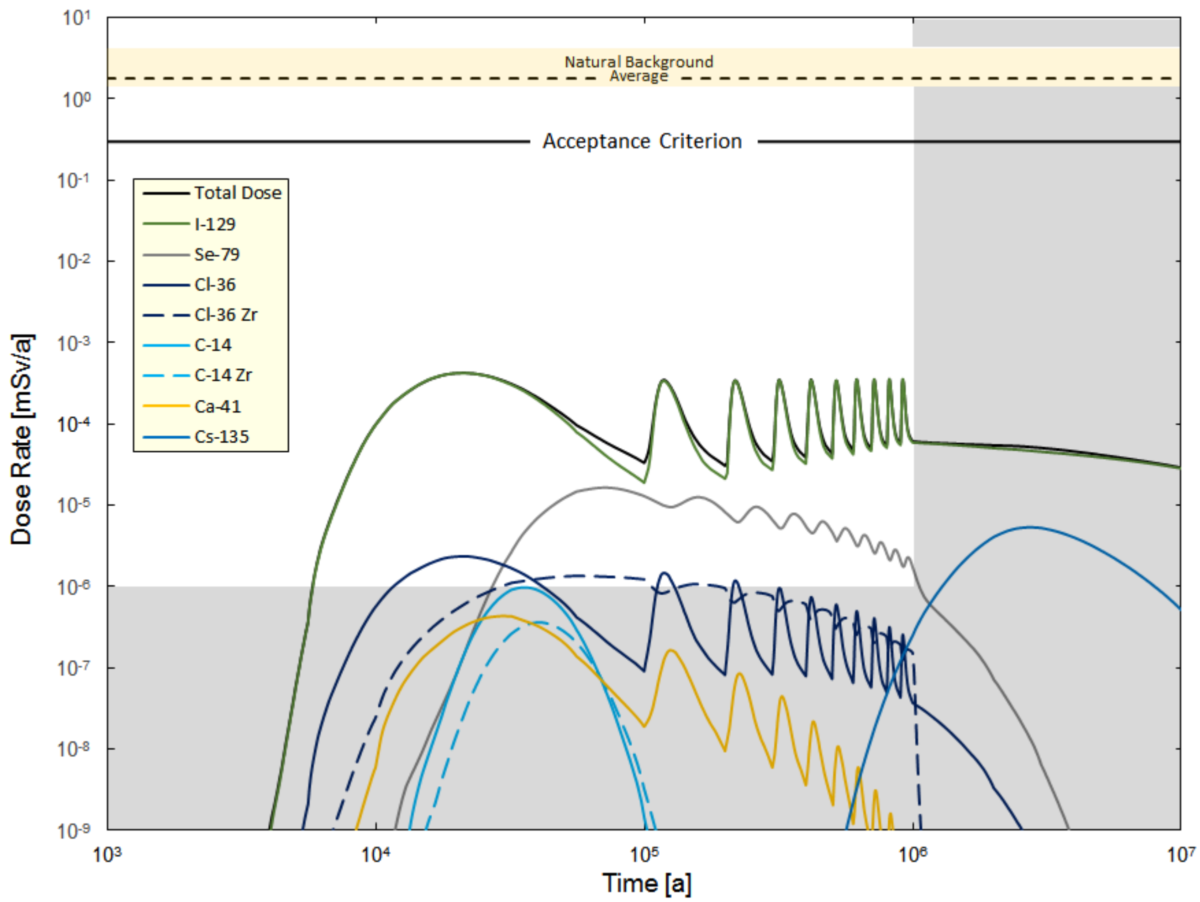

Figure 7-156: System Model: Sensitivity to Fuel Instant Release Fractions Set to 10%

7.8.2.3.2 Zircaloy Sheath Barrier Sensitivity

No credit is taken in the postclosure safety assessment for the presence of the Zircaloy fuel sheath as a barrier to contaminant release from the fuel. However, because the sheath itself contains contaminants and because the screening analysis identifies some of these contaminants as potentially important, the following Zircaloy specific sensitivity cases are simulated:

- Zircaloy dissolution rate increased by a factor of 10; and
- Instant release fractions for Zircaloy sheath contaminants set to 0.10.

Figure 7-157 shows the individual contributions to the total dose rate from the most significant radionuclides for the sensitivity case with the Zircaloy dissolution rate increased by a factor of 10.

As in the Base Case, I-129 is the dominant dose rate contributor, followed to a much lesser extent by Se-79, Cl-36 and C-14. The peak dose rate occurs at about 23,900 years and reaches a value of 2.6×10^{-4} mSv, similar to that of the Base Case. The results show a greater contribution of C-14 and Cl-36 due to increased Zircaloy dissolution; however, the effect on the total dose rate is almost negligible.

Actinide dose rates are zero because they are strongly sorbed in the buffer and geosphere and do not reach the biosphere during the simulation time.

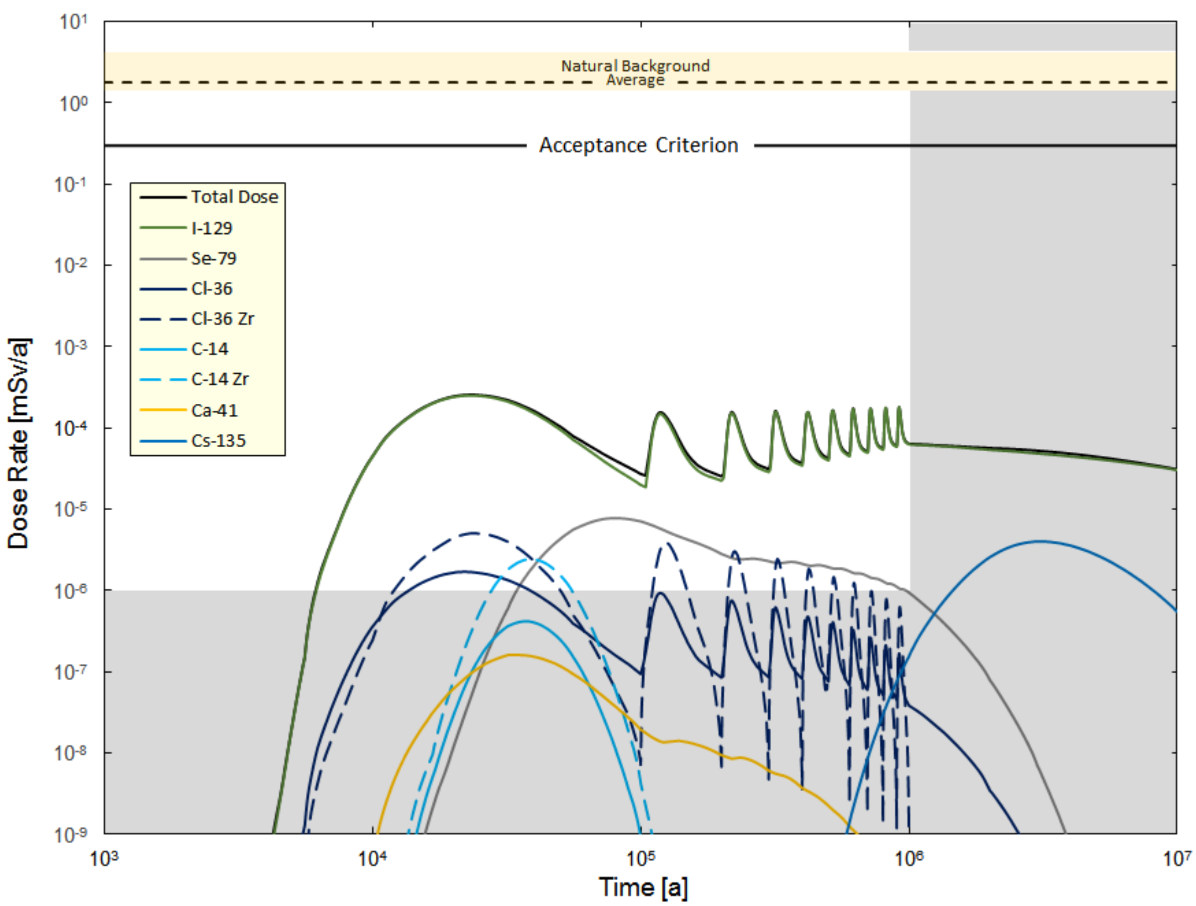

Figure 7-157: System Model: Sensitivity to a Factor of 10 Increase in Zircaloy Corrosion Rate

Figure 7-158 shows the individual contributions to the total dose rate from the most significant radionuclides for the sensitivity case with the Zircaloy instant release fractions set to 10%.

As in the Base Case, I-129 is the main dose contributor. The peak total dose rate occurs at about 23,400 years and reaches a value of about 2.5x10^{-4} mSv. This is the same as for the Base Case; however, the contributions from C-14 and Cl-36 are slightly increased relative to the Base Case results shown in Figure 7-153.

Actinide dose rates are zero because they are strongly sorbed in the buffer and geosphere and do not reach the biosphere during the simulation time.

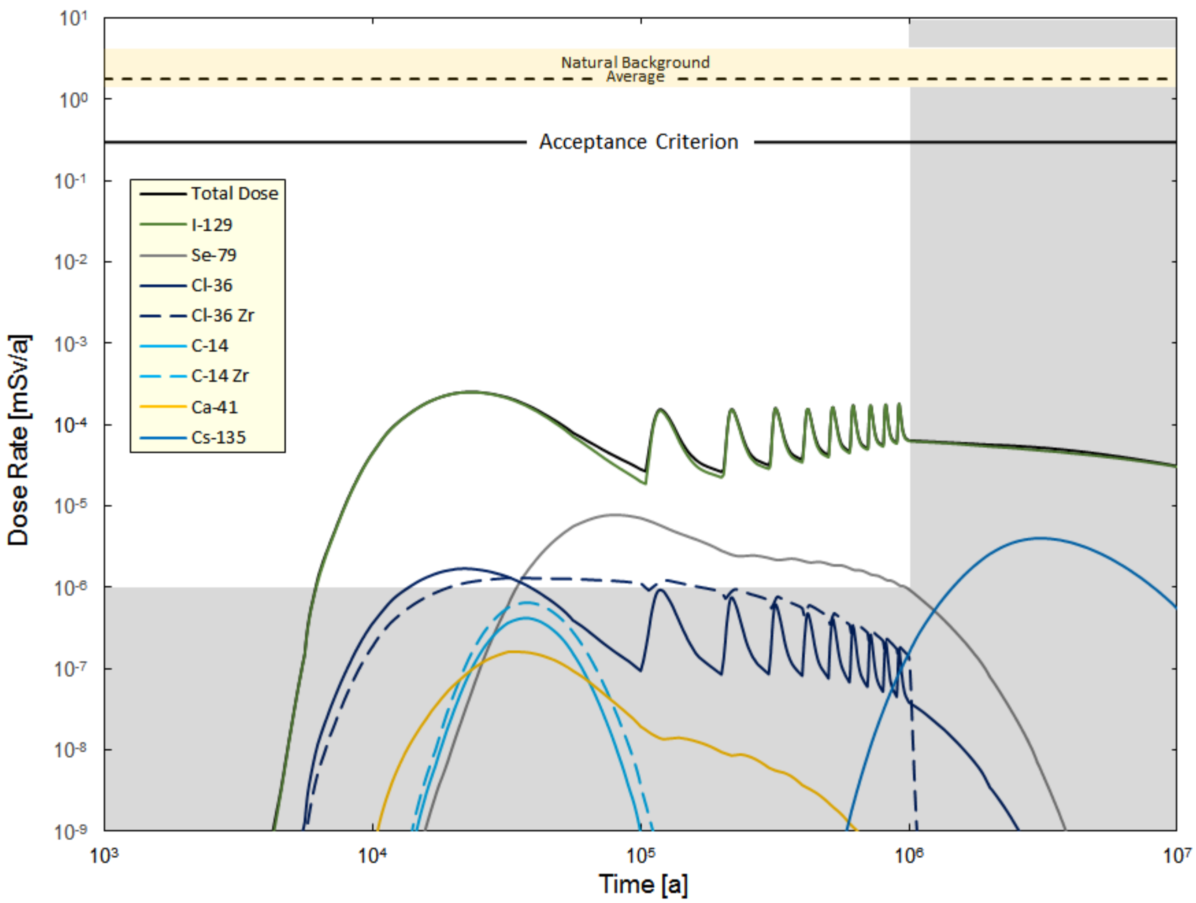

Figure 7-158: System Model: Sensitivity to Zircaloy Instant Release Fractions Set to 10%

7.8.2.3.3 Container Barrier Sensitivity

Sensitivity studies illustrating the effect of variations in the container barrier are:

- All 10 containers fail at 1000 years;
- 50 containers fail at 1000 years;
- 50 containers and 1000 containers fail at 10,000 years;
- Low sorption in the engineered barrier materials with coincident high solubility limits in the container;
- No solubility limits in the container.

Figure 7-159 shows the individual contributions to the total dose rate from the most significant radionuclides for the sensitivity case in which all 10 containers fail at 1000 years. Table 7-3 shows that the 1000 year failure time is quite conservative compared to what might be expected at a real site.

As in the Base Case, I-129 is the dominant dose rate contributor, followed to a lesser extent by Se-79, Cl-36 and C-14. The peak dose rate occurs at about 23,100 years and reaches a value of 2.6×10^{-3} mSv or about 10 times that of the Base Case.

Actinide dose rates are zero because they are strongly sorbed in the buffer and geosphere and do not reach the biosphere during the simulation time.

The effect of a slightly larger number of container failures can be illustrated by scaling these results. For example, if 50 containers are assumed to fail early, and all of these containers are assumed to be clustered in the location that maximizes the dose consequence, a conservative estimate of the dose rate is 0.013 mSv/a, or about 50 times that of the Base Case.

To illustrate the effect of an even greater number of container failures, a different approach must be used because it is not possible for all defective containers to simultaneously be in the location that maximizes the dose consequence. For large numbers of assumed defective containers, there are millions of potential arrangements; however, to provide a simple illustration, the consequences of the All Containers Fail at 10,000 years Disruptive Event Scenario (discussed in Section 7.9.2) can be used. These results can be scaled to illustrate repository performance for a uniform distribution of defective containers, given that there are 95,834 containers for 4.6 million bundles.

Applying the above approach for 1000 containers, the dose rate for a uniform distribution of defective containers failing at 10,000 years is 8.5×10^{-3} mSv/a. Similarly, the dose rate for a uniform distribution of 50 containers failing at 10,000 years is 4.2×10^{-4} mSv/a. Note that there is a large difference in dose rate between the two 50 container cases, with the dose rate for 1000 years with clustered containers 30 times higher than that for 10,000 years with uniformly distributed containers. Part of the difference is due to the longer decay time resulting in a slightly lower source term; however, the main reason is due to different assumed distribution of failed containers.

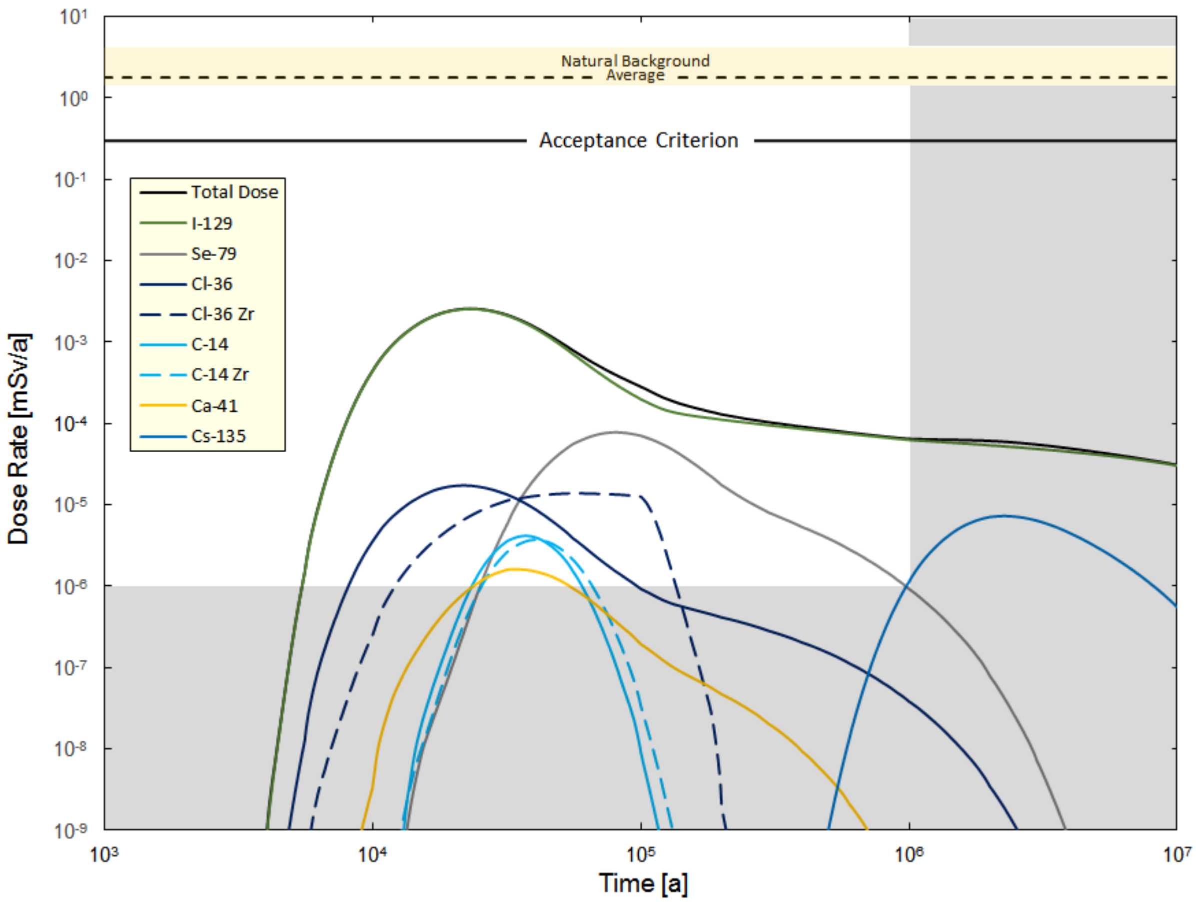

Figure 7-159: System Model: Sensitivity to All 10 Containers Fail at 1000 years

Figure 7-160 shows the individual contributions to the total dose rate from the most significant radionuclides for the sensitivity case with low sorption in the engineered barrier materials with coincident high solubility in the containers.

As in the Base Case, I-129 remains the dominant dose rate contributor, followed to a lesser extent by Se-79 and Cl-36. The peak dose rate occurs at about 23,900 years and reaches a value of 2.5×10^{-4} mSv, the same as of the Base Case. The I-129 release is unaffected because I-129 is non-sorbing and has no solubility limit.

Actinide dose rates are zero because they remain strongly sorbed in the geosphere despite the reduction of sorption in the engineered barriers, and do not reach the biosphere during the simulation time.

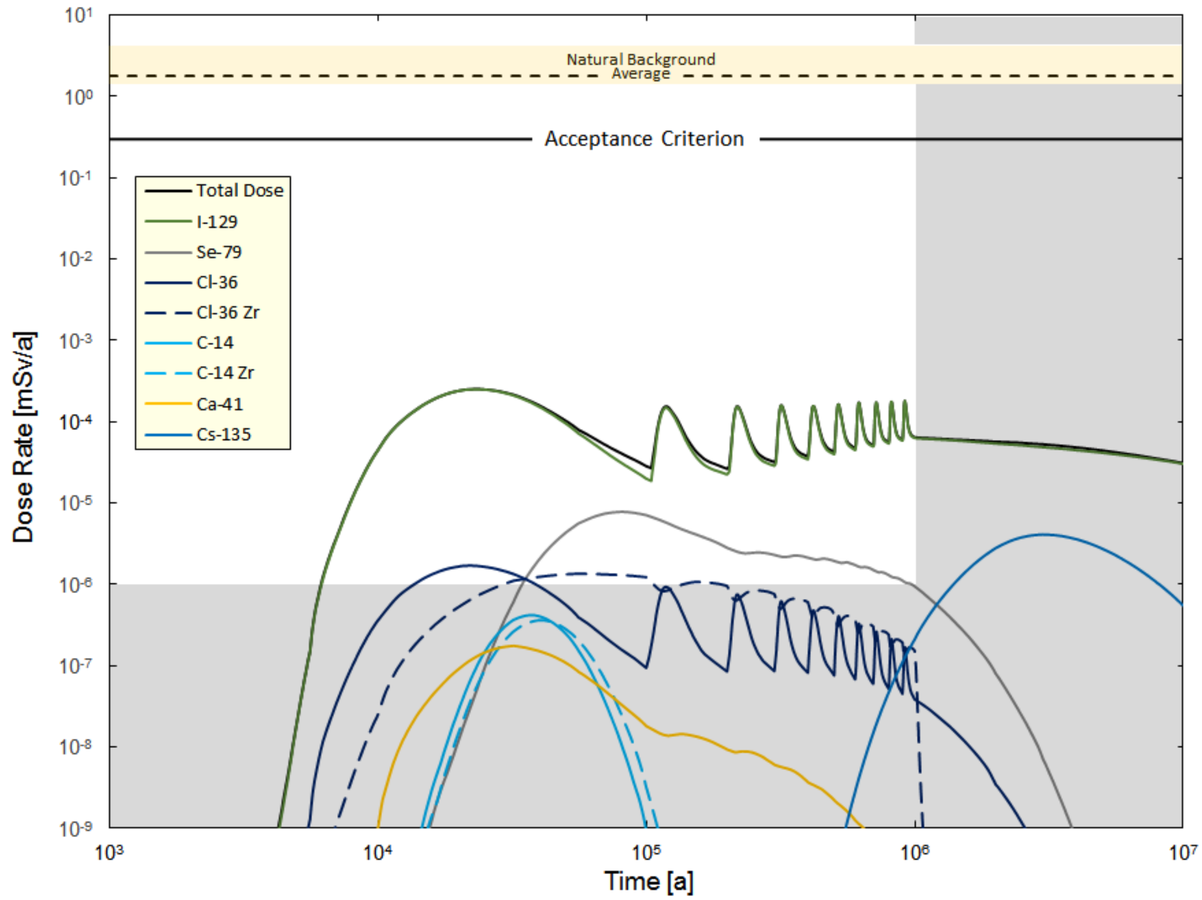

Figure 7-160: System Model: Sensitivity to Low Sorption in the EBS with Coincident High Solubility Limits in the Container

Figure 7-161 shows the individual contributions to the total dose rate from the most significant radionuclides for the sensitivity case with no solubility limits in the containers.

As in the Base Case, I-129 remains the dominant dose rate contributor, followed to a lesser extent by Se-79 and Cl-36. The peak dose rate occurs at about 23,900 years and reaches a value of 2.5×10^{-4} mSv, the same as that of the Base Case. The I-129, Cl-36 and Cs-135 releases are unaffected because these nuclides have no solubility limit. C-14 has a solubility limit but doesn't reach it, and a small amount of Se-79 is precipitated with essentially no effect on the Se-79 dose contribution.

Actinide dose rates are zero because they are strongly sorbed in the geosphere and do not reach the biosphere during the simulation time.

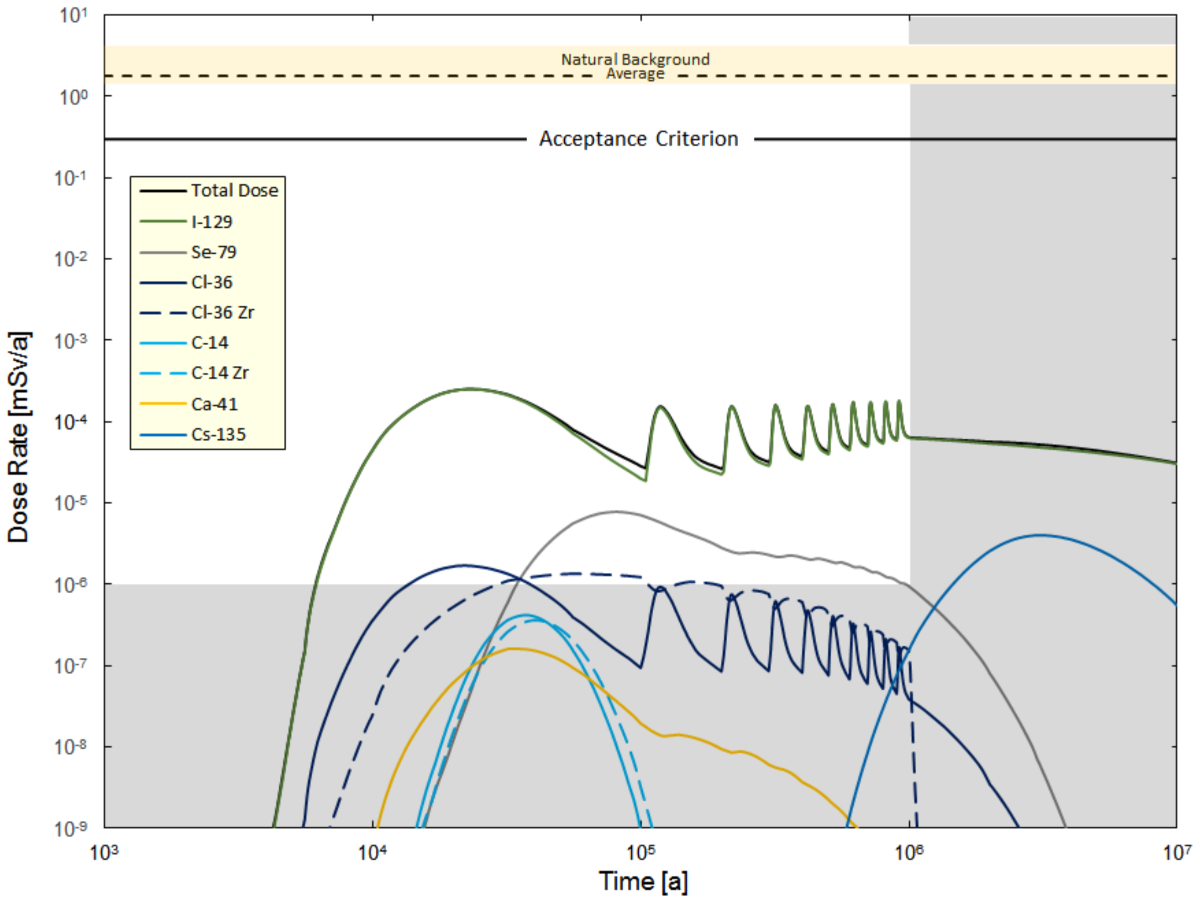

Figure 7-161: System Model: Sensitivity to No Solubility Limits

7.8.2.3.4 Buffer, Backfill, and Seals Barrier Sensitivity

Sensitivity studies illustrating the effect of variations in the buffer, backfill and seals barrier are:

- Low sorption in the engineered barrier materials with coincident high solubility limits in the container; and
- No sorption in the near field.

The sensitivity study with low sorption in the engineered barrier materials with coincident high solubility limits in the container is discussed in Section 7.8.2.3.3.

Figure 7-162 shows the individual contributions to the total dose rate from the most significant radionuclides for the sensitivity case with no sorption in the near field.

As in the Base Case, I-129 remains the dominant dose rate contributor, followed to a lesser extent by Se-79 and Cl-36. The peak dose rate occurs at about 23,800 years and reaches a value of 2.5×10^{-4} mSv, the same the Base Case. The I-129 and C-14 releases are unaffected because these radionuclides are non-sorbing in the barrier materials.

Actinide dose rates are zero because they are strongly sorbed in geosphere and do not reach the biosphere during the simulation time.

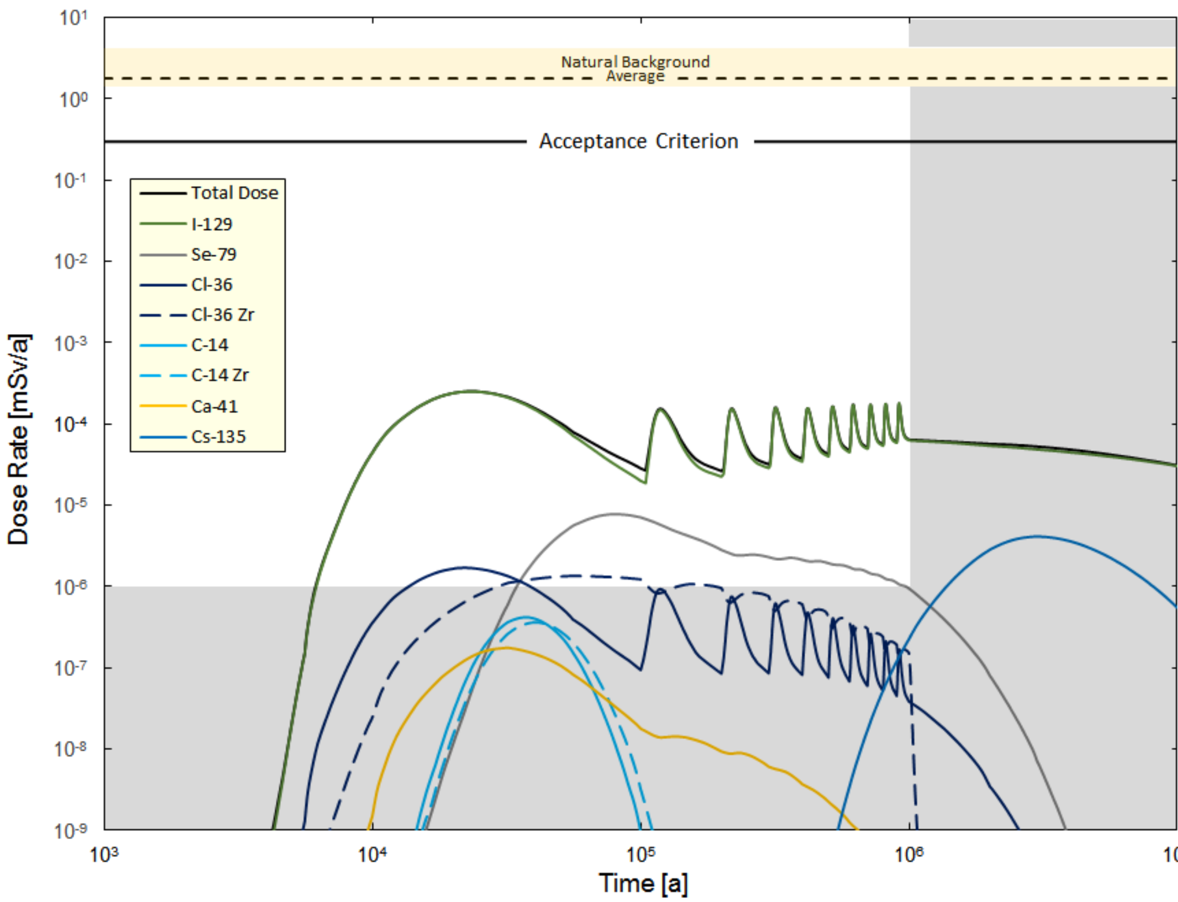

Figure 7-162: System Model: Sensitivity to No Sorption in the Near Field

7.8.2.3.5 Geosphere Barrier Sensitivity

The sensitivity study illustrating the effect of variations in the geosphere barrier is:

- Sorption parameters set to two standard deviations (low) values.

Figure 7-163 shows the individual contributions to the total dose rate from the most significant radionuclides for this sensitivity case. The peak dose rate is 2.6×10^{-4} mSv occurring at

24,200 years. In comparison to the Base Case, the dose contribution from some radionuclides is increased (e.g., C-14, Cs-135 and Sn-126); however, the peak dose rate and associated timing are essentially unaffected.

At very long times (i.e.; well beyond 1 Ma) U-238 daughters begin to appear. This is similar to what would occur should a natural uranium ore body be subjected to the same conditions.

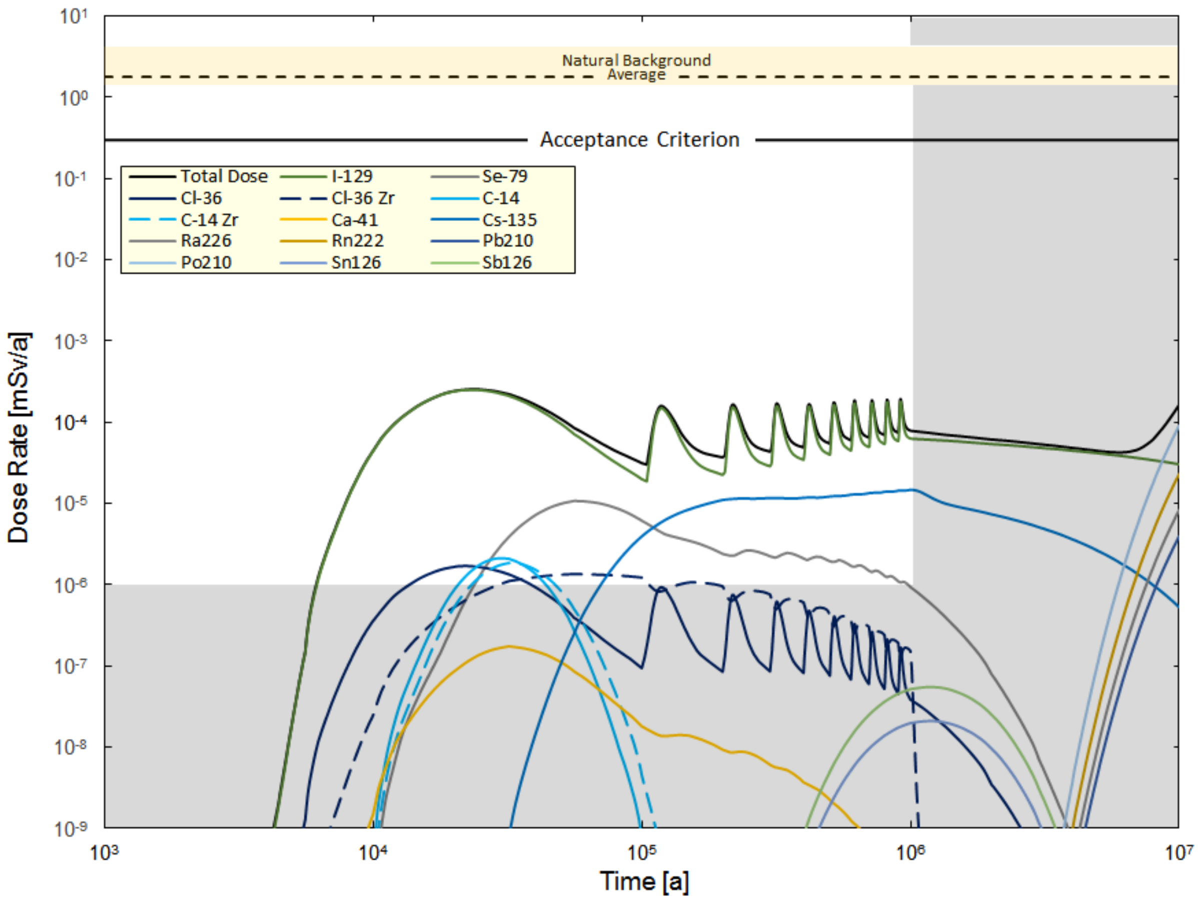

Note: For clarity, only the top four U-238 daughters are shown; however, 19 others are also above the lower bound value of 10^{-9} mSv

Figure 7-163: System Model: Sensitivity to Two Standard Deviations (Low) Sorption in the Geosphere

7.8.2.4 Glaciation Sensitivity

The effect of glaciation is discussed quantitatively based on the analysis of a glaciation scenario carried out as part of the Third Case Study (Garisto et al. 2010; Walsh and Avis 2010). The important features of this glaciation study are described here and its applicability to the current study is discussed.

7.8.2.4.1 Glacial Cycle

To explore the possible effects of glaciation, a representative future glacial cycle has been defined in terms of climate and surface boundary conditions using models of past glacial behaviour (Peltier 2003, 2006).

Specifically, Peltier (2006) developed a set of reference glacial system models that are consistent with evidence from the past glacial cycle and the Laurentide Ice Sheet that covered Canada and northern United States. The model results include surface boundary conditions (e.g., ice thickness and permafrost depth) across North America on a scale of grid size 50 km on a side. Simulation nn2 778 was selected for the glaciation sensitivity study since it produced a “warm-based” glacier at the hypothetical site (i.e., liquid water is sometimes present at the base of the ice sheet that periodically covers the site). A warm-based glacier is of interest because there is a greater opportunity for deep groundwater flow to be affected by passage of the ice sheet. Data extracted from Simulation nn2778 for a location representative of the study site are shown in Figure 7-164. The last glacial cycle lasted about 120,000 years.

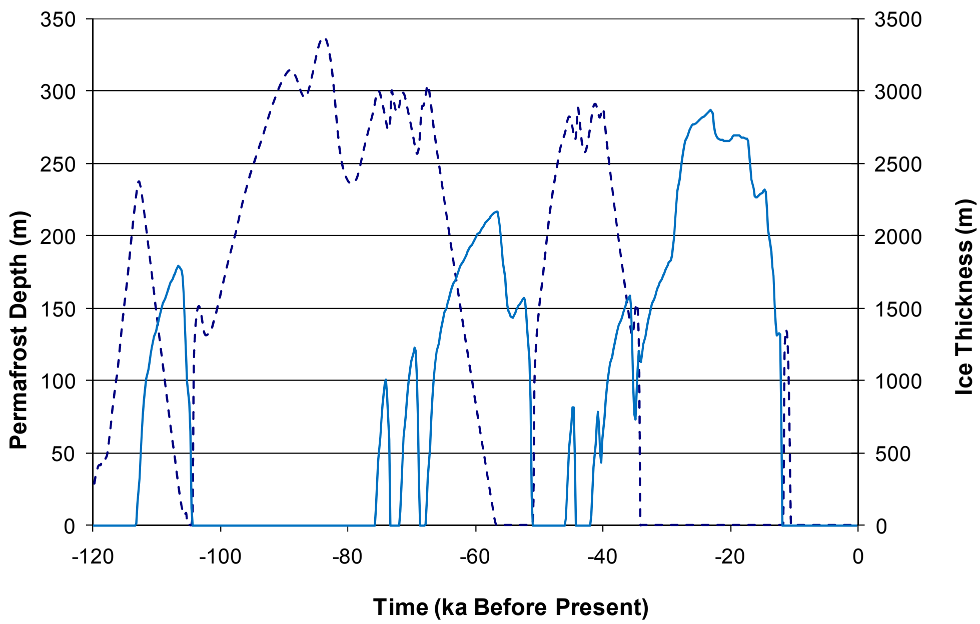

Note: Permafrost depth is represented by (- - - -) and ice sheet thickness by (——).

Figure 7-164: Permafrost Depth and Ice Sheet Thickness for Simulation nn2778

In the glaciation study, it is assumed that the present interglacial (temperate) period lasts a further 50,000 years. Following this long interglacial period, the climate at the repository site is represented by repeated cycles of a simplified version of Simulation nn2778 from Peltier (2006). A total of eight glacial cycles are assumed over the next million years.

A simplified glacial cycle was implemented to make the hydrogeological calculations feasible. This simplified cycle is shown in Figure 7-165 (ice height curves) and Figure 7-166 (permafrost depth profile). The time periods during which different glacial states occur at the study site are shown in Table 7-41.

The transient behaviour of the groundwater flow field during ice sheet movement across the site is of key interest. The time needed for the ice sheet to cross the model domain was estimated as follows:

- The ice sheet profile is specified by an analytical equation; and
- The ice height curves from Simulation nn2778 were fitted with the ice profile curve to determine advance and retreat rates, assuming that the ice sheet travels at a constant speed over the site. The ice speed was varied until a good match was obtained.

The fitted ice height over the site is compared to Simulation nn2778 in Figure 7-165. The ice sheet advance and retreat speeds ranged from 50 to 60 m/a and from 100 to 200 m/a respectively, which compare well with literature field data (Garisto et al. 2010).

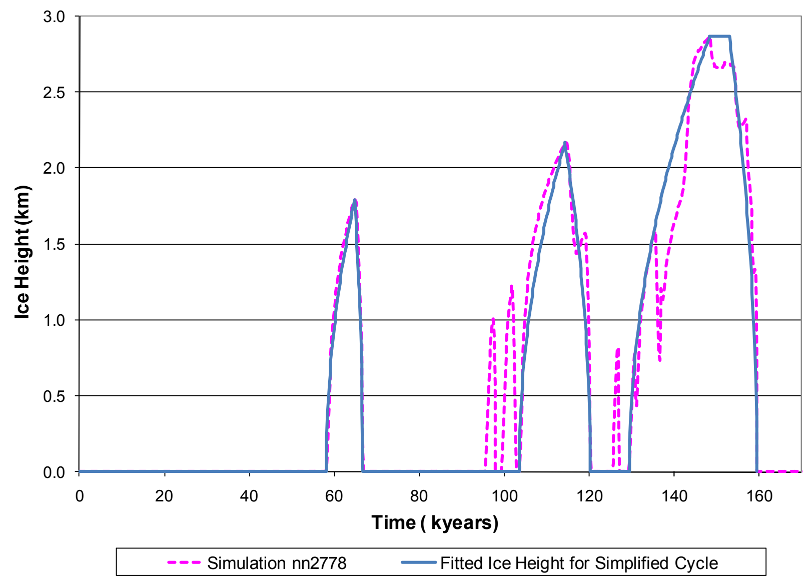

Note: The short periods of ice sheet cover at the site just before the 2nd and 3rd major ice sheet advances are neglected.

Figure 7-165: Comparison of Ice Sheet Height for the Reference Glacial Cycle with Simulation nn2778

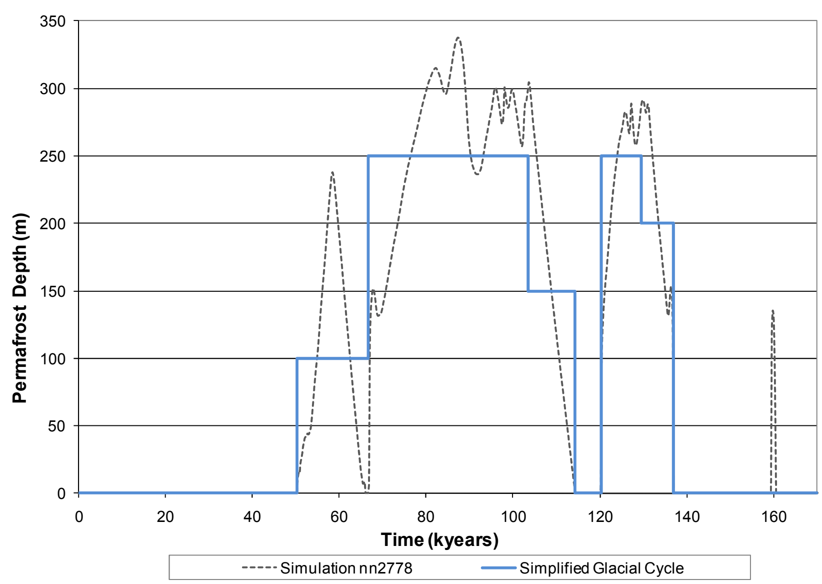

Figure 7-166: Comparison of Permafrost Depths for the Reference Glacial Cycle with Simulation nn2778

Table 7-41: Time History for Reference Glacial Cycle

Relative Time Period (years)[1]	Actual Times During First Cycle (years)	Duration of State (years)	Description of Glaciation State
------------------	0 – 50,300		Temperate (current Interglacial)
0 – 7800	50,300 – 58,100	7800	Permafrost
7800 – 14,500	58,100 – 64,800	6700	Ice Sheet Advance, permafrost underneath
14,500 – 16,400	64,800 – 66,700	1900	Ice Sheet Retreat, permafrost underneath
16,400 – 53,200	66,700 – 103,500	36,800	Permafrost
53,200 – 64,000	103,500 – 114,300	10,800	Ice Sheet Advance, permafrost underneath
64,000 – 70,000	114,300 – 120,300	6000	Ice Sheet Retreat, no permafrost underneath
70,000 – 79,200	120,300 – 129,500	9200	Permafrost
79,200 – 86,600	129,500 – 136,900	7400	Ice Sheet Advance, permafrost underneath
86,600 – 102,700	136,900 – 153,000	16,100	Ice Sheet Advance, no permafrost underneath
102,700 – 109,200	153,000 - 159,500	6500	Ice Sheet Retreat, no permafrost underneath
109,200 – 110,400	159,500 – 160,700	1200	Proglacial Lake
110,400 – 121,200	160,700 – 171,500	10,800	Temperate

Notes: [1] In the glaciation study the current interglacial period is assumed to extend 50,000 years into the future and immediately precedes the start of the first glacial cycle at 50,300 years. The glacial cycle repeats itself starting at: 171,500; 292,700; 413,900; etc. years.

7.8.2.4.2 Hydrogeological Modelling

The study area for the glaciation study is shown in Figure 7-167. Also shown for comparison purposes are the locations for the repository in the glaciation study and the repository in this postclosure safety assessment.

The hypothetical watershed is about 250 km^2, with a river crossing the domain and a topographic high along the northern boundary. The area is characterized by mild topographic changes. There are two major lakes within the model domain, the North and South lakes. The large scale (~100 m) fracture network was generated using a geostatistical fracture procedure, based on Canadian Shield lineament / fracture statistics and the results of a surface lineament analysis (Srivastava 2002).

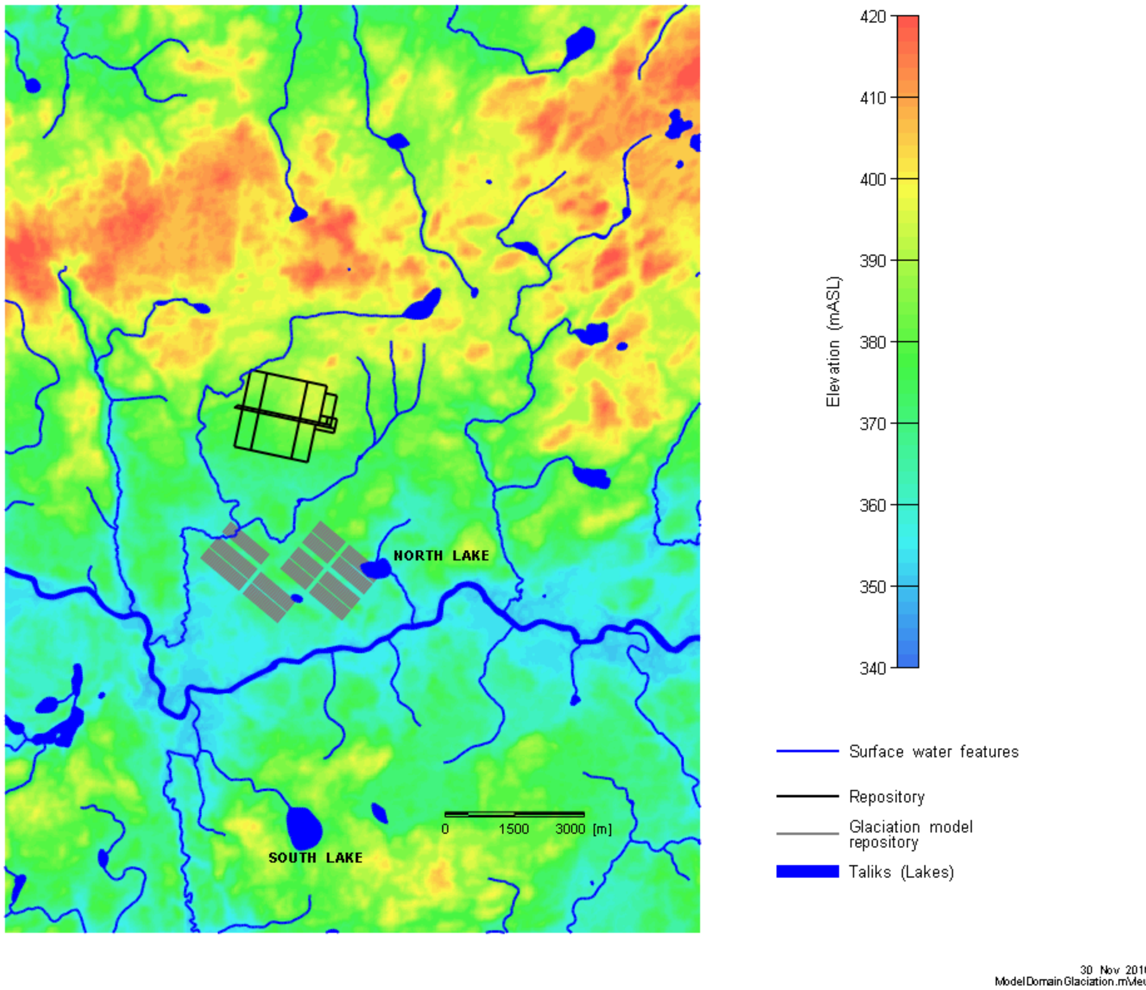

Note: The Glaciation Study considered a repository at a depth of 670 m.

Figure 7-167: Hydrogeological and Transport Model Domain for Glaciation Study

The numeric flow modelling was performed using 3D models implemented in FRAC3DVS-OPG and included the 1-D hydromechanical (HM) coupling model, which is based on the work of Neuzil (2003) and assumes purely vertical strain. The modelling assumed constant density water flow. The absence of salinity is generally viewed as a conservative assumption (i.e., there is more flow at depth than would occur if salinity effects were included, Normani 2009).

The North Lake at the eastern edge of the repository was identified as a discharge zone and is the terminus of the shortest flow pathline from the radionuclide source (i.e., assumed to be two defective containers each holding 360 used fuel bundles) which are located at the east corner of the repository). The North and South Lakes were designated as open taliks. A talik is a region of perennially unfrozen ground that may exist within a permafrost environment. Otherwise, the permafrost formed during the glacial cycle is assumed to be continuous across the study site.

The groundwater modelling is described in detail in Walsh and Avis (2010), where a general approach is developed that captures the impact of glacial cycles on a complex, fractured flow system. The modelling was performed using a 50 m grid model, which precluded direct incorporation of repository features and required use of a large dispersivity value (80 m). Even with these simplifications, execution time for eight glacial cycles (one million years) required more than six months. The main points are summarized below.

Unlike the constant climate case, the groundwater flow field is transient in the glaciation study due to the advance and retreat (along the north-south direction) of ice sheets over the model domain. Results of the simulations show the range of advective velocities that occur at the repository horizon. The modelling results indicated that the glaciation related changes to surface boundary conditions and permafrost formation had an extensive effect on the groundwater flow system, affecting direction and magnitude of flow.

In the glaciation flow model, the taliks were a significant factor, focussing flow from a large portion of the model domain at discrete locations. These isolated gaps in the permafrost acted as pathways for the dissipation of hydraulic pressure generated from preceding glacial events. The system reached equilibrium after the stored glacial pressure was drained. The presence of additional taliks and / or formation of discontinuous permafrost could significantly reduce the duration of glacially induced overpressures and perhaps also the volume of water flowing through individual taliks, decreasing the influence of an individual talik.

The effect of glaciation on the groundwater velocities at the glaciation study repository level is illustrated in Figure 7-168 which shows how the average vertical component of the advective velocity within the repository footprint at repository depth changes with time and varying boundary conditions. The plot makes clear how the different hydraulic boundary conditions affect the flow field in the repository. Advancing glaciers lead to larger negative or downward vertical velocities. Retreating glaciers have the reverse effect, and this effect persists into the following permafrost stages, as the rapid retreat does not allow all the pressure stored during the glacial advance to dissipate.

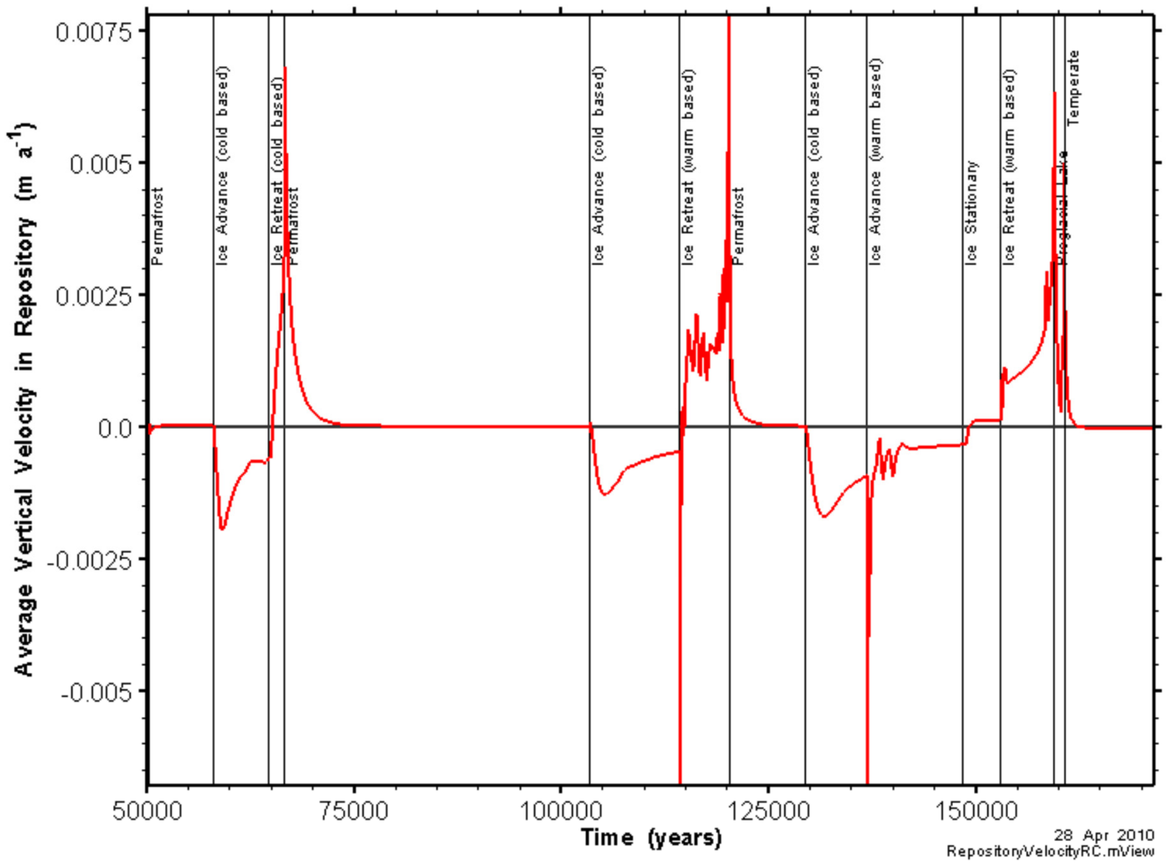

Note: Positive velocities are up, negative velocities are down.

Figure 7-168: Average Vertical Component of Velocity

Integrating the velocities shown in Figure 7-168 gives the average vertical travel distance of a particle within the repository footprint during one glacial cycle as shown in Figure 7-169. The cumulative vertical distance travelled is only about one meter after a 121,000 year long glacial sequence. This means that although the glacial cycling leads to increases in velocity and changes in flow direction, within the repository the hydraulic impacts of glacial advances and retreats almost cancel each other out. However, a caveat needs to be added. Although average velocities are very low within the repository, there is significant variation so that, at certain locations, particles need travel only a short distance from the repository before they encounter a fracture zone of higher permeability.

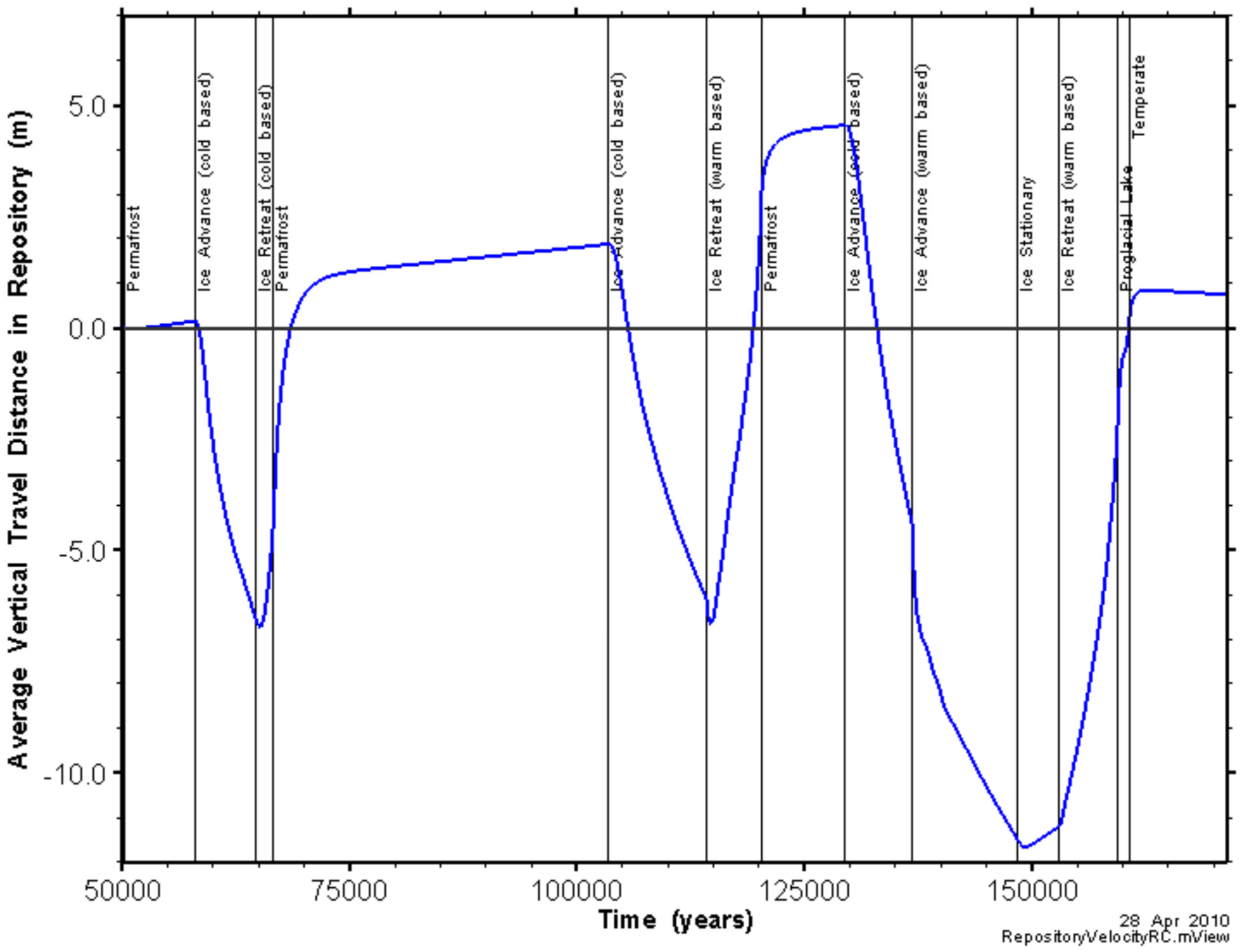

Figure 7-169: Cumulative Average Vertical Advective Flow Distance

7.8.2.4.3 Transport Modelling

The glaciation study further assumed that the repository was built to design specifications, except that two containers, each containing 360 used fuel bundles, were unknowingly placed in the repository with small undetected defects in the copper shell (Garisto et al. 2010). The defective containers are assumed located at the repository location with the shortest groundwater travel time to surface based on the initial temperate climate flow field.

The dose consequences were determined using the SYVAC3-CC4 system model; however, unlike the constant climate case, the groundwater flow field is transient. Since the SYVAC3-CC4 model cannot handle transient flows, it was necessary to approximate the transient groundwater flow field using a series of fixed groundwater flow fields. A different fixed groundwater flow field was selected for each of the nine unique geosphere states defined in the glaciation study (Garisto et al. 2010). Generally the groundwater flow field at around the mid-point of the state was used to represent the groundwater flow during the entire state.

The groundwater flow field for each unique geosphere state was then used to generate the corresponding geosphere network model for each state using the same methodology described in Section 7.8.1.2. Comparison of the I-129 transport results and calculated dose rates obtained using FRAC3DVS-OPG and SYVAC3-CC4 indicated that the approximation of the transient groundwater flow field worked fairly well, given the differences in the models (Garisto et al. 2010, Appendix C). Furthermore, although the I-129 mass flow curves to the biosphere are quite different for the transient model compared to the constant climate case, the overall trend is similar and by the end of the simulation period the transient model shows roughly similar cumulative mass flows into, for example, the North Lake (Figure 7-170).

The effects of a typical glacial advance-retreat cycle on a contaminant plume were largely confined to the upper part of the plume in the more permeable, shallower units. The core of the plume remained relatively unaffected by the hydraulic perturbations induced by the advancing and retreating ice field (Walsh and Avis 2010, Garisto et al. 2010). This is largely due to the low permeability of the deeper geosphere, and the roughly equal and opposite effects of the glacial advance and retreat stages.

7.8.2.4.4 Biosphere Model and Dose Calculations

For the purposes of biosphere modelling, the glacial cycle was divided into temperate, permafrost, ice sheet and proglacial lake states. The occurrence of these states during the reference glacial cycle is shown in Table 7-41. Biosphere parameters are dependent on the climate (i.e., the glacial state (Garisto et al. 2010, Appendix A)). Because the biosphere is so different, a different critical group was defined for each state.

In the temperate state, a Self-Sufficient Farmer household is the critical group. This group is assumed to spend their entire lives in the vicinity of the site and to obtain all their needs locally. All water needs (including irrigation and drinking) are met by a well that intercepts the contaminant plume from the repository. This is similar to the critical group assumed in this postclosure safety assessment report.

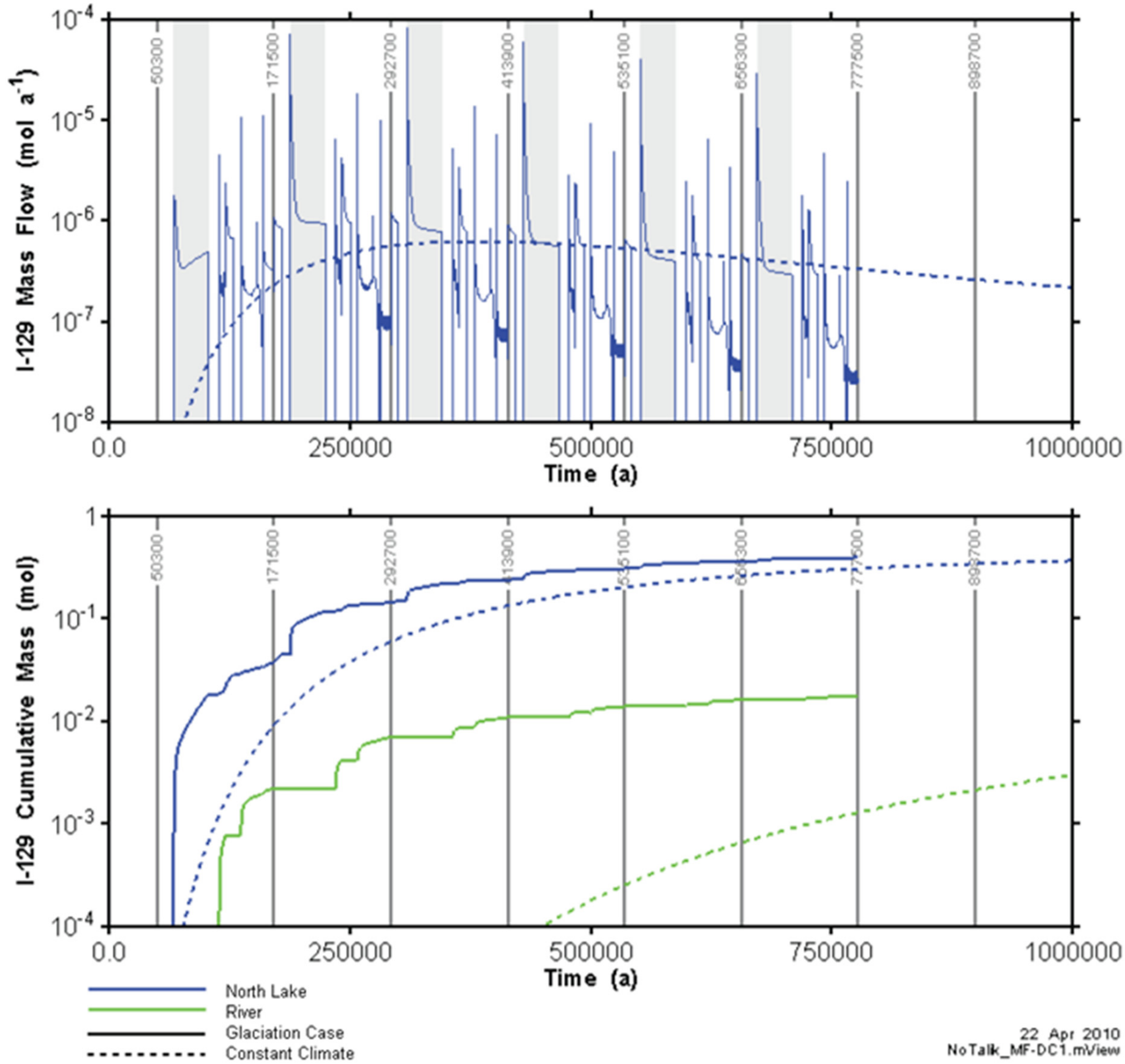

Notes: Compared to equivalent constant climate case (without a well). Mass flow only plotted for North Lake to improve legibility of plot. The vertical lines indicate the start of a glacial cycle. Shaded regions show the second permafrost state in each glacial cycle.

Figure 7-170: I-129 Mass Flow Rate and Cumulative Mass Flow from the Glaciation Study

The biosphere features of the permafrost state are based on the Southern Arctic Ecozone (Environment Canada 2008). This region has a periglacial climate with soils underlain by continuous permafrost and active (thaw) layers that are usually moist or wet throughout the summer. Caribou herds graze in this area in the summers and use it as calving grounds. Migratory birds use this ecozone as a major breeding and nesting ground.

An open talik was assumed to exist below the North and South lakes during permafrost states. Therefore, these lakes become the primary discharge area for groundwater from the repository during permafrost periods. The North lake is assumed to be the primary water source for the critical group living during permafrost states.

During permafrost states, farming is not possible so a Self-Sufficient Hunter, characteristic of the inland tundra region, is the critical group. This group is assumed to spend their entire lives in the vicinity of the site and to obtain all of their needs from that area. Their diet consists mainly of caribou meat, augmented with wild birds and plants. Caribou eat lichens which grow near the repository and are contaminated via air deposition. The atmosphere becomes contaminated due to aquatic degassing and aerosol suspension from the nearby lake. Because lichens live for long periods of time and retain deposited radionuclides effectively, they can accumulate contamination over an extended period.

During ice sheet states, the region near the repository site is covered by an ice sheet and the area is assumed to be uninhabited. Dose rates during the ice sheet state are zero.

The proglacial lake state climate is assumed to resemble that of the permafrost state. The main difference is the presence of a large proglacial lake created by rapid melting of the retreating ice sheet which supplies the critical group with all its water needs. In the proglacial lake state, the critical group is a Self-Sufficient Fisher who moved into the area after the last glaciation. This group resembles the Hunter critical group in that it hunts local mammals such as caribou and wild fowl; however, due to the availability of fish in the proglacial lake, the self-sufficient Fisher diet contains a greater proportion of fish.

Dose rates have been calculated up to one million years to determine the long-term impact of the repository. The dose pathways considered are climate state dependant and include water ingestion and immersion, plant ingestion, animal (fish, bird, milk, cattle, caribou, etc.) ingestion, and air inhalation and immersion.

The calculated I-129 dose rates are shown in Figure 7-171 for the reference case of the glaciation study and for the corresponding constant climate case. These doses were calculated using FRAC3DVS-OPG I-129 transport to the biosphere and the SYVAC3-CC4 biosphere submodel. (Dose rates are zero during the ice sheet states, as discussed above.) Calculated total dose rates are shown Figure 7-172. These latter dose rates were calculated with the SYVAC3-CC4 system model.

Calculated dose rates are well below the 0.3 mSv/a interim dose rate acceptance criterion established in Section 7.1.1 for this postclosure safety assessment.

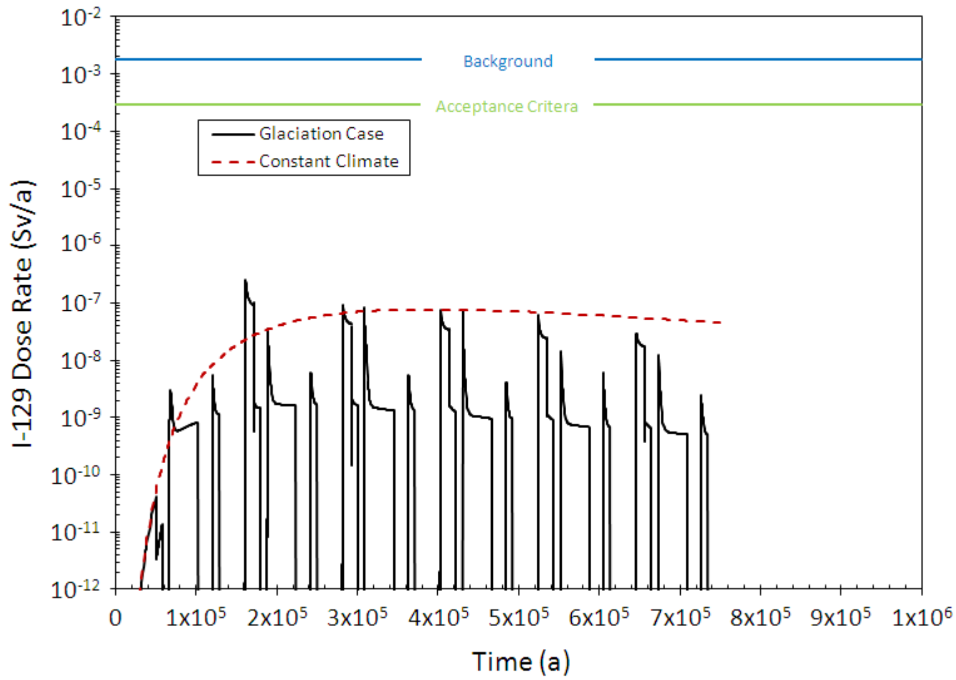

Figure 7-171: I-129 Dose Rate with Glacial Cycles

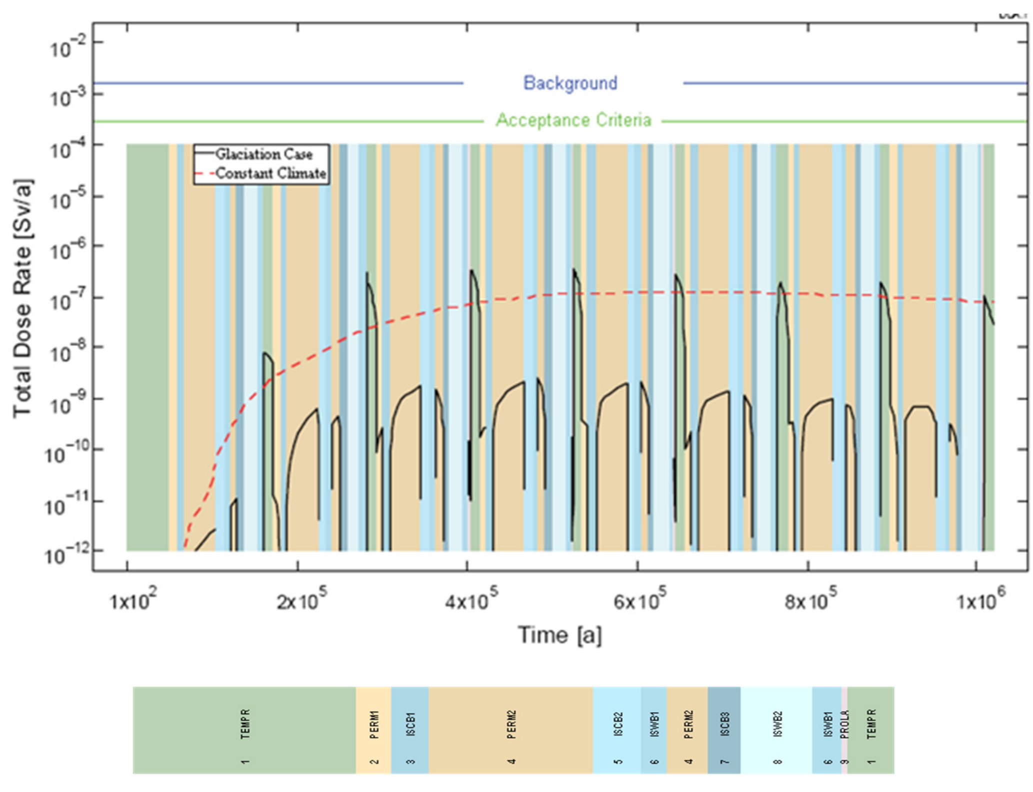

Figure 7-172: Total Dose Rate with Glacial Cycles

The two different models give similar results except for the sharp peaks in the FRAC3DVS-OPG dose rates that occur at the beginning of the second permafrost state of each glacial cycle. These sharp peaks are absent from the system model because this model only uses snap-shots of the transient groundwater flow field as discussed above.

Dose rates during the temperate state are much higher than during the other states mainly because the Farmer critical group uses a well for its water needs whereas the other critical groups use lake water. Radionuclide concentrations in well water are much higher than in lake water because of the lower dilution.

The most important exposure pathway for the Hunter and Fisher critical groups is ingestion of caribou meat because caribou ingest large quantities of lichens which can be contaminated by air deposition.

Besides the reference glaciation case, various sensitivity cases and probabilistic cases were also examined in the glaciation study (Garisto et al. 2010), including an All Containers Fail case similar to that investigated in this postclosure safety assessment. For all sensitivity cases, except the All Containers Fail case, the calculated peak dose rate was well below 0.3 mSv/a. For the All Containers Fail case, the total dose rate was 0.41 mSv/a for a brief period; however, this is below the 1 mSv/a interim dose acceptance criterion for Disruptive Event Scenarios used in this postclosure safety assessment.

It can therefore be concluded that for the hypothetical glaciation study site, the impacts of a deep geological repository would be below regulatory limits when the effects of glaciation are considered.

7.8.2.4.5 Applicability to the Current Postclosure Safety Assessment

The glaciation study illustrates the analysis methods and techniques that could be used in support of a quantitative discussion of the relative impacts of glaciation at a real repository site.

Because the repositories are located in the same watershed, the climate would evolve similarly and the glacial cycle described in Section 7.8.2.4.1 would be representative of the future climate at the postclosure safety assessment site. This means that the critical exposure groups defined for the glaciation cycle are also appropriate. The Farmer critical group present during the temperate period of the glaciation study has similar characteristics to the critical group used to calculate exposure doses in the current study. In particular, both groups use water from a well for drinking, irrigation, etc. and this well captures most of the radionuclide plume from the repository.

There are other substantial differences between the two studies however. These are:

- The glaciation study assumes two defective used fuel containers, with each container holding 360 used fuel bundles. The current study assumes 10 defective containers, with each container holding 48 used fuel bundles.
- The two defective containers are assumed to fail at 100 years. In the current study the first container fails after 1000 years and subsequent containers fail at a rate of one container every 100,000 years.

- The glaciation study assumes a pinhole failure in each container whereas the current study takes no credit for the container inhibiting contaminant movement.
- The repository depth in the glaciation study is 670 m whereas the repository in the current study is 500 m. The shallower repository could lead to an increased impact of ice sheet retreat / advance over the repository site on the groundwater velocities in the repository.
- While the surface lineaments are the same, different fracture networks are used.
- The Geosphere hydraulic conductivity profile in the glaciation study has six depth dependent categories of bedrock compared to three in the current study. Additionally, fracture hydraulic conductivity varied with depth, while the current study uses a single fracture hydraulic conductivity. At the repository level, for example, the hydraulic conductivity of the host rock is $7x10^{-12}$ m/s in the glaciation study versus $4x10^{-11}$ m/s in the current study.
- The horizontal borehole placement method is assumed in the glaciation study whereas stacked buffer boxes are assumed in the current study.
- The current study repository has a large water conducting feature intersecting the repository footprint.

In spite of the differences outlined above, it is anticipated that the relative effects of glaciation will be similar given that the two repositories are located at the same general location on the Canadian Shield. The glaciation study shows that the calculated peak dose rate could be an order of magnitude greater (depending on the glacial cycle) than the peak dose rate for a constant temperate climate case. Given that the dose rate for the Base Case is almost 1200 times less than the interim dose rate criterion of 0.3 mSv/a, it can be inferred that the anticipated dose consequences for the Base Case would also likely be well below regulatory limits when the effects of glaciation are considered.

A discussion of the potential effects of glaciation on the deep groundwater system for the current study geosphere is provided in Chapter 2.

7.8.2.5 Probabilistic Analysis

In the previous sections, deterministic analyses are performed for the Base Case and a series of sensitivity studies to illustrate the effect of degraded barrier performance on radionuclide transport.

Many of the modelling parameters are uncertain or have a natural degree of variability, and are therefore more generally characterized by a range or distribution of values. Simultaneous accounting of these uncertainties is achieved by using the System Model in probabilistic mode.

Probabilistic mode uses a random sampling strategy that considers the full range of possible parameter values. The results presented here draw from 100,000 simulations in which parameter values are randomly sampled from their probability density functions. Each of these thousands of simulations produces a unique estimate of impact that is used to collectively generate a distribution that reflects the underlying uncertainty. An important caveat is that parameter values that could affect groundwater flow are not varied in these simulations.

Two probabilistic cases are simulated. These are:

1) Number, locations and failure times for the defective containers fixed at their Base Case values, with all other available parameters varied; and
2) Number, locations and failure times for the defective containers varied, with all other parameters maintained at their Base Case values.

A selection of biosphere parameters represented by probability distributions is shown in Table 7-32 through Table 7-35. A detailed description of the probability distributions for all parameters is provided in Gobien et al. (2016).

<u>Container Assumptions</u>

In the Base Case, 10 defective containers are assumed present in the repository. For the probabilistic case in which the number of defective containers is varied, the number of defective containers is described by a binomial distribution with the individual container failure probability selected such that 10 failed containers is the 95th percentile value. This is representative of the anticipated successful manufacturing process and robust quality assurance program that will be implemented to ensure the likelihood of placing off-specification containers in the repository is very low. As noted in Section 7.2.2.1, studies are underway to better define this likelihood and the analysis would be updated when that information becomes available.

In the Base Case, the defective containers are all clustered in the location that maximizes contaminant uptake to the well. For the probabilistic case in which container locations are varied, defective containers can be in any of the 14 sectors of the Full Geosphere Submodel (see Section 7.8.1.2.2). Container failures in multiple sectors can also occur.

In the Base Case, the first defective container fails at 1000 years, with subsequent containers failing at a rate of one failure for every additional 100,000 years. In the probabilistic case in which container failure times are varied, the failure times are defined using a uniform distribution ranging between 1 and 1,000,000 years. In the model, containers in different sectors can fail at different times; however all defective containers in a given sector fail at the same time.

The well location is fixed at its Base Case location.

7.8.2.5.1 Results for Container Failure Assumptions Fixed

In this probabilistic case, the number, locations and failure times of the containers are fixed at their Base Case values, with all other available parameters varied.

This is simulated using the Simple Model described in Section 7.8.1.2.1.

<u>Dose Rate Results</u>

Figure 7-173 presents a histogram of the peak dose rates obtained over the 100,000 simulations, while Table 7-42 presents a summary of the histogram statistics. The median, 95th percentile and 99th percentile values are 1.1×10^{-4} mSv/a, 9.1×10^{-4} mSv/a and 2.1×10^{-3} mSv/a. The median and 95th percentile values are marked on the figure. For comparison, the Base Case deterministically determined peak dose rate is 2.5×10^{-4} mSv/a (Section 7.8.2.1). This falls between the median and 95th percentile values.

Figure 7-173 is lognormally distributed and has approximately 50% of the maximum dose rate results occuring within a factor of 3 of the Base Case value. This suggests that a large number of the parameter value changes in the probabilistic simulations do not have a significant effect on the maximum dose rate.

There are some higher dose simulations on the right hand side of Figure 7-173, with the maximum of these having a dose rate of 0.10 mSv/a. These higher dose cases are discussed in a later part of this section.

All values are below the interim dose rate acceptance criterion of 0.3 mSv/a established in Section 7.1.1.

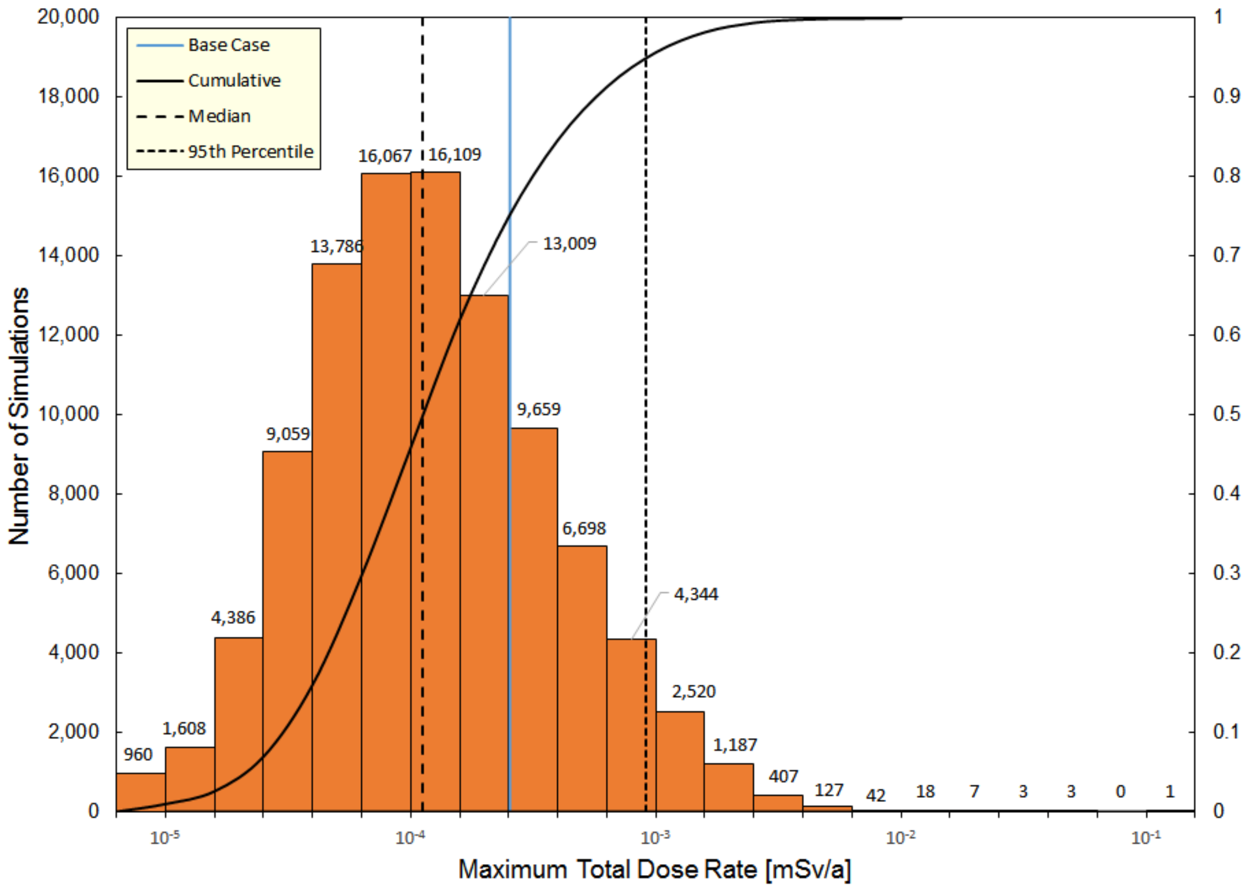

Note: The leftmost bin includes all simulations (960) that resulted in a dose less than 10^{-5} mSv/a

Figure 7-173: Probabilistic Assessment: Peak Dose Rate Histogram with Container Assumptions Fixed

Table 7-42: Statistical Information for the Peak Dose Rate Histogram with Container Assumptions Fixed

Statistic	Value (mSv/a)	Bootstrap 95% Confidence Bounds[1]	
		Lower Bound (mSv/a)	Upper Bound (mSv/a)
Median	1.1×10^{-4}	1.1×10^{-4}	1.2×10^{-4}
95th Percentile	9.1×10^{-4}	8.7×10^{-4}	9.6×10^{-4}
99th Percentile	2.1×10^{-3}	1.9×10^{-3}	2.2×10^{-3}

Notes:

[1] Based on 10 sets of 10,000 replicates of the dataset obtained using the bootstrap methodology. The confidence intervals are calculated using the bootstrap method (with replacement). Since the distribution of peak dose rates is skewed, the bootstrap BC_a methodology described by DiCiccio and Efron (1996) is used.

Table 7-43 shows the median, 95th percentile and 99th percentile values for those radionuclides that contribute more than 0.001% of the total dose rate. As in the Base Case, I-129 is the dominant dose contributor.

Table 7-43: Probabilistic Assessment: Individual Radionuclides Dose Contributions for Container Assumptions Fixed

Radionuclide	Median (mSv/a)	95th Percentile (mSv/a)	99th Percentile (mSv/a)
I-129	9.91×10^{-5}	7.53×10^{-4}	1.64×10^{-3}
Se-79	2.95×10^{-6}	6.34×10^{-5}	2.76×10^{-4}
Cs-135	2.23×10^{-6}	1.15×10^{-4}	6.33×10^{-4}
Cl-36	8.47×10^{-7}	4.05×10^{-5}	3.00×10^{-4}
Cl-36 Zr	6.46×10^{-7}	2.91×10^{-5}	1.54×10^{-4}
Ca-41	6.19×10^{-8}	1.08×10^{-6}	3.09×10^{-6}
C-14	5.48×10^{-8}	6.27×10^{-7}	1.72×10^{-6}
C-14 Zr	4.65×10^{-8}	2.56×10^{-7}	4.58×10^{-7}
Sb-126	0	0	7.86×10^{-8}
Np-237	0	0	6.54×10^{-8}
Sn-126	0	0	4.37×10^{-8}

Note: (1) only those radionuclides with values greater than 0.001% of the maximum column value are shown.

(2): Values less than 0.001% of the maximum column value are set to zero.

Figure 7-174 shows the distribution of dose rates from all 100,000 simulations showing the time dependence of the dose bands for the 25th, 50th, 75th, 90th, 95th and 99th percentiles.

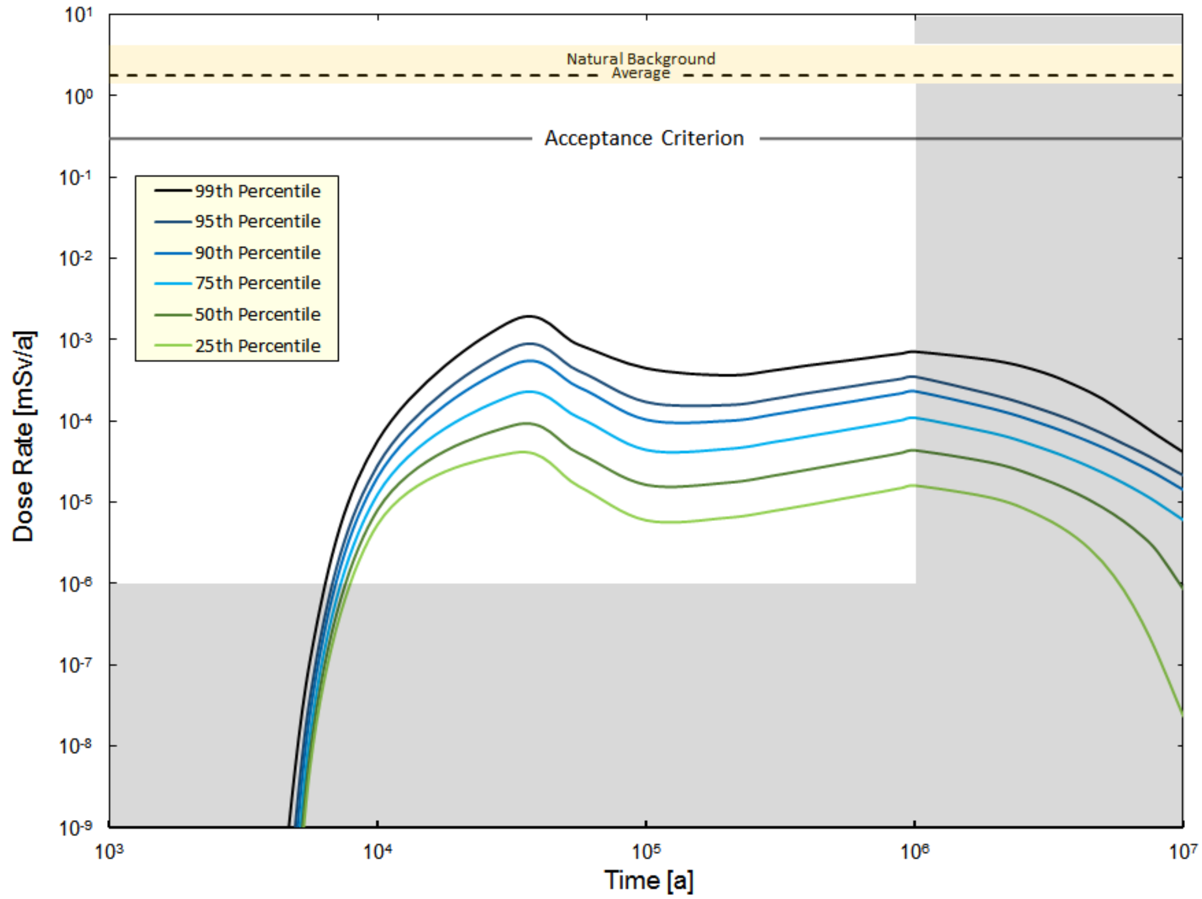

Figure 7-174: Probabilistic Assessment: Time Dependence of Percentile Values with Container Assumptions Fixed

<u>Maximum Value Simulations</u>

Figure 7-173 shows that there are a number of cases with dose rates considerably higher than the 95th percentile value (9.1×10^{-4} mSv/a), with the maximum value reported over all 100,000 simulations as 0.10 mSv/a.

The cases with the 6 highest dose rates have been extracted and studied to identify the causal factors. Table 7-44 summarizes each of these six cases, showing the peak dose rates, the time of the peak, the dominant radionuclide, how much the dominant radionuclide contributes to the total and the main exposure pathway.

Table 7-44: Probabilistic Assessment: Results for Top 6 High-Dose Simulations with Container Assumptions Fixed

Simulation	Peak Dose [mSv/a]	Time of Max Dose [Ma]	Dominant Radionuclide	% of total dose from Cs-135	Dominant Pathway
98653	1.0×10^{-1}	2.54	Cs-135	99.9	Food Ingestion – Leafy Veg Ingestion
45685	5.6×10^{-2}	1.53	Cs-135	100	Food Ingestion – Fish Ingestion
95774	4.1×10^{-2}	3.23	Cs-135	100	Food Ingestion – Root Veg Ingestion
28531	4.0×10^{-2}	1.69	Cs-135	99.4	Food Ingestion – Leafy Veg Ingestion
85471	3.9×10^{-2}	1.73	Cs-135	100	Food Ingestion – Root Veg Ingestion
32353	3.0×10^{-2}	1.51	Cs-135	99.2	Food Ingestion – Root Veg Ingestion

Table 7-44 shows that Cs-135 (and not I-129) is the dominant dose contributor in these cases, with the dominant exposure pathway being uptake of food. Five cases are controlled by ingestion of vegetables and one case is controlled by fish ingestion. The following observations can be made about these cases:

- The dose rates in cases whose dominant dose pathway is ingestion of garden vegetables are primarily due to high sorption in soils. Table 7-45 shows the soil types and Kd values for these simulations. The Kd values are many times higher than those of the Base Case.

Table 7-45: Probabilistic Assessment: Cs-135 Pathway

Simulation	Soil Type	Soil Kd [L/kg]	Ratio of Soil Kd to the Base Case Value*
98653	Clay	5.3×10^{5}	1950
95774	Sand	1.9×10^{5}	700
28531	Organic	8.7×10^{4}	320
85471	Loam	2.0×10^{5}	760
32353	Clay	1.8×10^{5}	650

*: The Base Case assumes a sandy soil with a Cs Kd of 2.7×10^{2} L/kg.

  Note that a number of other biosphere parameters (e.g., plant ingestion rate, soil irrigation rate, plant concentration ratio, soil washout ratio, atmospheric deposition rate and atmospheric dust loading) further increase the plant ingestion dose rate in these cases and determine whether the plant ingestion pathway is dominated by leafy or root vegetables.

- Simulation #45685 is unique in that the dominant dose pathway is ingestion of fish. This dose is entirely due to an extremely high sampled value for the aquatic concentration ratio for Cs-135 ($1.7x10^8$ L_{water}/kg_{wetbio} or 48,600 times the Base Case value).

- The soil Kd and aquatic concentration ratio are both described by lognormal distributions. Neither of these distributions have upper or lower bounds defined.

Although none of these simulations exceeded the dose rate criterion, the basis for Cs sorption in soils and concentration in the food chain should be reviewed for future studies and upper and lower bounds to probabilistic distributions should generally be applied. In the absence of such probability distribution bounds, extreme unrealistic values could be selected in the sampling process.

7.8.2.5.2 Results for Container Failure Parameters Varying

In this probabilistic case, the number, locations and failure times of the containers are varied, with all other available parameters fixed at their Base Case values.

This is simulated using the Full Model described in Section 7.8.1.2.2.

Number of Defective Containers

Figure 7-175 presents a histogram of the number of container failures over the 100,000 simulations. The minimum number of failures is 0 (in 209 simulations) and the maximum number is 20 (in one simulation). The median is 6, the 95th percentile is 11 (which is close to the value of 10 that was used to derive the failure distribution), and the 99th percentile is 13.

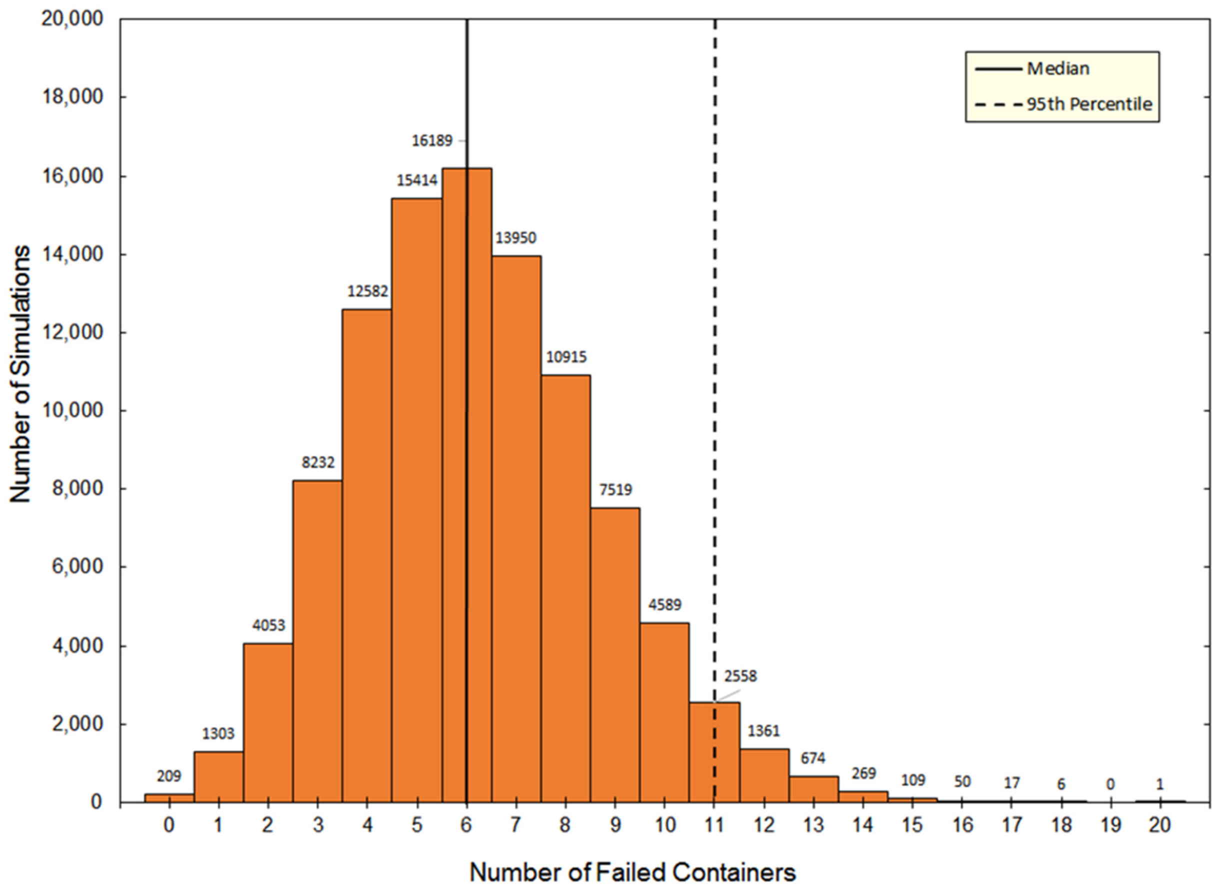

Figure 7-175: Probabilistic Assessment: Distribution of Container Failures with Container Assumptions Varying

<u>Dose Rate Results</u>

Figure 7-176 presents a histogram of the peak dose rates obtained over the 100,000 simulations, while Table 7-46 presents a summary of the histogram statistics. The median, 95th percentile and 99th percentile values are 4.4×10^{-5} mSv/a, 2.2×10^{-4} mSv/a and 3.2×10^{-4} mSv/a. The median and 95th percentile values are marked on the figure. The maximum over all simulations 6.2×10^{-4} mSv/a. For comparison, the Base Case deterministically determined peak dose rate is 2.5×10^{-4} mSv/a (Section 7.8.2.1). This is between the 95th and 99th percentile values.

Figure 7-176 has three primary peaks, with the first occurring between 1×10^{-5} mSv/a and 3×10^{-5} mSv/a, the second occurring between 4×10^{-5} mSv/a and 6×10^{-5} mSv/a and the third (and largest peak) occurring between 1×10^{-4} mSv/a and 2×10^{-4} mSv/a. These peaks correspond to transport being directed to one of the primary discharge zones. The largest peak occurs because the bulk of the transport reaches the well, and therefore the dose rates are comparable to that of the Base Case. The lower two peaks represent simulations in which the majority of the failed containers are located in regions of the repository where the discharge is to either the East or West rivers. There are very few simulations in which the primary discharge is to the Central Wetland due to the well being active and thereby capturing the bulk of the transport that would otherwise reach Central Wetland. The spread in the peaks is due to a variable number of failed containers in a given simulation.

There are some higher dose simulations on the right hand side of Figure 7-176, with the maximum of these having a dose rate of 6.2×10^{-4} mSv/a. These higher dose cases are discussed in a later part of this section.

All values are well below the interim dose rate acceptance criterion of 0.3 mSv/a established in Section 7.1.1.

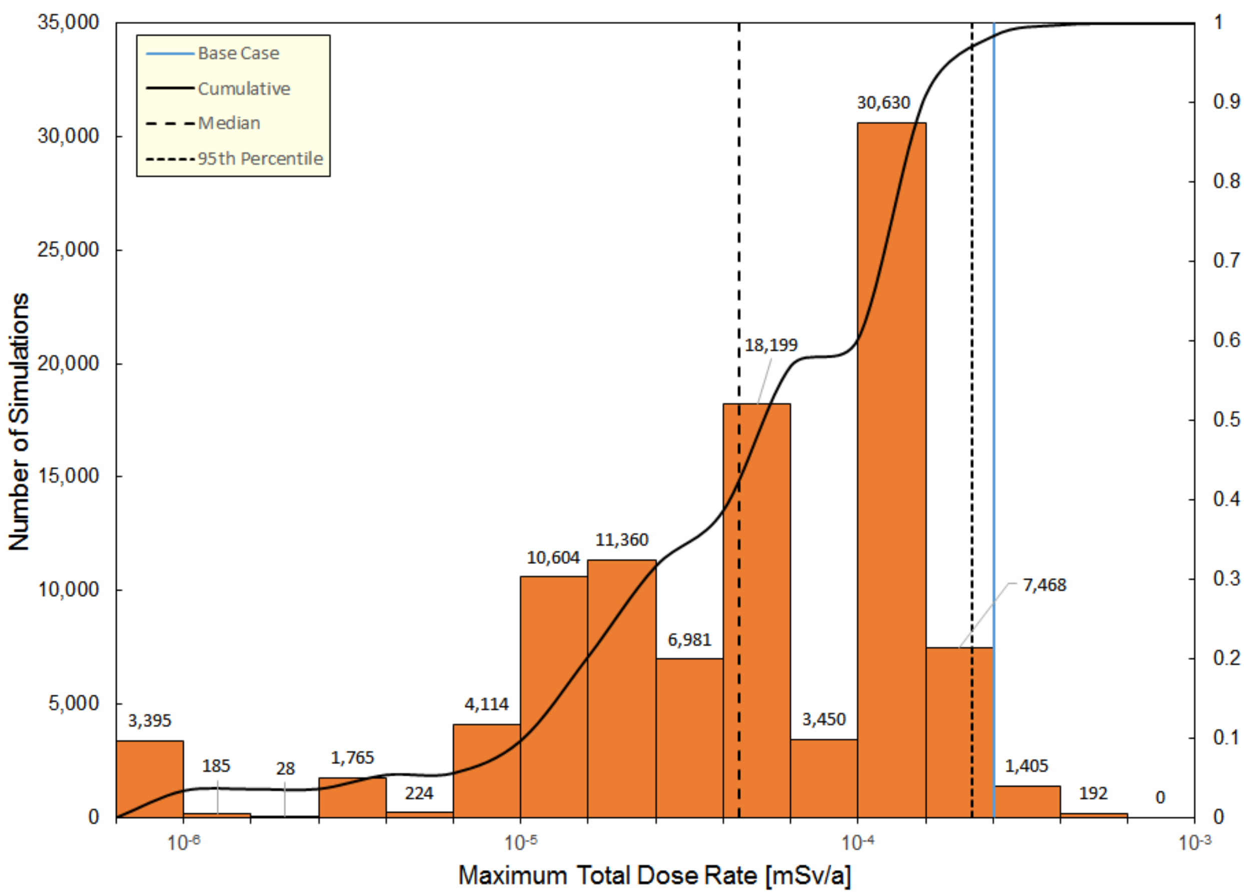

Note: The leftmost bin at 10^{-6} mSv/a includes all simulations (3395) that resulted in a dose less than 10^{-6} mSv/a

Figure 7-176: Probabilistic Assessment: Peak Dose Rate Histogram with Container Assumptions Varying

Table 7-46: Statistical Information for the Peak Dose Rate Histogram with Container Assumptions Varying

Statistic	Value (mSv/a)	Bootstrap 95% Confidence Bounds[1]	
		Lower Bound (mSv/a)	Upper Bound (mSv/a)
Median	$4.4x10^{-5}$	$4.3x10^{-5}$	$5.5x10^{-5}$
95th Percentile	$2.2x10^{-4}$	$2.2x10^{-4}$	$2.2x10^{-4}$
99th Percentile	$3.2x10^{-4}$	$3.2x10^{-4}$	$3.2x10^{-4}$

Notes:

[1] Based on 10 sets of 10,000 replicates of the dataset obtained using the bootstrap methodology. The confidence intervals are calculated using the bootstrap method (with replacement). Since the distribution of peak dose rates is skewed, the bootstrap BC_a methodology described by DiCiccio and Efron (1996) is used.

Table 7-47 shows the median, 95th percentile and 99th percentile values for those radionuclides that contribute more than 0.001% of the total dose rate. As in the Base Case, I-129 is the dominant dose contributor.

Table 7-47: Individual Radionuclide Dose Rates with Container Assumptions Varying

Radionuclide	Median (mSv/a)	95th Percentile (mSv/a)	99th Percentile (mSv/a)
I-129	$4.41x10^{-5}$	$2.18x10^{-4}$	$3.20x10^{-4}$
Cl-36 Zr	$1.09x10^{-7}$	2.52x10-7	$3.18x10^{-7}$
Cl-36	$7.90x10^{-8}$	2.91x10-7	$3.73x10^{-7}$
Cs-135	$7.20x10^{-8}$	4.48x10-7	$6.56x10^{-7}$
Se-79	$5.41x10^{-8}$	1.86x10-7	$2.24x10^{-7}$

Note: only those radionuclides with values greater than 0.001% of the maximum column value are shown

Figure 7-177 shows the distribution of dose rates from all 100,000 simulations showing the time dependence of the dose bands for the 25th, 50th, 75th, 90th, 95th and 99th percentiles. The peak dose rates occur much later than in the Base Case simulation because of the uniform distribution (1 to 1,000,000 years) adopted for container failure, and because the transport times to the well for repository sectors, other than the one represented in the Base Case, are much longer.

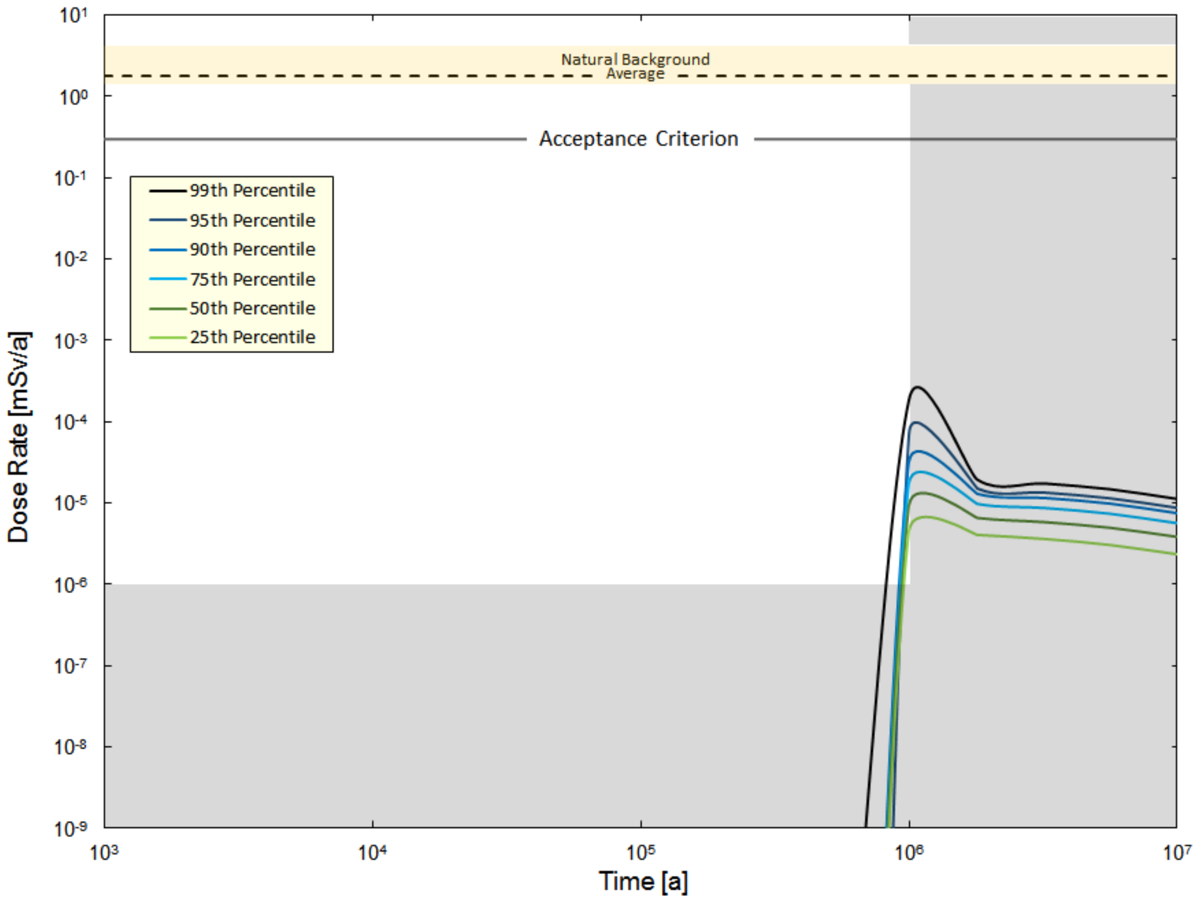

Figure 7-177: Probabilistic Assessment: Time Dependence of Percentile Values with Container Assumptions Varying

<u>Maximum Value Simulations</u>

Figure 7-176 shows there are cases with dose rates higher than the 95th percentile value (2.2×10^{-4} mSv/a), with the maximum value reported over all 100,000 simulations as 6.2×10^{-4} mSv/a. While these results are not substantially different from the Base Case value of 2.5×10^{-4} mSv/a, they are investigated further below to develop an improved understanding of the simulations.

Table 7-48 presents results from the 6 simulations with the highest dose rates.

Table 7-48: Probabilistic Assessment: Results for Top 6 High Dose Simulations with Container Assumptions Varying

Run ID	Peak Dose [mSv/a]	Time of Peak Dose [a]	Main Contributor	% of total from I-129	Number of Failed Containers	Number of Failures in Sector 10
57623	6.2×10^{-4}	1.02×10^{6}	I-129	99.9	14	5
96371	5.6×10^{-4}	1.02×10^{6}	I-129	99.8	16	5
56452	5.6×10^{-4}	1.02×10^{6}	I-129	99.8	11	5
9434	5.4×10^{-4}	1.02×10^{6}	I-129	99.9	15	5
45715	5.4×10^{-4}	1.02×10^{6}	I-129	99.8	8	5
62918	5.4×10^{-4}	1.02×10^{6}	I-129	99.9	12	5

All of these cases each have 5 containers failing in Sector 10 of the System Model, which is a sector that leads directly to the well. Unlike the Base Case, all of these containers have the same failure times. The highest dose case also has 3 containers failing in Sector 11, which is also a pathway to the well, with transport depending on the well pumping rate.

The main reason the dose is higher in some cases is due to the simultaneous failure of multiple containers. This results in an I-129 instant release term that is greater than that for a single container failure (as assumed in the Base Case), which then leads to a higher dose rate.

7.8.2.6 Summary of Results for System Modelling

Table 7-49 summarizes results for all of the cases described in Section 7.8.2. The results emphasize the importance of the well and its assumed location, with the fuel dissolution rate and the occurrence of common mode container failure also having a significant effect.

A greater number of failed containers can also have a significant effect; however, the magnitude of the effect depends strongly on where the additional defective containers are distributed within the repository with respect to the well.

Table 7-49: Summary of Results for System Model

Case	Peak Dose Rate (mSv/a)	Ratio to Base Case	Time of Peak Dose Rate (a)
REFERENCE CASE	**0**	**-**	**-**
Sensitivity Cases			
Base Case	2.5×10^{-4}	-	23,300
Base Case – No Well	1.4×10^{-7}	1/1800	27,700
Fuel Barrier Sensitivity*			
Fuel Dissolution Rate Increased by a Factor of 10	1.6×10^{-3}	6.4	27,900
Fuel Instant Release Fractions Set to 10%	4.3×10^{-4}	1.7	21,200
Zircaloy Sheath Barrier Sensitivity			
Zircaloy Dissolution Rate Increased by a Factor of 10	2.6×10^{-4}	1	23,900
Zircaloy Instant Release Fractions Set to 10%	2.5×10^{-4}	1	23,400
Container Barrier Sensitivity			
All 10 Containers Fail at 1000 Years	2.6×10^{-3}	10	23,100
Low Sorption in the EBS With Coincident High Solubility Limits in the Container	2.5×10^{-4}	1	23,900
No Solubility Limits in the Container	2.5×10^{-4}	1	23,900
50 Containers Fail at 1000 Years, all in worst location**	1.3×10^{-2}	50	23,100
50 Containers Fail at 10,000 Years, uniform distribution**	4.2×10^{-4}	1.7	36,300
1000 Containers Fail at 10,000 Years, uniform distribution**	8.5×10^{-3}	34	36,300
Buffer, Backfill and Seal Barrier Sensitivity			
Low Sorption in the EBS With Coincident High Solubility Limits in the Container	2.5×10^{-4}	1	23,900
No Sorption in the Near Field	2.5×10^{-4}	1	23,800
Geosphere Barrier Sensitivity			
Two Sigma (Low) Sorption in the Geosphere	2.6×10^{-4}	1	24,200
Glaciation Sensitivity			
Glaciation Case	Could be up to 10 times greater than temperate climate case		
Probabilistic Sensitivity			
Containers Assumptions Fixed (95th Percentile)	9.1×10^{-4}	3.6	-
Containers Assumptions Vary (95th Percentile)	2.2×10^{-4}	0.88	-

*: as discussed in Section 7.2.2.3, not credit is taken for the fuel sheath acting as a barrier to prevent the fuel from coming into contact with water

**: results obtained from scaling of other cases (see Section 7.8.2.3.3)

7.9 Modelling and Results for Disruptive Event Scenarios

Disruptive Event Scenarios postulate the occurrence of unlikely events leading to possible penetration of barriers and abnormal loss of containment. Chapter 6 describes how the Disruptive Scenarios are identified and concludes that the following are relevant to the hypothetical site and conceptual repository design:

- Inadvertent Human Intrusion;
- All Containers Fail;
- Repository Seals Failure;
- Poorly Sealed Borehole;
- Undetected Fault;
- Container Failure[1]; and
- Partially Sealed Repository.

As noted in Section 7.2, a limited scope of work has been adopted in this illustrative postclosure safety assessment, and as such, only the first three scenarios are examined in detail. It is recognized that for an actual site, the full set of scenarios would need to be evaluated.

Section 7.2.3 and Table 7-7 contain a description of these three scenarios

Regarding the excluded scenarios:

- For the Poorly Sealed Borehole Scenario, as long as the boreholes are sufficiently far from the repository footprint, they are unlikely to be important due to the small size of the borehole and the limits of transport in low permeability rock. Care would be taken to position the boreholes in locations that have minimal impact. The potential effects of the boreholes would be analyzed as part of a real site investigation, when the borehole distances are known.
- For the Undetected Fault Scenario, it is anticipated that any large fractures intercepting the repository not identified during site characterization would be discovered during construction such that appropriate mitigating measures could be taken. These measures could include possible rerouting of the repository layout to avoid large transmissive features.
- For the Container Failure Scenario, the peak dose arising from this event is anticipated to be similar to the Base Case of the Normal Evolution Scenario and significantly less than that arising from the All Containers Fail Disruptive Event Scenario due to the much smaller number of affected containers.
- The Partially Sealed Repository scenario considers the consequences if the repository is abandoned and the shafts are not sealed, thereby implying a near-future loss-of-society.

Analysis results and dose consequences for the first three Scenarios are discussed below.

---

[1] This considers delayed but substantive failure of a few containers due to unexpected in-situ conditions, and is different from the Normal Evolution Scenario which considers a small defect unknowingly present in some containers as the initiating event.

7.9.1 Inadvertent Human Intrusion

The Inadvertent Human Intrusion Scenario considers the same evolution of the repository system as for the Normal Evolution Scenario, with the only difference being the occurrence of human intrusion sometime after institutional control of the site is no longer effective. In this scenario, an exploratory borehole is assumed to be drilled through the geosphere and into the repository.

In an exploratory borehole, the investigators would most likely collect samples or conduct measurements at the repository level, which would then lead to identification of any significant residual radioactivity (e.g., gamma logging is a standard borehole measurement). The investigators would then initiate precautions to prevent further exposure, including cleanup and appropriate disposal of any surface-released materials. The borehole would also be properly sealed, so that under normal drilling circumstances, there would be little impact.

Nevertheless, the Inadvertent Human Intrusion Scenario assumes that the presence of radioactivity is not immediately recognized and safety restrictions are therefore not imposed. It further assumes that the drill site is not managed according to current standards, and that material from the borehole is released onto the surface.

The assessment does not include the variant case in which the borehole is poorly sealed thereby providing a long-term pathway for contaminants to escape the repository. Such a case has been considered in SKB (2010a), which shows that the consequences are orders of magnitude less than the SKB acute exposure dose rate for the Inadvertent Human Intrusion Scenario. Although not calculated here, a similar conclusion is expected because there is little driving force to transport contaminated material up the (narrow) borehole, and any such release would be further diluted in the groundwater flowing in the upper geosphere.

7.9.1.1 Description

Figure 7-178 presents an event tree defining the possible outcomes associated with drilling in a repository location.

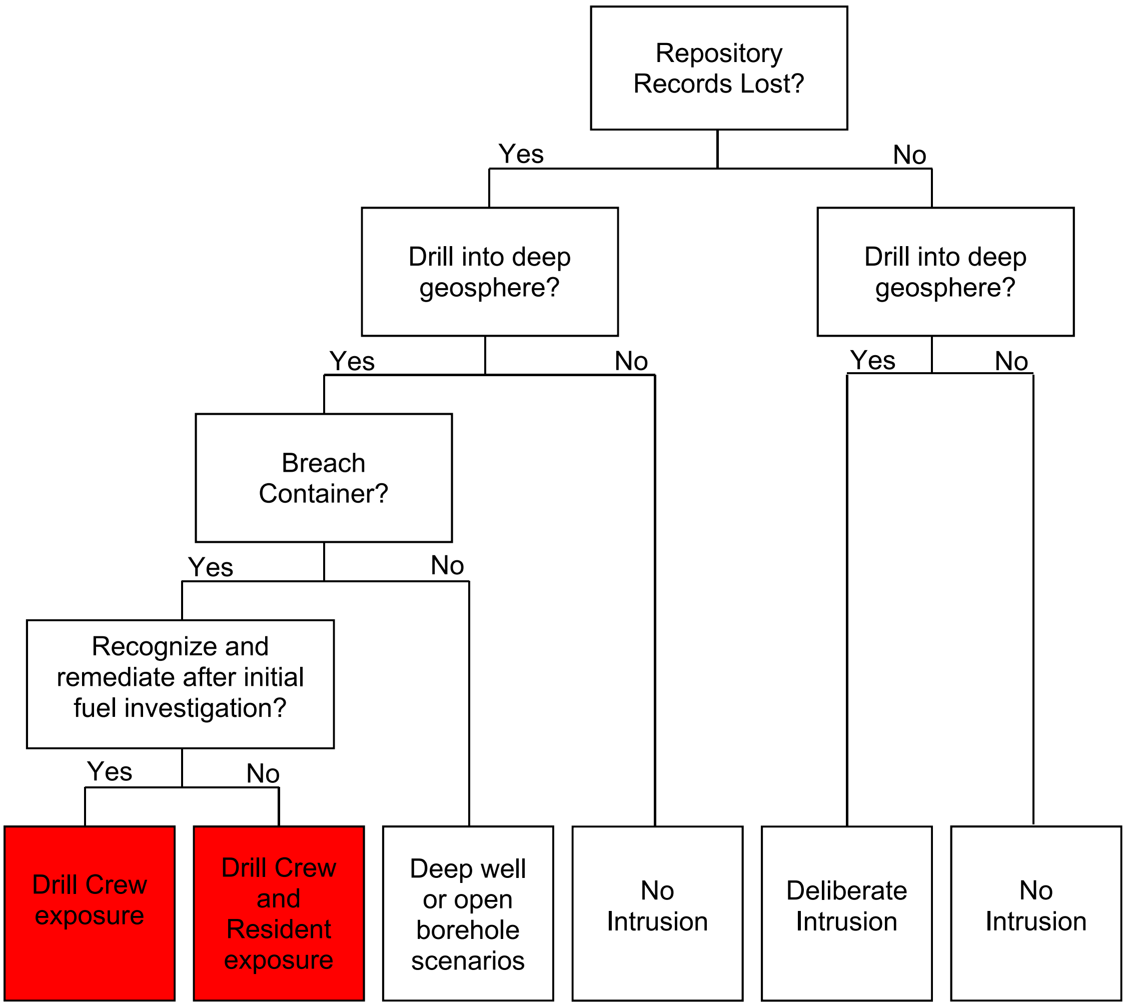

Figure 7-178: General Sequence of Events for Inadvertent Human Intrusion

Of interest to this discussion is the outcome in which:

- The repository records are lost;
- There is drilling into the deep geosphere; and
- The drilling breaches a used fuel container such that used fuel is inadvertently and unknowingly brought to the surface. Note that the early occurrence of such an event is unlikely given today's technology because drilling through a container wall without detecting it on the surface is not thought possible.

This then leads to the potential exposure of the following two groups:

- The Drill Crew, exposed to contaminated drill slurry spread on the surface around the drill rig and to a core section containing used fuel; and
- A Resident at the site, exposed by living nearby and growing food on soil contaminated by drill slurry[2].

To provide context, Table 7-50 presents a summary of the exposure groups considered in recent national and international inadvertent human intrusion safety assessments.

Table 7-50: Human Intrusion Pathways Considered in Recent Safety Assessments

Assessment	Scenario / Exposure Cases Considered
Medri 2012 (Canada)	Drill crew exposed to extracted core and slurry spread around the drill rig. Resident living and growing crops on contaminated soil from drilling slurry*
Posiva Oy 2014 (Finland)	Drill crew exposed while drilling into used fuel container* Geologist exposed to used fuel core sample Drill crew exposed while drilling into buffer material Geologist exposed to buffer material sample Drill crew exposed while drilling into backfill material Geologist exposure to backfill material sample Resident exposed through use of deep borehole for drinking water Resident exposed through use of deep borehole for drinking water, irrigation of crops and watering of livestock.
SKB 2014 (Sweden)	Drill crew exposed while working at the drill site* Construction worker exposed to the contaminated soil from drilling waste at the drill site after redevelopment of the land for commercial or residential construction. Residents exposed from growing a garden in soil contaminated by the drilling wastes.
DOE 2008 (USA)	Reasonable Maximally Exposed Individual (Resident) exposed as a result of direct pathway to the groundwater made accessible by the borehole.
Nagra 2002 (Switzerland)	Resident exposed as result of open borehole into buffer or waste creating pathway for radionuclide to reach aquifer
JNC 2000 (Japan)	Excavation workers (exposed externally to core sample and internally by inhalation)

Note: * Represents most limiting exposure case.

[2] Note that current drilling standards would not permit drill slurry to be left at the drill site, but it is conservatively assumed here that such standards are not applied.

Intrusion Likelihood

Regulatory document G-320 (CNSC 2006) recognizes that inadvertent human intrusion events could result in dose rates that exceed the regulatory limit and it states that reasonable efforts should be made to limit the probability of such high consequence scenarios. The following repository characteristics have therefore been assumed at this hypothetical site to minimize the likelihood of this event:

- A deep location;
- Site selection based on an absence of known groundwater resources at repository depth that could be used for drinking, agricultural or industrial purposes;
- Site selection based on an absence of economically exploitable natural resources; and
- The use of records and markers to preserve institutional memory to the extent practicable.

Furthermore, compartmentalizing the used fuel into containers is a design measure that mitigates the impact of intrusion. Another mitigating factor is the strength of the containers, which means unknowing penetration is unlikely.

7.9.1.2 Model and Assumptions

Computer Code

The radiological consequences are determined using HIMv2.1 (Medri 2015a), a human intrusion computer model developed using the AMBER v5.7.1 platform.

Prior to the detailed assessment, screening calculations are done to identify the potentially radiologically significant radionuclides. In this screening, hypothetical doses are calculated for ingestion and inhalation of the radionuclides in an entire fuel bundle, and for a one-year groundshine exposure to the contents of a fuel bundle mixed into 1 kg of soil. For each type of exposure, all radionuclides whose dose contributions are within six orders of magnitude of the maximum dose contributor are screened in. The calculations are done for 30, 500, and 1,000,000 year old fuels with discharge burnups of 220 MWh/kgU. As a result, 79 radionuclides emerged from the screening and are tracked in the HIMv2.1 model. Short-lived radionuclides are included through the dose coefficients of their parents. Doses are obtained using inhalation, ingestion, groundshine and external dose coefficients.

A detailed description of the parameters and equations used in HIMv2.1 is available in Medri (2015a).

Exposure Scenarios

The HIMv2.1 model determines the dose consequences to both exposure groups from the pathways illustrated in Figure 7-179. It models the acute dose to the Drill Crew at the time the material is brought to the surface and the annual chronic dose to Residents who are assumed to live nearby and grow crops on the site after the intrusion has occurred.

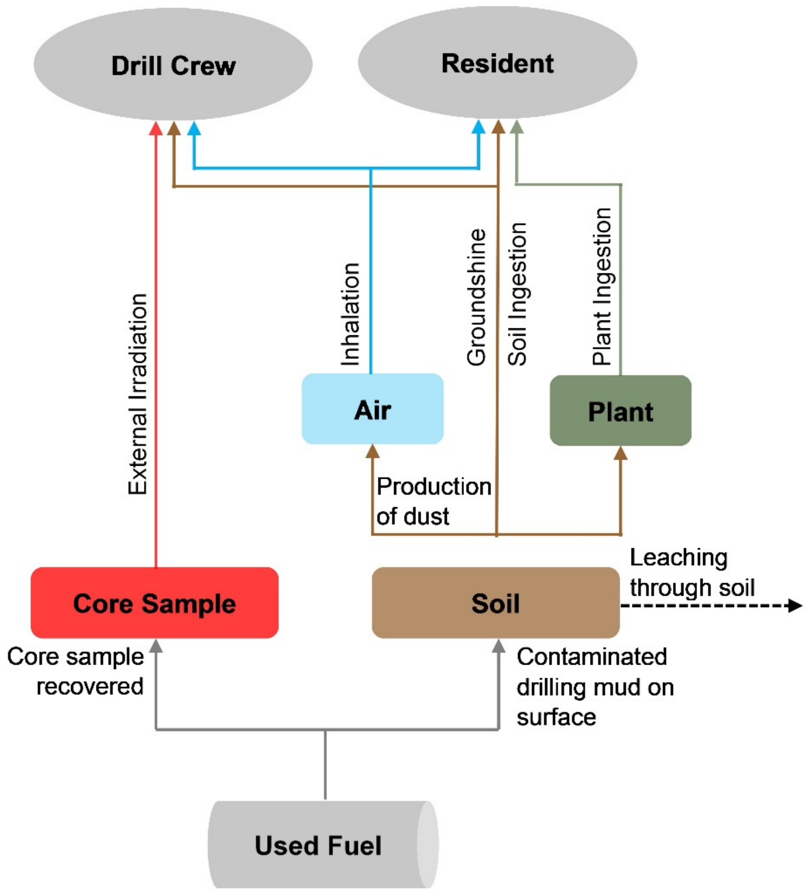

Figure 7-179: Inadvertent Human Intrusion - General Conceptual Model

Three different exposure scenarios are considered. In each scenario, used fuel is brought to the surface in the form of drill core and drill mud / slurry. Normal practice is for drill slurry to be contained at the site and ultimately be disposed of according to regulatory requirements; however, in this assessment, the drill slurry is conservatively assumed to be spilled around the drill rig without containment. The contaminated slurry would become mixed with surface material, as well as with subsequent drilled material. The waste is assumed to be uniformly mixed through a small near-surface volume of soil around the rig. The Drill Crew member handles the core sample for an hour, leading to a direct external exposure. The Drill Crew member is also exposed to the waste through groundshine, inhalation of contaminated dust and ingestion of contaminated soil from the mixed volume of near-surface material. The Drill Crew member is assumed to not wear a mask.

The exposure scenarios are stylized; they include approximate representations of inhalation, ingestion and direct exposure pathways such that the overall dose estimates are indicative of potential doses. The exposure scenarios are:

Scenario 1: Drilling operations take place for two days after the intrusion event (two 12-hour shifts), at which point the Drill Crew becomes aware of the hazard, immediately ceases operations and vacates the site.

The site is then completely remediated by qualified experts, and thus the Resident is unaffected by the incident. The dose to the remediation experts is not considered because they are assumed to take appropriate precautions.

Scenario 2: In Scenario 2, drilling operations continue for 14 workings days, at which point the Drill Crew vacates the site without identifying the hazard. Debris deposited on the surface around the drilling rig remains in place without remediation, subject only to radioactive decay and leaching.

The Resident lives at the contaminated site immediately after the original intrusion, and grows food on the contaminated soil. The Resident is exposed to contaminants through groundshine, dust inhalation and through ingestion of contaminated plants and soil. It is assumed that the contaminated land is limited in extent (and therefore has a higher concentration of contaminants), and so an allowance is made for the fraction of time that the Resident is exposed to the contaminated site on an annual basis.

Leaching considers the portion of precipitation that draws downward into the deeper soil (i.e., not the portion within the plant rooting depth that evapotranspires). As a conservative estimate, the Resident exposure is assumed to begin in the first year after intrusion, before leaching has any significant effect on the soil contaminant levels. Leaching is therefore conservatively ignored in this case. However, the Resident's annual dose is also examined for an assumed arrival time of 100 years after the original intrusion, in which case the effect of leaching is included.

Scenario 3: Scenario 3 is the same as Scenario 1, except that a higher fuel burnup is assumed (i.e., 280 MWh/kgU instead of 220 MWh/kgU). Table 3-1 in Chapter 3 shows that the 220 MWh/kgU value corresponds to roughly the 63rd to 93rd percentile value over all used CANDU fuel bundles (depending on the nuclear station), while the 280 MWh/kgU value similarly corresponds to the 95th to the 99.9th percentile value (again depending on the nuclear station).

<u>Key Assumptions and Parameters</u>

Key assumptions are:

- Institutional control is maintained for a minimum of 300 years after closure, at which point intrusion becomes possible;
- Decay and ingrowth calculations start at the time of placement, at which point the used fuel is 30 years old;
- There is a minimum period of 70 years of extended monitoring and 25 years of decommissioning and closure following placement, which means the fuel is 425 years old (i.e., 30 + 70 + 25 +300) at the earliest time of intrusion. This is conservative in that the fuel will likely be older at a real site;
- The drill intercepts a container in the repository and brings used fuel debris to the surface, either mixed with the drill slurry or as a section of intact drill core; and
- The biosphere is unchanging; that is, radioactive material is not carried away by wind, by water erosion or other external forces and airborne material is not assumed to deposit on top of the contaminated soil.

Table 7-51 lists important parameters used in the assessment. Source references for these values can be found in Medri (2015a).

Table 7-51: Parameters for Human Intrusion Scenario

Parameter	Value
Parameters related to used fuel quantities	
Fraction of used fuel per container that is damaged by borehole	0.17
Mass of used fuel in a container (kg)	1150
Fraction of U intercepted brought to surface as core	0.4
Fraction of U intercepted brought to surface as slurry	0.3
Instant release fractions (selected radionuclides)	Table 7-13
Radionuclide Inventory (mol/kgU or mol/kgZr)	See Medri (2015a)
Parameters related to soil and air	
Soil type	Clay
Soil density (kg/m^3)	1400
Soil water content (m^3/m^3)	0.3
Net infiltration rate of water through soil (m/a)	0.325
Depth of contaminated soil (m)	0.2
Contaminated soil fraction	0.1
Slurry area (m^2)	Drill Crew: 30 Resident: 80
Thickness of contaminated soil (m)	0.2
Dust loading in air (kg_{soil}/m^3)	Drill Crew: 1.0×10^{-7} Resident: 3.2×10^{-8}
Soil distribution coefficients for clay (m^3/kg)	See Medri (2015a)
Plant/Soil Concentration Ratios ($kg_{drysoil}/kg_{wetsoil}$)	See Medri (2015a)
Parameters related to human behavior	
Air inhalation rate (m^3/a)	8400
Plant ingestion (kg/a)	291
Resident annual soil ingestion (kg)	0.12
Drill Crew soil ingestion amount per intrusion event (g)	Scenario 1: 0.66 Scenario 2: 4.62 Scenario 3: 0.66
Contaminated food fraction	0.1
Exposure time of Drill Crew to core sample (hr)	1
Exposure time of Drill Crew to contaminated site (hr)	Scenario 1: 24 Scenario 2: 168 Scenario 3: 24
Exposure time for Resident each year (a)	0.1
Ingestion, Inhalation, groundshine and external dose coefficients (Sv/Bq or (Sv/a)/(Bq/kg))	See Medri (2015a)

7.9.1.3 Results

Dose Impact: Scenario 1 (Hazard Identified and Site Vacated after 2 Days)

Scenario 1 is described in Section 7.9.1.2. Figure 7-180 shows the calculated acute dose to a Drill Drew member as a function of time after closure, showing a breakdown of contributing pathways. The Resident is unaffected by this scenario because the site is assumed to be completely remediated. The maximum one-time dose to the Drill Crew, occurring at the earliest time of intrusion, is 90 mSv.

The total dose is dominated by Am-241 for the first 300 to 1000 years, by Pu-239 and Pu-240 from 10^3 to 10^5 years, and by the U-238 decay chain for longer times.

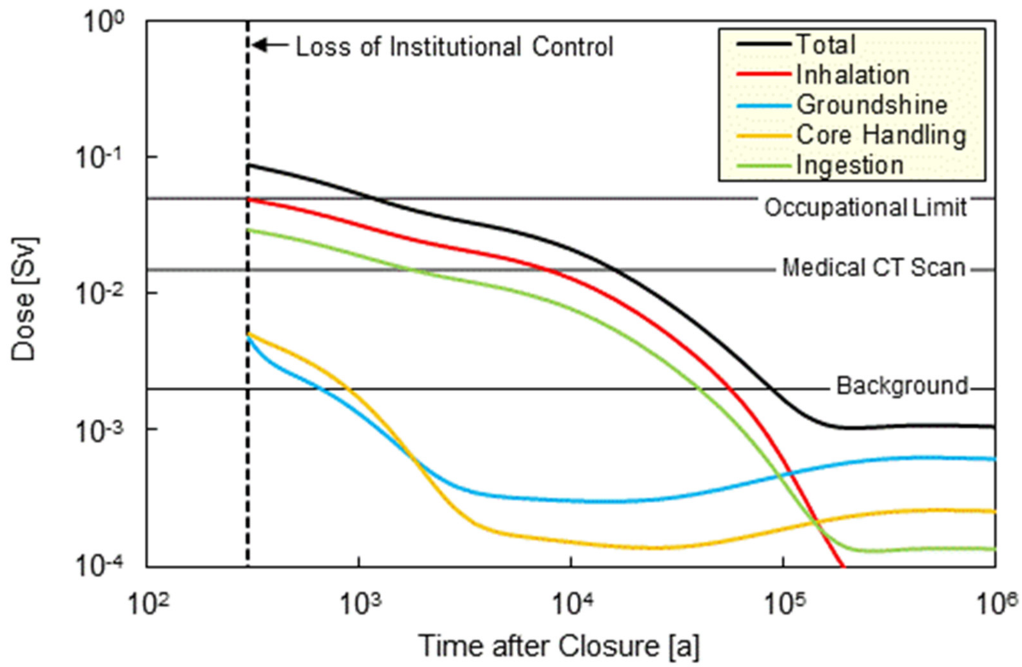

Note: Drill Crew receives a one-time (acute) dose.

Figure 7-180: Inadvertent Human Intrusion: Exposure Pathways to the Drill Crew – Hazard Identified and Site Vacated after 2 Days

Dose Impact: Scenario 2

Scenario 2 is also described in Section 7.9.1.2. Figure 7-181 shows the calculated acute dose to the Drill Crew member and chronic dose rate to the Resident as a function of the assumed time of intrusion after repository closure. The Resident's annual dose is also examined for an assumed arrival time of 100 years after intrusion, in which case the effect of leaching is included.

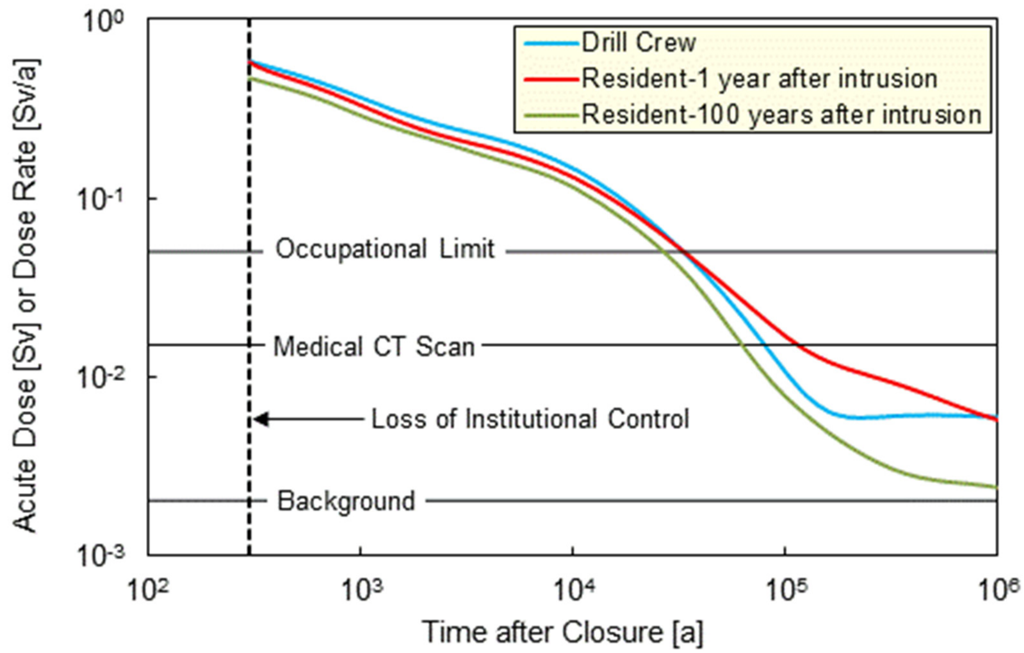

Note: The Drill Crew receives a one-time (acute) dose, while the Resident receives a (chronic) dose rate.

Figure 7-181: Inadvertent Human Intrusion: Summary of Exposures – Hazard Not Identified and Site Vacated after 14 Days

The principal results are:

- The maximum one-time dose to the Drill Crew member is 590 mSv.
- The maximum annual chronic dose to the Resident is 580 mSv.
- After 100 years of leaching, the maximum annual dose to the Resident is 470 mSv.
- Doses decrease as a function of the assumed time of intrusion due to radioactive decay. Intrusion doses after about 100,000 years are in the range of 10 to 20 mSv.

Figure 7-182 and Figure 7-183 show the breakdown of pathways for the Drill Crew member and the Resident. The total dose for both groups tends to be dominated by Am-241 for the first 300 to 1000 years, by Pu-240 and Pu-239 from 1000 to 100,000 years, and by the U-238 and Pu-241 decay chains for longer times. After about 100,000 years, the consequences are similar to those that might result from similar inadvertent drilling into an equivalent amount of natural uranium.

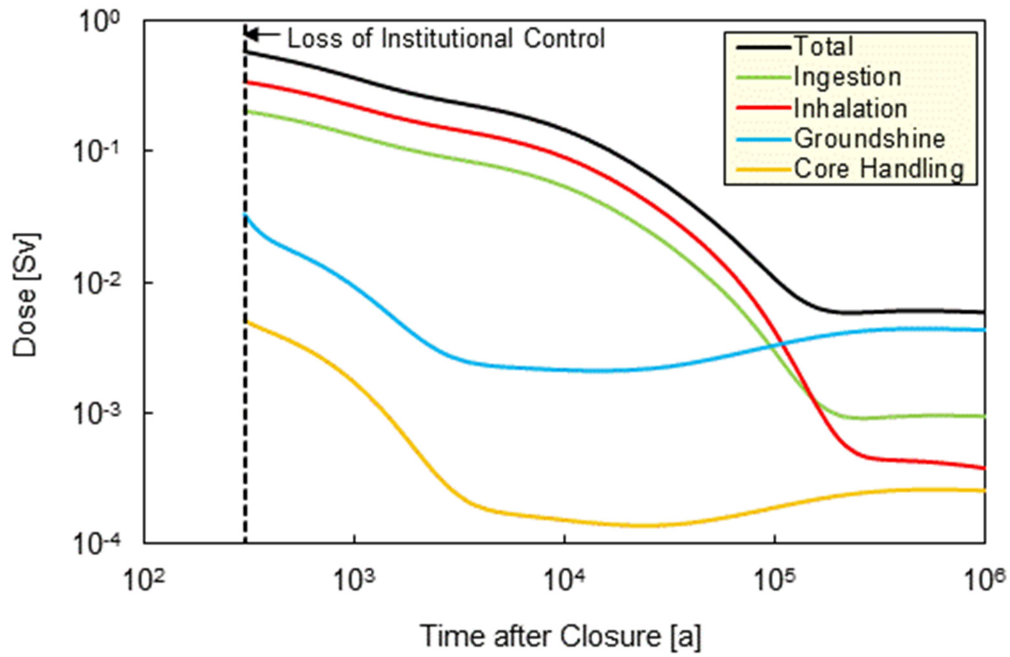

Note: Drill Crew receives a one-time (acute) dose

Figure 7-182: Inadvertent Human Intrusion: Exposure Pathways to the Drill Crew – Hazard Not Identified and Site Vacated after 14 Days

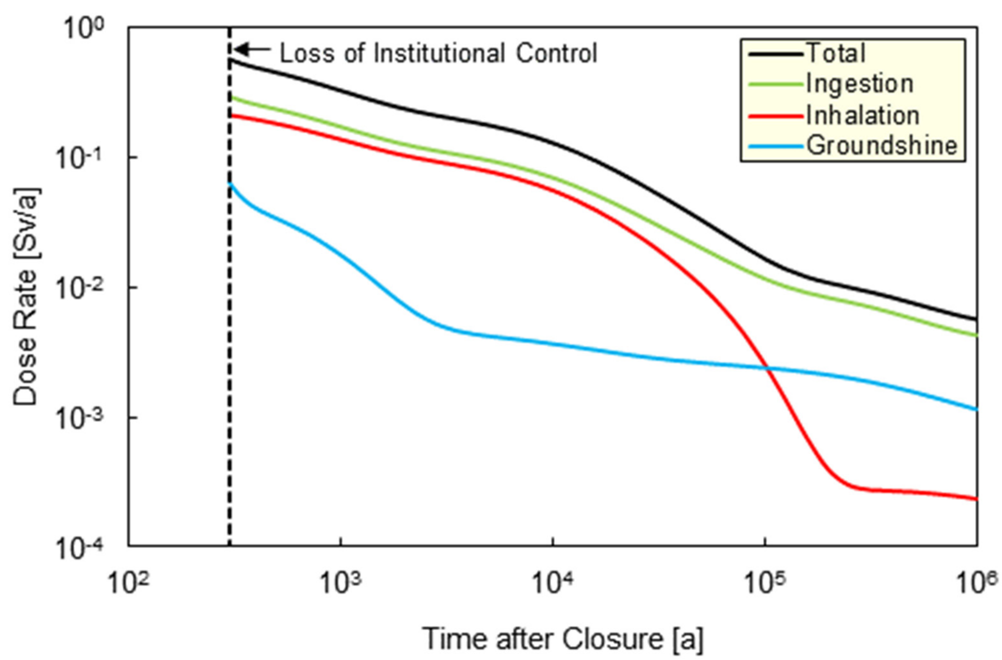

Note: Resident receives a chronic dose rate

Figure 7-183: Inadvertent Human Intrusion: Exposure Pathways for the Resident – Hazard Not Identified and Site Vacated after 14 Days

The Resident's exposure could potentially occur much later after the used fuel is inadvertently brought to the surface, assuming that the site is not remediated in the meantime. In this case, the exposure would be lower due to radioactive decay and to leaching of contaminants from the near-surface. Figure 7-184 shows the dose rate to a Resident living near and growing crops on the contaminated site as a function of time following an intrusion that occurs 300 years after repository closure. Leaching is not a significant factor in reducing potential doses until after about 1000 years.

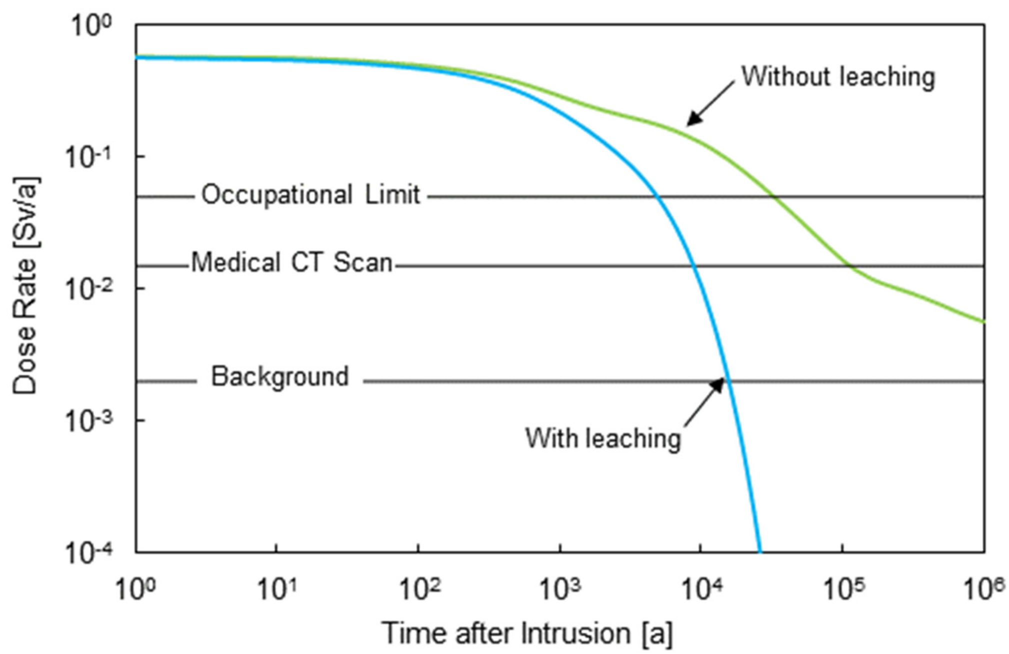

Figure 7-184: Inadvertent Human Intrusion: Effect of Leaching on Exposure to the Resident – Hazard Not Identified and Site Vacated after 14 Days

<u>Dose Impact: Scenario 3</u>

Scenario 3 is described in Section 7.9.1.2. This is identical to Scenario 1, except that it considers the unlikely case of a container loaded entirely with 280 MWh/kgU burnup fuel. As shown in Figure 7-185, increasing the burnup increases the maximum one-time acute dose to the Drill Crew member from 90 mSv to 110 mSv. This is because the amount of actinides increases with burnup due to the increased time for neutron absorption while the fuel is in the reactor.

The increase in dose is due mainly to the higher initial inventory of Am-241, Pu-241 (which decays to Am-241) and Pu-240. The total dose rate to the Drill Crew member in Scenario 1 is included in Figure 7-185 for comparison.

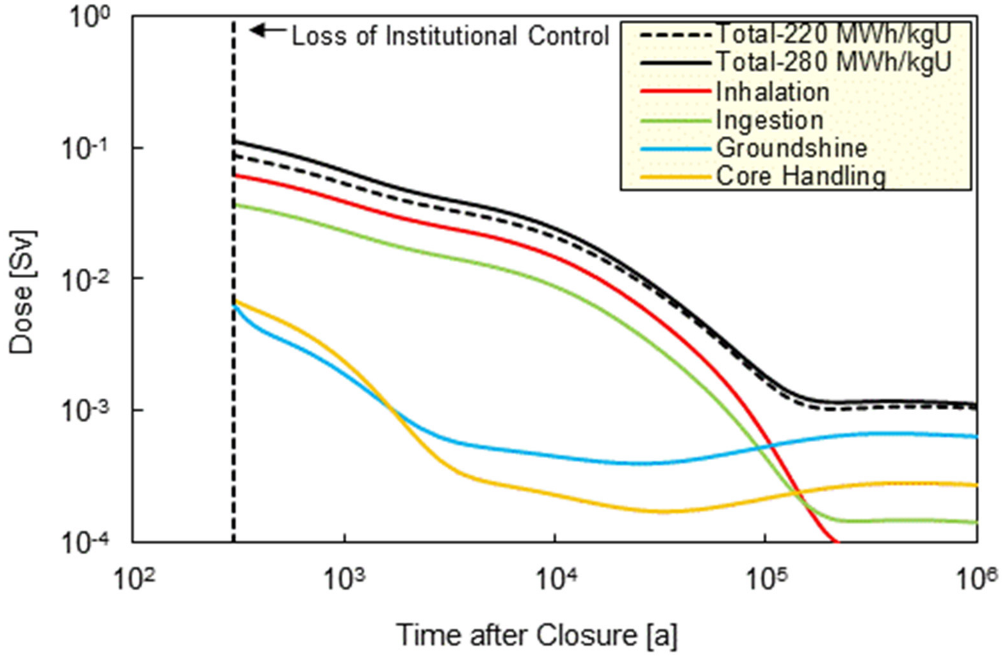

Note: Drill Crew receives a one-time (acute) dose.

Figure 7-185: Inadvertent Human Intrusion: Pathways for Drill Crew Exposure – Hazard Identified and Site Vacated after 2 Days with Higher Burnup

Annual Risk

To provide context for the dose rates, the annual risk to the most exposed individual can be estimated.

The annual risk to the Drill Crew (R_{DC}) is determined via:

$$R_{DC} = \Upsilon \cdot H \cdot P \quad (7\text{-}2)$$

where: Υ is the probability coefficient for stochastic effects per Sv or 0.057 according to ICRP (2007);

H is the highest dose in the time period of concern; and

P is the intrusion frequency.

While the intrusion frequency could in principle be estimated by assigning numerical values to each of the events in Figure 7-178, in practice these values are, to a large extent, non-quantifiable. Consequently, a more simplistic approach is adopted to illustrate the frequency with which an intrusion event may occur. This approach considers only the frequency of drilling.

Specifically, given that the area around the repository has no significant mineral resources, a deep drilling frequency to resurvey or update the geological information of about once every 100 years is assumed. Assuming each borehole characterizes an area of 10 km × 10 km, this results in a drilling frequency of $10^{-10}/m^2a$. Since the repository consists of 284 rooms, with each room having a projected area of 973 m^2, the frequency of inadvertent human intrusion into a room can be estimated as 2.8×10^{-5}/a. If only the container area is used, the intrusion frequency is estimated as 1.9×10^{-5}/a.

With Υ = 0.057/Sv, H = 0.59 Sv and P = 2.8 x 10^{-5}/a, the annual risk to the Drill Crew from an inadvertent human intrusion event is 9.4×10^{-7}/a. This is below the risk target of 10^{-5}/a for Disruptive Event Scenarios identified in Section 7.1.1.

The intrusion probability does not take into account the beneficial effect of institutional memory. Institutional memory could decrease with time, but at earlier times when high doses are more likely, ongoing institutional memory could significantly reduce the intrusion probability (and the risk) of such an event.

The repository might also be detected through surface geophysical measurements, but not recognized as a used fuel facility. In this case exploration drilling would specifically aim for the repository and the intrusion probability could be higher than the above random drilling frequency. But since the drilling program would be specifically designed to explore the anomaly, it is also more likely that the repository would be recognized before or shortly after the repository level was reached and the consequences would therefore be less than those estimated above.

At long times, the cumulative probability of intrusion increases, but the consequences also decrease until eventually they are similar to those for inadvertent intrusion into a uranium ore body.

7.9.2 All Containers Fail

The long-lived used fuel containers are an important feature of the multi-barrier concept. As discussed in Chapter 5, the containers are anticipated to remain intact for well in excess of one million years, based on consideration of the copper corrosion barrier, their sturdy mechanical design, and favourable site attributes. Nevertheless, the All Containers Fail Disruptive Event Scenario considers the hypothetical case in which all the containers fail simultaneously and relatively early.

The scenario assumes failure at 60,000 years. This is correlated with the earliest possible timeframe for an ice sheet to cover the site, and it assumes that some unanticipated effect of the ice sheet causes failure.

The sensitivity to earlier failure times is examined in a sensitivity case in which all containers are assumed to fail at 10,000 years.

7.9.2.1 Model and Assumptions

The dose assessment is performed using the System Model with the Full Geosphere Submodel described in Section 7.8.1.2.2. All model parameters are identical to those in the Base Case except:

- All 95,834 containers fail simultaneously; and
- The potential presence of a few containers with small initial defects is not included. This modelling simplification does not affect the peak dose rate.

The behaviour of hydrogen gas generated through corrosion of the internal steel container is discussed in Section 7.12.

7.9.2.2 Results

<u>All Containers Fail at 60,000 Years</u>

Figure 7-186 shows the dose rate for the case in which all containers fail at 60,000 years. Also included for comparison is the dose rate for the Base Case of the Normal Evolution Scenario.

The maximum dose rate is 1.01 mSv/a, occurring at 84,100 years. This is slightly greater than the interim dose rate criterion of 1 mSv/a for Disruptive Events defined in Section 7.1.1; however, Section 7.8.1.4.2 notes that I-129 transport to the well as determined using the Full Geosphere Submodel is overestimated by a factor of 1.6 as compared to the more detailed 3D groundwater transport model. Provided I-129 transport to the well is the dominant dose contributor for this event, the System Model results may be adjusted downwards to account for the overprediction.

The following examines whether I-129 is indeed the dominant dose contributor.

Figure 7-187 shows the dose contributions from the most significant radionuclides. As in the Base Case, I-129 is dominant.

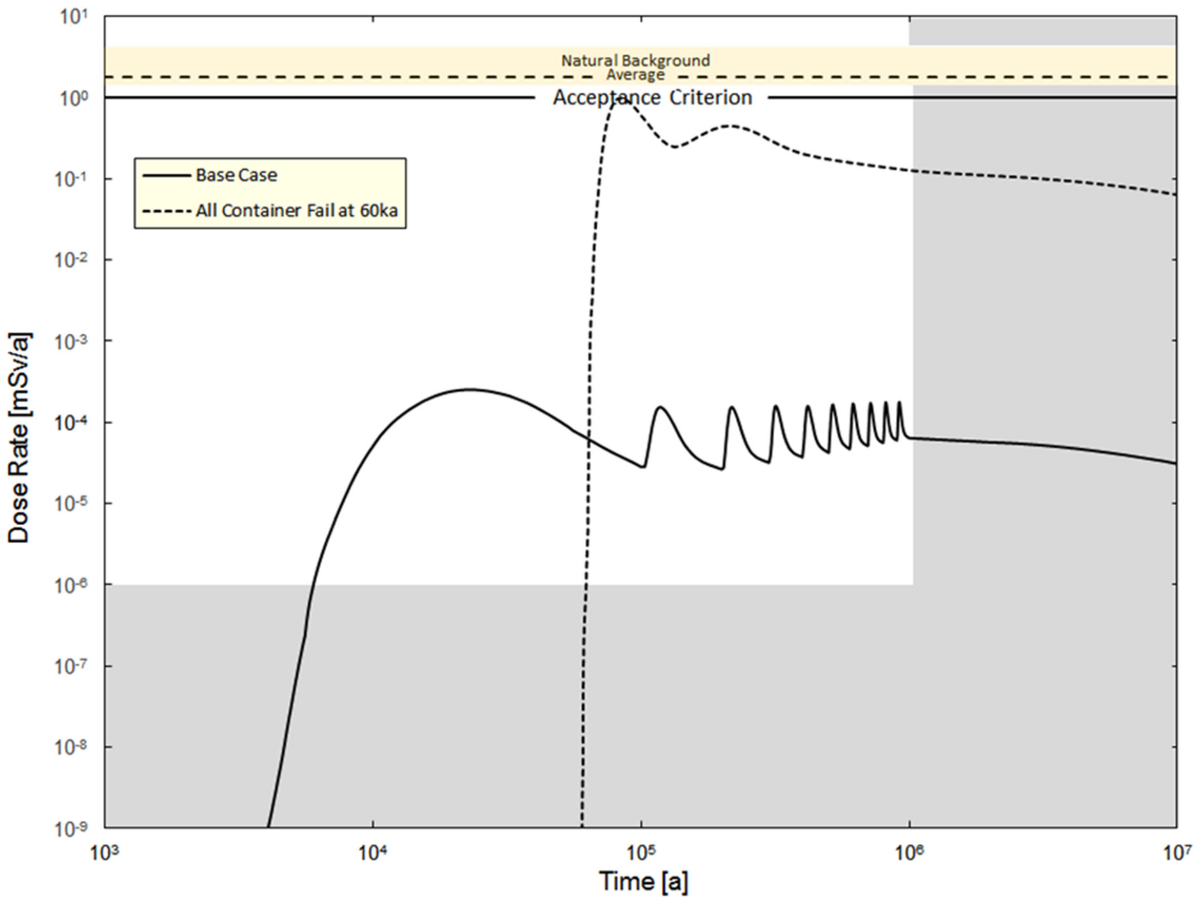

Figure 7-186: Full System Model: All Containers Fail at 60,000 Years: Dose Rate

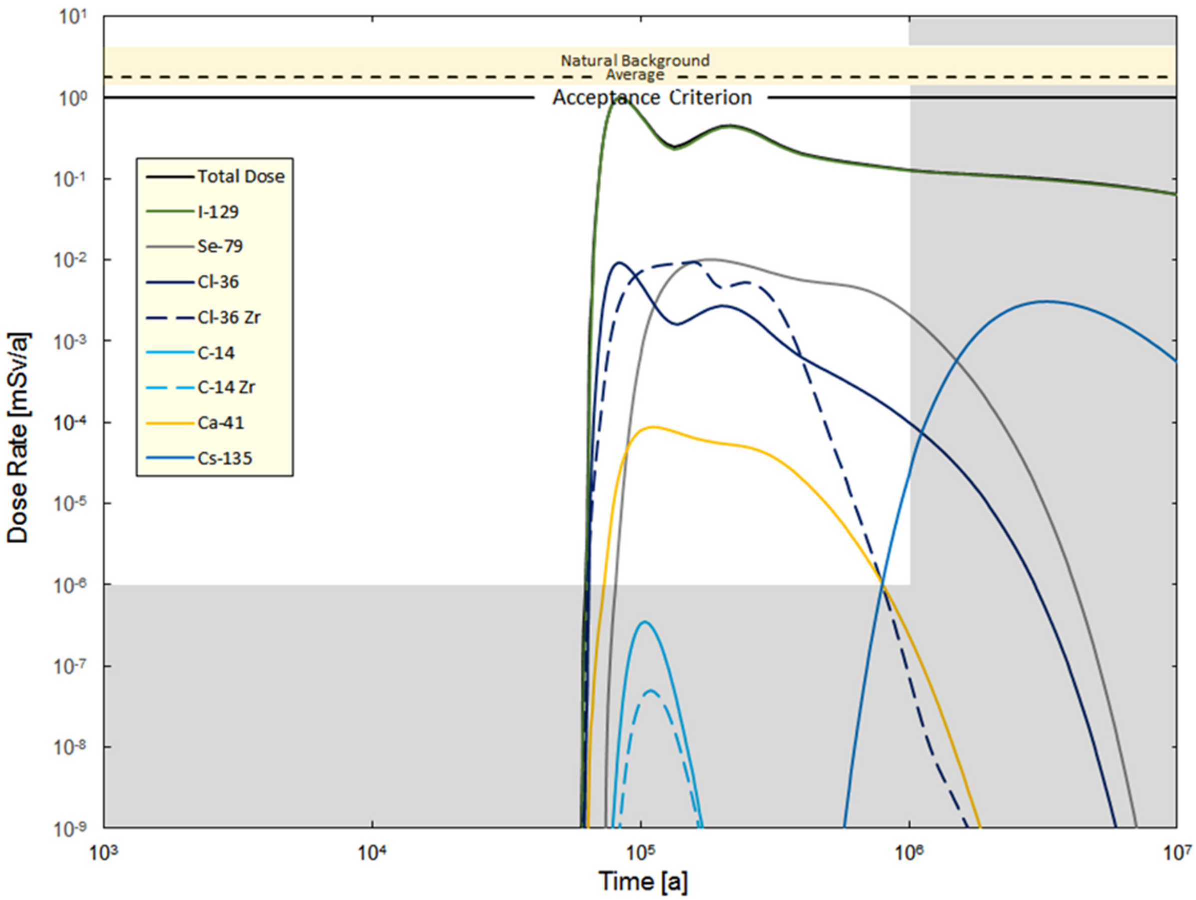

Figure 7-187: Full System Model: All Containers Fail at 60,000 Years: Contributing Radionuclides

Table 7-52 shows a breakdown of radionuclide contributions to the peak dose rate. I-129 is responsible for almost 99% of the peak.

Table 7-52: Radionuclide Dose Contributors for All Containers Fail at 60,000 Years

Radionuclide	Peak Dose Contribution [mSv/a]*	Percentage of Peak Dose [%]
I-129	9.97×10^{-1}	98.8
Cl-36	9.23×10^{-3}	0.92
Cl-36 Zr	3.25×10^{-3}	0.32
Ca-41	2.60×10^{-5}	0.0026
Se-79	5.71×10^{-6}	0.0006
C-14	1.77×10^{-8}	0.000002
C-14 Zr	1.18×10^{-9}	0.0000001
Other	0	0

* System Model

Table 7-53 shows a breakdown of the I-129 dose pathways. Essentially all of the I-129 dose is due to internal dose pathways, with drinking water and food ingestion accounting for essentially all of the dose. Drinking water is taken from the well, and well water is used to irrigate crops and water animals used as food sources.

Table 7-53: Radionuclide Dose Pathways for All Containers Fail at 60,000 Years

Pathway	Peak I-129 Dose Contribution [mSv/a]*	Percentage of the I-129 Peak Dose [%]
Total Dose From all Routes	9.97×10^{-1}	-
Internal Dose Pathways	$\mathbf{9.97 \times 10^{-1}}$	**100**
Drinking Water	5.59×10^{-1}	56.1
Food Ingestion	4.32×10^{-1}	43.4
Inhalation	3.66×10^{-3}	0.37
Soil Ingestion	1.53×10^{-3}	0.15
External Dose Pathways	$\mathbf{3.61 \times 10^{-5}}$	**0.0036**
Building Materials	1.63×10^{-5}	0.0016
Ground Exposure	1.44×10^{-5}	0.0014
Water Immersion	5.26×10^{-6}	0.0005
Air Immersion	1.07×10^{-7}	0.00001

* System Model

Because I-129 is dominant and because essentially all of the I-129 dose is due to the use of well water, the System Model result can be adjusted downwards by the factor of 1.6 mentioned above. This results in a dose rate for this scenario of 0.63 mSv/a, which is below the interim dose rate criterion.

<u>All Containers Fail at 10,000 Years</u>

Figure 7-188 compares the dose rate for the sensitivity case in which all containers fail at 10,000 years with that of the case with all containers failing at 60,000 years. The results are not substantially different, with a maximum dose rate of 1.3 mSv/a (or 1.3 times the 60,000 year value value) occurring at 36,300 years. The increase in dose rate occurs as a result of the higher fuel dissolution rates at 10,000 years (compared to 60,000 years) due to the higher radiation fields from the fuel.

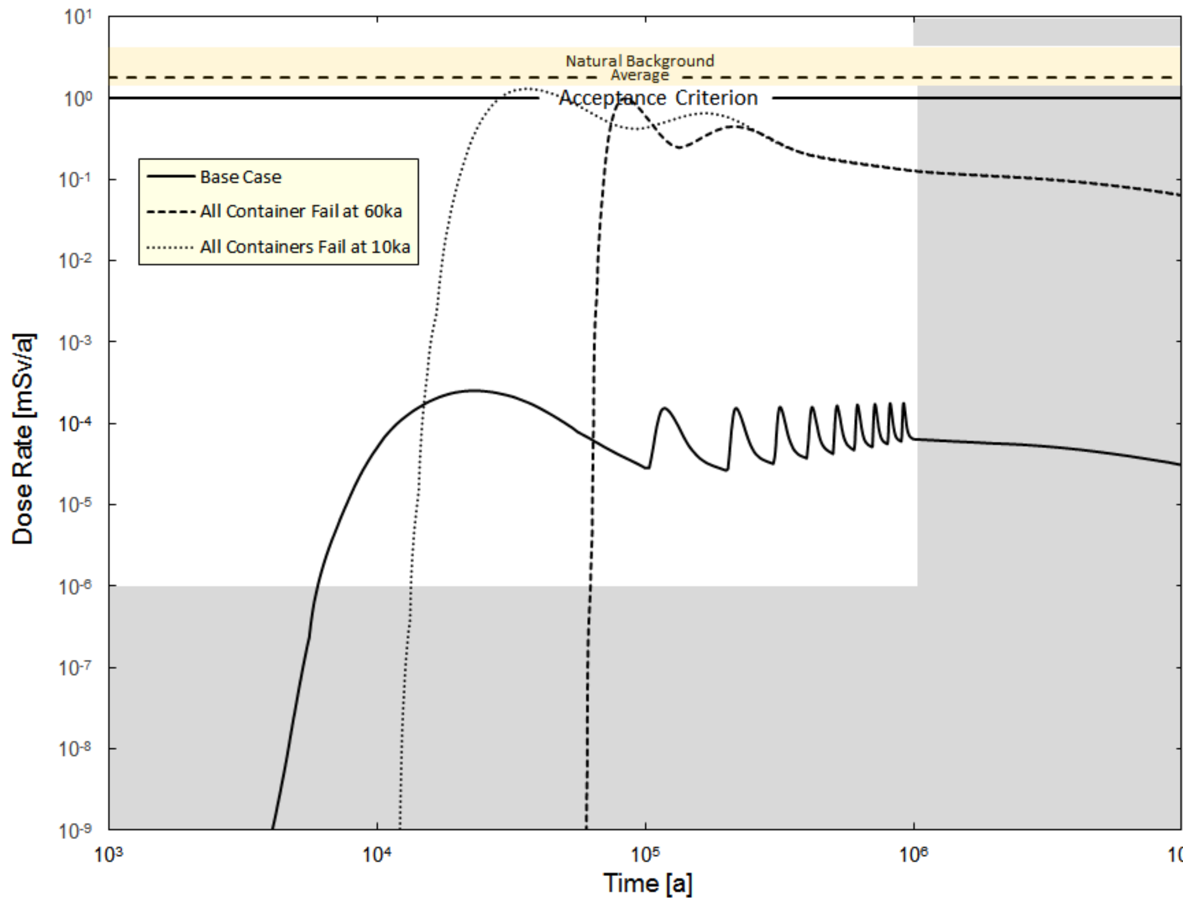

Figure 7-188: All Containers Fail at 10,000 Years: Sensitivity Case Dose Rate

As before, the System Model dose result is likely conservative by a factor of 1.6 based on comparison of I-129 results with the 3D groundwater transport model. Accounting for this factor reduces the dose rate to 0.81 mSv/a, which is below the interim dose rate criterion.

7.9.3 Repository Seals Failure

The Normal Evolution Scenario considers the likely behaviour of the shaft and repository seals and their associated excavation damaged zones. The Repository Seal Failure Scenario considers the same evolution of the repository system and the same exposure pathways as in the Base Case of the Normal Evolution Scenario, except that rapid and extensive degradation of the repository seals is assumed. For conservatism, it is assumed that this degradation occurs at the time of repository closure.

Simulations are performed using the Full Repository-Scale Model with the individual container source term described in Section 7.7.1.2. This model is used (instead of the System Model) because the groundwater flow field in the repository and vicinity could be affected by the assumed seal degradation.

Two simulations have been performed, with all model parameters the same as in the Base Case, except as noted below.

- Degraded Shaft Seal: All shaft components (i.e., bentonite / sand, asphalt, and concrete) are assigned a hydraulic conductivity of 1×10^{-7} m/s and a diffusivity of 3×10^{-10} m^2/s. This is equivalent to the Extreme Case described in Table 7-7. The shaft inner and Outer EDZ hydraulic conductivities are also increased by a factor of 100 and 10 respectively.
- Degraded Fracture Seal: The central and perimeter tunnel seals on either side of the main fracture are assumed degraded. All seal materials (i.e., highly compacted bentonite, dense backfill between seals, and concrete) are assigned a hydraulic conductivity of 1×10^{-9} m/s and a diffusivity of 3×10^{-10} m^2/s. The immediately adjacent Inner and Outer EDZ hydraulic conductivities are also increased by a factor of 100 and 10 respectively.

The locations of the 10 defective containers and the well are not changed in the cases described above; however, sensitivity cases are also performed to assess whether well and container locations closer to the shaft could result in higher dose consequences.

Figure 7-189 shows the results for I-129 transport to the well for both cases. There is essentially no change as compared to the Base Case. This is due to a combination of the distance to the shaft, the direction of groundwater flow, the hydraulic conductivity of the host rock and the effectiveness of the other intact seals.

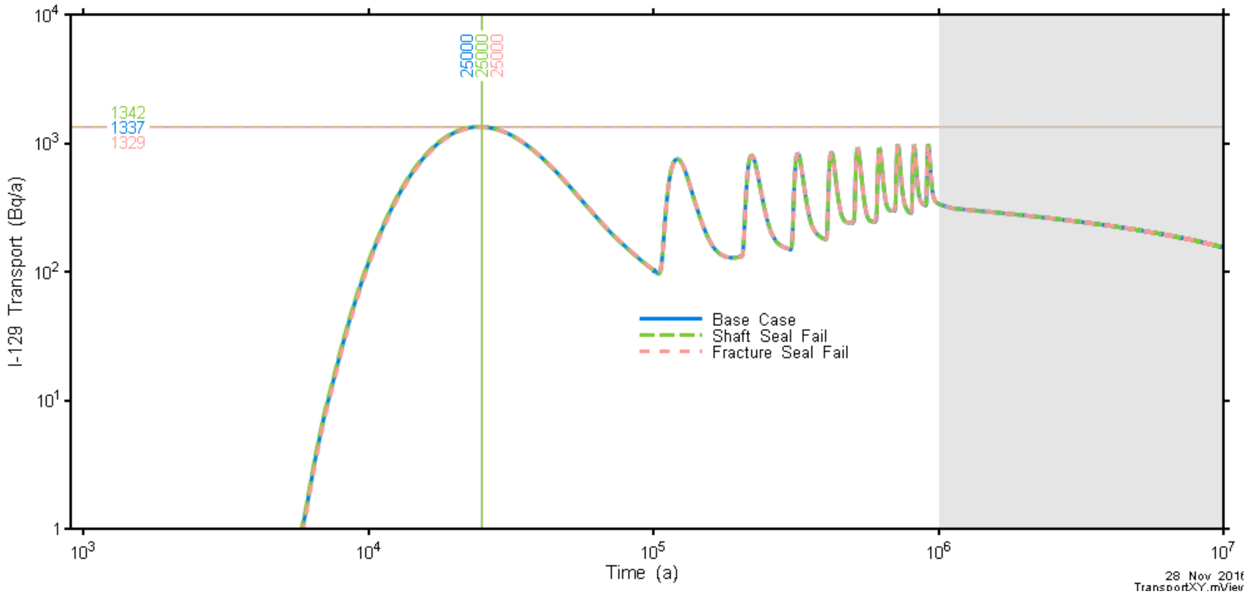

Figure 7-189: Full Repository-Scale Model: Repository Seal Failure – I-129 Transport to the Well

Sensitivity Case With Different Well / Defective Container Location

Sensitivity cases have been developed for the Main and Vent shafts to determine if higher dose consequences could be achieved with different well and defective container locations. In these sensitivity cases, the well is located at the shaft and the defective containers are placed in the location with minimum transport time to the well. The Service shaft is not considered because defective containers are further away than for the Main shaft.

Scoping calculations indicate that wells located at the interface between the shaft Inner EDZ and the shaft seal material could meet the required well demand without excessive drawdown.

To position the containers, locations of minimum transport time were based on MLE simulations conducted using Base Case and degraded shaft properties. The selected Main shaft defective container location is at the end of the eighth placement room in Panel H, approximately 300 m from the shaft, with an MLE of 241 ka for degraded shaft properties and 881 ka for Base Case shaft properties. The Vent shaft defective container location is at the end of the first placement room in Panel B, approximately 270 m from the shaft, with an MLE of 265 ka with degraded shaft properties and 456 ka for Base Case shaft properties.

Figure 7-190 shows the results for I-129 transport to the two well locations. Transport is shown for the Base Case, and for the revised well / defective container locations using both Base Case shaft properties and degraded shaft properties. The effect of the degraded shaft properties can be seen by comparing same colour solid and dashed lines; however, neither of the revised locations results in greater I-129 transport than in the Base Case. This is due to a reduced well capture fraction for the revised locations.

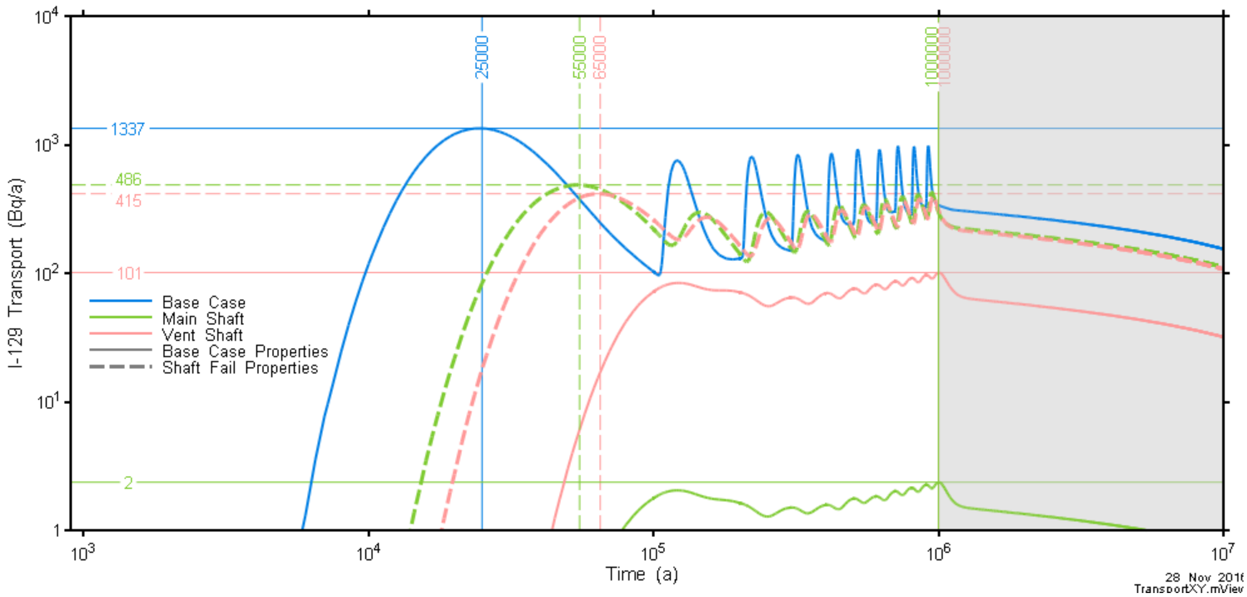

Figure 7-190: Full Repository Scale-Mode: Container Source Term – Main Shaft and Vent Shaft Fail Disruptive Event Scenarios - I-129 Transport to the Well

7.10 Modelling and Results for the Radiological Protection of the Environment

The results presented in Section 7.7 through Section 7.9 address the potential radiological effect of releases from the repository on persons. This section addresses the potential radiological effect on the environment.

For the Reference Case of the Normal Evolution Scenario, there is no effect because there are no releases from the repository. The approach taken here is therefore to compare results obtained for the Base Case and for the All Containers Fail at 60,000 Years Disruptive Event Scenario against the interim acceptance criteria established in Section 7.1.3 for the radiological protection of the environment.

The All Containers Fail Scenario is the limiting disruptive event and results in the greatest release of contaminants.

7.10.1 Method

The dose rates to non-human biota are assessed using the equations and data described in Medri and Bird (2015). The calculation method accounts for contamination by various radionuclides and pathways to different organisms, and considers two approaches to calculating the biota tissue radionuclide concentrations: the Concentration Ratio approach and the Transfer Factor approach.

Concentration Ratios estimate the radionuclide concentrations in all organisms based on the radionuclide concentrations in appropriate substrate media (soil, water, sediment or air). In Europe, calculation of dose consequences to non-human biota are largely performed using Concentration Ratios, often using the ERICA Tool (Brown et al. 2008).

Transfer Factors estimate the radionuclide concentration in mammals and birds based on the intake rate of food, soil, water and sediment. In previous work, the NWMO has used Transfer Factors to assess the radiological impact on mammals and birds and Concentration Ratios for all other biota (Garisto et al. 2008).

Figure 7-191 shows the dose calculation flow chart for the assessment. Input media concentrations are provided as a function of time by the System Model for the cases of interest.

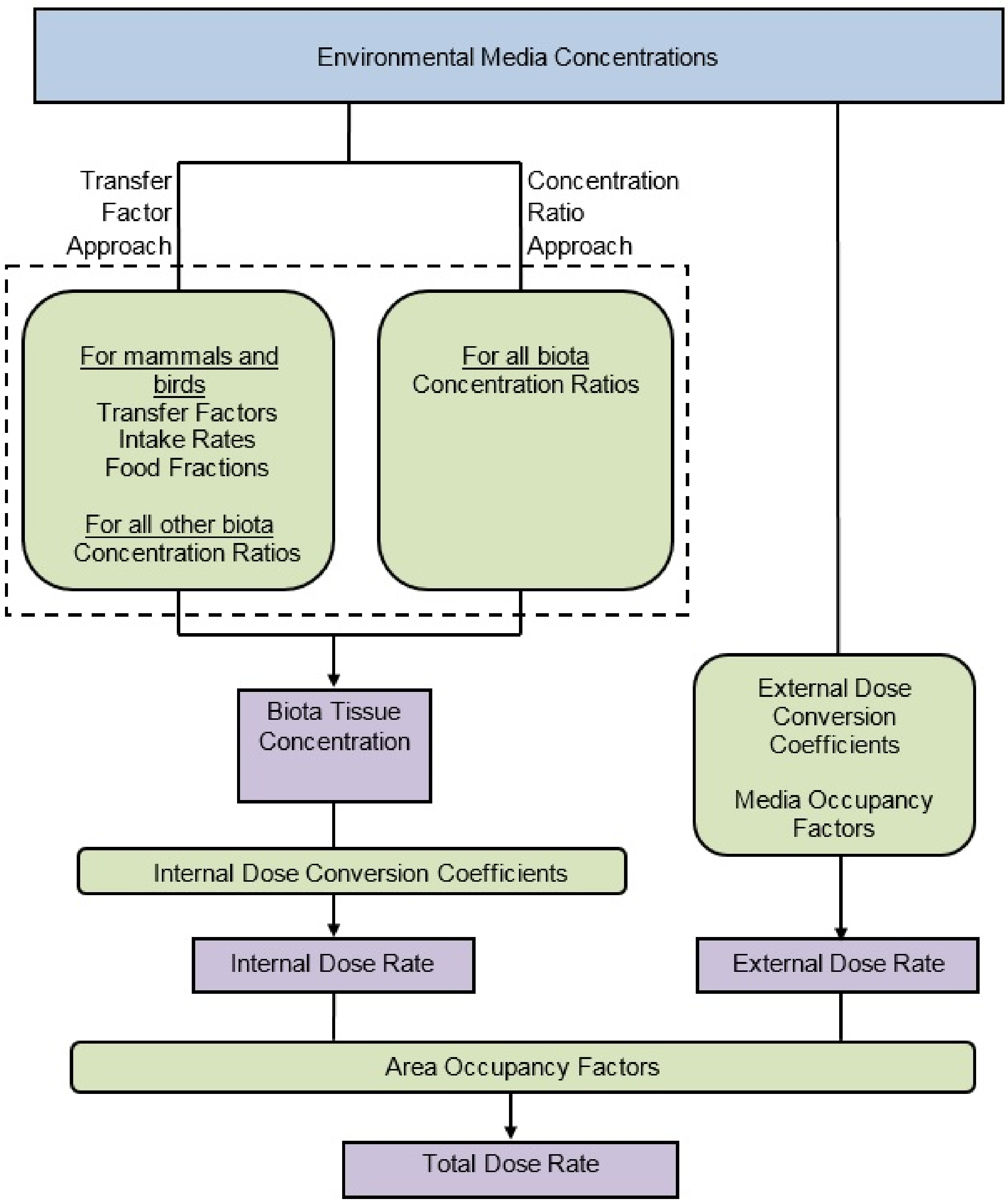

Note: Purple boxes represent calculated quantities, green boxes represent model parameters and the blue box represents inputs

Figure 7-191: Non-Human Biota Dose Assessment Flow Chart

The assessment is carried out using AMBER (Quintessa 2014). Two different sets of dose rate estimates for mammals and birds are generated, corresponding to the two different approaches (i.e., Transfer Factors and Concentration Ratios). The dose rate to all other non-human biota (i.e., reptiles, amphibians, plants, fish and invertebrates) are evaluated using Concentration Ratios.

Dose rate results are compared against the Interim Acceptance Criteria provided in Table 7-2 to judge whether the exposures are of radiological concern.

For the evaluation of potential future impacts, three representative ecosystems have been defined: the Southern Canadian Deciduous Forest, the Boreal Forest and the Inland Tundra (Garisto et al. 2008). These ecosystems are analysed through representative biota and simple biological exposure pathways. Selection of representative biota species for each of these ecosystems is detailed in Medri and Bird (2015).

The Boreal Forest ecosystem is most appropriate for the hypothetical site on the Canadian Shield, while the two other ecosystems represent potential future ecosystems depending on possible climate change in the longer term. Environmental conditions appropriate to these other ecosystems have not been modelled in this postclosure safety assessment (i.e., a constant temperate climate is assumed); however, to explore potential future implications, dose consequences to biota in these ecosystems are also calculated using the same environmental media concentrations as for the Boreal Forest.

7.10.2 Results

Table 7-54 presents the peak dose rates for the superset of representative biota across all three ecosystems identified in Medri and Bird (2015).

Table 7-54: Peak Dose Rates to Non-Human Biota

Scenario	Base Case (µGy/h)		All Containers Fail[3] (µGy/h)	
Non-Human Biota	**CR[1]**	**TF[2]**	**CR[1]**	**TF[2]**
Arctic Fox	$1.0×10^{-5}$	$9.3×10^{-6}$	$7.8×10^{-3}$	$1.2×10^{-2}$
Arctic Ground Squirrel	$3.0×10^{-7}$	$1.2×10^{-6}$	$1.2×10^{-3}$	$2.2×10^{-3}$
Arctic Hare	$3.0×10^{-7}$	$1.1×10^{-6}$	$1.2×10^{-3}$	$2.1×10^{-3}$
Arctic Wolf	$5.1×10^{-6}$	$2.2×10^{-5}$	$3.9×10^{-3}$	$1.7×10^{-2}$
Barren Ground Caribou	$2.0×10^{-6}$	$5.1×10^{-6}$	$1.5×10^{-3}$	$3.8×10^{-3}$
Beaver	$4.2×10^{-4}$	$1.0×10^{-4}$	$6.7×10^{-1}$	$7.4×10^{-2}$
Berries	$4.2×10^{-8}$	-	$1.5×10^{-4}$	$1.5×10^{-4}$
Brown Lemming	$2.9×10^{-7}$	$1.2×10^{-6}$	$1.2×10^{-3}$	$2.3×10^{-3}$
Brush Wolf	$2.6×10^{-6}$	$5.4×10^{-7}$	$2.0×10^{-3}$	$8.4×10^{-4}$
Canada Goose (SCDF & BF) [4]	$2.1×10^{-4}$	$2.2×10^{-5}$	$3.4×10^{-1}$	$4.2×10^{-2}$
Canada Goose (IT) [4]	$2.1×10^{-4}$	$2.2×10^{-5}$	$3.4×10^{-1}$	$4.2×10^{-2}$
Chironomid Larvae	$1.2×10^{-4}$	-	$1.3×10^{-1}$	$1.3×10^{-1}$
Common Garter Snake	$3.0×10^{-7}$	-	$1.2×10^{-3}$	$1.2×10^{-3}$

Scenario	Base Case (µGy/h)		All Containers Fail[3] (µGy/h)	
Non-Human Biota	**CR[1]**	**TF[2]**	**CR[1]**	**TF[2]**
Common Loon	4.2×10^{-4}	8.5×10^{-4}	6.7×10^{-1}	3.8×10^{-1}
Dwarf Arctic Willow	5.5×10^{-8}	-	1.9×10^{-4}	1.9×10^{-4}
Earthworm	5.8×10^{-7}	-	9.4×10^{-4}	9.4×10^{-4}
Eastern Cottontail Rabbit	3.0×10^{-7}	1.2×10^{-6}	1.2×10^{-3}	2.4×10^{-3}
Gray Wolf	2.6×10^{-6}	2.5×10^{-5}	2.0×10^{-3}	1.9×10^{-2}
Great Horned Owl (SCDF & BF)[4]	8.1×10^{-7}	2.3×10^{-5}	1.2×10^{-3}	3.0×10^{-2}
Great Horned Owl (IT)[4]	8.1×10^{-7}	3.5×10^{-6}	1.2×10^{-3}	5.4×10^{-3}
Groundhog	3.0×10^{-7}	1.1×10^{-6}	1.2×10^{-3}	2.2×10^{-3}
Lake Trout	8.3×10^{-4}	-	1.3×10^{0}	1.3×10^{0}
Lake Whitefish	8.3×10^{-4}	-	1.3×10^{0}	1.3×10^{0}
Lichen	1.3×10^{-6}	-	1.0×10^{-3}	1.0×10^{-3}
Mallard	4.2×10^{-4}	1.6×10^{-4}	6.7×10^{-1}	1.5×10^{-1}
Meadow Vole	2.9×10^{-7}	1.2×10^{-6}	1.2×10^{-3}	2.3×10^{-3}
Mink	8.3×10^{-4}	2.6×10^{-3}	1.3×10^{0}	5.5×10^{-1}
Moose	1.7×10^{-4}	5.6×10^{-5}	2.7×10^{-1}	4.6×10^{-2}
Muskrat	4.2×10^{-4}	3.1×10^{-4}	6.7×10^{-1}	2.2×10^{-1}
Northern Leopard Frog	8.3×10^{-4}	-	1.3×10^{0}	1.3×10^{0}
Pondweeds	7.2×10^{-5}	-	2.4×10^{-1}	2.4×10^{-1}
Red Fox	1.0×10^{-5}	2.5×10^{-6}	7.8×10^{-3}	3.9×10^{-3}
Red Throated Loon	4.2×10^{-4}	8.5×10^{-4}	6.7×10^{-1}	3.8×10^{-1}
Ruffed Grouse	8.1×10^{-7}	1.5×10^{-6}	1.2×10^{-3}	3.3×10^{-3}
Sedge Species	1.3×10^{-6}	-	6.1×10^{-3}	6.1×10^{-3}
Snowshoe Hare	3.0×10^{-7}	1.2×10^{-6}	1.2×10^{-3}	2.2×10^{-3}
Water Sedge	7.4×10^{-5}	-	2.5×10^{-1}	2.5×10^{-1}
White Cedar	5.3×10^{-8}	-	2.0×10^{-4}	2.0×10^{-4}
White-Tailed Deer	3.7×10^{-7}	9.1×10^{-7}	1.3×10^{-3}	2.6×10^{-3}
Willow Ptarmigan	8.1×10^{-7}	1.5×10^{-6}	1.2×10^{-3}	3.2×10^{-3}

1. Results using Concentration Ratios
2. Results using Transfer Factors
3. All Containers Fail Disruptive Event Scenario
4. SCDF: Southern Canadian Deciduous Forest, CF: Boreal Forest and IT: Inland Tundra.
5. '-' means the TF method does not apply to these biota

All dose rates are below the Tier 1 Interim Acceptance Criteria for both cases considered. It is therefore concluded that there is no concern about adverse impacts to non-human biota due from the potential release of radioactive contaminants from the repository.

For added context, the Tier 1 Interim Acceptance Criteria in Table 7-2 can also be used to determine a "Tier 1 Quotient", where this is the ratio formed by dividing the dose rates in Table 7-54 by the appropriate Tier 1 Interim Acceptance Criteria. Figure 7-192 shows the resulting Tier 1 Quotients for species with quotients greater than 10^{-2} for the All Containers Fail event. Base Case Tier 1 Quotients are much lower and are not shown.

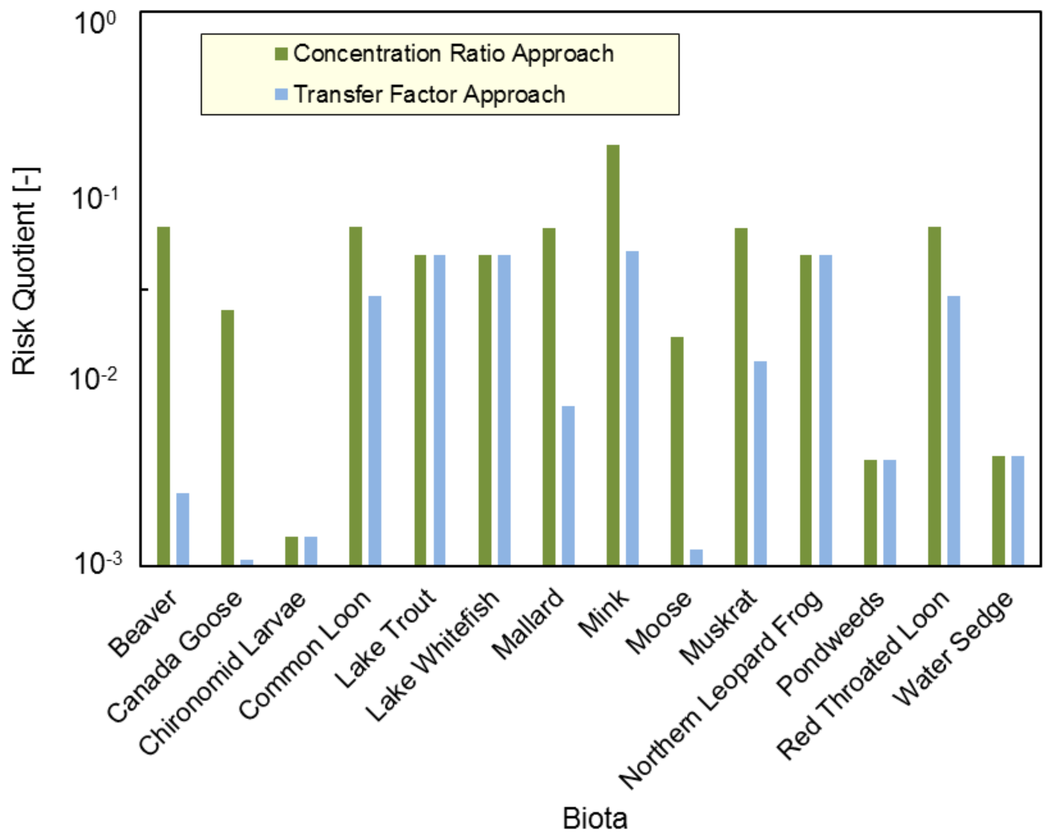

Figure 7-192: Tier 1 Quotients that exceed 10^{-2} in the All Containers Fail Disruptive Event Scenario

As expected, the Tier 1 quotients are all below 1, with the highest value occurring for the mink.

The mink exposure is further explored in Figure 7-193 to Figure 7-195. Figure 7-193 compares the time dependent dose rates to the mink for both radionuclide partitioning approaches and for both cases considered. Although there is some variation between the results calculated with Transfer Factors and those with Concentration Ratios, the use of either approach does not affect the conclusion of the current analysis, since all exposures are below the Tier 1 Interim Acceptance Criterion.

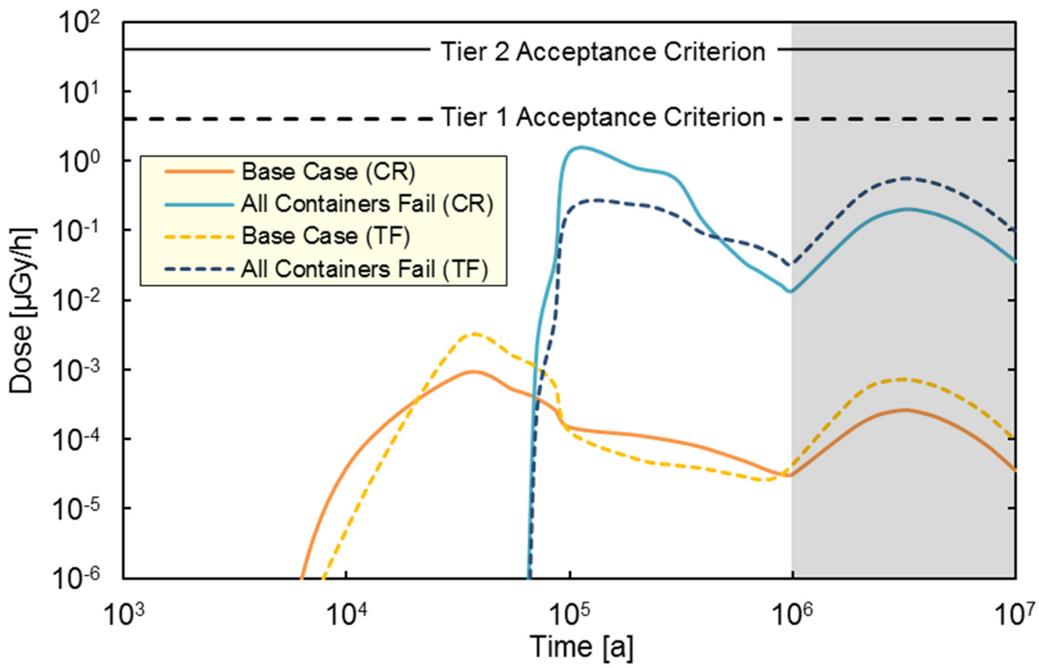

CR: Concentration Ratio Approach TF: Transfer Factor Approach

Figure 7-193: Dose Rates to the Mink as a Function of Time

Figure 7-194 and Figure 7-195 show the contribution from each radionuclide to the total dose rate for both radionuclide partitioning approaches for the All Containers Fail Disruptive Event Scenario. For the Concentration Ratio approach, the initial peak dose rate (occurring around 100,000 years) is due to internally deposited Cl-36, which is dictated by the water Concentration Ratio. For the Transfer Factor approach, the initial peak dose rate is due to internally deposited Se-79 (55%) and Cl-36 (45%), principally from the consumption of fish, muskrat and sediment. For both radionuclide partitioning approaches, the dose rate at later times is dominated by Cs-135.

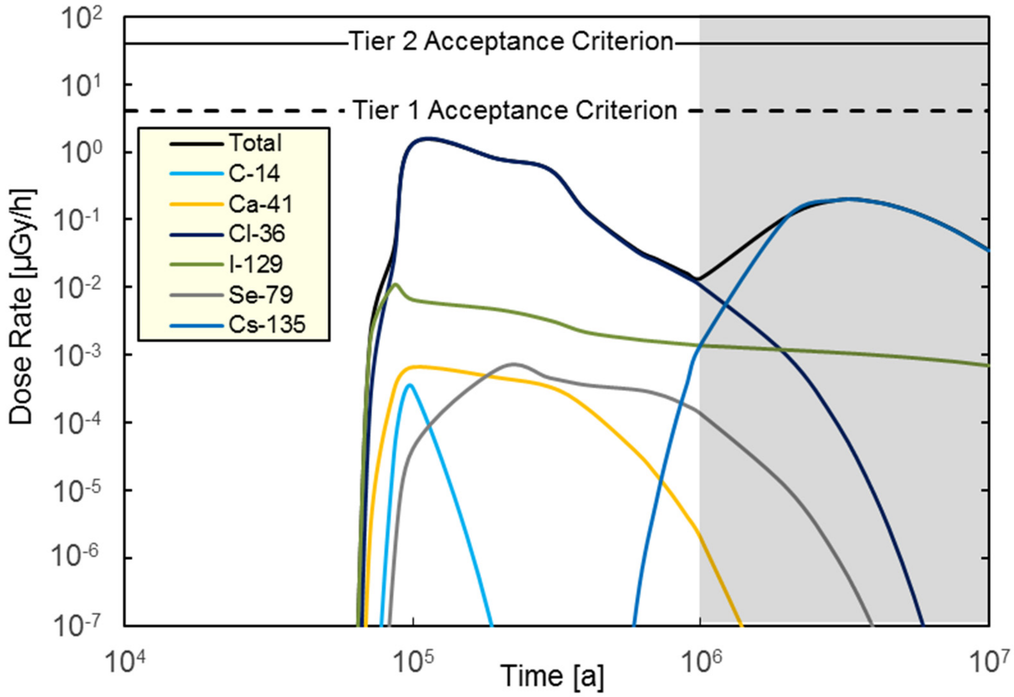

Note: C-14 and Cl-36 dose rates result from the sum of releases originating from both the fuel and the fuel sheath.

Figure 7-194: Radionuclide Breakdown of Dose Rate to Mink using Concentration Ratios for the All Containers Fail Disruptive Event Scenario

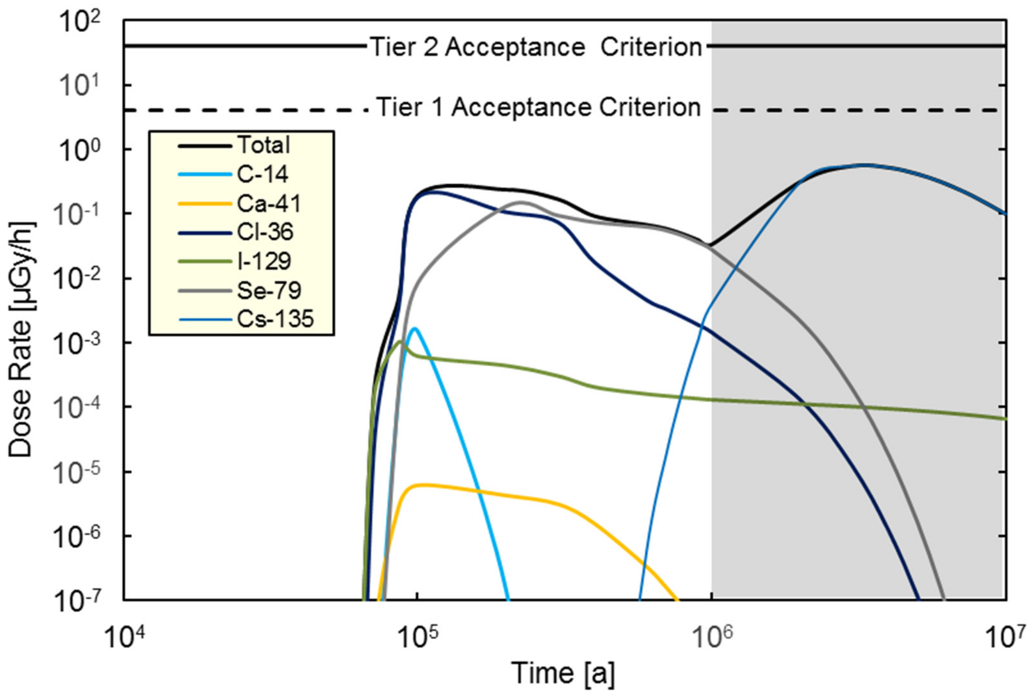

Note: C-14 and Cl-36 dose rates result from the sum of releases originating from both the fuel and the fuel sheath.

Figure 7-195: Radionuclide Breakdown of Dose Rate to the Mink using Transfer Factors for the All Containers Fail Disruptive Event Scenario

7.11 Modelling and Results for the Protection of Persons and the Environment from Hazardous Substances

This section addresses the potential non-radiological consequences of contaminants arising from the used fuel bundles and from the container on the health and safety of persons and the environment. The potentially significant chemically hazardous elements from the used fuel bundles considered in this study are Ag, Bi, Br, Cd, Hg, I, Mo, Sb, Se, Tc, Te, U and W, as identified in Section 7.6.2.

Chemical elements of potential concern could also be released from the copper containers and the engineered sealing materials. While the hazard from the sealing materials is expected to be very low because the components tend to be natural clay materials, an assessment is performed to determine the hazard associated with the copper containers.

Section 7.1.2 describes the applicable interim acceptance criteria, and Table 7-1 presents the criteria for groundwater, surface water, sediment, soil and air.

The ratio determined by dividing an element concentration by its acceptance criterion is called the ‘Concentration Quotient’. Concentration Quotients less than 1.0 indicate the interim acceptance criterion is not exceeded.

7.11.1 Contaminants from the Used Fuel Bundles

There are no releases for the Reference Case of the Normal Evolution Scenario.

To illustrate the potential consequences of contaminant releases, the approach compares results obtained for the Base Case and for the All Containers Fail at 60,000 Disruptive Event Scenario against the interim acceptance criteria. All Containers Fail scenario is selected because it is the disruptive event that results in the greatest contaminant release.

Surface water, sediment, soil and air concentrations in the System Model biosphere are compared to the corresponding acceptance criteria. Groundwater concentrations are taken to be those in the well.

In the Base Case, all contaminants enter the well and therefore sediment concentrations for surface water features are not calculated. Instead, Base Case sediment values are estimated by multiplying the surface water concentrations by sediment sorption coefficients taken from Gobien et al. (2016). As noted in Section 7.3.4, the System Model conservatively overestimates the amount of radionuclides in the biosphere by assuming all radionuclides transferred to the well are also simultaneously transferred to surface water features. Therefore, surface water concentrations are generated by the System Model even though there is no direct discharge to the surface.

Table 7-55 shows the Concentration Quotients for the Base Case. These are the maximum values achieved throughout the one million year time frame of interest. The highest value is 2.67×10^{-4} for Mo in groundwater. Wide margins are available to the interim acceptance criteria.

Table 7-56 shows the Concentration Quotients for the All Containers Fail Disruptive Scenario. These are also the maximum values achieved throughout the one million year time frame of interest. As expected, the quotients are higher than in the Base Case due to the significantly greater source term, with the highest value being 0.47 for Mo in groundwater.

The Table 7-55 and Table 7-56 results are also represented visually in Figure 7-196 to Figure 7-200.

Based on these results, it is concluded that the repository would not pose a non-radiological health and safety hazard to persons or to the environment for contaminants released from the used fuel bundles.

Table 7-55: System Model: Concentration Quotients for the Base Case

Element	Groundwater	Surface Water	Soil	Sediment*	Air
Ag	$8.05x10^{-5}$	$2.28x10^{-7}$	$1.24x10^{-5}$	$6.85x10^{-7}$	$2.39x10^{-7}$
Bi	-	-	$2.83x10^{-7}$	-	$1.97x10^{-9}$
Br	-	-	$6.20x10^{-8}$	-	$7.20x10^{-9}$
Cd	$1.21x10^{-5}$	$6.66x10^{-8}$	$1.45x10^{-6}$	$7.99x10^{-9}$	$1.26x10^{-5}$
Hg	$3.98x10^{-5}$	$2.81x10^{-7}$	$2.71x10^{-7}$	$1.28x10^{-9}$	$2.36x10^{-8}$
I	-	$7.09x10^{-10}$	$3.61x10^{-7}$	-	$1.11x10^{-6}$
Mo	$2.67x10^{-4}$	$6.31x10^{-8}$	$9.55x10^{-6}$	$1.90x10^{-9}$	$6.61x10^{-8}$
Sb	$1.58x10^{-6}$	$3.73x10^{-10}$	$3.04x10^{-7}$	$4.03x10^{-10}$	$9.38x10^{-10}$
Se	$3.55x10^{-6}$	$8.38x10^{-9}$	$5.20x10^{-7}$	$1.68x10^{-8}$	$8.79x10^{-9}$
Tc	-	-	0	-	-
Te	-	-	$1.36x10^{-7}$	-	$9.48x10^{-8}$
U	0	0	0	0	0
W	-	$1.81x10^{-10}$	$4.09x10^{-9}$	-	$8.48x10^{-10}$

Note: * Values are estimated using the surface water concentration as described in Section 7.11.3.
- Indicates there is not acceptance criteria for a given element in that media
Concentration Quotients below $1x10^{-15}$ are listed as zero

Table 7-56: System Model: Concentration Quotients for the All Containers Fail Case

Element	Groundwater	Surface Water	Soil	Sediment	Air
Ag	$6.35x10^{-2}$	$2.34x10^{-4}$	$9.78x10^{-3}$	$5.24x10^{-3}$	$1.89x10^{-4}$
Bi	-	-	$1.25x10^{-3}$	-	$8.67x10^{-6}$
Br	-	-	$3.83x10^{-4}$	-	$4.44x10^{-5}$
Cd	$1.59x10^{-2}$	$1.55x10^{-4}$	$1.90x10^{-3}$	$9.92x10^{-3}$	$1.66x10^{-2}$
Hg	$1.92x10^{-1}$	$1.36x10^{-3}$	$1.31x10^{-3}$	$1.36x10^{-3}$	$1.14x10^{-4}$
I	-	$5.94x10^{-7}$	$3.00x10^{-4}$	-	$9.15x10^{-4}$
Mo	$4.65x10^{-1}$	$1.74x10^{-4}$	$1.66x10^{-2}$	$7.22x10^{-3}$	$1.15x10^{-4}$
Sb	$2.40x10^{-3}$	$1.03x10^{-6}$	$4.62x10^{-4}$	$3.29x10^{-4}$	$1.43x10^{-6}$
Se	$8.98x10^{-2}$	$4.39x10^{-5}$	$1.32x10^{-3}$	$2.48x10^{-2}$	$2.23x10^{-5}$
Tc	-	-	0	-	-
Te	-	-	$2.07x10^{-4}$	-	$1.44x10^{-4}$
U	0	0	0	0	0
W	-	$5.79x10^{-7}$	$7.12x10^{-6}$	-	$1.48x10^{-6}$

Note: - Indicates there is not acceptance criteria for a given element in that media
Concentration Quotients below $1x10^{-15}$ are listed as zero

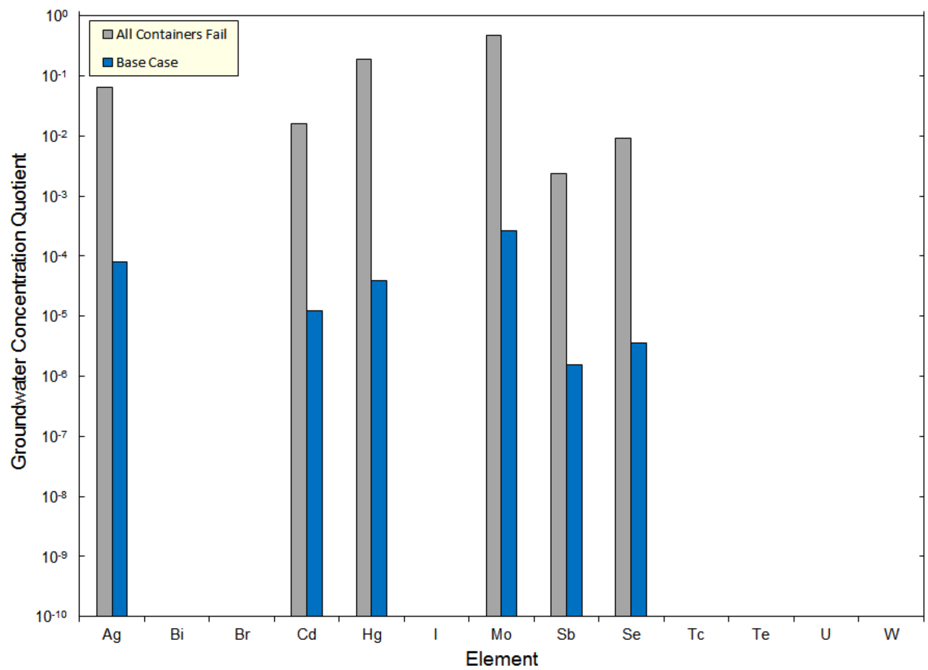

Note: Bi, Br, I, Tc, Te and W do not have acceptance criteria for groundwater, U results are off scale low

Figure 7-196: Non-Radiological Hazard: Groundwater Results

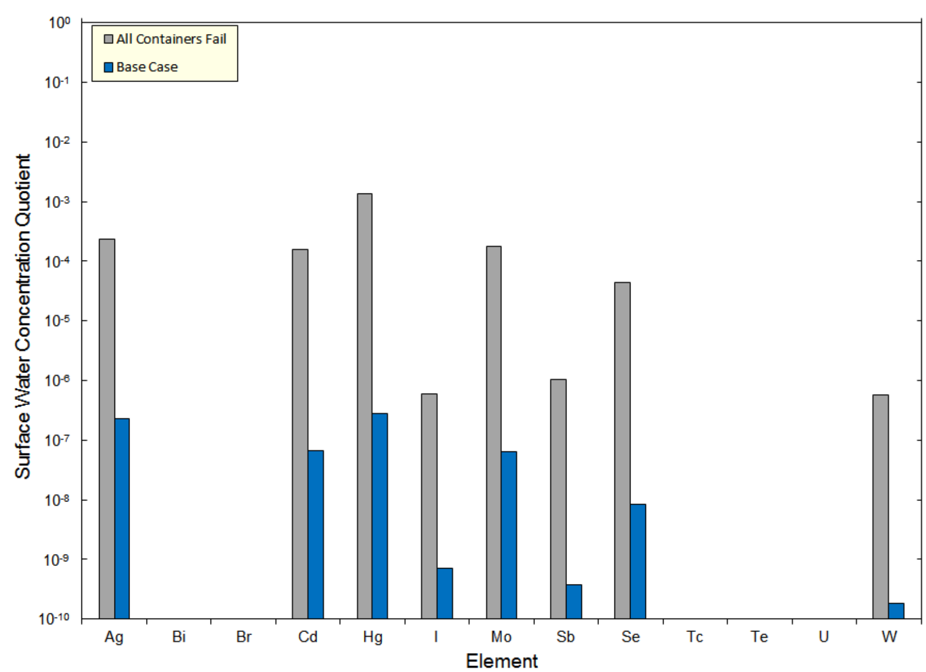

Note: Bi, Br, Tc, and Te do not have acceptance criteria for surface water, U results are off scale low

Figure 7-197: Non-Radiological Hazard: Surface Water Results

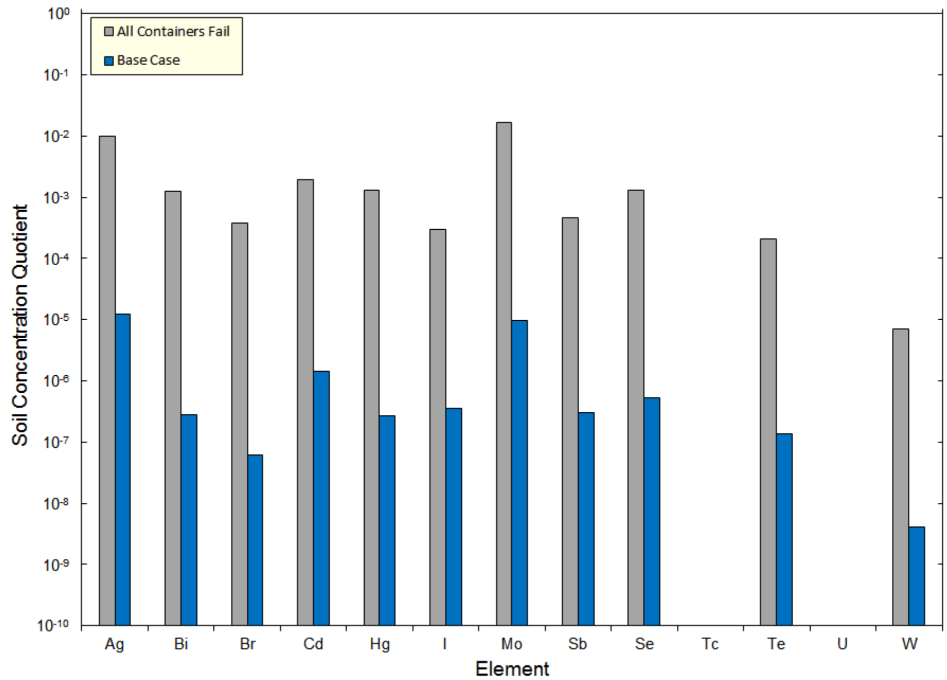

Note: Tc and U results are off scale low.

Figure 7-198: Non-Radiological Hazard: Soil Results

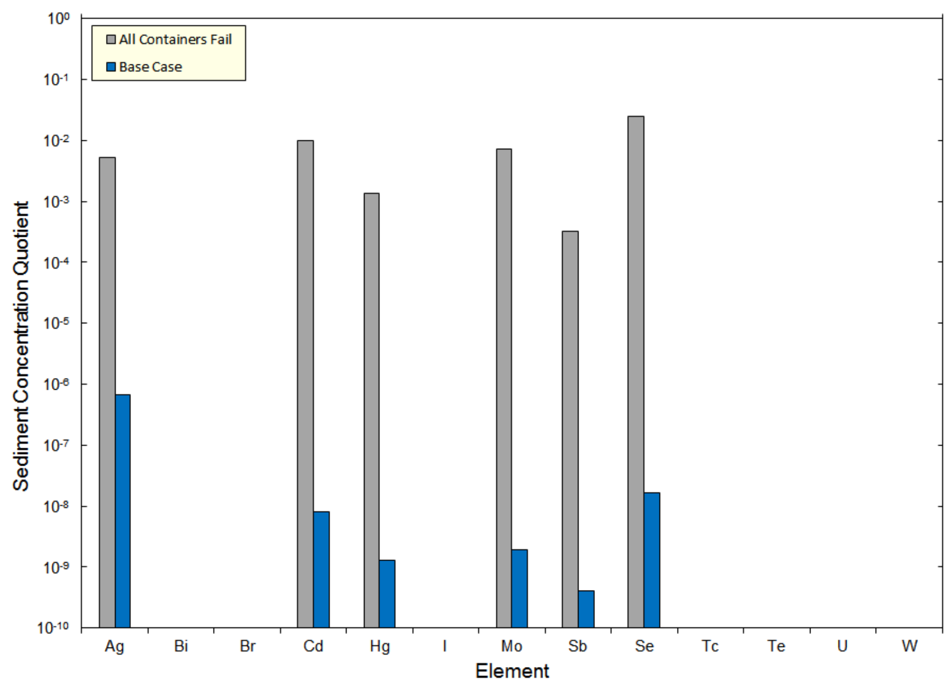

Note: Bi, Br, I, Tc, Te and W do not have acceptance criteria for Sediment, U results are off scale low.

Figure 7-199: Non-Radiological Hazard: Sediment Results

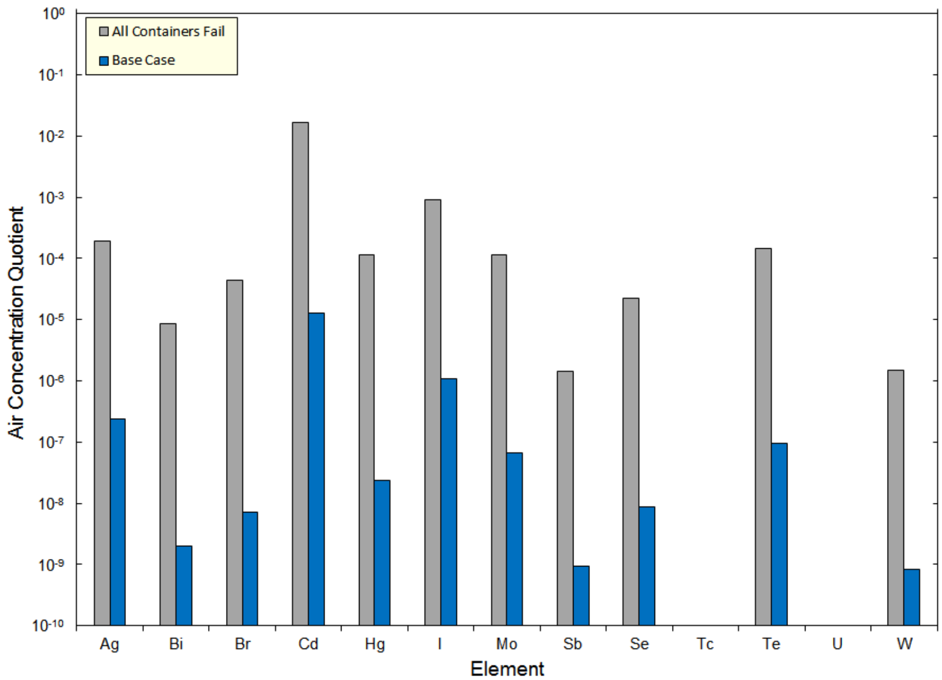

Note: Tc does not have an acceptance criterion in Air, U results are off scale low

Figure 7-200: Non-Radiological Hazard: Air Results

7.11.2 Copper Container Chemical Hazard Assessment

Chemical elements of potential concern could also be released from the copper container and the engineered sealing materials. While the hazard from the sealing materials is expected to be very low because the components are natural clay materials, an assessment is performed to determine the hazard associated with the copper containers.

The release rate of contaminants from the copper metal depends on the copper corrosion or dissolution rate. Although reducing conditions are expected after closure, a small amount of copper corrosion can still occur as discussed in Chapter 5.

For the purpose of this assessment, a solubility-limited dissolution model is used to determine the rate of copper release. The Rooms-Only Repository-Scale Model (see Section 7.7.1.2) is used to model copper transport to the biosphere.

The transport of copper away from the container is simulated by applying a constant concentration boundary condition of 1.4×10^{-4} mol/m^3 at every grid node intersecting containers in the repository. This concentration corresponds to the measured copper solubility limit increased by a factor of 10 (Table 7-16) to account for uncertainties in temperature and chemical conditions near the container. This conservatively results in a continuous input of copper into the model over the course of the 10 million year simulation.

Figure 7-201 illustrates groundwater copper concentrations within surface materials, one million years postclosure. Transport is primarily to surface sediments beneath surface waters.

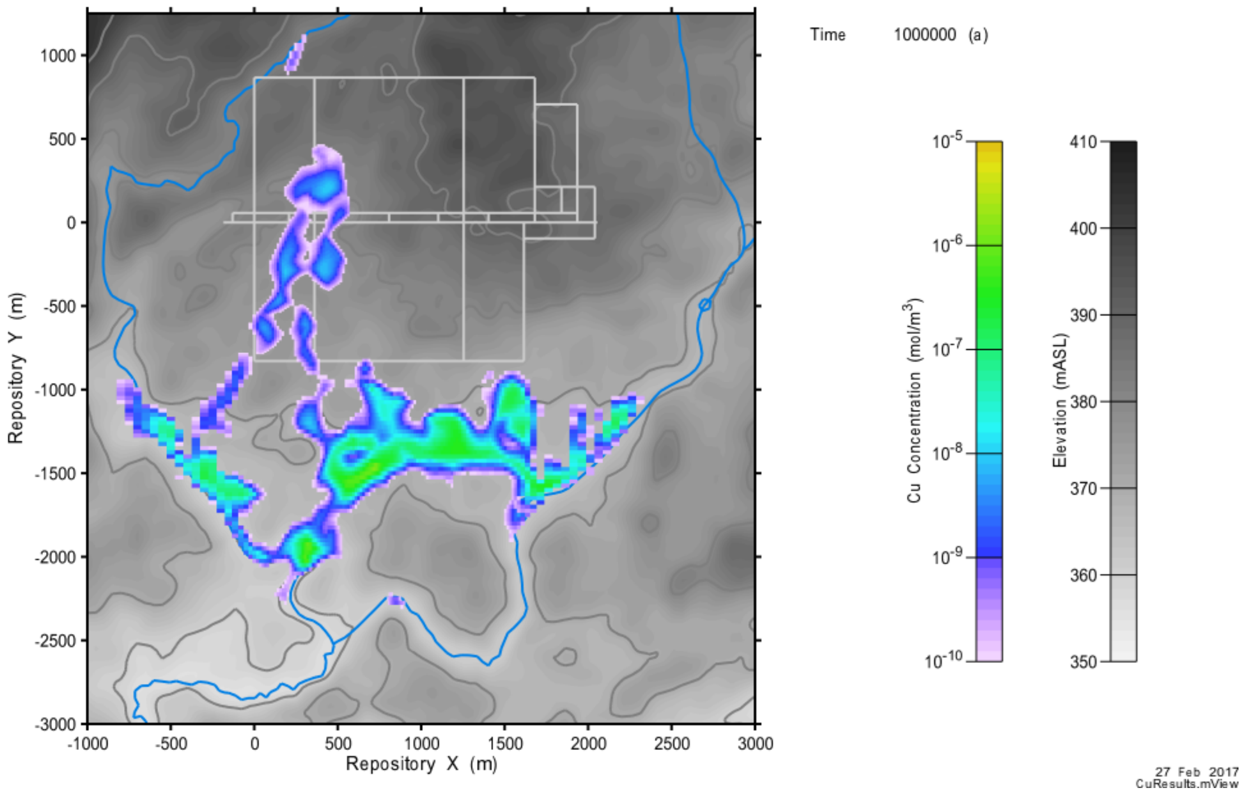

Figure 7-201: Rooms-Only Repository-Scale Model: Copper Concentration across the Repository Site (with well)

Figure 7-202 shows the transport of copper to the surface as a function of time.

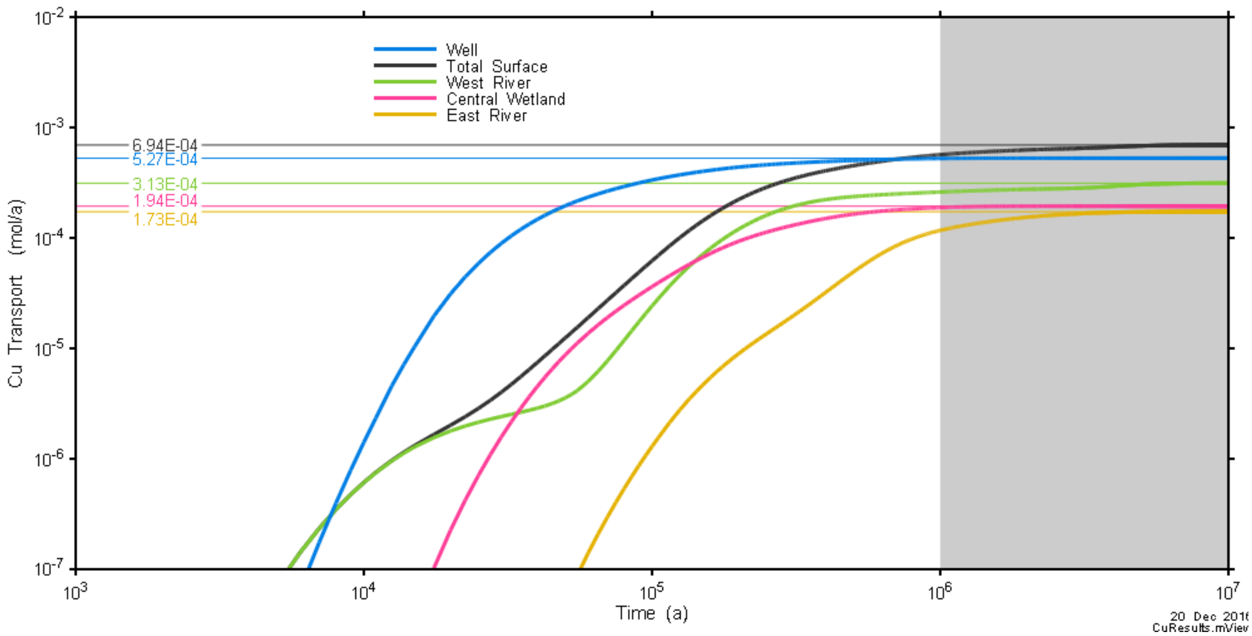

Figure 7-202: Rooms-Only Repository-Scale Model: Copper Transport to the Surface

To determine the groundwater Concentration Quotient, the maximum copper transport to the well (i.e., 5.27×10^{-4} mol/a) is assumed, with the well pumping at the reference rate of 911 m^3/a. The resulting well water concentration is 5.79×10^{-7} mol/m^3.

For simplicity, the surface water and groundwater concentrations are conservatively assumed to be the same as the well water concentration. The maximum soil and sediment concentrations are determined by multiplying the well water concentration by the applicable sorption coefficients for soil (0.11 m^3/kg) and sediment (0.37 m^3/kg).

Chemical element impurities present in the copper are not currently known; however, given that the copper will be at least 99.9% pure, the contaminant levels will be very low. To allow for an assessment, the impurity levels in Table 7-57 (SKB 1998 and SKB 2010b) are adopted. The calculation of impurity concentrations assumes the impurities are transported away at the same rate as the copper. Element specific K_d values for impurities in the buffer and geosphere may produce some variation in the transport times but because chemical species do not decay, peak impurity concentrations are largely independent of transport time.

Table 7-57 shows the computed surface water, groundwater, soil and sediment Concentration Quotients for copper and for the assumed impurity elements. Since these quotients are all well below 1.0, it is concluded that these elements would not pose a health and safety hazard to persons or to the environment.

Table 7-57: Concentration Impurity Levels in Copper and Estimated Element Concentration Quotients

Element	Impurity Level[1] [mol/mol Cu]	Maximum Element Conc in Well Water [mol/m^3]	Surface Water Conc Quotient[2]	Groundwater Conc Quotient[3]	Soil Conc Quotient[4]	Sediment Conc Quotient[5]
Cu	-	5.78×10^{-7}	3.68×10^{-2}	5.33×10^{-4}	6.66×10^{-5}	1.13×10^{-3}
Ag	1.47×10^{-5}	8.52×10^{-12}	9.19×10^{-6}	7.66×10^{-7}	4.04×10^{-6}	2.76×10^{-5}
As	4.24×10^{-6}	2.45×10^{-12}	3.68×10^{-8}	1.84×10^{-8}	7.80×10^{-11}	3.12×10^{-10}
Bi	3.04×10^{-7}	1.76×10^{-13}	-	-	7.97×10^{-10}	-
Cd	5.65×10^{-7}	3.27×10^{-13}	4.08×10^{-7}	1.75×10^{-8}	1.08×10^{-8}	4.90×10^{-8}
Co	2.16×10^{-5}	1.25×10^{-11}	1.23×10^{-6}	1.93×10^{-7}	1.23×10^{-8}	1.46×10^{-8}
Cr	1.83×10^{-5}	1.06×10^{-11}	5.51×10^{-7}	1.13×10^{-7}	3.66×10^{-7}	5.73×10^{-9}
Fe	1.14×10^{-5}	6.58×10^{-12}	1.23×10^{-9}	1.23×10^{-9}	1.64×10^{-9}	8.58×10^{-11}
Hg	3.17×10^{-7}	1.83×10^{-13}	9.19×10^{-6}	3.06×10^{-7}	1.09×10^{-8}	4.20×10^{-8}
Mn	5.78×10^{-7}	3.35×10^{-13}	3.68×10^{-10}	3.68×10^{-10}	3.23×10^{-11}	1.96×10^{-11}
Ni	1.08×10^{-5}	6.26×10^{-12}	1.47×10^{-8}	3.68×10^{-9}	5.54×10^{-9}	2.53×10^{-8}
[6]O	1.99×10^{-5}	1.15×10^{-11}	-	-	-	-
P	2.05×10^{-4}	1.19×10^{-10}	9.19×10^{-7}	-	-	-
Pb	1.53×10^{-6}	8.87×10^{-13}	6.13×10^{-9}	1.84×10^{-8}	1.70×10^{-8}	1.44×10^{-7}
S	2.97×10^{-5}	1.72×10^{-11}	2.90×10^{-7}	1.10×10^{-8}	4.50×10^{-11}	-
Sb	2.09×10^{-6}	1.21×10^{-12}	2.45×10^{-8}	2.45×10^{-8}	2.45×10^{-8}	2.65×10^{-8}
Se	2.41×10^{-6}	1.40×10^{-12}	1.10×10^{-7}	1.10×10^{-8}	4.96×10^{-8}	2.21×10^{-7}
[7]Si	4.53×10^{-5}	2.62×10^{-11}	-	-	-	-
Sn	1.07×10^{-6}	6.19×10^{-13}	1.01×10^{-9}	-	7.08×10^{-9}	-
Te	9.96×10^{-7}	5.76×10^{-13}	-	-	1.57×10^{-10}	-
Zn	9.72×10^{-7}	5.62×10^{-13}	5.13×10^{-11}	5.76×10^{-11}	1.73×10^{-10}	6.84×10^{-10}

Note: ’-‘ indicates that there are no defined criteria for that element in the given medium.
[1]Impurity levels are maximum values taken from SKB (1998), P impurity level is taken from SKB (2010b).
[2]Surface water concentration quotients are estimates based on the maximum element concentration in the well compared against the surface water criteria from Table 7-1.
[2]Groundwater concentration quotients are estimates based on the maximum element concentration in the well compared against the groundwater criteria from Table 7-1.
[4]Soil concentration quotients are estimated using the maximum element concentration in the well, the soil Kd values from Gobien and Garisto (2012) and the soil acceptance criteria from Table 7-1.
[5]Sediment concentration quotients are estimated using the maximum element concentration in the well, the sediment Kd values from Gobien and Garisto (2012) and the sediment acceptance criteria from Table 7-1.
[6]This element is considered non-hazardous and does not have criteria in Medri (2015c) as it is essential to life and is abundant..

7.12 Modelling and Results for Gas Generation and Migration

Gas will be generated in the repository due to corrosion of metals, degradation of organic materials, radiolysis of water, and radioactive decay. The potential impacts of gas generation have been studied internationally (ANDRA 2005, Nagra 2008, Mallants and Jacques 2004, SKB 1999). Among the potential impacts, the key ones are mechanical damage of the engineered barriers and host rock due to high gas pressures, modifications to groundwater flow and contaminant transport, gas release to the biosphere, and chemical effects of the gas on repository conditions.

This section describes calculations performed to estimate the potential effects of gas generation on the calculated dose consequences. The Base Case of the Normal Evolution Scenario and the All Containers Fail Disruptive Event Scenario are considered because these cases also include gas generation from failed containers. The calculations assume all gas generated in a given placement room is confined to only that room due to the presence of the room seal at the end of the room. Additional void volume present in the tunnels and access drifts is assumed to be inaccessible and the gas generated is discussed on a per room basis.

The Base Case assumes 10 containers fail within the first one million years, with the first failure occurring at 1000 years and subsequent failures occurring at a rate of one additional container every 100,000 years. However, as a conservative and simplifying assumption, the current analysis of gas generation assumes that all 10 containers fail simultaneously at 1000 years.

The All Containers Fail Scenario examines the case where all containers fail 60,000 years after repository closure. The analysis assumes the maximum number of containers in a placement room, which is 375 containers.

7.12.1 Gas Generation

This section considers the gas generation rate from:

- Metals and organics;
- Radiolysis and decay; and
- Volatilization of H_2S.

<u>From Metals and Organics</u>

In the Base Case, approximately 14,500 kg of steel (Gobien et al. 2016) is available for gas generation in a placement room containing 10 defective containers. In the All Containers Fail Disruptive Event Scenario, approximately 543,000 kg of steel (Gobien et al. 2016) is available for gas generation in a placement room containing 375 containers. No rock bolts are assumed present.

The steel surface area available for corrosion for each container is approximately 26 m^2 (Gobien et al. 2016). This includes all surfaces of the basket (69%) and the inner and outer surfaces of the steel vessel (31%). The total surface area of metal is thus 260 m^2 for 10 containers and 9.7×10^3 m^2 for 375 containers.

As discussed in Chapter 5, under the anaerobic conditions expected in the repository, hydrogen is produced by corrosion of steel following the reaction:

$$Fe+CO_3^{2-}\rightarrow FeCO_3+H_2+2OH^-$$

Organic carbon is also present, almost all of which is found in the highly compacted bentonite buffer boxes, the highly compacted bentonite spacer blocks, the gap fill and the bentonite seal. An estimated 4,200 kg of organic carbon is present, based on an organic carbon content in MX-80 bentonite of 1120 ppm (Marshall and Simpson 2014) and volumes of bentonite given in Gobien et al. (2016). Both the highly compacted bentonite (for the buffer boxes and seal) and the gap fill are composed of MX-80 bentonite.

Organic materials will also degrade under anaerobic conditions. Degradation of organics in clay is modelled as:

$$C_{org} + \text{Reactant} \rightarrow + ½\ CO_2 + ½\ CH_4 + \text{Residual}$$

where C_{org} denotes initial organics.

For simplicity, equal amounts of CO_2 and CH_4 are assumed to be produced and for conservatism, it is assumed that all organic carbon is consumed (i.e., all the organics are decomposable and no residual organic is formed). This is conservative since most of these organics would have been present in the natural clay materials for millions of years, and so are probably recalcitrant.

Gas generation rates depend on the steel corrosion rate and the bentonite degradation rate. According to the best estimate value for Equation 5.13, the steel corrosion rate is 6.8 μm/a at 1000 years (for the Base Case) and 1.7 μm/a at 60,000 years (for the All Containers Fail Scenario). Since the rate of bentonite degradation is not known, a very conservative value of 10^{-6}/a is assumed based on the age of natural bentonite deposits in North America (about 100 million years according to AECL 1992). The estimated maximum H_2 gas generation rates are therefore 245 mol/a for the Base Case and 2296 mol/a for the All Containers Fail Scenario. The total CO_2 and CH_4 from degradation of organics is 0.35 mol/a. The total maximum gas generation rate from metal corrosion and degradation of organics is 5.9 m^3@STP/a for the Base Case and 55 m^3@STP/a for the All Containers Fail Scenario.

Gas generation is assumed to continue at these rates until all steel inside the placement room has corroded (after an additional 6800 years for the Base Case and an additional 27,000 years for the All Containers Fail Scenario) and all organic material has degraded (after 10^6 years).

Note that this assessment conservatively ignores the methanogenesis reaction, $4H_2 + CO_2 \rightarrow CH_4 + 2H_2O$. This exothermic reaction, used by methanogenic bacteria as an energy source, has the potential to reduce the total inventory of gas.

From Radiolysis

Radiolysis can also generate gas. Radiolysis of water inside the defective containers could contribute a significant amount of hydrogen gas at early times; however, due to diminishing radiation fields, the production rate rapidly decreases with time. For example, 1000 years after closure, radiolysis could contribute an additional 10 mol/a (roughly 4% of the maximum gas generation rate from corrosion and degradation of organics) while 60,000 years after closure, radiolysis would contribute an additional 0.4 mol/a with 10 failed containers (0.1% of the maximum generation rate). If all containers fail at 60,000 years the rate would increase to 13 mol/a (0.5% of the maximum gas generation rate) for the All Containers Fail Scenario. This conservatively assumes that the Zircaloy cladding and steel components in the container do not stop alpha and beta particles.

Because the amount of gas generated by radiolysis is significant on times scales relevant for steel corrosion, the maximum gas generation rate from radiolysis is conservatively added to the total gas generation rate. As a result the maximum Base Case gas generation rate is increased by 10 mol/a to 255 mol/a (6.1 m^3@STP/a) and the maximum All Containers Fail Scenario gas generation rate is minimally increased by roughly 13 mol/a to 2309 mol/a (56 m^3@STP/a).

Outside the containers, radiation fields are lower because the thick container walls stop the alpha and beta particles and attenuate the gamma radiation. Gas generation by radiolysis occurring outside the containers is therefore neglected.

<u>Other Sources of Gas</u>

While the primary contributors to the gas pressure in the repository are expected to be H_2, CO_2 and CH_4, it is possible that hydrogen sulphide (H_2S), helium (He) and radon (Rn) could also be present.

Hydrogen sulphide is slightly soluble in water and is formed by the reduction of sulphate in the groundwater by microbes. Detailed characterization of specific sites will include comprehensive assessments of the deep groundwater, including dissolved sulphide concentrations. Calculations presented here assume the groundwater sulphide concentration is 1 μM, the 50th percentile of values reported by SKB for groundwaters at Forsmark (SKB 2010) and significantly higher than concentrations typically found in groundwaters in the Canadian Shield (see discussion in Chapter 5).

The vapour pressure of $H_2S(g)$ in equilibrium with a given concentration of $H_2S(aq)$ can be determined by using Henry's law:

$$H^{cp} = \frac{c[H_2S(aq)]}{p[H_2S(g)]}$$

Where H^{cp} is Henry's law solubility constant for H_2S, c is the molarity of the aqueous solution and p is the partial pressure of the gas.

The volatility of an aqueous solution of hydrogen sulphide will be highest when $H_2S(aq)$ is the dominant species in solution (i.e., at pH values less than about 6). Based on a Henry's law solubility constant of 0.1 M/atm (Sander 2015) and the groundwater sulphide concentration of 1 μM, the partial pressure of $H_2S(g)$ would be 1.0×10^{-5} atm or 1 Pa. This partial pressure is very small compared to the total gas pressure in the repository and can therefore be neglected.

The initial **Helium (He)** content of the fuel is very small, according to Tait et al. (2000). This initial amount is therefore neglected in comparison to the much larger amounts of hydrogen gas arising from steel corrosion, degradation of organic material and radiolysis.

In addition to the He initially present, alpha decay also results in the formation of He atoms. According to the inventories as a function of time presented in Tait et al. (2000), the greatest rates of He generation are 0.03 mol/a for the Base Case and 0.9 mol/a for the All Containers Fail Disruptive Event Scenario. These rates are negligible in comparison to the rates of gas generated in a placement room (255 mol/a for the Base Case and 2309 mol/a for the All Containers Fail Scenario).

The initial **Radon (Rn)** content of the fuel is also very small, according to Tait et al. (2000). This is therefore neglected in comparison to the much larger amounts of hydrogen gas arising from steel corrosion and decay of organic material. However, Rn is also produced as part of the 4N+2 decay chain. The greatest rate of Rn production, which occurs between 1000 and 10,000 years, is $6x10^{-13}$ mol/a for the Base Case and $1x10^{-9}$ mol/a for the All Containers Fail Scenario. This amount is insignificant relative to the gas produced via corrosion, degradation of organics and radiolysis.

For the reasons above, the contributions from H_2S, He and Rn have been neglected.

7.12.2 Gas Release and Migration

A number of mechanisms exist through the gas can escape into the host rock. To evaluate the relative importance of the different release mechanisms, scoping calculations have been done with results compared against the gas generation rates.

Gas Migration by Diffusion and Advection

Gas generated in the repository may dissolve in the groundwater and then diffuse or advect away. For the conceptual repository in this study, the engineered barrier system has a very low hydraulic conductivity and there is a small head differential across the repository.

The maximum amount of dissolved gas that can be removed by diffusion and advection can be estimated using Henry's Law. The diffusive transport of dissolved gas to the surface is calculated by taking the product of the effective diffusivity, Henry's Law constant, the water density and the gravitational constant. Based on a Henry's law constant for H_2 of $2x10^{-7}$ m^3@STP/m^3/Pa, and an effective diffusivity for the host rock of 10^{-12} m^2/s, the diffusive transfer rate is estimated as $6x10^{-8}$ m^3@STP/m^2/a.

The advective transport of dissolved gas to the surface is calculated by taking the product of the average linear velocity, the porosity, Henry's constant and the pressure at the repository horizon. Based on an average linear velocity of $6.8x10^{-2}$ m/a (calculated in the System Model model**)**, a porosity of 0.003 (see Table 7-20) and a pressure at the repository horizon of 4.9 MPa (based on the repository depth, gravity and the water density), the advective transfer rate is estimated as $2x10^{-5}$ m^3@STP/m^2/a. The total gas generation rates (approximately $1.9x10^{-3}$ m^3@STP/m^2 /a for the Base Case and $1.7x10^{-2}$ m^3@STP/m^2/a for the All Containers Fail Scenario) are greater than the rate at which dissolved gases can escape and it is therefore concluded that a H_2 gas phase is likely to be formed. A similar conclusion can be drawn for the CO_2 and CH_4 gases generated by degradation of organics in the sealing materials.

This conclusion is consistent with other studies that show, in general, that diffusion of dissolved gas in groundwater does not provide a significant contribution to bulk gas transport through the near field and does not prevent gas phase formation (ANDRA 2005, Nagra 2008, Mallants and Jacques 2004, and SKB 1999).

Gas Formation and Transport

Because the groundwater diffusive and advective processes are insufficient to remove the gases, a gas phase will form in the repository after the porewater becomes saturated with dissolved gas. The gas pressure could likely then build up until it is sufficient to overcome the threshold pressure of the repository engineered materials (buffer and backfill) and the surrounding host rock. The escaping gas can then enter the geosphere, and permeate (two-phase flow) through the rock.

Gas Transport through Bentonite

Gas transport through clay-based buffer and backfill materials is a complex process. It is known that a certain threshold pressure must be exceeded for gas to move through these materials when they are saturated or near-saturated. Gas propagation and penetration may be controlled by capillary retention, by the tension strength of the clay matrix, and by the swelling pressure (Pusch 2003). Early experiments and models suggested that the threshold pressure for water-saturated bentonite is approximately the sum of the hydrostatic and swelling pressures (SKB 1999).

While later experiments, such as LASGIT at the Äspö Hard Rock Laboratory in Sweden, have indicated this is too simple a model, the threshold pressure is in this range. Also, after the gas passes through the water-saturated bentonite buffer, evidence from laboratory tests suggest that the buffer will reseal (Hoch et al. 2004), with restoration of the hydraulic and transport properties that it possessed prior to the passage of gas.

Based on this information, it is anticipated that a gas transport pathway will be formed through the buffer annulus after the pressure around the container exceeds a threshold value. Once the gas passes through, the pressure near the container decreases significantly and the pathway is anticipated to close. If gas generation continues, a cycle may occur with successive periods of pressure build up and gas release.

Gas Transport through Host Rock

The host rock is a porous medium, with existing fractures and bulk rock porosity. Gas flow can occur in a porous medium if the following resistances are overcome:

- The capillary resistance as the gas-water interface moves through the pore or fracture constrictions, and
- The hydrostatic head and viscous resistances to water flow, so that water is displaced from the pathways.

For the bulk granitic rock at the repository level, the estimated threshold capillary pressure ranges from about 0.5 to 3 MPa, depending on the permeability (European Commission 2003). Given the permeability at repository depth, a reference capillary pressure of 3 MPa is adopted. In contrast, the estimated threshold capillary pressure for fractures is of the order of a few kPa, substantially lower than for bulk rock. Therefore, fractures, if encountered, would be the dominant gas migration pathway.

If it is assumed that the gas travels vertically through the homogeneous rock from which water has been at least partially displaced, a simple model, based on Darcy's law, can be used to estimate the migration of gas (Rodwell and Nash 1992). The model depends on the repository pressure (taken as the hydrostatic pressure) and surface pressure (taken as the atmospheric pressure), the gas viscosity and the effective rock permeability (taking into account the presence of water), which in turn depends on the hydraulic conductivity of the host rock.

Because the gas permeability of the host rock is not known, it is assumed that the gas permeability is 10% of the water permeability. If the repository gas pressure exceeds the threshold capillary pressure of the overlying rock, the estimated gas release flux through the host rock is approximately 0.3 m^3@STP/m^2/a (assuming the Base Case hydraulic conductivity of water of 4×10^{-11}m/s as shown in Table 7-27). If the hydraulic conductivity is reduced to that of Hydraulic Conductivity Sensitivity Case 2 (i.e., by a factor of 10), the gas flux through the host rock could be reduced to 0.03 m^3@STP/m^2/a.

Even with this lower value of hydraulic conductivity and the variety of simplifying and conservative assumptions described here that over-estimate the gas generation rate (e.g., simultaneous failure of multiple containers, simultaneous corrosion of all metal surfaces of failed containers, etc.), the gas release flux exceeds the estimated gas generation flux by a factor of 16 for the Base Case and by a factor of 1.8 for the All Containers Fail Scenario. It is therefore anticipated that most of the gas reaching the buffer / rock interface will escape via the host rock after the gas overpressure in the repository exceeds the gas threshold pressure.

The results from this assessment are consistent with other calculations that show that gas generated in a geological repository is likely to escape through most fractured crystalline rocks without an extreme gas pressure build up (SKB 1999).

It is therefore concluded that gas release via the host rock is sufficient to remove gas generated in the repository for both the Base Case and the All Containers Fail Disruptive Event Scenario. Pressure outside the buffer and backfill will be limited by the threshold capillary pressure in the host rock. To damage the host rock, the gas pressure will have to approach the lithostatic pressure which is estimated to be about 13 MPa. For this reason, it is also concluded that gas build up in the repository is insufficient to mechanically damage the host rock.

7.12.3 Evaluation of Potential Gas Generation Impacts

The possible impacts of gas generation in geological repositories have been previously identified in a number of review studies and safety assessments (European Commission 2003, Cool et al. 2004). Based on the assessment described above, some impacts are likely to be insignificant (e.g., mechanical damage to the host rock), so that only the potential impacts due to fires / explosions, releases of radioactive gases and the effect on container evolution need be considered further.

Fire and Explosion Impact

If the repository pressure exceeds the capillary threshold pressure of the bulk granitic rock, gases could be released via the bulk rock / fractures to the surface. This assessment assumes that a direct path from the repository to the surface could be created and that a house is situated on top of the repository. Gases released to the surface can infiltrate into this house, which is assumed to have a volume of 228 m^3, a floor area of 95 m^2, and an air exchange rate of $7x10^5$ m^3/a (Gobien et al. 2016).

Hydrogen and methane pose a potential explosion hazard in air if they accumulate to a level within the flammable range and if there is an ignition source. The flammable range in air (by volume) is between 4% and 74% for hydrogen (Air Product and Chemicals, 1994), and between 5% and 15% for methane (Air Products and Chemicals, 1999).

The gas inflow rate needed to achieve the lower limits of flammability is $2.8x10^4$ m^3@STP/a for H_2 and $3.5x10^4$ m^3@STP/a for CH_4. These rates are substantially higher than the maximum total gas generation rate from the whole repository for the Base Case (about 6.1 m^3@STP/a) and slightly greater than that for the All Containers Fail Scenario ($1.6x10^4$ m^3@STP/a).

Given the conservative nature of this assessment, it is therefore highly unlikely that significant flammable concentrations of hydrogen or methane would be produced and it is therefore concluded that a significant fire or explosion hazard in the biosphere does not exist.

Potential Dose Impact of Gas Release to Accessible Environment

The radiological impact of a release of C-14 gas (as CO_2 and CH_4) into the biosphere is considered here. The radiological impact of Rn-222 releases are not calculated because Rn-222 has a short half-life (3.8 days) and is expected to decay to negligible concentrations before reaching the surface.

To calculate C-14 doses, a very conservative and simplistic approach is taken whereby the C-14 released from the containers is assumed to be released directly into the house. However, the high flux from the instant release of C-14 is ignored because it occurs before the formation of a gas phase in the repository, which is required to support the formation of C-14 gas. Therefore, the small amount of C-14 that is instantly released is assumed to dissolve in the water. The maximum C-14 release rate for 10 containers is 8.7×10^5 Bq/a (at 1000 years) in the Base Case and 2.3×10^5 Bq/a for all containers in the All Containers Fail Scenario (at 60,000 years).

As in the fire and explosion assessment, the house is assumed to have a volume of 228 m^3 and an air exchange rate of $7x10^5$ m^3/a (Gobien et al. 2016). The equilibrium concentration of radionuclides in the house can be calculated from the volume of the building, the rate of entry of radioactive gases into the house and the building exchange rate. The adult house dweller has a breathing rate of 8400 m^3/a and spends roughly 80% of the year indoors (Gobien et al. 2016). The adult inhalation dose coefficient for C-14 (as CO_2) is $1.2x10^{-11}$ Sv/Bq (CSA 2014).

The estimated house C-14 concentration neglects the effects of dilution and dispersion, decay during transport through geosphere, and formation of soluble compounds. Based on these very conservative assumptions, the Base Case C-14 concentration in the house is 1.2 Bq/m^3 and the

C-14 inhalation dose rate for an adult living in the house is $1.0x10^{-4}$ mSv/a. In the All Containers Fail Disruptive Event Scenario, the concentration in the house is 0.32 Bq/m^3 and the C-14 inhalation dose rate for an adult living in the house is $2.6x10^{-5}$ mSv/a. These dose rates are well below the applicable interim dose rate acceptance criteria of 0.3 mSv/a for the Base Case and 1.0 mSv/a for the All Containers Fail Scenario.

Given the conservative nature of the dose calculation, it can be concluded that the potential airborne release of C-14 from the repository is not of concern.

Effect of Gas Generation on Container Evolution

Ingress of water into the failed containers will cause anaerobic corrosion of the inner steel vessel and generation of hydrogen, as discussed in Chapter 5. If the gas pressure in the container becomes sufficiently high, it could affect the evolution of the container (i.e., it could delay water inflow and potentially affect the evolving size of the defect). Experimental evidence also exists to show that the presence of hydrogen in the failed containers causes the dissolution rate of the used fuel to decrease (Shoesmith 2008, King and Shoesmith 2004, Spahiu and Sellin 2001, Spahiu et al. 2000). These effects have been conservatively neglected in this report.

7.13 Modelling and Results for Complementary Indicators

An “indicator” is a characteristic or consequence of a repository which can be used to indicate the overall safety or performance of the system. The most widely used indicator is the peak radiological dose rate, which is calculated from the characteristics of the waste and repository, the properties of the geosphere and biosphere, and the characteristics of the critical group.

The relevance of the calculated dose rates as indicators of potential exposure tends to decrease with time, in part because of uncertainties in the models and data used to calculate them. In particular, assumptions concerning the biosphere (e.g., climate), human lifestyles (i.e., critical group characteristics) and water flows in the near-surface environment become increasingly uncertain. The purpose of complementary long-term indicators is to supplement the dose rate indicator using system characteristics that are much less sensitive to such assumptions.

The types of complementary indicators considered are:

- Concentrations in the biosphere; and
- Transport to the biosphere.

Indicators of the first type avoid assumptions about biosphere pathways but make assumptions about flow rates in surface water bodies (i.e., dilution rates). Indicators of the second type avoid assumptions about surface water flows. Concentration type indicators are useful on medium timeframes (about 10^4 to 10^5 years), while transport type indicators are useful for very long timeframes (> 10^5 years) when there is more uncertainty about surface conditions.

The specific complementary indicators considered for radiological contaminants have been selected based on the recommendations of the SPIN project (Becker et al. 2002). The indicators are:

- Radiotoxicity concentration in a water body, for medium time scales; and

- Radiotoxicity transport from the geosphere, for longer time scales.

Radiotoxicity concentration (in mSv/m^3) is the sum over all radionuclides of the activity concentrations in the water body (in Bq/m^3) multiplied by the corresponding radionuclide ingestion dose coefficient. Radiotoxicity transport from the geosphere (in mSv/a) is similarly defined.

Although these complementary indicators are expressed in units of mSv/m^3 or mSv/a, they do not represent a dose; rather, they are radiotoxicity-weighted concentration or transport indicators.

Results are shown for the Base Case and for the All Containers Fail at 60,000 Years Disruptive Event Scenario.

7.13.1 Reference Values

To make use of indicators, reference values are required for comparison purposes. These are derived below.

Radiotoxicity Concentration in a Water Body

A reference value for the radiotoxicity concentration in a water body can be derived using information on present-day natural background radionuclide concentrations in Canadian surface waters. Table 7-58 shows these concentrations for a variety of radionuclides. Data representative of Canadian surface waters are taken from Sheppard and Sanipelli (2011a) while Southern Ontario data are taken from a subset of samples in Sheppard and Sanipelli (2011b).

Table 7-58: Background Concentration of Radionuclides in Surface Waters

Surface Water Concentration [Bq/L]					Ingestion DCF [Sv/Bq]	Radiotoxicity (Canadian) [mSv/m^3]
Radionuclide	Canadian		Southern Ontario			
H-3	3.2×10^{0}		3.7×10^{0}		1.8×10^{-11}	5.8×10^{-5}
Cl-36	5.1×10^{-6}		2.0×10^{-6}		9.3×10^{-10}	4.7×10^{-9}
K-40	3.3×10^{-2}		3.4×10^{-2}	a	6.2×10^{-9}	2.0×10^{-4}
Rb-87	2.6×10^{-4}		1.1×10^{-3}	b	1.5×10^{-9}	3.9×10^{-7}
I-129	1.0×10^{-7}		8.7×10^{-8}		1.1×10^{-7}	1.1×10^{-8}
Bi-210	6.4×10^{-3}	c	2.0×10^{-2}	c	1.3×10^{-9}	8.3×10^{-6}
Pb-210	6.4×10^{-3}		2.0×10^{-2}		6.9×10^{-7}	4.4×10^{-3}
Po-210	7.1×10^{-3}		2.0×10^{-2}	c	1.2×10^{-6}	8.5×10^{-3}
Rn-222	2.7×10^{-3}	d	5.8×10^{-3}	d	2.5×10^{-10}	6.8×10^{-7}
Ra-223	2.0×10^{-7}	f	4.8×10^{-7}	f	1.0×10^{-7}	2.0×10^{-8}
Ra-224	7.8×10^{-3}	h	6.3×10^{-3}	h	7.1×10^{-8}	5.6×10^{-4}
Ra-226	2.7×10^{-3}		5.8×10^{-3}		2.8×10^{-7}	7.6×10^{-4}
Ac-227	2.0×10^{-7}	f	4.8×10^{-7}	f	1.1×10^{-6}	2.2×10^{-7}
Th-227	2.0×10^{-7}	f	4.8×10^{-7}	f	8.8×10^{-9}	1.8×10^{-9}

Ra-228	2.9×10^{-4}		3.1×10^{-4}	g	6.9×10^{-7}	2.0×10^{-4}
Th-228	9.6×10^{-4}		3.1×10^{-4}	g	7.2×10^{-8}	6.9×10^{-5}
Th-230	1.9×10^{-3}		5.1×10^{-3}	e	2.1×10^{-7}	4.0×10^{-4}
Pa-231	2.0×10^{-7}	f	4.8×10^{-7}	f	7.1×10^{-7}	1.4×10^{-7}
Th-231	1.5×10^{-7}		4.8×10^{-7}	f	3.4×10^{-10}	5.1×10^{-11}
Th-232	3.9×10^{-4}		3.1×10^{-4}		2.3×10^{-7}	9.0×10^{-5}
Th-234	3.3×10^{-3}	e	5.1×10^{-3}	e	3.4×10^{-9}	1.1×10^{-5}
U-234	7.3×10^{-3}		5.1×10^{-3}	e	4.9×10^{-8}	3.6×10^{-4}
U-235	9.3×10^{-5}		2.4×10^{-4}		4.7×10^{-8}	4.4×10^{-6}
U-238	3.3×10^{-3}		5.1×10^{-3}		4.5×10^{-8}	1.5×10^{-4}
					Total	1.6×10^{-2}

Notes:
(a) Estimated using stable K concentration
(b) Estimated using stable Rb concentration
(c) Assumed to be in secular equilibrium with Pb-210
(d) Assumed to be in secular equilibrium with Ra-226
(e) Assumed to be in secular equilibrium with U-238
(f) Values are 500 times lower than for U-235 in water, as recommended by Amiro (1992, 1993)
(g) Assumed to be in secular equilibrium with Th-232
(h) Values are 20 times higher than for Th-232 in water, as recommended by Amiro (1992, 1993)

Sheppard and Sanipelli (2011a) suggest that the background concentration of radioactive species in surface water remains fairly homogeneous across Canada. Data extracted specifically for Southern Ontario appears to verify this with most radionuclide concentrations within a factor of two of the Canadian values. Canadian surface water data have therefore been selected as representative of the surface waters applicable to this hypothetical site.

Radiotoxicity concentration is determined by multiplying the surface water concentrations by the appropriate ingestion dose conversion factor (Gobien et al. 2016). The results are shown in the rightmost column of Table 7-58, with the total value of 1.6×10^{-2} mSv/m^3 indicated at the bottom right. For comparison, use of data specific to Southern Ontario results in a higher radiotoxicity concentration of 4.2×10^{-2} mSv/m^3. Thus, the selected reference value is conservative when used as a comparative baseline.

Dose impacts associated with these natural background levels are not of public concern so it follows that any dose impacts from the repository that are small in comparison should also not be of concern.

Radiotoxicity Transport from the Geosphere

Natural transport processes continuously carry small amounts of naturally occurring radioactivity from within the geosphere to the biosphere. The most important processes are groundwater flow and erosion (IAEA 2002). The natural radioactivity discharged to the biosphere with groundwater flow has been calculated in Garisto et al. (2004) from groundwater flow rates and radionuclide concentrations in groundwater. The result is a value of 7×10^5 mSv/a over a 100 km^2 subregional watershed area.

Alternatively, radiotoxicity transport to the surface can be calculated from the elemental composition of Canadian Shield granites and the erosion rate of granite over long time periods.

Table 7-22 in Section 7.6.1.2 presents values for elemental concentrations in granite used in the screening assessment for potentially hazardous chemical elements. Using this information, the subset of elemental concentrations for radioactive elements shown in Table 7-59 can be generated. From this, the elemental concentrations of their associated radioactive progeny can be determined, assuming secular equilibrium, as noted in Table 7-60.

Table 7-59: Radioactive Element Concentrations in Granites

Element	Granite Concentration [g/kg Granite]
U	0.0049
Th	0.031
K	38
Rb	0.16

Table 7-60: Radiotoxicity Concentration in Granite

Nuclide	Activity Concentration [Bq/kg]	Ingestion DCF [Sv/Bq]	Radiotoxicity Concentration [mSv/kg]
U-238	60	4.50×10^{-8}	2.7×10^{-3}
Th-234	60	3.40×10^{-9}	2.0×10^{-4}
U-234	60	4.90×10^{-9}	2.9×10^{-4}
Th-230	60	2.10×10^{-7}	1.3×10^{-2}
Ra-226	60	2.80×10^{-7}	1.7×10^{-2}
Rn-222	60	2.50×10^{-10}	1.5×10^{-5}
Pb-210	60	6.90×10^{-7}	4.1×10^{-2}
Bi-210	60	1.30×10^{-9}	7.8×10^{-5}
Po-210	60	1.20×10^{-6}	7.2×10^{-2}
U-235	3	4.70×10^{-8}	1.3×10^{-4}
Th-231	3	3.40×10^{-10}	9.5×10^{-7}
Pa-231	3	7.10×10^{-7}	2.0×10^{-3}
Ac-227	3	1.10×10^{-6}	3.1×10^{-3}
Th-227	3	8.80×10^{-9}	2.5×10^{-5}
Ra-223	3	1.00×10^{-7}	2.8×10^{-4}
Th-232	124	2.30×10^{-7}	2.8×10^{-2}
Ra-228	124	6.90×10^{-7}	8.6×10^{-2}
Th-228	124	7.20×10^{-8}	8.9×10^{-3}
Ra-224	124	7.13×10^{-8}	8.8×10^{-3}
K-40	1200	6.20×10^{-9}	7.4×10^{-3}
Rb-87	146	1.50×10^{-9}	2.2×10^{-4}
		Total	2.9×10^{-1}

By adopting the same values for erosion rate ($6.5x10^{-6}$ m/a), watershed area (59 km^2 for the hypothetical site) and granite density (2700 m^3/kg) used in Section 7.6.1.2 for the screening assessment, a total erosion rate of about $1.0x10^6$ kg/a can be estimated. By applying the ingestion dose conversion factors from Gobien et al. (2016) to the Table 7-60 values, a radiotoxicity transport value of about $3x10^5$ mSv/a can be determined.

This erosion value is similar to, but slightly less than, the $7x10^5$ mSv/a radiotoxicity transport value estimated for groundwater flow. It is adopted as the reference value for the radiotoxicity transport indicator.

Indicator Summary

Table 7-61 summarizes the reference values for the dose rate indicator and the complementary long-term indicators developed for use in this study. The reference values proposed in the EC SPIN project (Becker et al. 2002) are also shown for comparison. The higher value of the radiotoxicity transport indicator is likely due to the higher uranium content of Canadian Shield granite.

Table 7-61: Reference Values for Indicators

Indicator	Reference Value	
	Current Study	SPIN
Dose rate (m /a)	0.3	0.1 to 0.3
Radiotoxicity concentration in surface water (mSv/m^3)	$1.6x10^{-2}$	$2x10^{-2}$
Radiotoxicity transport from the geosphere (mSv/a)	$3x10^5$	$6x10^4$

7.13.2 Results for Complementary Indicators

Figure 7-203 shows the indicator values for the Base Case together with the dose rate indicator for comparison. The indicators have the same general shape because they both depend on radionuclide transport to the biosphere. The figure shows very large margins to the associated criteria for both complementary indictors.

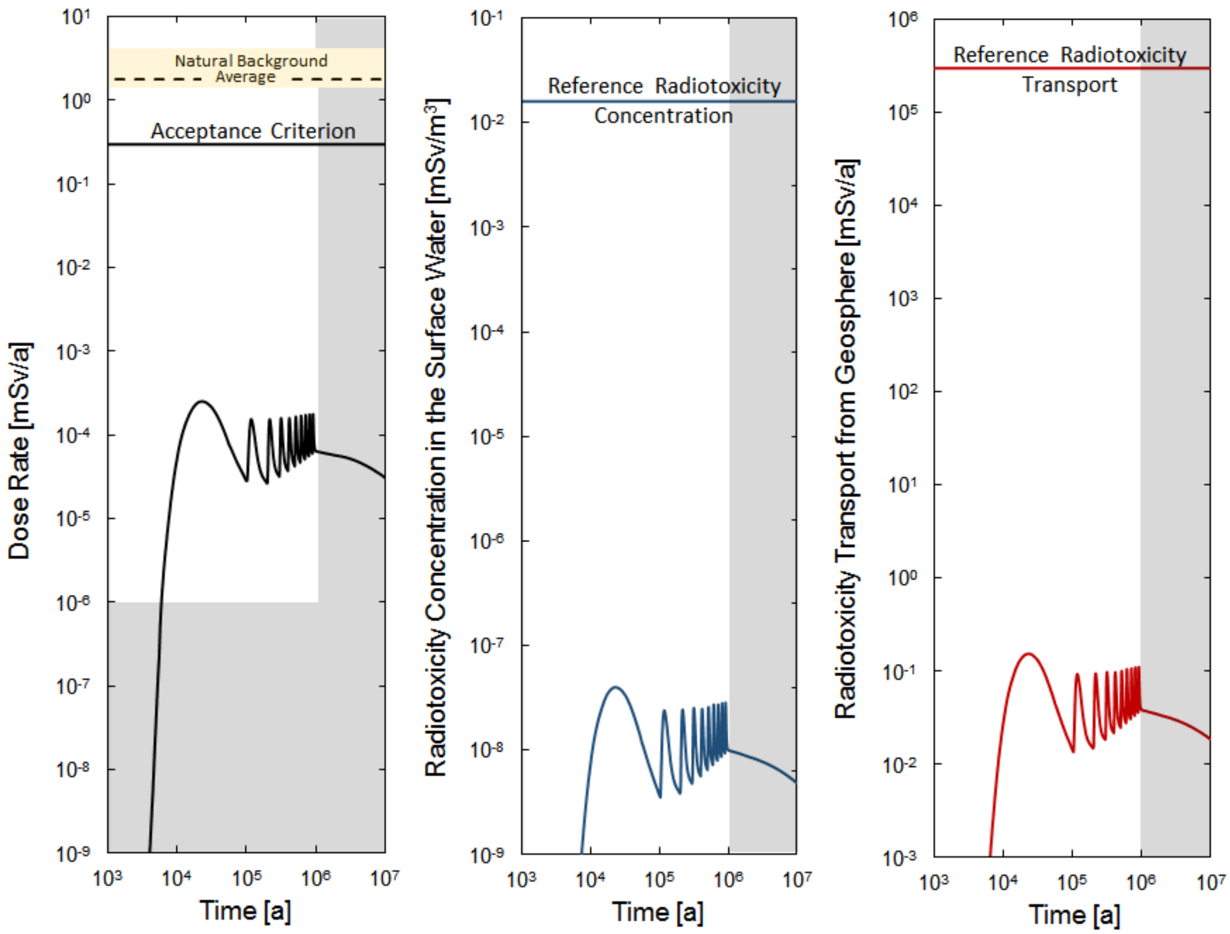

Figure 7-203: System Model: Base Case – Results for Indicators

Figure 7-204 through Figure 7-207 show the distribution of the radiotoxicity transport and radiotoxicity concentration indicators over the 100,000 probabilistic simulations described in Section 7.8.2.5. Results are shown for cases with container assumptions fixed and with container assumptions varying.

Figure 7-204 shows the radiotoxicity transport indicator with container assumptions fixed. The broad shape of this figure is similar to that of the probabilistic Base Case dose rate figure with container assumptions fixed (Figure 7-173), with differences due mainly to the effect of the biosphere transport parameters. Similarly, differences between Figure 7-204 and the radiotoxicity concentration results in Figure 7-205 are due mainly to the effect of surface water parameters.

Figure 7-206 and Figure 7-207 show results for the radiotoxicity transport and concentration indicators with container assumptions varying. The broad shape of these figures is similar to that of the probabilistic Base Case dose rate figure with container assumptions varying (Figure 7-176), with differences due mainly to the variations in the transport pathway to the discharge locations.

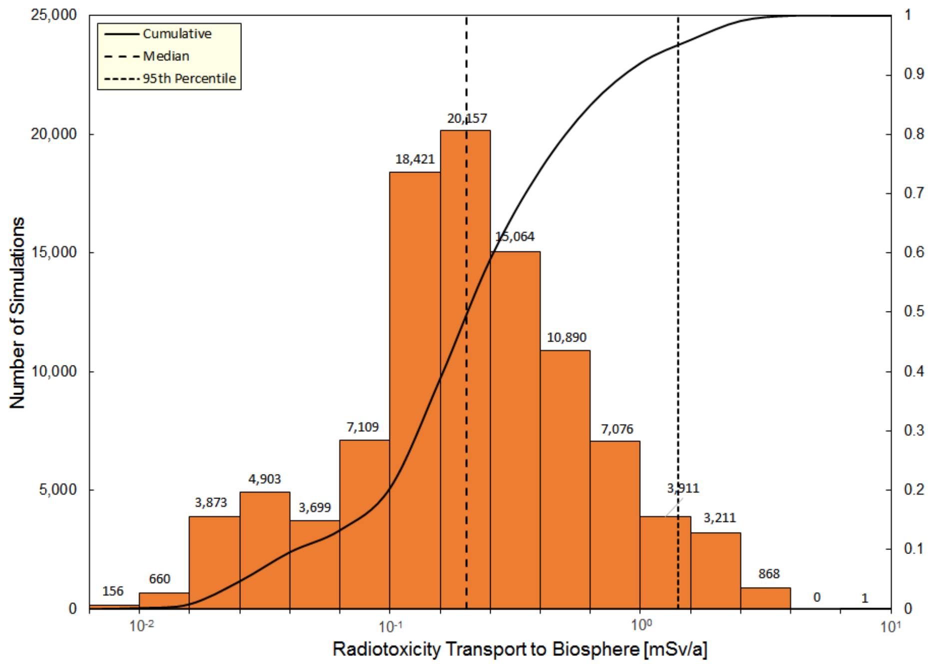

Note: The leftmost bin includes all simulations (156) that resulted in transport less than 10^{-2} mSv/a

Figure 7-204: System Model: Probabilistic Assessment for Radiotoxicity Transport Complementary Indicator – Container Assumptions Fixed

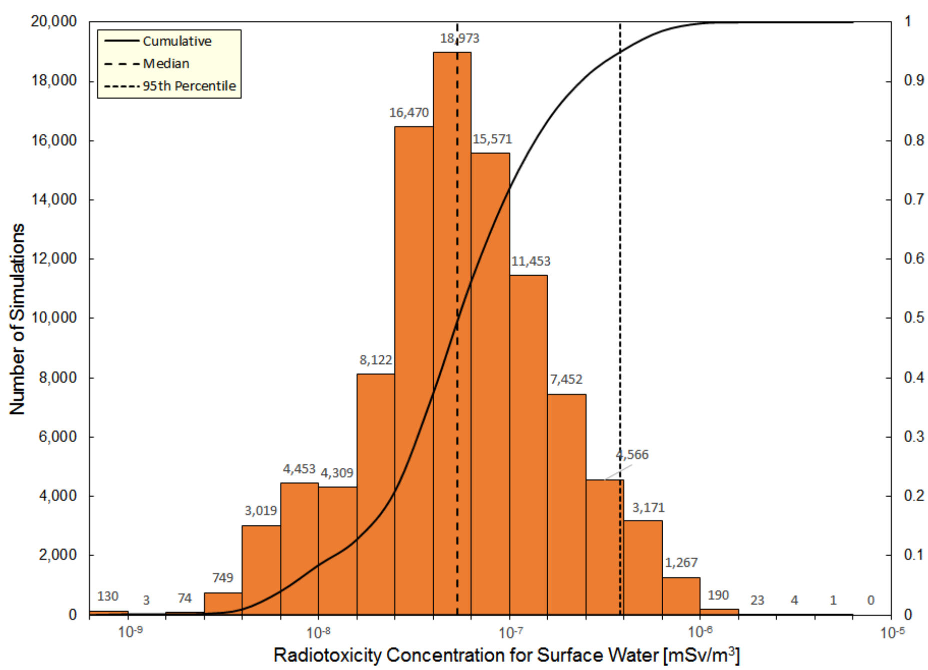

Note: The leftmost bin includes all simulations (130) that resulted in a concentration less than 10^{-9} mSv/m^3

Figure 7-205: System Model: Probabilistic Assessment for Radiotoxicity Concentration Complementary Indicator – Container Assumptions Fixed

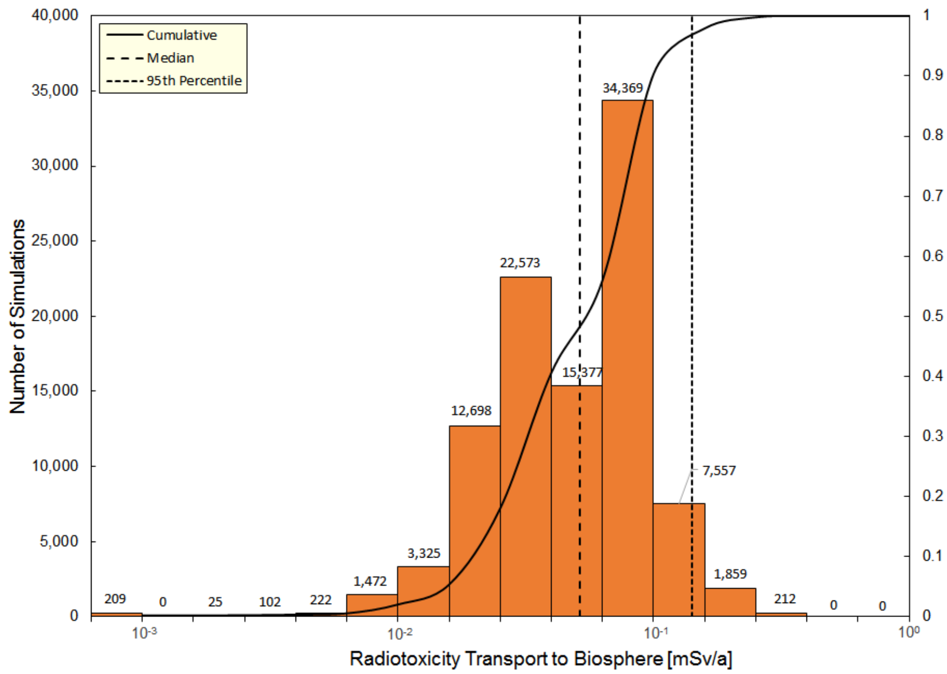

Note: The leftmost bin includes all simulations (209) that resulted in transport less than 10^{-3} mSv/a

Figure 7-206: System Model: Probabilistic Assessment for Radiotoxicity Transport Complementary Indicator – Container Assumptions Varying

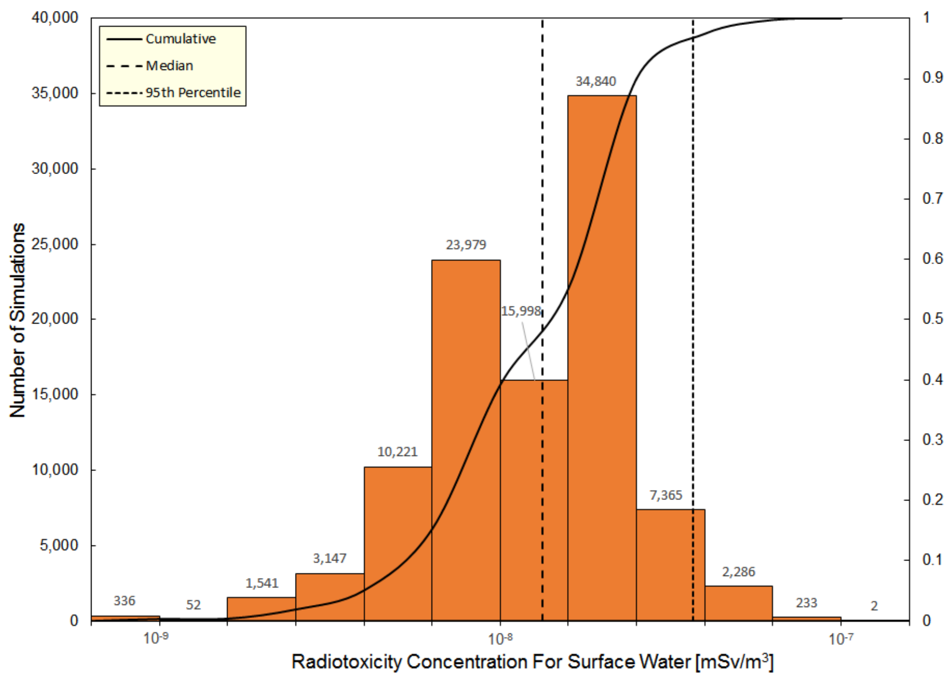

Note: The leftmost bin includes all simulations (336) that resulted in a concentration less than 10^{-9} mSv/m^3

Figure 7-207: System Model: Probabilistic Assessment for Radiotoxicity Concentration Complementary Indicator – Container Assumptions Varying

Figure 7-208 shows the indicator values for the All Containers Fail at 60,000 Years Disruptive Event Scenario together with the dose rate indicator for comparison. The indicators have the same general shape because they both depend on radionuclide transport to the biosphere. The figure shows very large margins to the associated criteria for both complementary indictors. The smaller margin for the dose rate criterion is indicative of the conservative nature of the dose acceptance criterion and the adoption of a worst-case person for the dose rate calculation.

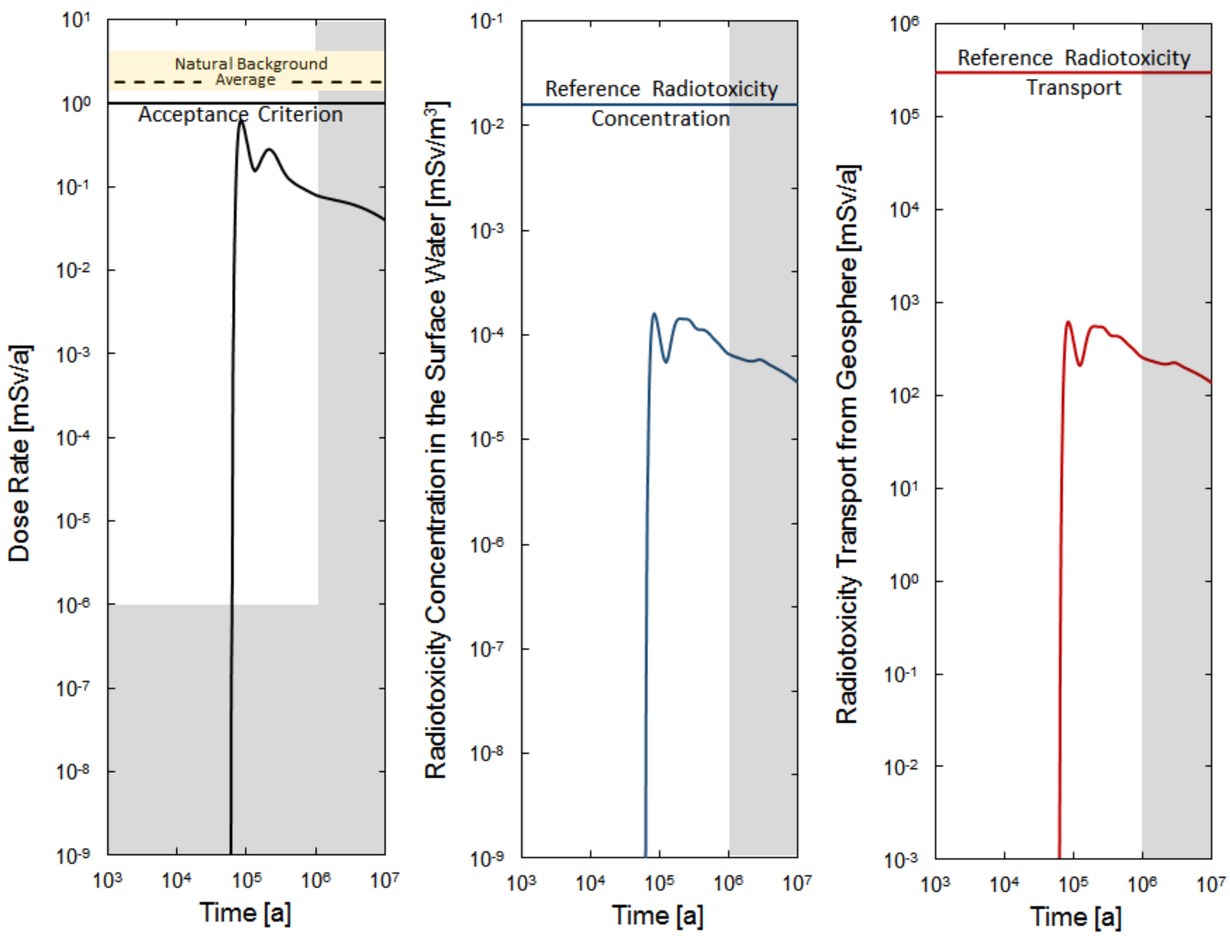

Note: Dose rate results have been reduced by a factor of 1.6 (see Section 7.9.2.2)

Figure 7-208: System Model: All Containers Fail at 60,000 Years – Results for Indicators

Table 7-62 summarizes the full suite of results for the two complementary indicators. Since both indicators are well below their acceptance / reference values shown in Table 7-61, additional confidence is provided that at long times (i.e., when the dose rate indicator is more uncertain) the impacts of the repository are likely to be very small.

Table 7-62: Results for Complementary Indicators

Case	Value	Radiotoxicity Concentration in Surface Water [mSv/m^3]	Radiotoxicity Transport from Geosphere [mSv/a]
-	**Reference Indicator Value***	**1.6×10^{-2}**	**3×10^{5}**
Reference Case	-	0	0
Base Case	Peak	4.0×10^{-8}	0.16
Probabilistic Container Assumptions Fixed	Median	5.5×10^{-8}	0.20
	95th Percentile	3.8×10^{-7}	1.4
	99th Percentile	7.1×10^{-7}	2.5
Probabilistic Container Assumptions Varying	Median	1.3×10^{-8}	0.051
	95th Percentile	3.7×10^{-8}	0.14
	99th Percentile	5.3×10^{-8}	0.20
All Containers Fail at 60,000 Years	Peak	1.6×10^{-4}	6.2×10^{2}

Note: * from Table 7-61.

7.14 Summary and Conclusions

This section summarizes the postclosure safety assessment.

7.14.1 Scope Overview

The Normal Evolution Scenario represents the normal (or expected) evolution of the site and facility. Disruptive Event Scenarios consider the effects of unlikely events that lead to possible penetration of barriers and abnormal degradation and loss of containment.

Section 7.2 presents the detailed scope of the assessment. Both Normal Evolution and Disruptive Event Scenarios are considered. The cases considered are illustrated in Figure 7-1.

The Reference Case of the Normal Evolution Scenario represents the situation in which all repository components meet their design specification and function as anticipated. As such, the used fuel containers remain intact essentially indefinitely (see Chapter 5) and no contaminant releases occur in the one million year time period of interest to the safety assessment.

Sensitivity studies are performed on the Reference Case to illustrate repository performance for a range of reasonably foreseeable deviations from key assumptions. These deviations arise from components that are unknowingly placed in the repository that either (a) do not meet their design specification or (b) do not fully function as anticipated.

Both deterministic and probabilistic simulations are performed.

The “Base Case” sensitivity study assumes a small number of containers have been fabricated with sizeable defects in their copper coating, and that 10 of these off-specification containers escape detection by the quality assurance program and are unknowingly placed in the repository. The effects of other types of fabrication and placement failures that might eventually lead to container failure (such as poorly fabricated and / or placed buffer boxes) are also described by the Base Case results.

The Base Case adopts a number of simplifying and bounding assumptions describing the container failure model, as described in Section 7.2.2.1. Key assumptions are:

- Geosphere properties as per Chapter 2;
- Used fuel inventories as per Chapter 3;
- Repository design as per Chapter 4;
- 10 containers with defects are present in the repository. The first container fails at 1000 years, with one additional container failing every 100,000 years;
- No other container failures occur;
- Constant temperate climate and steady-state groundwater flow;
- A self-sufficient farming family is unknowingly living on top of the repository, growing crops and raising livestock;
- Drinking and irrigation water for the family is obtained from a 100 m deep well. The well / defective container locations are such that contaminant release to the well is maximized;
- The well is pumping at a rate of 911 m^3/a. This is sufficient for drinking water and irrigation of household crops;
- Input parameters that are represented by probability distributions are set to either the most probable value (when there is one) or to the median value otherwise.

Deterministic sensitivity studies are performed about the Base Case to illustrate the effect of well assumptions, the effect of deviations in barrier performance, the effect of various FRAC3DVS-OPG modelling parameter assumptions, and the effect of glaciation. The full suite of deterministic sensitivity cases is described below:

<u>Cases Illustrating the Effect of Well Assumptions</u>

- No well;
- Intermittent well operation; and
- Random well location.

The well cases are described in Section 7.2.2.2 and Table 7-4.

<u>Cases Illustrating the Effect of Deviations in Barrier Performance</u>

Fuel Barrier:

- Fuel dissolution rate increased by a factor of 10; and
- Instant release fractions for fuel contaminants set to 0.10 for all radionuclides.

Zircaloy Sheath Barrier:

No credit is taken in the postclosure safety assessment for the presence of the Zircaloy fuel sheath as a barrier to contaminant release from the fuel. However, because the sheath itself contains contaminants and because the screening analysis (Section 7.6) identifies some of these contaminants as potentially important, the following Zircaloy specific sensitivity cases are simulated:

- Zircaloy dissolution rate increased by a factor of 10; and
- Instant release fractions for Zircaloy sheath radionuclide contaminants set to 0.10.

Container Barrier:

- All 10 containers fail at 1000 years;
- 50 containers fail at 1000 years;
- 50 and 1000 containers fail at 10,000 years;
- Low sorption in the engineered barrier materials with coincident high solubility limits in the container; and
- No solubility limits in the container.

The cases with 50 and 1000 containers illustrate repository performance for a greater assumed number of failed containers. For the two 50 container cases, the first case assumes all containers are clustered in the location that maximizes dose consequence, while the second case assumes the containers are uniformly distributed across the repository. The 1000 container case also assumes the containers are uniformly distributed across the repository.

Buffer and Backfill and Seals Barrier:

- Hydraulic conductivities of all EBS materials increased by a factor of 10;
- Low sorption in the engineered barrier materials with coincident high solubility limits in the container; and
- No sorption in the near field.

Geosphere Barrier:

- Hydraulic conductivities increased by a factor of 10;
- Hydraulic conductivities decreased by a factor of 10;
- Hydraulic conductivity in the excavation damaged zones (EDZ) increased by a factor of 10;
- Fracture standoff distance reduced to 50, 25 and 10 m;
- Sorption parameters set to their two sigma (low) values; and
- Dispersivity increased and decreased by a factor of 5.

The barrier sensitivity cases are described in Section 7.2.2.3 and Table 7-5.

Cases Illustrating the Effect of Modelling Attributes and Parameters on the Base Case

- Increased spatial resolution to confirm model convergence;
- Increased and decreased number of time steps to confirm model results are not sensitive to temporal resolution; and
- Discrete Fracture Network modelling in lieu of Equivalent Porous Media.

The modelling attribute cases are described in Section 7.2.2.4 and Table 7-6.

None of these modelling choices had any material effect on the results and they are therefore not discussed further.

The Effects of Glaciation

The effects of glaciation are discussed quantitatively based on the analysis of a glaciation scenario carried out as part of the Third Case Study (Garisto et al. 2010; Walsh and Avis 2010).

The glaciation study is described in Section 7.2.2.5.

Probabilistic Studies

For the probabilistic simulations (Section 7.2.2.3 and Table 7-5), random sampling is used to simulate 100,000 realizations of the following two cases:

- Number, locations and failure times for defective containers fixed at their Base Case values, with all other available parameters varied; and
- Number, locations and failure times for the defective containers varied, with all other parameters maintained at their Base Case values.

Parameter values that could affect the groundwater flow distribution are not varied in the simulations.

Disruptive Event Scenarios

The Disruptive Event Scenarios examined are described in Section 7.2.3 and Table 7-7. The cases considered are:

- Inadvertent Human Intrusion;
- All Containers Fail at 60,000 Years (with a sensitivity case that has the failure occurring at 10,000 years); and
- Repository Seals Failure.

Disruptive Scenarios are analysed with deterministic methods only.

Other Calculations

The main focus of the above is on the radiological protection of persons. The following are also addressed for the Base Case and for the All Containers Fail at 60,000 Years Disruptive Event Scenario:

- The radiological protection of the environment ;
- The protection of persons and the environment from hazardous substances; and
- The effects of gas generation and migration.

Finally, results are also generated for two complementary indicators of radiological safety for the Base Case and for the All Containers Fail at 60,000 Years Disruptive Event Scenario.

7.14.2 Result Summary

This section presents a summary of the results.

7.14.2.1 Radiological Protection of Persons

Results for the Normal Evolution Scenario and for the Disruptive Event Scenarios are described here.

7.14.2.1.1 Normal Evolution Scenario

Table 7-63 presents the result summary for the Normal Evolution Scenario. This table is an amalgam of results in Section 7.7.2 generated with the detailed 3D models (and summarized in Table 7-30) and results in Section 7.8.2 generated with the System Model (and summarized in Table 7-49). Cases with results in Bq/a have been simulated with the 3D models while cases with results in mSv/a have been simulated with the System Model. Three-dimensional modelling is used for cases that have the potential to affect the groundwater flow distribution because the System Model assumes the groundwater flow field is constant.

Results are shown for the Reference Case, the Base Case sensitivity study, the sensitivity studies performed on the Base Case to illustrate the effects of well assumptions, the sensitivity studies performed on the Base Case to illustrate the effect of deviations in barrier performance, and the sensitivity study performed to illustrate the effects of glaciation. The times of peak transport, the dose ratio (compared to the Base Case) and the factor by which the doses are below the 0.3 mSv/a interim dose rate acceptance criterion are shown. Both deterministic and probabilistic results are included in the table.

A brief discussion of the main results is provided following the table.

Table 7-63: Normal Evolution Result Summary

Case	Time of Peak Impact (a)	Peak Impact		Ratio to Base Case	Factor to Dose Limit*
		I-129 (Bq/a)	Dose (mSv/a)		
REFERENCE CASE	**-**	**0**	**0**	**-**	**-**
Sensitivity Cases					
Base Case** **(3D: Full Model)**	**25,000**	**1337**	**-**	**-**	**-**
Base Case (3D: Rooms-Only Model)	**24,200**	**1400**	**-**	**-**	**-**
Base Case (System Model)**	**23,300**	**-**	**$2.5x10^{-4}$**	**-**	**1200**
Sensitivity Cases for Well Model					
Base Case - No Well	27,700	-	$1.4x10^{-7}$	1/1800	$2.1x10^{6}$
Base Case - Intermittent Well	No effect for most times but up to a 1.8 times increase if the well is turned on at the time of peak I-129 transport				
Base Case - Random Well	Could be many orders of magnitude less than the Base Case depending on the well location				
Sensitivity Cases Illustrating the Effect of Deviations in Barrier Performance on the Base Case					
Fuel Barrier					
Fuel Dissolution Rate 10 Times Higher	27,900	-	$1.6x10^{-3}$	6.4	190
Instant Release Fraction set to 10%	21,200	-	$4.3x10^{-4}$	1.7	70
Zircaloy Sheath Barrier****					
Zr Dissolution Rate 10 Times Higher	23,900	-	$2.6x10^{-4}$	1.0	1200
Instant Release Fraction set to 10%	23,400	-	$2.5x10^{-4}$	1.0	1200
Container Barrier					
All 10 Containers Fail at 1000 Years	23,100	-	$2.6x10^{-3}$	10	120
Low Sorption in the EBS Materials With Coincident High Solubility Limits	23,900	-	$2.5x10^{-4}$	1.0	1200
No Solubility Limits	23,900	-	$2.5x10^{-4}$	1.0	1200
50 Containers Fail at 1000 Years, all in worst location++	23,100	-	$1.3x10^{-2}$	50	24
50 Containers Fail at 10,000 Years, uniform distribution++	36,300	-	$4.2x10^{-4}$	1.7	705
1000 Containers Fail at 10,000 Years, uniform distribution++	36,300	-	$8.5x10^{-3}$	34	35
Buffer, Backfill and Seals Barrier					
Hydraulic Conductivity of all EBS Materials 10 Times Higher**	24,100	1374	-	1.0	1200
Low Sorption in the EBS Materials With Coincident High Solubility Limits	23,900	-	$2.5x10^{-4}$	1.0	1200

Case	Time of Peak Impact (a)	Peak Impact		Ratio to Base Case	Factor to Dose Limit*
		I-129 (Bq/a)	Dose (mSv/a)		
No Sorption in the Near Field	23,800	-	2.5×10^{-4}	1.0	1200
Geosphere Barrier					
Hydraulic Conductivities 10 Times Higher***	5000	3679	-	2.6	460
Hydraulic Conductivities 10 Times Lower	1,020,000	460	-	0.3	4000
EDZ Conductivity 10 Times Higher**	20,000	1540	-	1.2	1000
50 m Fracture Standoff Distance	17,000	1538	-	1.1	1090
25 m Fracture Standoff Distance	13,400	1526	-	1.1	1090
10 m Fracture Standoff Distance	11,200	1473	-	1.1	1090
10 m Fracture Standoff Distance***	9,000	2046	-	1.5	800
Two Sigma (Low) Sorption	24,200	-	2.6×10^{-4}	1.0	1200
Dispersivity Increased by Factor of 5+	17,000	902	-	0.6	2000
Dispersivity Decreased by Factor of 5+	25.000	2131	-	1.5	800
Glaciation Sensitivity					
Glaciation Case	Could be up to 10 times greater than temperate climate case				
Probabilistic Cases (95th Percentiles)					
Container Assumptions Fixed	-	-	9.1×10^{-4}	3.6	330
Container Assumptions Vary	-	-	2.2×10^{-4}	0.88	1400

Notes:

* Peak impacts are determined from simulations performed with either the 3D models or the System Model. The 3D models do not include biosphere and dose representations and therefore results are presented for I-129 transport to the well. This is a reasonable surrogate for dose because System Model simulations show that I-129 transport to the well is the dominant dose contributor.

** Two FRAC3DVS-OPG Repository-Scale models have been used – the Rooms-Only Model and the Full Model. The Full Model contains more detail but takes longer to run. Items marked with '**' should be compared against Full Model results, whereas other items should be compared against Rooms-Only Model results.

*** Result is for the case with the well / defective containers locations revised to ensure maximum transport.

****As discussed in Section 7.2.2.3, no credit is taken for the fuel sheath acting as a barrier to prevent the fuel from coming into contact with water.

\+ Shown for illustration only as the Base Case values are already conservatively selected.

++ Results obtained by scaling other cases as discussed in Section 7.8.2.3.3)

\- Not applicable.

Deterministic Results

The dose rate is zero for the Reference Case.

For the other cases, the results shows that I-129 is the dominant dose contributor. This is because I-129 has a sizeable initial inventory, a non-zero instant release fraction, a very long half-life, no solubility limit, is non-sorbing in the buffer, backfill and geosphere and has a radiological impact on humans. All other fission products and actinides either decay away, or are released very slowly as the fuel dissolves and are thereafter sorbed in the engineered barriers and geosphere.

Dose rates for the cases simulated with the 3D groundwater flow and transport models can be inferred from the I-129 transport results by developing a scaling factor for the Base Case simulation in which both I-129 transport (in Bq/a) and dose rates (in mSv/a) are calculated.

For the Base Case, the peak dose rate is 2.5×10^{-4} mSv/a occurring at 23,300 years. This is well below the average Canadian background dose rate of 1.8 mSv/a and is a factor of 1200 times less than the 0.3 mSv/a interim dose rate acceptance criterion established in Section 7.1.1 for the radiological protection of persons.

The sensitivity cases that illustrate the effect of well assumptions indicate that the Base Case dose rate could actually be many orders of magnitude lower, depending on the location of the defective containers, whether or not a well is present, and where that well is located with respect to the defective containers.

Of the remaining sensitivity cases illustrating the effect of deviations in barrier performance, most have little to no effect on the dose consequence. Sensitivity cases that lead to higher dose rates are:

- Fuel Dissolution Rates increased by a Factor of 10, leading to a potential dose increase of 6.2 times;
- All 10 Containers Fail at 1000 Years, leading to a potential dose increase of 10 times.
- Geosphere Hydraulic Conductivities increased by a factor of 10, leading to a potential dose increase of 2.6 times;
- Fracture Standoff Distance reduced to 10 m, leading to a potential dose increase of about 1.5 times; and
- Geosphere Dispersivity Decreased by a Factor of 5, leading to a potential dose increase of 1.5 times.

For the 10 Containers Fail case, the actual dose would be less if fewer containers fail simultaneously, or if those failures are spread out in time, or if those failures occur at times later than 1000 years.

For the cases with 50 and 1000 failed containers, the dose rate could be higher; however, the actual dose would depend strongly on where the failed containers are located in the repository with respect to the well.

For the Geosphere Dispersivity case, these results are included for illustration only because the dispersivity values selected for the Base Case are already conservative. For all cases, the actual dose rates would depend highly on the presence of a well and where that well is located in relation to the failed containers.

The Glaciation Sensitivity shows that a potential dose increase of 10 times could occur. This is caused by a similar effect to that examined in the Intermittent Well sensitivity case in Section 7.7.2.3.4, with results also highly dependent on the defective container locations, the presence of a well and where that well is located in relation to the failed containers.

Probabilistic Results

The probabilistic cases examine the effect of simultaneous variation in multiple parameters.

The first case, in which the number, location and failure times of the 10 defective containers are fixed at the same values as in the Base Case while all other available parameters are varied, gives a measure of the overall uncertainty in the Base Case. The 95th percentile dose rate emerging from 100,000 simulations is $9.1x10^{-4}$ mSv/a or 3.6 times the Base Case value. This is a factor of 330 times less than the interim dose rate criterion of 0.3 mSv/a.

The second probabilistic case, in which the number, location and failure times of the 10 defective containers are varied while all other available parameters are fixed, gives an indication of the effect of different container failure times and different container failure locations, relative to the well location adopted in the Base Case. The 95th percentile dose rate emerging from 100,000 simulations is $2.2x10^{-4}$ mSv/a, a value less than that of the Base Case.

7.14.2.1.2 Disruptive Event Scenarios

Table 7-64 presents summary results from Section 7.9 for the All Containers Fail Disruptive Event Scenario and the Repository Seals Failure Disruptive Event Scenario, and compares them against the 1.0 mSv/a interim dose rate acceptance criterion. Key features to note are:

- Failure of all containers at 60,000 years results in a maximum dose rate of 0.63 mSv/a while failure of all containers at 10,000 years results in a maximum dose rate 0.81 mSv/a. Both results are below the 1 mSv/a interim dose rate acceptance criterion for Disruptive Events established in Section 7.1.1
- The Repository Seals Failure Scenario has no effect on the dose consequence as compared to the Base Case if the well / defective container locations are maintained in their Base Case positions. Section 7.9.3 describes a sensitivity study in which the well and defective container locations are moved much closer to the shaft with degraded seals; however, this case results in lower doses than for the case reported here.

Table 7-64: Disruptive Event Scenarios Result Summary

Case	Time of Peak Impact (a)	Peak Impact*		Factor to Dose Limit*
		I-129 (Bq/a)	Dose (mSv/a)	
REFERENCE CASE	**-**	**0**	**0**	**-**
Normal Evolution Scenario				
Base Case** **(3D: Full Model)**	**25,000**	**1337**	**-**	**-**
Base Case (3D: Rooms-Only Model)	**24,200**	**1400**	**-**	**-**
Base Case (System Model)**	**23,300**	**-**	**2.5×10^{-4}**	**1200**
Disruptive Event Scenarios				
All Containers Fail at 60,000 Years (3D)	108,000	3.35×10^{6}	-	-
All Containers Fail at 60,000 Years (System Model)***	84,000	-	0.63	1.6
All Containers Fail at 10,000 Years***	36,300	-	0.81	1.2
Degraded Shaft Seal**	25,000	1342	-	1200
Degraded Fracture Seal**	25,000	1329	-	1200

Notes:
* Peak impacts are determined from simulations performed with either the 3D models code or the System Model. The 3D models do not include biosphere and dose representations and therefore results are presented for I-129 transport to the well. This is a reasonable surrogate for dose because SYVAC3-CC4 simulations show that I-129 to the well is the dominant dose contributor.
** Two FRAC3DVS-OPG Repository-Scale models have been used – the Rooms-Only Model and the Full Model. The Full Model contains more detail but takes longer to run. Items marked with '**' should be compared against the Full Model results, whereas other items should be compared against the Rooms-Only Model results.
*** Dose for these cases reduced by a factor of 1.6 to account for conservatism in System Model (Section 7.9.2.2)
\- Not applicable

Section 7.9.1 presents a stylized analysis for the Inadvertent Human Intrusion Scenario. This scenario is not included in Table 7-64 because it is a special case, as recognized in CNSC Regulatory Guide G-320 (CNSC 2006). The assumed intrusion bypasses all barriers, and therefore dose consequence may exceed the regulatory limit.

The risk of inadvertent human intrusion is minimized by placing the used fuel deep underground in a location with no viable mineral resources and no potable groundwater resources, and by the use of markers and institutional controls

Three illustrative human intrusion cases are considered, as follows:

Scenario 1: Drilling operations take place for two days after the intrusion event (two 12-hour shifts), at which point the Drill Crew becomes aware of the hazard, immediately ceases operations and vacates the site.

The site is then completely remediated by qualified experts, and thus the Resident is unaffected by the incident. The dose to the remediation experts is not considered because they are assumed to take appropriate precautions.

Scenario 2: In Scenario 2, drilling operations continue for 14 workings days, at which point the Drill Crew vacates the site without identifying the hazard. Debris deposited on the surface around the drilling rig remains in place without remediation, subject only to radioactive decay and leaching. The Resident lives at the contaminated site immediately after the original intrusion, and grows food on the contaminated soil.

Scenario 3: Scenario 3 is the same as Scenario 1, except that a higher fuel burnup is assumed (i.e., 280 MWh/kgU instead of 220 MWh/kgU).

The results are summarized in Table 7-65.

The likelihood of this event occurring cannot be accurately determined; however, Section 7.9.1 shows that based on simple estimates of deep drilling rates, a risk to the Resident of 9.4×10^{-7} per annum can be estimated. This is below the risk target of 10^{-5} per annum identified in Section 7.1.1.

Table 7-65: Inadvertent Human Intrusion Result Summary

Scenario Number	Maximum Dose to Drill Crew (mSv)	Maximum Dose Rate to Resident (mSv/a)
1	90	0
2	590	580
3	110	0

7.14.2.2 Radiological Protection of the Environment

Section 7.10 describes the modelling and results obtained for the assessment of the radiological protection of the environment. The results are compared against both the screening criterion and the interim acceptance criteria established in Section 7.1.3.

Table 7-54 shows the peak dose rates to non-human biota computed using both the Concentration Ratio approach and the Transfer Factor approach are all below the screening criterion of 10 μGy/h.

Figure 7-196 through Figure 7-200 show that the dose rates are also well below the interim acceptance criteria.

Based on this, it can be concluded that there is no concern about adverse environment impacts associated with the potential release of radioactive contaminants from the repository.

7.14.2.3 Protection of Persons and the Environment from Hazardous Substances

Section 7.11 describes the modelling and results for the assessment of the non-radiological impact of the repository on persons and the environment. Copper is also assessed due to the amount of copper associated with the large number of containers in the repository. The results are compared against the interim acceptance criteria established in Section 7.1.2 and Section 7.1.4.

The Section 7.11 results are expressed in terms of a “Concentration Quotient”, where this is the ratio formed by dividing the concentrations in specific environmental media by the applicable interim acceptance criterion.

Table 7-55 shows Concentration Quotient results for the Base Case. The highest value is 2.67×10^{-4} for Mo in groundwater. Wide margins are available to the interim acceptance criteria.

Table 7-56 shows the Concentration Quotients results for the All Containers Fail Disruptive Scenario. The quotients are higher than in the Base Case, as expected due to the significantly greater source term, with the highest value being 0.47 for Mo in groundwater. All values are below the interim acceptance criteria.

Table 7-57 shows Concentration Quotient results for copper and for copper impurities, for a solubility limited copper release rate. All values are below the interim acceptance criteria.

Based on this, it can be concluded that there is no concern about adverse impacts to persons and non-human biota from the potential release of non-radiological contaminants from the repository.

7.14.2.4 Gas Generation and Migration

Section 7.12 describes the modelling and results obtained for the gas generation and migration assessment. The results indicate that:

- It is highly unlikely that significant flammable concentrations of hydrogen or methane would be produced and the risk of a significant fire or explosion hazard in the biosphere is negligible; and
- The radiological consequences due to gas-mediated transport of C-14 are very low.

7.14.2.5 Complementary Indicators

Section 7.13 presents the modelling and results for two complementary indicators.

These indicators (i.e., radiotoxicity concentration in a water body and radiotoxicity transport from the geosphere) supplement the dose rate indicator using system characteristics that are much less sensitive to assumptions regarding the biosphere and human behaviour.

Results for the Base Case are illustrated in Figure 7-203 and results for the All Containers Fail at 60,000 Years Disruptive Event Scenario are shown in Figure 7-208. Table 7-62 summarizes the full set of results, including two Base Case related probabilistic assessments of the indicators.

Both indicators are well below their acceptance / reference values shown in Table 7-61, thereby providing additional confidence that at long times (i.e., when the dose rate indicator is more uncertain) the impacts of the repository are likely to be very small.

7.14.3 Conclusion

Figure 7-209 shows the dose rates for the Reference Case, the Normal Evolution Base Case, and the All Containers Fail after 60,000 Years Disruptive Event Scenario.

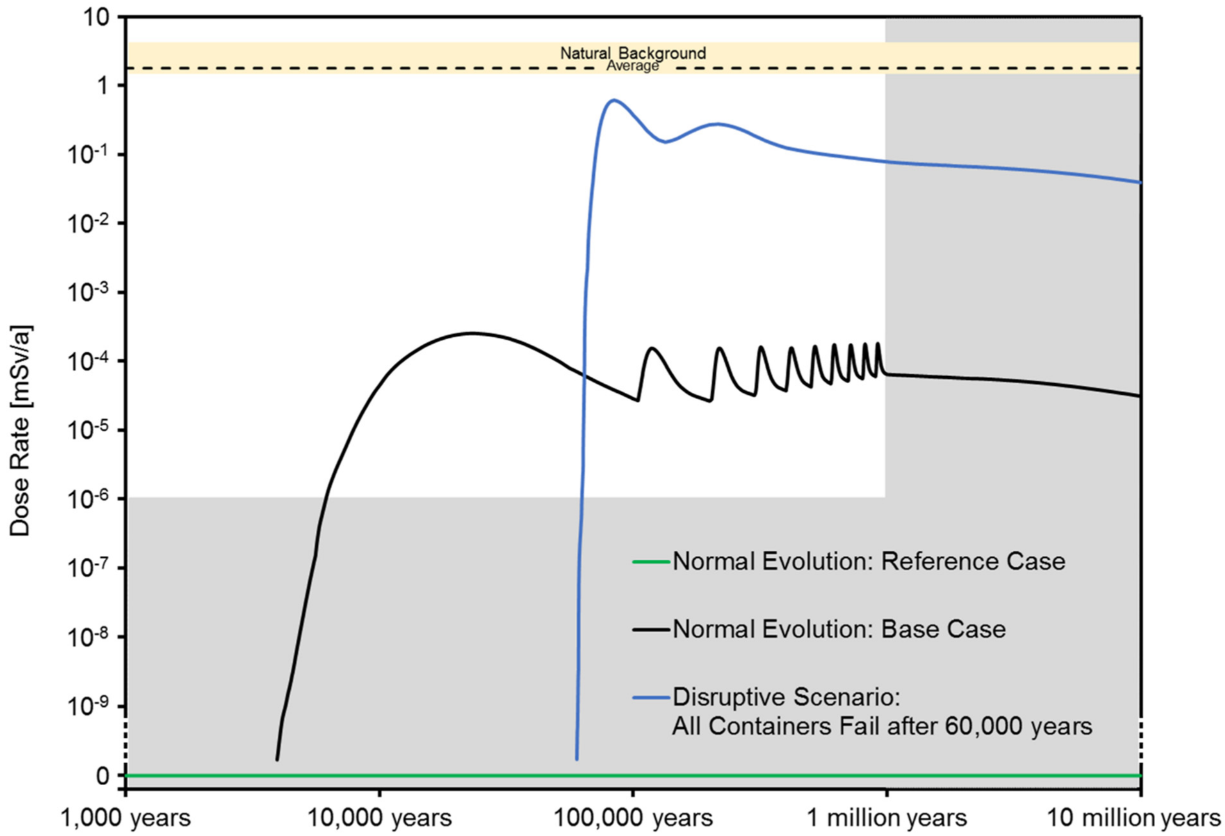

Figure 7-209: Dose Rate Result Summary

This postclosure safety assessment shows, for the Normal Evolution Scenario (and associated sensitivity cases), as well as for the analysed Disruptive Event Scenarios (excluding Inadvertent Human Intrusion), that all radiological and non-radiological interim acceptance criteria are met during the postclosure period. For the Inadvertent Human Intrusion Scenario, significant doses to the drill crew and significant dose rates to a resident may occur, but the likelihood of this scenario is very low. Furthermore, Regulatory Document G-320 (CNSC 2006) recognizes this as a special case which could potentially result in dose rates exceeding the regulatory limit.

7.15 References for Chapter 7

AECL. 1992. The Bentonite Industry in North America: Suppliers, Reserves, Processing Capacity and Products. Atomic Energy of Canada Limited. AECL-10587. Pinawa, Canada.

Air Products and Chemicals, Inc. 1999. *Methane Gas* [MSDS# 1070] http://avogadro.chem.iastate.edu/MSDS/methane.pdf (Accessed Oct 26, 2012). Allentown, PA, USA.

Air Products and Chemicals, Inc. 1994. *Hydrogen Gas* [MSDS# 1009]. http://avogadro.chem.iastate.edu/MSDS/hydrogen.pdf (Accessed Oct 26, 2012). Allentown, PA, USA.

Amiro, B.D. 1992. Baseline concentrations of nuclear fuel waste nuclides in the environment. Atomic Energy of Canada Limited, AECL10454, COG 91231. Pinawa, Canada.

Amiro, B.D. 1993. Protection of the environment from nuclear fuel waste radionuclides: a framework using environmental increments. Science of the Total Environment 128: 157-89.

Andersson, P., J. Garnier-Laplace, N.A. Beresform, D. Copplestone, J. Howard, P. Howe, D. Oughton, P. Whitehouse. 2009. Protection of the Environment From Ionising Radiation in a Regulatory Context (PROTECT): Proposed Benchmark Values. Journal of Environmental Radioactivity. 100(2009). 1100-1108.

ANDRA. 2005. Evaluation de Sûreté du Stockage Géologique. Paris, France

Baumgartner. P. 2000. Elemental Composition of Disposal Vault Sealing Materials. Ontario Power Generation Report 06819-REP-01300-10015 R00. Toronto, Canada.

Becker, D.-A., D. Buhmann, R. Storck, J. Alonso, J.-L. Cormenzana, M. Hugi, F. van Gemert, P. O'Sullivan, A. Laciok, J. Marivoet, X. Sillen, H. Nordman, T. Vieno and M. Niemeyer. 2002. Testing of Safety and Performance Indicators (SPIN). European Commission Report FIKW-CT2000-00081. European Commission, Brussels, Belgium.

Berger, A. and M.F. Loutre. 2002. An exceptionally long interglacial ahead? Science 297, 1287-1288.

Bowan, H.J. 1979. Environmental Chemistry of the Element. Academic Press Inc., London.

Brown, J.E., B. Alfonso, R. Avila, N.A. Beresford, D. Copplestone, G. Pröhl and A. Ulanovsky. 2008. The ERICA Tool. J. Environ. Radioactivity 99: 1371-1383.

Carbol, P., J. Cobos-Sabate, J-P. Glatz, C. Ronchi, V. Rondinella, D.H. Wegen, T. Wiss, A. Loida, V. Metz, B. Kienzler, K. Spahiu, B. Grambow, J. Quinones, A. Martinez Esparza Valiente. 2005. The effect of dissolved hydrogen on the dissolution of ^{233}U-doped UO_2 (s), high burn-up spent fuel and MOX fuel. Swedish Nuclear Fuel and Waste Management Company Technical Report TR-05-09.

Cool, W., M. Cunado, L. Johnson, M. Mantynen, W. Muller, S. Norris, W. Rodwell. 2004. EC GASNET Project: Gas issues in the safety assessment of deep repositories for nuclear waste. Material Research Society Symposium Proceedings Volume 807, 19-24.

CNSC. 2006. Regulatory Guide G-320: Assessing the Long Term Safety of Radioactive Waste Management. Canadian Nuclear Safety Commission. Ottawa, Canada.

CNSC. 2011. Setting Radiation Requirements on the Basis of Sound Science: The Role of Epidemiology. Canadian Nuclear Safety Commission, INFO-0812. Ottawa, Canada.

CNSC. 2013. Linear-Non-Threshold Model Fact Sheet. Canadian Nuclear Safety Commission. Ottawa, Canada. Available online: http://nuclearsafety.gc.ca/eng/pdfs/reading-room/healthstudies/Fact-Sheet-Linear-Non-Threshold-Model-2013.pdf

CSA. 2014. Guidelines for Calculating Derived Release Limits for Radioactive Material in Airborne and Liquid Effluents for Normal Operation of Nuclear Facilities. Canadian Standards Association. N288.1-14. Toronto, Canada.

Curti E. and P. Wersin. 2002. Assessment of Porewater Chemistry in the Bentonite Backfill for the Swiss SF/HLW Repository. Nagra Technical Report 02-09. Wettingen, Switzerland.

DiCiccio, T.J. and B. Efron. 1996. Bootstrap Confidence Intervals. Statistical Science Volume 11(3), 189-228.

DOE. 2008. Final Supplemental Environmental Impact Statement for a Geologic Repository for the Disposal of Spent Nuclear Fuel and High-Level Radioactive Waste at Yucca Mountain. US Department of Energy Report DOE/EIS-0250F-S1. Nevada, USA.

Eckerman, K.F. and R.W. Leggett. 1996. DCFPAK: Dose coefficients data file package for Sandia National Laboratory. Oak Ridge National Laboratory report ORNL/TM-13347. Oak Ridge, USA.

European Commission. 2003. GASNET: A Thematic Network on Gas Issues in Safety Assessment of Deep Repositories for Radioactive Waste. European Commission Report. Luxembourg.

Environment Canada. 2008. Southern Arctic Ecozone (http://www.ec.gc.ca/soer-ree/English/vignettes/Terrestrial/sa/default.cfm, accessed 2008).

Ferry, C., J.-P. Piron, A, Poulesquen, and C. Poinssot. 2008. Radionuclides Release from the Spent Fuel under Disposal Conditions: Re-evaluation of the Instant Release Fraction. Material Research Society Symposium Proceedings 1107, 447-454.

Flavelle, P. 1996. Perspectives of the Scale of the Canadian Nuclear Fuel Waste Disposal Concept. AECL INFO-0635. Ottawa, Canada.

Garisto, F. 1989. The Energy Spectrum of α-particles Emitted from Used CANDU Fuel, Annals of Nuclear Energy 16. 33-38.

Garisto, F. 2001. Radionuclide Screening Model (RSM) Version 1.1 Verification and Validation. Ontario Power Generation Report 06819-REP-01300-10029-R00. Toronto, Canada.

Garisto, F. and M. Gobien. 2013. SYVAC3-CC4 Verification and Validation Summary. Nuclear Waste Management Organization Report NWMO TR-2013-14. Toronto, Canada.

Garisto, F., J. Avis, N. Calder, A. D'Andrea, P. Gierszewski, C. Kitson, T. Melnyk, K. Wei, L. Wojciechowski. 2004. Third Case Study – Defective Container Scenario. Ontario Power Generation Report 06819-REP-01200-10126-R00. Toronto, Canada.

Garisto, F., T. Kempe, P. Gierszewski, K. Wei, C. Kitson, T. Melnyk, L. Wojciechowski, J. Avis and N. Calder. 2005. Horizontal Borehole Concept Case Study: Chemical Toxicity Risk. Ontario Power Generation Report 06819-REP-01200-10149-R00. Toronto, Canada.

Garisto, F., J. Avis., T. Chshyolkova, P. Gierszewski, M. Gobien, C. Kitson, T. Melnyk, J. Miller, R. Walsh and L. Wojciechowski. 2010. Glaciation Scenario: Safety Assessment for a Used Fuel Geological Repository. Nuclear Waste Management Organization Report NWMO TR-2010-10. Toronto, Canada.

Garisto, N., Z. Eslami and F. Bhesania, 2005. Ontario Power Generation Report 06819-REP-01200-10150, Alternative Exposure Groups, Toronto Canada.

Garisto, N.C., F. Copper and S.L. Fernandes. 2008. Non-Effect Concentrations for Screening Assessment of Radiological Impacts on Non-Human Biota. Nuclear Waste Management Organization. NWMO TR-2008-02. Toronto, Canada.

Garnier-Laplace, J., R. Gilbin, A. Agüero, F Alonzo, M. Björk, Ph. Ciffroy, D. Copplestone, M. Gilek, T. Hertel-Aas, A. Jaworska, C-M. Larsson, D. Oughton and I. Zinger. 2006. Deliverable 5: Derivation of Predicted-No-Effect-Dose-Rate values for ecosystems (and their sub-organisational levels) exposure to radioactive substances. ERICA.

Gobien, M., F. Garisto, E. Kremer and C. Medri. 2016. Sixth Case Study: Reference Data and Codes. Nuclear Waste Management Organization Technical Report NWMO TR-2016-10. Toronto, Canada.

Gobien, M., and F. Garisto. 2012. Data for Radionuclide and Chemical Element Screening. Nuclear Waste Management Organization Technical Report NWMO TR-2012-11. Toronto, Canada.

Goodwin, B.W., P. Gierszewski and F. Garisto. 2001. Radionuclide Screening Model (RSM) Version 1.1 - Theory. Ontario Power Generation Report 06819-REP-01200-10045-R00. Toronto, Canada.

Grambow, B., J. Bruno, L. Duro, J. Merino, A. Tamayo, C. Martin, G. Pepin, S. Schumacher, O. Smidt, C. Ferry, C. Jegou, J. Quiñones, E. Iglesias, N. Rodriguez Villagra, J. M. Nieto, A. Martínez-Esparza, A. Loida, V. Metz, B. Kienzler, G. Bracke (GRS), D. Pellegrini, G. Mathieu, V. Wasselin-Trupin, C. Serres, D. Wegen, M. Jonsson, L. Johnson, K. Lemmens, J. Liu, K. Spahiu, E. Ekeroth, I. Casas, J. de Pablo, C. Watson, P. Robinson, and D. Hodgkinson. 2010. MICADO Model Uncertainty for the Mechanism of

Dissolution of Spent Fuel in Nuclear Waste Repository. European Commission Report EUR 24597 EN. Brussels, Belgium.

Gras, J.M. 2014. State of the art of ^{14}C in Zircaloy and Zr alloys – ^{14}C release from zirconium alloy hulls. Carbon-14 Source Term (CAST) Report CAST-2014-D.3.1.

Grasty, R.L. and J.R. LaMarre. 2004. The Annual Effective Dose from Natural Sources of Ionising Radiation in Canada. Radiation Protection Dosimetry 108, No 3, 215-226.

Guo, R. 2015. Thermal Modelling of a Mark II Container. Nuclear Waste Management Organization Report NWMO-TR-2015-06. Toronto, Canada.

Guo, R. 2016. Thermal Response of a Mark II Conceptual Deep Geological Repository in Crystalline Rock. Nuclear Waste Management Organization Report NWMO-TR-2016-03. Toronto, Canada.

Hart D. and D. Lush. 2004. The Chemical Toxicity Potential of Candu Spent Fuel. NWMO Background Papers.

Health Canada. 2010. Part IV Guidance on Human Health Detailed Quantitative Radiological Risk Assessment. Health Canada. Ottawa, Canada.

Hermann, O.W. and R.M. Westfall. 1995. ORIGEN-S - SCALE System Module to Calculate Fuel Depletion, Actinide Transmutation, Fission Product Buildup and Decay, and Associated Radiation Source Terms. In: SCALE: A Modular Code System for Performing Standardized Computer Analyses for Licensing Evaluations. Oak-Ridge National Laboratory NUREG/CR-0200, Rev.4 (ORNL/NUREG/CSD-2/R4) Volume II, Part I. Oak-Ridge, USA.

Hoch, A. R., K.A. Cliffe, B.T. Swift and W.R. Rodwell. 2004. Modelling Gas Migration in Compacted Bentonite: GAMBIT Club Phase 3 Final Report, POSIVA Report 2004-02, Olkiluoto, Finland.

IAEA. 2002. Safety Indicators for the Safety Assessment of Radioactive Waste Disposal. International Atomic Energy Agency TECDOC-1372. Vienna, Austria.

IAEA. 2006. Safety Requirements: Geological Disposal of Radioactive Waste. International Atomic Energy Agency Safety Requirements WS-R-4. Vienna, Austria.

ICRP. 1991. 1990 Recommendations of the International Commission on Radiological Protection. International Commission on Radiological Protection Publication 60, Annals of the ICRP 21(1-3). Vienna, Austria.

ICRP. 1995. Age-dependent Doses to the Members of the Public from Intake of Radionuclides - Part 5 Compilation of Ingestion and Inhalation Coefficients. International Commission on Radiological Protection Publication 72, Annals of the ICRP 26(1). Vienna, Austria.

ICRP. 2007. The 2007 Recommendations of the International Commission on Radiological Protection. International Commission on Radiological Protection Publication 103, Annals of the ICRP (W2-4). Vienna, Austria.

ICRP. 2008. Environmental Protection: the Concept and Use of Reference Animals and Plants. ICRP Publication 108. Vienna, Austria.

ICRP. 2013. Radiological Protection in Geological Disposal of Long-lived Solid Radioactive Waste. International Commission on Radiological Protection Publication 122, Annals of the ICRP 42(3). Vienna, Austria.

ICRP. 2014. Protection of the environment under different exposure situations. ICRP Publication 124, Ann. ICRP 43(1). Vienna, Austria.

Jackson, D, K. Smith and M.D. Wood. 2014. Demonstrating Compliance with Protection Objectives for Non-Human Biota within Post-closure Safety Cases for Radioactive Waste Repositories. Journal of Environmental Radioactivity. Volume 133, Pages 60-68.

JNC. 2000. H12: Project to Establish the Scientific and Technical Basis for HLW in Japan. Japan Nuclear Cycle Development Institute JNC TN1410 2000-004. Tokai, Japan.

King, F. and D. Shoesmith. 2004. Electrochemical Studies of the Effect of H_2 on UO_2 Dissolution. Swedish Nuclear Fuel and Waste Management Company Report SKB TR 04-20. Stockholm, Sweden.

Kitson C.I., T.W. Melnyk, L.C. Wojciechowski, T. Chshyolkova. 2012. SYVAC3-CC4 User Manual, Version SCC409. Nuclear Waste Management Organization Report NWMO TR-2012-21. Toronto, Canada.

Liu, N., L. Wu, Z. Qin and D.W. Shoesmith. 2016. Roles of radiolytic and externally generated H_2 in the corrosion of fractured spent nuclear fuel. Environ. Sci. Technol. 50 (22), 12348-12344.

Mallants, D. and D. Jacques 2004. Performance Assessment for Deep Disposal of Low and Intermediate Level Short-lived Radioactive Waste in Boom Clay, SCK•CEN-R-3793. Mol, Belgium.

Marshall, M.H.M and M.J. Simpson. 2014. Characterization of Natural Organic Matter in Bentonite Clays. Nuclear Waste Management Organization. NWMO TR-2014-10. Toronto, Canada.

Medri, C. 2012. Human Intrusion Model for the Fourth and Fifth Case Studies: HIMv2.0. Nuclear Waste Management Organization. NWMO TR-2012-04. Toronto, Canada.

Medri, C. 2015a. Human Intrusion Model for the Mark II Container in Crystalline and Sedimentary Rock Environments: HIMv2.1. Nuclear Waste Management Organization Report NWMO TR-2015-04. Toronto, Canada.

Medri, C. 2015b. Non-Human Biota Dose Assessment Illustrative Results for Repositories in Crystalline and Sedimentary Rock. Nuclear Waste Management Report NWMO TR-2015-02. Toronto, Canada.

Medri, C. 2015c. Non-Radiological Interim Acceptance Criteria for the Protection of Persons and the Environment. Nuclear Waste Management Report NWMO TR-2015-03. Toronto, Canada.

Medri, C. and G.Bird. 2015. Non-Human Biota Dose Assessment Equations and Data. Nuclear Waste Management Organization. NWMO TR-2014-02 R001. Toronto, Canada.

Merrett, G.J. and P.A. Gillespie. 1983. Nuclear fuel waste disposal: long-term stability analysis. Atomic Energy of Canada Limited Report AECL-6820. Pinawa, Canada.

Muurinen, A. and J. Lehikoinen. 1999. Porewater chemistry in compacted bentonite. Engineering Geology 54, 207-214.

Nagra. 2002. Project Opalinus Clay: Safety Report, Demonstration of the Disposal Feasibility for Spent Fuel, Vitrified HLW and Long-lived ILW. Nagra Technical Report 02-05. Wettingen, Switzerland.

Nagra. 2008. Effects of Post-disposal Gas Generation in a Repository for Low- and Intermediate-level Waste Sited in the Opalinus Clay of Northern Switzerland. Nagra Technical Report NTB 08-07. Wettingen, Switzerland.

Neuzil, C. 2003. Hydromechancial coupling in geological processes. Hydrogeology Journal, 11, 41-83.

Normani, S.D. 2009. Paleoevolution of pore fluids in glaciated geologic settings. Ph.D. Thesis, University of Waterloo, Department of Civil Engineering. Waterloo, Canada.

NRC. 2006. Health Risks from Exposure to Low Levels of Ionizing Radiation: BEIR VII Phase 2. Committee on the Biological Effects of Ionizing Radiations (BEIR). The National Academies Press, Washington, DC, USA.

NWMO. 2012. SYVAC3-CC4 Theory, Version SCC409. Nuclear Waste Management Organization Report NWMO TR-2012-22. Toronto, Canada

Parkhurst, D.L. and C.A.J. Appelo. 1999. User's Guide to PHREEQC (Version 2) – A Computer Program for Speciation, Batch-Reaction, One-Dimensional Transport, and Inverse Geochemical Calculations. U.S Department of the Interior and U.S. Geological Survey Water-Resources Investigations Report 99-4259. Denver, USA.

Peltier, W.R. 2003. A refined model of the last deglaciation event of the current ice-age: ICE-5G. International Union for Quaternary Research (INQUA), XVI INQUA Congress Paper No. 9-3. Reno, USA.

Peltier, W.R. 2006. Boundary Conditions Data Sets for Spent Fuel Repository Performance Assessment. Ontario Power Generation Report 06819-REP-01200-10154-R00. Toronto, Canada.

Pickens, J. F., & Grisak, G. E. 1981. Modeling of scale-dependent dispersion in hydrogeologic systems. *Water Resources Research*, *17*(6), 1701-1711.

Posiva Oy. 2014. Safety Case for the Disposal of Spent Nuclear Fuel at Olkiluoto Radionuclide Transport and Dose Assessment for Humans in the Biosphere Assessment BSA-2012. POSIVA 2012-31. Eurajoki, Finland.

Pusch, R. 2003. The Buffer and Backfill Handbook. Part 3: Models for Calculation of Processes and Behaviour. Swedish Nuclear Fuel and Waste Management Company Report SKB TR-03-07. Stockholm, Sweden.

Quintessa Ltd. 2014. AMBER 5.7.1 Reference Guide. Henley-On-Thames, UK.

Razdan, M. and D.W. Shoesmith. 2015. The influence of hydrogen peroxide and hydrogen on the corrosion of simulated nuclear fuel. Faraday Discussions 180, 283-299.

Rollin, S., K. Spahiu and U.-B. Eklund. 2001. Determination of dissolution rates of spent fuel in carbonate solutions under different redox conditions with flow-through experiments. J. Nucl. Mat. 297, 231-243.

Rodwell, W.R. and P.J. Nash. 1992. Mechanisms and Modelling of Gas Migration from Deep Radioactive Waste Repositories. Nirex Report NSS/R250. Dorchester, U.K.

Sander, R. 2015. Compilation of Henry's law constants (version 4.0) for water as solvent. Atmos. Chem. Phys. 15, 4399-4981.

Sheppard, S.C. and B. Sanipelli. 2011a. Review of Environmental Radioactivity in Canada Nuclear Waste Management Organization report NWMO TR-2011-17. Toronto, Canada.

Sheppard, S.C. and B. Sanipelli. 2011b. Environmental radioactivity in Canada - Measurements. Nuclear Waste Management Organization report NWMO TR-2011-16. Toronto, Canada.

Shoesmith, D. 2008. The Role of Dissolved Hydrogen on the Corrosion/Dissoluton of Spent Nuclear Fuel. Nuclear Waste Management Organization Report NWMO TR-2008-19. Toronto, Canada.

Shoesmith. S. and D. Zagidulin. 2010. The corrosion of Zirconium under Deep Geological Repository Conditions. Nuclear Waste Management Organization Technical Report NWMO TR-2010-19. Toronto, Canada.

SKB. 1998. Design Premises for Canister for Spent Nuclear Fuel. Swedish Nuclear and Waste Management Company Technical Report TR-98-08. Stockholm, Sweden

SKB. 1999. Deep Repository for Spent Nuclear Fuel: SR 97 - Post-closure Safety: Main Report - Volume 1, Volume 2, and Summary. Swedish Nuclear Fuel and Waste Management Company Report SKB TR-99-06. Stockholm, Sweden.

SKB. 2010. Corrosion Calculations for the Safety Assessment SR-Site, TR-10-66. Stockholm, Sweden.

SKB. 2010a. Handling of future human actions in the safety assessment SR-Site. Swedish Nuclear and Waste Management Company Technical Report TR-10-53. Stockholm, Sweden.

SKB. 2010b. Design, Production and Initial State of the Canister. Swedish Nuclear and Waste Management Company Technical Report TR-10-14. Stockholm, Sweden

Smith, H.D. and D.L. Baldwin. 1993. An investigation of thermal release of carbon-14 from PWR Zircaloy spent fuel cladding. J. Nucl. Mat. 200, 128-137.

SKB. 2014. Handling of future human actions in the safety assessment SR-PSU. Swedish Nuclear Fuel and Waste Management Company Report. SKB TR-14-08. Stockholm, Sweden. 2011

Spahiu, K., L. Werme and U.-B. Eklund. 2000. The influence of near field hydrogen on actinide solubilities and spent fuel leaching. Radiochimica Acta 88, 507-511.

Spahiu, K. and P. Sellin. 2001. SR 97: Spent Fuel Alteration/Dissolution and the Influence of Near Field Hydrogen. In: Scientific Basis for Nuclear Waste Management XXIV. Material Research Society Symposium Proceedings Volume 663.

Srivastava, R.M. 2002. The Discrete Fracture Network Model in the Local Scale Flow System for the Third Case Study. Ontario Power Generation Report 06819-REP-01300-10061-R00. Toronto, Canada.

Sykes, J.F., S.D. Normani and E.A. Sudicky. 2003. Regional Scale Groundwater Flow in a Canadian Shield Setting. Ontario Power Generation Report 06819-REP-01200-10114-R00. Toronto, Canada.

Tait , J.C., I.C. Gauld and A.H. Kerr. 1995. Validation of the ORIGEN-S Code for Predicting Radionuclide Inventories in Used CANDU Fuel. Journal of Nuclear Materials 223, 109-121.

Tait, J.C., H. Roman and C.A. Morrison. 2000. Characteristics and Radionuclide Inventories of Used Fuel from OPG Nuclear Generating Stations. Volume 1 – Main Report and Volume 2 – Radionuclide Inventory Data. Ontario Power Generation Report 06819-REP- 01200-10029-R00. Toronto, Canada.

Therrien, R., R. G. McLaren, E. A. Sudicky, S.M. Panday and V. Guvanasen. 2010 FRAC3DVS-OPG: A Three-Dimensional Numerical Model Describing Subsurface Flow and Solute Transport. User's Guide, Groundwater Simulations Group, University of Waterloo. Waterloo, Canada.

Walsh, R. and J. Avis. 2010. Glaciation Scenario: Groundwater and Radionuclide Transport Studies. Nuclear Waste Management Organization Report NWMO TR-2010-09. Toronto, Canada.

Wu, L., N. Liu , Z. Qin and D.W. Shoesmith. 2014. Modeling the radiolytic corrosion of fractured nuclear fuel under permanent disposal conditions. J. Electrochem. Soc. 161, E3259-E3266.

Yamaguchi, I., S. Tanuma, I. Yasutomi, T. Nakayama, H. Tanabe, K. Katsurai, W. Kawamura, K. Maeda, H. Katao, and M. Saigusa. 1999. A study on chemical forms and migration behaviour of radionuclides in hull wastes. In ICEM'99 Conference Proceedings, Nagoya, Japan, Sept. 26-30. American Society of Mechanical Engineers. New York, USA.

8. TREATMENT OF UNCERTAINTIES

All analysis calculations have an associated uncertainty. CNSC Regulatory Guide G-320 (CNSC 2006) expects that uncertainty will be taken into account.

8.1 Approach

Many organizations use the following three broad categories[1] to structure the analysis of uncertainties in postclosure safety assessments (e.g., Marivoet et al. 2008):

- **Scenario Uncertainty**: Arises from uncertainty in the evolution of the repository system and human behaviour over the time scales of interest.
- **Model Uncertainty**: Associated with uncertainty in the conceptual, mathematical and computer models used to simulate the behaviour of the repository system (i.e., due to approximations used to represent the system).
- **Data Uncertainty**: Arises from uncertainty in the data and parameters used as input in the models (e.g., due to incomplete site-specific data or due to parameter estimation errors from interpretation of test results).

The following briefly discusses the approach adopted for uncertainties in this assessment report.

Scenario Uncertainty

Uncertainty in the future evolution of the site is addressed by assessing a range of scenarios that describe the potential evolution of the system. The scenario identification process, described in Chapter 6, ensures that key uncertainties are identified and scenarios are defined to explore their consequences.

The scenarios defined include the Normal Evolution Scenario (which describes the expected evolution of the repository) and a series of Disruptive Event Scenarios that postulate the occurrence of unlikely events leading to possible penetration of barriers and abnormal loss of containment.

To estimate potential future impacts, a stylized representation[2] of the biosphere and human receptors is adopted. A stylized representation is used rather than a detailed assessment based on current conditions because:

- Human behaviour may change over the time scale of relevance to the repository system,

---

[1] The boundaries between these categories can overlap. Depending upon how models are formulated, an uncertainty may be classed as a model or a data uncertainty.

[2] A stylized representation of the biosphere and human habits and behaviour is a representation that has been simplified to reduce the natural complexity to a level consistent with the objectives of the analysis; that is, using assumptions that are intended to be plausible and internally consistent but that tends to err on the side of conservatism.

- The surface and near-surface environment are likely to change as a result of natural causes such as ice ages and / or as a result of future human actions, and
- Societal and technological changes are unpredictable over such timescales.

In the stylized representation, while the exposure models are more general, it is assumed that future humans are generally similar to present-day humans with behaviors consistent with current or past human practice. People are assumed to live on the repository site in the future in a manner that maximizes their potential dose from exposure to releases from the repository.

Since assumptions concerning the biosphere (e.g., climate), human lifestyles (e.g., critical group characteristics) and water flows in the near-surface environment become increasingly uncertain with time, two complementary long-term indicators are also used to supplement the dose rate indicator using system characteristics that are much less sensitive to such assumptions.

Model Uncertainty

Conceptual and mathematical model uncertainties are identified in the model development process. Key uncertainties are addressed by using alternative conceptual representations of the system. This is facilitated by the use of different computer codes (e.g., FRAC3DVS-OPG and SYVAC3-CC4) that provide different conceptualizations and mathematical descriptions.

Some conceptual and mathematical model uncertainties are amenable to representation with parameter values, and these are investigated using the methods applied to data uncertainties. For example, uncertainties in the representation of sorption are treated by considering extreme bounding cases in which the sorption values are set to zero.

Data Uncertainty

Data uncertainties are identified in Gobien et al. (2016). These are accounted for through:

- Deterministic Calculations – alternative specific sets of parameter values. In particular, see the sensitivity cases in this assessment (Chapter 7, Section 7.2.2) that explore the effect of variations in key parameters affecting the performance of the multi-barrier system.
- Results are compared to the Base Case. This approach provides clear information on the effects of specific parameter variations. A limitation of this approach is that there is often no systematic or complete coverage of the uncertainty space in parameter values.
- Probabilistic Calculations – parameters are assigned probability distribution functions that describe their inherent uncertainty. The model is evaluated a large number of times, with each case using input values randomly selected from the distribution functions. The model output is a distribution of results. The strength of the probabilistic approach lies in its ability to better explore the parameter space of the phenomena considered. Its weakness is the need to make use of simplified models.

Conservatisms

Throughout the assessment process, it is necessary to make various assumptions relating to scenarios, models or data. Assumptions are often categorized as 'realistic'[3] or 'conservative'[4], although care needs to be taken when using such terms. The key is to ensure that each major assumption used in the assessment is considered and documented, and that the potential implications are understood.

While it may appear sensible to adopt a conservative approach to ensure the potential effects are not under-estimated, care is needed because the net effect of many conservative assumptions can be an unrealistic estimate of impact. Thus, the postclosure safety assessment adopts scientifically informed, physically realistic assumptions for processes and data that are understood and can be justified on the basis of the results of research and / or site investigation. Where there are high levels of uncertainty, conservative assumptions are adopted to allow the effects of uncertainties to be bounded.

In particular, Table 7-3 in Chapter 7 (reproduced below as Table 8-1) contrasts many of the conservative assumptions adopted in the Normal Evolution Scenario Base Case sensitivity study with what is likely to occur in reality. Further discussion of each item can be found in Chapter 7 in the text that follows Table 7-3.

[3] Realism is defined as "the representation of an element of the system (scenario, model or data), made in light of the current state of system knowledge and associated uncertainties, such that the safety assessment incorporates all that is known about the element under consideration and leads to an estimate of the expected performance of the system attributable to that element" (IAEA 2006).

[4] Conservatism is defined as "the conscious decision, made in light of the current state of system knowledge and associated uncertainties, to represent an element of the system (scenario, model or data) such that it provides an under-estimate of system performance attributable to that element and thereby an over-estimate of the associated radiological impact (i.e., dose or risk)" (IAEA 2006).

Table 8-1: Base Case Sensitivity Study Assumptions

Parameter	Realistic Assumption	Base Case Assumption
When can contaminants escape the container?	After the container is breached and large amounts of water contact the fuel	After the container is breached
Defect Parameters		
What is the defect of concern?	Undetected defect in the copper corrosion barrier	Undetected defect in the copper corrosion barrier
How large is the defect in the copper corrosion barrier?	Random sizes below the Detection Threshold (0.8 mm depth)	>>0.8mm Large enough to cause container failure at the assumed times
Where is the defect located?	Random location • < 1% chance over 8 mm weld • ~5% chance over weld area (8-30 mm steel) • ~25% chance over container head (30 mm steel) • ~70% chance over container body (46 mm steel)	Not applicable Complete container failure occurs at the assumed times
How long does an impaired copper barrier remain effective?	> 74 million years for defects below the 0.8 mm Detection Threshold (see Chapter 5) *Based on an assumed groundwater sulphide concentration of 1* μM	1000 years for the first container One additional container fails every 100,000 years
How many containers are breached prior to 1 million years?	0	10
Container Parameters		
Once the copper barrier is penetrated, how long before the steel inner shell is penetrated due to corrosion?	140,000 years for 8 mm 1,300,000 years for 30 mm 2,000,000 years for 46 mm *Based on 1 mm diameter hole in the copper barrier* *It is anticipated that there will be insufficient amounts of carbonate to promote siderite producing corrosion reactions (see Chapter 5)*	0 years
Once the steel barrier is penetrated, how long before large amounts of water enter the container?	It could take many tens of thousands of years for the container to fill with water	0 years

Parameter	Realistic Assumption	Base Case Assumption
Do the Zr fuel sheaths prevent water from contacting fuel elements?	Possibly Some fuel sheaths may still be intact when water enters the container	No
For fuel elements that are contacted by water, how large is the instant release source term?	Depends on the power experienced while in the reactor and on the physical condition of each fuel pellet	Conservative Value
Does H_2 released during steel corrosion and radiolysis inhibit the fuel dissolution rate (and thereby inhibit the contaminant release rate)?	Most likely Yes	No
Do corrosion products accumulate in the defect and obstruct the migration of contaminants?	Yes	No
After the steel barrier is penetrated, how long before the container wall corrodes away and no longer presents any resistance to contaminant release	120,000 years for 8 mm 460,000 years for 30 mm 710,000 years for 46 mm *It is anticipated that there will be insufficient amounts of carbonate to promote siderite producing corrosion reactions (see Chapter 5)*	0 years
Dose Parameters		
Are people living close to the facility?	Unknown The repository footprint is small and the location may be far from populated areas	Yes Living on top of the repository
Are the nearby people using a deep well to obtain their drinking water?	Unlikely Surface water sources or a shallow well are more likely	Yes A 100 m deep well is assumed
If used, where is the well located in relation to the defective containers?	Random	Worst location The location that maximizes contaminant uptake
Where are the hypothetical defective containers located in the repository?	Random	Clustered In the location that maximizes uptake to the well

8.2 Key Uncertainties

The postclosure safety assessment summarized in Section 7.14 indicates that the deep geological repository in geologic settings similar to the assumed site could tolerate large changes in the properties of key barrier parameters without challenging the interim dose acceptance criteria.

The key uncertainties in terms of their importance to modify potential impacts are:

- **Fracture Characterization**: For a real site in a Canadian Shield setting, there will be uncertainty in the fracture network and in the properties of the fractures. Site characterization may also not identify all existing significant fractures. A local network of small-scale fractures may provide a potential faster pathway through the rock mass than modelled here. These uncertainties can be reduced through site selection and repository location and depth, and any residual uncertainties can be handled through the adoption of conservative assumptions and / or Disruptive Scenarios (such as the Undetected Fault Scenario) within the postclosure analysis.

- **Glaciation Effects**: Although geological evidence at a real site is expected to indicate the deep geosphere has not been affected by past glaciation events and that the deep groundwater system has remained stagnant, glaciation will have a major effect on the surface and near-surface environment that is not entirely predictable. However, glaciation is not likely to occur before 60,000 to 100,000 years, and by that time there would have been significant radionuclide decay.

- **Number of Container Failures**: The Base Case of the Normal Evolution Scenario assumes 10 containers fail relatively early due to undetected defects in their copper coating. There is uncertainty in this number, and work is ongoing to better quantify the likelihood of a defect escaping the rigorous quality inspection program that will be implemented.

8.3 References for Chapter 8

CNSC. 2006. Regulatory Guide G-320: Assessing the Long Term Safety of Radioactive Waste Management. Canadian Nuclear Safety Commission. Ottawa, Canada.

Gobien, M., F. Garisto, E. Kremer and C. Medri. 2016. Sixth Case Study: Reference Data and Codes. Nuclear Waste Management Organization Technical Report NWMO TR-2016-10. Toronto, Canada.

IAEA. 2006. Safety Requirements: Geological Disposal of Radioactive Waste. International Atomic Energy Agency Safety Requirements WS-R-4. Vienna, Austria.

Marivoet, J., T. Beuth, J. Alonso and D.-A. Becker. 2008. Safety Functions, Definition and Assessment of Scenarios, Uncertainty Management and Uncertainty Analysis, Safety Indicators and Performance/Function Indicators. PAMINA Deliverable D-No. 1.1.1, European Commission. Brussels, Belgium.

9. NATURAL ANALOGUES

Natural analogues are natural features (materials or processes) that are similar to those expected in some part of a deep geological repository. Natural analogues can include both natural and anthropogenic materials, provided the processes that affect them are natural. They provide understanding or demonstration of how a repository may behave over time scales ranging up to many millions of years. Analogues exist for most features of the repository system, including the used fuel, engineered and natural containment systems, and key processes such as transport of contaminants.

The use of natural analogues in supporting key assumptions in safety assessment and adding credibility to its findings is recommended in IAEA (1999) and in Regulatory Guide G-320 (CNSC 2006). G-320 states: "*Natural analogue information should be used to build confidence that the system will perform as predicted by demonstrating that natural processes will limit the long-term release of contaminants to the biosphere to levels well below target criteria.*"

The natural analogues presented here can assist in understanding many of the underlying principles relevant to the long-term isolation and containment of used nuclear fuel. The present summary focusses on the engineered barriers; the use of geosphere analogues would be described in the Geosynthesis that would be prepared as part of the analysis of a real site.

9.1 Analogues for Used Nuclear Fuel

9.1.1 Natural Uranium Deposits

Natural uranium is relatively abundant. Like all other elements, it is cycled through biological and geological systems and tends to concentrate in some locations by natural processes. Uranium will slowly dissolve under oxidizing conditions and precipitate under reducing conditions. Most uranium ore bodies form by this process. Uranium ore bodies that are being mined today were formed hundreds of millions of years ago. The stability of these uranium ores provides information on the stability of used fuel.

Used fuel consists predominantly of uranium dioxide, with about 2% of the total being fission and activation products resulting from the nuclear reactions occurring in the fuel during power production. Natural uranium minerals are comparable in that many also consist of uranium dioxide along with uranium decay products.

One gram of natural uranium, as it is extracted from the earth in equilibrium with its progeny, contains a little less than 2×10^5 Bq of radioactivity. In comparison, after discharge from a reactor and 30 years of cooling, used fuel has an inventory of 2.7×10^9 Bq per gram of uranium, principally in the form of fission and activation products (Tait et al. 2000), and is considerably more radioactive than the original uranium ore. Due to the decay of most of the fission product isotopes present in used fuel, radioactivity decreases to 2.3×10^7 Bq per gram after 1000 years, while after approximately one million years, radioactivity decreases to a level similar to that in natural uranium.

The Cigar Lake uranium deposit found in Northern Saskatchewan (Figure 9-1) provides a Canadian example of an analogue for geological placement of used nuclear fuel. The Cigar Lake deposit is under development as a uranium mine and has been well studied as a natural analogue (Cramer and Smellie 1994, Miller et al. 2000). The ore body formed about 1.3 billion years ago.

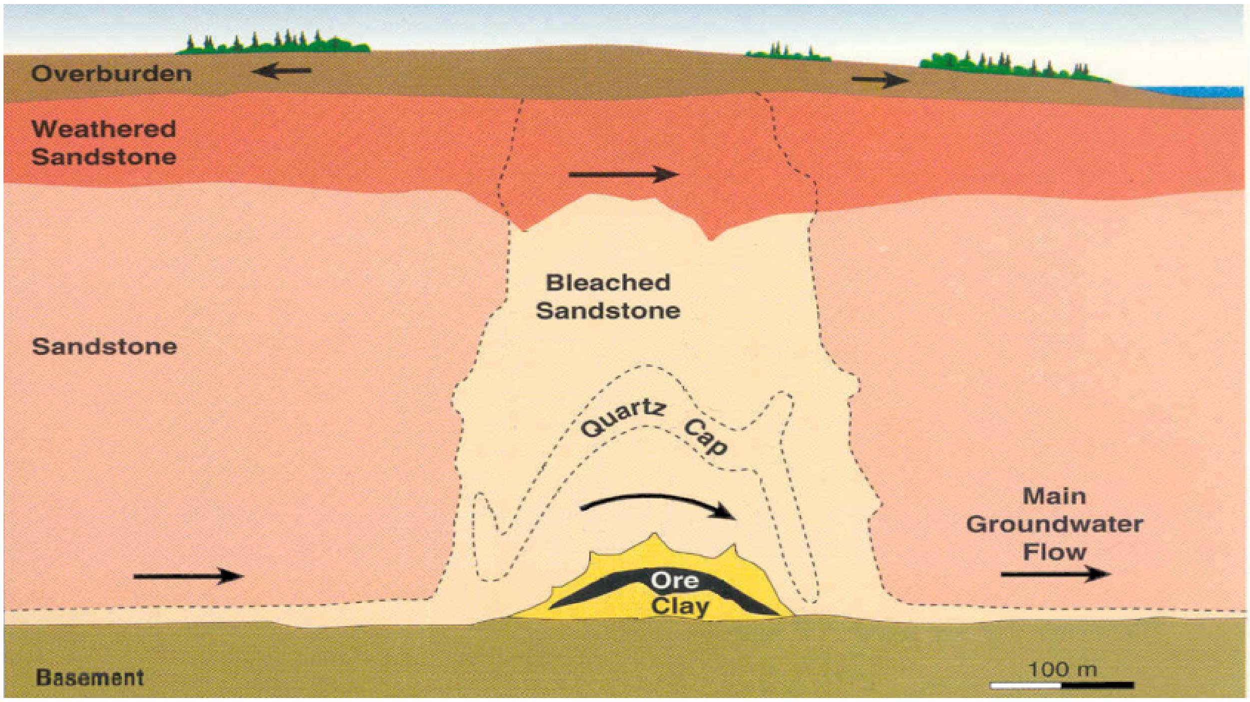

Figure 9-1: Cigar Lake Ore Deposit

The Cigar Lake uranium deposit is located about 430 m below surface, similar in depth to the repository considered in this study (i.e., 500 metres underground). The uranium is primarily in the form of uranium dioxide, so is similar in general composition to used fuel. The ore is also very rich in uranium, with much of the ore body at around 20% uranium and portions even higher. The total amount of uranium is roughly comparable to that to be placed in a Canadian repository. Also, the ore is surrounded by a clay envelope somewhat similar to the clay buffer specified in the repository design. It can be considered analogous to a “worst case” simulation, as it lacks any analogue for the used fuel containers and the host rock above the ore body is highly permeable sandstone.

Insufficient radionuclide migration has occurred around Cigar Lake to produce any detectible concentration anomalies in the soil, surface water and lake sediments and waters overlying the ore body. Environmental and geological exploration in the area has shown no surface expression of the ore body, and it had to be discovered by geophysical techniques. Indeed, on a map of surface radioactivity in Canada, the area of the Saskatchewan deposits generally shows up as having below-average surface radioactivity (McKee and Lush 2004).

Based on studies of the Cigar Lake ore body (Cramer and Smellie 1994), it was concluded that:

- uranium dioxide will remain stable over 100 million year time scales under the chemically-reducing conditions found adjacent to the Cigar Lake ore body, with very little uranium migrating from the deposit;
- the natural clay surrounding the ore has provided an effective long-term seal, preventing migration of radionuclides from the deposit;
- dissolved organic matter in groundwater migrating past the ore has not played a significant role in mobilizing radionuclides from the deposit; and
- natural hydrologic barriers and appropriate geochemical conditions found at the site are effective in preventing significant radionuclide migration from the deposit.

A different type of uranium ore body found in permeable rocks are the roll-front ore bodies, named because they are slowly but continuously migrating or "rolling" through the permeable host rock. The front of the ore body is in a reduced state, while the rear of the ore body is in a more oxidized state as a consequence of oxidizing groundwaters that are slowly driving the ore body through the rock formation. This creates a condition at the rear of the ore body in which the uranium becomes soluble and migrates to the front of the ore body where it again precipitates. Although used fuel would not be located in a permeable rock formation, these ore bodies are further indication of the importance of redox conditions to the long-term stability of uranium underground.

A well-studied example of a roll-front uranium deposit is the Osamu Utsumi mine in Brazil (Hofmann 1999). Hoffman reported that migration of uranium, along with palladium and selenium, was strongly inhibited at a redox front, causing immobilization. Results indicated that reducing conditions inhibit transport of these elements under most natural low-temperature conditions.

Roll-front uranium deposits illustrate how migration of uranium and many elements through locally oxidizing conditions in the container (assuming groundwater infiltration of used fuel containers and subsequent radiolysis of this water near the used fuel) would be effectively suppressed by the reducing conditions of the placement rooms and repository host rock.

9.1.2 Natural Fissioned Uranium

Nuclear fission occurred naturally on Earth over two billion years ago. In Gabon, Africa, there are 15 deposits of uranium ore that have acted as natural nuclear reactors (Miller et al. 2000), sometimes referred to as the Oklo fossil reactors (Figure 9-2). These remnants of natural uranium fission provide a close natural analogue for used nuclear fuel over long time periods in a geologic environment.

Approximately two billion years ago, when the Oklo ore bodies formed, the fraction of U-235 present in natural uranium was about 5%, much greater than the current value of about 0.7% (due to natural decay over time). With this level of U-235, and under the groundwater and pressure conditions in the Oklo ore bodies, sustained nuclear chain reactions occurred. The Oklo reactors operated at low power over about one million years. Approximately 6 to 12 tonnes of U-235 underwent fission, producing fission products, plutonium and other actinides, and generating temperatures in the natural reactors of up to 350°C.

Oklo reactor studies provide data regarding the stability of uranium dioxide in the presence of fission products, and on the transport of radionuclides within the surrounding geology. These studies indicate that more than 90% of the uranium "fuel" present in the reactors 2 billion years ago has remained in place. The transuranic elements, most of the fission products and their decay products were trapped in the uranium ore or the surrounding clay; the plutonium moved less than 3 metres. This is in absence of any analogues for the engineered barriers incorporated into a geological repository; containment and isolation of the Oklo reactors was achieved by the ore body and the surrounding sandstone and sedimentary formations. The rock has proved to be a well-sealed vault.

The stability of the Oklo used fuel has lasted through two billion years of continental drift and groundwater movement. This is particularly impressive considering the present day near-surface location of these natural reactors.

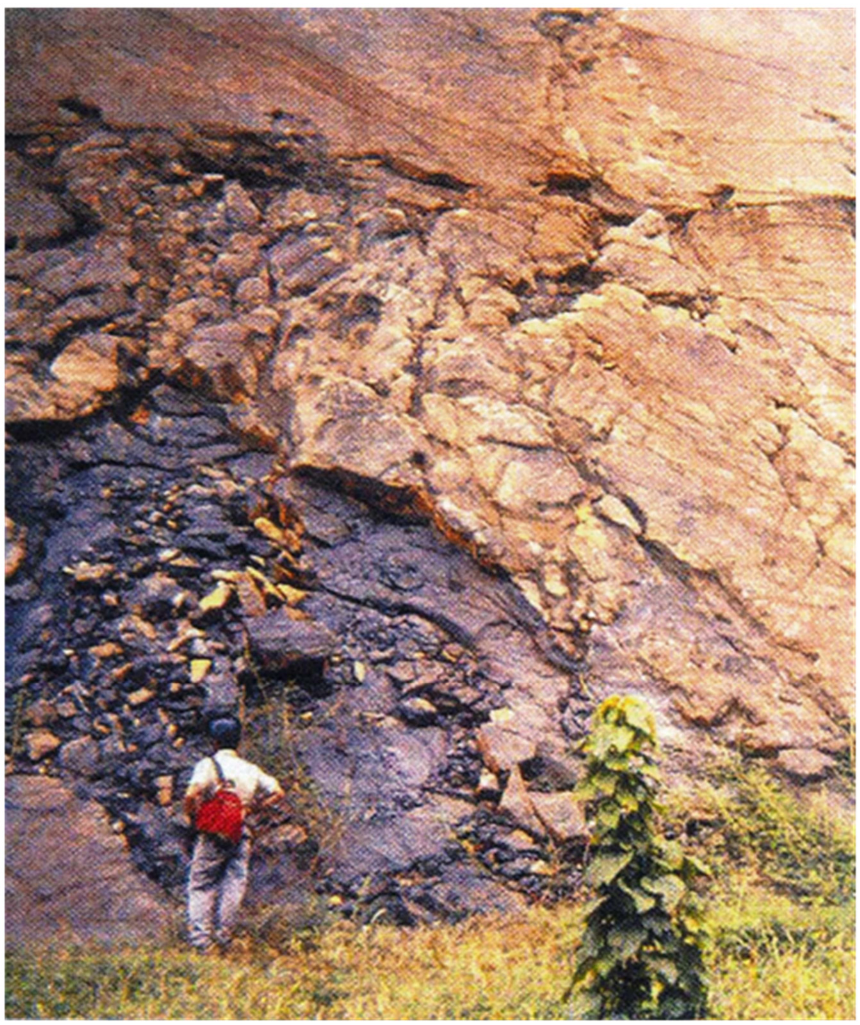

Notes: In Oklo, Gabon, the remains of an ancient natural nuclear reactor indicate the resulting plutonium has moved less than 3 metres over two billion years (from Miller et al., 2000).

Figure 9-2: Naturally Occurring Fission Reactor

The Oklo fossil reactors provide a snapshot in time of the condition of a natural used fuel repository two billion years after decommissioning. Information is obtained through indirect evidence such as the quantity and location of fission products and their decay products, and the actinides that can still be found in association with these natural reactors. This evidence indicates that careful selection of the host rock formation for a used fuel deep geological repository can render many fission products and actinides largely immobile.

9.1.3 Fractured Uranium Deposits

The Tono uranium deposit, located near Tokyo, has been the subject of analogue studies relating to transport of uranium (Miller et al. 2000). The uranium deposit, formed approximately 10 million years ago, lies between underlying crystalline bedrock and overlying sedimentary formations. The area is tectonically active and between 5 and 10 million years ago, the deposit was split by a fault. This displaced a portion of the ore body 30 m upward. Despite this large fault, many other nearby faults, and the occurrence of frequent tremors, Yoshida (1994) found that no significant uranium transport has occurred along the fault. Detailed examination of the host rock found substantial matrix diffusion, providing a very large surface area for sorption of radionuclides. Consequently, no substantial remobilisation of the uranium has occurred, despite the faulting history of the area.

The preferred location for a used fuel repository will include a minimum distance separating the repository from significant fracture zones, because large faults are considered the most consequential pathway for transport of any hypothetical release of radioactivity from the repository to the surface. Nonetheless, it is important to note that the Tono uranium deposit was split by a large fault and no significant fracture-based transport has occurred.

9.2 Analogues for Barriers

The repository design uses multiple barriers, including materials such as iron, copper, clays, concrete and asphalt to inhibit or prevent movement of radioactive elements and other materials from the facility into the surrounding environment.

In particular, the used fuel will be sealed inside a container made from steel and covered in copper, and surrounded by a clay-based buffer layer. Placement rooms, underground tunnels and the shafts will be sealed closed with a combination of clay, concrete and asphalt-based materials.

9.2.1 Copper

Copper is one of the relatively few metals that naturally occurs in their metallic state, indicating that it is stable under geological conditions. Solid pieces of native copper have been found containing more than 99% copper. The largest known deposit of metallic copper is in the Keweenaw Peninsula of Michigan (Crissman and Jacobs 1982), where large pieces of almost pure copper were either mined or found in glacial outwash.

Copper “plates” found in the mudstones from South Devon in England (Figure 9-3) provide a natural analogue for the corrosion of used fuel containers placed in a clay backfill. These copper plates are up to 4 mm thick, comprising stacks of thin copper sheets that are between a few tens of microns to a couple of millimetres in thickness. The plates were formed 200 million years ago and show little corrosion since that time, due in part to the protection of the clay-rich mudstone (Milodowski et al. 2000).

Data from these natural coppers help bound long-term copper corrosion rates for both reducing and oxidizing environments, which are useful in assessing the longevity of the used fuel containers.

Note: From Milodowski et al. (2000).

Figure 9-3: Copper Plate and Mudstone Covering

9.2.2 Iron

There are both archaeological and natural analogues for the long-term behavior of iron underground. These provide information on the corrosion rate of iron that can be expected over long time frames underground, as well as on the role of iron in maintaining favorable reducing conditions.

Recorded use of iron dates to Egypt in 1900 BCE (Miller et al. 2000). Johnson and Francis (1980) studied the corrosion of artifacts under a wide range of environmental conditions. From this work they have reported annual corrosion ranging from 0.1 to 10 microns, lasting over timescales of several thousand years.

The large amounts of iron (carbon steel) in the used fuel containers may buffer redox conditions in the repository, preventing oxidizing conditions near the used fuel. The Inchtuthil Roman nails found in Scotland provide an interesting analogue for this. At a Roman fortress that was abandoned in 87 CE (Angus et al. 1962; Pitts and St. Joseph 1985), over 1 million nails were buried in a 5-m deep pit under 3 m of earth. When the nails were unearthed in the 1950s, the nails on the outside of the mass were found to have corroded and formed a solid crust of iron oxides (rust) around the remaining mass of nails. The outside layer of nails formed a sacrificial redox sink, consuming oxygen before it could penetrate to the interior of the mass of nails. The physical expansion of the rust also served to self-seal the remaining nails from intruding groundwater and water vapour. As a result, the nails inside the rusty barrier experienced minimal-to-no corrosion over nearly 2,000 years.

In Greenland, on Disko Island, magmatic conditions within a crystalline rock formation (basalt) promoted deposition of native iron over a period of volcanism spanning from about 63 to 30 million years ago. An estimated 10 million tons of iron were deposited. Mass transport limitations (low diffusivity of reactants combined with high redox capacity) favoured preservation of the native iron. Native iron has survived millions of years in the rock matrix (Hellmuth 1991).

The natural redox buffering capacity of the clay and rock surrounding the Cigar Lake ore body is due mainly to ferrous compounds in the mafic mineral phases (Smellie and Karlsson 1996). These reducing conditions have suppressed transport of uranium and other oxidising species. The combination of slow groundwater flow and reducing conditions resulted in a very stable ore body.

9.2.3 Clays

<u>Sealing capacity</u>

The primary sealing material within the engineered containment system is bentonite clay. Bentonite (Figure 9-4) is a type of naturally occurring clay, containing a swelling component referred to as smectite or, more specifically, montmorillonite. Bentonite swells when exposed to water, minimizing water seepage and making an excellent sealing material when physically confined. It also has a high chemical sorption capacity, able to bind many elements to its crystalline surfaces, which greatly slows the migration of radionuclides. Bentonite is also very stable, typically formed millions to hundreds of millions of years ago. Clay materials can act as a very robust physical and chemical barrier, as illustrated in the discussion above of Cigar Lake where naturally formed clays acted as a protective barrier for geological time periods.
Laine and Karttunen (2010) recently produced a wide-ranging review of natural analogues for bentonite.

Each used fuel container will be surrounded by compacted bentonite clay and all excavated spaces will be filled with mixtures of clay, sand, and crushed rock. As the closed and sealed repository is slowly infiltrated by groundwater, the bentonite will swell and fill any remaining void spaces. The clay will prevent groundwater flow, and provide a chemically stable (“buffered”) environment around the container that will help it last a long time. Even after a container fails, radionuclides will only be able to move out through the bentonite by diffusion, greatly restricting their migration. In addition, the clay’s high adsorption capacity for many elements will significantly inhibit their movement.

Note: From EUBA (2011).

Figure 9-4: Bentonite Clay

The Dunarobba Forest in Italy (Figure 9-5) provides a natural analogue of the effectiveness of clays in minimizing groundwater movement (Benvegnú et al. 1988; Ambrosetti et al. 1992). The sequoia-like Dunarobba trees were buried in clay for 1.5 million years. The clay minimized the flow of water to the trees and prevented oxygen from reaching the wood. This maintained reducing conditions around the wood, protecting the wood from bacterial or fungal decay or chemical oxidation. As a result, the trees did not decay. They also did not fossilize - they are still made of wood.

Similar analogues have been found in the Canadian Arctic on Axel Heiberg Island (Greenwood and Basinger 1994) and at the Strathcona Fiord on Ellesmere Island (Francis 1988), where shale deposits over 40 million years old were found to contain preserved specimens of redwood, walnut, elm, birch and alder; also, gingko and katsura, now native to eastern Asia. The shale, which is consolidated clay, provided an effective barrier to oxygen and preserved the wood such that the wood grain and bark are preserved without chemical alteration – the cellular structure and most of its molecular structure remain intact.

Note: Retrieved Nov 23 2015 from http://it.wikipedia.org/wiki/File:Dunarobba.jpg.

Figure 9-5: 1.5 Ma Sequoia-like Tree Stumps at Dunarobba, Italy

Sensitivity to Temperature

Thermal alteration of bentonite has been studied, with a focus on higher temperatures of relevance to the near field. These studies indicate little reaction or degradation of bentonite physical properties below 150°C (Wersin et al. 2007). This compares well with repository temperatures (see Chapter 5), where the temperature at the surface of the container is predicted to peak at less than 100°C within 10 years of closure, then steadily decrease to 90°C after 100 years and ultimately return to ambient temperature by approximately 100,000 years.

For example, the bentonite beds at Kinnekulle in Southern Sweden were exposed to temperature of 140-160°C over a period of about 1000 years as a result of a basaltic intrusion (Pusch et al. 1998). For this bentonite, 350 million years after the intrusion event, the measured swelling pressures are still substantial and hydraulic conductivities are reasonably low, indicating that the sealing properties of the bentonite remain favourable.

Laine and Karttunen (2010) report on the Ishirini bentonite body in Libya. Some of the bentonite formations were crosscut by basaltic intrusions about 20 million years ago, causing local thermal alteration near the intrusions. Kolaříková and Hanus (2008) found that the minimum temperature experienced by the bentonite during the intrusions was probably higher than 190°C. The impact of raised temperatures, however, appears minimal: while some local cementation occurred, the majority of the bentonite remains unaltered.

Sensitivity to Salinity:

The effects of potential saline groundwaters have been studied. High salinity, such as is likely to occur in the sedimentary rocks of Southern Ontario (not likely in crystalline rocks), is expected to affect the swelling properties of the bentonite; however, it is not expected to alter the mineral stability of the bentonite.

For example, Alexander and Milodowski (2014) observe that the Perapedhi bentonites studied under the Cyprus Natural Analogue Project likely remained in a marine, saline environment for nearly 90 million years. Figure 9-6 compares the swelling pressure of the Cyprus bentonite with a range of industrial bentonites, showing that the swelling behavior is about what would be expected for a bentonite material of this nature (with an inherent low amount of montmorillonite). This indicates that exposure of this bentonite to marine saline conditions for nearly 90 million years had no significant impact on its swelling capacity. This analogue is at lower salinity than w ould be seen in sedimentary rock repository settings; however the exposure was also for a very long period of time and yet there was no significant impact.

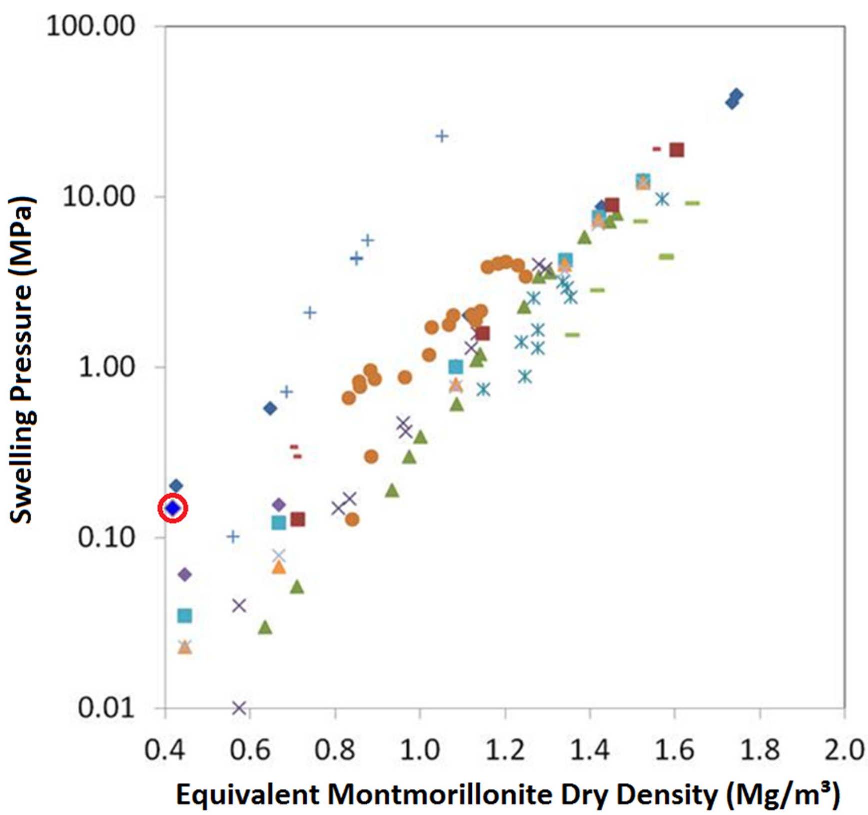

Figure 9-6: Swelling Performance of Various Bentonites (Cyprus is circled in red)

Sensitivity to Alkalinity

Bentonite, particularly the swelling clay component (smectite), is unstable under high pH conditions. In the repository, concrete may produce alkaline conditions locally, affecting adjacent bentonite. However, as the low-heat high-performance concrete leachates will have a lower pH (10 - 11) than Ordinary Portland Cement, it is expected that any reaction with the bentonite will be local. Furthermore, the concrete plugs are placed at a distance from the bentonite buffer around the containers.

Significant degradation of smectite has been observed in conditions with large amounts of alkaline groundwater; however, in natural analogue systems with limited groundwater flow, the reaction is limited. For example, results from the International Philippines Natural Analogue Project (Fujii et al. 2010) show that reaction with alkaline water (pH ~11) in the bentonite is restricted to the contact interface, with the width of the reaction zone a maximum of 5 cm. In another example, at the Cyprus Natural Analogue Project (Alexander and Milodowski, 2014), the groundwater ($9 < pH < 11$) appears to have been circulating under the bentonite for approximately 500,000 to 800,000 years. In this time, less than 1% of the smectite in the bentonite has reacted, indicating very slow reaction times. The authors note that sufficient swelling pressure remains in the reacted bentonite to minimize further reaction due to pore throat reduction (see also Wilson et al. 2011).

9.2.4 Concrete

Low-heat, high-performance concrete may be used to close container placement rooms. The concrete bulkheads will counteract the swelling pressure of the bentonite components and maintain the tunnel backfill materials in their intended position. Concrete bulkheads could also be used to provide structural support and confinement to the column of shaft sealing materials. Low-heat high-performance concrete is designed to minimize effects on the adjacent clay (Dixon et al. 2001).

Analogue studies of natural cements suggest that, within tectonically stable systems, the material is durable, with the oldest reported cements at Maqarin in north Jordan being some 2 million years old (Alexander 1992). Milodowski et al. (1989) also reported the presence of unreacted natural cements from the Scawt Hill and Carneal Plug sites in Northern Ireland. These cements were produced during the thermal metamorphism of the host limestone and are estimated to be some 58 million years old. In both examples, the natural cements are effectively impermeable and remain unchanged until accessed by groundwaters (through tectonic damage, for example). If damaged, the tendency is for these systems to reseal, either with secondary calcium silicate hydrate phases (Linklater 1998) or carbonates (Clark et al. 1994).

Of the natural analogue studies reported to date on cements, it is important to note that the natural cements examined are more akin to Ordinary Portland Cement, not low-heat high-performance cement (Gray and Shenton 1998). Low-heat high-performance cement is essentially the same as the pozzolanic cements developed by the Romans in the 3rd century BCE, or perhaps in Tiryns and Mycenae a millennium earlier (Middleton 1888). Recent studies of Roman cements exposed to marine salinities for about 2000 years tend to suggest little degradation of the cement (Oleson et al. 2004, Vola et al. 2011).

9.2.5 Asphalt

Bitumens are meltable substances distilled from fossil fuels while asphalts are solid bitumens containing various mineral materials[1]. The shaft seal design concept includes a layer of asphalt, providing a redundant low-permeability seal. The reference asphalt is the same as proposed for use in the Waste Isolation Pilot Plant (WIPP 2009).

Natural asphalts and bitumens have been used as glue or mastic for water-proofing for many thousands of years. In almost all cases where archaeological artifacts have been found coated in asphalt, they have been well preserved when mechanical disruption of the bitumen has not occurred: one example is provided by Babylonian buildings from 1300 BCE, where asphalt was used to coat floors and as a building material in river banks and piers (Hellmuth 1989); another comes from remains within the caves of Lascaux in France, approximately 15,000 years old (Nagra 1988).

Natural asphalts are found in a number of geological environments and in all climatic zones. Examples include the asphalt lakes of Trinidad and Guanoco, Venezuela, impregnated sandstones and limestones in Athabasca (Canada), Utah (USA), Val de Travers (Switzerland), and Hannover (Germany), and hydrothermal veins in Derbyshire (England).

The Athabasca oil sands located in the McMurray Formation in Athabasca are the largest known reservoir of crude bitumen in the world. The host formation is of early Cretaceous age and composed of numerous lenses of unconsolidated oil-bearing sand. Isotopic studies show the oil deposits to be about 112 million years old (Selby and Creaser 2005). The study by Longstaffe (1993) indicates that the bitumen has remained stable for over 10 million years.

The bitumen deposits in sandstone rocks in the Uinta Basin in Utah are believed to be from the late Cretaceous to Eocene period, 70 to 30 million years ago (Schamel 2009), formed under basin waters that were likely comparable to marine salinity. This natural analogue provides another example of the long-term stability of bitumen under likely saline conditions.

Also within the Uinta Basin in Utah, extensive veins of another natural asphalt called gilsonite were formed by hydrothermal fluids during the Eocene period, 56 to 34 million years ago, and have subsequently remained little altered for several tens of millions of years (Boden and Tripp 2012).

Drake et al. (2006) report natural asphalt (asphaltite) in open and closed fractures at the Forsmark site in Sweden. This asphalt was exposed to saline water (45 g/L at present) for at least several million years, suggesting very long-term stability of asphalt under saline conditions.

9.3 Analogue for Geosphere

Natural analogues for the behavior of the geosphere are also available. The site itself is an important analogue for the future behaviour of the geosphere at the site. In particular, geoscientific evidence of the past history of the site provides a direct analogue for future

---

[1] Local preference may reverse this terminology (e.g., United Kingdom vs. United States); similarly, common usage may not align with preferred geological terminology.

behaviour. This will be gathered for a real site as part of the site characterization, and presented in the geosynthesis. While this is not available for this hypothetical site, the Canadian Shield in general has low seismicity and no volcanism, with evidence that oxygen does not penetrate to any great depth during glaciation.

9.4 Natural Analogue Summary

Performance of repositories cannot be verified by experiment for time scales relevant to their long-term safety. Natural analogues provide qualitative and quantitative illustrations of long-term behaviour. While they do not prove that the performance of the various repository components will continue indefinitely, as they are not repository replicates, natural analogues provide support for key model assumptions and for the identification of processes that need to be represented and those that can be excluded. The natural analogues identified here provide additional understanding of the materials and processes that influence the behaviour of radionuclides in a deep geological repository. They provide supporting arguments and increase confidence in the long-term performance of the repository.

9.5 References for Chapter 9

Alexander, W.R. (ed). 1992. A natural analogue study of cement-buffered, hyperalkaline groundwaters and their interaction with a sedimentary host rock - I: Source-term description and geochemical code database validation. Nagra Technical Report Series NTB 91-10. Nagra, Wettingen, Switzerland.

Alexander, W.R. and A.E. Milodowski (eds). 2014. Cyprus Natural Analogue Project (CNAP) Phase IV Final Report. Posiva Working Report. Posiva, Eurajoki, Finland.

Ambrosetti, P., G. Basilici, S. Gentili, E. Biondi, Z. Cerquaglia and O. Girotti. 1992. La Foresta Fossile di Dunarobba. Ediart, Todi, Italy.

Angus, N.S., G.T. Brown and H.F. Cleere. 1962. The Iron Nails from the Roman Legionary Fortress at Inchtuthil, Perthshire. Journal of Iron and Steel Institute <u>200</u>, 956-968.

Benvegnú, F., A. Brondi and C. Polizzano. 1988. Natural Analogues and Evidence of Long-term Isolation Capacity of Clays Occurring in Italy: Contribution to the Demonstration of Geological Disposal Reliability of Long-lived Wastes in Clay. CEC Nuclear Science and Technology Report EUR 11896. Luxembourg.

Boden, T. and B.T. Tripp. 2012. Gilsonite veins of the Uinta Basin, Utah. Utah Geological Survey, Special Study 141. Utah Dept. of Natural Resources, Salt Lake City, USA.

Clark, I.D., R. Dayal and H.N. Khoury. 1994. The Maqarin (Jordan) natural analogue for 14C attenuation in cementitious barriers. Waste Management 14, 467-477.

CNSC. 2006. Regulatory Guide G-320: Assessing the Long Term Safety of Radioactive Waste Management. Canadian Nuclear Safety Commission. Ottawa, Canada.

Cramer, J.J. and J.A.T. Smellie. 1994. Final Report for the AECL/SKB Cigar Lake Analog Study. Atomic Energy of Canada Limited Report AECL-10851, COG-93-00147, SKB-TR-94-00004. Pinawa, Canada.

Crissman, D. and G Jacobs. 1982. Native Copper Deposits of the Portage Lake Volcanics, Michigan: Their Implications with Respect to Canister Stability for Nuclear Waste Isolation in Columbia River Basalts beneath the Hanford Site, Washington. Rockwell Hanford Operations Technical Report RHO-BW-ST- 26P. Hanford, USA.

Dixon, D.A., N.A. Chandler and P.M. Thompson. 2001. The selection of sealing system components in AECL's 1994 Environmental Impact Statement. Ontario Power Generation Report 06819-REP-01200-10074-R00. Toronto, Canada.

Drake, H., B. Sandström and E-L. Tullborg. 2006. Mineralogy and geochemistry of rocks and fracture fillings from Forsmark and Oskarshamn: Compilation of data for SR-Can. SKB R-06-109. SKB, Stockholm, Sweden.

EUBA. 2011. Fact Sheet on Bentonite. The European Association of the Bentonite Producers (EUBA: Member of IMA-Europe). Brussels, Belgium.

Francis, J.E. 1988. A 50 million-year old fossil forest from Strathcona Fiord, Ellesmere Island, Arctic Canada: evidence for a warm polar climate. Arctic. 41 314-318.

Fujii, N., C.A. Arcilla, M. Yamakawa, C. Pascua, K. Namiki, T. Sato, N. Shikazono and W.R. Alexander. 2010. Natural analogue studies of bentonite reaction under hyperalkaline conditions: overview of ongoing work at the Zambales Ophiolite, Philippines. Proc. ICEM 2010 Conference, ASME, Washington, USA.

Gray, M.N. and B.S. Shenton. 1998. For better concrete, take out some of the cement. In Proc. 6th ACI/CANMET Symposium on the Durability of Concrete, Bangkok, Thailand.

Greenwood, D.R. and J.F. Basinger. 1994. The paleoecology of high latitude Eocene swamp forests from Axel Heiberg Island, Canadian High Arctic. Review of Palaeobotany and Palynology. 81 83-97.

Hellmuth, K-H. 1989. Natural analogues of bitumen and bitumenized waste. Finnish Centre for Radiation and Nuclear Safety, STUK-B-VALO 58, Helsinki, Finland.

Hellmuth, K-H. 1991. The existence of native iron – Implications for nuclear waste management. Helsinki, Finland: Finnish Centre for Radiation and Nuclear Safety. Report STUK-B-VALO 68.

Hofmann, B.A. 1999. Geochemistry of Natural Redox Fronts – A Review. Nagra Technical Report NTB 99-05. Wettingen, Switzerland.

IAEA. 1999. Use of Natural Analogues to Support Radionuclide Transport Models for Deep Geological Repositories for Long Lived Radioactive Wastes. International Atomic Energy Agency TECDOC-1109. Vienna, Austria.

Johnson, A.B. and B. Francis. 1980. Durability of Metals from Archaeological Objects, Metal Meteorites, and Native Metals. Battelle Pacific Northwest Laboratory PNL-3198. Hanford, USA.

Kolaříková, I. and R. Hanus. 2008. Geochemistry and mineralogy of bentonites from Ishirini (Libya). Chemie der Erde-Geochemistry. 68 (1) 61-68.

Laine, H. and P. Karttunen. 2010. Long-Term Stability of Bentonite: A Literature Review. Posiva Working Report WR 2010-53, Posiva, Eurajoki, Finland.

Linklater, C.M. (ed). 1998. A natural analogue study of cement buffered, hyperalkaline groundwaters and their interaction with a repository host rock II. Nirex Science Report, S-98-003, NDA-RWMD, Harwell, UK.

Longstaffe, F. 1993. Meteoric Water and Sandstone Diagenesis in the Western Canada Sedimentary Basis, in SG36: Diagenesis and Basin Hydrodynamics. American Association of Professional Geologists AAPG Special Volume. Tulsa, USA.

McKee, P. and D. Lush. 2004. Natural and Anthropogenic Analogues - Insights for Management of Spent Fuel. Nuclear Waste Management Organization Report APM-REF-06110-24105. Toronto, Canada.

Middleton, J.H. 1888. On the chief methods of construction used in ancient Rome. Archaeologie LI, 41 – 60.

Miller, W., R. Alexander, N. Chapman, I McKinley and J. Smellie. 2000. Geologic Disposal of Radioactive Wastes & Natural Analogues Volume 2. Elsevier/ Pergamon Press. Oxford, UK.

Milodowski, A.E., P.H.A. Nancarrow and B. Spiro. 1989. A mineralogical and stable isotope study of natural analogues of Ordinary Portland Cement (OPC) and CaO–SiO2–H2O (CSH) compounds. United Kingdom Nirex Safety Studies Report, NSS/R240, NDA, Moor Row, UK.

Milodowski, A.E., M.T. Styles and V.L. Hards. 2000. A Natural Analogue for Copper Waste Canisters: The Copper-uranium Mineralised Concretions in the Permian Mudrocks of South Devon, United Kingdom. Swedish Nuclear Fuel and Waste Management Company Report SKB TR-02-09. Stockholm, Sweden.

Nagra. 1988. Solidification of Swiss Radioactive Waste with Bitumen. National Cooperative for the Disposal of Radioactive Waste (Nagra). NTB 85-28. Baden, Switzerland (in German).

Oleson, J.P., C. Brandon, S.M. Cramer, R. Cucitore, E. Gotti and R.L. Hohlfelder. 2004. The ROMACONS Project: a Contribution to the Historical and Engineering Analysis of Hydraulic Concrete in Roman Maritime Structures. Intern. J. Nautical Archaeol., 33.2, 199–229. doi: 10.1111/j.1095-9270.2004.00020.x

Pitts, L. and A. St. Joseph. 1985. Inchtuthil Roman Legionary Fortress Excavation 1952-1965. Society for the Promotion of Roman Studies. Britannia Monographs Series 6. London, England.

Pusch, R., H. Takase and S. Benbow. 1998. Chemical processes causing cementation in heat-affected smectite – the Kinnekulle bentonite. SKB Technical Report TR-98-25, Stockholm, Sweden.

Schamel, S. 2009. Strategies for in situ recovery of Utah’s heavy oil and bitumen resources. Utah Geological Survey, Open File Report 551. Salt Lake City, USA.

Selby D. and R.A. Creaser. 2005. Direct Radiometric Dating of Hydrocarbon Deposits Using Rhenium-Osmium Isotopes. Science 308, 1293-1295.

Smellie, J.A.T. and F. Karlsson. 1996. A reappraisal of some Cigar Lake issues of importance to performance assessment. SKB Technical Report TR 96-08, SKB, Stockholm, Sweden.

Tait, J.C., H. Roman and C.A. Morrison. 2000. Characteristics and Radionuclide Inventories of Used Fuel from OPG Nuclear Generating Stations Volumes 1 and 2. Ontario Power Generation Report 06819-REP-01200-10029-R00. Toronto, Canada.

Vola, G., E. Gotti, C. Brandon, J.P. Oleson and R.L. Hohlfelder. 2011. Chemical, mineralogical and petrographic characterization of Roman ancient hydraulic concretes cores from Santa Liberata, Italy, and Caesarea Palestinae, Israel. Periodico di Mineralogia 80, 317–338.

Wersin, P., L.H. Johnson and I.G. McKinley. 2007. Performance of the bentonite barrier at temperatures beyond 100°C: A critical review. Physics and Chemistry of the Earth 32 780-788.

Wilson, J., D. Savage, A. Bond, S. Watson, R. Pusch and D. Bennett (2011). Bentonite: a review of key properties, processes and issues for consideration in the UK context. Quintessa Report QRS-1378ZG-1.1 for the NDA-RWMD, Quintessa, Henley - on - Thames, UK.

WIPP. 2009. Waste isolation pilot plant hazardous waste facility permit renewal application September 2009: Appendix I2, Appendix A, Material specification shaft sealing system compliance submittal design report. Waste Isolation Pilot Plant, U.S. Department of Energy, Carlsbad, USA.

Yoshida, H. 1994. Relation between U-series nuclide migration and microstructural properties of sedimentary rocks. Applied Geochemistry, 9 (5), 479-490.

10. QUALITY ASSURANCE

10.1 Introduction

The NWMO defines the organization and the governance of the organization in the Governance Process Description, NWMO-PD-AD-0001-R009 (NWMO 2015a), which is authorized by the President. The Governance Process Description includes management's commitment to safety and quality as expressed in Sections 5.2 Management Commitment and 5.3 Quality Policy. This chapter describes how project activities important to safety in this illustrative postclosure safety assessment were conducted under an appropriate quality assurance framework.

10.2 APM Safety Case Project Quality Plan

The APM Safety Case Project Quality Plan (PQP) APM-PLAN-00120-0002-R003 (NWMO 2015b) was prepared in accordance with the Quality Policy by the NWMO Director, Performance Assurance and approved by the Project Manager for use during the preparation of this safety assessment. The quality plan was superseded by the APM Technical and Design Project Quality Plan, APM-PLAN-01913-0222-R000 (NWMO 2016), which was followed for work completed since its issue in 2016. Both of these APM PQPs meet the requirements of both CSA N286-12 and ISO 9001:2008.

The quality program applies to all organizational units with responsibilities for the preparation of the safety assessment. The following processes implement the program:

- A managed system consisting of governing documents that prescribe controls and responsibilities to ensure activities are carried out in a quality assured, effective manner by qualified personnel;
- Individual accountability for implementing and adhering to the managed system elements;
- A specific APM Work Plan identifying project scope, work breakdown, responsibilities and controls; and
- Evaluation and enhancement of the program elements through continuous improvement processes.

Selected vendors and suppliers are required to be qualified to appropriate quality assurance standards defined by the NWMO. Each of these vendors and suppliers selected is required to submit a detailed quality assurance and inspection plan for review and approval.

The quality program includes provisions for planned audits and assessments designed to provide a comprehensive, critical and independent evaluation of project activities. These audits and assessments cover the overall quality program, sub-tier programs, and interfaces between programs. The audits and assessments monitor compliance with governing procedures, standards and technical requirements, and confirm that quality program requirements are being effectively implemented. Audit and assessment results are documented, reported to and evaluated by a level of management having sufficient breadth of responsibility to assure actions are taken to address the findings.

Additional oversight of activities is provided through regular project monitoring and reporting, self-assessment conducted directly by the accountable managers and use of the non-conformance and corrective action program. In particular, the corrective action program assures that non-conformance conditions are identified, documented, reported, evaluated and corrected in a timely manner. Self-assessments are used by managers to evaluate conformance with procedures and plans and to improve the quality of the work execution.

The applicable APM PQP is supported by NWMO governance that establishes expectations for engineering and design, safety assessment, procurement, occupational health and safety, environmental protection, product and services approval, document control and record keeping.

The following are key elements of the APM PQP:

- Project specific quality objectives are established.
- Each person working on the project is responsible for achieving and maintaining quality and management is responsible for providing adequate resources and evaluating the quality of the work.
- APM project work is performed in accordance with applicable NWMO governing documents and established processes and procedures.
- Specific requirements for design, safety assessment and technical studies involving computer modeling are described.
- All work is conducted by qualified individuals.
- When work within the scope of the APM project is performed by another organization, the consultant/contractor performs work in compliance with ISO 9001:2008 or CSA N286-12 as appropriate and in compliance with an approved work specific quality plan and APM project-specific governing documents. When a consultant/contractor provides a specialized technical service, and their quality management system is not based on a recognized system, their quality management system may be accepted if it meets internal quality objectives and requirements.
- APM work is verified. Furthermore for work conducted by contractors, project quality plans are approved and include appropriate verification procedures for deliverables including verification process documentation.
- Experience from related industries is obtained through planned activities including information exchanges with other nuclear waste management organizations, participation in technical conferences, contracting with organizations and obtaining independent expert review and input.
- NWMO APM project personnel have access to observe and verify consultants/contractors' quality processes and examine quality assurance documentation.
- Documents considered to be quality assurance records as per APM-LIST-08133-0001-R001, Quality Assurance Documents (NWMO 2014), are transmitted into NWMO records.
- Targeted periodic assessments of work are performed on the APM project. Work performed by NWMO project personnel is assessed for compliance with the APM PQP and applicable procedures. Work performed by consultants/contractors and their subcontractors are assessed to confirm that it is being performed in compliance with their work specific quality plans.

10.3 Examples of Peer Review and Quality Assurance

Experienced contractors worked with NWMO to carry out the illustrative postclosure safety assessments for the APM project under approved project specific quality plans. The contractors committed to provide high quality work through effective application of a quality system that fostered best practice and included processes for continual improvement.

Safety assessments were conducted consistent with NWMO's governance, NWMO-PROC-EN-0003-R003 Safety Assessment Procedure (NWMO 2015c). For this illustrative safety case, formally accepted data clearance forms were used between the geoscience, engineering and safety assessment teams to ensure agreement on pertinent information and data. A final authorized data clearance form was also used to confirm data freeze. Software and reference datasets were procured, developed and maintained consistent with NWMO's governance, NWMO-PROC-EN-0002-R002 Technical Computer Software Procedure (NWMO 2013). The sensitivity cases examined in this safety assessment provide an indication of the potential range of variability of the base case. The disruptive event scenarios illustrate the upper boundaries of these unlikely compromises of the multiple safety barriers. The confidence in the software models used for this illustrative safety assessment is further reinforced by the consistency in terms of nuclide transport observed between the simple and complex models as described in Section 7.8.1.4, and the consistency between the deterministic and probabilistic results.

NWMO and independent peer review of key results and conclusions in the illustrative postclosure safety assessment was planned by the NWMO and completed. The comments and suggested improvements provided by the independent reviewers have been addressed and incorporated as appropriate into this illustrative safety assessment.

10.4 Future Safety Case Quality Assurance

Once an actual repository site is selected, on-site work will commence to characterize the site in terms of its geophysical and environmental properties. Simultaneously, the conceptual design will progress towards the detailed design required for licensing and ultimately container manufacture and facilities construction. The project quality assurance plan will necessarily expand in scope to ensure that the site characterization, detailed repository design, detailed container design, associated preclosure and postclosure safety assessments and environmental assessment are prepared under a comprehensive and robust quality assurance regime. At an appropriate time in the future, specific quality assurance plans will be prepared and implemented for the manufacturing and qualification of the used fuel containers and the construction and commissioning of the used fuel transfer facility and the repository.

10.5 References for Chapter 10

CSA N286-12. Management System Requirements for Nuclear Facilities. Canadian Standards Association. Canada.

ISO 9001:2008. Quality Management Systems Requirements. International Organization for Standardization.

NWMO. 2013. Technical Computer Software Procedure. Nuclear Waste Management Organization Procedure NWMO-PROC-EN-0002-R002. Toronto, Canada.

NWMO. 2014. APM Deep Geological Repository Project Quality Assurance Documents. Nuclear Waste Management Organization List APM-LIST-08133-0001-R001. Toronto, Canada.

NWMO. 2015a. Governance Process Description. Nuclear Waste Management Organization NWMO-PD-AD-0001-R009. Toronto, Canada.

NWMO. 2015b. APM Safety Case Project Quality Plan. Nuclear Waste Management Organization Plan APM-PLAN-00120-0002-R003. Toronto, Canada.

NWMO. 2015c. Safety Assessment Procedure. Nuclear Waste Management Organization Procedure NWMO-PROC-EN-0003-R003. Toronto, Canada.

NWMO. 2016. APM Design and Technical Project Quality Plan. Nuclear Waste Management Organization Plan APM-PLAN-01913-0222-R000. Toronto, Canada.

11. SUMMARY AND CONCLUSIONS

11.1 Safety Case

This report presents an illustrative case study of a postclosure safety assessment applied to examine the long-term safety of a multi-barrier deep geological repository design for Canada's used nuclear fuel within a hypothetical crystalline Canadian Shield setting.

The safety case for a repository is a set of arguments or attributes that collectively define the basis for the safety of the repository. Table 11-1 summarizes the safety attributes or arguments considered within the present hypothetical case study, and where further information on these is presented.

The purpose of this case study is to present a postclosure safety assessment and to illustrate how expectations, documented in CNSC Guide G-320 (CNSC 2006), subsequently referred to as G-320, are satisfied. Table 1-4 provides links between G-320 and sections of this report.

It should be recognized that this report is not intended to provide a full deep geological repository safety case as described in G-320. Aspects of G-320 that are relevant to this case study are extracted from this guidance document and included in grey 'text' boxes throughout this chapter.

> ***Developing a long-term safety case, G-320 Section 5.0:***
>
> *Demonstrating long term safety consists of providing reasonable assurance that waste management will be conducted in a manner that protects human health and the environment. This is achieved through the development of a safety case, which includes a safety assessment complemented by various additional arguments...*

This summary chapter is intended to highlight the means by which a safety assessment methodology has been applied to evaluate the safety and the associated uncertainty in the performance of a repository for nuclear used fuel in a crystalline setting. The strategy adopted is based, in part, on a defence-in-depth approach consistent with current international practice. The results of the safety assessment provide useful insight into the performance of the multi-barrier repository design and specific features of the design that could influence long-term performance.

Table 11-1: Summary of Key Safety Attributes

1. The geologic setting provides isolation and containment.	**Section**
1.1. The repository depth isolates the waste and repository components from surface changes created by human activities or natural events.	Assumed, Section 1.6.3.1
1.2. The repository is enclosed by stable, competent and low permeability rock.	Assumed, Section 1.6.3.1; also Section 2.2
1.3. The hydrogeologic setting that encloses the repository restricts groundwater and radionuclide movement.	Section 2.3
1.4. The mineralogy of the host rock, and the composition of the ground/porewater, are compatible with the engineered barriers.	Section 5.4 and Section 5.5
1.5. The host rock mineralogy and the composition of the ground/porewater are favourable for mitigating radionuclide movement.	Section 7.5.2
1.6. Natural resource potential is low within the repository geologic setting.	Assumed, Section 1.6.3.1
1.7. Seismic hazard is low.	Assumed, Section 1.6.3.1
1.8. The host rock is predictable and amenable to characterization.	Assumed, Section 1.6.3.1
2. The site geology has long-term stability.	
2.1. The hydrogeologic conditions at repository depth are stable and resilent to internal and external perturbations, including glaciation.	Section 2.3 and Section 5.1
2.2. The host rock is capable of withstanding thermal and mechanical stresses induced by internal and external perturbations, including glaciation.	Section 5.2
2.3. The repository conditions including chemistry and physical condition important for safety are not influenced by internal and external perturbations, including glaciation.	Section 5.2 and Section 5.5
2.4. Rate of erosion is low.	Section 5.1.2.3
2.5. Repository safety is not influenced by strong ground motions associated with rare earthquakes.	Section 5.1.1 and Section 5.2.6.3
3. The site supports robust construction and operation.	
3.1. Repository host rock conditions allow safe construction and operation.	Not covered in this study
3.2. Safe transportation route to site.	Not covered in this study
3.3. Frequency of severe natural events at site during construction and operation is low.	Not covered in this study
3.4. Robust facility design for safe construction and operation.	Not covered in this study
3.5. The site is not located in a sensitive ecological environment.	Not covered in this study

4. The used fuel wasteform is a barrier which contributes to the containment of radionuclides.	
4.1. Most radionuclides are immobile within the uranium oxide grains of the used CANDU fuel.	Section 5.3.3
4.2. The used CANDU fuel grains are mechanically durable and not materially impacted by radiation damage or helium gas buildup.	Section 5.3.3
4.3. The used fuel has low solubility under conditions of a failed container with contact with ground/porewater.	Section 5.4.4.7
4.4. The Zircaloy cladding provides a barrier to contact between ground/porewater and used fuel in a failed container.	Section 5.3.5
4.5. The Zircaloy cladding corrodes slowly under conditions of a failed container in contact with ground/porewater.	Section 5.4.4.6
5. Container and sealing systems are barriers which contribute to the isolation and containment of radionuclides.	
5.1. The container is designed for the underground conditions at timeframes relevant to repository safety.	Section 4.3.1 and Section 5.4
5.2. Inspection methods would ensure the container is built consistent with design specifications.	Not covered in this study
5.3. The in-room buffer system holds and protects the containers.	Section 4.3.2, 4.8.2 and Section 5.5
5.4. Engineered seals isolate the placement rooms from the access tunnels.	Section 4.3.2, 4.8.2
5.5. Shaft backfill and seals isolate the repository from the surface.	Section 4.3.2, 4.12
6. **Repository construction, operation and closure supports the long term repository performance objective.**	
6.1. Repository layout and spacing are designed for long-term structural stability.	Section 4.8 and Section 5.2.6
6.2. Repository design and construction methods minimize the excavation damaged zone.	Section 5.2.5
6.3. Materials used in repository construction and operation will not compromise long-term performance.	Section 5.2.4
6.4. Institutional controls and monitoring will verify performance.	Section 1.6.3.4
7. **The repository is robust to accidents and unexpected events.**	
7.1. Credible accident during operations would have low effects on public and environment.	Not covered in this study
7.2. Postclosure analyses show low effect from normal or expected scenarios, with large safety margin to regulatory criteria.	Section 7.14
7.3. Postclosure analyses show risk from disruptive scenarios to be acceptable.	Section 7.14

11.2 Repository System

System description, G-320 Section 7.3:

It is recognized that the system description may be less complete and rigorous early in the licensing lifecycle, and that the information used in long term assessments of safety for the purpose of design optimization or to support an environmental assessment or a licence application may therefore need to use some default or generic data. As licensing progresses through the facility's lifecycle, as-built information and operational data are acquired, and the site characteristics become better understood. It is expected that assessments of long term safety that are made later in the licensing lifecycle will be based on updated and refined models and data, with less reliance on default, generic, or assumed information, resulting in more reliable model results.

Section 4 of G-320 identifies several methods for long-term waste management, including surface facilities, near-surface facilities and deep geological facilities. As previous mentioned, this report describes the currently envisioned deep geological multiple barrier repository design. This design and waste management approach is commensurate with the waste's radiological, chemical, and biological hazard to the health and safety of persons and the environment.

The deep geological repository system is described in Chapters 2 through 5 of this report where:

- Chapter 2 describes the hypothetical geosphere setting;
- Chapter 3 describes the characteristics of the used nuclear fuel;
- Chapter 4 describes the repository design concept; and
- Chapter 5 describes how key components of the system will interact with each other and with the environment in the long term.

The key points from these chapters are summarized in this section along with parameters identified in the safety assessment as being influential to repository performance.

11.2.1 Geologic Description of the Hypothetical Site

Information related to the geologic characteristics of the site necessary to perform the illustrative safety assessment is presented in Chapters 1 and 2. Site-specific characterization activities at a candidate site would be designed to gather information on a broad range of geologic characteristics that would be used to develop a Descriptive Geosphere Site Model and support a repository safety case. For the purpose of this illustrative case study several key attributes have been assumed for the site as listed in Chapter 1 (Section 1.6.3.1).

Such attributes that normally would be confirmed through site-specific investigation include:

- The repository is positioned nominally at a depth of 500 m below ground surface;
- The repository is located in an area of low seismic hazard;
- The repository location is not associated with potable groundwater resources;
- The repository location is not associated with economically viable natural resources;
- The groundwater system at repository depth is electrochemically reducing;
- The host rock formation can withstand transient thermal and mechanical stresses; and

- The rates of site uplift and erosion are sufficiently small so as not to influence repository safety.

Specific site characteristics for the case study are described in Chapter 2. In particular, this chapter describes the spatial distribution: geologic, structural, physical and chemical hydrogeologic and geomechanical properties of the rock mass. The selection of these properties has been informed by historic work conducted within the Canadian Nuclear Fuel Waste Management Program. The information presented in Chapter 2 outlines the properties and long-term behaviour of the groundwater system for the reference case site. In addition to the reference case, alternative conceptual models are described with the intent of outlining a range of possible characteristics and properties at a crystalline site. The uncertainty associated with these alternative models is explored through sensitivity, bounding and 'what-if' simulations performed as part of the case study safety assessment.

11.2.2 Used Fuel

The characteristics of the used fuel are described in Chapter 3. The durability of used fuel and distribution of radionuclides within the fuel are identified as characteristics of the multi-barrier system. These characteristics contribute to the low dissolution rate of the fuel and hence the low release rate of radionuclides from the fuel matrix.

11.2.3 Design Concept

Licensing considerations, G-320 Section 4.3:

The design of a nuclear facility should be optimized to exceed all applicable requirements. In particular, a radioactive waste management facility should more than meet the regulatory limits, remaining below those limits by a margin that provides assurance of safety for the long term.

The repository design concept is presented in Chapter 4. As part of the multi-barrier system, two engineered barriers are included in this concept; a copper-coated container and a clay-based sealing system. The design will be further refined and optimized for a licence application. This approach is consistent with G-320, which identifies that the repository facility should more than meet the regulatory limits and remain below those limits by a margin that provides assurance of safety for the long term.

Waste management system, G-320 Section 4.1:

Waste management system for long term storage and disposal of waste refer to the combination of natural and engineered barriers and operational procedures that contribute to safely managing the waste. Long term assessment of these systems can provide information that can be used when making decisions concerning:

1. *Selection of an appropriate site;*
2. *Site characterization;*
3. *Selection of suitable design options during planning;*
4. *Optimization of selected design(s), including minimization of operational and post-operational impacts; and*
5. *Development of construction, operation, and decommissioning strategies and plans.*

Key assumptions in this case study include:

- The repository was positioned at a depth of 500 m. In an actual siting process, the repository location and footprint geometry would be designed to improve safety based on site-specific host rock conditions.
- The repository was positioned such that 100 m of intact crystalline rock existed between the placement room and a transmissive (10^{-6} m/s) structural feature connected to the ground surface.
- A long-lived container is envisaged with a 3 mm copper corrosion barrier. Research indicates that 1.3 mm would be sufficient for corrosion protection for 1 million years under reducing conditions. The thicker copper-coated containers provide a greater margin of safety.
- Highly compacted low permeability bentonite encloses the containers.
- The sealing systems have a low permeability.

The influence of these design features and their properties on repository performance is explored through the safety assessment summarized in Section 7.14. For example, sensitivity and complementary bounding analyses are used to illustrate the effects of distance to a discrete transmissive fracture (i.e., 10 m), increased fuel release parameters, increased container failure and sorption.

Chapter 5 describes the repository system, and how key components of the system will interact with each other and the environment in the long term, consistent with the G-320 guidance.

The long-term safety assessment presented in this report provides information that can be used to support and inform future decision making as described in G-320.

11.3 Safety Assessment

A structured approach is used to conduct the postclosure safety assessment where two classes of scenarios are assessed, consistent with Sections 5 and 7 of G-320. More specifically, the expectation to demonstrate the understanding of the system through a well-structured, transparent, and traceable methodology is described in this report.

> ***Performing long term assessments, G-320 Section 7.0:***
>
> *The CNSC expects the applicant to use a structured approach to assess the long term performance of a waste management system. Although long term assessments are done with different levels of detail and rigor for different purposes, the overall methodology for performing them should include the following elements:*
>
> 1. *Selection of appropriate methodology;*
> 2. *Assessment context;*
> 3. *System description;*
> 4. *Timeframes;*
> 5. *Assessment scenarios; and*
> 6. *Development of assessment models.*

The approach uses a systematic scenario identification process that acknowledges the timeframes of interest and that identifies features, events, and processes, which could have an impact on the repository's safety features, as described in Chapter 6. The different assessment strategies, including key assumptions and rationale, are described and complementary indicators are presented in Chapter 7, and summarized in this section.

The **normal evolution scenario** is based on a reasoned extrapolation of the hypothetical site and repository features, events and processes. The reference case accounts for the expected degradation of the site and repository over time, and it involves no release of radionuclides. The computer models and key assumptions are discussed in Chapter 7 and analyses of impacts are presented for a Base Case and a range of variant cases in which the effects of changes in physical and chemical conditions are examined.

Disruptive event scenarios examine the occurrence of unlikely events leading to the unexpected circumvention of barriers and loss of containment. Chapter 7 presents the methods, assumptions and results associated with the analysis of disruptive events.

> ***Criteria for protection of persons and the environment, G-320 Section 6.2:***
>
> The regulatory requirements for protection of persons and the environment from both radiological and non-radiological hazards of radioactive wastes lead to four distinguishable sets of acceptance criteria for a long term assessment:
>
> 1. *Radiological protection of persons;*
> 2. *Protection of persons from hazardous substances;*
> 3. *Radiological protection of the environment; and*
> 4. *Protection of the environment from hazardous substances.*

The results from the normal evolution scenario and disruptive events are compared against interim acceptance criteria in Chapter 7 consistent with the guidance of G-320. Interim acceptance criteria selected to meet the expectations in Section 6 of G-320 are proposed in Section 7.1 for each of the following categories:

- Radiological protection of persons;
- Protection of persons from hazardous substances;
- Radiological protection of the environment; and
- Protection of the environment from hazardous substances.

11.3.1 Assessment Strategies

Use of different assessment strategies, G-320 Section 5.2:

The strategy used to demonstrate long term safety may include a number of approaches, including, without being limited to:

1. Scoping assessments to illustrate the factors that are important to long term safety;
2. Bounding assessments to show the limits of potential impact;
3. Calculations that give a realistic best estimate of the performance of the waste management system, or conservative calculations that intentionally over-estimate potential impact; and
4. Deterministic or probabilistic calculations, appropriate for the purpose of the assessment, to reflect data uncertainty.

Any combination of these or other appropriate assessment strategies can be used in a complementary manner to increase confidence in the demonstration of long term safety.

Key elements are included in the approach to provide relevant information to assess long-term safety, as follows:

- Performing a screening exercise to identify potentially significant dose contributing radionuclides and hazardous substances so that subsequent assessments can focus on these.
- Conducting 3-dimensional hydrogeological modelling of the groundwater system(s) hosting the repository.
- Conducting a realistic best estimate of performance in the reference case (i.e., containers remain intact with no releases).
- Performing deterministic and probabilistic calculations of radionuclide transport from fuel to surface. This includes analysis of both normal and disruptive scenarios accompanied by sensitivity cases and bounding assessments.
- Estimating dose consequences for a critical group assumed to be farming on the surface biosphere directly above the repository.

11.3.2 Modelling Tools and Computer Codes

As discussed in Sections 7.3 and 7.4, appropriate modelling tools and computer codes are applied to assess key aspects of the repository's components and specific scenarios, consistent with the expectations in Section 7.6 of G-320.

The main computer models are FRAC3DVS-OPG v1.3 and SYVAC3-CC4 v4.09.2. These codes and the reference datasets are maintained under a NWMO software quality assurance system. They are codes that have been in use for Canadian repository assessments for many years, with FRAC3DVS being a commercially available code.

Developing and using assessment models, G-320 Section 7.6:

An assessment model should be consistent with the site description, waste properties, and receptor characteristics, and with the quality and quantity of data available to characterize the site, waste, exposure pathways, and receptors. A systematic process should be used to ensure that the set of data used for developing the assessment model is accurate and representative. Complex models should not be developed if there is not sufficient data to support them. The use of generic or default data in place of site-specific data in developing the conceptual and computer models may be acceptable when there is no site-specific data available, such as in early stages of development; however, with the acquisition of as-built information and operational data, and increased understanding of site characteristics throughout the facility lifecycle, site-specific data should be used.

Confidence in assessment models:

Confidence in the assessment model can be enhanced through a number of activities, including (without being limited to):

1. *Performing independent predictions using entirely different assessment strategies and computing tools;*
2. *Demonstrating consistency between the results of the long term assessment model and complementary scoping and bounding assessments;*
3. *Applying the assessment model to an analog of the waste management system;*
4. *Performing model comparison studies of benchmark problems;*
5. *Scientific peer review by publication in open literature; and*
6. *Widespread use by the scientific and technical community.*

The codes are used in a complementary manner, with FRAC3DVS-OPG providing detailed 3-dimensional flow and transport results for a limited number of cases, and SYVAC3-CC4 extending the results to a broad range of nuclides and sensitivity cases. The simplified SYVAC-CC4 model has been derived from the detailed FRAC3DVS-OPG transport results for I-129, and then verified for other specific radionuclides that represent a range of decay and transport parameters (i.e., C-14, Cl-36, Ca-41, Se-79, Cs-135, U-238/U-234).

To explore uncertainties arising from variability in the data used in the assessment predictions, SYVAC3-CC4 is also used to carry out probabilistic safety assessments of the entire repository system. Over 100,000 simulations are performed in which hundreds of input variables are simultaneously varied according to user defined parameter distributions.

11.3.2.1 Key Assumptions and Conservatisms in Modelling

Conservative over-estimates, G-320 Section 5.2.2:

A *conservative approach should be used when developing computer codes and models, and assumptions and simplifications of processes to make them more amenable for inclusion in computer models should not result in under-estimation of the potential risks or impacts*.

Chapter 7 describes the key attributes for the Base Case of the normal evolution scenario. The illustrative assessment presented in this report uses different strategies consistent with expectations in G-320. The assessment of the Base Case includes the following conservatisms as described in Chapter 7, Table 7-3:

- Containers with undetected defects are assumed in the normal evolution scenario, with the defects present at the time of container placement;
- The penetrated containers fill with water immediately;
- No credit is taken for the presence of the fuel sheath in maintaining fuel integrity and in preventing contact of the fuel matrix with water that may enter the container;
- No credit is taken for the effect of hydrogen gas (H_2) (produced by corrosion of the container) on the dissolution rate of the uranium oxide fuel (UO_2) fuel;
- No credit is taken for the effect of iron oxides (produced by corrosion of the container) in reducing the container internal void volume and providing a high surface area for adsorption of some of the radionuclides released from the fuel;
- No credit is taken for the likely filling of the defect with bentonite and/or corrosion products which could significantly increase the transport resistance;
- The defective containers are positioned in the repository location with the shortest travel time to the surface;
- A 100 m deep well is included in the assessment. It is positioned in the location that maximizes the dose consequence;
- All major fractures extending to depth have high hydraulic conductivity (10^{-6} m/s); and
- Conservative properties are assigned to the critical group (e.g., daily energy need, obtaining all food, fuel, water and building material locally, all drinking and irrigation water taken from the well, etc.).

Since this Base Case assumes a constant temperate climate, Section 7.8.1.4 also discusses the anticipated effects of glaciation on the assessment.

Analyzing uncertainties, G-320 Section 8.2:

A formal uncertainty analysis of the predictions should be performed to identify the sources of uncertainty. This analysis should distinguish between uncertainties arising from:

1. *Input data;*
2. *Scenario assumptions;*
3. *The mathematics of the assessment model; and*
4. *The conceptual models.*

These conservatisms are further described as part of the approach to assess uncertainties in Chapter 8. The division of uncertainties into scenario, model and data uncertainties is consistent with the guidance of G-320.

11.3.3 Normal Evolution Scenario

Normal evolution scenario, G-320 Section 7.5.1:

A normal evolution scenario should be based on reasonable extrapolation of present day site features and receptor lifestyles. It should include expected evolution of the site and degradation of the waste disposal system (gradual or total loss of barrier function) as it ages.

Depending on site-specific conditions and the timeframe for the assessment, a normal evolution scenario may need to include extreme conditions such as climate shifts or the onset of glaciations.

Consistent with the expectations in Section 7.5 of G-320, the Reference Case of the normal evolution scenario illustrates the expected evolution where all repository components meet their design specification and function as anticipated. As such, the used fuel containers remain intact essentially indefinitely (see Chapter 5) and no contaminant releases occur in the one million year time period of interest to the safety assessment.

The Base Case results are described in Section 7.7.2.3.3 and Section 7.8.2.1. The assessment illustrates repository performance for a scenario in which 10 containers are assumed to fail, with the first failure occurring after 1000 years and subsequent failures occurring at a rate of one container every 100,000 years thereafter.

For the Base Case, the primary dose contributor from the defective containers is determined to be I-129. These radionuclides are instantly released from the gap and grain boundary inventory in the fuel. They are relatively long-lived and mobile in the sub-surface environment. Other radionuclides, including actinides in particular, are only released by the very slow dissolution of the fuel and are retarded by sorption on the enclosing barrier systems.

The calculated peak total dose for this case is determined to be about 0.00025 mSv/year and occurs at about 23,000 years. The dose applies to a person living directly above the repository and as shown in Figure 7-152, I-129 is responsible for this dose consequence. It is about 1200 times less than the dose constraint of 0.3 mSv/year, and is a small fraction of the average natural background dose.

Section 7.8.2.1 also shows that the dose consequence for the Base Case is largely due to the use of well water. In the SYVAC3-CC4 biosphere model, well water is used for drinking, irrigation of food crops and for watering animals. Therefore, well sensitivity cases are presented in Section 7.8.2.2 to illustrate the effect of this assumption on safety assessment results. In particular, the dose consequence drops by approximately three orders of magnitude when it is assumed that water would be obtained by other means as opposed to using a well directly above the repository (i.e., positioned to receive maximum dose). The peak dose rate in this case drops to 1.4×10^{-7} mSv/year occurring at 28,000 years.

11.3.3.1 Results from Sensitivity Analyses and Bounding Assessments

Deterministic calculations, G-320 Section 5.2.3:

The mathematical approach to analyzing the scenarios in the safety case is guided by the purpose of the long term assessment. A deterministic model uses single-valued input data to calculate a single-valued result that will be compared to an acceptance criterion. Variations in input data values are taken into account in these calculations. To account for data variability, individual deterministic calculations must be done using different values of input parameters.

This is the approach used for performing sensitivity analyses (determining the response of model predictions to variations in input data) and importance analyses (calculating the range of predicted values that corresponds to the range of input values) of deterministic models.

To account for the variation in key input data values used in the Base Case, a number of sensitivity analyses are completed for key parameters as described in Section 7.2.2 and illustrated in Figure 7-1 (repeated as Figure 11-1 in this chapter). Some parameters are also pushed beyond the reasonable range of variations by setting their values to zero or by removing limits and running a set of bounding assessments, where a specific parameter is completely ignored. The identified parameters, the variation in their values and the rationale for selecting these cases are summarized in Chapter 7, Table 7-5.

The impacts are determined from simulations performed with either the FRAC3DVS-OPG or the SYVAC3-CC4 codes. The FRAC3DVS-OPG code does not have a biosphere model and therefore its results are presented in terms of I-129 transport to the surface. This provides a reasonable estimate of potential impacts by comparison with the I-129 transport to surface for the normal evolution scenario, since SYVAC3-CC4 simulations show that I-129 dominates the dose consequence.

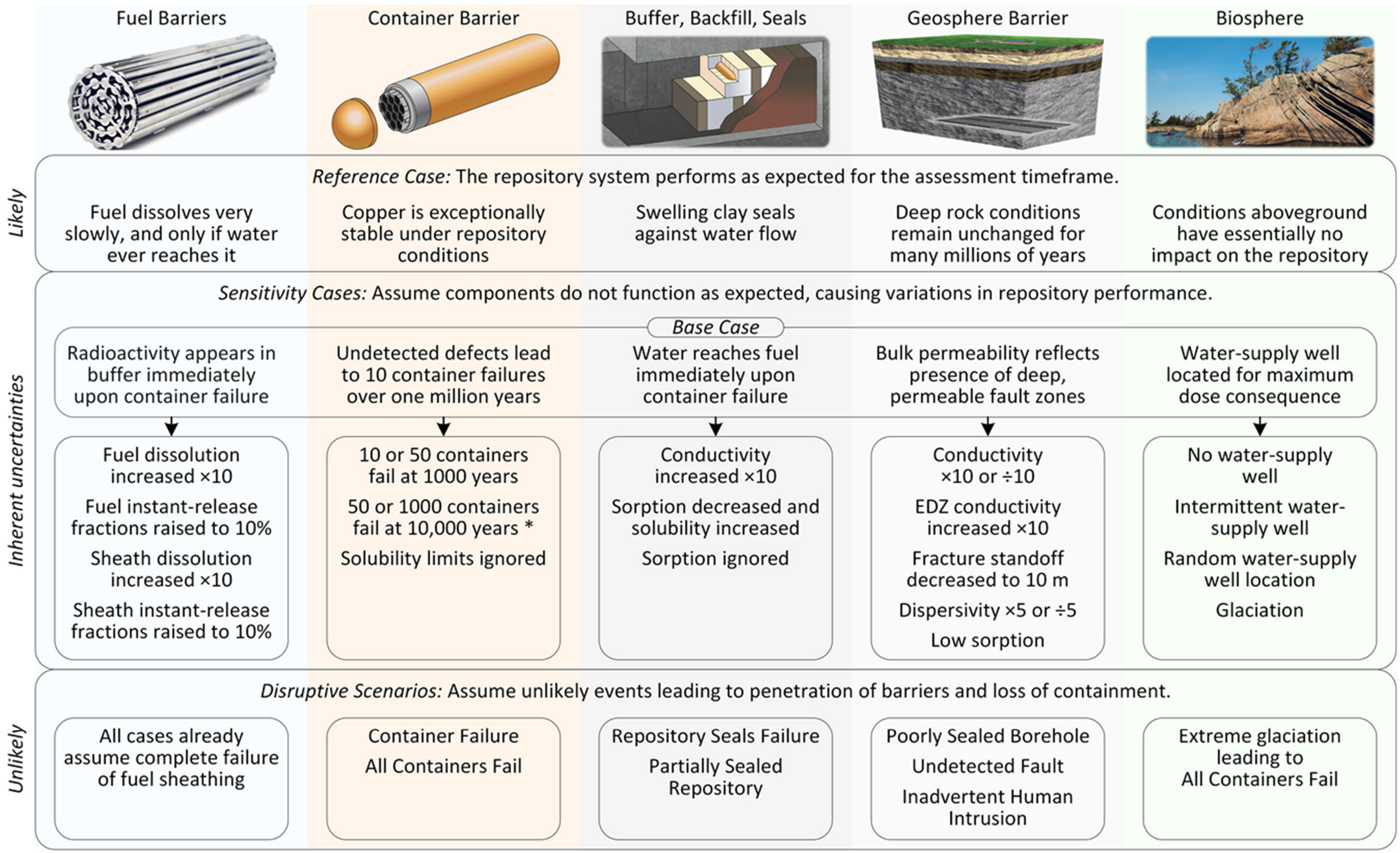

Note: Hypothetical container failures all occur in the one location that would yield the largest dose consequence. The case marked '*' is an exception, where hypothetical container failures are equally likely to occur at all locations across the repository.

Figure 11-1: Illustration Showing Normal Evolution Scenario, Sensitivity Studies, and Disruptive Event Scenarios

A summary of the key cases, a comparison against the interim acceptance criterion and the key findings are presented in Chapter 7, Table 7-62 and illustrated in Figure 11-2. The comparison of assessment results with interim acceptance criteria is consistent with the guidance in Section 8 of G-320.

The sensitivity analyses show that the impact on dose remains acceptable when key parameters are varied. The sensitivity analyses with the most significant impact on dose are from failing more containers earlier, increasing the dissolution rate of used fuel and assessing the effects of glaciation. The dose consequence is 50 times greater than the Base Case when 50 containers fail early and it is 6.2 times greater than the Base Case when the fuel dissolution is increased by a factor of ten. These remain 23 and 191 times below the interim dose acceptance criterion of 0.3 mSv/year respectively with the peak dose arrival time not materially changed from the Base Case, i.e., slightly longer than 23,000 years.

When the hydraulic conductivity of the rock mass enclosing the repository is varied, the peak dose consequence relative to the Base Case is directly affected and the peak time is inversely affected. For the highest case when the hydraulic conductivity is 10 times higher, the peak dose is 2.6 times greater than the Base Case and occurs at 5000 years.

Some sensitivity cases are found to have a minimal to no impact on dose in this case study as shown in Chapter 7, Table 7-62 and illustrated in Figure 11-2.

11.3.3.2 Results from the Probabilistic Analysis

> ***Probabilistic calculations, G-320 Section 5.2.3:***
>
> *Probabilistic models can explicitly account for uncertainty arising from variability in the data used in assessment predictions. Such models may also be structured to take account of different scenarios (as long as they are not mutually exclusive) or uncertainty within scenarios. Probabilistic models typically perform repeated deterministic calculations based on input values sampled from parameter distributions, with the set of results expressed as a frequency distribution of calculated consequences. Frequency multiplied by consequence is interpreted as the overall potential risk of harm from the waste management system.*

The results from the probabilistic cases are presented in Chapter 7, consistent with the expectations of G-320 in Section 5.2 on the use of different assessment strategies, where all parameters represented by probability distributions are simultaneously varied. In this case study, relevant parameters for contaminant release and transport were varied whereas the parameters associated with groundwater flow were not.

The first case, in which the number, location and failure times of the 10 defective containers are fixed at the same values as in the Base Case while all other available parameters are varied, gives a measure of the overall uncertainty in the Base Case. The 95th percentile dose rate emerging from 100,000 Monte Carlo simulations is 9.1×10^{-4} mSv/year or 3.6 times the Base Case value. This is a factor of 330 times less than the interim dose rate criterion of 0.3 mSv/year.

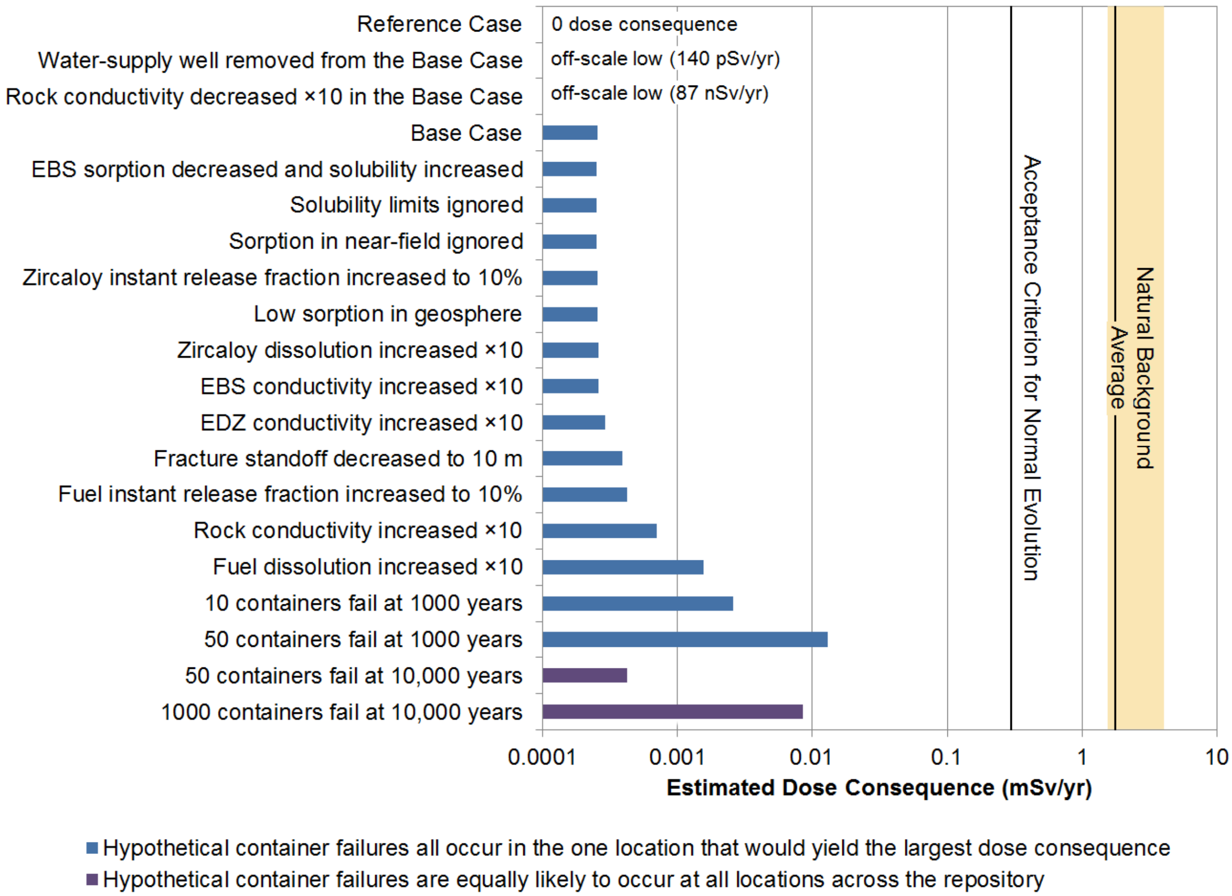

Figure 11-2: Key Results from Sensitivity Analyses and Bounding Assessments

The second probabilistic case, in which the number, location and failure times of the 10 defective containers are varied while all other available parameters are fixed, gives an indication of the effect of different container failure times and different container failure locations, relative to the well location adopted in the Base Case. The 95th percentile dose rate emerging from 100,000 Monte Carlo simulations is 2.2x10^{-4} mSv/year, a value less than that of the Base Case.

11.3.3.3 Results from Complimentary Indicators

> ***Complementary indicators of safety, G-320 Section 5.4:***
>
> *Several other safety indicators, such as those that reflect containment barrier effectiveness of site-specific characteristics that can be directly related to contaminant release and transport phenomena, can also be presented to illustrate the long term performance of a waste management system. Some examples of additional parameters include:*
>
> 1. *Container corrosion rates;*
> 2. *Waste dissolution rates;*
> 3. *Groundwater age and travel time;*
> 4. *Fluxes of contaminants from a waste management facility;*
> 5. *Concentrations of contaminants in specific environmental media (for example, concentration of radium in groundwater); or*
> 6. *Changes in toxicity of the waste.*

Complimentary indicators other than dose to an assumed human group are described in Section 7.13. Two indicators considered in this study are:

- Radiotoxicity concentration in a water body, for medium time scales; and
- Radiotoxicity transport from the geosphere, for longer time scales.

The results presented in Chapter 7 show that the indicators are well below reference values based on natural concentrations and fluxes. Other items were evaluated in the safety assessment but were not defined as “complimentary indicators.”

11.3.4 Disruptive Event Scenarios

> ***Disruptive event scenarios, including human intrusion, G-320 Section 7.5.2***
>
> *Disruptive event scenarios postulate the occurrence of unlikely events leading to possible penetration of barriers and abnormal loss of containment.*

Disruptive scenarios are assessed where barriers are assumed to fail due to unlikely failure mechanisms, as described in Section 6.2 of this report and consistent with Section 7.5 of G-320.

Chapter 6 also includes a review of the scenarios considered in assessments of deep repositories in other countries. The results, summarized in Table 6-5 of this report, show that most assessments have identified a limited number of additional scenarios that consider the degradation / failure of engineered and natural barriers by natural processes (e.g., earthquakes, climate change) and human actions (e.g., drilling, poor quality control). Although there are some scenarios identified that are not considered in the current study, these are either not relevant to a Canadian Shield site or were identified as relevant but not analyzed in this case study.

The scenarios considered in this study and key findings are summarized in Table 11-2.

The peak impacts are determined from simulations performed with either the FRAC3DVS-OPG or the SYVAC3-CC4 codes. The FRAC3DVS-OPG code does not have a biosphere model and therefore its results are presented in terms of I-129 transport to the surface. This provides a reasonable estimate of potential impacts by comparison with the I-129 transport to surface for the normal evolution scenario, since SYVAC3-CC4 simulations show that I-129 dominates the dose consequence, by more than two orders of magnitude at its peak.

Table 11-2: Summary of Key Findings from Disruptive Events

Scenario	Key Findings
All Containers Fail at 60,000 Years	Impact is significant • Peak dose rate occurs at 84,000 years • Dose consequence is 1.6 times below the disruptive events dose acceptance criterion of 1 mSv/a
All Containers Fail at 10,000 Years	Impact is significant • Peak dose rate occurs at 36,000 years • Dose consequence is 1.2 times below the disruptive events dose acceptance criterion of 1 mSv/a
Shaft Seal Failure	Impact is negligible • Peak dose rate occurs at 25,000 years • Dose consequence is 1200 times below the disruptive events dose acceptance criterion of 1 mSv/a
Fracture Seal Failure	Impact is negligible • Peak dose rate occurs at 25,000 years • Dose consequence is 1200 times below the disruptive events dose acceptance criterion of 1 mSv/a

The results from the all container failure scenarios, identified in Table 11-2, indicate that the containers are an important part of the multiple barriers in crystalline rock. The total peak impact is roughly proportional to the number of failed containers (a little less as some containers have long pathways to release). However the peak results are not highly sensitive to the time of container failure beyond 10,000 years. This occurs since the container failure time in both cases is larger than the fission product decay time and shorter than the half-life of I-129. The remaining actinides and most of any remaining fission products are retained and delayed in the other engineered and natural barriers so that the peak dose rate does not substantially change between these two cases.

The various seal failure scenarios have shown no effect on the predicted dose consequence in this study due to the distance between the containers with undetected defects and the degraded seals.

Disruptive event scenarios, including human intrusion, G-320 Section 7.5.2

Scenarios assessing the risk from inadvertent intrusion should be case-specific, based on the type of waste and the design of the facility, and should consider both the probability of intrusion and its associated consequences. Surface and near-surface facilities (e.g., tailings sites) are more likely to experience intrusion than deep geological facilities.

Scenarios concerning inadvertent human intrusion into a waste facility could predict doses that are greater than the regulatory limit. Such results should be interpreted in light of the degree of uncertainty associated with the assessment, the conservatism in the dose limit, and the likelihood of the intrusion. Both the likelihood and the risk from the intrusion should therefore be reported.

As described in Chapter 7, Section 7.9.1 presents a stylized analysis for the Inadvertent Human Intrusion Scenario. This scenario is a special case, as recognized in Section 7.5.2 of G-320, since it bypasses all the barriers put in place, and therefore the associated dose consequence could exceed the regulatory limit.

The results from the human intrusion assessment show a potential maximum dose to the drill crew of about 590 mSv, and to a site resident (i.e., someone farming on the site) of about 580 mSv, assuming early intrusion and improper management of the drill site.

This scenario is addressed through making it very unlikely; in part through placing the used fuel deep underground in a geologic setting with low mineral resource potential, poor prospects for potable groundwater resources, and by the use of institutional controls.

The likelihood of this event occurring is roughly estimated as 3×10^{-5} per year, which implies a risk of serious health effects of 9.4×10^{-7} per year. This is significantly less than the annual risk of 7×10^{-5} per year noted in G-320 for stochastic effects associated with the current regulatory limit of 1 mSv per year for dose to members of the public.

11.4 Future Work

The conceptual design and illustrative postclosure assessment presented in this report for a hypothetical site represent a single case study in crystalline rock. Other design concepts and other site conditions have been explored in other Canadian and international case studies.

Since this report is prepared for a hypothetical site and thus is not a full safety case, a number of aspects are not covered in detail. These are noted in Chapter 1. Also, the postclosure safety assessment illustrated the method and approach, but did not assess all scenarios or aspects of relevance for a full safety case (see Section 7.2.4).

There is ongoing work at NWMO to support siting activities, design development and other research. Findings will continue to be incorporated in case studies.

11.5 Conclusion

The current case study work, done at a very early stage in the APM Project, supports the continuing development of a deep geological repository for used fuel in crystalline rock. The current repository design concept and a corresponding postclosure safety assessment are included to illustrate methodology.

11.6 References for Chapter 11

CNSC. 2006. Regulatory Guide G-320: Assessing the Long Term Safety of Radioactive Waste Management, Canadian Nuclear Safety Commission. Ottawa, Canada.

THIS PAGE HAS BEEN LEFT BLANK INTENTIONALLY

12. SPECIAL TERMS

12.1 Units

a	annum
Bq	becquerel
°C	degree Celsius
cm	centimetre
d	day
dm	decimetre
g	gram
Gy	gray
GPa	gigapascal
h	hour
K	Kelvin
kg	kilogram
kgU	kilogram of Uranium
kJ	kilojoule
km	kilometre
kW	kilowatt
L	litre
m	metre
Ma	million years
mASL	metres above sea level
mBGS	metres below ground surface
mg	milligram
Mg	megagram
MJ	megajoule
mL	millilitre
mm	millimetre
mol	mole
MPa	megapascal
mSv	millisievert
mV	millivolt

mW	milliwatt
MW	megawatt
n	neutron (associated with neutron fluence)
nm	nanometre
nSv	nanosievert
Pa	pascal
ppm	parts per million
s	second
Sv	sievert
W	watt
wt%	mass percentage
µg	microgram
µm	micrometre
µSv	microsieverts

12.2 Abbreviations and Acronyms

1D	One Dimensional
2D	Two Dimensional
3D	Three Dimensional
ADS	Adsorbed
AECL	Atomic Energy of Canada
ALARA	As Low as Reasonably Achievable
APM	Adaptive Phased Management
AQ or (aq)	Aqueous
BCE	Before Common Era
BSB	Bentonite-Sand Buffer
CANDU	CANada Deuterium Uranium
CANLUB	Thin graphite coating between the fuel pellet and the fuel sheath
CC4	Canadian Concept Generation 4
CC	Constant Climate
CCME	Canadian Council of the Environment
CCM-UC	Copper Corrosion Model for Uniform Corrosion

CE	Common Era
CEAA	Canadian Environmental Assessment Act
CFU	Colony Forming Units
CNSC	Canadian Nuclear Safety Commission
CRT	Container Retrieval Test
C-S-H	In the C-S-H term, the “C” stands for Ca, “S” for Si, and “H” for H_2O. The hyphens indicate that no specific solid phases or proportions are implied.
CSA	Canadian Standards Association
C Steel	Carbon Steel
DBF	Dense Backfill
DDW	Dry Density Weight
DEM	Digital Elevation Model
DFN	Discrete Fracture Network
DGR	Deep Geological Repository
DGSM	Descriptive Geosphere Site Model
EA	Environmental Assessment
EBS	Engineered Barrier System
EBW	Electron-Beam Welding
EC	Environment Canada
E_{CORR}	Corrosion Potential
EDZ	Excavation Damage Zone
Eh	Oxidation Potential
EIS	Environmental Impact Statement
EMDD	Effective Montmorillonite Dry Density
ENEVs	Estimated No Effect Values
EPM	Equivalent Porous Media
ERICA	Environmental Risks from Ionising Contaminants Assessment
FEPs	Features, Events and Processes
FP	Fission Product
FSW	Friction-Stir Welding
GGM	Gas Generation Model
GLFA	Glycol-Lipid Fatty Acid
GM	Geometric Mean

GSD	Geometric Standard Deviation
GSM	Glacial Systems Model
HC	Health Canada
HCB	Highly-Compacted Bentonite
HEPA	High-Efficiency Particulate Air
HIM	Human Intrusion Model
HM	Hydromechanical
IAEA	International Atomic Energy Agency
ICRP	International Commission on Radiological Protection
ID	Inner Diameter
Imp	Impurity
ISO	International Organization for Standardization
LBF	Light Backfill
LGM	Last Glacial Maximum
LHHPC	Low-Heat, High-Performance Concrete
MIC	Microbiologically Influenced Corrosion
MLE	Mean Life Expectancy
NDE	Non-Destructive Examination
NDT	Non-Destructive Testing
NEA	Nuclear Energy Agency
NLFA	Neutral-Lipid Fatty Acid
NOAA	National Oceanic and Atmospheric Administration
NTS	National Topographic System
NWMO	Nuclear Waste Management Organization
NSCA	Nuclear Safety and Control Act
OD	Outer Diameter
OFP	Oxygen-Free Phosphorus-doped
O/M	Oxygen/Metal
OPG	Ontario Power Generation
PDF	Probability Density Function
PLFA	Phospho-Lipid Fatty Acid
PPT	Precipitate
PQP	Project Quality Plan

PWR	Pressurized Water Reactor
RH	Relative Humidity
RSM	Radionuclide Screening Model
SCC	Stress Corrosion Cracking
SKB	Swedish Nuclear Fuel and Waste Management Company (Svensk Kärnbränslehantering AB)
SRTM	Shuttle Radar Topography Mission
SSM	Swedish Radiation Safety Authority
STP	Standard Temperature and Pressure
SYVAC3	System Variable Analysis Code
TDS	Total Dissolved Solids
TDZ	Thermal Damage Zone
THM	Thermal-hydraulic-mechanical
TWI	The Welding Institute
UDF	Underground Demonstration Facility
UFC	Used Fuel Container
UFPP	Used Fuel Packaging Plant
UFTP	Used Fuel Transportation Package
UofT GSM	University of Toronto Glacial Systems Model
URL	Underground Research Lab
WRA	Whiteshell Research Area

THIS PAGE HAS BEEN LEFT BLANK INTENTIONALLY